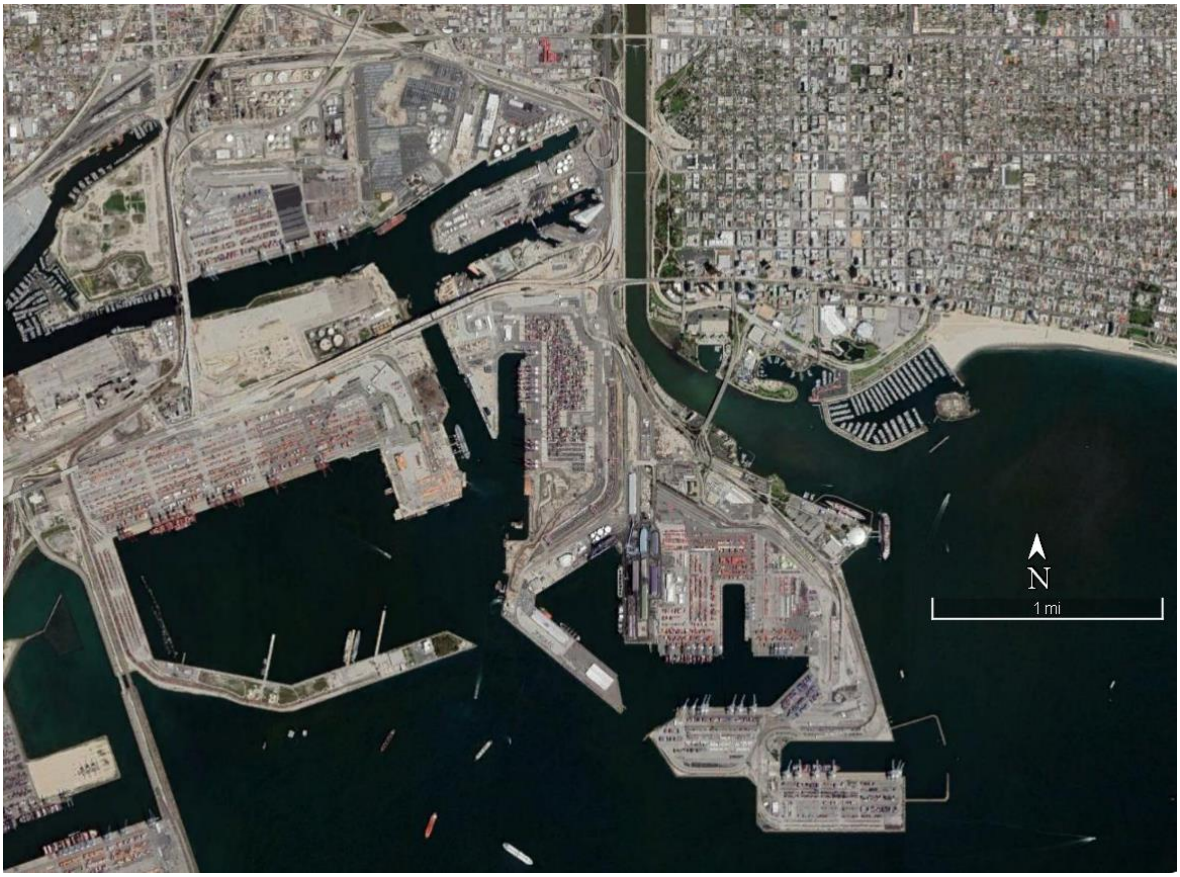
PORT-WIDE GROUND MOTION STUDY UPDATE
PORT OF LONG BEACH, CALIFORNIA

FINAL REPORT



Prepared For:

Port of LONG BEACH
THE PORT OF CHOICE

The Port of Long Beach
415 West Ocean Blvd.
Long Beach, CA 90802

Prepared By:

Earth Mechanics, Inc.
Geotechnical and Earthquake Engineering

Earth Mechanics, Inc.
17800 Newhope Street, Suite B
Fountain Valley, CA 92708

EMI Project No. 19-158

October 26, 2020

Earth Mechanics, Inc.
Geotechnical & Earthquake Engineering

October 26, 2020 EMI Project No. 19-158

The Port of Long Beach
415 West Ocean Blvd.
Long Beach, CA 90802

Attention: Mr. Joel Aguilar, S.E.
Deputy Chief Harbor Engineer

Subject: **Final Port-Wide Ground Motion Study Update Report, Port of Long Beach, California**

Dear Mr. Aguilar,

Attached please find the Final Port-Wide Ground Motion Study Update Report for the Port of Long Beach, California. This report contains the methodology and findings of our study and the resulting recommendations for design of port structures. All review comments received from the Port of Long Beach on previous versions of the report have been incorporated in this report.

On behalf of the entire project team, we appreciate the opportunity to work with you on this project. If you have any questions or comments on this report, please do not hesitate to call us.

Sincerely,
EARTH MECHANICS, INC.



Amir Zand, Ph.D., GE
Senior Engineer



Amin Rahmani, Ph.D., PE
Project Engineer



(Raj) S. Varatharaj, GE
Principal Engineer



(Arul) K. Arulmoli, Ph.D., GE
Project Manager

17800 Newhope Street, Suite B, Fountain Valley, California 92708 Tel: (714) 751-3826 Fax: (714) 751-3928

Copy: Dr. Geoffrey Martin, Emeritus Professor, University of Southern California Technical Advisor
Dr. Nick Gregor, Independent Consultant, Seismologist and Technical Advisor
Mr. Cheng Lai, Moffatt & Nichol, Technical Reviewer
Dr. Omar Jaradat, Moffatt & Nichol, Technical Reviewer

TABLE OF CONTENTS

Section **Page**

ACRONYMS / DEFINITIONS 7

EXECUTIVE SUMMARY 8

1.0 INTRODUCTION 10

1.1 Background 10
1.2 Scope 11
1.3 Basis of Study 12
1.4 Outline of Report 12

2.0 GEOLOGICAL AND GEOTECHNICAL OVERVIEW 15

2.1 Regional Physiography 15
2.2 Regional Stratigraphy 16
2.3 Regional Geologic Structure 17
2.4 Regional Seismicity 18
2.5 Wilmington Blind Thrust Fault 19
2.6 Ground Conditions 19
2.6.1 Information Sources 20
2.6.2 Soil Profiles for Site Response Analysis 20

3.0 PROBABILISTIC SEISMIC HAZARD ANALYSIS (PSHA) 30

3.1 Overview 30
3.2 Uniform Hazard Spectra for Firm (Improved) Ground 30
3.3 Firm (Improved) ground MCE_R ARS per ASCE 7-16 Standards 37
3.3.1 Probabilistic MCE_R ARS for Firm Ground 38
3.3.2 Deterministic MCE_R ARS for Firm Ground 38
3.3.3 Site-Specific MCE_R ARS for Firm Ground 39
3.4 Selected Spectrally-Matched Ground Motion Time Histories For Firm Ground 39
3.5 Methodology Used for Estimation of Sloping Ground Displacements 41

4.0 EARTHQUAKE SITE RESPONSE 44

4.1 Methodology 44
4.2 Soil Profiles and Properties 44
4.3 Shear Modulus Reduction and Damping Ratio Models 45
4.4 Site Response Analysis Results 45
4.5 Unimproved Ground DE ARS per ASCE 7-16 Standards 46

5.0 SUMMARY AND DESIGN RECOMMENDATIONS 50

5.1 Overview 50
5.2 Horizontal Response Spectra for OLE, CLE, 975-yr, and DE Events 50

5.3 Vertical Response Spectra for OLE, CLE, 975-yr, and DE Events 51
5.4 Newmark Displacements 51
5.5 Seismic Parameters for Geotechnical Evaluations 52
5.6 Spectrally-Matched Ground Motion Time Histories 52

6.0 LIMITATIONS 77

7.0 REFERENCES 77

8.0 BIBLIOGRAPHY 89

LIST OF FIGURES

Figure **Title** **Page**

Figure 1-1 Site Location Map 14
Figure 2-1 Regional Fault And Physiography Map 22
Figure 2-2 Geologic Structure Map Of The POLB Area 23
Figure 2-3 Geological Cross Section A-A' 24
Figure 2-4 Geological Cross Section B-B' 25
Figure 2-5 Regional Map Showing Inferred Projected Surface Fault Trace For The Wilmington Blind Thrust Fault (Source: Figure 2 of Wolfe et al., 2019) 26
Figure 2-6 Three-Dimensional (3D) Perspective Of The Wilmington Blind-Thrust Showing Correspondence Between Horizons Mapped From The Offshore 3D Seismic Survey (Source: Figure 6 of Wolfe et al., 2019) 27
Figure 2-7 Soil Zones Used for Seismic Response Analyses 28
Figure 2-8 Idealized Soil Profiles Used for Seismic Response Analyses 29
Figure 3-1 Firm (Improved) Ground ARS and DRS for Earthquakes with Various Return Periods 42
Figure 3-2 Firm (Improved) Ground MCE_R ARS Curve Based on ASCE 7-16 - Section 21.2 43
Figure 4-1 Areas A & B Extents within the Port of Long Beach 47
Figure 4-2 Unimproved Ground DE ARS Curve for Area A Based on ASCE 7-16 - Section 21.3 48
Figure 4-3 Unimproved Ground DE ARS Curve for Area B Based on ASCE 7-16 - Section 21.3 49
Figure 5-1 Recommended Firm (Improved) and Unimproved Ground ARS Curves - Area A - OLE Event 54
Figure 5-2 Recommended Firm (Improved) and Unimproved Ground ARS Curves - Area B - OLE Event 55
Figure 5-3 Recommended Firm (Improved) and Unimproved Ground ARS Curves - Area A - CLE Event 56
Figure 5-4 Recommended Firm (Improved) and Unimproved Ground ARS Curves - Area B - CLE Event 57

Figure 5-5 Recommended Firm (Improved) and Unimproved Ground ARS Curves - Area A - 975 Yr Return Period Event 58
Figure 5-6 Recommended Firm (Improved) and Unimproved Ground ARS Curves - Area B - 975 Yr Return Period Event 59
Figure 5-7 Recommended Firm (Improved) and Unimproved Ground ARS Curves - Area A - ASCE 7-16 Based DE Event 60
Figure 5-8 Recommended Firm (Improved) and Unimproved Ground ARS Curves - Area B- ASCE 7-16 Based DE Event 61
Figure 5-9 Recommended Firm (Improved) and Unimproved Ground DRS Curves - Area A - OLE Event 62
Figure 5-10 Recommended Firm (Improved) and Unimproved Ground DRS Curves - Area B - OLE Event 63
Figure 5-11 Recommended Firm (Improved) and Unimproved Ground DRS Curves - Area A - CLE Event 64
Figure 5-12 Recommended Firm (Improved) and Unimproved Ground DRS Curves - Area B - CLE Event 65
Figure 5-13 Recommended Firm (Improved) and Unimproved Ground DRS Curves - Area A - 975 Yr Return Period Event 66
Figure 5-14 Recommended Firm (Improved) and Unimproved Ground DRS Curves - Area B - 975 Yr Return Period Event 67
Figure 5-15 Recommended Firm (Improved) and Unimproved Ground DRS Curves - Area A - ASCE 7-16 Based DE Event 68
Figure 5-16 Recommended Firm (Improved) and Unimproved Ground DRS Curves - Area B- ASCE 7-16 Based DE Event 69
Figure 5-17 Recommended Firm (Improved) Ground ARS Curves – Areas A and B - OLE, CLE, 975-yr, and ASCE 7-16 Based DE 70
Figure 5-18 Recommended Unimproved Ground ARS Curves – Area A - OLE, CLE, 975-yr, and ASCE 7-16 Based DE 71
Figure 5-19 Recommended Unimproved Ground ARS Curves – Area B - OLE, CLE, 975-yr, and ASCE 7-16 Based DE 72
Figure 5-20 Spectral Amplification Factors (Ratio of Unimproved Ground ARS Over Improved Ground ARS) - Area A - OLE, CLE, 975-yr, and ASCE 7-16 Based DE 73
Figure 5-21 Spectral Amplification Factors (Ratio of Unimproved Ground ARS Over Improved Ground ARS) - Area B - OLE, CLE, 975-yr, and ASCE 7-16 Based DE 74
Figure 5-22 Recommended Firm (Improved) and Unimproved Ground Vertical ARS Curves – OLE, CLE, 975-Yr Return Period and ASCE 7-16 Based DE Event 75
Figure 5-23 Recommended Newmark Displacement Curves for Site Screening for OLE, CLE, 975-yr, DE_G, and MCE_G level Events 76

LIST OF TABLES

Table **Title** **Page**

Table 3-1 Firm (Improved) Ground ARS and DRS for Earthquakes with Various Return Periods 32
Table 3-2 Damping Scaling Factors to Determine Horizontal Component of Spectral Accelerations For Damping Ratios (ξ) 1, 2, 10, 15, 20, and 25% for 72 yr (OLE) event 35
Table 3-3 Damping Scaling Factors to Determine Horizontal Component of Spectral Acceleration For Damping Ratios (ξ) 1, 2, 10, 15, 20, and 25% for 475 yr (CLE), 975 yr and 2475 yr events 35
Table 3-4 Damping Scaling Factors to Determine Vertical Component of Spectral Accelerations For Damping Ratios (ξ) 1, 2, 10, 15, 20, and 25% for 72 yr (OLE) event 36
Table 3-5 Damping Scaling Factors to Determine Vertical Component of Spectral Accelerations For Damping Ratios (ξ) 1, 2, 10, 15, 20, and 25% for 475 yr (CLE), 975 yr and 2475 yr events 36
Table 3-6 Input Seismic Parameters Used to Determine the DE level ARS Curve for Site Class D per Section 21.3 of ASCE 7-16..... 38
Table 3-7 Selected Startup Motions for 72 yr Return Period (OLE) Event..... 40
Table 3-8 Selected Startup Motions for 475-yr (CLE), 975-yr, and 2475-yr Return Period Events 40
Table 4-1 Input Seismic Parameters Used to Develop Code-based ARS Curves for Site Class E and D per Section 21.3 of ASCE 7-16..... 46
Table 5-1 Recommended Seismic Parameters for Geotechnical Evaluations..... 52

APPENDICES

Appendix A Probabilistic Seismic Hazard Analysis (PSHA)
Appendix B OLE, CLE, 975-yr, MCE_R, and DE Level Firm (Improved) Ground Motion Time Histories
Appendix C Details of Site Response Analysis Results
Appendix D Newmark Displacement Anlaysis Results
Appendix E OLE, CLE, 975-yr, and DE Level Unimproved Ground Motion Time Histories

ACRONYMS / DEFINITIONS

ARS: Acceleration Response Spectrum
CBC: California Building Code
CGS: California Geological Survey
CLE: Contingency Level Earthquake having a return period of 475 years
DE: Code-based Design Earthquake (per ASCE 7)
DRS: Displacement Response Spectrum (pseudo-relative displacement)
DSF: Damping Scaling Factor
DSHA: Deterministic Seismic Hazard Analysis
FG: Firm (Improved) Ground
GMC: Ground Motion Characterization
MCE: Maximum Considered Earthquake; Most severe earthquake considered by ASCE 7 (MCE_R or MCE_G)
MCE_G: Geometric Mean Maximum Considered Earthquake
MCE_R: Risk-targeted Maximum Considered Earthquake
Newmark Displacement: Seismically-induced slope movements estimated based on Newmark sliding block method
NISZ: Newport-Inglewood Structural Zone
OLE: Operating Level Earthquake having a return period of 72 years
PEER: Pacific Earthquake Engineering Research Center
POLB: Port of Long Beach
PSHA: Probabilistic Seismic Hazard Analysis
PWGM: Port-Wide Ground Motion
RP: Return Period
SCEC: Southern California Earthquake Center
SRA: Site Response Analysis
SSC: Seismic Source Characterization
UCERF3: Uniform California Earthquake Rupture Forecast, Version 3
UG: Unimproved Ground
USGS: United States Geological Survey
WDC: Wharf Design Criteria
975-yr Event: Earthquake having a return period of 975 years

EXECUTIVE SUMMARY

This report presents an update to the original 2006 port-wide ground motion (PWGM) study and the 2015 addenda to the PWGM study completed by Earth Mechanics, Inc. (EMI, 2006, 2015) for the Port of Long Beach (POLB). The purpose of the present study is to update PWGM Study Report to incorporate the significant advancements that have been made in the understanding of the California earthquake rupture mechanisms, ground motion predictions, and site response evaluations.

The probabilistic seismic hazard analysis (PSHA) efforts were conducted by Dr. Nick Gregor and Dr. Linda Al Atik as consultants to EMI, with EMI providing an independent check. This port-wide ground motions study update was peer reviewed by Dr. Geoffrey Martin, Emeritus Professor, Department of Civil Engineering, University of Southern California. The structural review team included Dr. Omar Jaradat and Mr. Cheng Lai from Moffatt & Nichol (M&N). The primary aim of the study was to develop consistent seismic ground motion recommendations for structures within the POLB area for four different earthquake levels: the operating level earthquake (OLE), having a return period of 72 years, contingency level earthquake (CLE), having a return period of 475 years, 975-year return period earthquake, and code-based design earthquake (DE) per the current California Building Code (CBC, 2019).

Regional and site geology and seismicity were reviewed and summarized to establish the latest understanding on geological features and faults contributing to the seismic hazard at the POLB. Geotechnical ground conditions affecting site response were interpreted from review of available geotechnical data reports for numerous project sites located throughout the port area (no field investigations were undertaken for the purpose of the study). Four generalized site soil profiles representative of the POLB area were developed for site response assessment.

The PSHA was performed using the latest NGA-West 2 ground motion models commonly used in California, including the latest version of seismic source models; Uniform California Earthquake Rupture Forecast, Version 3 (UCERF3)–The Time Independent Model (USGS, 2013). The UCERF3 (USGS, 2013) database as well as the CBC 2019 ground motion maps do not include the recently characterized Wilmington Blind Thrust Fault (Wolfe et al., 2019), located within the San Pedro Bay. The present study considers this fault as an additional seismic source to the UCERF3 (USGS, 2013) seismic source model. The main trace of the Wilmington fault may potentially combine with the Huntington Beach segment, Compton Thrust and Newport-Inglewood faults to potentially generate less frequent larger magnitude events. However, multiple fault rupture scenarios associated with the Wilmington fault have not been researched to date; therefore, these scenarios were not considered in this study. Due to its relatively low slip rate of 0.14-0.18 mm/yr and low recurrence interval of 3,490 to 4,490 years, the contribution of Wilmington fault in the PSHA study was found to be negligible for hazard levels of 2,475 years and less. In general, the inclusion of this source led to an increase of up to 4 percent in the ground motions.

Epistemic uncertainties in earthquake source and ground motion model parameters were addressed through the use of logic tree methodology. Local site conditions were incorporated by performing nonlinear site response analyses using the computer program, DeepSoil (Hashash et al., 2020). Four idealized soil profiles were considered in the analyses. To incorporate uncertainties in soil profiles, the nonlinear time history analysis for each site was conducted using lower-bound, upper-bound, and liquefied soil properties.

This report provides horizontal and vertical components of uniform hazard spectra (UHS) for firm (improved) ground and unimproved ground conditions within the Port for various earthquake levels. The recommended acceleration response spectra can be used by structural designers utilizing modal response spectrum analysis techniques. Damping values ranging from 1% to 25% were considered in the study. A total of seven (7) sets of mutually orthogonal (two horizontal and one vertical) spectrum-compatible acceleration-time histories are provided for unimproved and firm (improved) ground conditions for the selected earthquake events. Simplified Newmark sliding block analyses were performed to develop the corresponding Newmark displacement screening charts, providing estimates of ground displacement as a function of yield acceleration.

The report will need an update of the ground motion criteria presented when significant changes in the state of practice in the seismological, geological, and geotechnical framework occur. Addenda may be issued at future dates to incorporate CBC changes if any.

1.0 INTRODUCTION

1.1 Background

The Port of Long Beach (POLB) commissioned a port-wide ground motion (PWGM) study in 2004 to develop consistent earthquake ground motion recommendations for design of structures within the entire Port area. The two-year PWGM Study was performed by Earth Mechanics, Inc. (EMI), and at the conclusion of the study in August 2006, EMI issued a PWGM Study Report (EMI, 2006). The report included recommendations for two levels of earthquakes: operating level earthquake (OLE), having a return period of 72 years, and contingency level earthquake (CLE), having a return period of 475 years. The CLE corresponds to the design earthquake defined in the 2001 California Building Code (CBC, 2001). The PWGM Study Report was referenced in the first version of the POLB's Wharf Design Criteria (WDC) that outlines the guidelines, recommendations, and requirements for design of new wharves at the POLB (POLB, 2007).

In the 2007 version of the CBC (CBC, 2007), the definition of the Design Earthquake (DE) was revised that invalidated the use of CLE for structures that must be designed per CBC. The new definition was based on the American Society of Civil Engineers' ASCE 7-05 standard (ASCE, 2006). To incorporate the new DE requirements, and also to confirm the validity of the PWGM Study Report using the latest advancements in ground motion predictions New Generation Attenuation (NGA) Study (Abrahamson and Silva, 2008; Boore and Atkinson, 2008; Campbell and Bozorgnia, 2008; Chiou and Youngs, 2008), an Addendum to the PWGM Study Report was prepared by EMI in 2008 (EMI, 2008). This addendum was referenced in the second version of the POLB WDC (POLB, 2009).

Subsequent changes to DE required by the updated versions of the CBC (CBC, 2010; CBC, 2013), and as triggered by changes in the later version of ASCE 7 (ASCE 7-10) were incorporated in Addendum No. 2 (EMI, 2011) and Addendum No. 3 (EMI, 2015) and referenced in Versions 3 and 4 of the WDC (POLB, 2012; POLB, 2015). The requirements for DE in the 2016 CBC (CBC, 2016) remained the same as in the CBC 2013. However, the current CBC (CBC, 2019) incorporates the recommendations from the latest version of ASCE 7 (ASCE, 2016), that will also require revisions to the DE recommendations.

Since the completion of the first NGA Study in 2008, significant advancements in ground motion predictions have been made through the NGA-West2 Project, sponsored by the Pacific Earthquake Engineering Research Center (PEER) that was completed in 2014 (Bozorgnia, et al., 2014; EERI, 2014). Similarly, significant advancements have also been made in the understanding of the California earthquake rupture mechanisms through the project sponsored jointly by the United States Geological Survey (USGS), California Geological Survey (CGS), and the Southern California Earthquake Center (SCEC) and the Working Group of California Earthquake Probabilities. The team completed a report titled "Uniform California Earthquake Rupture Forecast, Version 3 (UCERF3)–The Time Independent Model" (USGS, 2013). In addition, a

recent technical publication suggested the presence of a new fault, the Wilmington Fault, within the San Pedro Bay (Wolfe et al., 2019) that could have an impact on the seismicity within the POLB.

The POLB selected the EMI-Moffatt & Nichol team to complete the current PWGM Study Update to address the above significant advancements in the scientific and engineering communities.

1.2 Scope

The scope of the study includes the following tasks:

- Collect and review available geologic and geotechnical documents and update geologic and ground conditions at the POLB as necessary.
- Perform Probabilistic Seismic Hazard Analysis (PSHA) for firm (improved)-ground conditions for OLE, CLE, 975-year return period earthquake, and DE per the Uniform California Earthquake Rupture Forecast, Version 3 (UCERF3) (USGS, 2013) including the newly characterized Wilmington Fault (Wolfe et al., 2019). Perform sensitivity studies to incorporate uncertainties in firm-ground conditions.
- Develop Acceleration Response Spectra (ARS) and Displacement Response Spectra (DRS) for 5 percent damping for firm (improved)-ground conditions for OLE, CLE, 975-yr event and DE and additional earthquake events having return periods of 25, 50, 100, 200, 300, 400, 1,500, and 2,000 years.
- Develop seven (7) sets of spectrum-compatible acceleration-time histories for OLE, CLE, 975-yr and DE for firm (improved) ground conditions.
- Review ground conditions and update soil profiles as necessary to represent existing (unimproved) subsurface soil conditions.
- Perform one-dimensional Site Response Analysis for various soil profiles developed above for OLE, CLE, 975-yr event, and DE. Perform sensitivity studies to incorporate uncertainties in ground conditions.
- Develop ARS and DRS for 5% damping for unimproved-ground conditions for OLE, CLE, 975-yr event, and DE.
- Develop seven (7) sets of spectrum-compatible acceleration-time histories for OLE, CLE, 975-yr event, and DE for unimproved ground conditions.
- Perform Newmark displacement analyses for OLE, CLE, 975-yr event, DE, and maximum considered earthquake geometric mean (MCE_G) for firm (improved) ground conditions.
- Develop ARS and DRS for various damping values (1%, 2%, 10%, 15%, 20%, and 25%) for unimproved and firm (improved) ground conditions for OLE, CLE, 975-yr event, and DE.

- Document the results and recommendations in a Port-Wide Ground Motion Study Update Report.

Deliverable items produced in accordance with the scope of work were as follows:

- Three (3) hard copies of the Stamped/Signed Report.
- Two (2) Flash Drives of the Report and Time History Native Files.
- One (1) fully editable and searchable PDF of the Stamped/Signed Report.

1.3 Basis of Study

The ground motion study was performed by EMI as a subconsultant to M&N under a contract with the POLB (contract HD-9136). The study was performed using available data and office-based procedures. Geologic and seismicity information was reviewed on a regional and site-specific basis to establish the latest understanding on geological features contributing to the seismic hazard at the POLB. Ground conditions affecting site response within the POLB area were assessed from review of available geotechnical reports for project sites located throughout the POLB area. No field investigations were undertaken for the purpose of the study.

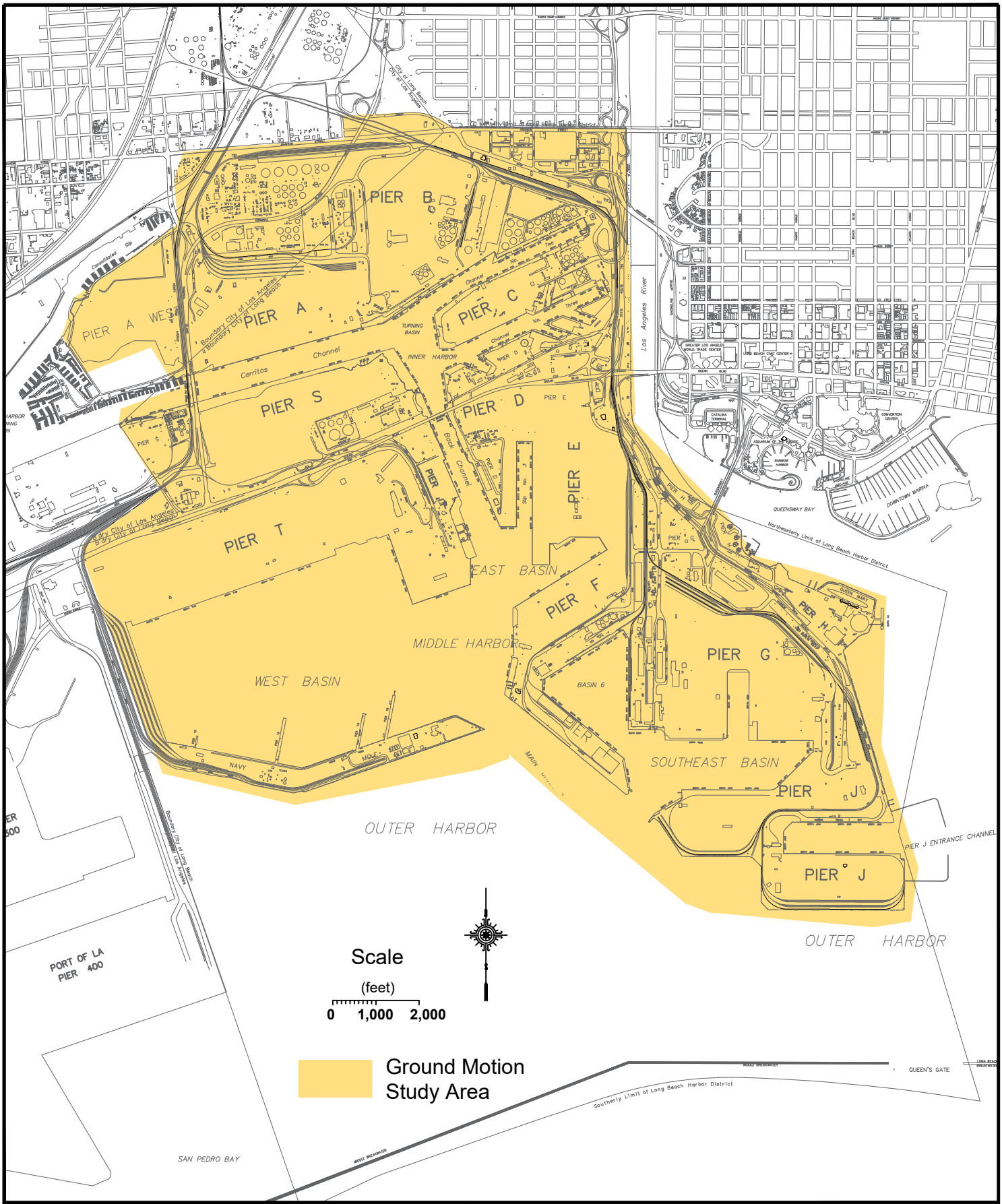
A probabilistic seismic hazard framework based upon the latest California seismic source models, i.e., UCERF3, and NGA-West 2 ground motion models was adopted to perform site-specific seismic hazard analysis. The probabilistic seismic hazard analysis (PSHA) efforts were led by Dr. Nick Gregor and Dr. Linda Al Atik, as consultants to EMI, with EMI providing an independent check. The recently characterized Wilmington fault (Wolfe et al., 2019), located within the San Pedro Bay was also included in the PSHA. The results from the PSHA were used to develop recommendations for firm ground (FG) conditions. Local site conditions were incorporated by performing nonlinear site response analyses (SRA) using the computer program, DeepSoil (Hashash et al., 2020). Four idealized soil profiles were considered to represent site conditions at the Port. Nonlinear time history analysis for each site was conducted by using lower-bound, upper-bound, and liquefied soil properties. The results from the SRA were used to develop recommendations for unimproved ground (UG) conditions. Simplified Newmark Sliding Block analyses were performed to develop the corresponding Newmark displacement charts, providing estimates of ground displacement as a function of yield acceleration.

1.4 Outline of Report

Section 2.0 provides the geological and geotechnical overview. Section 3.0 includes the discussion on PSHA and Newmark displacement evaluation approach. Appendix A includes detailed discussion on PSHA and FG time histories for OLE, CLE, 975-yr, and DE are presented in Appendix B. The Newmark displacement analysis results are presented in Appendix D. Section 4.0 details the earthquake site response evaluation. Appendix C includes the site response analysis

results. The UG time histories for OLE, CLE, 975-yr, and DE are presented in Appendix E. Summary of results and design recommendations are included in Section 5.0.

The report targets those parties involved with the seismic design of all structures located within the POLB area. Key design inputs provided are uniform hazard spectra for OLE, CLE, 975-year return period, and DE excitation levels. These are intended for direct use by structural designers utilizing modal response spectrum analysis techniques. Also provided are spectrum-compatible acceleration-time histories for both unimproved and firm (improved) ground conditions.



Earth Mechanics, Inc.
Geotechnical and Earthquake Engineering

Port-Wide Ground Motion Study Update, Port of Long Beach, California

Site Location Map

Project No. 19-158 | Date: 10-26-20 | Figure 1-1

2.0 Geological and Geotechnical Overview

2.1 Regional Physiography

The POLB area is in the Los Angeles Basin near the juncture of two major physiographic/ geologic provinces, the Peninsular Ranges to the south and the Western Transverse Ranges to the north. In very simple terms the Peninsular Ranges comprise a series of northwest-southeast trending ranges and valleys whereas the Transverse Ranges comprise east-west trending ranges and valleys. Both of these provinces extend into the offshore area and include the Santa Barbara Basin and the Continental Borderland. In both of the provinces the valleys and ranges are separated by major fault zones; these faults trend subparallel to the ranges, that is, northwest-southeast within the Peninsular Ranges and east-west in the Transverse Ranges. The area between the two provinces comprises the Santa Monica Bay, Los Angeles, San Gabriel, and Upper Santa Ana River Valley basins which contain a complex mixture of faults and folds with orientations typical of both provinces.

The POLB is within the coastal area of the Los Angeles Basin which is a large low-lying coastal plain bordered by the Santa Monica Mountains on the north, the Repetto and Puente Hills on the northeast, the Santa Ana Mountains on the east, and the San Joaquin Hills on the south (see Figure 2-1). The southwestern margin of the basin is open to the Pacific Ocean except for one prominent hill, the Palos Verdes Hills or Peninsula. The offshore area to the southwest is characterized by a broad, relatively shallow, shelf or bench that extends about 5 to 15 km where it drops off steeply to deep ocean basins, the Santa Monica Basin north of the Palos Verdes Hills and the San Pedro Basin south of the hills. The offshore area is characterized by a series of islands and submarine shoal areas, or banks, separated by deep basins, and commonly referred to as the Southern California Continental Borderland.

The floor of the Los Angeles Basin is a relatively flat surface rising gently from sea level along the coastline to the surrounding mountains which then rise abruptly to a few thousand feet above the plain. The flat basin floor is interrupted in a few localities by small hills such as the northwesterly alignment of hills and mesas extending from the Newport Beach area on the south to the Beverly Hills area on the north. This northwest-trending alignment of hills divides the basin floor into two major plains, the Downey-Tustin Plain northeast of the hills and the Torrance Plain on the southwest.

The inland margins of the Los Angeles Basin are commonly elevated somewhat above the general level of the basin floor within an apron of higher elevation surfaces such as the Santa Monica Plain, La Brea Plain, Montebello Plain, Santa Fe Springs Plain, and the Coyote Hills (see Figure 2-1). These elevated plains generally comprise slightly dissected older alluvial surfaces.

The major drainages in the Los Angeles Basin enter the basin through narrow passes or gaps in the hills and then flow southerly to the ocean. The major drainages are the Los Angeles River, the San Gabriel River, and the Santa Ana River. Other local significant drainages are Rio Hondo, Coyote Creek, Ballona Creek, Compton Creek, and San Diego Creek. The Port of Long Beach lies

within the coastal delta of the Los Angeles and San Gabriel rivers, but this drainage system has been highly modified by channelization of the streams within a network of concrete and rip-rap lined aqueducts.

2.2 Regional Stratigraphy

The floor of the Los Angeles Basin, the marginal plains, and the adjacent submarine shelf are directly underlain by Quaternary-age sandy sediments with local silts, clays, and gravels. These generally can be subdivided into nonindurated, loose Holocene-age sediments that cover the bulk of the basin and shelf, and Pleistocene-age materials which are exposed only locally within some of the uplifts within the Newport-Inglewood Structural Zone and the marginal plains.

Onshore, the uppermost Pleistocene materials are generally non-marine deposits referred to as the Lakewood Formation which is on the order of 125,000 to 500,000 years old (California Department of Water Resources, 1961). These late- to middle-Pleistocene sediments overlie older early Pleistocene marine sediments referred to as the San Pedro Formation which is more than 500,000 years old. The San Pedro Formation overlies marine Tertiary-age (> 2 million years) sediments and sedimentary rocks. These include the Pico, Repetto, Fernando, Puente, and Monterey formations. The Tertiary-age sediments and rocks, in turn, overlie Mesozoic-age (~100 million years) crystalline basement rocks at depths ranging from about 1,500 to 3,000 m west of the Newport-Inglewood Structural Zone (NISZ) to as much as 10,000 m in the deepest part of the central basin east of the NISZ (Yerkes et al., 1965). The basement west of the NISZ is primarily metamorphic rock (schist) whereas the basement to the east includes both metamorphic and igneous rocks.

A geologic structure map is shown in Figure 2-2 and characteristic geological cross sections in Figure 2-3 and Figure 2-4 that typify site stratigraphy and geologic structure in the POLB area. Surficial geology is characterized by Holocene-age, near-shore, marine and non-marine strata, including beach, estuary, tidal flat, lagoon, shallow-water bay sediments, and shoreline terrace deposits. Deposited as sea level rose during the Pleistocene age, these deposits have been significantly modified by dredging and filling operations for the numerous harbor facilities. The approximate location of the natural shoreline before harbor and urban development is partially shown on Figure 2-2 indicating that most of the harbor facilities south of the coastal bluffs have been constructed on fill.

Both the fill and the native near-shore sediments overlie similar older deposits of the late-Pleistocene-age Lakewood Formation, which in turn overlies the early Pleistocene San Pedro Formation (see Figure 2-3 and Figure 2-4). Differentiating the young sediments from the Lakewood or San Pedro formations is difficult in boreholes because of their similar origin and characteristics. Except for density, which is generally greater in the older Lakewood and San Pedro formations, the units can only be confidently differentiated by fossil analysis. Underlying strata comprise folded and faulted Pliocene- and Miocene-age formations, and the major angular Pico unconformity,

separating the Quaternary and upper Pliocene sediments from lower Pliocene-Miocene deposits and Catalina Schist basement (see Figure 2-3 and Figure 2-4).

2.3 Regional Geologic Structure

The present-day tectonic stress field is one of north-northeasterly compression. This is seen in the geologic structure, and is indicated by earthquake focal-mechanism solutions and by geodetic measurements. These data suggest compression rates of between 5 and 9 mm/yr across the greater Los Angeles area.

Except for a few marginal zones, the geologic structure of the Los Angeles basin is characterized by relatively flat-lying, late-Quaternary strata overlying slightly folded early-Pleistocene strata, which in turn overlie gently to moderately dipping Pliocene strata of the Fernando, Pico, and Repetto formations and the Miocene Puente/Monterey Formation.

The central part of the basin is a deep trough that rises rather abruptly due to faulting and folding. The principal faulting zones are the NISZ-Los Alamitos system on the west and the Puente Hills fault system (Los Angeles-Santa Fe Springs-Coyote Hills-Peralta Hills faults) on the east.
Except for the Newport-Inglewood Structural Zone, most surface geological faults such as the Santa Monica, Hollywood, and Whittier faults occur along the basin margins. In addition to these known surface faults, the Los Angeles region is underlain by subsurface thrust and reverse faults (commonly referred to as "blind" faults and shown on Figure 2-1 as dotted lines). These are poorly understood features with poorly known locations and orientations. Most of the known subsurface faults underlie the higher-standing plains along the inland margin of the basin, but others have been proposed (for example, the San Joaquin Hills thrust fault). Most large earthquakes associated with these subsurface features are most likely to originate at depths between 10 and 15 km. The 1987 Whittier earthquake occurred on one of these buried faults that dips northerly under the Repetto Hills and San Gabriel Basin northeast of the site.

The Los Angeles region has a complicated history. Within much of the area, the basement is buried beneath sedimentary and volcanic rocks no older than Miocene. Apparently, basement rocks in the region were unroofed and exposed across wide areas when the ancient Farallon oceanic plate, which was being subducted from the west, stopped subducting below the area (Atwater and Stock, 1998). Upon cessation of subduction, regional rifting and strike-slip faulting occurred oblique to the continental margin leading to clockwise rotation of the Transverse Ranges (Luyendyk et al., 1980) involving the existing faults. In late Pliocene and Quaternary time (the past 4 million years), faults that previously formed by extension were involved in regional crustal compression (Wright 1991; Crouch and Suppe, 1993). During the transition from extension to compression, some middle Miocene normal faults were reactivated as reverse and strike-slip faults (Rivero et al., 2000). Blind thrust faults and folds may have begun to form about this time. In the project area, evidence for the Pliocene onset of the compressive deformation comes from the large Wilmington anticline which deforms rocks deposited since lower Pliocene

time. The folding and faulting that formed this anticline apparently was largely completed before the end of the late Pliocene (Truex, 1974).

The present tectonic regime appears to have been in place since middle Pleistocene time and the present-day configuration of the Los Angeles basin would have been recognizable about 200,000 to 300,000 years ago, although the sea may have still occasionally migrated into some low-lying coastal channels (Ponti, 1989). The bulk of tectonic activity in the Long Beach region during Quaternary time appears to have occurred along the Palos Verdes fault and the NISZ, both of which form the most prominent uplifts in the Los Angeles Basin. The Signal Hill uplift within the NISZ, for example, formed in the past couple hundred thousand years (Ponti and Lajoie, 1992). If these deformation characteristics can be applied basin wide, the greatest tectonic activity within late Pleistocene time has occurred primarily in proximity to the major surface faults such as the Palos Verdes, Malibu-Santa Monica-Hollywood, Newport-Inglewood, Whittier, and Sierra Madre faults. The subsurface thrust faults within the region have not been active enough to create similar prominent uplifts and only a few (e.g. Santa Fe Springs) even have subtle recognizable surface expression.

The Pico unconformity shown on Figure 2-3 and Figure 2-4 is a feature of tectonic significance. This unconformity indicates that the major folding of the Wilmington Anticline occurred prior to the Quaternary time. High-resolution, 3-dimensional, seismic-reflection data from the THUMS oil operations (Prior, 2004) clearly show that the THB fault is truncated at the Pico unconformity indicating that the fault has not been active since late Tertiary time. In contrast to the THB fault, the Palos Verdes and Newport-Inglewood faults extend to the surface and are associated with abundant Quaternary deformation and prominent surface uplifts such as the Palos Verdes Hills and Signal Hill. Increased activity on the NISZ in latest Tertiary and Quaternary time appears to coincide with the end of major activity on the THB fault.

A small amount of uplift has occurred in the area of the Wilmington Anticline since late Pliocene time, and some of this uplift appears to be Quaternary in age (Ponti, 2004; Edwards et al., 2002). This uplift is compatible with the regional compressional forces acting across the Los Angeles region. The compression can result in transpressional strike slip faulting, thrust faulting, and/or folding. Both the NISZ and the Palos Verdes faults are transpressional strike slip faults whereas the Wilmington anticline-syncline and Gardena syncline represent folding between the major faults. The documented uplift (Castle and Buchanan-Banks, 1989) in the Wilmington anticline area is associated with the 1933 Long Beach earthquake on the NISZ and represents evidence that at least some Quaternary-age folding of the Wilmington anticline is due to tectonics of the adjacent faults. Alternatively, thrusting on the subsurface Compton thrust ramp has been proposed as a cause of folding of the Wilmington anticline (Shaw, 1993).

2.4 Regional Seismicity

Details of the fault systems at the Port based on the Uniform California Earthquake Rupture Forecast, Version 3 (UCERF3)–The Time Independent Model (USGS, 2013) including the newly

characterized Wilmington fault (Wolfe et al., 2019) are elaborated in Appendix A. On average, the greater Los Angeles area (i.e. the Los Angeles basin and the adjoining basins such as the San Fernando and San Gabriel valleys) is experiencing compression at rates of between 5 and 9 mm/yr as a result of north-northeasterly tectonic shortening. This compressional tectonic behavior results in a complex mixture of strike-slip and reverse (thrust) faulting and folding. Some of the reverse and thrust faults are poorly located and poorly understood, but earthquakes such as the 1987 Whittier Narrows and 1994 Northridge earthquakes are testimony to the existence of the subsurface reverse faults and for their importance to seismic design. Nevertheless, the bulk of tectonic activity in the Long Beach region during Quaternary time appears to have occurred along the nearby Palos Verdes fault and Newport-Inglewood Structural Zone (NISZ), both of which are primarily strike-slip faults and represent the most significant seismic potential for the POLB.

2.5 Wilmington Blind Thrust Fault

The inferred projected surface trace of the recently characterized Wilmington fault is shown in Figure 2-5. Also plotted in the figure as thin red lines are the fault traces of the seismic fault sources contained in the UCERF3 database. Wolfe et al. (2019) estimate the slip rate of the Wilmington fault to be in the range of 0.14 to 0.18 mm/yr, which is lower than the other faults in the immediate region. According to Wolfe et al. (2019), the range in recurrence intervals for the fault is estimated to be 3490 – 4490 years. Given this range, equally weighted recurrence intervals values of 3490, 3990, and 4490 years were assumed for this fault.

Three-dimensional representation of the fault is shown in Figure 2-6. The main trace of the Wilmington fault may potentially combine with the Huntington Beach segment, Compton Thrust and Newport-Inglewood faults to potentially generate larger magnitude events but the recurrence intervals of these events is as expected longer and thus their potential impact on the seismic hazard results for hazard levels of 2,500 years and less would be expected to be reduced.

2.6 Ground Conditions

Pier facilities at the POLB have been formed from natural coastal and man-made land masses, creating wide variations in ground conditions throughout the POLB area. Dredged fill materials have been used extensively in the construction of the man-made land masses. These materials generally are not considered representative of firm-ground conditions assumed in probabilistic hazard studies. An assessment of ground conditions was therefore undertaken to establish appropriate depths to firm-ground conditions and to assess appropriate site response behavior for design.

Firm-ground conditions were defined on the basis of time-averaged shear wave velocity. The average shear wave velocity $\bar{v}_s$ was calculated as follows:

$$\bar{v}_s = \frac{\sum_{i=1}^{n} d_i}{\sum_{i=1}^{n} \frac{d_i}{v_{si}}} \tag{2.1}$$

Where:

d_i = thickness of layer i (in ft), and

v_{si} = shear wave velocity in layer i (in ft/sec).

The depth to firm ground was defined at the top of a 100-ft (30-m) depth interval that has a minimum time-averaged shear wave velocity $\bar{v}_{s30}$ of approximately 1,000 ft/sec (≈300 m/sec):

$$\bar{v}_{s30} = 1{,}000\ ^{ft}/_{sec} = \frac{100\,ft}{\sum_{i=1}^{n} \frac{d_i}{v_{si}}} \tag{2.2}$$

Information sources and the methodology for the development of these depths at various locations at the POLB are described below.

2.6.1 Information Sources

The primary source of information for ground conditions at the POLB was past project-specific reports made available by the POLB. These comprised mainly geotechnical reports undertaken at berths, piers and other structures as listed in the bibliography in Section 7. The ground information contained in these geotechnical reports was in the form of boring investigations with Standard Penetration Test (SPT) data generally provided at 5-foot intervals, and Cone Penetration Test (CPT) soundings. Depths investigated were typically on the order of 100 ft.

Other sources of ground investigation information included shear wave velocities obtained from the ROSRINE database (ROSRINE, 2001) and several of the projects listed in the bibliography where geophysical testing was also performed.

2.6.2 Soil Profiles for Site Response Analysis

Soil profiles were established through evaluation of the available information to determine appropriate response parameters (shear wave velocity and density) and to establish expected depths to firm-ground conditions. As boring investigations represented most of the available information, evaluation efforts were largely concerned with assimilation of the various soil descriptions, SPT blowcount, and density data indicated. CPT sounding and shear wave velocity data served to supplement and support this information. Findings suggested a demarcation of the POLB into four areas denoted as Zones I, II, III and IV in which similar soil profiles were apparent. The approximate extents of these zones are shown in Figure 2-7.

The four idealized soil profiles and shear wave velocity profiles corresponding to each zone are shown in Figure 2-8. Shear wave velocity profiles were established by reconciling SPT blowcount

and density data with available shear wave measurements and drawing on experience with similar ground conditions in the area. Density values assigned varied between 115 pcf (harbor sediments), 120 pcf (alluvial fill) and 125 pcf (alluvial/Gaspur deposits). Depths to firm-ground conditions were based on $\bar{v}_s$ calculations using available shear wave velocity data and interpretation of SPT blowcounts in a similar manner. The profiles shown in Figure 2-8 end at depths corresponding to the defined firm-ground condition.

It should be noted that the available boring investigations, CPT soundings, and shear-wave velocity measurements provided data representative of ground conditions at specific locations only, and were not of sufficient extent to permit a comprehensive characterization. Therefore, the soil profiles presented are therefore only considered to be generally representative of local site conditions at the POLB. Specific ground investigations undertaken as part of a routine site investigation program are expected to establish which soil profile(s) are most appropriate on a site-by-site basis. This will also allow for the possibility of peculiar ground conditions that may require special attention.

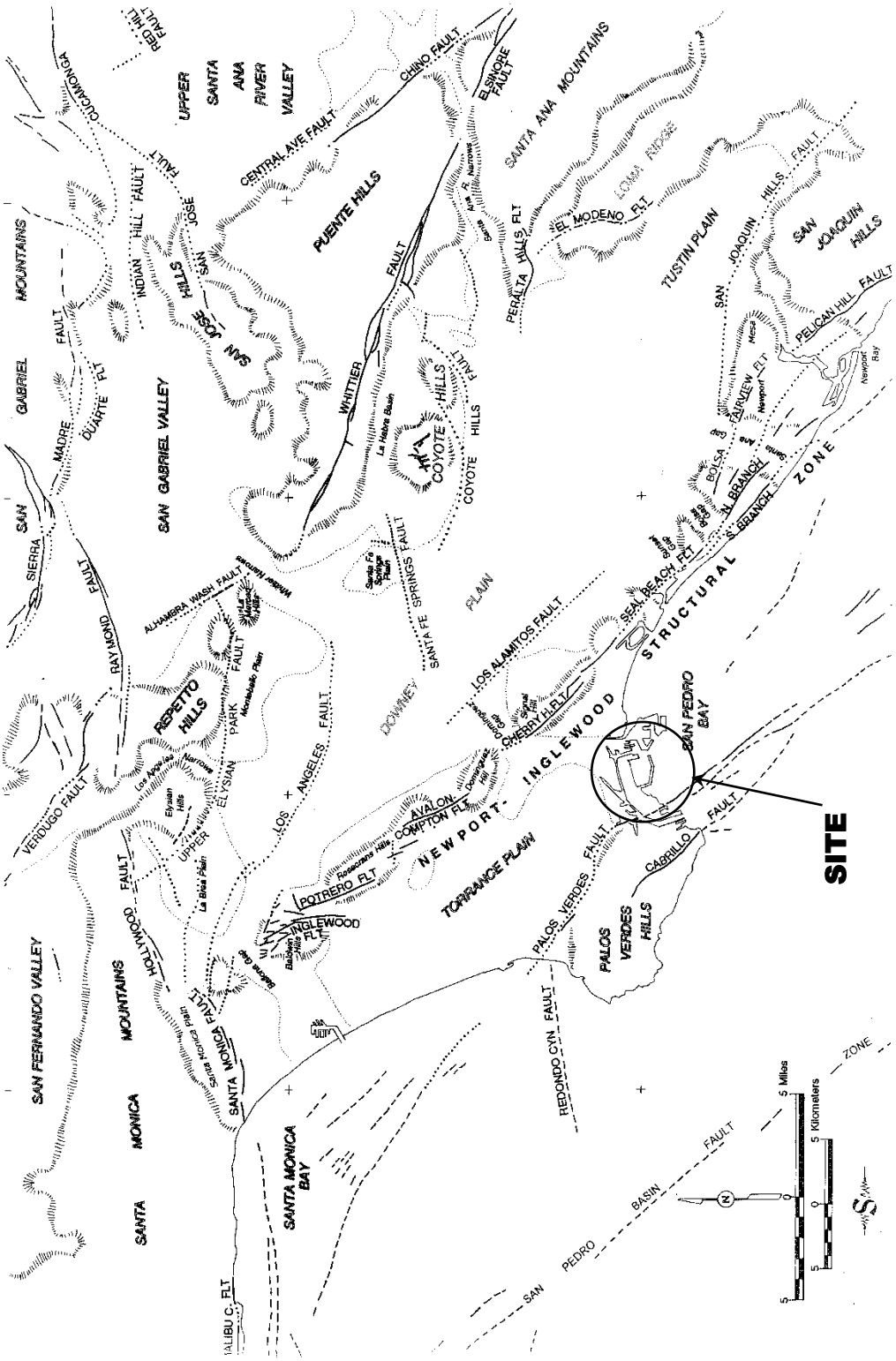


FIGURE 2-1 REGIONAL FAULT AND PHYSIOGRAPHY MAP

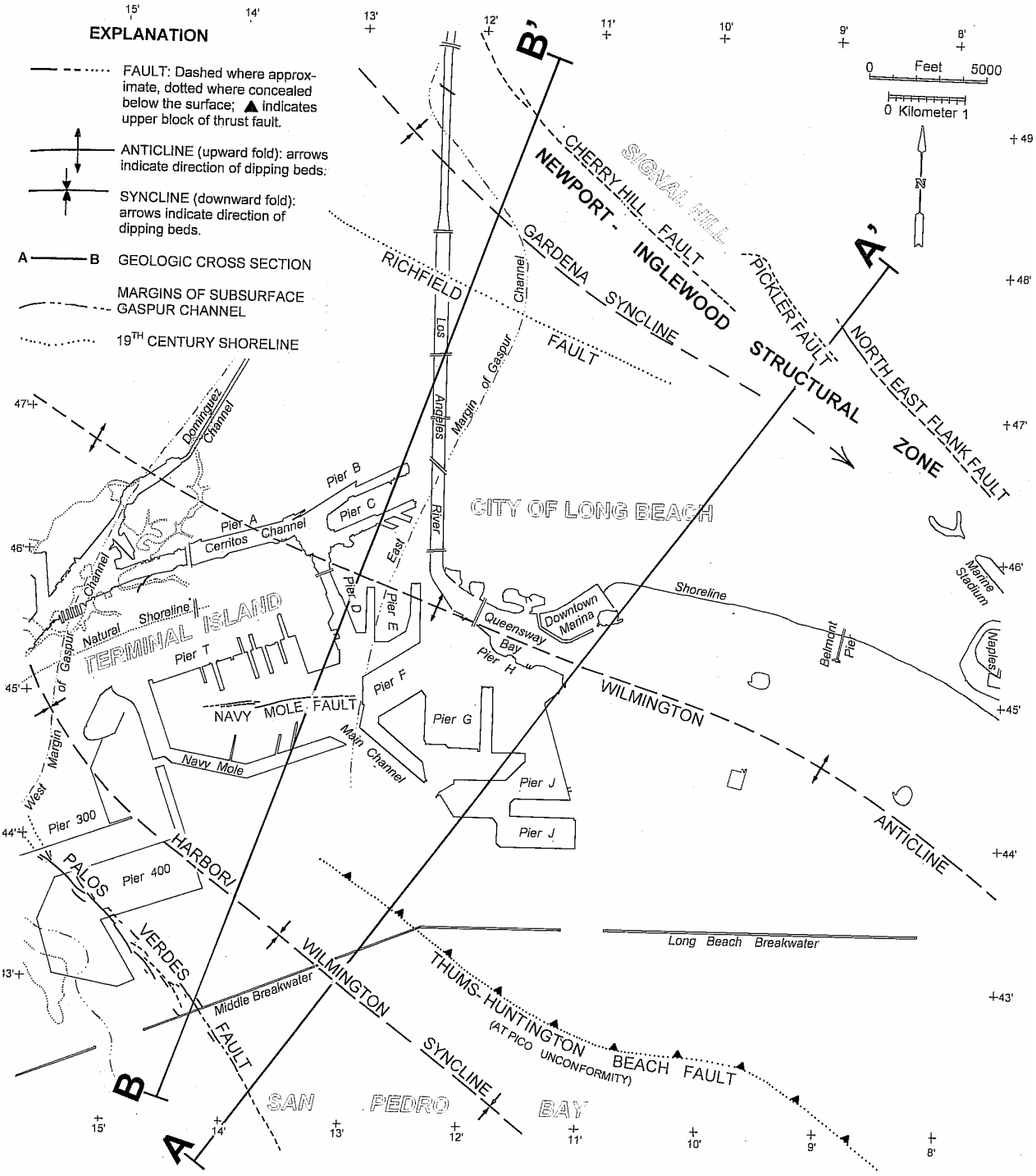


FIGURE 2-2 GEOLOGIC STRUCTURE MAP OF THE POLB AREA

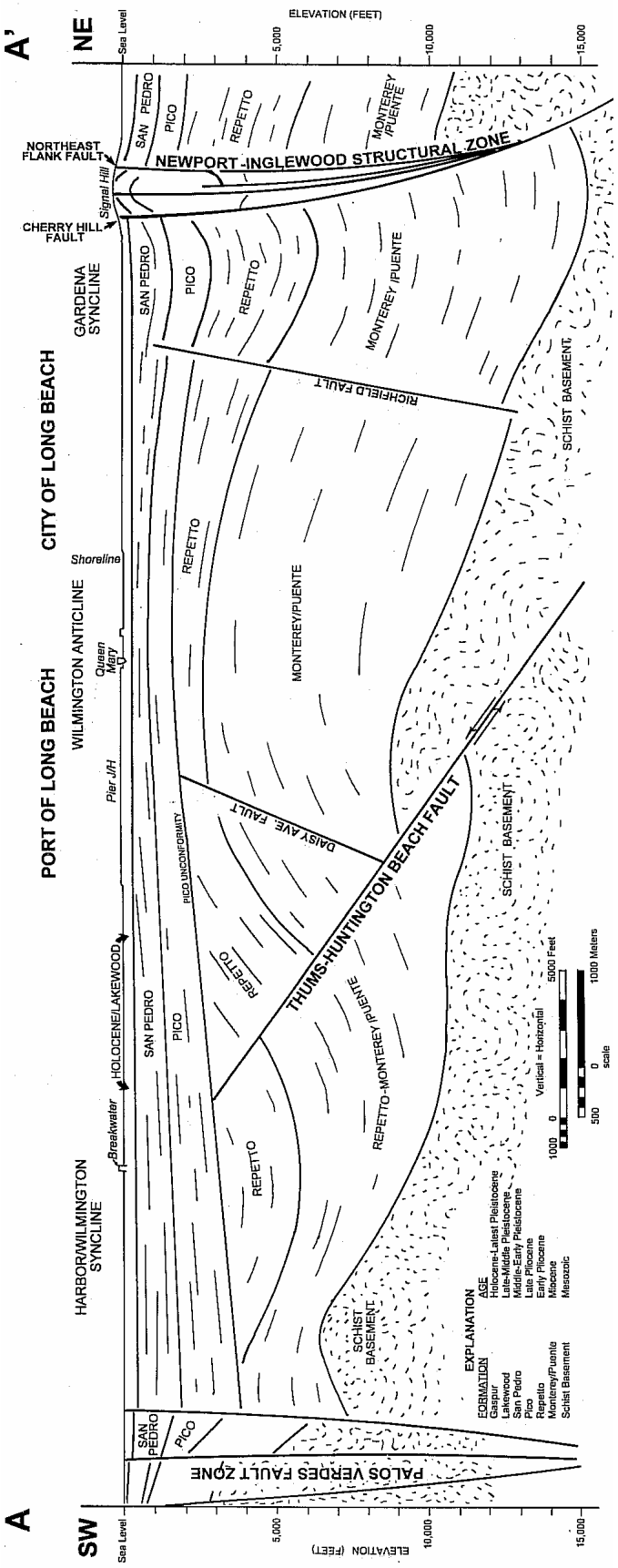


FIGURE 2-3 GEOLOGICAL CROSS SECTION A-A'

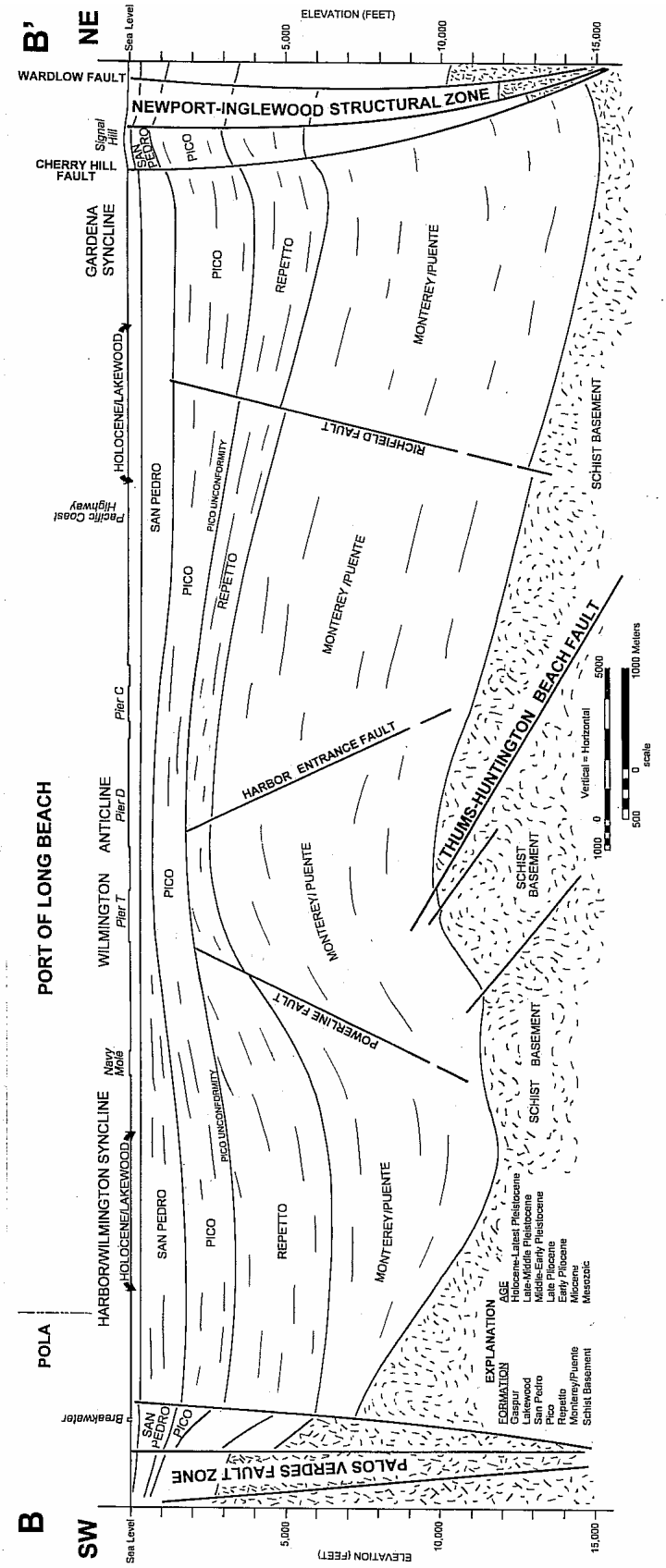


FIGURE 2-4 GEOLOGICAL CROSS SECTION B-B'

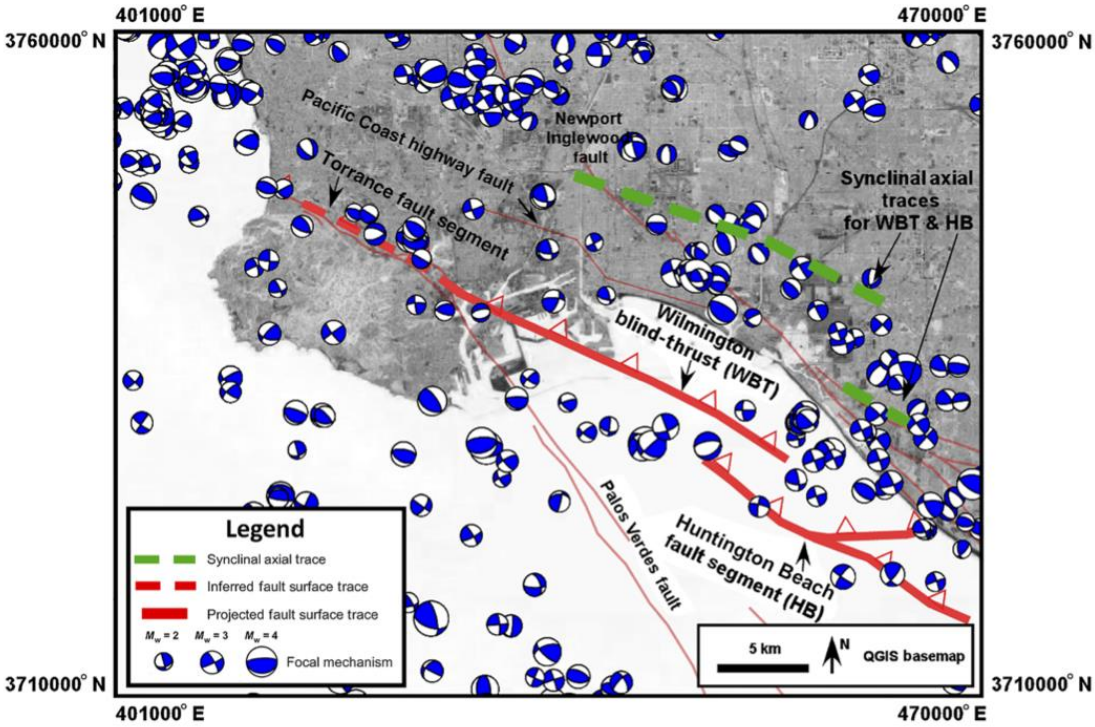


FIGURE 2-5 REGIONAL MAP SHOWING INFERRED PROJECTED SURFACE FAULT TRACE FOR THE WILMINGTON BLIND THRUST FAULT (SOURCE: FIGURE 2 OF WOLFE ET AL., 2019)

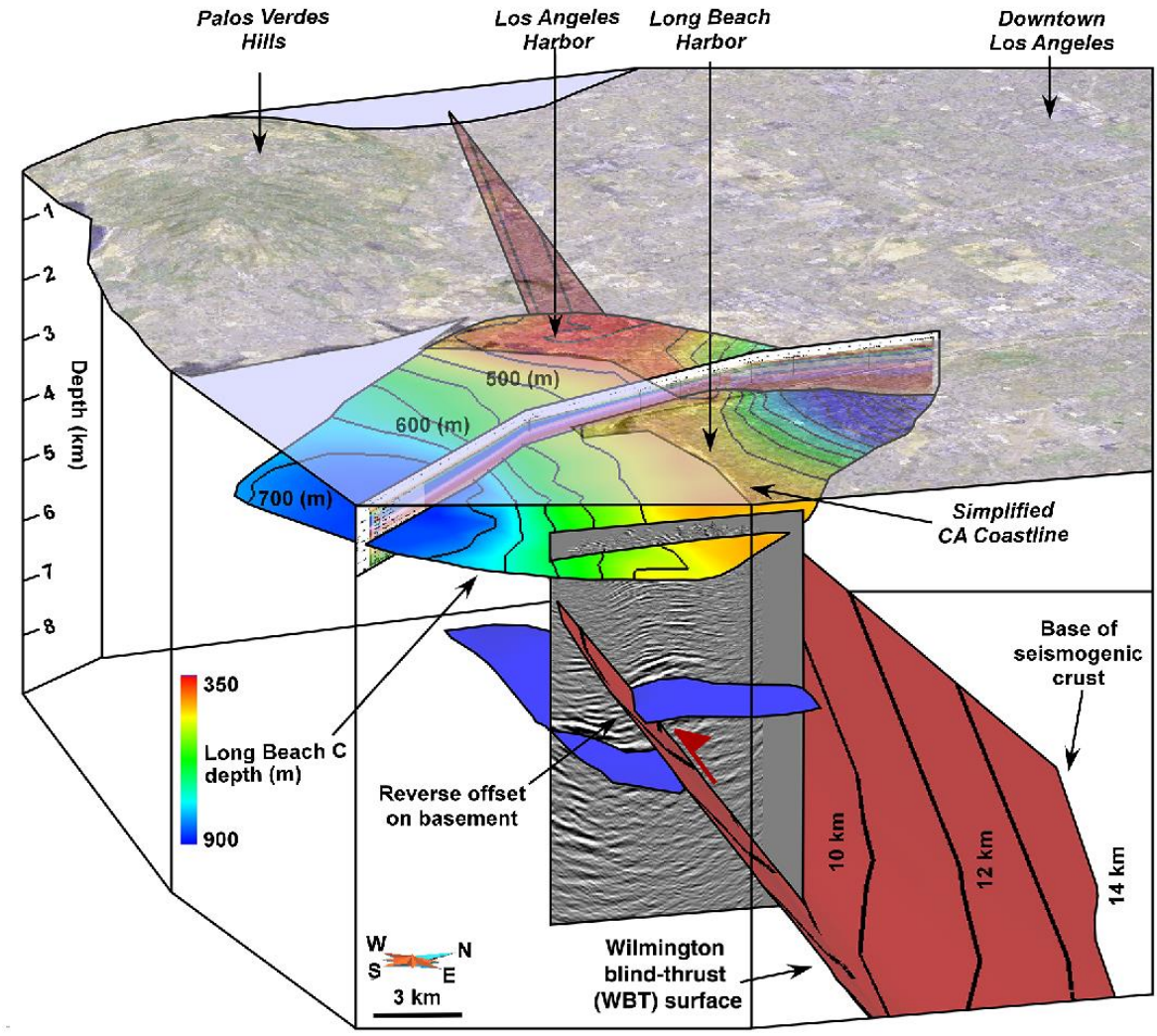
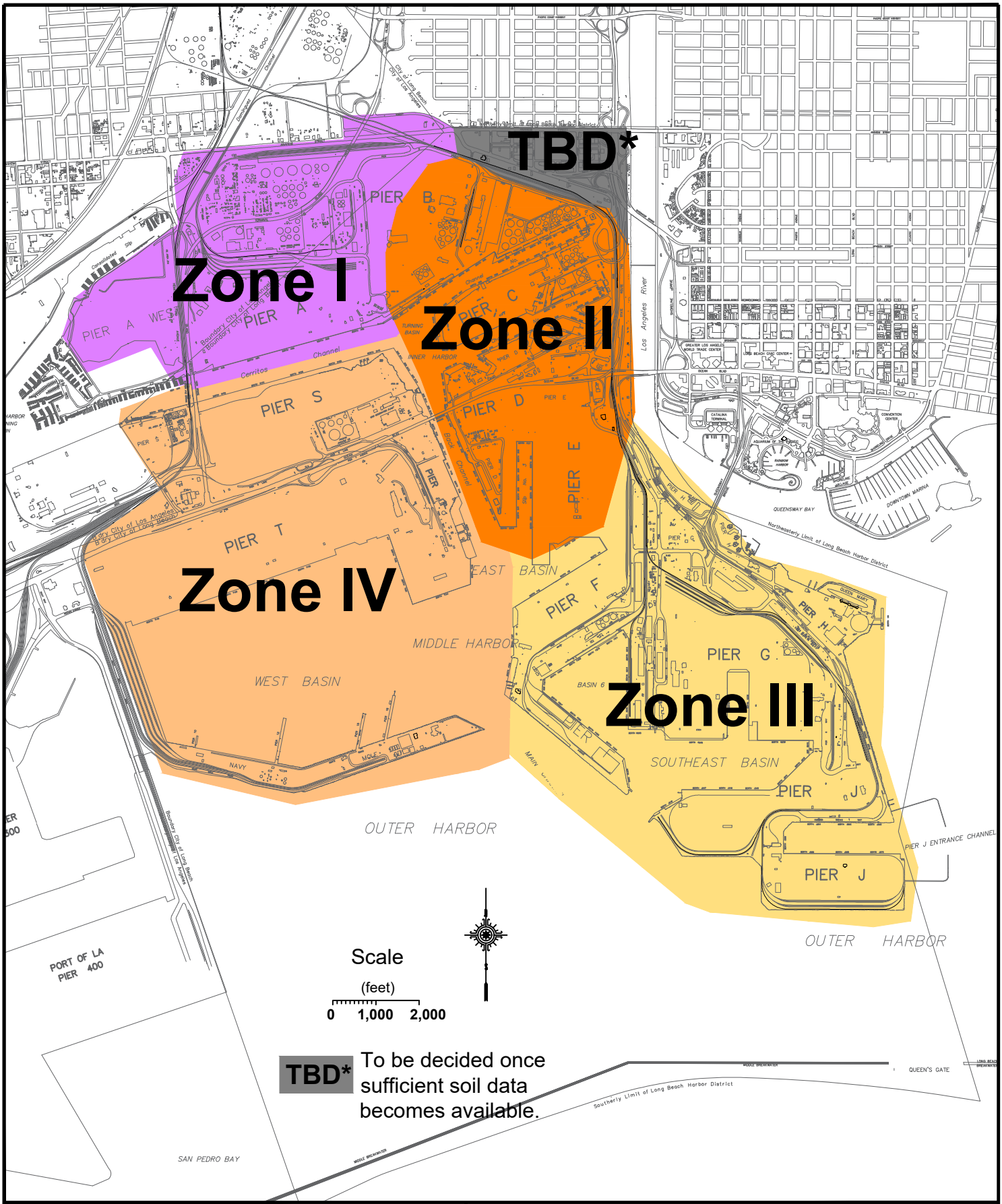


FIGURE 2-6 THREE-DIMENSIONAL (3D) PERSPECTIVE OF THE WILMINGTON BLIND-THRUST SHOWING CORRESPONDENCE BETWEEN HORIZONS MAPPED FROM THE OFFSHORE 3D SEISMIC SURVEY (SOURCE: FIGURE 6 OF WOLFE ET AL., 2019)



Earth Mechanics, Inc.
Geotechnical and Earthquake Engineering

Port-Wide Ground Motion Study Update, Port of Long Beach, California

Soil Zones Used For Seismic Response Analyses

Project No. 19-158 | Date: 10-26-20 | Figure 2-7

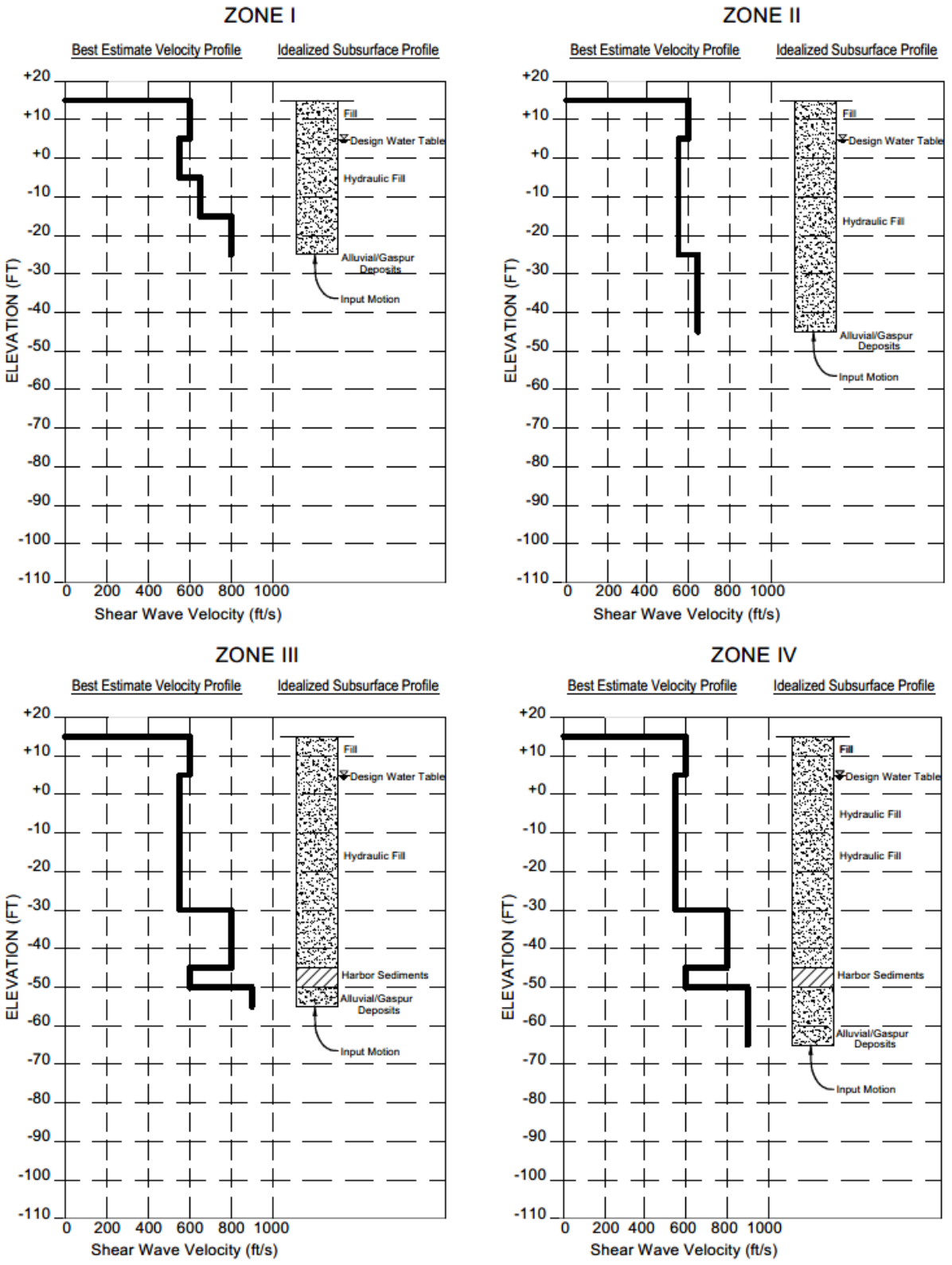


FIGURE 2-8 IDEALIZED SOIL PROFILES USED FOR SEISMIC RESPONSE ANALYSES

3.0 PROBABILISTIC SEISMIC HAZARD ANALYSIS (PSHA)

3.1 Overview

The probabilistic seismic hazard analysis (PSHA) followed the standard approach initially developed by Cornell (1968). This approach has been expanded to fully treat both the randomness (aleatory variability) and the scientific uncertainty (epistemic uncertainty). The PSHA analyses were previously developed as part of a port-wide seismic hazard study for the Port of Long Beach (POLB) (EMI, 2006). These ground motions were developed following a standard PSHA methodology and the current state of knowledge and practice input models at the time of the study. These models include the seismic source characterization (SSC) and the ground motion characterization (GMC). During the last decade with the collection and understanding of vast amounts of geological and seismological data, these SSC and GMC models have evolved and subsequently the models used in the 2006 study have been updated and replaced with current PSHA practice.

The SSC was based on the current state of knowledge for crustal seismic source characterization for California developed in the Uniform California Earthquake Rupture Forecast Version 3 (UCERF3). The newly characterized Wilmington fault (Wolfe et al., 2019) located in the immediate area around the POLB was also included in SSC. Due to its relatively low recurrence interval of 3,490 to 4,490 years and also low slip rate of 0.14-0.18 mm/yr, the contribution of Wilmington fault in the PSHA study was found to be negligible for hazard levels of 2,475 years and less. In general, the inclusion of the Wilmington fault in the UCERF 3 database led to an increase of up to 4 percent in the ground motion spectral accelerations. Further discussions regarding the Wilmington Fault characteristics are provided in Section 2.3 of Appendix A.

Four equally weighted Next Generation Attenuation models for Western US (NGA-West2) were used to predict ground motions for the PSHA study. The NGA-West 2 models are: Abrahamson et al. (2014) (referred to as ASK14), Boore et al. (2014) (referred to as BSSA14), Campbell and Bozorgnia (2014) (referred to as CB14), and Chiou and Youngs (2014) (referred to as CY14). A $V_{S,30}$ value of 300 m/sec was used to represent firm (improved) ground conditions. The Idriss (2014) ground motion model was not used in this study due to the site-specific $V_{S,30}$ value of 300 m/sec being less than the minimum recommended value of 450 m/sec for this model. Further details of the SSC, GMC, and methodologies used to consider ground motion directivity effects and develop vertical component of spectral responses are explained in Appendix A.

3.2 Uniform Hazard Spectra for Firm (Improved) Ground

The PSHA was performed for firm (improved) ground conditions to determine the uniform hazard spectra of earthquake events having return periods of 72, 475, 975 and 2,475 years. The analysis was extended to develop uniform hazard spectra for additional earthquake events having return periods of 25, 50, 100, 200, 300, 400, 1,500, and 2,000 years. The firm (improved) ground five (5) percent damping acceleration and pseudo relative displacement response spectra (ARS, DRS) for

the earthquake return periods (RP): 25, 50, 72 (OLE), 100, 200, 300, 400, 475 (CLE), 975, 1,500, 2,000 and 2,475 years are presented in Figure 3-1. Table 3-1 presents the spectral values for each of the events.

The spectral responses for other damping ratios can be correlated from the 5% damping spectral responses using the methodology outlined in the Pacific Earthquake Engineering Research Center (PEER) report by Rezaeian et al. (2012). The approach outlines a procedure to determine a Damping Scaling Factor (DSF) that is expressed as:

$$\text{DSF} = \frac{\text{Spectral acceleration for a } \xi\% \text{ damping ratio } (\text{Sa}_{\xi})}{\text{Spectral acceleration for a 5\% damping ratio } (\text{Sa}_{\xi=5\%)}}$$

The DSFs as a function of vibration periods were determined for 72 (OLE), 475 (CLE), 975 and 2,475 yr return period events for damping ratios of 1%, 2%, 10%, 15%, 20%, and 25%. The DSFs are presented in Tables 3-2 and 3-3. These values are applicable for horizontal component of ground motions. For vertical component, the DSFs presented in Tables 3-4 and 3-5 should be used.

Per the definition, spectral responses for a given damping ratio can be obtained by multiplying the spectral acceleration for 5% damping by the corresponding DSF presented in the tables.

TABLE 3-1 Firm (Improved) Ground ARS and DRS for Earthquakes with Various Return Periods

Period (sec)	25 yr RP		50 yr RP		72 yr RP		100 yr RP	
	Accel (g)	Disp. (in) *	Accel (g)	Disp. (in) *	Accel (g)	Disp. (in) *	Accel (g)	Disp. (in) *
0.010	0.090	0.000	0.144	0.000	0.179	0.000	0.217	0.000
0.020	0.090	0.000	0.144	0.001	0.179	0.001	0.217	0.001
0.030	0.093	0.001	0.149	0.001	0.186	0.002	0.225	0.002
0.040	0.101	0.002	0.161	0.003	0.201	0.003	0.242	0.004
0.050	0.109	0.003	0.174	0.004	0.217	0.005	0.262	0.006
0.075	0.140	0.008	0.222	0.012	0.276	0.015	0.333	0.018
0.100	0.171	0.017	0.270	0.026	0.335	0.033	0.404	0.040
0.150	0.211	0.047	0.333	0.073	0.413	0.091	0.494	0.109
0.200	0.226	0.088	0.357	0.140	0.443	0.173	0.530	0.208
0.250	0.227	0.139	0.359	0.219	0.446	0.273	0.536	0.328
0.300	0.222	0.195	0.350	0.308	0.436	0.384	0.525	0.463
0.400	0.198	0.309	0.312	0.489	0.390	0.611	0.473	0.741
0.500	0.175	0.428	0.277	0.679	0.348	0.851	0.423	1.036
0.750	0.124	0.680	0.199	1.096	0.250	1.378	0.307	1.692
1.000	0.091	0.887	0.147	1.441	0.187	1.828	0.230	2.251
1.500	0.055	1.220	0.092	2.029	0.118	2.592	0.146	3.220
2.000	0.038	1.473	0.063	2.472	0.082	3.198	0.102	3.996
3.000	0.022	1.908	0.037	3.256	0.048	4.265	0.061	5.378
4.000	0.014	2.167	0.024	3.829	0.032	5.064	0.041	6.440
5.000	0.010	2.332	0.017	4.170	0.023	5.599	0.030	7.230
7.500	0.005	2.606	0.009	4.915	0.012	6.707	0.016	8.820
10.000	0.003	2.666	0.005	5.196	0.007	7.252	0.010	9.702

** Pseudo relative spectral displacement.*

TABLE 3-1 CONT'D

Period (sec)	200 yr RP		300 yr RP		400 yr RP		475 yr RP	
	Accel (g)	Disp. (in) *	Accel (g)	Disp. (in) *	Accel (g)	Disp. (in) *	Accel (g)	Disp. (in) *
0.01	0.315	0.000	0.387	0.000	0.442	0.000	0.479	0.000
0.02	0.316	0.001	0.387	0.002	0.443	0.002	0.480	0.002
0.03	0.327	0.003	0.401	0.004	0.458	0.004	0.495	0.004
0.04	0.351	0.005	0.429	0.007	0.490	0.008	0.528	0.008
0.05	0.380	0.009	0.462	0.011	0.527	0.013	0.566	0.014
0.075	0.477	0.026	0.575	0.032	0.654	0.036	0.706	0.039
0.10	0.570	0.056	0.690	0.068	0.779	0.076	0.836	0.082
0.15	0.698	0.154	0.835	0.184	0.944	0.208	1.011	0.223
0.20	0.753	0.295	0.909	0.356	1.027	0.402	1.097	0.429
0.25	0.768	0.470	0.934	0.571	1.058	0.647	1.136	0.695
0.30	0.760	0.669	0.930	0.819	1.061	0.935	1.143	1.007
0.40	0.695	1.088	0.859	1.345	0.994	1.556	1.076	1.685
0.50	0.626	1.532	0.780	1.909	0.908	2.221	0.991	2.424
0.75	0.464	2.554	0.586	3.225	0.690	3.801	0.759	4.178
1.0	0.354	3.462	0.453	4.436	0.539	5.275	0.597	5.843
1.5	0.228	5.011	0.294	6.474	0.352	7.750	0.392	8.628
2.0	0.161	6.292	0.209	8.176	0.251	9.832	0.280	10.977
3.0	0.098	8.639	0.128	11.314	0.155	13.690	0.174	15.318
4.0	0.067	10.528	0.088	13.842	0.107	16.750	0.120	18.718
5.0	0.049	11.992	0.065	15.865	0.079	19.221	0.088	21.507
7.5	0.028	15.219	0.037	20.186	0.045	24.509	0.050	27.523
10.0	0.017	16.983	0.023	22.939	0.029	27.985	0.032	31.143

** Pseudo relative spectral displacement.*

TABLE 3-1 CONT'D

Period (sec)	975 yr RP		1500 yr RP		2000 yr RP		2475 yr RP	
	Accel (g)	Disp. (in) *	Accel (g)	Disp. (in) *	Accel (g)	Disp. (in) *	Accel (g)	Disp. (in) *
0.01	0.641	0.001	0.752	0.001	0.829	0.001	0.891	0.001
0.02	0.643	0.003	0.754	0.003	0.830	0.003	0.892	0.003
0.03	0.662	0.006	0.773	0.007	0.853	0.008	0.916	0.008
0.04	0.707	0.011	0.823	0.013	0.910	0.014	0.973	0.015
0.05	0.758	0.019	0.887	0.022	0.978	0.024	1.044	0.026
0.075	0.936	0.052	1.084	0.060	1.190	0.066	1.276	0.070
0.10	1.096	0.107	1.270	0.124	1.401	0.137	1.506	0.147
0.15	1.308	0.288	1.523	0.335	1.661	0.366	1.772	0.390
0.20	1.447	0.566	1.672	0.655	1.834	0.718	1.965	0.769
0.25	1.523	0.932	1.769	1.082	1.954	1.196	2.086	1.276
0.30	1.553	1.368	1.824	1.606	2.025	1.784	2.163	1.905
0.40	1.499	2.348	1.781	2.789	1.998	3.128	2.147	3.362
0.50	1.389	3.400	1.673	4.093	1.881	4.602	2.043	4.999
0.75	1.104	6.076	1.356	7.465	1.547	8.520	1.688	9.294
1.0	0.901	8.820	1.117	10.929	1.279	12.518	1.414	13.842
1.5	0.599	13.185	0.757	16.665	0.875	19.270	0.968	21.324
2.0	0.436	17.050	0.552	21.615	0.641	25.078	0.713	27.919
3.0	0.273	24.069	0.350	30.840	0.409	36.054	0.455	40.052
4.0	0.187	29.344	0.238	37.244	0.277	43.456	0.309	48.463
5.0	0.137	33.500	0.174	42.650	0.203	49.673	0.224	54.838
7.5	0.076	41.605	0.094	52.010	0.108	59.580	0.119	65.493
10.0	0.048	47.097	0.060	58.240	0.068	66.825	0.075	73.189

** Pseudo relative spectral displacement.*

TABLE 3-2 Damping Scaling Factors to Determine Horizontal Component of Spectral Accelerations For Damping Ratios (ξ) 1, 2, 10, 15, 20, and 25% for 72 yr (OLE) event

Period (sec)	Damping Scaling Factor ($Sa_\xi / Sa_{\xi=5\%}$)					
	ξ = 1%	ξ = 2%	ξ = 10%	ξ = 15%	ξ = 20%	ξ = 25%
0.01	1.000	1.000	1.000	1.000	1.000	1.000
0.05	1.192	1.097	0.948	0.923	0.909	0.899
0.075	1.354	1.180	0.899	0.849	0.818	0.795
0.1	1.475	1.245	0.857	0.784	0.736	0.702
0.2	1.616	1.333	0.789	0.679	0.608	0.557
0.3	1.611	1.339	0.777	0.660	0.584	0.529
0.4	1.594	1.336	0.772	0.652	0.574	0.517
0.5	1.580	1.332	0.769	0.648	0.569	0.512
0.75	1.549	1.319	0.773	0.653	0.573	0.516
1	1.533	1.313	0.775	0.654	0.575	0.517
1.5	1.510	1.301	0.782	0.664	0.586	0.530
2	1.475	1.283	0.788	0.673	0.596	0.541
3	1.436	1.266	0.795	0.682	0.607	0.551
4	1.392	1.245	0.801	0.690	0.615	0.560
5	1.357	1.229	0.803	0.692	0.617	0.561
7.5	1.296	1.199	0.814	0.708	0.635	0.580
10	1.203	1.143	0.851	0.761	0.696	0.647

TABLE 3-3 Damping Scaling Factors to Determine Horizontal Component of Spectral Acceleration For Damping Ratios (ξ) 1, 2, 10, 15, 20, and 25% for 475 yr (CLE), 975 yr and 2475 yr events

Period (sec)	Damping Scaling Factor ($Sa_\xi / Sa_{\xi=5\%}$)					
	ξ = 1%	ξ = 2%	ξ = 10%	ξ = 15%	ξ = 20%	ξ = 25%
0.01	1.000	1.000	1.000	1.000	1.000	1.000
0.05	1.225	1.115	0.932	0.898	0.877	0.862
0.075	1.356	1.186	0.889	0.831	0.793	0.766
0.1	1.421	1.226	0.858	0.782	0.732	0.695
0.2	1.539	1.299	0.800	0.694	0.624	0.573
0.3	1.515	1.295	0.793	0.681	0.608	0.554
0.4	1.505	1.295	0.788	0.674	0.598	0.542
0.5	1.486	1.287	0.789	0.674	0.598	0.542
0.75	1.467	1.282	0.785	0.666	0.588	0.530
1	1.415	1.257	0.794	0.679	0.602	0.545
1.5	1.399	1.249	0.802	0.690	0.614	0.558
2	1.357	1.224	0.812	0.705	0.632	0.578
3	1.314	1.200	0.829	0.730	0.662	0.610
4	1.284	1.184	0.838	0.742	0.675	0.624
5	1.249	1.167	0.841	0.746	0.680	0.629
7.5	1.239	1.160	0.851	0.761	0.697	0.648
10	1.160	1.114	0.877	0.800	0.743	0.699

TABLE 3-4 Damping Scaling Factors to Determine Vertical Component of Spectral Accelerations For Damping Ratios (ξ) 1, 2, 10, 15, 20, and 25% for 72 yr (OLE) event

Period (sec)	Damping Scaling Factor ($Sa_\xi / Sa_{\xi=5\%}$)					
	ξ = 1%	ξ = 2%	ξ = 10%	ξ = 15%	ξ = 20%	ξ = 25%
0.01	1.000	1.000	1.000	1.000	1.000	1.000
0.02	1.024	1.013	0.991	0.986	0.983	0.981
0.03	1.163	1.083	0.951	0.927	0.912	0.902
0.05	1.462	1.236	0.862	0.793	0.749	0.717
0.08	1.639	1.331	0.802	0.703	0.639	0.593
0.1	1.693	1.362	0.780	0.670	0.600	0.550
0.15	1.720	1.380	0.769	0.653	0.579	0.526
0.2	1.689	1.370	0.769	0.651	0.576	0.522
0.3	1.644	1.353	0.769	0.650	0.574	0.519
0.5	1.590	1.335	0.771	0.651	0.573	0.516
0.75	1.561	1.325	0.773	0.651	0.572	0.515
1	1.563	1.327	0.772	0.650	0.571	0.513
2	1.486	1.291	0.782	0.663	0.585	0.528
4	1.392	1.250	0.789	0.671	0.592	0.534
5	1.329	1.219	0.803	0.689	0.612	0.554
7.5	1.253	1.175	0.833	0.733	0.664	0.611
10	1.184	1.129	0.869	0.788	0.730	0.686

TABLE 3-5 Damping Scaling Factors to Determine Vertical Component of Spectral Accelerations For Damping Ratios (ξ) 1, 2, 10, 15, 20, and 25% for 475 yr (CLE), 975 yr and 2475 yr events

Period (sec)	Damping Scaling Factor ($Sa_\xi / Sa_{\xi=5\%}$)					
	ξ = 1%	ξ = 2%	ξ = 10%	ξ = 15%	ξ = 20%	ξ = 25%
0.01	1.000	1.000	1.000	1.000	1.000	1.000
0.02	1.044	1.025	0.982	0.972	0.965	0.960
0.03	1.210	1.111	0.930	0.893	0.869	0.851
0.05	1.494	1.260	0.841	0.758	0.703	0.664
0.08	1.621	1.335	0.788	0.678	0.607	0.556
0.1	1.664	1.358	0.772	0.656	0.582	0.528
0.15	1.677	1.366	0.766	0.648	0.572	0.517
0.2	1.618	1.342	0.775	0.658	0.582	0.528
0.3	1.574	1.321	0.781	0.666	0.591	0.537
0.5	1.524	1.302	0.786	0.670	0.595	0.539
0.75	1.486	1.290	0.784	0.666	0.588	0.530
1	1.478	1.287	0.786	0.668	0.590	0.533
2	1.414	1.258	0.792	0.676	0.598	0.541
4	1.303	1.203	0.814	0.706	0.631	0.575
5	1.271	1.186	0.824	0.718	0.645	0.590
7.5	1.179	1.129	0.866	0.781	0.721	0.673
10	1.146	1.103	0.897	0.830	0.780	0.742

3.3 Firm (Improved) ground MCE_R ARS per ASCE 7-16 Standards

Seismic design recommendations in California Building Code (CBC) 2019 are based on the seismic criteria in ASCE 7-16 standards where the Design Earthquake (DE) ground motion is based on the Risk-targeted Maximum Considered Earthquake (MCE_R) ground motion. According to Section 20.3.1 of ASCE 7-16, soils vulnerable to potential failure or collapse under seismic loading, such as liquefiable soils, quick and highly sensitive clays, and collapsible weakly cemented soils should be classified as Site Class F and a site response analysis in accordance with Section 21 of ASCE 7-16 shall be performed. Since most sites in POLB have high liquefaction potential due to presence of hydraulic fills, a site-specific procedure in accordance with Chapter 21 of the ASCE 7-16 was adopted to evaluate MCE_R ARS for firm ground conditions. The procedure for developing MCE_R ARS is as follows:

The MCE_R response acceleration at each period is the lesser of probabilistic and deterministic MCE_R response accelerations. The probabilistic MCE_R response acceleration shall be taken as the spectral response accelerations in the direction of maximum horizontal response represented by a 5 percent damped acceleration response spectrum that is expected to achieve a 1 percent probability of collapse within a 50-year period. For the purpose of this study, Method 1, as described in ASCE 7-16 Section 21.2.1.1, was adopted. In this method, ordinates of the probabilistic ground motion ARS at each period is determined as the product of the risk coefficient, C_R, and the spectral response acceleration from a 5 percent damped acceleration response spectrum having a 2 percent probability of exceedance within a 50-year period (2,475-Year average return period).

The value of the risk coefficient, C_R, is determined using values of C_{RS} and C_{R1} from Figures 22-18A and 22-19A of ASCE 7-16, respectively. Alternatively, the values can be obtained from the USGS website. At spectral response periods less than or equal to 0.2 sec., C_R is taken as equal to C_{RS}. At spectral response periods greater than or equal to 1.0 sec., C_R is taken as equal to C_{R1}. At response spectral periods greater than 0.2 sec. and less than 1.0 sec., C_R is based on linear interpolation of C_{RS} and C_{R1}.

The spectral response accelerations predicted by the NGA-West 2 ground motion models do not represent the maximum response in the horizontal plane. Therefore, the response spectral accelerations computed from the hazard analysis shall be scaled by factors to increase the motions to the maximum response. Per ASCE 7-16, the scale factors shall be 1.1 for periods less than or equal to 0.2 sec, 1.3 for a period of 1.0 sec, and 1.5 for periods greater than or equal to 5.0 sec.

The deterministic MCE_R response acceleration at each period is calculated as an 84th-percentile 5 percent damped ARS in the direction of maximum horizontal response computed at that period. The envelope of the ARS calculated for the characteristic earthquakes on all known active faults within the region shall be used. In addition, per ASCE 7-16 Section 21.2.2, if the largest spectral response acceleration of the resulting deterministic ground motion response spectrum is less than $1.5F_a$, then this response spectrum should be scaled by a single factor such that the maximum

response spectral acceleration equals $1.5F_a$. The firm (improved) ground is classified as site class D, therefore, F_a is equal to 1.0 per ASCE 7-16.

Per section 21.2.3 of ASCE 7-16, the site-specific MCE_R at any period should not be taken less than 150% of the site-specific DE spectrum. The site-specific DE ARS is defined as two-thirds of the MCE_R spectral response acceleration, but not less than 80% of the acceleration response determined for the code-based site class in accordance with Section 21.3 of ASCE 7-16. Site Class D with parameters presented in Table 3-6 was used to develop the lower bound (80% of site class D) ARS for the firm (improved) ground. It appeared that the 80% of site class D spectrum lie below the site-specific DE spectrum except at periods longer than 5.0 sec where spectral accelerations are slightly higher. The 150% of the envelope of these two spectra were considered as the site-specific MCE_R.

TABLE 3-6 Input Seismic Parameters Used to Determine the DE level ARS Curve for Site Class D (Firm Ground) per Section 21.3 of ASCE 7-16

Parameter	Values for Site Class D
S_s^*	1.694g
S_1^*	0.62g
F_a	1.0
F_v	2.5
S_{DS}	1.129g
S_{D1}	1.033g
T_L	8 sec

**S_s and S_1 are code-based mapped MCE_R spectral accelerations for site class B/C, i.e., Vs,30=760 m/s.*

3.3.1 Probabilistic MCE_R ARS for Firm Ground

The probabilistic MCE_R ARS for firm ground at each period was determined as the product of the maximum direction coefficient discussed in Section 3.3, risk coefficient, C_R, and the spectral response acceleration from a 5 percent damped acceleration response spectrum having a 2 percent probability of exceedance within a 50-year period (2,475-year average return period). The resulting probabilistic MCE_R ARS for firm ground, together with the original MCE ARS and corresponding spectral amplitudes are shown on Figure 3-2.

3.3.2 Deterministic MCE_R ARS for Firm Ground

The deterministic ARS was taken as the envelope of the 84th percentile ARS spectra for controlling faults, multiplied by the maximum direction factor discussed in Section 3.3. Deterministic MCE_R ARS was evaluated using three rupture scenarios on controlling faults (Palos Verdes fault,

Newport-Inglewood fault, and Compton thrust). For simplicity, the analysis was performed for the site with largest seismic hazard, i.e., site 5 (see Appendix A). The NGA-West 2 spreadsheet by PEER (Seyhan, 2015) was used to evaluate the deterministic 84th percentile spectra. Figure 3-2 shows the deterministic 84th percentile ARS for firm ground.

3.3.3 Site-Specific MCE$_R$ ARS for Firm Ground

The MCE$_R$ response acceleration at each period is the lesser of the probabilistic and deterministic MCE$_R$ ARS. Figure 3-2 shows the probabilistic, deterministic, and site-specific MCE$_R$ ARS for firm ground conditions. It can be seen that the probabilistic MCE$_R$ ARS is smaller than the deterministic MCE$_R$ ARS at all periods and therefore controlling the MCE$_R$ ARS. The site specific MCE$_R$ ARS, as shown on Figure 3-2, was used as the target spectrum to develop spectrum compatible MCE$_R$ level ground motions for site response analyses.

3.4 Selected Spectrally-Matched Ground Motion Time Histories For Firm Ground

Startup ground motions for spectrum compatible time histories were selected based on deaggregation results for different return periods, as presented in Appendix A. Based on the deaggregation results, the contributing earthquakes for the 72-yr return period (OLE) include events with magnitudes between 5 and 7 with distance of 15 to 20 km, as well as magnitude 7.5 to 8 earthquakes at distance of about 85 km, associated with San Andreas fault. For return periods of 475-yr (CLE), 975-yr, and 2,475-yr (MCE), the magnitude 6 to 7.5 events at distances up to 10 km have the most contribution, with decreasing contribution from magnitude 7.5 to 8 distant earthquakes on San Andreas fault for larger return periods.

Based upon the above results, seven sets of startup ground motions presented in Table 3-7 were selected for the 72-yr (OLE) return period, and different seven sets of startup ground motions presented in Table 3-8 were adopted for the 475-yr (CLE), 975-yr, and 2,475-yr (MCE) return periods. Majority of these startup motions were used in the 2006 study (EMI, 2006). For continuity of the present study with the 2006 study, the same motions were adopted herein with the exception of one set for the OLE (motion set no. 5 in Table 3-7) and two sets for the other return periods (motion set no. 3 and 5 in Table 3-8) which were selected from the more recent PEER NGA West 2 database (Ancheta et al., 2013).

The selected startup ground motions were modified to match the ARS curves using the computer program RSPMATCH (Abrahamson, 1992) which uses a time-domain approach to spectrally match input motion spectral responses to a target ARS curve. The goal of this approach is to preserve the general non-stationary characteristics of the ground motion in acceleration, velocity, and displacement while modifying the spectral response to match a given target response spectrum.

The initial three-component time histories, modified time histories, and comparison of the matched spectra with the firm-ground ARS for the OLE, CLE, 975-yr, and MCE$_R$ events are shown in Appendix B. The plots represent the estimated ground motions recorded at the ground surface, i.e., the finished grade within the Port.

TABLE 3-7 Selected Startup Motions for 72 yr Return Period (OLE) Event

Set	PEER RSN *	Earthquake	Mw	Pulse Motion	Station	Distance, R_{rup} (km)
1	802	1989 Loma Prieta	6.9	Yes	Saratoga – Aloha Ave.	8.5
2	729	1987 Superstition Hill	6.5	No	Wildlife Liquefaction Array	23.9
3	667	1987 Whittier	6.0	No	Northridge-Saticoy St.	41.7
4	170	1979 Imperial Valley	6.5	Yes	EC CO Center FF	7.3
5	4101	2004 Parkfield	6.0	Yes	Parkfield - Vineyard Canyon 3W	5.6
6	821	1992 Erzincan	6.7	No	Erzincan	4.4
7	988	1994 Northridge	6.7	No	Century City, LACC	23.4

* *PEER ground motion database (https://ngawest2.berkeley.edu/).*

Table 3-8 Selected Startup Motions for 475-yr (CLE), 975-yr, and 2475-yr Return Period Events

Set	PEER RSN *	Earthquake	Mw	Pulse Motion	Station	Distance, R_{rup} (km)
1	1787	1999 Hector Mine	7.1	No	Hector	11.7
2	767	1989 Loma Prieta	6.9	Yes	Gilroy Array 0#3	12.8
3	2114	2002 Denali, Alaska	7.9	Yes	TAPS Pump Station #10	2.7
4	1612	1999 Duzce, Turkey	7.1	No	Lamont 1059	4.2
5	6906	2010 Darfield, New Zealand	7.0	Yes	GDLC	1.2
6	6	1940 Imperial Valley	6.9	No	El Centro	6.1
7	1108	1995 Kobe, Japan	6.9	No	Kobe University	0.9

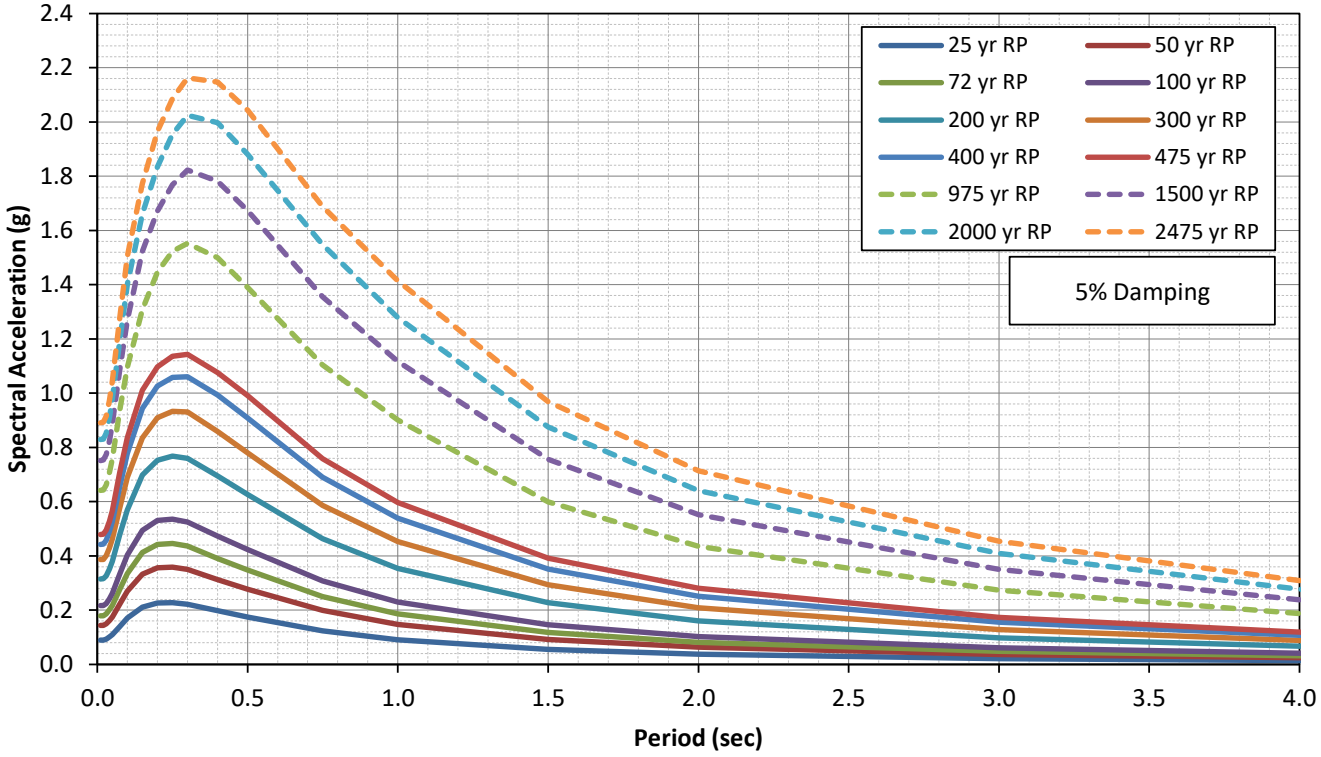
* *PEER ground motion database (https://ngawest2.berkeley.edu/).*

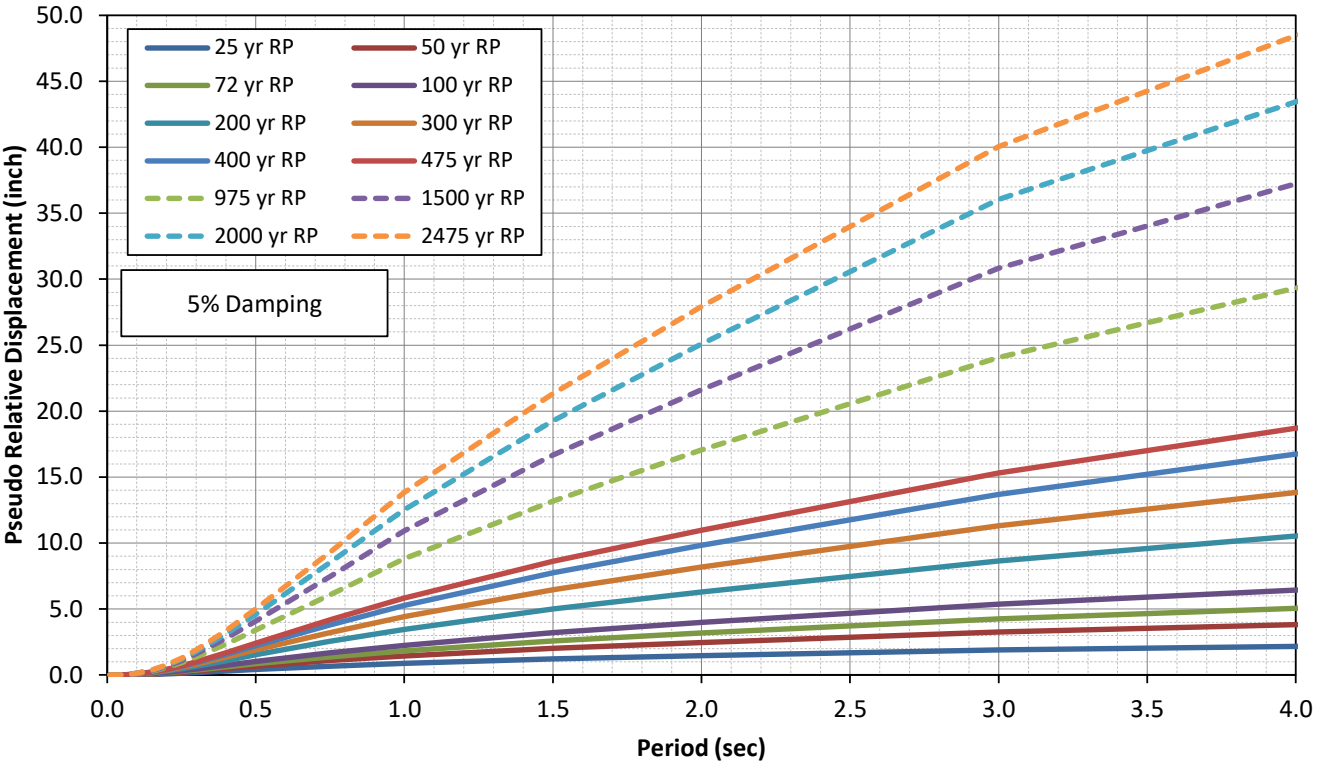
3.5 Methodology Used for Estimation of Sloping Ground Displacements

The Newmark sliding block method (Newmark, 1965) was adopted to estimate potential slope movements under earthquake loadings. Per the Newmark sliding block method, when the input ground motion induced along the failure plane exceeds a threshold acceleration, displacement of the sliding mass accumulates during shaking, resulting in residual slope displacement at the end of shaking. The magnitude of the slope displacement is obtained by double-integrating the difference of the applied acceleration and the threshold acceleration with respect to time. The threshold acceleration is often referred to as the yield acceleration (k_y) and is defined as the horizontal acceleration that results in a factor of safety of 1.0 in a pseudo-static limit equilibrium slope stability analysis.

Although the Newmark sliding block method treats the potential sliding soil mass as a rigid body and ignores the deformability of the sliding block, the method provides reasonable estimates of the slope deformation for liquefiable site conditions when the ground motion recorded at the base of the sliding mass is used and liquefaction is assumed to occur at the beginning of the earthquake shaking.

In this study, firm (improved) ground surface motions, instead of the ground motions at the base of the sliding mass, were used conservatively to determine the slope deformations. The estimated slope displacements for different earthquake events will be discussed later in Section 5.4. The analysis results are intended to be used as a screening tool to determine whether a particular project requires further evaluations such as site-specific site response and/or soil-structure interaction analysis.



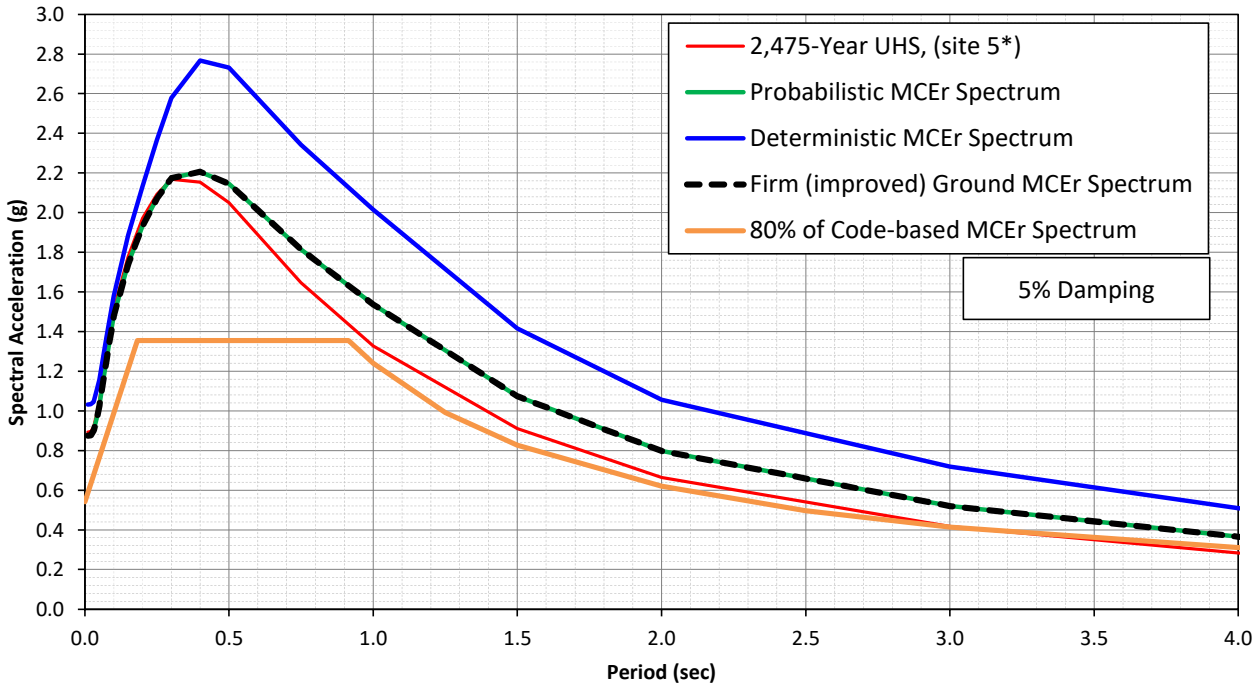


Earth Mechanics, Inc.
Geotechnical and Earthquake Engineering

Firm (Improved) Ground ARS and DRS for Earthquakes with Various Return Periods

POLB Port-Wide Ground Motion Study 2020

EMI Project No: 19-158	Date: 10/26/2020	Figure 3-1



Period (sec)	2,475-Year UHS, (site 5*)	Probabilistic MCEr Spectrum	Deterministic MCEr Spectrum	Firm (improved) Ground MCEr Spectrum	Period (sec)	80% of Code-based MCEr Spectrum
0.010	0.8937	0.876	1.032	0.876	0.000	0.542
0.020	0.8954	0.878	1.034	0.878	0.183	1.355
0.030	0.9188	0.901	1.045	0.901	0.915	1.355
0.040	0.9766	0.957	1.101	0.957	1.000	1.240
0.050	1.0474	1.027	1.156	1.027	1.250	0.992
0.075	1.2798	1.254	1.370	1.254	1.500	0.827
0.100	1.5103	1.480	1.580	1.480	2.000	0.620
0.150	1.7777	1.742	1.886	1.742	2.500	0.496
0.200	1.9712	1.932	2.132	1.932	3.000	0.413
0.250	2.0919	2.073	2.367	2.073	4.000	0.310
0.300	2.1696	2.174	2.579	2.174	5.000	0.248
0.400	2.1537	2.206	2.768	2.206	6.000	0.207
0.500	2.0501	2.145	2.732	2.145	6.500	0.191
0.750	1.6468	1.814	2.343	1.814	7.500	0.166**
1.000	1.3279	1.536	2.015	1.536	10.000	0.0992**
1.500	0.9104	1.074	1.416	1.074		
2.000	0.6639	0.798	1.056	0.798		
3.000	0.4174	0.520	0.720	0.520		
4.000	0.2828	0.365	0.509	0.365		
5.000	0.2068	0.276	0.380	0.276		
7.500	0.1107	0.148	0.183	0.166**		
10.000	0.0702	0.094	0.106	0.099**		

** Site 5 was used here since the site has the largest seismic hazard compared to other areas in the POLB (see Appendix A - PSHA study results).*

*** The spectral accelerations at periods of 7.5 and 10 sec were controled by 80% of code-based site class D ARS determined based on Section 21.3 of ASCE 7-16.*

Earth Mechanics, Inc.
Geotechnical and Earthquake Engineering

Firm (Improved) Ground MCE_R ARS Curve Based on ASCE 7-16 - Section 21.2

POLB Port-Wide Ground Motion Study 2020

EMI Project No: 19-158 | Date: 10/26/2020 | Figure 3-2

4.0 EARTHQUAKE SITE RESPONSE

4.1 Methodology

The site response analyses adopted herein was relatively similar to the analyses performed for the 2006 PWGM Study (EMI, 2006). However, instead of the equivalent linear site response analysis using the SHAKE91 program (Idriss and Sun, 1992), a more robust nonlinear total stress time-domain analysis methodology was used. Unlike the equivalent linear analysis which is performed in frequency domain, the nonlinear analysis solves the equations of motion in time domain, using the Newmark-β method.

Nonlinear time-domain analysis using the DeepSoil program (Hashash et al., 2020) is better suited for estimation of soil site response under earthquakes with larger intensity (e.g., 475, 975 and 2,475 yr events). It is to be noted that the shear modulus reduction and damping ratio data, available in the current literature/guidelines, is collected using resonant column tests at small strains, and towards the medium shear strain levels the torsional shear test results are used. The measured shear modulus and damping ratio curves are extrapolated at the large strain levels. This extrapolation may underestimate or overestimate the shear strength at large strains (Groholski et al., 2016 and Hashash et al., 2020). Therefore, a general quadratic/hyperbolic (GQ/H) backbone curve, as described by Groholski et al. (2016) and implemented in DeepSoil v7.0 computer program, was used herein to account for the correct shear strength magnitudes at large strains.

4.2 Soil Profiles and Properties

The soil profiles shown in Figure 2-8 for zones I, II, III, and IV were used in the computer program DeepSoil (Hashash et al., 2020). To account for spatial variability of soil properties and uncertainties associated with estimation of material stiffness and strength parameters, three different sets of soil properties were considered for each soil zone; lower-bound, upper-bound, and liquefied conditions. The lower- and upper-bound profiles considered shear wave velocity profiles that were respectively 12 percent lower and higher than the best estimate shear wave velocities shown in Figure 2-6. This amount of variation corresponded to about 25 percent variability in the magnitude of small-strain shear modulus (G_{max}). The analyses considered lower-bound and upper-bound friction angles of 32 and 35 degrees and lower-bound and upper-bound cohesions of 50 psf and 100 psf for the hydraulic fill. The lower- and upper-bound undrained shear strength of the harbor sediments encountered in zones III and IV were assumed to be 1,000 psf and 2,500 psf, respectively. For liquefied conditions, residual shear strength of 0.15 times the in-situ vertical effective stress (σ'_v) was estimated following the approach outlined in Idriss and Boulanger (2008). The shear wave velocity profile below the ground water table (liquefiable soils) was correlated using the equation of Dickenson (1994).

4.3 Shear Modulus Reduction and Damping Ratio Models

Similar to EMI study in 2006 (EMI, 2006), the dynamic shear modulus (G/G_{max}) and damping (D/D_{max}) curves for hydraulic fill were estimated using the empirical relationships by EPRI (1993). For harbor sediments, the shear modulus and damping curves of Vucetic and Dobry (1991) were adopted assuming plasticity index (PI) of 15. For liquefied soils, the curves of Vucetic and Dobry (1991) with PI of 0.0 were used.

In order to improve the model accuracy in large strain range, the reference backbone curves discussed above were used to fit a general quadratic/hyperbolic (GQ/H) backbone curve, as described by Groholski et al. (2016) and implemented in DeepSoil v7.0. In addition, the reference damping curves were used to fit unloading-reloading relationship using modulus reduction and damping curve fitting (MRDF)-Darendeli Model (Darendeli, 2001) as available in DeepSoil v7.0 soil model libraries. The fitting procedure was applied for every layer in the soil profile, resulting in a soil model that better estimates the small-strain behavior as well as the soil strength at larger strain levels.

4.4 Site Response Analysis Results

The suite of seed motions described in Section 3.4 were applied to the base of the soil profiles as outcropping motions. Four (4) levels of earthquake motions including OLE, CLE, 975-yr return period and MCE_R were considered in the analyses. Given that (i) each earthquake event comprised of fourteen (14) ground motion time histories, and (ii) three different soil properties, i.e., lower- and upper-bound, and liquefied conditions, were considered for each of the four soil zones, a total of 168 (=14×3×4) site response analyses were performed to develop unimproved ground response spectra at the ground surface.

As expected, for each soil zone and ground motion the upper-bound soil profile controlled the spectral responses at short periods and the lower-bound soil profile controlled the spectral response at long periods. Spectral responses were much smaller in the liquefied soil profile which just showed slightly larger spectral accelerations in periods greater than 1.0 second (see in Appendix C-Part I). The acceleration spectrum for each ground motion was taken as the envelope of the ARS curves of upper-bound, lower-bound, and liquefied soil conditions. The geometric mean of the fourteen enveloped ARS curves was then considered as the average ARS curve for each soil zone and earthquake level. These curves are presented in Appendix C. All ARS curves are developed for 5 percent damping ratio.

It was noted that the spectral responses at Zones II, III, and IV were similar (see Appendix C-Part II). Therefore, the ARS curves of these three zones were enveloped, and the three zones were combined and denoted as *Area A* hereafter in the report. Since the hydraulic fill depth in Zone I was 20 to 30 ft less than the other zones, the spectral responses in this zone were considerably different that those of the other zones. To this end, Zone I was not combined with the other zones. The zone is denoted as *Area B* hereafter in this report. Figure 4-1 shows the extents of the two

areas in the Port of Long Beach. The recommended ARS and DRS curves for Areas A and B under OLE, CLE, 975, DE level earthquakes are presented in Section 5.

4.5 Unimproved Ground DE ARS per ASCE 7-16 Standards

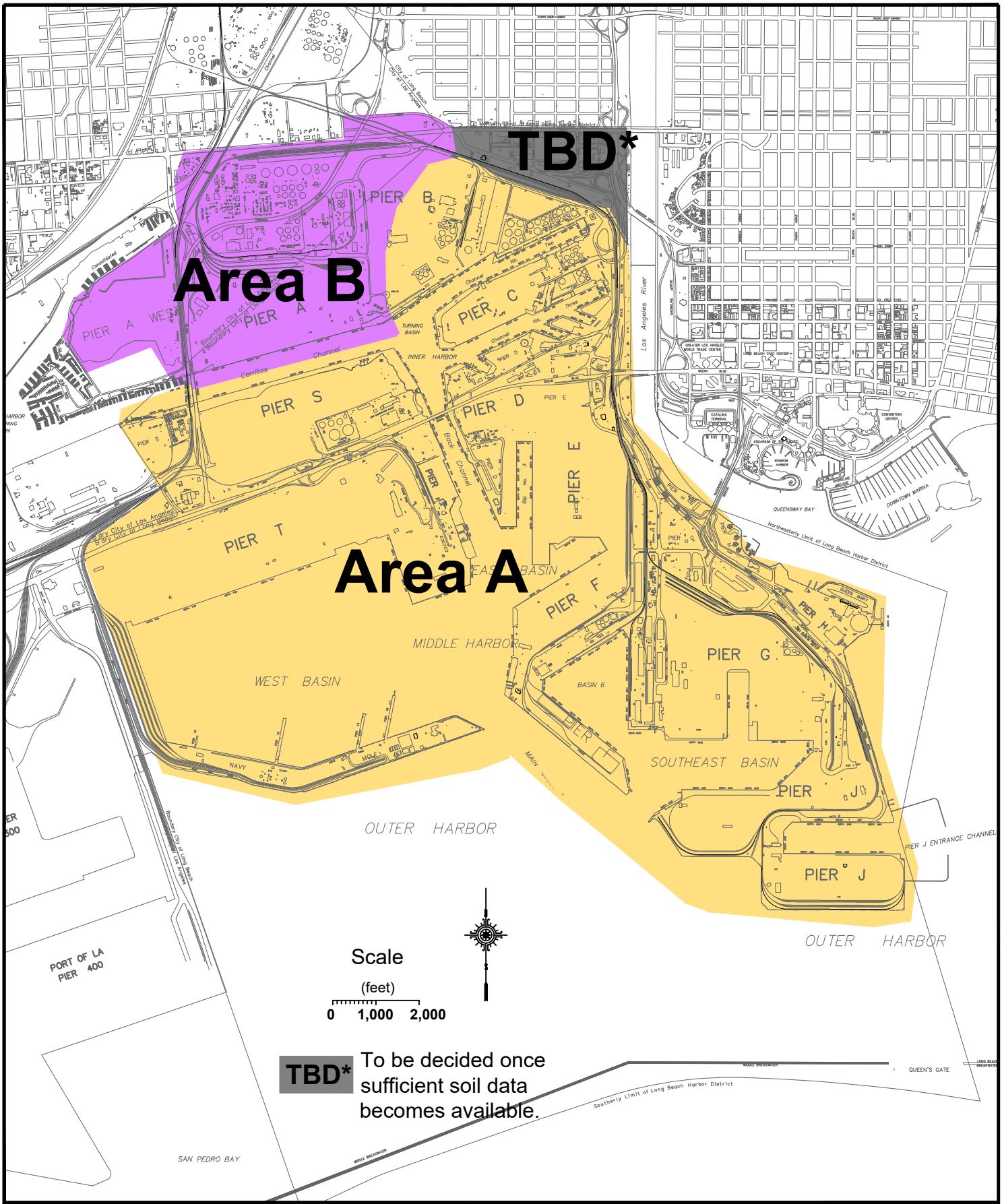
The provisions of Chapter 21 of ASCE 7-16 were adopted to develop DE ARS curve from the MCE_R level spectral accelerations. The ARS represent the spectral response of the ground motions recorded at the ground surface, i.e., the finished grade in POLB projects. Per Section 21.3 (ASCE 7-16), the DE ARS is defined as two-thirds of the MCE_R spectral response acceleration, but no less than 80% of the acceleration response determined for the same site class in accordance with Section 21.3 of ASCE 7-16. To account for uncertainties associated with characterization of hydraulic fills, the lower limit for DE acceleration response was calculated for both Site Classes D and E using the parameters presented in Table 4-1 below.

Considerable reduction in spectral accelerations was noted at periods less than 1.0 second compared to the firm ground spectral accelerations for the MCE_R event. This is because the MCE_R level ground motions impart large seismic forces into the unimproved ground (hydraulic fill) mobilizing excessive soil nonlinearity and energy damping which can be potentially overestimated in the site response analyses. In order to account for the uncertainties associated with estimation of soil nonlinearity under such extreme earthquake events, the unimproved DE ARS curve was enveloped with the firm (improved) ground ARS curve. Figures 4-2 and 4-3 compare the site-specific DE ARS with the ASCE 7-16 based lower limits (80% of site classes D and E) for areas A and B, respectively.

TABLE 4-1 Input Seismic Parameters Used to Develop Code-based ARS Curves for Unimproved Ground (Site Classes E and D) per Section 21.3 of ASCE 7-16

Parameter	Site Class E	Site Class D
S_s^*	1.694g	
S_1^*	0.62g	
F_a	1.0	1.0
F_v	4.0	2.5
S_{DS}	1.129g	1.129g
S_{D1}	1.653g	1.033g
T_L	8 sec	8 sec

** S_s and S_1 are code-based mapped MCE_R spectral accelerations for site class B/C, i.e., Vs,30=760 m/s.*

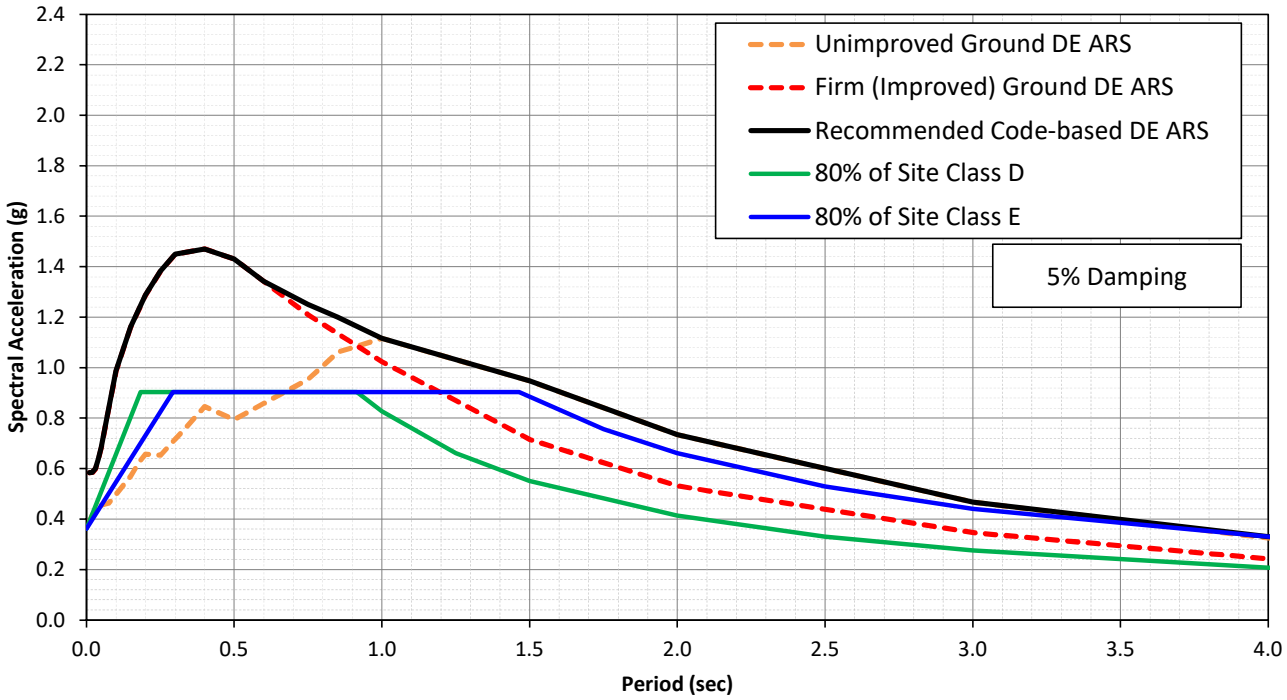


Earth Mechanics, Inc.
Geotechnical and Earthquake Engineering

Port-Wide Ground Motion Study Update, Port of Long Beach, California

Areas A & B Extents Within The Port of Long Beach
Figure 4-1

Project No. 19-158	Date: 10-26-20



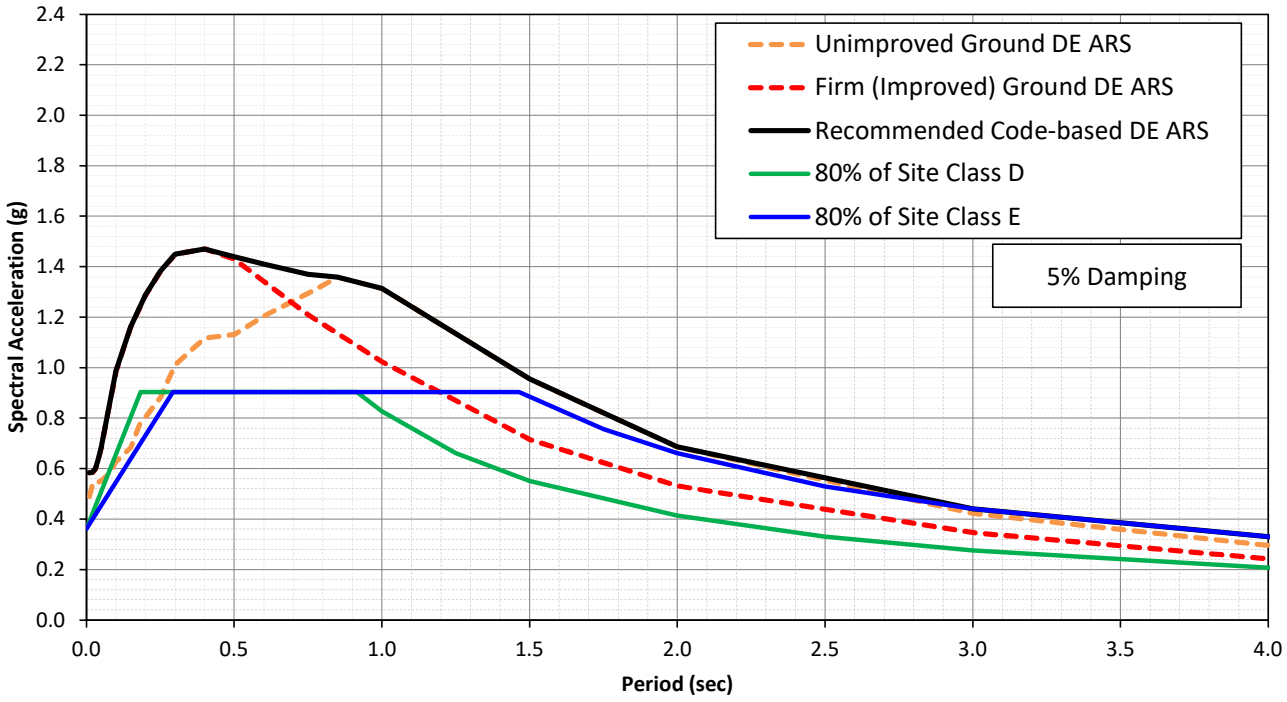
Period (sec)	Unimproved Ground DE ARS	Firm Ground DE ARS	Recommended Code-based DE ARS
0.01	0.390	0.584	0.584
0.02	0.417	0.585	0.585
0.03	0.433	0.600	0.600
0.04	0.439	0.638	0.638
0.05	0.456	0.684	0.684
0.08	0.463	0.836	0.836
0.10	0.499	0.987	0.987
0.15	0.572	1.162	1.162
0.18	0.629	1.237	1.237
0.20	0.658	1.288	1.288
0.25	0.653	1.382	1.382
0.30	0.717	1.450	1.450
0.40	0.846	1.471	1.471
0.50	0.794	1.430	1.430
0.60	0.859	1.342	1.342
0.75	0.954	1.210	1.250
0.85	1.061	1.135	1.200
1.00	1.116	1.024	1.116
1.50	0.948	0.716	0.948
2.00	0.734	0.532	0.734
3.00	0.467	0.347	0.467
4.00	0.325	0.243	0.331
5.00	0.245	0.184	0.265
7.50	0.172	0.111	0.177
10.00	0.088	0.066	0.106

Earth Mechanics, Inc.
Geotechnical and Earthquake Engineering

Unimproved Ground DE ARS Curve for Area A
Based on ASCE 7-16 - Section 21.3

POLB Port-Wide Ground Motion Study 2020

EMI Project No: 19-158 | Date: 10/26/2020 | Figure 4-2



Period (sec)	Unimproved Ground DE ARS	Firm Ground DE ARS	Recommended Code-based DE ARS
0.01	0.490	0.584	0.584
0.02	0.537	0.585	0.585
0.03	0.534	0.600	0.600
0.04	0.547	0.638	0.638
0.05	0.552	0.684	0.684
0.08	0.579	0.836	0.836
0.10	0.628	0.987	0.987
0.15	0.684	1.162	1.162
0.18	0.776	1.237	1.237
0.20	0.805	1.288	1.288
0.25	0.883	1.382	1.382
0.30	1.013	1.450	1.450
0.40	1.117	1.471	1.471
0.50	1.132	1.430	1.440
0.60	1.205	1.342	1.410
0.75	1.295	1.210	1.370
0.85	1.358	1.135	1.358
1.00	1.314	1.024	1.314
1.50	0.955	0.716	0.955
2.00	0.687	0.532	0.687
3.00	0.423	0.347	0.441
4.00	0.295	0.243	0.331
5.00	0.216	0.184	0.265
7.50	0.144	0.111	0.177
10.00	0.076	0.066	0.106

Earth Mechanics, Inc.
Geotechnical and Earthquake Engineering

Unimproved Ground DE ARS Curve for Area B
Based on ASCE 7-16 - Section 21.3

POLB Port-Wide Ground Motion Study 2020

EMI Project No: 19-158 | Date: 10/26/2020 | Figure 4-3

5.0 SUMMARY AND DESIGN RECOMMENDATIONS

5.1 Overview

Before the 2006 port-wide ground motion study (EMI, 2006), the Port's practice toward the development of ground motion criteria for design was to conduct site-specific studies for each project by the design teams selected for those projects. This approach had the benefit of site-specific data being utilized for each project. However, over the years, there had often been significant discrepancies among various recommendations among various consultants.

EMI's scope of work includes updating the 2006 port-wide ground motion study (EMI, 2006) based on the latest understanding of California seismic sources (UCERF3) and ground motion prediction models (NGA-West 2) and to develop a consistent set of ground motion recommendations that can be used for future POLB projects.

5.2 Horizontal Response Spectra for OLE, CLE, 975-yr, and DE Events

Firm (improved) ground acceleration response spectra were determined by performing site-specific probabilistic seismic hazard analysis (PSHA). The analysis details are presented in Appendix A. To develop ARS curves for unimproved ground nonlinear site response analysis were performed as described in Section 4. The site response analysis outputs are presented in Appendix C.

Firm (improved) and unimproved ground 5 percent damped ARS for Areas A and B are presented in Figures 5-1 through 5-8 for OLE, CLE, 975-yr and DE events. The ARS curves represent the spectral responses of the ground motions recorded at the ground surface, i.e., the finished grade in POLB projects. To better take into consideration site conditions spatial variability within the entire POLB area and to account for uncertainties associated with the numerical modeling of soil nonlinearity (stiffness/strength degradation) under moderate to strong earthquake shakings, the unimproved ground ARS curve for each event was determined by enveloping the ARS curve derived from the site response analyses with the corresponding firm (improved) ground ARS curve. The corresponding displacement response spectra (DRS) are presented in Figures 5-9 through 5-16. The ARS for all four earthquake events for firm (improved) ground and unimproved ground for Areas A and B are presented in Figures 5-17, 5-18, and 5-19, respectively. The ratio of the unimproved ground spectral accelerations over firm (improved) ground spectral accelerations, i.e., amplification factors for 5% damped spectral accelerations, for all four events are shown in Figures 5-20 and 5-21 for Areas A and B, respectively.

The ARS and DRS curves (horizontal component of ground motion) for damping ratios of 1%, 2%, 10%, 15%, 20%, and 25% can be estimated using the damping scaling factors (DSF) presented in Tables 3-2 and 3-3. For the DE event, the DSFs presented in Table 3-3 can be used. As discussed in Section 3.2, the DSFs were determined using the methodology outlined in the Pacific Earthquake Engineering Research Center (PEER) report prepared by Rezaeian et al. (2012).

It is to be noted that the provisions of Section 21.4 of ASCE 7-16 should be taken into consideration when determining the code-based S_{DS} and S_{D1} using the recommended DE ARS shown in Figures 5-7 and 5-8.

5.3 Vertical Response Spectra for OLE, CLE, 975-yr, and DE Events

Vertical ground motion ARS for firm ground condition and return periods of 72-yr (OLE), 475-yr (CLE), 975-yr, and 2,475-yr are evaluated and presented in Appendix A. For DE event, the vertical ARS was estimated by multiplying the firm ground horizontal DE ARS by V/H ratios of 2,475-yr level UHS. The V/H ratios presented in Appendix A were used herein.

The firm (improved) ground vertical ARS can also be used for unimproved ground conditions for both Area A and Area B. Recommended vertical response spectra for return periods of 72-yr (OLE), 475-yr (CLE), 975-yr, and DE for 5% damping are shown in Figure 5-22. Per ASCE 7-16 Section 11.9, the ordinates of the DE vertical ARS were checked to be; (i) greater than or equal to 80% of S_{av} values determined following Sections 11.9.2 and 11.9.3 of ASCE 7-16 for vibration periods equal to or less than 2.0 sec, and (ii) greater than or equal to one-half of corresponding horizontal spectral acceleration for periods greater than 2.0 sec.

The damping scaling factors (DSF) presented in Tables 3-4 and 3-5 can be used to determine the ARS curves (vertical component of ground motion) for damping ratios of 1%, 2%, 10%, 15%, 20%, and 25%. For the DE event, the DSFs presented in Table 3-5 can be used. Th vertical component DSFs were determined using the methodology outlined in the Pacific Earthquake Engineering Research Center (PEER) report prepared by Rezaeian et al. (2012).

5.4 Newmark Displacements

Simplified Newmark sliding block-type analyses were conducted to estimate lateral ground displacements under the OLE, CLE, 975-yr, and DE level earthquakes. For building structures, ASCE 7-16 (Chapters 12 and 15) requires determination of lateral ground movements induced by geometric mean maximum considered earthquake (MCE_G) events. To this end, in addition to the earthquake events above, Newmark analysis was completed for MCE_G level events.

Slope displacements were estimated using the suite of firm (improved) ground outcropping motions discussed in Section 3.4. The estimated displacement for all time histories are presented in Appendix D. Figure 5-23 provides the recommended average lateral ground displacement versus slope yield acceleration. Because these analyses are based on the firm-ground outcropping motions, the recommended curves are considered conservative and may be used as a screening tool to determine whether a particular project requires further evaluations such as site-specific soil-structure interaction analysis. The benefits of such analyses to the project should be clearly demonstrated. Approval for such analyses should be obtained from the Port before performing the analyses.

5.5 Seismic Parameters for Geotechnical Evaluations

Table 5-1 presents the recommended PGA and earthquake magnitudes (M_w) that can be used for liquefaction and lateral spread analyses for Areas A and B. The PGA for each earthquake event was taken as the larger of the PGA values estimated for firm (improved) ground and unimproved ground. MCE_G level parameters are additionally provided in the table below since per ASCE 7-16 (chapters 12 and 15) for any building structures, all geotechnical evaluations should be performed considering the geometric mean maximum considered earthquake (MCE_G). The DE level PGA was taken as two-thirds of the MCE_G level PGA. The DE level PGA values shown in Figures 5-7 and 5-8 at the period of 0.0 second were not used here because the values in the graphs were derived from maximum-direction acceleration spectrum with 1% probability of building collapse in 50 years (MCE_R) which is applicable for structural calculations only not for geotechnical evaluations such as liquefaction analysis. It should be noted that the DE level PGA for geotechnical evaluations is denoted as DE_G in this study to avoid confusion with two-thirds of MCE_R that is used in structural evaluations.

TABLE 5-1 Recommended Seismic Parameters for Geotechnical Evaluations

Parameter	72-yr Event (OLE)	475-yr Event (CLE)	975-yr Event	DE_G Event *	MCE_G
PGA (g)	0.20 (Area A) 0.23 (Area B)	0.48 (Area A) 0.52 (Area B)	0.64 (Area A) 0.64 (Area B)	0.59 (Area A) 0.59 (Area B)	0.89 (Area A)** 0.89 (Area B)**
M_w***	6.5	7.3	7.3	7.3	7.3

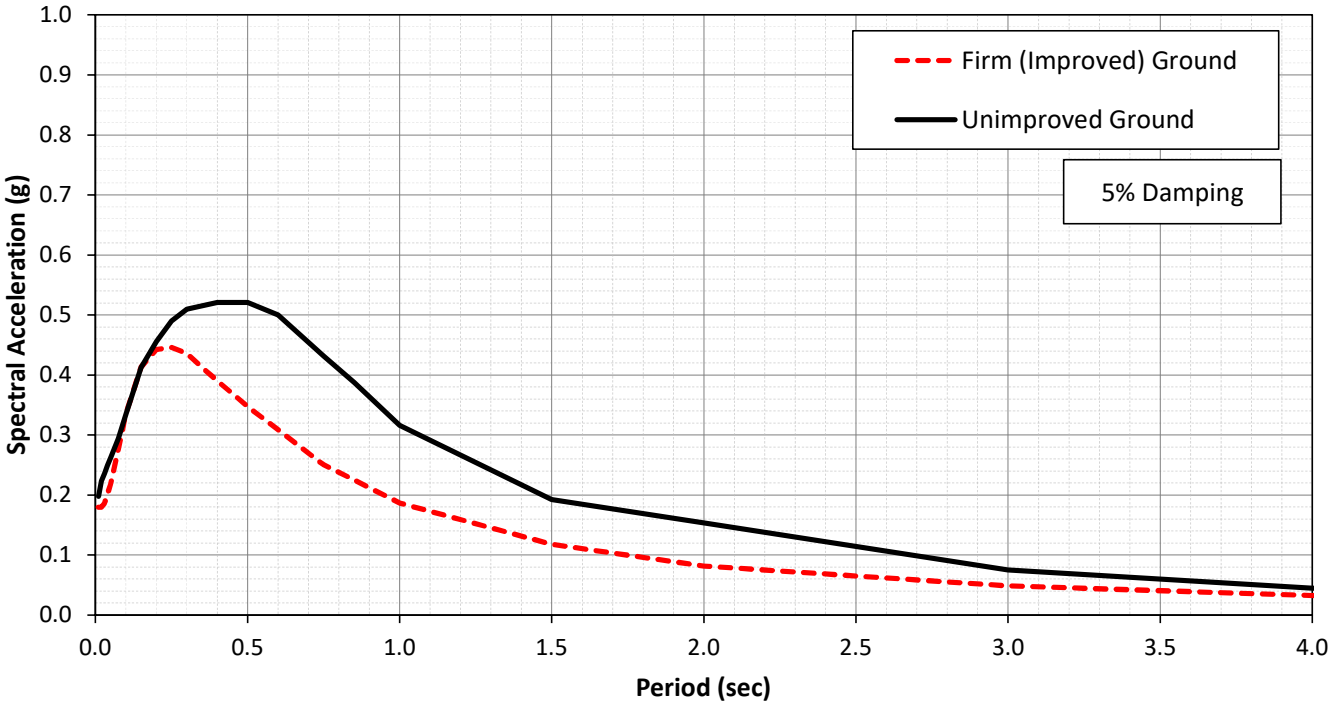
* *DE level PGA (DE_G) is considered as 2/3 of MCE_G PGA.*
** *MCE_G peak ground acceleration, i.e., PGA_M.*
*** *M_w was found to be similar in Areas A and B.*

5.6 Spectrally-Matched Ground Motion Time Histories

Firm ground spectrally-matched ground motion time histories are presented in Appendix B. The approach to develop the time histories were elaborated in Section 3.4. The same approach was adopted to spectrally match the seed ground motions listed in Tables 3-5 and 3-6 to the recommended OLE, CLE, 975-yr, and ASCE 7-16 based DE level unimproved ground ARS curves presented in Figures 5-1 through 5-8. The spectrally matched time history of ground motions for each event for Areas A and B are presented in Appendix E. In addition, digital format of the time histories both for the firm (improved) and the unimproved ground conditions are provided in an attachment to this report.

The above time histories (except those for DE event) can be used for both two-dimensional (2D) and three-dimensional (3D) geotechnical and structural analyses. The DE level time histories can be used for 2D analyses, only. For 3D analyses, spectral-matching of the seed time histories to the

DE spectrum is expected to be too conservative. Unlike the ARS of the other events that represent the *median* ground-motion response spectra of a motion when rotated over all horizontal orientations, the DE level ARS represents the *maximum* spectrum of all orientations; therefore, the design earthquake intensity can be potentially overestimated in a 3D analysis if both horizontal components of a motion are matched to the maximum-direction spectrum. The method outlined in ASCE 7-16 – Section 16.2 can be employed to develop the appropriate components of the DE level ground motions.



Period (sec)	Firm (Imporved) Ground ARS (g)	Unimproved Ground ARS (g)
0.010	0.179	0.198
0.020	0.179	0.224
0.030	0.186	0.236
0.040	0.201	0.249
0.050	0.217	0.262
0.075	0.276	0.295
0.100	0.335	0.335
0.150	0.413	0.413
0.200	0.443	0.456
0.250	0.446	0.490
0.300	0.436	0.510
0.400	0.390	0.521
0.500	0.348	0.521
0.600	0.309	0.500
0.750	0.250	0.432
0.850	0.225	0.388
1.000	0.187	0.316
1.500	0.118	0.192
2.000	0.082	0.153
3.000	0.048	0.075
4.000	0.032	0.045
5.000	0.023	0.029
7.500	0.012	0.015
10.000	0.007	0.007

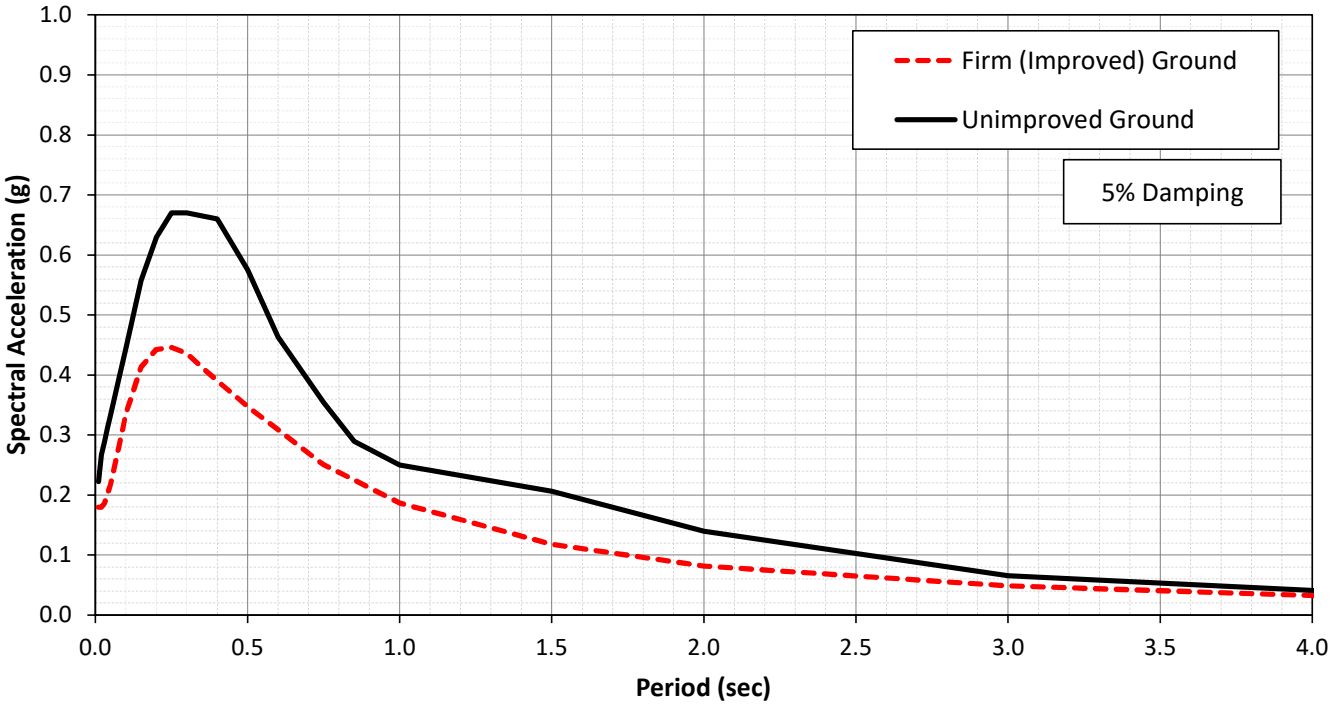
Earth Mechanics, Inc.
Geotechnical and Earthquake Engineering

Recommended Firm (Improved) and Unimproved Ground ARS Curves - Area A - OLE Event

POLB Port-Wide Ground Motion Study 2020

EMI Project No: 19-158 Date: 10/26/2020

Figure 5-1



Period (sec)	Firm (Imporved) Ground ARS (g)	Unimproved Ground ARS (g)
0.010	0.179	0.223
0.020	0.179	0.267
0.030	0.186	0.290
0.040	0.201	0.312
0.050	0.217	0.334
0.075	0.276	0.390
0.100	0.335	0.446
0.150	0.413	0.558
0.200	0.443	0.630
0.250	0.446	0.670
0.300	0.436	0.670
0.400	0.390	0.660
0.500	0.348	0.576
0.600	0.309	0.463
0.750	0.250	0.355
0.850	0.225	0.290
1.000	0.187	0.250
1.500	0.118	0.206
2.000	0.082	0.140
3.000	0.048	0.066
4.000	0.032	0.041
5.000	0.023	0.028
7.500	0.012	0.015
10.000	0.007	0.007

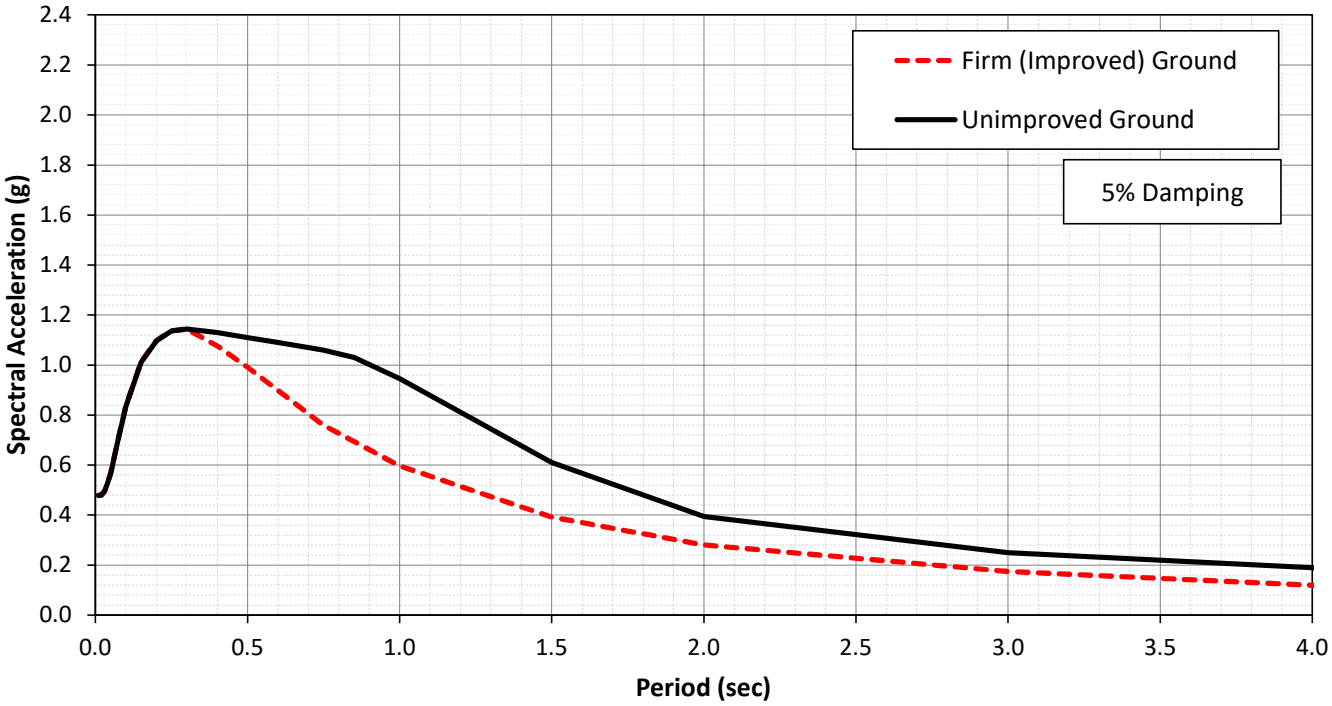
Earth Mechanics, Inc.
Geotechnical and Earthquake Engineering

Recommended Firm (Improved) and Unimproved Ground ARS Curves - Area B - OLE Event

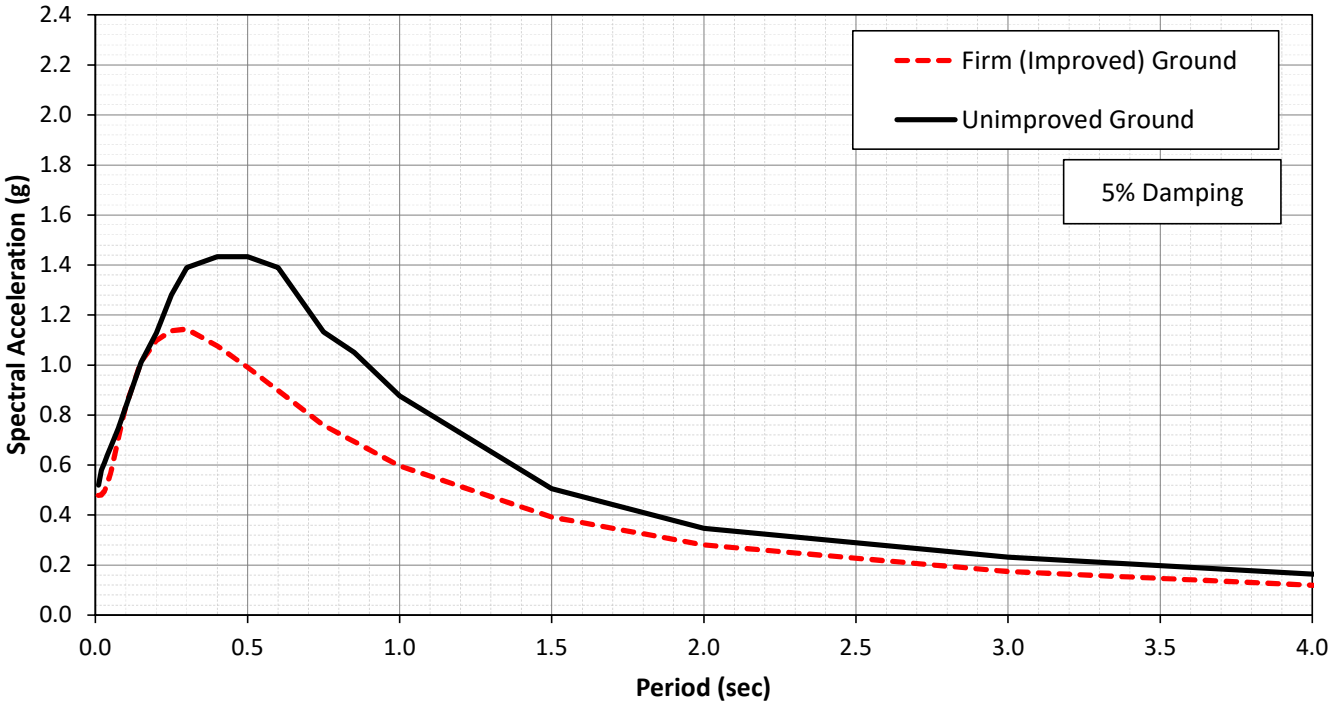
POLB Port-Wide Ground Motion Study 2020

EMI Project No: 19-158 Date: 10/26/2020

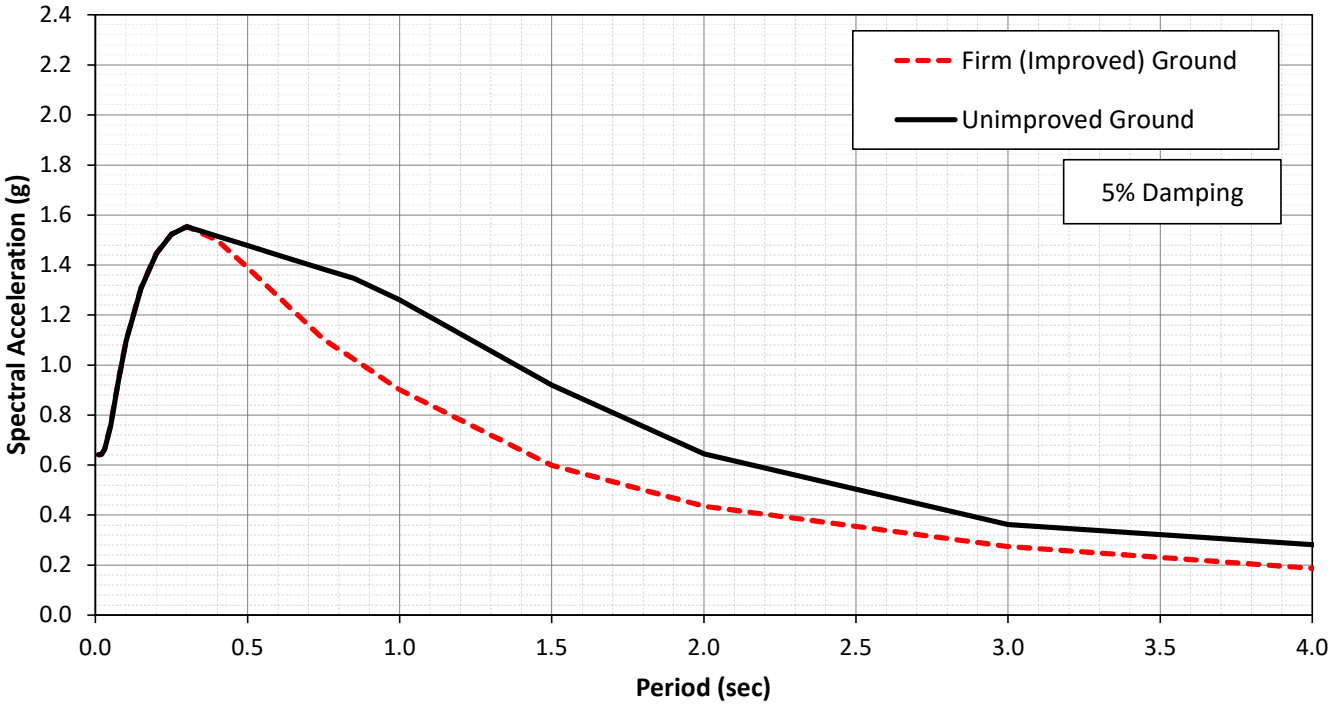
Figure 5-2



Period (sec)	Firm (Imporved) Ground ARS (g)	Unimproved Ground ARS (g)
0.010	0.479	0.479
0.020	0.480	0.480
0.030	0.495	0.495
0.040	0.528	0.528
0.050	0.566	0.566
0.075	0.706	0.706
0.100	0.836	0.836
0.150	1.011	1.011
0.200	1.097	1.097
0.250	1.136	1.136
0.300	1.143	1.143
0.400	1.076	1.130
0.500	0.991	1.110
0.600	0.898	1.090
0.750	0.759	1.060
0.850	0.694	1.030
1.000	0.597	0.946
1.500	0.392	0.610
2.000	0.280	0.394
3.000	0.174	0.249
4.000	0.120	0.190
5.000	0.088	0.135
7.500	0.050	0.078
10.000	0.032	0.040



Period (sec)	Firm (Imporved) Ground ARS (g)	Unimproved Ground ARS (g)
0.010	0.479	0.519
0.020	0.480	0.580
0.030	0.495	0.611
0.040	0.528	0.641
0.050	0.566	0.672
0.075	0.706	0.748
0.100	0.836	0.836
0.150	1.011	1.011
0.200	1.097	1.129
0.250	1.136	1.281
0.300	1.143	1.390
0.400	1.076	1.433
0.500	0.991	1.433
0.600	0.898	1.390
0.750	0.759	1.132
0.850	0.694	1.051
1.000	0.597	0.877
1.500	0.392	0.506
2.000	0.280	0.347
3.000	0.174	0.232
4.000	0.120	0.164
5.000	0.088	0.119
7.500	0.050	0.070
10.000	0.032	0.036



Period (sec)	Firm (Imporved) Ground ARS (g)	Unimproved Ground ARS (g)
0.010	0.641	0.641
0.020	0.643	0.643
0.030	0.662	0.662
0.040	0.707	0.707
0.050	0.758	0.758
0.075	0.936	0.936
0.100	1.096	1.096
0.150	1.308	1.308
0.200	1.447	1.447
0.250	1.523	1.523
0.300	1.553	1.553
0.400	1.499	1.516
0.500	1.389	1.478
0.600	1.275	1.440
0.750	1.104	1.384
0.850	1.023	1.346
1.000	0.901	1.261
1.500	0.599	0.920
2.000	0.436	0.645
3.000	0.273	0.362
4.000	0.187	0.282
5.000	0.137	0.210
7.500	0.076	0.123
10.000	0.048	0.064

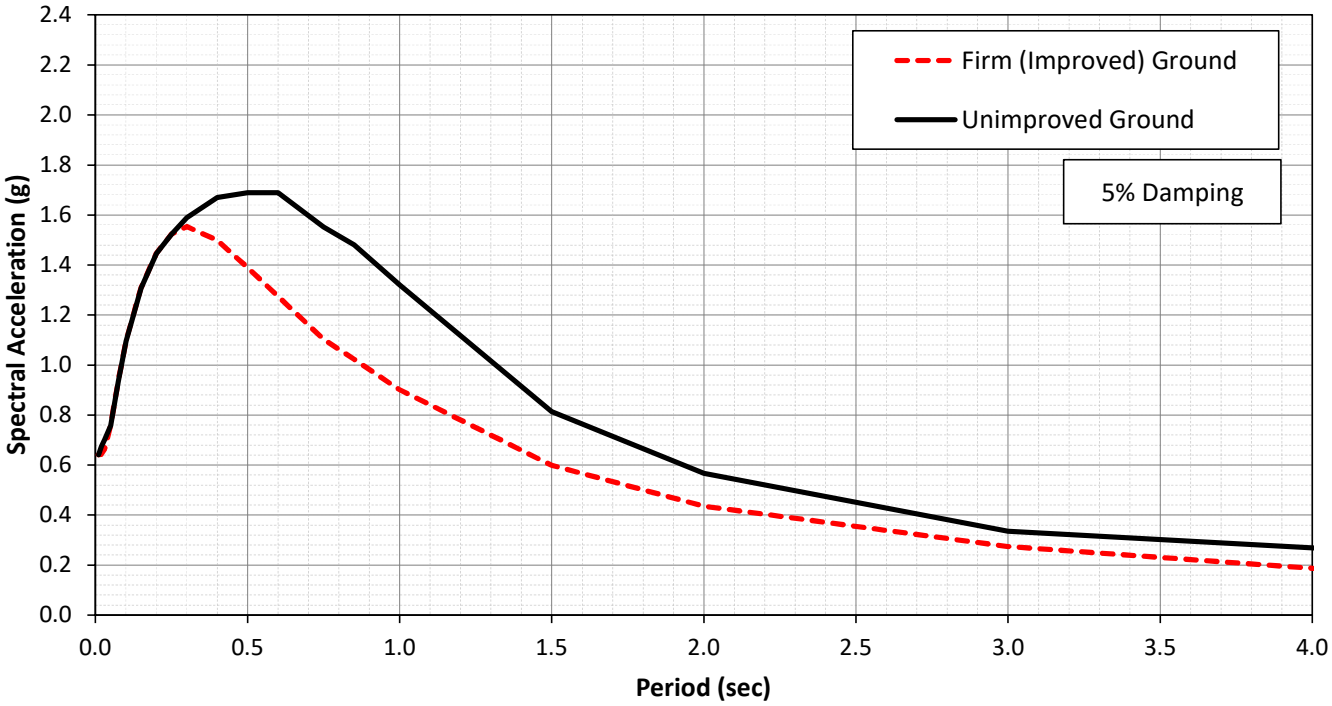
Earth Mechanics, Inc.
Geotechnical and Earthquake Engineering

Recommended Firm (Improved) and Unimproved Ground ARS Curves - Area A - 975-yr Return Period Event

POLB Port-Wide Ground Motion Study 2020

EMI Project No: 19-158 Date: 10/26/2020

Figure 5-5



Period (sec)	Firm (Imporved) Ground ARS (g)	Unimproved Ground ARS (g)
0.010	0.641	0.641
0.020	0.643	0.674
0.030	0.662	0.701
0.040	0.707	0.728
0.050	0.758	0.758
0.075	0.936	0.936
0.100	1.096	1.096
0.150	1.308	1.308
0.200	1.447	1.447
0.250	1.523	1.523
0.300	1.553	1.590
0.400	1.499	1.670
0.500	1.389	1.689
0.600	1.275	1.689
0.750	1.104	1.553
0.850	1.023	1.481
1.000	0.901	1.321
1.500	0.599	0.814
2.000	0.436	0.566
3.000	0.273	0.336
4.000	0.187	0.269
5.000	0.137	0.197
7.500	0.076	0.113
10.000	0.048	0.058

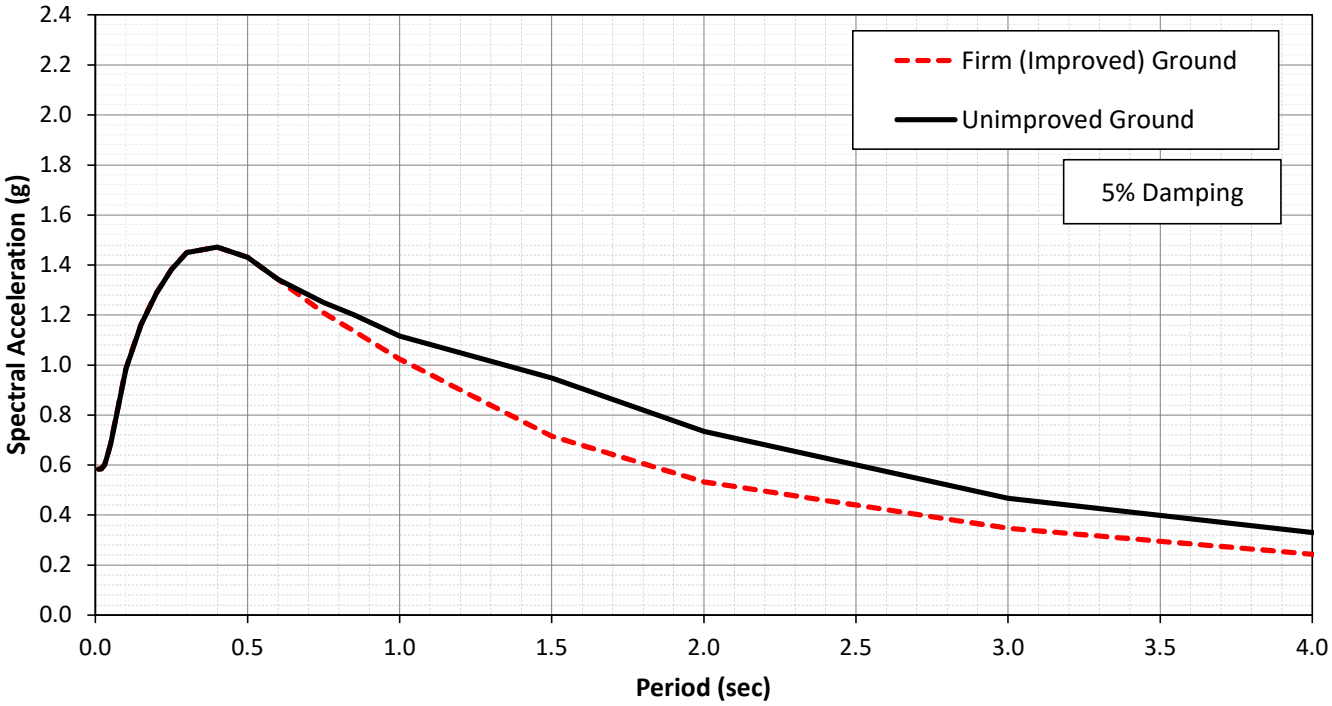
Earth Mechanics, Inc.
Geotechnical and Earthquake Engineering

Recommended Firm (Improved) and Unimproved Ground ARS Curves - Area B - 975-yr Return Period Event

POLB Port-Wide Ground Motion Study 2020

EMI Project No: 19-158 Date: 10/26/2020

Figure 5-6



Period (sec)	Firm (Imporved) Ground ARS (g)	Unimproved Ground ARS (g)
0.010	0.584	0.584
0.020	0.585	0.585
0.030	0.600	0.600
0.040	0.638	0.638
0.050	0.684	0.684
0.075	0.836	0.836
0.100	0.987	0.987
0.150	1.162	1.162
0.200	1.288	1.288
0.250	1.382	1.382
0.300	1.450	1.450
0.400	1.471	1.471
0.500	1.430	1.430
0.600	1.342	1.342
0.750	1.210	1.250
0.850	1.135	1.200
1.000	1.024	1.116
1.500	0.716	0.948
2.000	0.532	0.734
3.000	0.347	0.467
4.000	0.243	0.331
5.000	0.184	0.265
7.500	0.111	0.177
10.000	0.066	0.106

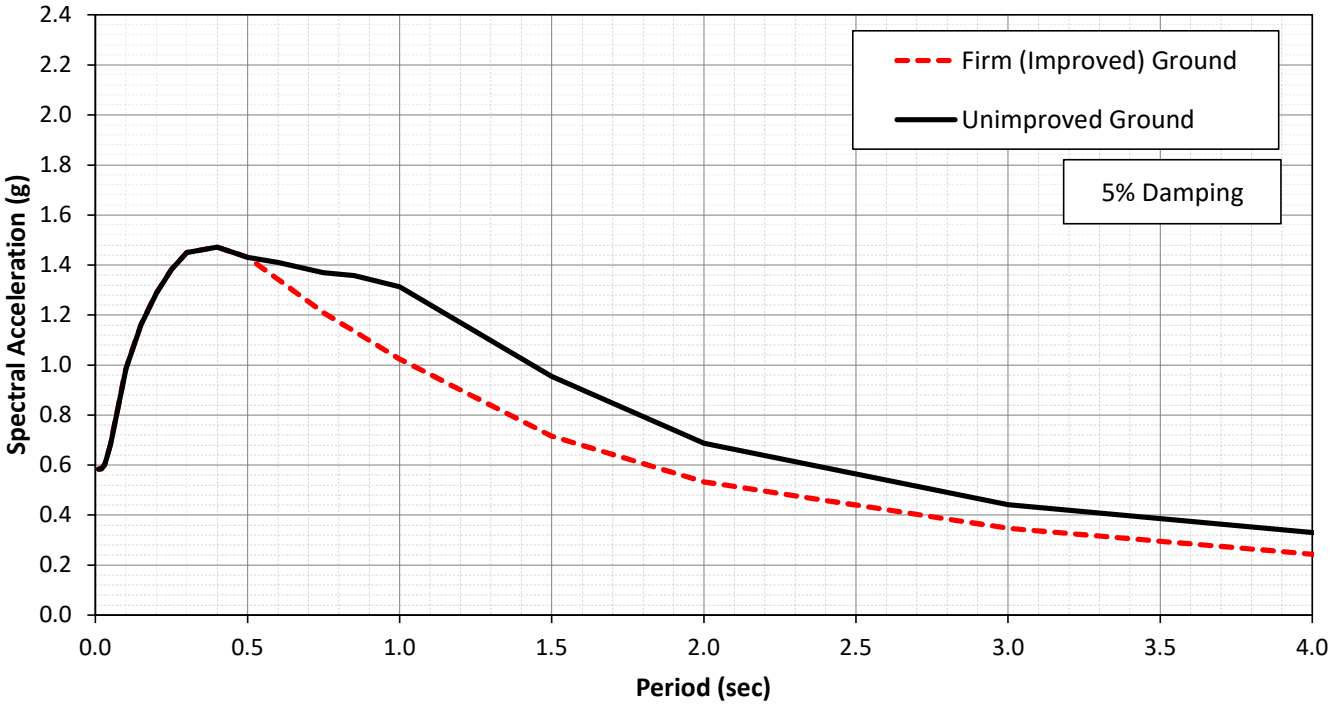
Earth Mechanics, Inc.
Geotechnical and Earthquake Engineering

Recommended Firm (Improved) and Unimproved Ground ARS Curves - Area A - ASCE 7-16 Based DE Event

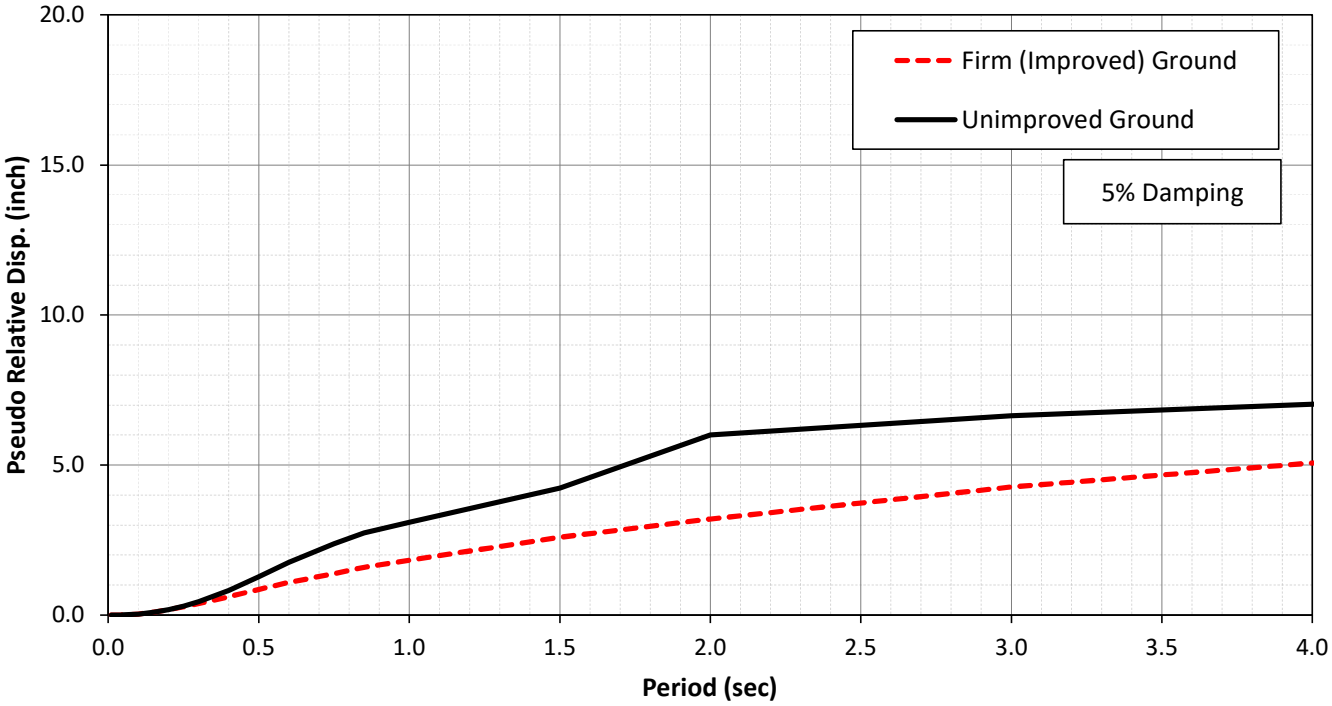
POLB Port-Wide Ground Motion Study 2020

EMI Project No: 19-158 Date: 10/26/2020

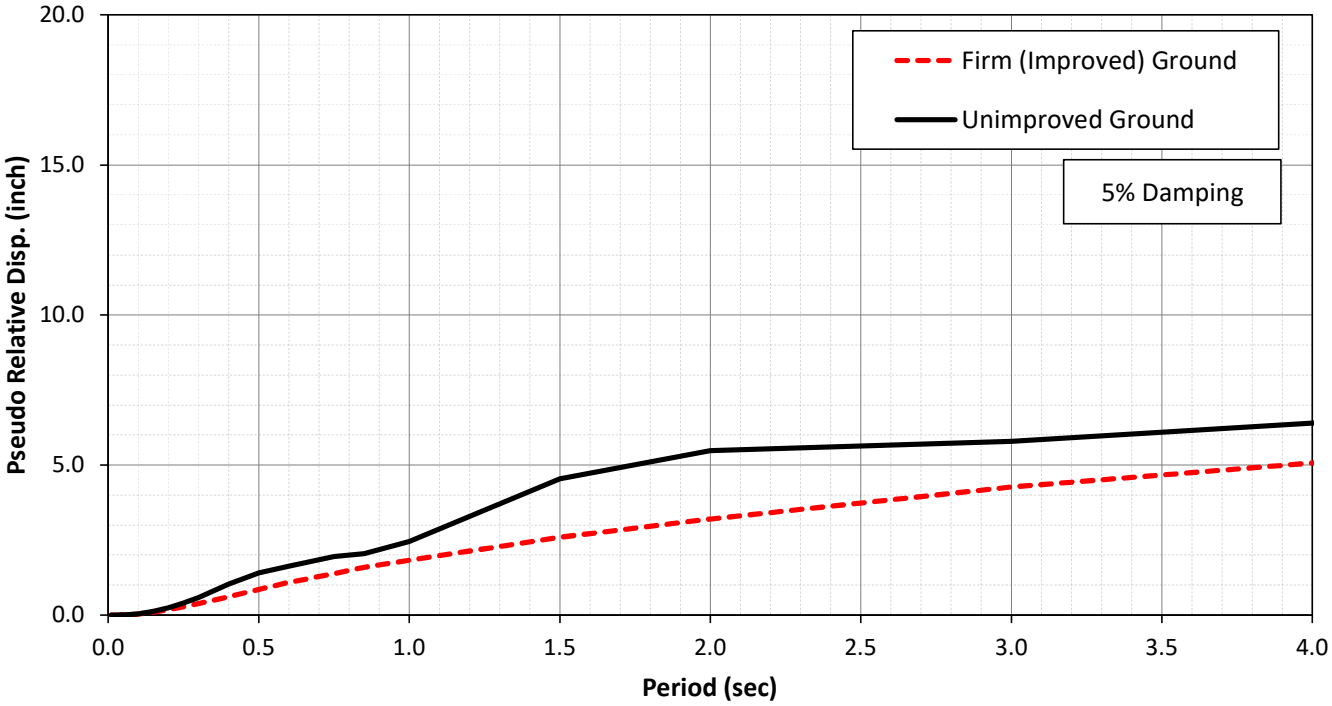
Figure 5-7



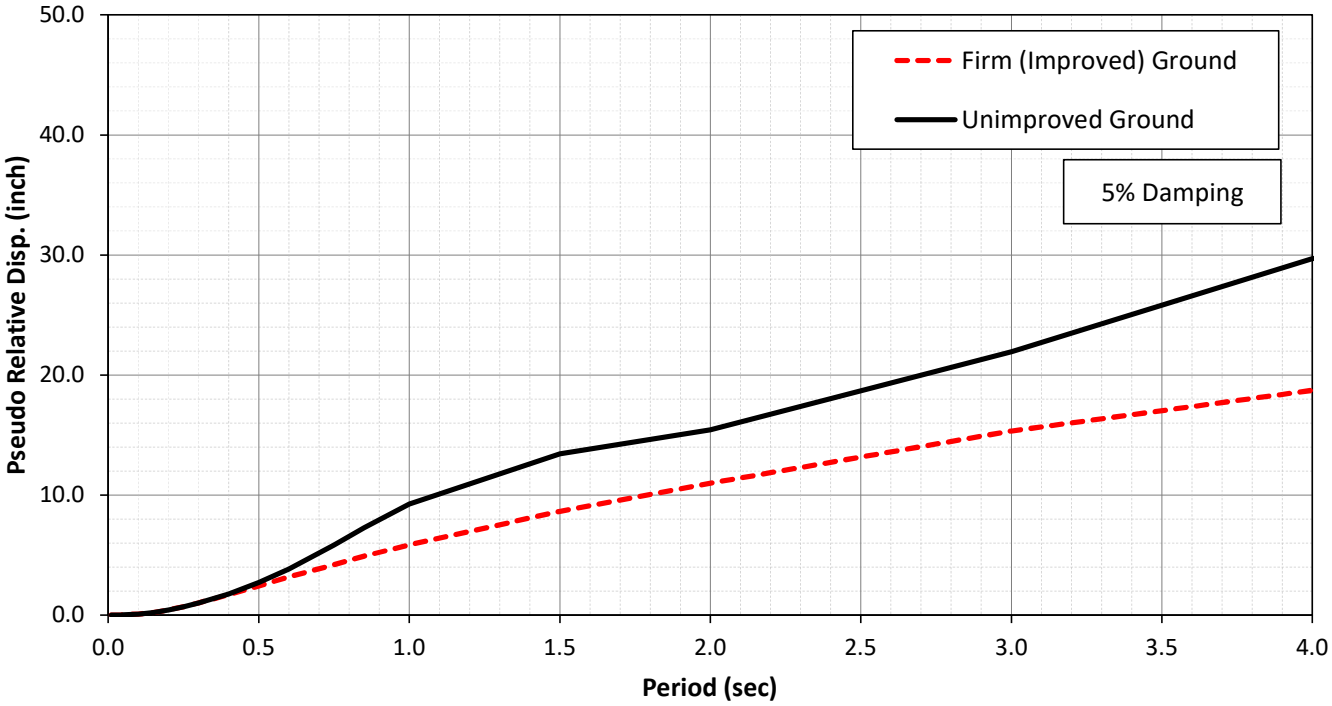
Period (sec)	Firm (Imporved) Ground ARS (g)	Unimproved Ground ARS (g)
0.010	0.584	0.584
0.020	0.585	0.585
0.030	0.600	0.600
0.040	0.638	0.638
0.050	0.684	0.684
0.075	0.836	0.836
0.100	0.987	0.987
0.150	1.162	1.162
0.200	1.288	1.288
0.250	1.382	1.382
0.300	1.450	1.450
0.400	1.471	1.471
0.500	1.430	1.430
0.600	1.342	1.410
0.750	1.210	1.370
0.850	1.135	1.358
1.000	1.024	1.314
1.500	0.716	0.955
2.000	0.532	0.687
3.000	0.347	0.441
4.000	0.243	0.331
5.000	0.184	0.265
7.500	0.111	0.177
10.000	0.066	0.106



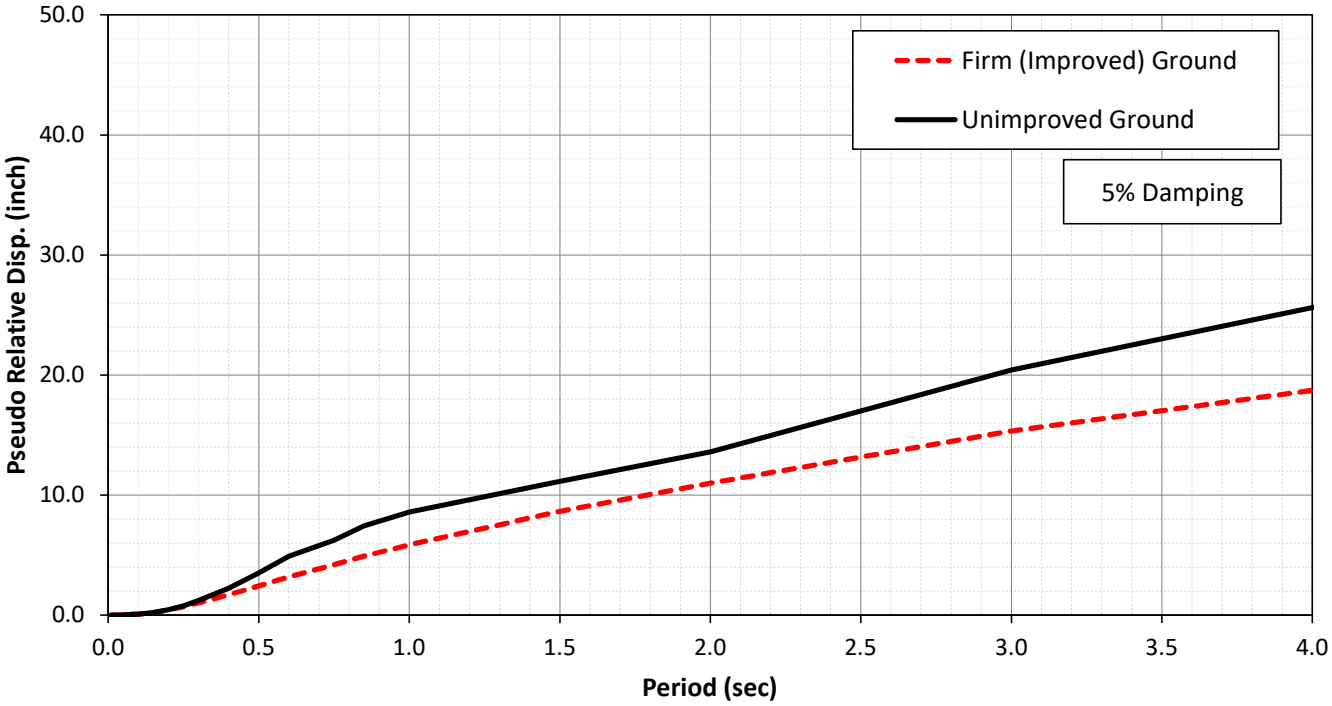
Period (sec)	Firm (Imporved) Ground ARS (inch)	Unimproved Ground ARS (inch)
0.010	0.000	0.000
0.020	0.001	0.001
0.030	0.002	0.002
0.040	0.003	0.004
0.050	0.005	0.006
0.075	0.015	0.016
0.100	0.033	0.033
0.150	0.091	0.091
0.200	0.173	0.179
0.250	0.273	0.300
0.300	0.384	0.449
0.400	0.611	0.816
0.500	0.851	1.275
0.600	1.088	1.762
0.750	1.378	2.379
0.850	1.590	2.743
1.000	1.828	3.094
1.500	2.592	4.238
2.000	3.198	6.007
3.000	4.265	6.640
4.000	5.064	7.025
5.000	5.599	7.194
7.500	6.707	8.443
10.000	7.252	7.252



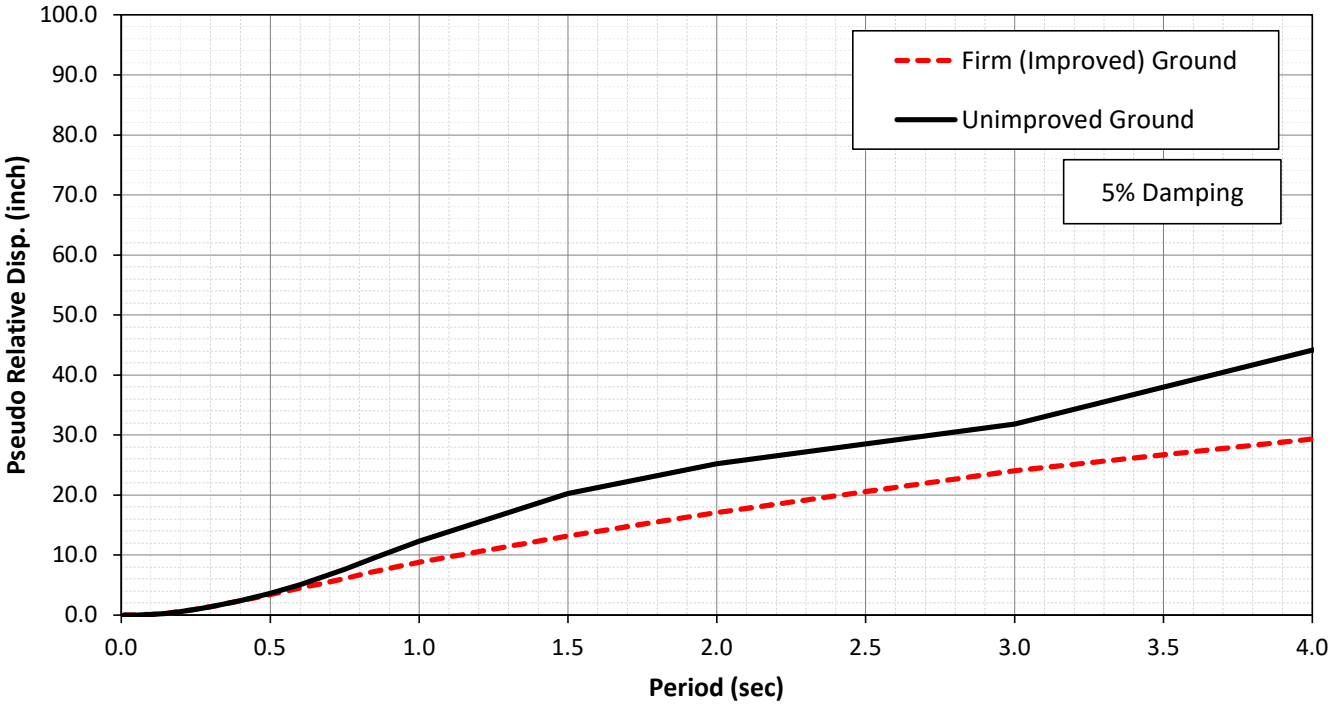
Period (sec)	Firm (Imporved) Ground ARS (inch)	Unimproved Ground ARS (inch)
0.010	0.000	0.000
0.020	0.001	0.001
0.030	0.002	0.003
0.040	0.003	0.005
0.050	0.005	0.008
0.075	0.015	0.021
0.100	0.033	0.044
0.150	0.091	0.123
0.200	0.173	0.247
0.250	0.273	0.410
0.300	0.384	0.590
0.400	0.611	1.034
0.500	0.851	1.408
0.600	1.088	1.632
0.750	1.378	1.953
0.850	1.590	2.049
1.000	1.828	2.447
1.500	2.592	4.542
2.000	3.198	5.477
3.000	4.265	5.793
4.000	5.064	6.398
5.000	5.599	6.781
7.500	6.707	8.089
10.000	7.252	7.252



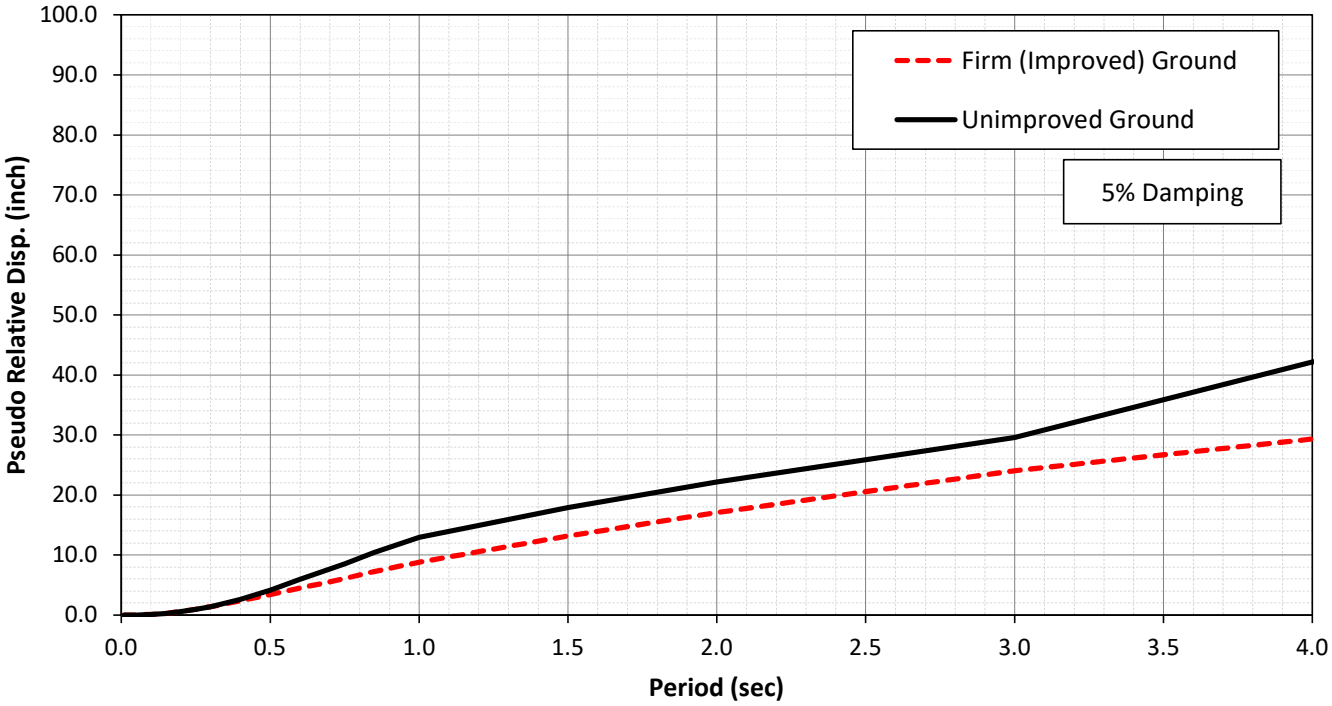
Period (sec)	Firm (Imporved) Ground ARS (inch)	Unimproved Ground ARS (inch)
0.010	0.000	0.000
0.020	0.002	0.002
0.030	0.004	0.004
0.040	0.008	0.008
0.050	0.014	0.014
0.075	0.039	0.039
0.100	0.082	0.082
0.150	0.223	0.223
0.200	0.429	0.429
0.250	0.695	0.695
0.300	1.007	1.007
0.400	1.685	1.770
0.500	2.424	2.716
0.600	3.164	3.841
0.750	4.178	5.836
0.850	4.908	7.284
1.000	5.843	9.256
1.500	8.628	13.433
2.000	10.977	15.435
3.000	15.318	21.934
4.000	18.718	29.690
5.000	21.507	32.967
7.500	27.523	42.954
10.000	31.143	38.774



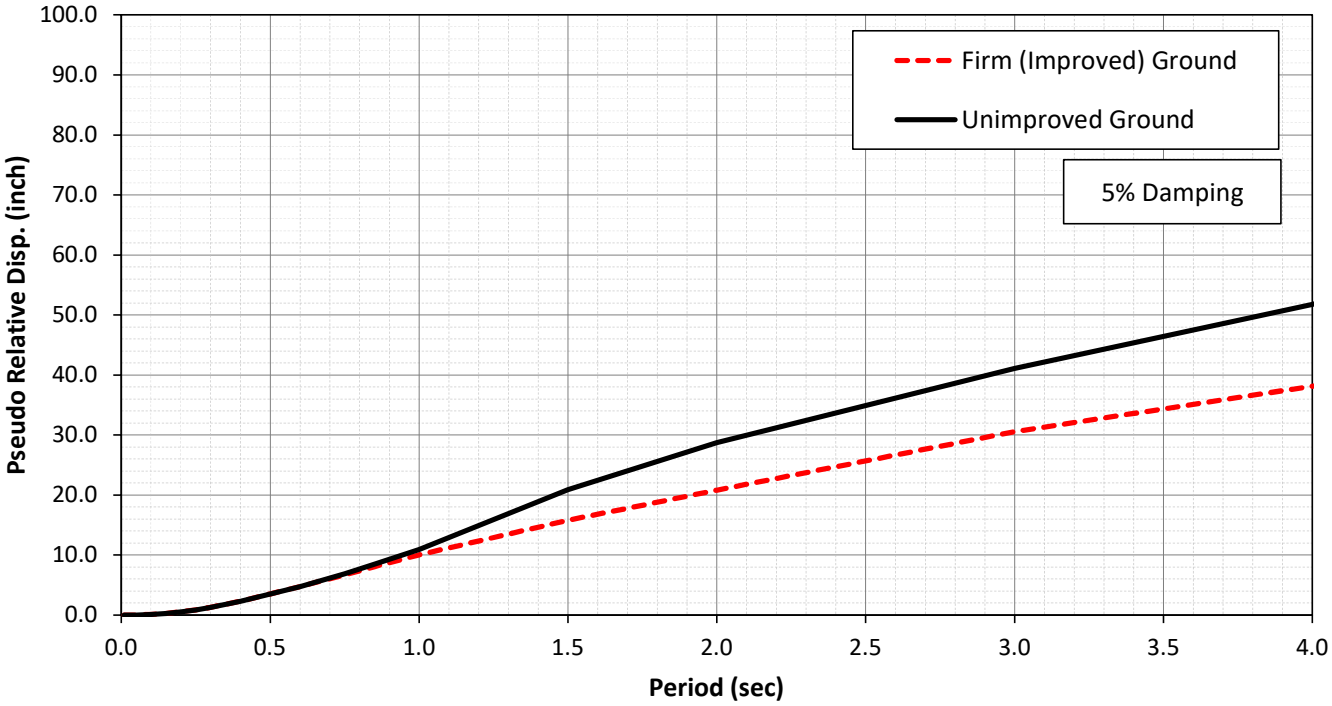
Period (sec)	Firm (Imporved) Ground ARS (inch)	Unimproved Ground ARS (inch)
0.010	0.000	0.001
0.020	0.002	0.002
0.030	0.004	0.005
0.040	0.008	0.010
0.050	0.014	0.016
0.075	0.039	0.041
0.100	0.082	0.082
0.150	0.223	0.223
0.200	0.429	0.442
0.250	0.695	0.784
0.300	1.007	1.224
0.400	1.685	2.244
0.500	2.424	3.506
0.600	3.164	4.898
0.750	4.178	6.233
0.850	4.908	7.433
1.000	5.843	8.586
1.500	8.628	11.142
2.000	10.977	13.591
3.000	15.318	20.434
4.000	18.718	25.633
5.000	21.507	29.051
7.500	27.523	38.689
10.000	31.143	35.184



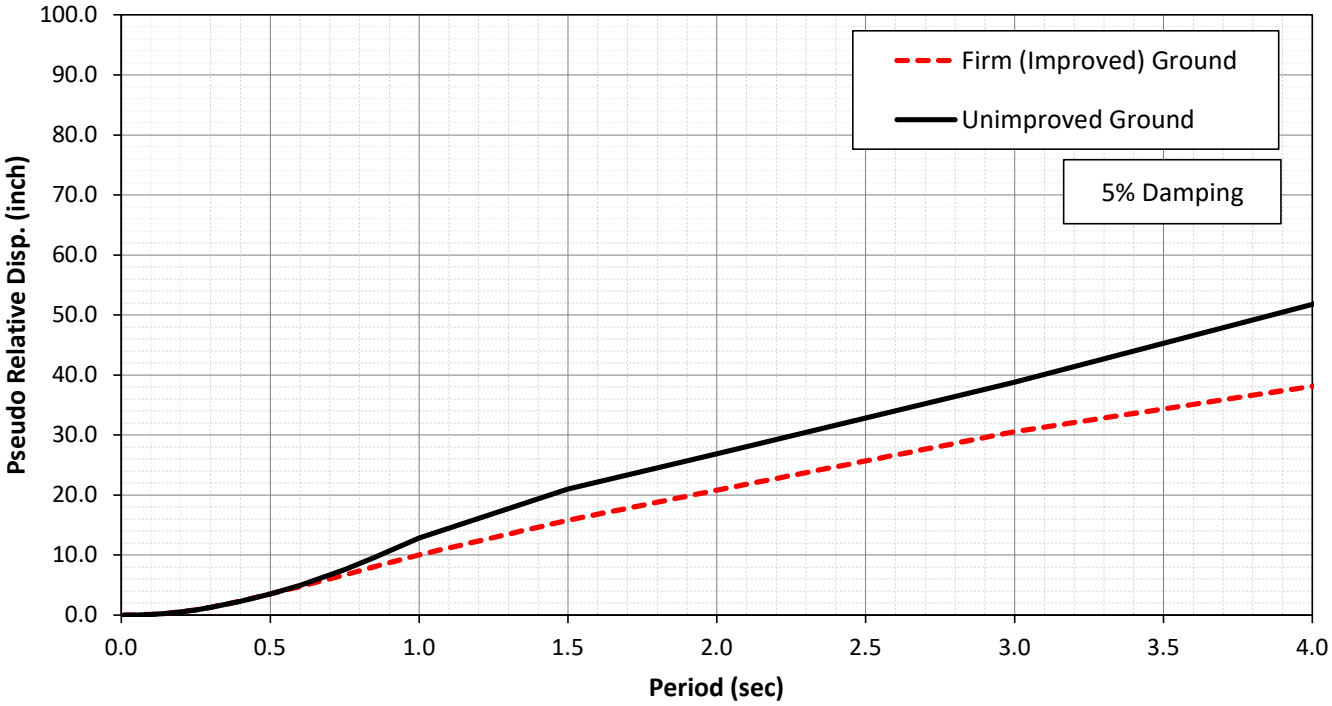
Period (sec)	Firm (Imporved) Ground ARS (inch)	Unimproved Ground ARS (inch)
0.010	0.001	0.001
0.020	0.003	0.003
0.030	0.006	0.006
0.040	0.011	0.011
0.050	0.019	0.019
0.075	0.052	0.052
0.100	0.107	0.107
0.150	0.288	0.288
0.200	0.566	0.566
0.250	0.932	0.932
0.300	1.368	1.368
0.400	2.348	2.374
0.500	3.400	3.617
0.600	4.493	5.075
0.750	6.076	7.619
0.850	7.232	9.520
1.000	8.820	12.340
1.500	13.185	20.267
2.000	17.050	25.246
3.000	24.069	31.845
4.000	29.344	44.161
5.000	33.500	51.498
7.500	41.605	67.856
10.000	47.097	62.231



Period (sec)	Firm (Imporved) Ground ARS (inch)	Unimproved Ground ARS (inch)
0.010	0.001	0.001
0.020	0.003	0.003
0.030	0.006	0.006
0.040	0.011	0.011
0.050	0.019	0.019
0.075	0.052	0.052
0.100	0.107	0.107
0.150	0.288	0.288
0.200	0.566	0.566
0.250	0.932	0.932
0.300	1.368	1.401
0.400	2.348	2.615
0.500	3.400	4.133
0.600	4.493	5.951
0.750	6.076	8.550
0.850	7.232	10.471
1.000	8.820	12.931
1.500	13.185	17.922
2.000	17.050	22.170
3.000	24.069	29.586
4.000	29.344	42.169
5.000	33.500	48.123
7.500	41.605	62.363
10.000	47.097	56.583



Period (sec)	Firm (Imporved) Ground ARS (inch)	Unimproved Ground ARS (inch)
0.010	0.001	0.001
0.020	0.002	0.002
0.030	0.005	0.005
0.040	0.010	0.010
0.050	0.017	0.017
0.075	0.046	0.046
0.100	0.097	0.097
0.150	0.256	0.256
0.200	0.504	0.504
0.250	0.846	0.846
0.300	1.277	1.277
0.400	2.303	2.303
0.500	3.500	3.500
0.600	4.729	4.729
0.750	6.659	6.882
0.850	8.029	8.486
1.000	10.025	10.924
1.500	15.762	20.880
2.000	20.820	28.737
3.000	30.542	41.101
4.000	38.102	51.783
5.000	45.036	64.729
7.500	60.954	97.527
10.000	64.729	103.566



Period (sec)	Firm (Imporved) Ground ARS (inch)	Unimproved Ground ARS (inch)
0.010	0.001	0.001
0.020	0.002	0.002
0.030	0.005	0.005
0.040	0.010	0.010
0.050	0.017	0.017
0.075	0.046	0.046
0.100	0.097	0.097
0.150	0.256	0.256
0.200	0.504	0.504
0.250	0.846	0.846
0.300	1.277	1.277
0.400	2.303	2.303
0.500	3.500	3.500
0.600	4.729	4.968
0.750	6.659	7.543
0.850	8.029	9.607
1.000	10.025	12.856
1.500	15.762	21.025
2.000	20.820	26.892
3.000	30.542	38.837
4.000	38.102	51.783
5.000	45.036	64.729
7.500	60.954	97.527
10.000	64.729	103.566

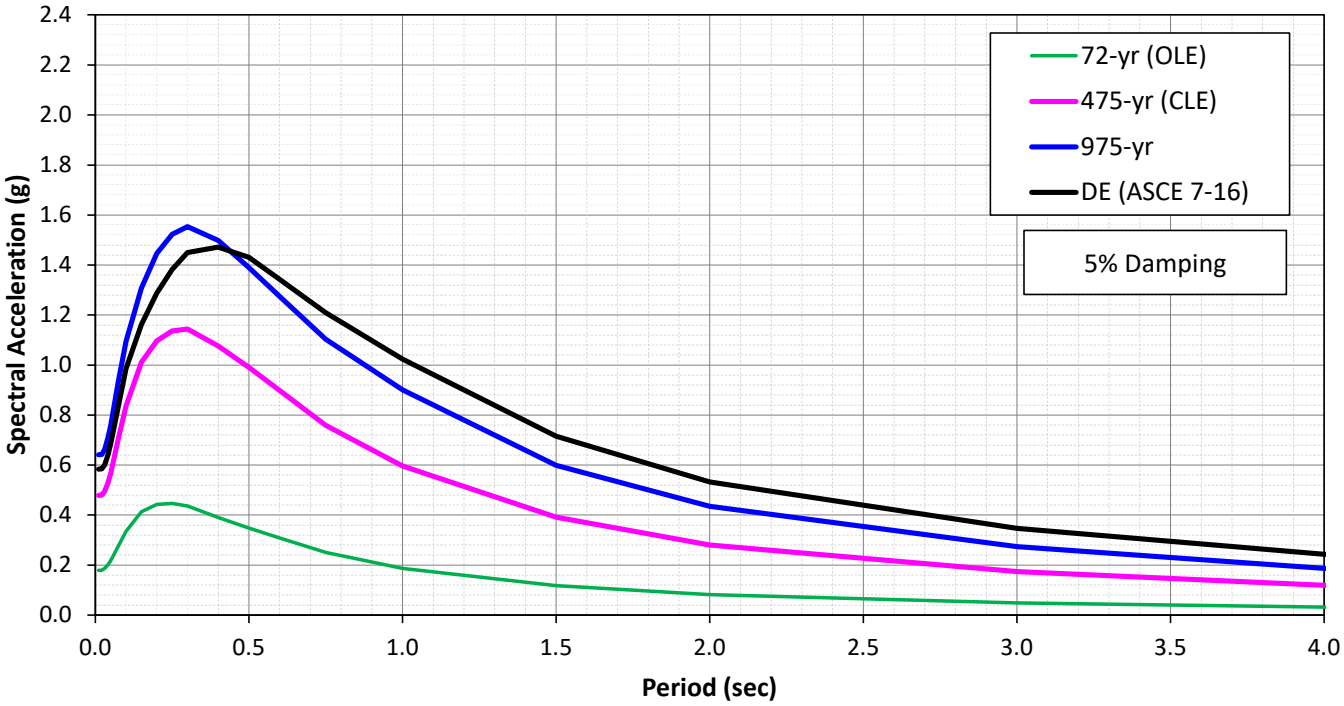
Earth Mechanics, Inc.
Geotechnical and Earthquake Engineering

Recommended Firm (Improved) and Unimproved Ground DRS Curves - Area B - ASCE 7-16 Based DE Event

POLB Port-Wide Ground Motion Study 2020

EMI Project No: 19-158 Date: 10/26/2020

Figure 5-16



Period (sec)	72-yr OLE ARS (g)	475-yr CLE ARS (g)	975-yr ARS (g)	ASCE 7-16 DE (g)
0.010	0.179	0.479	0.641	0.584
0.020	0.179	0.480	0.643	0.585
0.030	0.186	0.495	0.662	0.600
0.040	0.201	0.528	0.707	0.638
0.050	0.217	0.566	0.758	0.684
0.075	0.276	0.706	0.936	0.836
0.100	0.335	0.836	1.096	0.987
0.150	0.413	1.011	1.308	1.162
0.200	0.443	1.097	1.447	1.288
0.250	0.446	1.136	1.523	1.382
0.300	0.436	1.143	1.553	1.450
0.400	0.390	1.076	1.499	1.471
0.500	0.348	0.991	1.389	1.430
0.600	0.309	0.898	1.275	1.342
0.750	0.250	0.759	1.104	1.210
0.850	0.225	0.694	1.023	1.135
1.000	0.187	0.597	0.901	1.024
1.500	0.118	0.392	0.599	0.716
2.000	0.082	0.280	0.436	0.532
3.000	0.048	0.174	0.273	0.347
4.000	0.032	0.120	0.187	0.243
5.000	0.023	0.088	0.137	0.184
7.500	0.012	0.050	0.076	0.111
10.000	0.007	0.032	0.048	0.066

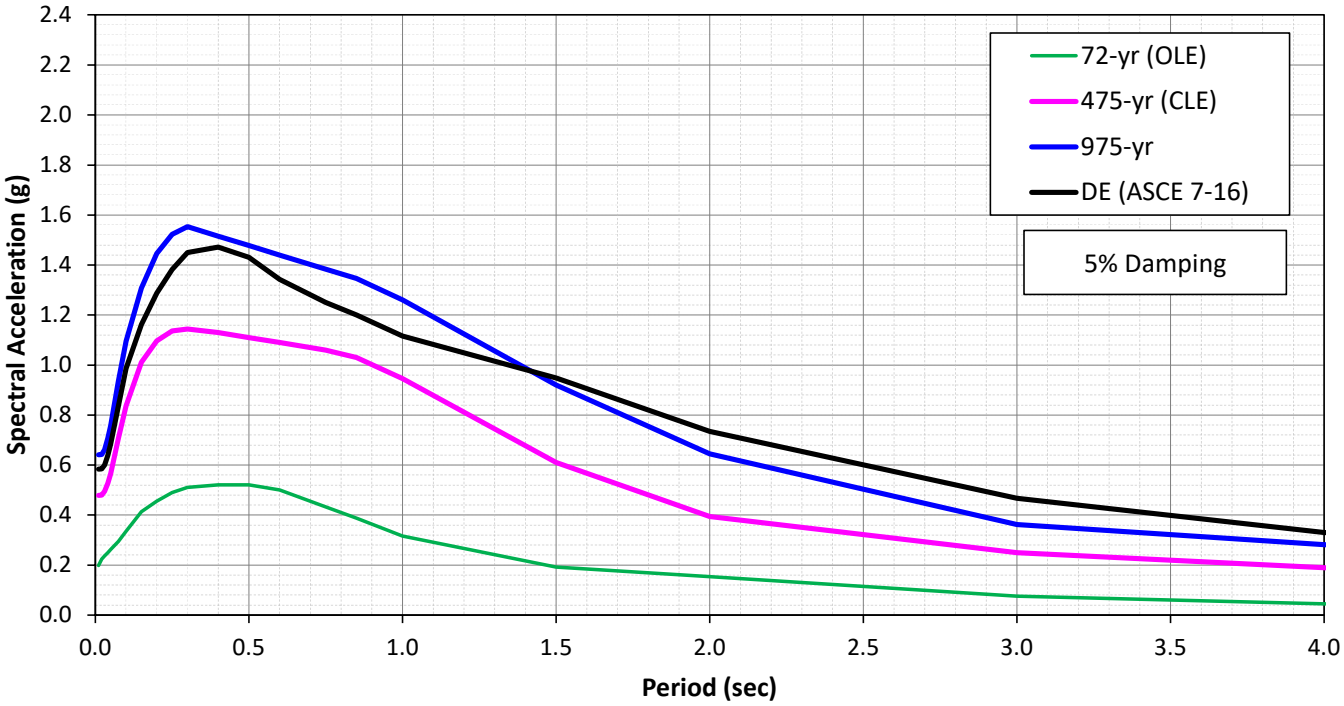
Earth Mechanics, Inc.
Geotechnical and Earthquake Engineering

Recommended Firm (Improved) Ground ARS Curves - Area A and B- OLE, CLE, 975-yr, and ASCE 7-16 Based DE

POLB Port-Wide Ground Motion Study 2020

EMI Project No: 19-158 Date: 10/26/2020

Figure 5-17



Period (sec)	72-yr OLE ARS (g)	475-yr CLE ARS (g)	975-yr ARS (g)	ASCE 7-16 DE (g)
0.010	0.198	0.479	0.641	0.584
0.020	0.224	0.480	0.643	0.585
0.030	0.236	0.495	0.662	0.600
0.040	0.249	0.528	0.707	0.638
0.050	0.262	0.566	0.758	0.684
0.075	0.295	0.706	0.936	0.836
0.100	0.335	0.836	1.096	0.987
0.150	0.413	1.011	1.308	1.162
0.200	0.456	1.097	1.447	1.288
0.250	0.490	1.136	1.523	1.382
0.300	0.510	1.143	1.553	1.450
0.400	0.521	1.130	1.516	1.471
0.500	0.521	1.110	1.478	1.430
0.600	0.500	1.090	1.440	1.342
0.750	0.432	1.060	1.384	1.250
0.850	0.388	1.030	1.346	1.200
1.000	0.316	0.946	1.261	1.116
1.500	0.192	0.610	0.920	0.948
2.000	0.153	0.394	0.645	0.734
3.000	0.075	0.249	0.362	0.467
4.000	0.045	0.190	0.282	0.331
5.000	0.029	0.135	0.210	0.265
7.500	0.015	0.078	0.123	0.177
10.000	0.007	0.040	0.064	0.106

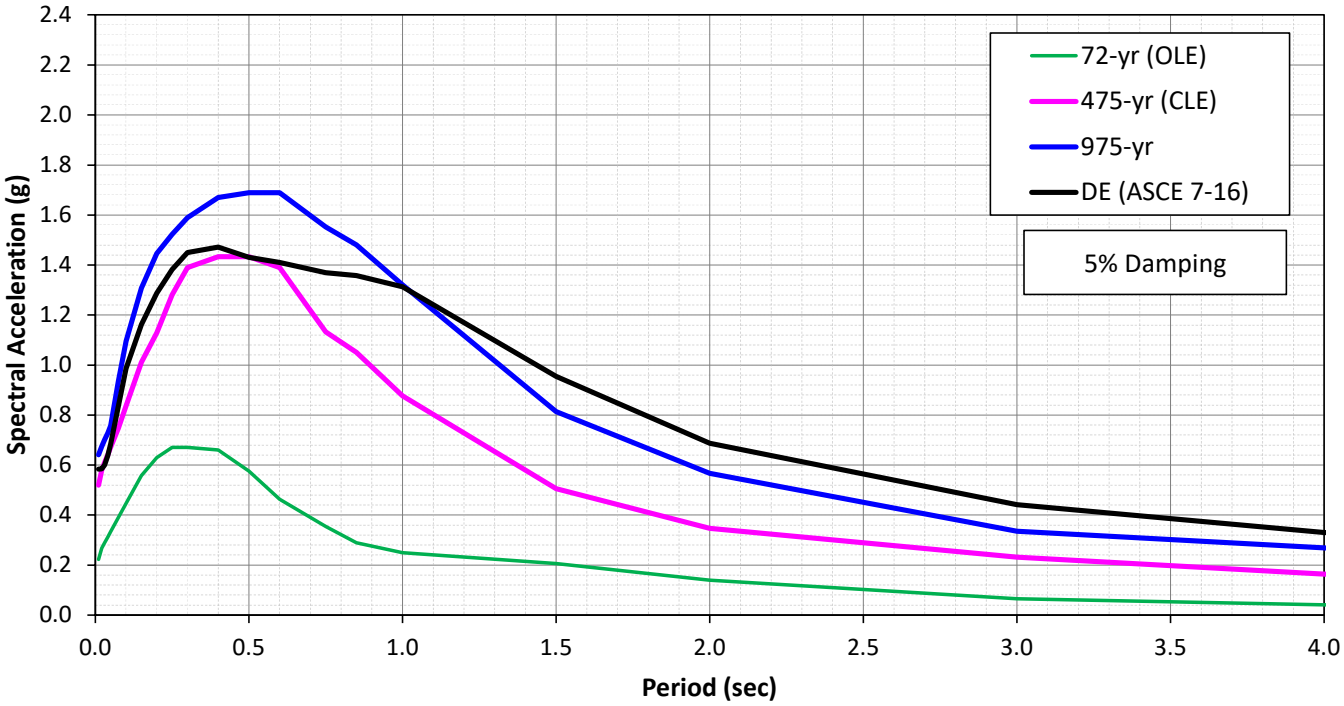
Earth Mechanics, Inc.
Geotechnical and Earthquake Engineering

Recommended Unimproved Ground ARS Curves - Area A - OLE, CLE, 975-yr, and ASCE 7-16 Based DE

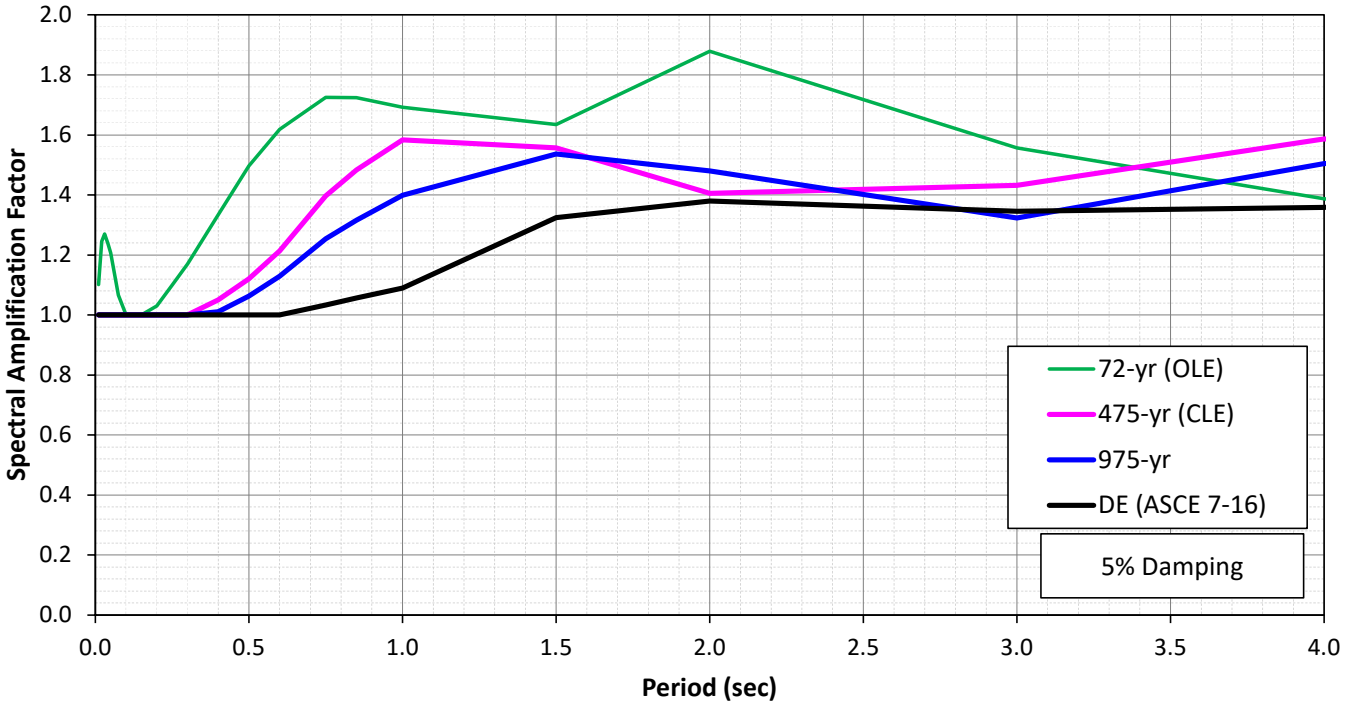
POLB Port-Wide Ground Motion Study 2020

EMI Project No: 19-158 Date: 10/26/2020

Figure 5-18



Period (sec)	72-yr OLE ARS (g)	475-yr CLE ARS (g)	975-yr ARS (g)	ASCE 7-16 DE (g)
0.010	0.223	0.519	0.641	0.584
0.020	0.267	0.580	0.674	0.585
0.030	0.290	0.611	0.701	0.600
0.040	0.312	0.641	0.728	0.638
0.050	0.334	0.672	0.758	0.684
0.075	0.390	0.748	0.936	0.836
0.100	0.446	0.836	1.096	0.987
0.150	0.558	1.011	1.308	1.162
0.200	0.630	1.129	1.447	1.288
0.250	0.670	1.281	1.523	1.382
0.300	0.670	1.390	1.590	1.450
0.400	0.660	1.433	1.670	1.471
0.500	0.576	1.433	1.689	1.430
0.600	0.463	1.390	1.689	1.410
0.750	0.355	1.132	1.553	1.370
0.850	0.290	1.051	1.481	1.358
1.000	0.250	0.877	1.321	1.314
1.500	0.206	0.506	0.814	0.955
2.000	0.140	0.347	0.566	0.687
3.000	0.066	0.232	0.336	0.441
4.000	0.041	0.164	0.269	0.331
5.000	0.028	0.119	0.197	0.265
7.500	0.015	0.070	0.113	0.177
10.000	0.007	0.036	0.058	0.106



Period (sec)	72-yr OLE ARS (g)	475-yr CLE ARS (g)	975-yr ARS (g)	ASCE 7-16 DE (g)
0.010	1.102	1.000	1.000	1.000
0.020	1.246	1.000	1.000	1.000
0.030	1.270	1.000	1.000	1.000
0.040	1.239	1.000	1.000	1.000
0.050	1.207	1.000	1.000	1.000
0.075	1.066	1.000	1.000	1.000
0.100	1.000	1.000	1.000	1.000
0.150	1.000	1.000	1.000	1.000
0.200	1.031	1.000	1.000	1.000
0.250	1.099	1.000	1.000	1.000
0.300	1.170	1.000	1.000	1.000
0.400	1.335	1.050	1.011	1.000
0.500	1.498	1.120	1.064	1.000
0.600	1.619	1.214	1.130	1.000
0.750	1.726	1.397	1.254	1.033
0.850	1.725	1.484	1.316	1.057
1.000	1.693	1.584	1.399	1.090
1.500	1.635	1.557	1.537	1.325
2.000	1.878	1.406	1.481	1.380
3.000	1.557	1.432	1.323	1.346
4.000	1.387	1.586	1.505	1.359
5.000	1.285	1.533	1.537	1.437
7.500	1.259	1.561	1.631	1.600
10.000	1.000	1.245	1.321	1.600

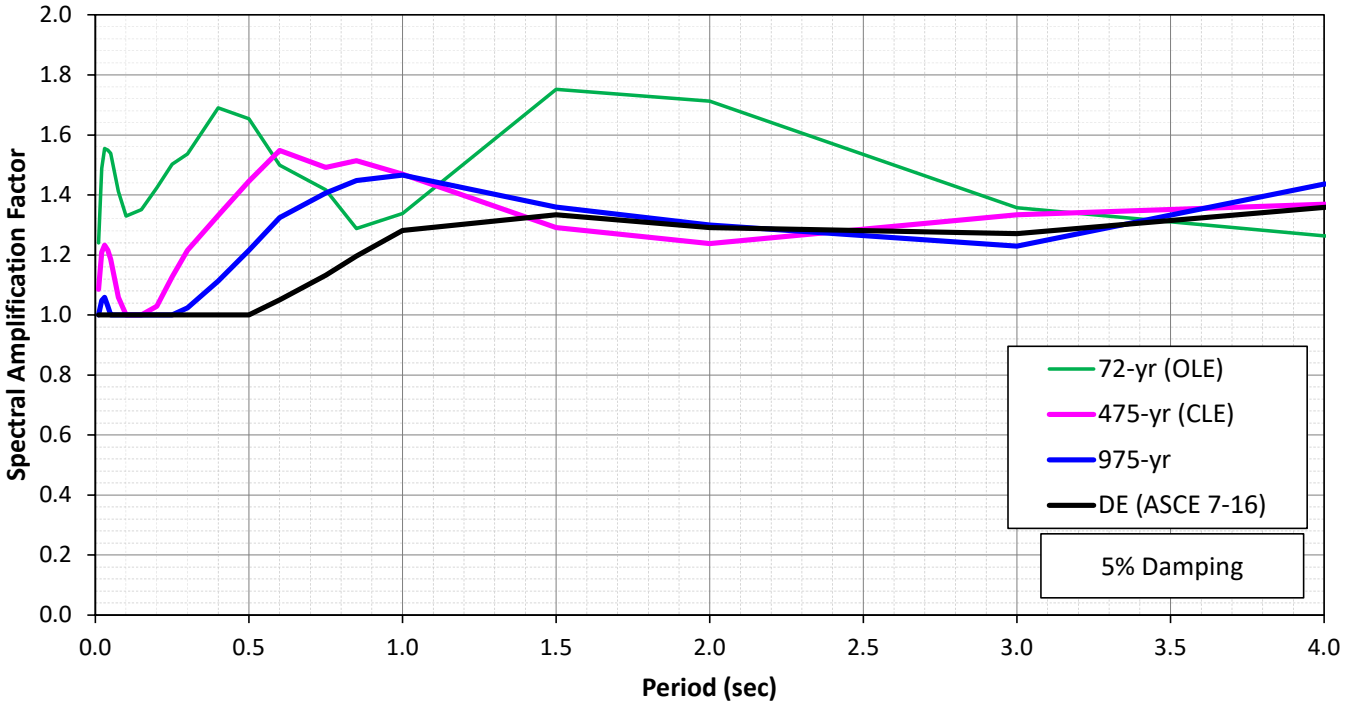
Earth Mechanics, Inc.
Geotechnical and Earthquake Engineering

Spectral Amplification Factors (Ratio of Unimproved Ground ARS Over Improved Ground ARS) - Area A - OLE, CLE, 975-yr, and ASCE 7-16 Based DE

POLB Port-Wide Ground Motion Study 2020

EMI Project No: 19-158 Date: 8/5/2020

Figure 5-20



Period (sec)	72-yr OLE ARS (g)	475-yr CLE ARS (g)	975-yr ARS (g)	ASCE 7-16 DE (g)
0.010	1.240	1.085	1.000	1.000
0.020	1.489	1.210	1.049	1.000
0.030	1.555	1.233	1.059	1.000
0.040	1.550	1.216	1.029	1.000
0.050	1.539	1.186	1.000	1.000
0.075	1.412	1.059	1.000	1.000
0.100	1.330	1.000	1.000	1.000
0.150	1.351	1.000	1.000	1.000
0.200	1.424	1.029	1.000	1.000
0.250	1.503	1.128	1.000	1.000
0.300	1.537	1.216	1.024	1.000
0.400	1.691	1.332	1.114	1.000
0.500	1.654	1.446	1.216	1.000
0.600	1.500	1.548	1.325	1.051
0.750	1.417	1.492	1.407	1.133
0.850	1.288	1.514	1.448	1.196
1.000	1.339	1.470	1.466	1.282
1.500	1.752	1.291	1.359	1.334
2.000	1.713	1.238	1.300	1.292
3.000	1.358	1.334	1.229	1.272
4.000	1.264	1.369	1.437	1.359
5.000	1.211	1.351	1.437	1.437
7.500	1.206	1.406	1.499	1.600
10.000	1.000	1.130	1.201	1.600

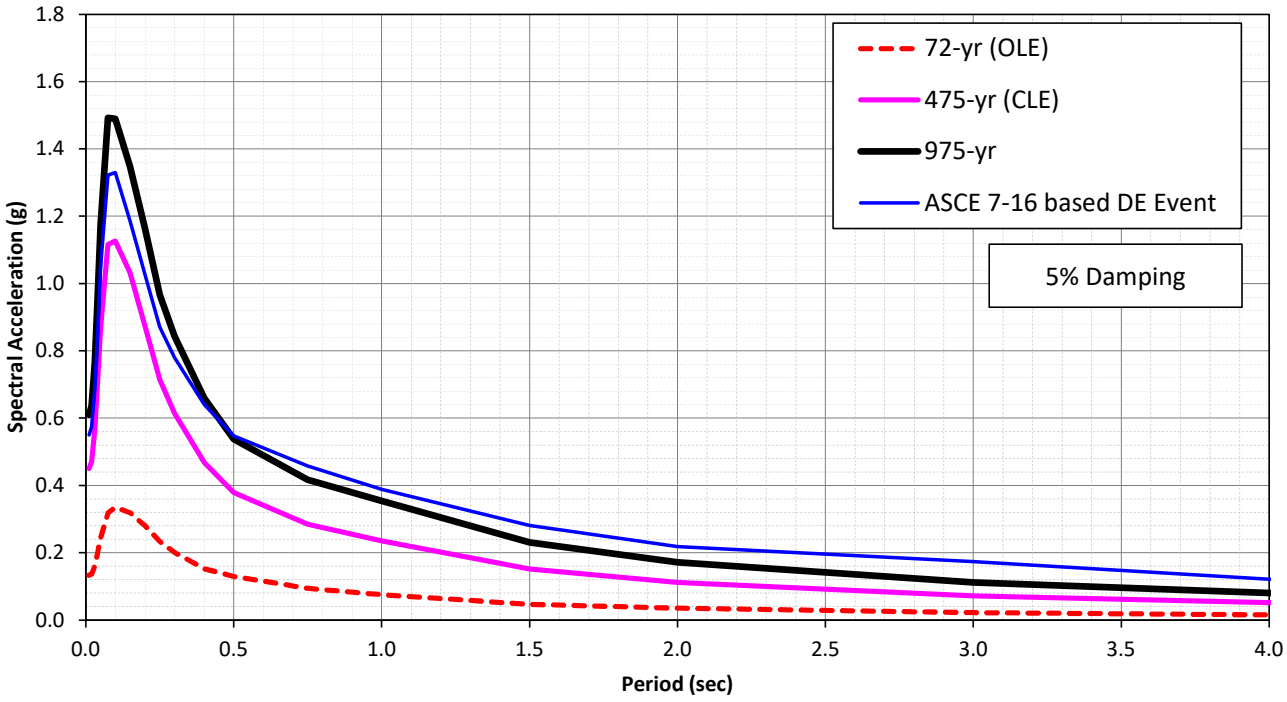
Earth Mechanics, Inc.
Geotechnical and Earthquake Engineering

Spectral Amplification Factors (Ratio of Unimproved Ground ARS Over Improved Ground ARS) - Area B - OLE, CLE, 975-yr, and ASCE 7-16 Based DE

POLB Port-Wide Ground Motion Study 2020

EMI Project No: 19-158 Date: 8/5/2020

Figure 5-21



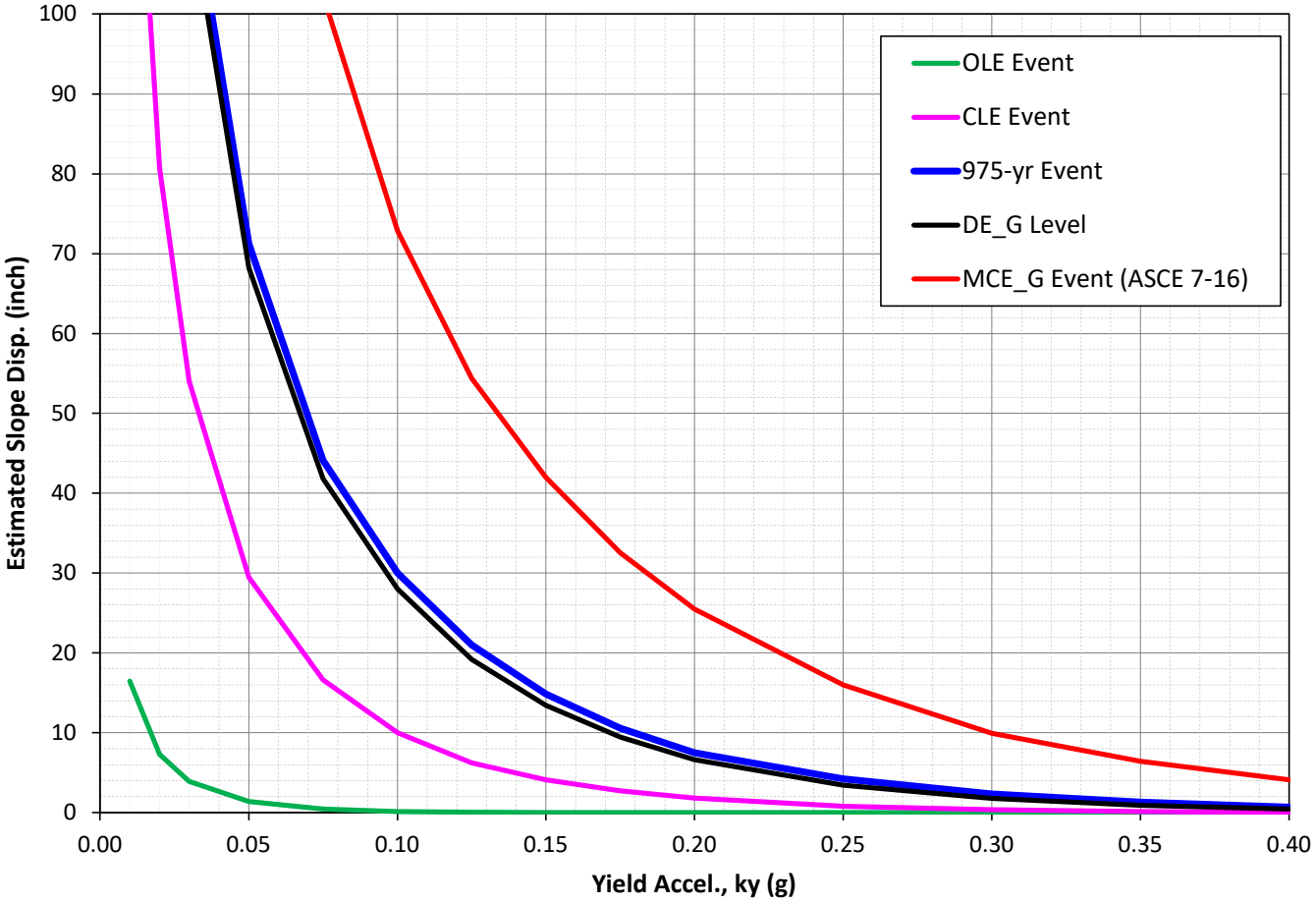
Period (sec)	72-yr (OLE) ARS	475-yr (CLE) ARS	975-yr ARS	ASCE7-16 based DE ARS
0.01	0.133	0.451	0.610	0.550
0.02	0.137	0.470	0.637	0.574
0.03	0.163	0.567	0.765	0.687
0.04	0.204	0.712	0.963	0.861
0.05	0.246	0.869	1.174	1.050
0.08	0.319	1.116	1.493	1.322
0.10	0.335	1.127	1.490	1.330
0.15	0.319	1.032	1.348	1.186
0.20	0.280	0.873	1.163	1.025
0.25	0.234	0.715	0.967	0.870
0.30	0.201	0.615	0.844	0.780
0.40	0.153	0.469	0.660	0.641
0.50	0.130	0.379	0.538	0.547
0.75	0.095	0.285	0.417	0.458
1.00	0.075	0.236	0.354	0.388
1.50	0.047	0.152	0.231	0.280
2.00	0.036	0.112	0.172	0.218
3.00	0.023	0.072	0.112	0.173
4.00	0.015	0.052	0.081	0.122
5.00	0.010	0.039	0.059	0.092
7.50	0.005	0.021	0.032	0.055
10.00	0.003	0.013	0.019	0.033

Earth Mechanics, Inc.
Geotechnical and Earthquake Engineering

Recommended Firm (Improved) and Unimproved Ground Vertical ARS Curves - OLE, CLE, 975-yr Return Period, and ASCE 7-16 based DE Events

POLB Port-Wide Ground Motion Study 2020

EMI Project No: 19-158 | Date: 10/26/2020 | Figure 5-22



Yield Accel., ky (g)	Slope Disp., OLE Event (inch)	Slope Disp., CLE Event (inch)	Slope Disp., 975Yr RP Event (inch)	Slope Disp., DE_G Event (inch)	Slope Disp., MCE_G Event (inch)
0.01	16.4	140	275	259	525
0.02	7.3	80.7	166	159	319
0.03	3.9	54.0	118	114	239
0.05	1.4	29.5	71.2	68.2	155
0.075	0.5	16.6	44.1	41.8	102
0.1	0.1	10.0	30.0	28.0	72.9
0.125	0.0	6.2	21.0	19.2	54.4
0.15	0.0	4.1	14.9	13.4	42.0
0.175	0.0	2.7	10.6	9.5	32.6
0.2	0.0	1.8	7.5	6.6	25.5
0.25	0.0	0.8	4.2	3.4	16.0
0.3	0.0	0.4	2.4	1.8	9.9
0.35	0.0	0.1	1.3	0.9	6.4
0.4	0.0	0.0	0.7	0.4	4.1

Earth Mechanics, Inc.
Geotechnical and Earthquake Engineering

Recommended Newmark Displacement Curves for Site Screening for OLE, CLE, 975-yr, DE_G, and MCE_G level Events

POLB Port-Wide Ground Motion Study 2020

EMI Project No: 19-158 Date: 10/26/2020

Figure 5-23

6.0 LIMITATIONS

This Port-Wide Ground Motion Study Update Report was prepared by Earth Mechanics, Inc. (EMI) under a contract with Moffatt & Nichol (M&N) and is intended for the sole use by the Port of Long Beach (POLB) and by engineering consultants working on POLB projects located within the Long Beach Harbor District (LBHD). The POLB, M&N, and EMI have no responsibility for the use of this report by any other entities for their projects within the LBHD unless it is specifically required by the POLB.

7.0 REFERENCES

Abrahamson , N. A. 1992, "Non-stationary spectral matching," Seismological Research Letters 63 (1), 30.

Abrahamson, N. A., 2000, "Effects of rupture directivity on probabilistic seismic hazard analysis," Proceedings of 6th International Conference on Seismic Zonation, November 12-15, Palm Springs, California, Earthquake Research Institute, Oakland, California.

Abrahamson, N. A., and Silva, W., 1997, "Empirical response spectral attenuation relations for shallow crustal earthquakes," Seismological Research Letters, Vol. 68, No. 1, January/ February.

Abrahamson, N. A. and Silva, W. J., 2008, "Summary of the Abrahamson & Silva NGA Ground-Motion," Earthquake Spectra, Volume 24, No. 1, February.

Abrahamson, N. A., Silva, W. J., and R. Kamai. 2014, Summary of the ASK14 ground motion relation for active crustal regions. Earthquake Spectra, Vol. 30, No. 3, pp. 1025-1055.

American Association of Petroleum Geologists, 1988, "Correlation section across Los Angeles Basin from Palos Verdes to San Gabriel Mountains," Pacific Section, CS3R.

American Society of Civil Engineers (ASCE), ASCE/SEI 7-05, 2006, "Minimum Design Loads for Building and Other Structures," ASCE Standard.

ASCE, ASCE/SEI 7-10, 2010, "Minimum Design Loads for Building and Other Structures," ASCE Standard.

ASCE, 2016, "Minimum Design Loads for Buildings and Other Structures", ASCE/SEI Standard 7-16.

Ancheta, T. D., Darragh, R. B., Stewart, J. P., Seyhan, E., Silva, W. J., Chiou, B. S. J., Wooddell, K. E., Graves, R. W., Kottke, A. R., Boore, D. M., Kishida, T., and Donahue, J. L., 2013, "PEER NGA-West2 Database," PEER Report 2013/03, Pacific Earthquake Engineering Research Center.

Atwater, T., and Stock, J., 1998, "Neogene plate tectonic history of southwestern United States: an update," New Zealand Geophysical Society, Joint Annual Conference, Programme and Abstracts, Geological Society of New Zealand Miscellaneous Publication 101A.

Benioff, H., 1938, "The determination of the extent of faulting with application to the Long Beach earthquake," Bulletin of the Seismological Society of America, Vol. 28, p. 77-84.

Bird, P., and Rosenstock, R.W., 1984, "Kinematics of present crust and mantle flow in southern California," Geological Society of America Bulletin, Vol. 95, p. 946-957.

Blake, F., 2000, "FRISKSP User's Manual - 4.00 Update," Documentation, April.

Bommer, J.J., Acevedo, A.B., Douglas, J., 2003, "The selection and scaling of real earthquake accelerograms for use in seismic design and assessment," ACI International Conference on Seismic Design and Retrofit for Earthquake Resistance, San Diego, California, December.

Bonilla, , M.G., 1973, "Trench exposures across surface fault ruptures associated with the San Fernando earthquake," *in* "San Fernando, California, earthquake of February 9, 1971, Vol. 3: Geological and Geophysical Studies," Murphy L.M., ed., Washington, D.C., National Oceanic and Atmospheric Administration, p. 173-182.

Boore, D.M., Joyner, W.B., and Fumal, T.E., 1997, "Equations for estimating horizontal response spectra and peak acceleration from western north American earthquakes: a summary a recent work," Seismological Research Letters, Vol. 68, No. 1, January/February.

Boore, D. M. and Atkinson, G. M., 2008, "Ground-Motion Prediction Equations for the Average Horizontal Component of PGA, PGV, and 5%-Damped PSA at Spectral Periods between 0.01 s and 10.0 s," Earthquake Spectra, Volume 24, No. 1, February.

Boore, D. M, Stewart, J. P., Seyhan, E. and G. M. Atkinson (2014), NGA-West2 equations for predicting PGA, PGV, and 5% damped PSA for shallow crustal earthquakes. Earthquake Spectra, Vol. 30, No. 3, pp. 1057-1085.

Bozorgnia, Y. et al., 2014, "NGA-West2 Research Project," Earthquake Spectra, Volume 30, Number 3, August, pp. 973-987.

Bozorgnia, Y., N. Abrahamson, L. Al Atik, T. D. Ancheta, G. M. Atkinson, J. W. Baker, A. Baltay, D.M. Boore, K. W. Campbell, B. S-J. Chiou, R. Darragh, S. Day, J. Donahue, R. W. Graves, N. Gregor, T. Hanks, I. M. Idriss, R. Kamai, T. Kishida, A. Kottke, S. A. Mahin, S. Rezaeian, B. Rowshandel, E. Seyhan, S. Shahi, T. Shantz, W. Silva, P. Spudich, J. P. Stewart, J. Watson-Lamprey, K. Wooddell, R. Youngs, 2014, NGA-West2 Research Project, Earthquake Spectra,Vol. 30, No. 3, pp. 973-987.

Bullard, T.F., and Lettis, W.R., 1993, "Quaternary fold deformation associated with blind thrust faulting, Los Angeles basin, California," Journal of Geophysical Research, Vol. 98, p. 8349-8369.

California Building Code (CBC) 2001, "California Building Code," California Code of Regulations, Title 24, Part 2.

CBC 2007, "California Building Code," California Code of Regulations, Title 24, Part 2.

CBC 2010, "California Building Code," California Code of Regulations, Title 24, Part 2.

CBC 2013, "California Building Code," California Code of Regulations, Title 24, Part 2.

CBC 2016, "California Building Code," California Code of Regulations, Title 24, Part 2.

CBC 2019, "California Building Code," California Code of Regulations, Title 24, Part 2.

California Department of Water Resources, 1961, "Planned utilization of the ground water basins of the Coastal Pain of Los Angeles County, Appendix A, Ground Water Geology," Department of Water Resources Bulletin No. 104.

California Geological Survey, 2003, "The revised 2002 California probabilistic seismic hazard maps," California Geological Survey website by Cao, T., Bryant, W.A., Rowshandel, B., Branum, D., and Wills, C.J., June 2003.

Campbell, K. W., 1997, "Empirical near-source attenuation relationships for horizontal and vertical components of peak ground acceleration, peak ground velocity, and pseudo-absolute acceleration response spectra," Seismological Research Letters, Vol. 68, No. 1, pp.154-179.

Campbell, K. W. and Bozorgnia, Y., 2008, "NGA Ground Motion Model for the Geometric Mean Horizontal Component of PGA, PGV, and PGD and 5% Damped Linear Elastic Response Spectra for Periods ranging from 0.01 s to 10.0 s," Earthquake Spectra, Volume 24, No. 1, February.

Campbell, K. W. and Y. Bozorgnia, 2014, NGA-West2 ground motion model for the average horizontal components of PGA, PGV, and 5% damped linear acceleration response spectra. Earthquake Spectra, Vol. 30, No. 3, pp. 1087-1115.

Castle, R.O., and Buchanan-Banks, J.M., 1989, "Vertical surface displacements along a part of the Newport-Inglewood zone of folds and faults, Los Angeles and Orange counties, California," U.S. Geological Survey Miscellaneous Field Studies Map MF 2088.

Chiou, B. S-J. and Youngs, R. R., 2008, "An NGA Model for the Average Horizontal Component of Peak Ground Motion and Response Spectra," Earthquake Spectra, Volume 24, No. 1, February.

Chiou, B. S.-J., and R. R. Youngs, 2014, Update of the Chiou and Youngs NGA model for the average horizontal component of peak ground motion and response spectra. Earthquake Spectra, Vol. 30, No. 3, pp. 1117-1153.

Clark, B.R., Zeiser, F.L., and Gath, E.M., 1986, "Evidence for determining activity level of the Pelican Hill fault, coastal Orange County, California." Association of Engineering Geologists, Annual Meeting, Abstracts with Program, p. 146.

Clarke, S.H., Greene, H.G., Kennedy, M.P. and Vedder, J.G., 1987, "Geological map of the inner-southern continental margin, California Continental Margin Geologic Map series: California," California Division of Mines and Geology.

Clarke, S.H., and Kennedy, M.P., 1998, "Analysis of Late Quaternary faulting in the Los Angeles harbor area and hazard to the Vincent Thomas bridge," California Department of Conservation, Division of Mines and Geology, Open-File Report 98-01.

Clarke, D., 2004, Geologist for the City of Long Beach, personal communication.

Cornell, C.A., 1968, "Engineering seismic risk analysis," Seismological Society of America Bulletin, v. 58, p. 1583-1606.

Crook, R., Jr., Allen, C.R., Kamb, B., Payne, C.M., and Proctor, R.J., 1987, "Quaternary geology and seismic hazard of the Sierra Madre and associated faults, western San Gabriel Mountains," *in* "Recent reverse faulting in the Transverse Ranges, California," U.S. Geological Survey, Professional Paper 1339, p. 27-64.

Crook R.C. Jr., and Proctor, R.J., 1992, "The Santa Monica and Hollywood faults and the southern boundary of the Transverse Ranges province," *in* "Engineering geology practice in southern California," Association of Engineering Geologists, Southern California Section, Special Publication 4, p. 233-246.

Crouch, J.K., and Suppe, J., 1993, "Late Cenozoic tectonic evolution of the Los Angeles basin and inner California borderland: a model for core complex-like crustal extension," Geological Society of America Bulletin, Vol. 105, p. 1415-1434.

Darendeli, M. B., 2001, Development of a New Family of Normalized Modulus Reduction and Material Damping Curves, Ph.D. Thesis, Department of Civil, Architectural and Environmental Engineering, The University of Texas, Austin, Texas.

Davis, T.L., and Namson, J., and Yerkes, 1989, "A cross section of the Los Angeles area: seismically active fold and thrust belt, the 1987 Whittier Narrows earthquake and earthquake hazard," Journal of Geophysical Research, Vol. 94, p. 9644-9664.

Dibblee, T.W., Jr., 1999, "Geologic Map of the Palos Verdes Peninsula and Vicinity, Redondo Beach, Torrance and San Pedro quadrangles," Dibblee Geological Foundation Map DF 70.

Dickenson, S.E., 1994, Dynamic Response of Soft and Deep Cohesive Soils during the Loma Prieta Earthquake of October 17, 1989, PhD thesis, Dept. of Civil and Enviro. Eng., University of California, Berkeley, CA.

Dolan, J.F., Sieh, K., Rockwell, T.K., Yeats, R.S., Shaw, J., Suppe, J., Huftile, G.J., and Gath, E.M., 1995, "Prospect for larger or more frequent earthquakes in the Los Angeles metropolitan region, California," Science, Vol. 267, p. 199-205.

Dolan, J.F., Sieh, K., Rockwell, T.K., Guptill, P. and Miller, G., 1997, "Active Tectonics, Paleoseismology, and Seismic Hazards of the Hollywood Fault, Northern Los Angeles Basin, California," Geological Society of America Bulletin, Vol. 109, p. 1595-1616.

Dolan, J.F., Stevens, D., Rockwell, T.K., 2000a, "Paleoseismologic evidence for an early- to mid-Holocene age of the most recent surface rupture on the Hollywood fault, Los Angeles, California," Bulletin of the Geological Society of America, Vol. 90, p. 334-344.

Dolan, J.F., Sieh, K., Rockwell, T.K., 2000b, "Late Quaternary activity and seismic potential of the Santa Monica fault system, Los Angeles, California," Geological Society of America Bulletin, Vol. 112, p. 1559-1581.

Dolan, J.F., Christofferson, S.A., and Shaw, J.H., 2003, "Recognition of paleoearthquakes on the Puente Hills blind thrust fault, California," science, Vol. 300, p. 115-118.

Drumm, P.L., 1992, Holocene displacement of the central splay of the Malibu Coast fault zone, Latigo Canyon, Malibu, *in* Engineering geology practice in southern California: Association of Engineering Geologists, Southern California Section, Special Publication 4, p. 247-254.

Earth Mechanics, Inc, 1993, "Probabilistic seismic-hazard assessment and free-field site Response, Port of Los Angeles, Pier 400," Report for Pier 400 Design Consultants, Carson, CA, EMI project No. 92-204.

Earth Mechanics, Inc, 1995, "Interim design response spectrum, Vincent Thomas bridge retrofit," Report for Moffatt & Nichol and Caltrans Translab, EMI project No. 95-126, August 14.

Earth Mechanics, Inc. 1998, "Seismic ground motion report for the San Francisco-Oakland Bay Bridge East Span Seismic Safety Project, Bridge No. 34-006, Contract No. 59A0053," Draft Report submitted to Caltrans, December 24.

Earth Mechanics, Inc, 2001, "Final ground motion and fault study report, West Basin, Port of Los Angeles, San Pedro, California," Report for Port of Los Angeles, San Pedro, CA, EMI project No. 00-115-8, April 27.

Earth Mechanics, Inc., 2006, Port-wide Ground Motion Study Port of Long Beach, California, Final Report, August 2006.

Earth Mechanics, Inc., 2008, "Addendum to Port-Wide Ground Motion Study, Port of Long Beach, California," Prepared for the Port of Long Beach, August 15.

Earth Mechanics, Inc. 2011, "Addendum No. 2 to Port-Wide Ground Motion Study, Port of Long Beach, California," Prepared for the Port of Long Beach, April 14.

Earth Mechanics, Inc., 2015, "Final Addendum No. 3 to Port-Wide Ground Motion Study, Site-Specific Ground Motion Recommendations per CBC 2013, Port of Long Beach, California," Prepared for Port of Long Beach, May 13.

Earthquake Engineering Research Institute (EERI), 2014, "Special Issue on the NGA-West2 Project," Earthquake Spectra, Volume 30, Number 3, August.

Edwards, B.D., Catchings, R.D., Hildebrand, T.G., Miller, M.S., Ponti, D.J., and Wolfe, S.C., 2001, "Quaternary sedimentary structure of the southwestern Los Angeles basin region," Geological Society of America Abstracts with Program, Vol. 33, PA-41.

Edwards, B.D., Ponti, D.J., Ehmann, K.D., Tinsley, J.C., III, and Reicherdt, E.G., 2002, "Offshore stratigraphic controls on saltwater intrusion in Los Angeles area coastal aquifers," American Geophysical Union Fall Meeting, San Francisco, CA, EOS, Vol. 83, p. F567.

Edwards, B.D., Ehmann, K.D., Ponti, D.J., Tinsley, J.C., III, and Reicherdt, E.G., 2003, "Offshore stratigraphic controls on saltwater intrusion in Los Angeles area coastal aquifers," *in* "LA Basin 2003, Original Urban Oil Field Legends, Conference Program and Abstracts," American Association of Petroleum Geologists, Pacific Section and Western Region Society of Petroleum Engineers, Abstract, p. 62.

Electric Power Research Institute (EPRI), 1993, "Guidelines for determining design basis ground motions." Palo Alto, Calif: Electric Power Research Institute, vol. 1-5, EPRI TR-102293.

Fall, E.W., Rzonca, G.F., Spellman, H.A., 1987, "Late Quaternary faulting, Malibu Coast fault zone, Malibu, California," Association of Engineering Geologists, Annual Meeting Abstracts with Program, p. 38.

Federal Emergency Management Agency (FEMA), 2003, NEHRP Recommended Provisions for Seismic Regulations for New Buildings and Other Structures (FEMA 450), Part 1–Provisions, 2003 Edition, Building Seismic Safety Council of the National Institute of Building Sciences, Washington, D.C.

Fischer, P.J., Rudat, J.H., Patterson, R.H., and Simila, G., 1987, "The Palos Verdes fault zone: onshore and offshore," *in* "Geology of the Palos Verdes Peninsula and San Pedro Bay," Society of Economic Paleontologists and Mineralogists, Pacific Coast Section, Guidebook 55, p. 91-133.

Fisher, M.A., Normark, W.R., Bohannon, R.G., Sliter, R.W., and Calvert, A.J., 2003, "Geology of the continental margin beneath Santa Monica Bay, Southern California, from seismic-reflection data," Bulletin of the Seismological Society of America, Vol. 93, p. 1955-1983.

Fisher, M.A., Normark, W.R., Langenheim, V.E., and Calvert, A.J., 2004, "The offshore Palos Verdes Fault zone near San Pedro, Southern California," Bulletin of the Seismological Society of America, Vol. 94, p. 506-530.

Freeman, S.T., Heath, E.G, Guptill, P.D., and Waggoner J.T., 1992, "Seismic hazard assessment, Newport-Inglewood Fault Zone," *in* "Engineering geology practice in Southern California," Association of Engineering Geologists, Southern California Section, Special Publication 4, p. 211-231.

Geomatrix Consultants, 1992, "Seismic Ground Motion Study for West Span San Francisco Bay Bridge," Report to California Department of Transportation, Contract No. 59N772.

Geomatrix Consultants, 1995, "Adjustments to rock spectra for Caltrans toll bridges in Northern California," Report prepared for Caltrans Division of Structures, Sacramento, California.

Groholski, D., Hashash, Y., Kim, B., Musgrove, M., Harmon, J., and Stewart, J., 2016, "Simplified Model for Small-Strain Nonlinearity and Strength in 1D Seismic Site Response Analysis." J. Geotech. Geoenviron. Eng., 10.1061/(ASCE)GT.1943-5606.0001496, 04016042.

Grant, L.B., Waggoner, J.T., Rockwell, T.K., and Von Stein, C., 1997, "Paleoseismicity of the north branch of the Newport-Inglewood fault zone in Huntington Beach, California, from cone penetrometer test data," Bulletin of the Seismological Society of America, Vol. 87, p 277-293

Greene, H.G., and Kennedy, M.P., 1986, "Geology of the mid-southern California continental margin," California Division of Mines and Geology, California Continental Margin Geologic Map Series, Area 2 of 7.

Gutenberg, B., and Richter, C.F., 1954, "Seismicity of the Earth and associated phenomena," Princeton University Press, Princeton, N.J.

Hanks, T.C., and Bakum, W.H., 2002, "A bilinear source-scaling model for M-log A observations of continental earthquakes," Bulletin of the Seismological Society of America, Vol. 92, p.1841-1846.

Harding Lawson Associates, 1989, "Seismic and Geotechnical Overview, 2020 Project, Ports of Los Angeles and Long Beach, San Pedro Bay, California," Report to Vickerman/Zachary/Miller, Oakland, HLA Job. No. 13134,015.11.

Harding, T.P. and Tuminas, A.C., 1988, "Interpretation of footwall (lowside) fault traps sealed by reverse faults and convergent wrench faults," American Association of Petroleum Geologists Bulletin, Vol. 72, p. 738-757.

Hashash, Y.M.A., Musgrove, M.I., Harmon, J.A., Ilhan, O., Xing, G., Groholski, D.R., Phillips, C.A., and Park, D., 2020, "DEEPSOIL 7.0, User Manual". Urbana, IL, Board of Trustees of University of Illinois at Urbana-Champaign.

Hauksson, E., 1987, "Seismotectonics of the Newport-Inglewood fault zone in the Los Angeles Basin, southern California." Bulletin of the Seismological Society of America, v. 77, p. 539-561.

Hauksson, E., 1990, "Earthquakes, faulting, and stress in the Los Angeles basin," Journal of Geophysical Research, Vol. 95, p. 15,365-15,394.

Hauksson, E., 1995, "Seismological overview of the 1994 Northridge earthquake sequence in California," *in* "The Northridge California earthquake of 17 January 1994," Woods, M.C., and Seiple, W.R., editors, California Department of Conservation, Division of Mines and Geology, Special Publication 116, p. 17-38.

Hauksson, E. and Gross, S., 1991, "Source parameters of the 1933 Long Beach earthquake," Bulletin of the Seismological Society of American, Vol. 81, p. 81-98.

Hummon, C., Schneider, C.L., Yeats, R.S., Dolan, J.F., Sieh, K.E., and Huftile, G.J., 1994, "Wilshire fault: earthquakes in Hollywood?," Geology, Vol. 22, p. 291-294.

Idriss, I.M, and Sun, J.I.,1992, "User's Manual for SHAKE91: A computer program for conducting equivalent linear seismic response analyses of horizontally layered soil deposits," User's Manual, Center for Geotechnical Modeling, Dept. of Civil & Environmental Engineering, University of California, Davis, CA, November.

Idriss, I. M., 2014, An NGA-West2 empirical model for estimating the horizontal spectral values generated by shallow crustal earthquakes. Earthquake Spectra, Vol. 30, No. 3, pp. 1155-1177.

Idriss, I. M., and Boulanger, R. W., 2008, Soil liquefaction during earthquakes. Monograph MNO-12, Earthquake Engineering Research Institute, Oakland, CA, 261 pp.

Jennings, C.W., 1994, "Fault activity map of California and adjacent areas with locations and ages of recent volcanic eruptions," Department of Conservation, Division of Mines and Geology, California Geologic Data Map Series, Map No. 6.

Lindvall S.C., and Rockwell, T.K., 1995, "The Rose Canyon fault and earthquake hazards of San Diego," Association of Engineering Geologists, Annual Meeting, Abstract, p. 58.

Los Angeles County Seismic Safety Element, 1990, "Technical appendix to the safety element of the Los Angeles County general plan, hazard reduction in Los Angeles County," Prepared for Department of Regional Planning by Leighton and Associates and Sedway Cooke Associates.

Luyendyk, B.P., Kamerling, M.J., and Terres, R.R., 1980, "Geometric model for Neogene crustal rotations in Southern California," Geological Society of America Bulletin, Vol. 91, p. 211-217.

McMurdie, D.S., 1973, "Geology and general history of the Dominguez oil field in an urban environment -Los Angeles County, California," Pacific Sections, American Society of

Petroleum Geologists- Society of Exploration Paleontologists and Mineralogists-Society of Exploration Geophysicists, Guidebook, Trip 1, p. 25-31.

McNeilan, T.W., Rockwell, T.K., and Resnick, G.S., 1996, "Style and rate of Holocene slip, Palos Verdes fault, Southern California," Journal of Geophysical Research, Vol. 101, p. 8317-8334.

Mualchin, L., 1996, "California seismic hazard map, 1996," California Department of Transportation, Revision 1, July 1996.

Mueller, K.J., 1997, "Recency of folding along the Compton-Los Alamitos trend: implications for seismic risk in the Los Angeles basin," EOS Transactions of the American Geophysical Union, Vol. 78, p. F702.

Nardin, T.R., and Henyey, T.L., 1978, "Pliocene-Pleistocene diastrophism of Santa Monica and San Pedro shelves, California continental borderland," American Association of Petroleum Geologists Bulletin, Vol. 62, p.247-272.

Newmark, N., 1965, "Effects of earthquakes on dams and embankments," Geotechnique, Vol. 15, No.2, pp. 139-160.

Oskin, M., and Sieh, K.E., 1998, "The Elysian Park anticlinorium; surficial evidence of an active blind reverse fault beneath downtown Los Angeles," Geological Society of America, Abstracts with Programs, Cordilleran Section, n. 6471, p. 57.

Oskin M., Sieh, K., Rockwell, T., Miller, G., Guiptill, P., Curtis M., McArdle, S. and Elliot, P., 2000, "Active parasitic folds on the Elysian Park anticline: implications for seismic hazard in central Los Angeles, California," Geological Society of America Bulletin, Vol. 113, p. 693-707.

Pacific Earthquake Engineering Research Center (PEER), 2014, "Enhancement of Next Generation Attenuation Relationships for Western US (NGA-West2)," http://peer.berkeley.edu/ngawest2/, Last retrieved on May 15.

Pacific Earthquake Engineering Research Center (PEER) Ground Motion Database, 2020, https://ngawest2.berkeley.edu/, Last retrieved on June 25.

Ponti, D. J., 1989, "Aminostratigraphy and chronostratigraphy of Pleistocene marine sediments, southwestern Los Angeles Basin, California," Ph. D. dissertation, Boulder, Co., University of Colorado.

Ponti, D.J., 2004, U.S. Geological Survey, Principal Investigator for Coastal Groundwater Investigation, personal communication.

Ponti, D.J., and LaJoie, K.R., 1992, "Chronostratigraphic implications for tectonic deformation of Palos Verdes and Signal Hills, Los Angeles Basin, California," Association of Engineering Geologists, 35th Annual Meeting, Proceedings, p. 617-620.

Port of Long Beach (POLB), 2007, "Wharf Design Criteria, Version 1.1," March 20.
POLB, 2009, "Wharf Design Criteria, Version 2.0," January 30.

POLB, 2012, "Wharf Design Criteria, Version 3.0," February 29.

POLB, 2015, "Wharf Design Criteria, Version 4.0," May 20.

Prior, S., 2004, THUMS Senior Geologist, personal communication.

Rezaeian, S., Bozorgnia, Y. , Idriss, I. M. , Campbell, K. , Abrahamson, N. , and Silva, W., 2012, Spectral Damping Scaling Factors for Shallow Crustal Earthquakes in Active Tectonic Regions. PEER Report 2012/102, Pacific Earthquake Engineering Research Center, Berkeley, CA.

Rivero, C., Shaw, J.H., and Mueller, K.L., 2000, "Oceanside and Thirtymile Bank blind thrusts: implications for earthquake hazards in coastal Southern California," Geology, Vol. 28, p. 891-894.

Rockwell, T.K., Hatch, M.E., and Schug, D.L., 1987, "Late Quaternary rates of Agua Blanca and Borderland faults," U.S. Geological Survey, Final Technical Report 14-08-0001-22012.

ROSRINE, 2001, "Resolution of site response from the Northridge Earthquake," Website: http://geoinfo.usc.edu/rosrine/

Rubin, C.M., Lindvall, S.C., and Rockwell, T.K., 1998, "Evidence for large earthquakes in metropolitan Los Angeles," Science, Vol. 281, p. 398-402.

Sadigh, K., Chang K.-Y., Egan, J.A., Makdisi, F., and Youngs, R.R., 1997, "Attenuation relationships for shallow crustal earthquakes based on California strong motion data," Seismological Research Letters, Vol. 68, No. 1, January/February.

Schell, B.A., 1991, "Seismotectonic zonation and seismic hazard analyses in Southern California," Fourth International Conference on Seismic Zonation, Proceedings, Vol. 2, p. 19-26.

Schell, B.A., 1997, "Seismotectonics of the Los Angeles Basin and seismic hazards associated with the Norwalk, Peralta Hills, El Modeno, and Los Alamitos faults, Southern California," Association of Engineering Geologists Annual Meeting, Portland, Oregon, Abstracts with Program, p. 145.

Schwartz, H.B., and Coppersmith, K.L., 1984, "Fault behavior and characteristic earthquakes; examples from the Wasatch and San Andreas fault zones," Journal of Geophysical Research, v. 89, p. 5681-5698.

Seyhan, E. 2015, "NGA West 2 GMPE Spreadsheet, Version 5.7," https://peer.berkeley.edu/peer-strong-ground-motion-databases, April 14.

Shaw, J.H., 1993, "Active blind-thrust faulting and strike-slip fault-bend folding in California," Princeton University (Ph.D. Thesis), Princeton, New Jersey, 216 p.

Shaw, J.H., Plesch, A., Dolan, J.F., Pratt, T.L., and Fiore, P., 2002, "Puente Hills blind-thrust system, Los Angeles, California," Bulletin of the Seismological Society of America, Vol. 92, p. 2946-2960.

Shaw, J.H., and Shearer, P.M., 1999, "An elusive blind-thrust fault beneath metropolitan Los Angeles," Science, Vol. 283, p.1516 (5 March)

Shaw, J.H., and Suppe, J., 1996, "Earthquake hazards of active blind thrust faults under the central Los Angeles basin, California," Journal of Geophysical Research, Vol. 101, p. 8623-8642.

Shlemon, R.J., Elliott, P., and Franzen, S., 1995, "Holocene displacement history of the Newport-Inglewood, North Branch fault splays, Santa Ana River floodplain, Huntington Beach, California," Geological Society of America, Abstracts with Programs, Vol. 27, p. A-375.

Somerville, P.G., Irikura, K., Graves, R.W., Sawasa, S., Wald, D., Abrahamson, N.A., Iwasaki, Y., Kagawa, T., Smith, N., and Kowada, A., 1999, "Characterizing crustal earthquake slip models for prediction of strong ground motion," Seismological Research Letters, Vol. 70, No. 59-80.

Somerville, P.G., Smith, N.F., Graves, R.W., and Abrahamson, N.A., 1997, "Modification of empirical strong ground motion attenuation relations to include the amplitude and duration effects of rupture directivity," Seismological Research Letters, Vol. 68, No. 1, January/ February.

Truex, J.N., 1974, "Structural evolution of Wilmington, California anticline," American Association of Petroleum Geologists Bulletin, Vol. 58, p. 2398-2410

Tsutsumi, H., Yeats, R.S., and Huftile, G.J., 2001, "Late Cenozoic tectonics of the northern Los Angeles fault system, California," Geological Society of America Bulletin, Vol. 113, p. 454-468.

Tucker, A.Z., and Dolan, J.F., 2001, "Paleoseismologic evidence for a >8ka age of the most recent surface rupture on the eastern Sierra Madre fault, northern Los Angeles metropolitan region, California," Bulletin of the Seismological Society of America, Vol. 91, p. 232-249.

United States Geological Survey (USGS), 2013, The Uniform California Earthquake Rupture Forecast, Version 3 (UCERF3) – The Time Independent Model, USGS Open File Report 2013-1165, CGS Special Report 228, Southern California Earthquake Center Publication 1792.

United States Geological Survey (USGS), 2020, "U.S. Seismic Design Maps Web-based Tool," https://earthquake.usgs.gov/hazards/interactive/, last retrieved on June 25.

Vedder, J.G., Greene, H.G., Clarke, S.H., and Kennedy, M.P., 1986, "Geologic map of the mid-Southern California continental margin," California Division of Mines and Geology, California Continental Margin Geologic Map Series, Map No. 2A.

Vucetic, M. and Dobry, R., 1991, Effect of Soil Plasticity on Cyclic Response. Journal of Geotechnical Engineering, 117, 89-107.

Ward, S.N., 1994, "A multidisciplinary approach to seismic hazard in Southern California," Bulletin of the Seismological Society of America, Vol. 84, p. 1293-1309.

Ward, S.N., and Valensise, G., 1994, "The Palos Verdes terraces, California: bathtub rings from a buried reverse fault," Journal of Geophysical Research, Vol. 99, p. 4485-4494.

Wells, D. and K. Coppersmith, 1994, "Updated empirical relationships among magnitude, rupture length, rupture area, and surface displacement," Bull Seism. Soc. Am., Vol. 84, 974-1002.

Wolfe, F.D., J.H. Shaw, A. Plesch, D. J. Ponti, J.F. Dolan and M. R. Legg, 2019, The Wilmington Blind-Thrust Fault: An Active Concealed Earthquake Source beneath Los Angeles, California, Bull. Seism. Soc. Am., Vol. 109, No. 5, pp. 1890-1906.

Woodring, W.P., Bramlette, M.N., and Kew, W.S.W., 1946, "Geology and Paleontology of Palos Verdes Hills, California," U.S. Geological Survey, Professional Paper 207.

Woodward Clyde Consultants, 1976, "Geotechnical Investigation, Los Angeles Outer Harbor, Port of Los Angeles, California," Report to POLA, Project No. A653I.

Wright, T.L., 1991, "Structural geology and tectonic evolution of the Los Angeles Basin, California," *in* "Active basin margins," Biddle, K.T., ed., American Association of Petroleum Geologists Memoir 52.

Yerkes, R.F., McColloch, T.H., Schoellhamer, J.E., and Vedder, J.G., 1965, "Geology of the Los Angeles Basin, California - an introduction," U.S. Geological Survey, Professional Paper 420-A.

Youngs, R. R. and K. Coppersmith, 1985, "Implications for fault slip rates and earthquake recurrence models to probabilistic seismic hazard estimates," Bull. Seism. Soc. Am., Vol. 75, 939-964.

Zielbauer, E.J., Kues, H.A., Burnham, W.L., and Keene, A.G., 1962, "Dominguez Gap Barrier Project Geologic Investigation," Los Angeles County Flood Control District, March 1962.

8.0 BIBLIOGRAPHY

Advanced Foundation Engineering Incorporated, 1968, "Foundation Investigation, Proposed Berthing and Mooring Facilities, Port of Long Beach, California," Report to National Molasses Company, Port of Long Beach, California, April 8.

Brown & Caldwell, 1996, "Results of Ocean Boulevard Widening Project Soil Sampling," Prepared for Port of Long Beach, July 12.

CH2M HILL (1991), "Port of Long Beach, Pier C Deepening, Report of Geotechnical Explorations and Analysis," December.

Converse Foundation Engineers (1966), "Pier F, Berth 204, Proposed Wharf and Warehouse Foundation Investigation," March.

Converse Ward Davis Dixon, Inc (1979), "Foundation Investigation, Shelter for Flying Boat Long Beach Dry Dock Site, Hughes Aircraft Company, Los Angeles, California.

Dames & Moore, 1952, "Progress Report, Foundation Investigation, Proposed Ocean Boulevard Bridge, Long Beach, California," Prepared for Port of Long Beach, December 12.

Dames & Moore, 1958, "Report of Foundation Investigation, Proposed Tanker Pier, Pier E, Long Beach Harbor, California," Prepared for Richfield Oil Corporation, March 19.

Dames & Moore, 1961a, "Report of Foundation and Hydraulic Fill Investigation, Proposed New Pier J and Extension of Pier F, Long Beach Harbor, Long Beach, California," Report to the Long Beach Harbor Department, July 27.

Dames & Moore, 1961b, "Preliminary Report of Foundation and Hydraulic Fill Investigation, Proposed Maritime and Commerce Museum, Rainbow Lagoon Area, Long Beach, California," Report to the City of Long Beach, October-November 27.

Dames & Moore, 1964, "Report of Foundation Investigation, Proposed Wharf Berth 83, Channel 2, Long Beach Harbor, Long Beach, California," Report to the Long Beach Harbor Department, April 28.

Dames & Moore, 1965, "Report of Foundation Investigation, Proposed Wharf Berths 232 Through 234, Pier J, Long Beach Harbor, Long Beach, California," Report to the Long Beach Harbor Department, June 17.

Dames & Moore, 1966, "Report of Foundation Investigation, Additional Tanks, Marine Terminal, Channel 2 – Berth 77, Long Beach Harbor, California," Report to the Atlantic Richfield Company, December 20.

Dames & Moore, 1967, "Report of Foundation Investigation, Proposed Wharf, Berths 245, 246 and 247, Pier J, Long Beach Harbor, California," Report to the Long Beach Harbor Department, June 7.

Dames & Moore, 1967, "Supplement No. 2 – Report Foundation Investigation, Proposed Magnolia Avenue Bridge, Long Beach, California," Report to the City of Long Beach, August l8.

Dames & Moore, 1968, "Additional Test Borings and Evaluation of Recently Placed Hydraulic Fill, Proposed Magnolia Avenue Bridge Long Beach, California," Report to the City of Long Beach, May 7.

Dames & Moore, 1968, "Report - Soil Stability Studies Berths 212 Through 214, Pier G, Long Beach Harbor, Long Beach, California," Report to the Long Beach Harbor Department, December 5.

Dames & Moore, 1969, "Report - Consultation and Soil Sampling Proposed Hydraulic Dredging Project, Extension of Pier G and Pier J, Long Beach Harbor, Long Beach, California," Report to the Long Beach Harbor Department, September 5.

Dames & Moore, 1970, "Report - Foundation Investigation Berths 243 and 244, Pier J, Long Beach Harbor, Long Beach, California," Report to the Long Beach Harbor Department, May 18.

Dames & Moore, 1972, "Report of Soil and Foundation Investigation, Proposed Sea-Land Container Terminal, Pier G Expansion, Berths 226-230, Long Beach Harbor, Long Beach, California," Report to the Long Beach Harbor Department, February 3.

Dames & Moore, 1972, "Report - Soil and Foundation Investigation, Proposed Tanker Terminal, Pier A, Berth 202, Long Beach, California," Report to the Long Beach Harbor Department, October 13.

Dames & Moore, 1979, "Report - Soil and Foundation Investigation, Proposed Wharf and Cargo Handling Facility, Berths 81 and 82, Long Beach, California," Report to the Port of Long Beach, October 11.

Dames & Moore, 1980, "Report, Soil and Foundation Investigation, Improvements to West Seventh Street Property (SP Parcel) Berths 62-67," Report to the Port of Long Beach, January 25.

Dames & Moore, 1981, "Report Geotechnical Engineering and Environmental Services, Proposed Marine Tanker Terminal and Crude Oil Transfer Facility Berth 121, Pier E, Long Beach, California," Report to the Port of Long Beach, February 26.

Dames & Moore, 1985, "Report Construction Monitoring Cantilever Bulkhead, Pier G, Berths 212-213, Long Beach Harbor District," Report to the Port of Long Beach, November 4.

Dames & Moore, 1989, "Geotechnical Investigation, West Seventh Street Development, Port of Long Beach, California," Report to Port of Long Beach, May 25.

Dames & Moore, 1990, "Seismic Stability Evaluation, Proposed North Wharf, Pier J Expansion Project for the Port of Long Beach," Report to Port of Long Beach, October 17.

Dames & Moore, 1993, "Report Geotechnical Investigation Proposed Scrap Metal Handling Facility Berths T-118 and T-119 Port of Long Beach," for Port of Long Beach, August 31.

Dames & Moore, 1994, "Geotechnical Investigation Proposed Landfill and Wharf Construction, Slip No. 2, Port of Long Beach," for the Port of Long Beach, December 23.

Dames & Moore, 1999, "Report, Phase I Geotechnical Investigation for Pier S Backland Development Port of Long Beach," for Port of Long Beach, January 20.

Diaz Yourman & Associates, 1997, "Geotechnical Investigation, Data Report, Naval Station Container Terminal, Long Beach, California", Report Prepared for KPFF Consulting Engineers, January 20.

Diaz Yourman & Associates, 1999, "Geotechnical Investigation, The Waterfront at the Queen Mary – Phase I, Long Beach, California", Report Prepared for Queen's Seaport Development Inc, May 28.

Diaz Yourman & Associates, 2002, "Geotechnical Investigation Dredging and Wharf Extension Phase II Pier T Marine Terminal," Report Prepared for KPFF Consulting Engineers, July 22.

Diaz Yourman & Associates, 2002, "Geotechnical Investigation Filling of Drydock No. 1 and Surrounding Area Pier T Marine Terminal, Port of Long Beach," Report Prepared for KPFF Consulting Engineers, June 27.

Diaz Yourman & Associates, 2003, "Geotechnical Data Report, Gerald Desmond Bridge Replacement Project, Long Beach, California," Report to Parsons/HNTB Joint Venture, September 29.

Diaz Yourman Associates (DYA), 2003, "Geotechnical Investigation Data Report – Pier T Container Terminal, Volume I", Prepared for KPFF Consulting Engineers, October 16.

Diaz Yourman Associates (DYA), 2003, "Geotechnical Investigation Data Report – Pier T Container Terminal, Volume II", Prepared for KPFF Consulting Engineers, January 18, 2001 and December 19, 2003.

Diaz Yourman Associates (DYA), 2003, "Geotechnical Investigation Data Report – Pier T Container Terminal, Volume III", Prepared for KPFF Consulting Engineers, October 19, 2001 and December 04, 2002.

Diaz Yourman Associates (DYA), 2003, "Geotechnical Investigation Dredging and Wharf Extension, Phase II, Pier T marine Terminal", Prepared for KPFF Consulting Engineers, October 01.

Diaz Yourman & Associates, 2004, " Geotechnical Data Report, Back Channel Navigation Safety Improvement Project, Port of Long Beach, Long Beach, California," Prepared for Han-Padron Associates, May 26.

Diaz Yourman & Associates, 2004, "Geotechnical Investigation, Liquefied Natural Gas and Liquid Bulk Terminals, Long Beach, California," Prepared for KPFF Consulting Engineers, Seattle, WA, August 5.

Diaz Yourman & Associates, 2005, "Geotechnical Investigation, POLB Security Command and Control Center, Long Beach, California," Prepared for POLB, June 6.

Diaz Yourman & Associates, 2010, "Geotechnical Service Offshore Borrow Source Study, Long Beach, California," Prepared for the Port of Long Beach, July 2.

Diaz Yourman & Associates, 2010, "Geotechnical Investigation Pavement Coring And New Pavement Section Long Beach, California," Prepared for the Port of Long Beach, August 12.

Diaz Yourman & Associates, 2011, "Preliminary Geotechnical Investigation, On-Dock Rail Support Facility, Los Angeles County, California," Prepared for HDR Engineering, Inc., February 22.

Diaz Yourman & Associates, 2012, "Geotechnical Investigation, North Operations and IT Management Building, Power/Crane Maintenance Shop and Marine Operations Building, Pier E, Port of Long Beach, California," Prepared for AECOM, January 20.

Diaz Yourman & Associates, 2016, "Preliminary Conclusions, Georgia-Pacific Pier D Terminal, Port of Long Beach, California," Prepared for COWI, November 18.

Earth Mechanics, Inc., 1991, "Port of Long Beach Feasibility Study for Deepening of Pier C, Seismic Response Analysis", Prepared for Port of Long Beach, September 20.

Earth Mechanics, Inc., 1996, "Foundation Report for Pier J Grade Separation, Port of Long Beach, California," Prepared for MK-Centennial.

Earth Mechanics, Inc., 1997, "Final Geotechnical Investigation Report, Ocean Boulevard Storm Pump station, Long Beach, California", Port of Long Beach, November 19.

Earth Mechanics, Inc., 2005, "Preliminary Ground Motion Criteria for Gerald Desmond Bridge for Caltrans Interim Review," Prepared for Caltrans, February 4.

Earth Mechanics, Inc., 2005, "Preliminary Geotechnical Report for Gerald Desmond Bridge Replacement Project, Long Beach," Prepared for PTG/HNTB Joint Venture, July.

Earth Mechanics, Inc., 2006, "Geotechnical Report for Pier T, Berth T121 BP Cold Ironing Project, Port of Long Beach," Prepared for DMJM HARRIS, February 8.

Earth Mechanics, Inc., 2006, "Final Preliminary Foundation Report (PFR), Schuler Heim Bridge (Replace), Los Angeles and Long Beach, California," Prepared for Alameda Corridor Transportation Authority, September 5.

Earth Mechanics, Inc. & Diaz Yourman Associates, 2005, "Preliminary Geotechnical Report for Gerald Desmond Bridge Replacement Project, Long Beach, California, Draft Report Prepared For PTG/HNTB Joint Venture, July.

Earth Mechanics, Inc. (EMI), 2009, "Port of Long Beach Terminal Island Rail Improvement Project, Nimitz Road Grade Separation, Structure Preliminary Geotechnical Report for Advance Planning Study", Prepared for Parsons, August 18.

Earth Mechanics, Inc. (EMI), 2009, "MOTEMS Audit Program, Geotechnical Study of Berths 82-83, Petro-Diamond Terminal Company Marine Oil Terminal, Port of Long Beach, California", EMI Project No 09-104, October 21.

Earth Mechanics, Inc. (EMI), 2009, "MOTEMS Audit Program, Geotechnical Study, Berths F209 and G211A, Chemoil Marine Oil Terminal, Port of Long Beach, California", EMI Project No 09-105, November 6.

Earth Mechanics, Inc. (EMI), 2009, "MOTEMS Audit Program, Geotechnical Study of Berths 84-87 Tesoro Marine Oil Terminal, Port of Long Beach, California", EMI Project No 08-149, November 16.

Earth Mechanics, Inc. (EMI), 2009, "Geotechnical Site Characterization, Pier E Development Project, Port of Long Beach, California", EMI Project No 09-133, December 15.

Earth Mechanics, Inc. (EMI), 2010, "Final Geotechnical Report, Track Realignment at Ocean Boulevard and Pier F Avenue Support Yard", Port of Long Beach, California, November.

Earth Mechanics, Inc. (EMI), 2010, "Final Geotechnical Engineering Report, Pier E Development Project, Port of Long Beach, California", EMI Project No 09-133, March 10.

Earth Mechanics, Inc. (EMI), 2010, "Final Foundation Report, NB SR 103 Off-Ramp, Bridge No. 53-3034K, Los Angeles County, California, (7-LA-47, PM 0.01, EA 238501)", EMI Project No. 06-123-03, May 7.

Earth Mechanics, Inc. (EMI), 2010, "Final Foundation Report, New Dock Street Off-Ramp, Bridge No. 53-3031, Los Angeles County, California, (7-LA-47, PM 3.74, EA 238501)", EMI Project No. 06-123-03, May 7.

Earth Mechanics, Inc. (EMI), 2010, "Final Foundation Report, New Dock Street On-Ramp, Bridge No. 53-3033, Los Angeles County, California, (7-LA-47, PM 3.74, EA 238501)", EMI Project No. 06-123-03, May 7.

Earth Mechanics, Inc. (EMI), 2010, "Final Foundation Report, New Dock Street On-Ramp, Bridge No. 53-3033, Los Angeles County, California, (7-LA-47, PM 3.74, EA 238501)", EMI Project No. 06-123-03, May 7.

Earth Mechanics, Inc. (EMI), 2010, "Final Foundation Report, SB SR 103 On-Ramp, Bridge No. 53-3035S, Los Angeles County, California, (7-LA-47, PM 0.01, EA 238501)", EMI Project No. 06-123-03, May 7.

Earth Mechanics, Inc., (EMI) 2010, "Final Foundation Report, Schuyler Heim Bridge (Replace), Bridge No. 53-3032, Los Angeles County, California, (7-LA-47, PM 3.58, EA 238501)," Prepared for Alameda Corridor Transportation Authority, May 10.

Earth Mechanics, Inc. (EMI), 2010, "Final Foundation Report, Retaining Wall A1, Bridge No. 53E0147, Mechanically Stabilized Earth (MSE) Wall, Los Angeles County, California, (7-LA-47, PM 3.55, EA 238501)", EMI Project No. 06-123-03, May 10.

Earth Mechanics, Inc. (EMI), 2010, "Final Foundation Report, Retaining Wall C1, Wall No. 53E0148, Mechanically Stabilized Earth (MSE) Wall, Los Angeles County, California (7-LA-47, PM 3.74, EA 238501))", EMI Project No. 06-123-03, May 10.

Earth Mechanics, Inc. (EMI), 2010, "Final Foundation Report, Retaining Wall C1, Wall No. 53E0148, Mechanically Stabilized Earth (MSE) Wall, Los Angeles County, California (7-LA-47, PM 3.74, EA 238501))", EMI Project No. 06-123-03, May 10.

Earth Mechanics, Inc. (EMI), 2010, "Final Foundation Report, Retaining Wall H1, Los Angeles County, California, (7-LA-47, PM 0.18, EA 238501)", EMI Project No. 06-123-03, May 10.

Earth Mechanics, Inc. (EMI), 2010, "Final Foundation Report, Retaining Wall G1, Wall No. 53E0151, Retaining Wall G2, Los Angeles County, California, (7-LA-47, PM 0.17, EA 238501)", EMI Project No. 06-123-03, May 10.

Earth Mechanics, Inc. (EMI), 2010, "Draft Foundation Report, Walls No. 1 & 2 and Walls No. 3 & 4 Mechanically Stabilized Earth (MSE) Walls and Associated Roadways, Terminal Island Rail Improvement Project, Port of Long Beach, Los Angeles County, California", Prepared for Parsons Transportation Group, September 30.

Earth Mechanics, Inc. (EMI), 2010, "Draft Foundation Report, Nimitz Grade Separation, Terminal Island Rail Improvement Project, Port of Long Beach, Los Angeles County, California", Prepared for Parsons Transportation Group, October 6.

Earth Mechanics, Inc. (EMI), 2010, "Geotechnical Report for Reconfiguration at Control Point (CP) Mole Project, Terminal Island Rail Improvement, Port of Long Beach, California", EMI Project No 09-128, Prepared for Parsons Transportation Group, December 9.

Earth Mechanics, Inc. (EMI), 2011 "Geotechnical Data Report for Slip 1, Middle Harbor Redevelopment Project, Port of Long Beach, California", EMI Project No. 09-133, Prepared for Moffatt & Nichol Engineers, March 22.

Earth Mechanics, Inc. (EMI), 2011, "Update on Gerald Desmond Bridge Ground Motions Studies", June 24.

Earth Mechanics, Inc. (EMI), 2011, "MOTEMS Geotechnical Study of United States Naval Facilities Command, DFSP San Pedro Pier 12, Port of Long Beach, California", EMI Project No. 10-150, June 24.

Earth Mechanics, Inc. (EMI), 2011, "Seismic Ground Motion Report for Gerald Desmond Bridge Replacement Project, Long Beach, California", Final Report Prepared for Parsons/HNTB Joint Venture, August 26.

Earth Mechanics, Inc. (EMI), 2011, "Replacement Pile Recommendations, Pier J247 Mooring Dolphin, Port of Long Beach, California", EMI Project No 10-148, September 19.

Earth Mechanics, Inc. (EMI), 2011, "Addendum No. 2 to "Final Geotechnical Report, Pier E Redevelopment Project, Port of Long Beach, California dated March 10, 2010" EMI Project No 09-133, April 8.

Earth Mechanics, Inc. & Diaz Yourman Associates, 2011, "Geotechnical Data Report for Gerald Desmond Bridge Replacement Project, Long Beach, California, Volume I – Main Bridge and Approach Structures, Draft Report Prepared for PTG/HNTB Joint Venture, July.

Earth Mechanics, Inc. & Diaz Yourman Associates, 2011, "Geotechnical Data Report for Gerald Desmond Bridge Replacement Project, Long Beach, California, Volume II – Connectors, Draft Report Prepared for PTG/HNTB Joint Venture, July.

Earth Mechanics, Inc. & Diaz Yourman Associates, 2011, "Supplemental Geotechnical Data Report for Gerald Desmond Bridge Replacement Project, Long Beach, California", Prepared for the Port of Long Beach, September.

Earth Mechanics, Inc., 2011, "Replacement Pile Recommendations, Pier J247 Mooring Dolphin, Port of Long Beach, California", Geotechnical Memorandum Prepared For PTG/HNTB Joint Venture, September 11.

Earth Mechanics, Inc. (EMI), 2012, "Geotechnical Data Report for Sewer Lift Stations # 110 and 112, Pier E North Gate Redevelopment - Middle Harbor Redevelopment Project, Port of Long Beach, California", EMI Project No 09-133, June 5.

Earth Mechanics, Inc. (EMI), 2012, "Final Geotechnical Report for Pier E Terminal Container Yard Redevelopment - Phase 1, Middle Harbor Terminal Development Program, Port of Long Beach, Long Beach, California", EMI Project No 09-133, June 8.

Earth Mechanics, Inc. (EMI), 2012, "Geotechnical Input for Seismic Pushover Analysis under Level 2 Earthquake 77-78 BP Marine Oil Terminal, Port of Long Beach, California", EMI Project No 12-122, July 31.

Earth Mechanics, Inc. (EMI), 2012, "Geotechnical Report, Pier E Terminal Intermodal Yard, Middle Harbor Terminal Development Program, Port of Long Beach, California", EMI Project No 10-122, February 28.

Earth Mechanics, Inc. (EMI), 2012, "Geotechnical Design Report for MOTEMS Upgrades, Berths B84-B87 Tesoro Marine Oil Terminal, Port of Long Beach, California", EMI Project No 11-139, December 12.

Earth Mechanics, Inc. (EMI), 2013, "Final Geotechnical Report, Pico Avenue Pavement Reconstruction Project, Port of Long Beach, California", EMI Project No 10-148, February 27.

Earth Mechanics, Inc. (EMI), 2013, "Geotechnical Recommendations for Berth F209 (Chemoil) Oil Terminal Fender System Replacement Project, Port of Long Beach, California", EMI Project No 13-124, May 8.

Earth Mechanics, Inc. (EMI), 2014, "Geotechnical Letter Report for Pier E Terminal VACIS Structure, Middle Harbor Terminal Development Program, Port of Long Beach, California", EMI Project No. 13-149, December 12.

Earth Mechanics, Inc. (EMI), 2014, "Geotechnical Investigation for Sewer Lift Station106, Port of Long Beach, California", EMI Project No. 13-150, March 14.

Earth Mechanics, Inc. (EMI), 2014, "Port of Long Beach Back Channel Dredging and Widening Project, Geotechnical Investigation Data Package, Port of Long Beach, California", EMI Project No. 13-133, May 01.

Earth Mechanics, Inc. (EMI), 2014, "Geotechnical Input for Seismic Pushover Analysis under Level 2 Earthquake, Berth 76 Tesoro Marine Oil Terminal, Port of Long Beach, California", EMI Project No. 14-122, September 24.

Earth Mechanics, Inc. (EMI), 2014, "Final Geotechnical Report for B-1 Oil Field Set-Aside Area, Pier E Terminal Container Yard Redevelopment - Phase 2, Middle Harbor Terminal Development Program, Port of Long Beach, Long Beach, California", EMI Project No 09-133, October 16.

Earth Mechanics, Inc. (EMI), 2014, "Middle Harbor Terminal Development Program, Port of Long Beach, Long Beach, California, Slip 1 Fill (Area W3), Geotechnical Investigation Data Package", EMI Project No 09-133, October 16.

Earth Mechanics, Inc. (EMI), 2015, "Geotechnical Data Report, Inner Harbor Turning Basin Dredging Project, Port of Long Beach, California", EMI Project No 14-137, February 24.

Earth Mechanics, Inc. (EMI), 2015, "100% Design Geotechnical Data Report, Fireboat Station No. 15 Improvements, Port of Long Beach, California", EMI Project No 11-156, July 16.

Earth Mechanics, Inc. (EMI), 2015, "Design Geotechnical Data Report, Berths B84-85 Tesoro Oil Terminal Ground Improvement Project, Port of Long Beach, California", EMI Project No 14-137, July 27.

Earth Mechanics, Inc. (EMI), 2015, "100% Design Geotechnical Design Report for Fireboat Station No. 15 Improvements, Pier F Avenue, Port of Long Beach, California", EMI Project No 11-156, July 29.

Earth Mechanics, Inc. (EMI), 2015, "Final Geotechnical Report, Pier G Avenue Street Improvement Project, Port of Long Beach, California", EMI Project No 10-148 & 14-137, February 13.

Earth Mechanics, Inc. (EMI), 2015, "Geotechnical Report, Harbor Scenic Drive Street Improvement Project, Port of Long Beach, California", EMI Project No 14-137, February 13.

Earth Mechanics, Inc. (EMI), 2015, "Final Geotechnical Input for Berth and Channel Deepening (Revision 1), Port-Wide Dredge Plan and Federal Channel Expansion Study, Port of Long Beach, California", EMI Project No 15-152, March 24.

Earth Mechanics, Inc. (EMI), 2015, "Geotechnical Data Report, Back Channel Dredging Project, Port of Long Beach, California", EMI Project No 14-137, September 10.

Earth Mechanics, Inc. (EMI), 2015, "Seismically Induced Vertical Settlement and Lateral Movement Estimate Geotechnical Recommendations for Proposed Chemoil Pipeline Construction at Berth 211A, Port of Long Beach, California", EMI Project No 15-143, September 28.

Earth Mechanics, Inc. (EMI), 2016, "Geotechnical Evaluation of Proposed Dredge Slopes at Back Channel Dredging Project, Port of Long Beach, California", EMI Project No 14-137, March 15.

Earth Mechanics, Inc. (EMI), 2016, "Final Geotechnical Report for Marine Maintenance Dock Facilities at Berth D48 Project, Port of Long Beach, California", EMI Project No 15-136, May 20.

Earth Mechanics, Inc. (EMI), 2016, "Geotechnical Memorandum for Preliminary Design, Pier J Berths 245-247 Landside Crane Rail Upgrade Project, Port of Long Beach, California", EMI Project No 16-118, October 14.

Earth Mechanics, Inc. (EMI), 2016, "Seismic Design Criteria for Demolition of the Existing Gerald Desmond Bridge, City of Long Beach, California", EMI Project No 16-141, November 21.

Earth Mechanics, Inc. (EMI), 2017, "Geotechnical Data Report, Pier F Buried "Cyclopean" Quay Wall, Middle Harbor Terminal, Port of Long Beach, California", EMI Project No 09-133, February 17.

Earth Mechanics, Inc. (EMI), 2017, "Geotechnical Data Report, Pier E Berth 22 Wharf and Stage 3 Container Yard Development, Middle Harbor Terminal, Port of Long Beach, California", EMI Project No 09-133, February 16.

Earth Mechanics, Inc. (EMI), 2017, "Geotechnical Design Report, Pier E Berth 22 Wharf and Stage 3 Container Yard Development, Middle Harbor Terminal, Port of Long Beach, California", EMI Project No 09-133, February 14.

Earth Mechanics, Inc. (EMI), 2017, "Geotechnical Memorandum for Pier G215, Mooring Bollard Project, Port of Long Beach, California", EMI Project No 17-110, June 1.

Earth Mechanics, Inc. (EMI), 2017, "Geotechnical Design Report, Pier E Stage 3 Container Yard Developments, Port of Long Beach, California", EMI Project No 09-133, June 19.

Earth Mechanics, Inc. (EMI), 2017, "Preliminary Geotechnical Input for Pier J Breakwater Dredging, Port-Wide Dredge Plan and Federal Channel Expansion Study, Port of Long Beach, California", EMI Project No 15-152, September 5.

Earth Mechanics, Inc. (EMI), 2019 "Geotechnical Report for Terminal Island Wye Track Realignment Project, Port of Long Beach, California", EMI Project No 16-102, November 21.

Earth Mechanics, Inc. (EMI), 2019, "Geotechnical Design Report for the South Battery Exchange Building (SBXB), Pier E Middle Harbor Development, Port of Long Beach, California", EMI Project No 18-112, May 20.

Earth Mechanics, Inc. (EMI), 2019, "Slope Stability Evaluation for Berths J245, J246, and J247, Pier J Long Beach Harbor, Port of Long Beach, California", EMI Project No 19-128, September 24.

Earth Mechanics, Inc. (EMI), 2019, "Geotechnical Memorandum, Foundation Recommendations for the Proposed Vehicle Charging Station, Pier T Terminal, Port of Long Beach, California", EMI Project No 18-123, November 19.

Earth Mechanics, Inc. (EMI), 2019, "Geotechnical Data Report, Ocean Boulevard Coastal Bike Trail Connector, Port of Long Beach, California", EMI Project No 18-138, November 4.

Earth Mechanics, Inc. (EMI), 2019, "Final Geotechnical Design Report, Ocean Boulevard Coastal Bike Trail Connector, Port of Long Beach, California", EMI Project No 18-138, November 21.

Earth Mechanics, Inc. (EMI), 2019, "Post-Construction Geotechnical Memorandum for MOTEMS Upgrades, Berths B84-B87 Marathon Marine Oil Terminal, Port of Long Beach, California", EMI Project No 18-143, December 27.

Earth Mechanics, Inc. (EMI), 2020, "Geotechnical Data Report, Pier G Wharf Improvement, Berth G236 Wharf Extension and Backlands, Port of Long Beach, California", EMI Project No 17-104, April 15.Earth Mechanics, Inc. (EMI), 2020, "Geotechnical Memorandum for Pier G Wharf Improvement, Berth G236 Wharf Extension and Backlands (Final Submittal), Port of Long Beach, California", EMI Project No 17-104, April 26.

Earth Mechanics, Inc. (EMI), 2020, "Draft Geotechnical Design Report, Fourth Track at Ocean Boulevard, Rail and Roadway Improvement Project, Port of Long Beach, California", EMI Project No 20-102, June 24.

Earth Mechanics, Inc. (EMI), 2020, "Geotechnical Memorandum – Foundation Support for the Proposed Lighting Poles, Pier G Metro Railyard Lighting Project, Port of Long Beach, California", EMI Project No 19-150, July 29.

Ertec Western, Inc., 1982, "Report (Draft) Geotechnical Investigation Proposed Long Beach International Coal Project Long Beach, California", for The Port of Long Beach, April 23.

Fugro-McClelland, 1992, "Post-Improvement Geotechnical Study, 122-Acre Hydraulic Landfill Ground Improvement Project, Contract B - Phase III Areas, Terminal Island, Port of Los Angeles, San Pedro, CA."

Fugro West, Inc., 1978, "Geotechnical Investigation, Proposed Sohio Terminal, Long Beach, California," Report Prepared for Port of Long Beach, July 11.

Fugro West, Inc., 1997, "Geotechnical Study Report, Channel 2 Access Upgrade Project, Port of Long Beach," Prepared for Moffatt & Nichol Engineers, May.

Fugro West, Inc., 2002, "Dike Design, Pier 300 Extension, Port of Los Angeles, California," Report to the U.S. Army Corps of Engineers.

Fugro West, Inc., 2004, "Preliminary Geotechnical Engineering Study, California United Terminal, Port of Long Beach, California," Prepared for Moffatt & Nichol Engineers, February 26.

Fugro West, Inc., 2006, "Geotechnical Site Characterization, Pier E Redevelopment Project, Port of Long Beach, California," Revised Draft Report for Moffatt & Nichol Engineers, March.

Fugro West, Inc., 2009, "Geotechnical Engineering Report Pier E Redevelopment Project, Port of Long Beach, California," Prepared for Moffatt & Nichol Engineers, May.

G. A. Nicoll and Associates, Inc., 1998, "Geotechnical Investigation 6th Street Utility Long Beach, California," Prepared for EDM Services, Inc.

Geofon, Inc., 1984, "Geotechnical Investigation Pier A Expansion, Berths 5 to 10, Port of Long Beach, Long Beach, California," Prepared for the Port of Long Beach, May 31.

Geofon, Inc., 1986, "Geotechnical Investigation, Pier J Expansion Project, Port of Long Beach, Long Beach, California," Prepared for the Port of Long Beach, October 29.

Geofon, Inc., 1987, "Geotechnical Data Collection, Pier J Expansion Project Port of Long Beach," Submitted to Port of Long Beach, August 26.

Geofon, Inc., 1989, "Geotechnical Investigation, Wharf Modification Pier J, Berths 245-247, Port of Long Beach, California," December 18.

Geofon, Inc., 1991a, "Geotechnical Investigation, 100-Acre Surcharge Area, Pier J Expansion Project – Phase II, Port of Long Beach, California," Final Report to Port of Long Beach, April 11.

Geofon, Inc., 1991b, "Final Report Geotechnical Investigation, Pier J Expansion Project - Phase 2 Lagoon Area Port of Long Beach," Prepared for The Port of Long Beach, December 30.

Geofon, Inc., 1994, "Geotechnical Report, Anaheim Street Grade Separation, Port of Long Beach," Prepared for De Lew Cather, Inc., November 21.

Geofon, Inc., 1995, "Borrow Area Evaluation Report, Port of Long Beach Stockpile, Port of Los Angeles, Los Angeles, California," Prepared for Parsons Brinckerhoff Quade and Douglas, Inc., January 11.

Geofon, Inc., 1996, "Geotechnical Investigation, Storm Drain, Sanitary Sewer, and Pump Stations, Pier A Back Area, Berths A88-A96, Port of Long Beach, California," Prepared for Moffatt & Nichol Engineers, Inc, February 15.

GeoSyntec Consultants, 2002, "Summary Geotechnical Report, Pier G, Berths G214-G215 Wharf Upgrade, Port of Long Beach, California," Prepared for Sandwell Engineering, Inc., September.

Geotechnical Professionals, Inc., 2002, "Draft Report Geotechnical Investigation for Pier S Wharf, Port of Long Beach," Prepared for the Port of Long Beach, September 16.

Geotechnical Professionals, Inc., 2003a, "Draft Marine Geotechnical Investigation for Pier S Wharf Dredging Port of Long Beach," Prepared for Port of Long Beach, March 5.

Geotechnical Professionals, Inc., 2003b, "Geotechnical Studies for Pier S Wharf, Port of Long Beach," Report to Port of Long Beach, July 21.

Geotechnical Professionals, Inc., 2012, "Geotechnical Investigation, Pier S Dike Realignment, HD-S2161, Port of Long Beach," April 26.

Group Delta Consultants, Inc., 2001, "Draft Structure Foundation Report, Pier S/Pier T connector UC (Br. No. 53-2940), Pier S/Pier T W/B Connector Ramp UC (Br. No. 53-2941), Pier S/Pier T E/B Connector Ramp UC (Br. No. 53-2942), Terminal Island/Ocean Blvd. Interchange Project, Port of Long Beach, California," Prepared for the Port of Long Beach, March 8.

Group Delta Consultants, Inc., 2001, "Geotechnical Investigation, Wharf Design and Construction Pier S, Berths S102-S108, Port of Long Beach," Prepared for the Port of Long Beach, May 17.

Group Delta Consultants, Inc., 2001, "Final Structure Foundation Report, Terminal Island Freeway Separation Terminal Island/Ocean Blvd. Interchange Project, Port of Long Beach, California," Prepared for the Port of Long Beach, August 17.

Group Delta Consultants, Inc., 2001, "Final Structure Foundation Report, Henry Ford Avenue Undercrossing Terminal Island/Ocean Blvd. Interchange Project, Port of Long Beach," Prepared for the Port of Long Beach, August 17.

Group Delta Consultants, Inc., 2002, "Geotechnical Design Report, Ocean Boulevard/ Terminal Island Freeway Interchange Project, Port of Long Beach, Long Beach, California," Prepared for the Port of Long Beach, October 22.

Harding Lawson Associates, 1990, "Field and Laboratory Data, Pier J Expansion Project, North Wharf, Port of Long Beach, California," Report to the Port of Long Beach, January 31.

Kleinfelder, 1996, "Report of Geotechnical Investigation for the Proposed New Container Wharf at Pier J, Berths J235 and J236, Port of Long Beach, California," Report to the Port of Long Beach, Long Beach, California, March 29.

Kleinfelder, 2000a, "Geotechnical Investigation, Volume 1 – Soil Data Report, Port of Long Beach, Pier G Terminal Development Project," Prepared for the Port of Long Beach, Long Beach, California, June.

Kleinfelder, 2000b, "Geotechnical Investigation, Volume 2 – Geotechnical Design Guidelines, Port of Long Beach, Pier G Terminal Development Project," Prepared for the Port of Long Beach, July.

Kleinfelder, 2003, "Report of Geotechnical Feasibility Investigation, Proposed New Port of Long Beach Administration and Maintenance Buildings, 669 Harbor Plaza, Long Beach, California," Prepared for the Port of Long Beach, August.

Law/Crandall, Inc., 1994a, "Final Report of Geotechnical Investigation Proposed Railroad Bridge and Railway Improvements Portion of the Anaheim Street Viaduct Widening Project Los Angeles, CA," Report to the Port of Los Angeles, September 1.

Law/Crandall, Inc., 1994b, "Revised Final Report of Geotechnical Investigation Proposed Anaheim Street Viaduct Widening Project Los Angeles, CA," Report to the Port of Los Angeles, October 31.

Leighton and Associates, Inc., 1990, "Geotechnical Investigation, Berth 95-97 Development Project, Port of Long Beach," Prepared for the Port of Long Beach, May 4.

Leighton and Associates, Inc., 1995, "Draft Report of Geotechnical investigation for Berths A88-A98 Development Project, Port of Long Beach, Volume I," Prepared for the Port of Long Beach, September 29.

Leighton and Associates, Inc., 1995, "Draft Report of Geotechnical investigation for Berths A88-A98 Development Project, Port of Long Beach, Volume II," Prepared for the Port of Long Beach, September 29.

Leighton and Associates, Inc., 1996, "Geotechnical Investigation for Wharf Design and Construction at Pier A, Berths A88-A96, Port of Long Beach," Report to the Port of Long Beach, January 19.

LeRoy Crandall and Associates, 1977, "Report of Geotechnical Investigation, Proposed Modernization of Bulk Loading Facilities, Pier D, Port of Long Beach, Long Beach, California," Report to the Port of Long Beach, February 23.

Long Beach Harbor Consultants, 1976, "Volume 1 Final Report - Environmental and Geotechnical Sampling Program, The Port of Long Beach, California," Prepared for the Port of Long Beach, March 23.

L. T. Evans, 1949a, "Soil Investigation for Long Beach Harbor Department," Long Beach, California, January 12.

L. T. Evans, 1949b, "Soil Investigation for Long Beach Harbor Department," Long Beach, California, January 10.

L. T. Evans, 1952, "Soil Investigation for Long Beach Harbor Department," Long Beach, California, February 27.

L. T. Evans, 1953, "Foundation Investigation for Ninth Street Bridge, Long Beach, California," Report to the Port of Long Beach, January 26.

MAA Engineering Consultants, Inc., 1992, "42-Acre Site, Phase I Post-Surcharge Investigation, Port of Los Angeles." Prepared for the Port of Los Angeles.

MAA Engineering Consultants, Inc., 2000, "Geotechnical Report, Pier G, Berths G212-G215 Facilities, AQMD Rule 1158 Compliance Upgrade," Prepared for Sandwell Engineering, Inc., August.

Moore & Taber, 1983, "Geotechnical Investigation, Bulkhead and Wharf Improvements, Montar Gypsum Long Beach Plant, Long Beach, California," November 3.

Sea Surveyor Inc., 1994, "Queens Gate Dredging, Geotechnical and Chemical Investigation," Prepared for the Port of Long Beach, California, December 30.

URS, 2007, "Geotechnical Investigation Report, Pier A West/Area 2, Interim/Source Removal Action Project Wilmington, California," Prepared for the Port of Long Beach, California, October 15.

URS, 2011, "Data Report, Geotechnical Investigation, Back Channel Navigation Safety Improvements Project, Port of Long Beach, California," Prepared for the Port of Long Beach, California, March 21.

Woodward Clyde Consultants, 1996, "Ground motion evaluation, Long Beach Naval Station Container Terminal, Long Beach, California," Report to Diaz-Yourman & Associates, Tustin, California, Project No. 964G076, June 11.

APPENDIX A PROBABILISTIC SEISMIC HAZARD ANALYSIS (PSHA)

Seismic Hazard Analysis Including the Wilmington Fault for Port of Long Beach (POLB) Site Locations in Long Beach, CA

Draft Report

Prepared for:

Earth Mechanics, Inc.

Prepared by:

Nick Gregor and Linda Al Atik

Table of Contents

1. Introduction 1
2. Seismic Source Characterization 5
   - 2.1 Fault Sources 6
   - 2.2 Gridded Seismicity 13
   - 2.3 Wilmington Fault Characterization 16
3. Ground Motion Characterization 18
4. Probabilistic Seismic Hazard Analysis (PSHA) 20
   - 4.1 Methodology 20
   - 4.2 Site 1 – Horizontal 22
   - 4.3 Site 3 – Horizontal 44
   - 4.4 Site 5 – Horizontal 64
   - 4.5 Site 8 – Horizontal 84
   - 4.6 Comparison for POLB Sites – Horizontal 104
   - 4.7 Site 5 – Horizontal with Directivity 111
   - 4.8 Vertical Scenario Events and V/H Ratios 118
5. Summary 125
6. References 137

List of Tables

Table 1. Site locations and V_{S30} values used in the PSHA study for the POLB. 2
Table 2. Number of UCERF3 fault scenarios and distance to closest fault segment within 300 km from the four POLB sites. 7
Table 3. Estimated mean slip rates for selected faults from the UCERF3 grand inversion in the immediate vicinity of the four POLB site locations. 8
Table 4. Horizontal UHS for Site 1 at the four hazard levels not including the Wilmington fault. 26
Table 5. Horizontal UHS for Site 1 at the four hazard levels including the Wilmington fault. .. 27
Table 6. Mean magnitude for the four hazard levels for Site 1 including the Wilmington fault. 29
Table 7. Mean distance for the four hazard levels for Site 1 including the Wilmington fault. . 30
Table 8. Mean epsilon for the four hazard levels for Site 1 including the Wilmington fault. ... 31
Table 9. Horizontal UHS for Site 3 at the four hazard levels including the Wilmington fault. .. 47
Table 10. Mean magnitude for the four hazard levels for Site 3 including the Wilmington fault. 49
Table 11. Mean distance for the four hazard levels for Site 3 including the Wilmington fault. 50
Table 12. Mean epsilon for the four hazard levels for Site 3 including the Wilmington fault. . 51
Table 13. Horizontal UHS for Site 5 at the four hazard levels including the Wilmington fault. 67
Table 14. Mean magnitude for the four hazard levels for Site 5 including the Wilmington fault. 69
Table 15. Mean distance for the four hazard levels for Site 5 including the Wilmington fault. 70
Table 16. Mean epsilon for the four hazard levels for Site 5 including the Wilmington fault. . 71
Table 17. Horizontal UHS for Site 8 at the four hazard levels including the Wilmington fault. 87
Table 18. Mean magnitude for the four hazard levels for Site 8 including the Wilmington fault. 89
Table 19. Mean distance for the four hazard levels for Site 8 including the Wilmington fault. 90
Table 20. Mean epsilon for the four hazard levels for Site 8 including the Wilmington fault. . 91
Table 21. UHS including the Wilmington fault for the 72-year (OLE) return period hazard level at the four POLB site locations and the resulting envelope spectra. 105
Table 22. UHS including the Wilmington fault for the 475-year (CLE) return period hazard level at the four POLB site locations and the resulting envelope spectra. 106
Table 23. UHS including the Wilmington fault for the 975-year return period hazard level at the four POLB site locations and the resulting envelope spectra. 107
Table 24. UHS including the Wilmington fault for the 2,475-year return period hazard level at the four POLB site locations and the resulting envelope spectra. 108
Table 25. UHS for the 72-year (OLE) return period hazard level at Site 5 both with and without directivity and including the Wilmington fault. 112
Table 26. UHS for the 475-year (CLE) return period hazard level at Site 5 both with and without directivity and including the Wilmington fault. 113
Table 27. UHS for the 975-year return period hazard level at Site 5 both with and without directivity and including the Wilmington fault. 114

Table 28. UHS for the 2,475-year return period hazard level at Site 5 both with and without directivity and including the Wilmington fault. 115
Table 29. Scenario events for the 72-year (OLE) hazard level used to develop vertical to horizontal spectral ratios for POLB sites. 118
Table 30. Vertical to horizontal (V/H) spectral ratios for the envelope and scenarios associated with the 72-year (OLE) hazard level for POLB sites. 120
Table 31. Scenario events for the 475-year (CLE) and 975-year hazard levels used to develop vertical to horizontal spectral ratios for POLB sites. 121
Table 32. Vertical to horizontal (V/H) spectral ratios for the envelope and scenarios associated with the 475-year (CLE) and 975-year hazard levels for POLB sites. 122
Table 33. Scenario events for the 2,475-year hazard level used to develop vertical to horizontal spectral ratios for POLB sites. 123
Table 34. Vertical to horizontal (V/H) spectral ratios for the envelope and scenarios associated with the 2,475-year hazard level for POLB sites. 124
Table 35. UHS for the 72-year (OLE) return period hazard level at Site 5 with and without directivity and for the vertical component and including the Wilmington fault. 126
Table 36. UHS for the 475-year (CLE) return period hazard level at Site 5 with and without directivity and for the vertical component and including the Wilmington fault. 127
Table 37. UHS for the 975-year return period hazard level at Site 5 with and without directivity and for the vertical component and including the Wilmington fault. 128
Table 38. UHS for the 2,475-year return period hazard level at Site 5 with and without directivity and for the vertical component and including the Wilmington fault. 129
Table 39. UHS for the 72-year (OLE) return period hazard level for POLB from the previous study (Earth Mechanics Inc., 2006). 132
Table 40. UHS for the 475-year (CLE) return period hazard level for POLB from the previous study (Earth Mechanics Inc., 2006). 133

List of Figures

Figure 1. Schematic showing the elements of a probabilistic seismic hazard analysis (Source: Earthquake Engineering Research Institute, 1989). 4
Figure 2. Regional map showing the UCERF3 fault segments (red traces) associated with all rupture scenarios within a closest maximum distance of 300 km from the four POLB site locations (black stars). 9
Figure 3. Map showing the four site locations (red circles) and fault traces from UCERF3 used in the analysis. Red fault traces are strike-slip faults and black fault traces are reverse faults... 10
Figure 4. Cumulative annual rate of earthquakes from the UCERF3 fault sources within 300 km from Site 1. 11
Figure 5. Cumulative annual rate of earthquakes from the UCERF3 fault sources within 300 km from Site 3. 11
Figure 6. Cumulative annual rate of earthquakes from the UCERF3 fault sources within 300 km from Site 5. 12
Figure 7. Cumulative annual rate of earthquakes from the UCERF3 fault sources within 300 km from Site 8. 12
Figure 8. Cumulative annual rate of earthquakes from the UCERF3 gridded sources within 300 km from Site 1. 14
Figure 9. Cumulative annual rate of earthquakes from the UCERF3 gridded sources within 300 km from Site 3. 14
Figure 10. Cumulative annual rate of earthquakes from the UCERF3 gridded sources within 300 km from Site 5. 15
Figure 11. Cumulative annual rate of earthquakes from the UCERF3 gridded sources within 300 km from Site 8. 15
Figure 12. Regional map showing inferred projected surface fault trace for the Wilmington blind thrust fault. (Taken from Figure 2 of Wolfe et al., 2019). 16
Figure 13. Ground-motion logic tree showing the different branches and associated weights; μ and σ are median prediction and epistemic standard deviation of the natural-logarithmic values of the ground-motion parameter of interest. 19
Figure 14. Mean horizontal component hazard curves from the UCERF3 gridded and fault sources, the Wilmington fault, and total hazard for PGA for Site 1. 23
Figure 15. Mean horizontal component hazard curves from the UCERF3 gridded and fault sources, the Wilmington fault, and total hazard for T = 0.2 sec for Site 1. 23
Figure 16. Mean horizontal component hazard curves from the UCERF3 gridded and fault sources, the Wilmington fault, and total hazard for T = 0.5 sec for Site 1. 24
Figure 17. Mean horizontal component hazard curves from the UCERF3 gridded and fault sources, the Wilmington fault, and total hazard for T = 1.0 sec for Site 1. 24
Figure 18. Mean horizontal component hazard curves from the UCERF3 gridded and fault sources, the Wilmington fault, and total hazard for T = 2.0 sec for Site 1. 25
Figure 19. Uniform hazard spectra for Site 1 not including the Wilmington fault. 28
Figure 20. Uniform hazard spectra for Site 1 including the Wilmington fault. 28
Figure 21. Horizontal mean magnitude for Site 1 including the Wilmington fault. 32
Figure 22. Horizontal mean distance for Site 1 including the Wilmington fault. 32

Figure 23. Horizontal mean epsilon for Site 1 including the Wilmington fault. 33
Figure 24. Magnitude-distance contribution for the 72-year (OLE) hazard level for PGA for Site 1 including the Wilmington fault. 34
Figure 25. Magnitude-distance contribution for the 72-year (OLE) hazard level for T = 0.2 sec for Site 1 including the Wilmington fault. 34
Figure 26. Magnitude-distance contribution for the 72-year (OLE) hazard level for T = 0.5 sec for Site 1 including the Wilmington fault. 35
Figure 27. Magnitude-distance contribution for the 72-year (OLE) hazard level for T = 1.0 sec for Site 1 including the Wilmington fault. 35
Figure 28. Magnitude-distance contribution for the 72-year (OLE) hazard level for T = 2.0 sec for Site 1 including the Wilmington fault. 36
Figure 29. Magnitude-distance contribution for the 475-year (CLE) hazard level for PGA for Site 1 including the Wilmington fault. 36
Figure 30. Magnitude-distance contribution for the 475-year (CLE) hazard level for T = 0.2 sec for Site 1 including the Wilmington fault. 37
Figure 31. Magnitude-distance contribution for the 475-year (CLE) hazard level for T = 0.5 sec for Site 1 including the Wilmington fault. 37
Figure 32. Magnitude-distance contribution for the 475-year (CLE) hazard level for T = 1.0 sec for Site 1 including the Wilmington fault. 38
Figure 33. Magnitude-distance contribution for the 475-year (CLE) hazard level for T = 2.0 sec for Site 1 including the Wilmington fault. 38
Figure 34. Magnitude-distance contribution for the 975-year hazard level for PGA for Site 1 including the Wilmington fault. 39
Figure 35. Magnitude-distance contribution for the 975-year hazard level for T = 0.2 sec for Site 1 including the Wilmington fault. 39
Figure 36. Magnitude-distance contribution for the 975-year hazard level for T = 0.5 sec for Site 1 including the Wilmington fault. 40
Figure 37. Magnitude-distance contribution for the 975-year hazard level for T = 1.0 sec for Site 1 including the Wilmington fault. 40
Figure 38. Magnitude-distance contribution for the 975-year hazard level for T = 2.0 sec for Site 1 including the Wilmington fault. 41
Figure 39. Magnitude-distance contribution for the 2,475-year hazard level for PGA for Site 1 including the Wilmington fault. 41
Figure 40. Magnitude-distance contribution for the 2,475-year hazard level for T = 0.2 sec for Site 1 including the Wilmington fault. 42
Figure 41. Magnitude-distance contribution for the 2,475-year hazard level for T = 0.5 sec for Site 1 including the Wilmington fault. 42
Figure 42. Magnitude-distance contribution for the 2,475-year hazard level for T = 1.0 sec for Site 1 including the Wilmington fault. 43
Figure 43. Magnitude-distance contribution for the 2,475-year hazard level for T = 2.0 sec for Site 1 including the Wilmington fault. 43
Figure 44. Mean horizontal component hazard curves from the UCERF3 gridded and fault sources, the Wilmington fault, and total hazard for PGA for Site 3. 44

Figure 45. Mean horizontal component hazard curves from the UCERF3 gridded and fault sources, the Wilmington fault, and total hazard for T = 0.2 sec for Site 3. 45
Figure 46. Mean horizontal component hazard curves from the UCERF3 gridded and fault sources, the Wilmington fault, and total hazard for T = 0.5 sec for Site 3. 45
Figure 47. Mean horizontal component hazard curves from the UCERF3 gridded and fault sources, the Wilmington fault, and total hazard for T = 1.0 sec for Site 3. 46
Figure 48. Mean horizontal component hazard curves from the UCERF3 gridded and fault sources, the Wilmington fault, and total hazard for T = 2.0 sec for Site 3. 46
Figure 49. Uniform hazard spectra for Site 3 including the Wilmington fault. 48
Figure 50. Horizontal mean magnitude for Site 3 including the Wilmington fault. 52
Figure 51. Horizontal mean distance for Site 3 including the Wilmington fault. 52
Figure 52. Horizontal mean epsilon for Site 3 including the Wilmington fault. 53
Figure 53. Magnitude-distance contribution for the 72-year (OLE) hazard level for PGA for Site 3 including the Wilmington fault. 54
Figure 54. Magnitude-distance contribution for the 72-year (OLE) hazard level for T = 0.2 sec for Site 3 including the Wilmington fault. 54
Figure 55. Magnitude-distance contribution for the 72-year (OLE) hazard level for T = 0.5 sec for Site 3 including the Wilmington fault. 55
Figure 56. Magnitude-distance contribution for the 72-year (OLE) hazard level for T = 1.0 sec for Site 3 including the Wilmington fault. 55
Figure 57. Magnitude-distance contribution for the 72-year (OLE) hazard level for T = 2.0 sec for Site 3 including the Wilmington fault. 56
Figure 58. Magnitude-distance contribution for the 475-year (CLE) hazard level for PGA for Site 3 including the Wilmington fault. 56
Figure 59. Magnitude-distance contribution for the 475-year (CLE) hazard level for T = 0.2 sec for Site 3 including the Wilmington fault. 57
Figure 60. Magnitude-distance contribution for the 475-year (CLE) hazard level for T = 0.5 sec for Site 3 including the Wilmington fault. 57
Figure 61. Magnitude-distance contribution for the 475-year (CLE) hazard level for T = 1.0 sec for Site 3 including the Wilmington fault. 58
Figure 62. Magnitude-distance contribution for the 475-year (CLE) hazard level for T = 2.0 sec for Site 3 including the Wilmington fault. 58
Figure 63. Magnitude-distance contribution for the 975-year hazard level for PGA for Site 3 including the Wilmington fault. 59
Figure 64. Magnitude-distance contribution for the 975-year hazard level for T = 0.2 sec for Site 3 including the Wilmington fault. 59
Figure 65. Magnitude-distance contribution for the 975-year hazard level for T = 0.5 sec for Site 3 including the Wilmington fault. 60
Figure 66. Magnitude-distance contribution for the 975-year hazard level for T = 1.0 sec for Site 3 including the Wilmington fault. 60
Figure 67. Magnitude-distance contribution for the 975-year hazard level for T = 2.0 sec for Site 3 including the Wilmington fault. 61
Figure 68. Magnitude-distance contribution for the 2,475-year hazard level for PGA for Site 3 including the Wilmington fault. 61

Figure 69. Magnitude-distance contribution for the 2,475-year hazard level for T = 0.2 sec for Site 3 including the Wilmington fault. 62
Figure 70. Magnitude-distance contribution for the 2,475-year hazard level for T = 0.5 sec for Site 3 including the Wilmington fault. 62
Figure 71. Magnitude-distance contribution for the 2,475-year hazard level for T = 1.0 sec for Site 3 including the Wilmington fault. 63
Figure 72. Magnitude-distance contribution for the 2,475-year hazard level for T = 2.0 sec for Site 3 including the Wilmington fault. 63
Figure 73. Mean horizontal component hazard curves from the UCERF3 gridded and fault sources, the Wilmington fault, and total hazard for PGA for Site 5. 64
Figure 74. Mean horizontal component hazard curves from the UCERF3 gridded and fault sources, the Wilmington fault, and total hazard for T = 0.2 sec for Site 5. 65
Figure 75. Mean horizontal component hazard curves from the UCERF3 gridded and fault sources, the Wilmington fault, and total hazard for T = 0.5 sec for Site 5. 65
Figure 76. Mean horizontal component hazard curves from the UCERF3 gridded and fault sources, the Wilmington fault, and total hazard for T = 1.0 sec for Site 5. 66
Figure 77. Mean horizontal component hazard curves from the UCERF3 gridded and fault sources, the Wilmington fault, and total hazard for T = 2.0 sec for Site 5. 66
Figure 78. Uniform hazard spectra for Site 5 including the Wilmington fault. 68
Figure 79. Horizontal mean magnitude for Site 5 including the Wilmington fault. 72
Figure 80. Horizontal mean distance for Site 5 including the Wilmington fault. 72
Figure 81. Horizontal mean epsilon for Site 5 including the Wilmington fault. 73
Figure 82. Magnitude-distance contribution for the 72-year (OLE) hazard level for PGA for Site 5 including the Wilmington fault. 74
Figure 83. Magnitude-distance contribution for the 72-year (OLE) hazard level for T = 0.2 sec for Site 5 including the Wilmington fault. 74
Figure 84. Magnitude-distance contribution for the 72-year (OLE) hazard level for T = 0.5 sec for Site 5 including the Wilmington fault. 75
Figure 85. Magnitude-distance contribution for the 72-year (OLE) hazard level for T = 1.0 sec for Site 5 including the Wilmington fault. 75
Figure 86. Magnitude-distance contribution for the 72-year (OLE) hazard level for T = 2.0 sec for Site 5 including the Wilmington fault. 76
Figure 87. Magnitude-distance contribution for the 475-year (CLE) hazard level for PGA for Site 5 including the Wilmington fault. 76
Figure 88. Magnitude-distance contribution for the 475-year (CLE) hazard level for T = 0.2 sec for Site 5 including the Wilmington fault. 77
Figure 89. Magnitude-distance contribution for the 475-year (CLE) hazard level for T = 0.5 sec for Site 5 including the Wilmington fault 77
Figure 90. Magnitude-distance contribution for the 475-year (CLE) hazard level for T = 1.0 sec for Site 5 including the Wilmington fault. 78
Figure 91. Magnitude-distance contribution for the 475-year (CLE) hazard level for T = 2.0 sec for Site 5 including the Wilmington fault. 78
Figure 92. Magnitude-distance contribution for the 975-year hazard level for PGA for Site 5 including the Wilmington fault. 79

Figure 93. Magnitude-distance contribution for the 975-year hazard level for T = 0.2 sec for Site 5 including the Wilmington fault. 79
Figure 94. Magnitude-distance contribution for the 975-year hazard level for T = 0.5 sec for Site 5 including the Wilmington fault. 80
Figure 95. Magnitude-distance contribution for the 975-year hazard level for T = 1.0 sec for Site 5 including the Wilmington fault. 80
Figure 96. Magnitude-distance contribution for the 975-year hazard level for T = 2.0 sec for Site 5 including the Wilmington fault. 81
Figure 97. Magnitude-distance contribution for the 2,475-year hazard level for PGA for Site 5 including the Wilmington fault. 81
Figure 98. Magnitude-distance contribution for the 2,475-year hazard level for T = 0.2 sec for Site 5 including the Wilmington fault. 82
Figure 99. Magnitude-distance contribution for the 2,475-year hazard level for T = 0.5 sec for Site 5 including the Wilmington fault. 82
Figure 100. Magnitude-distance contribution for the 2,475-year hazard level for T = 1.0 sec for Site 5 including the Wilmington fault. 83
Figure 101. Magnitude-distance contribution for the 2,475-year hazard level for T = 2.0 sec for Site 5 including the Wilmington fault. 83
Figure 102. Mean horizontal component hazard curves from the UCERF3 gridded and fault sources, the Wilmington fault, and total hazard for PGA for Site 8. 84
Figure 103. Mean horizontal component hazard curves from the UCERF3 gridded and fault sources, the Wilmington fault, and total hazard for T = 0.2 sec for Site 8. 85
Figure 104. Mean horizontal component hazard curves from the UCERF3 gridded and fault sources, the Wilmington fault, and total hazard for T = 0.5 sec for Site 8. 85
Figure 105. Mean horizontal component hazard curves from the UCERF3 gridded and fault sources, the Wilmington fault, and total hazard for T = 1.0 sec for Site 8. 86
Figure 106. Mean horizontal component hazard curves from the UCERF3 gridded and fault sources, the Wilmington fault, and total hazard for T = 2.0 sec for Site 8. 86
Figure 107. Uniform hazard spectra for Site 8 including the Wilmington fault. 88
Figure 108. Horizontal mean magnitude for Site 8 including the Wilmington fault. 92
Figure 109. Horizontal mean distance for Site 8 including the Wilmington fault. 92
Figure 110. Horizontal mean epsilon for Site 8 including the Wilmington fault. 93
Figure 111. Magnitude-distance contribution for the 72-year (OLE) hazard level for PGA for Site 8 including the Wilmington fault. 94
Figure 112. Magnitude-distance contribution for the 72-year (OLE) hazard level for T = 0.2 sec for Site 8 including the Wilmington fault. 94
Figure 113. Magnitude-distance contribution for the 72-year (OLE) hazard level for T = 0.5 sec for Site 8 including the Wilmington fault. 95
Figure 114. Magnitude-distance contribution for the 72-year (OLE) hazard level for T = 1.0 sec for Site 8 including the Wilmington fault. 95
Figure 115. Magnitude-distance contribution for the 72-year (OLE) hazard level for T = 2.0 sec for Site 8 including the Wilmington fault. 96
Figure 116. Magnitude-distance contribution for the 475-year (CLE) hazard level for PGA for Site 8 including the Wilmington fault. 96

Figure 117. Magnitude-distance contribution for the 475-year (CLE) hazard level for T = 0.2 sec for Site 8 including the Wilmington fault. 97
Figure 118. Magnitude-distance contribution for the 475-year (CLE) hazard level for T = 0.5 sec for Site 8 including the Wilmington fault. 97
Figure 119. Magnitude-distance contribution for the 475-year (CLE) hazard level for T = 1.0 sec for Site 8 including the Wilmington fault. 98
Figure 120. Magnitude-distance contribution for the 475-year (CLE) hazard level for T = 2.0 sec for Site 8 including the Wilmington fault. 98
Figure 121. Magnitude-distance contribution for the 975-year hazard level for PGA for Site 8 including the Wilmington fault. 99
Figure 122. Magnitude-distance contribution for the 975-year hazard level for T = 0.2 sec for Site 8 including the Wilmington fault. 99
Figure 123. Magnitude-distance contribution for the 975-year hazard level for T = 0.5 sec for Site 8 including the Wilmington fault. 100
Figure 124. Magnitude-distance contribution for the 975-year hazard level for T = 1.0 sec for Site 8 including the Wilmington fault. 100
Figure 125. Magnitude-distance contribution for the 975-year hazard level for T = 2.0 sec for Site 8 including the Wilmington fault. 101
Figure 126. Magnitude-distance contribution for the 2,475-year hazard level for PGA for Site 8 including the Wilmington fault. 101
Figure 127. Magnitude-distance contribution for the 2,475-year hazard level for T = 0.2 sec for Site 8 including the Wilmington fault. 102
Figure 128. Magnitude-distance contribution for the 2,475-year hazard level for T = 0.5 sec for Site 8 including the Wilmington fault. 102
Figure 129. Magnitude-distance contribution for the 2,475-year hazard level for T = 1.0 sec for Site 8 including the Wilmington fault. 103
Figure 130. Magnitude-distance contribution for the 2,475-year hazard level for T = 2.0 sec for Site 8 including the Wilmington fault. 103
Figure 131. UHS including the Wilmington fault for the 72-year (OLE) return period hazard level at the four POLB site locations and the resulting envelope spectrum. 109
Figure 132. UHS including the Wilmington fault for the 475-year (CLE) return period hazard level at the four POLB site locations and the resulting envelope spectrum. 109
Figure 133. UHS including the Wilmington fault for the 975-year return period hazard level at the four POLB site locations and the resulting envelope spectrum. 110
Figure 134. UHS including the Wilmington fault for the 2,475-year return period hazard level at the four POLB site locations and the resulting envelope spectrum. 110
Figure 135. UHS for the 72-year (OLE) return period hazard level at Site 5 with and without directivity and including the Wilmington fault. 116
Figure 136. UHS for the 475-year (CLE) return period hazard level at Site 5 with and without directivity and including the Wilmington fault. 116
Figure 137. UHS for the 975-year return period hazard level at Site 5 with and without directivity and including the Wilmington fault. 117
Figure 138. UHS for the 2,475-year return period hazard level at Site 5 with and without directivity and including the Wilmington fault. 117

Figure 139. Vertical to horizontal (V/H) spectral ratios for the scenarios and resulting envelope associated with the 72-year (OLE) hazard level for POLB sites. 119
Figure 140. Vertical to horizontal (V/H) spectral ratios for the scenarios and resulting envelope associated with the 475-year (CLE) and 975-year hazard levels for POLB sites. 121
Figure 141. Vertical to horizontal (V/H) spectral ratios for the scenarios and resulting envelope associated with the 2,475-year hazard level for POLB sites. 123
Figure 142. UHS for the 72-year (OLE) return period hazard level at Site 5 with and without directivity and for the vertical component and including the Wilmington fault. 130
Figure 143. UHS for the 475-year (CLE) return period hazard level at Site 5 with and without directivity and for the vertical component and including the Wilmington fault. 130
Figure 144. UHS for the 975-year return period hazard level at Site 5 with and without directivity and for the vertical component and including the Wilmington fault. 131
Figure 145. UHS for the 2,475-year return period hazard level at Site 5 with and without directivity and for the vertical component and including the Wilmington fault. 131
Figure 146. Comparison of the 72-year (OLE) hazard level UHS for POLB from the current and previous PSHA studies. 134
Figure 147. Spectral ratio of the current UHS divided by the previous UHS for the 72-year (OLE) hazard level UHS. 134
Figure 148. Comparison of the 475-year (CLE) hazard level UHS for POLB from the current and previous PSHA studies. 135
Figure 149. Spectral ratio of the current UHS divided by the previous UHS for the 475-year (CLE) hazard level UHS. 136

1. Introduction

Vibratory ground motions were previously developed as part of a site-wide seismic hazard study for the Port of Long Beach (POLB) (Earth Mechanics Inc., 2006). These ground motions were developed following a standard probabilistic seismic hazard (PSHA) methodology and the current state of knowledge and practice input models at the time of the study. These models include the seismic source characterization (SSC) and the ground motion characterization (GMC). During the last decade with the collection and understanding of vast amounts of geological and seismological data, these SSC and GMC models have evolved and subsequently the models used in the 2006 study have been updated and replaced with current PSHA practice.

Recently a seismic hazard study was performed (Gregor and Al Atik, 2019) using the current state of practice and state of knowledge SSC and GMC models for a suite of sites in the Port of Long Beach following a standard PSHA methodology. As this seismic hazard study was being concluded a recent geologic fault study of the Wilmington fault was released (Wolfe et al., 2019). This newly characterized fault is located in the immediate area around the POLB and was not explicitly considered as a fault source in the UCERF3 seismic source characterization. This report presents the analysis of the seismic hazard including this additional seismic source with the UCERF3 seismic source model. The same methodology and approach performed in the Gregor and Al Atik (2019) study are implemented for this study.

The PSHA was performed for four POLB site locations (see Table 1) in Long Beach California. These four site locations were selected to be representative of the expected variation in ground motions from the PSHA study given their relative location to the faults in the immediate vicinity of the POLB. Ground motions were computed for the horizontal component of motion based on an assigned average shear wave velocity value for the top 30 m (V_{S30}) of 300 m/sec for all four site locations. The PSHA was performed for the full range of spectral periods up to 10 sec (peak ground acceleration PGA, 0.02, 0.03, 0.05, 0.075, 0.1, 0.15, 0.2, 0.25, 0.3, 0.4, 0.5, 0.75, 1, 1.5, 2, 3, 4, 5, 7.5, 10 sec).

Given the close proximity of the Palos Verdes fault and other faults in the immediate region around the POLB, a recently developed directivity model was also implemented in the PSHA for the horizontal component of motion. The model from Bayless and Somerville (as presented in Spudich et al., 2013) is an updated directivity model from the original Somerville et al. (1997) model. Note that this original model was also modified by Abrahamson (2000) and used in the previous PSHA study (Earth Mechanics Inc., 2006). This current updated model is similar to the previous model in that it predicts changes to the estimated median ground motions for an average directivity component, a fault normal and a fault parallel component. This model is based on the geometry of either a strike-slip fault or a dip-slip fault and modifies ground motions for spectral periods greater than 0.5 seconds. Note that for the inclusion of the Wilmington fault, the Bayless and Somerville directivity model was not applied given the relatively low maximum magnitude (i.e., 6.4) assigned to the fault. In addition, based on the relative contribution of the Wilmington fault to the total hazard which will be presented later in this report, the decision of not applying the directivity model to the Wilmington fault is not

expected to under-represent the hazard given the uncertainty in the calculated ground motions.

Design ground-motion response spectra were developed based on two specific seismic design levels: OLE defined as the 50% probability of exceedance in 50 years; and CLE defined as the 10% probability of exceedance in 50 years. These two hazard levels approximately correspond to 72-year (OLE) and 475-year (CLE) return periods. Additionally, ground motions were developed for the 975- and 2,475-year return period hazard levels. Vertical design spectra were developed based on the selection of controlling scenario events from the PSHA deaggregation and the application of empirically based vertical to horizontal spectral ratios. Complete spectra were developed for Site 5 for the horizontal component both with and without directivity and the vertical component of motion. A comparison of the horizontal ground motions will be provided for the two cases in which the Wilmington fault is not included in the analysis and is included in the analysis.

Table 1. Site locations and V_{S30} values used in the PSHA study for the POLB.

Site	Longitude	Latitude	V_{S30} (m/sec)
Site 1 – Navy Mole (West)	-118.24	33.743	300
Site 3 – Pier T	-118.237	33.753	300
Site 5 – Pier A	-118.239	33.772	300
Site 8 – Pier E	-118.213	33.76	300

The basic elements of a PSHA are shown in Figure 1 (Earthquake Engineering Research Institute, 1989). The SSC and GMC models constitute the input to the PSHA. The SSC model defines the earthquake source seismicity and geometry while the GMC model defines the ground-motion scaling as a function of the earthquake source parameters, propagation parameters, and local site conditions. The primary output of a PSHA is a set of seismic hazard curves for the ground motion parameters of interest from which uniform hazard spectra (UHS) are developed using equations given in McGuire (2004). A deaggregation of the seismic hazard using equations given in Bazzurro and Cornell (1999) is used to define controlling events (design earthquake scenarios) required to develop the vertical design spectra and design time histories.

The primary SSC model implemented in this study is the Uniform California Earthquake Rupture Forecast, Version 3 (UCERF3) (USGS, 2013) which represents an update from the SSC used in the previous study (Earth Mechanics Inc., 2006) and is recognized as the current state of knowledge for crustal seismic source characterization in California. As noted earlier, the recent characterization of the Wilmington fault (Wolfe et al., 2019) is also included as part of the SSC model. The current Next Generation Attenuation for Western US (NGA-West2) suite of ground motion models (Bozorgnia et al., 2014) are used in this study and also represent an update to the models used in the previous study (Earth Mechanics Inc., 2006). These seismic source and ground motion models represent the best available earthquake science for performing PSHA at

sites located in California. The PSHA was computed for this study using the HAZ45-HSR computer program (Gregor and Al Atik, 2017a). This computer program was validated for calculating seismic hazard by successfully passing the test cases developed as part of the Pacific Earthquake Engineering Research Center (PEER) PSHA code verification project (Hale et al., 2018). This validation study is described in Gregor and Al Atik (2017b).

In this report, we present an overview of the SSC and GMC models as implemented in HAZ45-HSR. The PSHA results are presented in terms of mean hazard curves at select spectral periods (i.e., 0.01, 0.2, 0.5, 1, and 2 sec). The uniform hazard spectra (UHS) are presented at the specified design levels for each of the four site locations for the full spectral period range of 0.01 (PGA) to 10 sec for the horizontal component. For each site and design level, deaggregation plots are presented for the same selected spectral period values of 0.01, 0.2, 0.5, 1, and 2 sec. Finally, the horizontal component ground motions including the implementation of the directivity model are provided for Site 5.

Based on the deaggregation results, controlling scenario events were estimated for each hazard level. Given the relatively small contribution of the Wilmington fault to the total hazard, these scenarios are applicable for either case in which the Wilmington fault was considered. These scenario events and their parameters were developed to be consistent with the SSC model used in the analysis. Given these controlling events, vertical to horizontal (V/H) spectral ratios were estimated from two empirical models (Gulerce and Abrahamson, 2011; Bozorgnia and Campbell, 2016) each assigned equal weights. Rather than develop multiple vertical design spectra for a given site and hazard level, the final V/H ratio which is applied to the horizontal design spectrum was selected to be the envelop of the suite of estimated scenario V/H ratios.

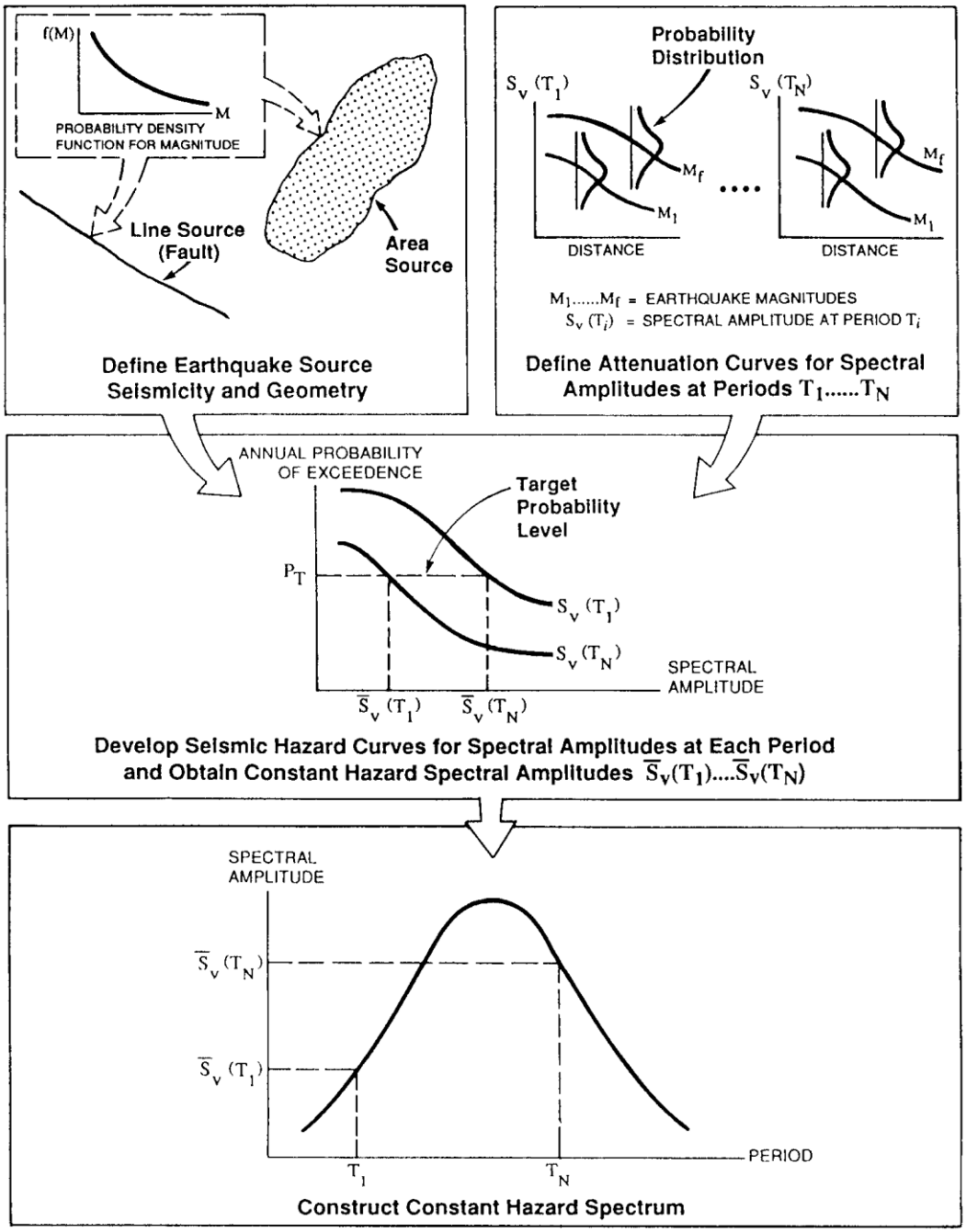


Figure 1. Schematic showing the elements of a probabilistic seismic hazard analysis (Source: Earthquake Engineering Research Institute, 1989).

2. Seismic Source Characterization

A complete tectonic, geology and seismicity summary for the POLB area, and Southern California is provided in Appendix A and B of the previous report (Earth Mechanics Inc., 2006). In general, the POLB is located within the coastal area of the Los Angeles basin where the present-day tectonic stress is in a north-northeasterly compressional regime. The area contains basin bounding faults, dipping buried thrust faults and more vertically dipping strike-slip faults.

The previous PSHA study (Earth Mechanics Inc., 2006) implemented a combination of the Frankel et al. (2003) and the Southern California Earthquake Center (SCEC) Community Fault model. For those faults in the immediate area of the POLB and expected to contribute significantly to the total hazard, a logic tree approach was applied to capture the epistemic uncertainty in the estimated parameters. For the more distant and regional faults a more simplified model of the faults was applied based on the mean estimates from the Frankel et al. (2003) model.

The current state of knowledge for crustal seismic source characterization for California developed in the Uniform California Earthquake Rupture Forecast Version 3 (UCERF3) seismic source model (USGS, 2013) was implemented in HAZ45-HSR and used for evaluating the hazard at the four POLB site locations. This regionally developed SSC model is not expected to fully contain any smaller scale site-specific seismic sources, especially those that were characterized after the development of the UCERF3 SSC model. It would be expected that any of these potentially uncharacterized seismic sources would be included in the gridded seismicity distribution associated with the UCERF3 SSC model. This, however, assumes that any of these potentially unknown seismic sources have been seismically active in the duration of the historical seismicity catalog.

The UCERF3 SSC model is a complex source model accounts for potential seismic events associated with both mapped and unmapped faults. This newly developed SSC model for the California region is different from previous SSC models (e.g., UCERF2) in that the strict fault segmentation breaks were relaxed allowing for multiple fault segment ruptures. These multiple segment ruptures can develop into large magnitude earthquakes (e.g., magnitudes larger than 8) but with a low probability of occurrence. As part of the UCERF3 SSC model, a broad range of data was used to perform a grand inversion which estimates the long-term rate of occurrence of all earthquakes of magnitude 5.0 and larger. Both planar fault segments and gridded smooth seismicity point sources were considered in this grand inversion. Mathematically, this grand inversion is somewhat straightforward; however, based on the volume of input data and as importantly the number of logic tree branches (i.e., 1,440 logic tree branches) considered for the epistemic uncertainty (e.g., see Figure 3 of USGS, 2013), the grand inversion was performed on super computers. Two notable features of the UCERF3 SSC model are the removal of the over-prediction of earthquakes in the magnitude 6.5-7.0 range when compared to the historical seismicity catalogs and the potential for earthquake ruptures associated with multiple fault systems as have been observed in large crustal earthquakes. A brief overview of the important features of the UCERF3 model pertinent to this study are summarized herein.

As part of the implementation of the UCERF3 SSC model for this study, only seismic sources associated with fault segments and gridded point sources located within a maximum distance of 300 km from a site were included in the PSHA study. Note that this maximum distance of 300 km is larger than is typically used (e.g., 200 km) for a given seismic source model in California. This cutoff distance is based on sensitivity studies for sites in California where the UCERF3 seismic source model indicated limited contributions from sources out to a maximum distance of 300 km. The use of a maximum distance of 300 km allows subsampling the full dataset of rupture scenarios while capturing the events expected to contribute to the seismic hazard at a given site location. This maximum distance used in the analysis is also within the acceptable distance range of the ground-motion prediction equations discussed later in this report.

2.1 Fault Sources

The UCERF3 SSC model consists of a total of 3,412 individual fault segments for the entire region of California. These individual segments were estimated based on a rupture length of approximately 7 km. Within the framework of the UCERF3 model, a minimum of at least two fault segments must rupture together to create an earthquake rupture scenario. In addition to this minimum number of rupture segments, multiple segments are allowed to rupture as part of a single earthquake scenario based on the assigned rules for multiple rupturing segments. Note that segments do not need to be continuous but must be within a close proximity of each other (e.g., about 5 km) for multiple segments to rupture in a given scenario. This allowance for the joining of close but not continuous fault segments is a feature of the UCERF3 SSC that was not allowed in earlier versions of the UCERF SSC model.

Two fault models (FM3.1 and FM3.2) were developed for the UCERF3 SSC model and the recommended weights for these two models are 50% each. As part of the available data for the UCERF3 model, a combined dataset for both the FM3.1 and FM3.2 was used in this study. This combined dataset is provided to allow for the calculation of the mean hazard curves without the need to separately compute and combine the hazard results from FM3.1 and FM3.2. With this combined UCERF3 SSC fault model, there are a total of 1,634,466 individual earthquake rupture scenarios associated with combinations of the 3,412 individual fault segments for the entire region of California. For this study, the closest distance (rupture distance) from the site to the stitched fault segments associated with each fault rupture scenario was measured and scenarios with closest distance of less than 300 km from the site were included in the site-specific PSHA. Based on the cutoff distance of 300 km, the number of fault rupture scenarios included in the PSHA study for the four site locations in this study is listed in Table 2. Given the same 300 km cut off distance and the close location of the four sites used in the analysis, the number of fault ruptures used in the analysis for all four sites is similar (see Table 2).

The individual UCERF3 fault segments within 300 km of the four site locations are plotted in Figure 2. As can be observed in the map of Figure 2, the UCERF3 SSC model contains rupture scenarios in which multiple segments rupture together, therefore spanning a large area around and away from the site. Based on this long fault rupture length, the associated magnitude for these scenarios can be large, however, their estimated rate of occurrence is generally low.

The closest individual segment contained in the UCERF3 database to each of the four sites is also provided in Table 2. These four sites are located above the buried trace of the Compton Thrust fault which is a northeast dipping thrust fault with the top trace of the fault at a depth of approximately 5 km. The closest fault to these four site locations is the Palos Verdes fault. The faults in the immediate area around each of the four POLB site locations are shown in Figure 3. The sites are indicated with the red circles and the faults are plotted based on their style of faulting with red traces being strike-slip faults and black traces being reverse faults.

For the closest faults to the four site locations labeled in Figure 3, a summary of the mean slip rates computed from the UCERF3 model is provided in Table 3. Note, however, that these slip rates from the UCERF3 database are estimated based on the grand inversion and segmentation grouping of fault systems but are not used in the traditional method of performing a PSHA where the magnitude recurrence of a fault is estimated based on the slip rate and an assumed magnitude recurrence relationship. These values listed in Table 3, however, allow for a rough assessment of the relative activity rates and contribution to the seismic hazard for the sites from these closely located faults. The mean weighted slip rate estimates from the previous study (Earth Mechanics Inc., 2006) are also listed in Table 3. Both the Cabrillo and Los Alamitos fault were not directly modeled as part of the UCERF3 model. However, any potential seismic activity associated with these smaller and low slip rate faults would either be accounted for in the background seismicity rates of the UCERF3 source model or through the seismic moment release of the other faults in the area as part of the grand inversion. For the other faults listed in Table 3, the comparison of the slip rates is favorable with a decrease in the Palos Verdes fault slip rate but an increase in the Newport/Inglewood fault slip rate of approximately the same relative amount. Given the observation that the hazard at the POLB sites is primarily controlled by the Palos Verdes fault (Earth Mechanics Inc., 2006), a reduction of the slip rates as noted in Table 3 for the Palos Verdes fault would be expected to lead to a reduction in the estimated ground motions assuming the same ground motion models are used.

Table 2. Number of UCERF3 fault scenarios and distance to closest fault segment within 300 km from the four POLB sites.

Site	Number of Fault Scenarios	Closest Fault Segment	Distance to Closest Segment, Rrup (km)
Site 1	1,121,861	Palos Verdes 11 (section ID = 1912)	1.09
Site 3	1,121,951	Palos Verdes 11 (section ID = 1912)	1.70
Site 5	1,128,992	Palos Verdes 11 (section ID = 1912)	3.07
Site 8	1,121,341	Palos Verdes 11 (section ID = 1912)	4.05

Table 3. Estimated mean slip rates for selected faults from the UCERF3 grand inversion in the immediate vicinity of the four POLB site locations.

Fault	UCERF3 Mean Slip Rate (mm/yr)	2006 Study Slip Rate (mm/yr)
Palos Verdes	2.28	2.7
Newport/Inglewood	1.22	1.0
Compton Thrust	0.82	0.75
San Pedro Basin	0.77	0.7
Cabrillo	---	0.1
Los Alamitos	---	0.375

Wilmington fault slip rate: 0.14 to 0.18 mm/yr.

For UCERF3 rupture scenarios in which multiple fault segments are included each with potentially different dip angle, a weighted-average dip angle is computed. This average dip angle is calculated based on the area-weighted dip angles for the individual fault segments relative to the total area of the entire rupture scenario (total area of all associated segments). Similarly, the average depth-to-top of rupture was calculated based on the area-weighted average of the depth-to-top of rupture of the individual fault segments associated with a particular rupture.

Based on the selected scenario fault ruptures within 300 km from each of the sites, the summed annual rate of earthquakes as a function of magnitude is shown in Figures 4 – 7 for the four site locations. Note that for this cut off distance of 300 km, approximately 69% of the total scenarios from the UCERF3 seismic source model are included in the selection. The annual rates are plotted for all distances (red line) and for four distance bins. For the sites in this study, Figures 4 – 7 indicate that the largest contribution to the total rates of scenario fault ruptures is primarily from scenarios with distance of 50 to 100 km for magnitude greater than 7.8 and greater than 100 km range for smaller magnitudes.

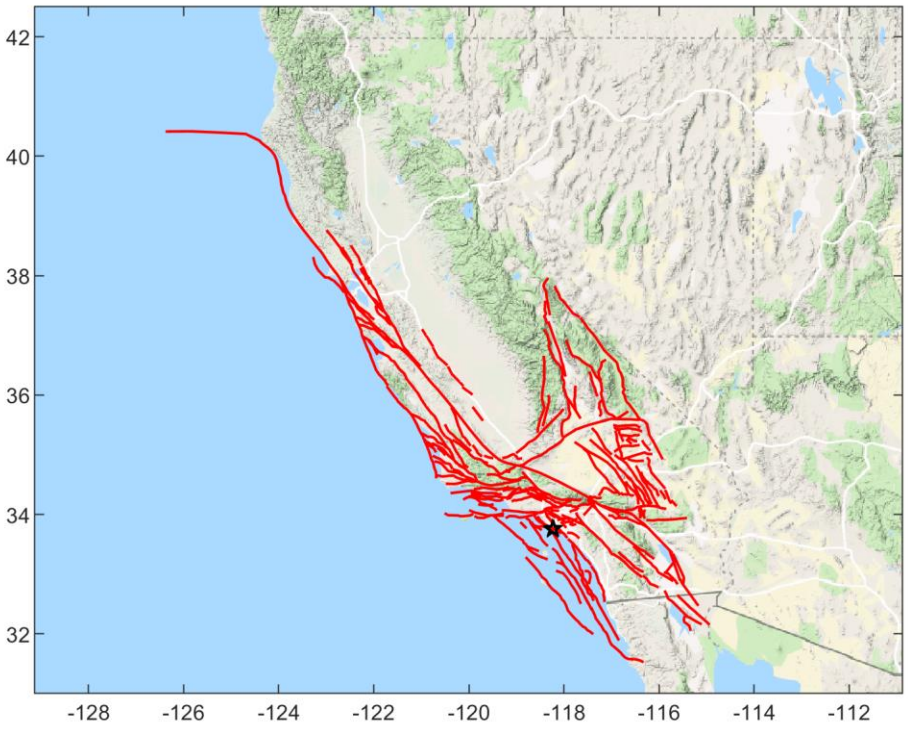


Figure 2. Regional map showing the UCERF3 fault segments (red traces) associated with all rupture scenarios within a closest maximum distance of 300 km from the four POLB site locations (black stars).

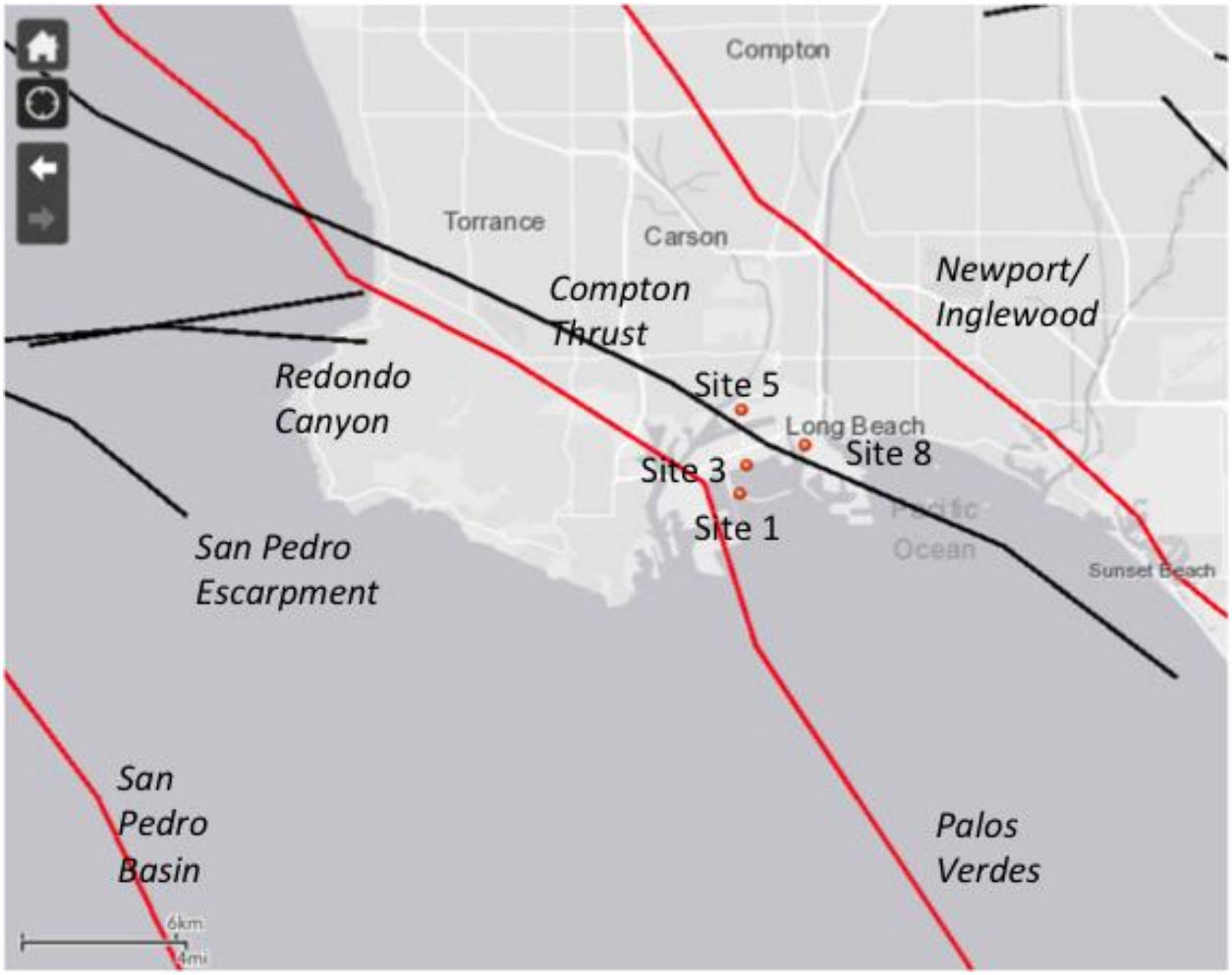


Figure 3. Map showing the four site locations (red circles) and fault traces from UCERF3 used in the analysis. Red fault traces are strike-slip faults and black fault traces are reverse faults.

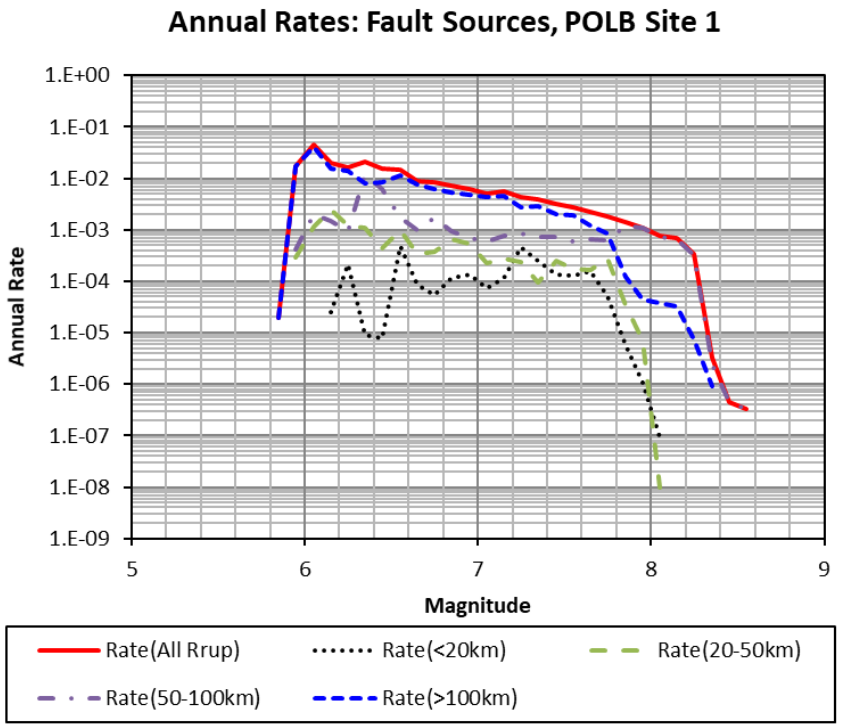


Figure 4. Cumulative annual rate of earthquakes from the UCERF3 fault sources within 300 km from Site 1.

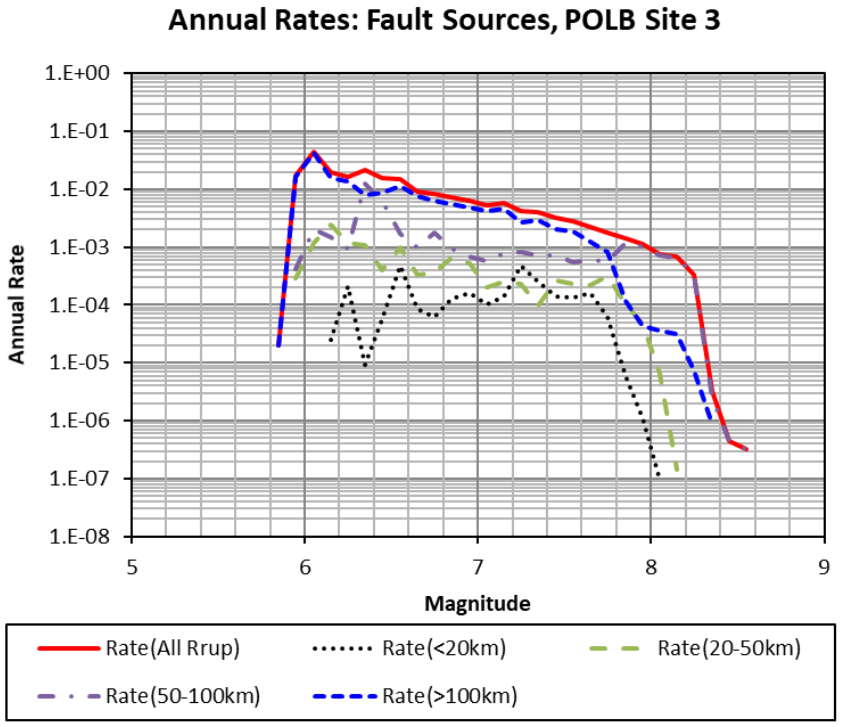


Figure 5. Cumulative annual rate of earthquakes from the UCERF3 fault sources within 300 km from Site 3.

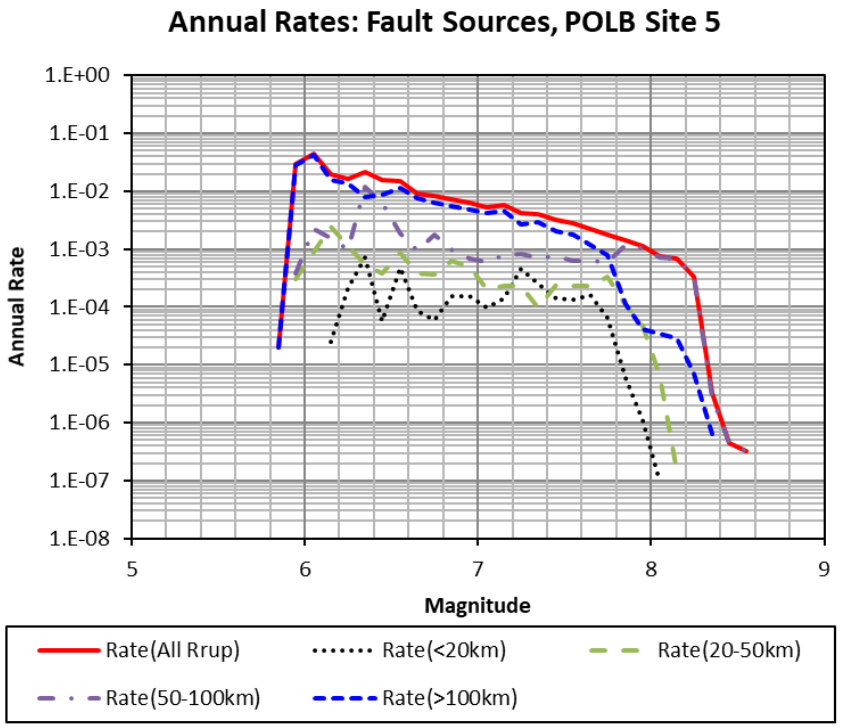


Figure 6. Cumulative annual rate of earthquakes from the UCERF3 fault sources within 300 km from Site 5.

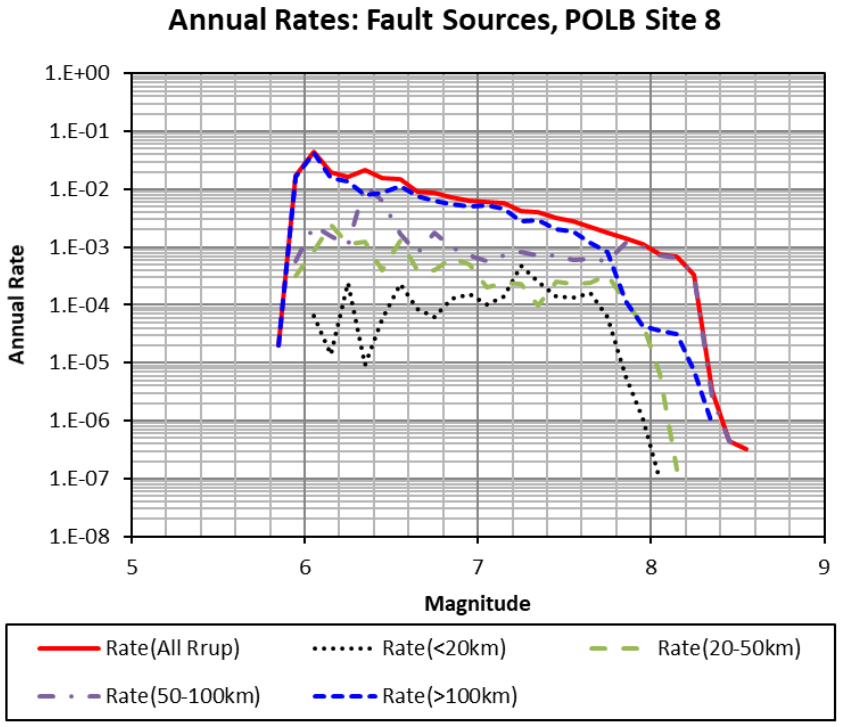


Figure 7. Cumulative annual rate of earthquakes from the UCERF3 fault sources within 300 km from Site 8.

2.2 Gridded Seismicity

For the gridded point sources, a standard approach in analyzing and smoothing the historical earthquake catalog was employed in the development of the UCERF3 model. Gridded point source locations are defined at 0.1x0.1 degree latitude and longitude intervals and the UCERF3 SSC model provides a weighting scheme for each defined point location for the strike-slip, reverse, and normal earthquake mechanisms. These fault mechanism weights are used with the ground motion prediction equations when estimating the ground motions from the grid point sources.

For the implementation of the gridded source model, distance corrections are computed based on the modeling of virtual faults centered at each grid point. For this distance correction, three virtual faults are considered: a vertical strike-slip fault and reverse and normal dipping faults with a dip angle of 50 degrees. For the two dipping fault cases, both the hanging wall and footwall cases are considered with equal weights between the two cases. To account for the potential strike orientation of these virtual faults, three azimuthal orientations of perpendicular, parallel, and rotated by 45 degrees related to the site location are considered.

The number of gridded point sources within the cutoff distance of 300 km from the four POLB sites are 2,112 (Site 1), 2,114 (Site 3), 2,124 (Site 5) and 2,127 (Site 8), respectively. Similar to the fault sources, the cumulative annual rate of earthquakes from gridded sources versus magnitude is shown in Figures 8 – 11. The annual rates are shown for all distances (red line) and for four different distance bins. For the gridded sources, the largest contribution to the total rates of gridded scenarios are coming from the grid points with distances greater than 100 km from the site. This largest contribution from the largest distance bin is expected based on the number of grid points which fall within each distance bin. As an example for Site 1 site, the total number of grid points of 2,112 are distributed as 12 for distances less than 20 km, 61 for distances of 20 – 50 km, 233 for distances of 50 – 100 km, and 1,806 for distances greater than 100 km. However, this does not indicate that the more distant grid points will control the seismic hazard at the site since the attenuation and estimation of ground motions is not considered in these comparison figures. Comparing the cumulative annual rates of earthquakes from fault sources and gridded sources for the site, we note that the fault rupture scenarios have higher annual rate of occurrence than the gridded sources earthquakes for magnitude larger than about 6.25.

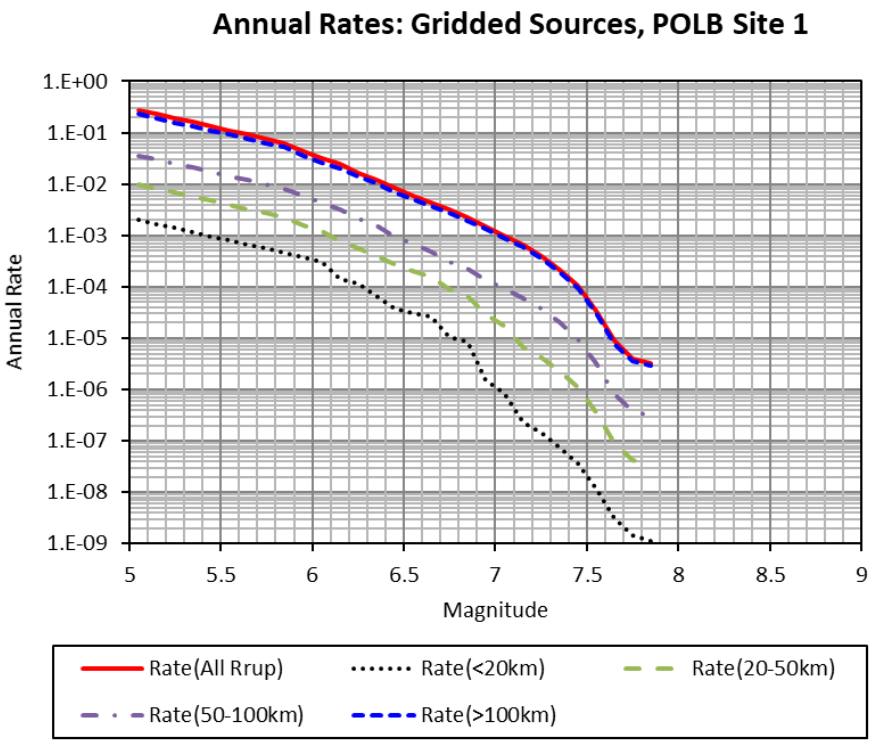


Figure 8. Cumulative annual rate of earthquakes from the UCERF3 gridded sources within 300 km from Site 1.

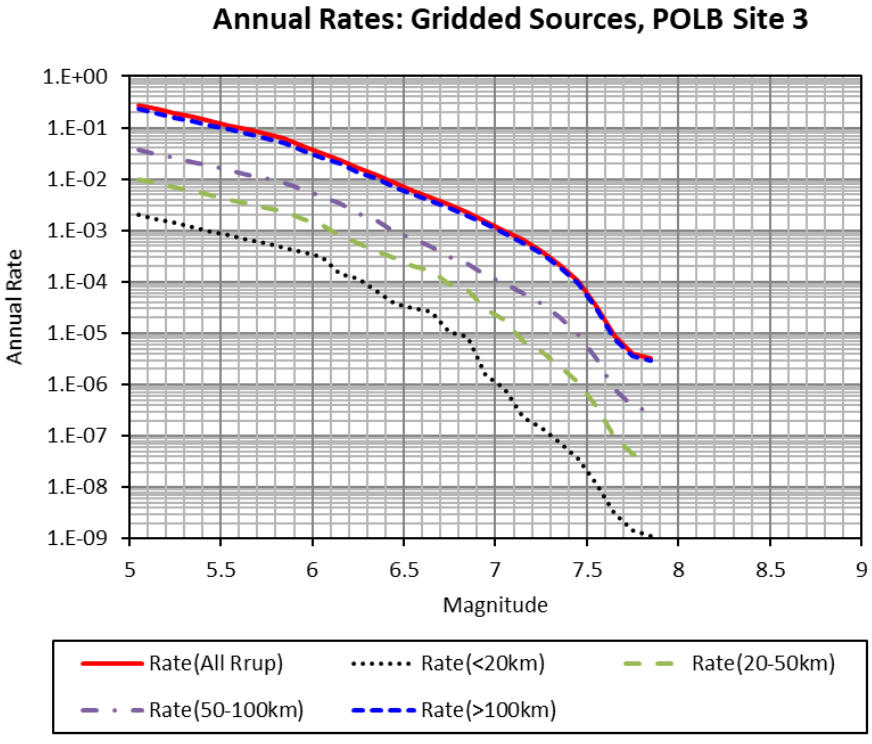


Figure 9. Cumulative annual rate of earthquakes from the UCERF3 gridded sources within 300 km from Site 3.

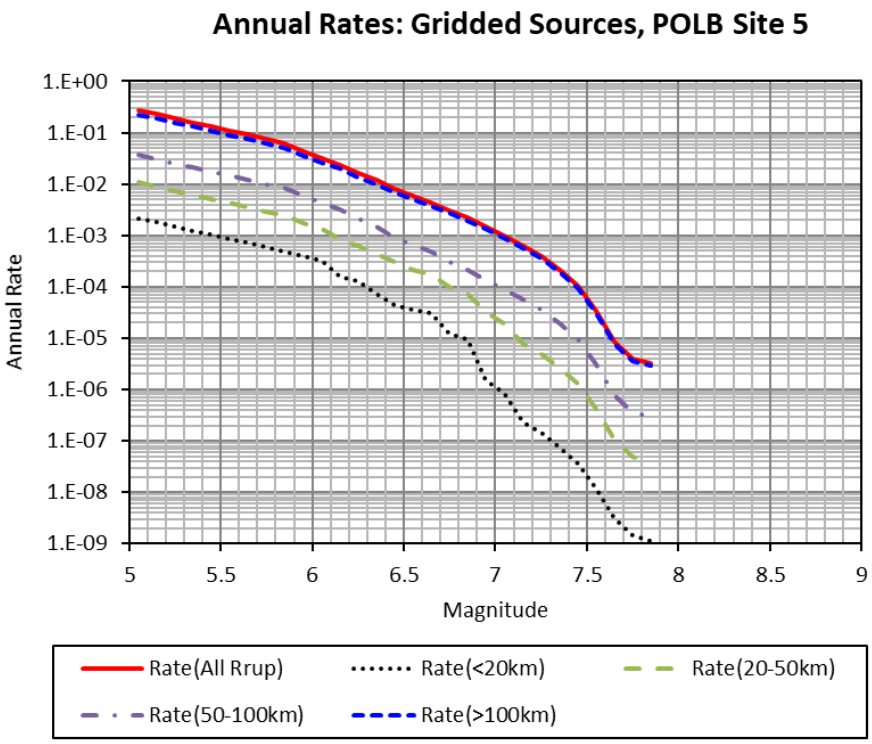


Figure 10. Cumulative annual rate of earthquakes from the UCERF3 gridded sources within 300 km from Site 5.

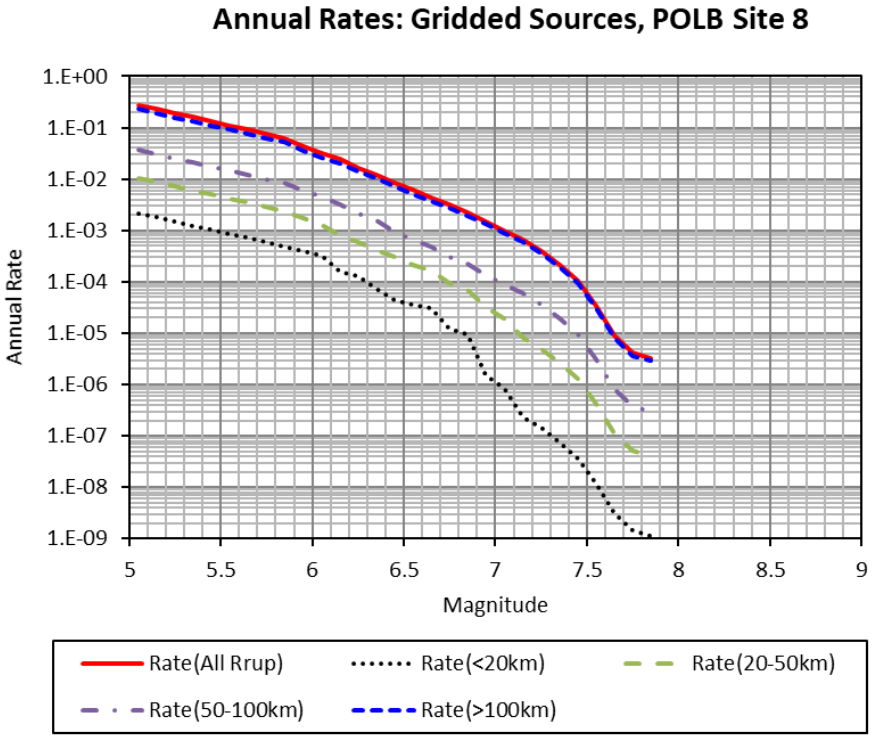


Figure 11. Cumulative annual rate of earthquakes from the UCERF3 gridded sources within 300 km from Site 8.

2.3 Wilmington Fault Characterization

Wolfe et al. (2019) proposed that the Wilmington fault is active and should be considered for seismic hazard studies in the Los Angeles region. The inferred projected surface trace of the fault is shown in Figure 12 (taken from Figure 2 of Wolfe et al., 2019). Note that Site 3 for the POLB is located directly above the projected surface trace of the fault. Also plotted in the figure as thin red lines are the fault traces of the seismic fault sources contained in the UCERF3 database. As noted in Gregor and Al Atik (2019) study, the Palos Verdes, Newport-Inglewood and Compton Thrust faults are the closest faults to the POLB sites.

Wolfe et al. (2019) estimate the slip rate of the Wilmington fault to be in the range of 0.14 – 0.18 mm/yr, which is lower than the other faults in the immediate region as listed in Table 3. Based on the comparisons of these slip rates it should not be expected that the inclusion of the Wilmington fault will have a large impact on the PSHA results but it could have a large impact on deterministic ground motion calculations as noted in Wolfe et al., 2019.

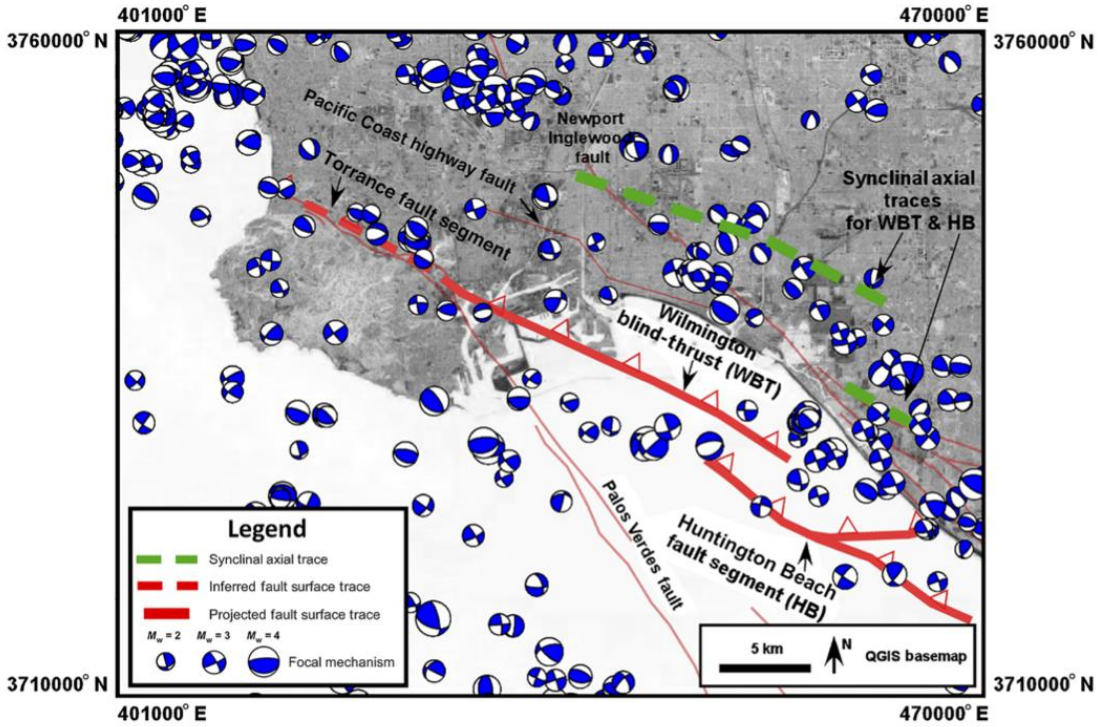


Figure 12. Regional map showing inferred projected surface fault trace for the Wilmington blind thrust fault. (Taken from Figure 2 of Wolfe et al., 2019).

For this seismic hazard study, the preferred dip angle of 53 degrees was adopted with the top of the fault at a depth of 1.25 km and the bottom at a depth of 12 km. As provided in Table 2 of

Wolfe et al. (2019), the range in recurrence intervals for the fault is estimated to be 3490 – 4490 years. Given this range, equally weighted recurrence intervals values of 3490, 3990, and 4490 years were assumed for this fault. For the magnitude recurrence model, a maximum magnitude distribution with a maximum magnitude of 6.4 was assumed with a b-value of 0.8.

As was previously discussed, the Wilmington fault was considered as an additional seismic source to the UCERF3 seismic source model. Given this additional seismic source without the consideration of any reduction or modification of the UCERF3 seismic source model, there is a potential that the seismic hazard and results may be conservative based on double counting from the seismic sources in this immediate area. However, the use of the assumed maximum magnitude distribution will limit this potential conservatism given that any expected smaller magnitude events associated with the Wilmington fault would not be modeled and would be assumed to be included in the UCERF3 background seismic source.

It should also be noted that as the Wolfe et al. (2019) study presents, the main trace of the Wilmington fault may potentially combine with the Huntington Beach segment, Compton Thrust and Newport-Inglewood faults to potentially generate larger magnitude events but the recurrence intervals of these events is as expected longer and thus their potential impact on the seismic hazard results for hazard levels of 2,475 years and less would be expected to be reduced. Geometrically, for these multi-segment events, the geometry of the Wilmington fault is postulated to be truncated at depth from these other faults. The results presented in this report do not include these more complex aspects of the seismic source characterization of the Wilmington fault. The impact of including these more complex rupture scenarios would be expected to be more significant for any deterministic study than probabilistic study based on the potential increase in the associated maximum magnitudes.

3. Ground Motion Characterization

Four equally weighted Next Generation Attenuation for Western US (NGA-West2) GMPEs were used to predict RotD050 (Boore, 2010) ground motions for the PSHA study. These GMPEs are: Abrahamson et al. (2014) (referred to as ASK14), Boore et al. (2014) (referred to as BSSA14), Campbell and Bozorgnia (2014) (referred to as CB14), and Chiou and Youngs (2014) (referred to as CY14). The RotD050 ground motion measure corresponds to the 50^{th} percentile of the response spectra over all rotation angles. A V_{S30} value of 300 m/sec was assigned for all four POLB sites. We note that the Idriss (2014) model was not used in this study due to the site-specific V_{S30} value of 300 m/sec being less than the minimum recommended value of 450 m/sec for this model.

For the ASK14 and CY14 models, the functional form of the models based on an "estimated V_{S30}" value was implemented in this study. Note that the difference between the estimated and measured V_{S30} flag only impacts the uncertainty of two of the four GMPE models (ASK14 and CY14) but does not impact the median ground-motion estimates. Based on the V_{S30} value of 300 m/sec for the four POLB sites, the default Z1 and Z2.5 parameter values used in this study for the GMPEs are 0.456 and 1.757 km, respectively.

Because the NGA-West2 GMPEs were developed in a collaborative effort with interactions and exchange of ideas among the developers, the NGA-West2 developers indicated that additional epistemic uncertainty should be incorporated into the median ground-motion estimation from their GMPEs. The additional epistemic uncertainty model of Al Atik and Youngs (2014) developed as part of the NGA-West2 project is used in this study. The Al Atik and Youngs (2014) epistemic uncertainty model is distance-independent but depends on magnitude, style-of-faulting, and spectral period. The logic tree for the ground-motion characterization model is shown in Figure 13.

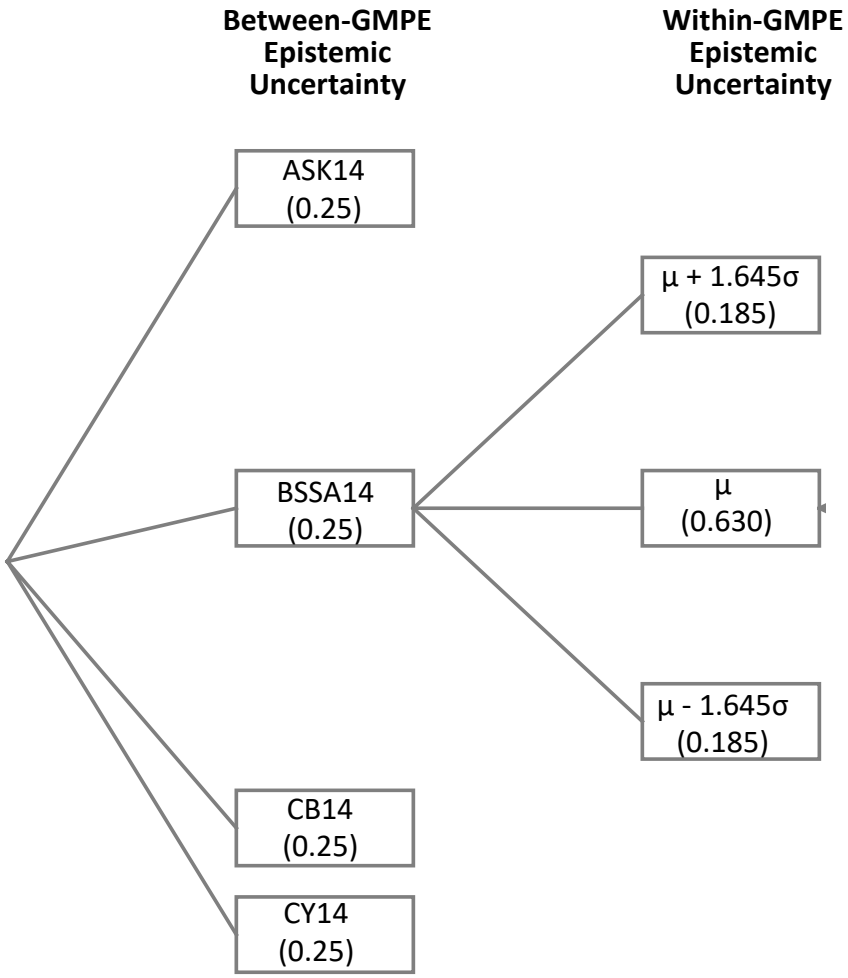


Figure 13. Ground-motion logic tree showing the different branches and associated weights; μ and σ are median prediction and epistemic standard deviation of the natural-logarithmic values of the ground-motion parameter of interest.

4. Probabilistic Seismic Hazard Analysis (PSHA)

4.1 Methodology

Probabilistic seismic hazard calculations were carried out using the computer program HAZ45-HSR. This PSHA program is based on the HAZ45 computer program (Abrahamson and Gregor, 2015) and follows a standard state of practice approach for probabilistic seismic hazard analysis. HAZ45-HSR was specifically developed to implement the UCERF3 source model for the California High Speed Rail (HSR) project and is documented in Gregor and Al Atik (2017a). It has successfully passed the validation test cases associated with the recent PEER PSHA Validation testing program (Gregor and Al Atik, 2017b).

A sigma truncation value of 8.0 was used for the PSHA. The minimum magnitude used in the analysis was 5.0. Mean Hazard curves were computed for the four separate sites in this study for the following suite of spectral periods: PGA (0.01 sec), 0.02, 0.03, 0.04, 0.05, 0.075, 0.1, 0.15, 0.2, 0.25, 0.3, 0.4, 0.5, 0.75, 1.0, 1.5, 2.0, 3.0, 4.0, 5.0, 7.5 and 10.0 sec. Based on the GMPEs used in the analysis, these mean hazard curves are defined for the RotD050 component (Boore, 2010). As stated earlier, given the potential significance of longer period design motions, the observed impact of rupture directivity on longer period ground motions, and the close proximity of several faults near the sites, a rupture directivity model was implemented within the PSHA framework. The directivity model by Bayless and Somerville is presented in Spudich et al. (2013). This model applies an adjustment to the median ground motion estimate for a given event depending on the parameters of the event. This model was applied to the full UCERF3 seismic source database but was not applied to the Wilmington fault based on its relatively small maximum magnitude (**M**6.4) compared to directivity models which tend to reduce the amount of directivity for earthquakes with magnitudes less than about 6.5. The directivity model was also not applied given the expected and confirmed lesser contribution of the Wilmington fault to the total hazard. This implementation choice would not necessarily be used if deterministic ground motions were being computed as part of this project consistent with the conclusion stated in Wolfe et al. (2019).

Although Bayless and Somerville in Spudich et al. (2013) discusses the potential need for a reduction in the associated aleatory uncertainty when including the directivity model adjustments, no recommendation is provided. In addition, a preliminary analysis of near field data from the NGA West2 dataset indicates that the reduction in the aleatory uncertainty due to the directivity adjustment of median ground motions is small.

For the implementation of the directivity model using the UCERF3 source model, the necessary directivity parameters were computed for each scenario within a rupture distance of 80 km. The as-published directivity model does not contain this additional tapering as a function of closest rupture distance but it was implemented based on a recommendation from Bayless (personal communication, 2016) and is consistent with the distance limitations of the other directivity models presented in Spudich et al. (2013).

For the modeling of the potential locations of the hypocenters needed to estimate the directivity parameters for the strike-slip cases, hypocenters were randomized and assumed to occur at each of the multiple segments within a given scenario rupture with a strike-slip mechanism and with a total number of 20 or fewer fault segments. For scenario ruptures with strike-slip faulting mechanism and total number of fault segments greater than 20, hypocenters were placed on every other fault segment. The rate for a given scenario was equally divided among the number of randomized hypocenters for this scenario. For the dip-slip cases, a total of six hypocentral locations down-dip were assigned.

Based on this suite of mean hazard curves, uniform hazard spectra (UHS) were computed initially for the horizontal component of motion for each of the four POLB site locations both without the Wilmington fault (Gregor and Al Atik, 2019) and with the Wilmington fault. A comparison of the UHS for these four POLB site locations indicates that the ground motion results from Site 5 approximately equal the envelop of the results from the all four site locations. Given this observation, the results from Site 5 are selected as being representative for the POLB sites and the additional mean hazard curves and ground motion spectra for the average horizontal component with directivity (FD), the fault normal (FN) and the fault parallel (FP) components were computed for Site 5.

For each of the four POLB sites, ground motion values were computed for a suite of four hazard levels. The OLE is defined as the 50% probability of exceedance in 50 years, which corresponds to a return period of approximately 72-year. The CLE is defined as the 10% probability of exceedance in 50 years, which corresponds to a return period of approximately 475-year. The other two hazard levels were a 975-year and 2,475-year return period. Note that the previous ground motion study (Earth Mechanics Inc., 2006) only computed ground motions for the OLE and CLE hazard levels.

For the given hazard levels at each site location, estimates of the mean magnitude, distance and epsilon values were computed and presented in the report including the Wilmington fault. Binned magnitude and distance contributions (i.e., deaggregation) to the hazard for the return periods of interest were computed and presented below for each of the four POLB sites at a select number of spectral periods. As expected, given the relative location of the four sites, these deaggregation results are very similar from one site location to the next. It can also be stated that in comparing the previous results without the Wilmington fault (Gregor and Al Atik, 2019) and these current results with the Wilmington fault, the deaggregation results are very similar.

For the vertical component design spectra, controlling scenario events were selected based on the deaggregation results and the seismic source faults in the area. These scenario events are applicable for both cases in which the Wilmington fault was and was not considered. For each scenario, the necessary event parameters were estimated to allow for the calculation of vertical to horizontal spectral ratios from two empirically based V/H models: Gulerce and Abrahamson (2011) and Bozorgnia and Campbell (2016). The Gulerce and Abrahamson (2011) model is based on the NGA-West1 database whereas the Bozognia and Campbell (2016) model is based

on the more recent NGA-West2 database. The results from these two models were assigned equal weights. In general, when developing vertical spectra following this methodology multiple vertical spectra could be developed depending on the controlling scenario events and their respective V/H ratio values. However, typically, the vertical design motion is not as critical for design decisions (i.e., as compared to the horizontal design motions) and V/H ratios typically tend to be somewhat similar. For these reasons, the envelop of the V/H ratio from the scenario events was taken to apply to the horizontal design spectra for the development of the vertical spectra. This is a conservative approach for the vertical design spectra. If, however, in future analyses it is demonstrated that the vertical component design motions are important and or critical, a refinement of the vertical motions developed and presented in this report can be performed. In addition, given the similar results from the closely located sites, the development of the scenario events and associated V/H spectral ratio is applicable to all four site locations.

4.2 Site 1 – Horizontal

The mean hazard curves including the Wilmington fault for Site 1 are shown in Figures 14 through 18 for PGA and spectral periods of 0.2, 0.5, 1.0, and 2.0 sec. For the longer spectral periods (i.e., 1 and 2 sec) these plots are showing the horizontal component without the inclusion of the directivity model. In these plots, individual hazard curves from the scenario fault ruptures, gridded sources, the Wilmington fault and the combined total hazard are presented. For the 72-year return period (OLE) hazard level, the hazard curve plots indicate that the hazard is primarily controlled by the contribution from the gridded point sources and to a lesser amount the contribution from the fault sources. At the 475-year (CLE) hazard level the contribution from the fault sources increases relative to the contribution form the gridded point sources. At the lower hazard levels of 975-year and 2,475-year return periods, the results indicate an increase in the relative contribution from the fault sources over the gridded point sources. Also based on these plots the contribution from the Wilmington fault is not significant, especially at the shorter return periods.

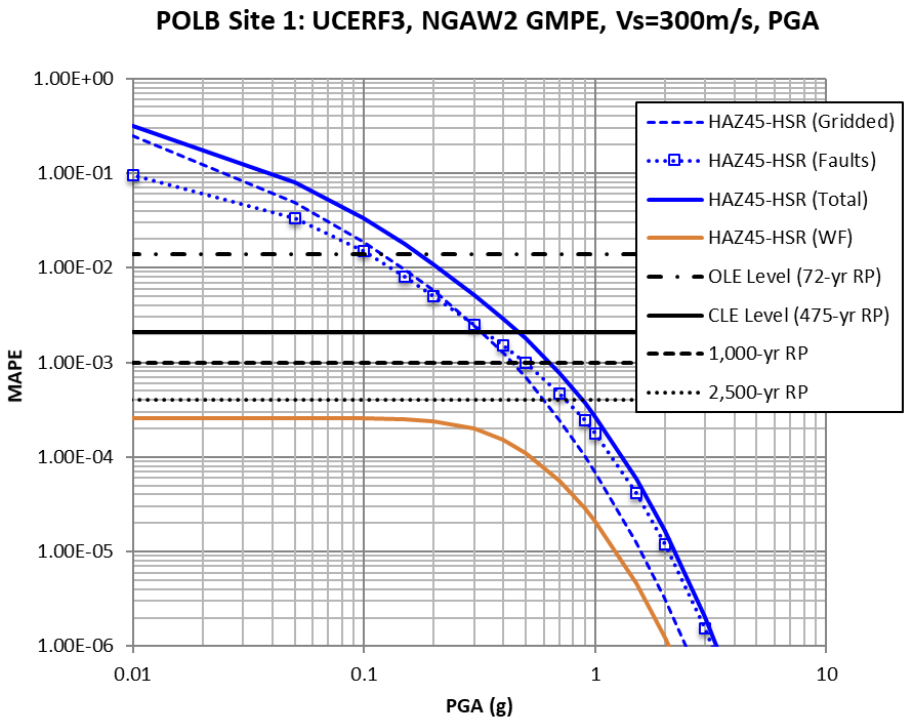


Figure 14. Mean horizontal component hazard curves from the UCERF3 gridded and fault sources, the Wilmington fault, and total hazard for PGA for Site 1.

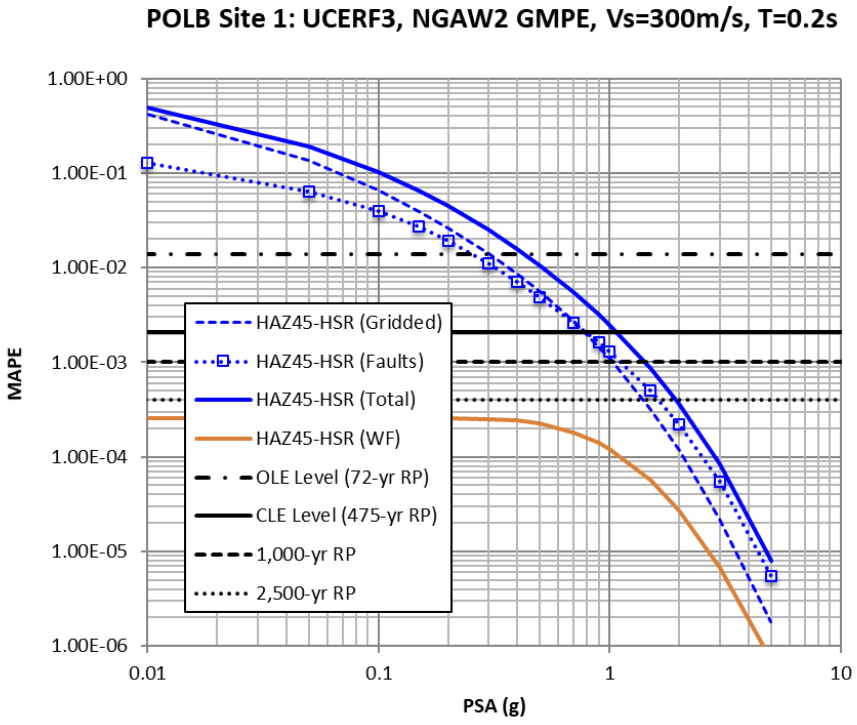


Figure 15. Mean horizontal component hazard curves from the UCERF3 gridded and fault sources, the Wilmington fault, and total hazard for T = 0.2 sec for Site 1.

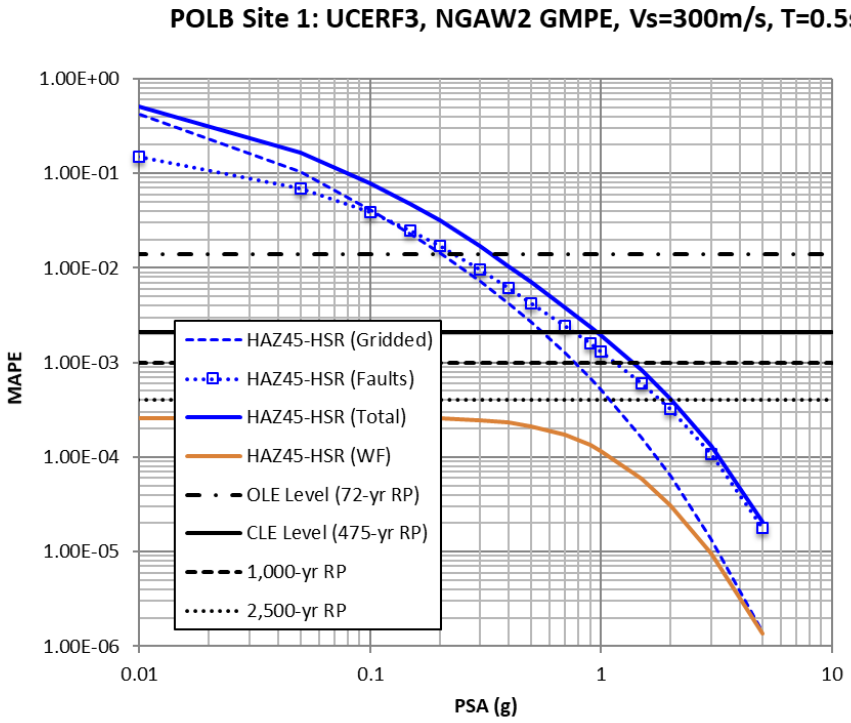


Figure 16. Mean horizontal component hazard curves from the UCERF3 gridded and fault sources, the Wilmington fault, and total hazard for T = 0.5 sec for Site 1.

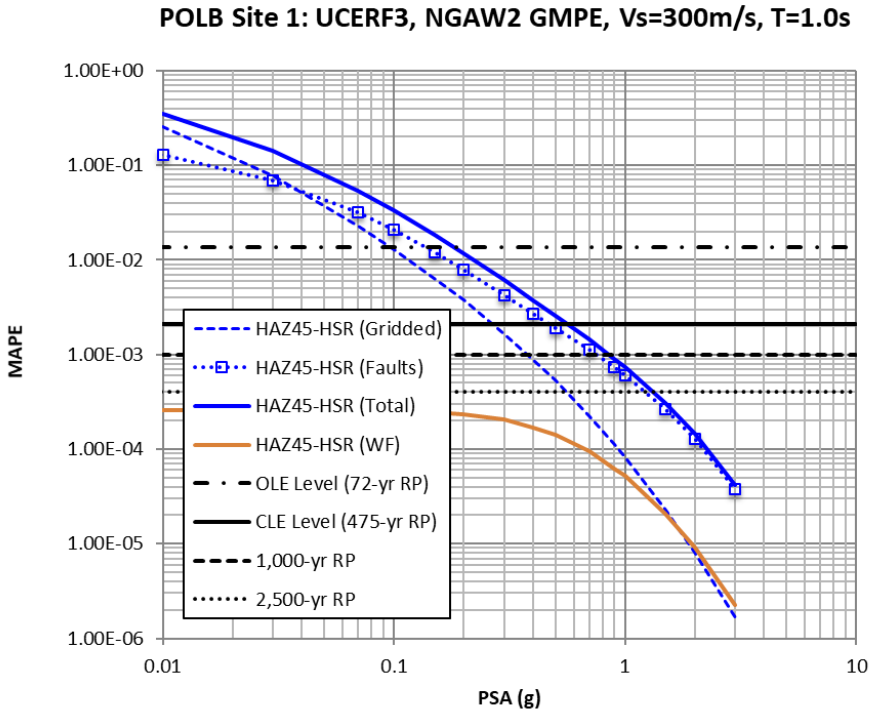


Figure 17. Mean horizontal component hazard curves from the UCERF3 gridded and fault sources, the Wilmington fault, and total hazard for T = 1.0 sec for Site 1.

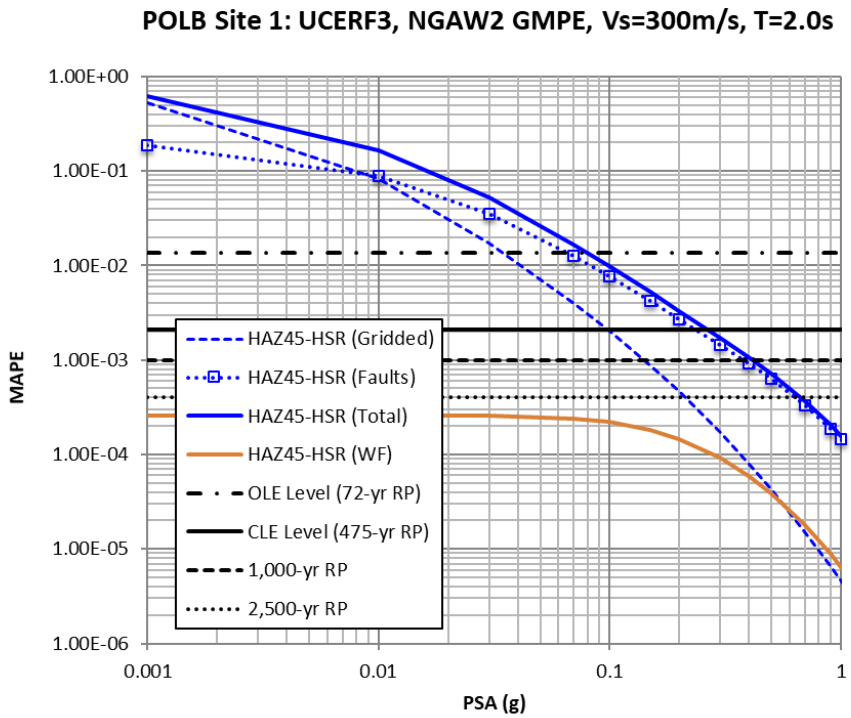


Figure 18. Mean horizontal component hazard curves from the UCERF3 gridded and fault sources, the Wilmington fault, and total hazard for T = 2.0 sec for Site 1.

Given the hazard curves for the full suite of spectral periods, the computed uniform hazard spectra (UHS) for the 72-year (OLE), 475-year (CLE), 975-year and 2,475-year return period hazard levels are plotted in Figure 19 for the case without the Wilmington fault (Gregor and Al Atik, 2019) and in Figure 20 for the case with the Wilmington fault. The horizontal UHS values at all spectral periods are given in Table 4 without the inclusion of the Wilmington fault (Gregor and Al Atik, 2019) and in Table 5 with the inclusion of the Wilmington fault. On average the inclusion of the Wilmington fault leads to a slight increase in the ground motions on the order of approximately 3-4% or less.

Table 4. Horizontal UHS for Site 1 at the four hazard levels not including the Wilmington fault.

Period (sec)	72-year (OLE) Horizontal PSA (g)	475-year (CLE) Horizontal PSA (g)	975-year Horizontal PSA (g)	2,475-year Horizontal PSA (g)
0.01	0.1717	0.4511	0.6140	0.8558
0.02	0.1714	0.4521	0.6155	0.8574
0.03	0.1781	0.4671	0.6340	0.8815
0.04	0.1925	0.5008	0.6778	0.9371
0.05	0.2085	0.5376	0.7290	1.0084
0.075	0.2645	0.6706	0.9015	1.2279
0.1	0.3222	0.7973	1.0596	1.4473
0.15	0.3967	0.9662	1.2640	1.7124
0.2	0.4251	1.0487	1.3928	1.8943
0.25	0.4280	1.0821	1.4647	2.0187
0.3	0.4185	1.0848	1.4933	2.0863
0.4	0.3742	1.0168	1.4288	2.0661
0.5	0.3339	0.9311	1.3262	1.9659
0.75	0.2398	0.7024	1.0356	1.5864
1	0.1785	0.5429	0.8211	1.2843
1.5	0.1128	0.3574	0.5501	0.8877
2	0.0784	0.2564	0.4008	0.6506
3	0.0465	0.1599	0.2514	0.4153
4	0.0312	0.1111	0.1744	0.2839
5	0.0221	0.0822	0.1284	0.2077
7.5	0.0118	0.0472	0.0720	0.1107
10	0.0072	0.0304	0.0458	0.0702

Table 5. Horizontal UHS for Site 1 at the four hazard levels including the Wilmington fault.

Period (sec)	72-year (OLE) Horizontal PSA (g)	475-year (CLE) Horizontal PSA (g)	975-year Horizontal PSA (g)	2,475-year Horizontal PSA (g)
0.01	0.1735	0.4635	0.6317	0.8792
0.02	0.1733	0.4646	0.6334	0.8811
0.03	0.1800	0.4798	0.6521	0.9051
0.04	0.1945	0.5127	0.6973	0.9605
0.05	0.2105	0.5502	0.7470	1.0310
0.075	0.2673	0.6859	0.9221	1.2558
0.1	0.3252	0.8135	1.0812	1.4814
0.15	0.4007	0.9859	1.2916	1.7499
0.2	0.4291	1.0700	1.4275	1.9409
0.25	0.4323	1.1068	1.5055	2.0651
0.3	0.4225	1.1119	1.5347	2.1394
0.4	0.3781	1.0448	1.4773	2.1231
0.5	0.3374	0.9596	1.3716	2.0256
0.75	0.2424	0.7252	1.0710	1.6357
1	0.1805	0.5617	0.8532	1.3271
1.5	0.1141	0.3695	0.5695	0.9132
2	0.0793	0.2647	0.4138	0.6674
3	0.0471	0.1643	0.2581	0.4226
4	0.0316	0.1135	0.1778	0.2874
5	0.0224	0.0837	0.1302	0.2093
7.5	0.0119	0.0477	0.0724	0.1111
10	0.0073	0.0306	0.0459	0.0703

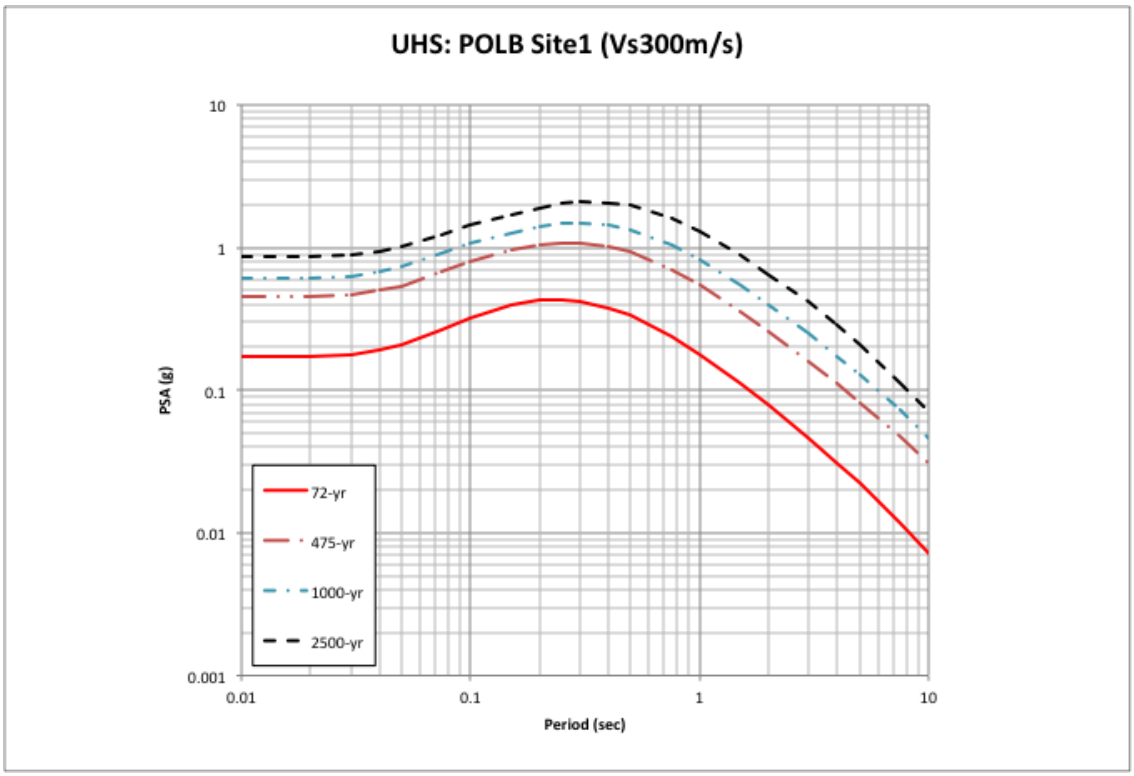


Figure 19. Uniform hazard spectra for Site 1 not including the Wilmington fault.

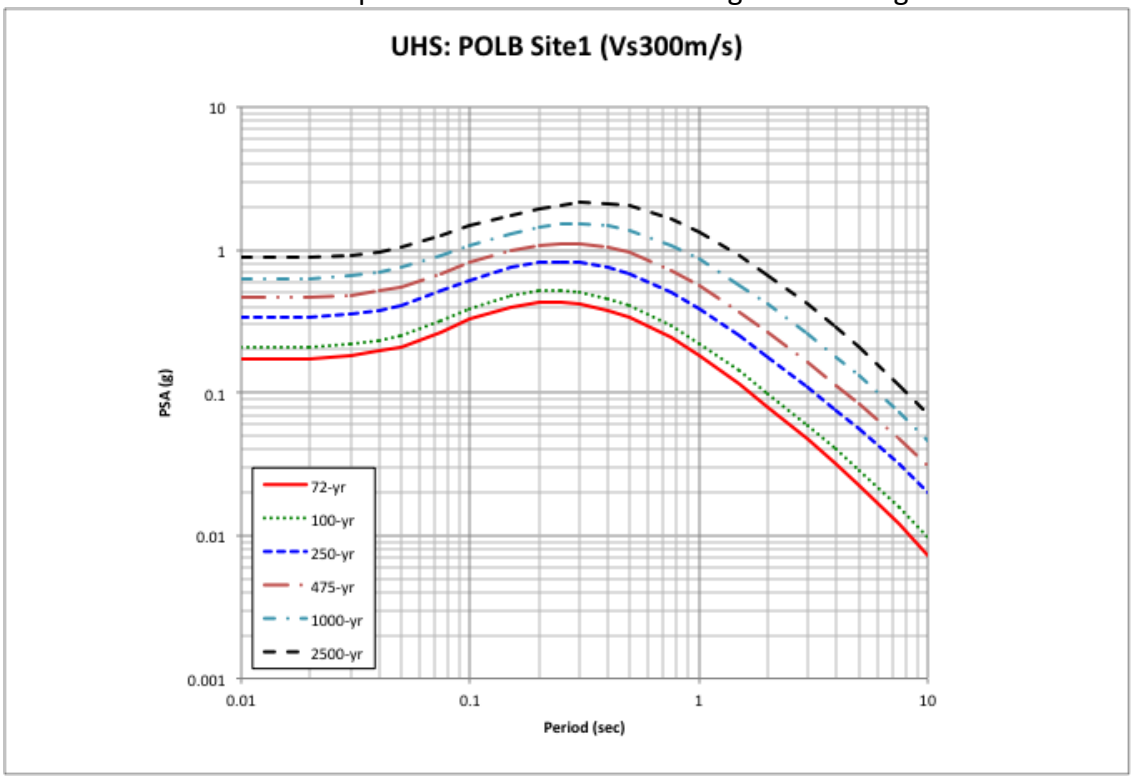


Figure 20. Uniform hazard spectra for Site 1 including the Wilmington fault.

The mean magnitude, distance and epsilon values for the horizontal component including the Wilmington fault but without the directivity model are plotted in Figures 21 to 23 for the four hazard levels. These plots are shown as a function of spectral period. As expected, the magnitude increases and the distance decreases with the increasing return period hazard levels. Also observed in these plots is the expected increase in the mean epsilon values between the four hazard levels with the 2,475-year results greater than approximately 1 over the full spectral period range. The mean magnitude, distance and epsilon values are listed in Tables 6 through 8 for the four hazard levels including the Wilmington fault. These mean values are very similar for the two cases in which the Wilmington fault was or was not considered in the analysis.

Table 6. Mean magnitude for the four hazard levels for Site 1 including the Wilmington fault.

Period (sec)	72-year (OLE) Magnitude	475-year (CLE) Magnitude	975-year Magnitude	2,475-year Magnitude
0.01	6.36	6.58	6.68	6.78
0.02	6.36	6.58	6.68	6.78
0.03	6.34	6.57	6.66	6.76
0.04	6.33	6.55	6.64	6.73
0.05	6.32	6.52	6.61	6.68
0.075	6.28	6.46	6.55	6.61
0.1	6.26	6.44	6.51	6.58
0.15	6.28	6.48	6.54	6.62
0.2	6.33	6.54	6.63	6.72
0.25	6.38	6.61	6.71	6.80
0.3	6.43	6.67	6.78	6.86
0.4	6.52	6.78	6.88	6.97
0.5	6.59	6.85	6.94	7.03
0.75	6.70	6.95	7.03	7.11
1	6.77	7.01	7.09	7.15
1.5	6.90	7.13	7.17	7.22
2	6.99	7.19	7.22	7.26
3	7.11	7.28	7.30	7.30
4	7.19	7.36	7.35	7.36
5	7.24	7.41	7.40	7.39
7.5	7.30	7.53	7.53	7.52
10	7.35	7.58	7.59	7.59

Table 7. Mean distance for the four hazard levels for Site 1 including the Wilmington fault.

Period (sec)	72-year (OLE) Distance (km)	475-year (CLE) Distance (km)	975-year Distance (km)	2,475-year Distance (km)
0.01	27.17	10.58	7.74	5.61
0.02	26.94	10.39	7.62	5.53
0.03	26.90	10.57	7.80	5.71
0.04	26.60	10.80	7.84	5.94
0.05	26.82	11.51	8.45	6.45
0.075	26.92	12.20	9.33	7.62
0.1	26.71	12.75	10.05	7.85
0.15	26.67	12.78	10.39	7.93
0.2	27.71	13.18	9.99	7.47
0.25	28.85	13.29	9.55	7.15
0.3	30.13	13.57	9.49	6.97
0.4	33.09	14.23	9.74	6.78
0.5	35.86	15.09	10.50	6.68
0.75	40.94	16.76	10.79	6.57
1	43.22	17.56	10.52	6.47
1.5	49.48	20.21	12.23	6.60
2	53.00	22.23	12.65	7.07
3	58.91	24.98	15.05	7.59
4	62.39	28.48	17.27	9.42
5	65.02	31.46	20.75	11.78
7.5	74.61	42.46	33.02	24.73
10	80.04	49.69	42.11	34.15

Table 8. Mean epsilon for the four hazard levels for Site 1 including the Wilmington fault.

Period (sec)	72-year (OLE) Epsilon	475-year (CLE) Epsilon	975-year Epsilon	2,475-year Epsilon
0.01	0.148	0.607	0.867	1.230
0.02	0.146	0.605	0.868	1.233
0.03	0.176	0.649	0.909	1.267
0.04	0.211	0.694	0.957	1.303
0.05	0.249	0.746	1.001	1.328
0.075	0.316	0.863	1.112	1.400
0.1	0.358	0.917	1.153	1.465
0.15	0.346	0.914	1.144	1.450
0.2	0.306	0.832	1.071	1.393
0.25	0.284	0.758	0.999	1.323
0.3	0.288	0.710	0.936	1.247
0.4	0.284	0.634	0.847	1.165
0.5	0.296	0.603	0.804	1.132
0.75	0.300	0.539	0.718	1.052
1	0.276	0.473	0.651	0.994
1.5	0.230	0.424	0.602	0.965
2	0.180	0.394	0.568	0.930
3	0.090	0.356	0.536	0.897
4	-0.007	0.349	0.548	0.903
5	-0.076	0.362	0.582	0.931
7.5	-0.205	0.446	0.742	1.090
10	-0.311	0.435	0.761	1.163

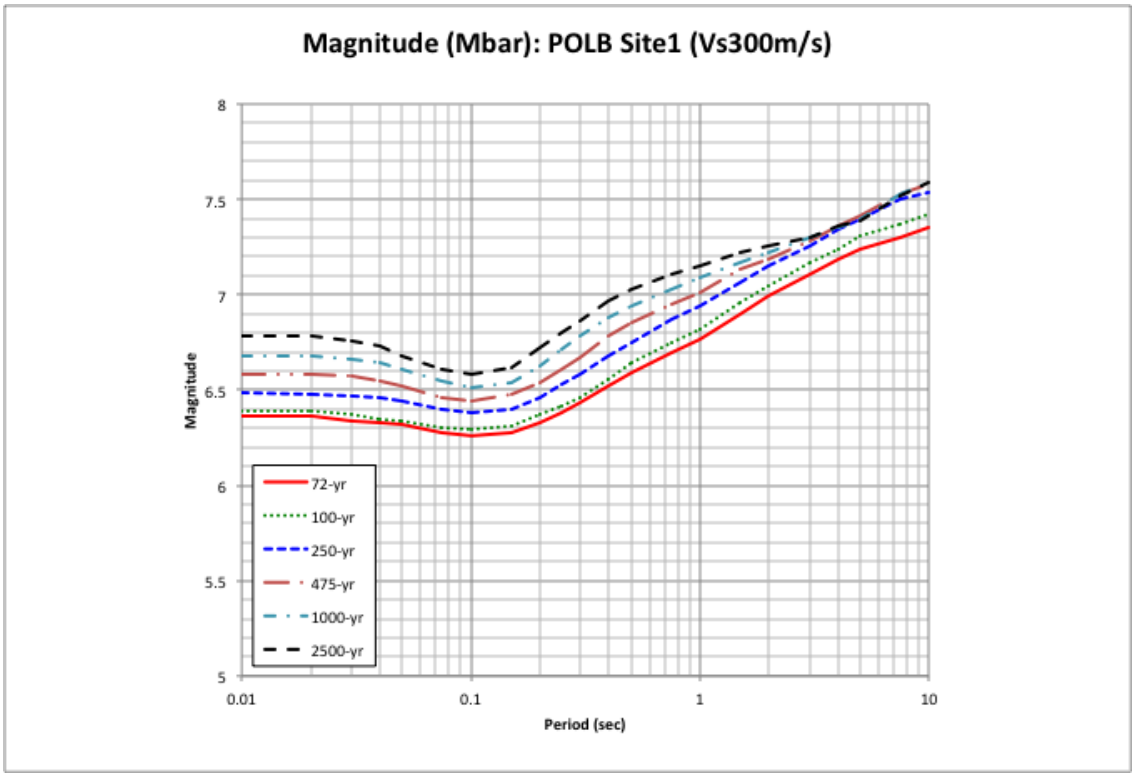


Figure 21. Horizontal mean magnitude for Site 1 including the Wilmington fault.

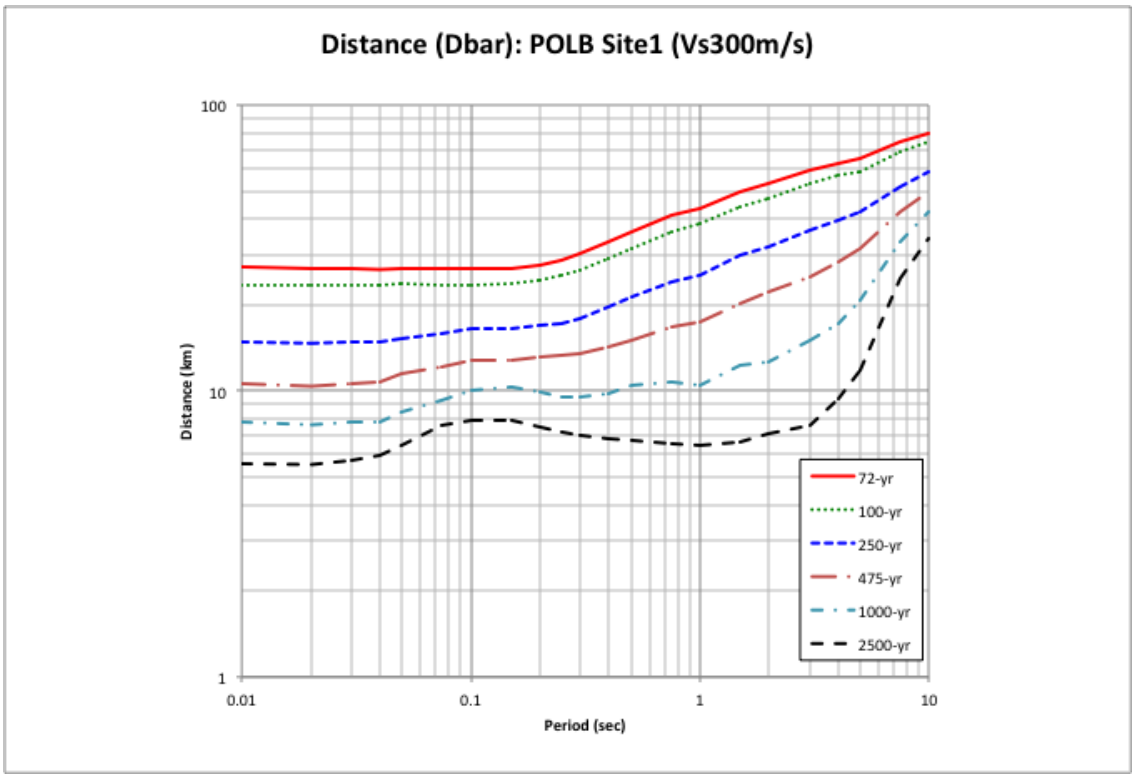


Figure 22. Horizontal mean distance for Site 1 including the Wilmington fault.

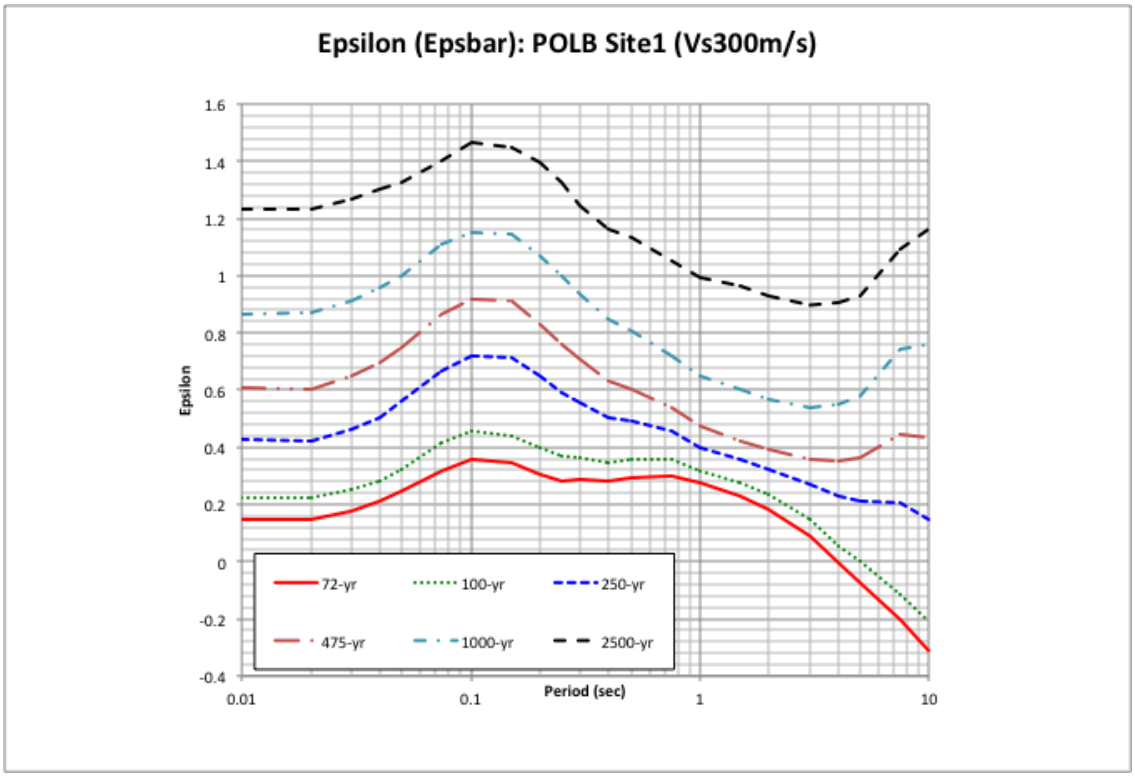


Figure 23. Horizontal mean epsilon for Site 1 including the Wilmington fault.

The binned magnitude and distance contributions including the Wilmington fault to the 72-year (OLE) hazard level are shown in Figures 24 to 28 for Site 1 for PGA and spectral periods of 0.2, 0.5, 1.0, and 2.0 sec. Similar plots are shown in Figures 29 to 33 for the 475-year (CLE) hazard level, Figures 34 to 38 for the 975-year hazard level, and Figures 39 to 43 for the 2,475-year hazard level. At the shortest return period level of 72-years (OLE), the hazard is being contributed to from small to moderate magnitude events over a broad distance of less than about 100 km. At the longer spectral periods a relative increase in the amount of contribution to the total hazard is observed for the larger magnitude (i.e., greater than 7.0) in the distance bin of 50 – 100 km. This corresponds to the contribution from the San Andreas fault. At the longer return period hazard levels, the relative contribution of the local Palos Verdes and Newport/Inglewood faults to the total hazard is observed in the deaggregation plots. Based on this increase in these local faults, the relative contribution from the San Andreas fault is decreased at the longer spectral periods. These results are similar to the results without the Wilmington fault and the same conclusions on the controlling seismic sources are applicable for both cases.

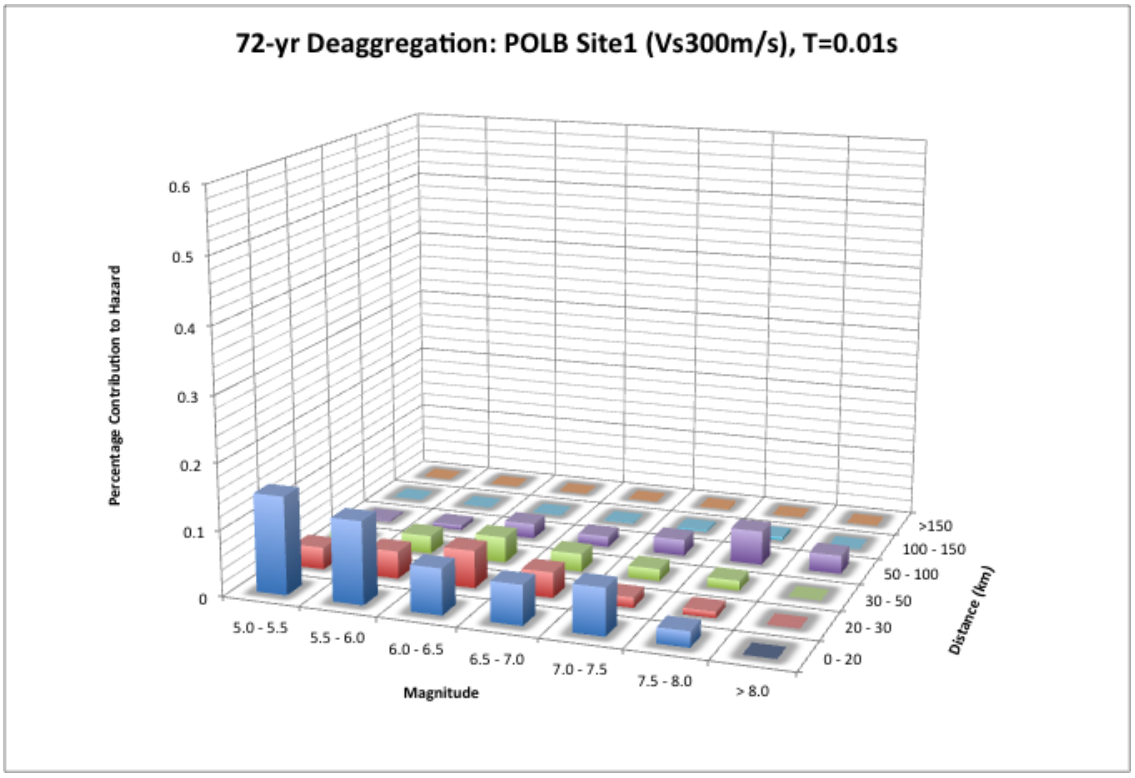


Figure 24. Magnitude-distance contribution for the 72-year (OLE) hazard level for PGA for Site 1 including the Wilmington fault.

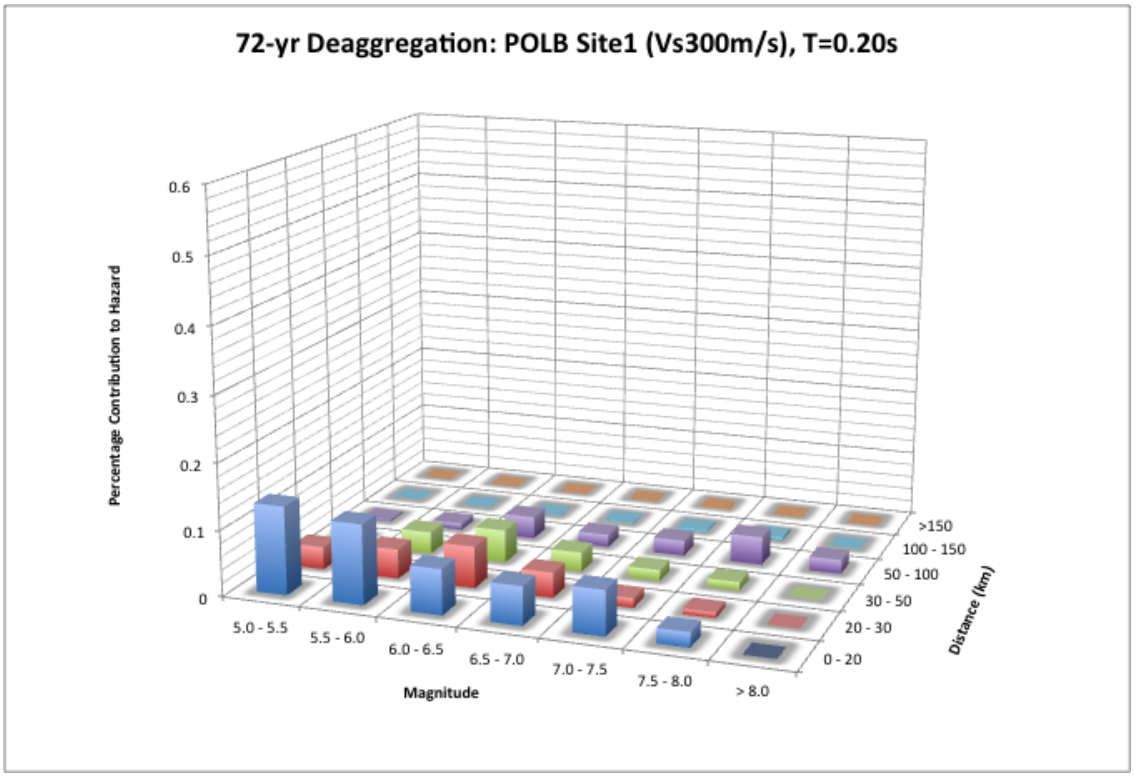


Figure 25. Magnitude-distance contribution for the 72-year (OLE) hazard level for T = 0.2 sec for Site 1 including the Wilmington fault.

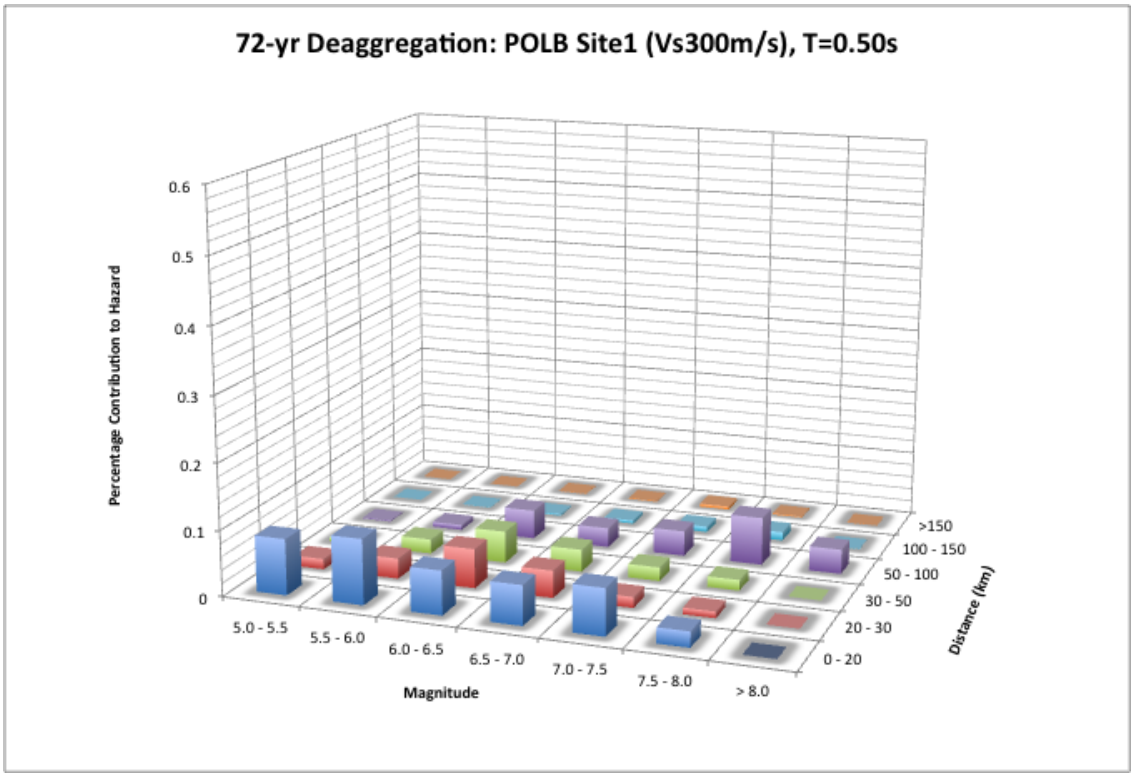


Figure 26. Magnitude-distance contribution for the 72-year (OLE) hazard level for T = 0.5 sec for Site 1 including the Wilmington fault.

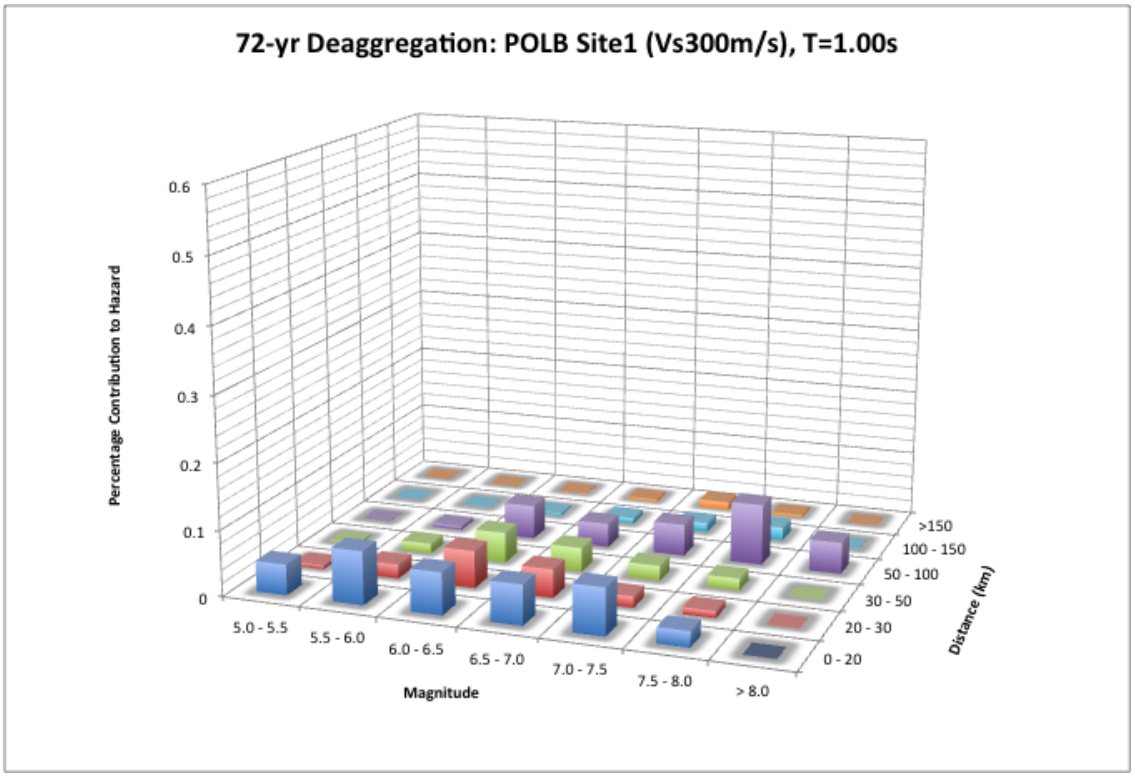


Figure 27. Magnitude-distance contribution for the 72-year (OLE) hazard level for T = 1.0 sec for Site 1 including the Wilmington fault.

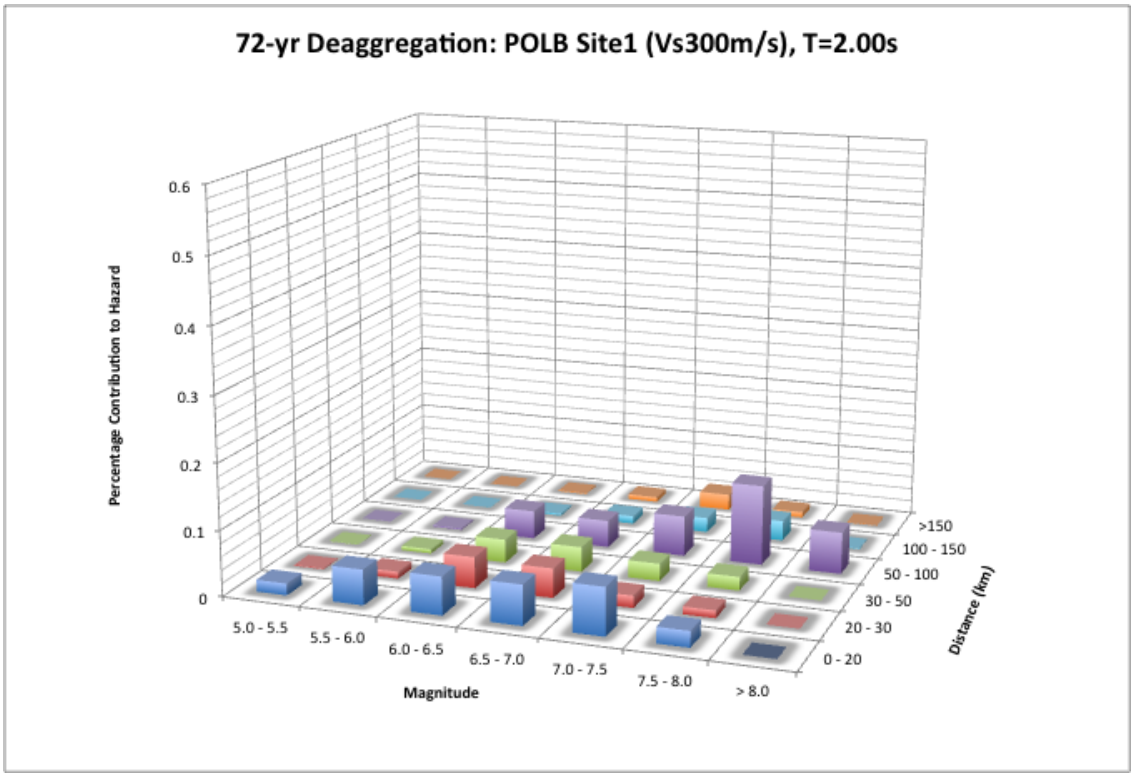


Figure 28. Magnitude-distance contribution for the 72-year (OLE) hazard level for T = 2.0 sec for Site 1 including the Wilmington fault.

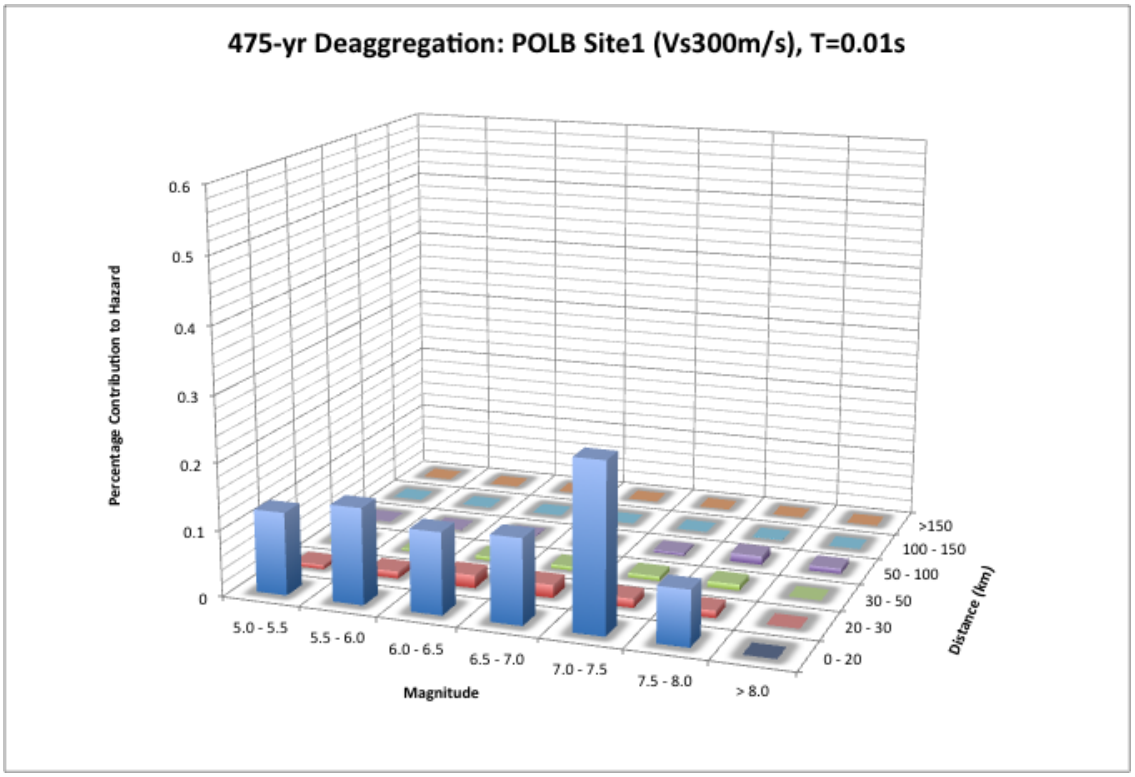


Figure 29. Magnitude-distance contribution for the 475-year (CLE) hazard level for PGA for Site 1 including the Wilmington fault.

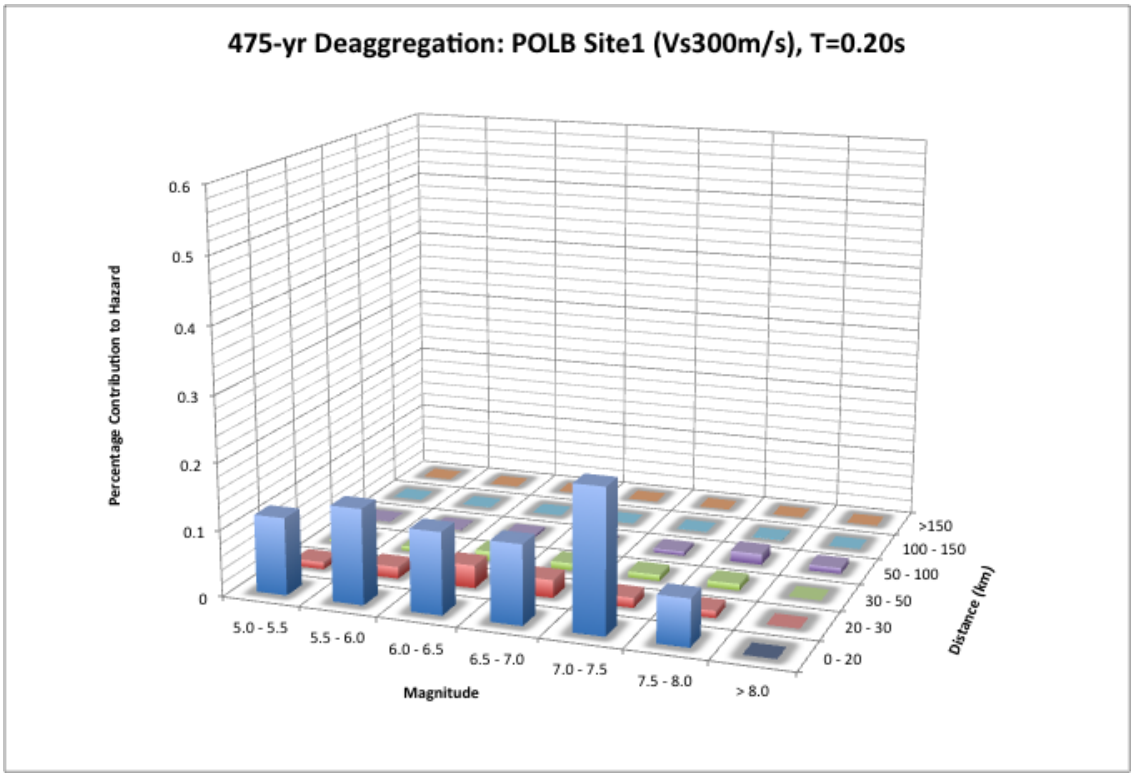


Figure 30. Magnitude-distance contribution for the 475-year (CLE) hazard level for T = 0.2 sec for Site 1 including the Wilmington fault.

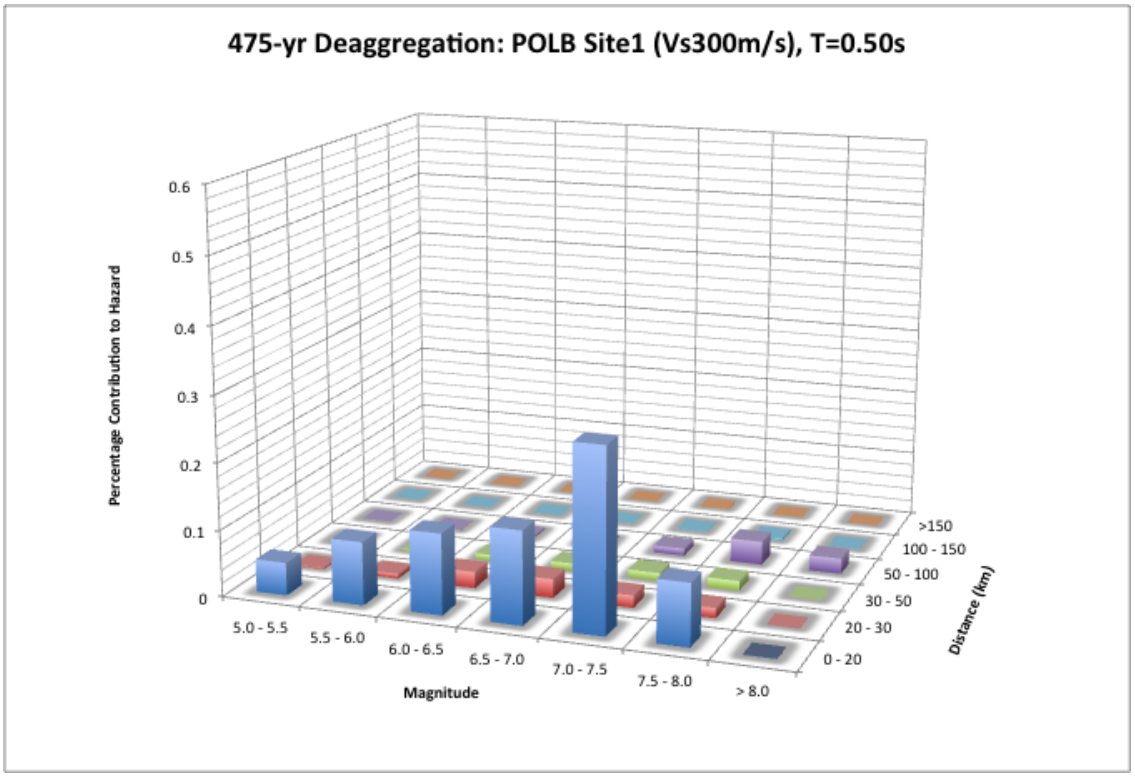


Figure 31. Magnitude-distance contribution for the 475-year (CLE) hazard level for T = 0.5 sec for Site 1 including the Wilmington fault.

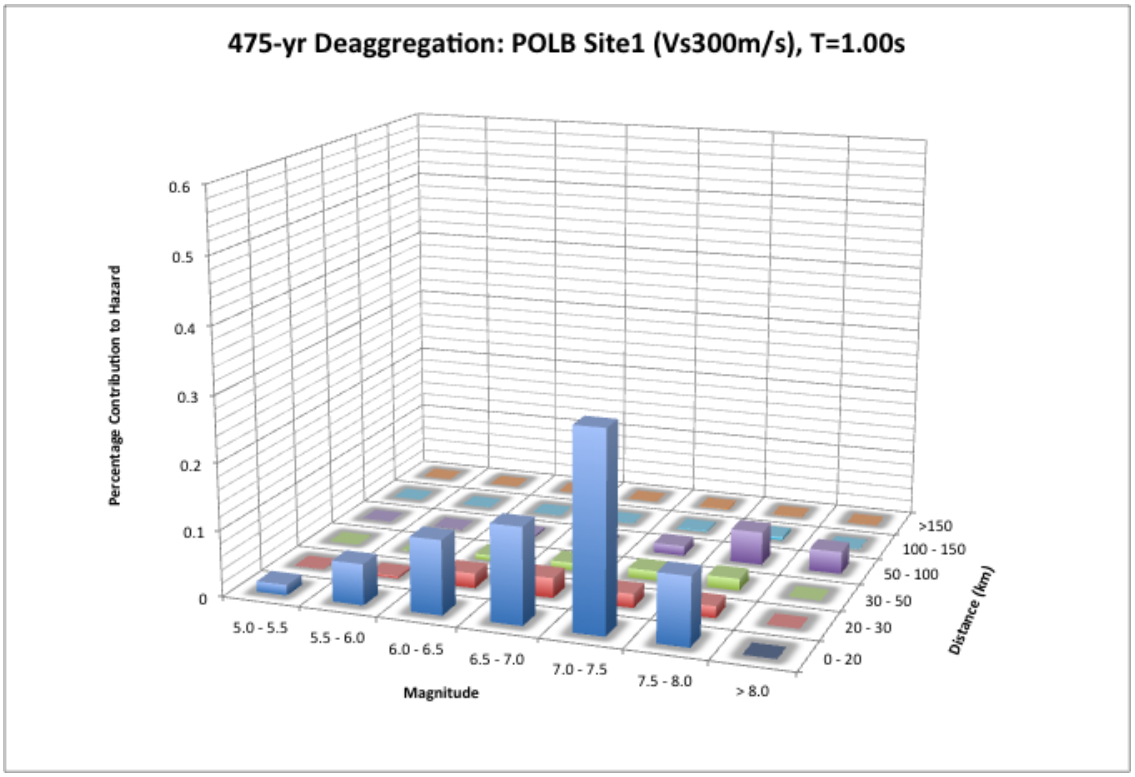


Figure 32. Magnitude-distance contribution for the 475-year (CLE) hazard level for T = 1.0 sec for Site 1 including the Wilmington fault.

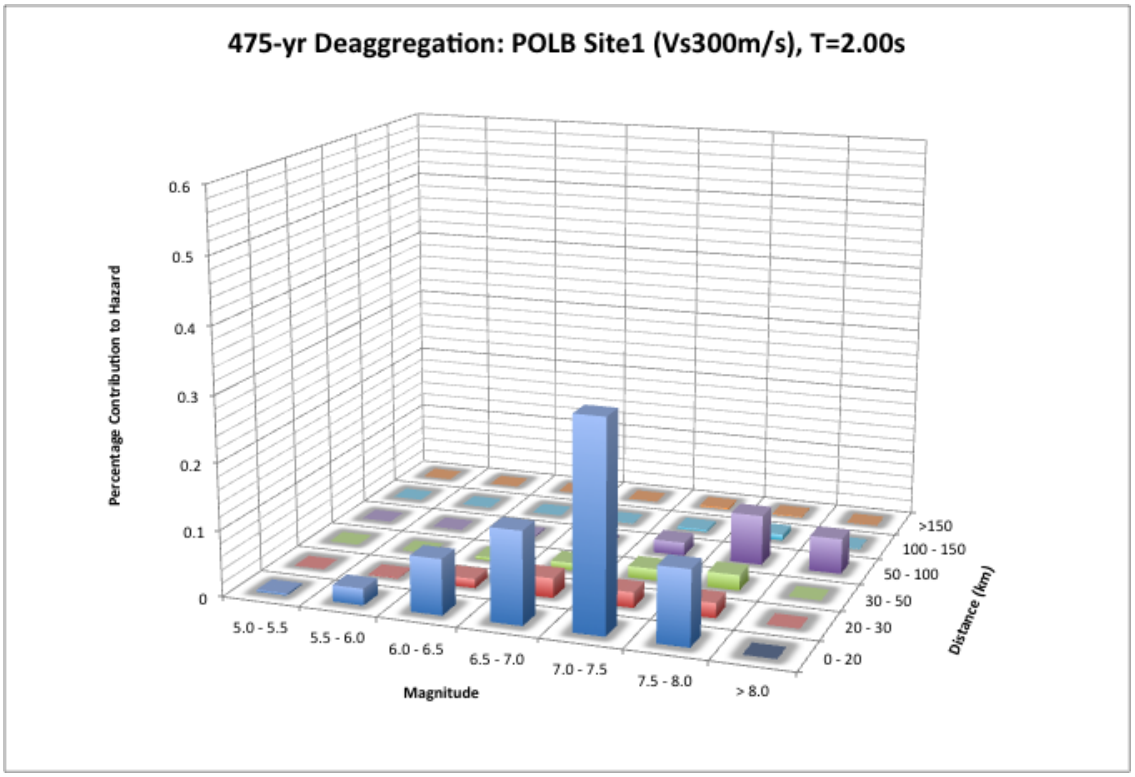


Figure 33. Magnitude-distance contribution for the 475-year (CLE) hazard level for T = 2.0 sec for Site 1 including the Wilmington fault.

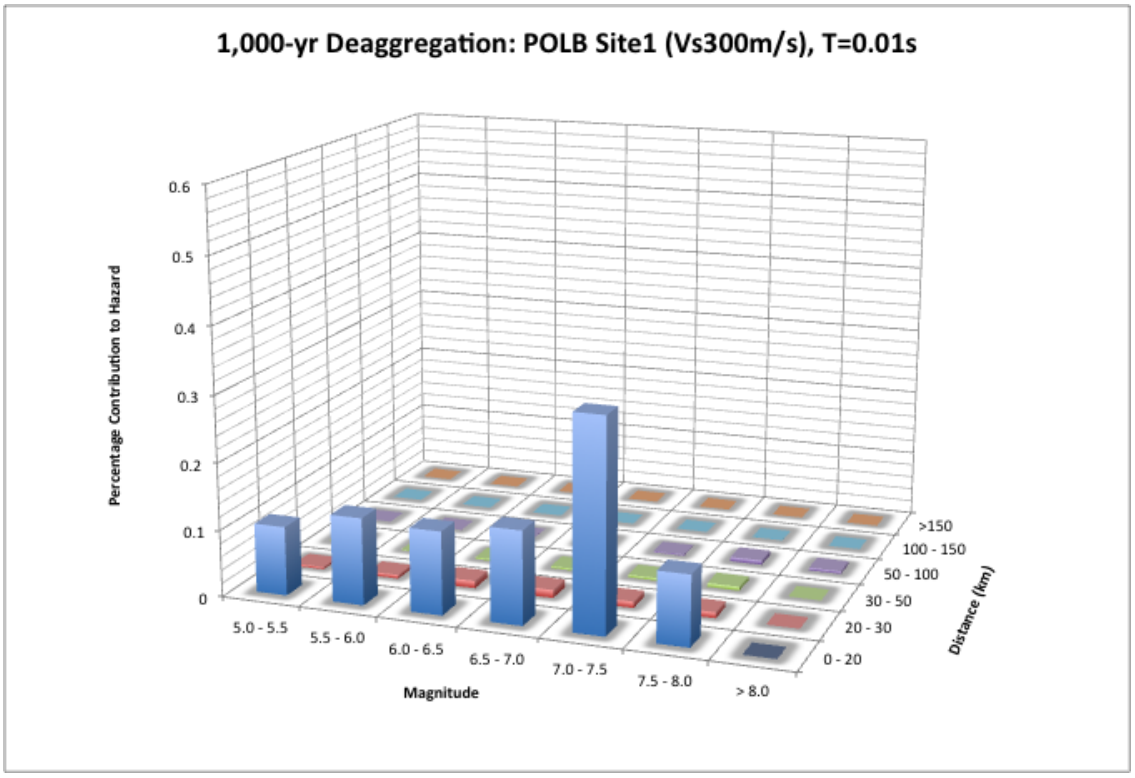


Figure 34. Magnitude-distance contribution for the 975-year hazard level for PGA for Site 1 including the Wilmington fault.

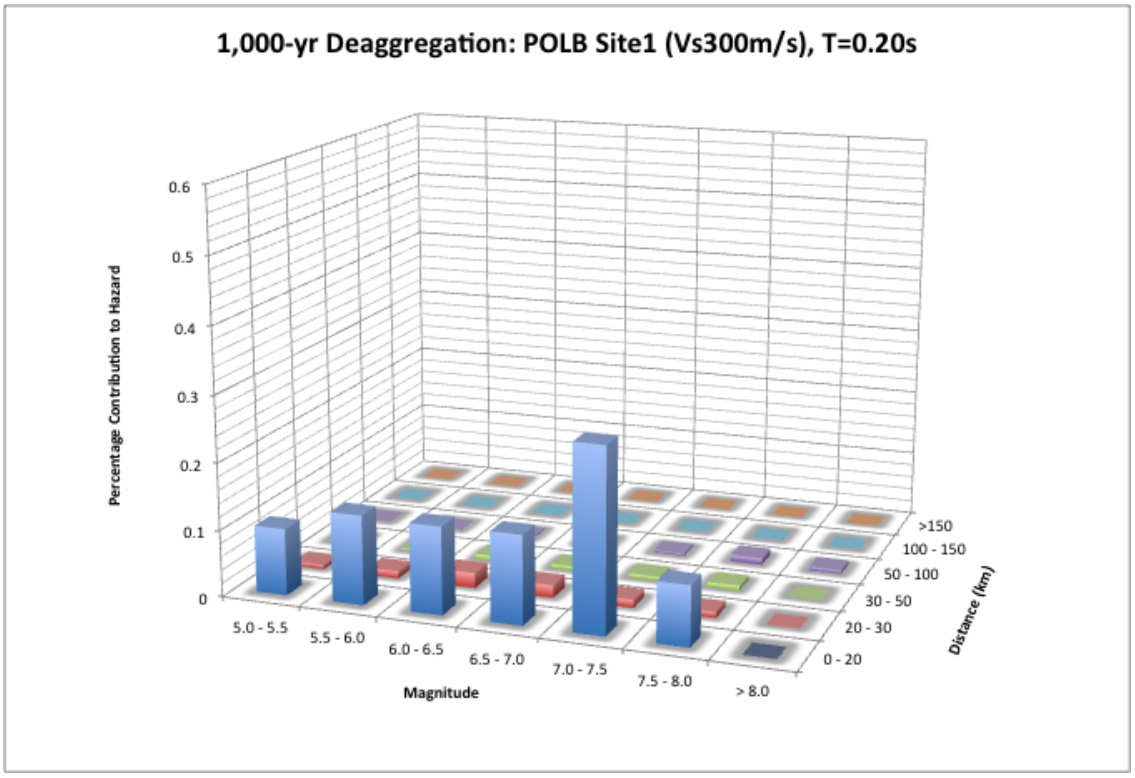


Figure 35. Magnitude-distance contribution for the 975-year hazard level for T = 0.2 sec for Site 1 including the Wilmington fault.

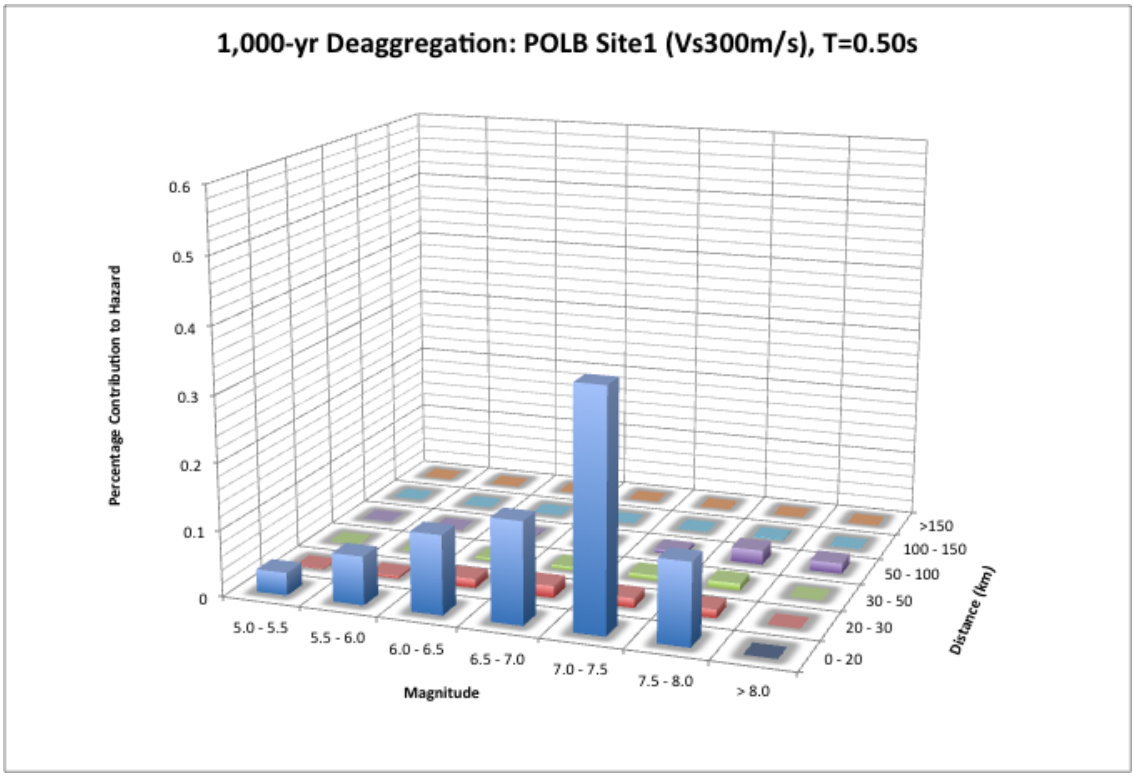


Figure 36. Magnitude-distance contribution for the 975-year hazard level for T = 0.5 sec for Site 1 including the Wilmington fault.

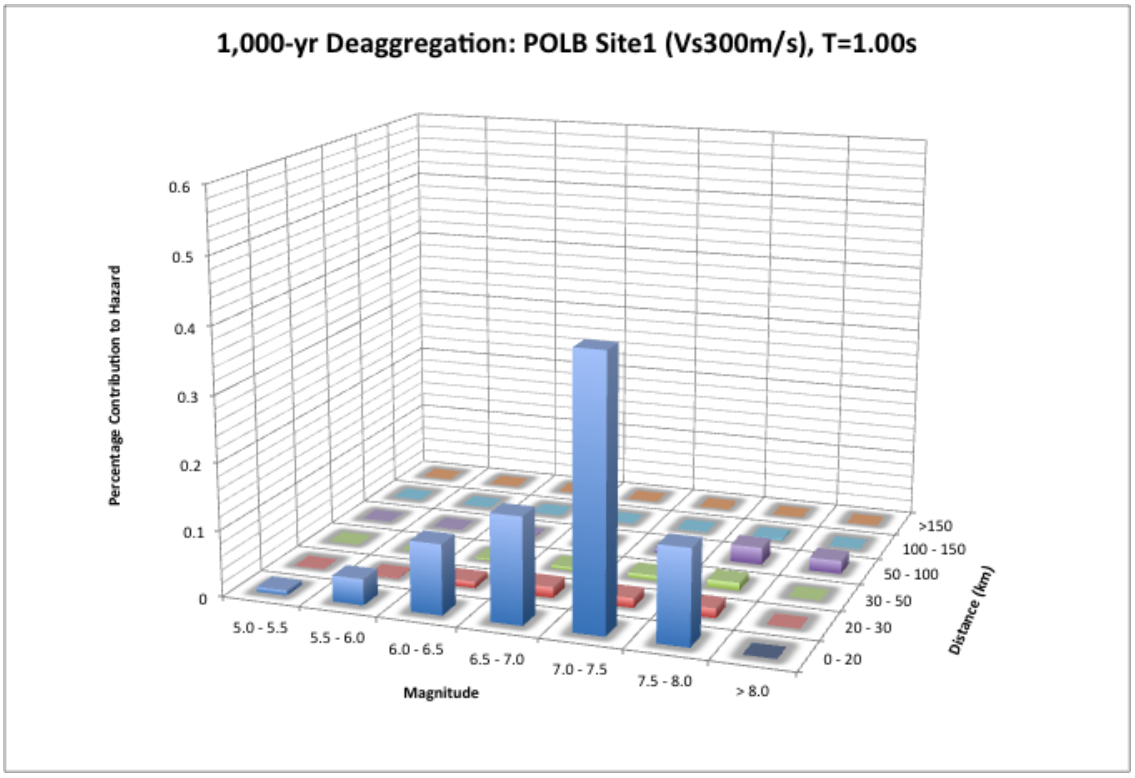


Figure 37. Magnitude-distance contribution for the 975-year hazard level for T = 1.0 sec for Site 1 including the Wilmington fault.

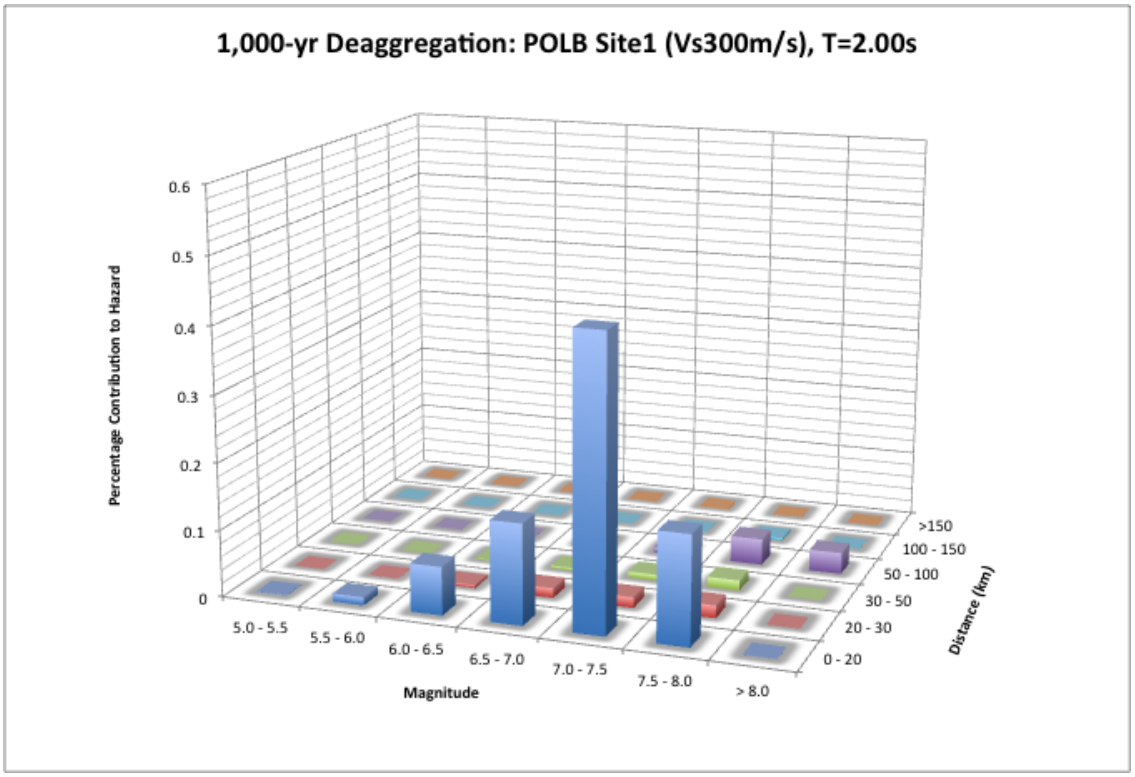


Figure 38. Magnitude-distance contribution for the 975-year hazard level for T = 2.0 sec for Site 1 including the Wilmington fault.

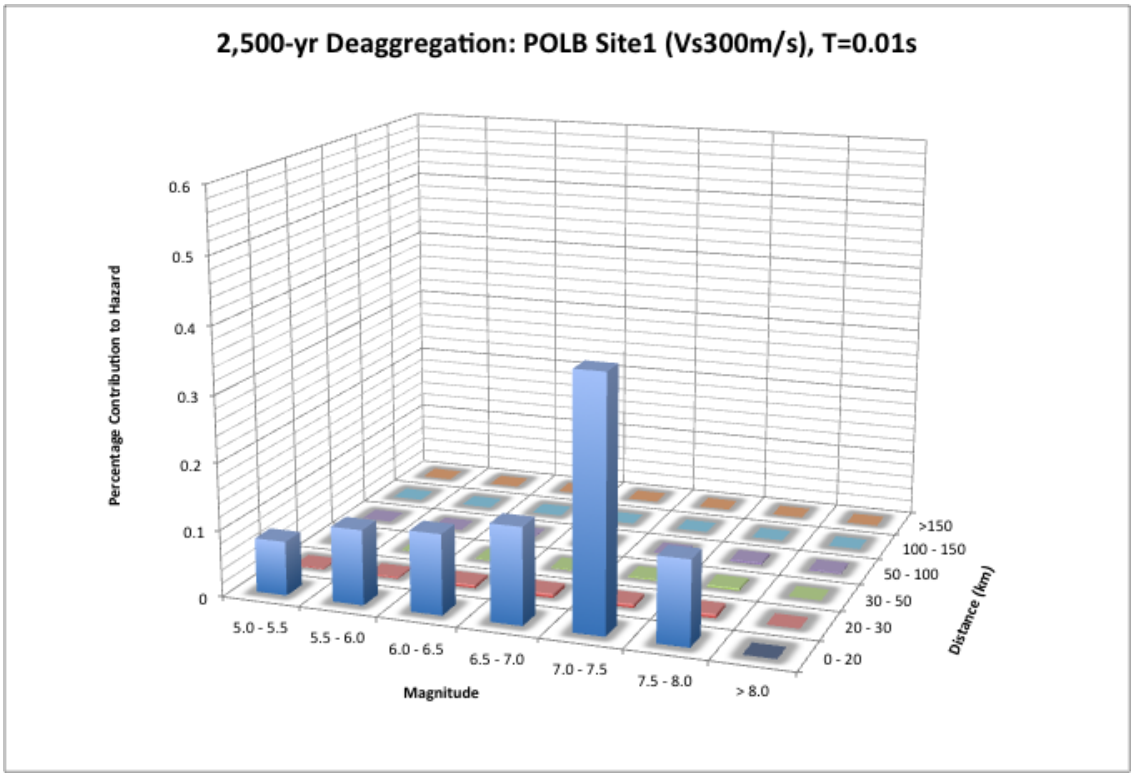


Figure 39. Magnitude-distance contribution for the 2,475-year hazard level for PGA for Site 1 including the Wilmington fault.

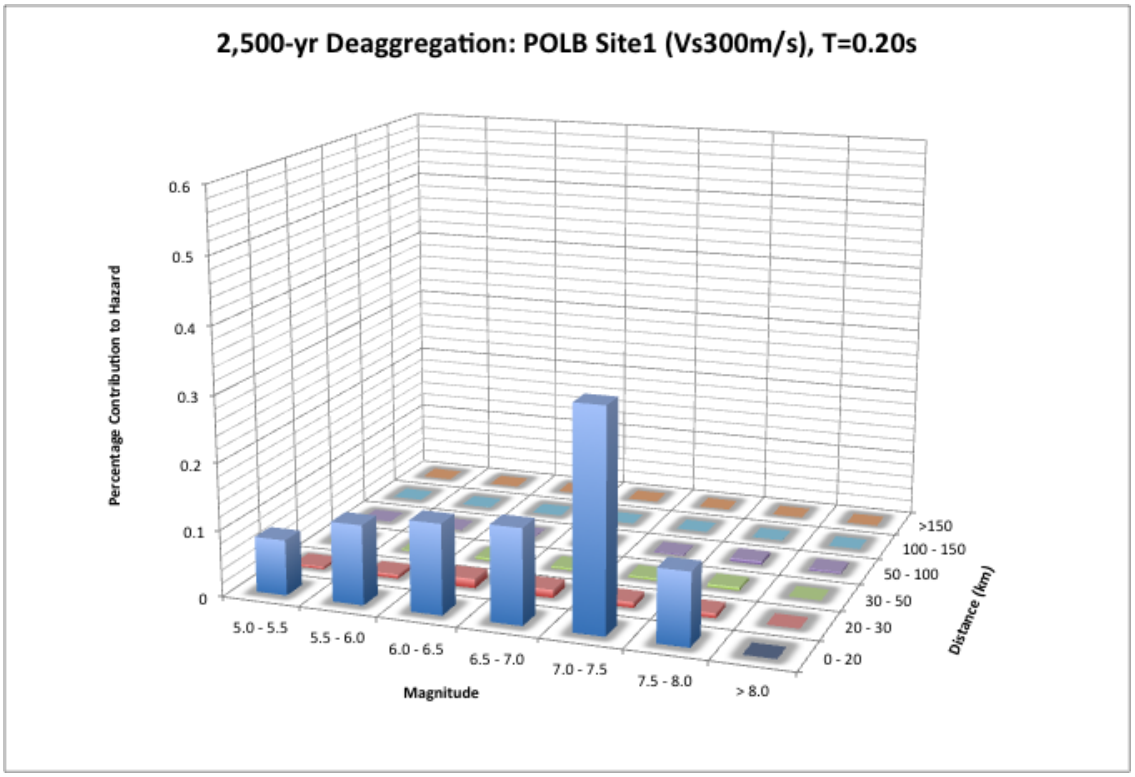


Figure 40. Magnitude-distance contribution for the 2,475-year hazard level for T = 0.2 sec for Site 1 including the Wilmington fault.

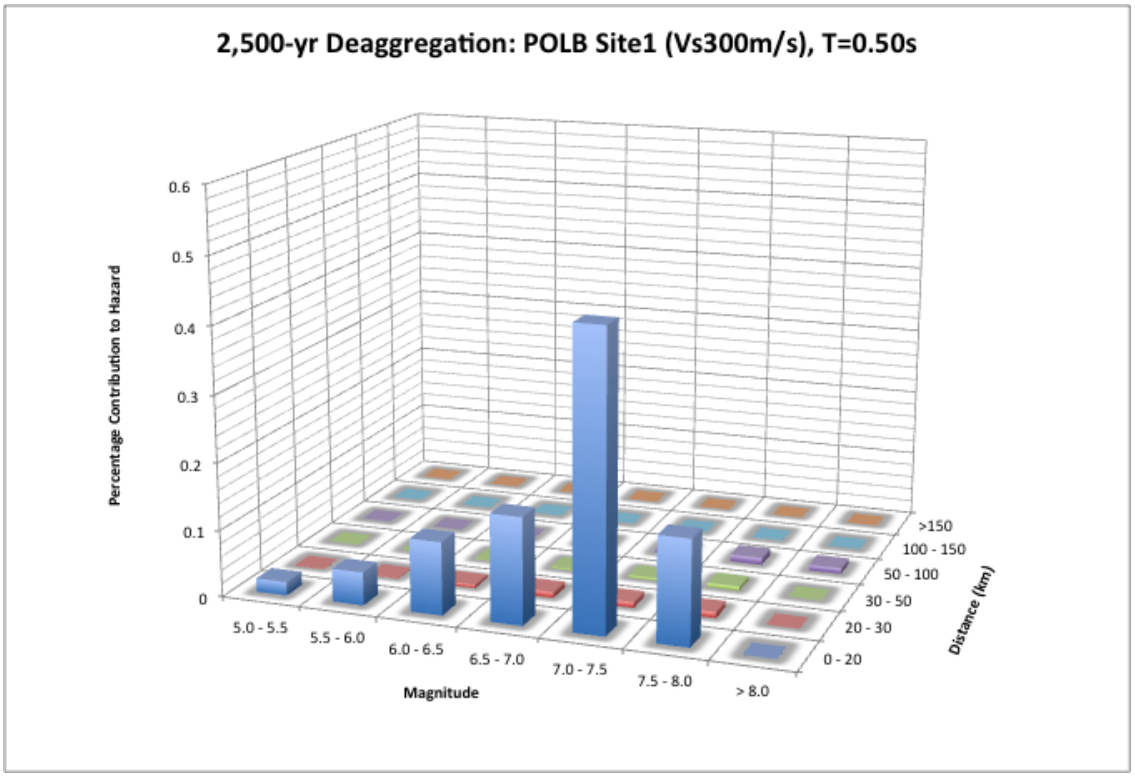


Figure 41. Magnitude-distance contribution for the 2,475-year hazard level for T = 0.5 sec for Site 1 including the Wilmington fault.

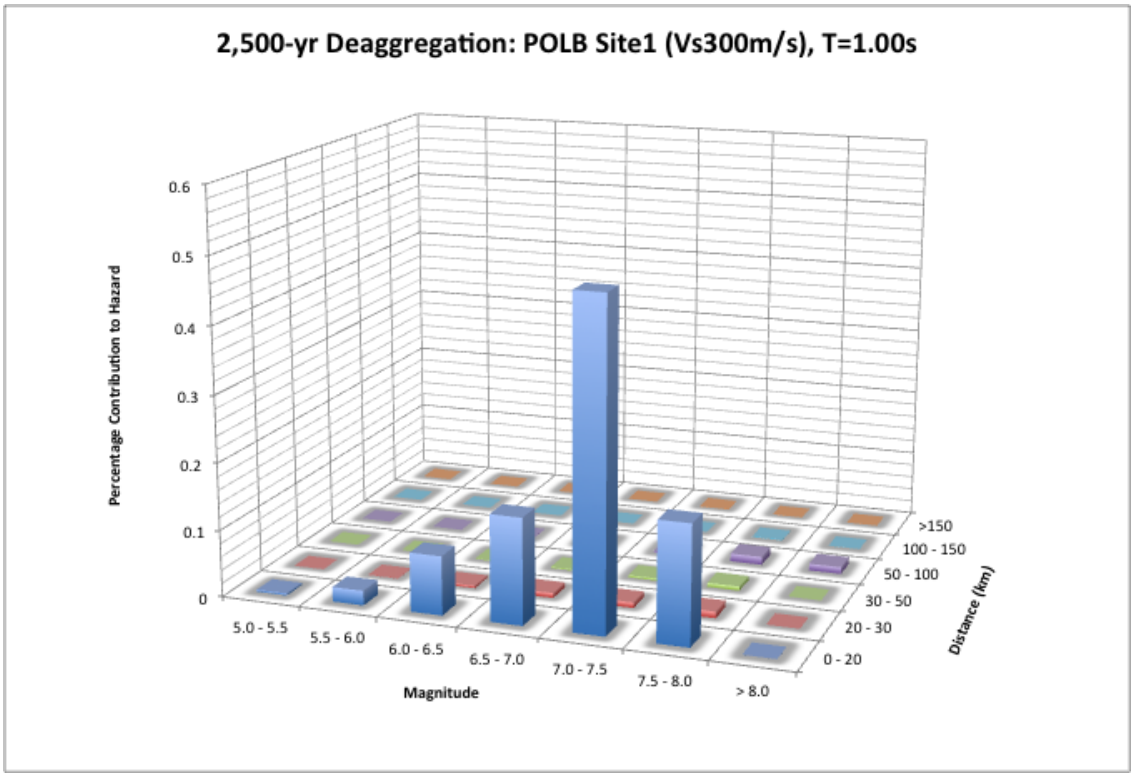


Figure 42. Magnitude-distance contribution for the 2,475-year hazard level for T = 1.0 sec for Site 1 including the Wilmington fault.

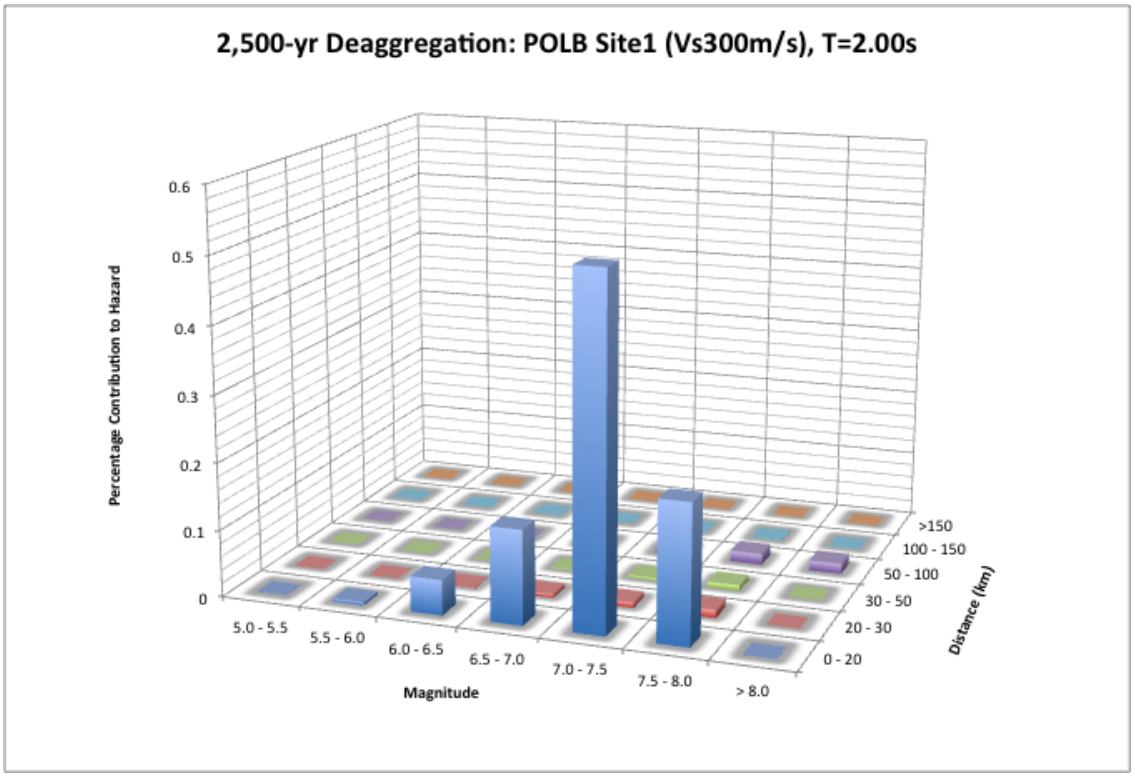


Figure 43. Magnitude-distance contribution for the 2,475-year hazard level for T = 2.0 sec for Site 1 including the Wilmington fault.

4.3 Site 3 – Horizontal

The mean hazard curves including the Wilmington fault for Site 3 are shown in Figures 44 through 48 for PGA and spectral periods of 0.2, 0.5, 1.0, and 2.0 sec. For the longer spectral periods (i.e., 1 and 2 sec) these plots are showing the horizontal component without the inclusion of the directivity model. In these plots, individual hazard curves from the scenario fault ruptures, gridded sources, the Wilmington fault, and the combined total hazard are presented. For the 72-year return period (OLE) hazard level, the hazard curve plots indicate that the hazard is primarily controlled by the contribution from the gridded point sources and to a lesser amount the contribution from the fault sources. At the 475-year (CLE) hazard level the contribution from the fault sources increases relative to the contribution form the gridded point sources. At the lower hazard levels of 975-year and 2,475-year return periods, the results indicate an increase in the relative contribution from the fault sources over the gridded point sources. As was observed for the Site 1 results, the contribution from the Wilmington fault is not significant to the total hazard.

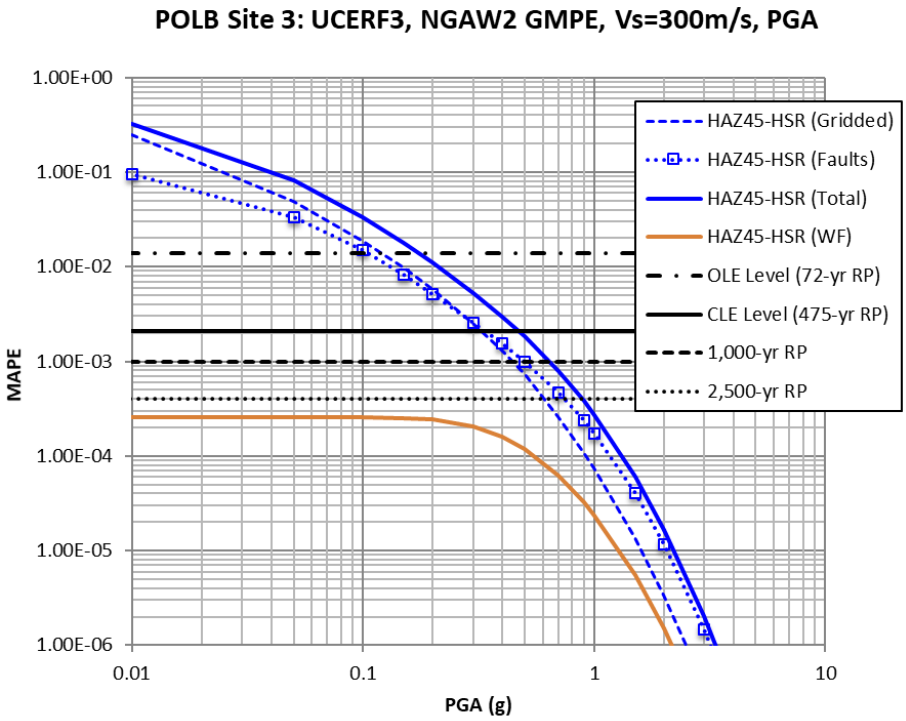


Figure 44. Mean horizontal component hazard curves from the UCERF3 gridded and fault sources, the Wilmington fault, and total hazard for PGA for Site 3.

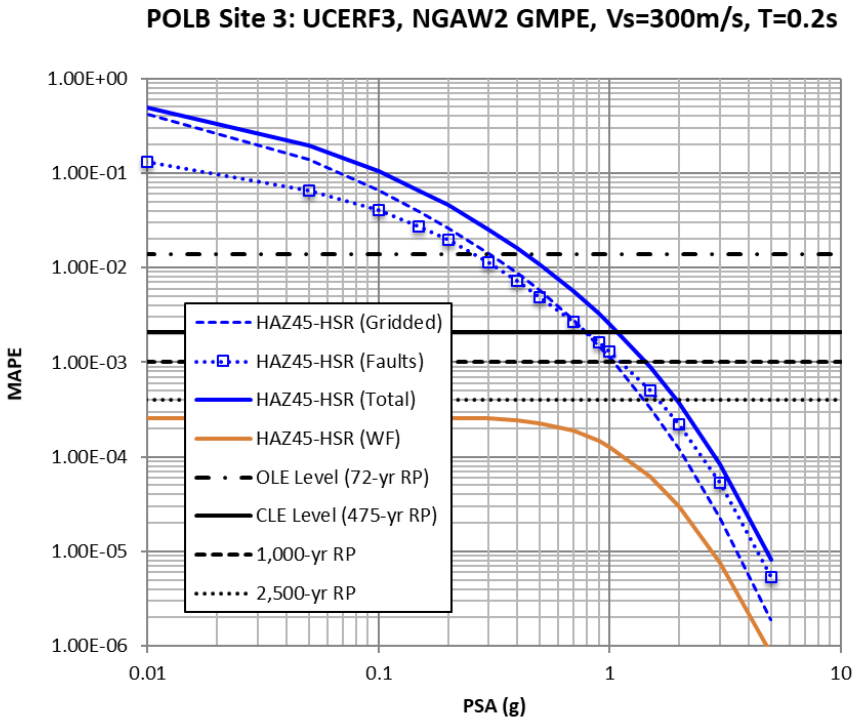


Figure 45. Mean horizontal component hazard curves from the UCERF3 gridded and fault sources, the Wilmington fault, and total hazard for T = 0.2 sec for Site 3.

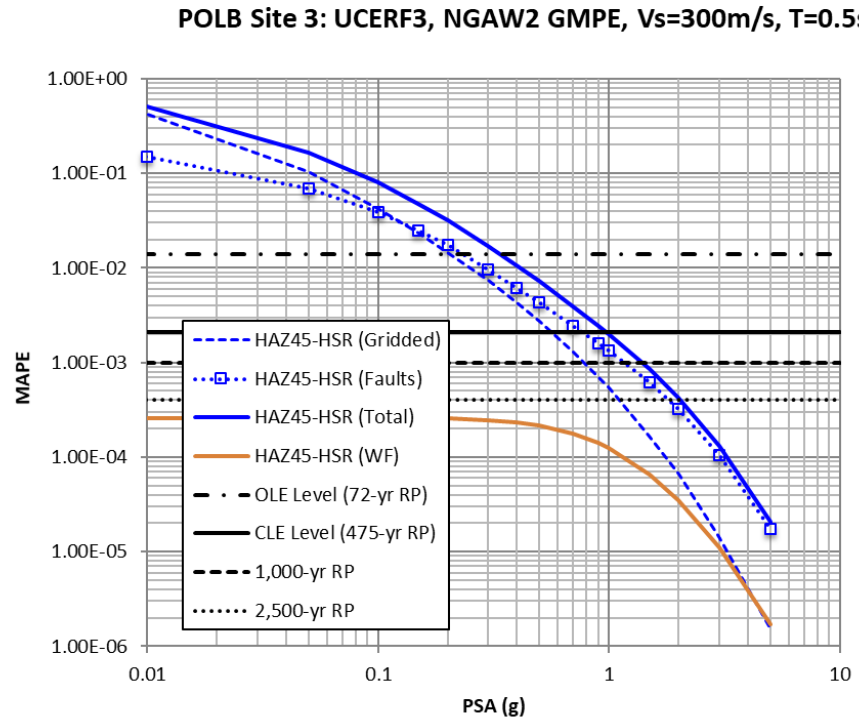


Figure 46. Mean horizontal component hazard curves from the UCERF3 gridded and fault sources, the Wilmington fault, and total hazard for T = 0.5 sec for Site 3.

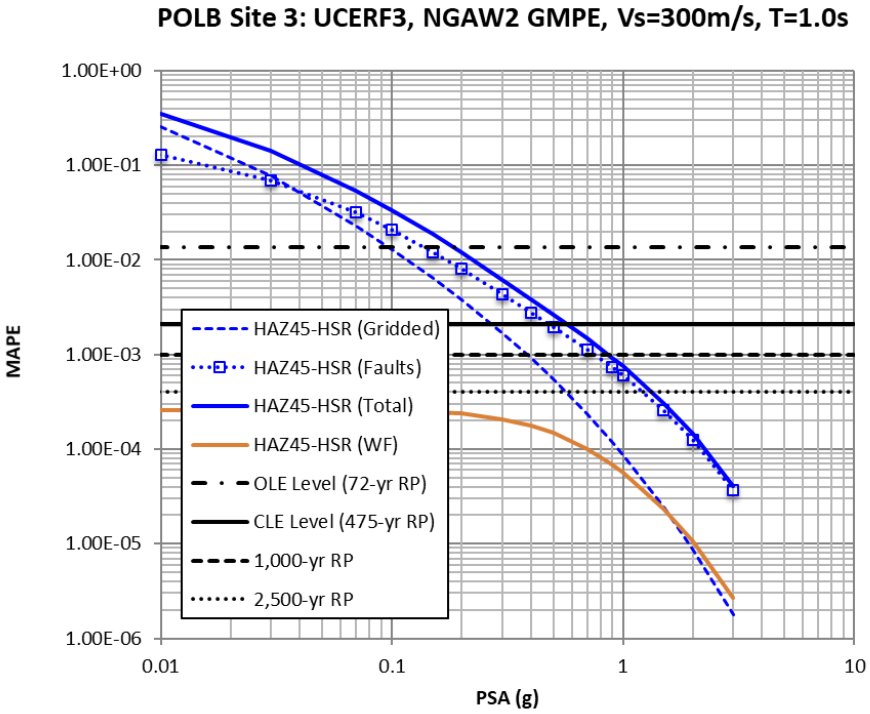


Figure 47. Mean horizontal component hazard curves from the UCERF3 gridded and fault sources, the Wilmington fault, and total hazard for T = 1.0 sec for Site 3.

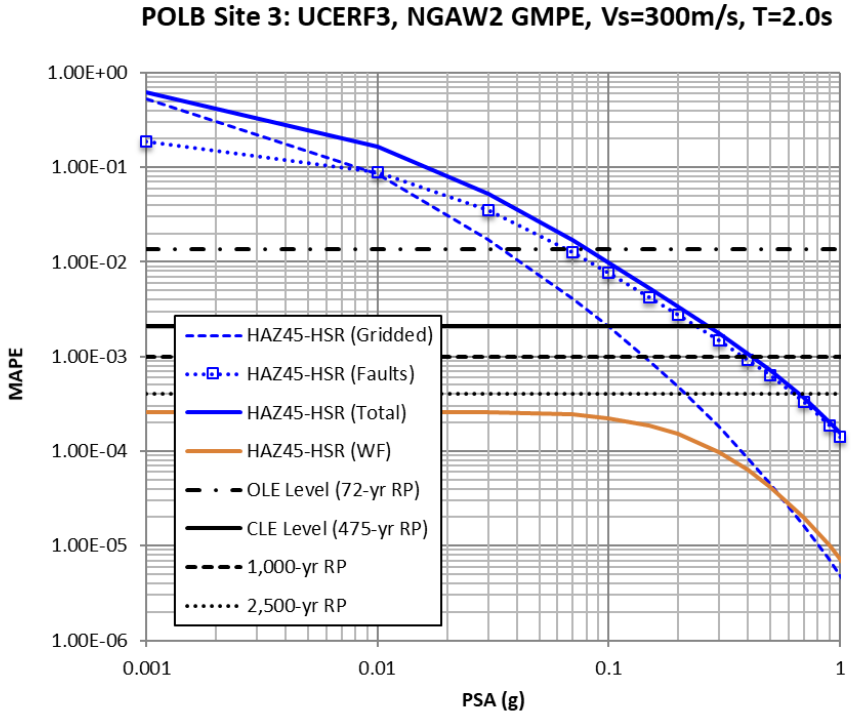


Figure 48. Mean horizontal component hazard curves from the UCERF3 gridded and fault sources, the Wilmington fault, and total hazard for T = 2.0 sec for Site 3.

Given the hazard curves with the inclusion of the Wilmington fault for the full suite of spectral periods, the computed uniform hazard spectra (UHS) for the 72-year (OLE), 475-year (CLE), 975-year and 2,475-year return period hazard levels are plotted in Figure 49. The horizontal UHS values at all spectral periods are given in Table 9. Similar increase in the ground motions on the order of 3-4% or less is observed for Site 3 for the inclusion of the Wilmington fault.

Table 9. Horizontal UHS for Site 3 at the four hazard levels including the Wilmington fault.

Period (sec)	72-year (OLE) Horizontal PSA (g)	475-year (CLE) Horizontal PSA (g)	975-year Horizontal PSA (g)	2,475-year Horizontal PSA (g)
0.01	0.1753	0.4690	0.6379	0.8853
0.02	0.1750	0.4701	0.6395	0.8871
0.03	0.1819	0.4855	0.6585	0.9109
0.04	0.1966	0.5182	0.7038	0.9671
0.05	0.2125	0.5559	0.7538	1.0376
0.075	0.2699	0.6933	0.9303	1.2653
0.1	0.3283	0.8214	1.0900	1.4932
0.15	0.4042	0.9953	1.3023	1.7615
0.2	0.4331	1.0796	1.4401	1.9538
0.25	0.4363	1.1174	1.5174	2.0767
0.3	0.4266	1.1232	1.5475	2.1519
0.4	0.3818	1.0562	1.4923	2.1352
0.5	0.3405	0.9709	1.3850	2.0359
0.75	0.2446	0.7338	1.0808	1.6424
1	0.1821	0.5685	0.8613	1.3314
1.5	0.1151	0.3740	0.5744	0.9154
2	0.0800	0.2678	0.4173	0.6689
3	0.0475	0.1662	0.2600	0.4228
4	0.0318	0.1147	0.1789	0.2874
5	0.0225	0.0845	0.1310	0.2094
7.5	0.0120	0.0480	0.0727	0.1113
10	0.0073	0.0308	0.0461	0.0704

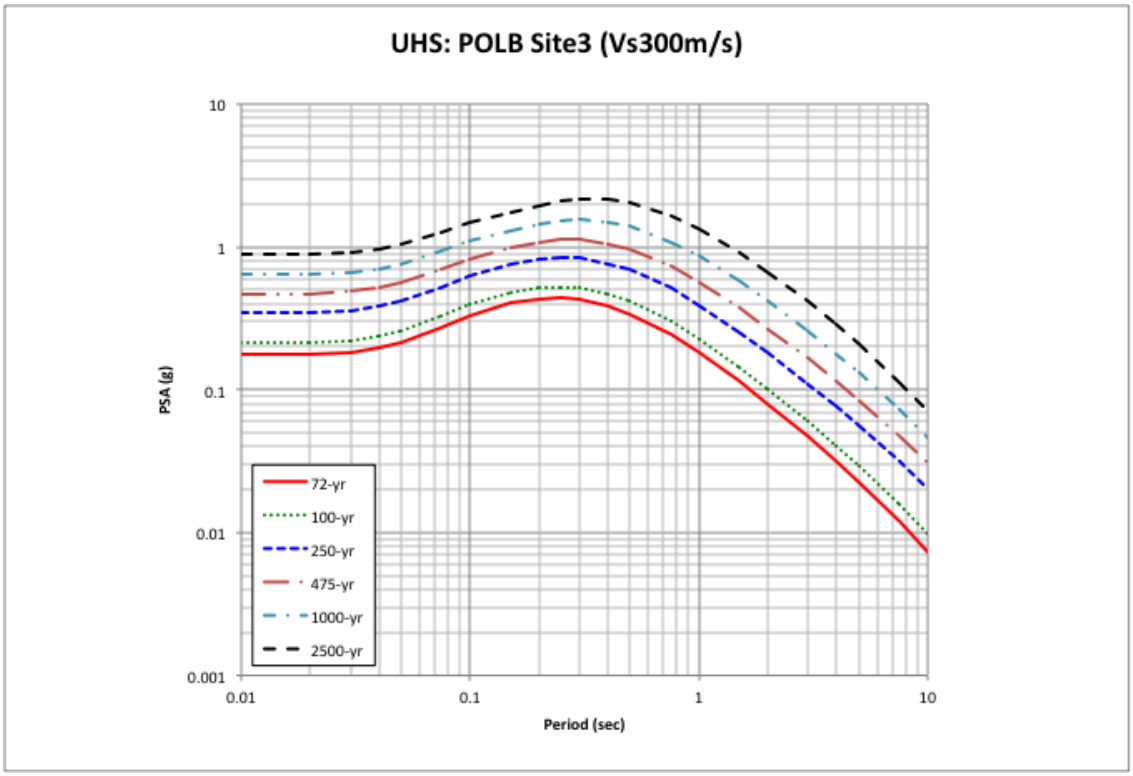


Figure 49. Uniform hazard spectra for Site 3 including the Wilmington fault.

The mean magnitude, distance and epsilon values for the horizontal component including the Wilmington fault but without the directivity model are plotted in Figures 50 to 52 for the four hazard levels. These plots are shown as a function of spectral period. As expected, the magnitude increases and the distance decreases with the increasing return period hazard levels. Also observed in these plots is the expected increase in the mean epsilon values between the four hazard levels with the 2,475-year results greater than approximately 1 over the full spectral period range. The mean magnitude, distance and epsilon values are listed in Tables 10 through 12 for the four hazard levels. Similar to the results for Site 1, these mean values are in close agreement for the two cases in which the Wilmington fault was or was not considered.

Table 10. Mean magnitude for the four hazard levels for Site 3 including the Wilmington fault.

Period (sec)	72-year (OLE) Magnitude	475-year (CLE) Magnitude	975-year Magnitude	2,475-year Magnitude
0.01	6.36	6.58	6.67	6.76
0.02	6.36	6.58	6.67	6.77
0.03	6.35	6.56	6.65	6.74
0.04	6.33	6.54	6.63	6.71
0.05	6.32	6.52	6.60	6.67
0.075	6.28	6.47	6.54	6.59
0.1	6.26	6.44	6.50	6.57
0.15	6.28	6.48	6.54	6.62
0.2	6.33	6.54	6.63	6.70
0.25	6.38	6.60	6.70	6.79
0.3	6.43	6.66	6.77	6.85
0.4	6.52	6.77	6.88	6.96
0.5	6.58	6.84	6.93	7.02
0.75	6.70	6.95	7.02	7.10
1	6.76	7.01	7.08	7.14
1.5	6.90	7.12	7.17	7.22
2	6.99	7.19	7.22	7.26
3	7.11	7.28	7.29	7.30
4	7.19	7.36	7.35	7.36
5	7.24	7.41	7.40	7.40
7.5	7.30	7.53	7.53	7.53
10	7.35	7.58	7.60	7.60

Table 11. Mean distance for the four hazard levels for Site 3 including the Wilmington fault.

Period (sec)	72-year (OLE) Distance (km)	475-year (CLE) Distance (km)	975-year Distance (km)	2,475-year Distance (km)
0.01	26.82	10.49	7.81	5.81
0.02	26.65	10.35	7.70	5.74
0.03	26.49	10.49	7.87	5.92
0.04	26.27	10.81	7.92	6.15
0.05	26.57	11.44	8.52	6.64
0.075	26.60	12.04	9.37	7.74
0.1	26.46	12.70	10.11	7.94
0.15	26.44	12.66	10.38	8.04
0.2	27.44	13.11	9.98	7.60
0.25	28.48	13.22	9.61	7.33
0.3	29.76	13.49	9.57	7.17
0.4	32.66	14.13	9.73	7.01
0.5	35.37	14.90	10.50	6.94
0.75	40.45	16.59	10.92	6.86
1	42.60	17.41	10.60	6.78
1.5	48.79	19.87	12.28	6.96
2	52.30	21.82	12.75	7.41
3	58.06	24.60	15.12	8.01
4	61.64	28.15	17.39	9.88
5	64.25	31.06	20.85	12.28
7.5	73.81	42.02	32.96	25.04
10	79.23	49.33	41.96	34.42

Table 12. Mean epsilon for the four hazard levels for Site 3 including the Wilmington fault.

Period (sec)	72-year (OLE) Epsilon	475-year (CLE) Epsilon	975-year Epsilon	2,475-year Epsilon
0.01	0.142	0.617	0.885	1.249
0.02	0.140	0.615	0.886	1.261
0.03	0.171	0.659	0.927	1.284
0.04	0.206	0.703	0.973	1.321
0.05	0.243	0.753	1.015	1.345
0.075	0.312	0.870	1.120	1.413
0.1	0.354	0.923	1.160	1.475
0.15	0.341	0.921	1.152	1.457
0.2	0.301	0.838	1.088	1.411
0.25	0.279	0.765	1.010	1.339
0.3	0.283	0.717	0.951	1.273
0.4	0.278	0.643	0.864	1.181
0.5	0.289	0.612	0.821	1.156
0.75	0.294	0.548	0.740	1.081
1	0.271	0.484	0.674	1.025
1.5	0.224	0.434	0.624	0.995
2	0.174	0.403	0.591	0.964
3	0.085	0.367	0.560	0.926
4	-0.012	0.361	0.571	0.931
5	-0.080	0.372	0.602	0.955
7.5	-0.207	0.456	0.754	1.104
10	-0.312	0.442	0.770	1.175

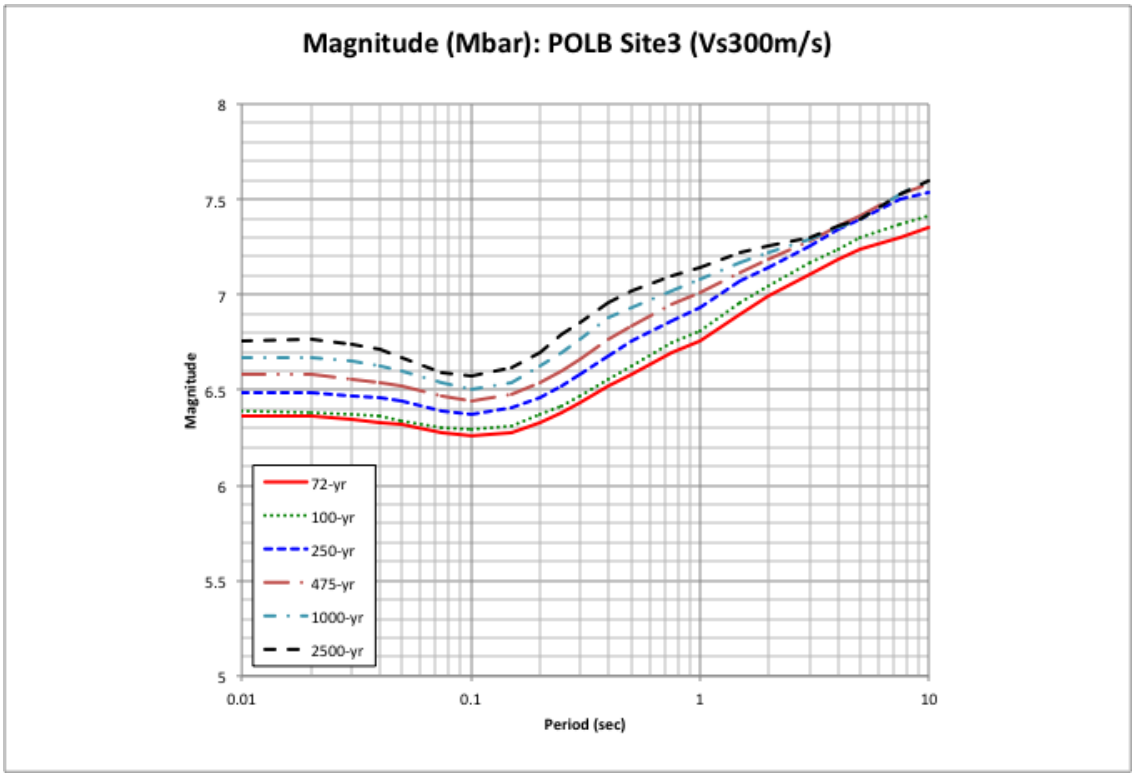


Figure 50. Horizontal mean magnitude for Site 3 including the Wilmington fault.

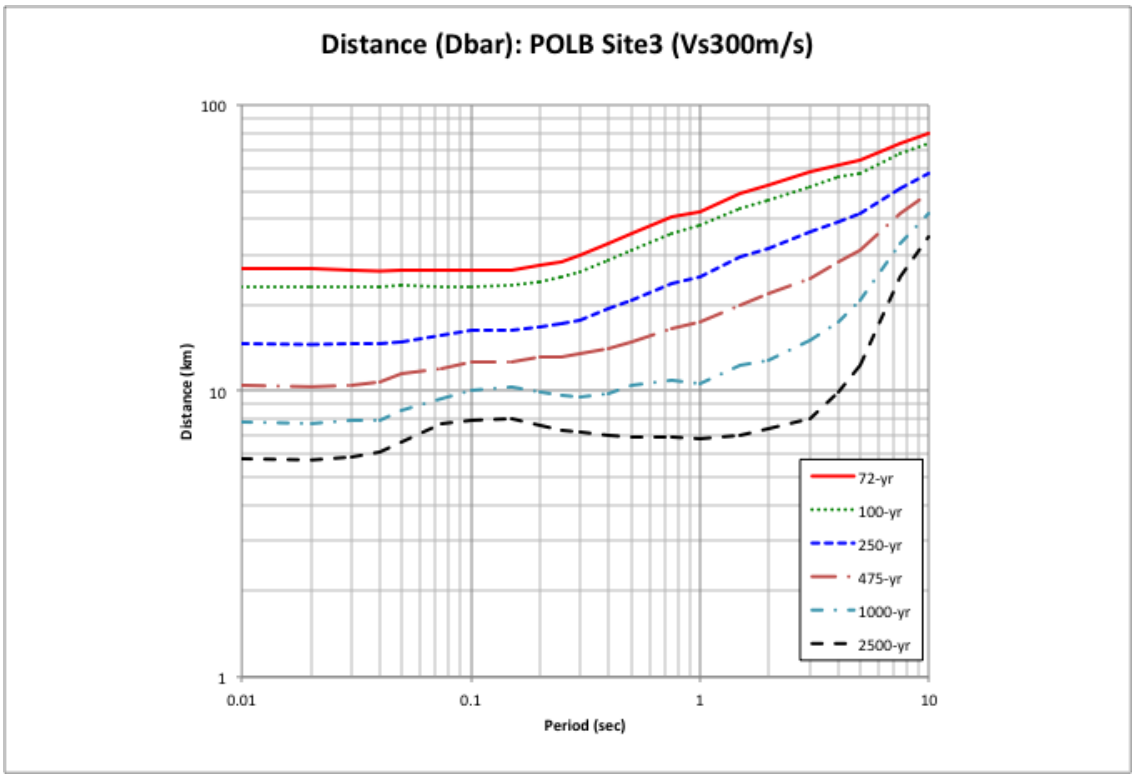


Figure 51. Horizontal mean distance for Site 3 including the Wilmington fault.

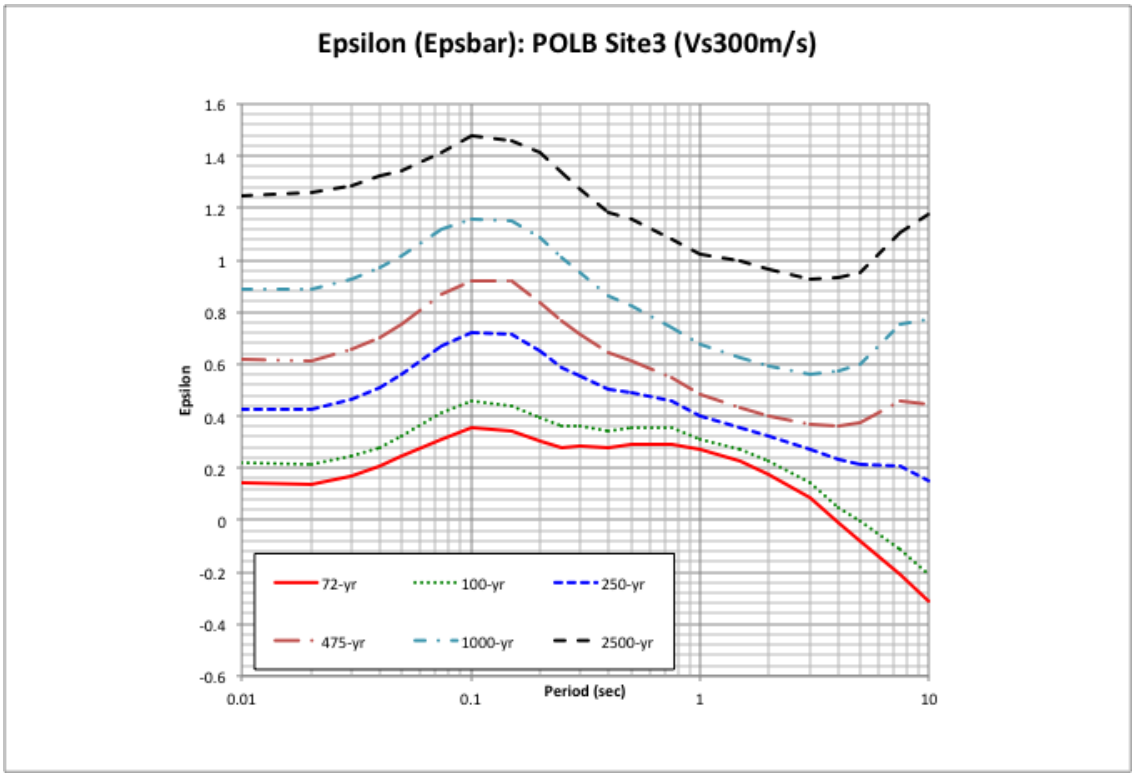


Figure 52. Horizontal mean epsilon for Site 3 including the Wilmington fault.

The binned magnitude and distance contributions to the 72-year (OLE) hazard level are shown in Figures 53 to 57 for the site for PGA and spectral periods of 0.2, 0.5, 1.0, and 2.0 sec. Similar plots are shown in Figures 58 to 62 for the 475-year (CLE) hazard level, Figures 63 to 67 for the 975-year hazard level, and Figures 68 to 72 for the 2,475-year hazard level. These deaggregation results are very similar to the previous results from Site 1 and the results without the Wilmington fault, with the same general observations and conclusions on the controlling sources for the total hazard.

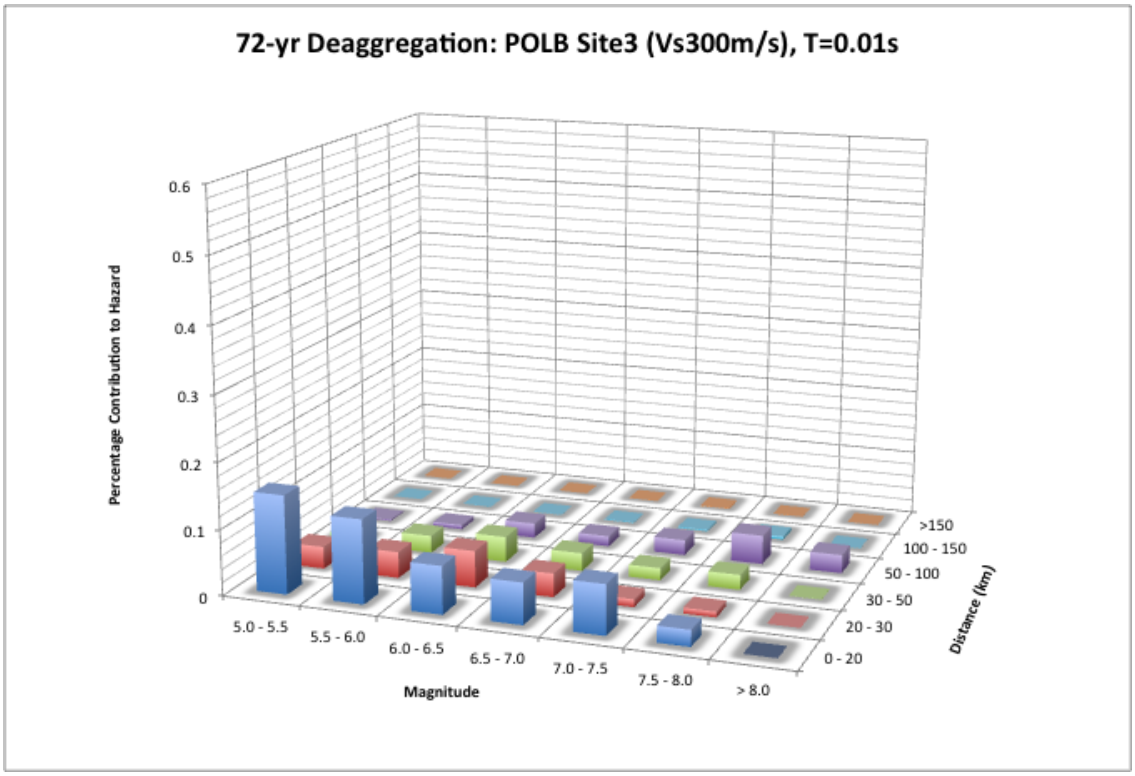


Figure 53. Magnitude-distance contribution for the 72-year (OLE) hazard level for PGA for Site 3 including the Wilmington fault.

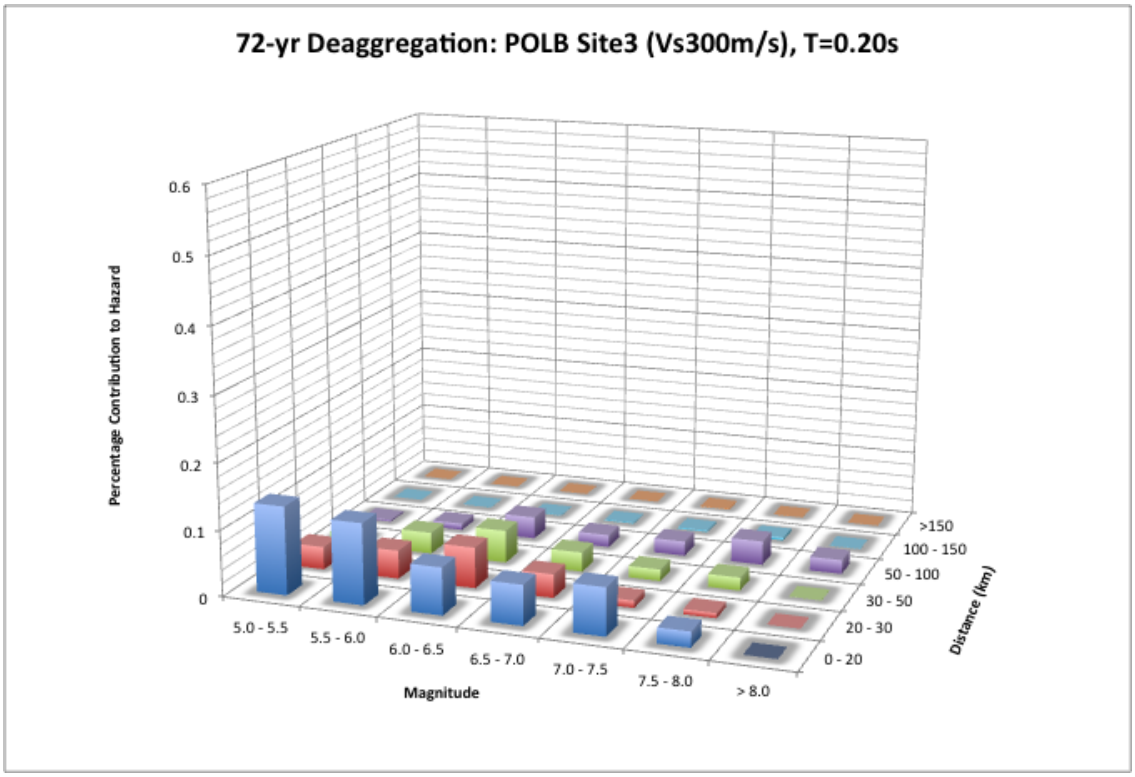


Figure 54. Magnitude-distance contribution for the 72-year (OLE) hazard level for T = 0.2 sec for Site 3 including the Wilmington fault.

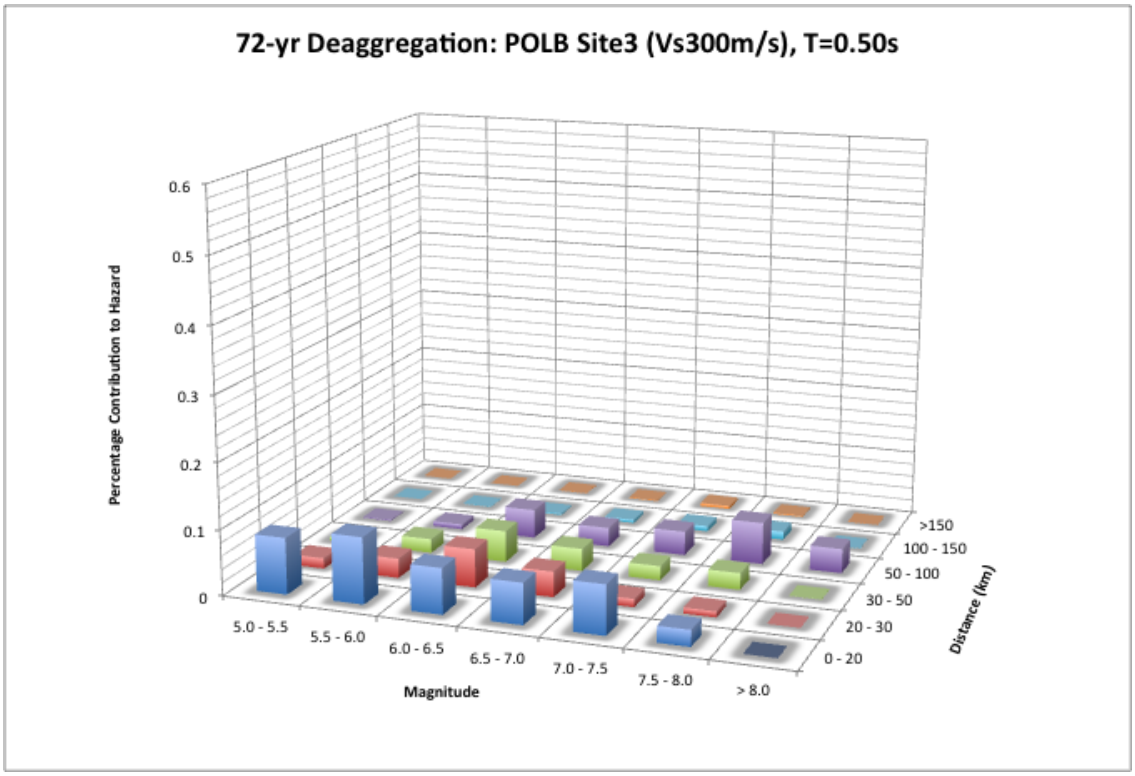


Figure 55. Magnitude-distance contribution for the 72-year (OLE) hazard level for T = 0.5 sec for Site 3 including the Wilmington fault.

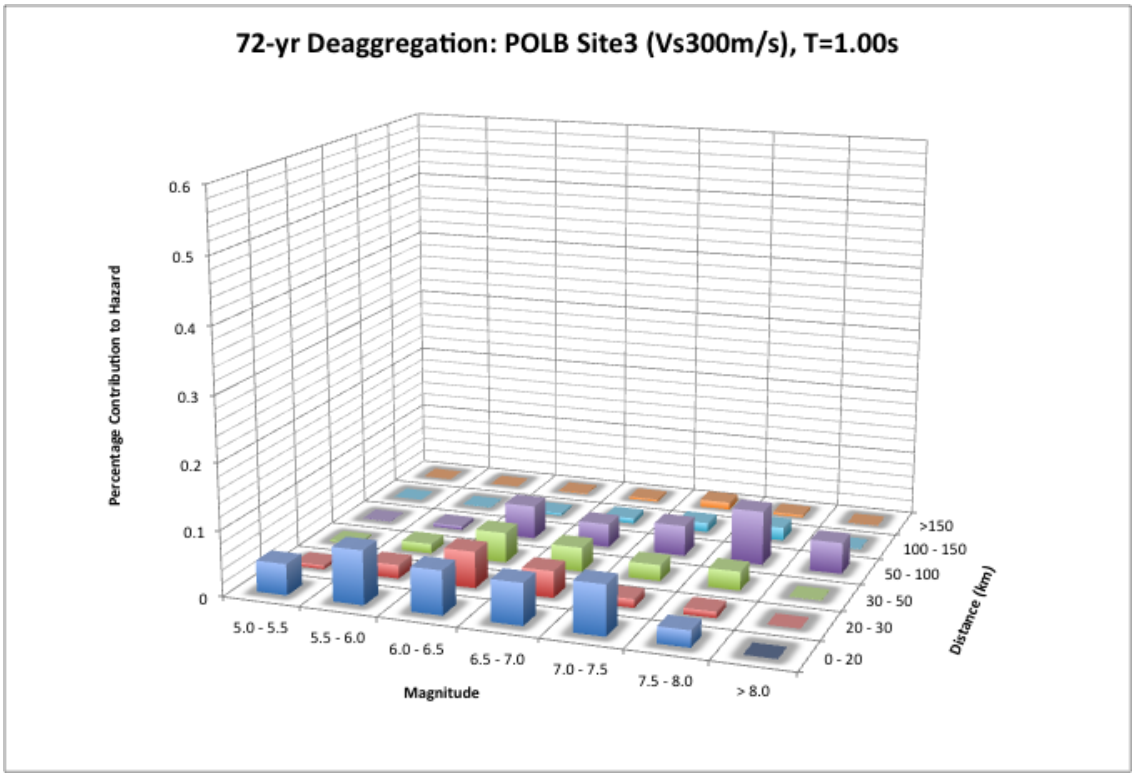


Figure 56. Magnitude-distance contribution for the 72-year (OLE) hazard level for T = 1.0 sec for Site 3 including the Wilmington fault.

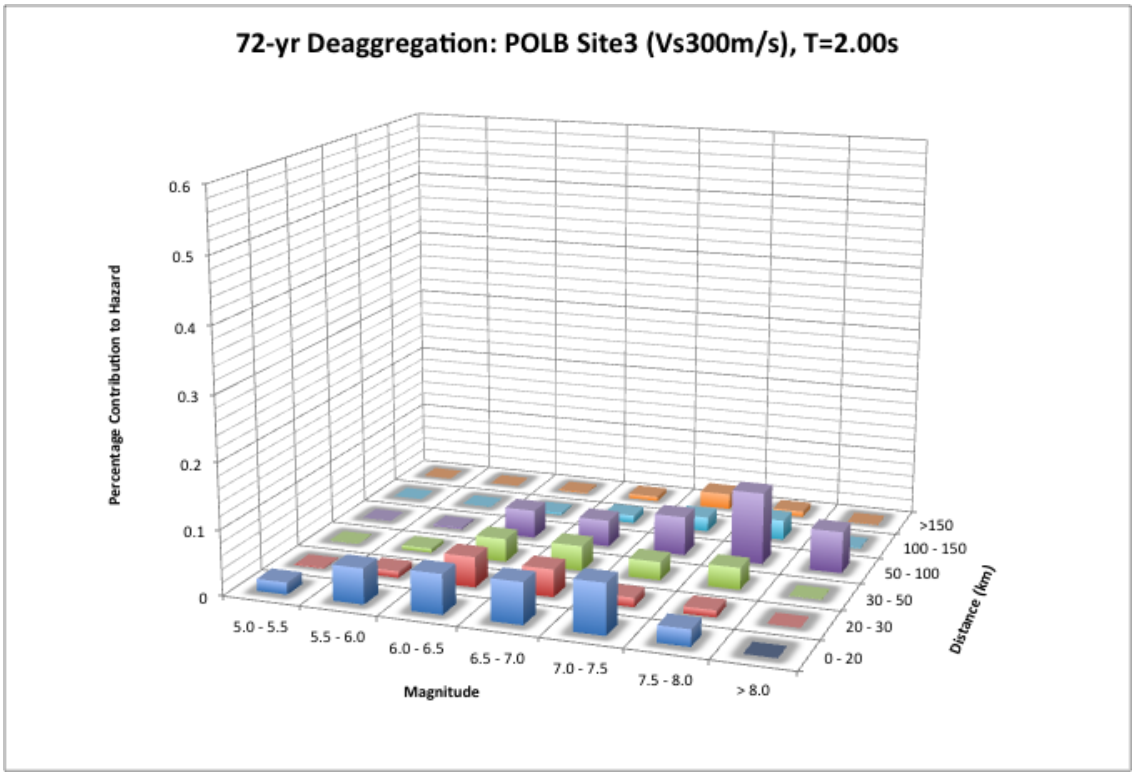


Figure 57. Magnitude-distance contribution for the 72-year (OLE) hazard level for T = 2.0 sec for Site 3 including the Wilmington fault.

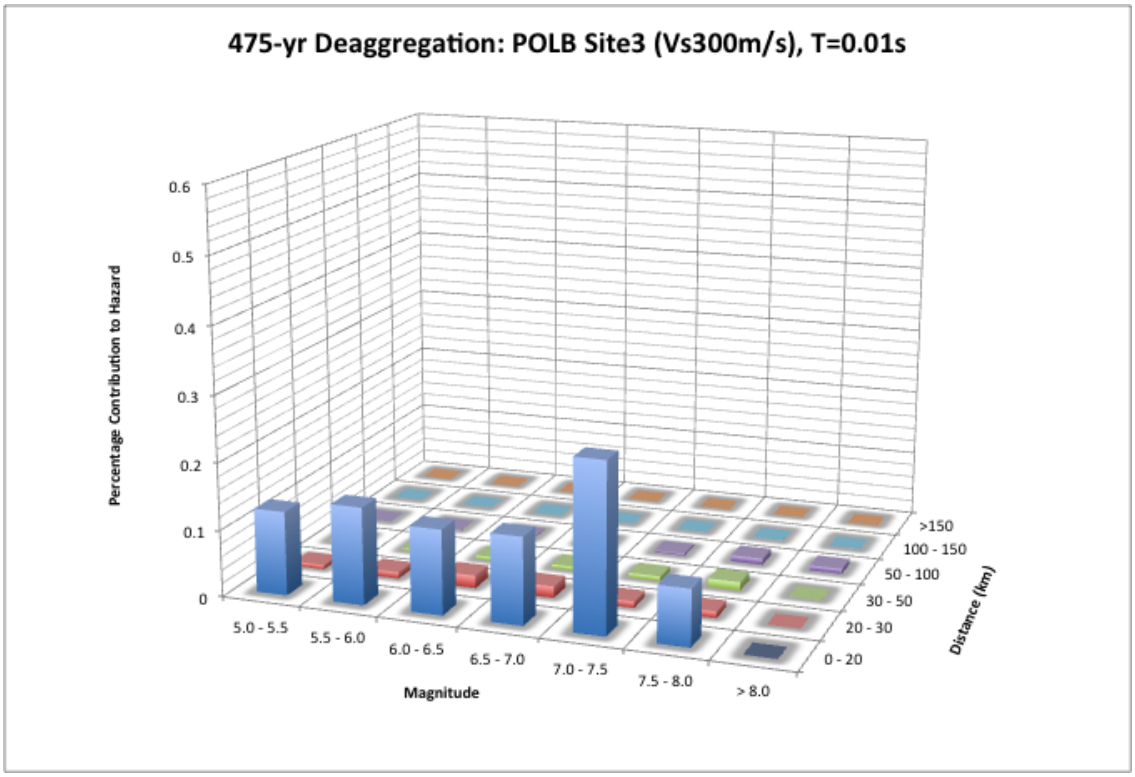


Figure 58. Magnitude-distance contribution for the 475-year (CLE) hazard level for PGA for Site 3 including the Wilmington fault.

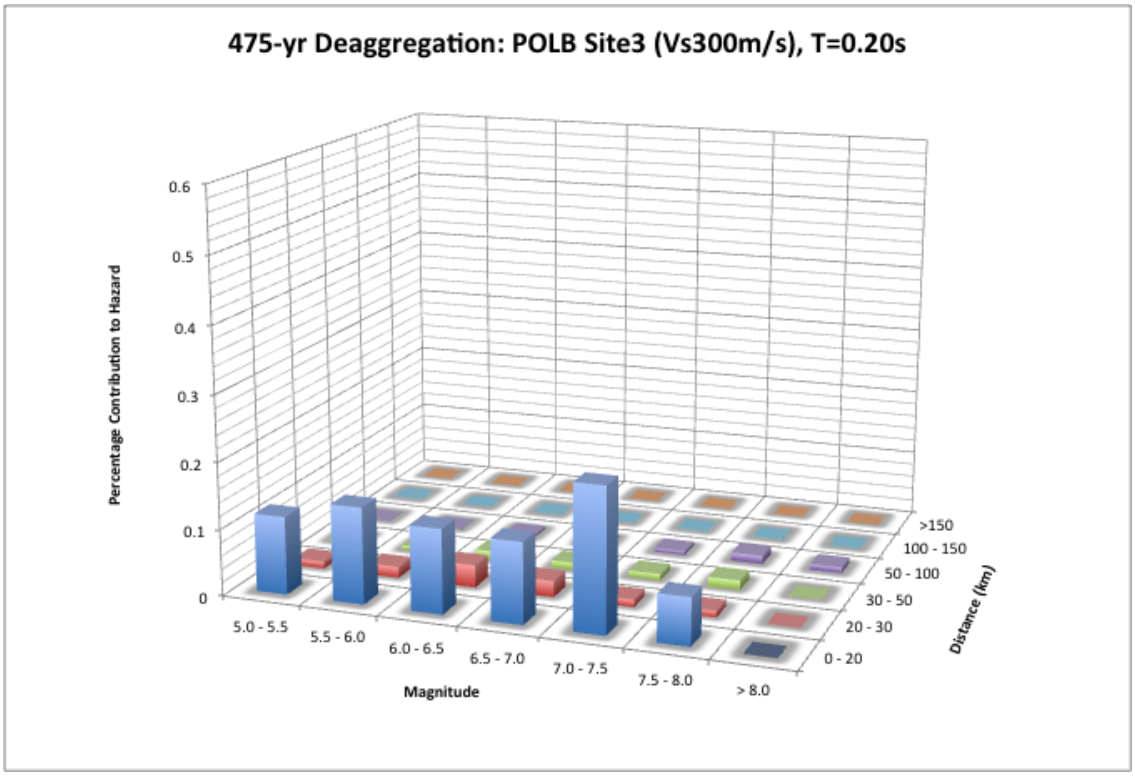


Figure 59. Magnitude-distance contribution for the 475-year (CLE) hazard level for T = 0.2 sec for Site 3 including the Wilmington fault.

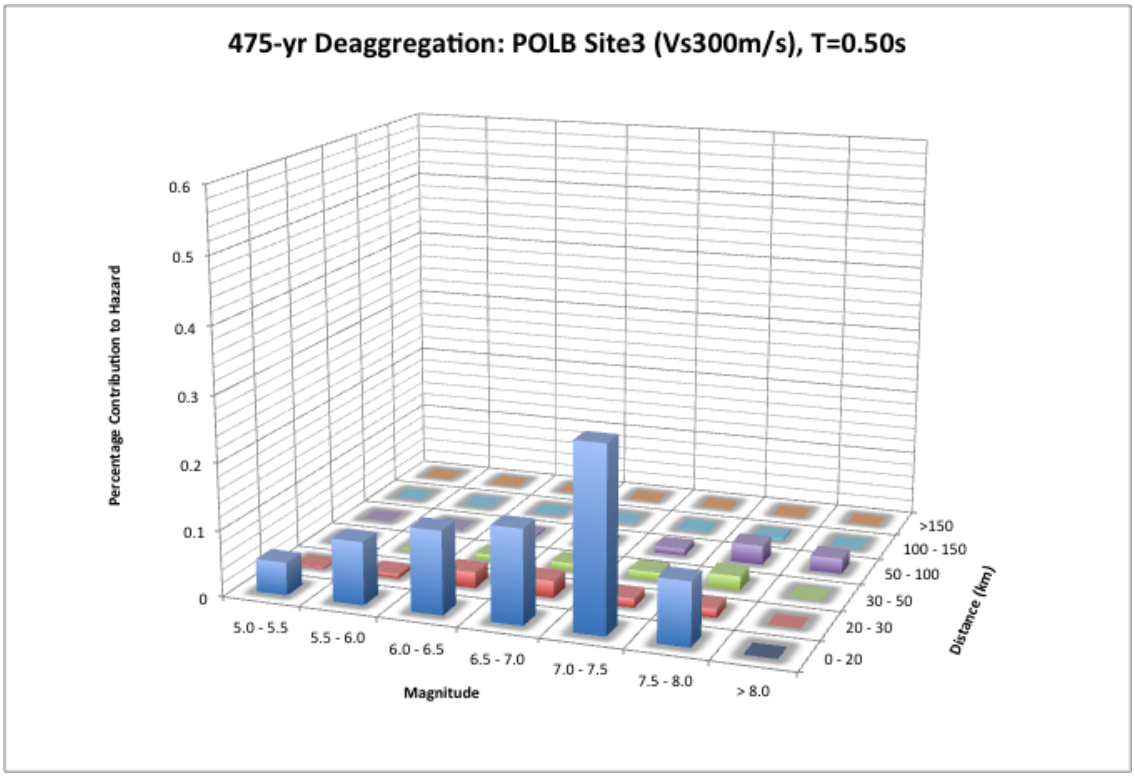


Figure 60. Magnitude-distance contribution for the 475-year (CLE) hazard level for T = 0.5 sec for Site 3 including the Wilmington fault.

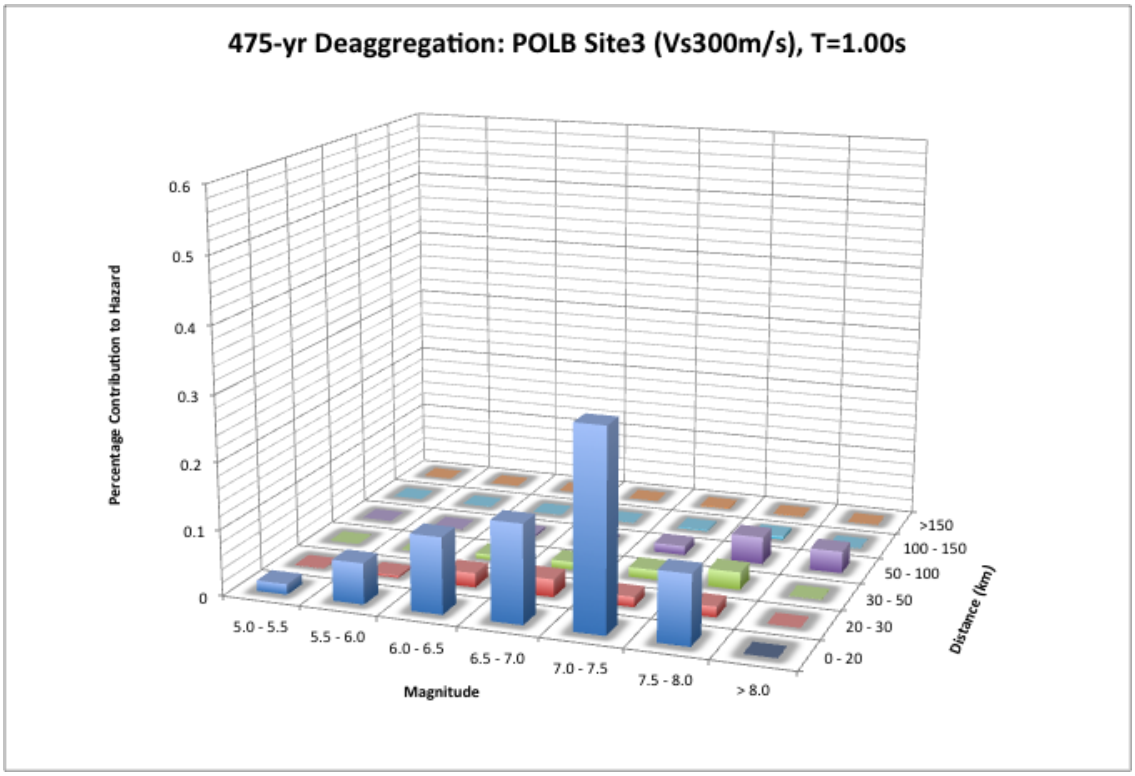


Figure 61. Magnitude-distance contribution for the 475-year (CLE) hazard level for T = 1.0 sec for Site 3 including the Wilmington fault.

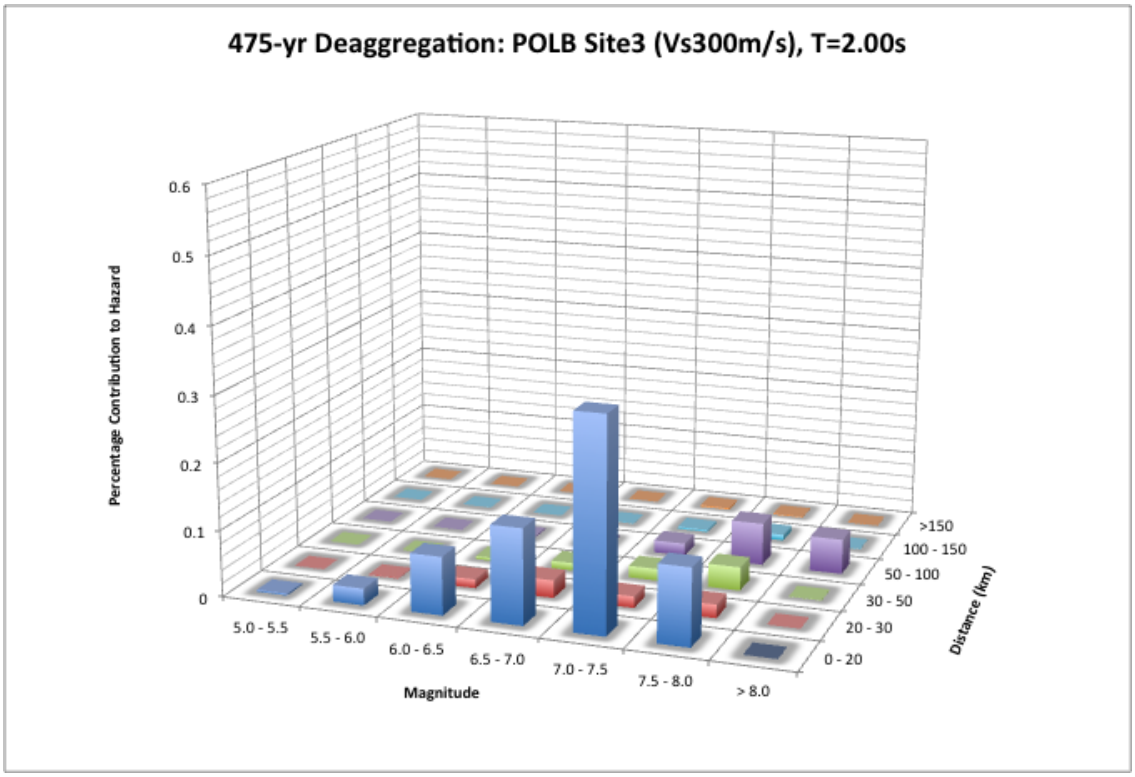


Figure 62. Magnitude-distance contribution for the 475-year (CLE) hazard level for T = 2.0 sec for Site 3 including the Wilmington fault.

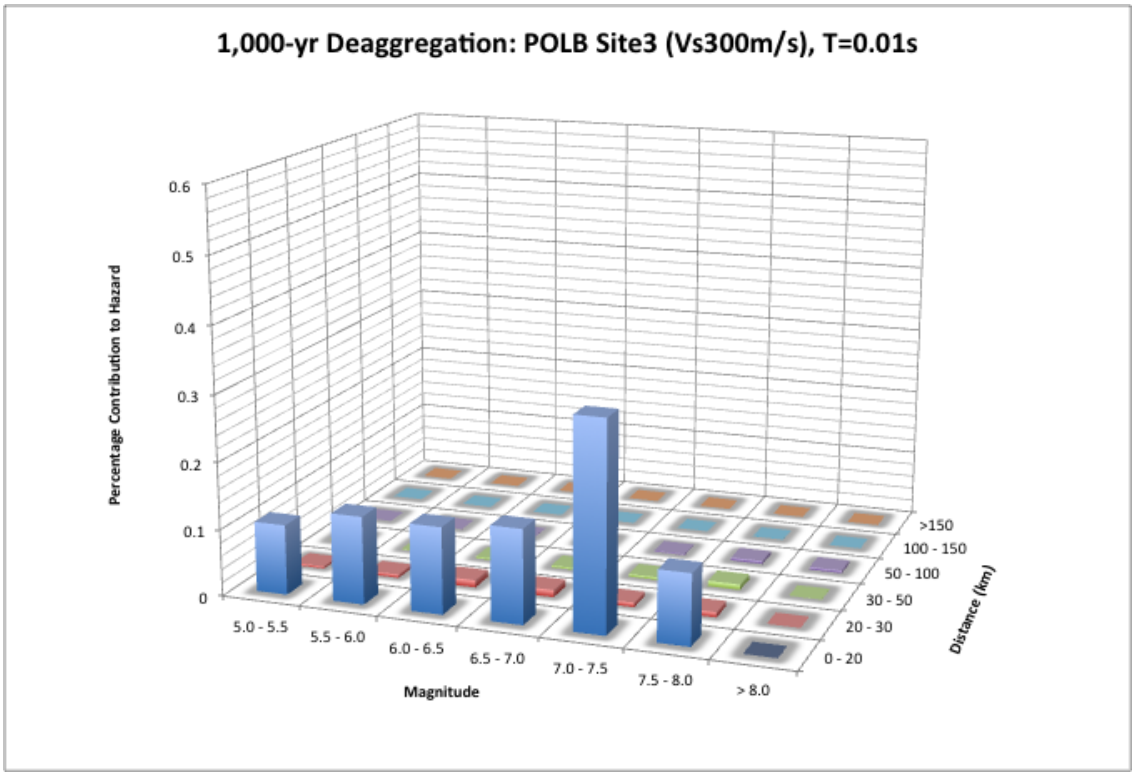


Figure 63. Magnitude-distance contribution for the 975-year hazard level for PGA for Site 3 including the Wilmington fault.

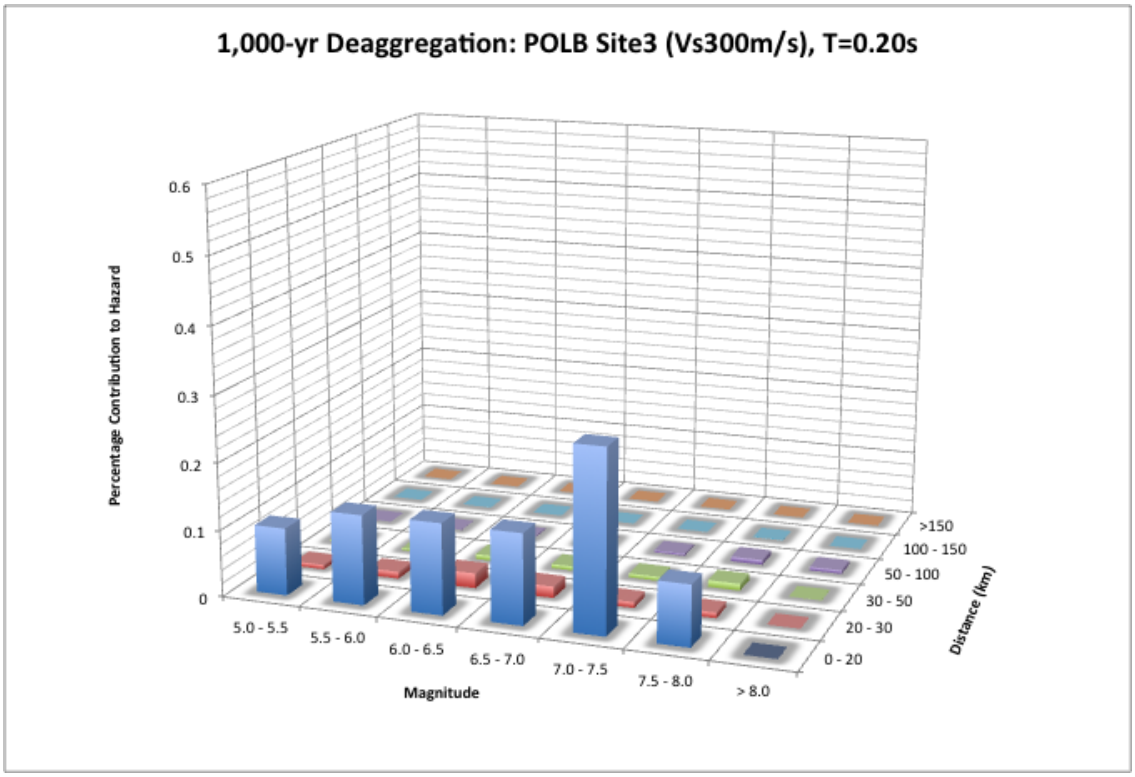


Figure 64. Magnitude-distance contribution for the 975-year hazard level for T = 0.2 sec for Site 3 including the Wilmington fault.

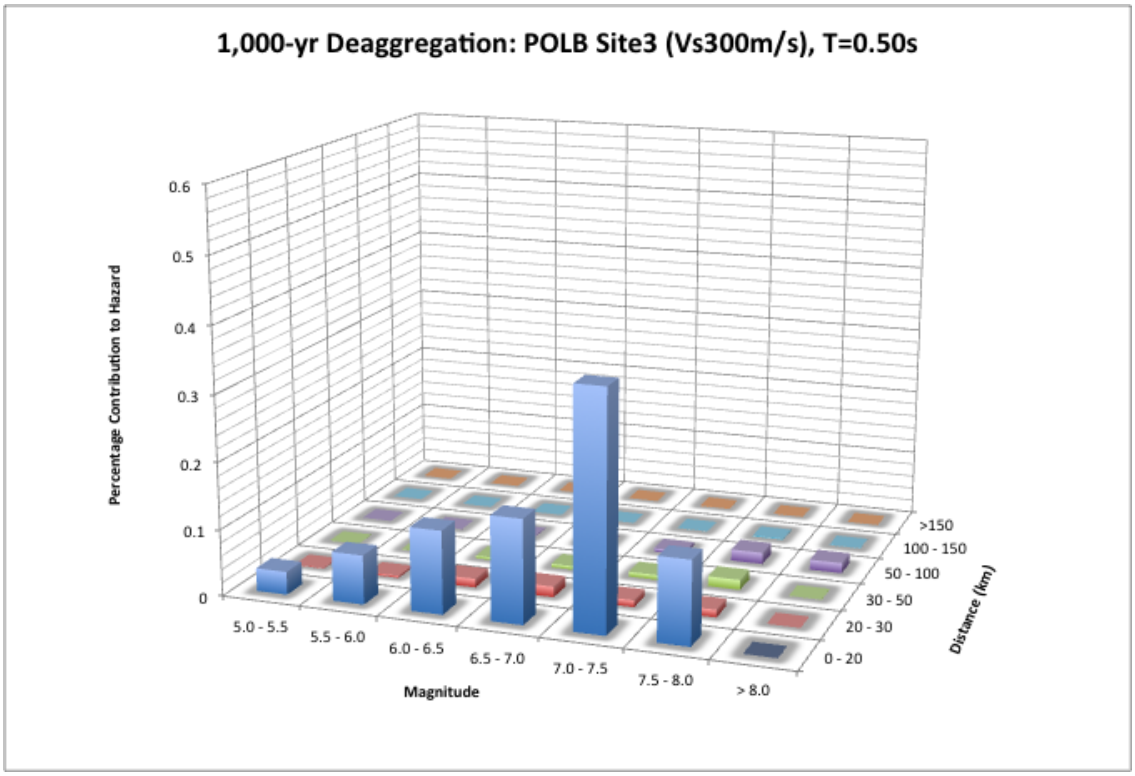


Figure 65. Magnitude-distance contribution for the 975-year hazard level for T = 0.5 sec for Site 3 including the Wilmington fault.

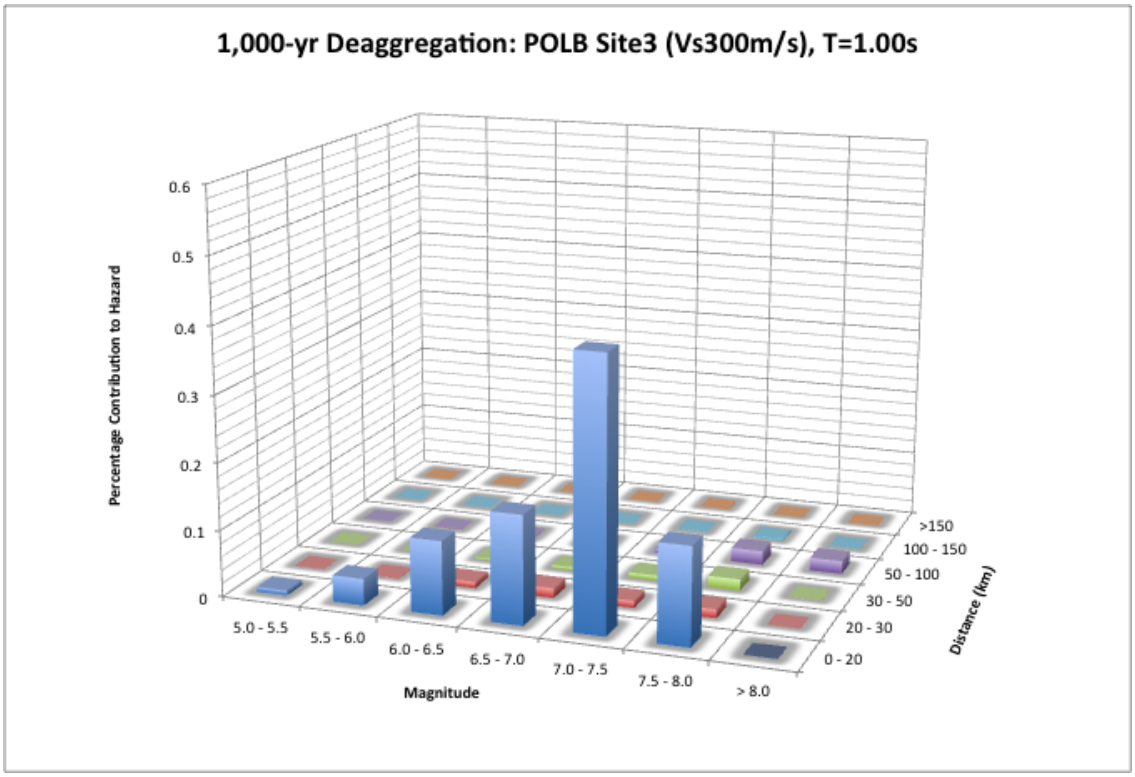


Figure 66. Magnitude-distance contribution for the 975-year hazard level for T = 1.0 sec for Site 3 including the Wilmington fault.

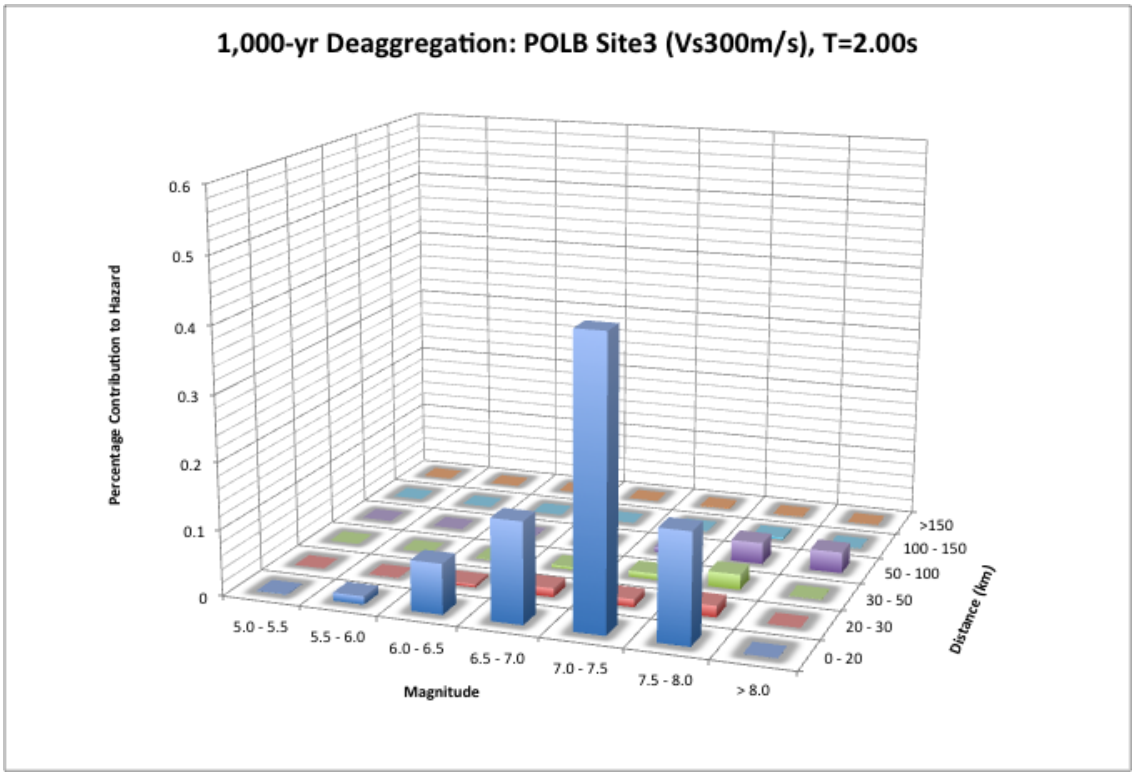


Figure 67. Magnitude-distance contribution for the 975-year hazard level for T = 2.0 sec for Site 3 including the Wilmington fault.

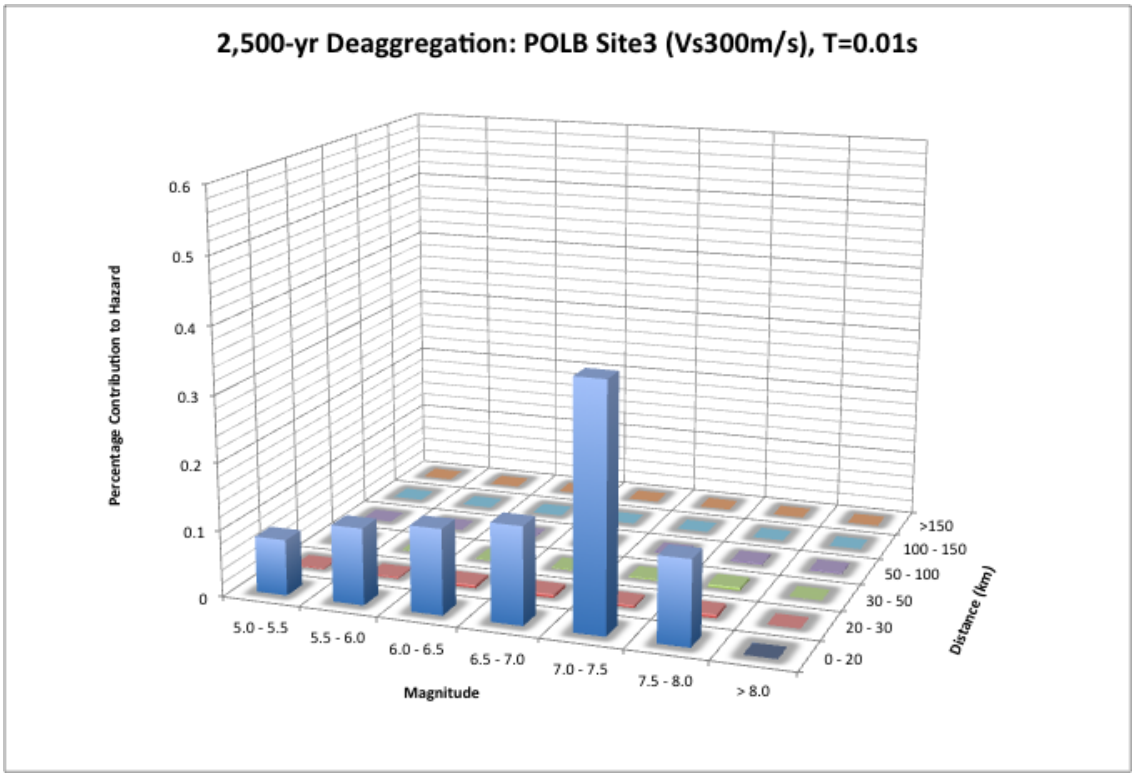


Figure 68. Magnitude-distance contribution for the 2,475-year hazard level for PGA for Site 3 including the Wilmington fault.

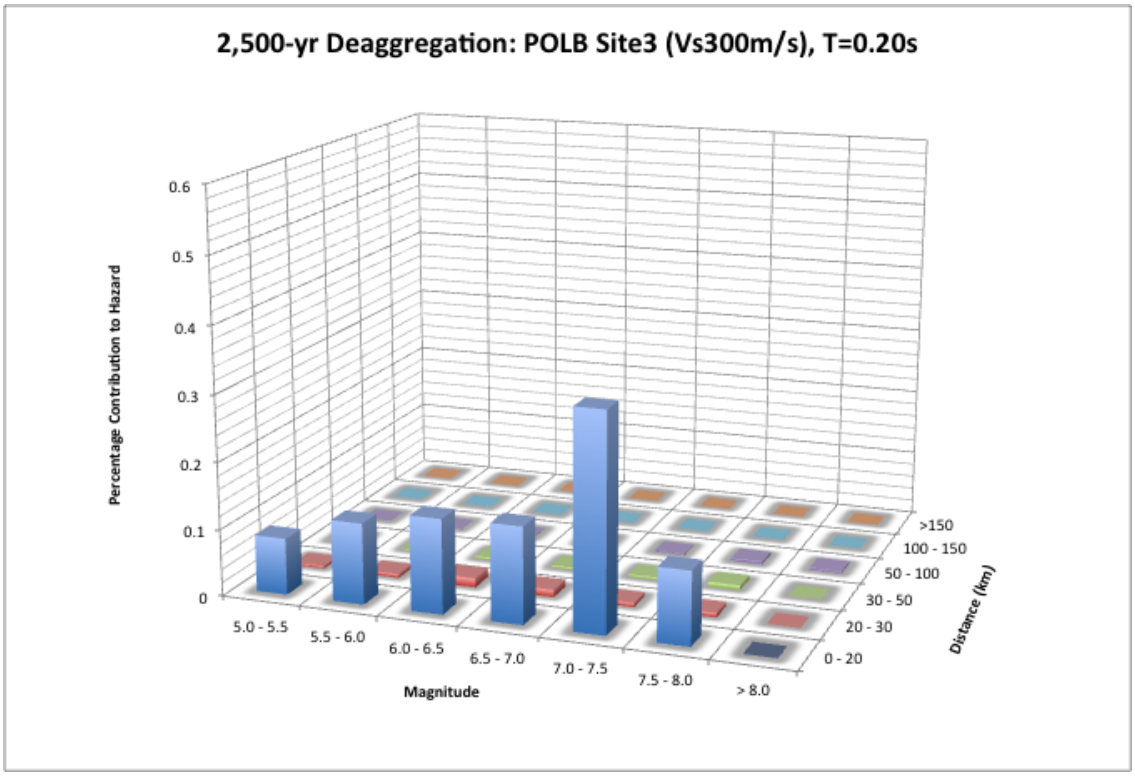


Figure 69. Magnitude-distance contribution for the 2,475-year hazard level for T = 0.2 sec for Site 3 including the Wilmington fault.

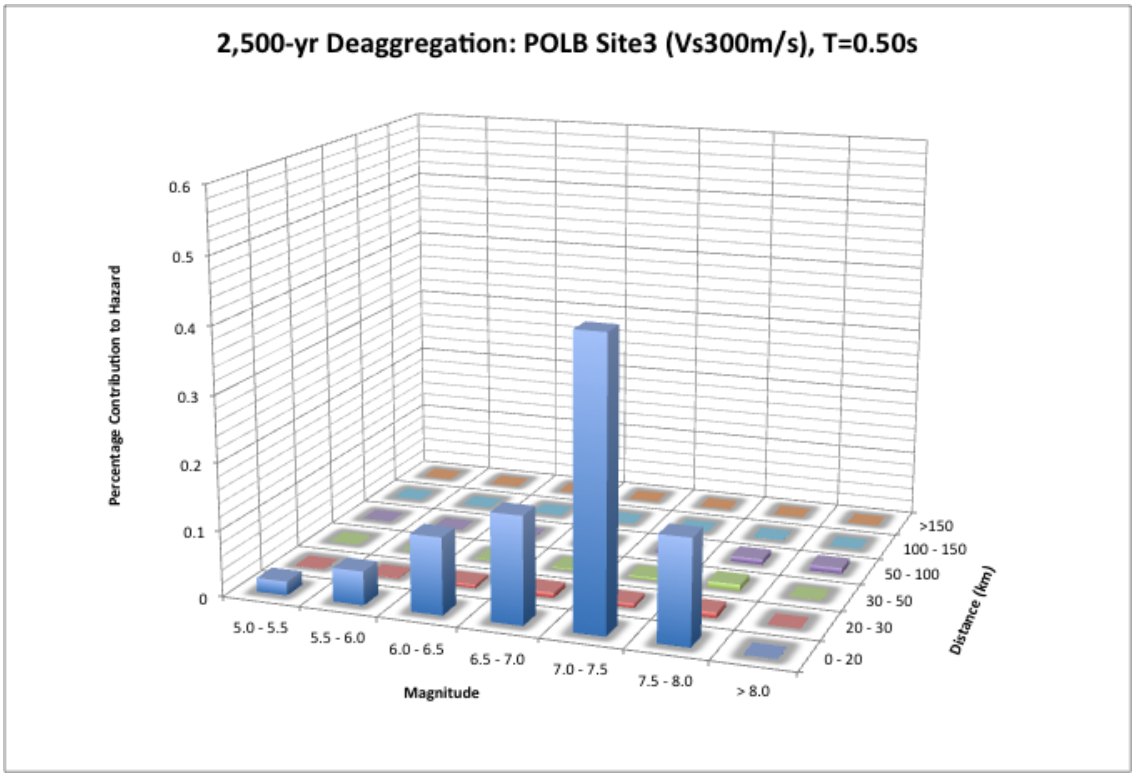


Figure 70. Magnitude-distance contribution for the 2,475-year hazard level for T = 0.5 sec for Site 3 including the Wilmington fault.

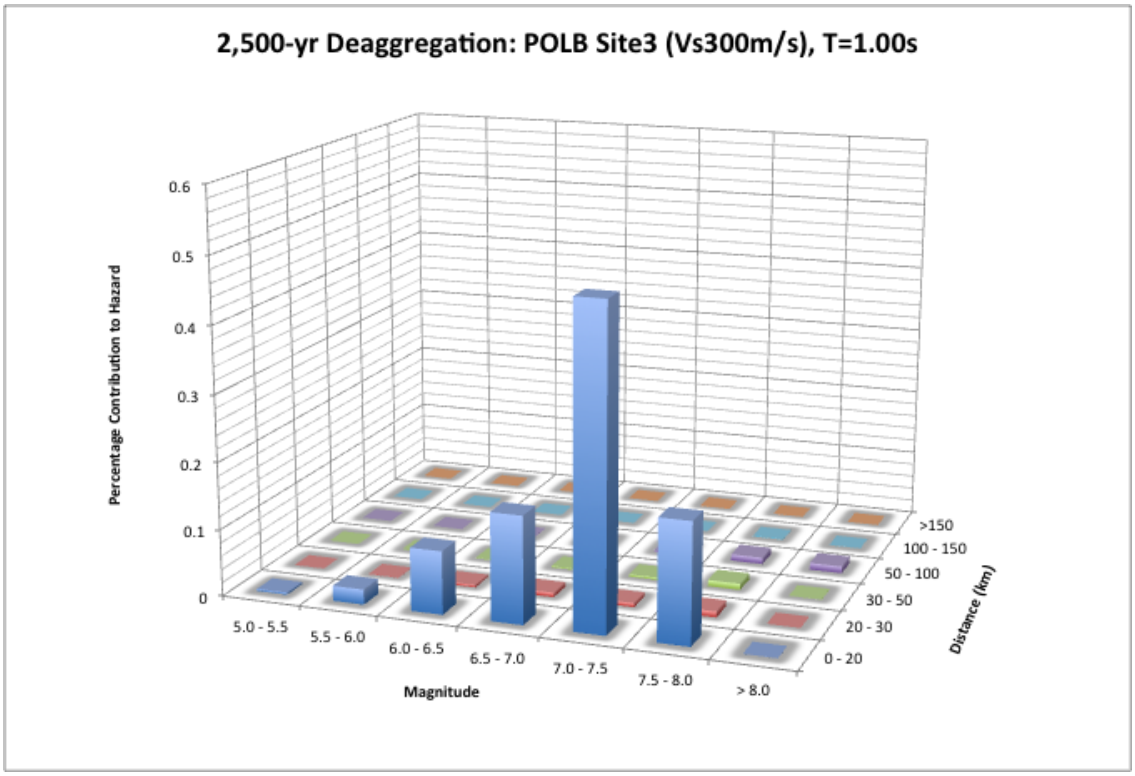


Figure 71. Magnitude-distance contribution for the 2,475-year hazard level for T = 1.0 sec for Site 3 including the Wilmington fault.

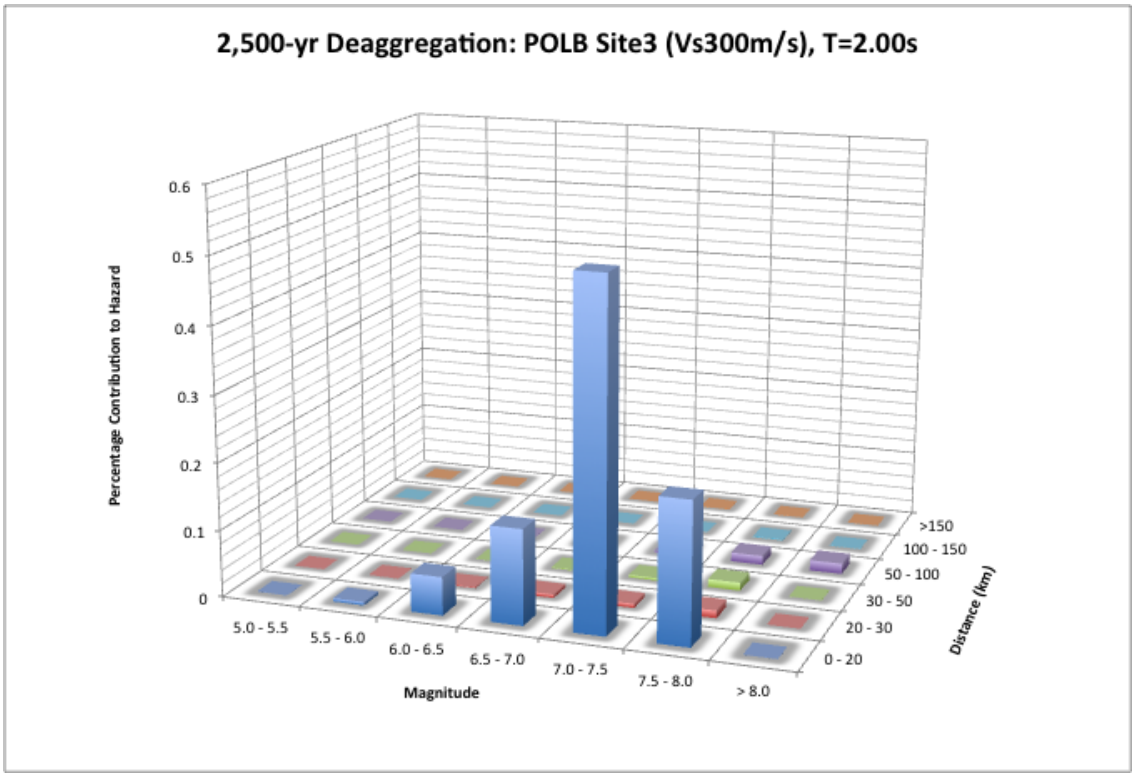


Figure 72. Magnitude-distance contribution for the 2,475-year hazard level for T = 2.0 sec for Site 3 including the Wilmington fault.

4.4 Site 5 – Horizontal

The mean hazard curves including the Wilmington fault for Site 5 are shown in Figures 73 through 77 for PGA and spectral periods of 0.2, 0.5, 1.0, and 2.0 sec. For the longer spectral periods (i.e., 1 and 2 sec) these plots are showing the horizontal component without the inclusion of the directivity model. In these plots, individual hazard curves from the scenario fault ruptures, gridded sources, the Wilmington fault, and the combined total hazard are presented. For the 72-year return period (OLE) hazard level, the hazard curve plots indicate that the hazard is primarily controlled by the contribution from the gridded point sources and to a lesser amount the contribution from the fault sources. At the 475-year (CLE) hazard level the contribution from the fault sources increases relative to the contribution form the gridded point sources. At the lower hazard levels of 975-year and 2,475-year return periods, the results indicate an increase in the relative contribution from the fault sources over the gridded point sources. These plots also show the relatively minor contribution of the Wilmington fault to the total hazard.

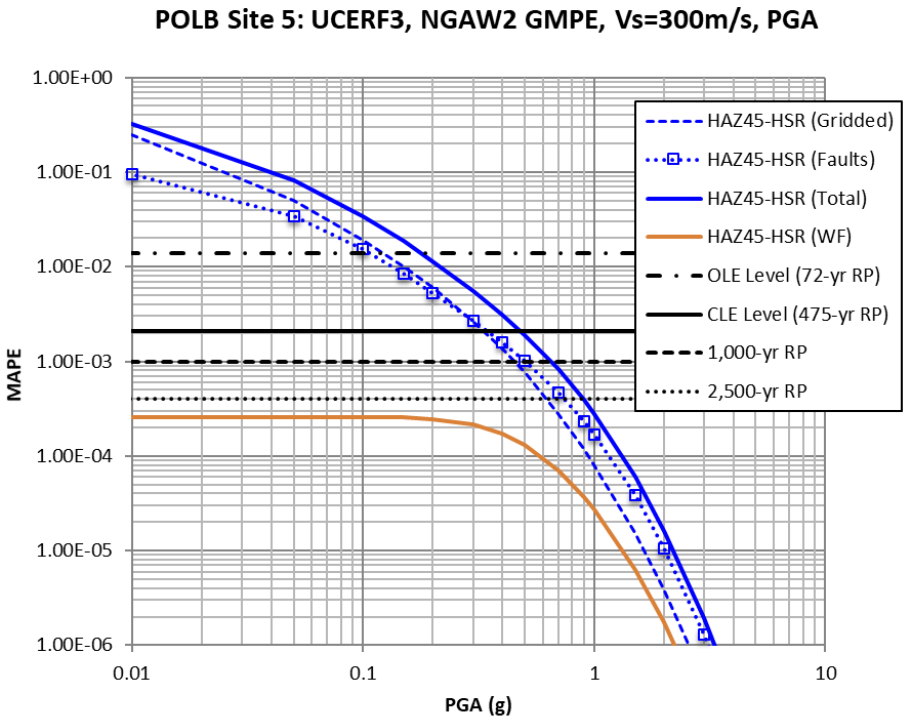


Figure 73. Mean horizontal component hazard curves from the UCERF3 gridded and fault sources, the Wilmington fault, and total hazard for PGA for Site 5.

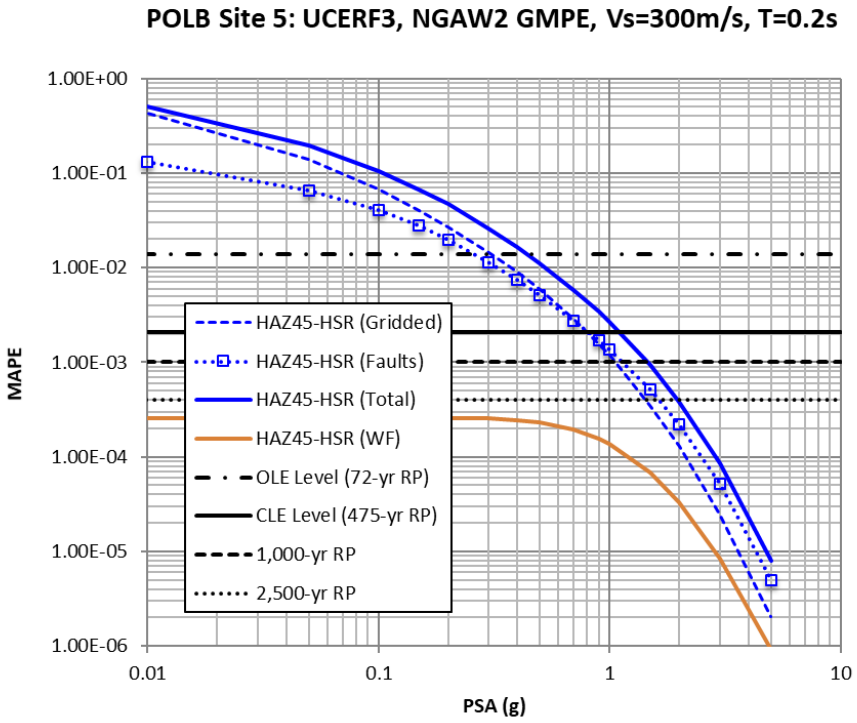


Figure 74. Mean horizontal component hazard curves from the UCERF3 gridded and fault sources, the Wilmington fault, and total hazard for T = 0.2 sec for Site 5.

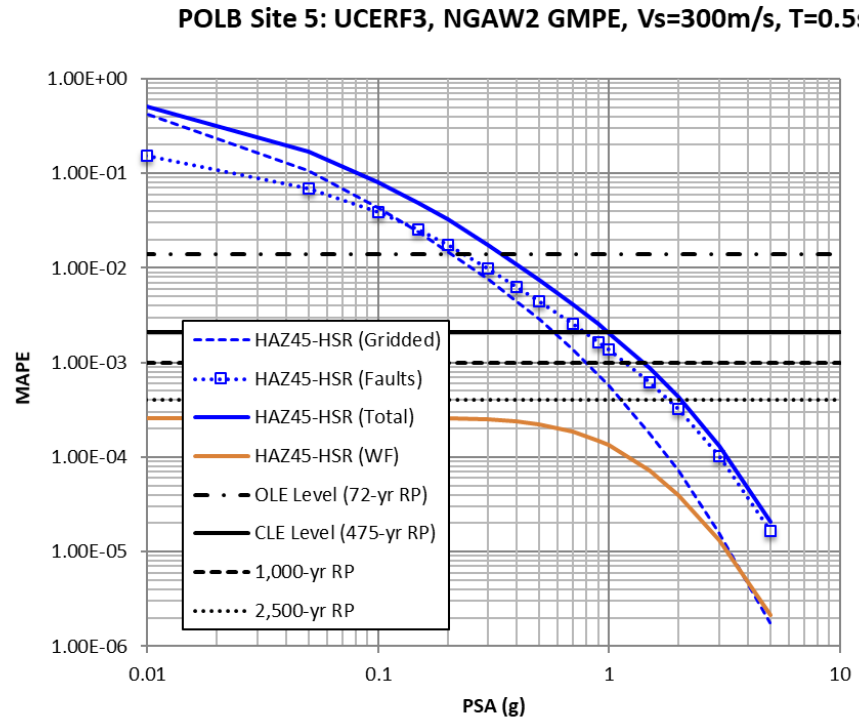


Figure 75. Mean horizontal component hazard curves from the UCERF3 gridded and fault sources, the Wilmington fault, and total hazard for T = 0.5 sec for Site 5.

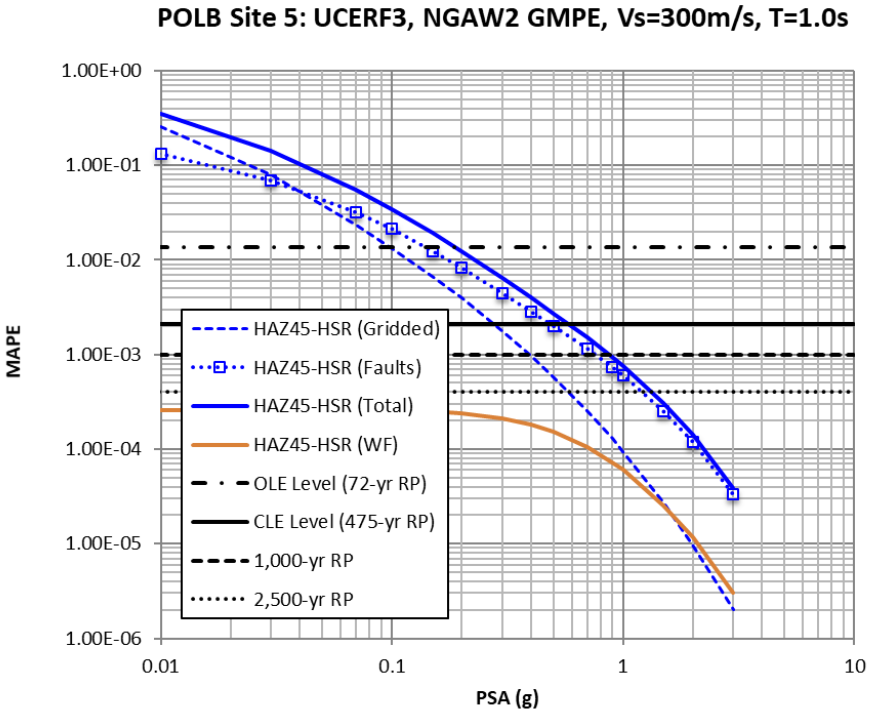


Figure 76. Mean horizontal component hazard curves from the UCERF3 gridded and fault sources, the Wilmington fault, and total hazard for T = 1.0 sec for Site 5.

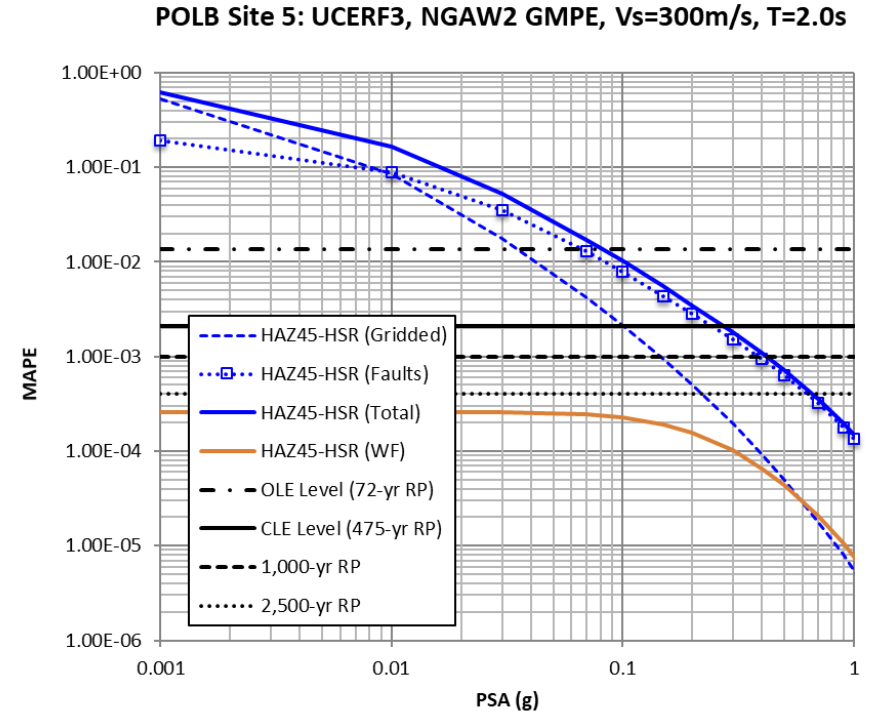


Figure 77. Mean horizontal component hazard curves from the UCERF3 gridded and fault sources, the Wilmington fault, and total hazard for T = 2.0 sec for Site 5.

Given the hazard curves for the full suite of spectral periods, the computed uniform hazard spectra (UHS) including the Wilmington fault for the 72-year (OLE), 475-year (CLE), 975-year and 2,475-year return period hazard levels are plotted in Figure 78. The horizontal UHS values at all spectral periods are given in Table 13. Similar to the other two sites, these UHS results including the Wilmington fault are slightly greater (i.e., 3-4% or less) than the previous results not including the Wilmington fault (Gregor and Al Atik, 2019).

Table 13. Horizontal UHS for Site 5 at the four hazard levels including the Wilmington fault.

Period (sec)	72-year (OLE) Horizontal PSA (g)	475-year (CLE) Horizontal PSA (g)	975-year Horizontal PSA (g)	2,475-year Horizontal PSA (g)
0.01	0.1787	0.4783	0.6476	0.8937
0.02	0.1784	0.4795	0.6493	0.8954
0.03	0.1854	0.4951	0.6687	0.9188
0.04	0.2005	0.5273	0.7136	0.9766
0.05	0.2164	0.5659	0.7647	1.0474
0.075	0.2751	0.7059	0.9442	1.2798
0.1	0.3342	0.8359	1.1053	1.5103
0.15	0.4112	1.0105	1.3198	1.7777
0.2	0.4408	1.0964	1.4606	1.9712
0.25	0.4441	1.1354	1.5359	2.0919
0.3	0.4341	1.1427	1.5680	2.1696
0.4	0.3888	1.0756	1.5140	2.1537
0.5	0.3465	0.9902	1.4058	2.0501
0.75	0.2487	0.7478	1.0931	1.6468
1	0.1852	0.5789	0.8696	1.3279
1.5	0.1169	0.3805	0.5785	0.9104
2	0.0813	0.2723	0.4199	0.6639
3	0.0482	0.1684	0.2605	0.4174
4	0.0322	0.1159	0.1788	0.2828
5	0.0228	0.0853	0.1308	0.2068
7.5	0.0121	0.0484	0.0728	0.1107
10	0.0074	0.0309	0.0461	0.0702

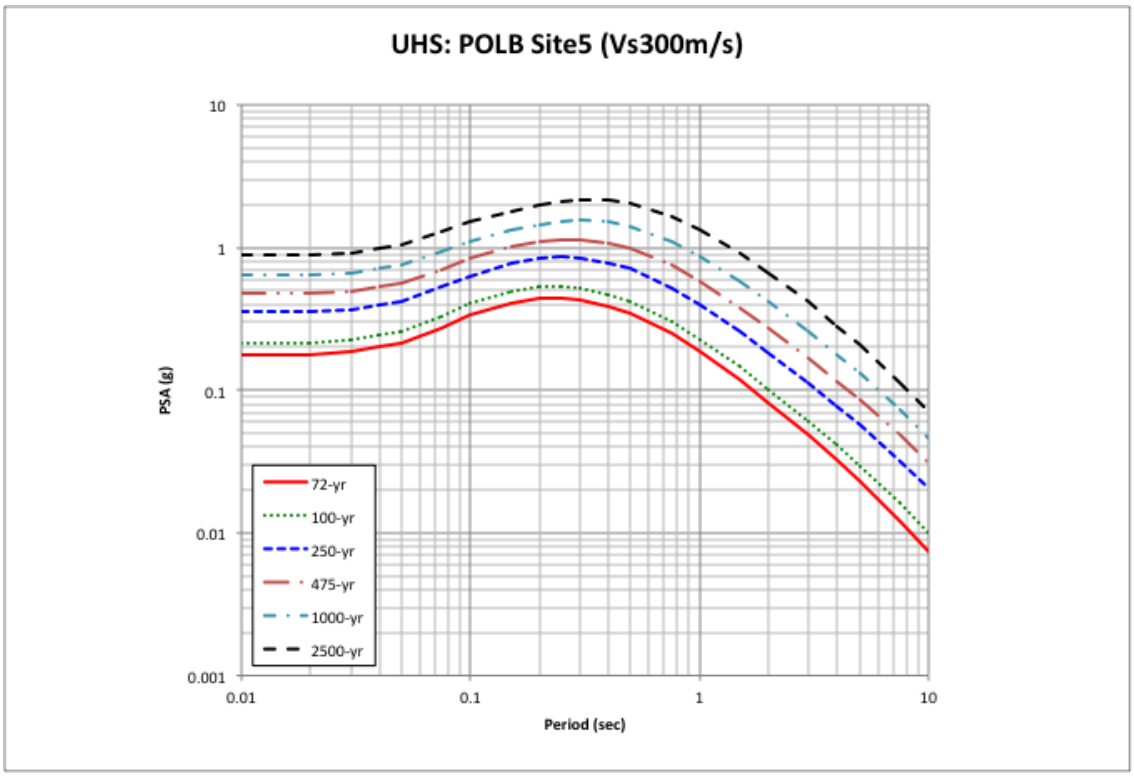


Figure 78. Uniform hazard spectra for Site 5 including the Wilmington fault.

The mean magnitude, distance and epsilon values including the Wilmington fault for the horizontal component without the directivity model are plotted in Figures 79 to 81 for the four hazard levels. These plots are shown as a function of spectral period. As expected, the magnitude increases and the distance decreases with the increasing return period hazard levels. Also observed in these plots is the expected increase in the mean epsilon values between the four hazard levels with the 2,475-year results greater than approximately 1 over the full spectral period range. The mean magnitude, distance and epsilon values are listed in Tables 14 through 16 for the four hazard levels and are similar to the results without the Wilmington fault (Gregor and Al Atik, 2019).

Table 14. Mean magnitude for the four hazard levels for Site 5 including the Wilmington fault.

Period (sec)	72-year (OLE) Magnitude	475-year (CLE) Magnitude	975-year Magnitude	2,475-year Magnitude
0.01	6.36	6.57	6.65	6.74
0.02	6.36	6.57	6.65	6.74
0.03	6.34	6.55	6.63	6.71
0.04	6.33	6.53	6.61	6.68
0.05	6.32	6.51	6.58	6.63
0.075	6.28	6.46	6.52	6.56
0.1	6.26	6.43	6.48	6.54
0.15	6.28	6.47	6.53	6.59
0.2	6.33	6.53	6.61	6.69
0.25	6.39	6.60	6.69	6.76
0.3	6.43	6.65	6.75	6.83
0.4	6.52	6.77	6.86	6.94
0.5	6.59	6.84	6.92	7.00
0.75	6.69	6.94	7.01	7.08
1	6.77	7.00	7.07	7.13
1.5	6.89	7.11	7.17	7.21
2	6.98	7.18	7.21	7.25
3	7.11	7.28	7.30	7.31
4	7.18	7.36	7.36	7.37
5	7.23	7.42	7.41	7.41
7.5	7.30	7.54	7.54	7.54
10	7.34	7.58	7.60	7.61

Table 15. Mean distance for the four hazard levels for Site 5 including the Wilmington fault.

Period (sec)	72-year (OLE) Distance (km)	475-year (CLE) Distance (km)	975-year Distance (km)	2,475-year Distance (km)
0.01	26.20	10.54	8.14	6.37
0.02	25.98	10.41	8.03	6.30
0.03	25.87	10.52	8.18	6.48
0.04	25.56	10.90	8.29	6.67
0.05	26.02	11.53	8.84	7.15
0.075	25.99	12.04	9.60	8.13
0.1	25.89	12.63	10.36	8.30
0.15	25.96	12.73	10.57	8.44
0.2	26.87	13.12	10.17	8.06
0.25	27.89	13.31	9.95	7.89
0.3	29.07	13.49	9.91	7.74
0.4	31.84	14.17	10.04	7.63
0.5	34.51	14.85	10.80	7.63
0.75	39.42	16.54	11.36	7.66
1	41.55	17.31	11.09	7.66
1.5	47.59	19.69	12.87	7.93
2	51.06	21.62	13.40	8.47
3	56.57	24.53	15.83	9.20
4	60.29	28.12	18.27	11.35
5	62.98	31.12	21.72	13.70
7.5	72.52	41.88	33.69	26.31
10	77.93	49.21	42.50	35.47

Table 16. Mean epsilon for the four hazard levels for Site 5 including the Wilmington fault.

Period (sec)	72-year (OLE) Epsilon	475-year (CLE) Epsilon	975-year Epsilon	2,475-year Epsilon
0.01	0.133	0.640	0.923	1.291
0.02	0.130	0.638	0.917	1.303
0.03	0.162	0.681	0.960	1.326
0.04	0.198	0.721	1.002	1.360
0.05	0.232	0.770	1.042	1.376
0.075	0.307	0.885	1.144	1.441
0.1	0.347	0.936	1.184	1.506
0.15	0.334	0.936	1.179	1.492
0.2	0.293	0.856	1.121	1.442
0.25	0.271	0.784	1.042	1.367
0.3	0.272	0.735	0.980	1.301
0.4	0.268	0.661	0.894	1.218
0.5	0.278	0.634	0.856	1.193
0.75	0.283	0.576	0.783	1.125
1	0.260	0.517	0.727	1.079
1.5	0.213	0.470	0.677	1.050
2	0.165	0.439	0.646	1.016
3	0.080	0.408	0.618	0.985
4	-0.017	0.402	0.629	0.982
5	-0.083	0.411	0.652	1.006
7.5	-0.207	0.481	0.784	1.131
10	-0.310	0.460	0.791	1.202

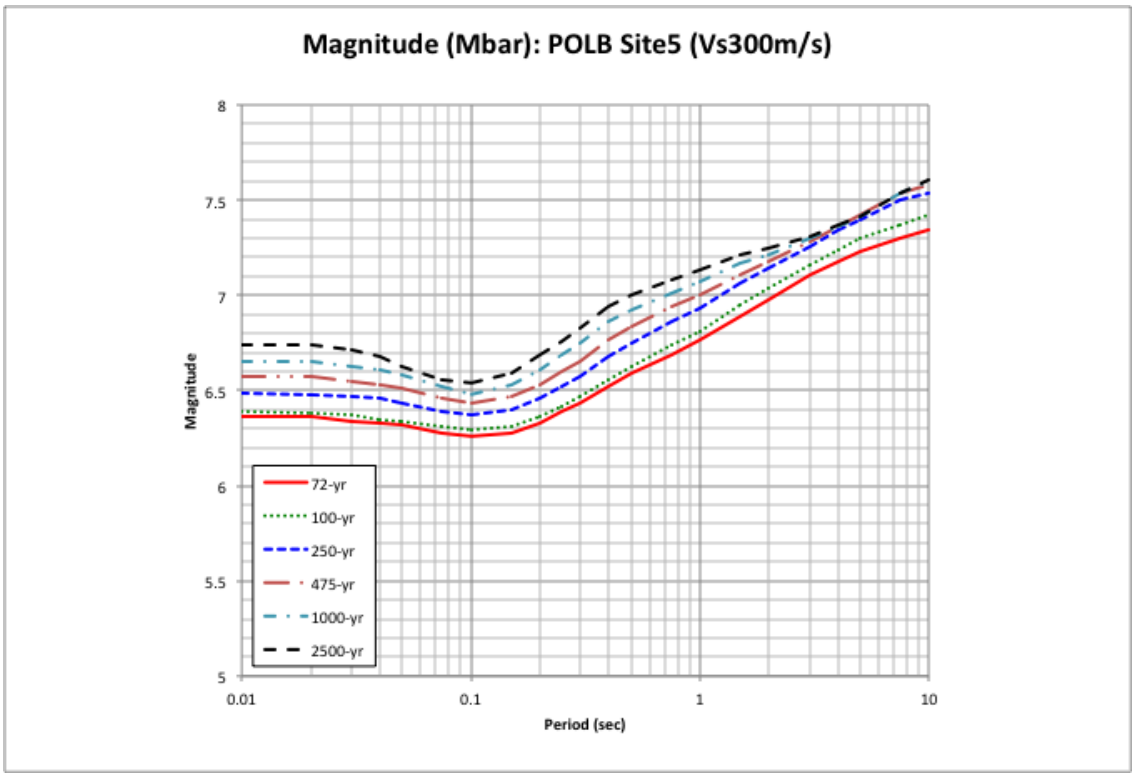


Figure 79. Horizontal mean magnitude for Site 5 including the Wilmington fault.

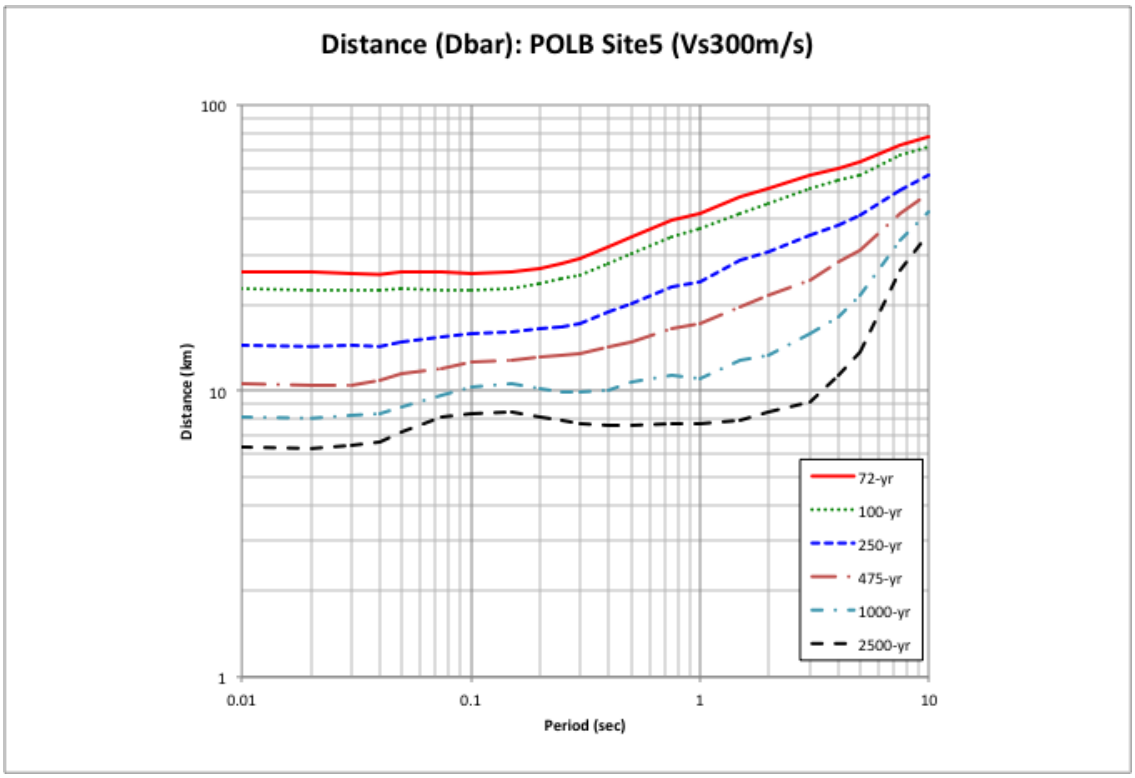


Figure 80. Horizontal mean distance for Site 5 including the Wilmington fault.

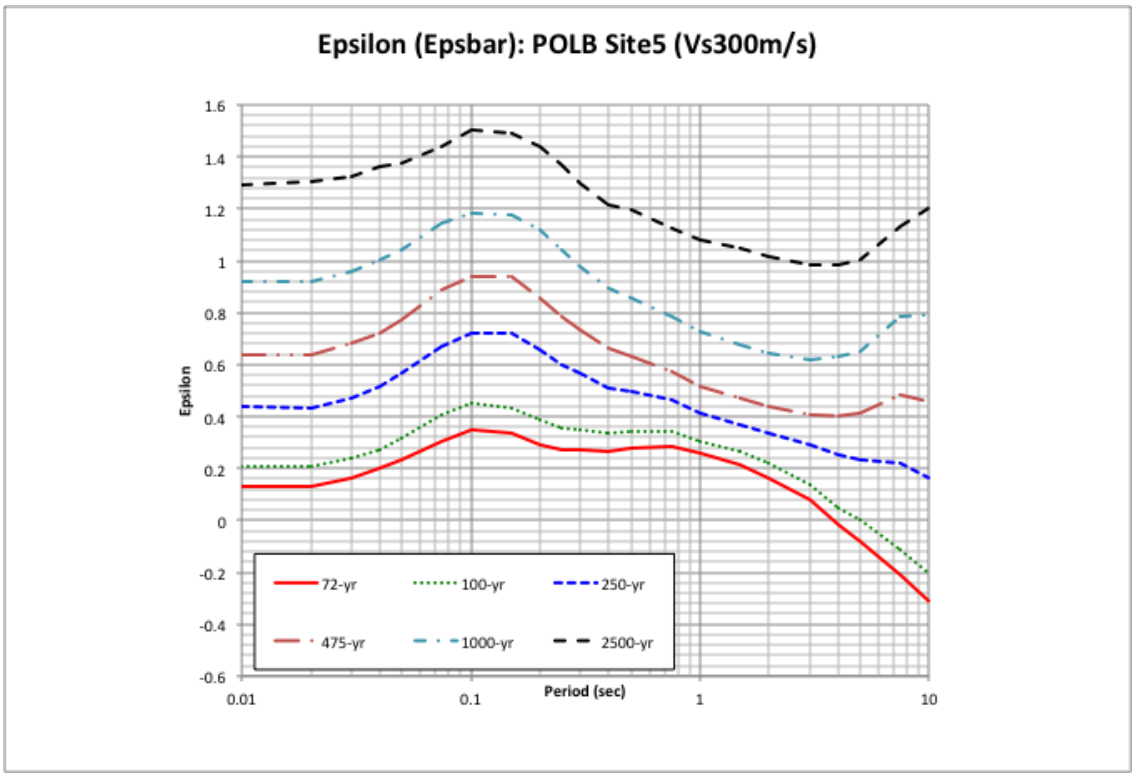


Figure 81. Horizontal mean epsilon for Site 5 including the Wilmington fault.

The binned magnitude and distance contributions to the 72-year (OLE) hazard level are shown in Figures 82 to 86 for the site for PGA and spectral periods of 0.2, 0.5, 1.0, and 2.0 sec. Similar plots are shown in Figures 87 to 91 for the 475-year (CLE) hazard level, Figures 92 to 96 for the 975-year hazard level, and Figures 97 to 101 for the 2,475-year hazard level. These deaggregation results are very similar to the previous results from the other sites and the case without the Wilmington fault (Gregor and Al Atik, 2019) with the same general observations and conclusions on the controlling sources for the total hazard.

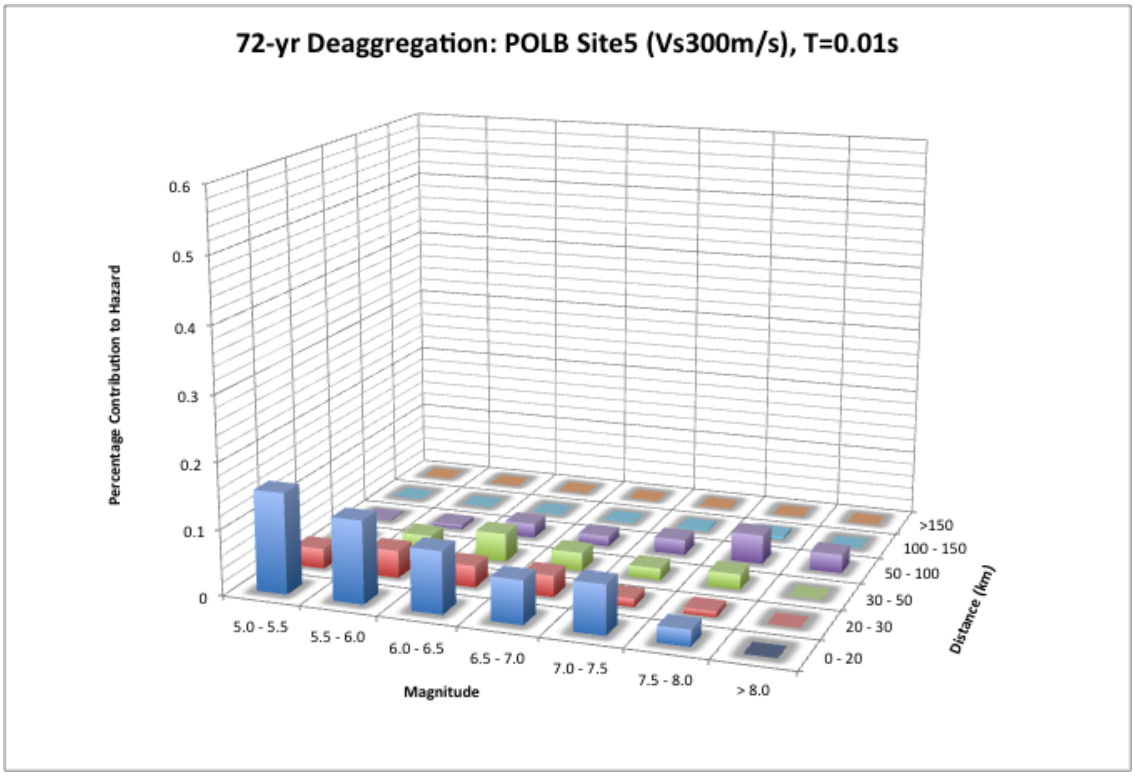


Figure 82. Magnitude-distance contribution for the 72-year (OLE) hazard level for PGA for Site 5 including the Wilmington fault.

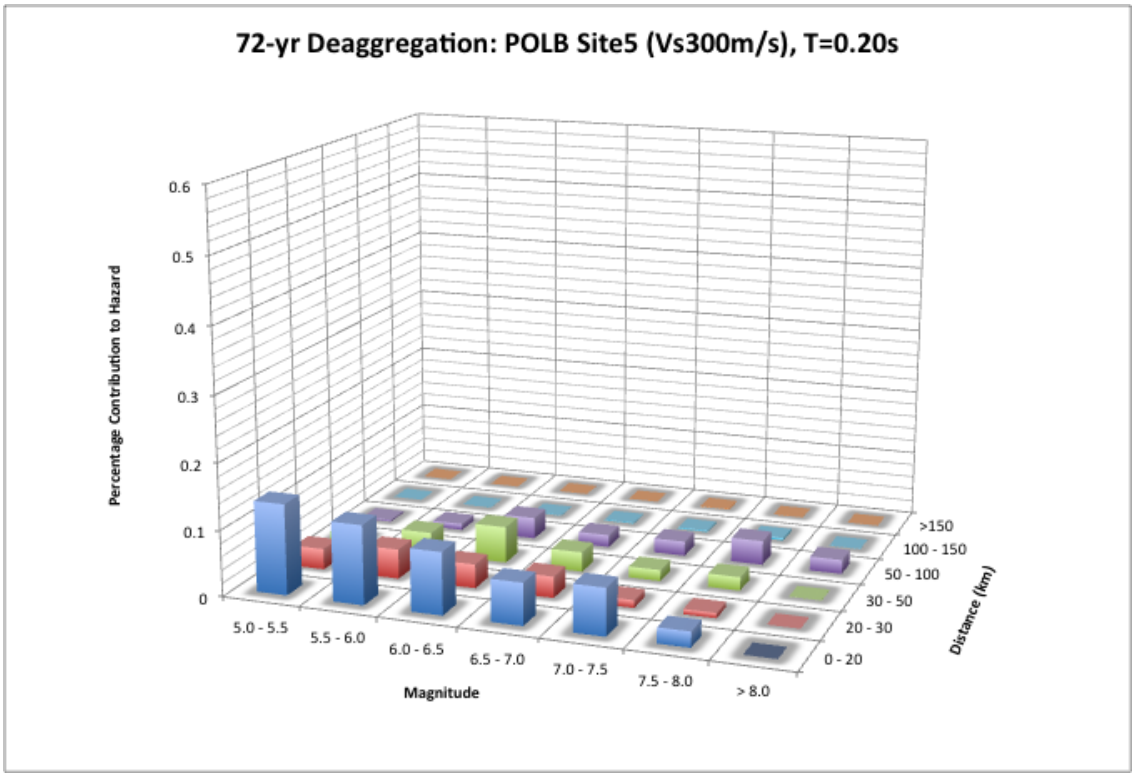


Figure 83. Magnitude-distance contribution for the 72-year (OLE) hazard level for T = 0.2 sec for Site 5 including the Wilmington fault.

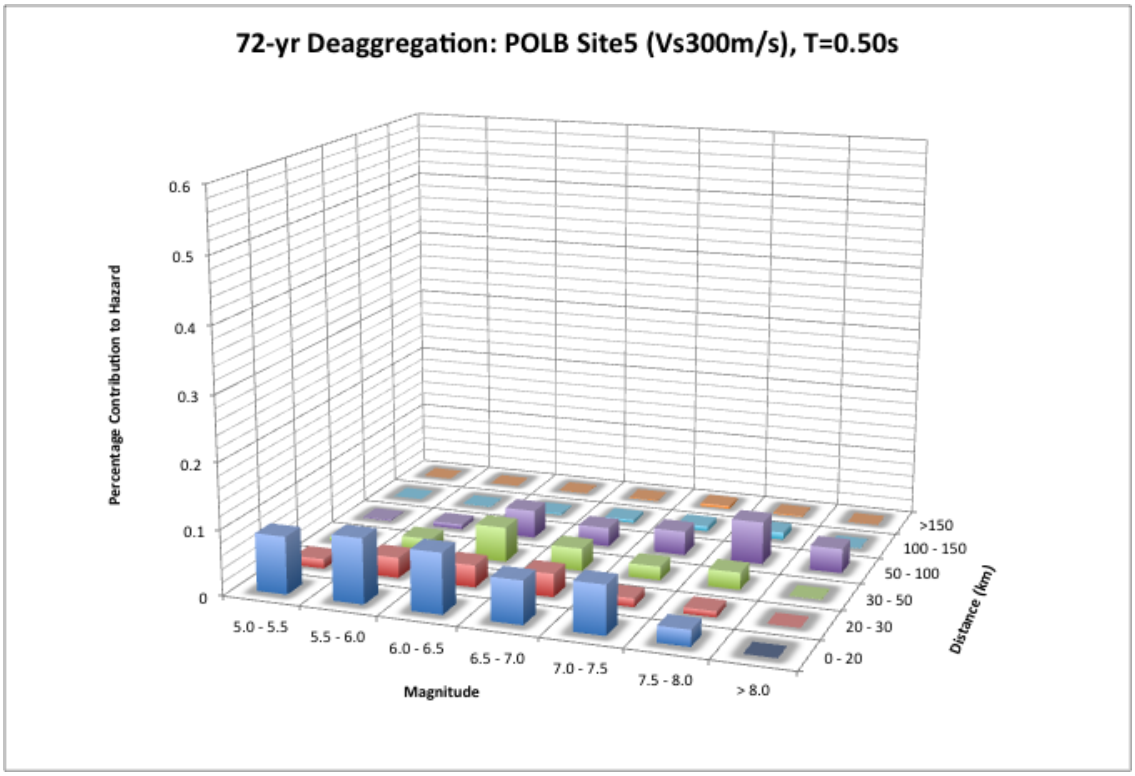


Figure 84. Magnitude-distance contribution for the 72-year (OLE) hazard level for T = 0.5 sec for Site 5 including the Wilmington fault.

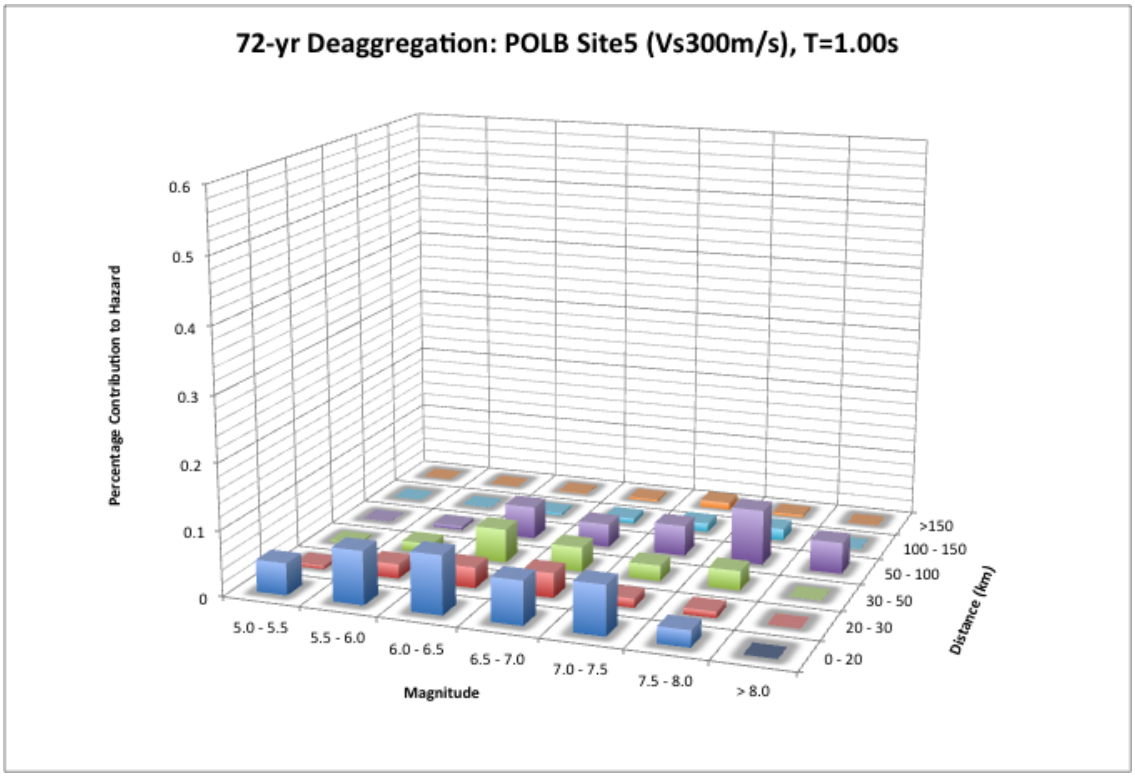


Figure 85. Magnitude-distance contribution for the 72-year (OLE) hazard level for T = 1.0 sec for Site 5 including the Wilmington fault.

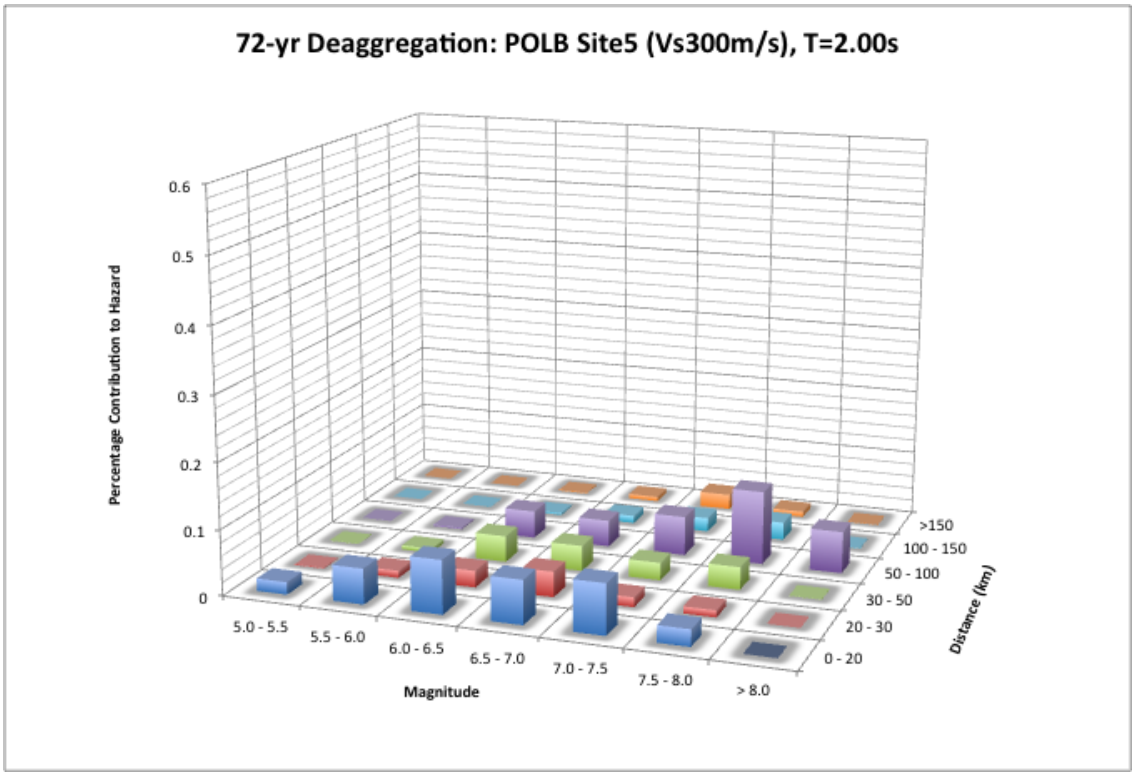


Figure 86. Magnitude-distance contribution for the 72-year (OLE) hazard level for T = 2.0 sec for Site 5 including the Wilmington fault.

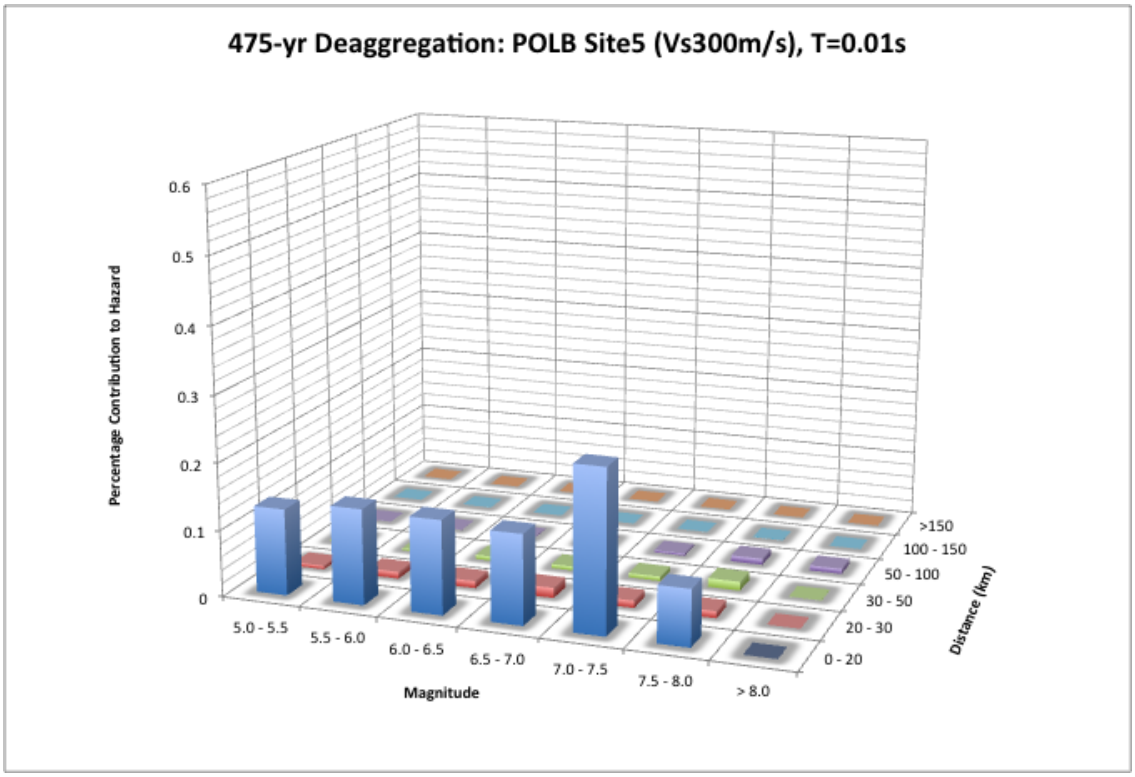


Figure 87. Magnitude-distance contribution for the 475-year (CLE) hazard level for PGA for Site 5 including the Wilmington fault.

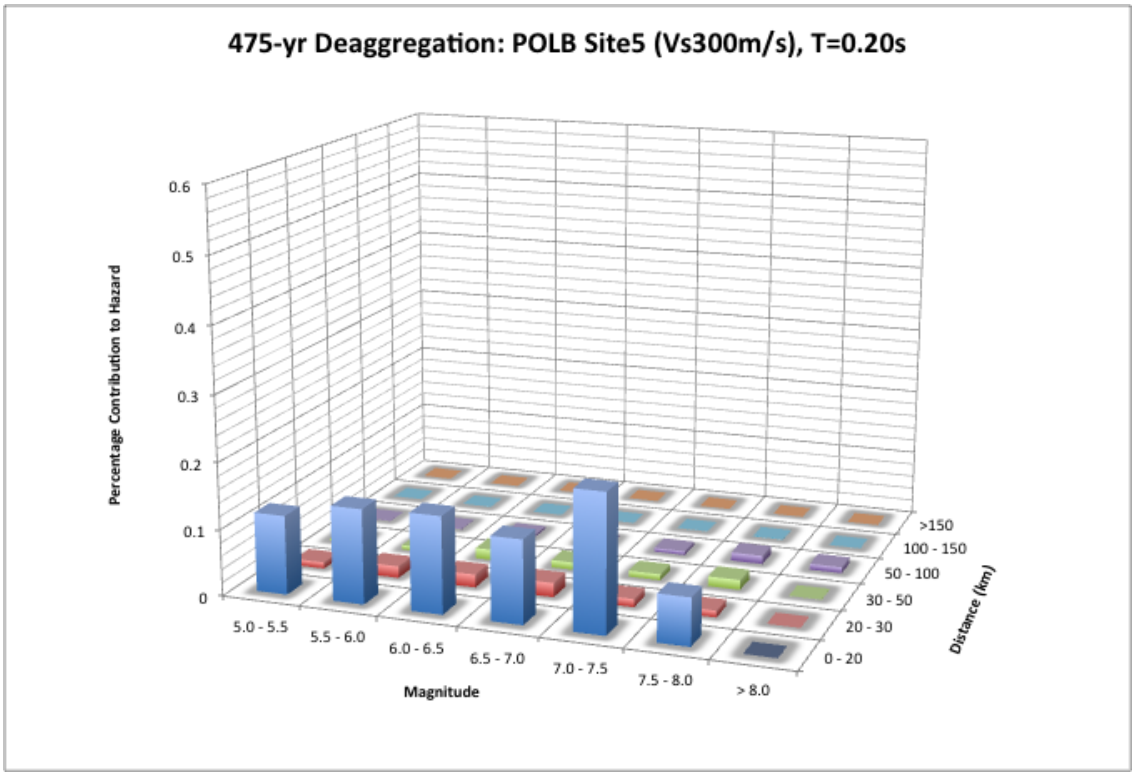


Figure 88. Magnitude-distance contribution for the 475-year (CLE) hazard level for T = 0.2 sec for Site 5 including the Wilmington fault.

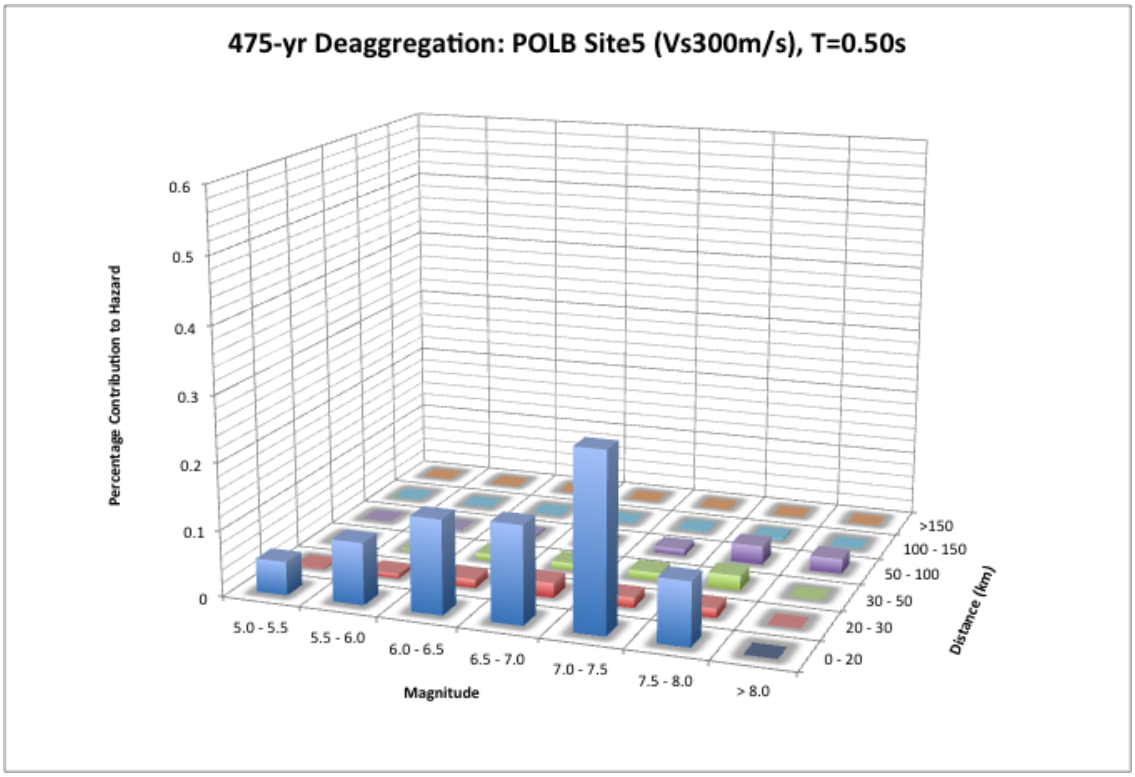


Figure 89. Magnitude-distance contribution for the 475-year (CLE) hazard level for T = 0.5 sec for Site 5 including the Wilmington fault .

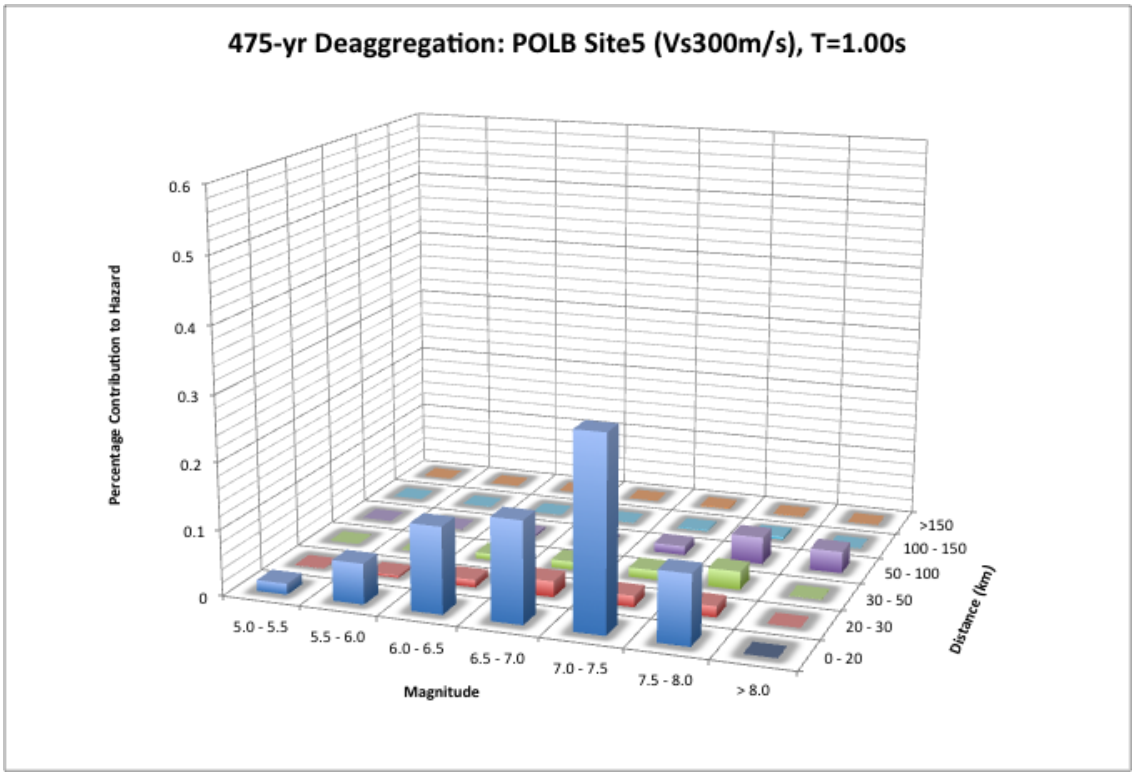


Figure 90. Magnitude-distance contribution for the 475-year (CLE) hazard level for T = 1.0 sec for Site 5 including the Wilmington fault.

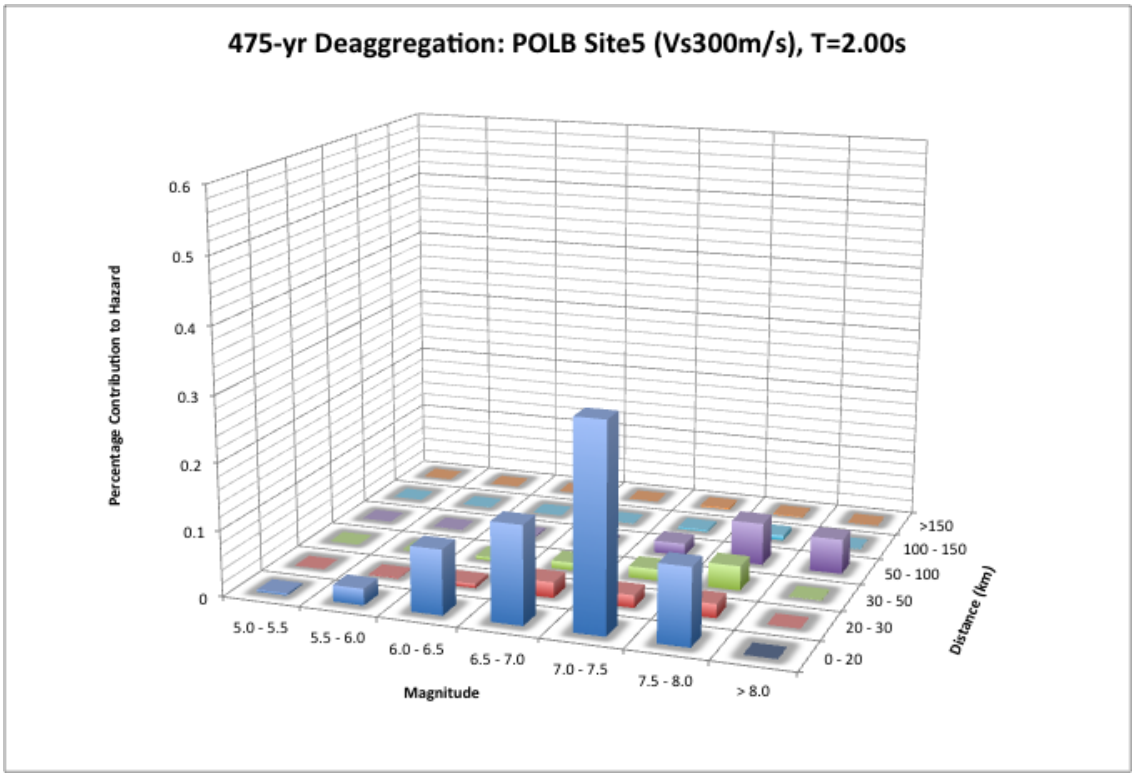


Figure 91. Magnitude-distance contribution for the 475-year (CLE) hazard level for T = 2.0 sec for Site 5 including the Wilmington fault.

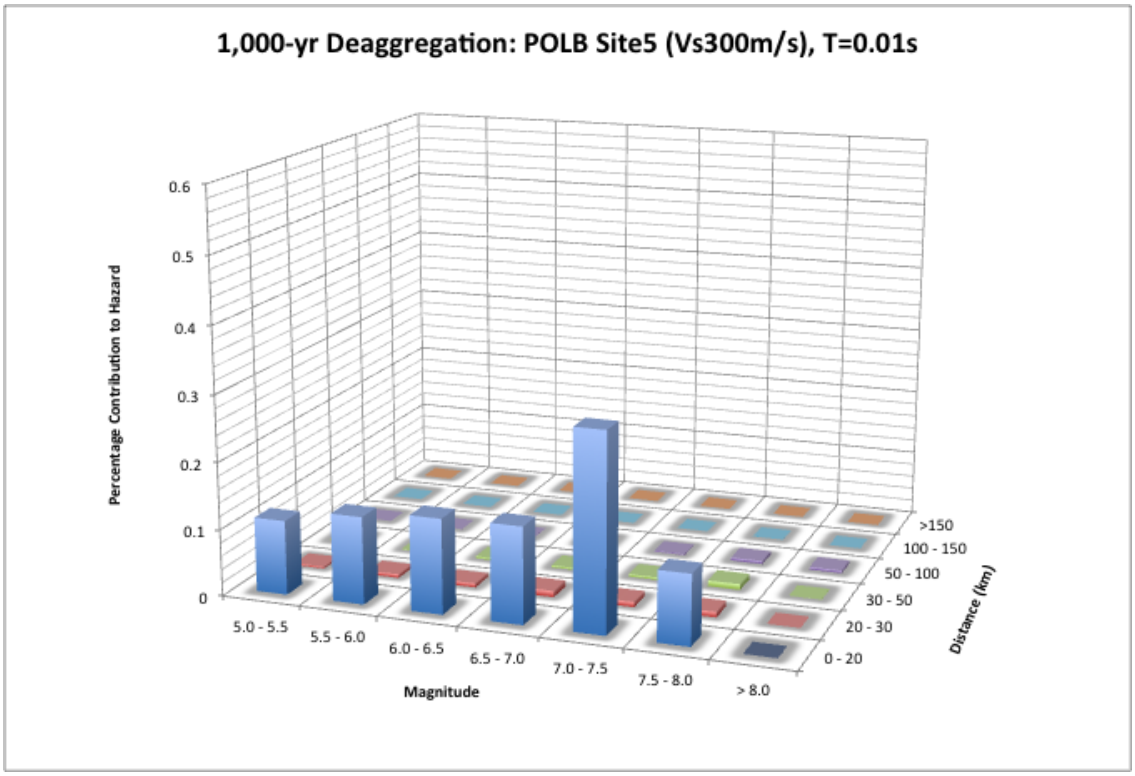


Figure 92. Magnitude-distance contribution for the 975-year hazard level for PGA for Site 5 including the Wilmington fault.

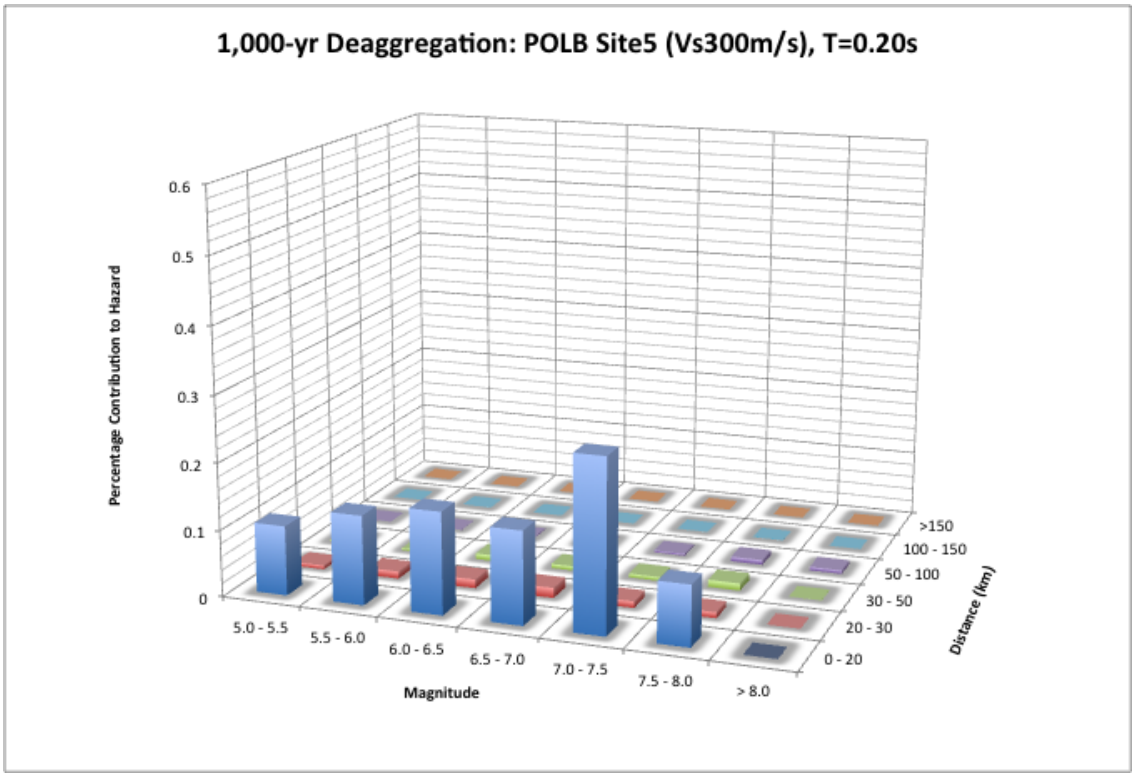


Figure 93. Magnitude-distance contribution for the 975-year hazard level for T = 0.2 sec for Site 5 including the Wilmington fault.

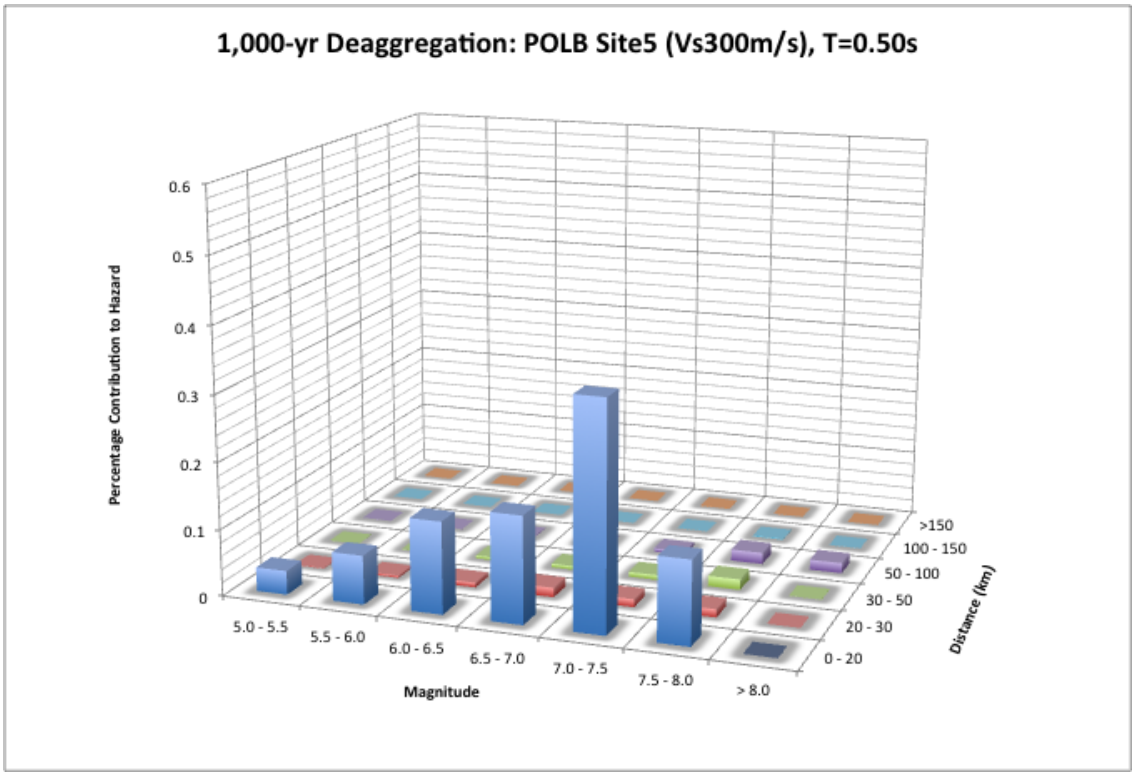


Figure 94. Magnitude-distance contribution for the 975-year hazard level for T = 0.5 sec for Site 5 including the Wilmington fault.

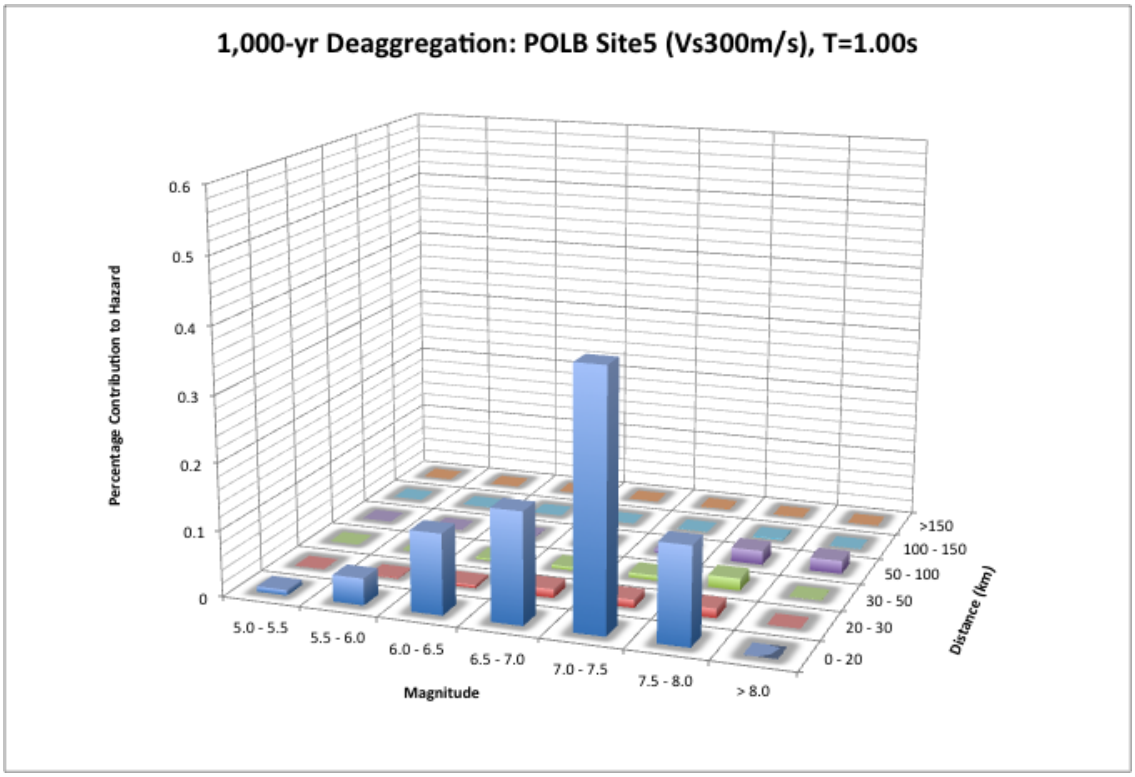


Figure 95. Magnitude-distance contribution for the 975-year hazard level for T = 1.0 sec for Site 5 including the Wilmington fault.

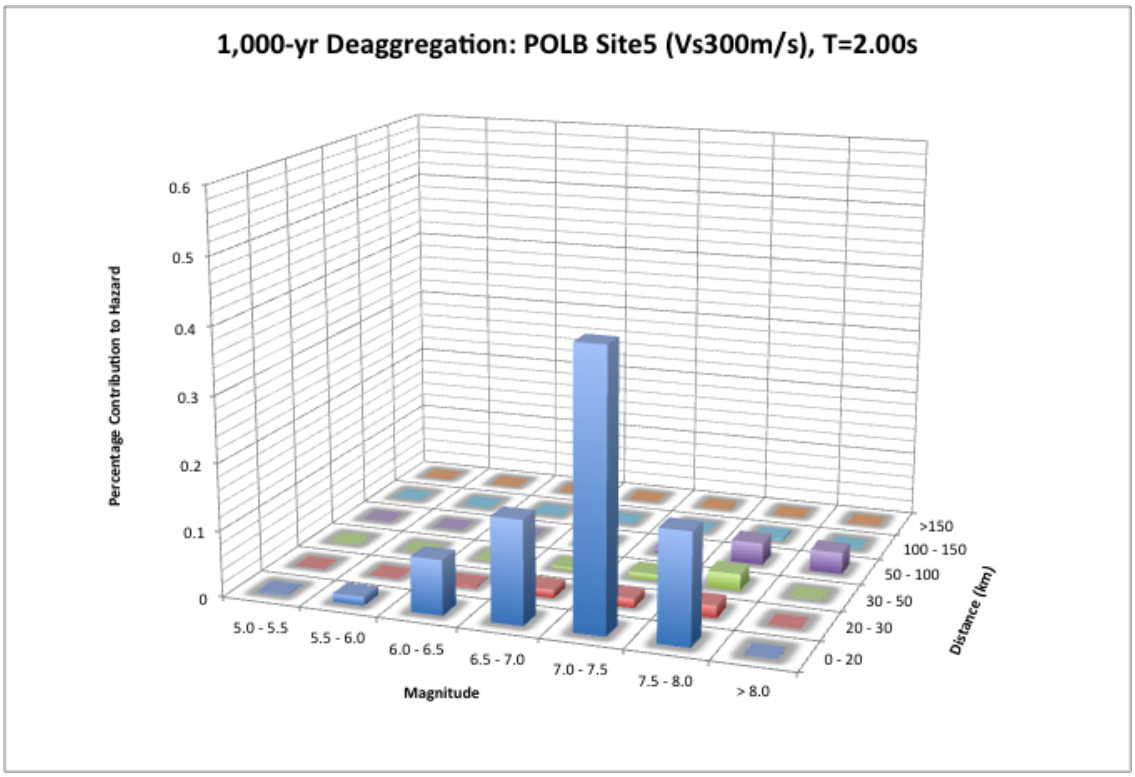


Figure 96. Magnitude-distance contribution for the 975-year hazard level for T = 2.0 sec for Site 5 including the Wilmington fault.

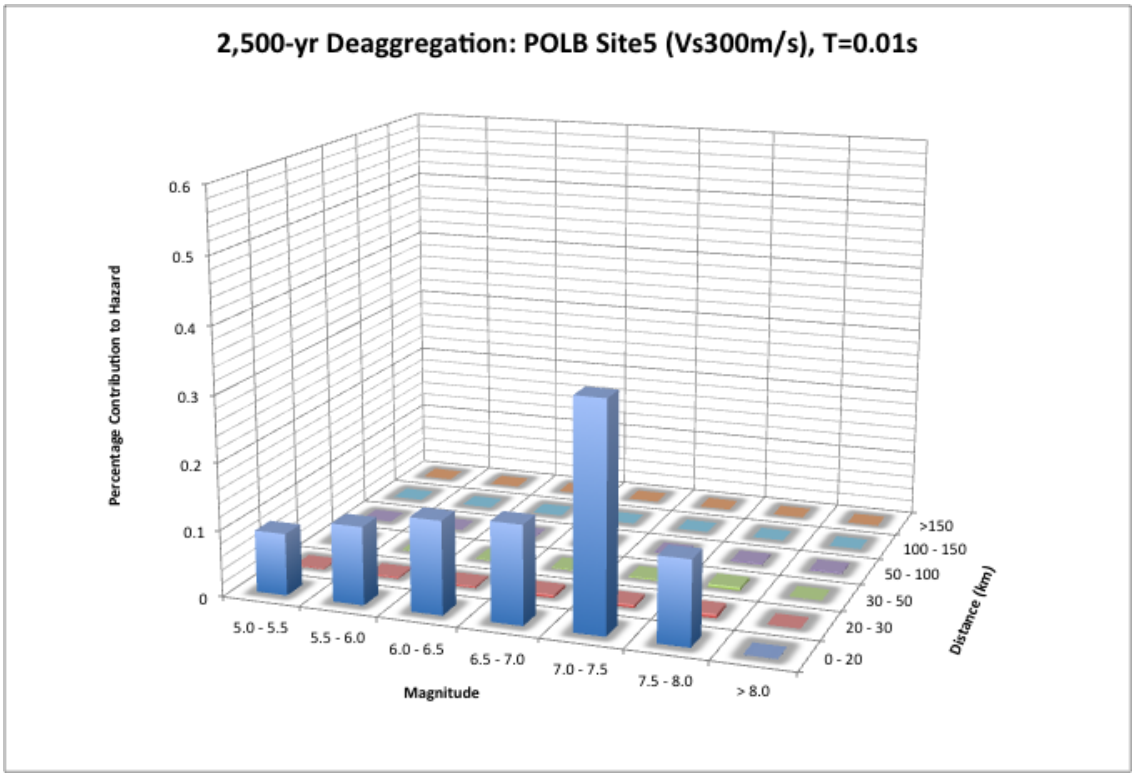


Figure 97. Magnitude-distance contribution for the 2,475-year hazard level for PGA for Site 5 including the Wilmington fault.

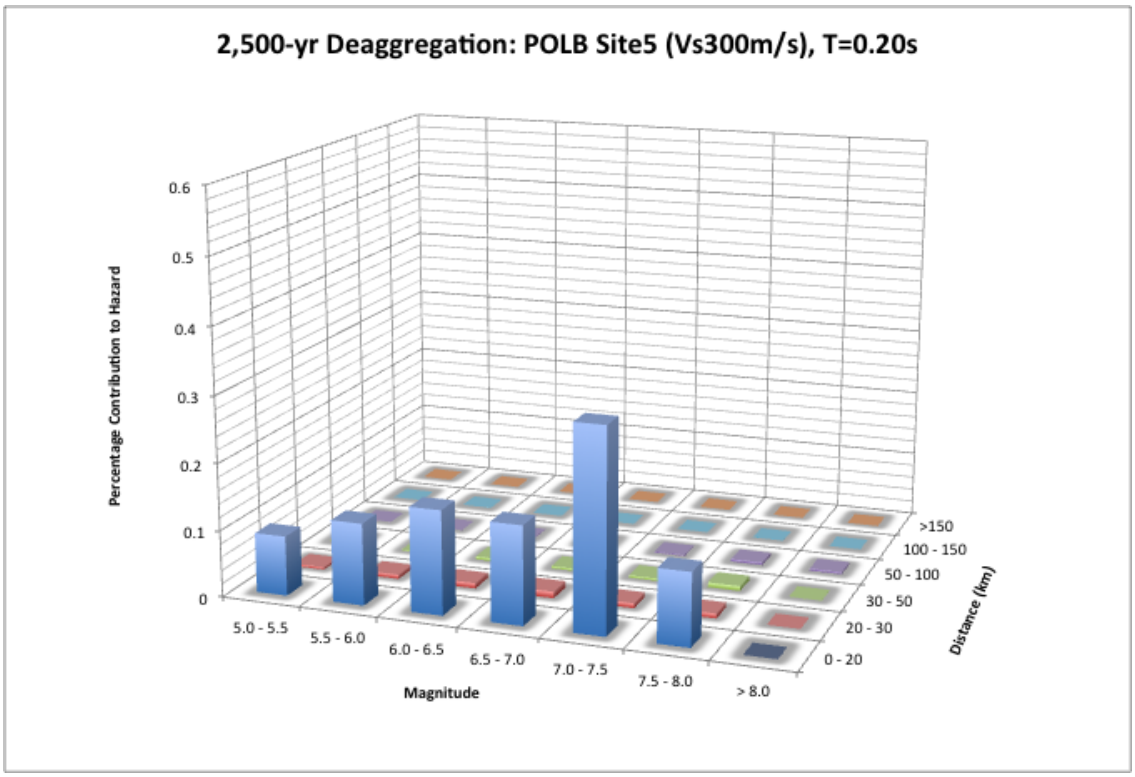


Figure 98. Magnitude-distance contribution for the 2,475-year hazard level for T = 0.2 sec for Site 5 including the Wilmington fault.

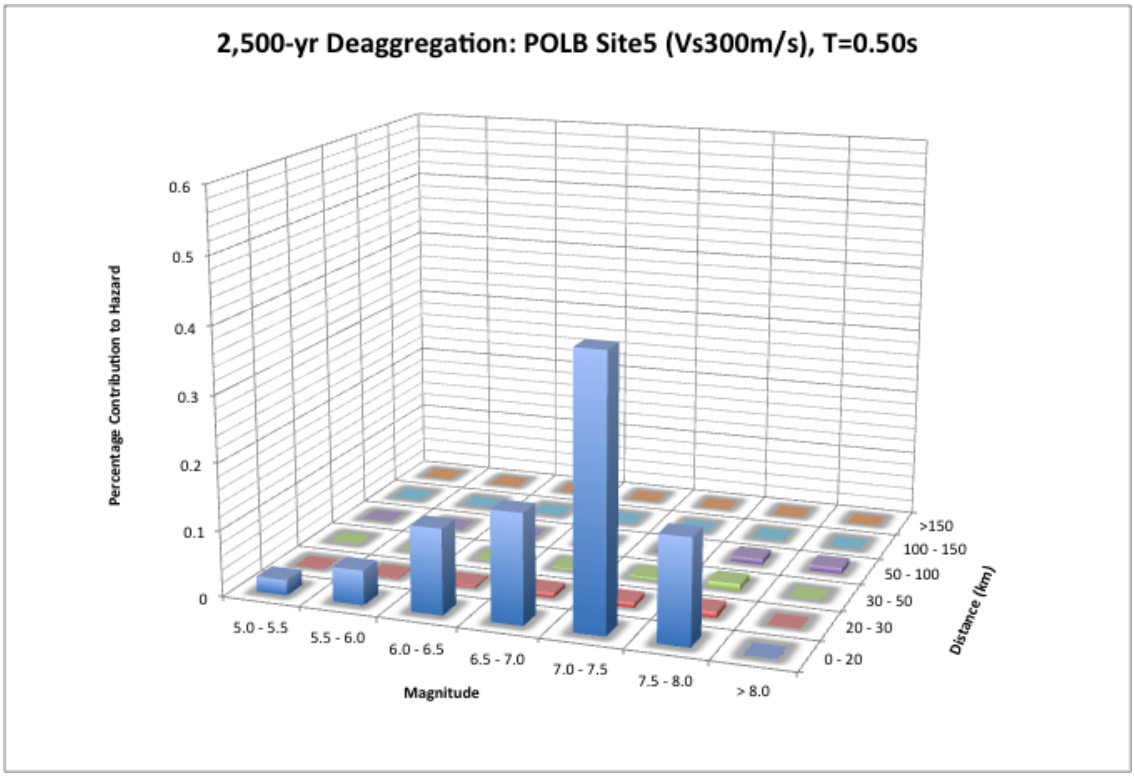


Figure 99. Magnitude-distance contribution for the 2,475-year hazard level for T = 0.5 sec for Site 5 including the Wilmington fault.

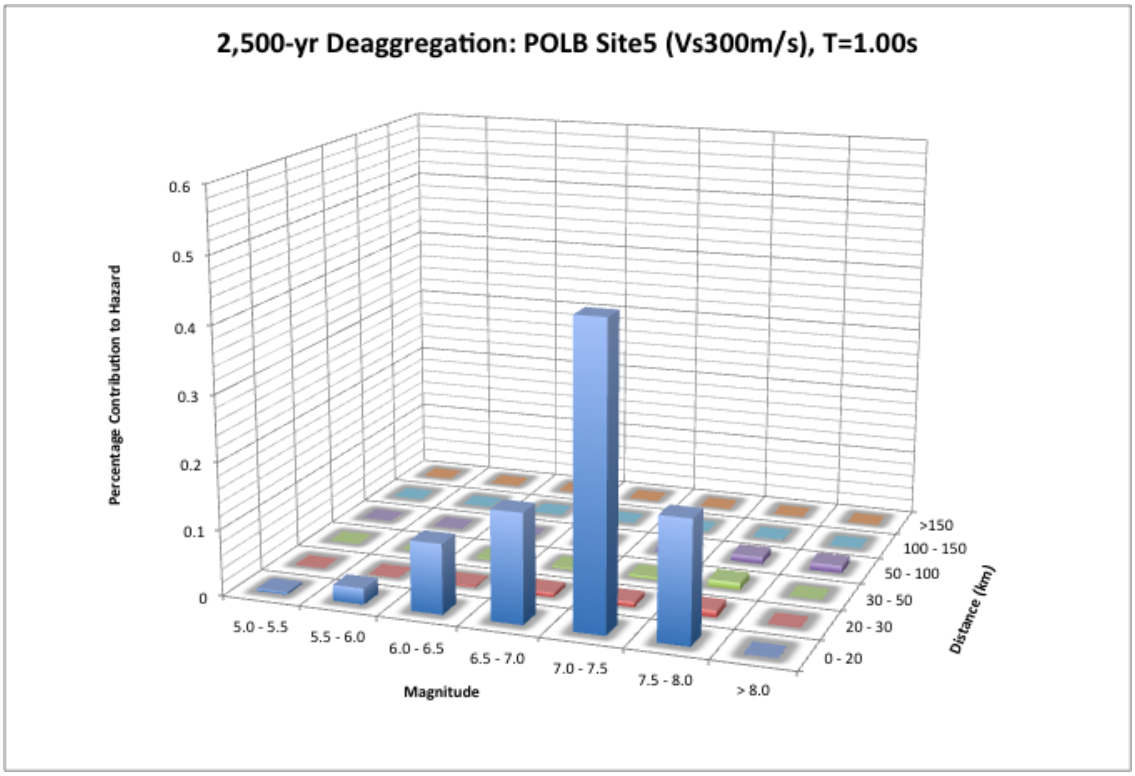


Figure 100. Magnitude-distance contribution for the 2,475-year hazard level for T = 1.0 sec for Site 5 including the Wilmington fault.

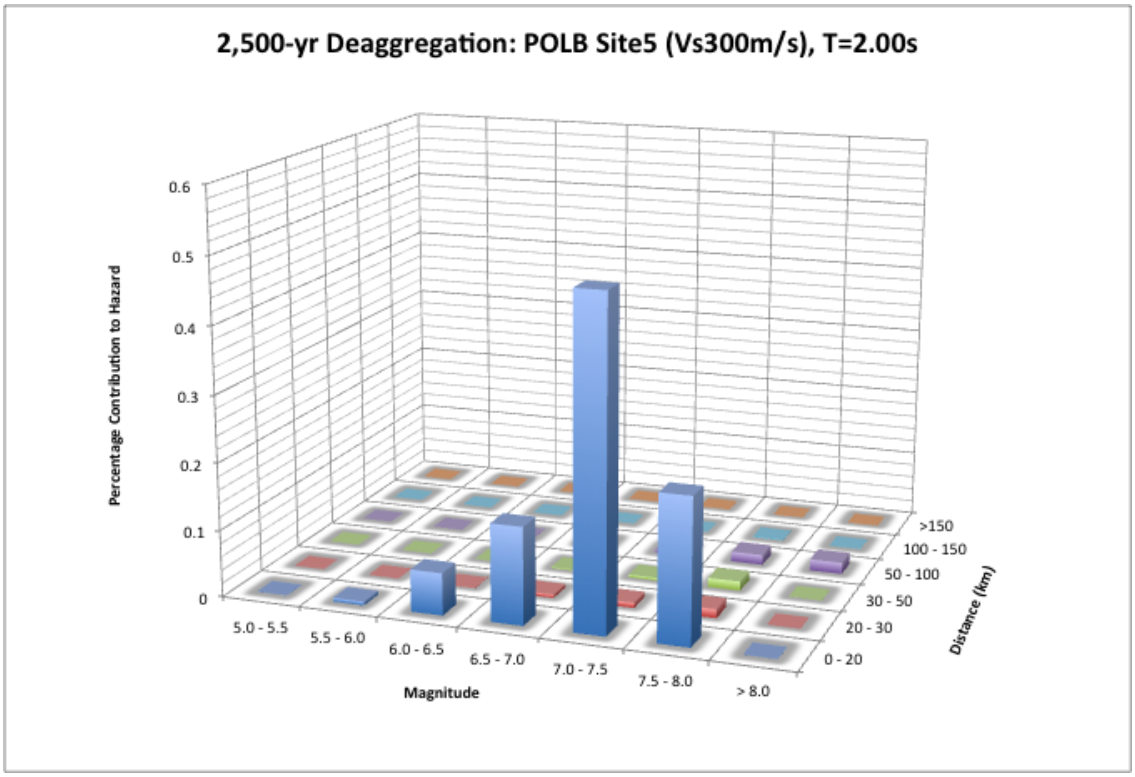


Figure 101. Magnitude-distance contribution for the 2,475-year hazard level for T = 2.0 sec for Site 5 including the Wilmington fault.

4.5 Site 8 – Horizontal

The mean hazard curves including the Wilmington fault for Site 8 are shown in Figures 102 through 106 for PGA and spectral periods of 0.2, 0.5, 1.0, and 2.0 sec. For the longer spectral periods (i.e., 1 and 2 sec) these plots are showing the horizontal component without the inclusion of the directivity model. In these plots, individual hazard curves from the scenario fault ruptures, gridded sources, the Wilmington fault, and the combined total hazard are presented. For the 72-year return period (OLE) hazard level, the hazard curve plots indicate that the hazard is primarily controlled by the contribution from the gridded point sources and to a lesser amount the contribution from the fault sources. At the 475-year (CLE) hazard level the contribution from the fault sources increases relative to the contribution form the gridded point sources. At the lower hazard levels of 975-year and 2,475-year return periods, the results indicate an increase in the relative contribution from the fault sources over the gridded point sources. Also observed in these hazard curve plots is the relatively small contribution from the Wilmington fault to the total hazard.

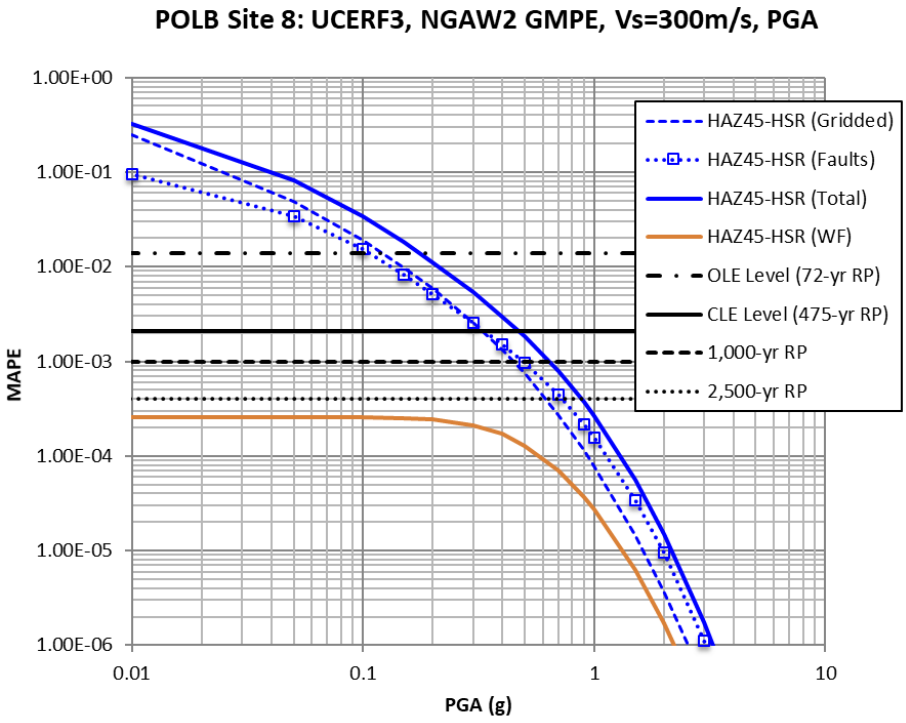


Figure 102. Mean horizontal component hazard curves from the UCERF3 gridded and fault sources, the Wilmington fault, and total hazard for PGA for Site 8.

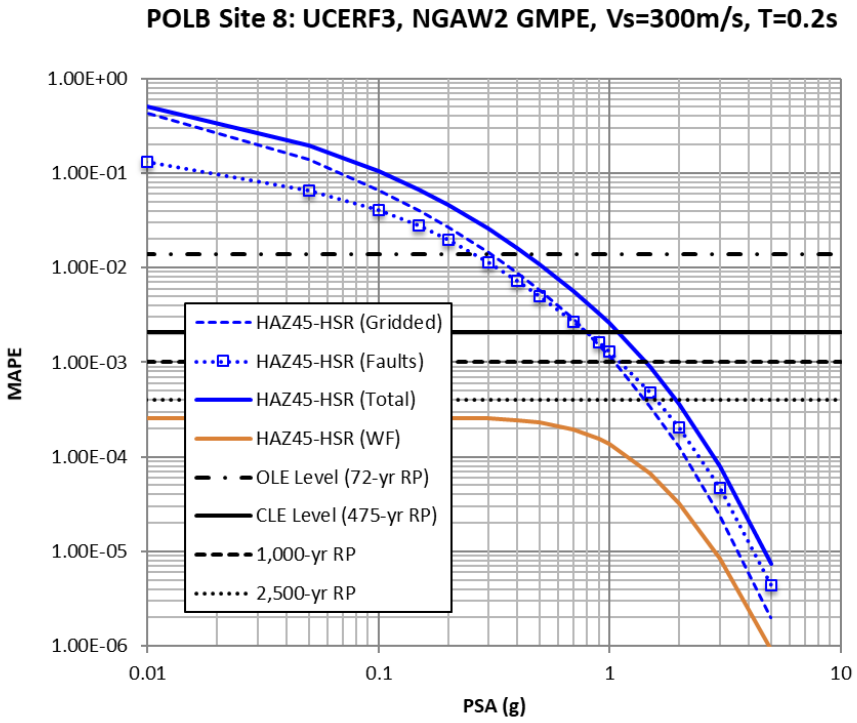


Figure 103. Mean horizontal component hazard curves from the UCERF3 gridded and fault sources, the Wilmington fault, and total hazard for T = 0.2 sec for Site 8.

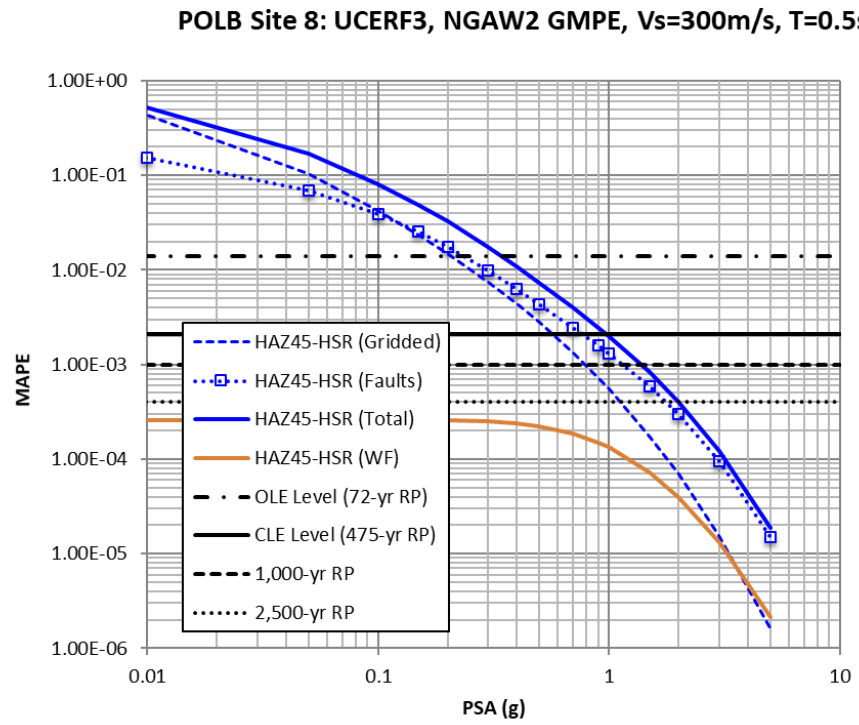


Figure 104. Mean horizontal component hazard curves from the UCERF3 gridded and fault sources, the Wilmington fault, and total hazard for T = 0.5 sec for Site 8.

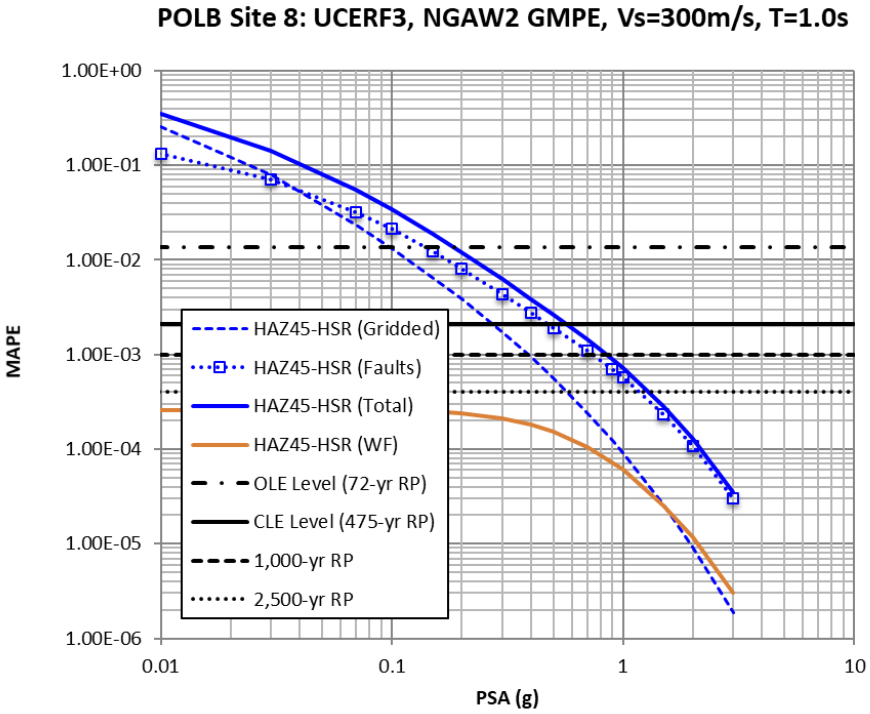


Figure 105. Mean horizontal component hazard curves from the UCERF3 gridded and fault sources, the Wilmington fault, and total hazard for T = 1.0 sec for Site 8.

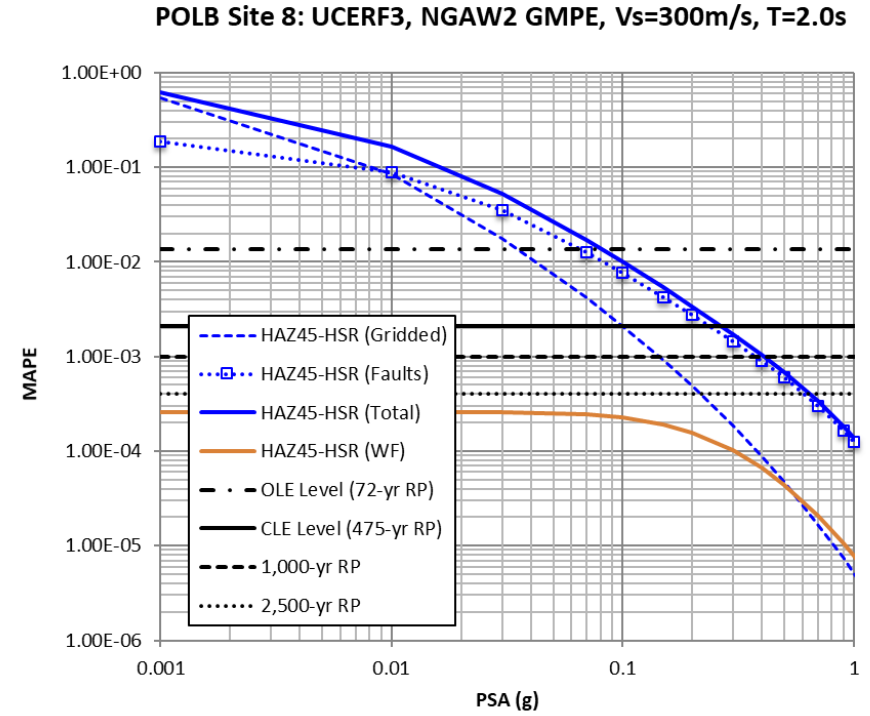


Figure 106. Mean horizontal component hazard curves from the UCERF3 gridded and fault sources, the Wilmington fault, and total hazard for T = 2.0 sec for Site 8.

Given the hazard curves for the full suite of spectral periods, the computed uniform hazard spectra (UHS) including the Wilmington fault for the 72-year (OLE), 475-year (OLE), 975-year and 2,475-year return period hazard levels are plotted in Figure 107. The horizontal UHS values at all spectral periods are given in Table 17 and these results are slightly higher (i.e., 3-4% or less) than the previous results without the Wilmington fault (Gregor and Al Atik, 2019).

Table 17. Horizontal UHS for Site 8 at the four hazard levels including the Wilmington fault.

Period (sec)	72-year (OLE) Horizontal PSA (g)	475-year (CLE) Horizontal PSA (g)	975-year Horizontal PSA (g)	2,475-year Horizontal PSA (g)
0.01	0.1764	0.4697	0.6354	0.8763
0.02	0.1762	0.4708	0.6369	0.8778
0.03	0.1831	0.4862	0.6560	0.9025
0.04	0.1979	0.5188	0.7018	0.9589
0.05	0.2139	0.5567	0.7519	1.0304
0.075	0.2717	0.6949	0.9292	1.2586
0.1	0.3303	0.8231	1.0892	1.4864
0.15	0.4067	0.9968	1.2997	1.7511
0.2	0.4358	1.0808	1.4362	1.9386
0.25	0.4390	1.1178	1.5120	2.0602
0.3	0.4293	1.1237	1.5413	2.1329
0.4	0.3845	1.0568	1.4839	2.1124
0.5	0.3428	0.9713	1.3751	2.0090
0.75	0.2462	0.7327	1.0687	1.6061
1	0.1834	0.5666	0.8476	1.2906
1.5	0.1158	0.3728	0.5645	0.8848
2	0.0805	0.2669	0.4103	0.6451
3	0.0478	0.1654	0.2545	0.4067
4	0.0320	0.1140	0.1753	0.2756
5	0.0227	0.0840	0.1284	0.2026
7.5	0.0121	0.0478	0.0719	0.1091
10	0.0074	0.0306	0.0456	0.0692

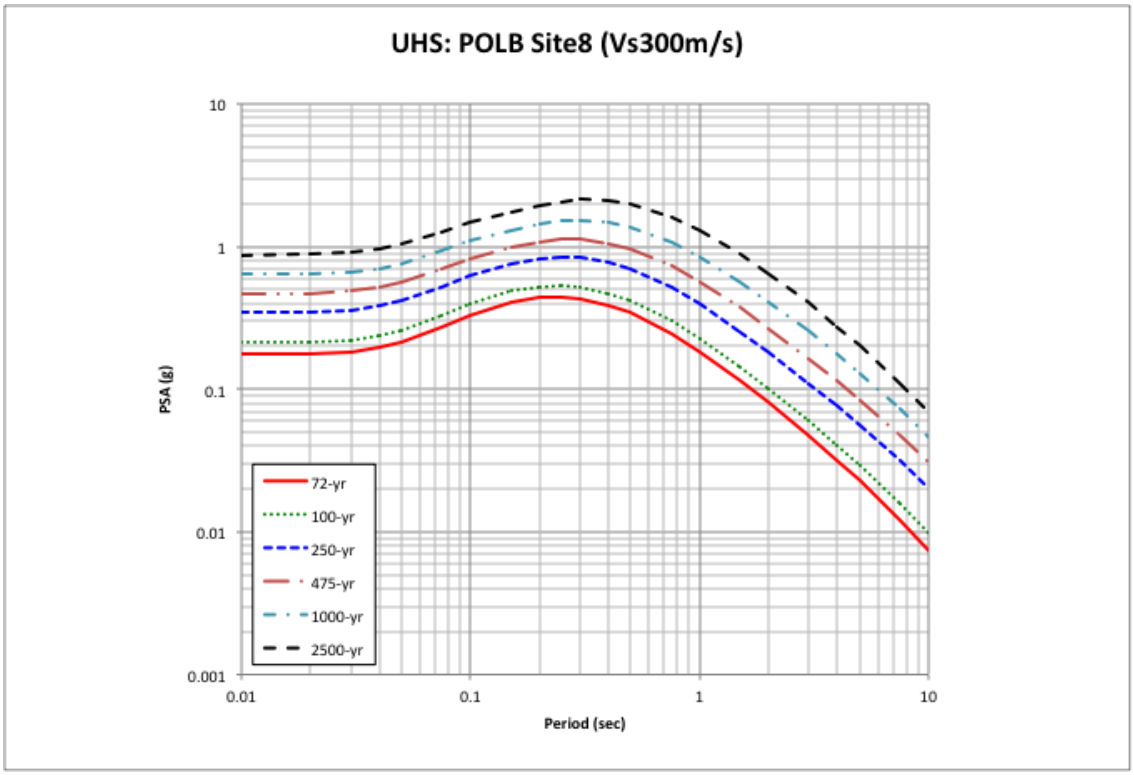


Figure 107. Uniform hazard spectra for Site 8 including the Wilmington fault.

The mean magnitude, distance and epsilon values for the horizontal component including the Wilmington fault but without the directivity model are plotted in Figures 108 to 110 for the four hazard levels. These plots are shown as a function of spectral period. As expected, the magnitude increases and the distance decreases with the increasing return period hazard levels. Also observed in these plots is the expected increase in the mean epsilon values between the four hazard levels with the 2,475-year results greater than approximately 1 over the full spectral period range. The mean magnitude, distance and epsilon values including the Wilmington fault are listed in Tables 18 through 20 for the four hazard levels. These values are similar to the previous results without the Wilmington fault (Gregor and Al Atik, 2019).

Table 18. Mean magnitude for the four hazard levels for Site 8 including the Wilmington fault.

Period (sec)	72-year (OLE) Magnitude	475-year (CLE) Magnitude	975-year Magnitude	2,475-year Magnitude
0.01	6.37	6.56	6.64	6.72
0.02	6.36	6.56	6.64	6.72
0.03	6.35	6.54	6.62	6.70
0.04	6.33	6.52	6.60	6.66
0.05	6.32	6.50	6.57	6.62
0.075	6.28	6.45	6.51	6.55
0.1	6.26	6.43	6.48	6.53
0.15	6.28	6.46	6.52	6.59
0.2	6.33	6.53	6.61	6.67
0.25	6.39	6.60	6.68	6.75
0.3	6.43	6.65	6.75	6.82
0.4	6.52	6.76	6.86	6.94
0.5	6.59	6.84	6.93	7.01
0.75	6.70	6.94	7.02	7.09
1	6.77	7.00	7.08	7.13
1.5	6.90	7.12	7.17	7.22
2	6.99	7.19	7.22	7.25
3	7.11	7.29	7.31	7.32
4	7.19	7.37	7.37	7.38
5	7.24	7.42	7.42	7.42
7.5	7.31	7.55	7.55	7.55
10	7.35	7.59	7.61	7.62

Table 19. Mean distance for the four hazard levels for Site 8 including the Wilmington fault.

Period (sec)	72-year (OLE) Distance (km)	475-year (CLE) Distance (km)	975-year Distance (km)	2,475-year Distance (km)
0.01	26.79	11.06	8.60	6.79
0.02	26.62	10.90	8.50	6.73
0.03	26.53	11.05	8.65	6.87
0.04	26.22	11.33	8.67	7.07
0.05	26.59	11.98	9.24	7.50
0.075	26.64	12.50	10.00	8.51
0.1	26.49	13.10	10.74	8.68
0.15	26.54	13.14	11.01	8.83
0.2	27.47	13.55	10.71	8.51
0.25	28.50	13.76	10.35	8.29
0.3	29.77	14.06	10.42	8.18
0.4	32.60	14.76	10.65	8.12
0.5	35.28	15.56	11.50	8.15
0.75	40.29	17.35	12.06	8.30
1	42.49	18.20	11.96	8.42
1.5	48.57	20.76	13.78	8.77
2	52.08	22.75	14.29	9.37
3	57.76	25.63	17.02	10.08
4	61.35	29.25	19.42	12.55
5	63.95	32.22	22.92	14.69
7.5	73.58	42.97	34.78	27.56
10	79.02	50.23	43.80	37.00

Table 20. Mean epsilon for the four hazard levels for Site 8 including the Wilmington fault.

Period (sec)	72-year (OLE) Epsilon	475-year (CLE) Epsilon	975-year Epsilon	2,475-year Epsilon
0.01	0.147	0.648	0.923	1.294
0.02	0.145	0.647	0.925	1.306
0.03	0.176	0.689	0.968	1.333
0.04	0.213	0.730	1.013	1.361
0.05	0.248	0.778	1.048	1.389
0.075	0.319	0.892	1.149	1.442
0.1	0.359	0.942	1.191	1.509
0.15	0.347	0.944	1.183	1.496
0.2	0.307	0.863	1.123	1.451
0.25	0.286	0.792	1.047	1.371
0.3	0.290	0.745	0.988	1.304
0.4	0.286	0.673	0.903	1.221
0.5	0.296	0.647	0.866	1.204
0.75	0.302	0.593	0.799	1.142
1	0.280	0.535	0.742	1.088
1.5	0.233	0.488	0.694	1.063
2	0.184	0.456	0.662	1.026
3	0.096	0.425	0.637	1.005
4	-0.001	0.417	0.647	1.004
5	-0.069	0.424	0.669	1.030
7.5	-0.197	0.489	0.797	1.149
10	-0.301	0.467	0.797	1.207

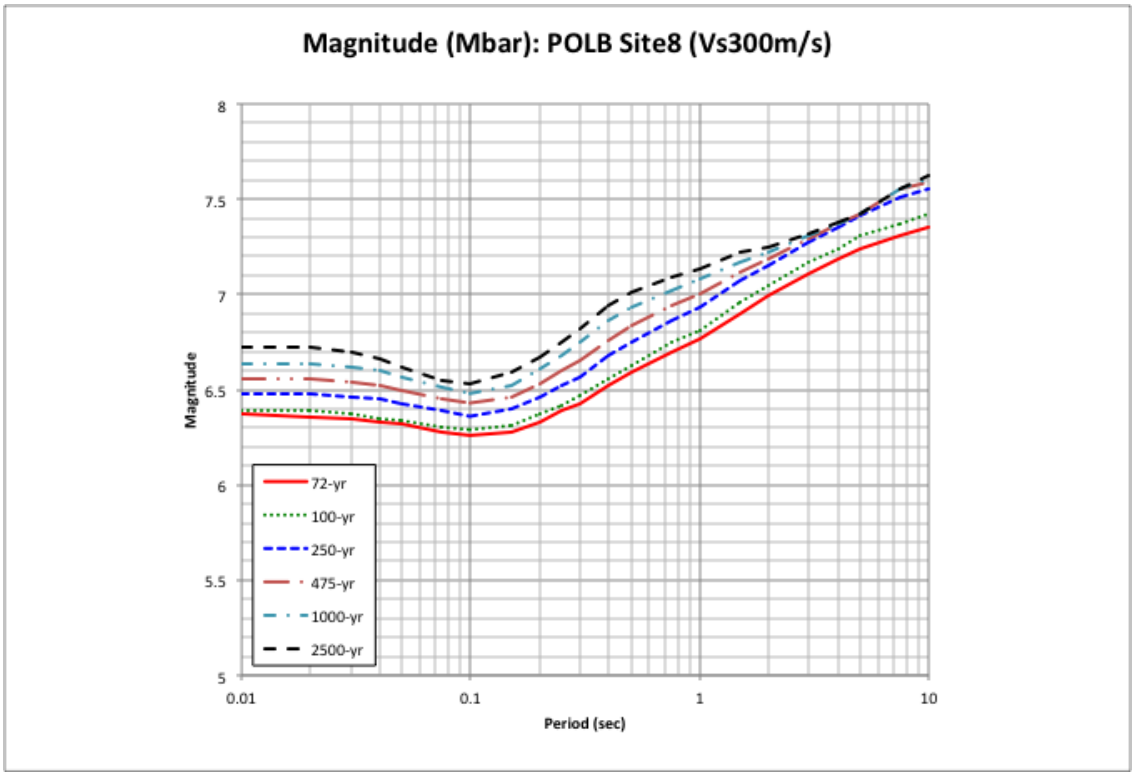


Figure 108. Horizontal mean magnitude for Site 8 including the Wilmington fault.

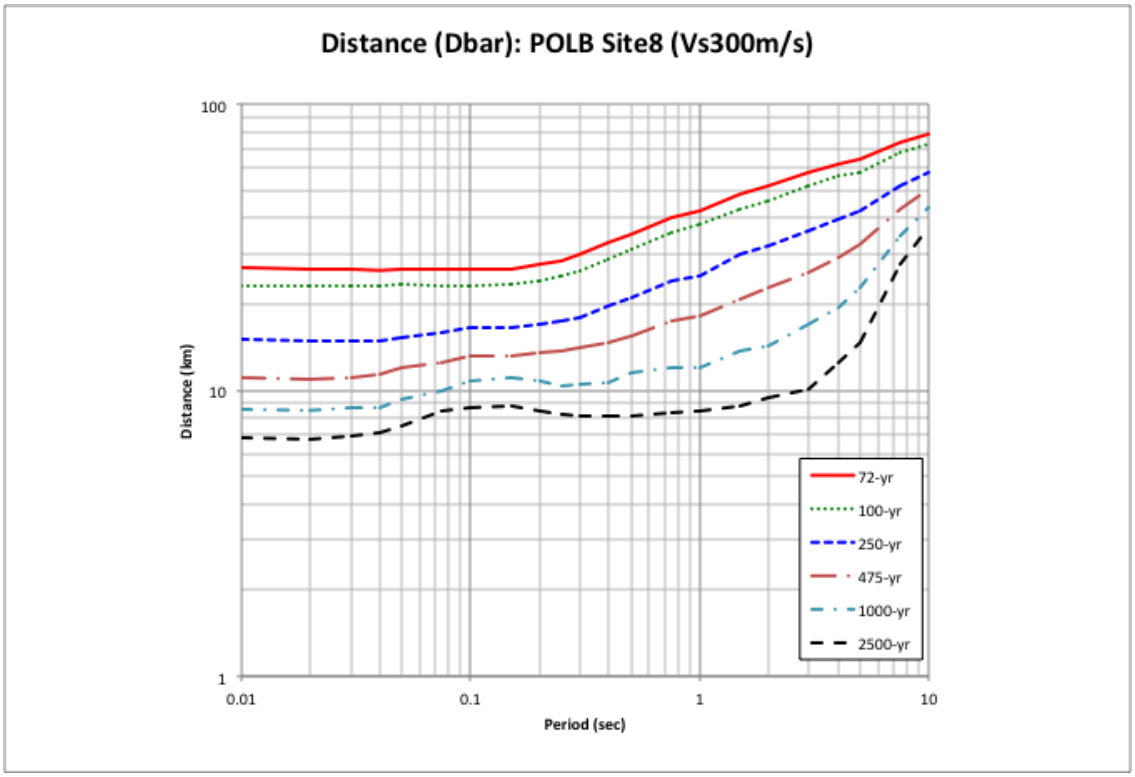


Figure 109. Horizontal mean distance for Site 8 including the Wilmington fault.

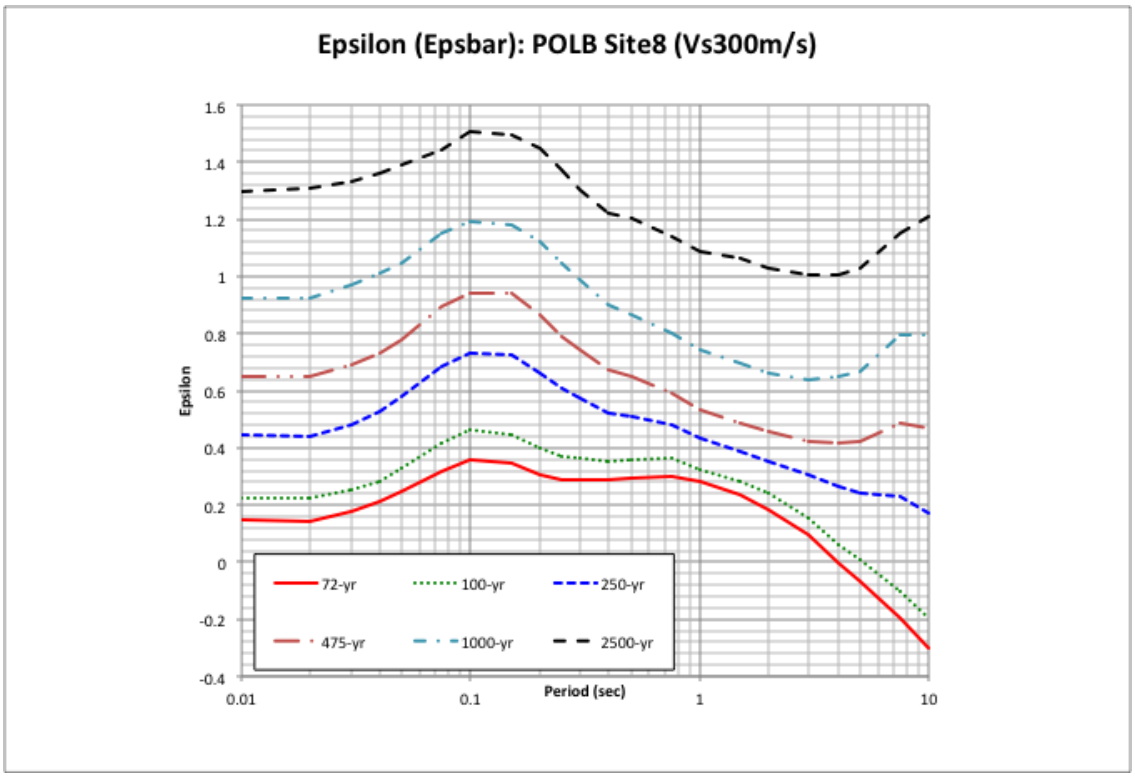


Figure 110. Horizontal mean epsilon for Site 8 including the Wilmington fault.

The binned magnitude and distance contributions including the Wilmington fault to the 72-year (OLE) hazard level are shown in Figures 111 to 115 for the site for PGA and spectral periods of 0.2, 0.5, 1.0, and 2.0 sec. Similar plots are shown in Figures 116 to 120 for the 475-year (CLE) hazard level, Figures 121 to 125 for the 975-year hazard level, and Figures 126 to 130 for the 2,475-year hazard level. These deaggregation results are very similar to the previous results for the other sites and for the case without the Wilmington fault (Gregor and Al Atik, 2019), with the same general observations and conclusions on the controlling sources for the total hazard.

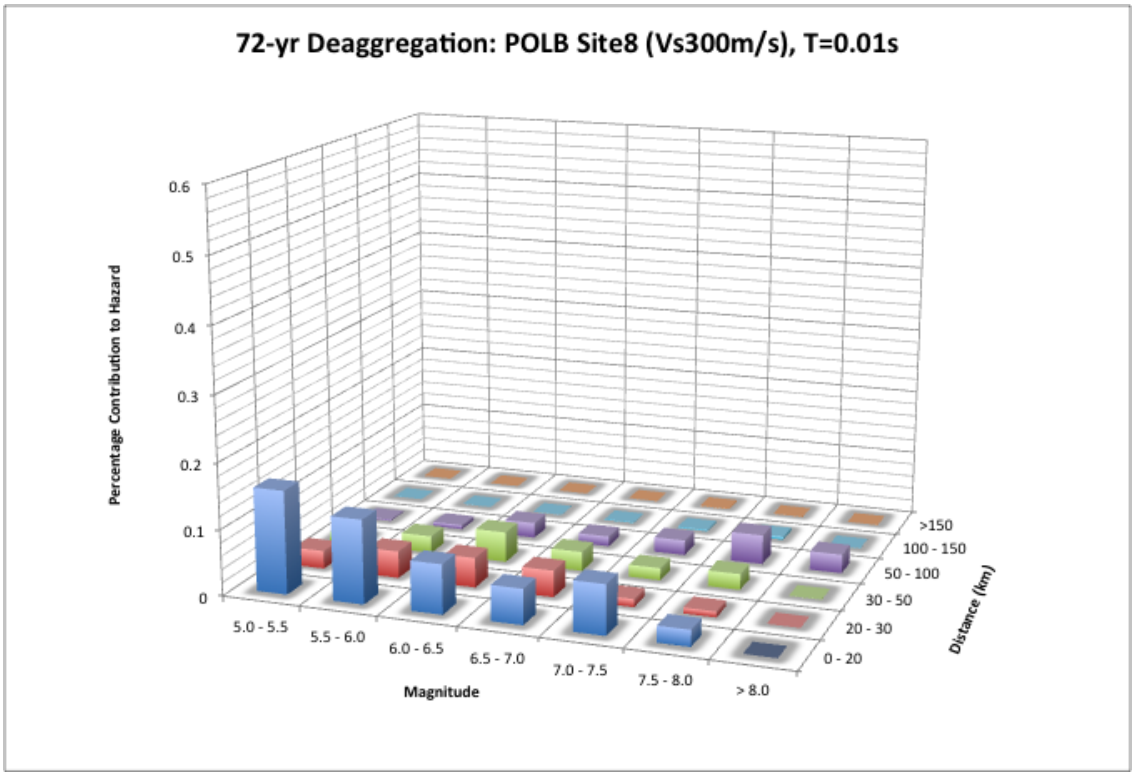


Figure 111. Magnitude-distance contribution for the 72-year (OLE) hazard level for PGA for Site 8 including the Wilmington fault.

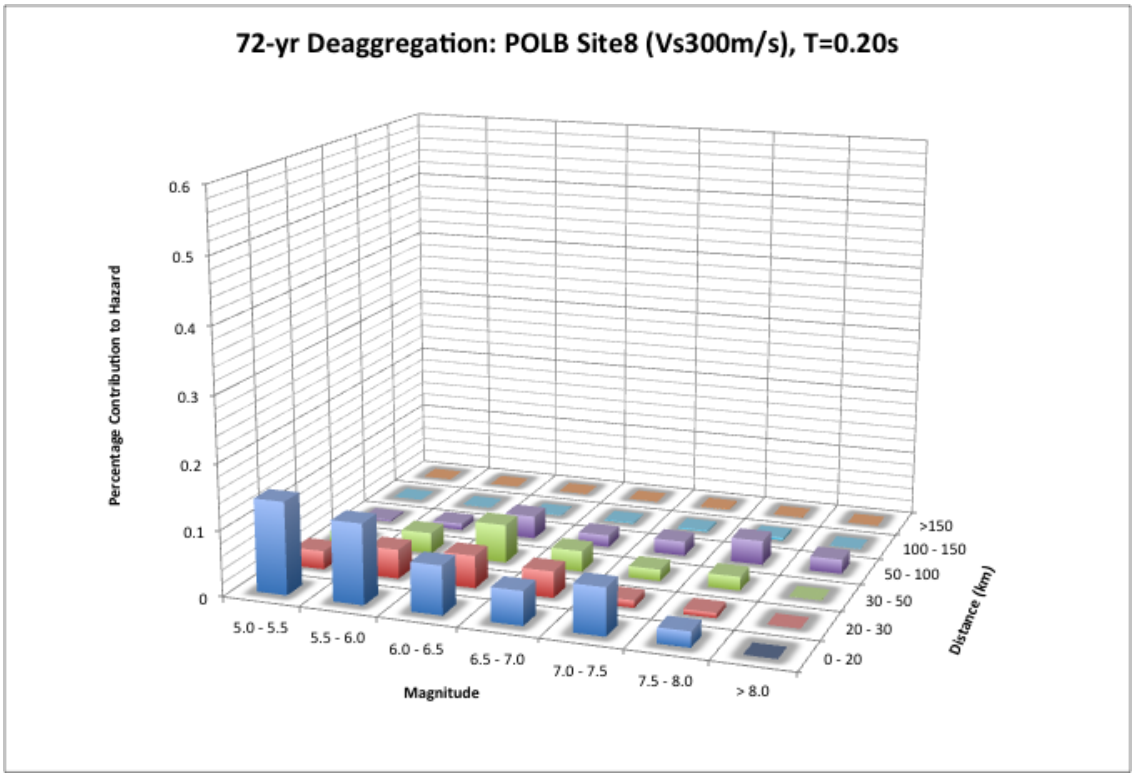


Figure 112. Magnitude-distance contribution for the 72-year (OLE) hazard level for T = 0.2 sec for Site 8 including the Wilmington fault.

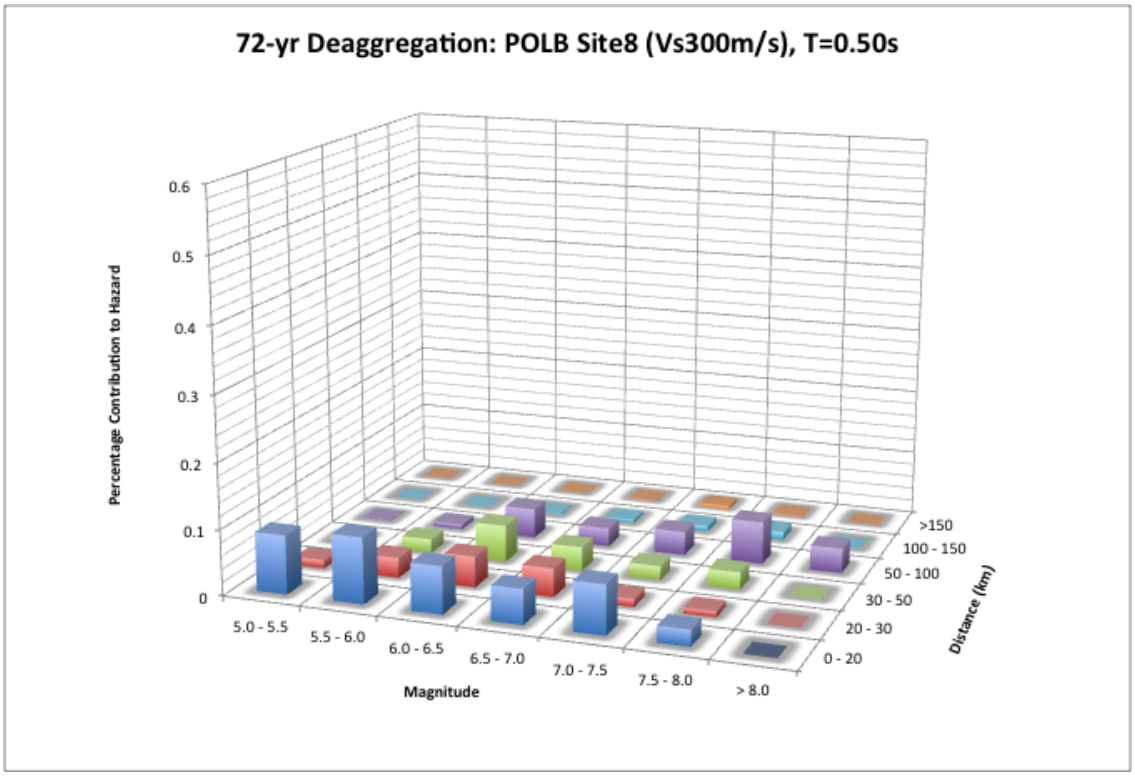


Figure 113. Magnitude-distance contribution for the 72-year (OLE) hazard level for T = 0.5 sec for Site 8 including the Wilmington fault.

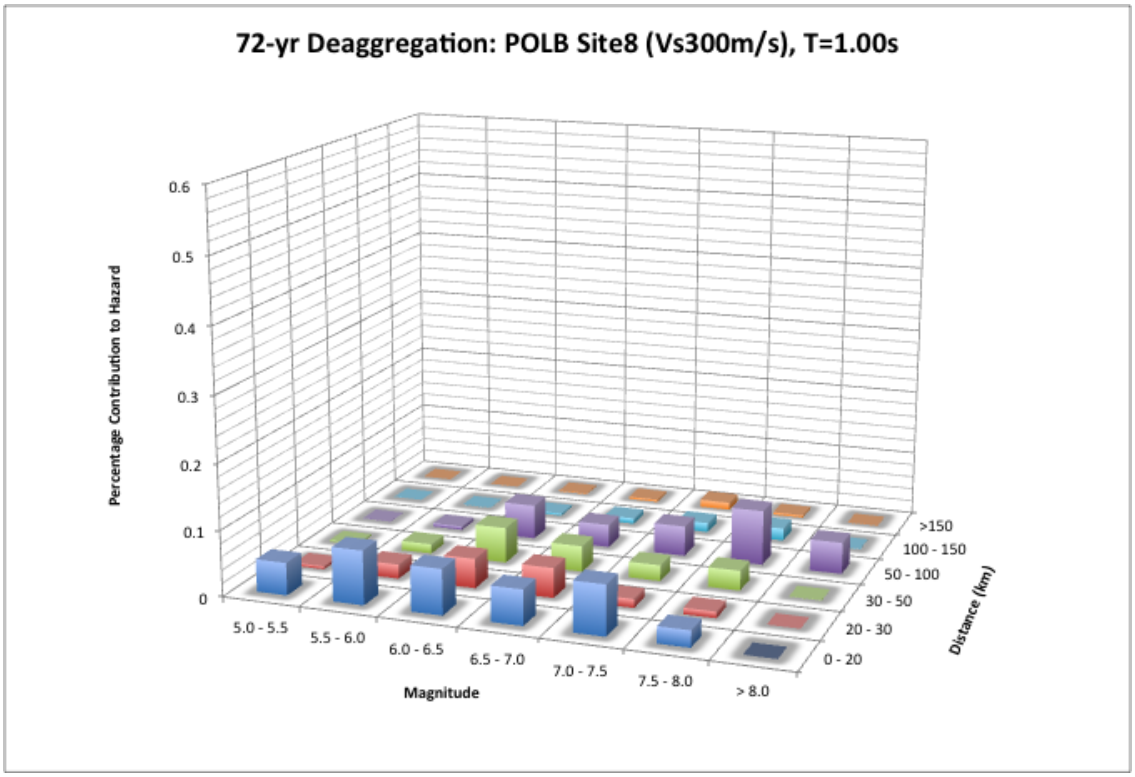


Figure 114. Magnitude-distance contribution for the 72-year (OLE) hazard level for T = 1.0 sec for Site 8 including the Wilmington fault.

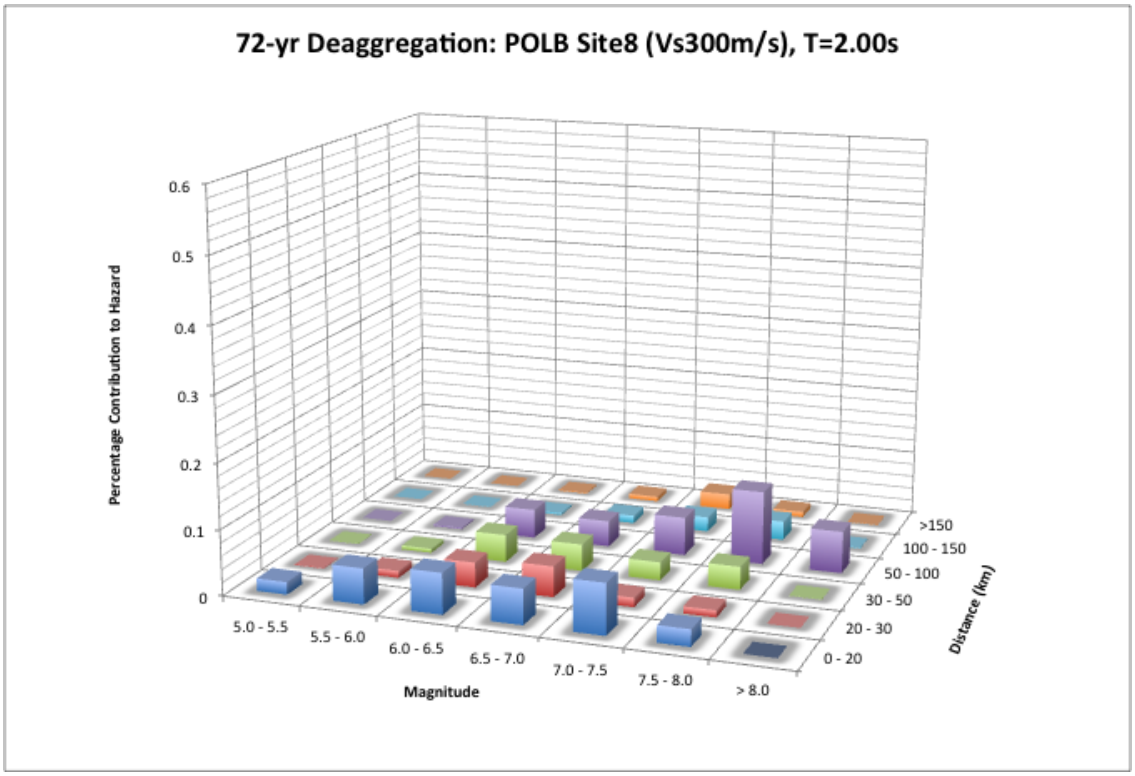


Figure 115. Magnitude-distance contribution for the 72-year (OLE) hazard level for T = 2.0 sec for Site 8 including the Wilmington fault.

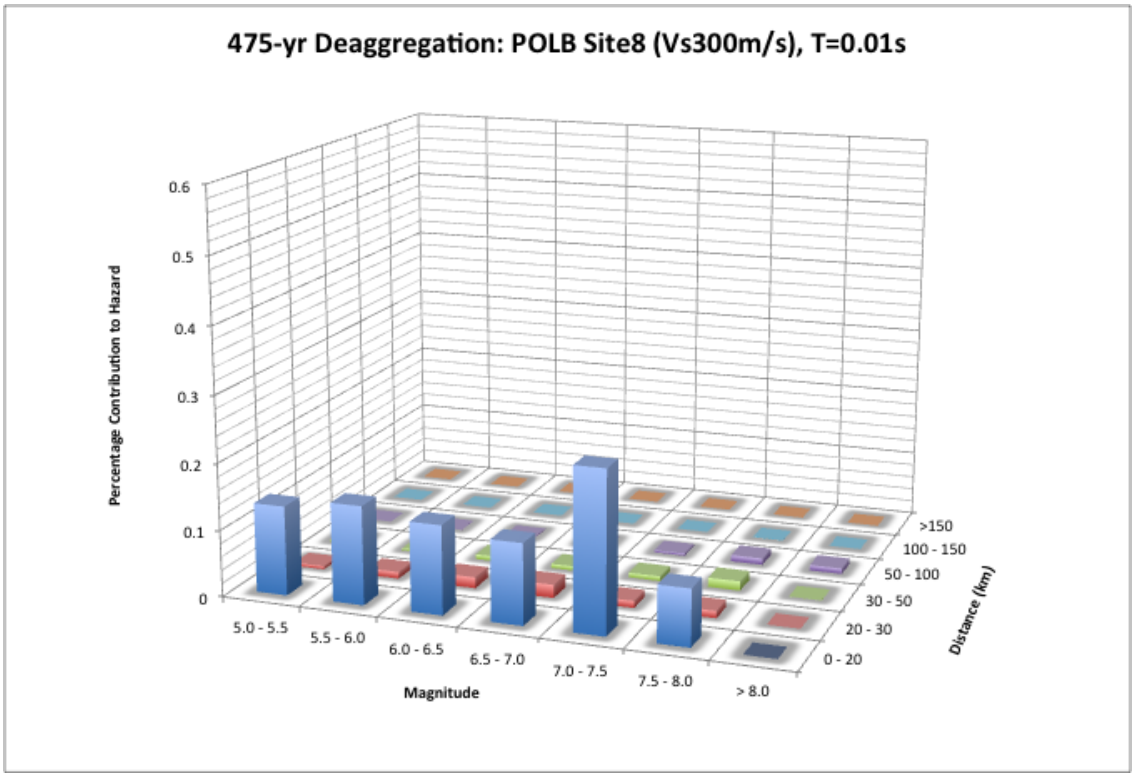


Figure 116. Magnitude-distance contribution for the 475-year (CLE) hazard level for PGA for Site 8 including the Wilmington fault.

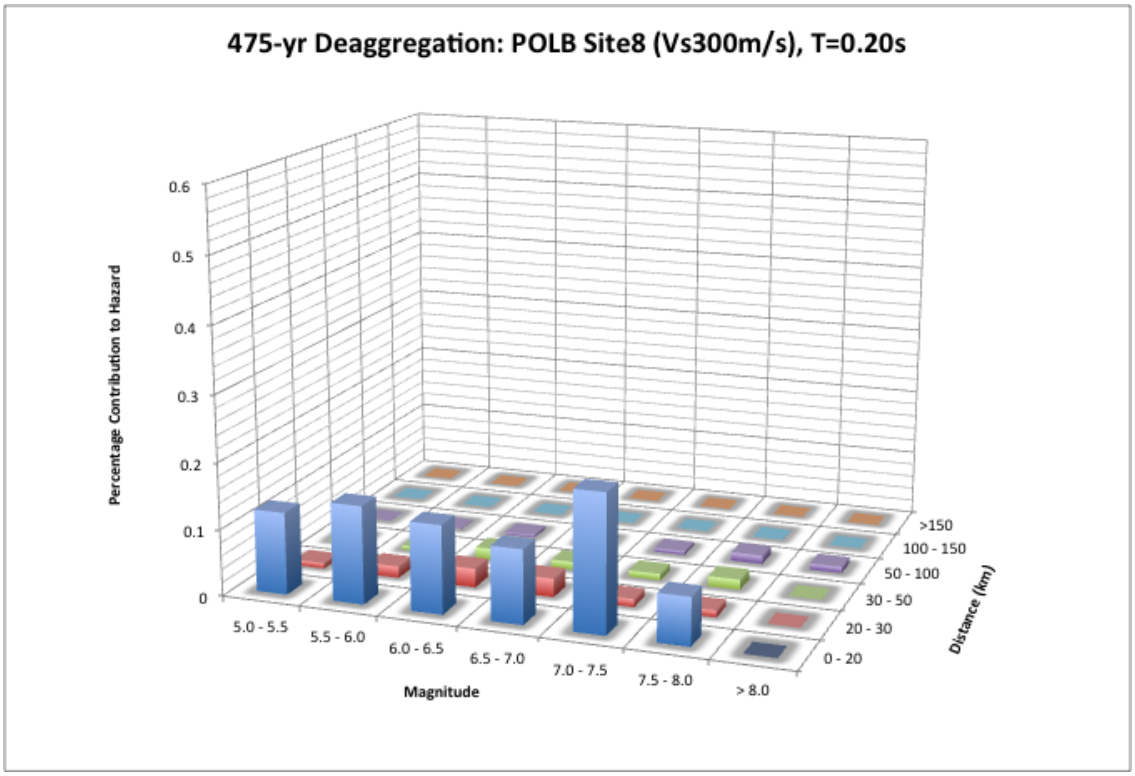


Figure 117. Magnitude-distance contribution for the 475-year (CLE) hazard level for T = 0.2 sec for Site 8 including the Wilmington fault.

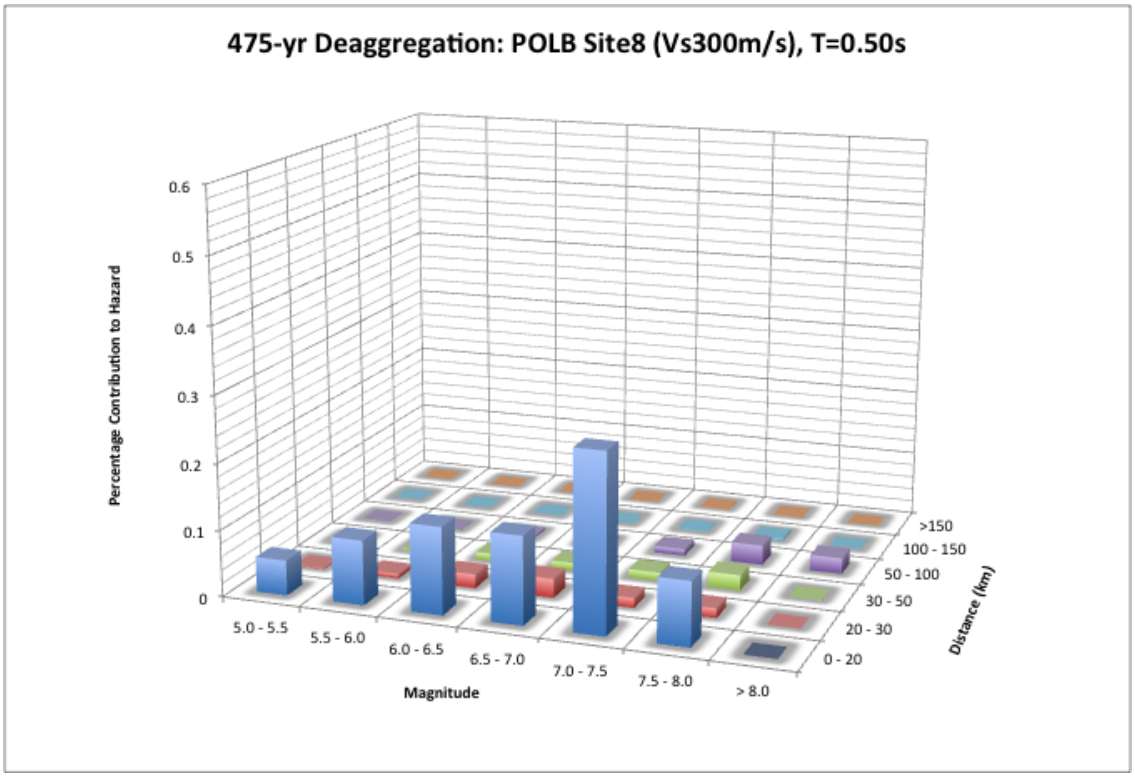


Figure 118. Magnitude-distance contribution for the 475-year (CLE) hazard level for T = 0.5 sec for Site 8 including the Wilmington fault.

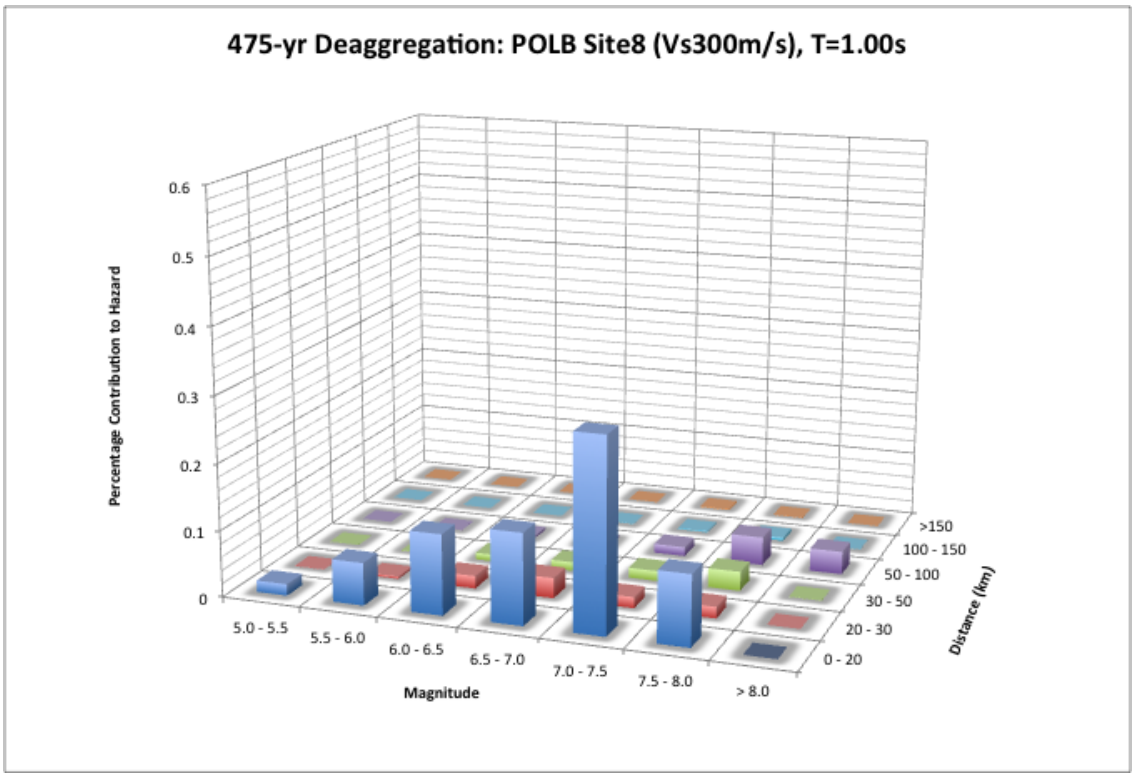


Figure 119. Magnitude-distance contribution for the 475-year (CLE) hazard level for T = 1.0 sec for Site 8 including the Wilmington fault.

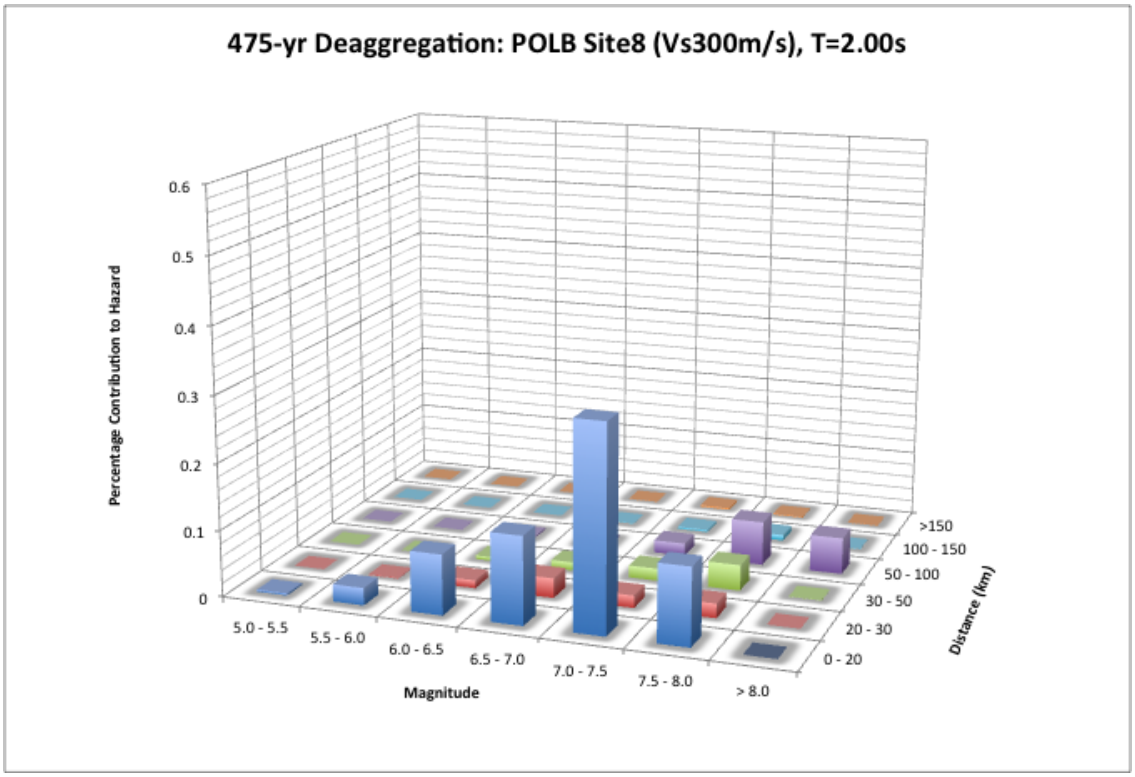


Figure 120. Magnitude-distance contribution for the 475-year (CLE) hazard level for T = 2.0 sec for Site 8 including the Wilmington fault.

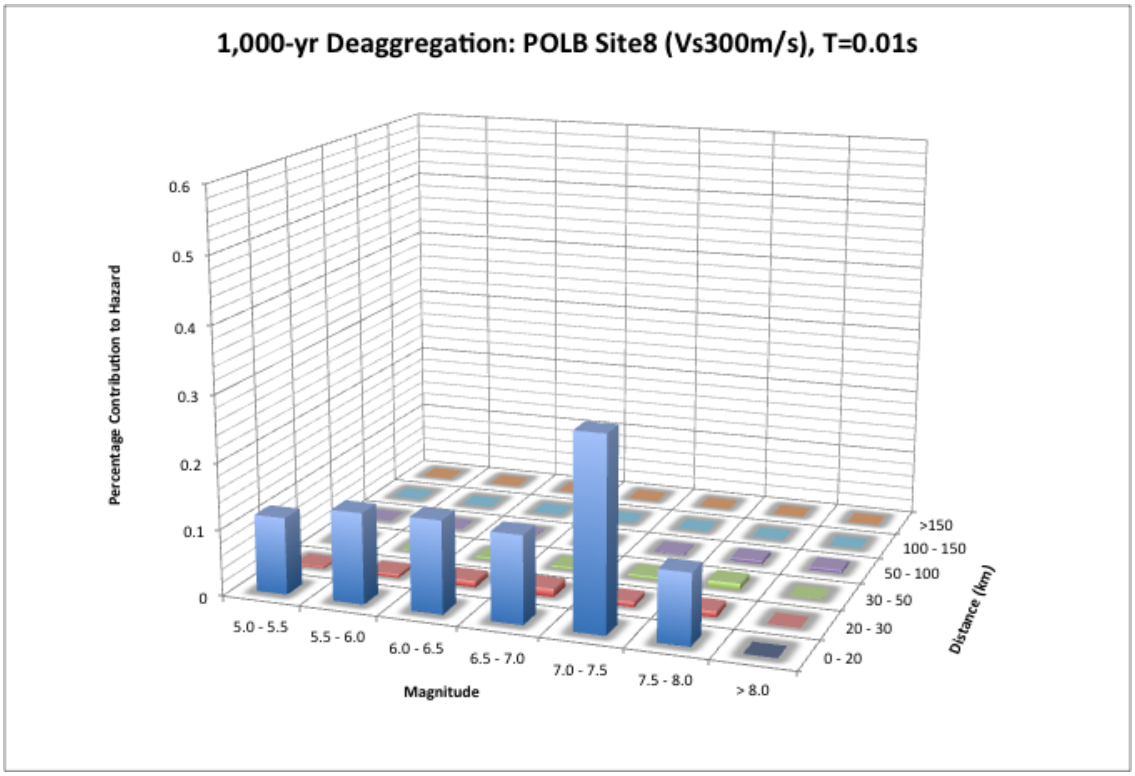


Figure 121. Magnitude-distance contribution for the 975-year hazard level for PGA for Site 8 including the Wilmington fault.

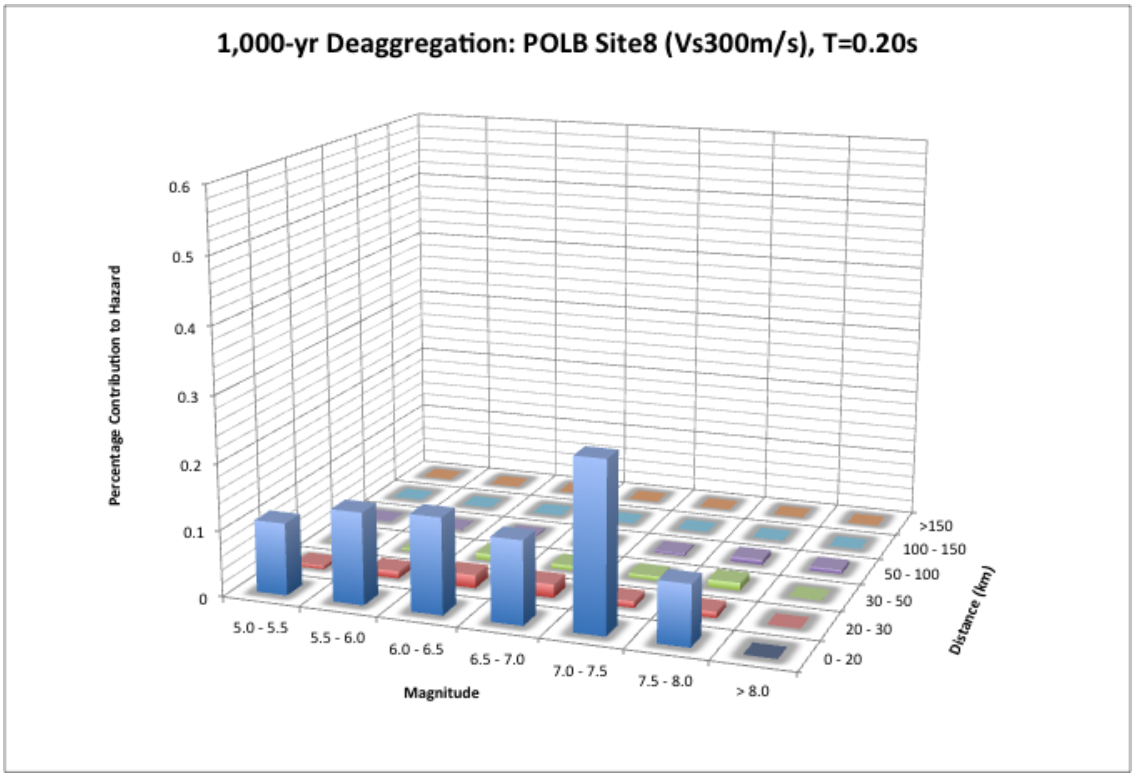


Figure 122. Magnitude-distance contribution for the 975-year hazard level for T = 0.2 sec for Site 8 including the Wilmington fault.

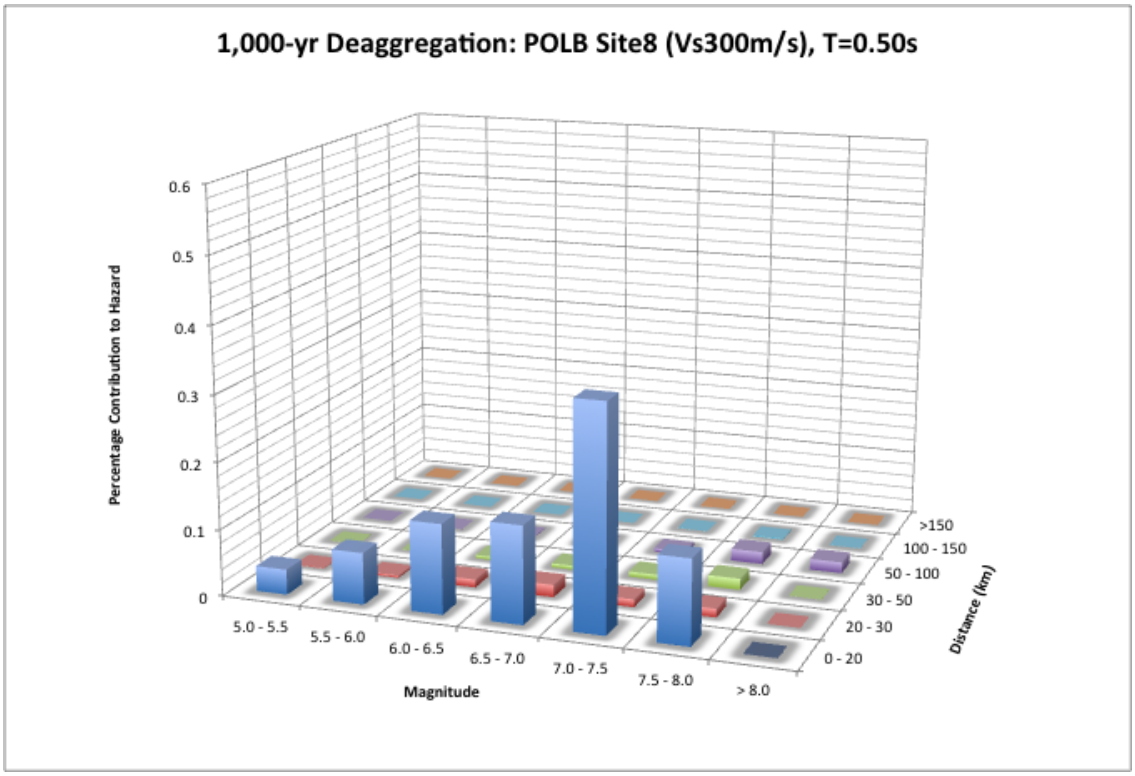


Figure 123. Magnitude-distance contribution for the 975-year hazard level for T = 0.5 sec for Site 8 including the Wilmington fault.

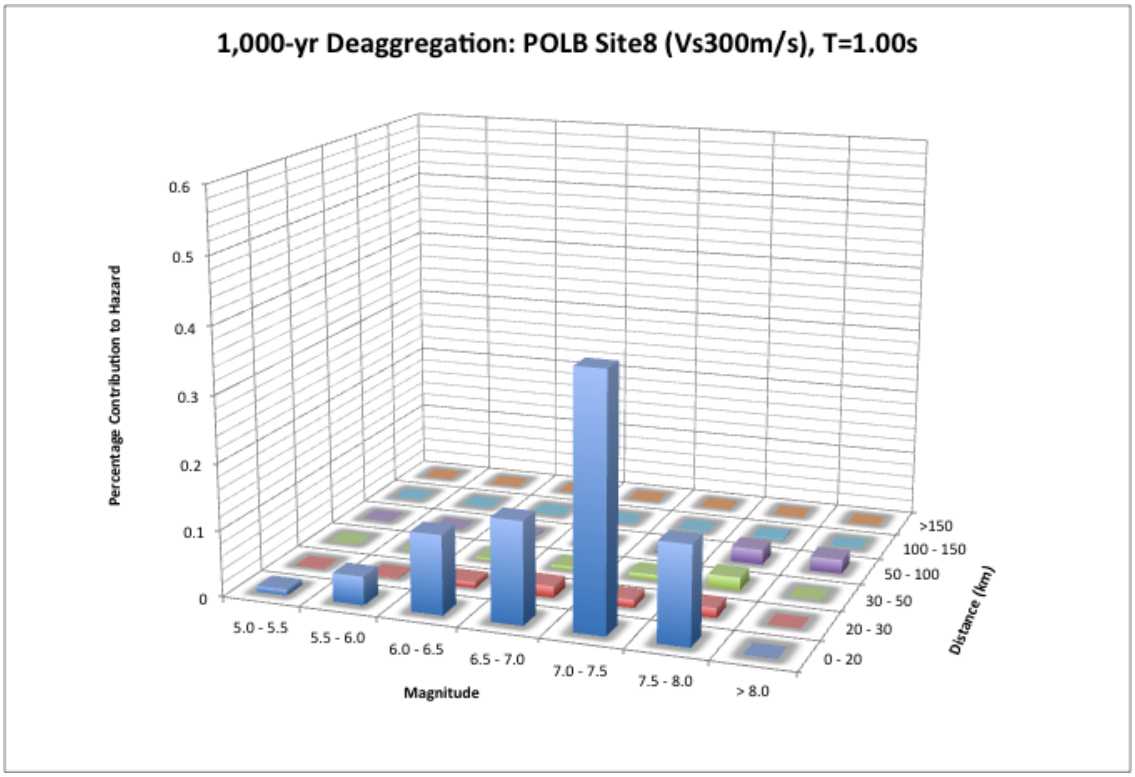


Figure 124. Magnitude-distance contribution for the 975-year hazard level for T = 1.0 sec for Site 8 including the Wilmington fault.

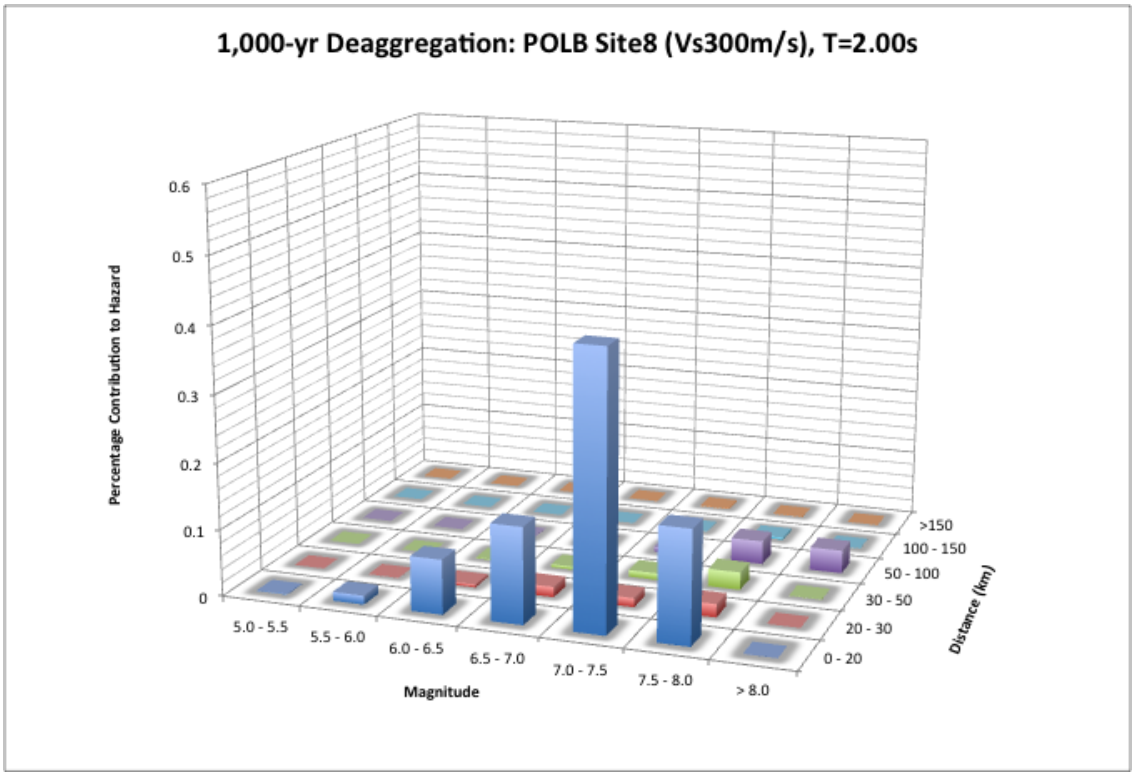


Figure 125. Magnitude-distance contribution for the 975-year hazard level for T = 2.0 sec for Site 8 including the Wilmington fault.

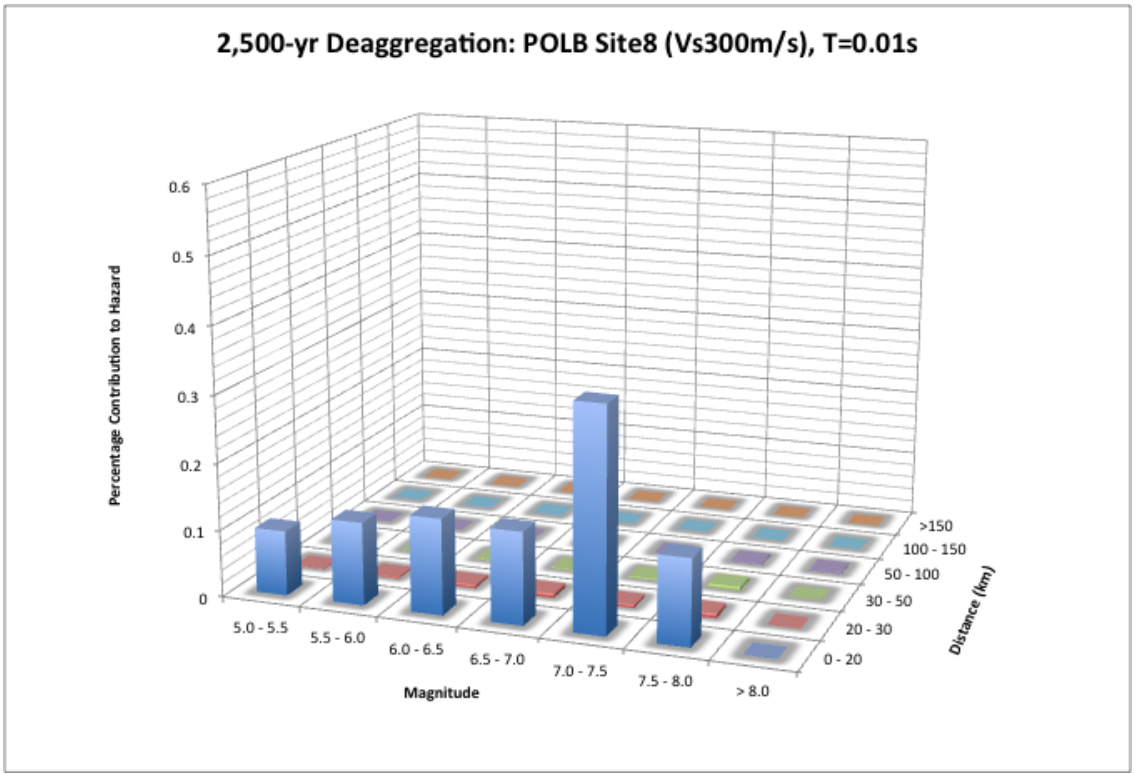


Figure 126. Magnitude-distance contribution for the 2,475-year hazard level for PGA for Site 8 including the Wilmington fault.

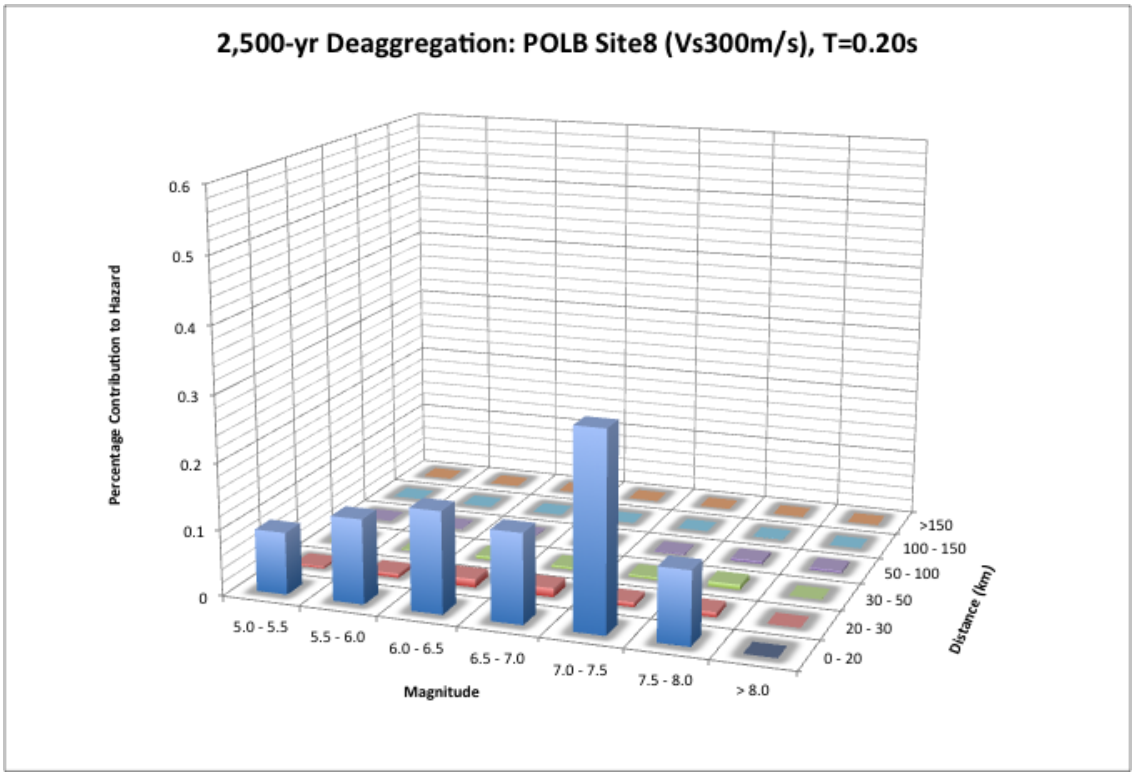


Figure 127. Magnitude-distance contribution for the 2,475-year hazard level for T = 0.2 sec for Site 8 including the Wilmington fault.

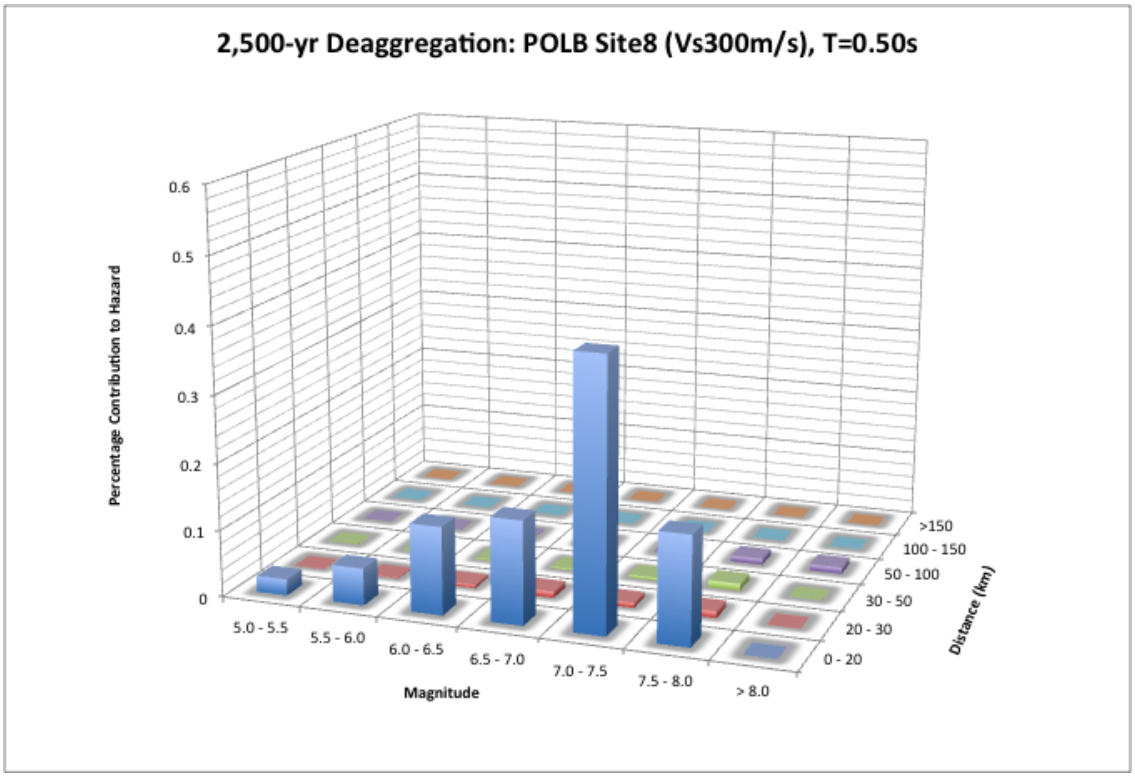


Figure 128. Magnitude-distance contribution for the 2,475-year hazard level for T = 0.5 sec for Site 8 including the Wilmington fault.

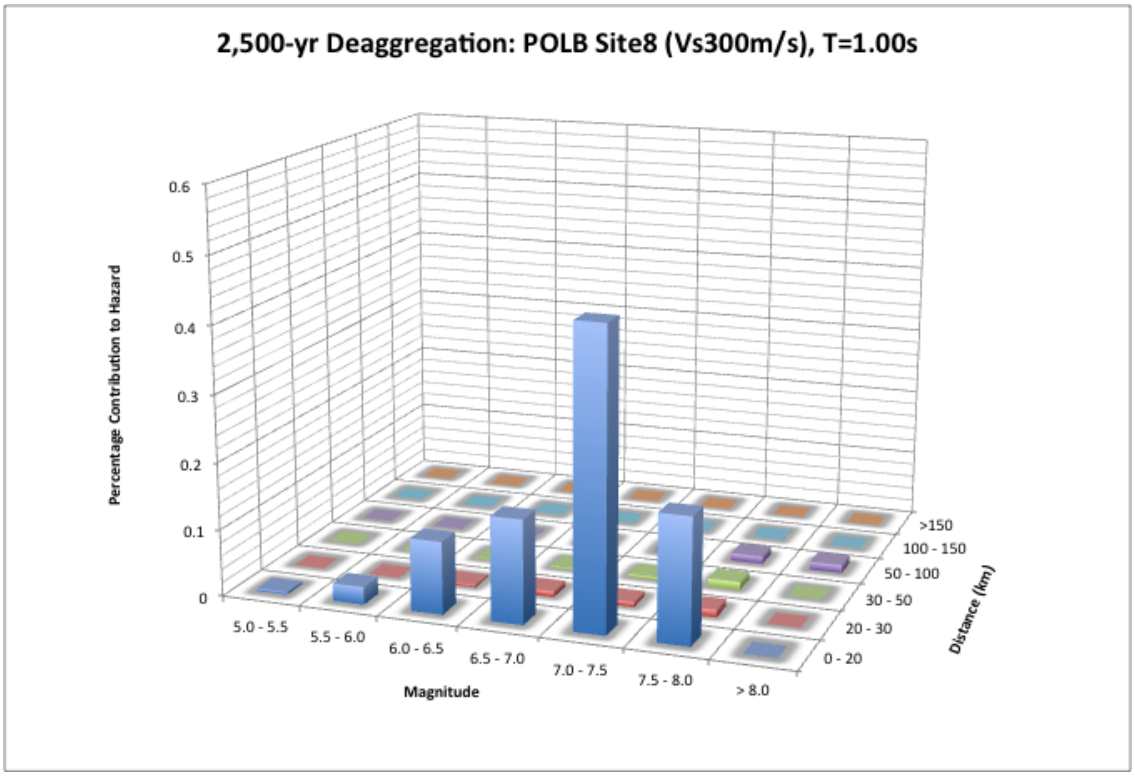


Figure 129. Magnitude-distance contribution for the 2,475-year hazard level for T = 1.0 sec for Site 8 including the Wilmington fault.

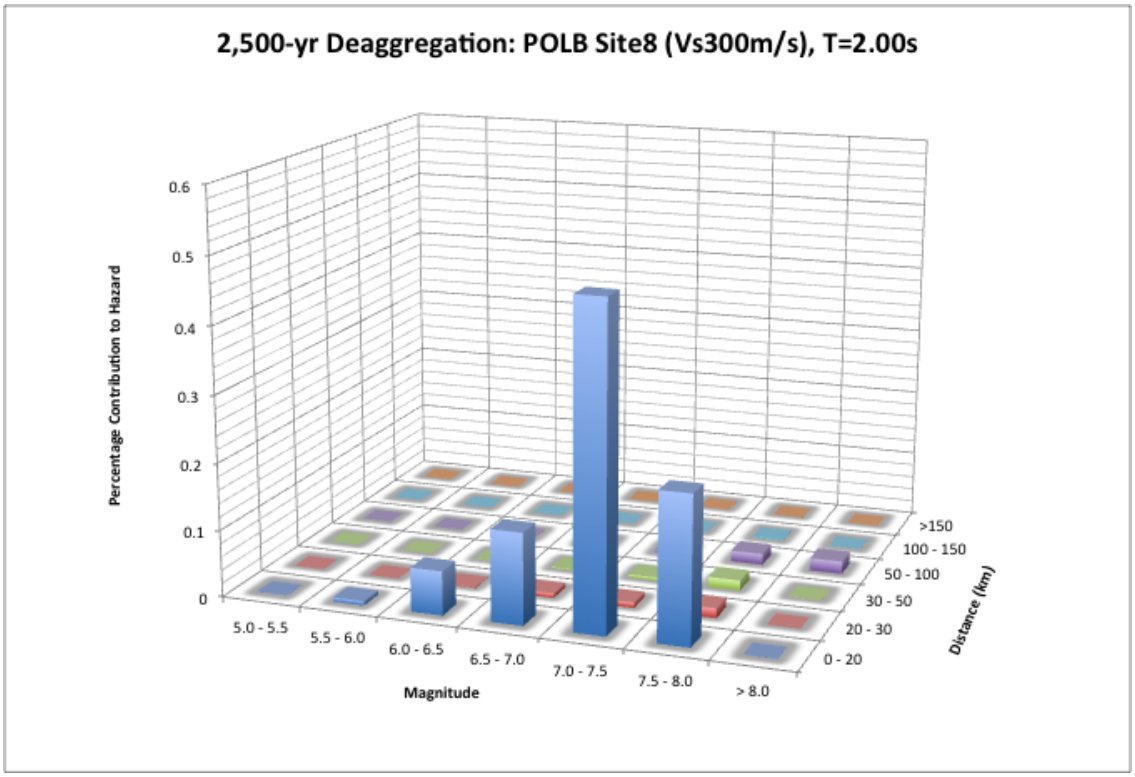


Figure 130. Magnitude-distance contribution for the 2,475-year hazard level for T = 2.0 sec for Site 8 including the Wilmington fault.

4.6 Comparison for POLB Sites – Horizontal

Given the results for the four POLB sites a comparison is presented of the resulting UHS for each of the four hazard levels all including the Wilmington fault. The digital values are listed in Tables 21 – 24 and plotted in Figures 131 – 133. Also listed in the tables is the envelop of the computed spectra with the controlling values bolded for the corresponding site. At the two lower hazard levels, the envelop spectra is controlled by the results from Site 5 for all spectral periods. For the 475-yr hazard level the results from Site 3 for spectral periods of 4 and 5 seconds are slightly larger than the results for Site 5. The results from Site 5 control at all other spectral periods. For the 2,475-year hazard level, the ground motions from Site 5 represent the envelop motions for spectral periods equal to and less than 1 sec. For longer spectral periods the results from Site 5 are within 2% or less of the controlling results from Site 3. Given this and the similar results across the four POLB site locations, the spectra from Site 5 can be assumed to representative for other site locations within the POLB area.

Table 21. UHS including the Wilmington fault for the 72-year (OLE) return period hazard level at the four POLB site locations and the resulting envelope spectra.

Period (sec)	Site 1 PSA (g)	Site 3 PSA (g)	Site 5 PSA (g)	Site 8 PSA (g)	Envelop PSA (g)
0.01	0.1735	0.1753	**0.1787**	0.1764	0.1787
0.02	0.1733	0.1750	**0.1784**	0.1762	0.1784
0.03	0.1800	0.1819	**0.1854**	0.1831	0.1854
0.04	0.1945	0.1966	**0.2005**	0.1979	0.2005
0.05	0.2105	0.2125	**0.2164**	0.2139	0.2164
0.075	0.2673	0.2699	**0.2751**	0.2717	0.2751
0.1	0.3252	0.3283	**0.3342**	0.3303	0.3342
0.15	0.4007	0.4042	**0.4112**	0.4067	0.4112
0.2	0.4291	0.4331	**0.4408**	0.4358	0.4408
0.25	0.4323	0.4363	**0.4441**	0.4390	0.4441
0.3	0.4225	0.4266	**0.4341**	0.4293	0.4341
0.4	0.3781	0.3818	**0.3888**	0.3845	0.3888
0.5	0.3374	0.3405	**0.3465**	0.3428	0.3465
0.75	0.2424	0.2446	**0.2487**	0.2462	0.2487
1	0.1805	0.1821	**0.1852**	0.1834	0.1852
1.5	0.1141	0.1151	**0.1169**	0.1158	0.1169
2	0.0793	0.0800	**0.0813**	0.0805	0.0813
3	0.0471	0.0475	**0.0482**	0.0478	0.0482
4	0.0316	0.0318	**0.0322**	0.0320	0.0322
5	0.0224	0.0225	**0.0228**	0.0227	0.0228
7.5	0.0119	0.0120	**0.0121**	0.0121	0.0121
10	0.0073	0.0073	**0.0074**	0.0074	0.0074

Table 22. UHS including the Wilmington fault for the 475-year (CLE) return period hazard level at the four POLB site locations and the resulting envelope spectra.

Period (sec)	Site 1 PSA (g)	Site 3 PSA (g)	Site 5 PSA (g)	Site 8 PSA (g)	Envelop PSA (g)
0.01	0.4635	0.4690	**0.4783**	0.4697	0.4783
0.02	0.4646	0.4701	**0.4795**	0.4708	0.4795
0.03	0.4798	0.4855	**0.4951**	0.4862	0.4951
0.04	0.5127	0.5182	**0.5273**	0.5188	0.5273
0.05	0.5502	0.5559	**0.5659**	0.5567	0.5659
0.075	0.6859	0.6933	**0.7059**	0.6949	0.7059
0.1	0.8135	0.8214	**0.8359**	0.8231	0.8359
0.15	0.9859	0.9953	**1.0105**	0.9968	1.0105
0.2	1.0700	1.0796	**1.0964**	1.0808	1.0964
0.25	1.1068	1.1174	**1.1354**	1.1178	1.1354
0.3	1.1119	1.1232	**1.1427**	1.1237	1.1427
0.4	1.0448	1.0562	**1.0756**	1.0568	1.0756
0.5	0.9596	0.9709	**0.9902**	0.9713	0.9902
0.75	0.7252	0.7338	**0.7478**	0.7327	0.7478
1	0.5617	0.5685	**0.5789**	0.5666	0.5789
1.5	0.3695	0.3740	**0.3805**	0.3728	0.3805
2	0.2647	0.2678	**0.2723**	0.2669	0.2723
3	0.1643	0.1662	**0.1684**	0.1654	0.1684
4	0.1135	0.1147	**0.1159**	0.1140	0.1159
5	0.0837	0.0845	**0.0853**	0.0840	0.0853
7.5	0.0477	0.0480	**0.0484**	0.0478	0.0484
10	0.0306	0.0308	**0.0309**	0.0306	0.0309

Table 23. UHS including the Wilmington fault for the 975-year return period hazard level at the four POLB site locations and the resulting envelope spectra.

Period (sec)	Site 1 PSA (g)	Site 3 PSA (g)	Site 5 PSA (g)	Site 8 PSA (g)	Envelop PSA (g)
0.01	0.6317	0.6379	**0.6476**	0.6354	0.6476
0.02	0.6334	0.6395	**0.6493**	0.6369	0.6493
0.03	0.6521	0.6585	**0.6687**	0.6560	0.6687
0.04	0.6973	0.7038	**0.7136**	0.7018	0.7136
0.05	0.7470	0.7538	**0.7647**	0.7519	0.7647
0.075	0.9221	0.9303	**0.9442**	0.9292	0.9442
0.1	1.0812	1.0900	**1.1053**	1.0892	1.1053
0.15	1.2916	1.3023	**1.3198**	1.2997	1.3198
0.2	1.4275	1.4401	**1.4606**	1.4362	1.4606
0.25	1.5055	1.5174	**1.5359**	1.5120	1.5359
0.3	1.5347	1.5475	**1.5680**	1.5413	1.5680
0.4	1.4773	1.4923	**1.5140**	1.4839	1.5140
0.5	1.3716	1.3850	**1.4058**	1.3751	1.4058
0.75	1.0710	1.0808	**1.0931**	1.0687	1.0931
1	0.8532	0.8613	**0.8696**	0.8476	0.8696
1.5	0.5695	0.5744	**0.5785**	0.5645	0.5785
2	0.4138	0.4173	**0.4199**	0.4103	0.4199
3	0.2581	0.2600	**0.2605**	0.2545	0.2605
4	0.1778	**0.1789**	0.1788	0.1753	0.1789
5	0.1302	**0.1310**	0.1308	0.1284	0.1310
7.5	0.0724	0.0727	**0.0728**	0.0719	0.0728
10	0.0459	0.0461	**0.0461**	0.0456	0.0461

Table 24. UHS including the Wilmington fault for the 2,475-year return period hazard level at the four POLB site locations and the resulting envelope spectra.

Period (sec)	Site 1 PSA (g)	Site 3 PSA (g)	Site 5 PSA (g)	Site 8 PSA (g)	Envelop PSA (g)
0.01	0.8792	0.8853	**0.8937**	0.8763	0.8937
0.02	0.8811	0.8871	**0.8954**	0.8778	0.8954
0.03	0.9051	0.9109	**0.9188**	0.9025	0.9188
0.04	0.9605	0.9671	**0.9766**	0.9589	0.9766
0.05	1.0310	1.0376	**1.0474**	1.0304	1.0474
0.075	1.2558	1.2653	**1.2798**	1.2586	1.2798
0.1	1.4814	1.4932	**1.5103**	1.4864	1.5103
0.15	1.7499	1.7615	**1.7777**	1.7511	1.7777
0.2	1.9409	1.9538	**1.9712**	1.9386	1.9712
0.25	2.0651	2.0767	**2.0919**	2.0602	2.0919
0.3	2.1394	2.1519	**2.1696**	2.1329	2.1696
0.4	2.1231	2.1352	**2.1537**	2.1124	2.1537
0.5	2.0256	2.0359	**2.0501**	2.0090	2.0501
0.75	1.6357	1.6424	**1.6468**	1.6061	1.6468
1	1.3271	**1.3314**	1.3279	1.2906	1.3314
1.5	0.9132	**0.9154**	0.9104	0.8848	0.9154
2	0.6674	**0.6689**	0.6639	0.6451	0.6689
3	0.4226	**0.4228**	0.4174	0.4067	0.4228
4	0.2874	**0.2874**	0.2828	0.2756	0.2874
5	0.2093	**0.2094**	0.2068	0.2026	0.2094
7.5	0.1111	**0.1113**	0.1107	0.1091	0.1113
10	0.0703	**0.0704**	0.0702	0.0692	0.0704

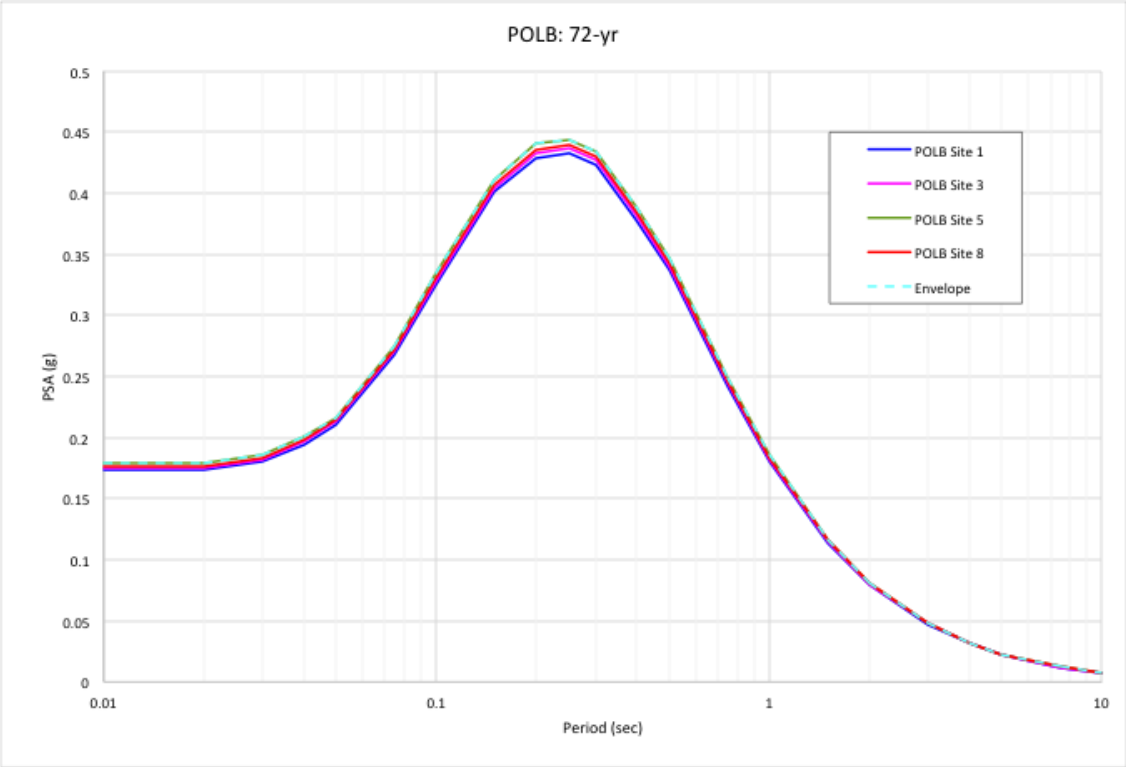


Figure 131. UHS including the Wilmington fault for the 72-year (OLE) return period hazard level at the four POLB site locations and the resulting envelope spectrum.

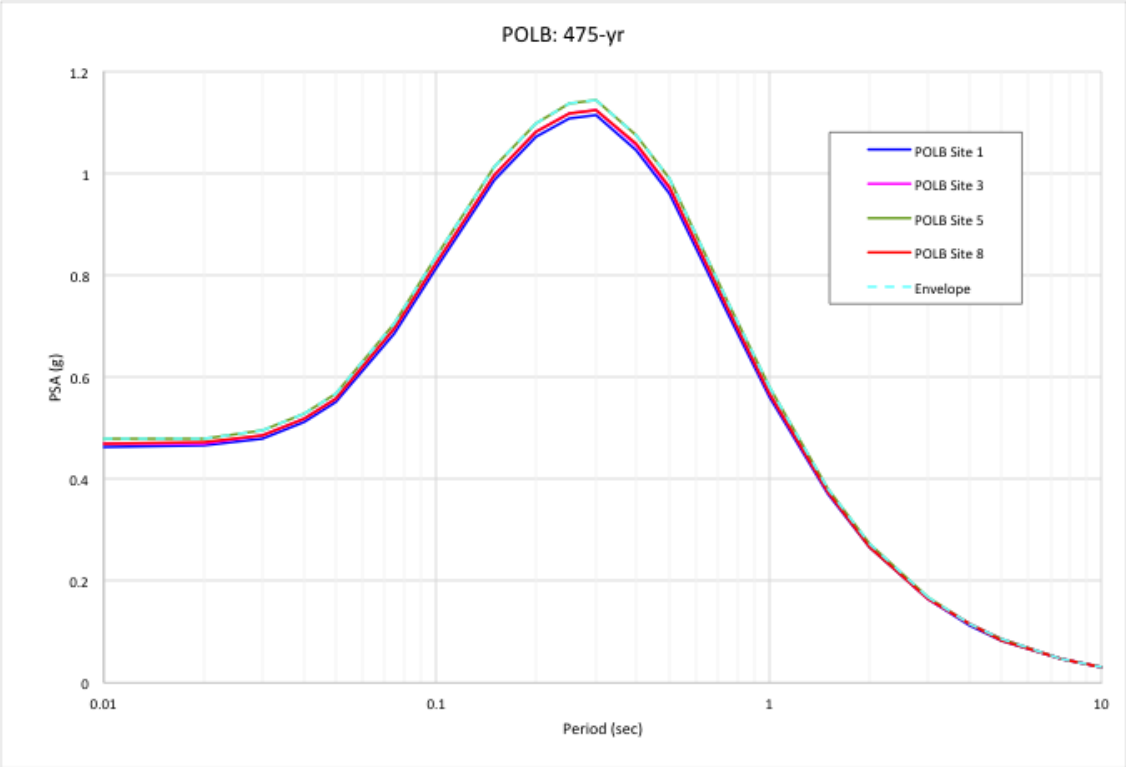


Figure 132. UHS including the Wilmington fault for the 475-year (CLE) return period hazard level at the four POLB site locations and the resulting envelope spectrum.

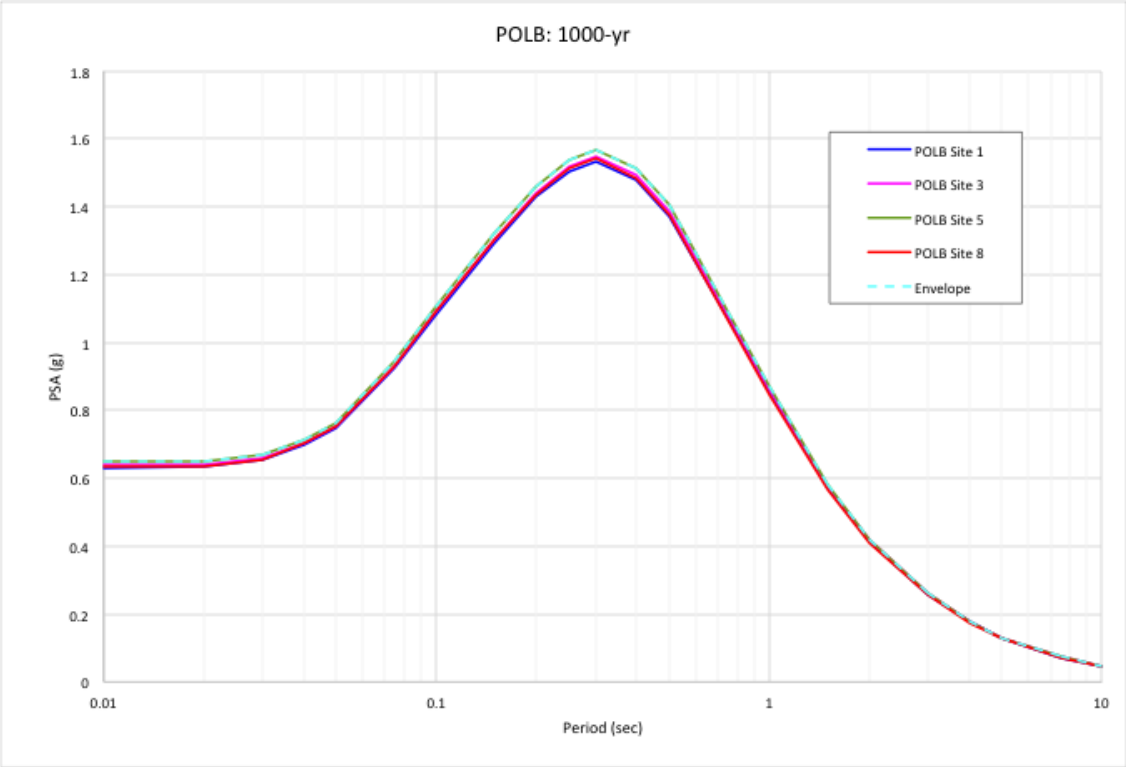


Figure 133. UHS including the Wilmington fault for the 975-year return period hazard level at the four POLB site locations and the resulting envelope spectrum.

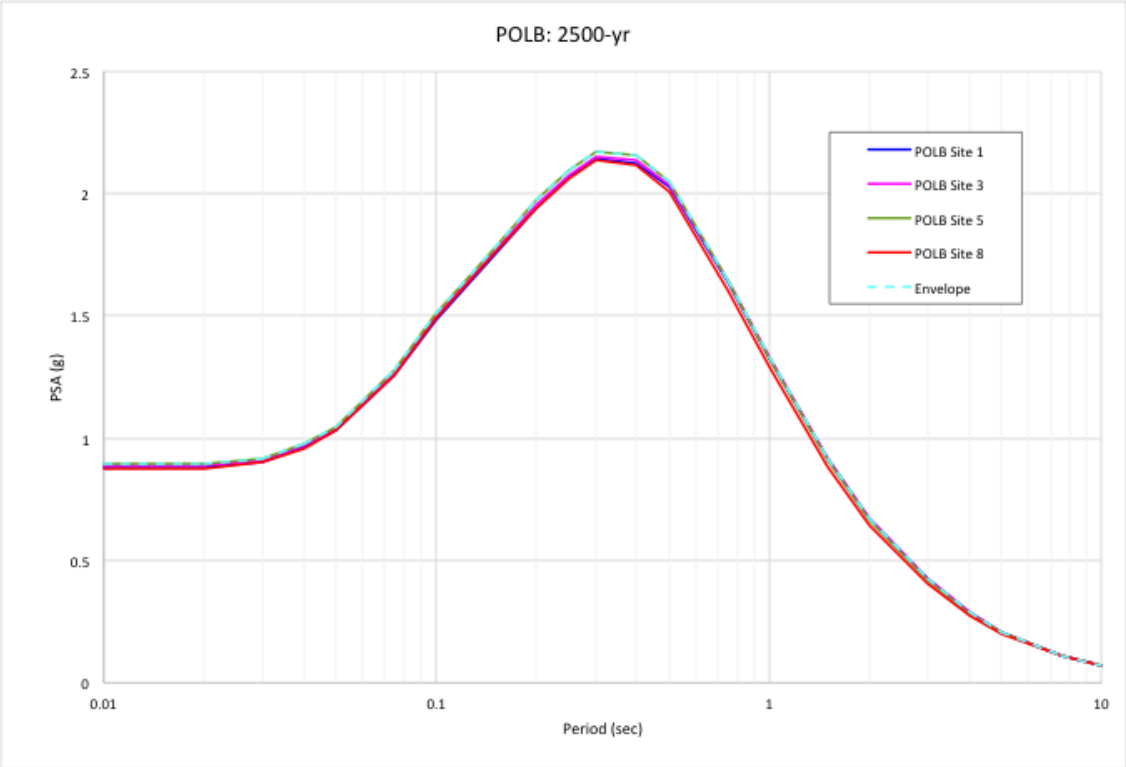


Figure 134. UHS including the Wilmington fault for the 2,475-year return period hazard level at the four POLB site locations and the resulting envelope spectrum.

4.7 Site 5 – Horizontal with Directivity

Based on the selection of the results from Site 5 to be representative of the ground motions for the POLB project area, additional PSHA calculations were performed for Site 5 to include the Bayless and Somerville (2013) directivity model. As discussed previously this directivity model was not applied to the Wilmington fault based on its relatively lower maximum magnitude and its observed limited contribution to the total hazard. The results presented in this section, however, do include the Wilmington fault for the total hazard. Note that the inclusion of this model only impacts spectral periods of greater than 0.5 sec. Mean hazard curves and UHS ground motions were computed for the average horizontal component with directivity (FD), the fault normal (FN) and fault parallel (FP) components of motions. The resulting UHS for the four hazard levels are provided in Tables 25 – 28. For completeness the UHS for the horizontal component without the consideration of directivity are also provided in the tables. Comparison plots of the resulting spectra are shown in Figure 135 – 138. As expected, the impact of including the directivity model has a minimal influence for the 72-year (OLE) return period case. However, for the longer return period cases, the influence of the directivity model becomes larger. At these longer return periods the fault normal component has the largest ground motions and the horizontal component without directivity is similar to the fault parallel component results. Similar deaggregation results are observed for these additional calculations with the incorporation of the directivity model.

Table 25. UHS for the 72-year (OLE) return period hazard level at Site 5 both with and without directivity and including the Wilmington fault.

Period (sec)	Hor PSA (g)	FD PSA (g)	FN PSA (g)	FP PSA (g)
0.01	0.1787	0.1794	0.1794	0.1794
0.02	0.1784	0.1792	0.1792	0.1792
0.03	0.1854	0.1862	0.1862	0.1862
0.04	0.2005	0.2013	0.2013	0.2013
0.05	0.2164	0.2173	0.2173	0.2173
0.075	0.2751	0.2763	0.2763	0.2763
0.1	0.3342	0.3355	0.3355	0.3355
0.15	0.4112	0.4128	0.4128	0.4128
0.2	0.4408	0.4425	0.4425	0.4425
0.25	0.4441	0.4459	0.4459	0.4459
0.3	0.4341	0.4359	0.4359	0.4359
0.4	0.3888	0.3904	0.3904	0.3904
0.5	0.3465	0.3479	0.3479	0.3479
0.75	0.2487	0.2504	0.2507	0.2498
1	0.1852	0.1867	0.1865	0.1862
1.5	0.1169	0.1177	0.1175	0.1172
2	0.0813	0.0817	0.0819	0.0814
3	0.0482	0.0484	0.0486	0.0484
4	0.0322	0.0323	0.0325	0.0323
5	0.0228	0.0229	0.0230	0.0229
7.5	0.0121	0.0122	0.0123	0.0121
10	0.0074	0.0074	0.0075	0.0074

Table 26. UHS for the 475-year (CLE) return period hazard level at Site 5 both with and without directivity and including the Wilmington fault.

Period (sec)	Hor PSA (g)	FD PSA (g)	FN PSA (g)	FP PSA (g)
0.01	0.4783	0.4785	0.4785	0.4785
0.02	0.4795	0.4797	0.4797	0.4797
0.03	0.4951	0.4954	0.4954	0.4954
0.04	0.5273	0.5275	0.5275	0.5275
0.05	0.5659	0.5662	0.5662	0.5662
0.075	0.7059	0.7062	0.7062	0.7062
0.1	0.8359	0.8363	0.8363	0.8363
0.15	1.0105	1.0108	1.0108	1.0108
0.2	1.0964	1.0969	1.0969	1.0969
0.25	1.1354	1.1360	1.1360	1.1360
0.3	1.1427	1.1432	1.1432	1.1432
0.4	1.0756	1.0762	1.0762	1.0762
0.5	0.9902	0.9908	0.9908	0.9908
0.75	0.7478	0.7589	0.7656	0.7481
1	0.5789	0.5969	0.5972	0.5818
1.5	0.3805	0.3918	0.3934	0.3760
2	0.2723	0.2804	0.2895	0.2682
3	0.1684	0.1739	0.1830	0.1668
4	0.1159	0.1195	0.1278	0.1145
5	0.0853	0.0879	0.0946	0.0836
7.5	0.0484	0.0500	0.0536	0.0472
10	0.0309	0.0318	0.0342	0.0303

Table 27. UHS for the 975-year return period hazard level at Site 5 both with and without directivity and including the Wilmington fault.

Period (sec)	Hor PSA (g)	FD PSA (g)	FN PSA (g)	FP PSA (g)
0.01	0.6476	0.6478	0.6478	0.6478
0.02	0.6493	0.6495	0.6495	0.6495
0.03	0.6687	0.6688	0.6688	0.6688
0.04	0.7136	0.7137	0.7137	0.7137
0.05	0.7647	0.7648	0.7648	0.7648
0.075	0.9442	0.9445	0.9445	0.9445
0.1	1.1053	1.1054	1.1054	1.1054
0.15	1.3198	1.3200	1.3200	1.3200
0.2	1.4606	1.4609	1.4609	1.4609
0.25	1.5359	1.5364	1.5364	1.5364
0.3	1.5680	1.5681	1.5681	1.5681
0.4	1.5140	1.5146	1.5146	1.5146
0.5	1.4058	1.4061	1.4061	1.4061
0.75	1.0931	1.1170	1.1319	1.0936
1	0.8696	0.9133	0.9165	0.8754
1.5	0.5785	0.6073	0.6139	0.5678
2	0.4199	0.4419	0.4672	0.4111
3	0.2605	0.2775	0.3040	0.2573
4	0.1788	0.1903	0.2125	0.1760
5	0.1308	0.1390	0.1574	0.1274
7.5	0.0728	0.0766	0.0858	0.0708
10	0.0461	0.0488	0.0545	0.0449

Table 28. UHS for the 2,475-year return period hazard level at Site 5 both with and without directivity and including the Wilmington fault.

Period (sec)	Hor PSA (g)	FD PSA (g)	FN PSA (g)	FP PSA (g)
0.01	0.8937	0.8938	0.8938	0.8938
0.02	0.8954	0.8955	0.8955	0.8955
0.03	0.9188	0.9188	0.9188	0.9188
0.04	0.9766	0.9766	0.9766	0.9766
0.05	1.0474	1.0475	1.0475	1.0475
0.075	1.2798	1.2799	1.2799	1.2799
0.1	1.5103	1.5104	1.5104	1.5104
0.15	1.7777	1.7779	1.7779	1.7779
0.2	1.9712	1.9713	1.9713	1.9713
0.25	2.0919	2.0920	2.0920	2.0920
0.3	2.1696	2.1697	2.1697	2.1697
0.4	2.1537	2.1538	2.1538	2.1538
0.5	2.0501	2.0502	2.0502	2.0502
0.75	1.6468	1.6951	1.7252	1.6469
1	1.3279	1.4210	1.4329	1.3382
1.5	0.9104	0.9728	0.9907	0.8878
2	0.6639	0.7163	0.7716	0.6462
3	0.4174	0.4569	0.5163	0.4129
4	0.2828	0.3109	0.3624	0.2778
5	0.2068	0.2252	0.2674	0.2010
7.5	0.1107	0.1195	0.1410	0.1071
10	0.0702	0.0751	0.0874	0.0680

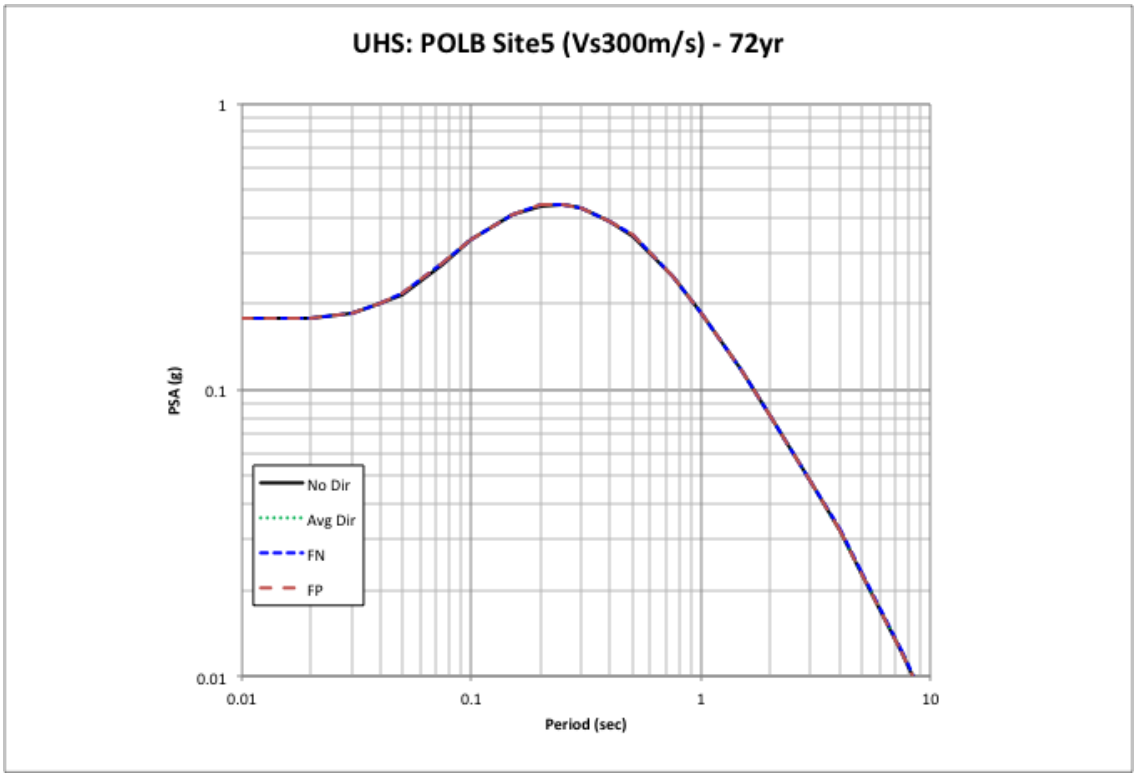


Figure 135. UHS for the 72-year (OLE) return period hazard level at Site 5 with and without directivity and including the Wilmington fault.

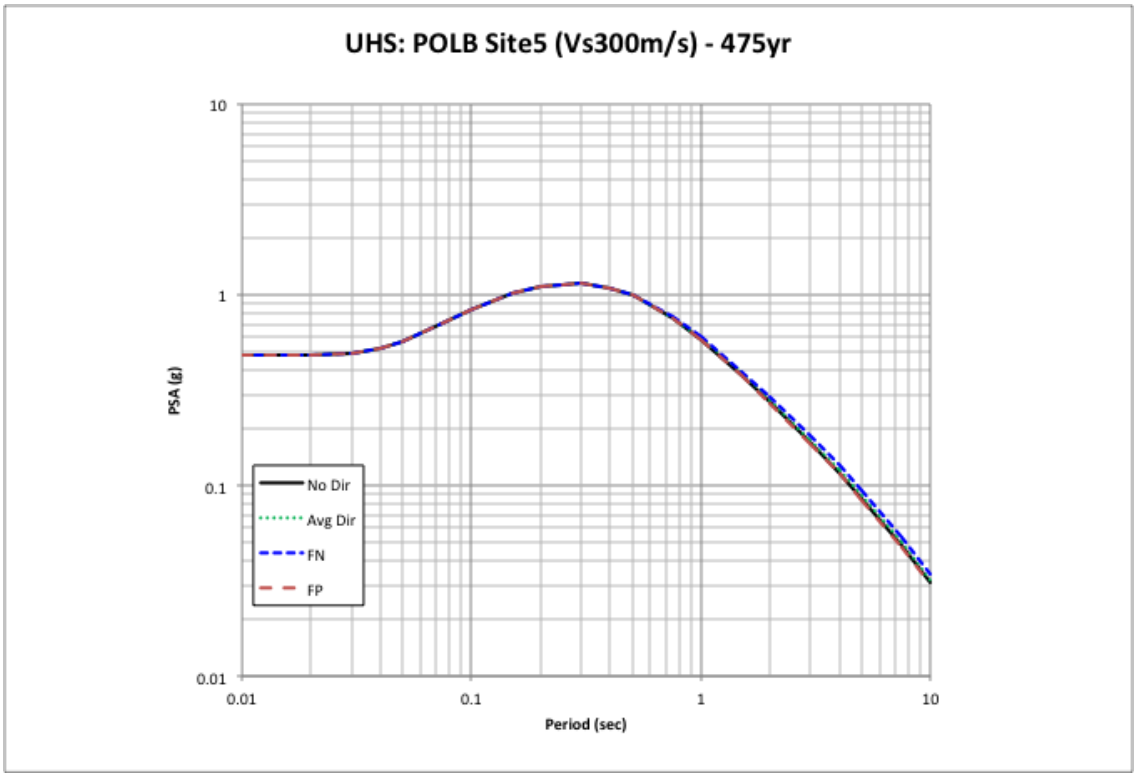


Figure 136. UHS for the 475-year (CLE) return period hazard level at Site 5 with and without directivity and including the Wilmington fault.

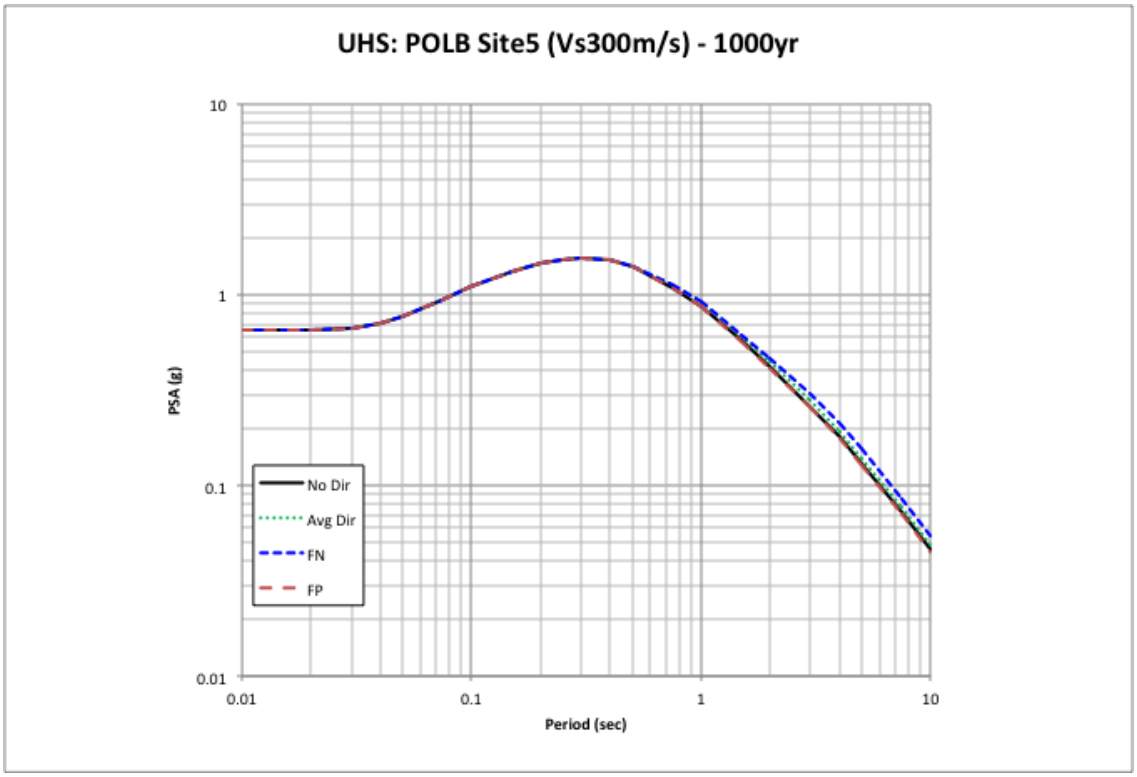


Figure 137. UHS for the 975-year return period hazard level at Site 5 with and without directivity and including the Wilmington fault.

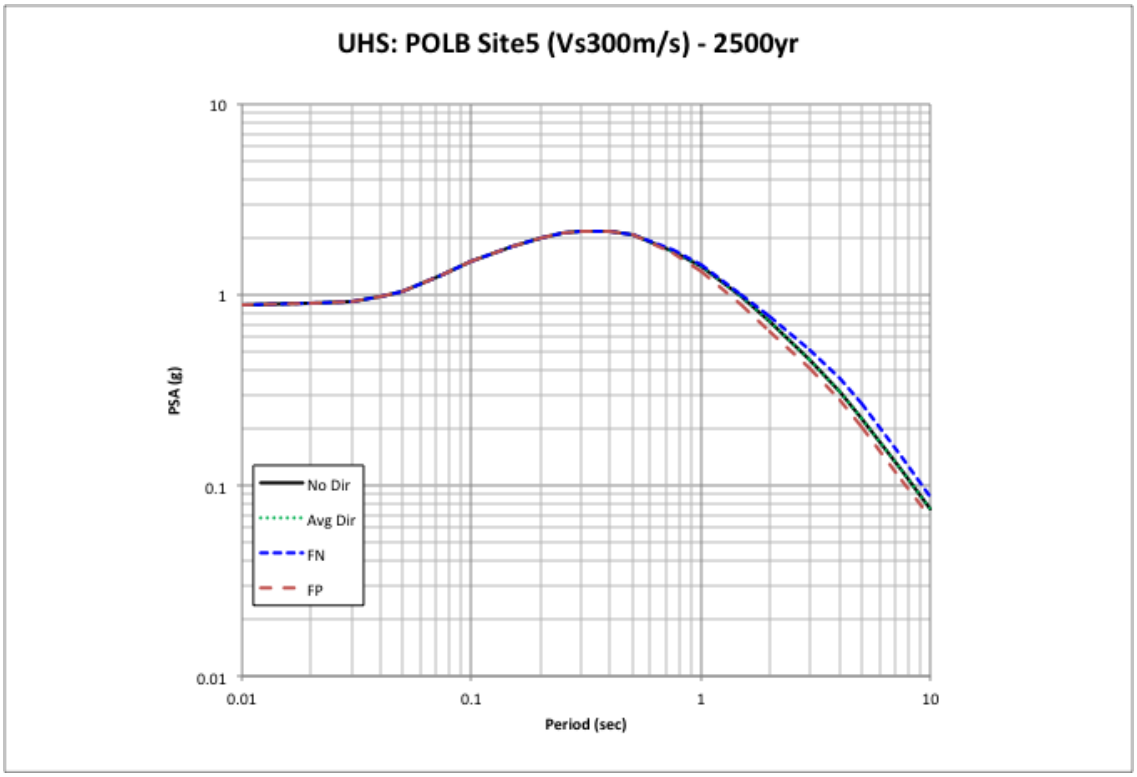


Figure 138. UHS for the 2,475-year return period hazard level at Site 5 with and without directivity and including the Wilmington fault.

4.8 Vertical Scenario Events and V/H Ratios

Given the results of the PSHA deaggregation and the seismic source model including the Wilmington fault used in the analysis a total of three scenario events were selected for the 72-year (OLE), 475-year (CLE) and 975-year hazard levels and two scenario events for the 2,475-year hazard level for the development of vertical ground motion. The three events associated with the 72-year (OLE) case are slightly different in terms of the magnitude and distance values than those for the 475-year (CLE) and 975-year cases. For the 2,475-year case, the third scenario associated with the San Andreas fault is dropped from consideration given the deaggregation results showing limited contribution to the total hazard from this seismic source.

The scenario events and specific parameters are listed in Table 29 for the 72-year (OLE) hazard level. Given these scenario events, the average V/H ratio from the two equally weighted empirical models (Gulerce and Abrahamson, 2011 and Bozorgnia and Campbell, 2016) is plotted in Figure 139 along with the envelope V/H values. These values are listed in Table 30. For periods less than 0.4 sec the envelope values are controlled by Scenario #2. For spectral periods equal to 5 sec and longer and between 0.4 and 1.5 sec, the envelope is based on the results from Scenario #3. Finally, for the other range of spectral periods (i.e., between 1.5 and 5 sec) the envelope values are based on the results from Scenario #1.

Table 29. Scenario events for the 72-year (OLE) hazard level used to develop vertical to horizontal spectral ratios for POLB sites.

Parameter	Scenario #1	Scenario #2	Scenario #3
Magnitude	6.0	7.25	7.75
Rupture Distance (km)	20	15	85
R_x Distance (km)	20	15	85
R_{jb} Distance (km)	20	15	85
Top of Rupture (km)	2.26	0	0
Dip	90	90	90
V_{S30} (m/sec)	300	300	300
Z_1 (km) for GA model[1]	0.453	0.453	0.453
Z_{25} (km) for BC model	1.757	1.757	1.757
Mechanism	Strike-Slip	Strike-Slip	Strike-Slip
Associated Fault	Palos Verdes	Newport/Inglewood	San Andreas

[1] Z_1 value based on recommended value from ASK14 ground motion model

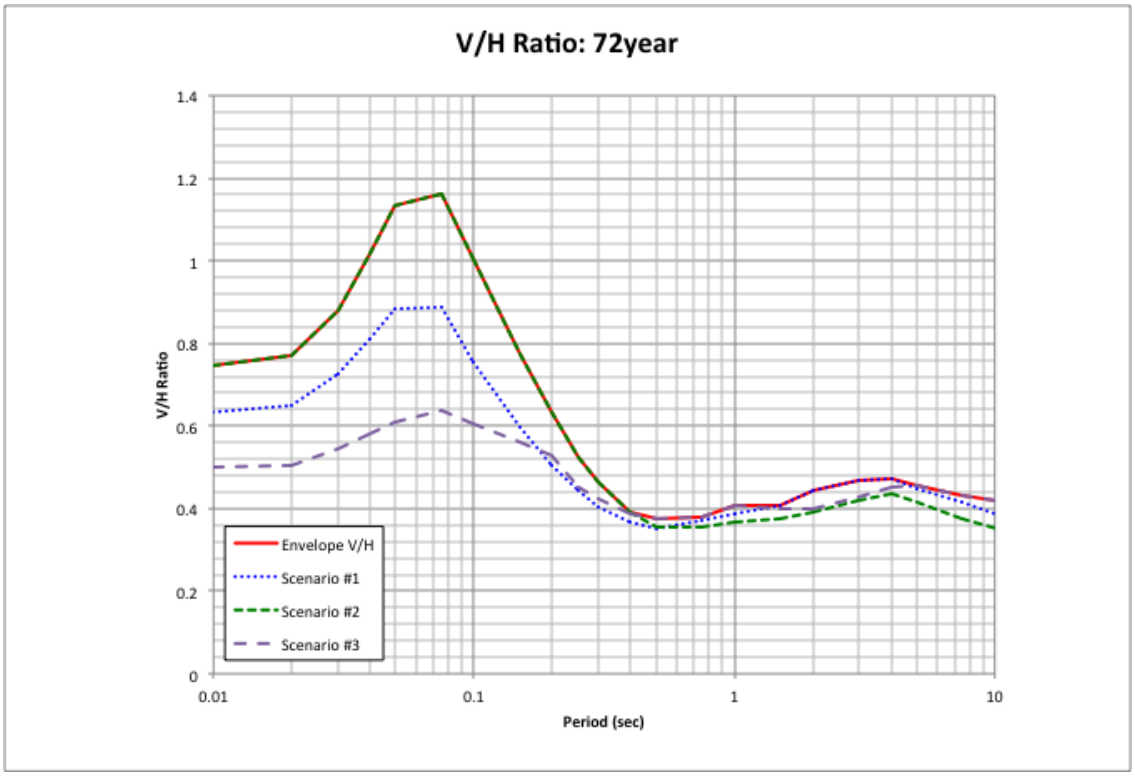


Figure 139. Vertical to horizontal (V/H) spectral ratios for the scenarios and resulting envelope associated with the 72-year (OLE) hazard level for POLB sites.

Table 30. Vertical to horizontal (V/H) spectral ratios for the envelope and scenarios associated with the 72-year (OLE) hazard level for POLB sites.

Period (sec)	Envelope V/H	Scenario #1 V/H	Scenario #2 V/H	Scenario #3 V/H
0.01	0.7464	0.6343	0.7464	0.5006
0.02	0.7691	0.6508	0.7691	0.5053
0.03	0.8812	0.7272	0.8812	0.5445
0.04	1.0165	0.8105	1.0165	0.5796
0.05	1.1356	0.8817	1.1356	0.6084
0.075	1.1603	0.8873	1.1603	0.6377
0.1	1.0037	0.7542	1.0037	0.6045
0.15	0.7758	0.5970	0.7758	0.5624
0.2	0.6347	0.5057	0.6347	0.5277
0.25	0.5265	0.4457	0.5265	0.4533
0.3	0.4632	0.4035	0.4632	0.4218
0.4	0.3926	0.3690	0.3926	0.3870
0.5	0.3755	0.3513	0.3566	0.3755
0.75	0.3811	0.3693	0.3546	0.3811
1	0.4069	0.3861	0.3663	0.4069
1.5	0.4057	0.4057	0.3753	0.3985
2	0.4420	0.4420	0.3912	0.3984
3	0.4663	0.4663	0.4216	0.4281
4	0.4726	0.4726	0.4357	0.4502
5	0.4543	0.4496	0.4175	0.4543
7.5	0.4326	0.4143	0.3773	0.4326
10	0.4184	0.3856	0.3528	0.4184

Given the envelope V/H spectral values in Table 30 the vertical spectrum is computed by scaling the horizontal spectra without the directivity model. This was applied to the results for Site 5 and will be presented in the Summary section of this report.

For the 475-year (CLE) and 975-year hazard levels, the same three scenario events were selected. These are similar to the 72-year (OLE) events but with a slight decrease in the distance value for Scenario #1 and Scenario #2. These scenario event parameters are listed in Table 31. Based on these parameters, the computed V/H spectral ratios are plotted in Figure 140 and listed in Table 32. For spectral periods less than 0.5 sec the controlling scenario is Scenario #2. For spectral periods greater than 0.5 sec the envelope is based on the larger of Scenario #1 and Scenario #3 which both have similar results in this spectral period range.

Table 31. Scenario events for the 475-year (CLE) and 975-year hazard levels used to develop vertical to horizontal spectral ratios for POLB sites.

Parameter	Scenario #1	Scenario #2	Scenario #3
Magnitude	6.0	7.25	7.75
Rupture Distance (km)	5	5	85
R_x Distance (km)	5	5	85
R_{jb} Distance (km)	5	5	85
Top of Rupture (km)	2.26	0	0
Dip	90	90	90
V_{S30} (m/sec)	300	300	300
Z_1 (km) for GA model[1]	0.453	0.453	0.453
Z_{25} (km) for BC model	1.757	1.757	1.757
Mechanism	Strike-Slip	Strike-Slip	Strike-Slip
Associated Fault	Palos Verdes	Palos Verdes	San Andreas

[1] Z_1 value based on recommended value from ASK14 ground motion model

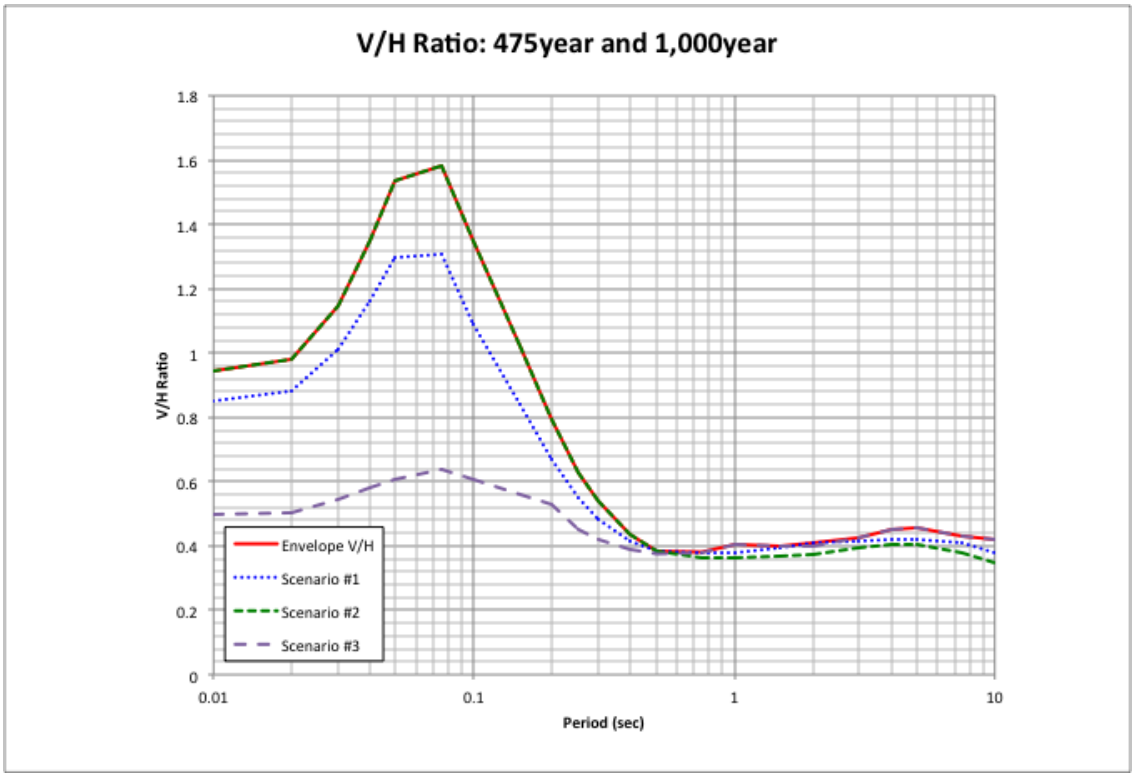


Figure 140. Vertical to horizontal (V/H) spectral ratios for the scenarios and resulting envelope associated with the 475-year (CLE) and 975-year hazard levels for POLB sites.

Table 32. Vertical to horizontal (V/H) spectral ratios for the envelope and scenarios associated with the 475-year (CLE) and 975-year hazard levels for POLB sites.

Period (sec)	Envelope V/H	Scenario #1 V/H	Scenario #2 V/H	Scenario #3 V/H
0.01	0.9420	0.8484	0.9420	0.5006
0.02	0.9809	0.8822	0.9809	0.5053
0.03	1.1446	1.0129	1.1446	0.5445
0.04	1.3494	1.1638	1.3494	0.5796
0.05	1.5349	1.2981	1.5349	0.6084
0.075	1.5808	1.3090	1.5808	0.6377
0.1	1.3477	1.0893	1.3477	0.6045
0.15	1.0211	0.8427	1.0211	0.5624
0.2	0.7961	0.6691	0.7961	0.5277
0.25	0.6295	0.5514	0.6295	0.4533
0.3	0.5380	0.4812	0.5380	0.4218
0.4	0.4356	0.4168	0.4356	0.3870
0.5	0.3825	0.3821	0.3825	0.3755
0.75	0.3811	0.3784	0.3628	0.3811
1	0.4069	0.3793	0.3619	0.4069
1.5	0.3985	0.3919	0.3687	0.3985
2	0.4097	0.4097	0.3747	0.3984
3	0.4281	0.4166	0.3935	0.4281
4	0.4502	0.4224	0.4048	0.4502
5	0.4543	0.4216	0.4024	0.4543
7.5	0.4326	0.4078	0.3765	0.4326
10	0.4184	0.3768	0.3466	0.4184

Finally, for the 2,475-year hazard level, the number of scenario events was reduced to two based on the limited contribution of the San Andreas fault to the total hazard. These two scenarios have the same parameters as the previous scenarios and these parameters are listed in Table 33. Based on these parameters, the computed V/H spectral ratios are plotted in Figure 141 and listed in Table 34. For spectral periods less than 0.5 sec the controlling scenario is Scenario #2. For spectral periods greater than 0.5 sec, the envelope is based Scenario #1.

Table 33. Scenario events for the 2,475-year hazard level used to develop vertical to horizontal spectral ratios for POLB sites.

Parameter	Scenario #1	Scenario #2
Magnitude	6.0	7.25
Rupture Distance (km)	5	5
R_x Distance (km)	5	5
R_{jb} Distance (km)	5	5
Top of Rupture (km)	2.26	0
Dip	90	90
V_{S30} (m/sec)	300	300
Z_1 (km) for GA model[1]	0.453	0.453
Z_{25} (km) for BC model	1.757	1.757
Mechanism	Strike-Slip	Strike-Slip
Associated Fault	Palos Verdes	Palos Verdes

[1] Z_1 value based on recommended value from ASK14 ground motion model

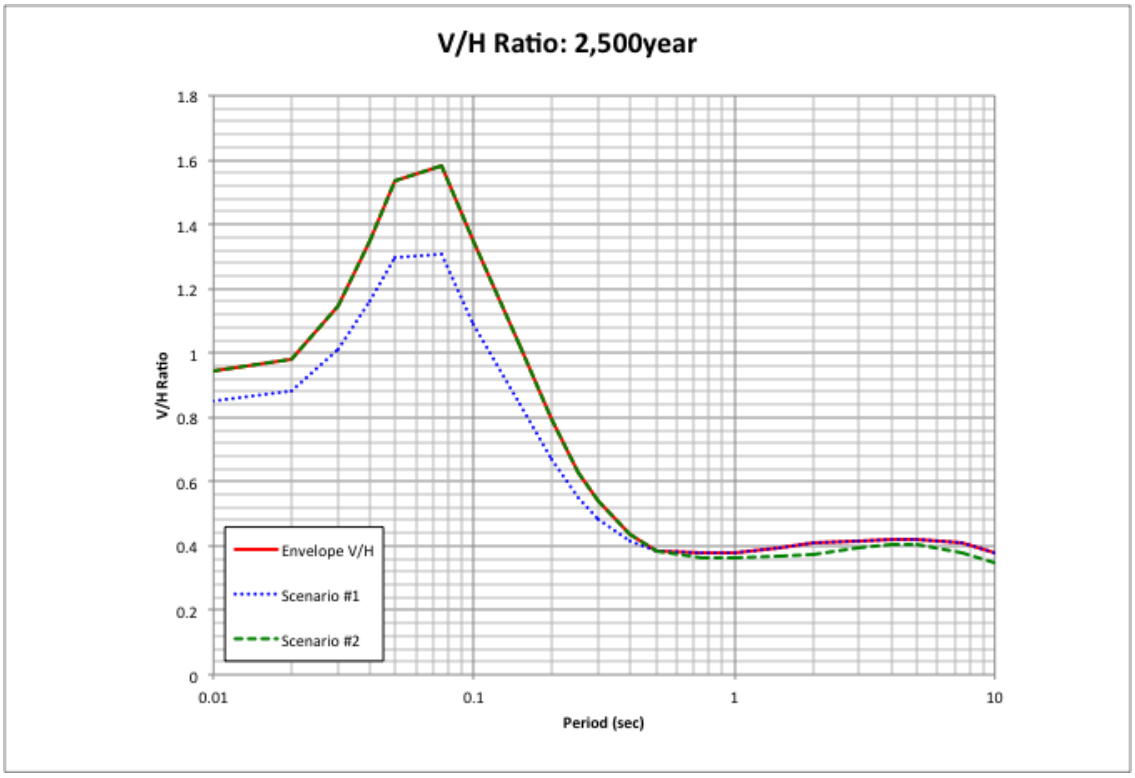


Figure 141. Vertical to horizontal (V/H) spectral ratios for the scenarios and resulting envelope associated with the 2,475-year hazard level for POLB sites.

Table 34. Vertical to horizontal (V/H) spectral ratios for the envelope and scenarios associated with the 2,475-year hazard level for POLB sites.

Period (sec)	Envelope V/H	Scenario #1 V/H	Scenario #2 V/H
0.01	0.9420	0.8484	0.9420
0.02	0.9809	0.8822	0.9809
0.03	1.1446	1.0129	1.1446
0.04	1.3494	1.1638	1.3494
0.05	1.5349	1.2981	1.5349
0.075	1.5808	1.3090	1.5808
0.1	1.3477	1.0893	1.3477
0.15	1.0211	0.8427	1.0211
0.2	0.7961	0.6691	0.7961
0.25	0.6295	0.5514	0.6295
0.3	0.5380	0.4812	0.5380
0.4	0.4356	0.4168	0.4356
0.5	0.3825	0.3821	0.3825
0.75	0.3784	0.3784	0.3628
1	0.3793	0.3793	0.3619
1.5	0.3919	0.3919	0.3687
2	0.4097	0.4097	0.3747
3	0.4166	0.4166	0.3935
4	0.4224	0.4224	0.4048
5	0.4216	0.4216	0.4024
7.5	0.4078	0.4078	0.3765
10	0.3768	0.3768	0.3466

5. Summary

A PSHA study update from a previous study (Earth Mechanics Inc., 2006) has been conducted for the POLB project. This initial update (Gregor and Al Atik, 2019) implemented a new and current state of knowledge seismic source model for California. This UCERF3 seismic source model is the current model being used for the national seismic hazard maps and building code maps in California and the results from this initial study are presented in Gregor and Al Atik (2019). More recently a newly characterization fault source (i.e., Wilmington fault) in the immediate region around the POLB was developed (Wolfe et al., 2019). As noted in Wolfe et al. (2019) this newly characterized fault may impact deterministic analyses in the area and its characterization was included in this study. The contribution of this seismic source in a PSHA study is limited based on the relatively low slip rate associated with this fault. In general, the inclusion of this source leads to an increase in the ground motions of about 3-4% and less. As noted earlier in the report, no adjustments were applied to the UCERF3 seismic source model in this immediate region based on the inclusion of the Wilmington fault and as such this observed slight increase could be attributable to potential double counting of the seismic sources in this region. These observed slight increases, however, fall well within the uncertainty in the mean ground motion estimates.

In addition to the use of this newer seismic source model, both the initial (Gregor and Al Atik, 2019) and the current study implemented the current state of knowledge for ground motion models (NGA West2). Both the seismic source model and the ground motion model represent updates and replacements to the models used in the previous 2006 study. A common V_{S30} value of 300 m/sec was used for all the sites.

Based on the calculations performed for four site locations for the horizontal component of ground motions, the ground motion results from Site 5 were selected to be representative for the POLB project. This selection was based on the observation that the Site 5 results envelope or are within 2% of the envelop of the ground motion results from the other three site locations. For the representative Site 5, additional calculations to include the Bayless and Somerville (2013) directivity model were performed.

Ground motions were computed for four hazard levels corresponding to the 72-year (OLE), 475-year (CLE), 975-year and 2,475-year return periods. Based on the deaggregation results, scenario events were selected for the calculation of applicable vertical to horizontal (V/H) spectral ratios.

A summary of the ground motion spectra for Site 5 are listed in Tables 35 – 38 for Site 5. These spectra are also plotted in Figures 142 – 145.

Table 35. UHS for the 72-year (OLE) return period hazard level at Site 5 with and without directivity and for the vertical component and including the Wilmington fault.

Period (sec)	Hor PSA (g)	FD PSA (g)	FN PSA (g)	FP PSA (g)	Vertical PSA (g)
0.01	0.1787	0.1794	0.1794	0.1794	0.1334
0.02	0.1784	0.1792	0.1792	0.1792	0.1372
0.03	0.1854	0.1862	0.1862	0.1862	0.1634
0.04	0.2005	0.2013	0.2013	0.2013	0.2038
0.05	0.2164	0.2173	0.2173	0.2173	0.2458
0.075	0.2751	0.2763	0.2763	0.2763	0.3192
0.1	0.3342	0.3355	0.3355	0.3355	0.3354
0.15	0.4112	0.4128	0.4128	0.4128	0.3190
0.2	0.4408	0.4425	0.4425	0.4425	0.2798
0.25	0.4441	0.4459	0.4459	0.4459	0.2338
0.3	0.4341	0.4359	0.4359	0.4359	0.2011
0.4	0.3888	0.3904	0.3904	0.3904	0.1526
0.5	0.3465	0.3479	0.3479	0.3479	0.1301
0.75	0.2487	0.2504	0.2507	0.2498	0.0948
1	0.1852	0.1867	0.1865	0.1862	0.0754
1.5	0.1169	0.1177	0.1175	0.1172	0.0474
2	0.0813	0.0817	0.0819	0.0814	0.0359
3	0.0482	0.0484	0.0486	0.0484	0.0225
4	0.0322	0.0323	0.0325	0.0323	0.0152
5	0.0228	0.0229	0.0230	0.0229	0.0104
7.5	0.0121	0.0122	0.0123	0.0121	0.0053
10	0.0074	0.0074	0.0075	0.0074	0.0031

Table 36. UHS for the 475-year (CLE) return period hazard level at Site 5 with and without directivity and for the vertical component and including the Wilmington fault.

Period (sec)	Hor PSA (g)	FD PSA (g)	FN PSA (g)	FP PSA (g)	Vertical PSA (g)
0.01	0.4783	0.4785	0.4785	0.4785	0.4506
0.02	0.4795	0.4797	0.4797	0.4797	0.4703
0.03	0.4951	0.4954	0.4954	0.4954	0.5667
0.04	0.5273	0.5275	0.5275	0.5275	0.7115
0.05	0.5659	0.5662	0.5662	0.5662	0.8687
0.075	0.7059	0.7062	0.7062	0.7062	1.1160
0.1	0.8359	0.8363	0.8363	0.8363	1.1265
0.15	1.0105	1.0108	1.0108	1.0108	1.0319
0.2	1.0964	1.0969	1.0969	1.0969	0.8728
0.25	1.1354	1.1360	1.1360	1.1360	0.7147
0.3	1.1427	1.1432	1.1432	1.1432	0.6148
0.4	1.0756	1.0762	1.0762	1.0762	0.4685
0.5	0.9902	0.9908	0.9908	0.9908	0.3787
0.75	0.7478	0.7589	0.7656	0.7481	0.2850
1	0.5789	0.5969	0.5972	0.5818	0.2355
1.5	0.3805	0.3918	0.3934	0.3760	0.1516
2	0.2723	0.2804	0.2895	0.2682	0.1116
3	0.1684	0.1739	0.1830	0.1668	0.0721
4	0.1159	0.1195	0.1278	0.1145	0.0522
5	0.0853	0.0879	0.0946	0.0836	0.0387
7.5	0.0484	0.0500	0.0536	0.0472	0.0209
10	0.0309	0.0318	0.0342	0.0303	0.0129

Table 37. UHS for the 975-year return period hazard level at Site 5 with and without directivity and for the vertical component and including the Wilmington fault.

Period (sec)	Hor PSA (g)	FD PSA (g)	FN PSA (g)	FP PSA (g)	Vertical PSA (g)
0.01	0.6476	0.6478	0.6478	0.6478	0.6101
0.02	0.6493	0.6495	0.6495	0.6495	0.6369
0.03	0.6687	0.6688	0.6688	0.6688	0.7654
0.04	0.7136	0.7137	0.7137	0.7137	0.9630
0.05	0.7647	0.7648	0.7648	0.7648	1.1738
0.075	0.9442	0.9445	0.9445	0.9445	1.4926
0.1	1.1053	1.1054	1.1054	1.1054	1.4896
0.15	1.3198	1.3200	1.3200	1.3200	1.3477
0.2	1.4606	1.4609	1.4609	1.4609	1.1627
0.25	1.5359	1.5364	1.5364	1.5364	0.9668
0.3	1.5680	1.5681	1.5681	1.5681	0.8436
0.4	1.5140	1.5146	1.5146	1.5146	0.6595
0.5	1.4058	1.4061	1.4061	1.4061	0.5377
0.75	1.0931	1.1170	1.1319	1.0936	0.4166
1	0.8696	0.9133	0.9165	0.8754	0.3538
1.5	0.5785	0.6073	0.6139	0.5678	0.2305
2	0.4199	0.4419	0.4672	0.4111	0.1720
3	0.2605	0.2775	0.3040	0.2573	0.1115
4	0.1788	0.1903	0.2125	0.1760	0.0805
5	0.1308	0.1390	0.1574	0.1274	0.0594
7.5	0.0728	0.0766	0.0858	0.0708	0.0315
10	0.0461	0.0488	0.0545	0.0449	0.0193

Table 38. UHS for the 2,475-year return period hazard level at Site 5 with and without directivity and for the vertical component and including the Wilmington fault.

Period (sec)	Hor PSA (g)	FD PSA (g)	FN PSA (g)	FP PSA (g)	Vertical PSA (g)
0.01	0.8937	0.8938	0.8938	0.8938	0.8419
0.02	0.8954	0.8955	0.8955	0.8955	0.8783
0.03	0.9188	0.9188	0.9188	0.9188	1.0516
0.04	0.9766	0.9766	0.9766	0.9766	1.3178
0.05	1.0474	1.0475	1.0475	1.0475	1.6077
0.075	1.2798	1.2799	1.2799	1.2799	2.0231
0.1	1.5103	1.5104	1.5104	1.5104	2.0354
0.15	1.7777	1.7779	1.7779	1.7779	1.8153
0.2	1.9712	1.9713	1.9713	1.9713	1.5693
0.25	2.0919	2.0920	2.0920	2.0920	1.3169
0.3	2.1696	2.1697	2.1697	2.1697	1.1673
0.4	2.1537	2.1538	2.1538	2.1538	0.9382
0.5	2.0501	2.0502	2.0502	2.0502	0.7842
0.75	1.6468	1.6951	1.7252	1.6469	0.6231
1	1.3279	1.4210	1.4329	1.3382	0.5037
1.5	0.9104	0.9728	0.9907	0.8878	0.3568
2	0.6639	0.7163	0.7716	0.6462	0.2720
3	0.4174	0.4569	0.5163	0.4129	0.1739
4	0.2828	0.3109	0.3624	0.2778	0.1195
5	0.2068	0.2252	0.2674	0.2010	0.0872
7.5	0.1107	0.1195	0.1410	0.1071	0.0451
10	0.0702	0.0751	0.0874	0.0680	0.0264

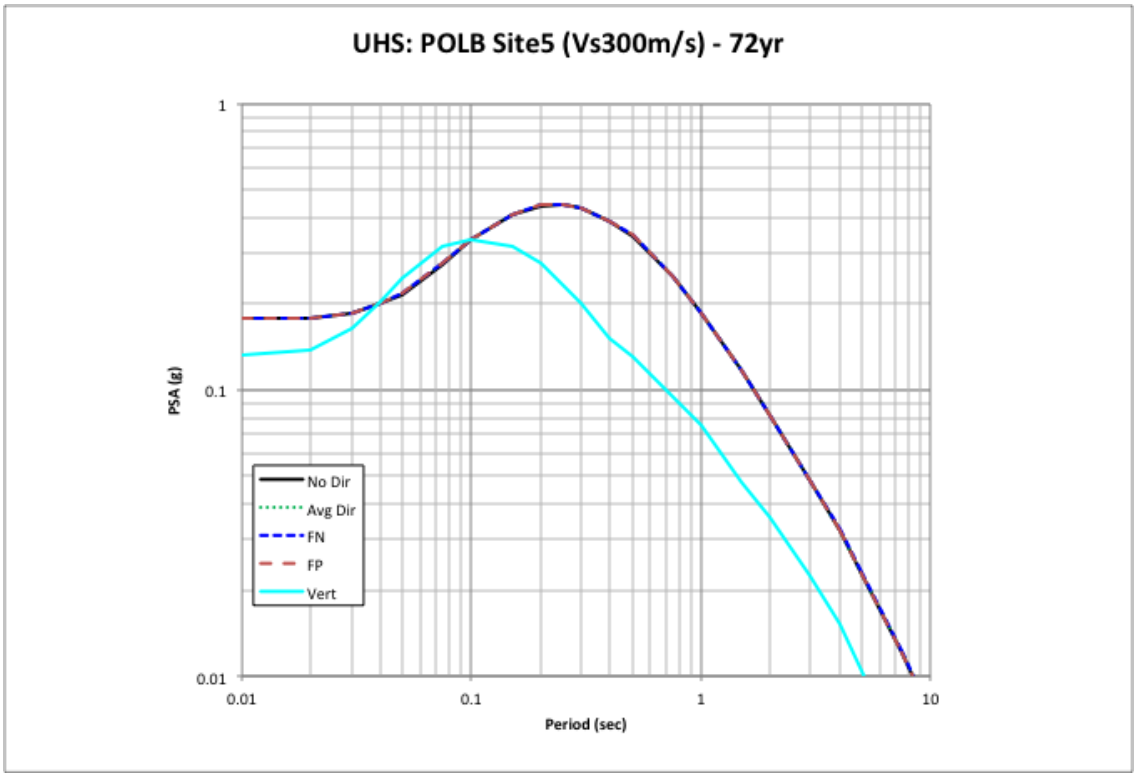


Figure 142. UHS for the 72-year (OLE) return period hazard level at Site 5 with and without directivity and for the vertical component and including the Wilmington fault.

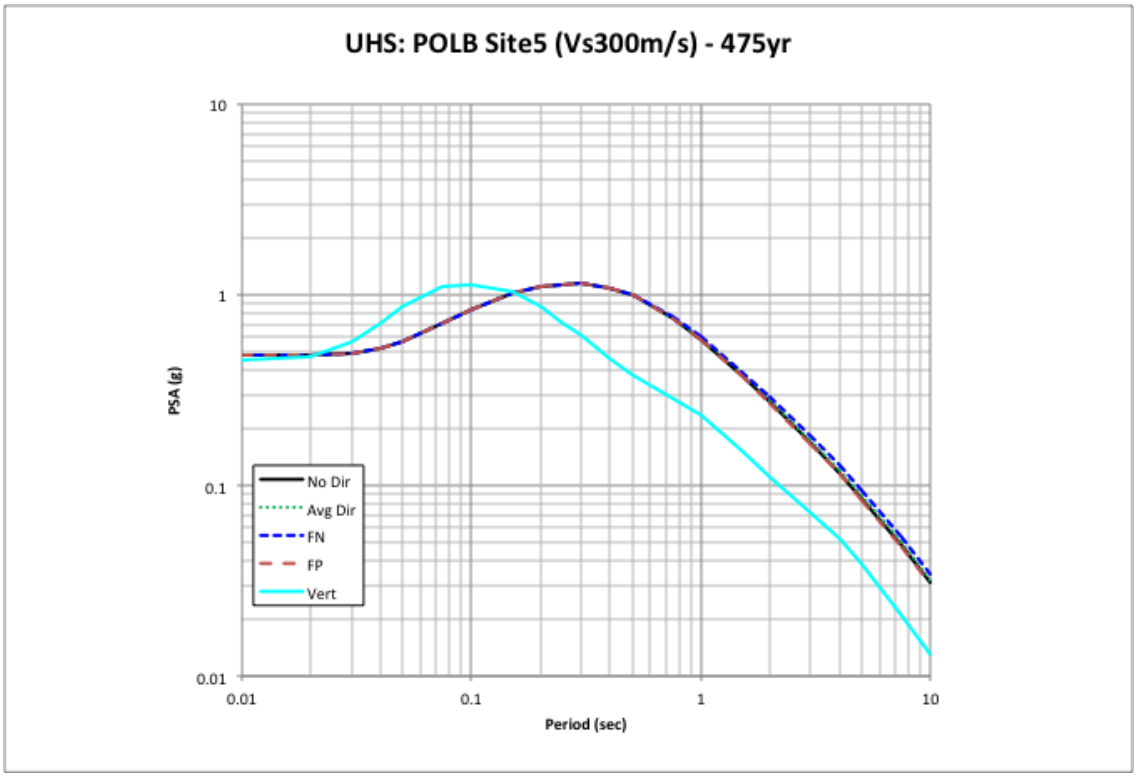


Figure 143. UHS for the 475-year (CLE) return period hazard level at Site 5 with and without directivity and for the vertical component and including the Wilmington fault.

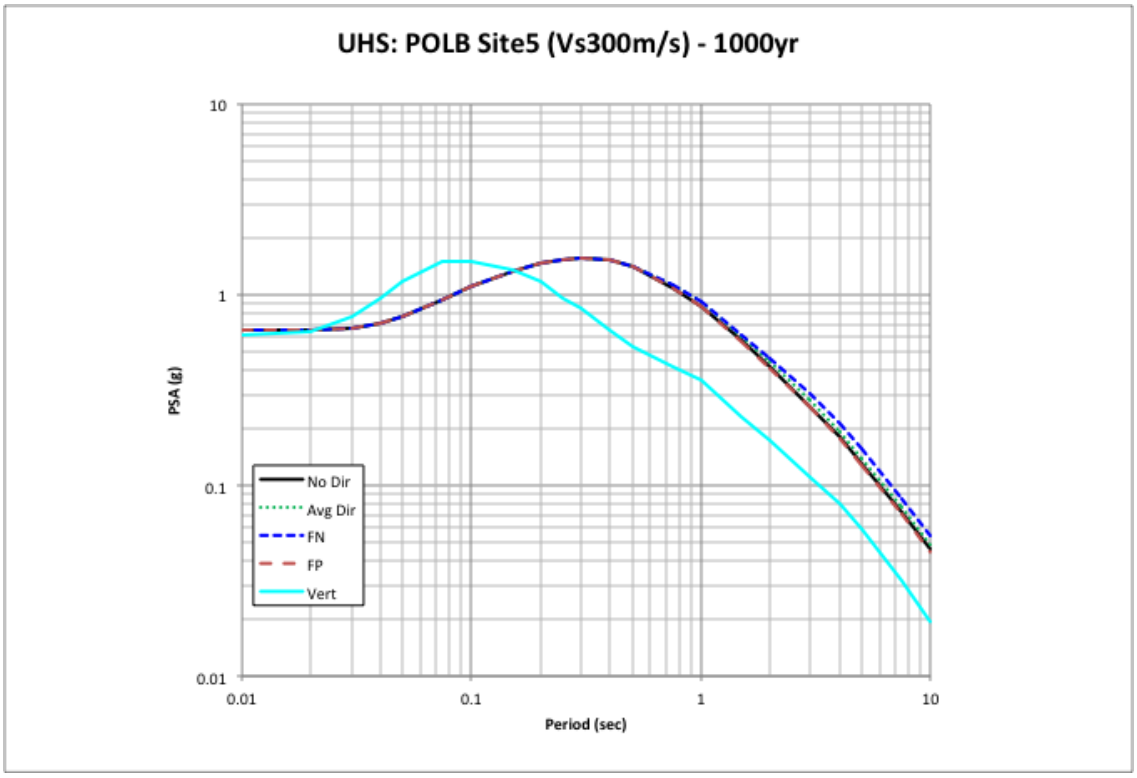


Figure 144. UHS for the 975-year return period hazard level at Site 5 with and without directivity and for the vertical component and including the Wilmington fault.

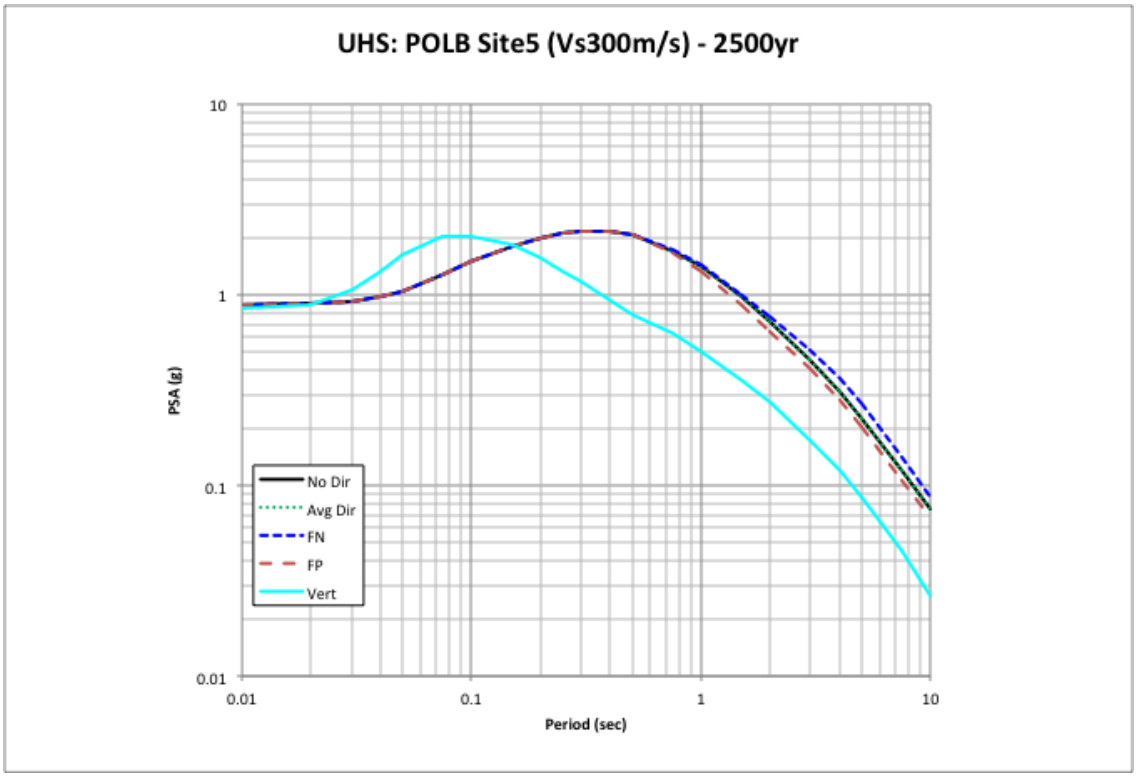


Figure 145. UHS for the 2,475-year return period hazard level at Site 5 with and without directivity and for the vertical component and including the Wilmington fault.

Given these ground motion results from the current PSHA study for the POLB including the Wilmington fault, a comparison is presented with the previous ground motion results (Earth Mechanics Inc., 2006). As has been noted before, the major difference between the two PSHA studies is in the different seismic source model and ground motion models used in the analysis. Previously, ground motions were computed for the 72-year (OLE) and 475-year (CLE) hazard levels for the fault normal (FN), fault parallel (FP) and vertical components. The subsurface site conditions are assumed to be the same between the two studies. The computed ground motions from the previous study (Earth Mechanics Inc., 2006) are listed in Table 39 for 72-year (OLE) hazard level and Table 40 for the 475-year (CLE) hazard level.

Table 39. UHS for the 72-year (OLE) return period hazard level for POLB from the previous study (Earth Mechanics Inc., 2006).

Period (sec)	FN PSA (g)	FP PSA (g)	Vertical PSA (g)
0.01	0.173	0.173	0.129
0.02	0.173	0.173	0.129
0.03	0.173	0.173	0.157
0.05	0.214	0.214	0.247
0.075	0.266	0.266	0.287
0.1	0.317	0.317	0.289
0.12	0.335	0.335	0.276
0.15	0.361	0.361	0.268
0.17	0.379	0.379	0.255
0.2	0.405	0.405	0.235
0.3	0.399	0.399	0.179
0.4	0.36	0.36	0.144
0.5	0.329	0.329	0.122
0.75	0.257	0.257	0.091
1	0.212	0.212	0.074
1.5	0.152	0.152	0.053
2	0.114	0.115	0.043
3	0.063	0.063	0.027
4	0.039	0.039	0.02
5	0.026	0.026	0.014
6	0.019	0.019	0.012
8	0.011	0.011	0.008
10	0.007	0.007	0.005

Table 40. UHS for the 475-year (CLE) return period hazard level for POLB from the previous study (Earth Mechanics Inc., 2006).

Period (sec)	FN PSA (g)	FP PSA (g)	Vertical PSA (g)
0.01	0.496	0.496	0.515
0.02	0.496	0.496	0.515
0.03	0.496	0.496	0.687
0.05	0.614	0.614	1.229
0.075	0.762	0.762	1.456
0.1	0.91	0.91	1.386
0.12	0.954	0.954	1.231
0.15	1.021	1.021	1.032
0.17	1.066	1.066	0.928
0.2	1.132	1.132	0.8
0.3	1.121	1.121	0.54
0.4	1.029	1.029	0.418
0.5	0.958	0.958	0.34
0.75	0.735	0.733	0.231
1	0.62	0.616	0.186
1.5	0.449	0.444	0.131
2	0.331	0.327	0.108
3	0.196	0.19	0.073
4	0.129	0.125	0.056
5	0.092	0.089	0.045
6	0.068	0.066	0.036
8	0.041	0.04	0.027
10	0.026	0.026	0.017

Graphically the comparisons between the spectra for the 72-year (OLE) hazard level are provided in Figure 146. The spectral ratio between the current results for Site 5 divided by the previous results is plotted in Figure 147. The ratio values are not computed for spectral periods greater than 4.0 sec based on the limitations of the ground motion models used in the previous PSHA study. In general, the current results are showing an increase of less than about 20% over the spectral period range of 0.01 sec (PGA) to about 1.0 sec for the three components of motion. For longer spectral periods, the current ground motion results are observed to be lower by as much as about 20-30%.

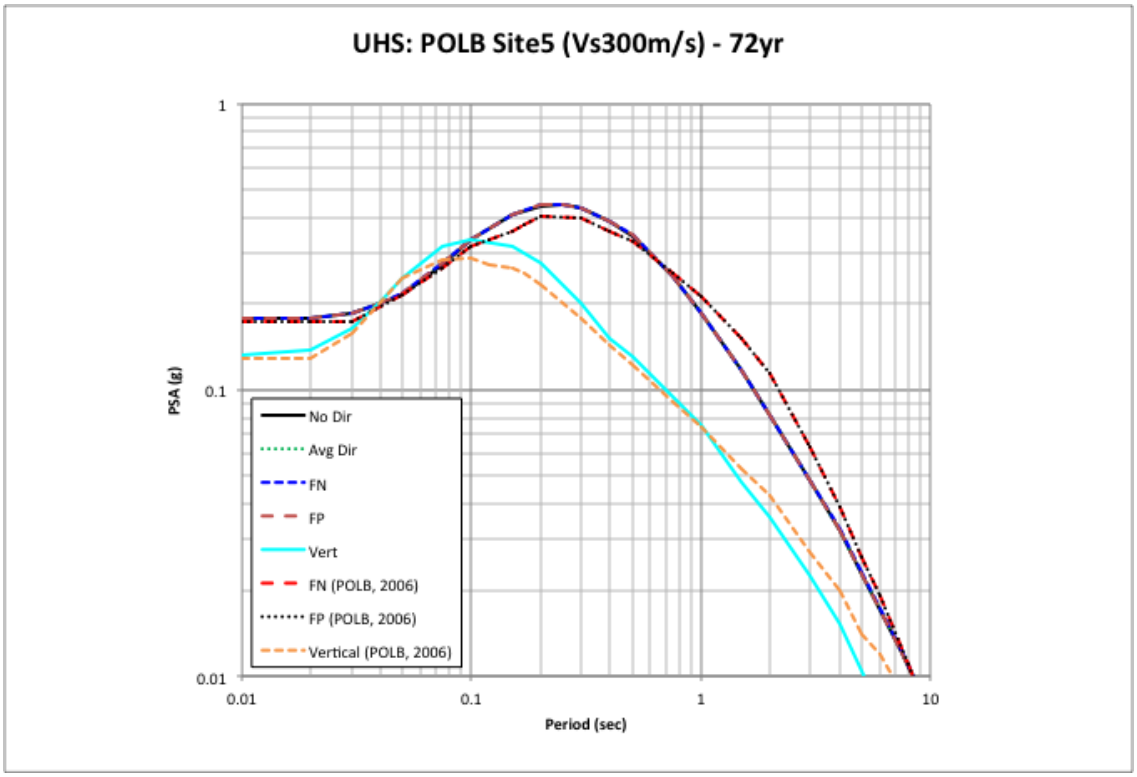


Figure 146. Comparison of the 72-year (OLE) hazard level UHS for POLB from the current and previous PSHA studies.

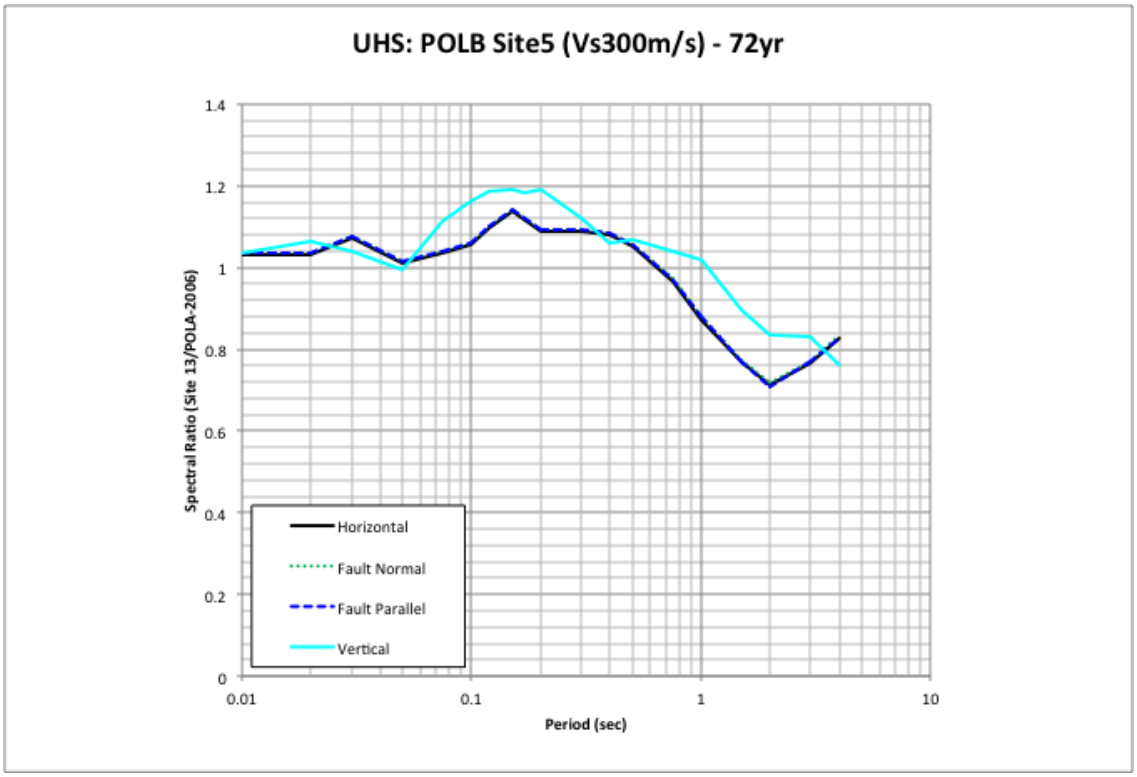


Figure 147. Spectral ratio of the current UHS divided by the previous UHS for the 72-year (OLE) hazard level UHS.

Similar comparisons between the spectra for the 475-year (CLE) hazard level are provided in Figure 148. The spectral ratio between the current results for Site 5 divided by the previous results is plotted in Figure 149. The ratio values are not computed for spectral periods greater than 4.0 sec based on the limitations of the ground motion models used in the previous PSHA study. In general, the current results are showing a decrease on the order of 10-20% over the spectral period range of 0.01 sec (PGA) to about 0.2 sec for the three components of motion. For longer spectral periods, the vertical component is showing an increase up to about 25% at 1.0 sec and then a decrease for longer spectral periods. For the two horizontal components of motion including directivity, the results are similar between the two studies with a slight reduction with the current values on the order of 10-20% or less.

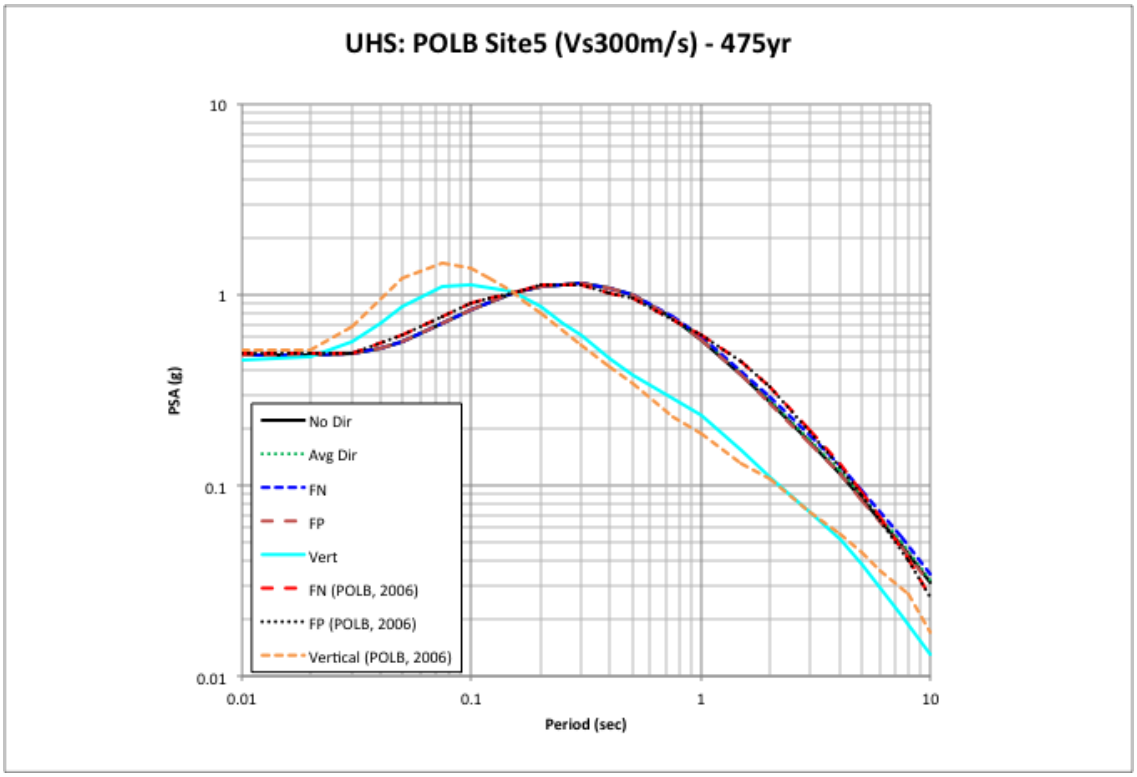


Figure 148. Comparison of the 475-year (CLE) hazard level UHS for POLB from the current and previous PSHA studies.

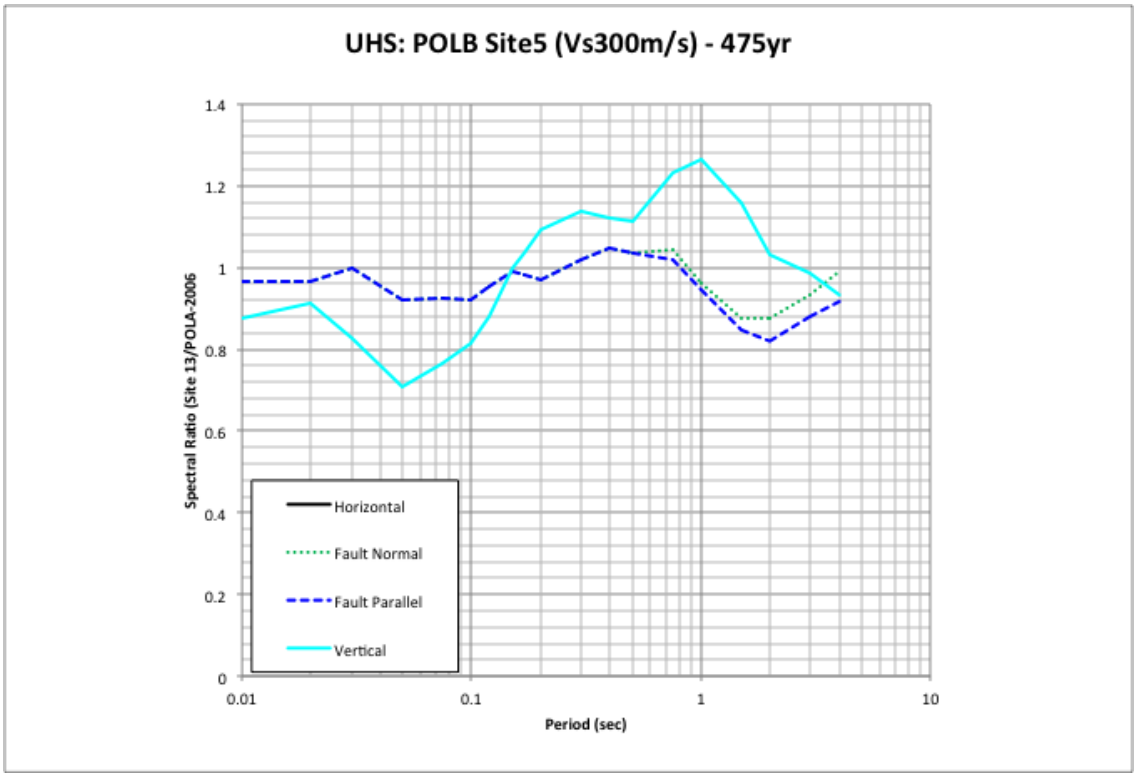


Figure 149. Spectral ratio of the current UHS divided by the previous UHS for the 475-year (CLE) hazard level UHS.

The observed differences between the two PSHA studies can be expected to be based on differences in the seismic source and ground motion models. Based on the similar comparison of the associated slip rates for the controlling faults in the immediate region around the POLB and the differences in the ground motion models including their aleatory sigma models, these observed differences are not unusual. The ground motion results presented in this report are based on the current state of knowledge seismic source and ground motion models and follows a standard state of practice PSHA methodology. The results from Site 5 are applicable for the assigned subsurface site conditions with a V_{S30} value of 300 m/sec. Any observations and or conclusions for other site conditions may not be applicable without additional sensitivity studies or calculations.

6. References

Abrahamson, N. A. and N. Gregor (2015). Haz45, Seismic Hazard Analysis Software.

Abrahamson, N. A., Silva, W. J., and R. Kamai. 2014. Summary of the ASK14 ground motion relation for active crustal regions. Earthquake Spectra, Vol. 30, No. 3, pp. 1025-1055.

Al Atik, L. and R. R. Youngs (2014). Epistemic uncertainty for NGA-West2 Models. Earthquake Spectra, Vol. 30, No. 3, pp. 1301-1318.

Bazzurro, P., and C. A. Cornell (1999). Disaggregation of seismic hazard, Bulletin of the Seismological Society of America, Vol. 89, pp. 501–520.

Boore, D. M, Stewart, J. P., Seyhan, E. and G. M. Atkinson (2014). NGA-West2 equations for predicting PGA, PGV, and 5% damped PSA for shallow crustal earthquakes. Earthquake Spectra, Vol. 30, No. 3, pp. 1057-1085.

Bozorgnia, Y., N. Abrahamson, L. Al Atik, T. D. Ancheta, G. M. Atkinson, J. W. Baker, A. Baltay, D. M. Boore, K. W. Campbell, B. S-J. Chiou, R. Darragh, S. Day, J. Donahue, R. W. Graves, N. Gregor, T. Hanks, I. M. Idriss, R. Kamai, T. Kishida, A. Kottke, S. A. Mahin, S. Rezaeian, B. Rowshandel, E. Seyhan, S. Shahi, T. Shantz, W. Silva, P. Spudich, J. P. Stewart, J. Watson-Lamprey, K. Wooddell, R. Youngs (2014). NGA-West2 Research Project, Earthquake Spectra, Vol. 30, No. 3, pp. 973-987.

Bozorgnia, Y., and K. W. Campbell (2016). NGA-West2 ground motion model for the vertical-to-horizontal ratio of PGA, PGV, and linear response spectra, Earthquake Spectra, Vol. 32, pp. 951–978.

Campbell, K. W. and Y. Bozorgnia (2014). NGA-West2 ground motion model for the average horizontal components of PGA, PGV, and 5% damped linear acceleration response spectra. Earthquake Spectra, Vol. 30, No. 3, pp. 1087-1115.

Chiou, B. S.-J., and R. R. Youngs (2014). Update of the Chiou and Youngs NGA model for the average horizontal component of peak ground motion and response spectra. Earthquake Spectra, Vol. 30, No. 3, pp. 1117-1153.

Earth Mechanics Inc. (2006). Port-wide Ground Motion Study Port of Long Beach, California, Final Report, August 2006.

Earthquake Engineering Research Institute (1989). The basics of seismic risk analysis, Earthquake Spectra, Vol. 5, pp. 675–699.

Frankel, A.D., Petersen, M.D., Mueller, C.S., Haller, K.M., Wheeler, R.L., Leyendecker, E.V., Wesson, R.L., Harmsen, S.C., Cramer, C.H., Perkins, D.M., Rukstales, K.S., 2002, Documentation for the 2002 update of the National Seismic Hazard Maps: U.S. Geological Survey Open-File Report 2002–420, 39 p.

Gregor, N. and L. Al Atik (2019). Seismic Hazard Analysis for Port of Long Beach (POLB) Site Locations in Long Beach, CA, report prepared for Earth Mechanics Inc., September 3, 2019.

Gregor, N., and L. Al Atik (2017a). UCERF3 Implementation for Probabilistic Seismic Hazard Assessment Using HAZ45-HSR, Report prepared for SC Solutions, Sunnyvale, California.

Gregor, N., and L. Al Atik (2017b). Validation Testing of the Probabilistic Seismic Hazard Program: HAZ45-HSR, Report prepared for SC Solutions, Sunnyvale, California.

Gregor, N. W. Silva, and B. Darragh (2002). Development of Attenuation Relations For Peak Particle Velocity and Displacement, PEARL Report to PG&E/CEC/Caltrans, Pacific Engineering and Analysis Report.

Gulerce, Z. and N.A. Abrahamson (2011). Site-Specific Design Spectra for Vertical Ground Motion, Earthquake Spectra, Vol. 27, No. 4, pp. 1023-1047.

Hale, C., N. Abrahamson, and Y. Bozorgnia (2018). Probabilistic Seismic Hazard Analysis Code Verification, PEER Report, Pacific Earthquake Engineering Research Center, University of California, Berkeley, California, PEER Report 2018/03.

Idriss, I. M. (2014). An NGA-West2 empirical model for estimating the horizontal spectral values generated by shallow crustal earthquakes. Earthquake Spectra, Vol. 30, No. 3, pp. 1155-1177.

McGuire, R. K. (2004). Seismic Hazard and Risk Analysis, Monograph NMO-10, Earthquake Engineering Research Institute, Oakland, California.

McGuire, R. K., W. J. Silva, and C. J. Costantino (2001). Technical Basis for Revision of Regulatory Guidance on Design Ground Motions: Hazard- and Risk-consistent Ground Motion Spectra Guidelines, Nuclear Regulatory Commission Report, NUREG/CR-6728.

Spudich, P., J. R. Bayless, J. W. Baker, B. S.J. Chiou, B. Rowshandel, S. K. Shahi and P. Somerville. 2013. Final Report of the NGA-West2 Directivity Working Group, PEER Report 2013/09, May 2013.

USGS (2013). The Uniform California Earthquake Rupture Forecast, Version 3 (UCERF3) – The Time Independent Model, USGS Open File Report 2013-1165.

Wolfe, F.D., J.H. Shaw, A. Plesch, D. J. Ponti, J.F. Dolan and M. R. Legg (2019). The Wilmington Blind-Thrust Fault: An Active Concealed Earthquake Source beneath Los Angeles, California, Bull. Seism. Soc. Am., Vol. 109, No. 5, pp. 1890-1906

APPENDIX B OLE, CLE, 975-YR, MCE$_R$, AND DE LEVEL FIRM (IMPROVED) GROUND MOTION TIME HISTORIES

The seven (7) sets of 3-component time histories discussed in Section 3.4 and listed below in Tables B1 and B2 are modified to match the firm-ground spectra using the time-domain approach. Each set has three (3) components (FN, FP and FV), resulting in a total of 21 time histories for each ground motion level. For each time history, the following is plotted:

- Initial acceleration, velocity and displacement time histories scaled to PGA,
- Modified (spectral-matched) acceleration, velocity and displacement time histories, and
- Comparison of the target acceleration and relative displacement spectra with the spectra of the initial and the modified time histories.

These plots are shown in Figure B1 through Figure B21 for the OLE, Figure B22 through Figure B42 for the CLE, Figure B43 through Figure B63 for the 975-yr., Figure B64 through Figure B84 for the MCE_R, and Figure B85 through Figure B105 for the DE ground motion levels.

Table B1. Selected Seed Motion for 72 yr Return Period (OLE) Event

Set	PEER RSN *	Earthquake	Mw	Pulse Motion	Station	Distance, R_{rup} (km)
1	802	1989 Loma Prieta	6.9	Yes	Saratoga – Aloha Ave.	8.5
2	729	1987 Superstition Hill	6.5	No	Wildlife Liquefaction Array	23.9
3	667	1987 Whittier	6.0	No	Northridge-Saticoy St.	41.7
4	170	1979 Imperial Valley	6.5	Yes	EC CO Center FF	7.3
5	4101	2004 Parkfield	6.0	Yes	Parkfield - Vineyard Canyon 3W	5.6
6	821	1992 Erzincan	6.7	No	Erzincan	4.4
7	988	1994 Northridge	6.7	No	Century City, LACC	23.4

* *PEER ground motion database (https://ngawest2.berkeley.edu/).*

Table B2. Selected Seed Motion for 475-yr (CLE), 975-yr, and 2475-yr Return Period Events

Set	PEER RSN *	Earthquake	Mw	Pulse Motion	Station	Distance, R_{rup} (km)
1	1787	1999 Hector Mine	7.1	No	Hector	11.7
2	767	1989 Loma Prieta	6.9	Yes	Gilroy Array 0#3	12.8
3	2114	2002 Denali, Alaska	7.9	Yes	TAPS Pump Station #10	2.7
4	1612	1999 Duzce, Turkey	7.1	No	Lamont 1059	4.2
5	6906	2010 Darfield, New Zealand	7.0	Yes	GDLC	1.2
6	6	1940 Imperial Valley	6.9	No	El Centro	6.1
7	1108	1995 Kobe, Japan	6.9	No	Kobe University	0.9

* *PEER ground motion database (https://ngawest2.berkeley.edu/).*

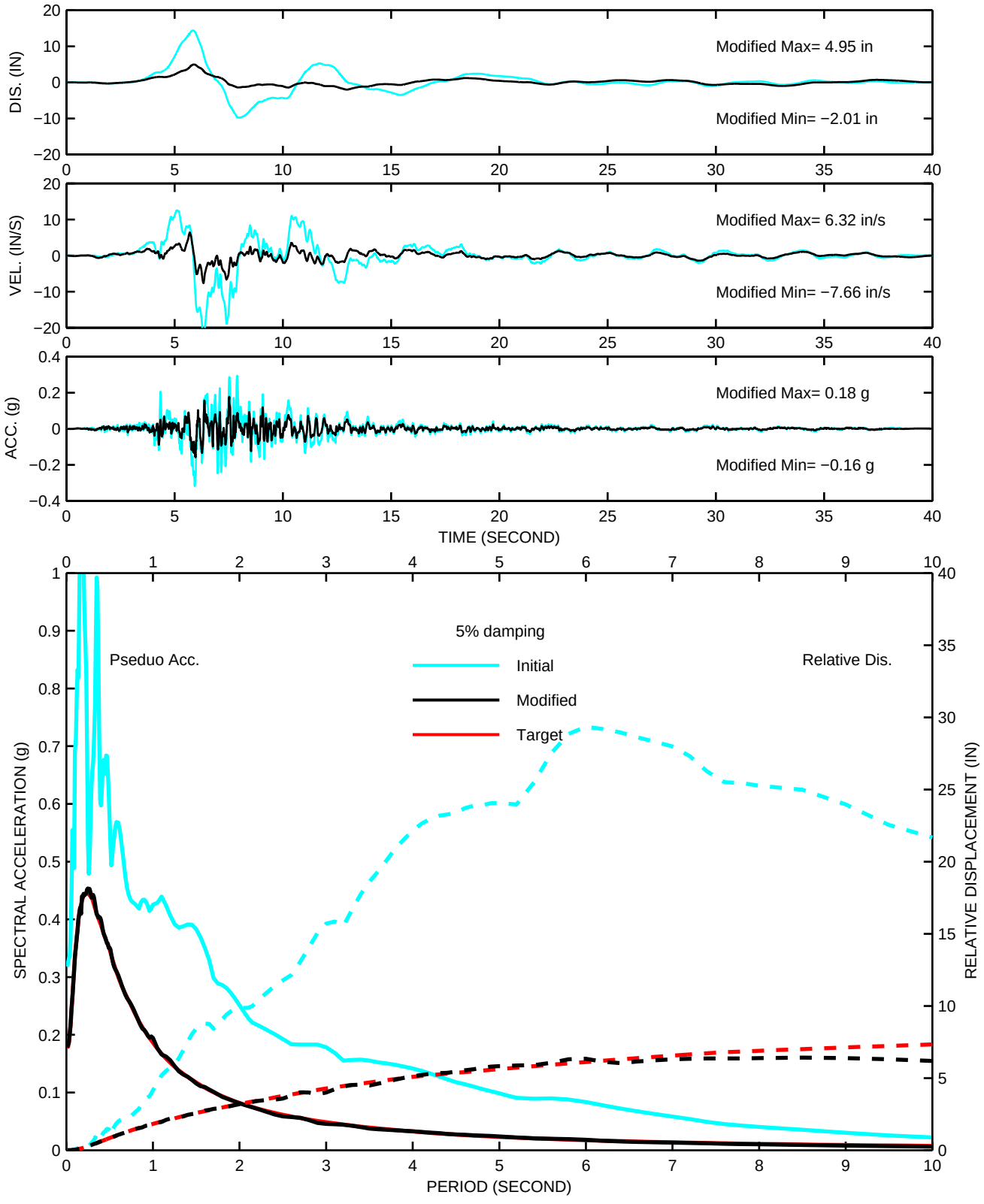


Figure B1. Firm−Ground OLE Spectrum Compatible Ground Motion (5% Damped) − Set 1 Fault Normal

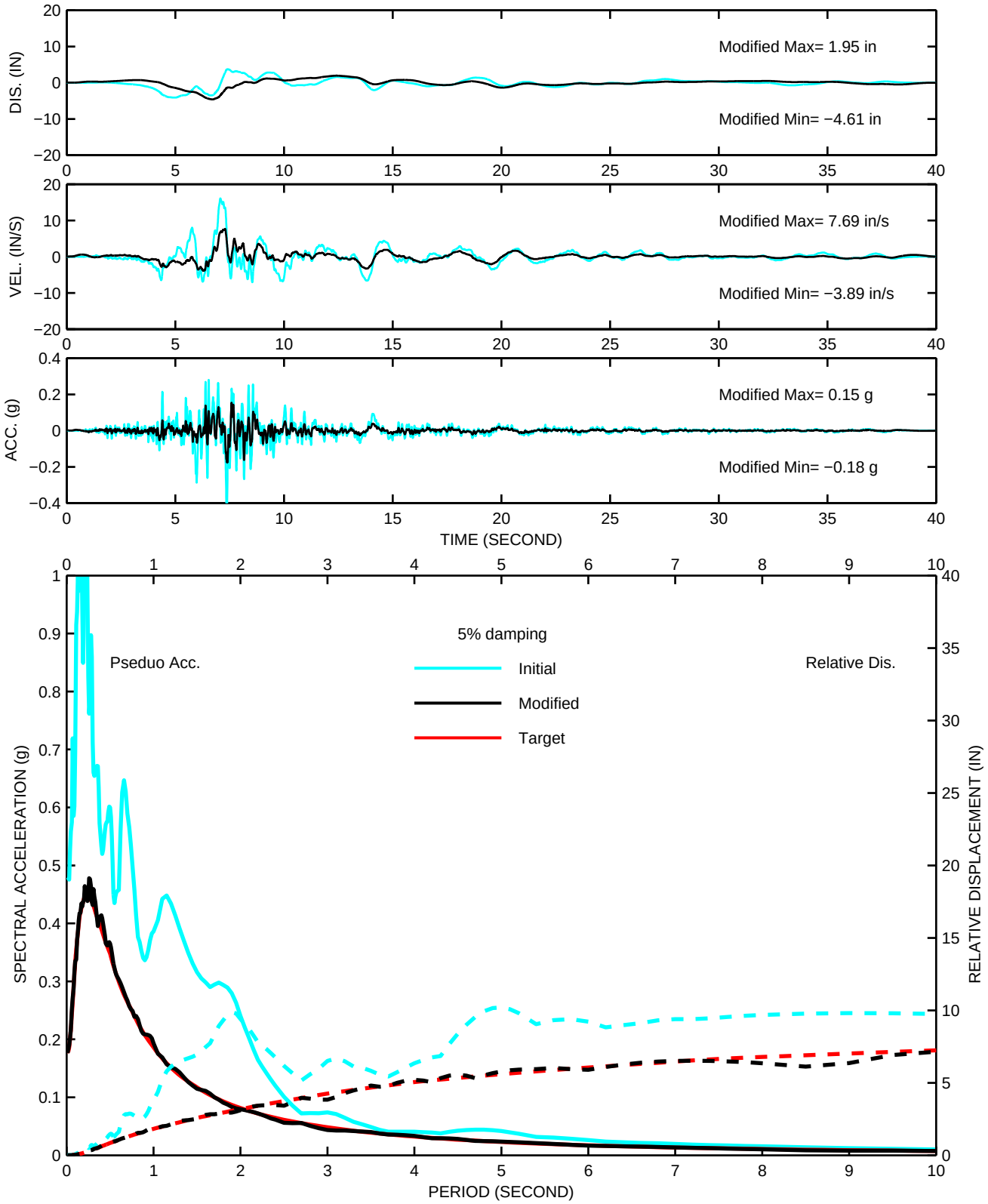


Figure B2. Firm−Ground OLE Spectrum Compatible Ground Motion (5% Damped) − Set 1 Fault Parallel

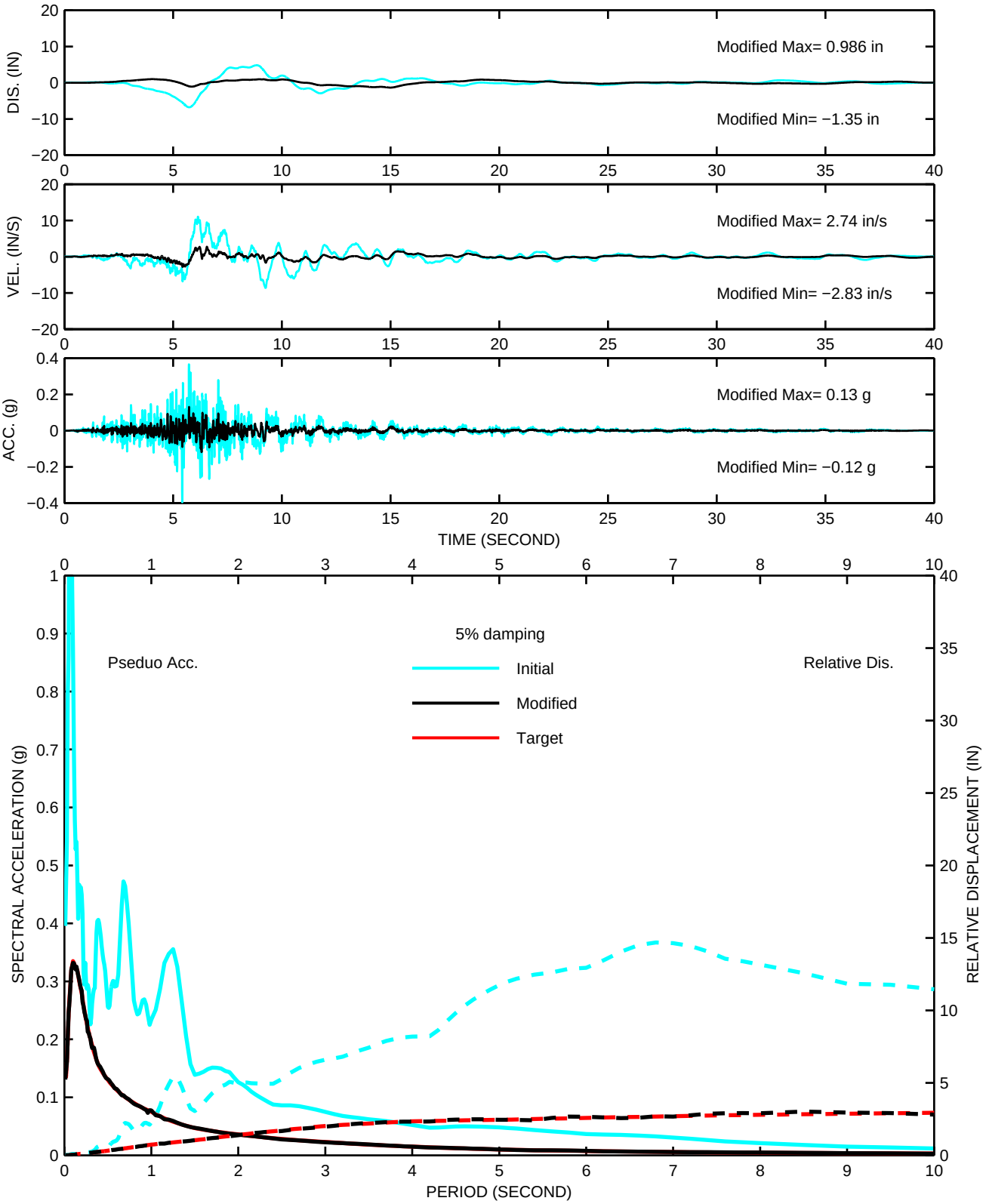


Figure B3. Firm−Ground OLE Spectrum Compatible Ground Motion (5% Damped) − Set 1 Vertical

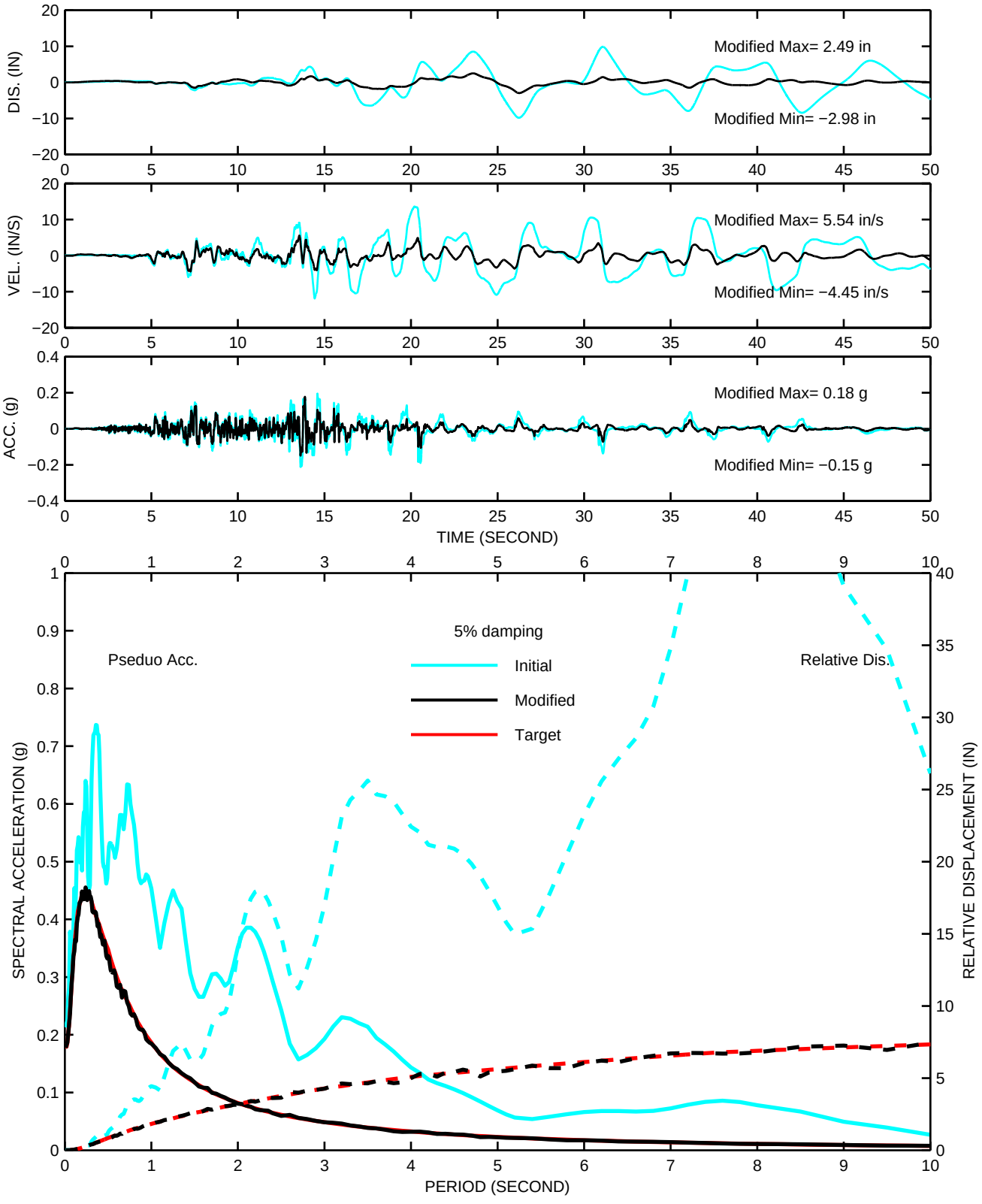


Figure B4. Firm−Ground OLE Spectrum Compatible Ground Motion (5% Damped) − Set 2 Fault Normal

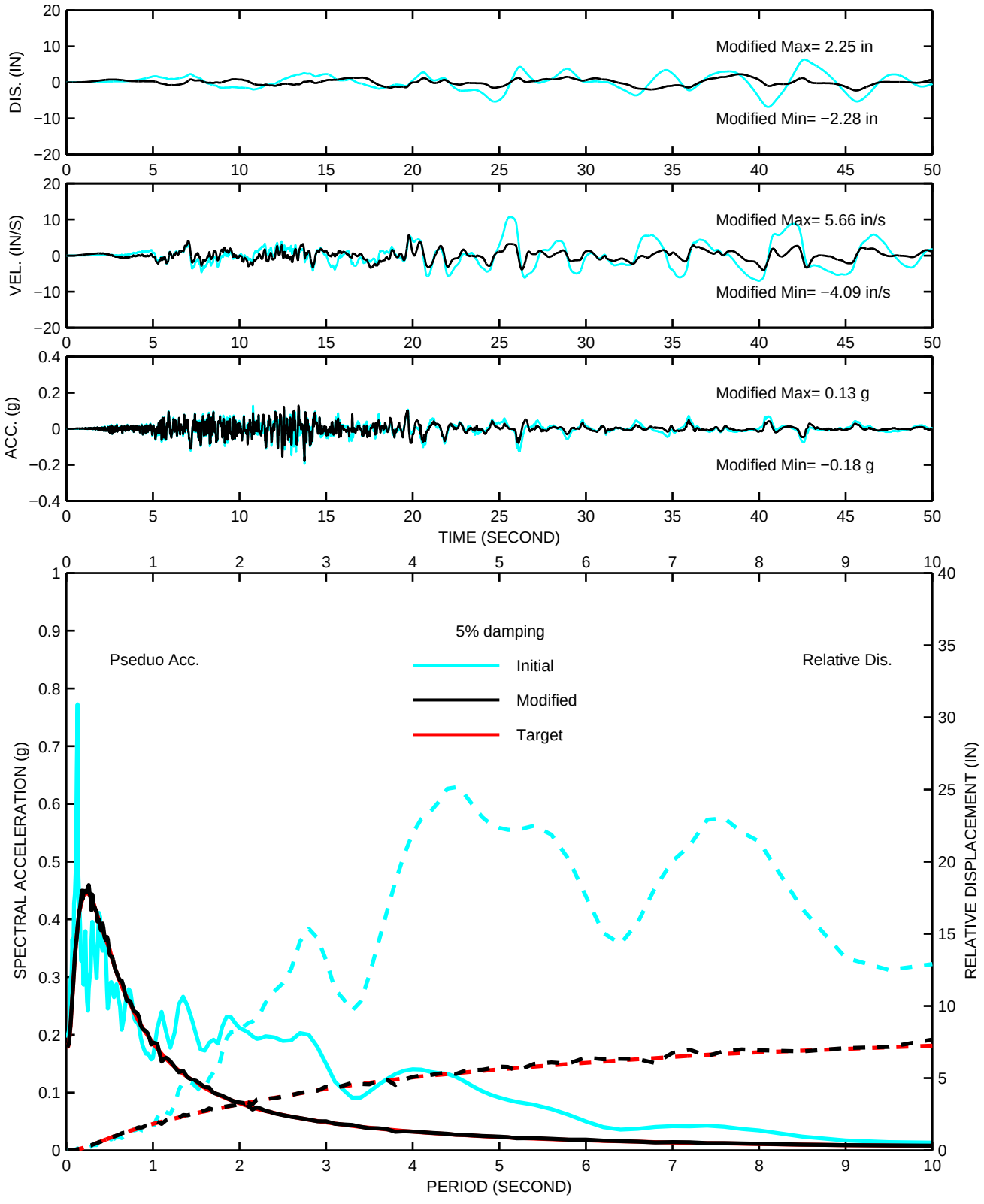


Figure B5. Firm−Ground OLE Spectrum Compatible Ground Motion (5% Damped) − Set 2 Fault Parallel

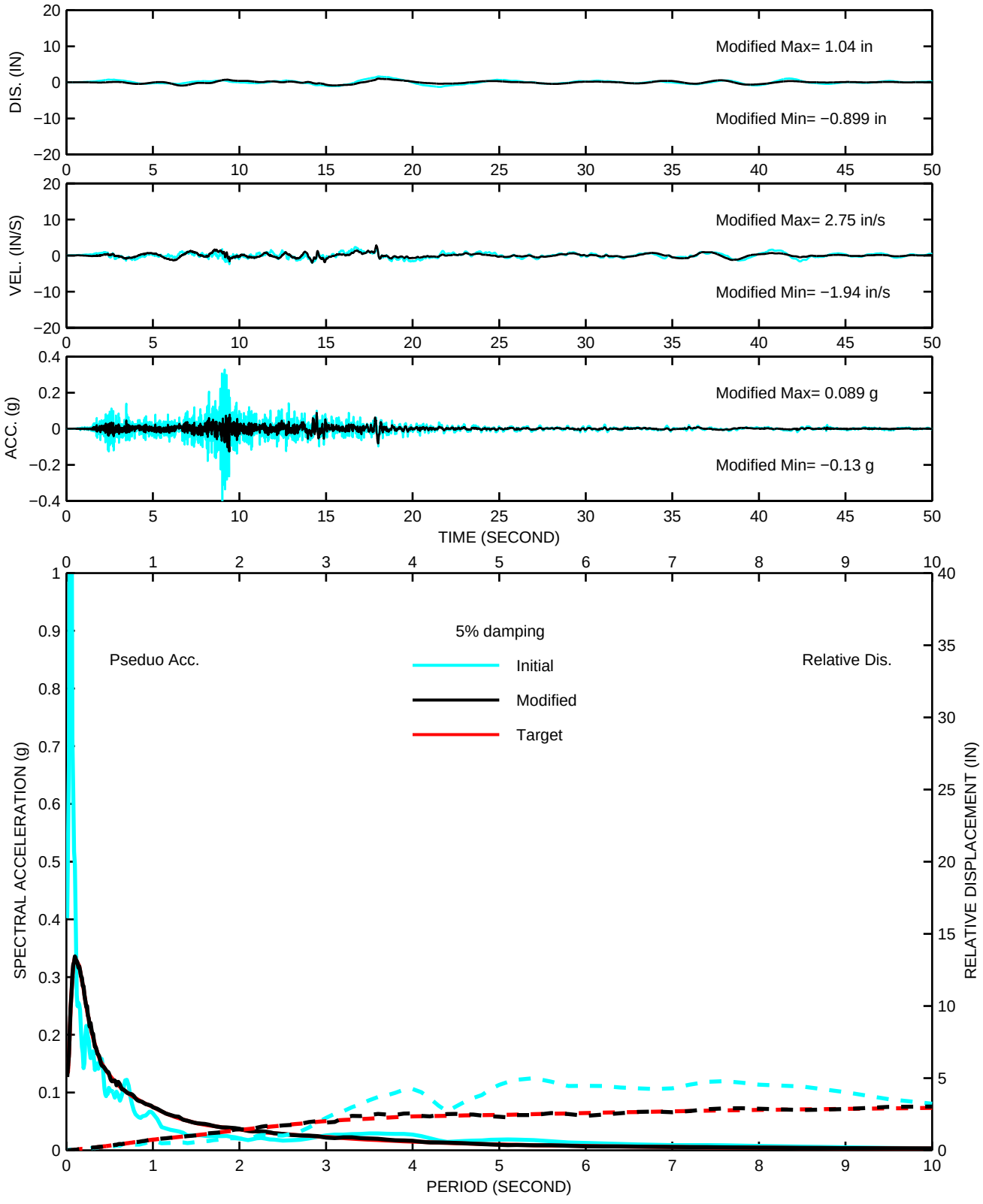


Figure B6. Firm−Ground OLE Spectrum Compatible Ground Motion (5% Damped) − Set 2 Vertical

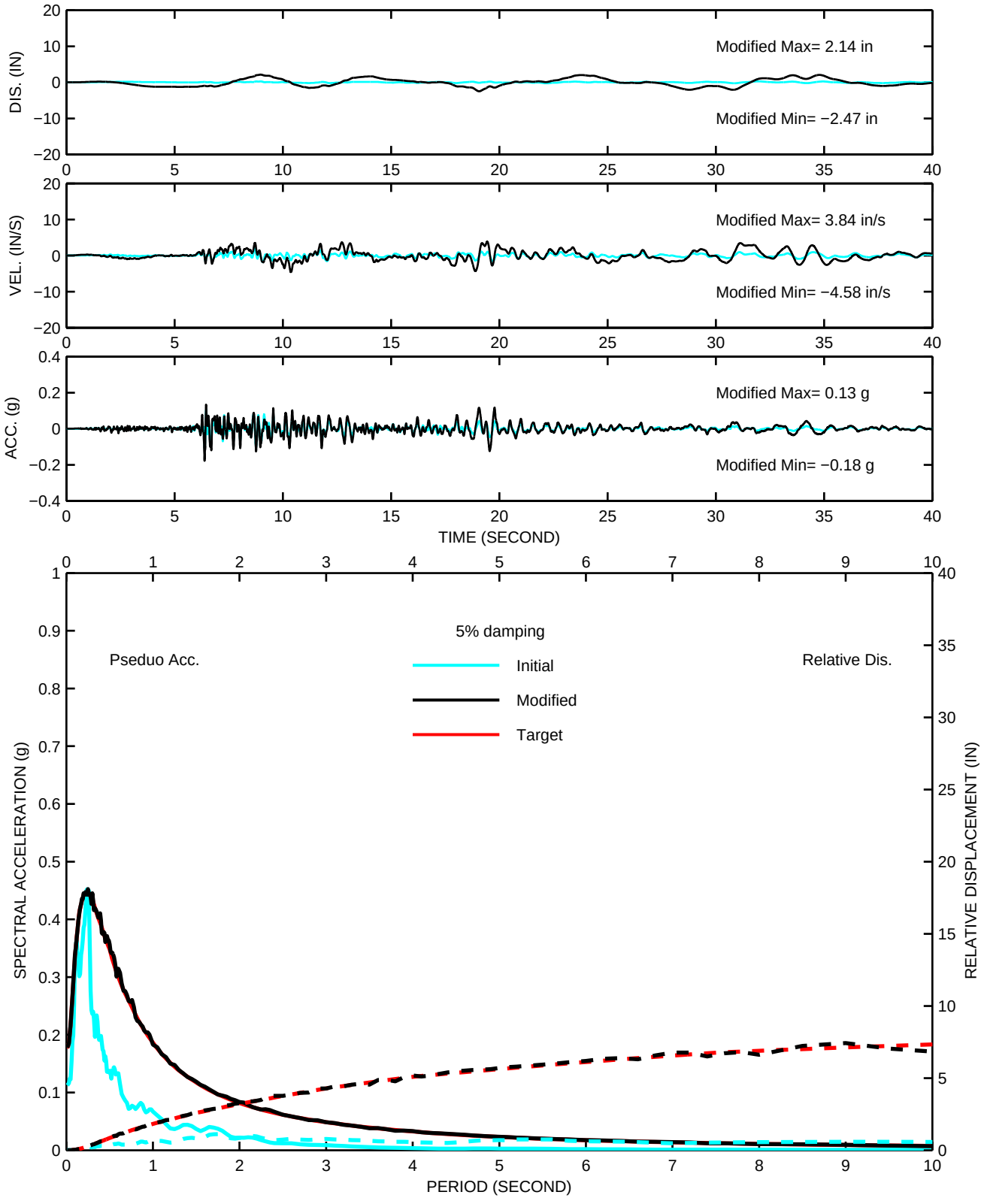


Figure B7. Firm−Ground OLE Spectrum Compatible Ground Motion (5% Damped) − Set 3 Fault Normal

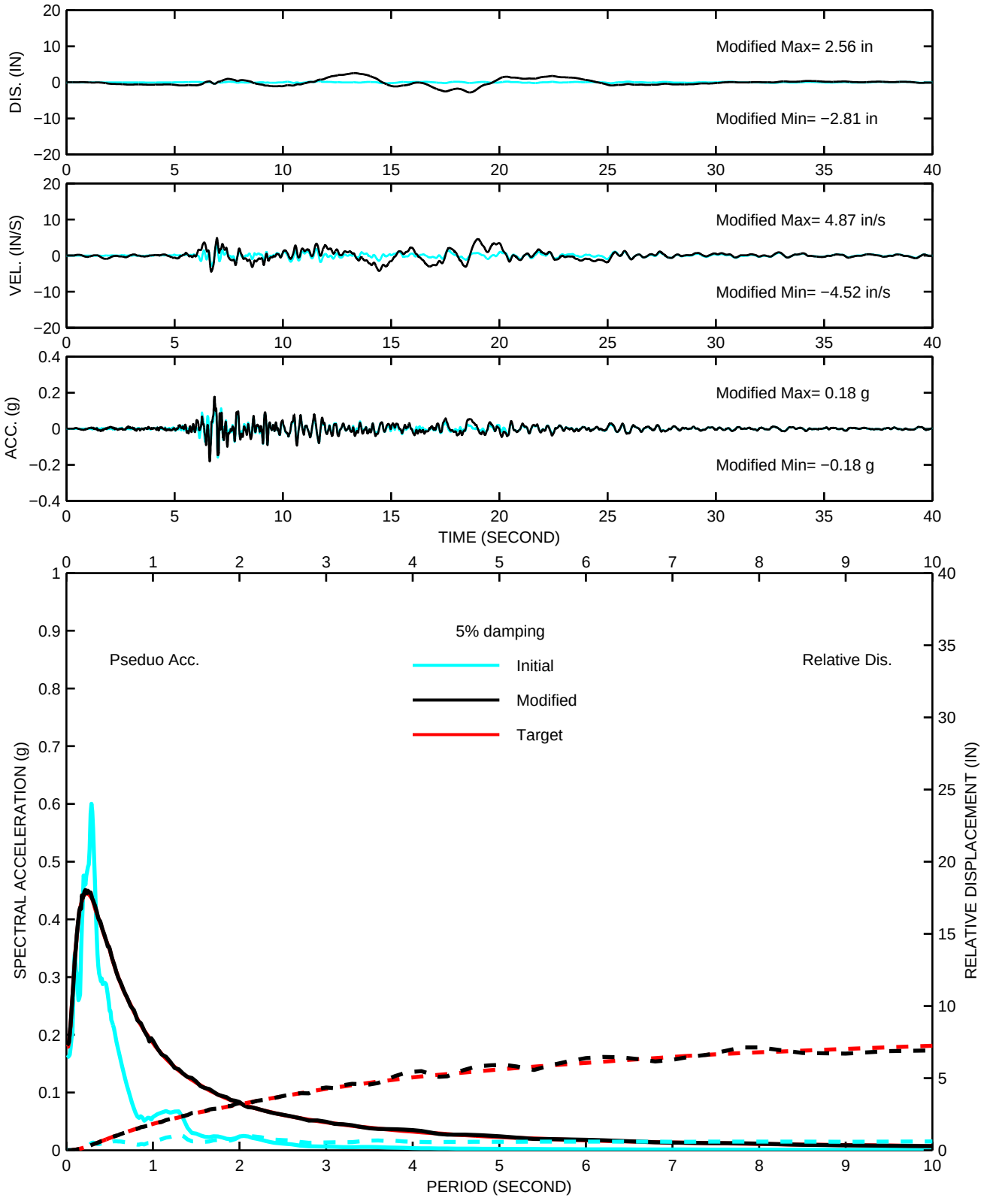


Figure B8. Firm−Ground OLE Spectrum Compatible Ground Motion (5% Damped) − Set 3 Fault Parallel

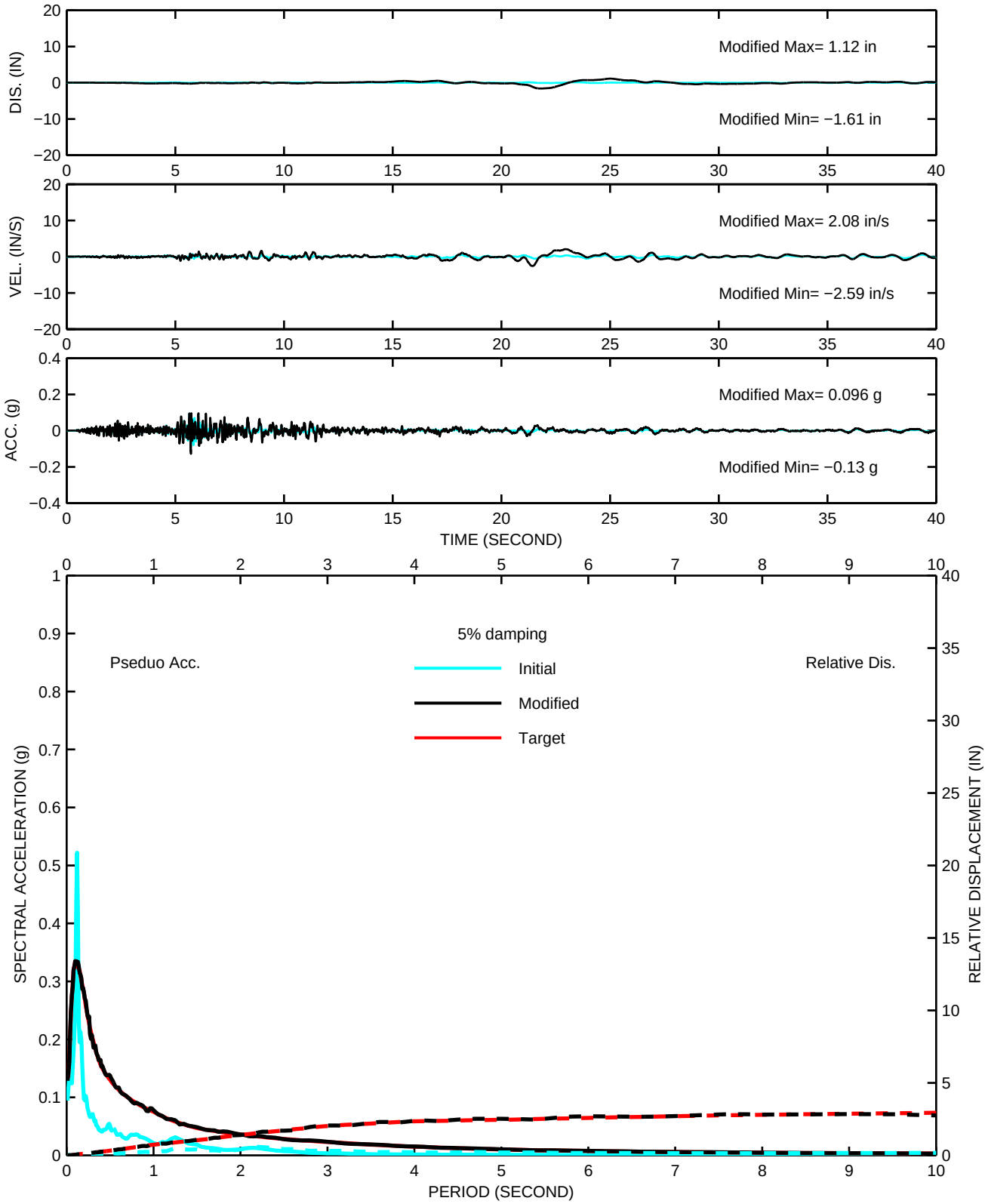


Figure B9. Firm−Ground OLE Spectrum Compatible Ground Motion (5% Damped) − Set 3 Vertical

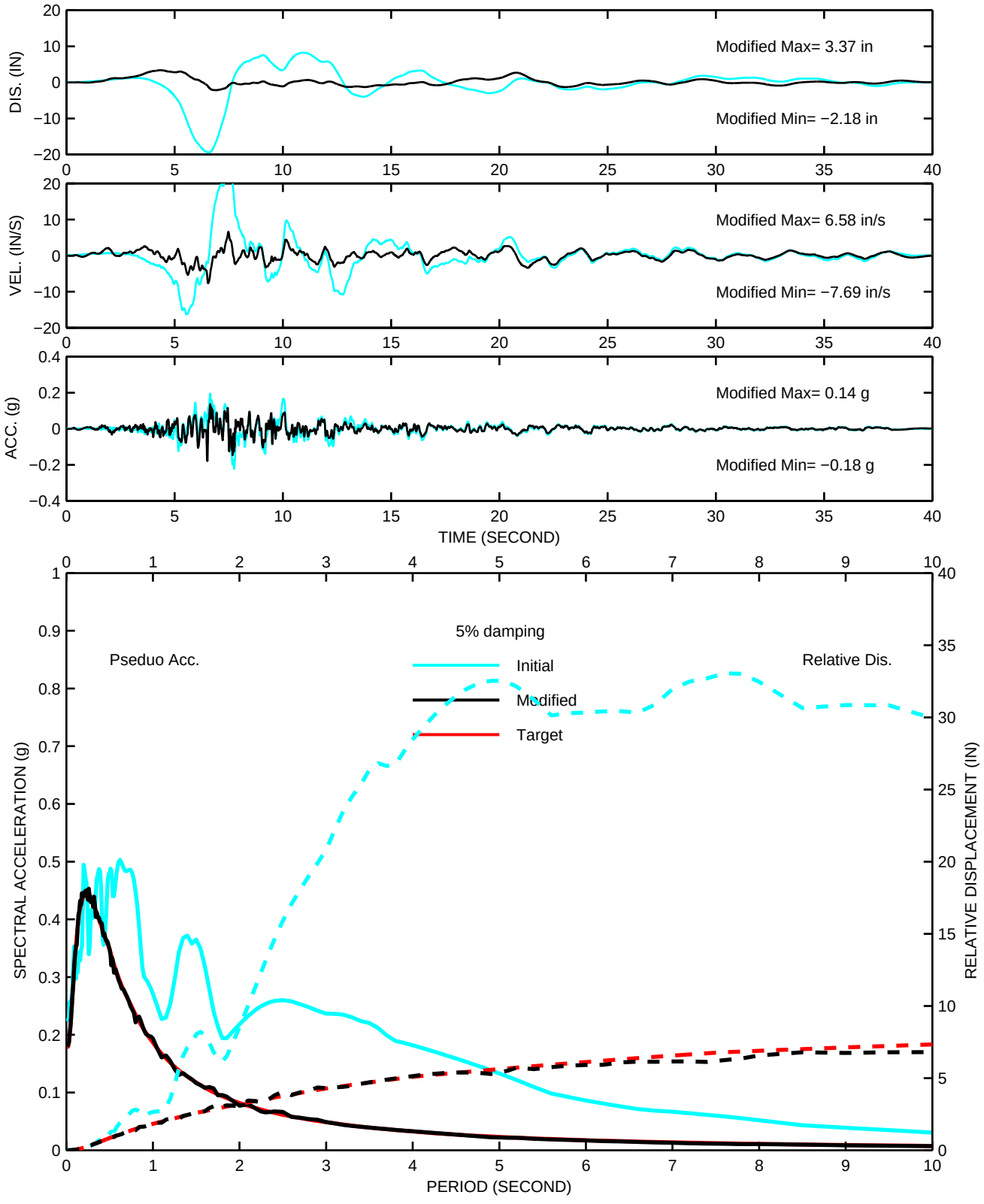


Figure B10. Firm−Ground OLE Spectrum Compatible Ground Motion (5% Damped) − Set 4 Fault Normal

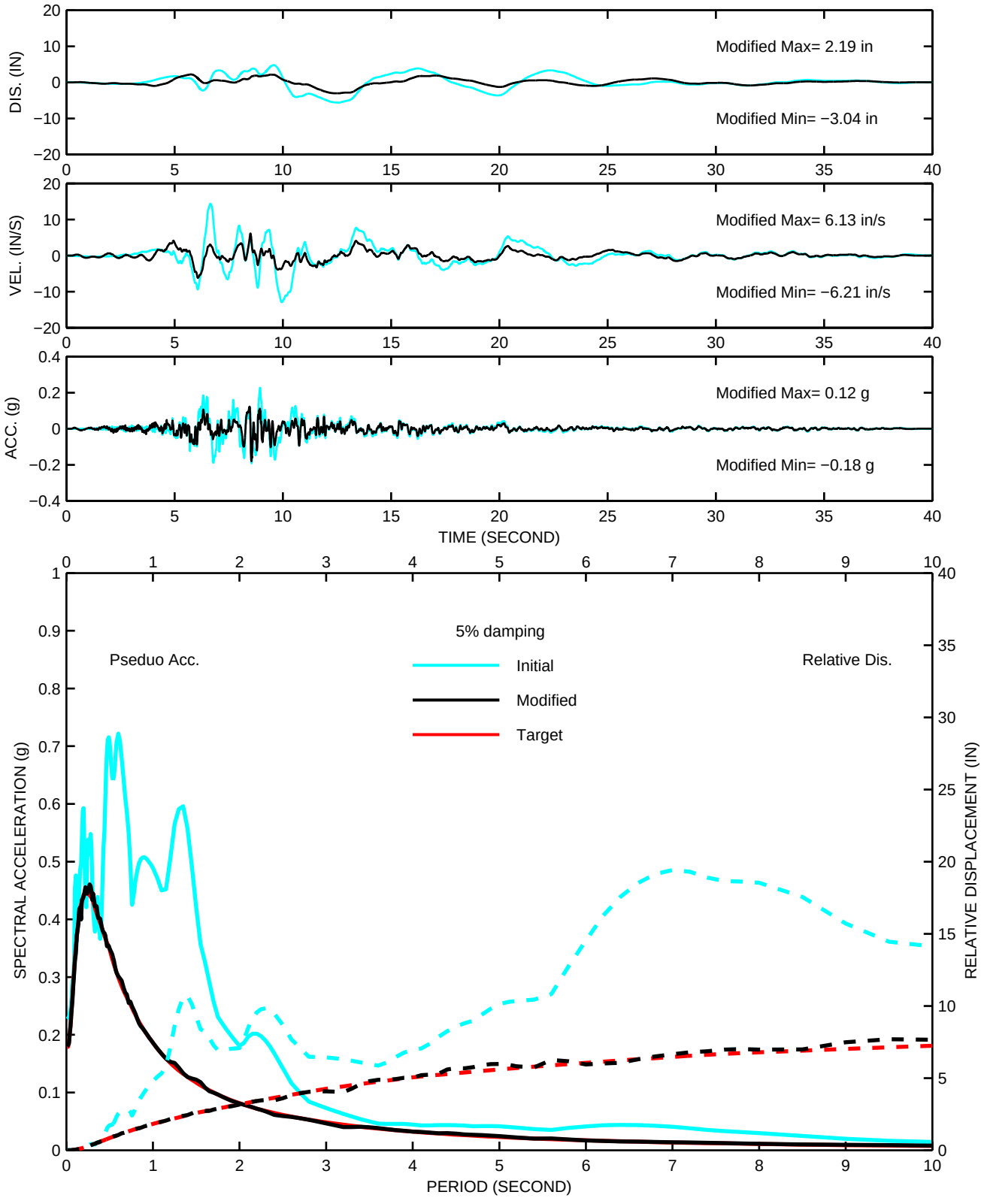


Figure B11. Firm−Ground OLE Spectrum Compatible Ground Motion (5% Damped) − Set 4 Fault Parallel

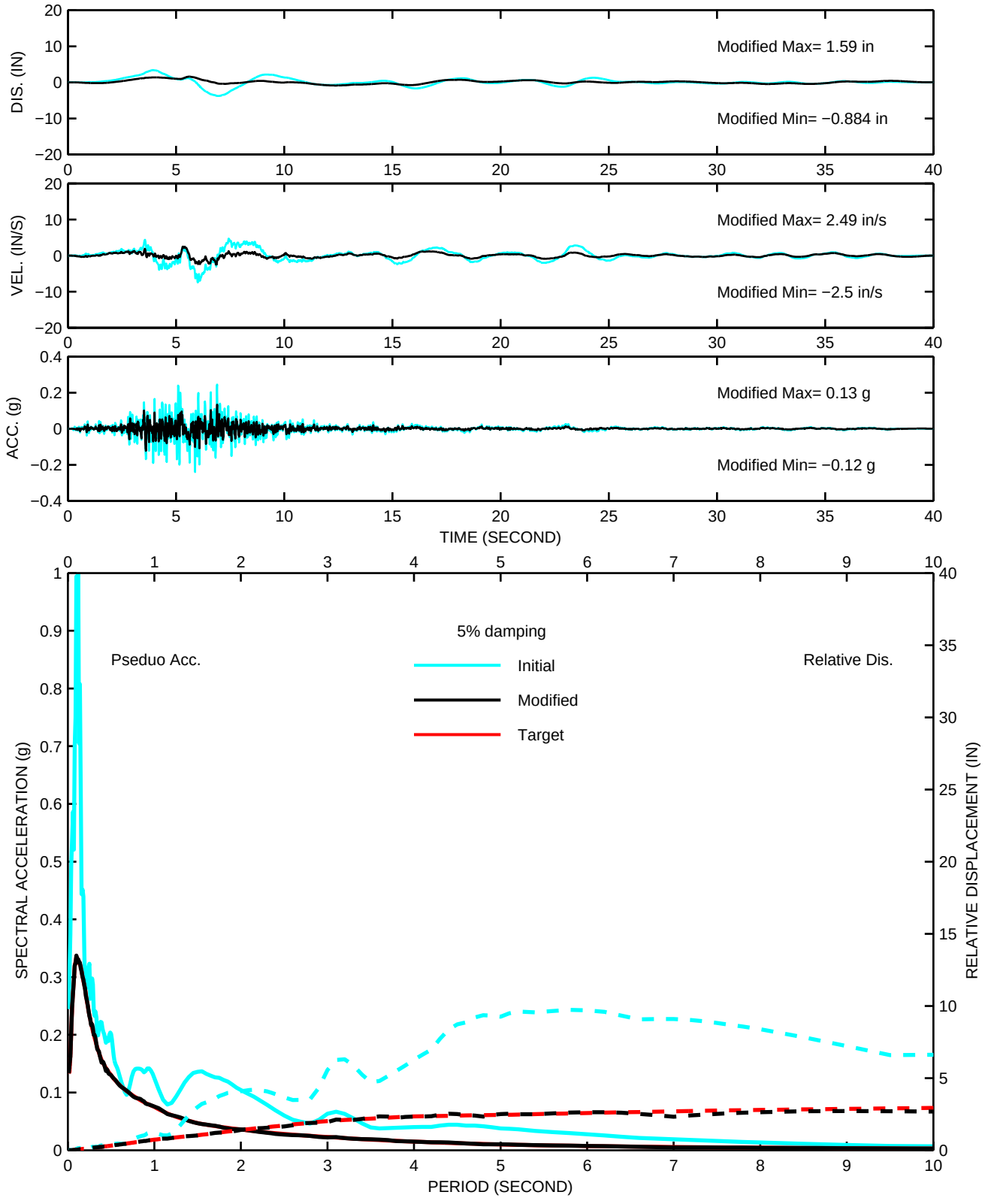


Figure B12. Firm−Ground OLE Spectrum Compatible Ground Motion (5% Damped) − Set 4 Vertical

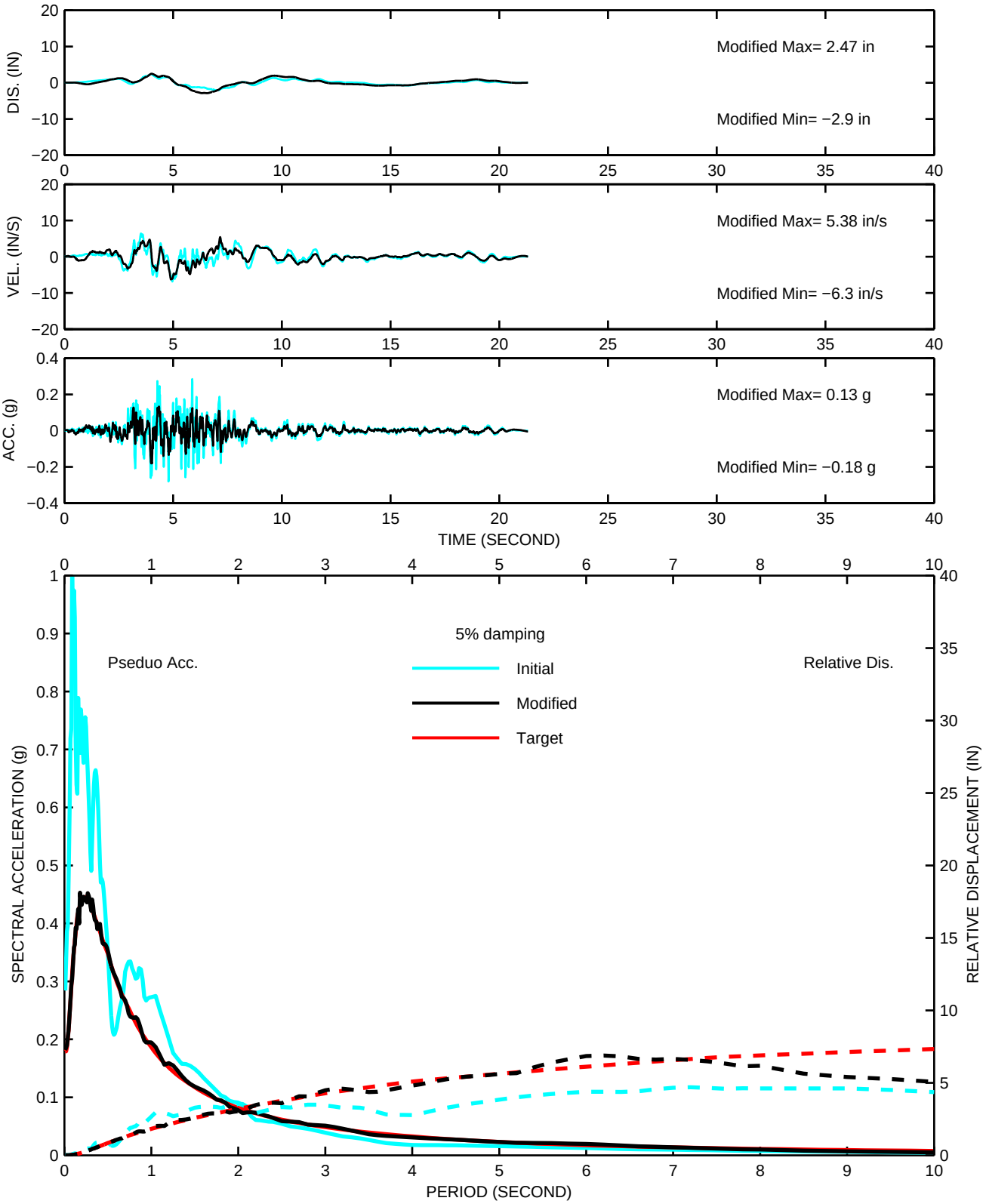


Figure B13. Firm−Ground OLE Spectrum Compatible Ground Motion (5% Damped) − Set 5 Fault Normal

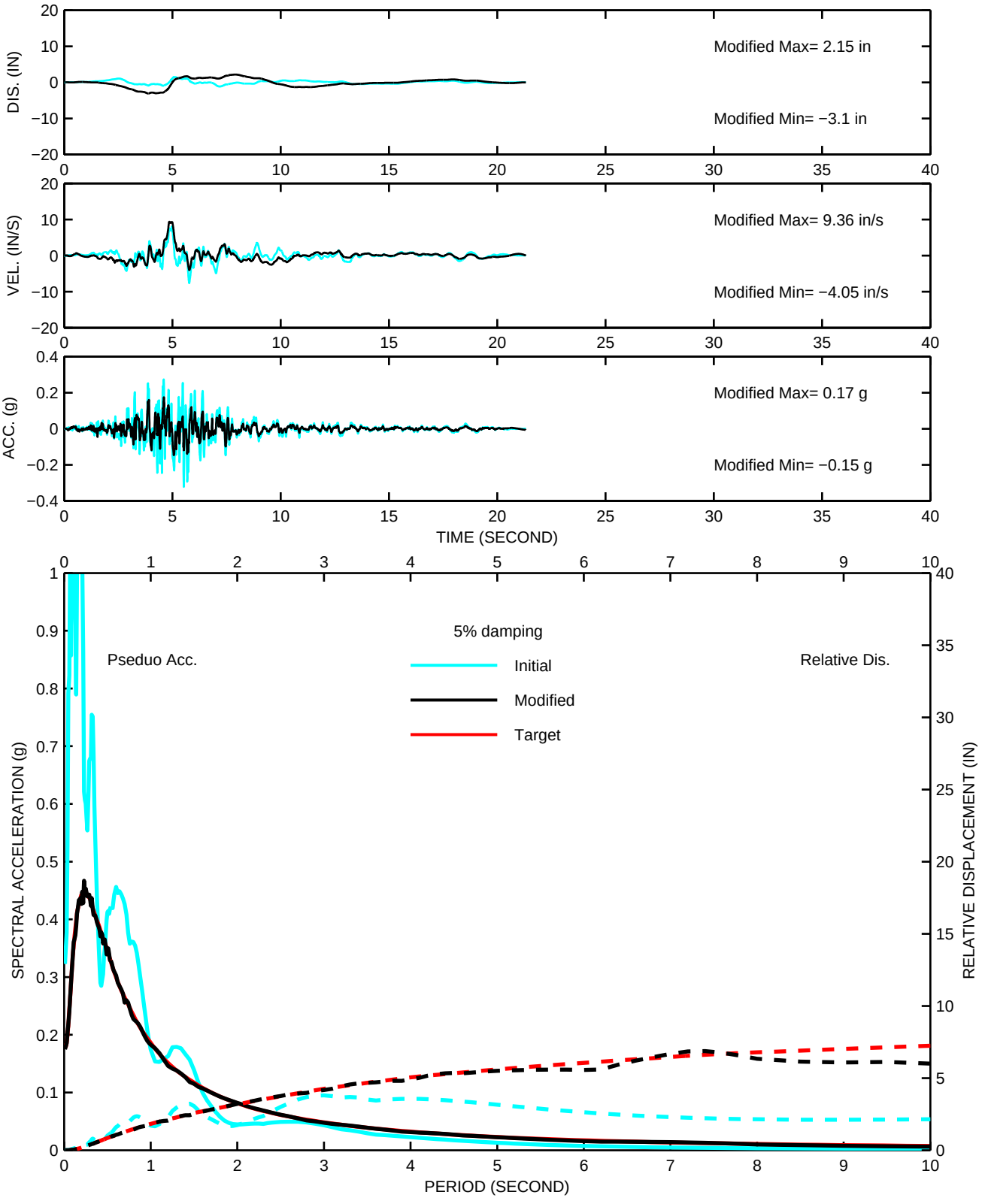


Figure B14. Firm−Ground OLE Spectrum Compatible Ground Motion (5% Damped) − Set 5 Fault Parallel

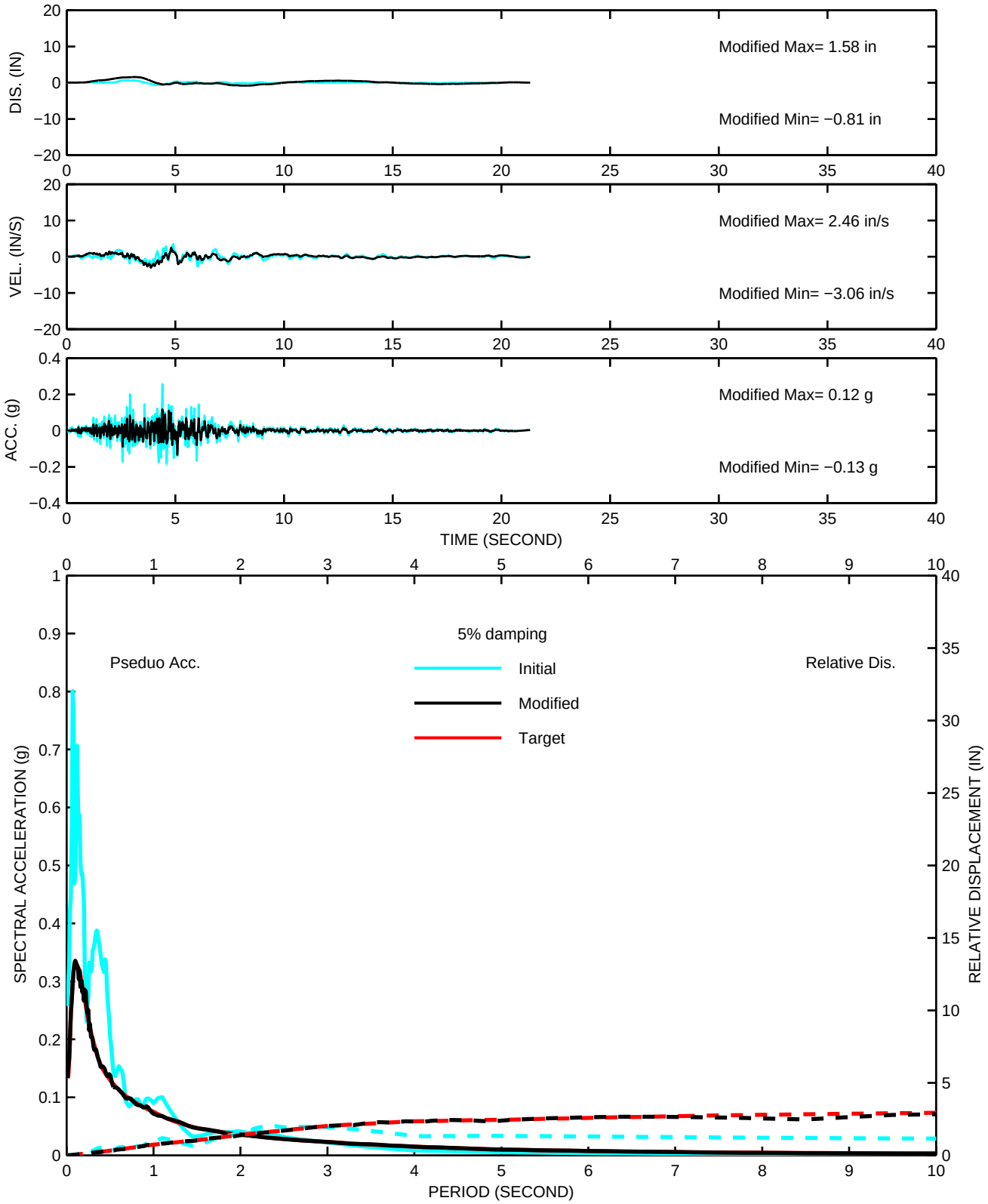


Figure B15. Firm−Ground OLE Spectrum Compatible Ground Motion (5% Damped) − Set 5 Vertical

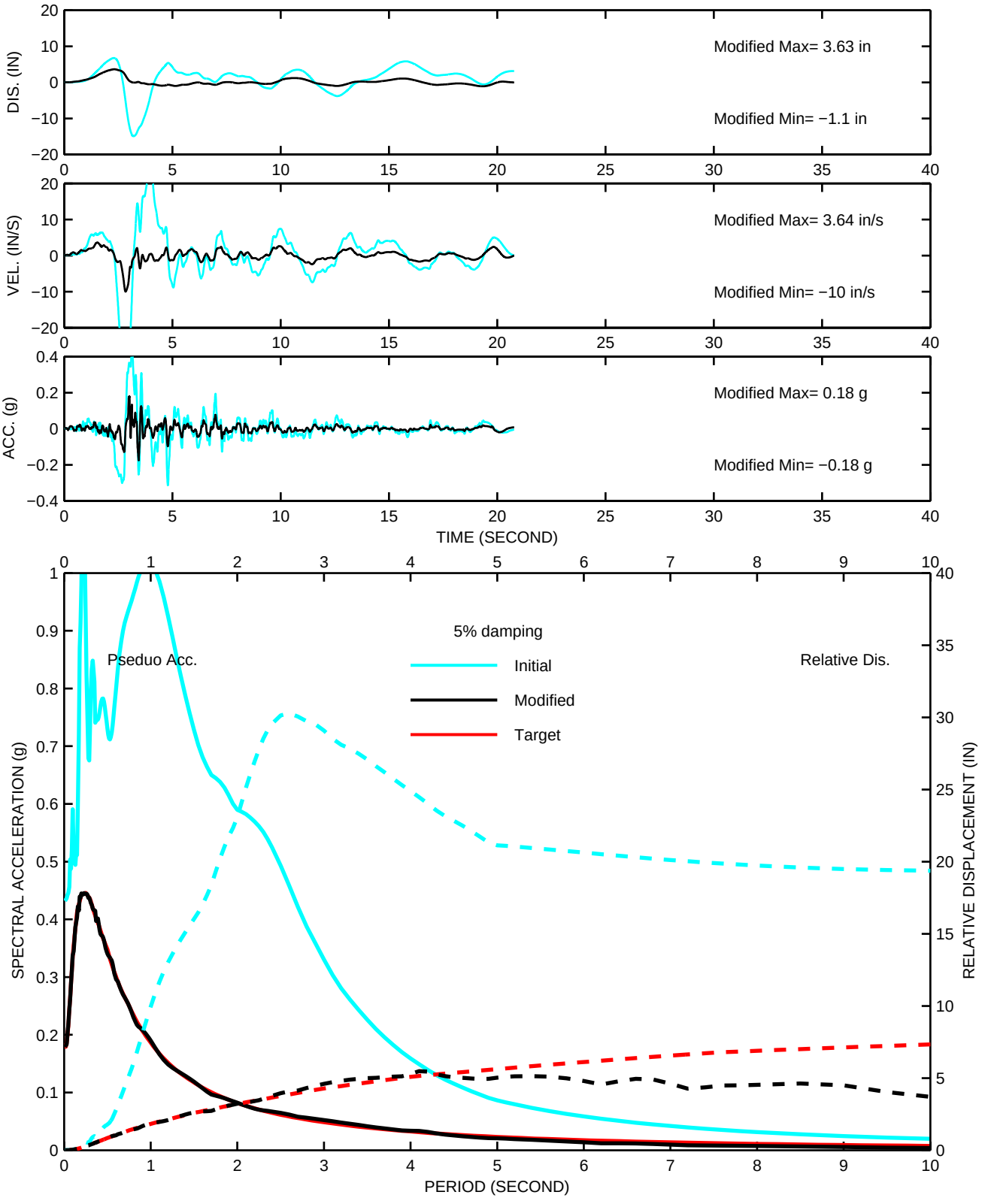


Figure B16. Firm−Ground OLE Spectrum Compatible Ground Motion (5% Damped) − Set 6 Fault Normal

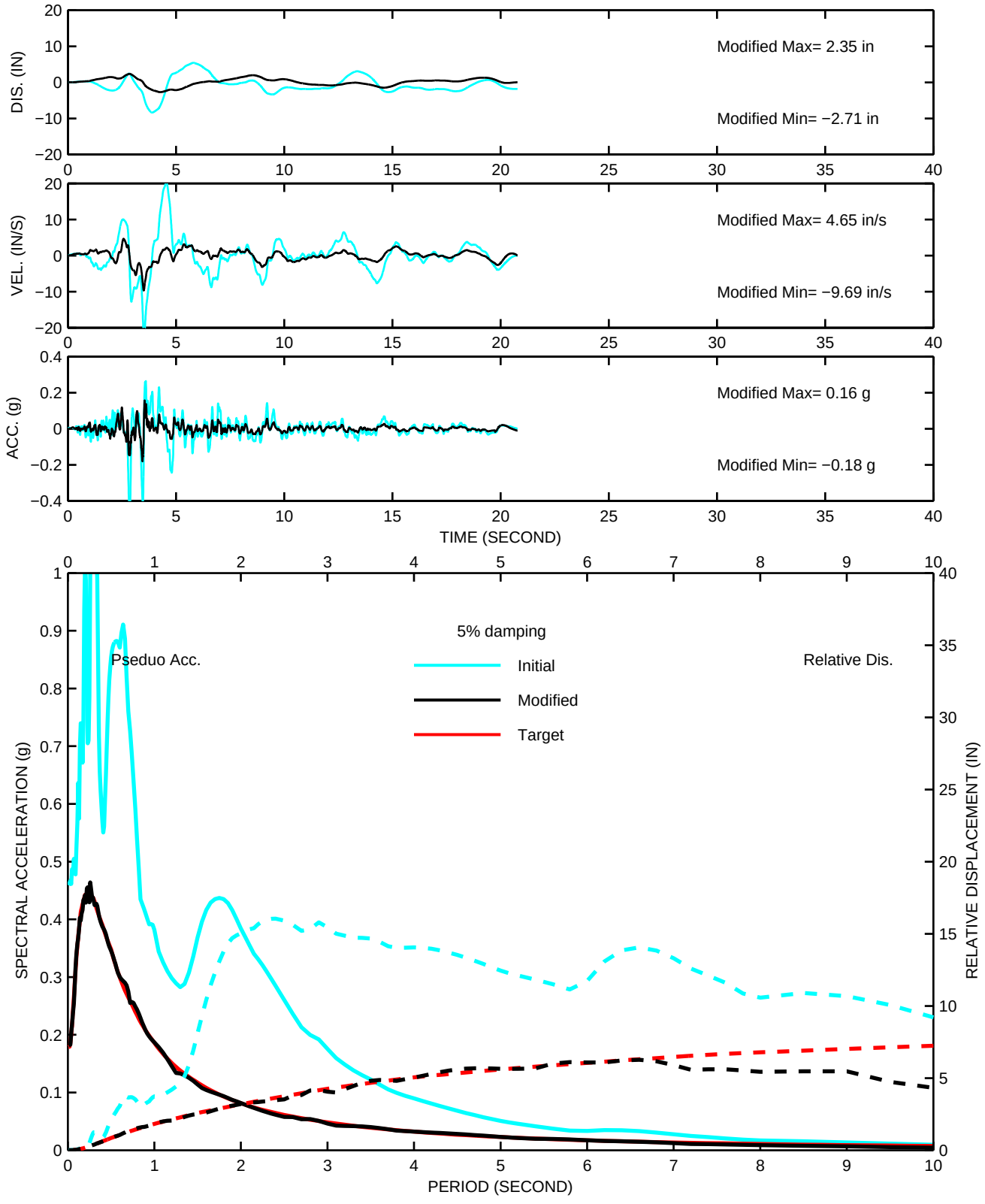


Figure B17. Firm−Ground OLE Spectrum Compatible Ground Motion (5% Damped) − Set 6 Fault Parallel

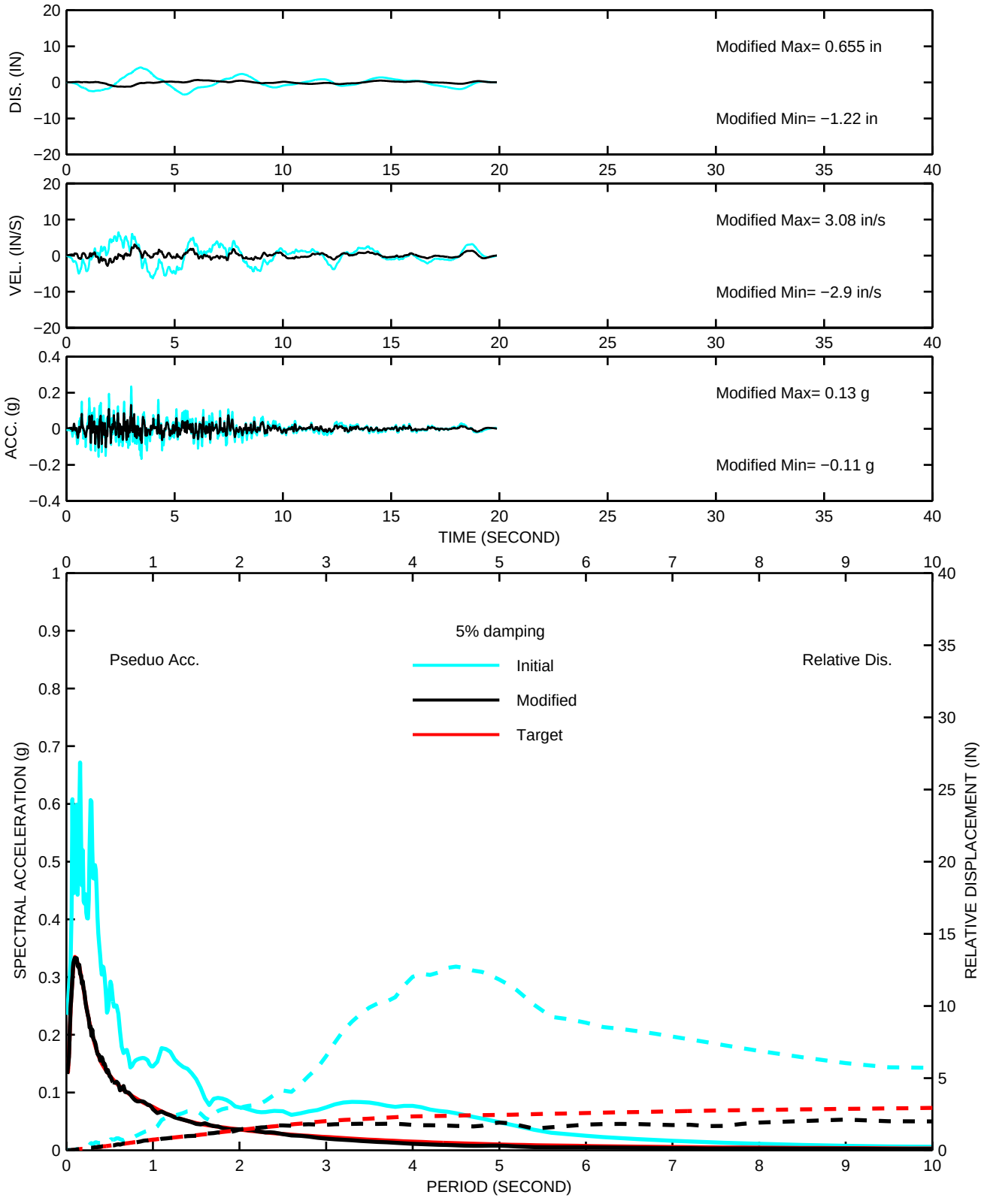


Figure B18. Firm−Ground OLE Spectrum Compatible Ground Motion (5% Damped) − Set 6 Vertical

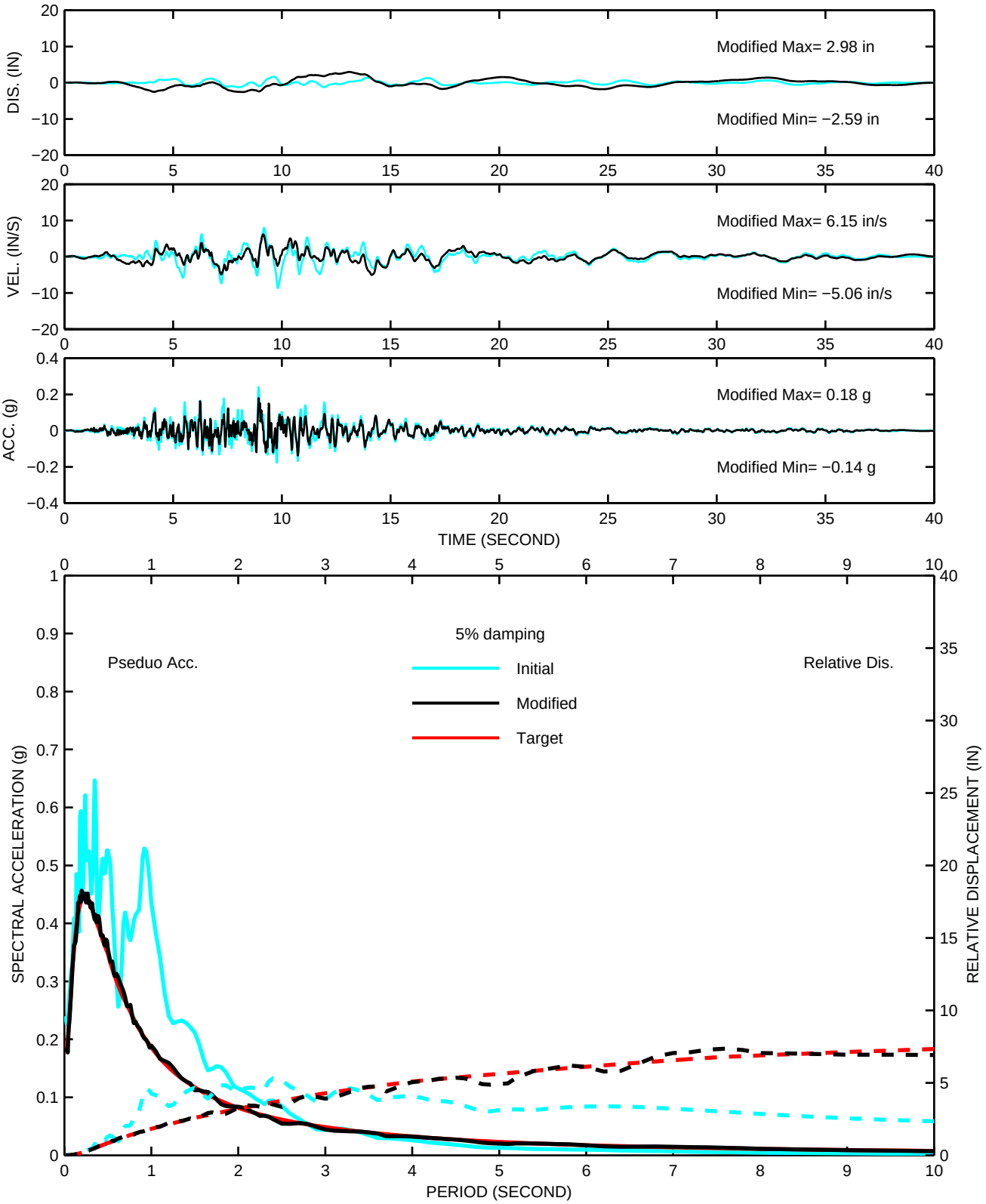


Figure B19. Firm−Ground OLE Spectrum Compatible Ground Motion (5% Damped) − Set 7 Fault Normal

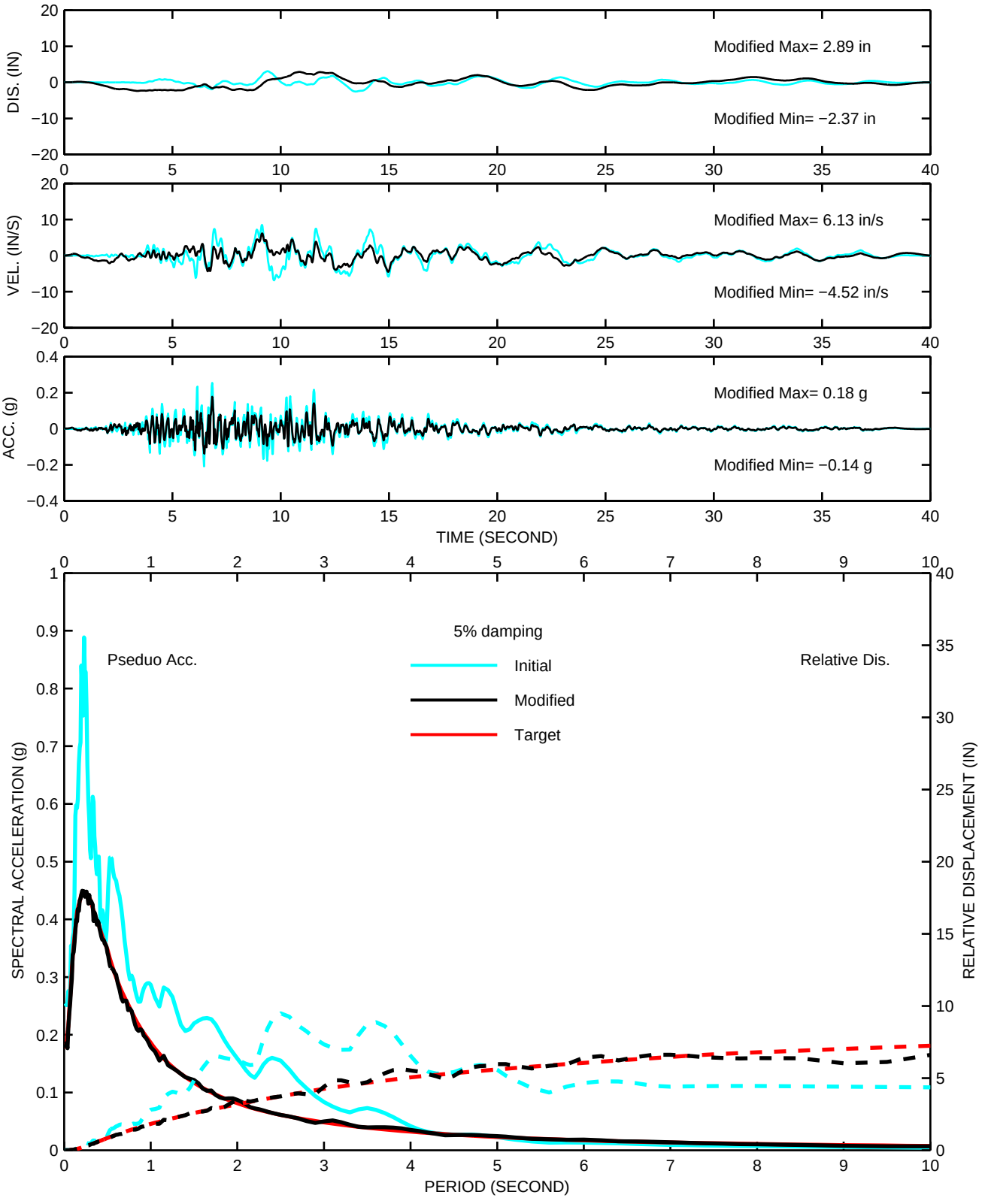


Figure B20. Firm−Ground OLE Spectrum Compatible Ground Motion (5% Damped) − Set 7 Fault Parallel

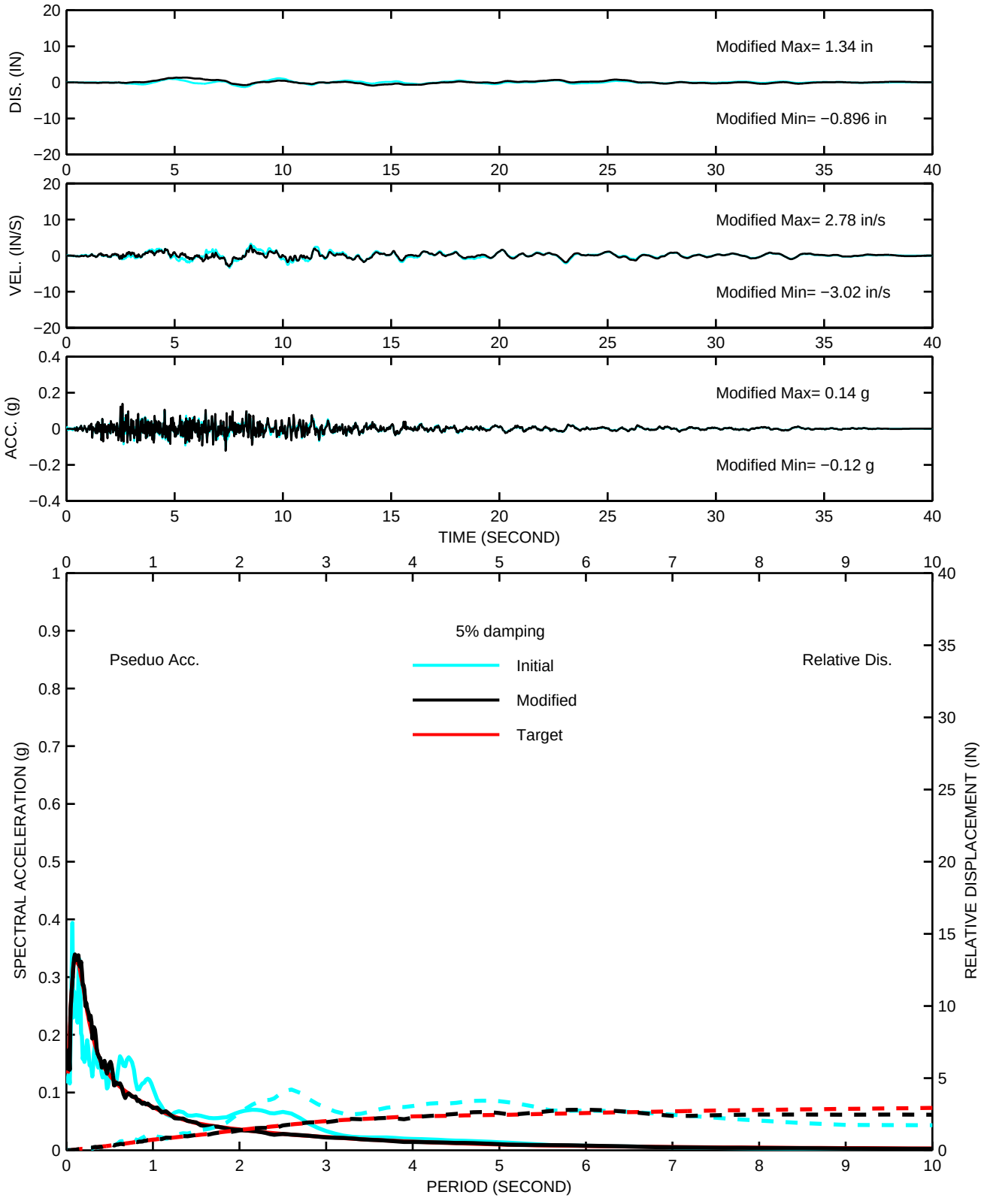


Figure B21. Firm−Ground OLE Spectrum Compatible Ground Motion (5% Damped) − Set 7 Vertical

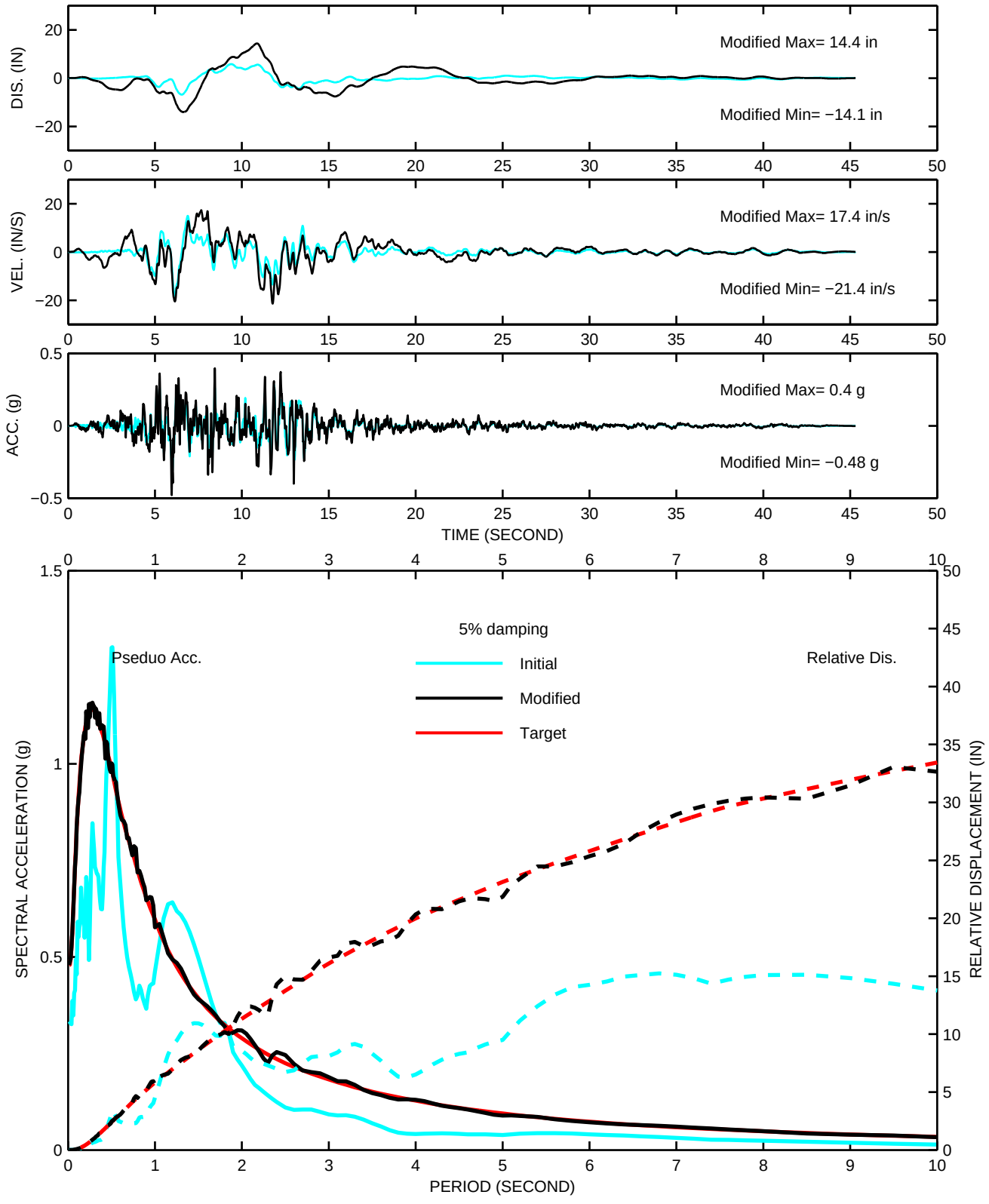


Figure B22. Firm−Ground CLE Spectrum Compatible Ground Motion (5% Damped) − Set 1 Fault Normal

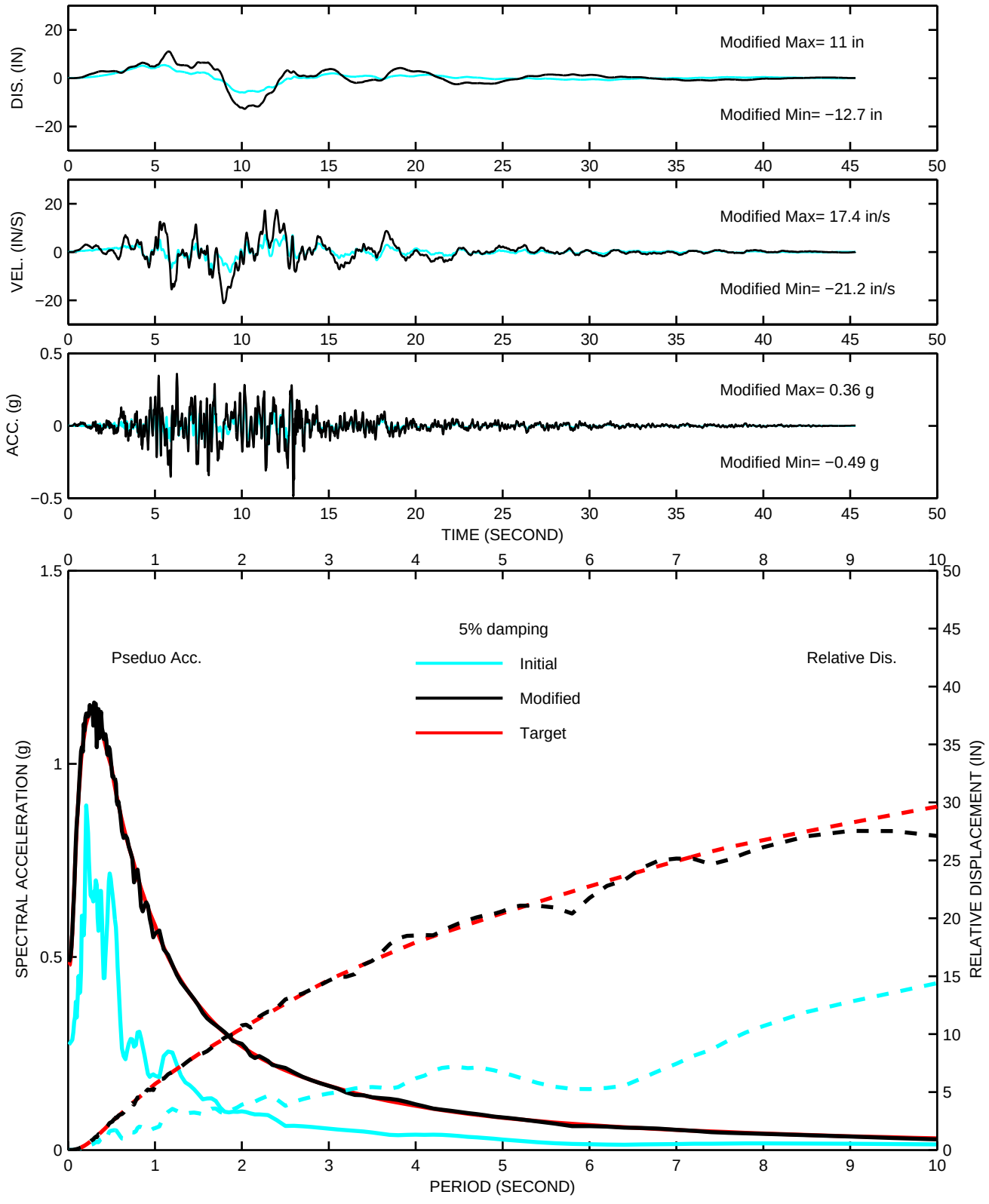


Figure B23. Firm−Ground CLE Spectrum Compatible Ground Motion (5% Damped) − Set 1 Fault Parallel

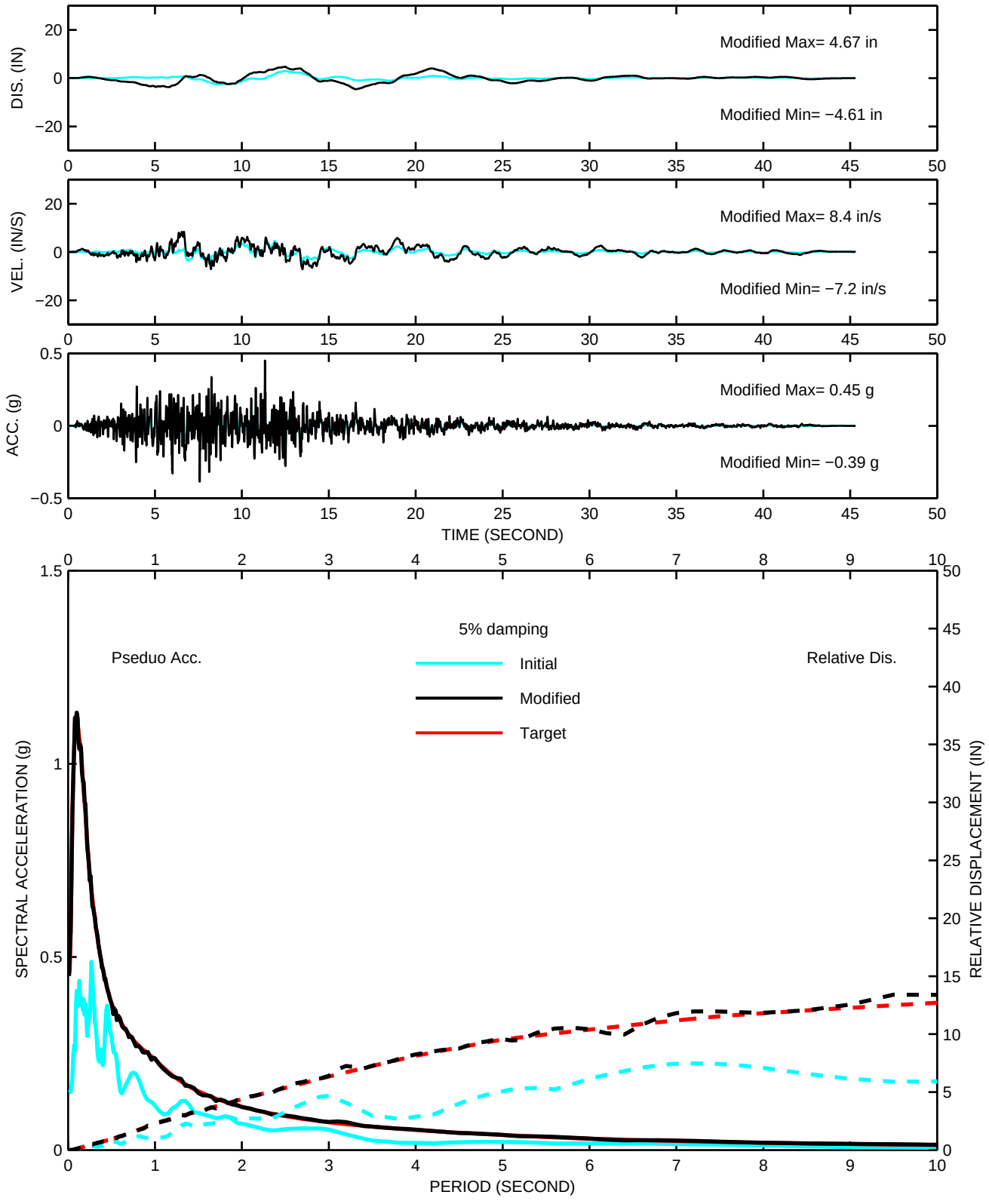


Figure B24. Firm−Ground CLE Spectrum Compatible Ground Motion (5% Damped) − Set 1 Vertical

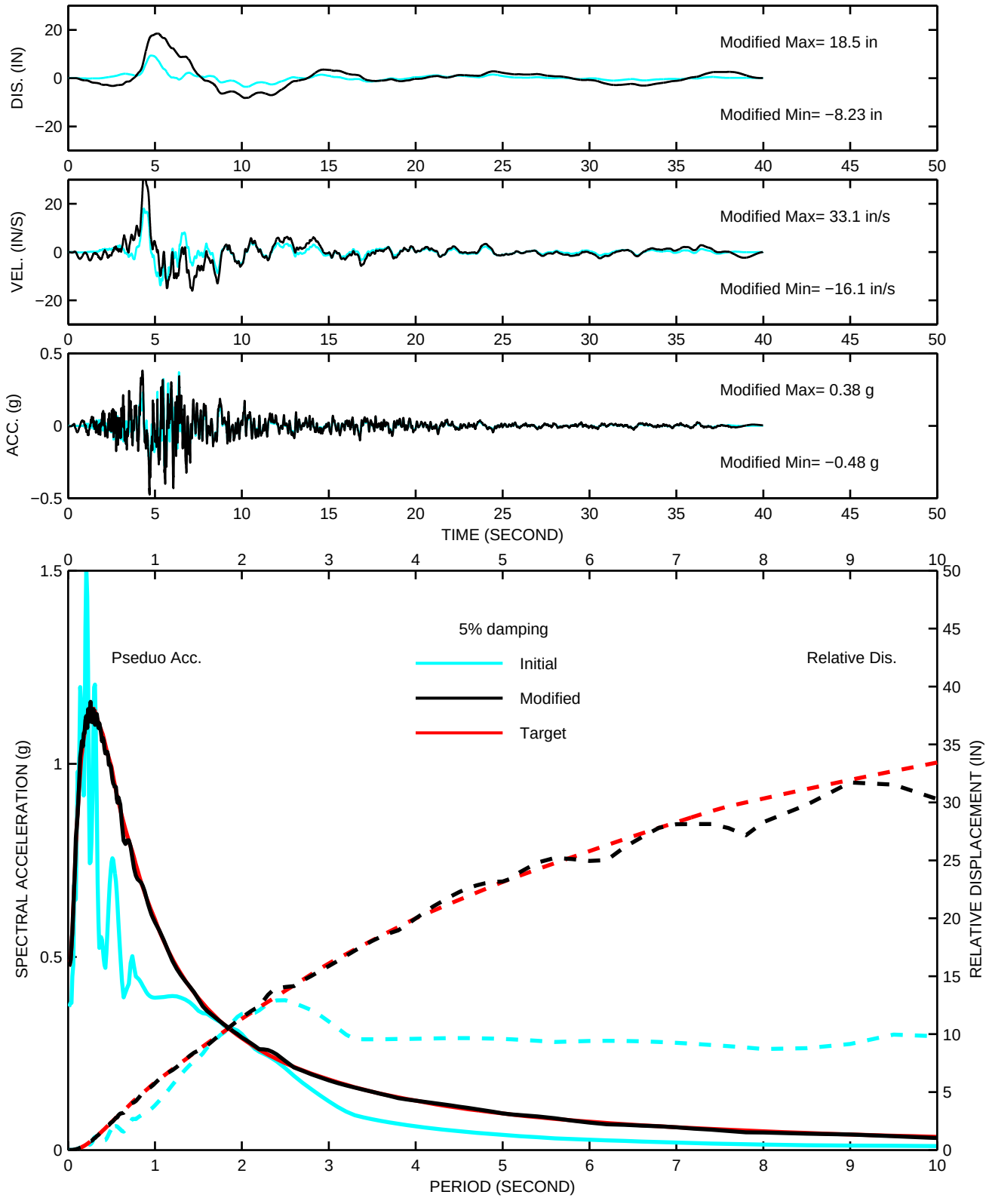


Figure B25. Firm−Ground CLE Spectrum Compatible Ground Motion (5% Damped) − Set 2 Fault Normal

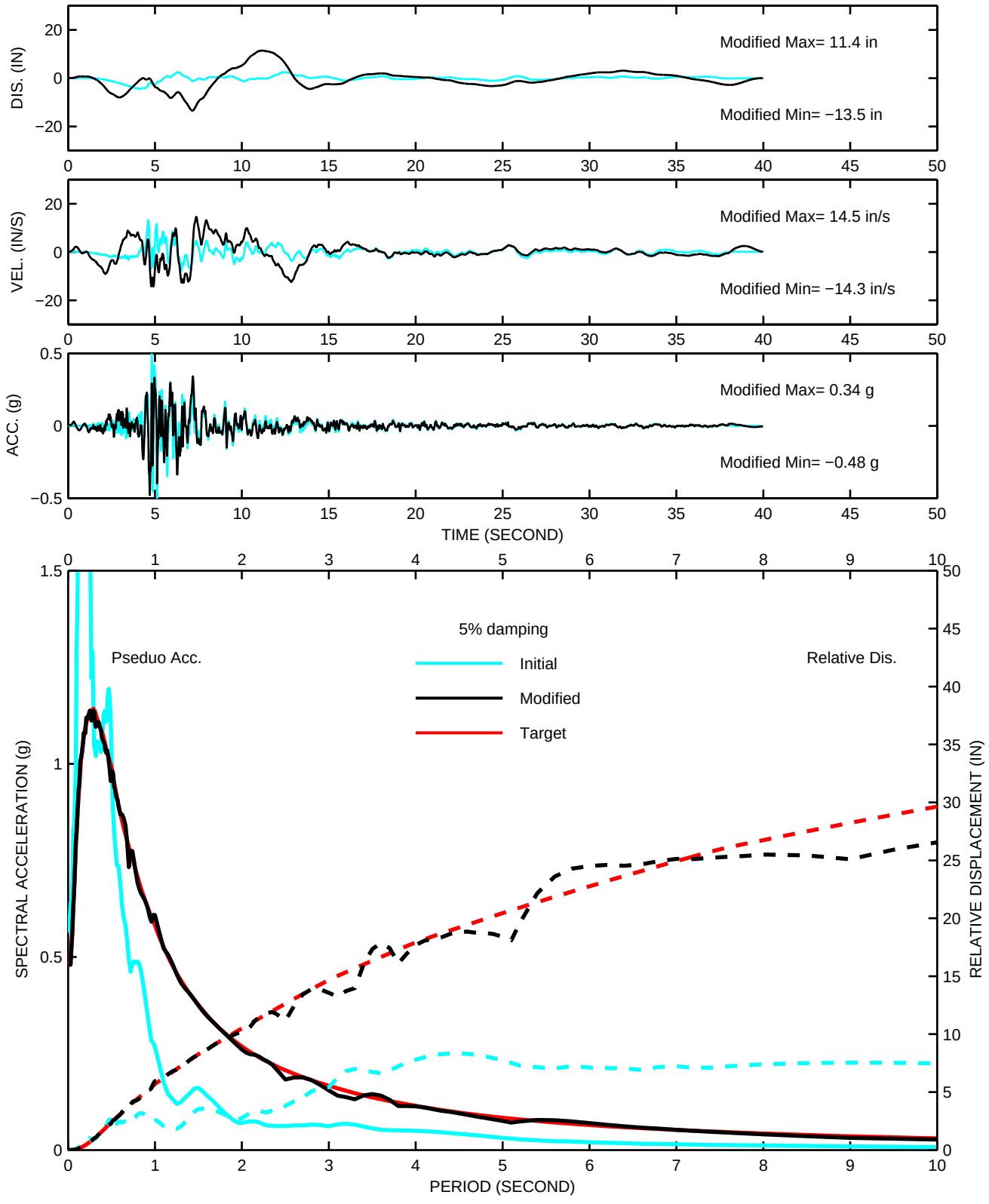


Figure B26. Firm−Ground CLE Spectrum Compatible Ground Motion (5% Damped) − Set 2 Fault Parallel

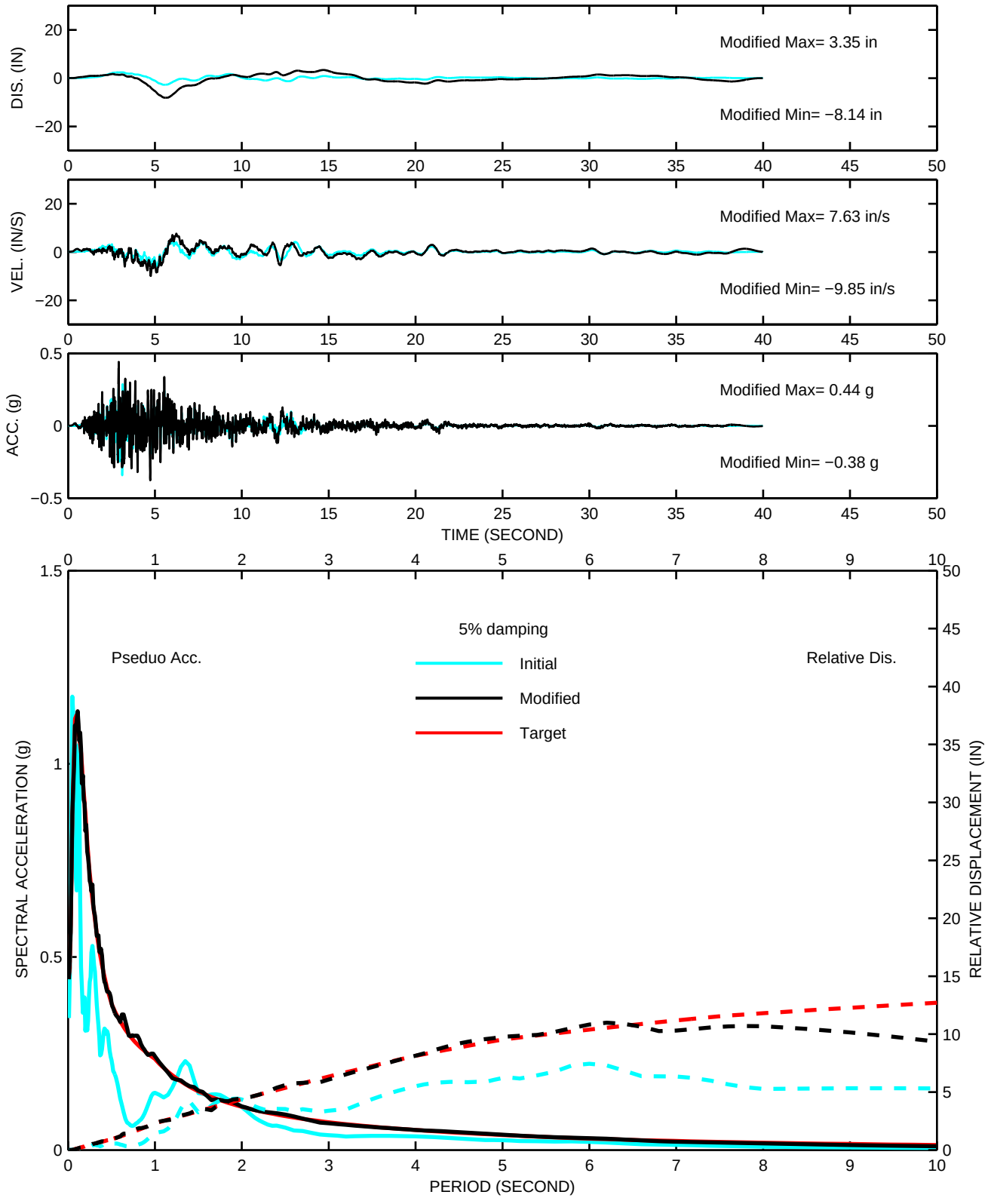


Figure B27. Firm−Ground CLE Spectrum Compatible Ground Motion (5% Damped) − Set 2 Vertical

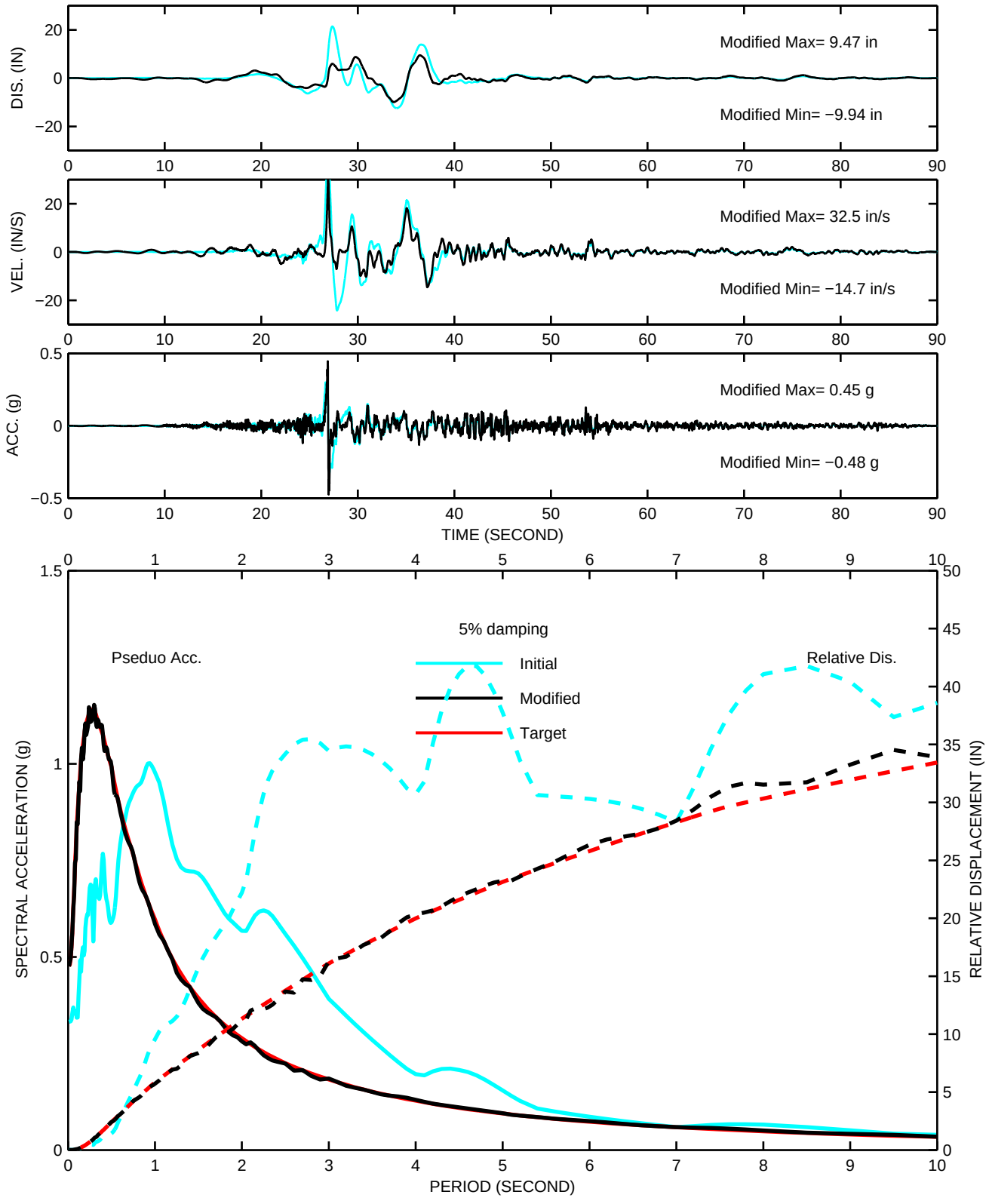


Figure B28. Firm−Ground CLE Spectrum Compatible Ground Motion (5% Damped) − Set 3 Fault Normal

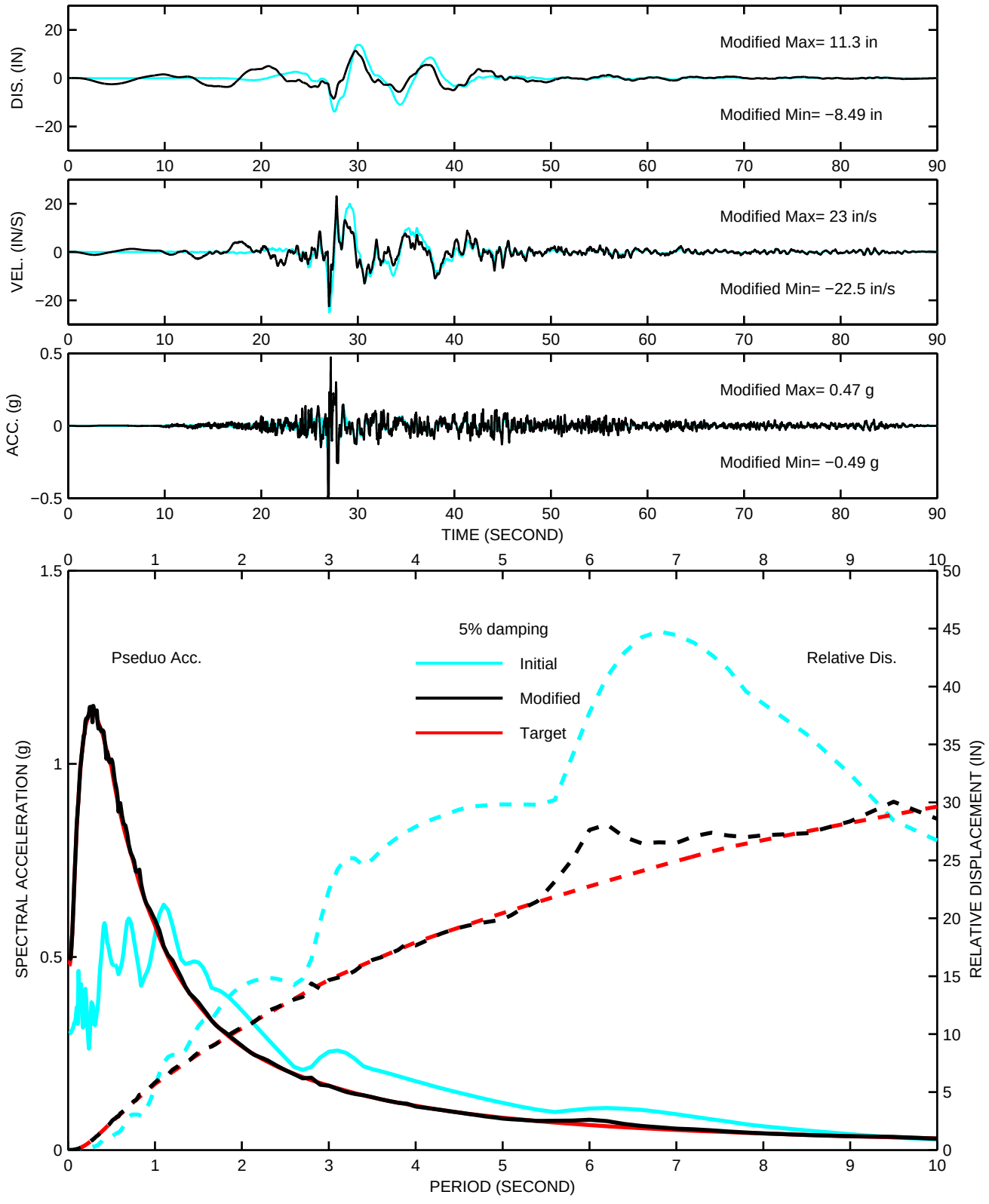


Figure B29. Firm−Ground CLE Spectrum Compatible Ground Motion (5% Damped) − Set 3 Fault Parallel

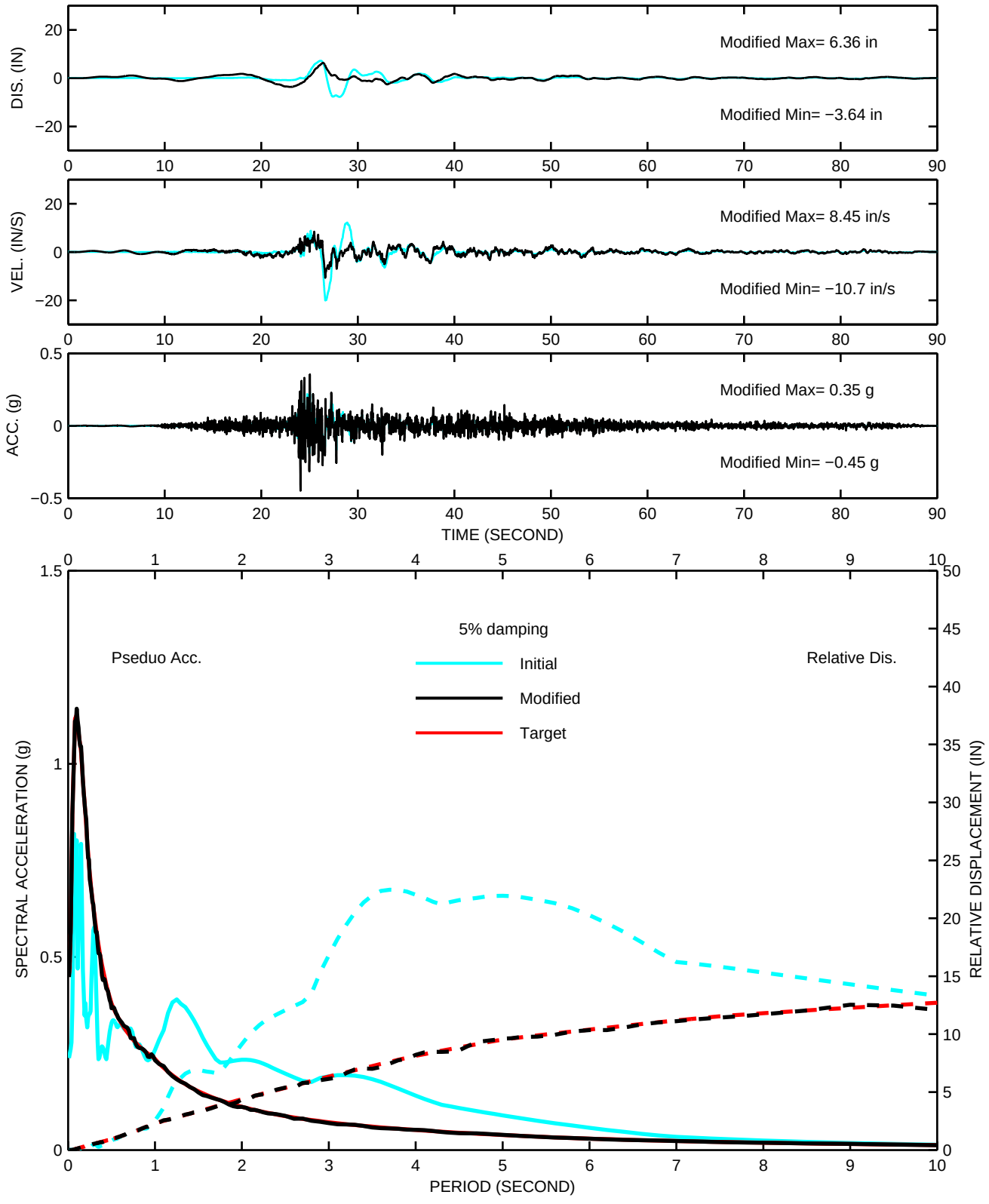


Figure B30. Firm−Ground CLE Spectrum Compatible Ground Motion (5% Damped) − Set 3 Vertical

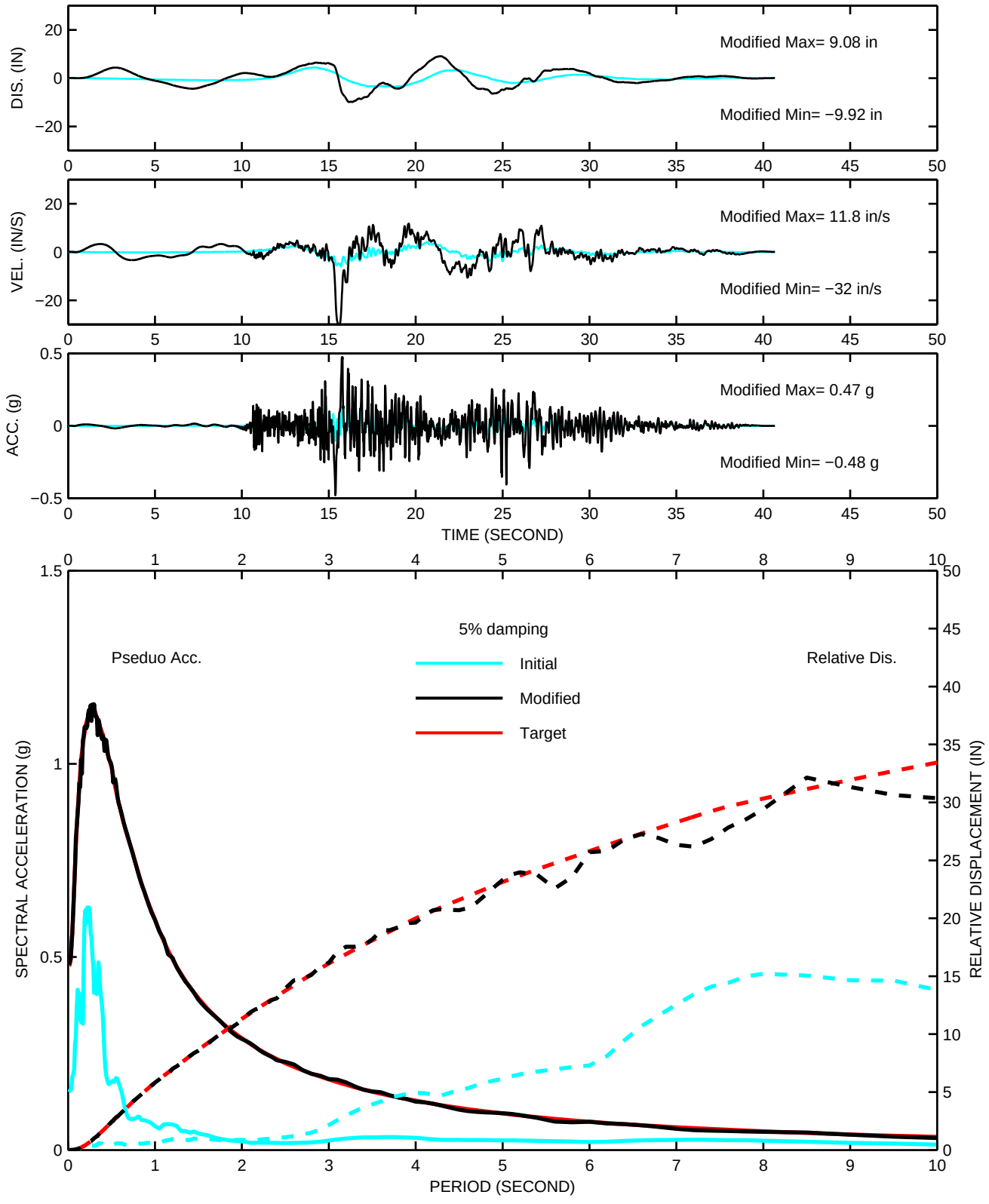


Figure B31. Firm−Ground CLE Spectrum Compatible Ground Motion (5% Damped) − Set 4 Fault Normal

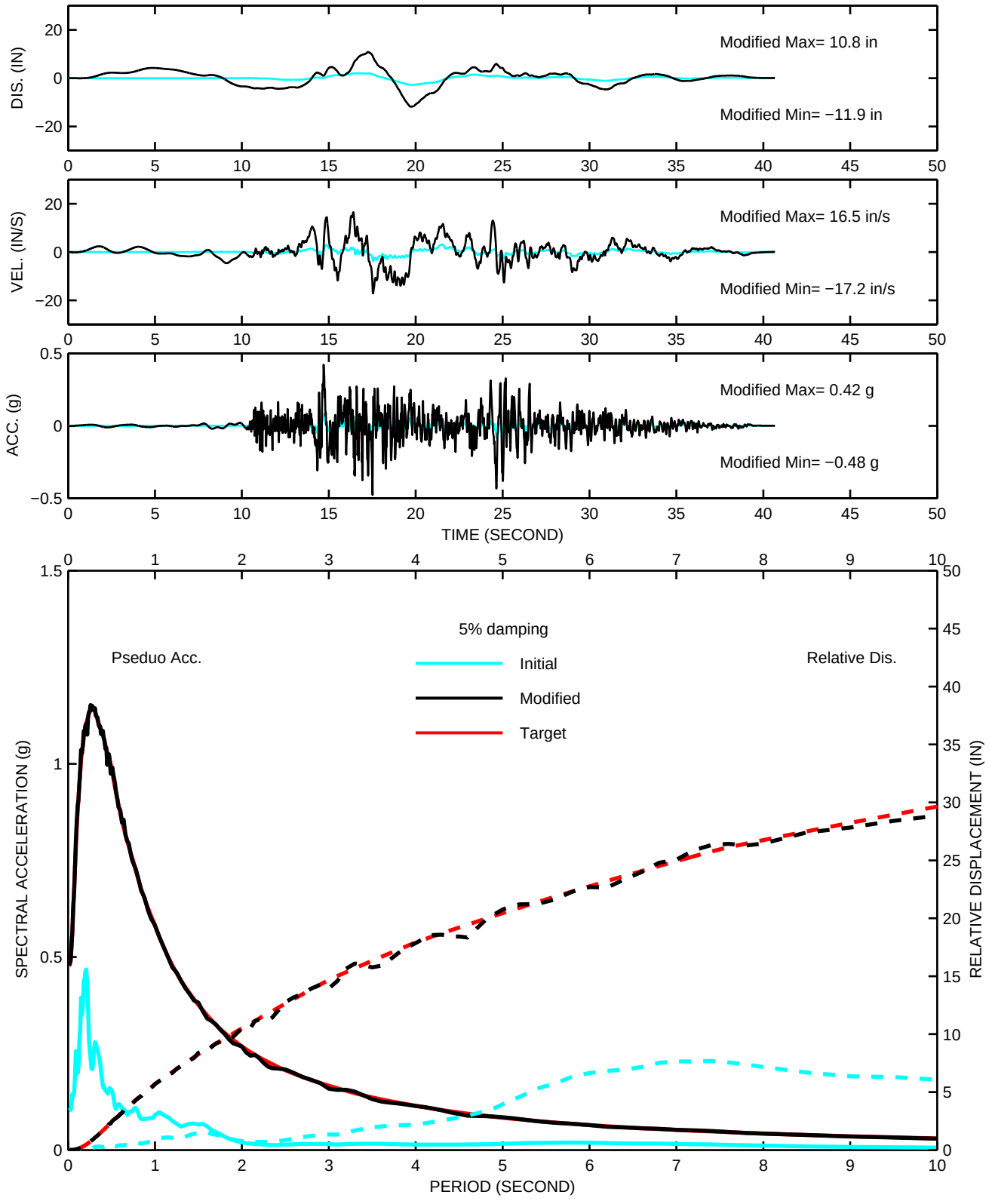


Figure B32. Firm−Ground CLE Spectrum Compatible Ground Motion (5% Damped) − Set 4 Fault Parallel

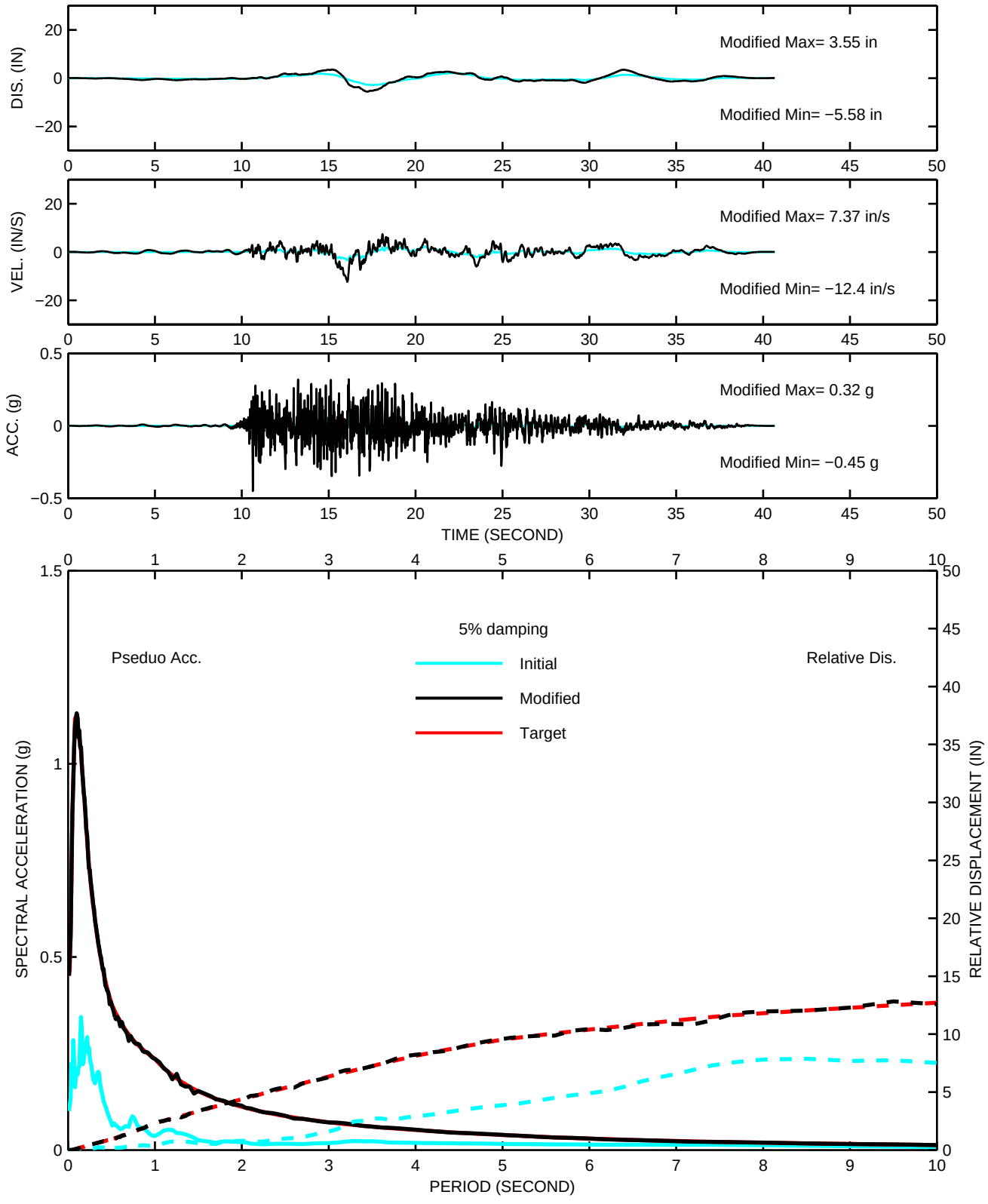


Figure B33. Firm−Ground CLE Spectrum Compatible Ground Motion (5% Damped) − Set 4 Vertical

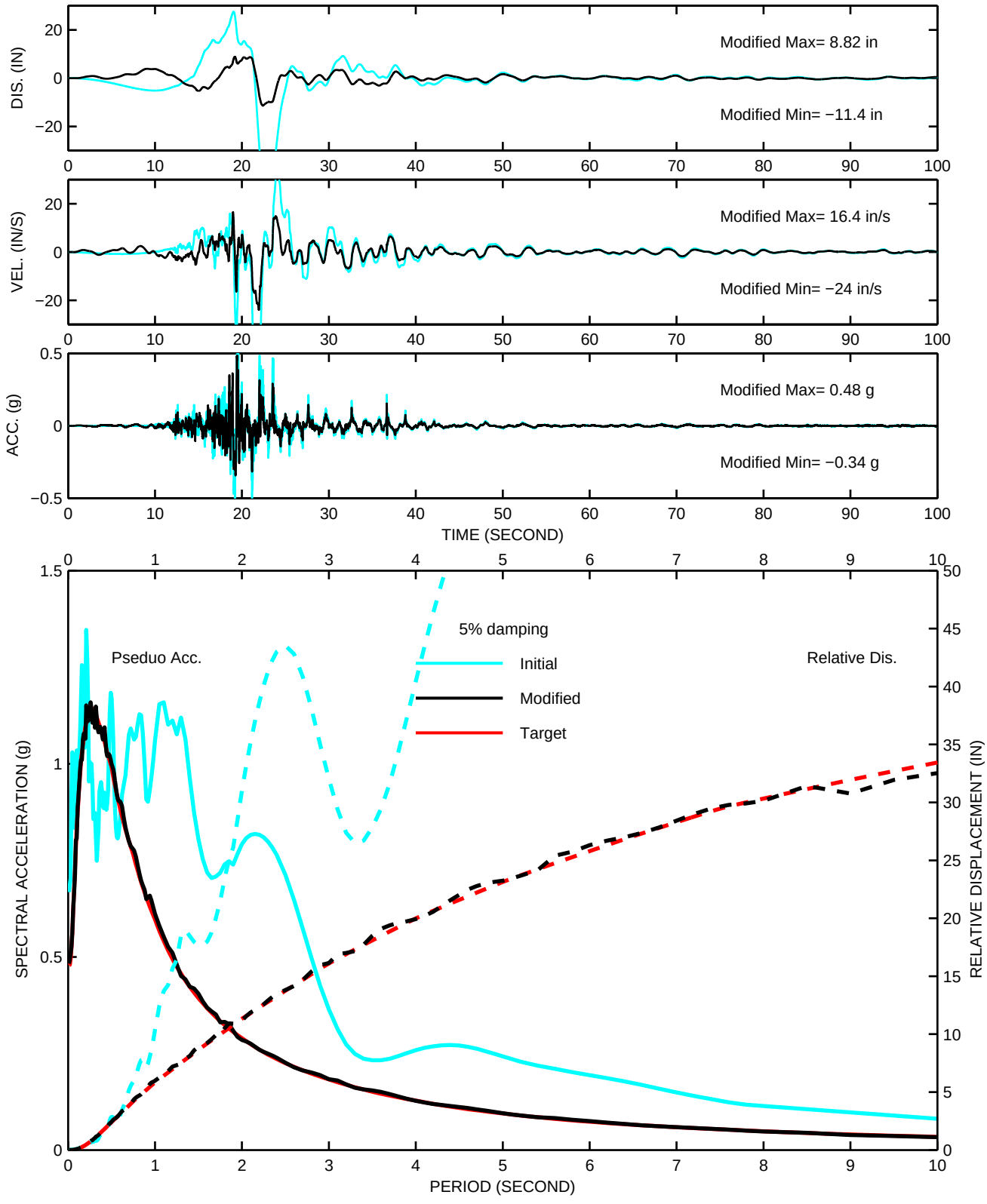


Figure B34. Firm−Ground CLE Spectrum Compatible Ground Motion (5% Damped) − Set 5 Fault Normal

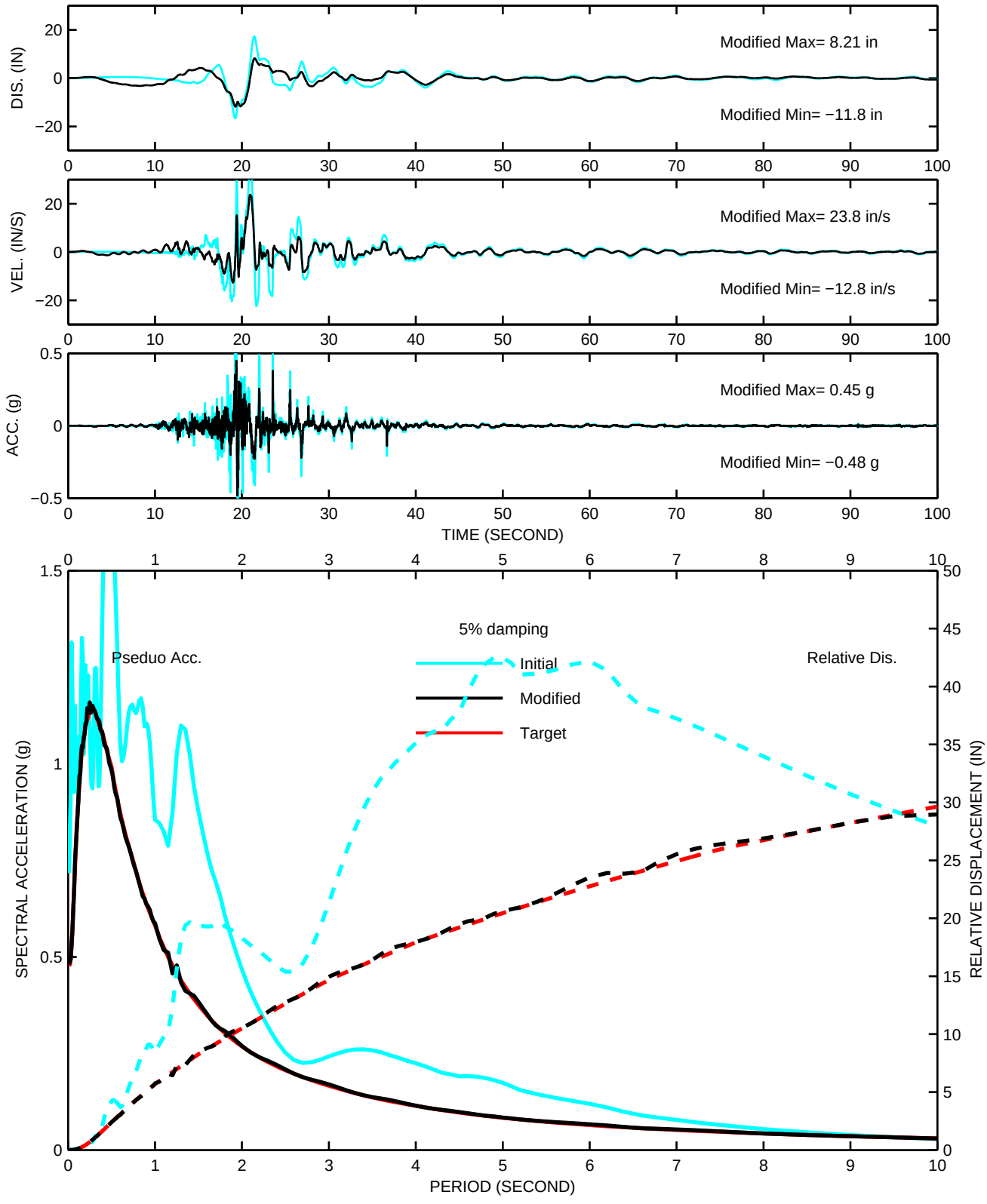


Figure B35. Firm−Ground CLE Spectrum Compatible Ground Motion (5% Damped) − Set 5 Fault Parallel

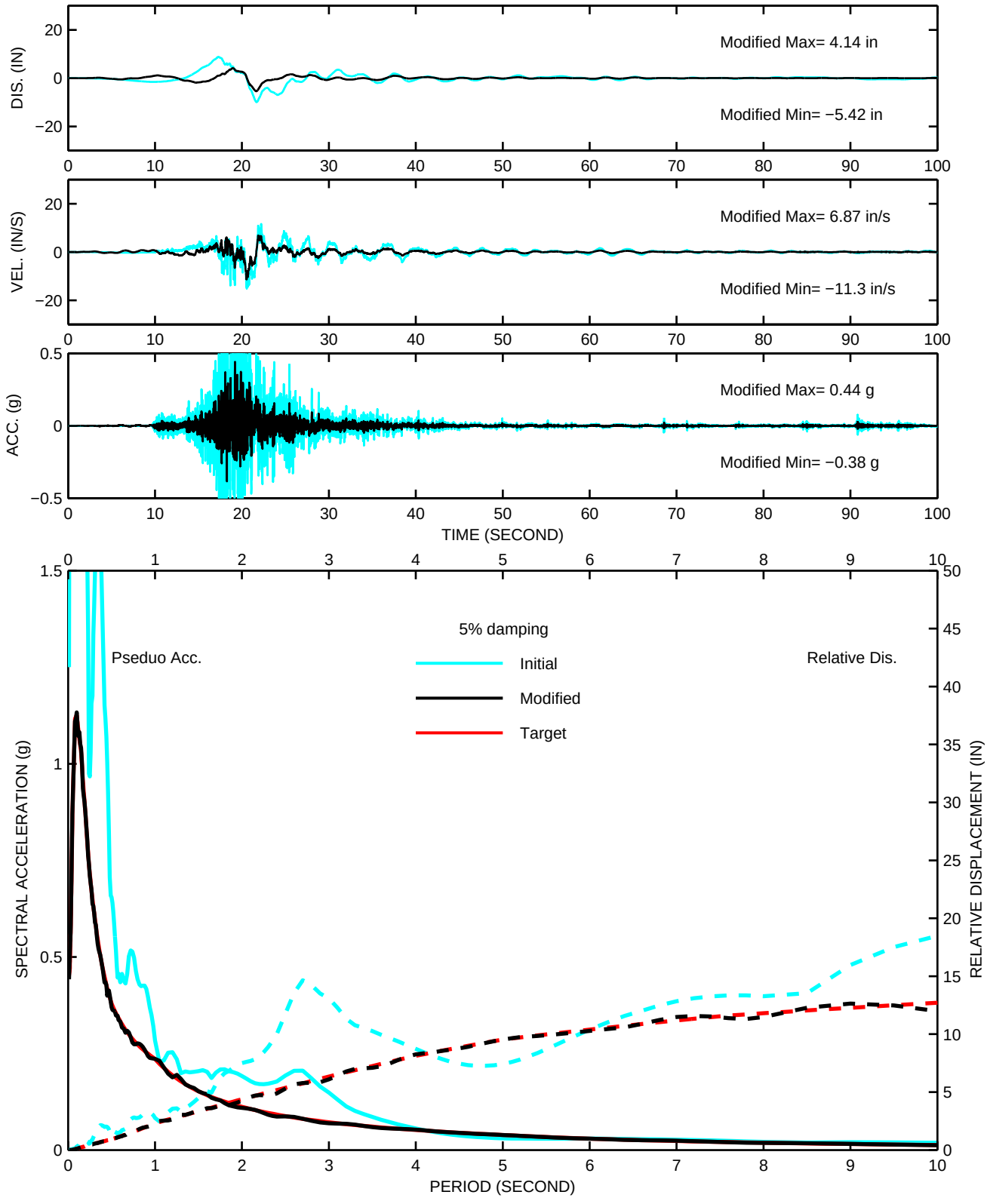


Figure B36. Firm−Ground CLE Spectrum Compatible Ground Motion (5% Damped) − Set 5 Vertical

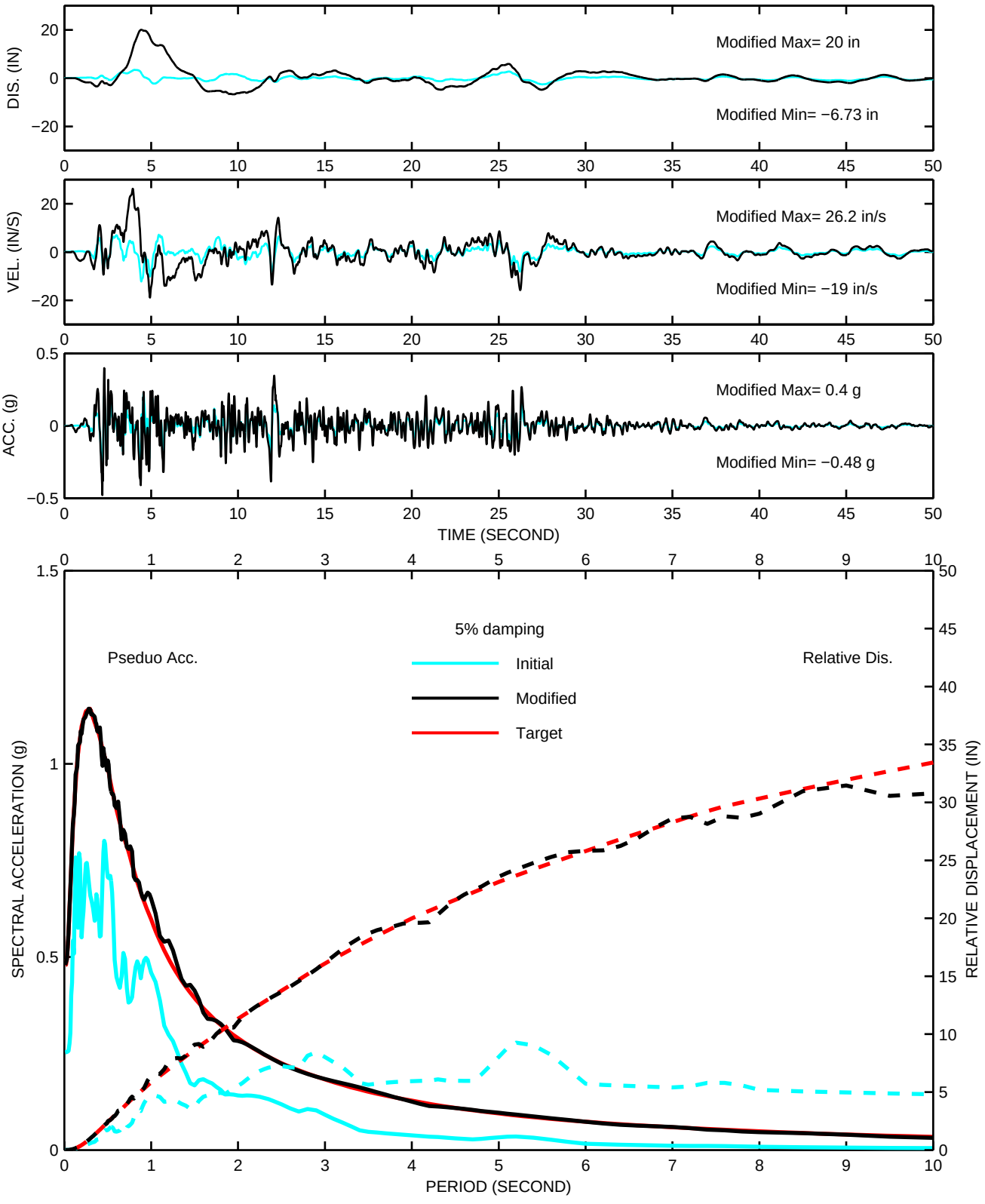


Figure B37. Firm−Ground CLE Spectrum Compatible Ground Motion (5% Damped) − Set 6 Fault Normal

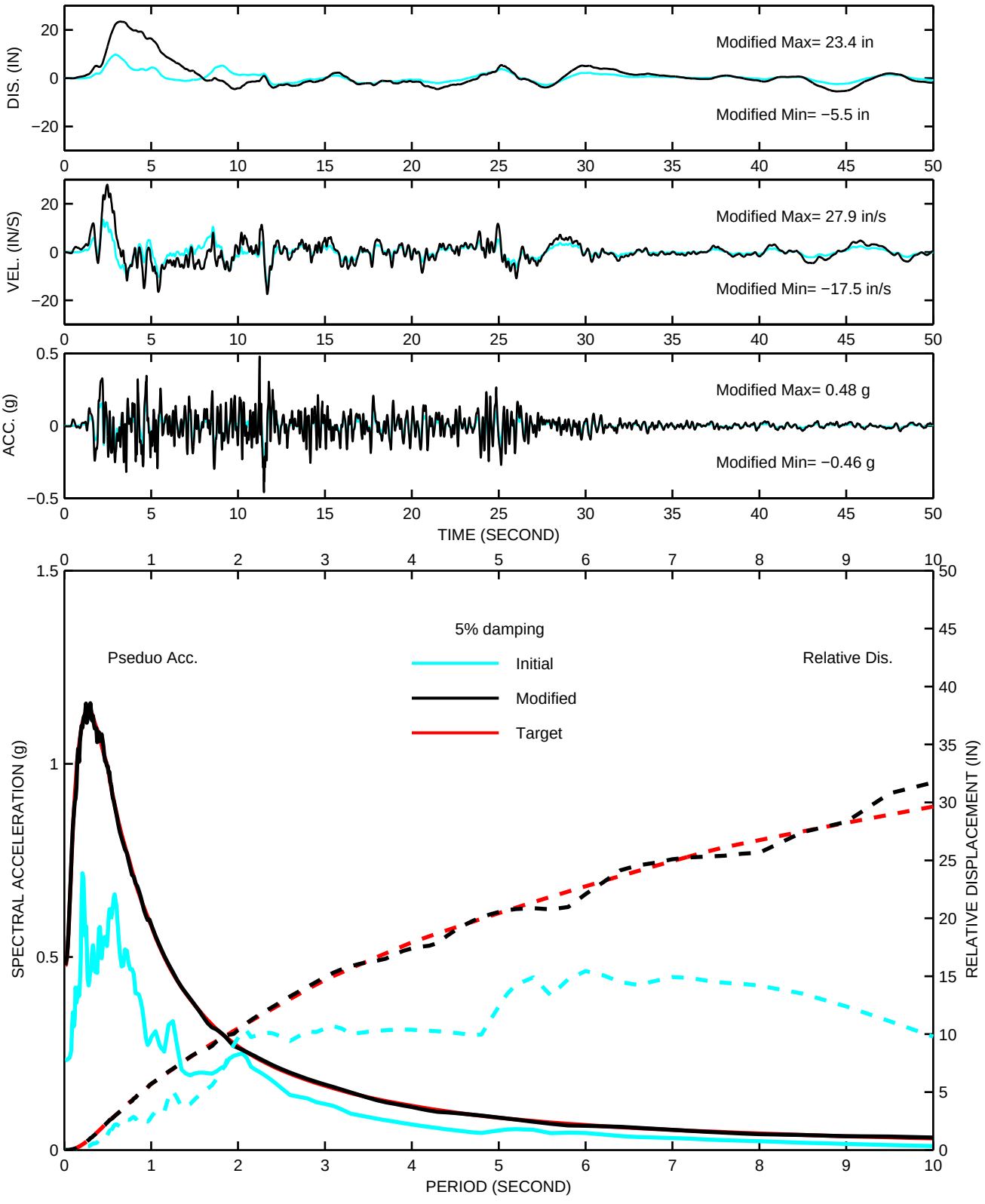


Figure B38. Firm−Ground CLE Spectrum Compatible Ground Motion (5% Damped) − Set 6 Fault Parallel

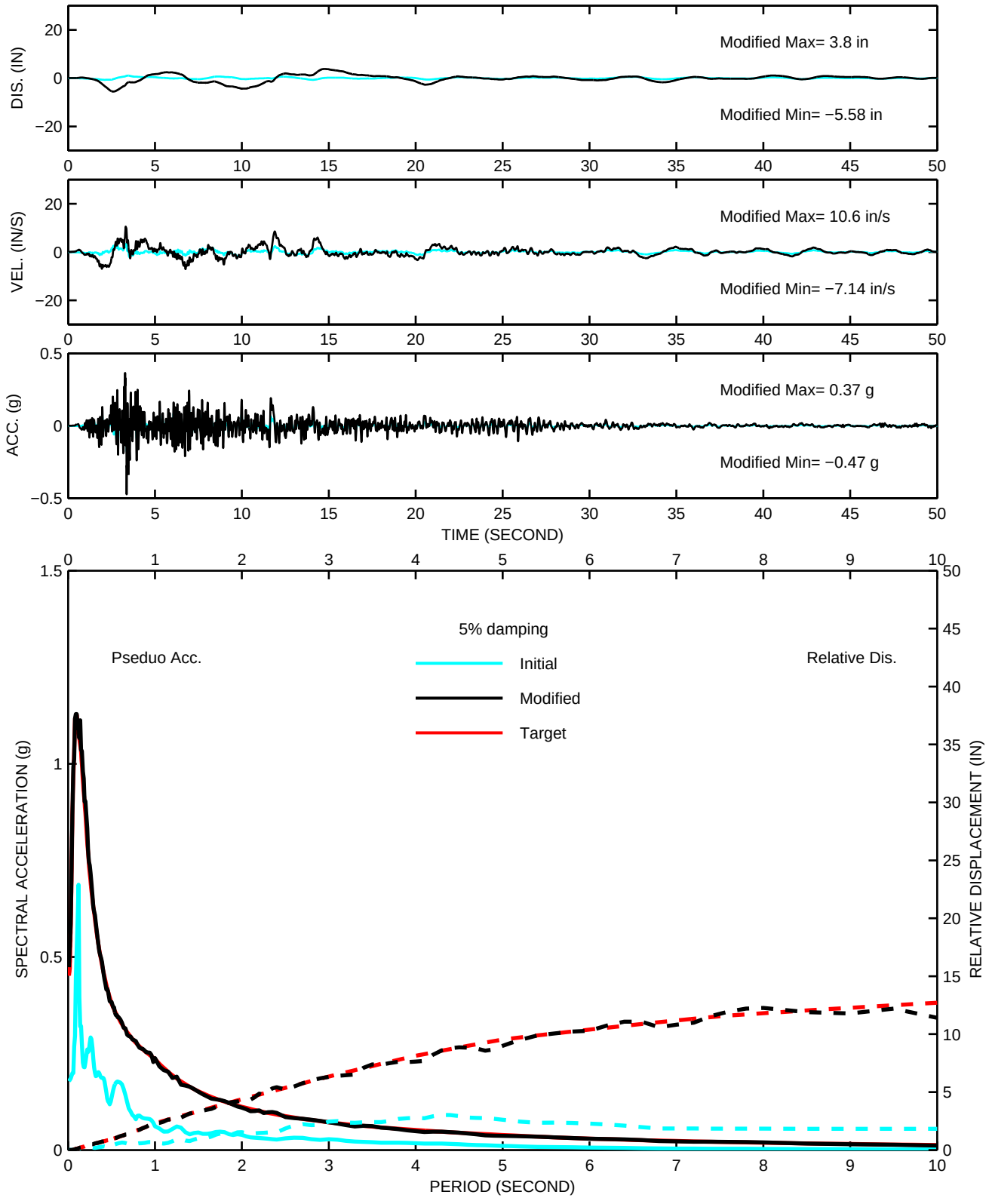


Figure B39. Firm−Ground CLE Spectrum Compatible Ground Motion (5% Damped) − Set 6 Vertical

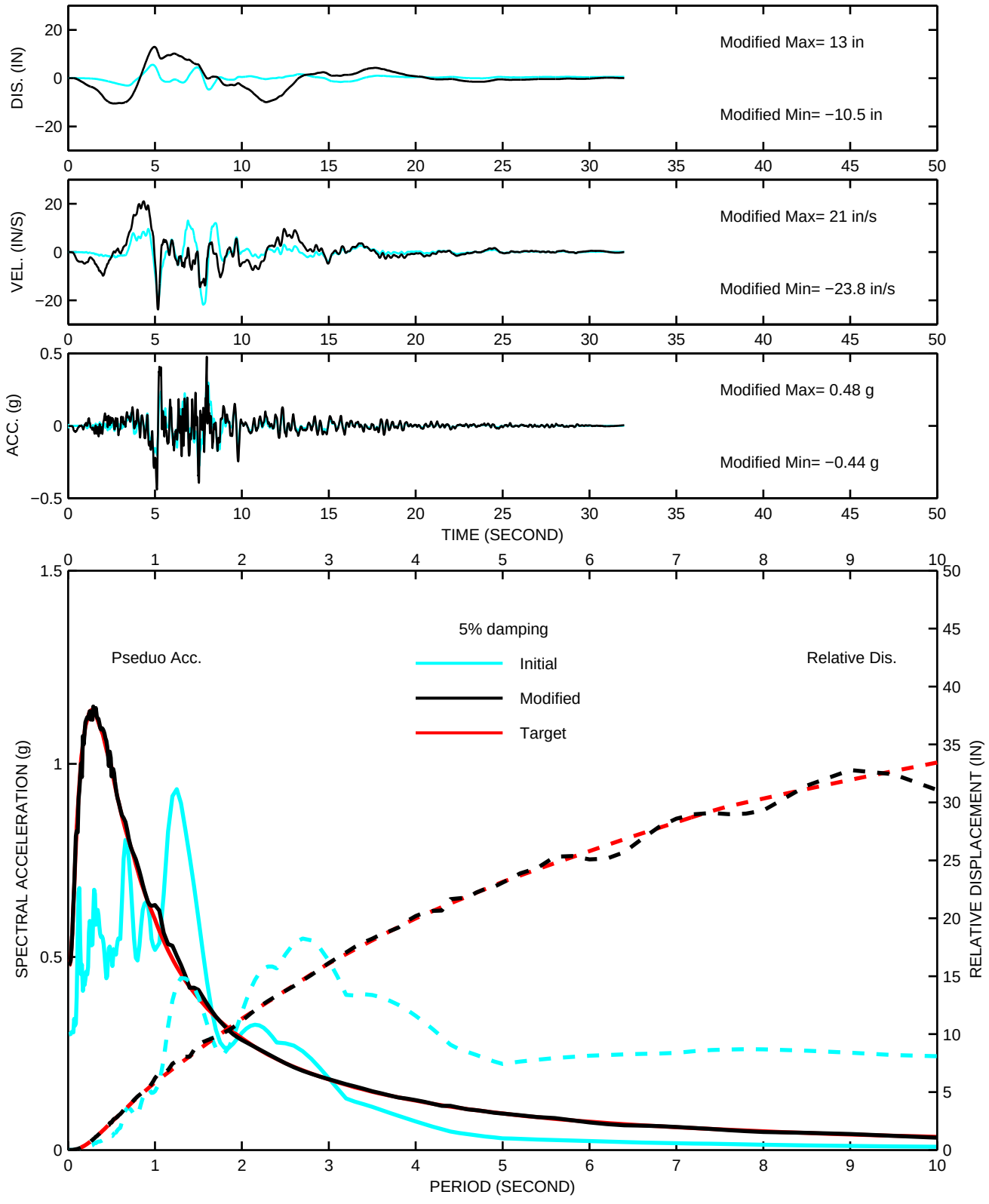


Figure B40. Firm−Ground CLE Spectrum Compatible Ground Motion (5% Damped) − Set 7 Fault Normal

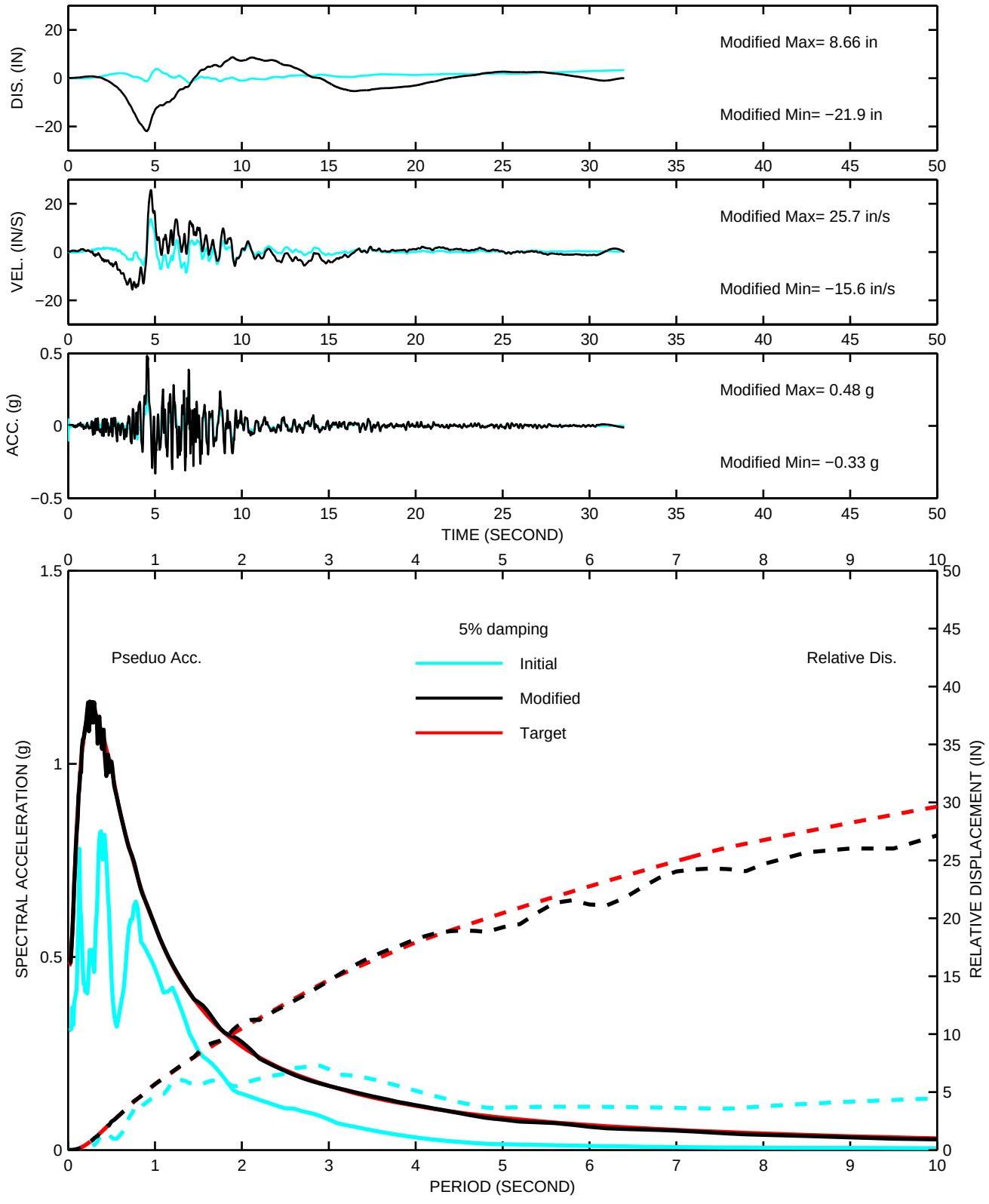


Figure B41. Firm−Ground CLE Spectrum Compatible Ground Motion (5% Damped) − Set 7 Fault Parallel

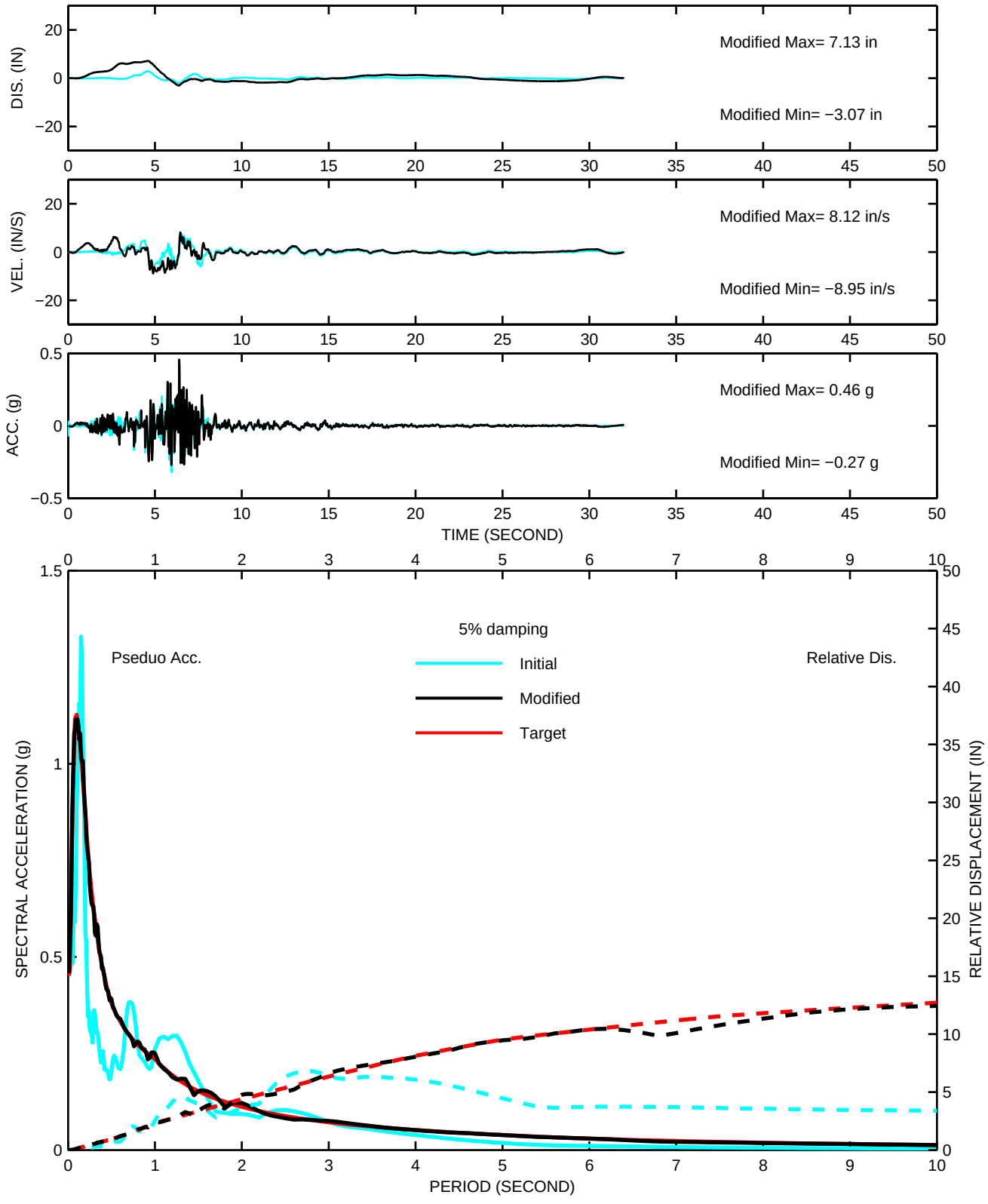


Figure B42. Firm−Ground CLE Spectrum Compatible Ground Motion (5% Damped) − Set 7 Vertical

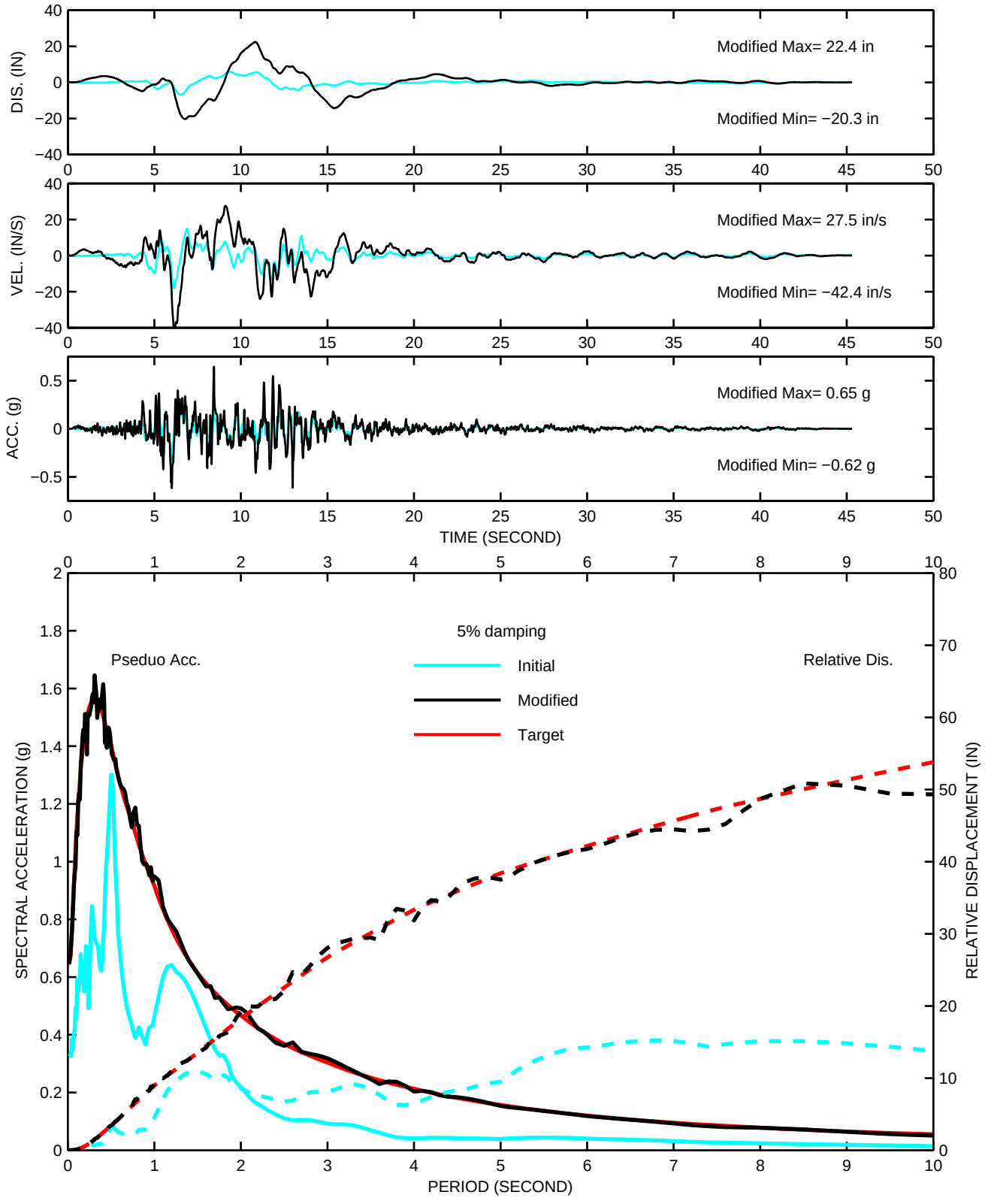


Figure B43. Firm−Ground 975−Yr Spectrum Compatible Ground Motion (5% Damped) − Set 1 Fault Normal

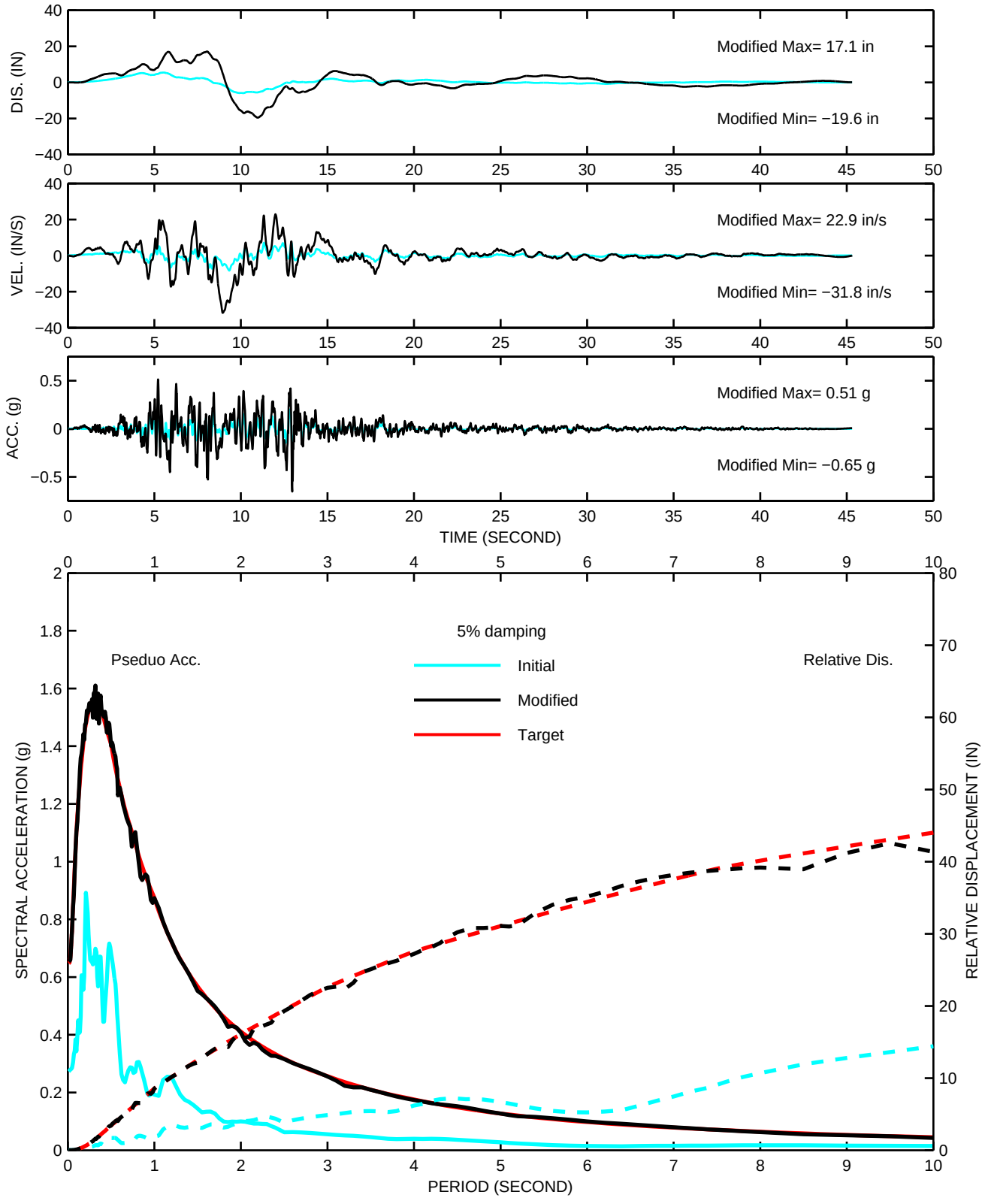


Figure B44. Firm−Ground 975−Yr Spectrum Compatible Ground Motion (5% Damped) − Set 1 Fault Parallel

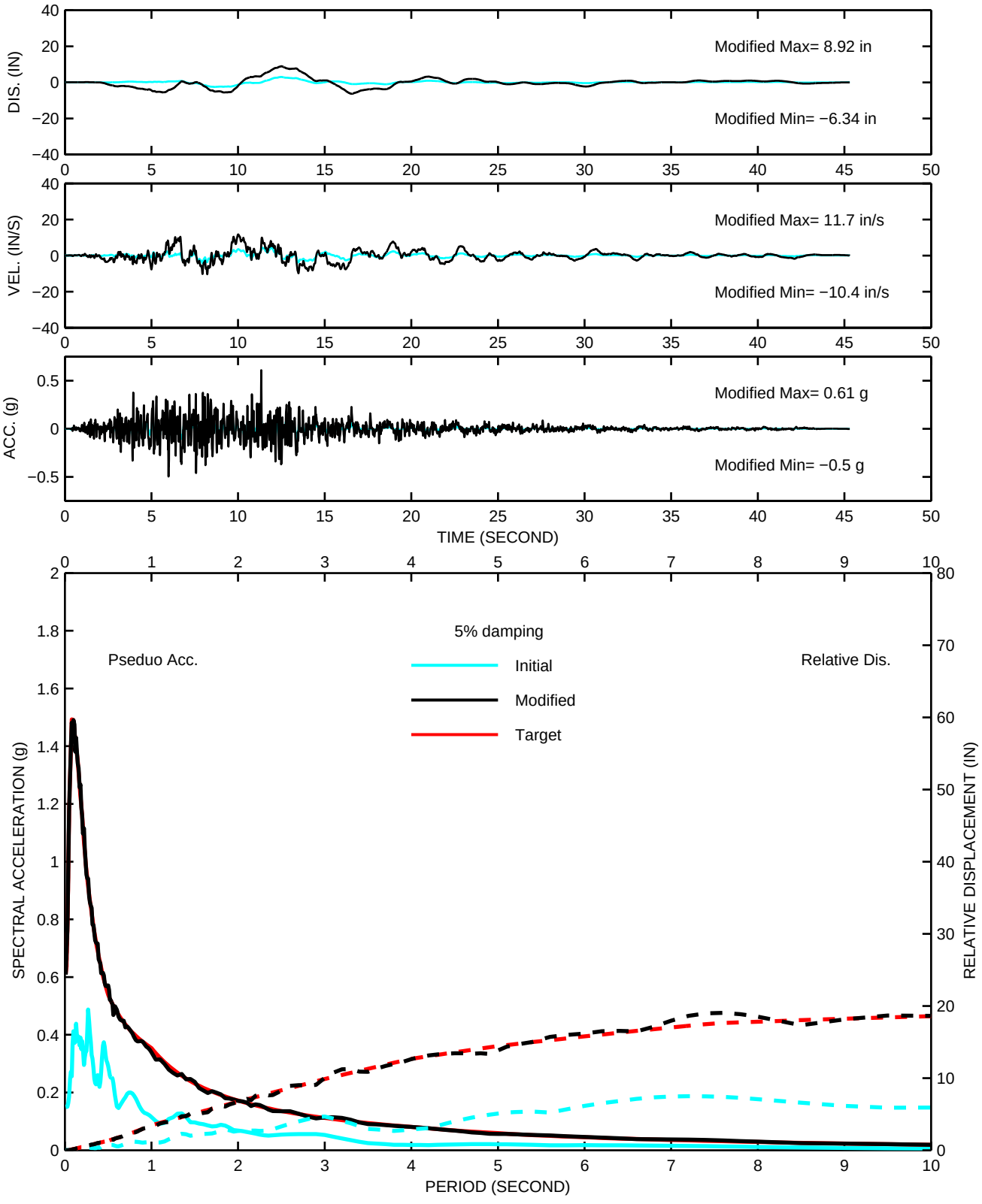


Figure B45. Firm−Ground 975−Yr Spectrum Compatible Ground Motion (5% Damped) − Set 1 Vertical

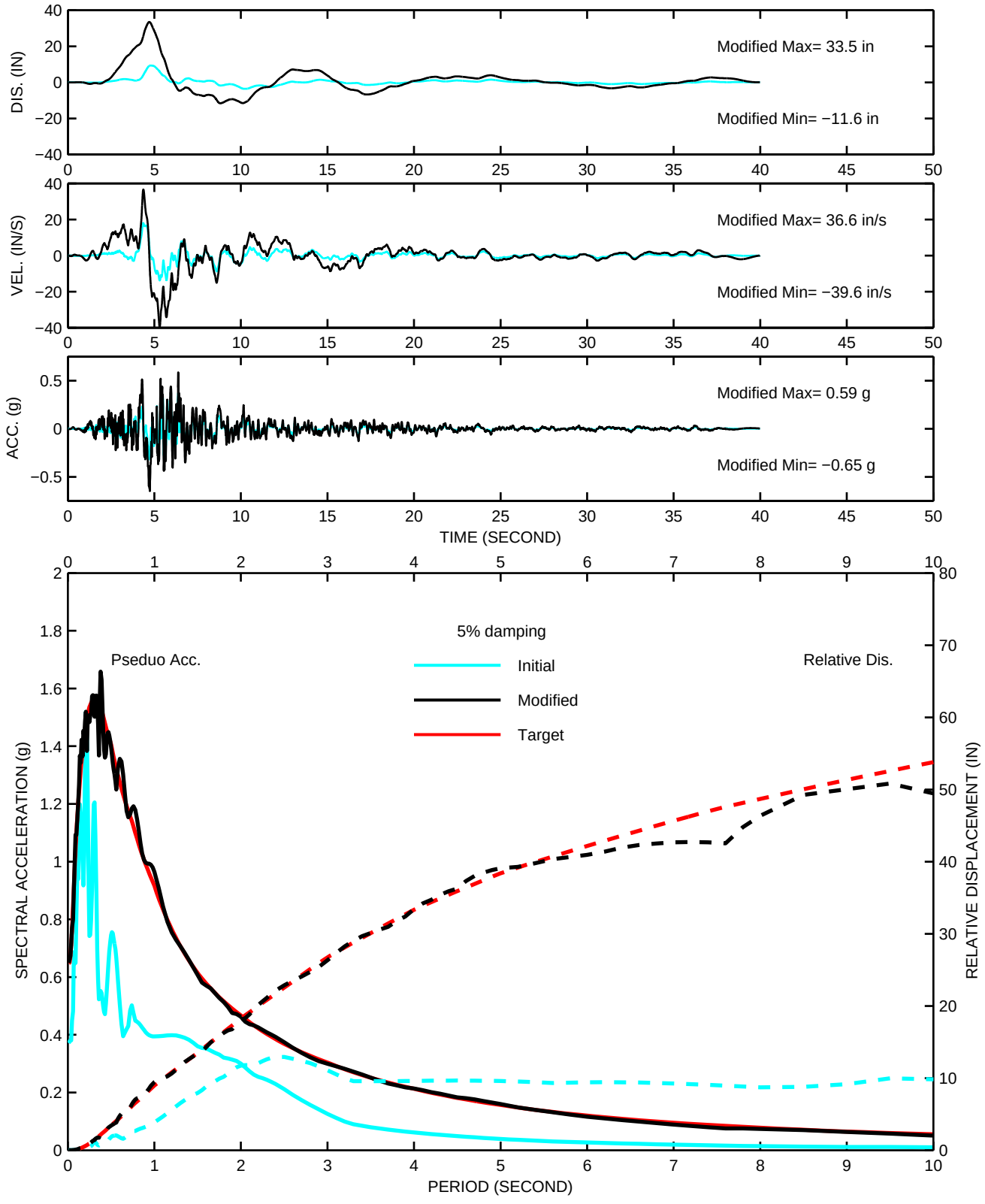


Figure B46. Firm−Ground 975−Yr Spectrum Compatible Ground Motion (5% Damped) − Set 2 Fault Normal

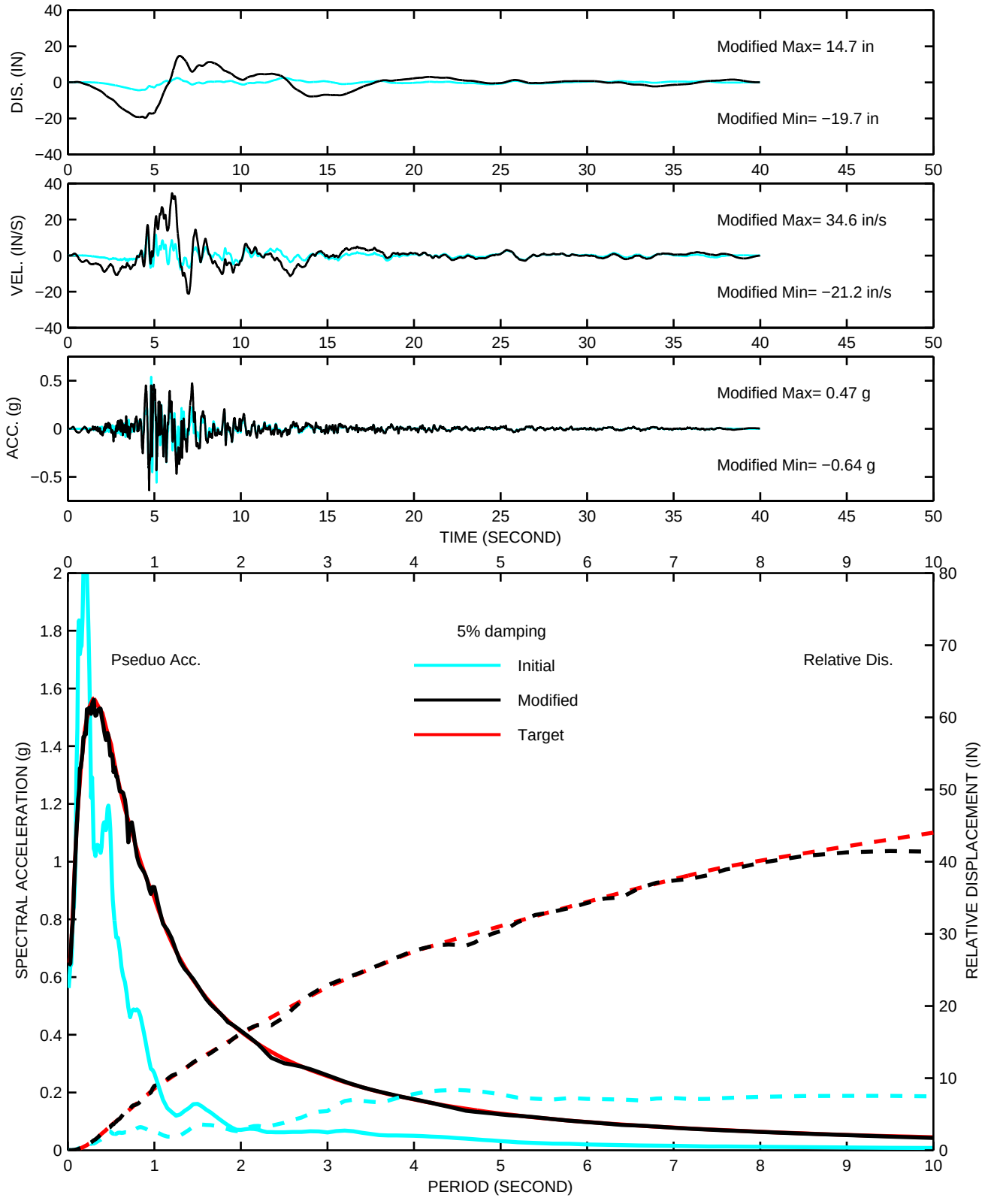


Figure B47. Firm−Ground 975−Yr Spectrum Compatible Ground Motion (5% Damped) − Set 2 Fault Parallel

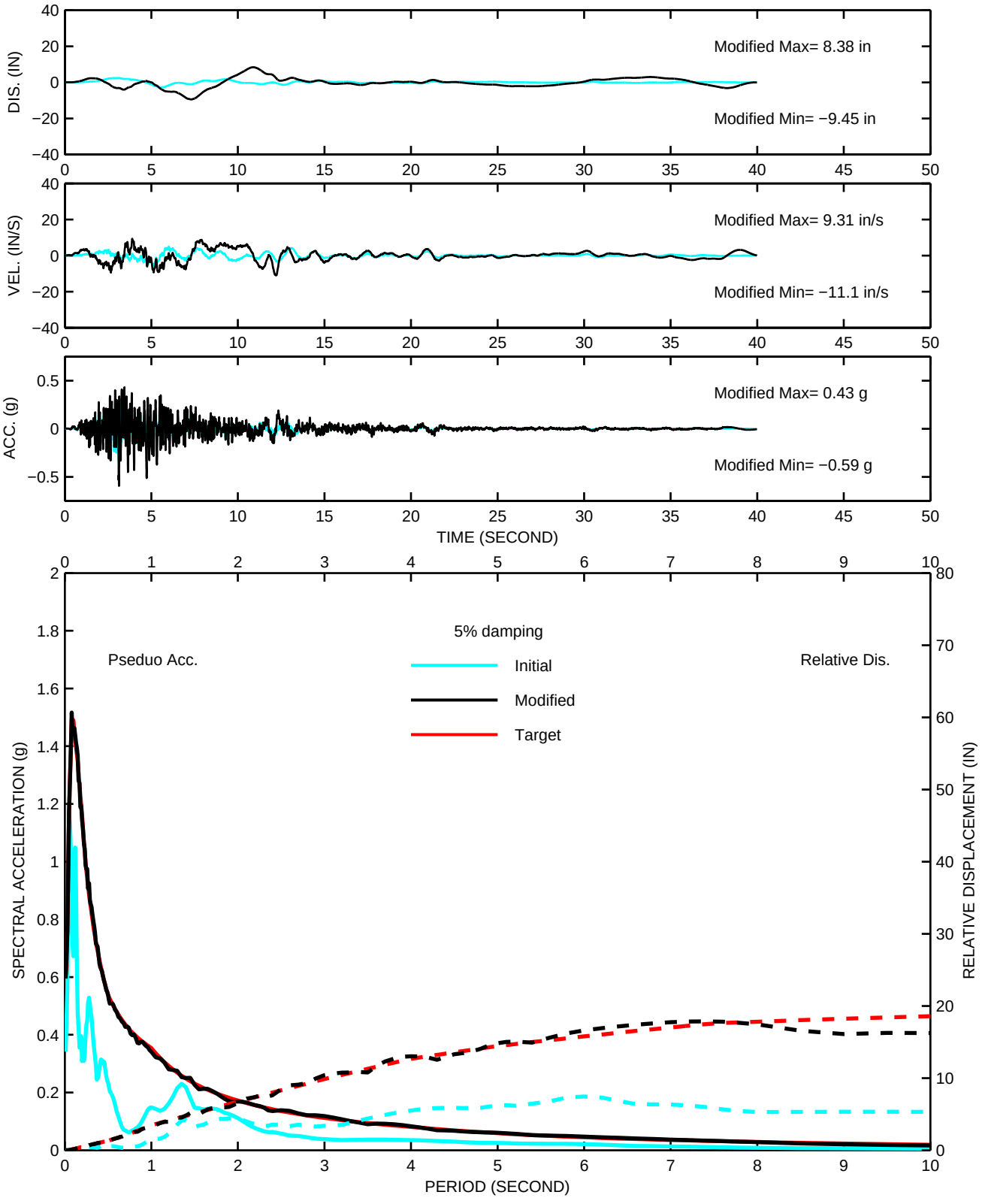


Figure B48. Firm−Ground 975−Yr Spectrum Compatible Ground Motion (5% Damped) − Set 2 Vertical

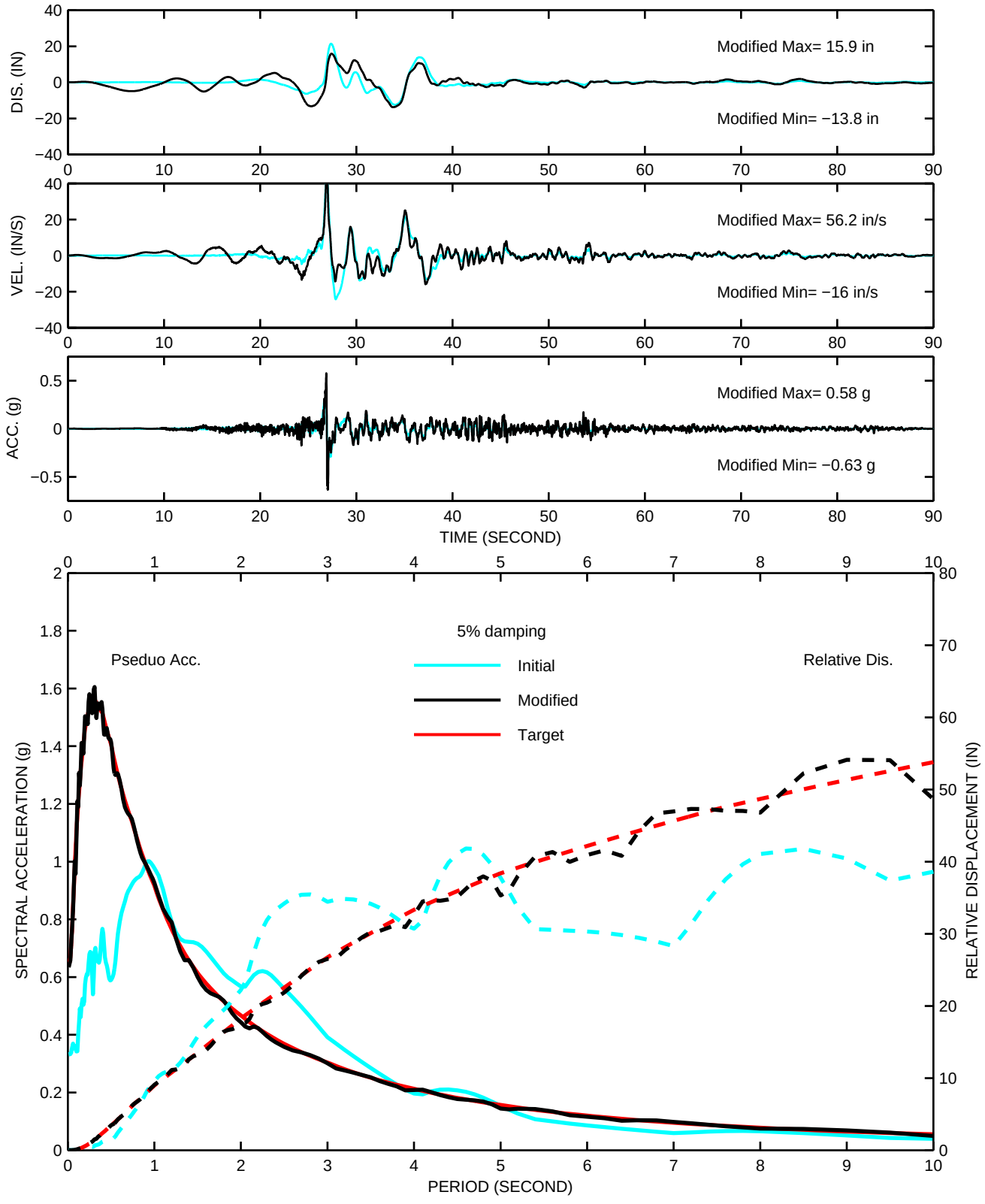


Figure B49. Firm−Ground 975−Yr Spectrum Compatible Ground Motion (5% Damped) − Set 3 Fault Normal

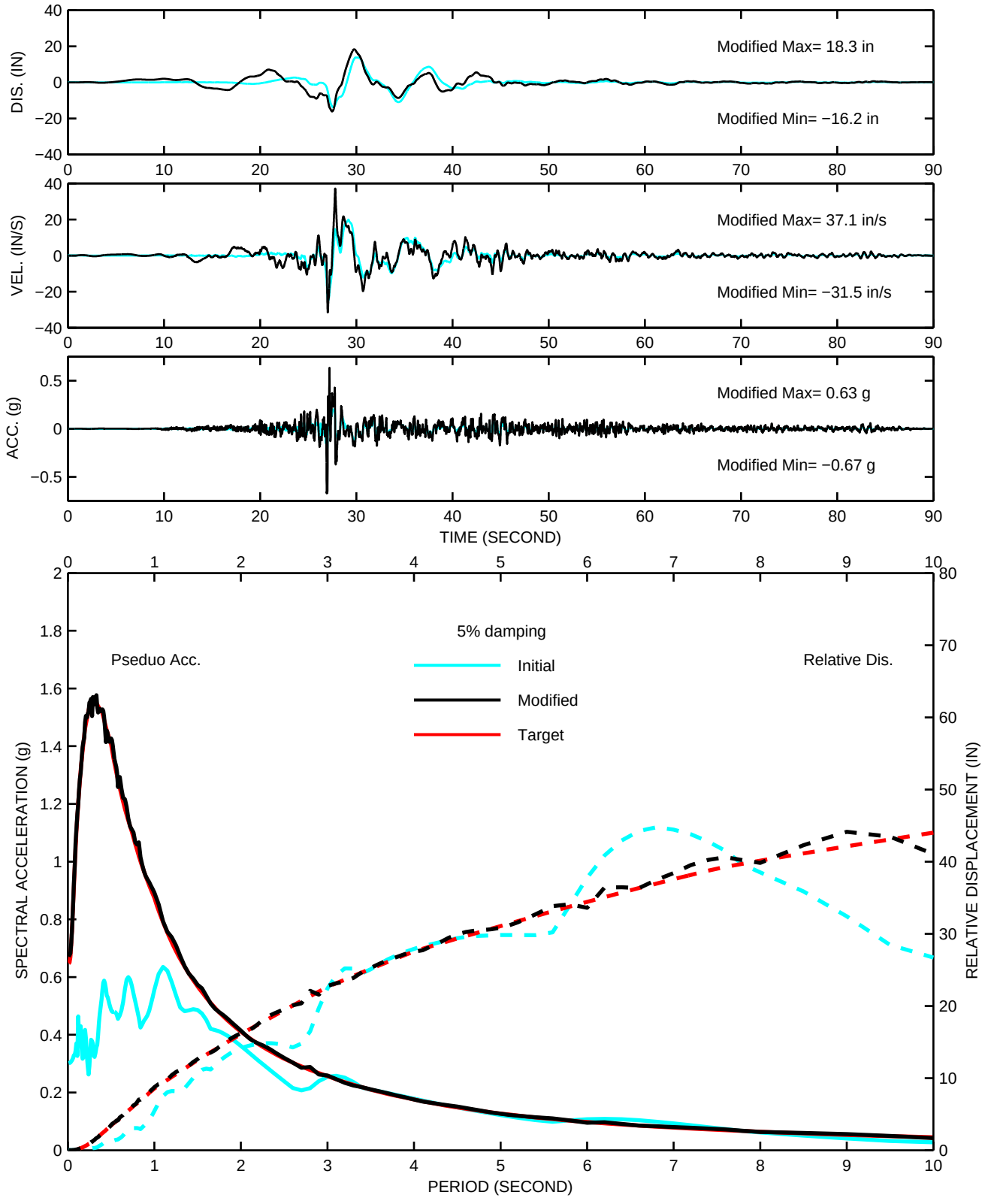


Figure B50. Firm−Ground 975−Yr Spectrum Compatible Ground Motion (5% Damped) − Set 3 Fault Parallel

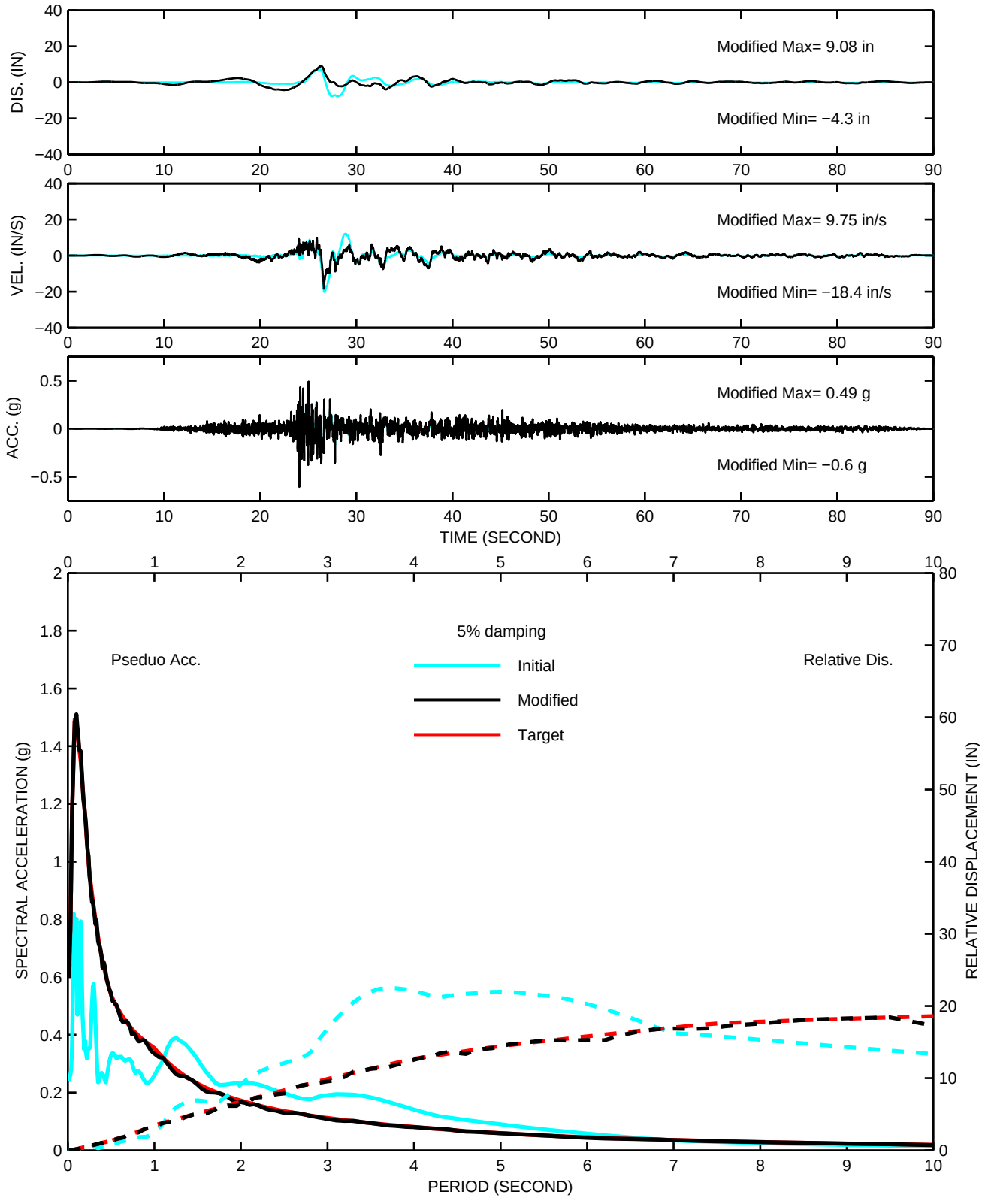


Figure B51. Firm−Ground 975−Yr Spectrum Compatible Ground Motion (5% Damped) − Set 3 Vertical

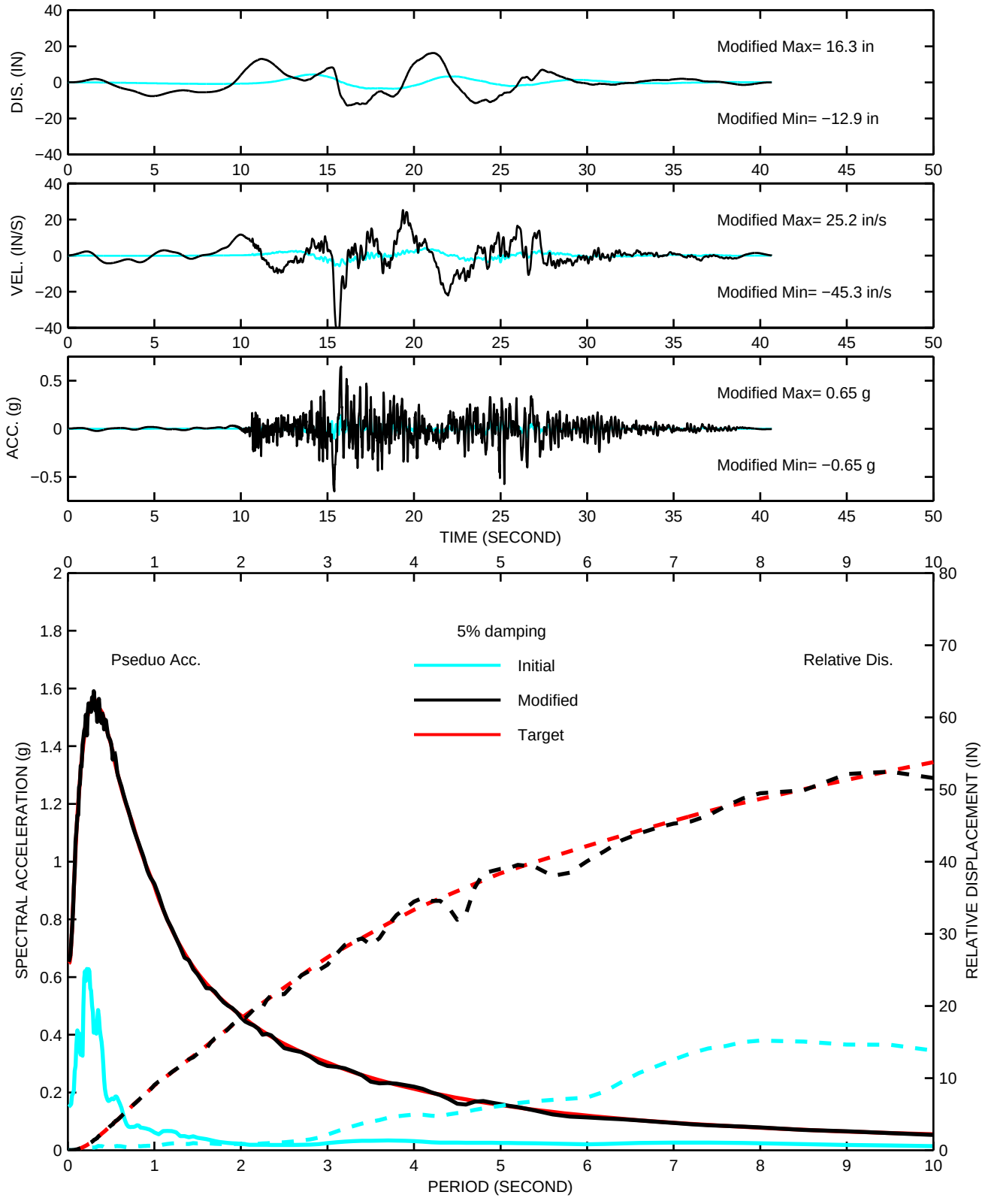


Figure B52. Firm−Ground 975−Yr Spectrum Compatible Ground Motion (5% Damped) − Set 4 Fault Normal

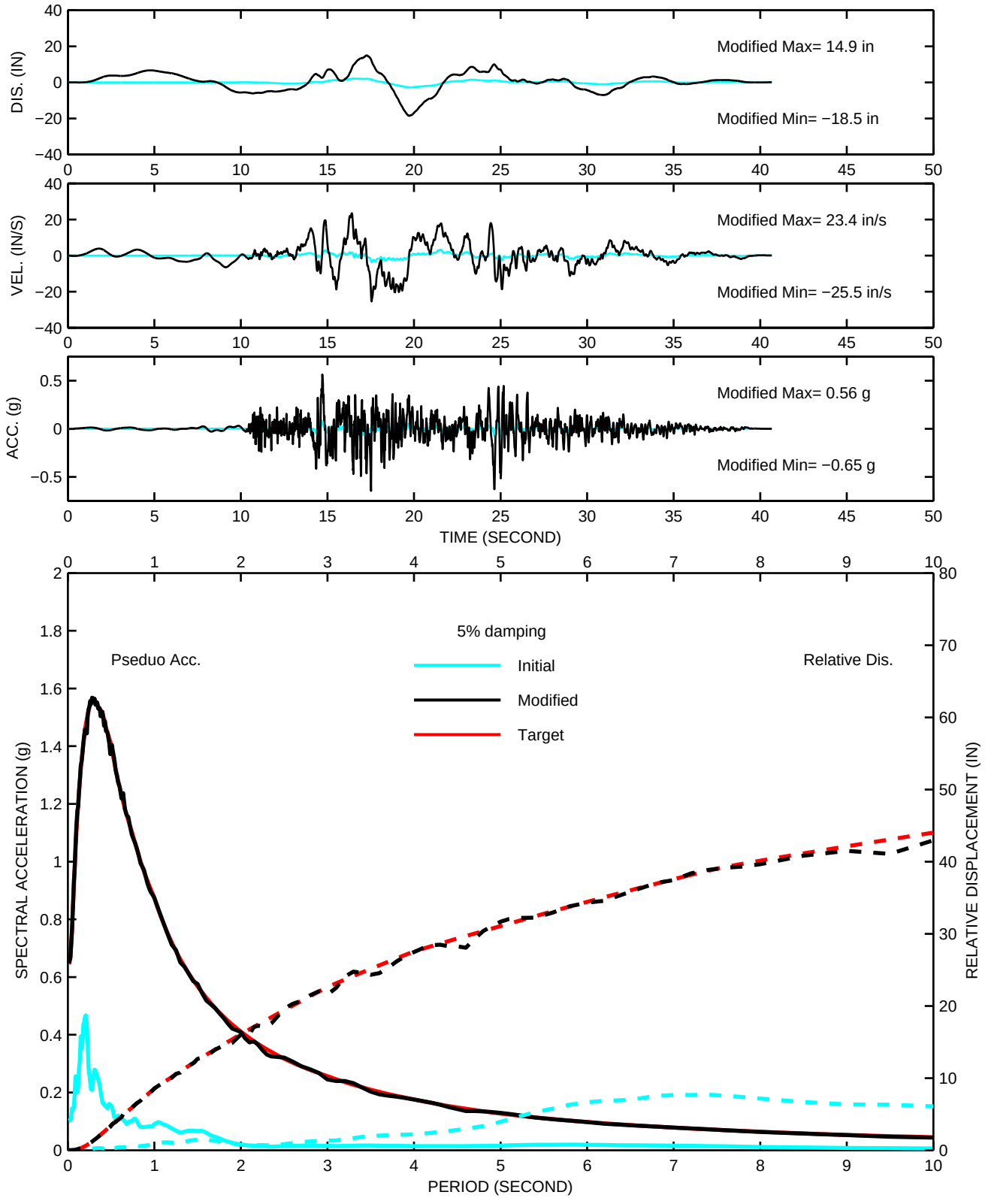


Figure B53. Firm−Ground 975−Yr Spectrum Compatible Ground Motion (5% Damped) − Set 4 Fault Parallel

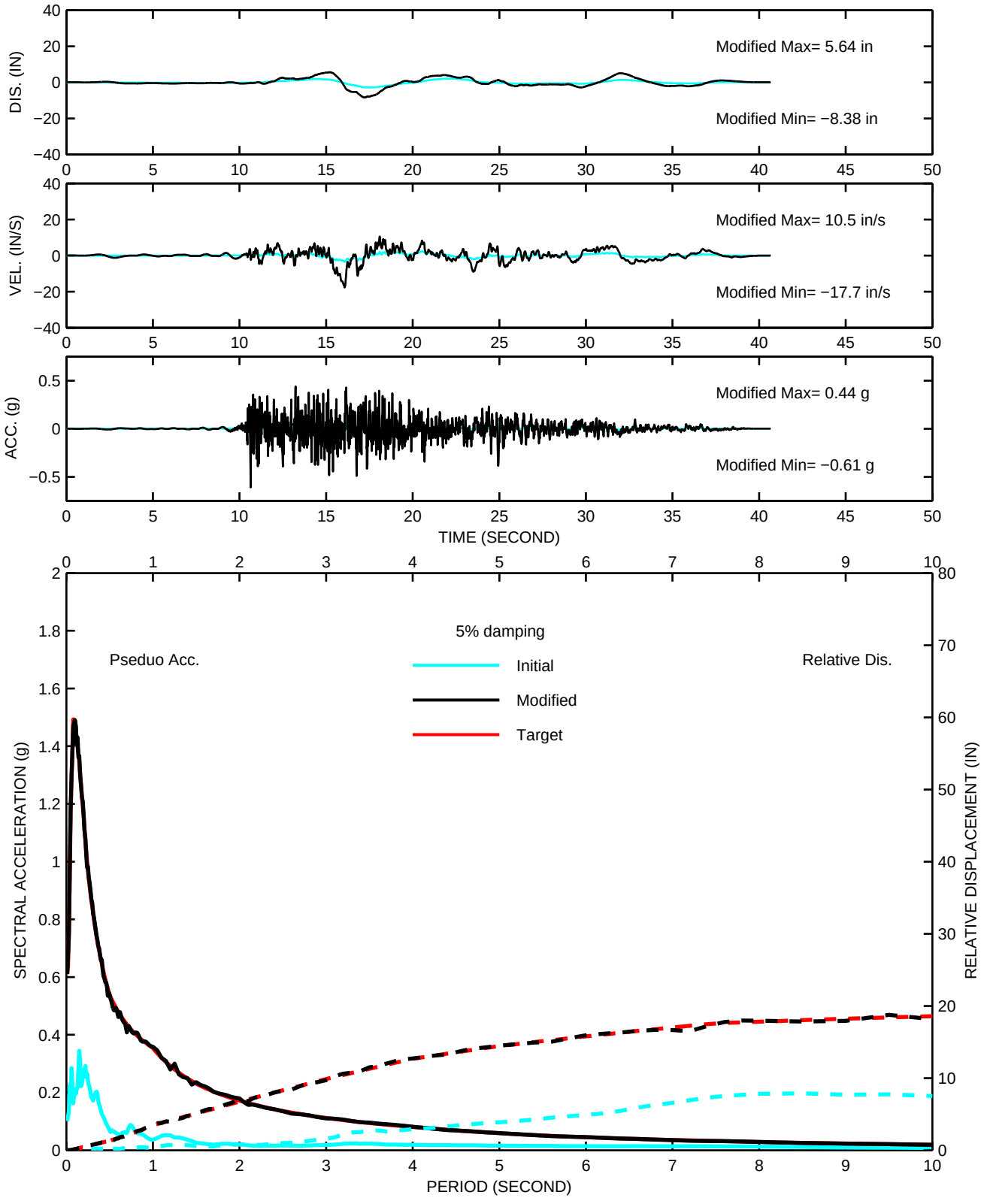


Figure B54. Firm−Ground 975−Yr Spectrum Compatible Ground Motion (5% Damped) − Set 4 Vertical

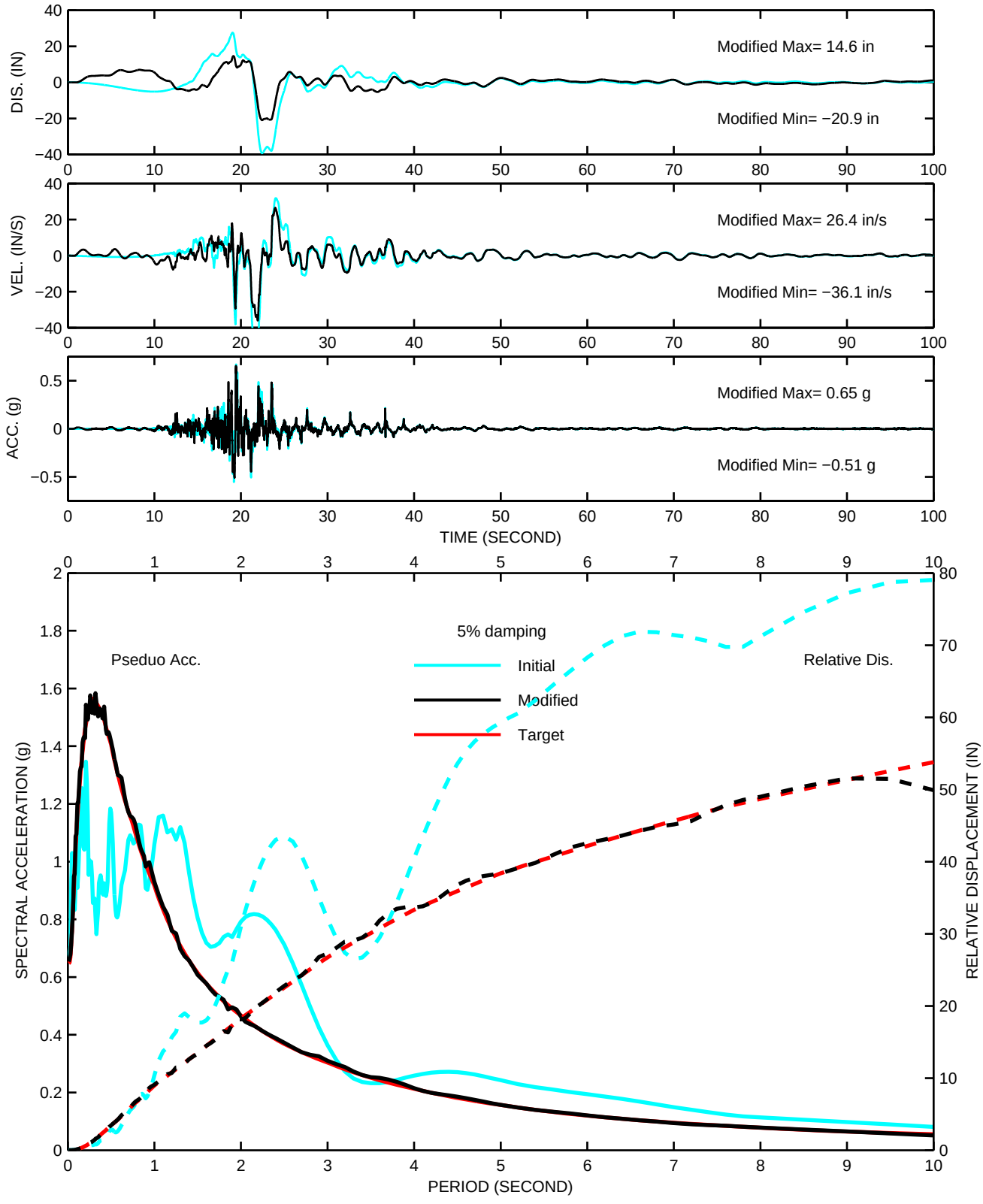


Figure B55. Firm−Ground 975−Yr Spectrum Compatible Ground Motion (5% Damped) − Set 5 Fault Normal

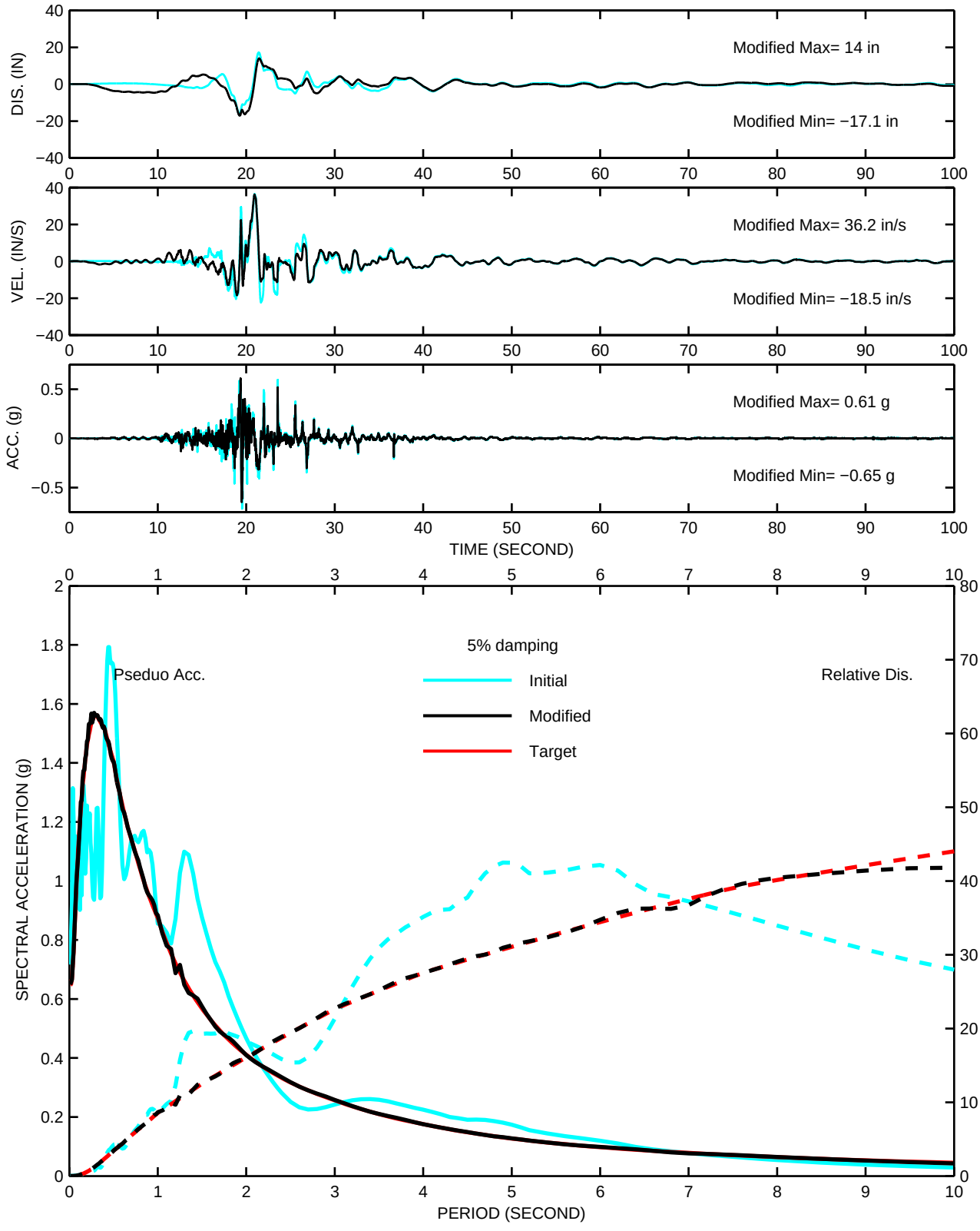


Figure B56. Firm−Ground 975−Yr Spectrum Compatible Ground Motion (5% Damped) − Set 5 Fault Parallel

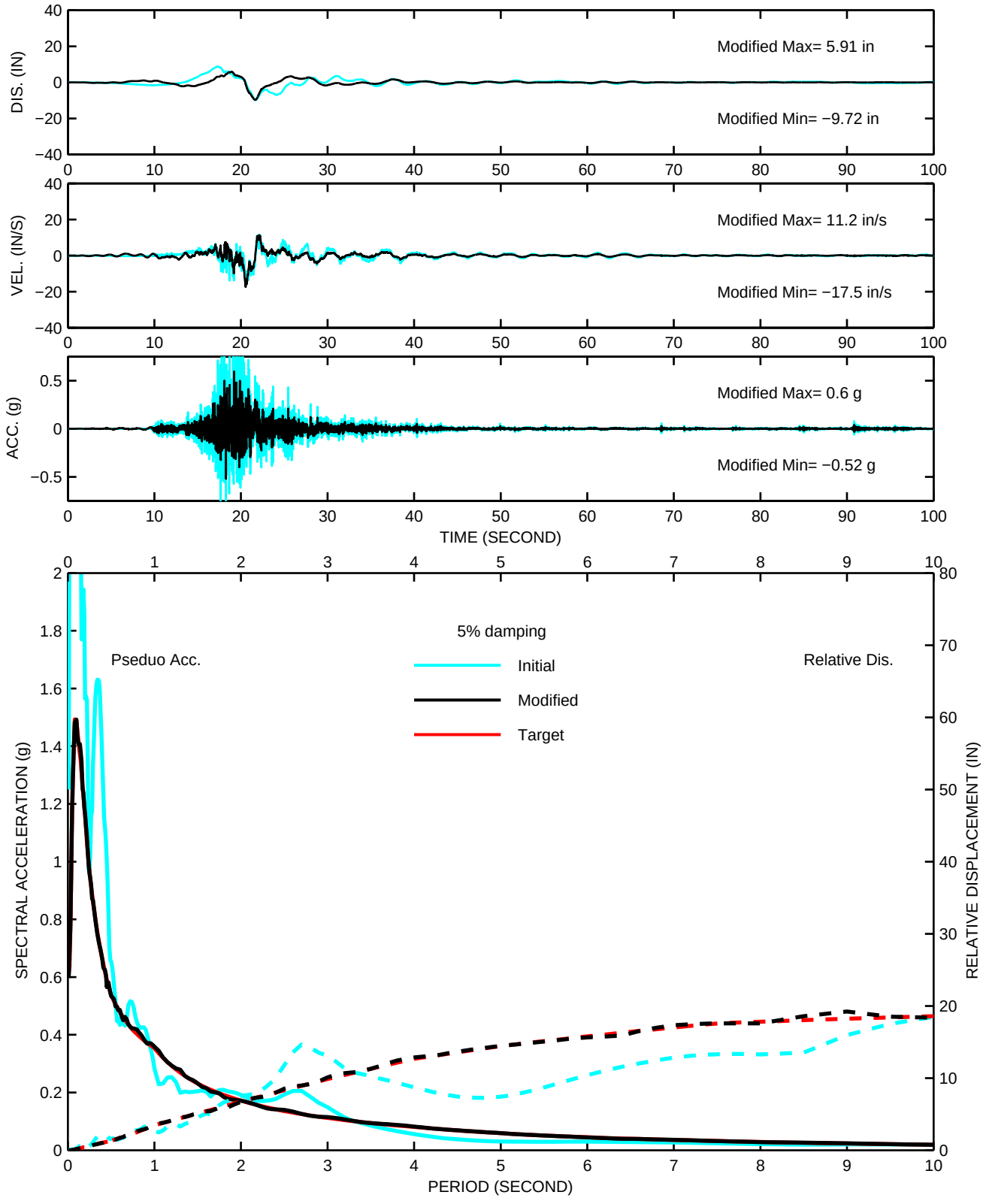


Figure B57. Firm−Ground 975−Yr Spectrum Compatible Ground Motion (5% Damped) − Set 5 Vertical

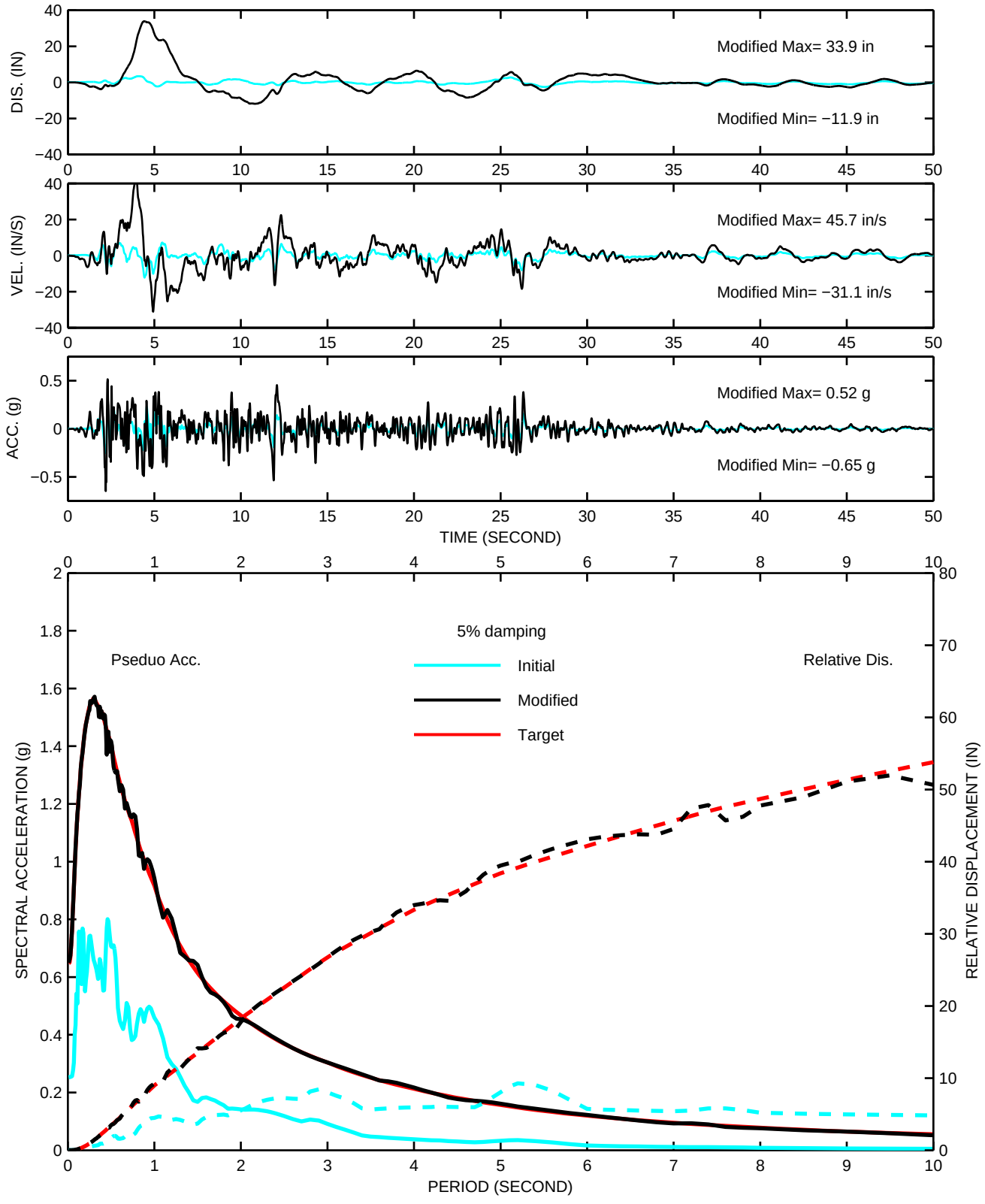


Figure B58. Firm−Ground 975−Yr Spectrum Compatible Ground Motion (5% Damped) − Set 6 Fault Normal

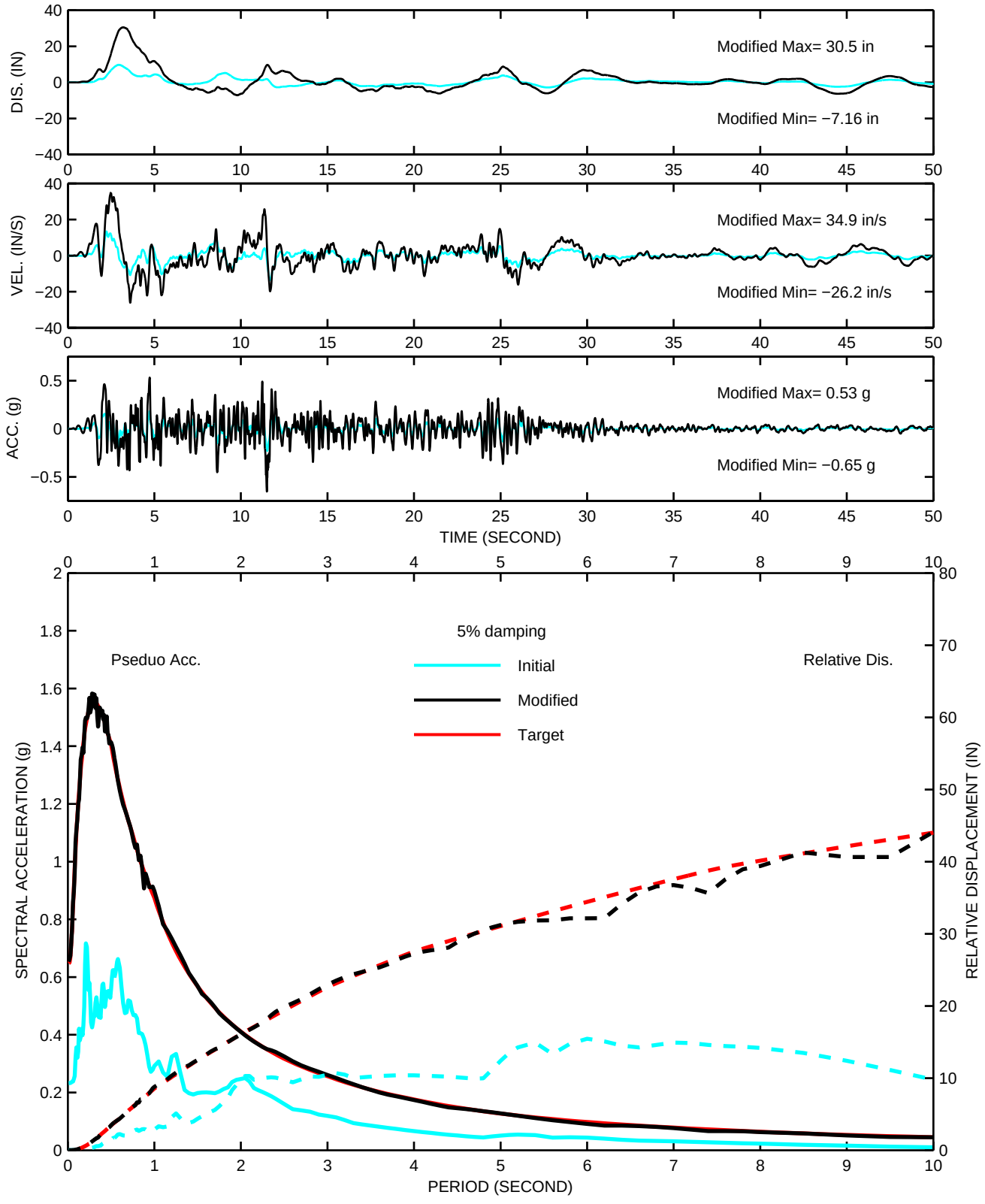


Figure B59. Firm−Ground 975−Yr Spectrum Compatible Ground Motion (5% Damped) − Set 6 Fault Parallel

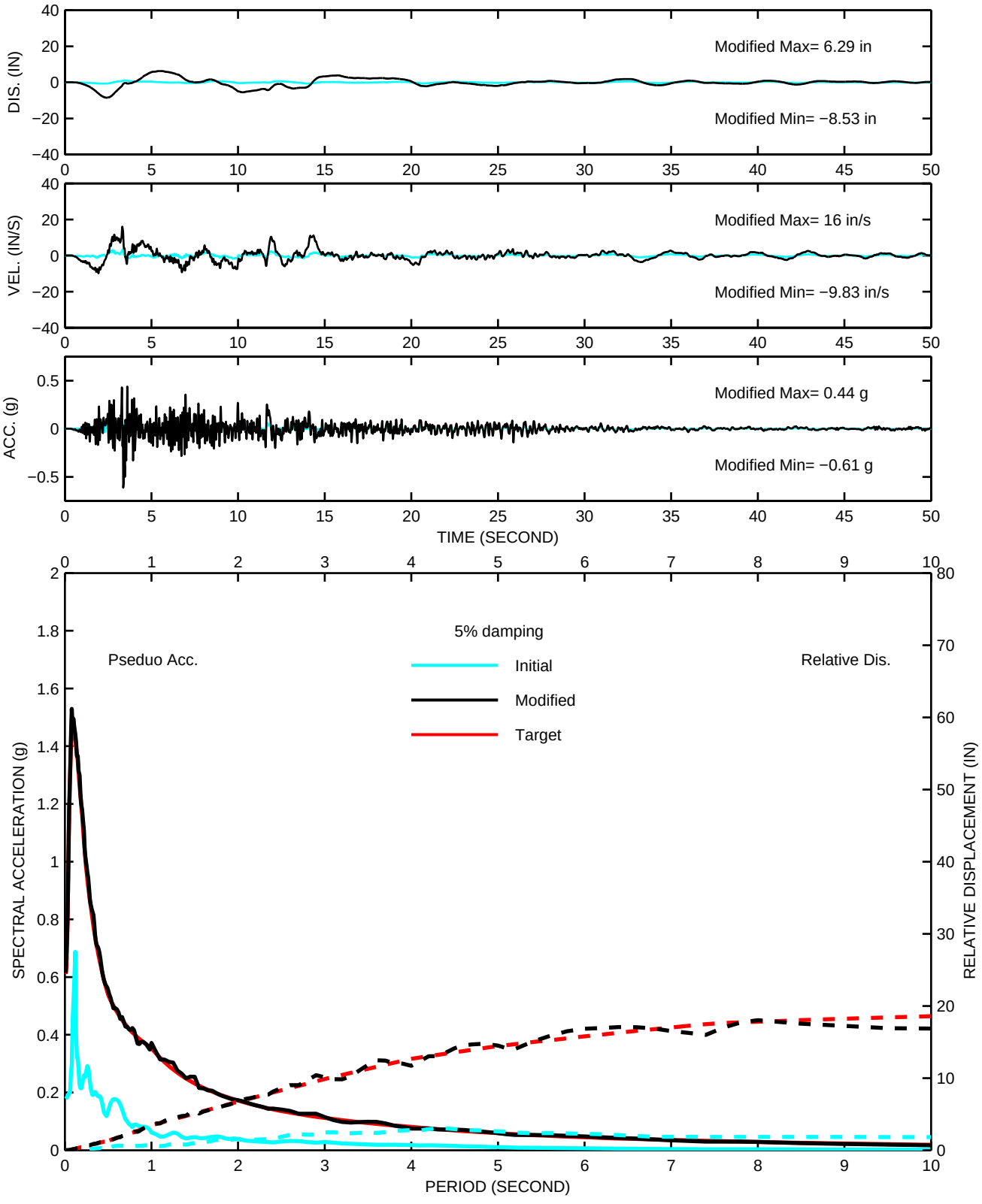


Figure B60. Firm−Ground 975−Yr Spectrum Compatible Ground Motion (5% Damped) − Set 6 Vertical

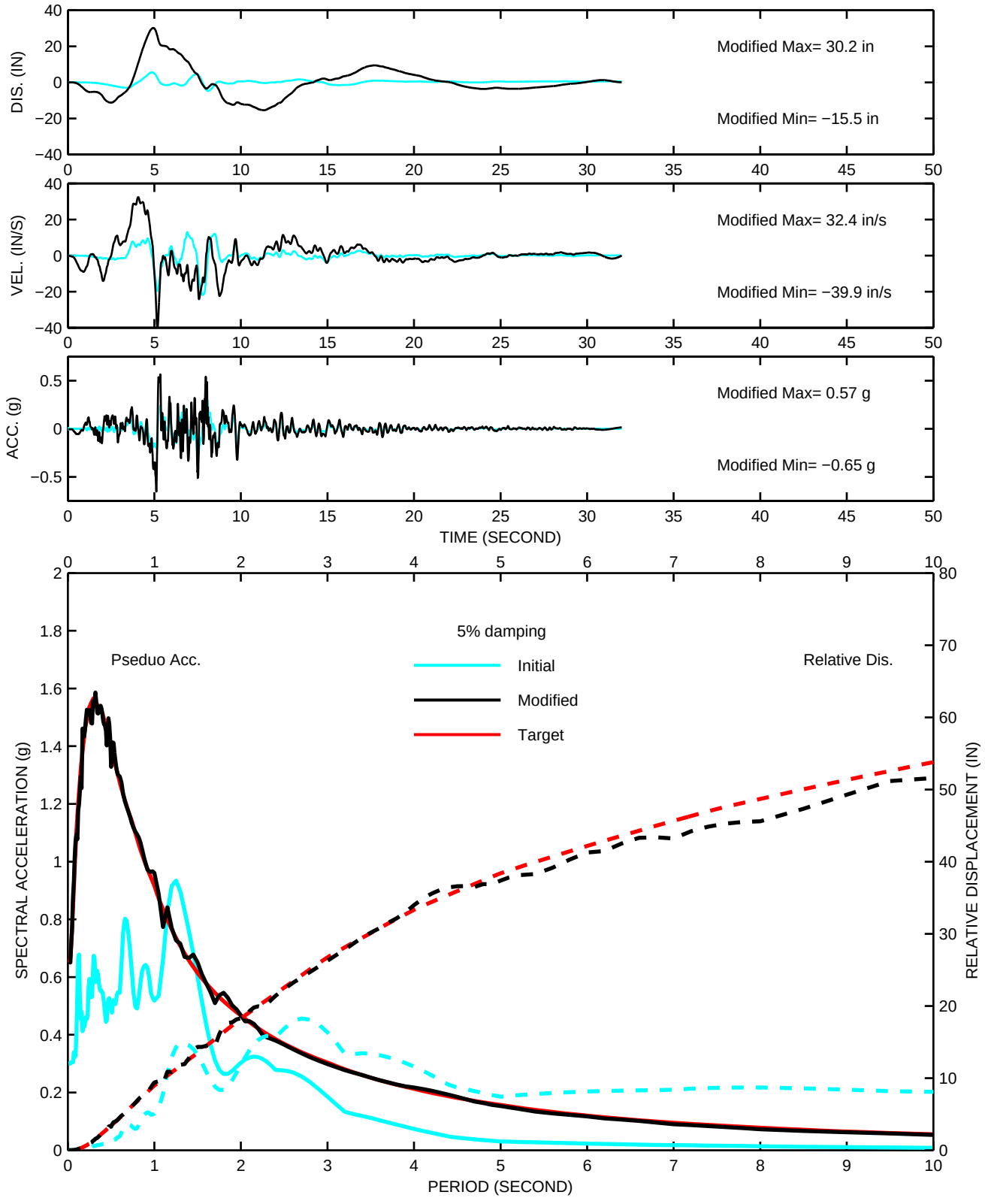


Figure B61. Firm−Ground 975−Yr Spectrum Compatible Ground Motion (5% Damped) − Set 7 Fault Normal

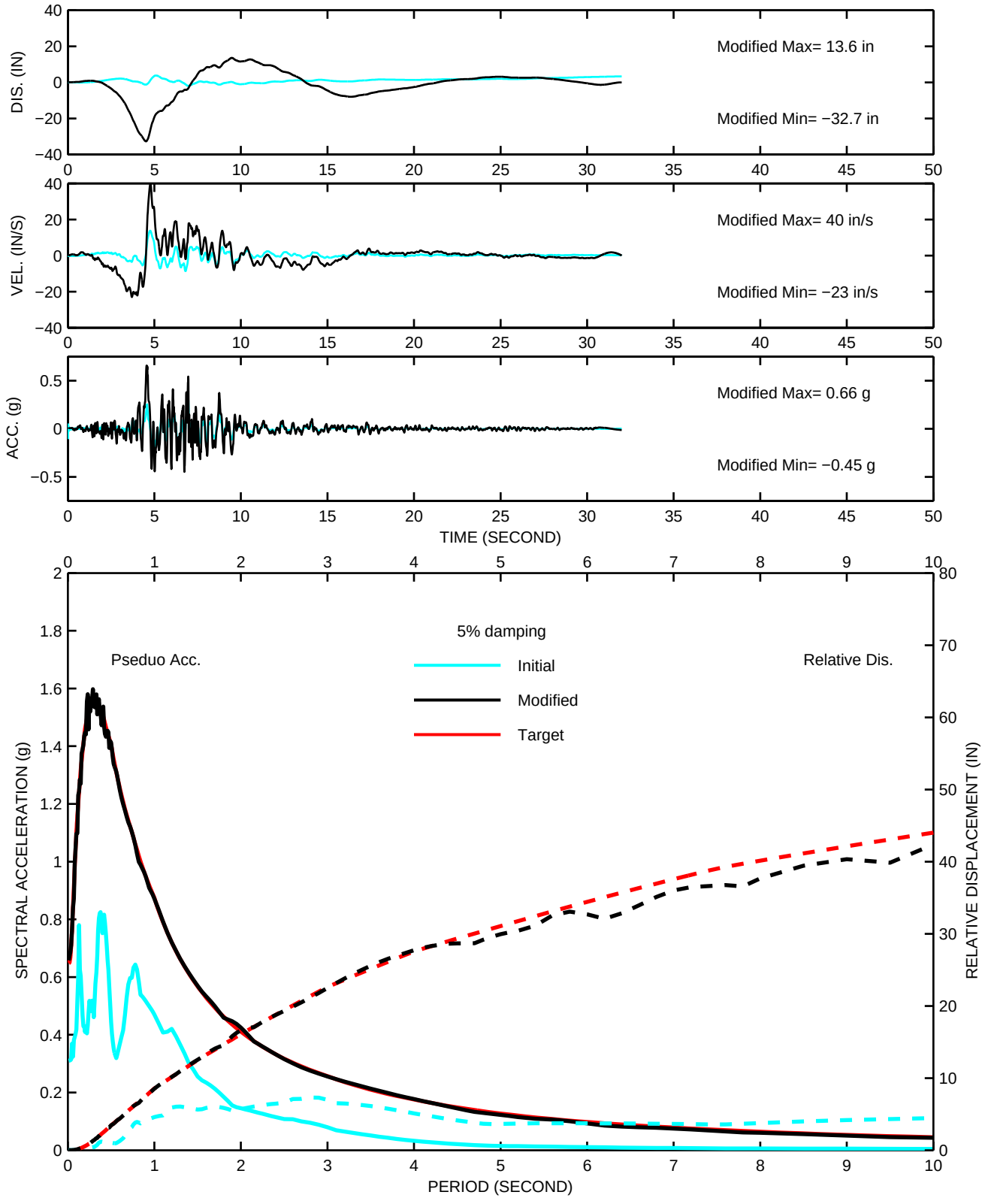


Figure B62. Firm−Ground 975−Yr Spectrum Compatible Ground Motion (5% Damped) − Set 7 Fault Parallel

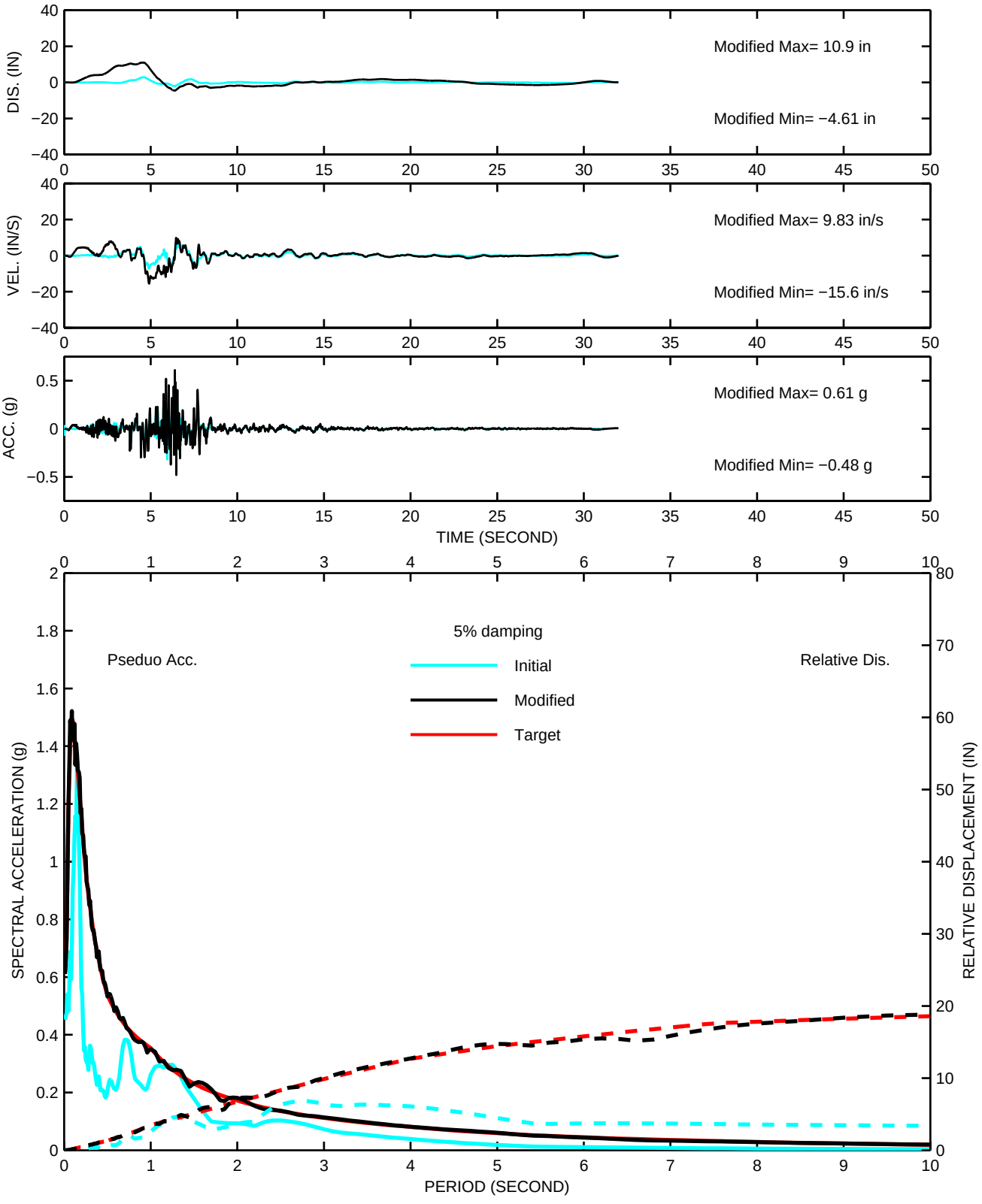


Figure B63. Firm−Ground 975−Yr Spectrum Compatible Ground Motion (5% Damped) − Set 7 Vertical

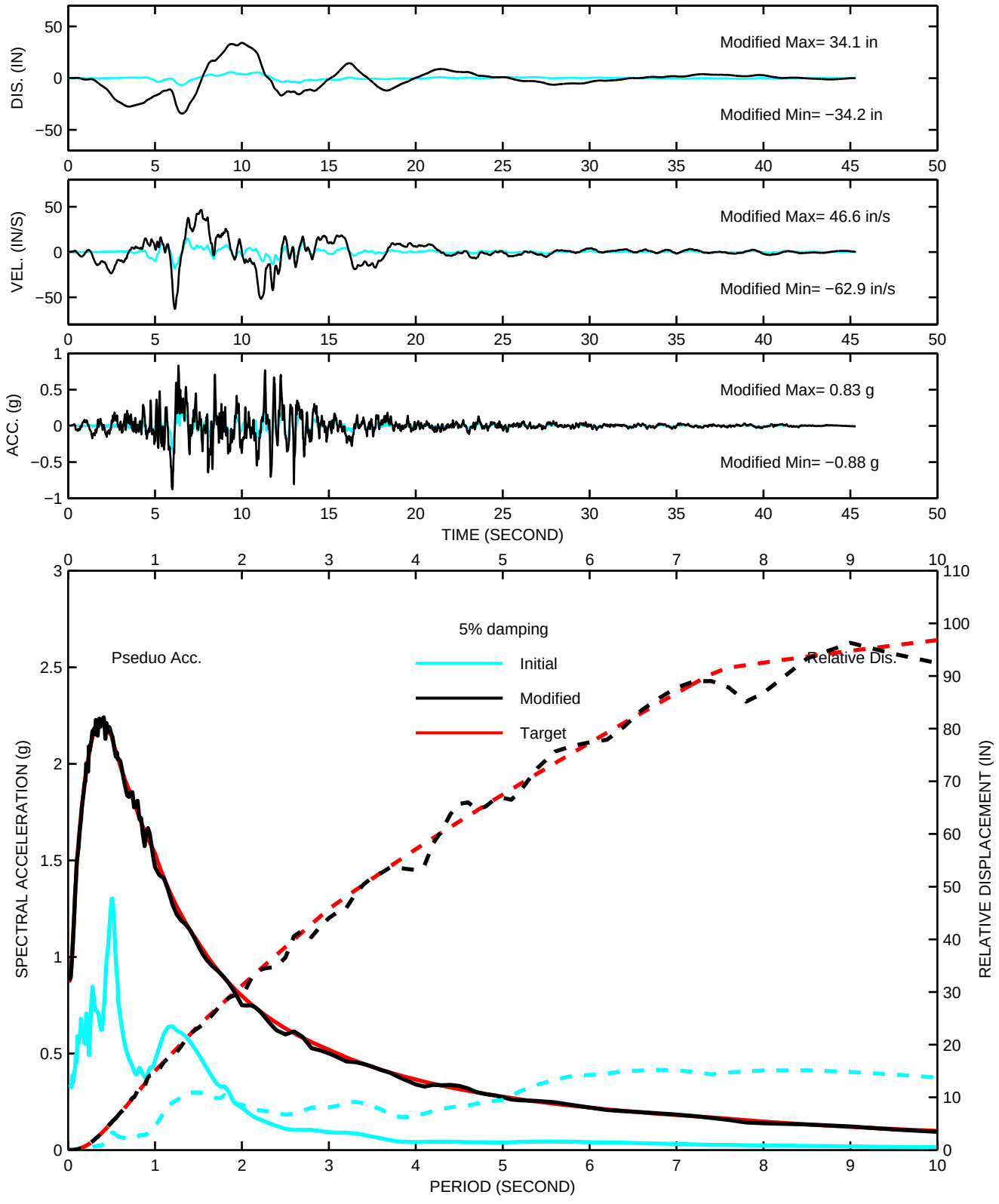


Figure B64. Firm−Ground MCEr Spectrum Compatible Ground Motion (5% Damped) − Set 1 Fault Normal

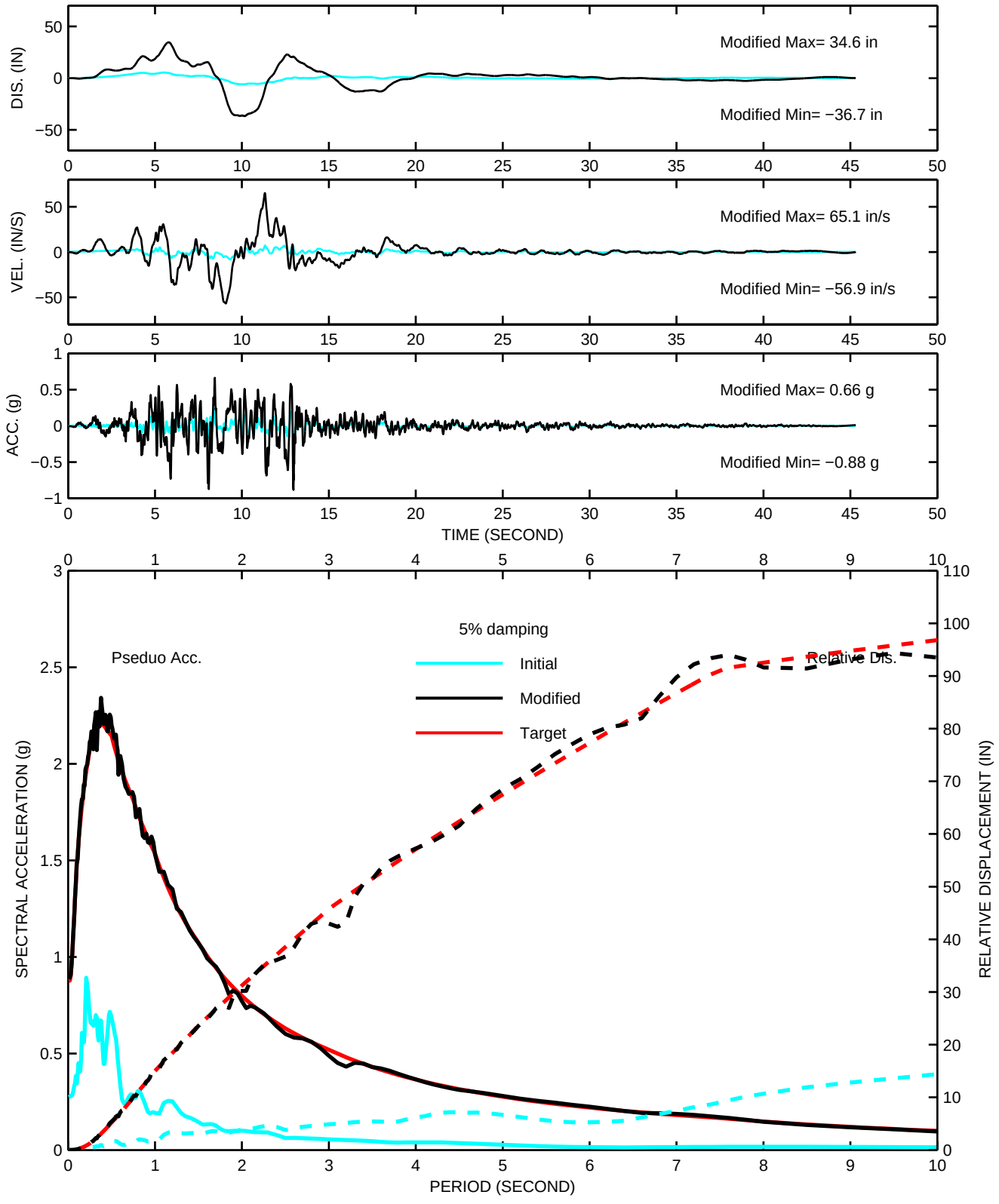


Figure B65. Firm−Ground MCEr Spectrum Compatible Ground Motion (5% Damped) − Set 1 Fault Parallel

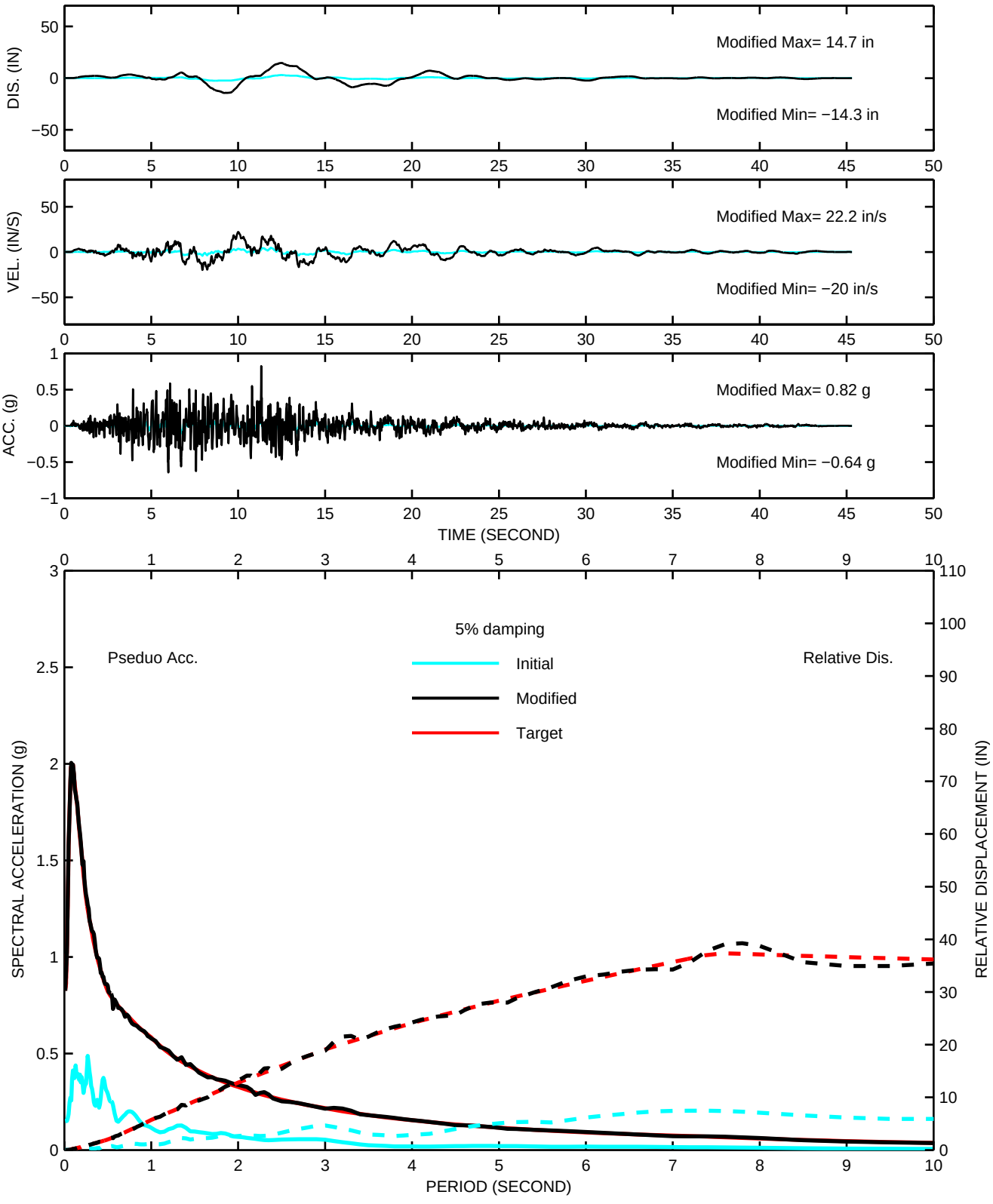


Figure B66. Firm−Ground MCEr Spectrum Compatible Ground Motion (5% Damped) − Set 1 Vertical

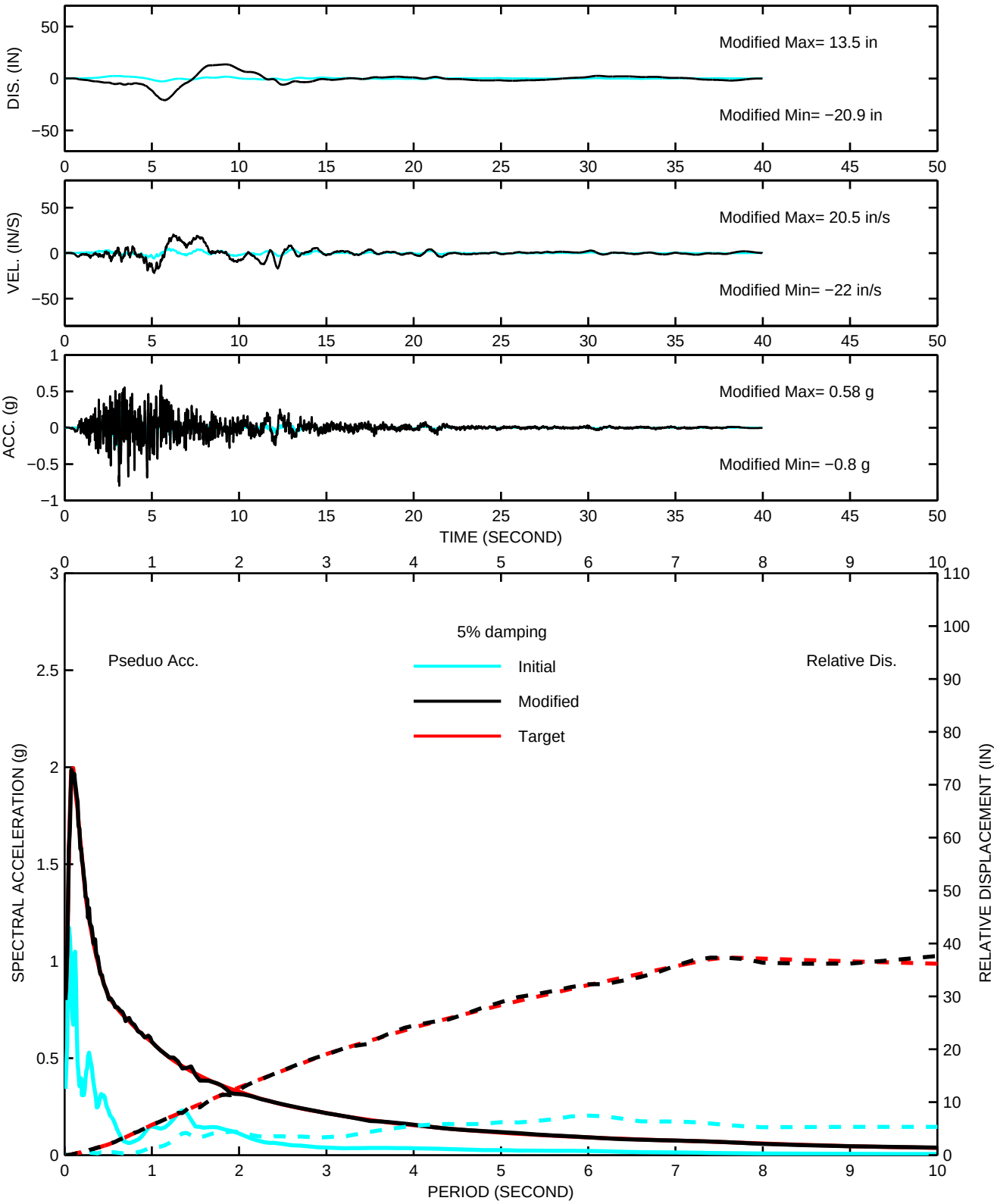


Figure B69. Firm−Ground MCEr Spectrum Compatible Ground Motion (5% Damped) − Set 2 Vertical

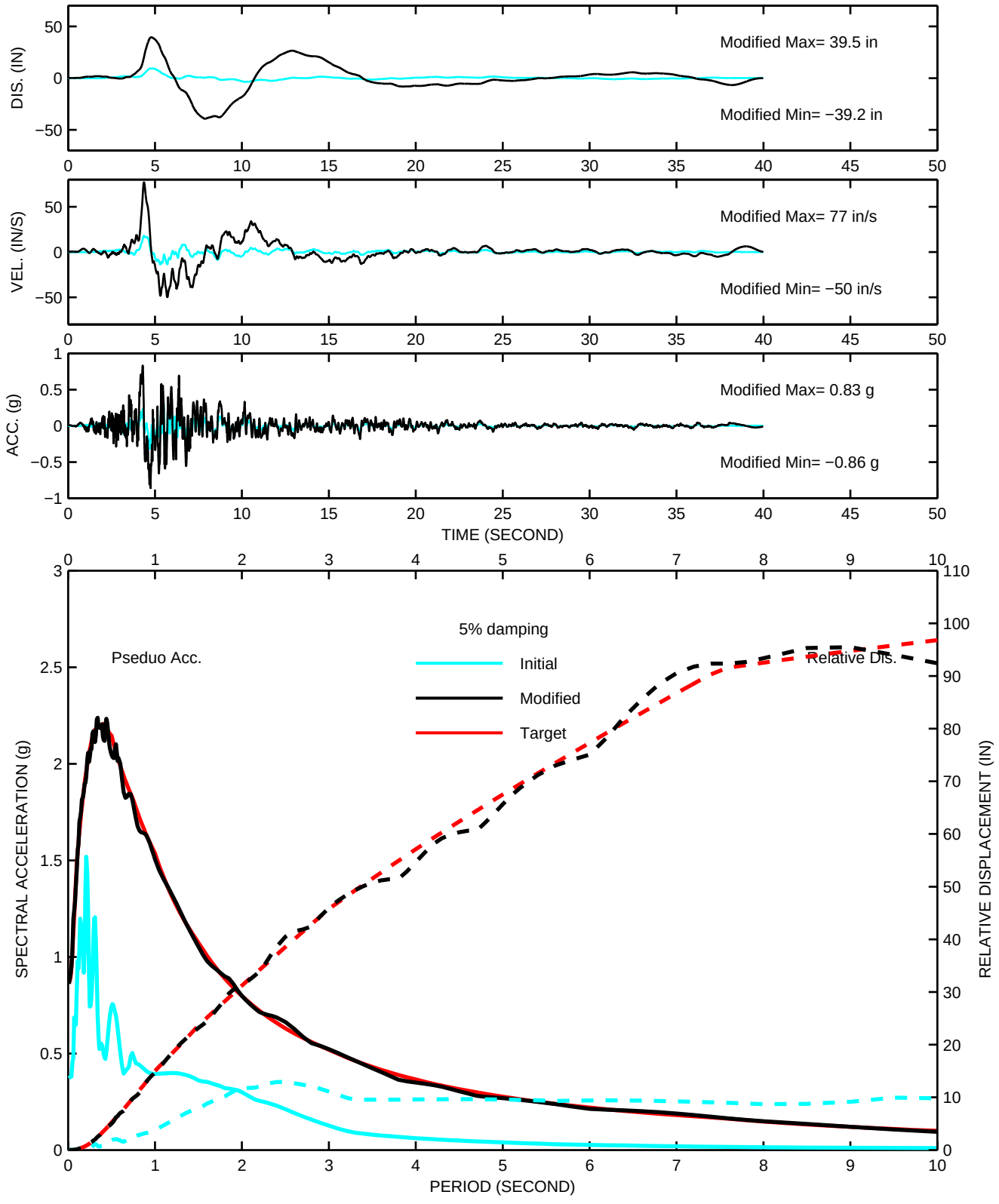


Figure B67. Firm−Ground MCEr Spectrum Compatible Ground Motion (5% Damped) − Set 2 Fault Normal

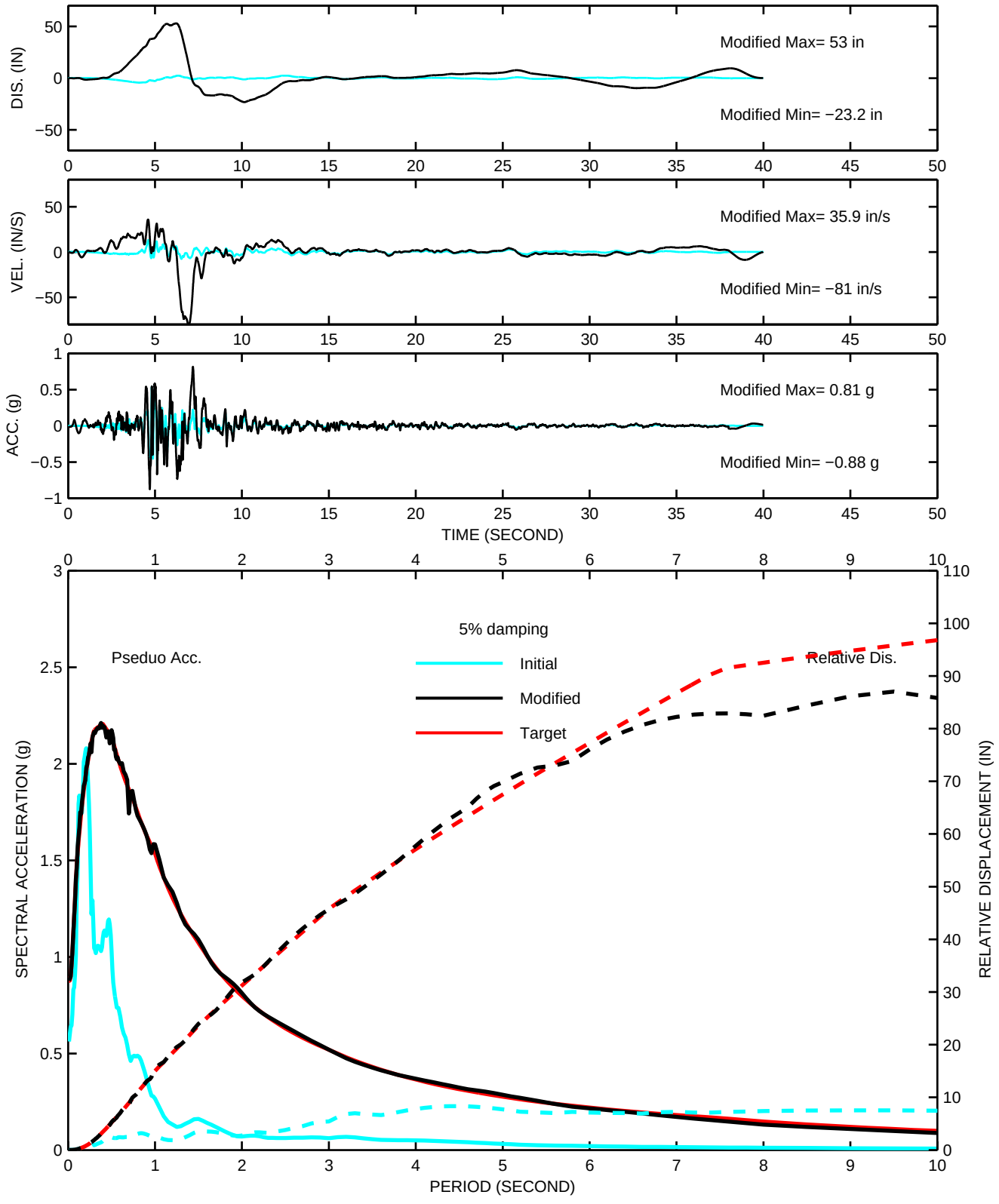


Figure B68. Firm−Ground MCEr Spectrum Compatible Ground Motion (5% Damped) − Set 2 Fault Parallel

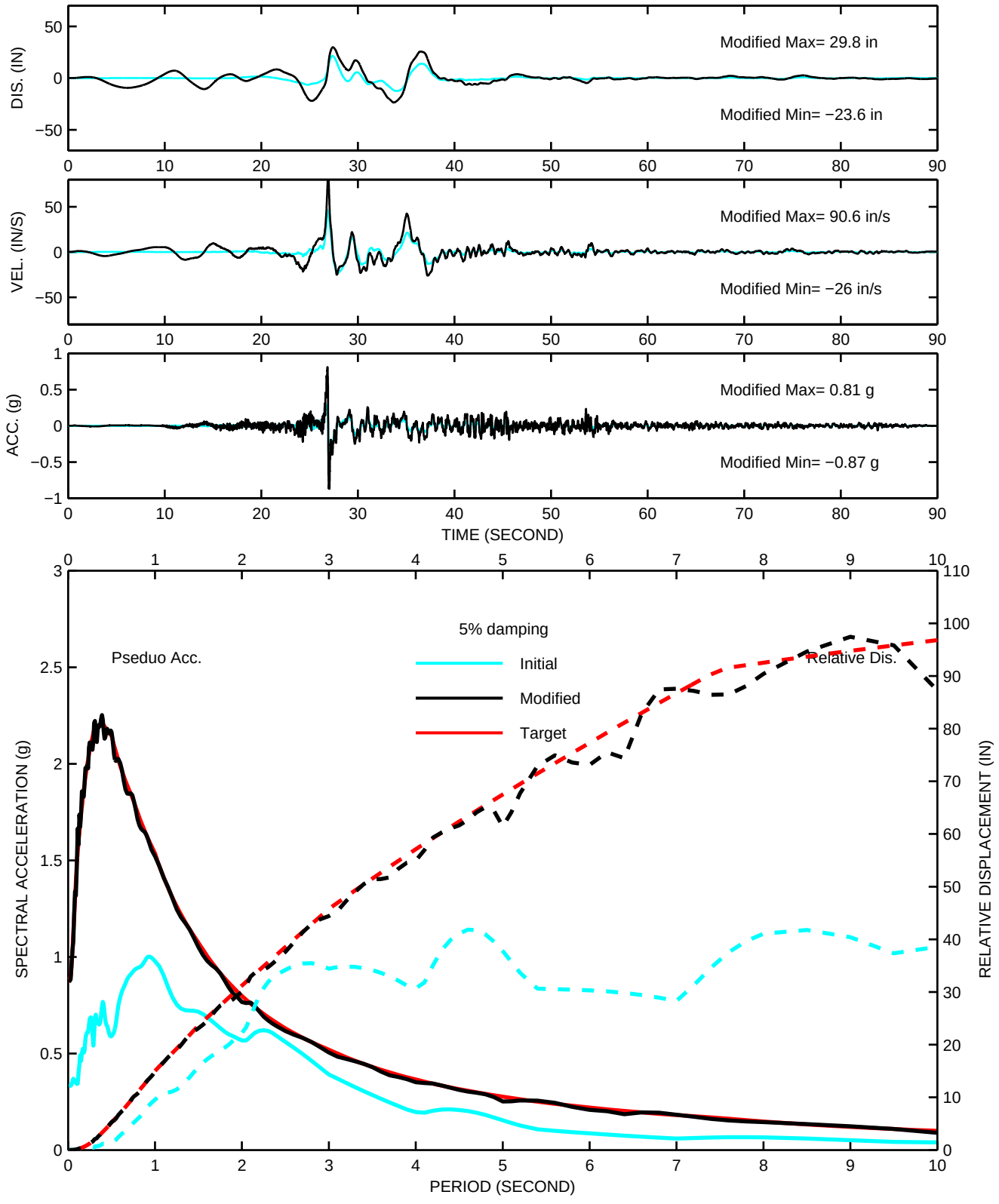


Figure B70. Firm−Ground MCEr Spectrum Compatible Ground Motion (5% Damped) − Set 3 Fault Normal

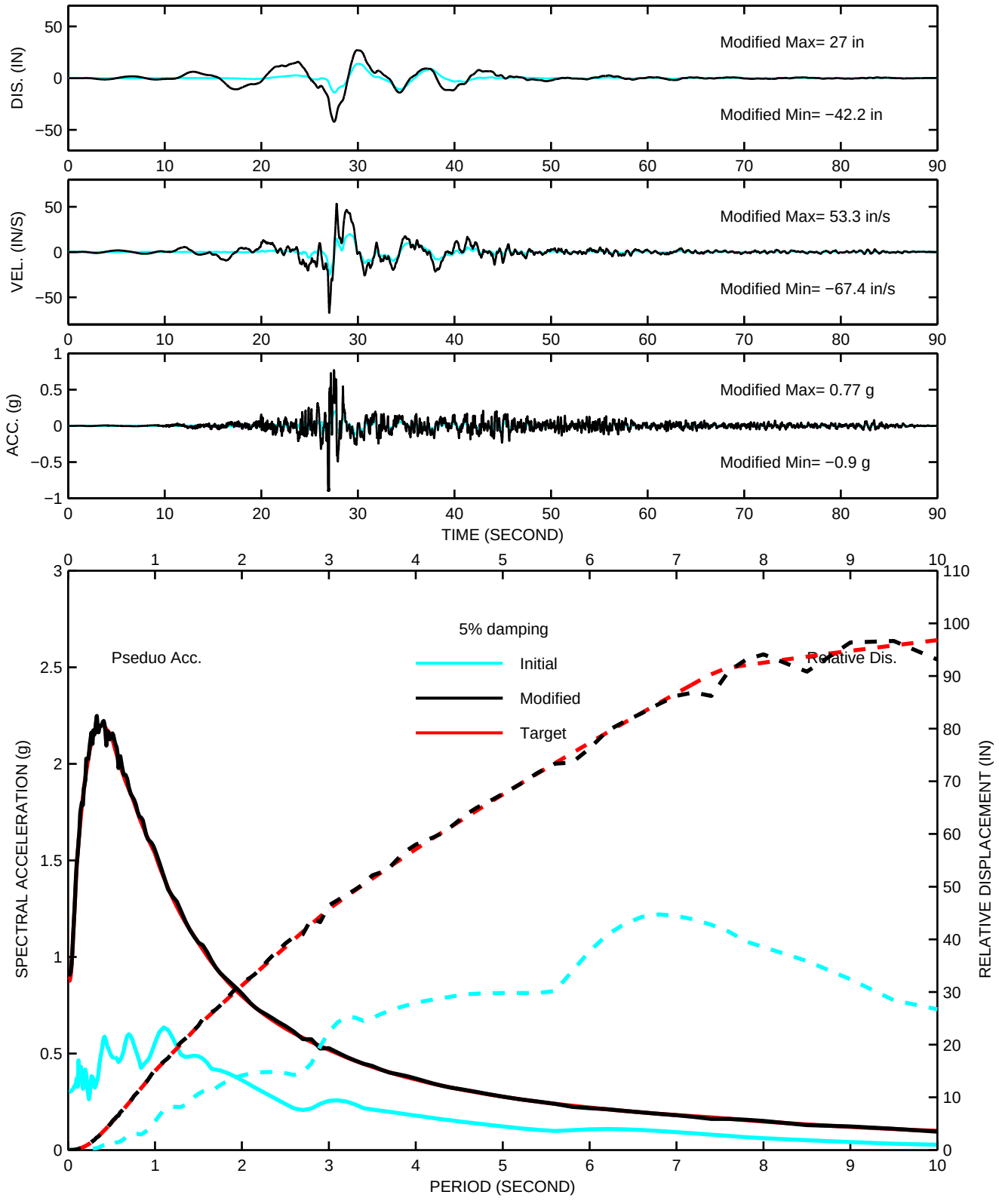


Figure B71. Firm−Ground MCEr Spectrum Compatible Ground Motion (5% Damped) − Set 3 Fault Parallel

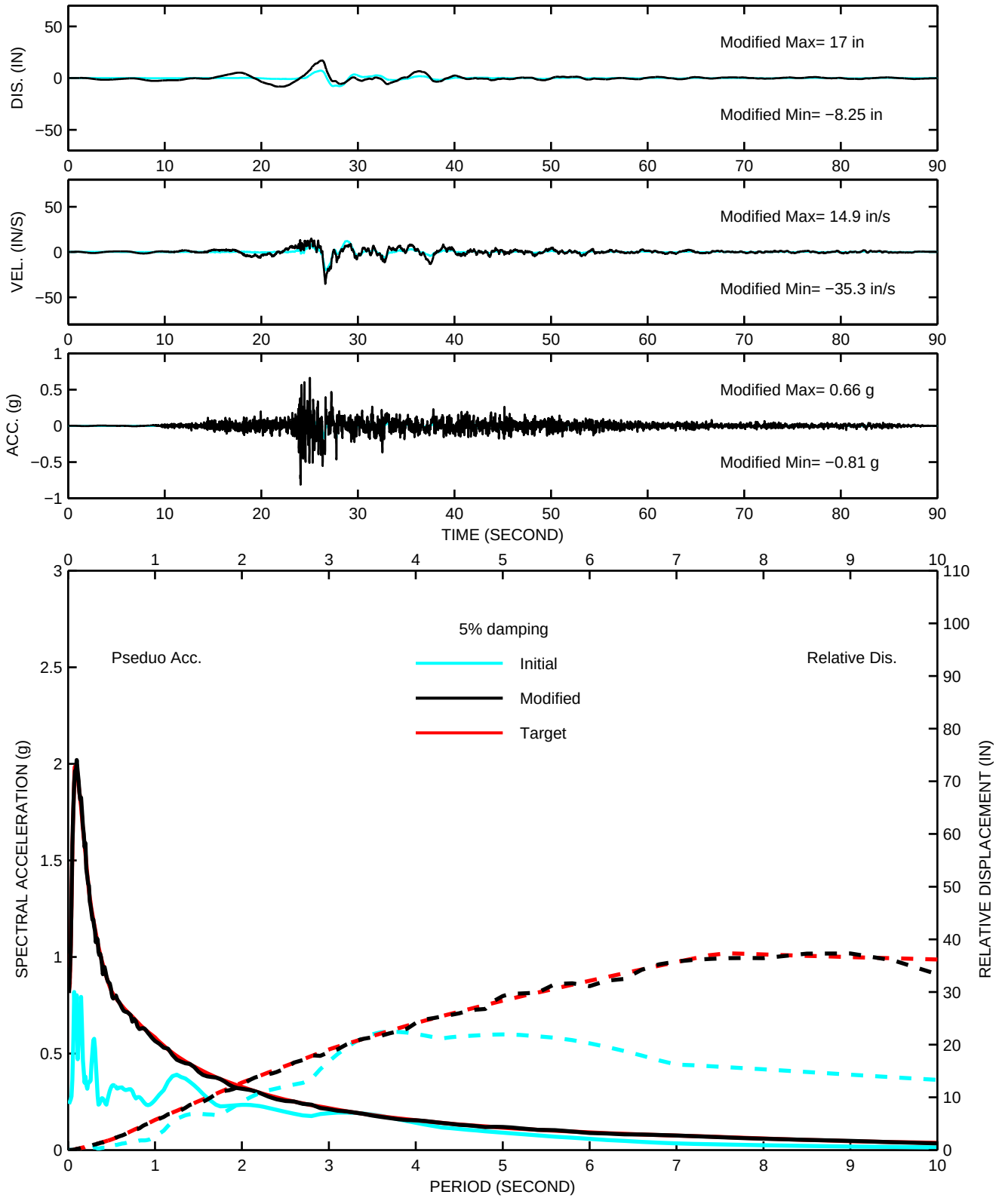


Figure B72. Firm−Ground MCEr Spectrum Compatible Ground Motion (5% Damped) − Set 3 Vertical

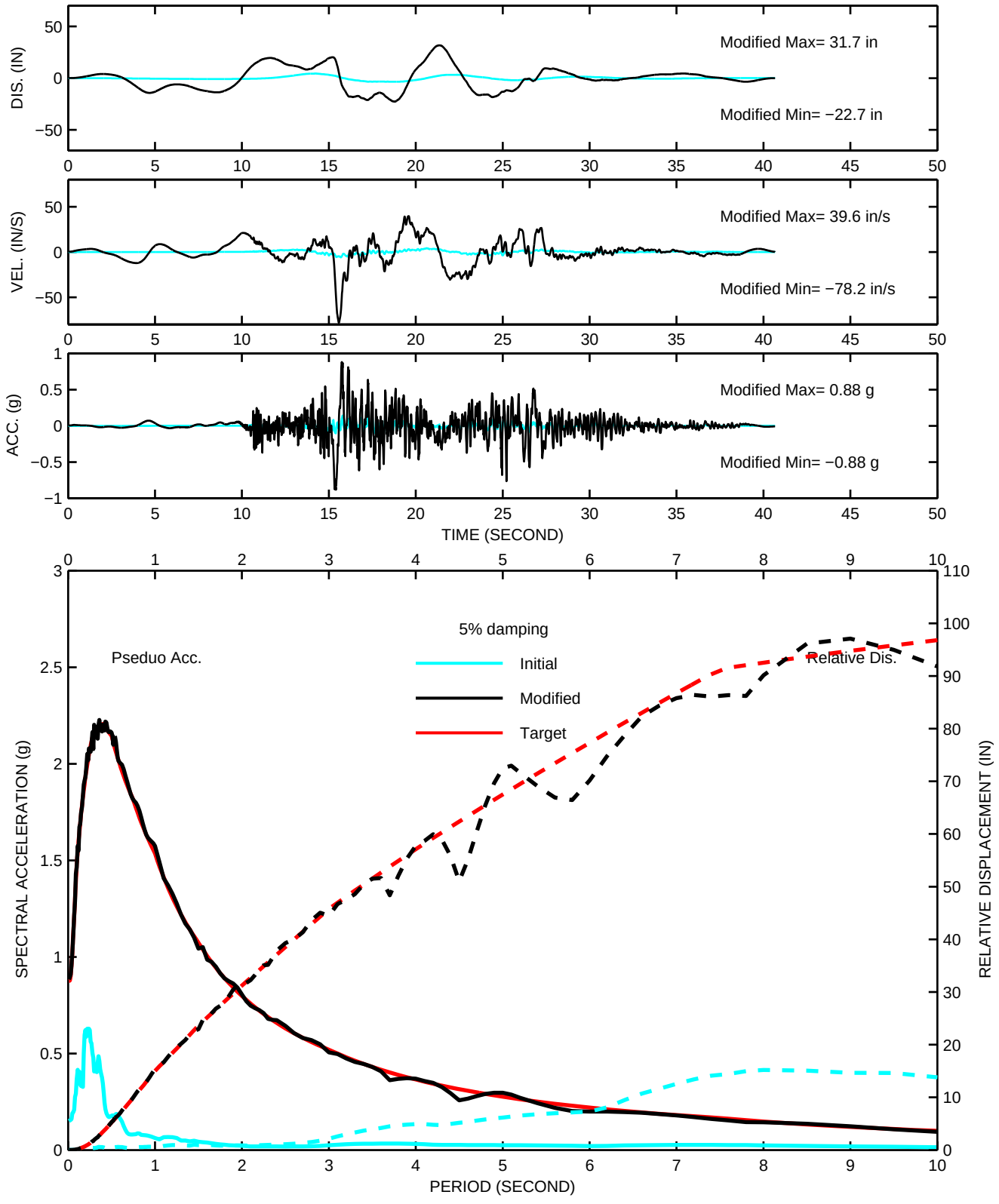


Figure B73. Firm−Ground MCEr Spectrum Compatible Ground Motion (5% Damped) − Set 4 Fault Normal

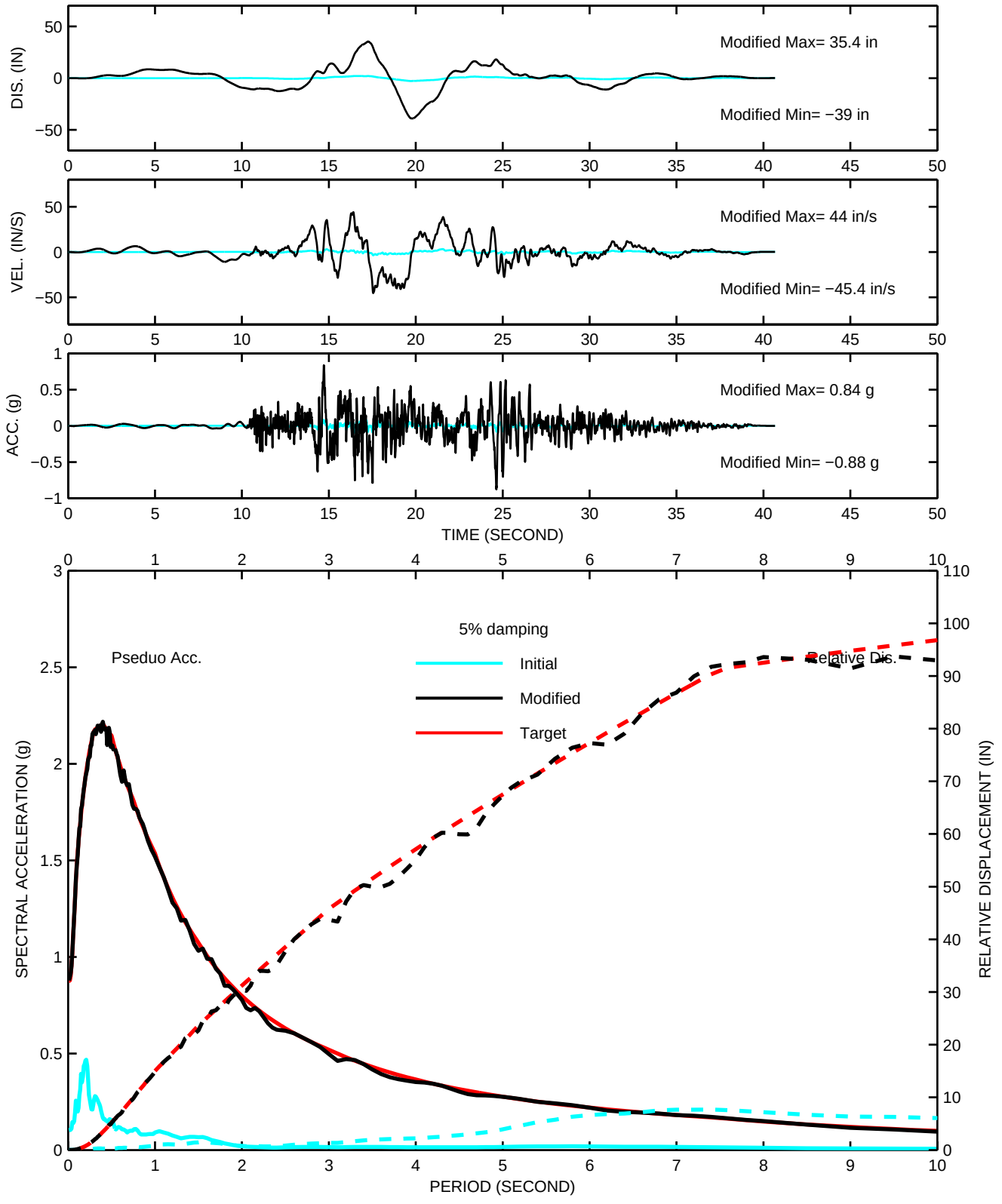


Figure B74. Firm−Ground MCEr Spectrum Compatible Ground Motion (5% Damped) − Set 4 Fault Parallel

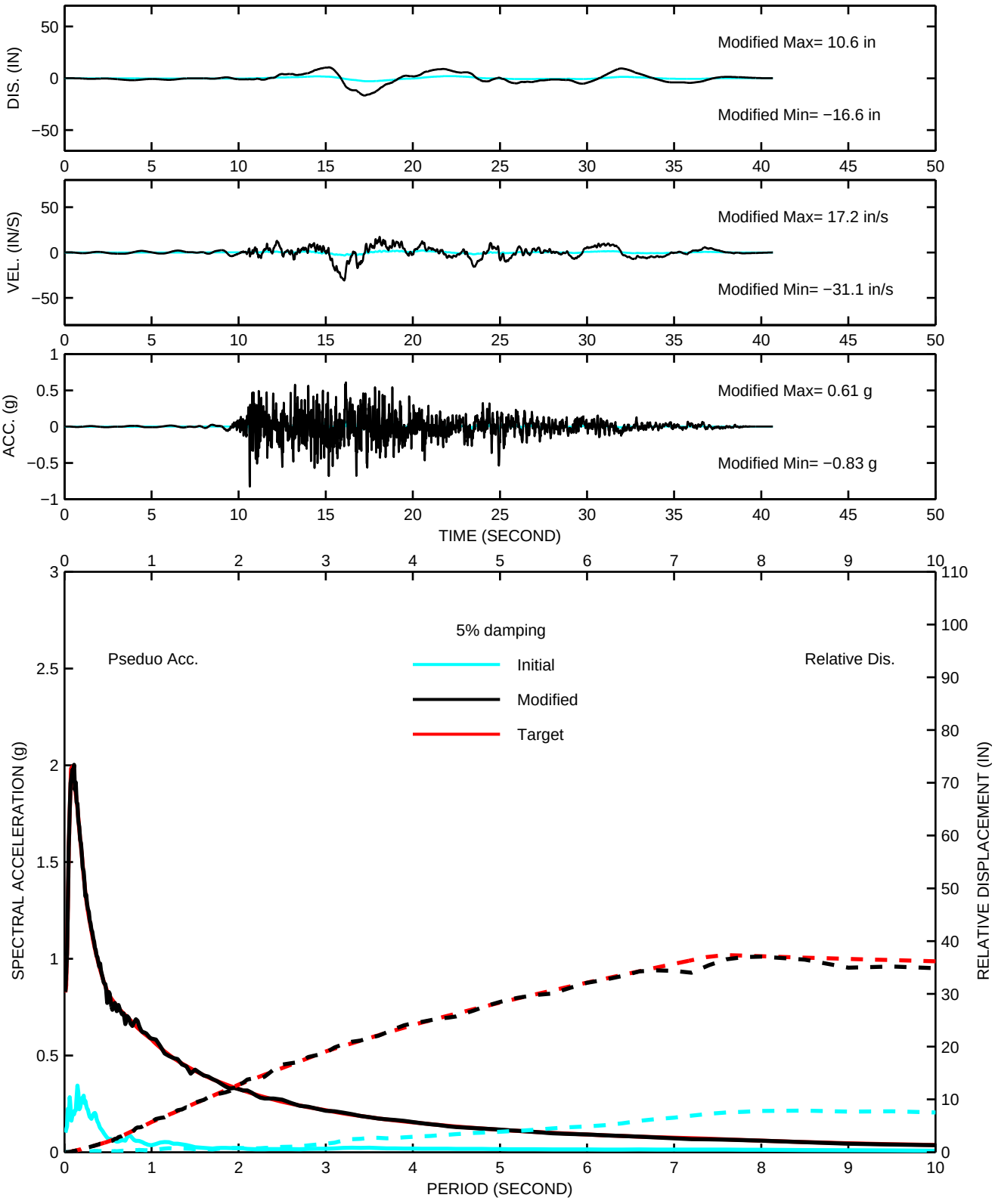


Figure B75. Firm−Ground MCEr Spectrum Compatible Ground Motion (5% Damped) − Set 4 Vertical

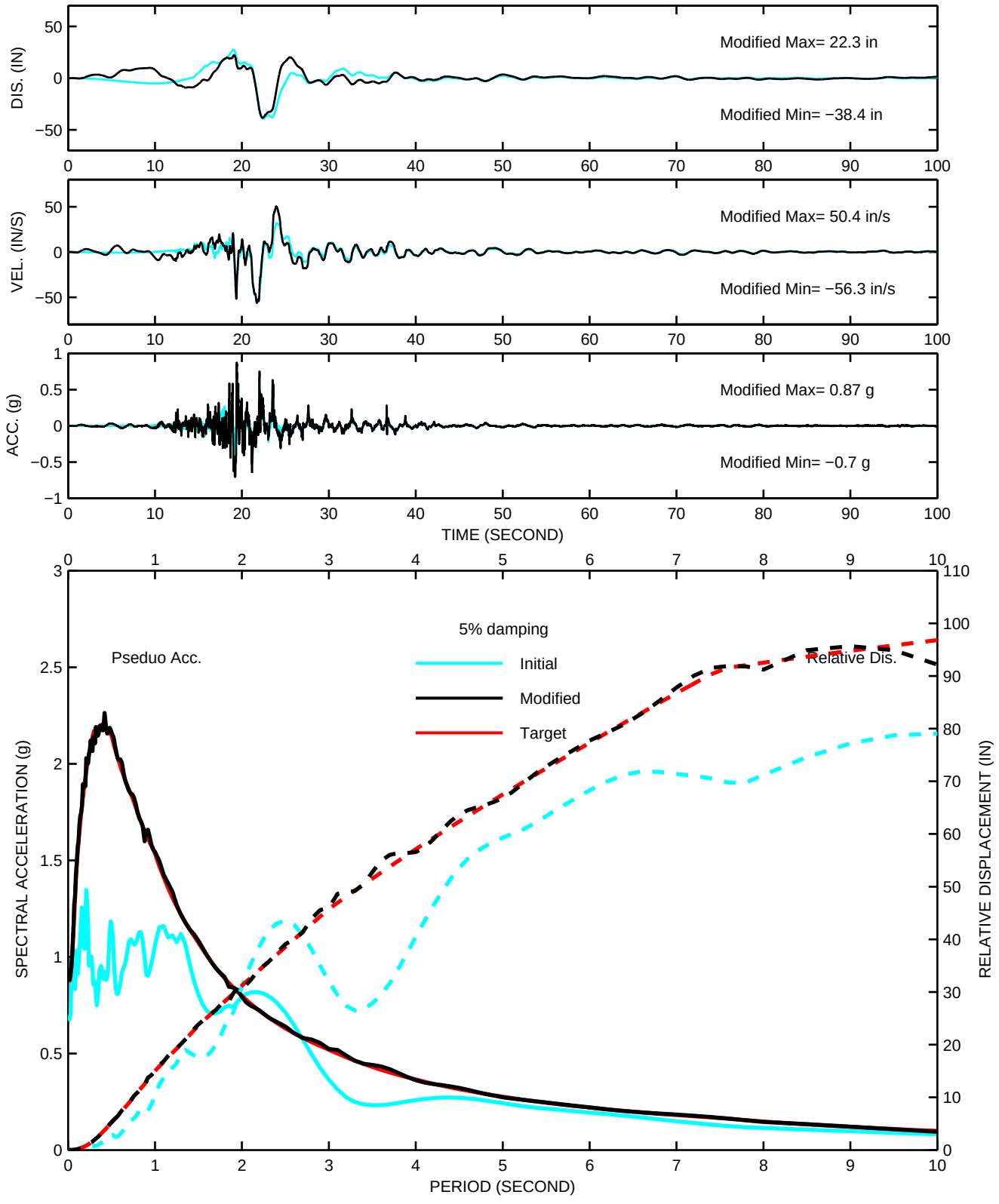


Figure B76. Firm−Ground MCEr Spectrum Compatible Ground Motion (5% Damped) − Set 5 Fault Normal

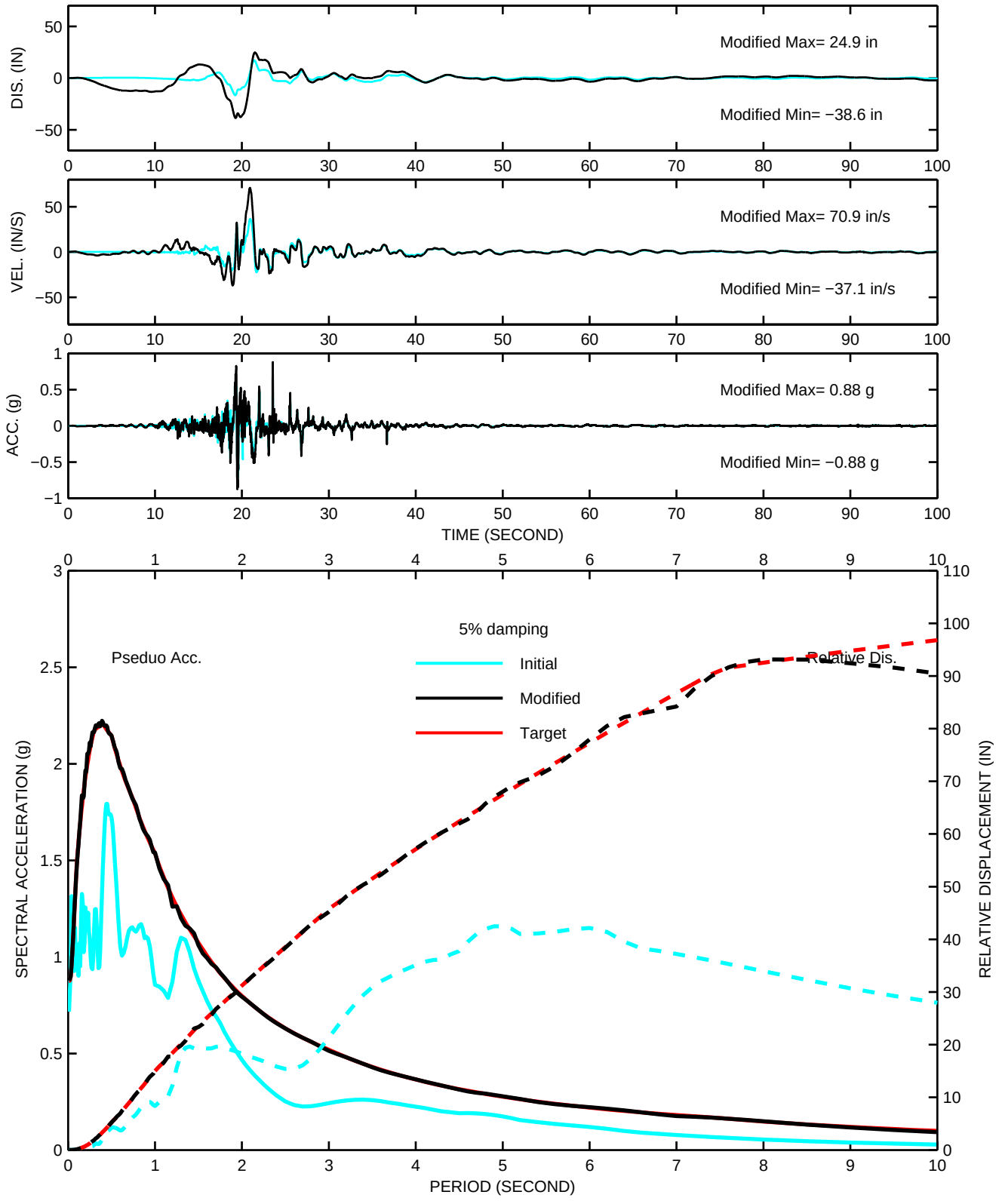


Figure B77. Firm−Ground MCEr Spectrum Compatible Ground Motion (5% Damped) − Set 5 Fault Parallel

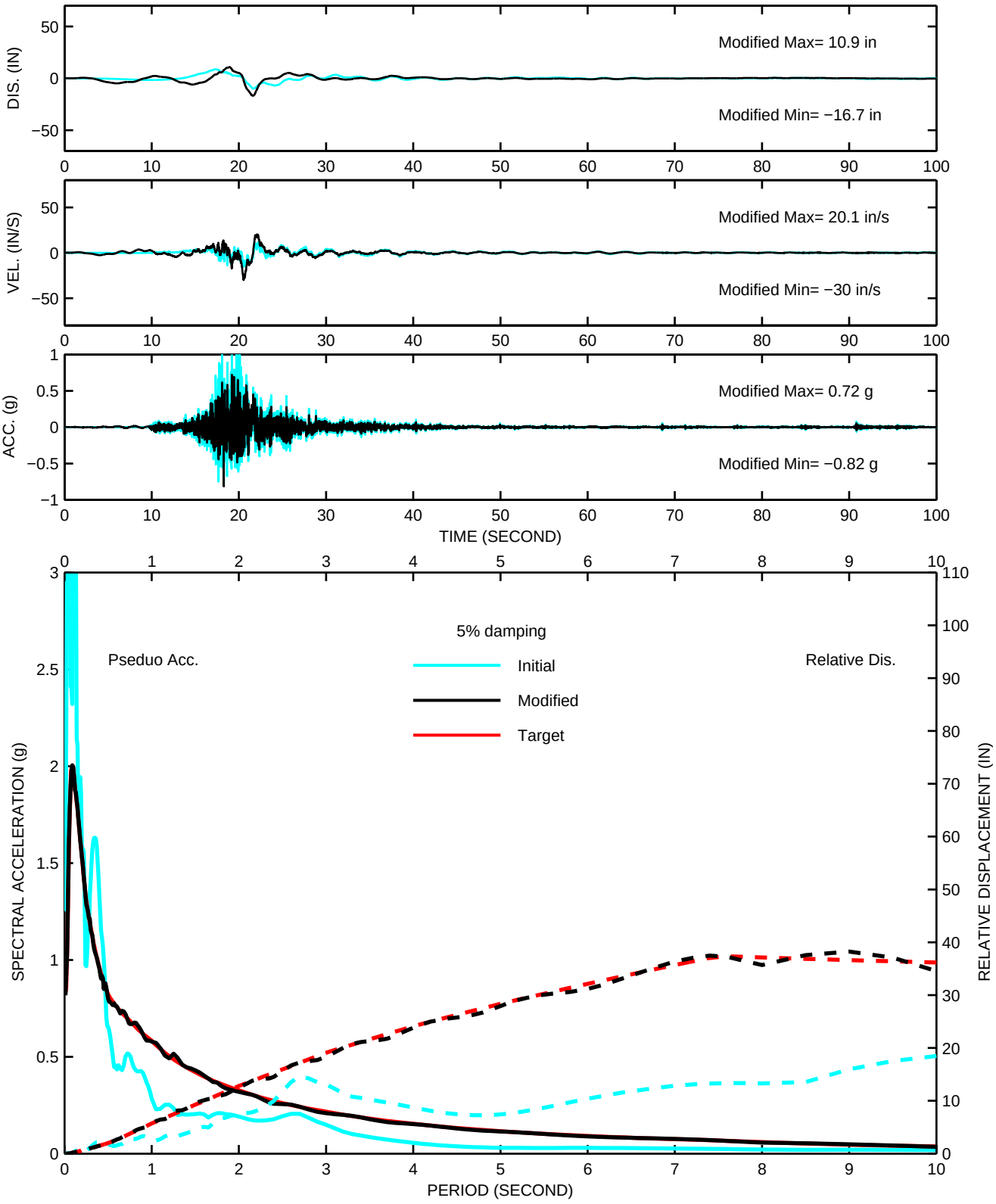


Figure B78. Firm−Ground MCEr Spectrum Compatible Ground Motion (5% Damped) − Set 5 Vertical

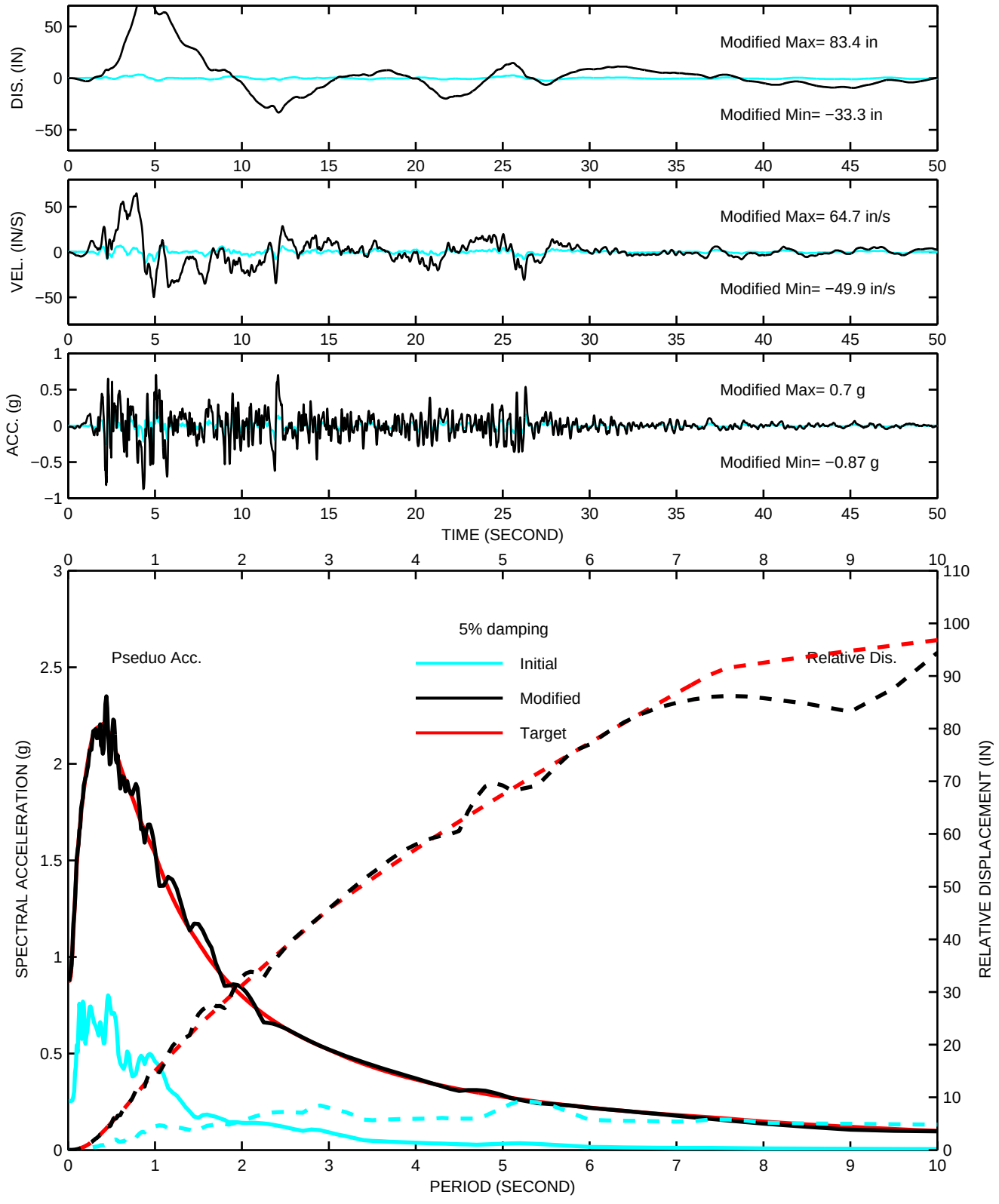


Figure B79. Firm−Ground MCEr Spectrum Compatible Ground Motion (5% Damped) − Set 6 Fault Normal

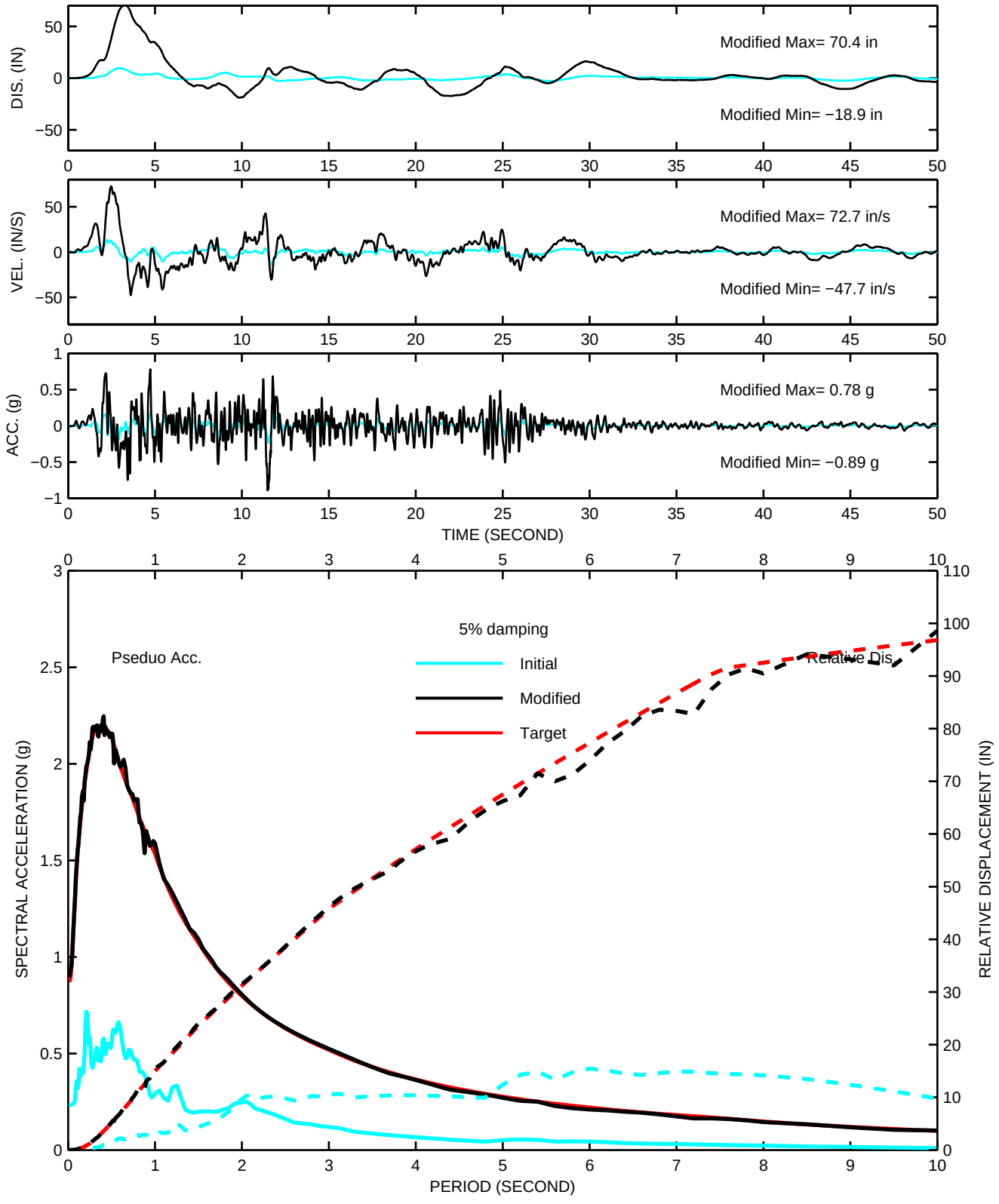


Figure B80. Firm−Ground MCEr Spectrum Compatible Ground Motion (5% Damped) − Set 6 Fault Parallel

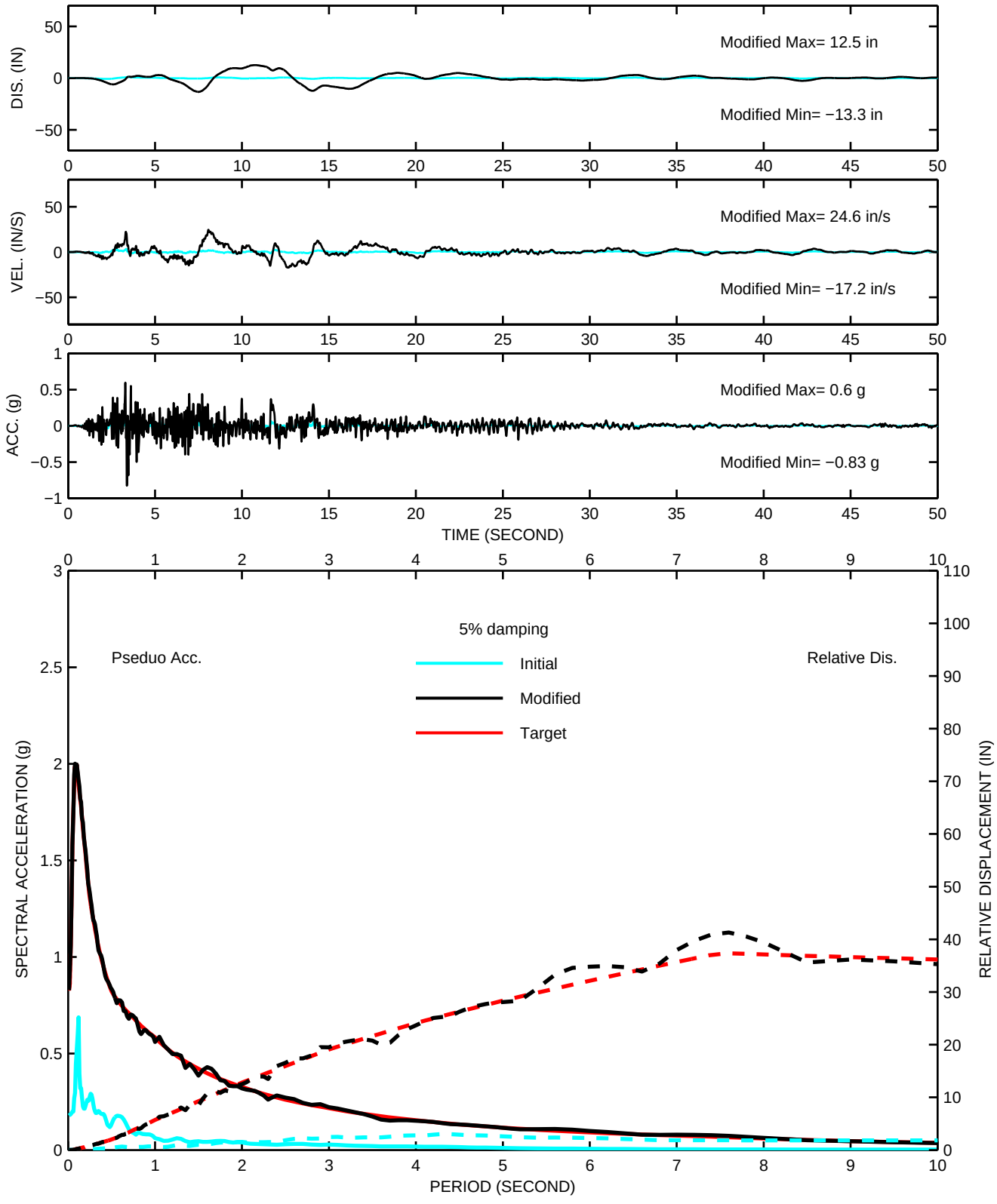


Figure B81. Firm−Ground MCEr Spectrum Compatible Ground Motion (5% Damped) − Set 6 Vertical

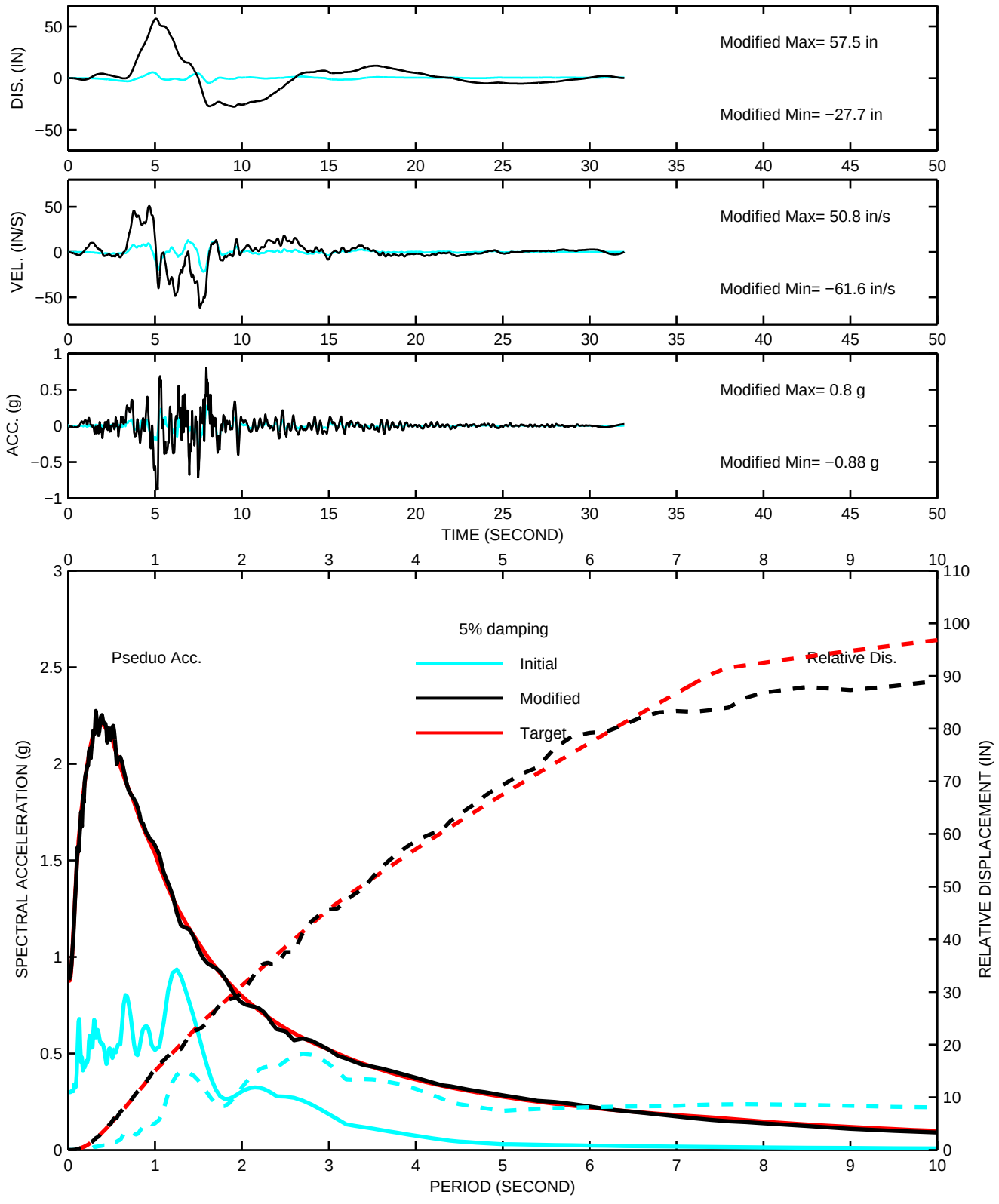


Figure B82. Firm−Ground MCEr Spectrum Compatible Ground Motion (5% Damped) − Set 7 Fault Normal

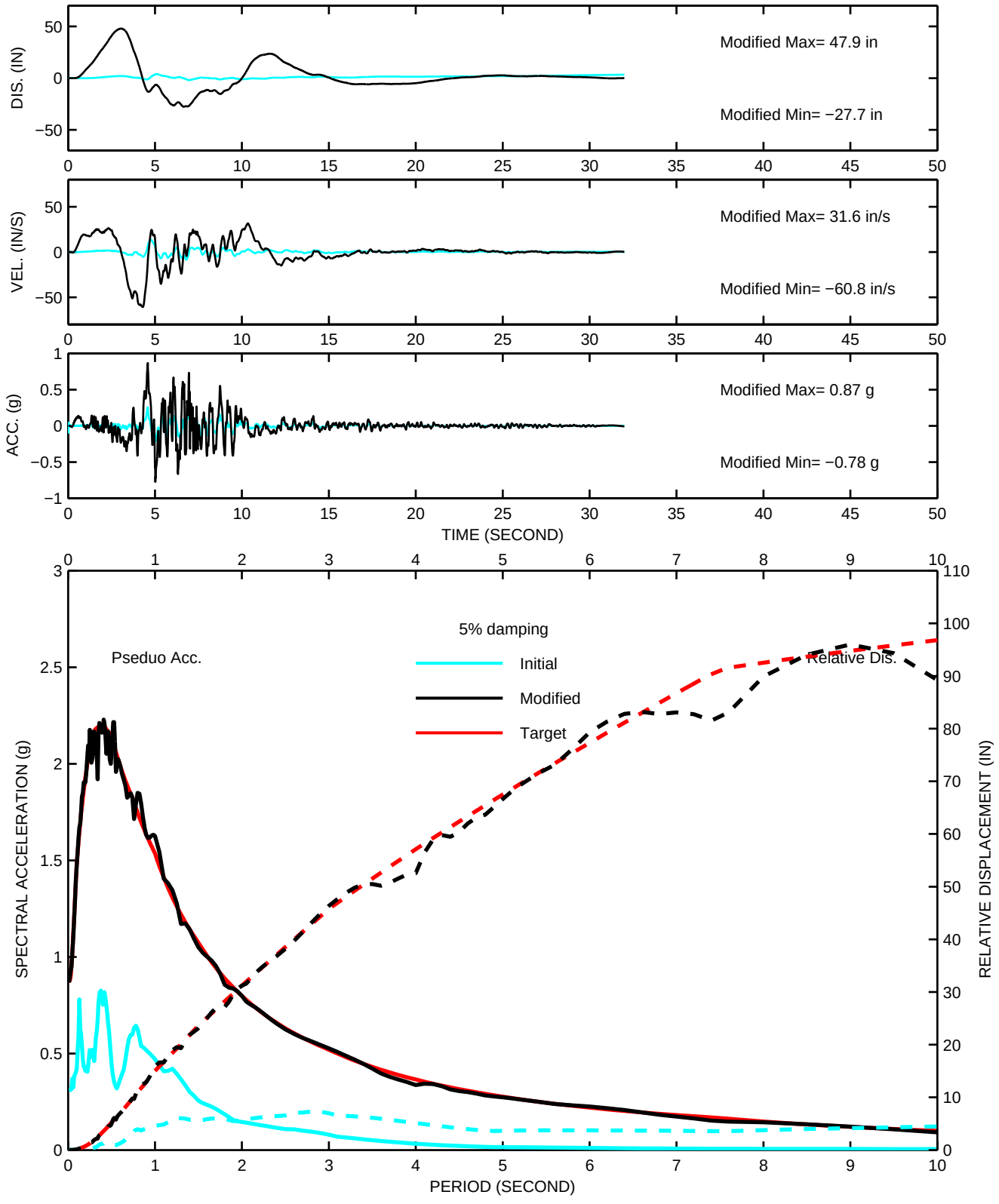


Figure B83. Firm−Ground MCEr Spectrum Compatible Ground Motion (5% Damped) − Set 7 Fault Parallel

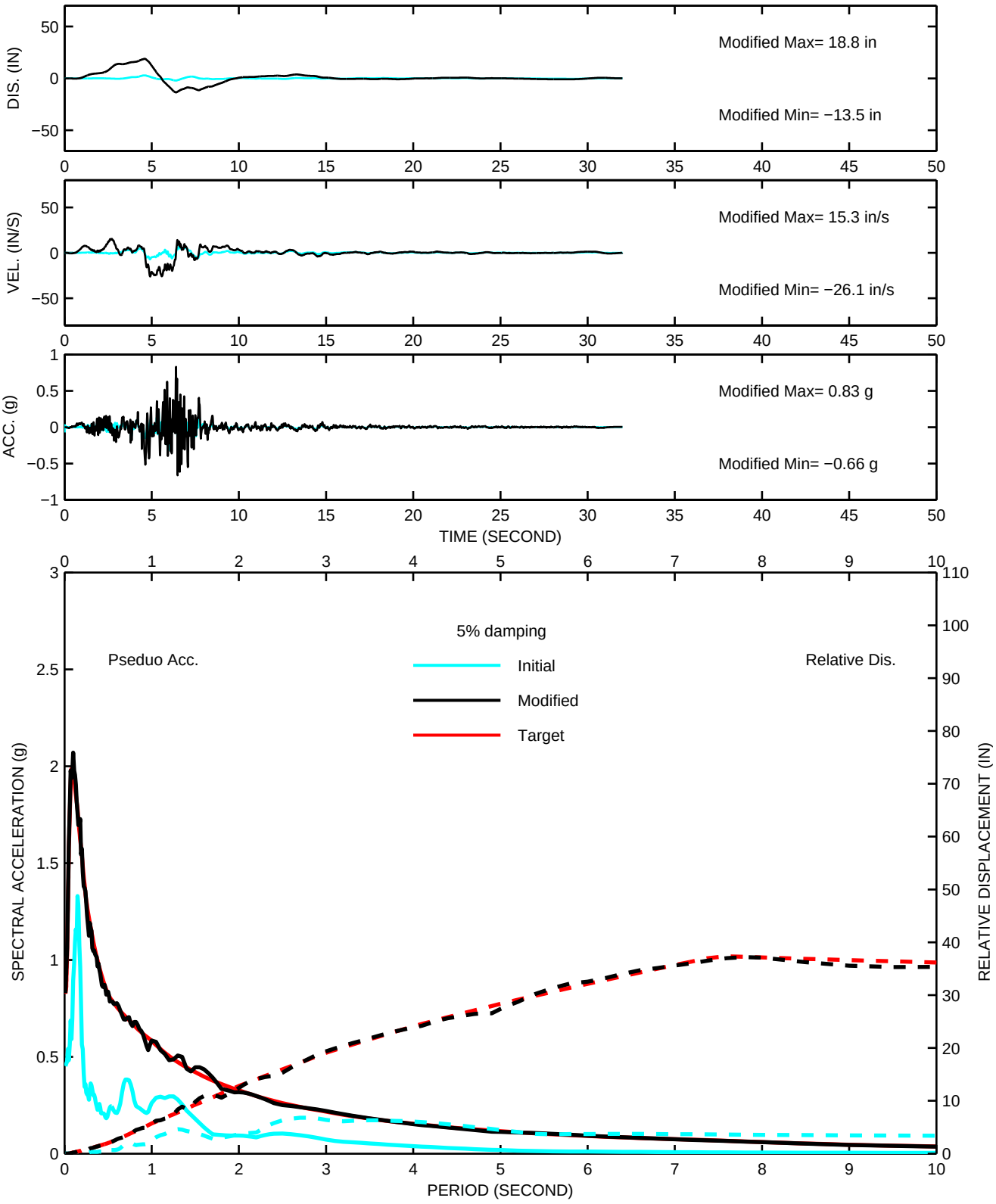


Figure B84. Firm−Ground MCEr Spectrum Compatible Ground Motion (5% Damped) − Set 7 Vertical

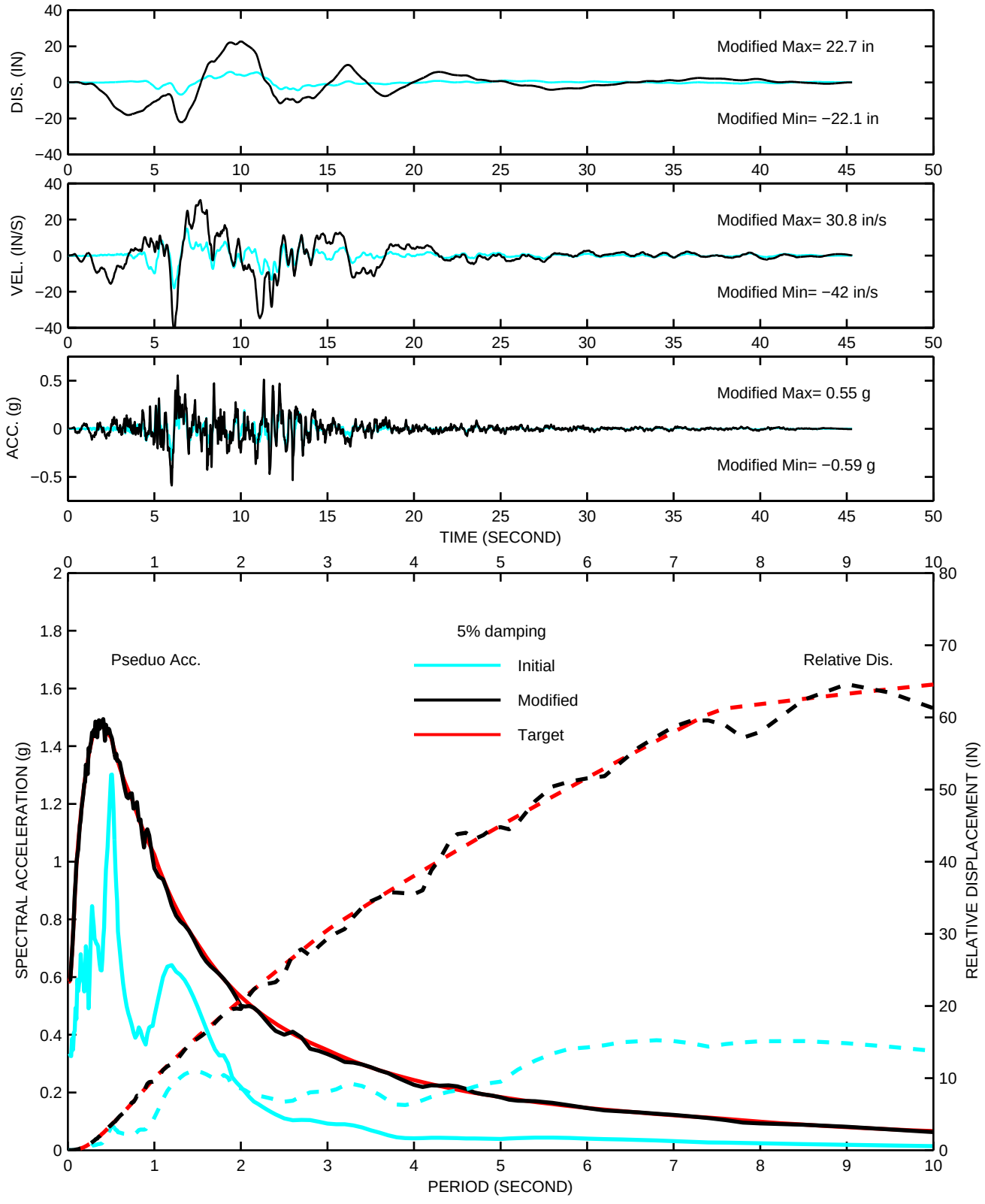


Figure B85. Firm−Ground DE Spectrum Compatible Ground Motion (5% Damped) − Set 1 Fault Normal

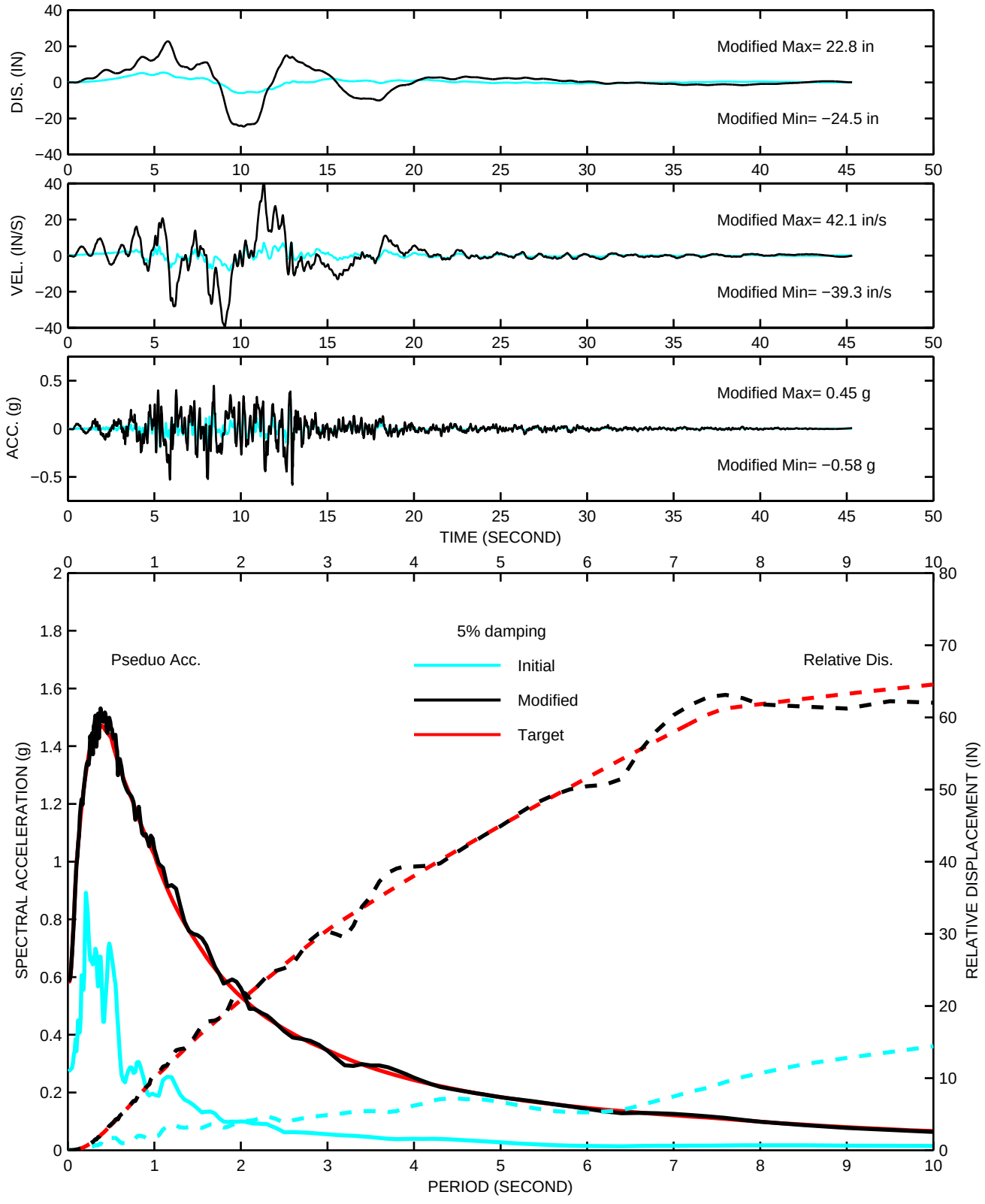


Figure B86. Firm−Ground DE Spectrum Compatible Ground Motion (5% Damped) − Set 1 Fault Parallel

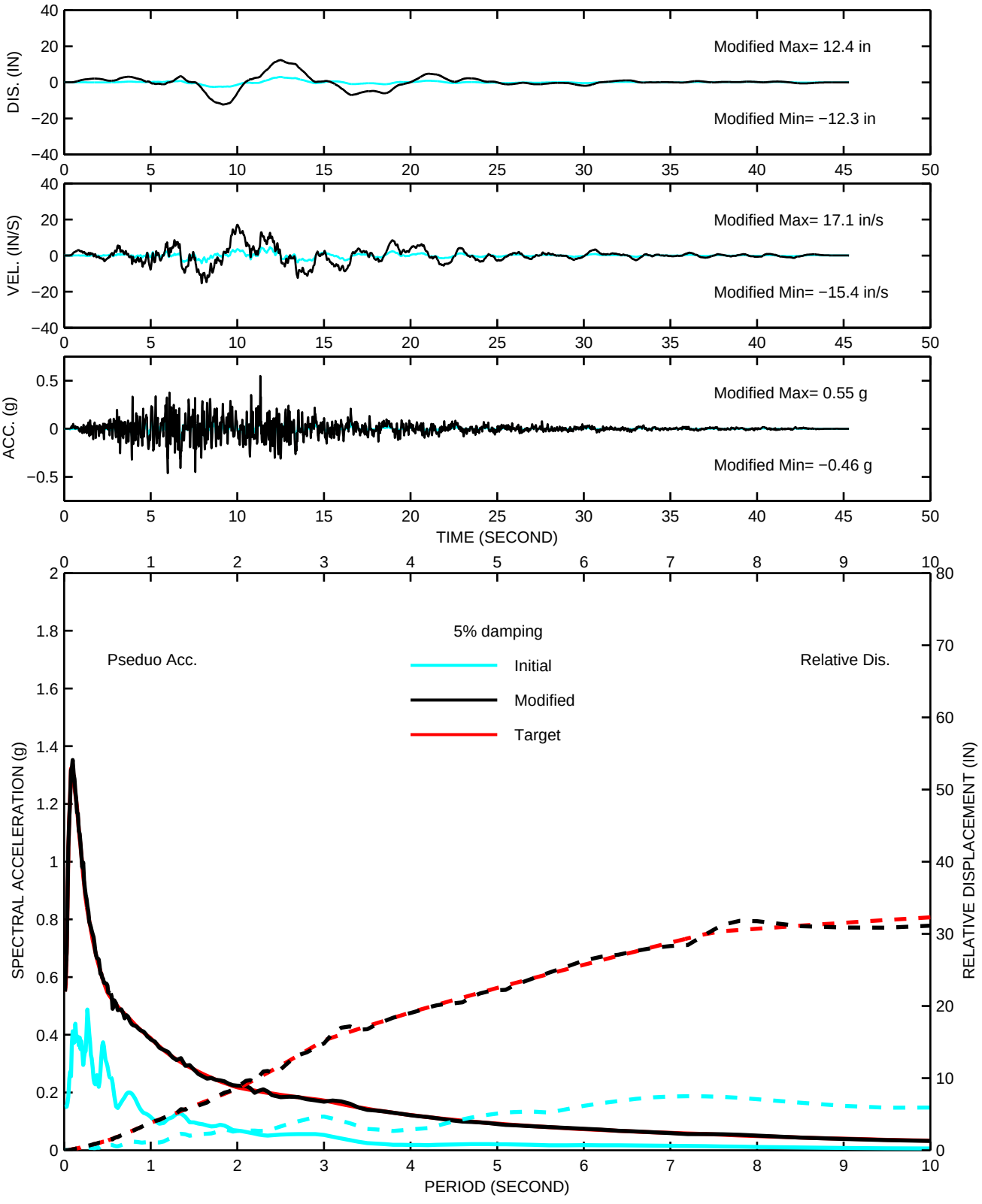


Figure B87. Firm−Ground DE Spectrum Compatible Ground Motion (5% Damped) − Set 1 Vertical

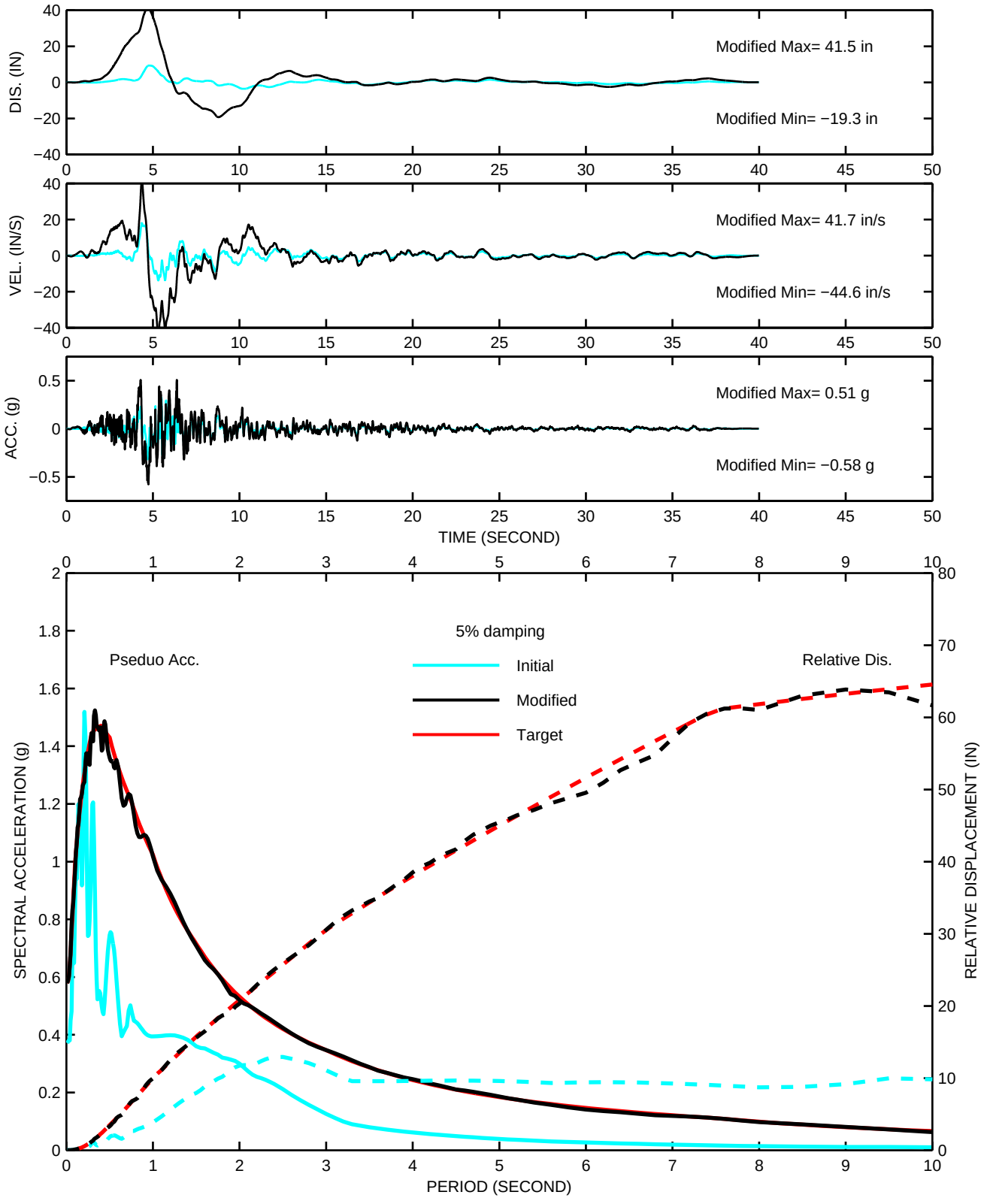


Figure B88. Firm−Ground DE Spectrum Compatible Ground Motion (5% Damped) − Set 2 Fault Normal

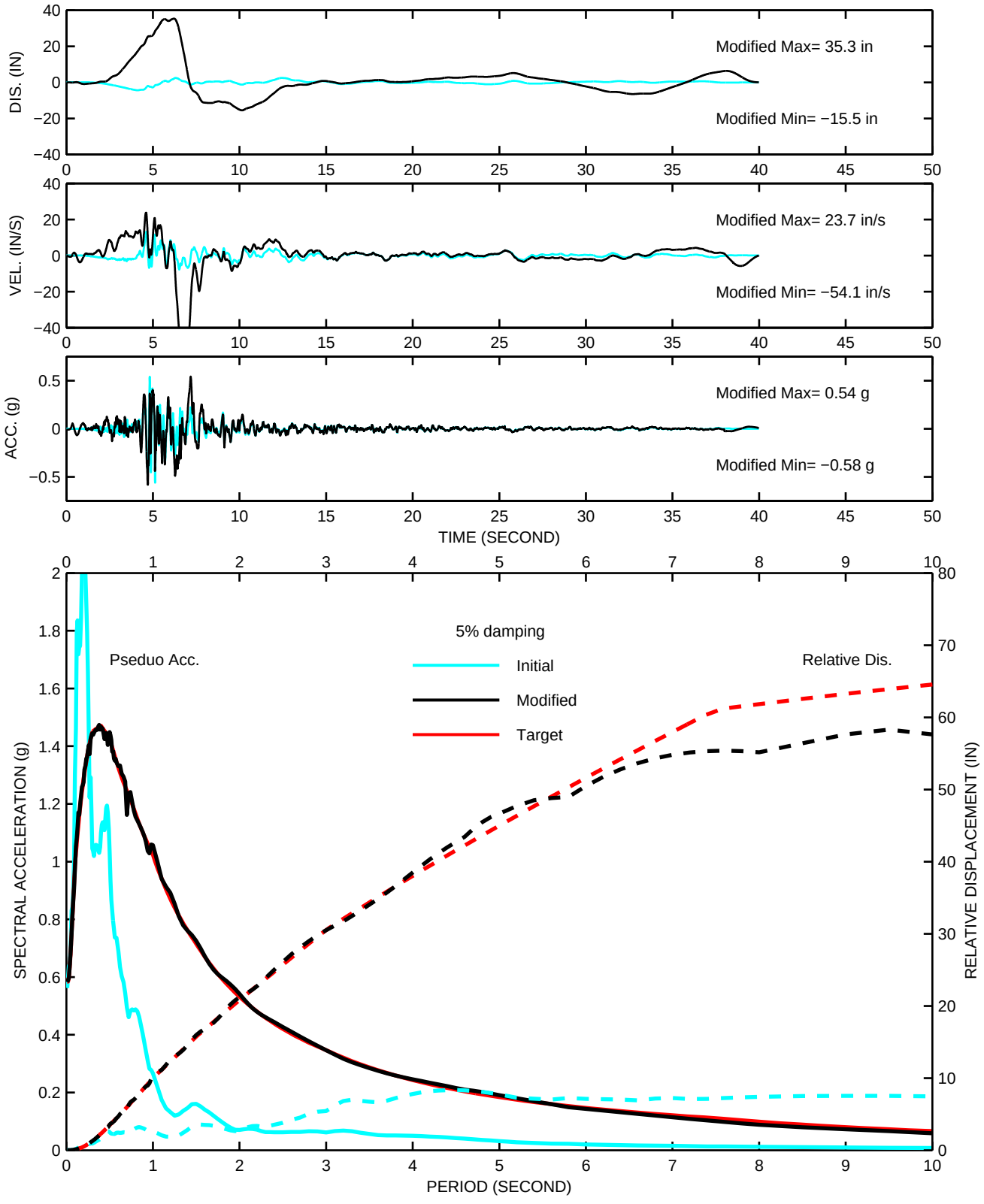


Figure B89. Firm−Ground DE Spectrum Compatible Ground Motion (5% Damped) − Set 2 Fault Parallel

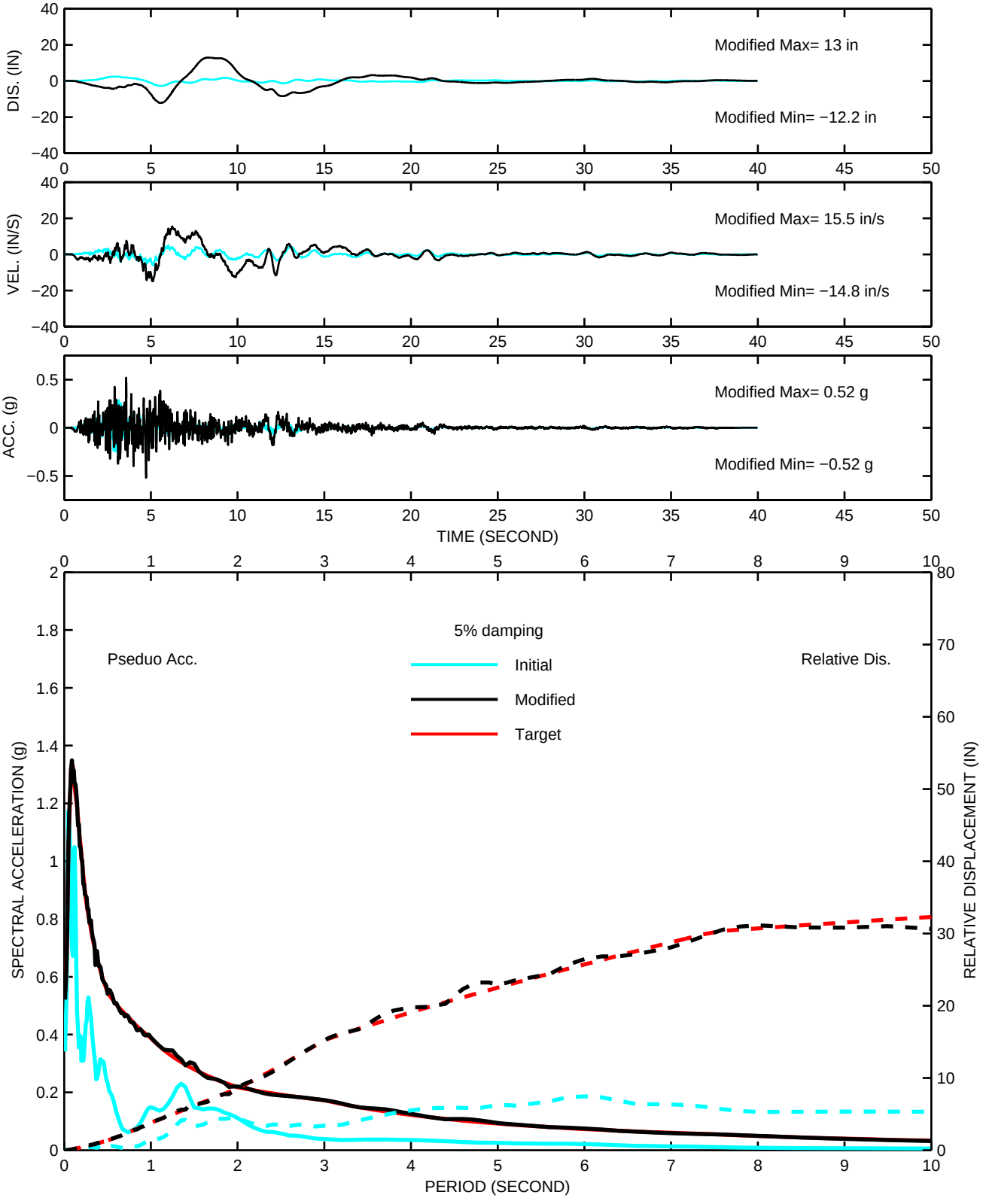


Figure B90. Firm−Ground DE Spectrum Compatible Ground Motion (5% Damped) − Set 2 Vertical

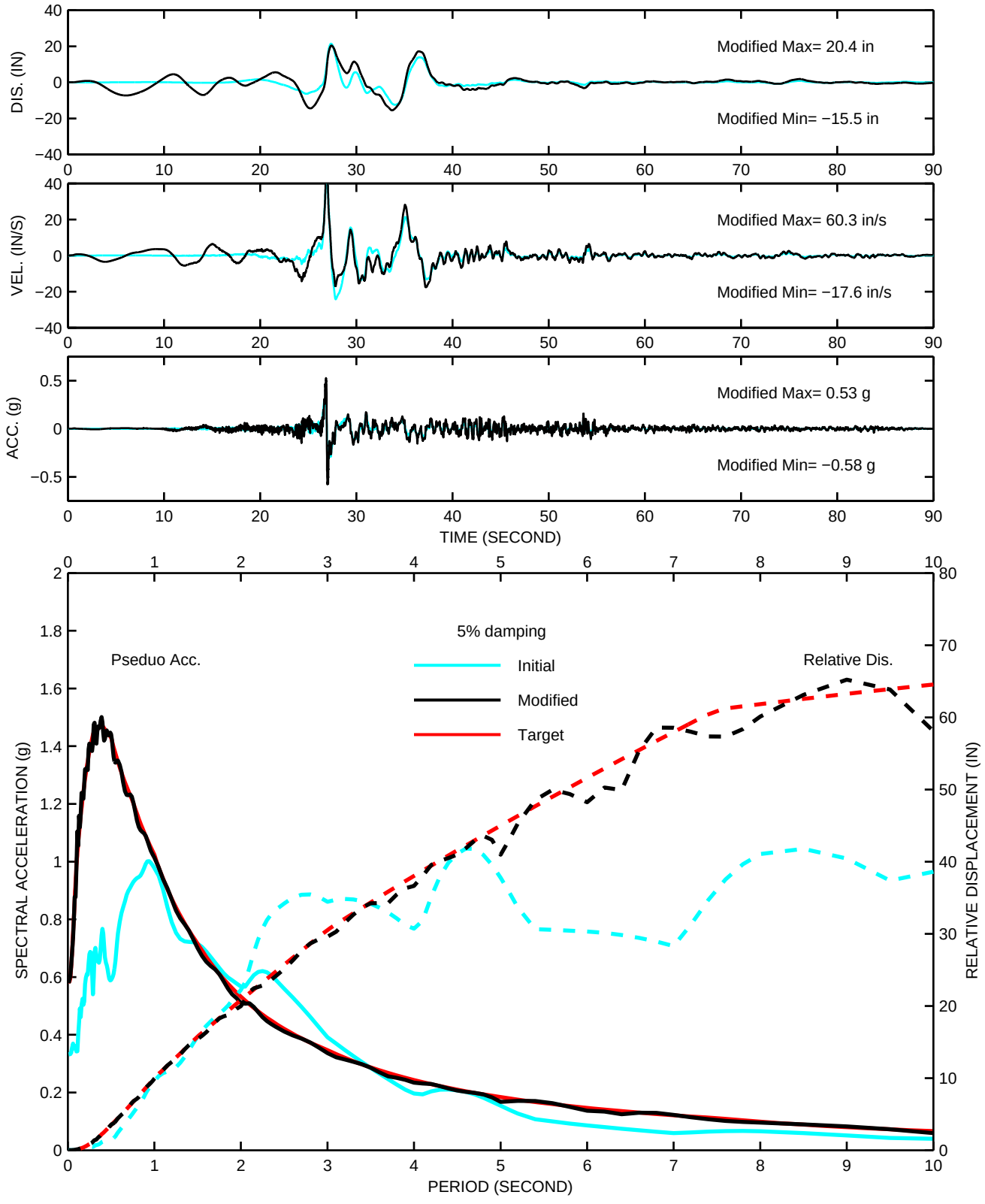


Figure B91. Firm−Ground DE Spectrum Compatible Ground Motion (5% Damped) − Set 3 Fault Normal

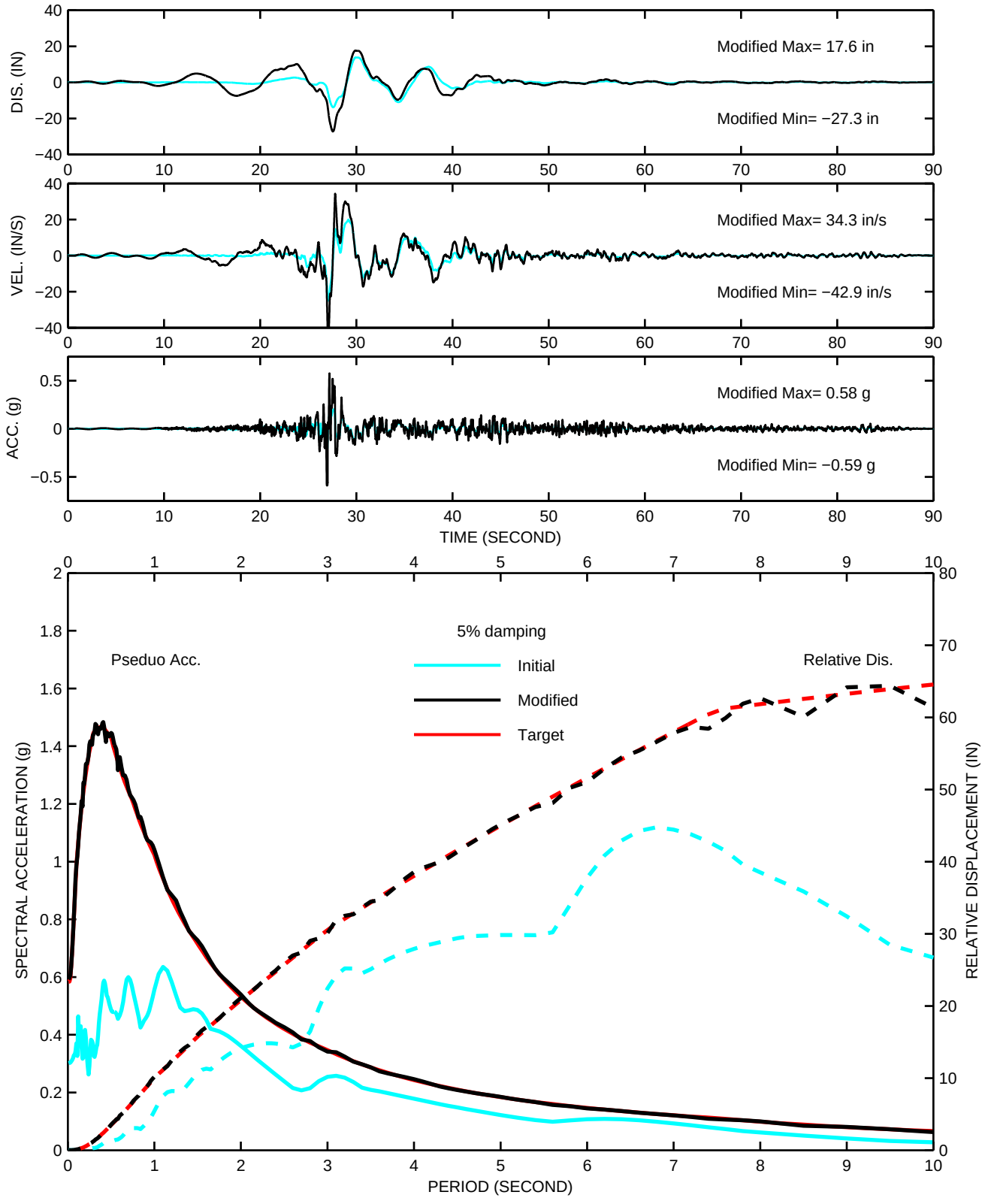


Figure B92. Firm−Ground DE Spectrum Compatible Ground Motion (5% Damped) − Set 3 Fault Parallel

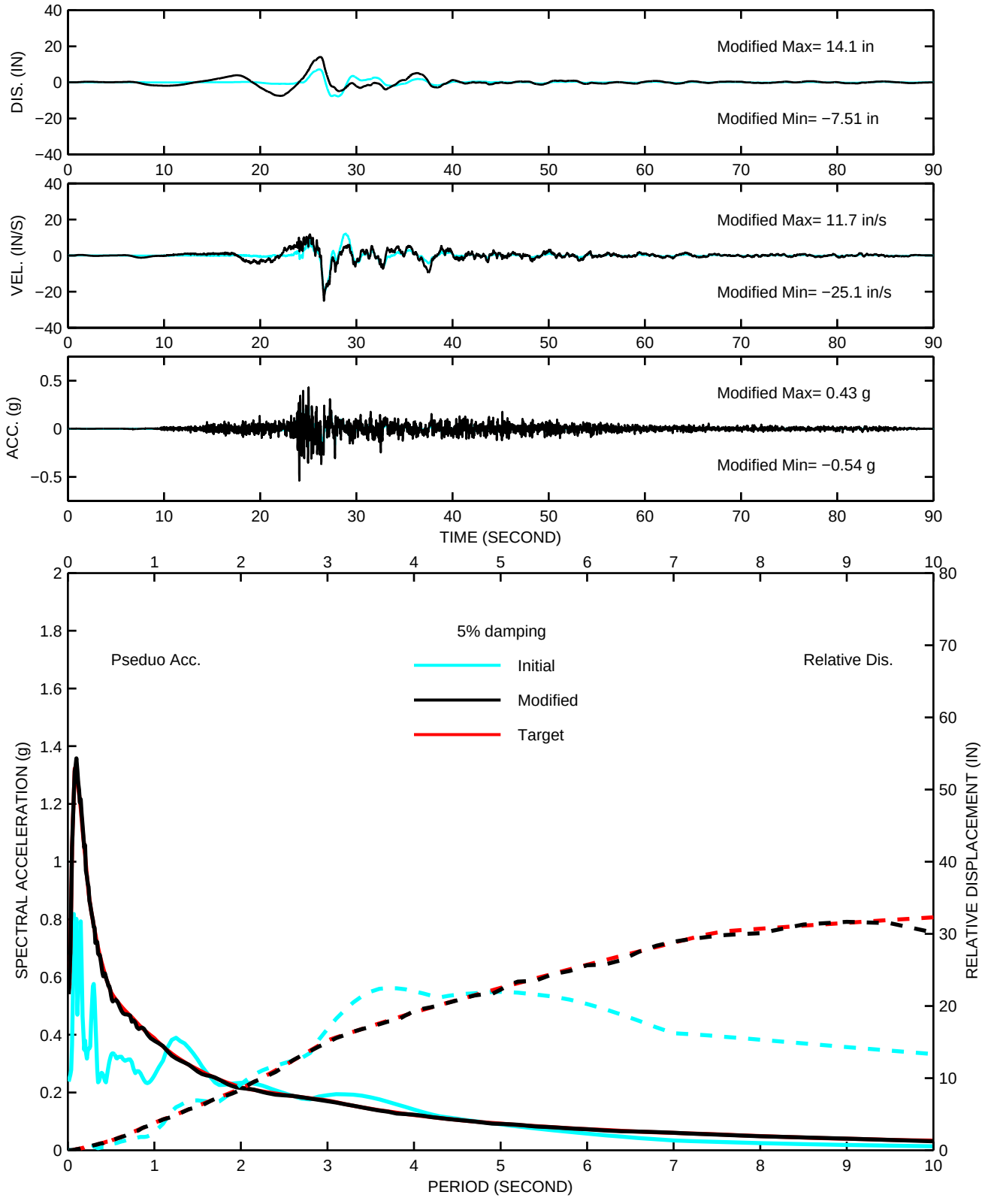


Figure B93. Firm−Ground DE Spectrum Compatible Ground Motion (5% Damped) − Set 3 Vertical

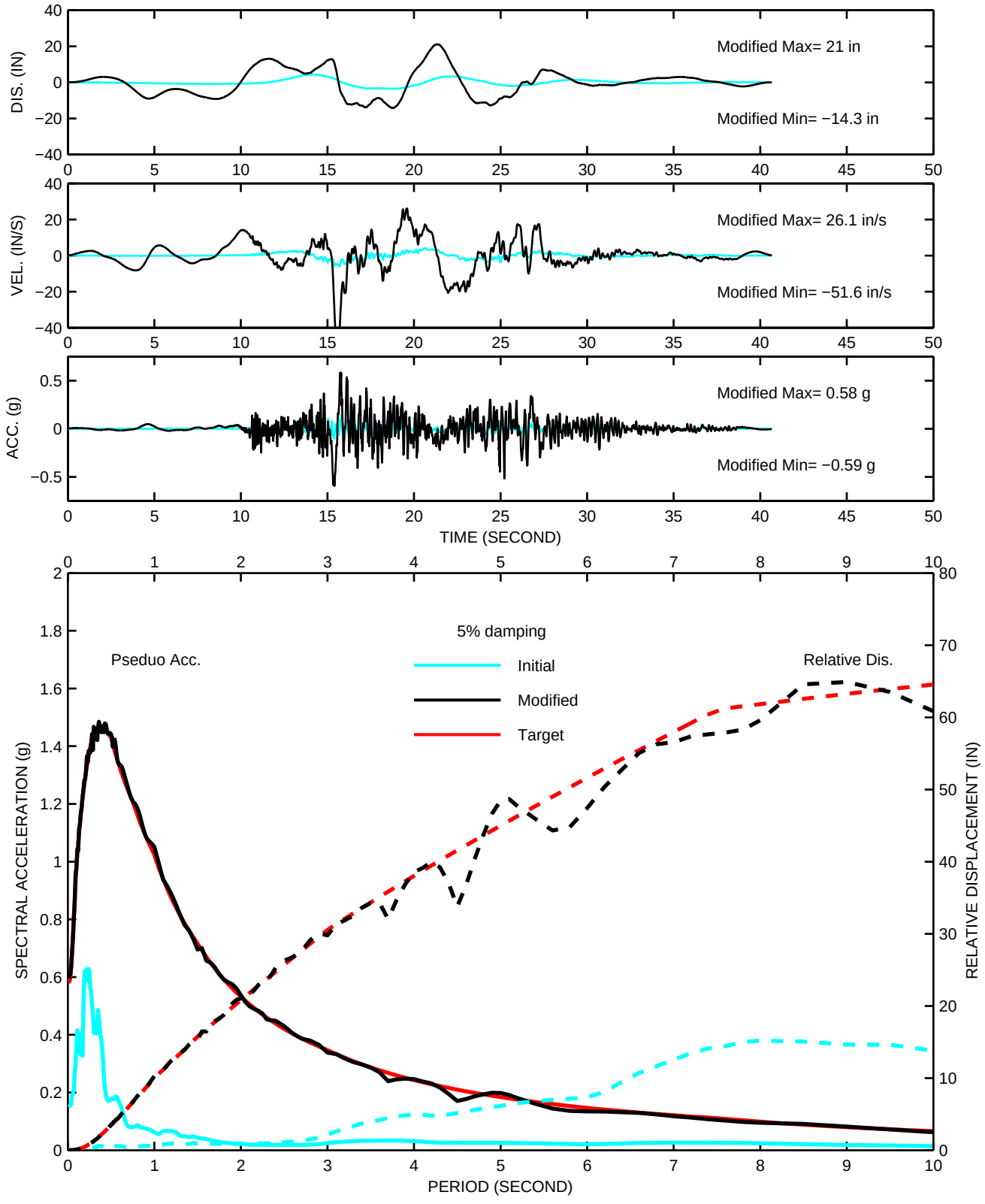


Figure B94. Firm−Ground DE Spectrum Compatible Ground Motion (5% Damped) − Set 4 Fault Normal

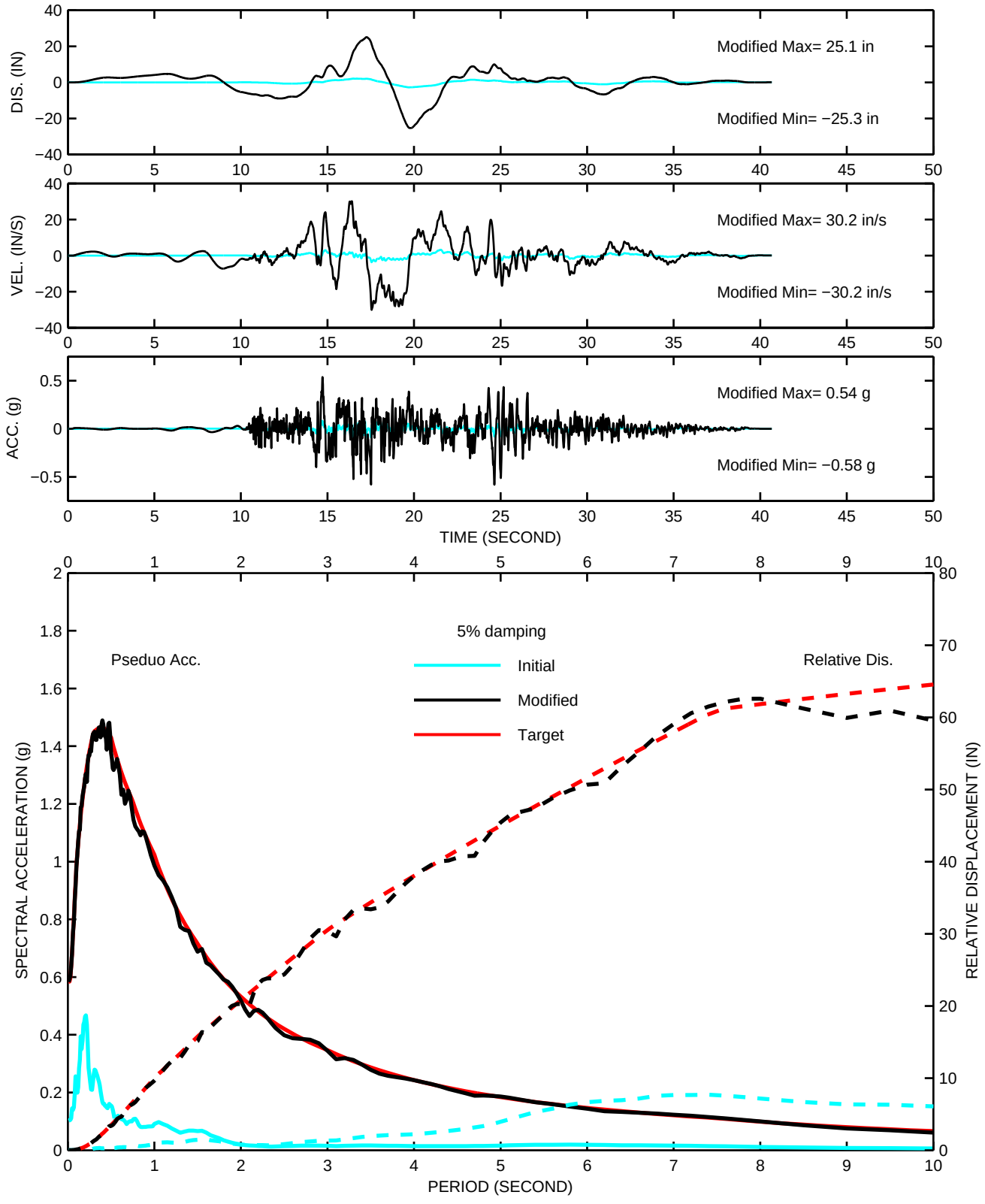


Figure B95. Firm−Ground DE Spectrum Compatible Ground Motion (5% Damped) − Set 4 Fault Parallel

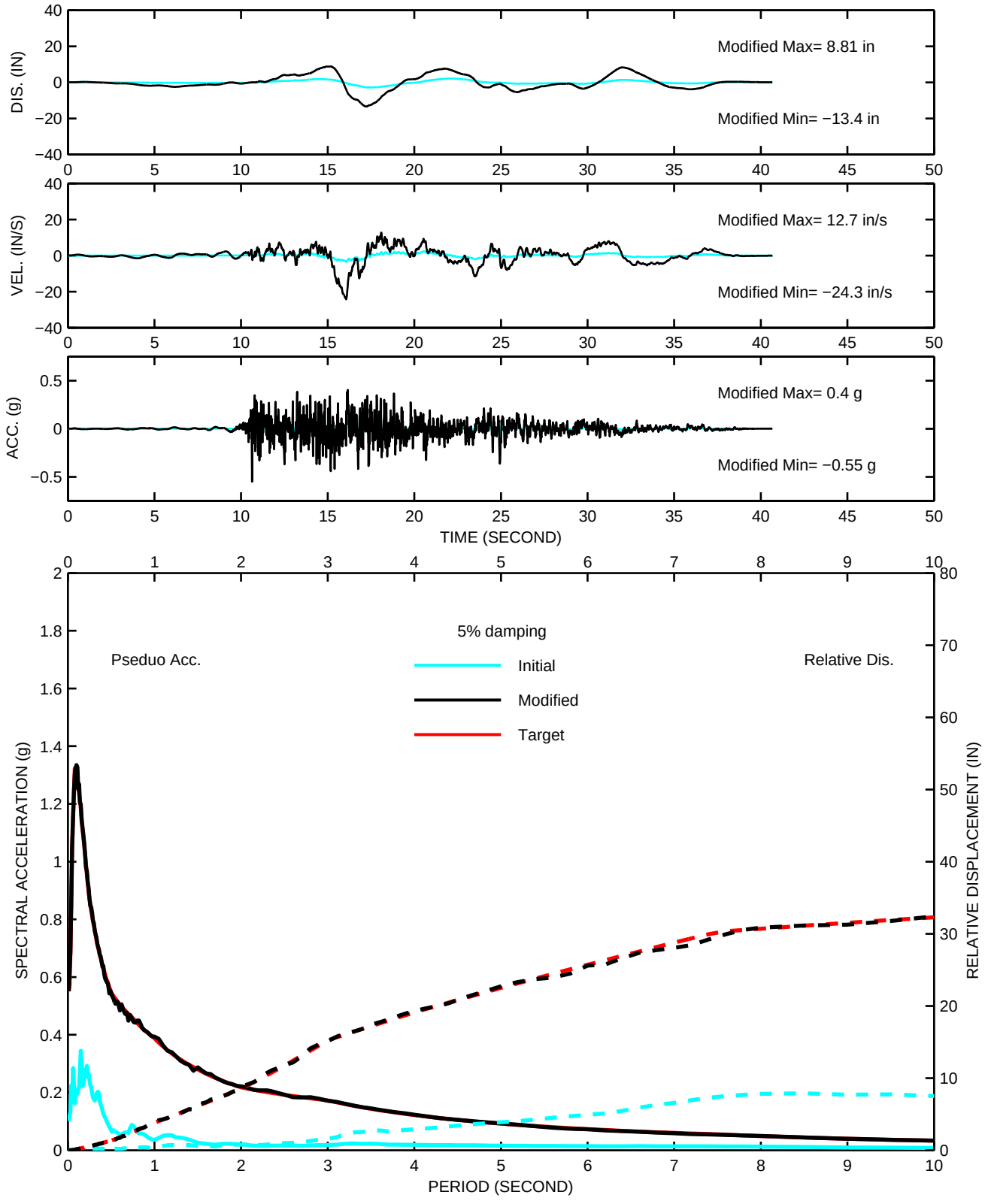


Figure B96. Firm−Ground DE Spectrum Compatible Ground Motion (5% Damped) − Set 4 Vertical

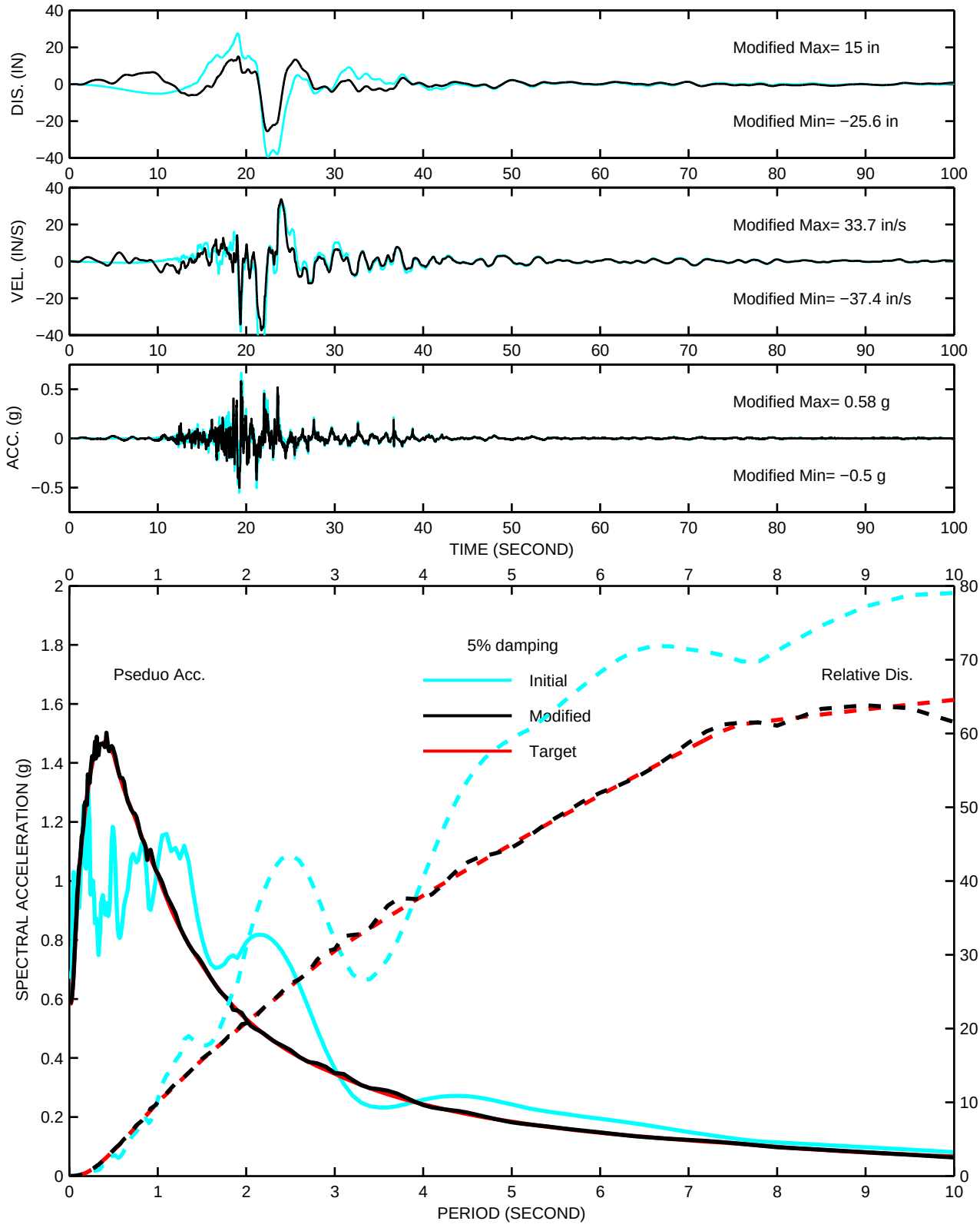


Figure B97. Firm−Ground DE Spectrum Compatible Ground Motion (5% Damped) − Set 5 Fault Normal

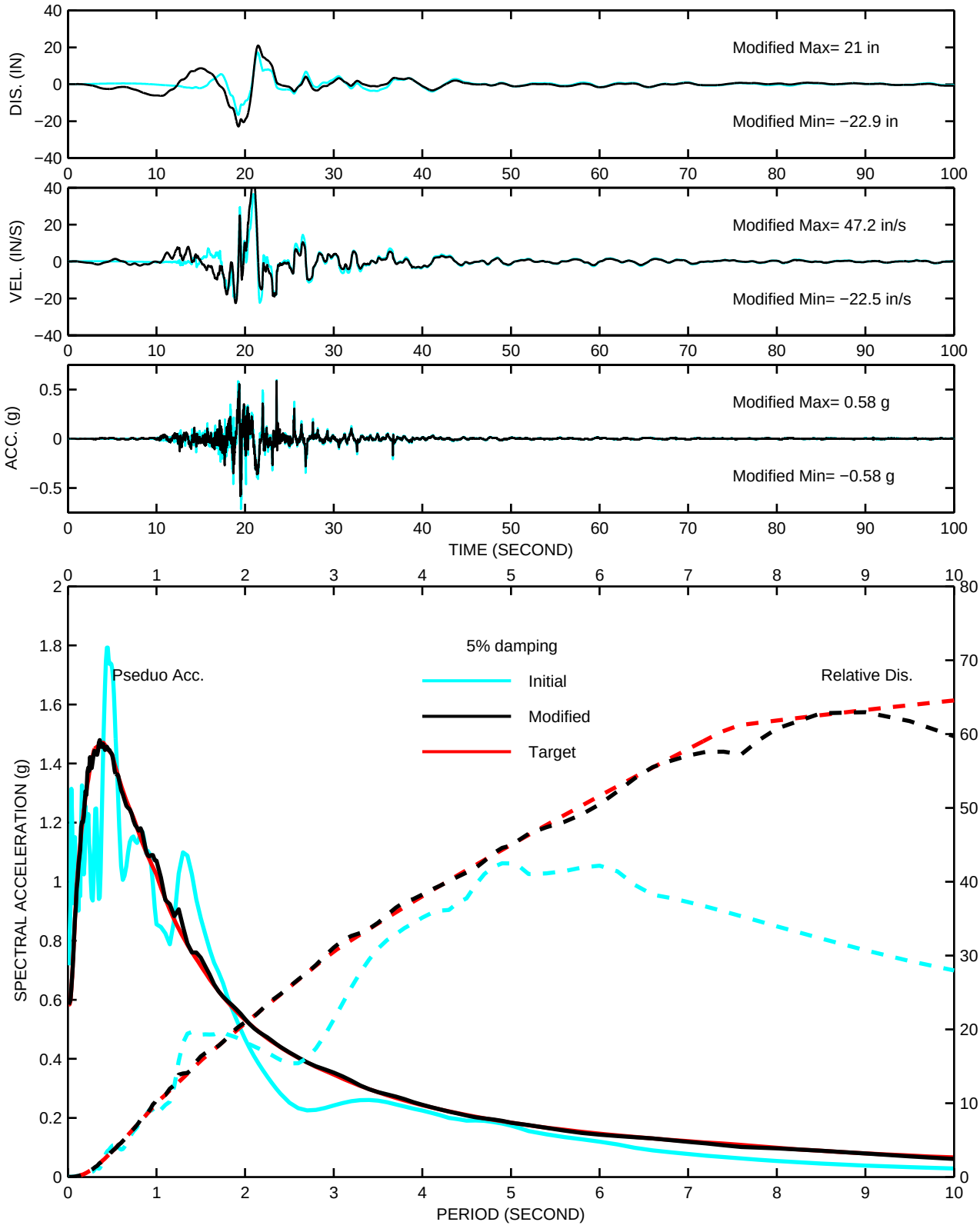


Figure B98. Firm−Ground DE Spectrum Compatible Ground Motion (5% Damped) − Set 5 Fault Parallel

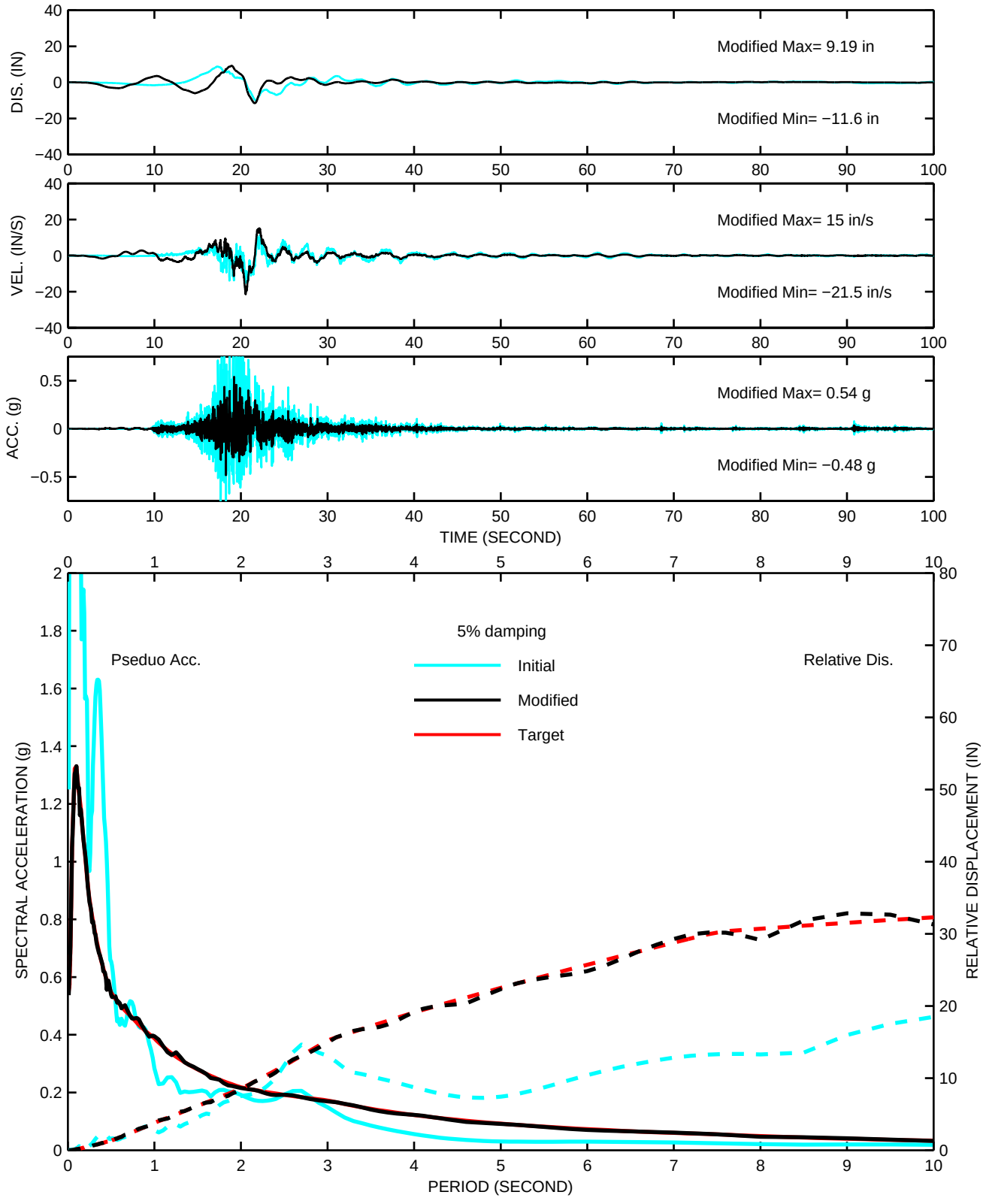


Figure B99. Firm−Ground DE Spectrum Compatible Ground Motion (5% Damped) − Set 5 Vertical

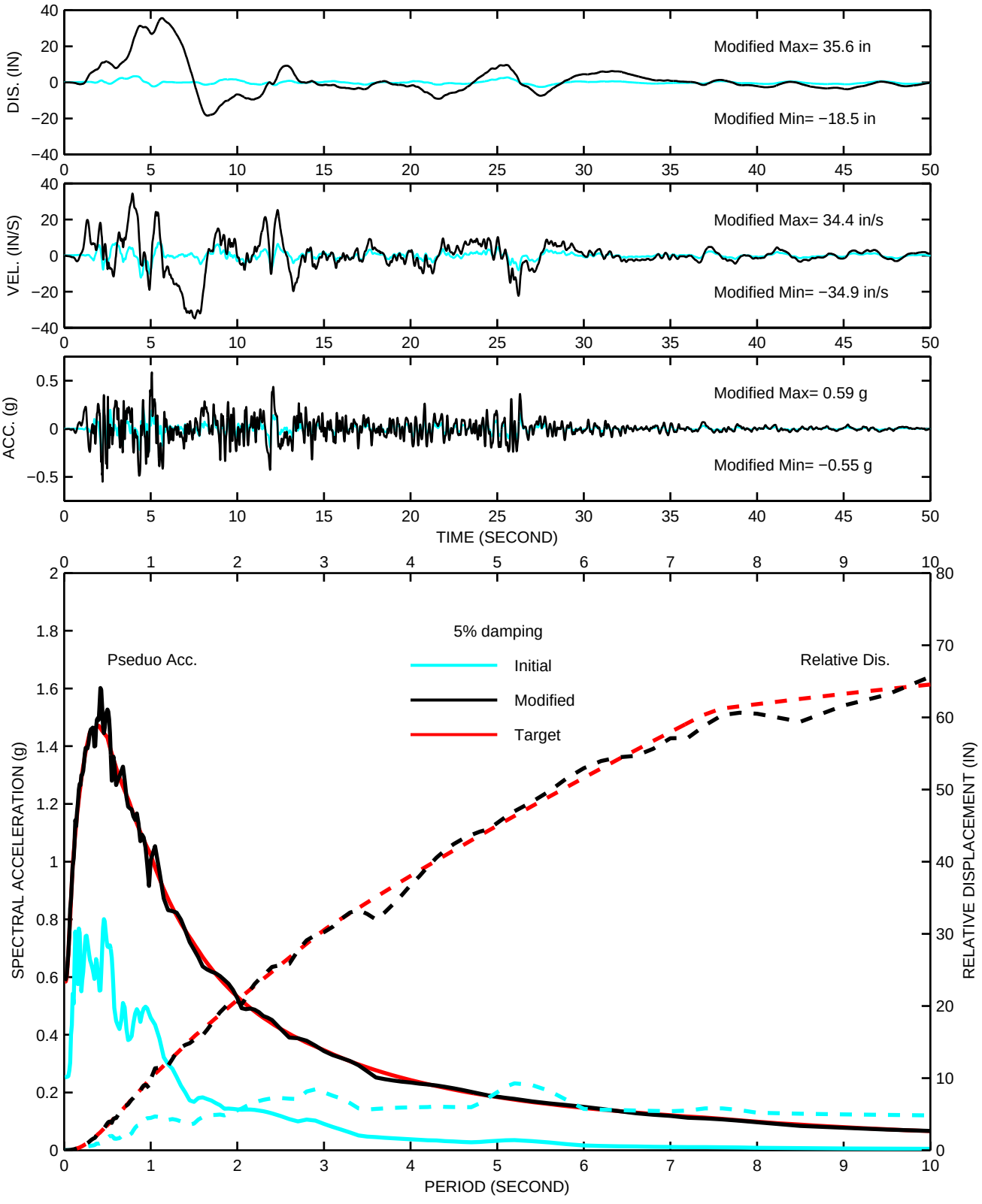


Figure B100. Firm−Ground DE Spectrum Compatible Ground Motion (5% Damped) − Set 6 Fault Normal

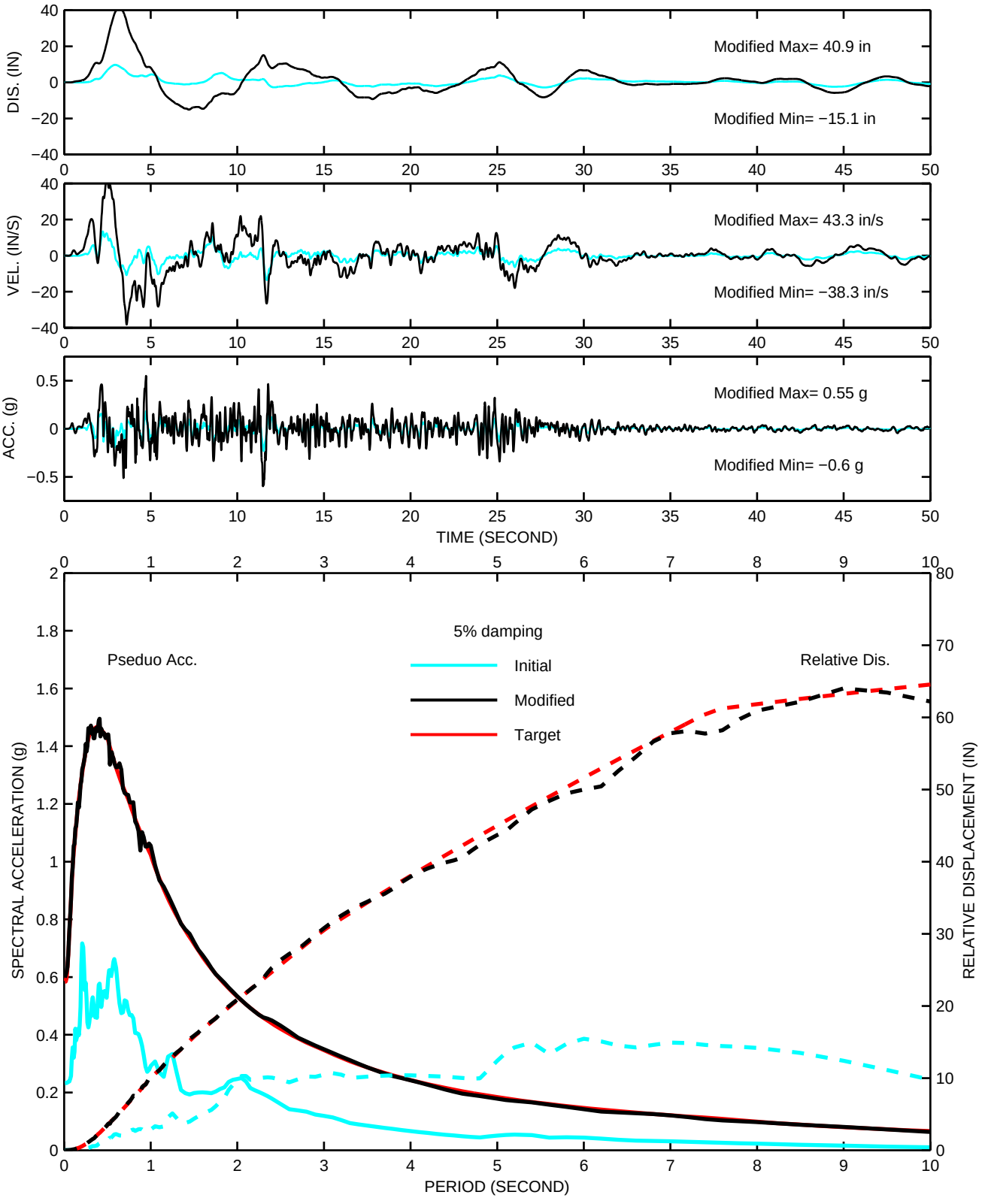


Figure B101. Firm−Ground DE Spectrum Compatible Ground Motion (5% Damped) − Set 6 Fault Parallel

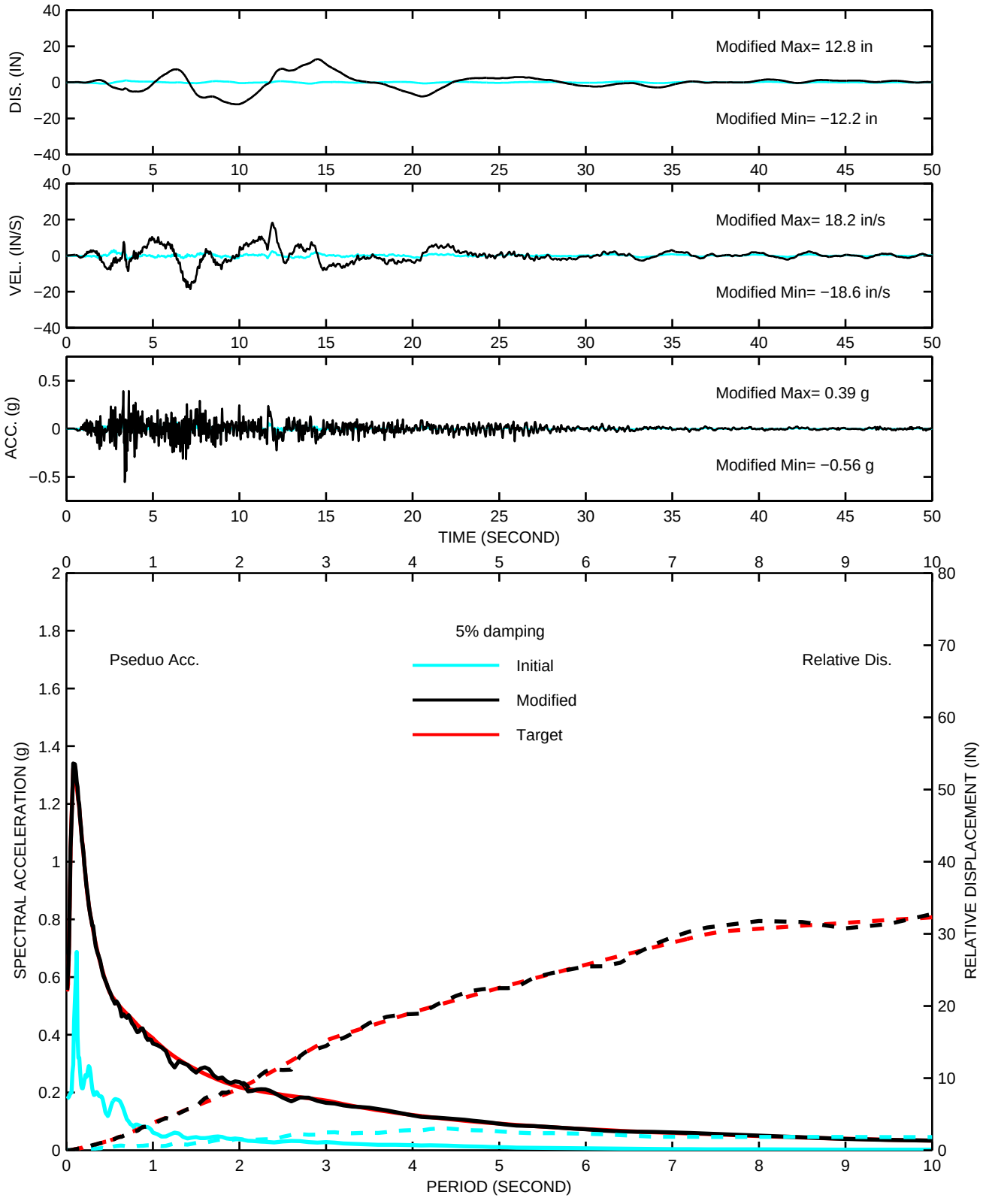


Figure B102. Firm−Ground DE Spectrum Compatible Ground Motion (5% Damped) − Set 6 Vertical

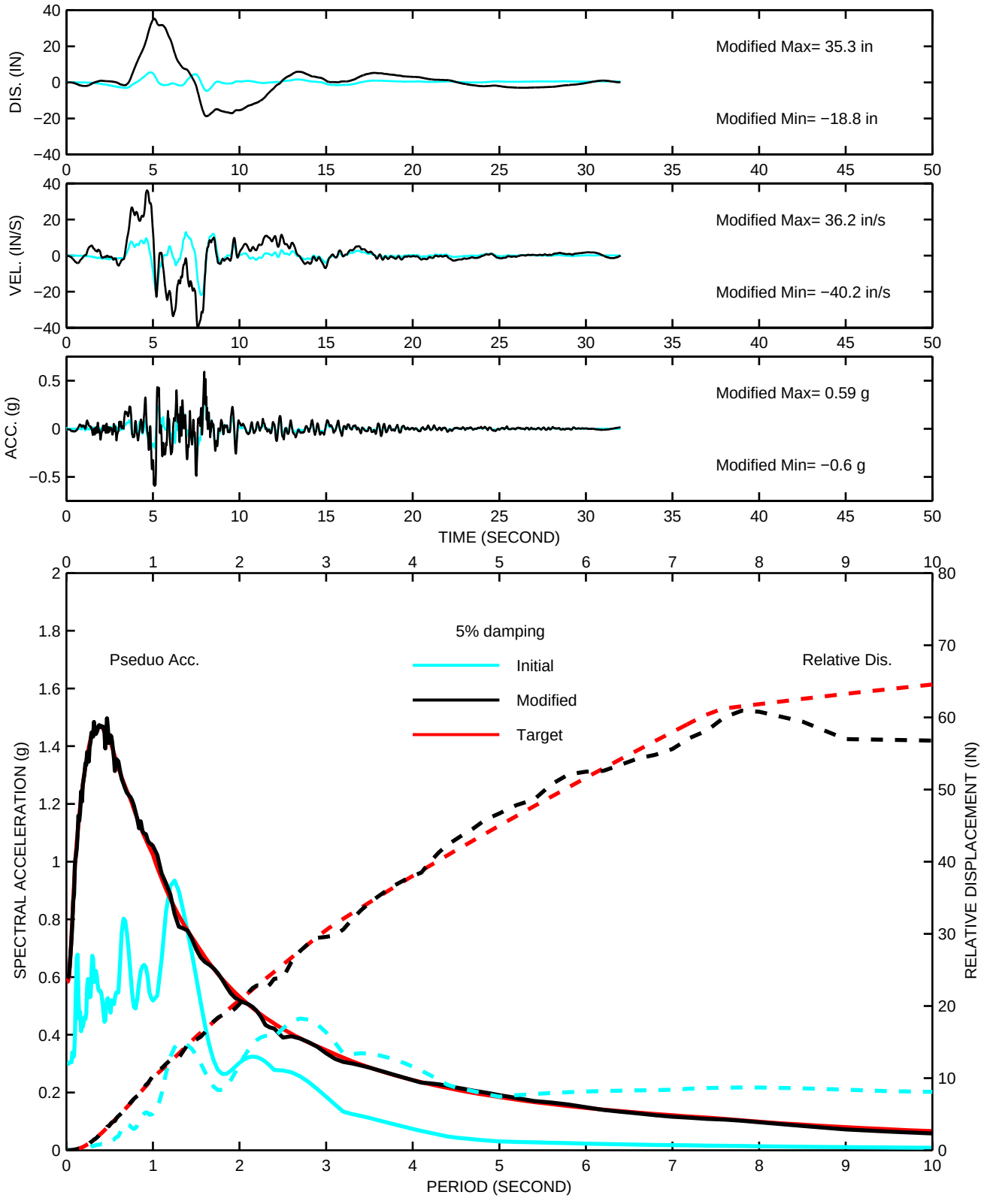


Figure B103. Firm−Ground DE Spectrum Compatible Ground Motion (5% Damped) − Set 7 Fault Normal

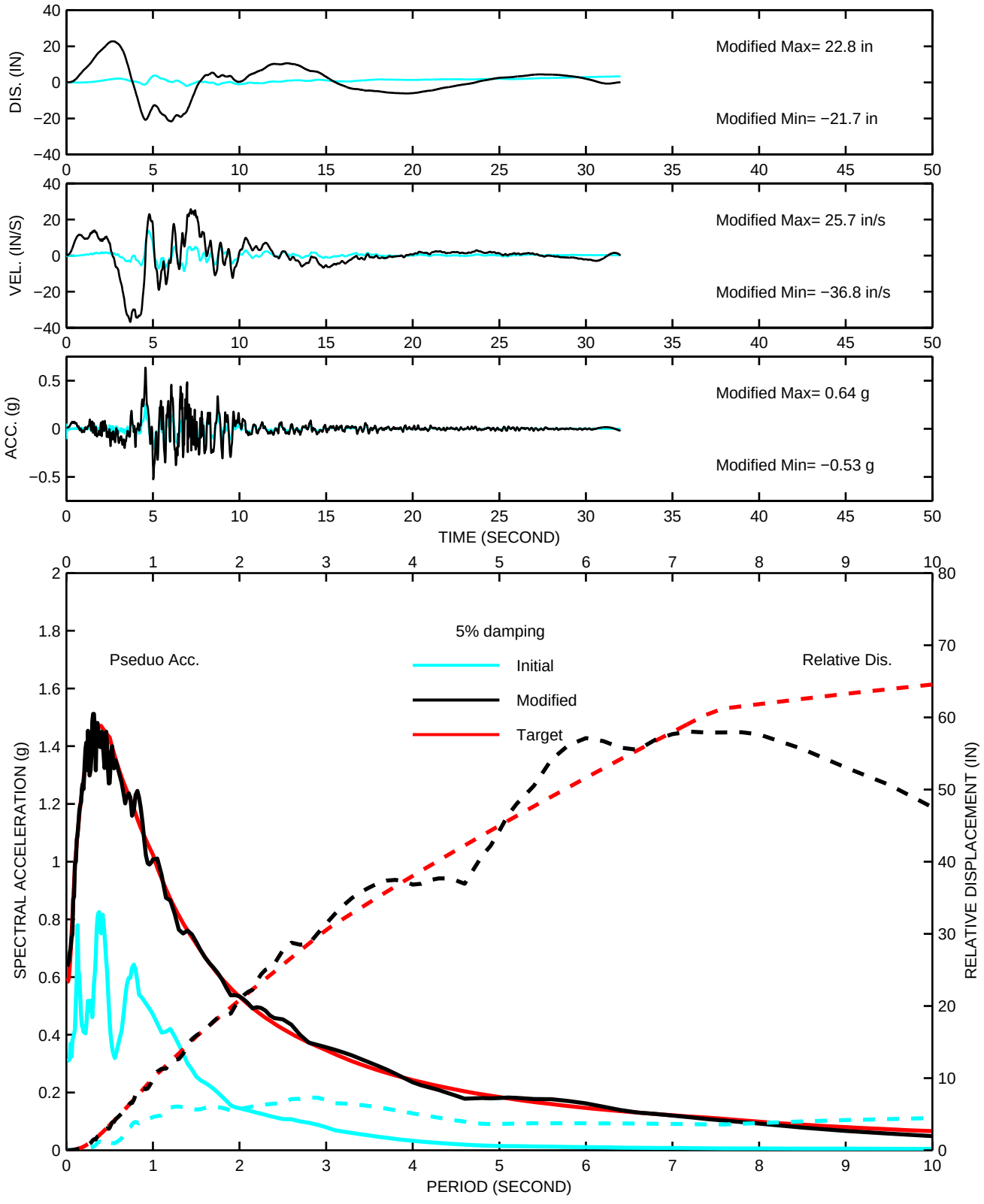


Figure B104. Firm−Ground DE Spectrum Compatible Ground Motion (5% Damped) − Set 7 Fault Parallel

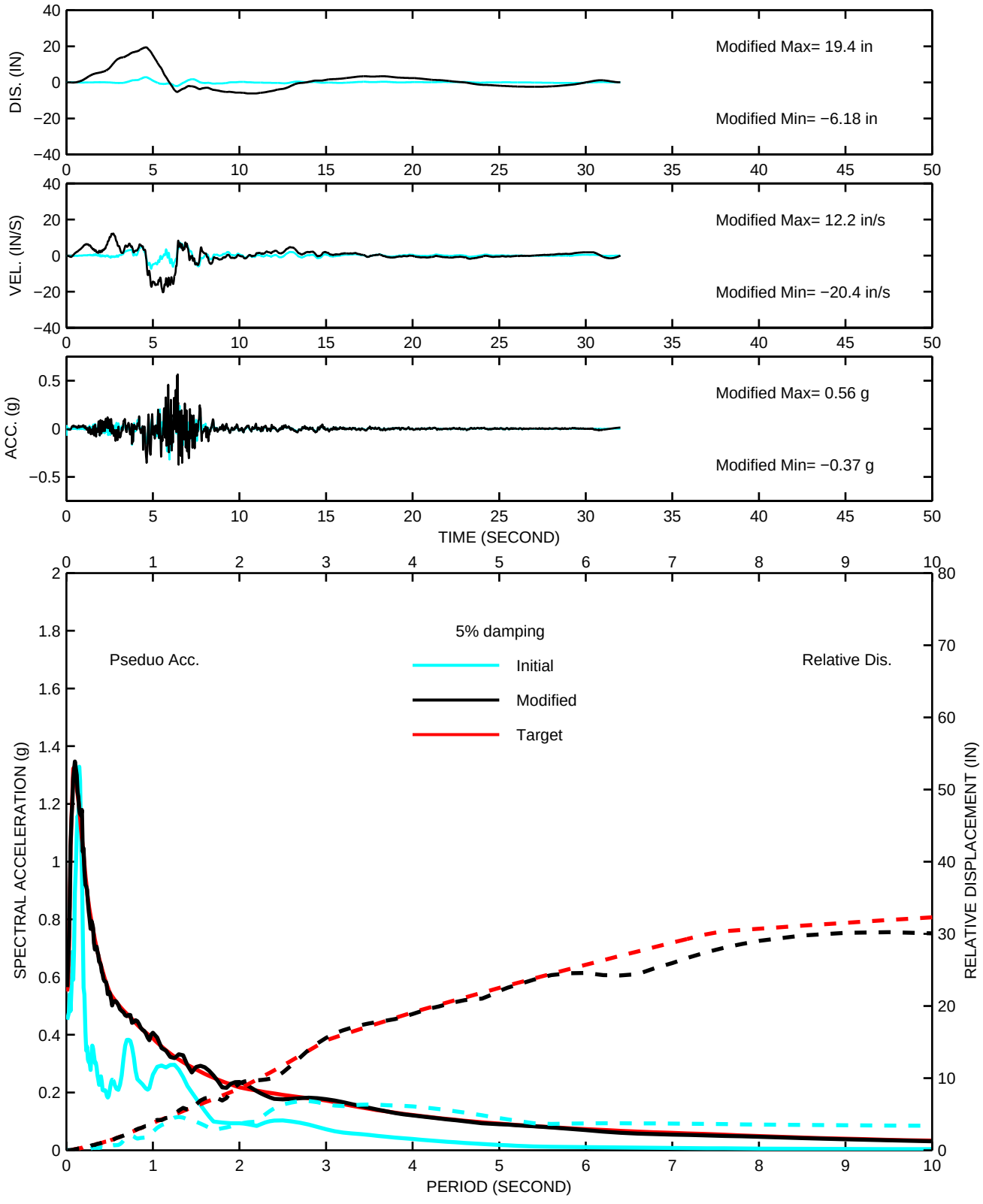


Figure B105. Firm−Ground DE Spectrum Compatible Ground Motion (5% Damped) − Set 7 Vertical

APPENDIX C DETAILS OF SITE RESPONSE ANALYSIS RESULTS

As discussed in Section 4 of this report, the computer program DeepSoil v7.0 (Hashash et al., 2020) was used to perform non-linear site response analysis. The spectrally matched start-up ground motions (as discussed in Section 3.4) were used as input acceleration time histories. The soil profiles shown in Figure 2-8 for zones I, II, III, and IV were considered to represent the subsurface conditions at the POLB area. The dynamic shear modulus (G/G_{max}) and damping (D/D_{max}) curves for hydraulic fill were estimated using the empirical relationships by EPRI (1993). For harbor sediments, the shear modulus and damping curves of Vucetic and Dobry (1991) were adopted assuming plasticity index (PI) of 15. For liquefied soils, the curves of Vucetic and Dobry (1991) with PI of 0.0 were used.

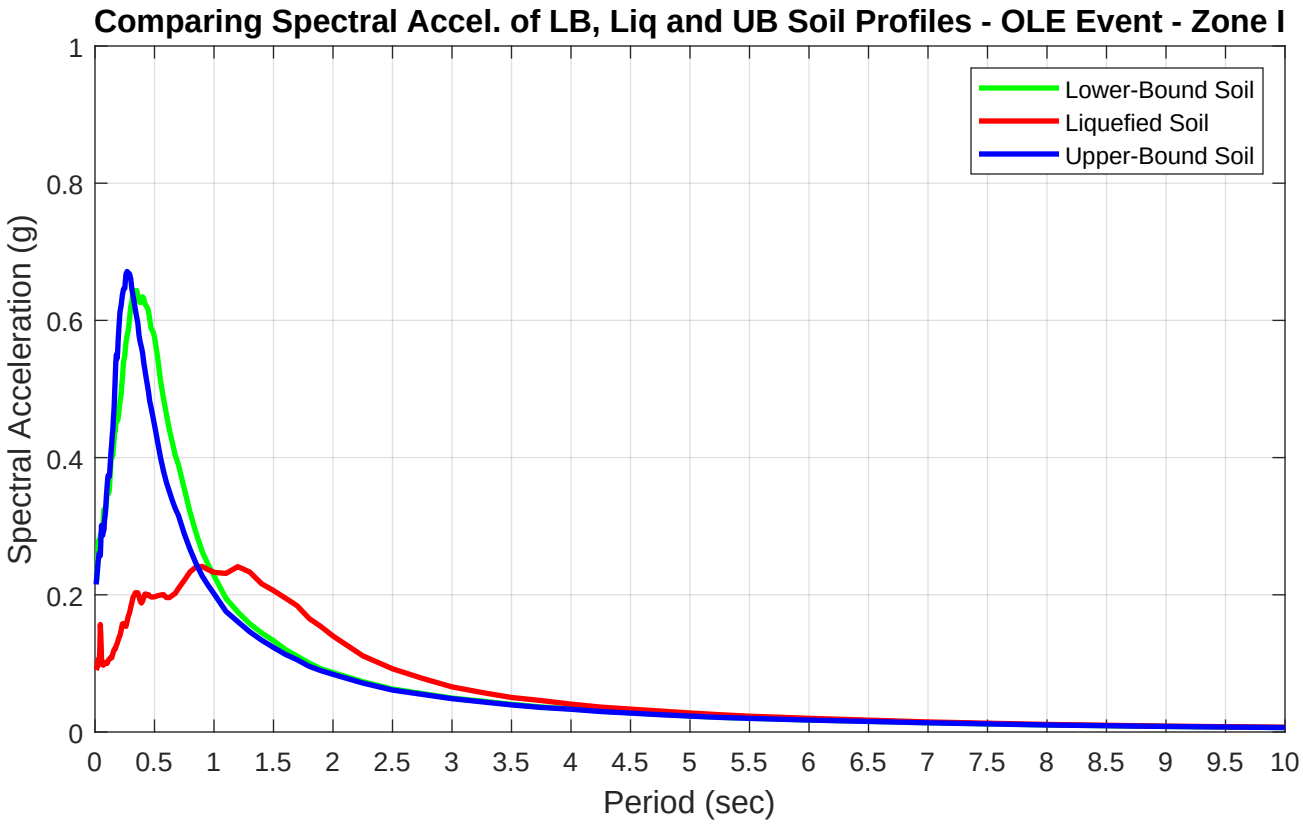
To account for spatial variability of soil properties and uncertainties associated with estimation of material stiffness and strength parameters, three different sets of soil properties were considered for each soil zone; lower-bound, upper-bound, and liquefied conditions. The lower- and upper-bound profiles considered shear wave velocity profiles that were respectively 12 percent lower and higher than the best estimate shear wave velocities shown in Figure 2-8 of the report. This amount of variation corresponded to about 25 percent variability in the magnitude of small-strain shear modulus (G_{max}). The analyses considered lower-bound and upper-bound friction angles of 32 and 35 degrees and lower-bound and upper-bound cohesions of 50 psf and 100 psf for the hydraulic fill. The lower- and upper-bound undrained shear strength of the harbor sediments encountered in zones III and IV were assumed to be 1,000 psf and 2,500 psf, respectively. For liquefied conditions, residual shear strength of 0.15 times the in-situ vertical effective stress (σ'_v) was estimated following the approach outlined in Idriss and Boulanger (2008). The shear wave velocity profile below the ground water table (liquefiable soils) was correlated using the equation of Dickenson (1994).

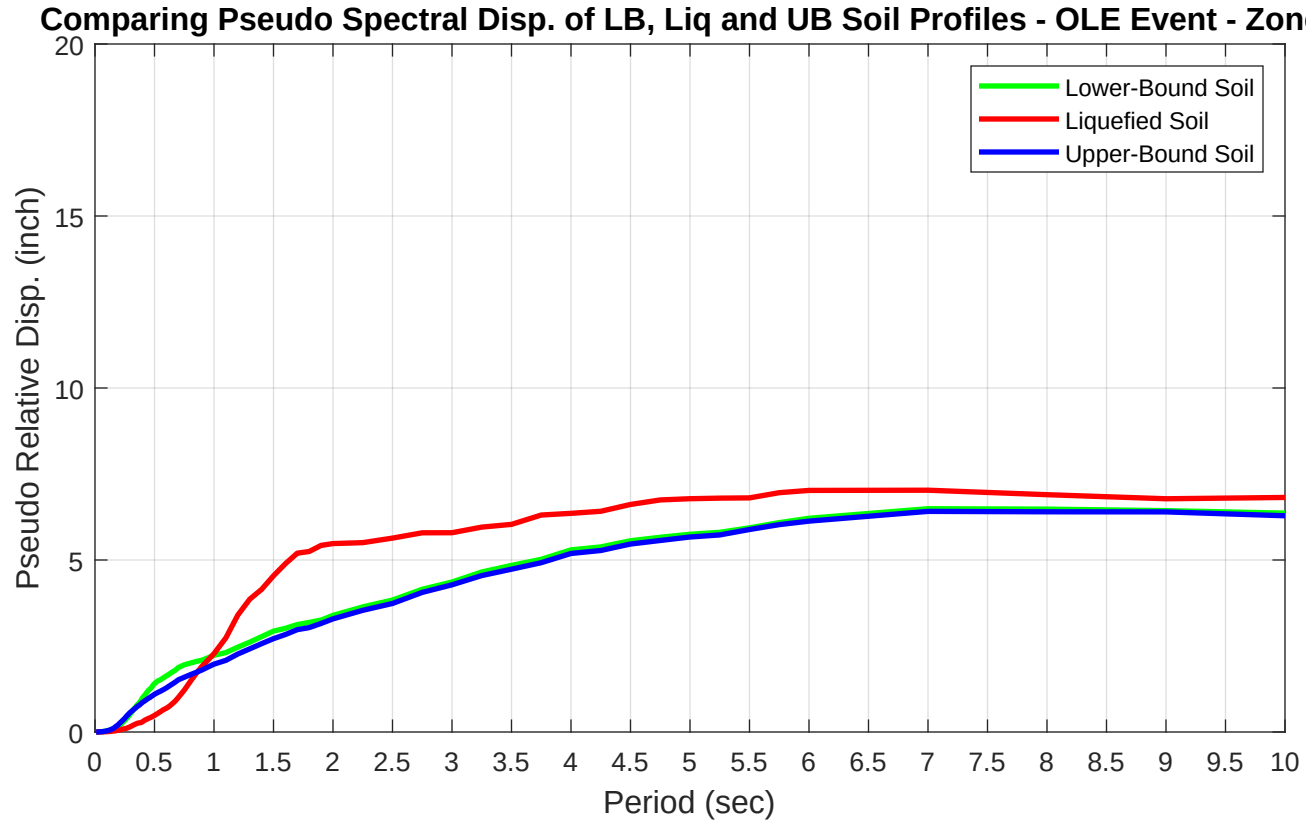
In order to improve the model accuracy in large strain range, the reference backbone curves discussed above were used to fit a general quadratic/hyperbolic (GQ/H) backbone curve, as described by Groholski et al. (2016) and implemented in DeepSoil v7.0. In addition, the reference damping curves were used to fit unloading-reloading relationship using modulus reduction and damping curve fitting (MRDF)-Darendeli Model (Darendeli, 2001) as available in DeepSoil v7.0 soil model libraries. The fitting procedure was applied for every layer in the soil profile, resulting in a soil model that better estimates the small-strain behavior as well as the soil strength at larger strain levels.

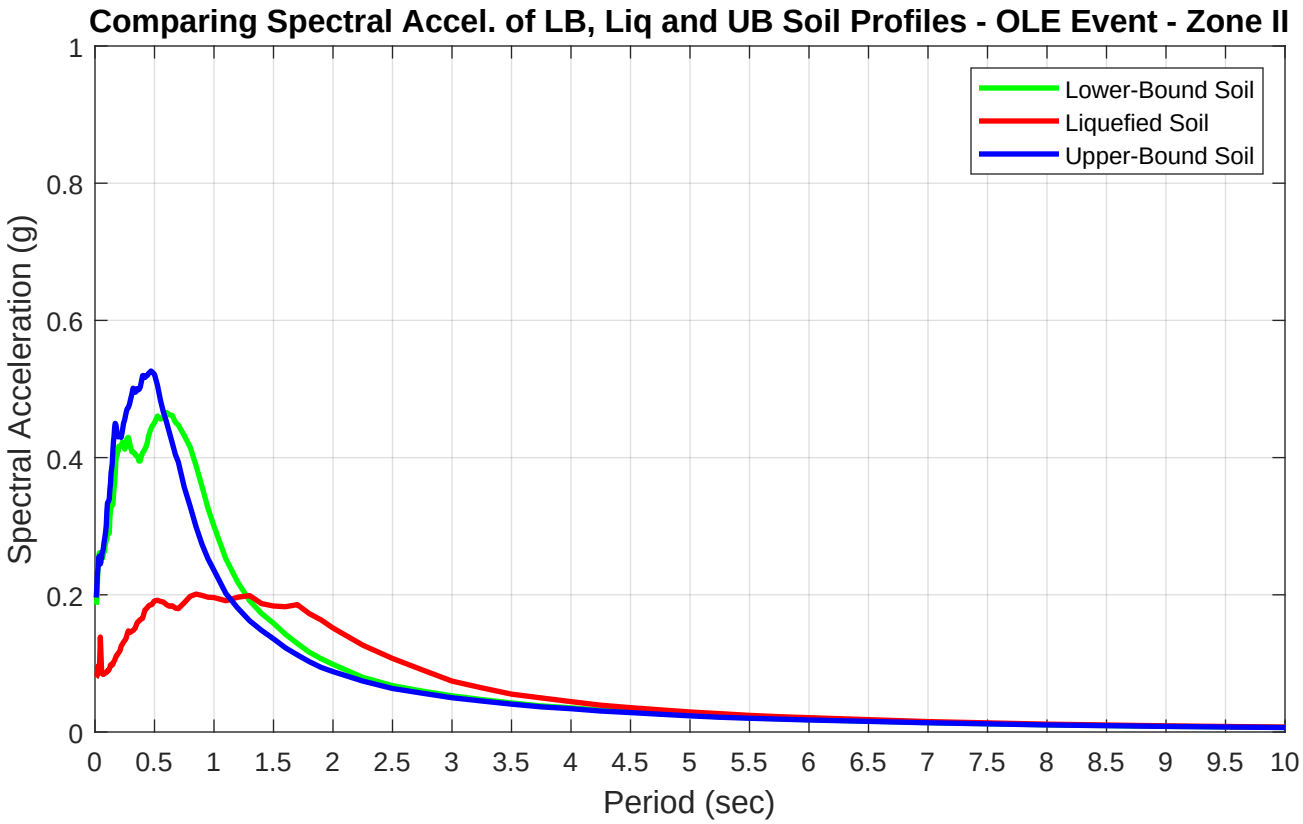
This appendix presents the computed spectral acceleration and displacement magnitude for the following cases:

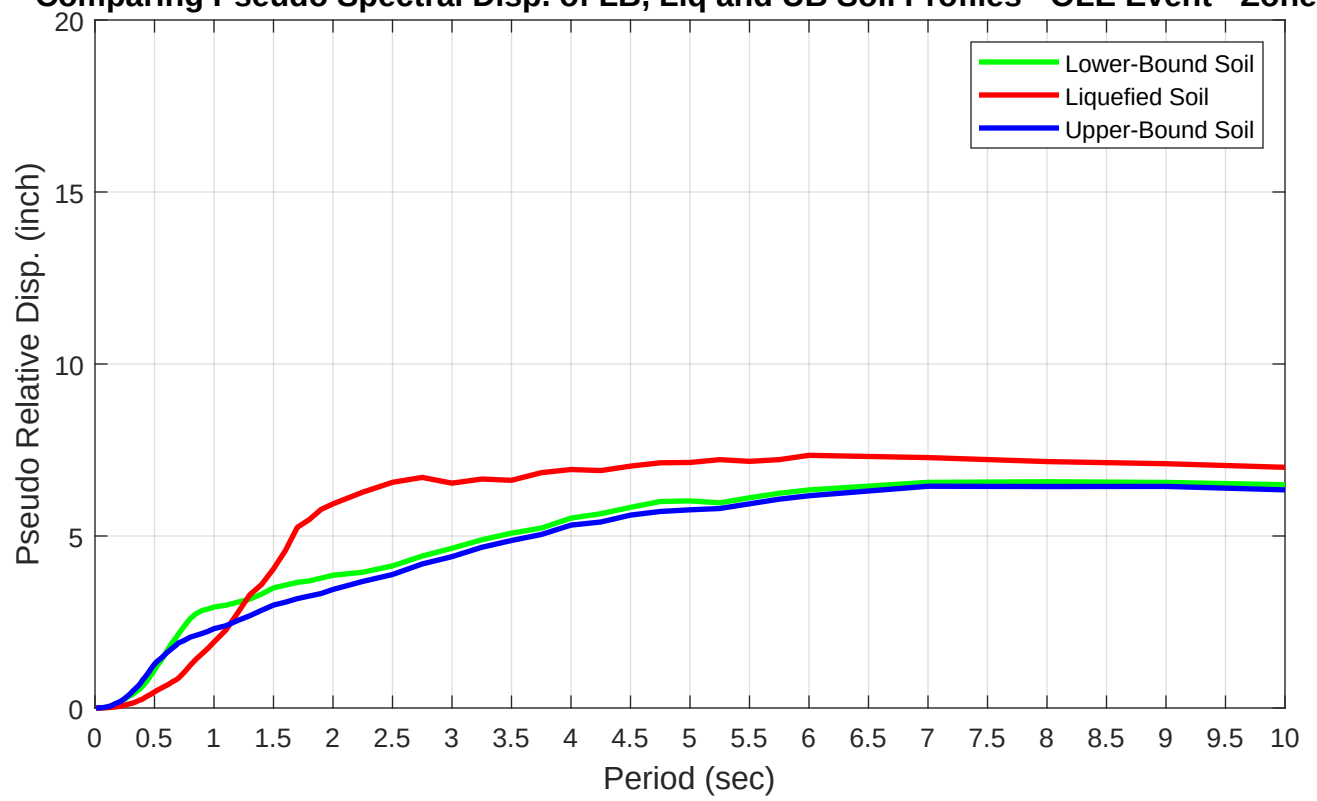
- Lower-bound, liquefied, and upper-bound soil profiles for soil zones I, II, III, and IV for OLE, CLE, 975-yr and MCE_R events. The results are presented in **Part I** of the appendix.
- The spectral responses for lower-bound, liquefied, and upper-bound soil profiles were enveloped representing one single acceleration and displacement spectrum for each soil zone and earthquake event. **Part II** of this appendix includes the spectral responses.
- The spectral responses at zones II, III, and IV were enveloped representing one single acceleration and displacement spectrum for Area A. Spectral responses at zone I was presented as Area B. The results are shown in **Part III** of this appendix.

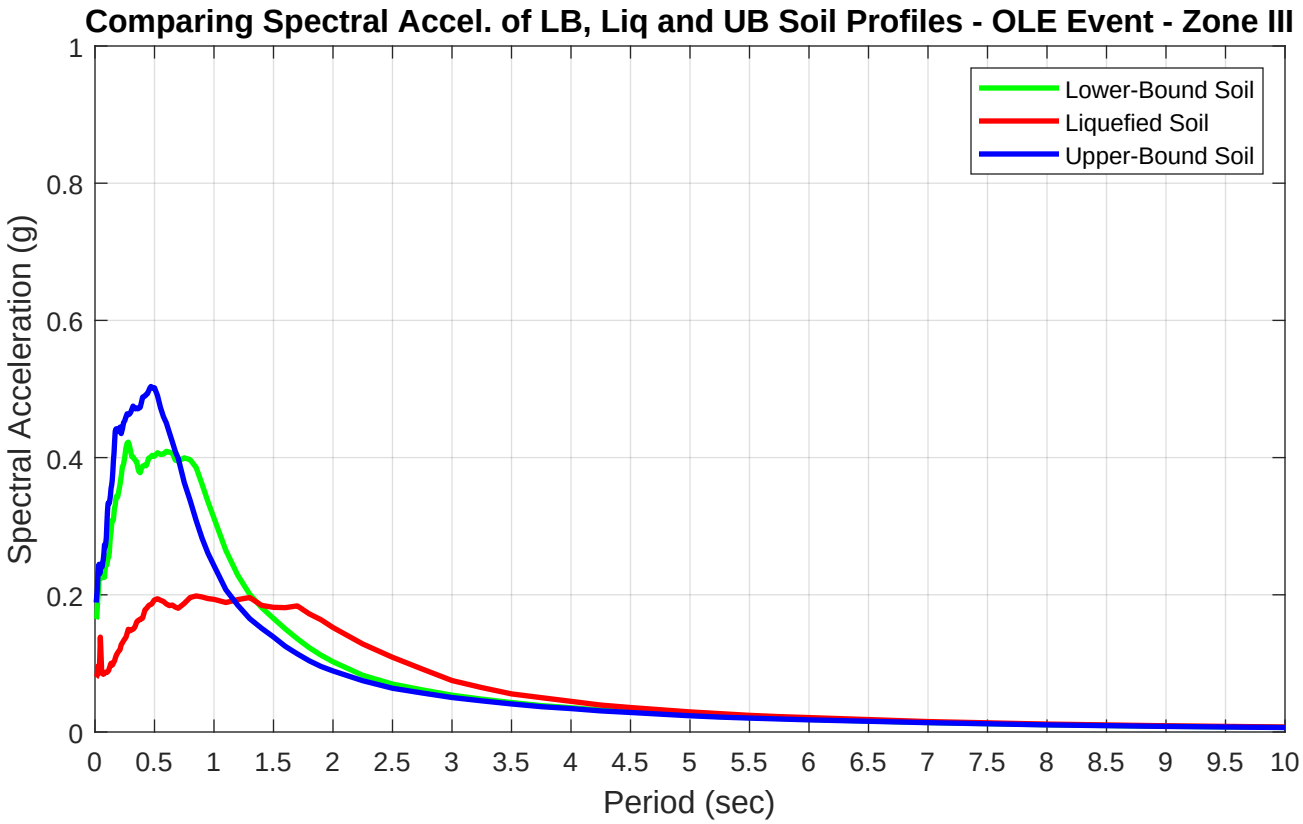
Part I: Spectral Acceleration and Pseudo Spectral Displacement Spectra for Lower-Bound, Liquefied, and Upper-Bound Soil Profiles

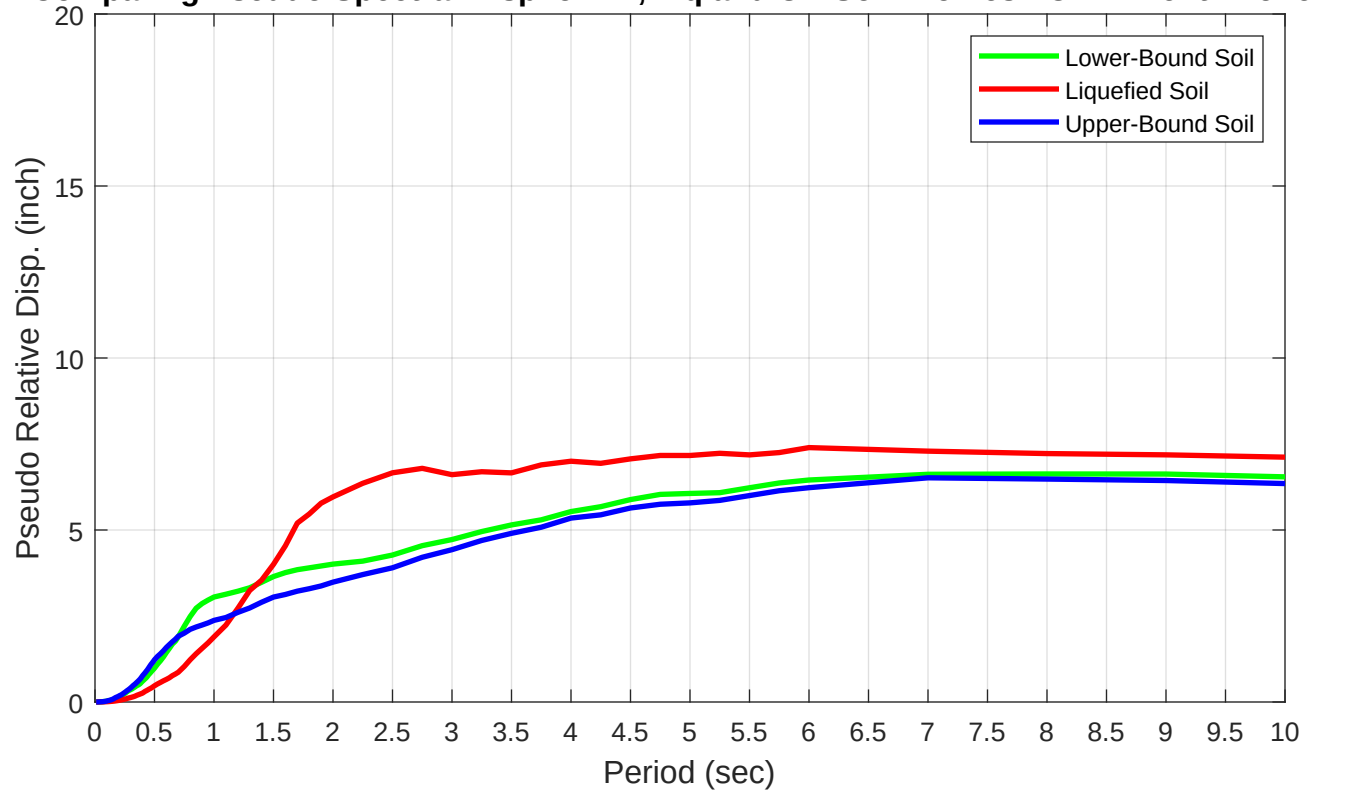

Comparing Spectral Accel. of LB, Liq and UB Soil Profiles - OLE Event - Zone I
Lower-Bound Soil
Liquefied Soil
Upper-Bound Soil
Spectral Acceleration (g)
Period (sec)
0
0.2
0.4
0.6
0.8
1
0 0.5 1 1.5 2 2.5 3 3.5 4 4.5 5 5.5 6 6.5 7 7.5 8 8.5 9 9.5 10

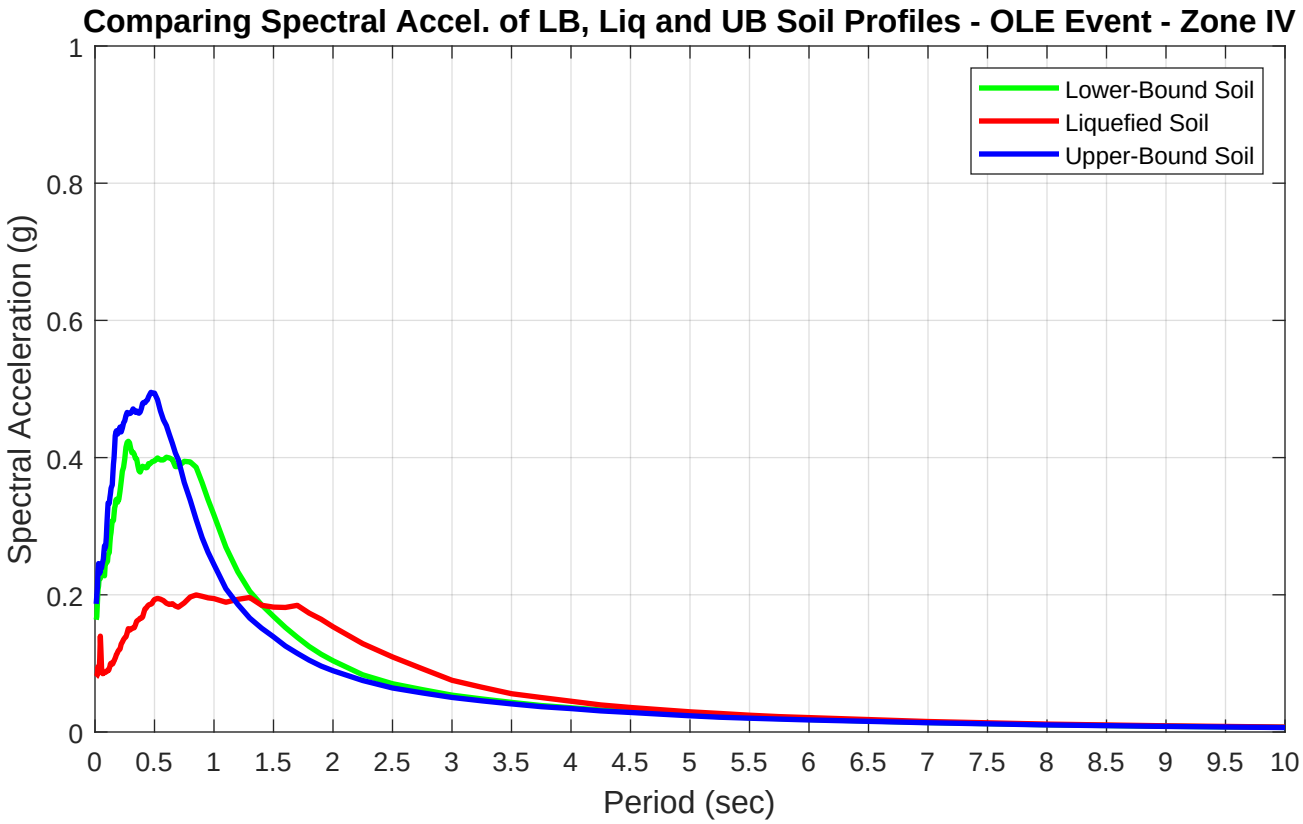

Comparing Pseudo Spectral Disp. of LB, Liq and UB Soil Profiles - OLE Event - Zone I
Lower-Bound Soil
Liquefied Soil
Upper-Bound Soil
Pseudo Relative Disp. (inch)
Period (sec)
0
5
10
15
20
0 0.5 1 1.5 2 2.5 3 3.5 4 4.5 5 5.5 6 6.5 7 7.5 8 8.5 9 9.5 10

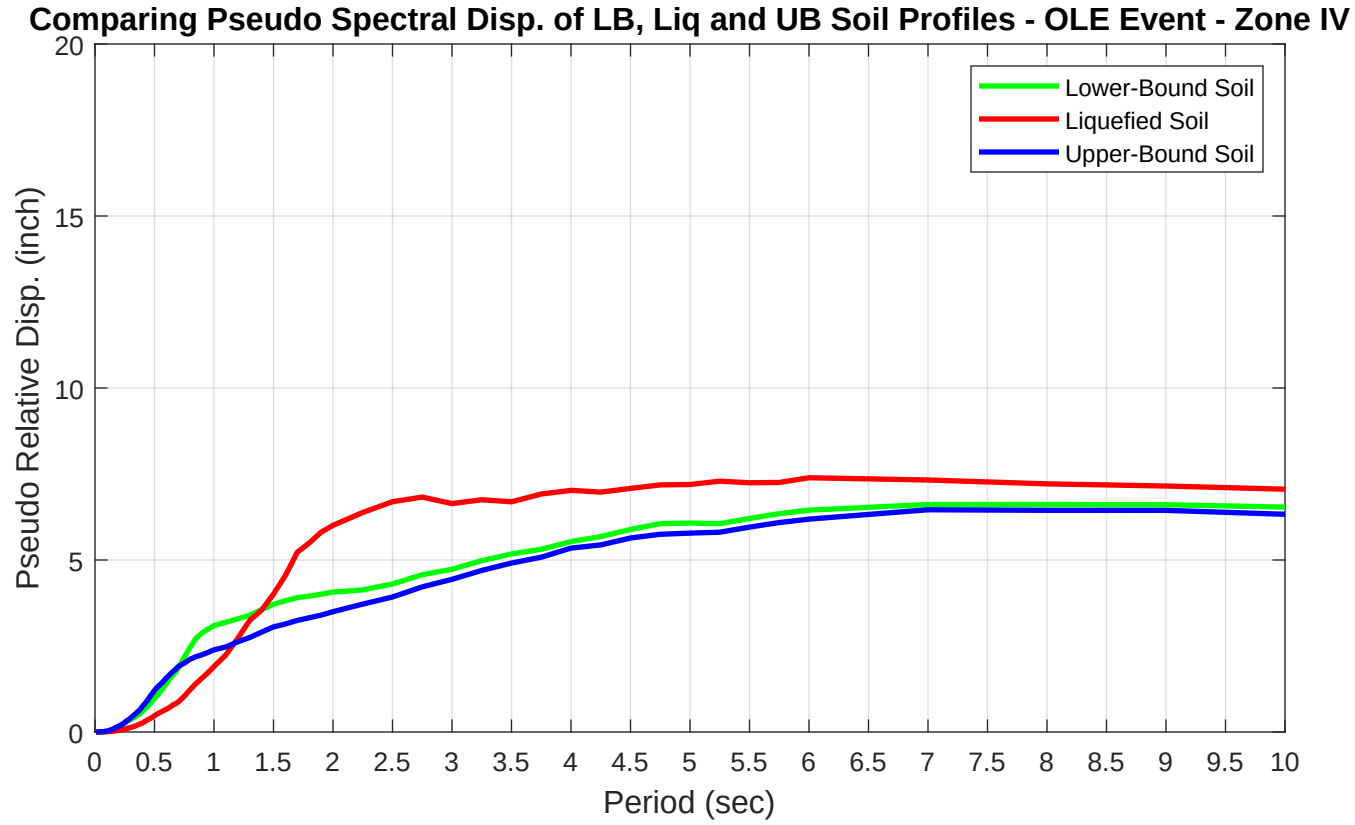

Comparing Spectral Accel. of LB, Liq and UB Soil Profiles - OLE Event - Zone II
Lower-Bound Soil
Liquefied Soil
Upper-Bound Soil
Spectral Acceleration (g)
Period (sec)
0
0.2
0.4
0.6
0.8
1
0 0.5 1 1.5 2 2.5 3 3.5 4 4.5 5 5.5 6 6.5 7 7.5 8 8.5 9 9.5 10

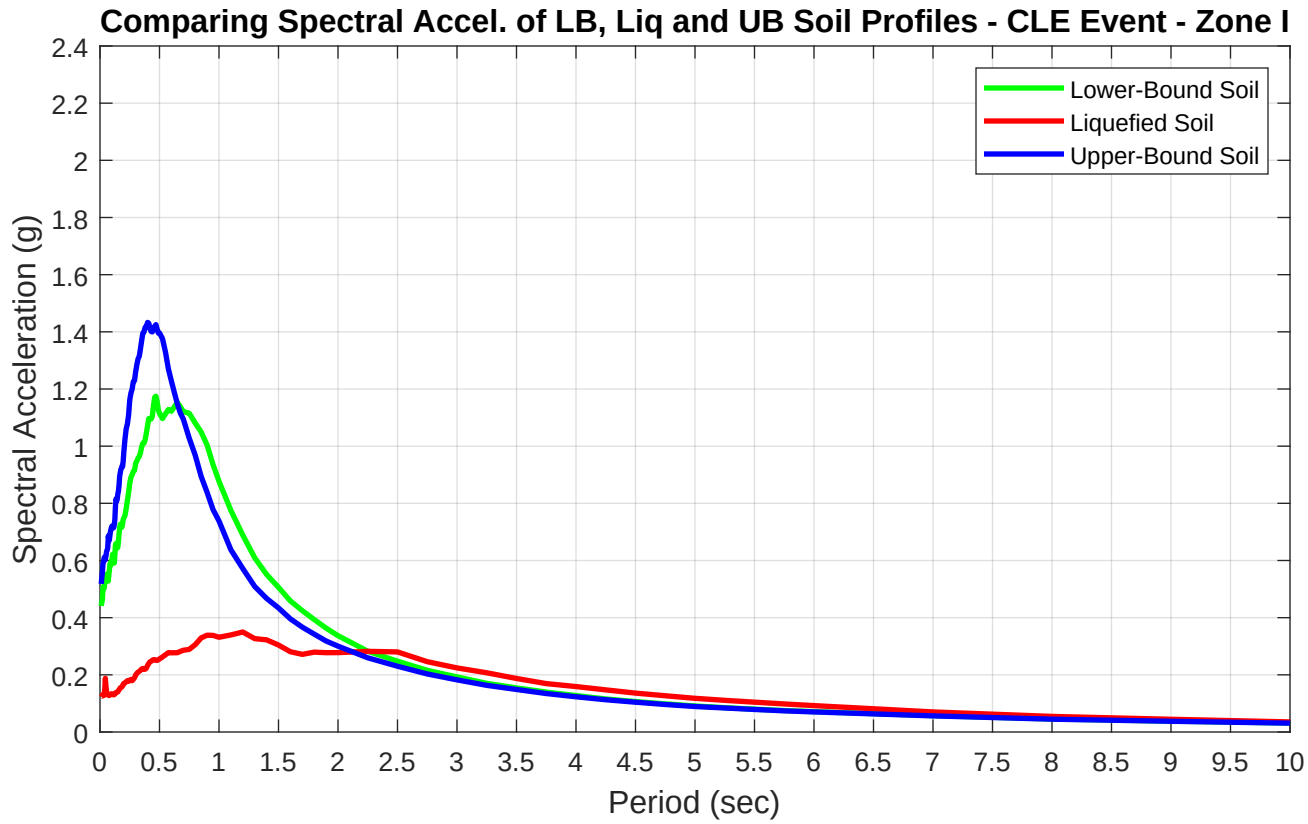

Comparing Pseudo Spectral Disp. of LB, Liq and UB Soil Profiles - OLE Event - Zone II
Lower-Bound Soil
Liquefied Soil
Upper-Bound Soil
Pseudo Relative Disp. (inch)
Period (sec)
0
5
10
15
20
0 0.5 1 1.5 2 2.5 3 3.5 4 4.5 5 5.5 6 6.5 7 7.5 8 8.5 9 9.5 10

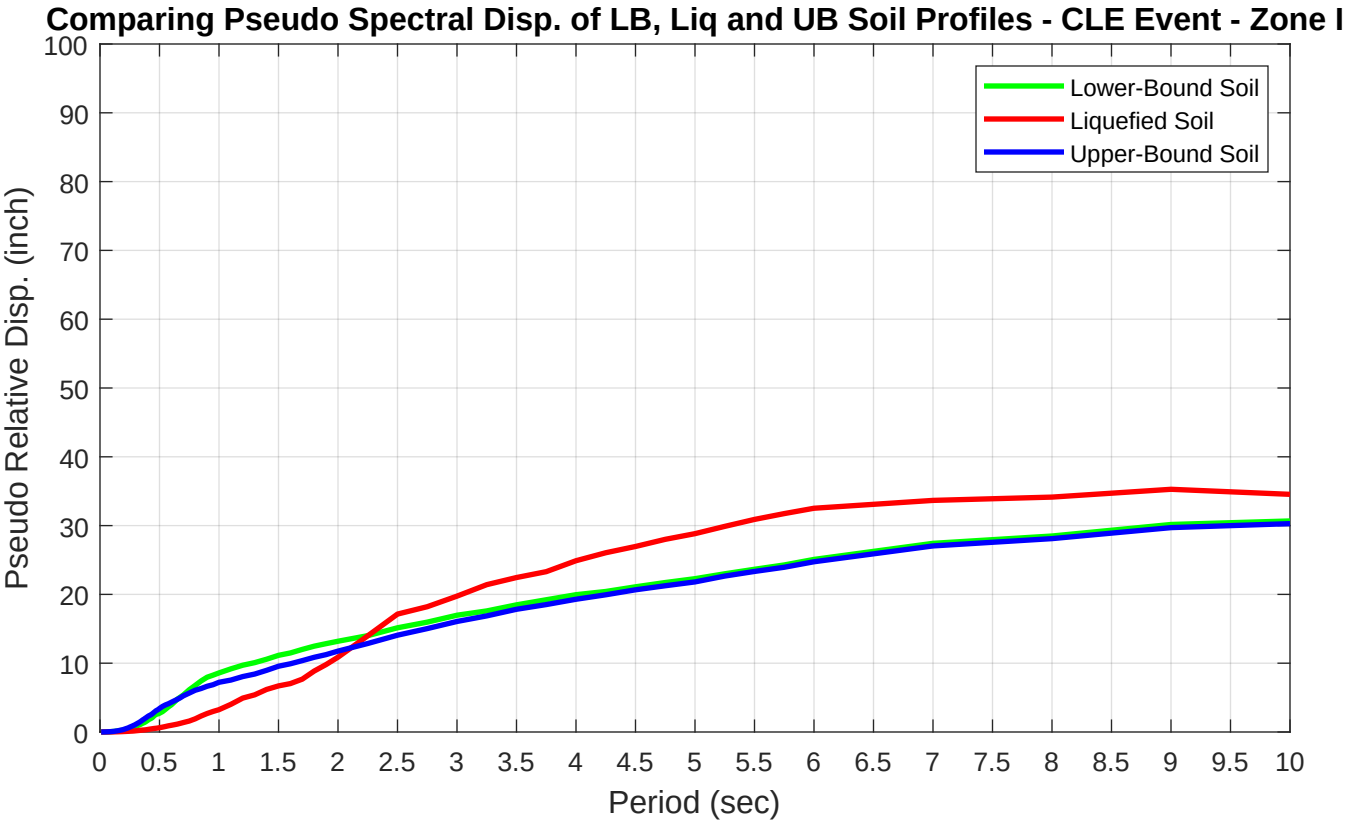

Comparing Spectral Accel. of LB, Liq and UB Soil Profiles - OLE Event - Zone III
Lower-Bound Soil
Liquefied Soil
Upper-Bound Soil
Spectral Acceleration (g)
Period (sec)
0
0.2
0.4
0.6
0.8
1
0 0.5 1 1.5 2 2.5 3 3.5 4 4.5 5 5.5 6 6.5 7 7.5 8 8.5 9 9.5 10

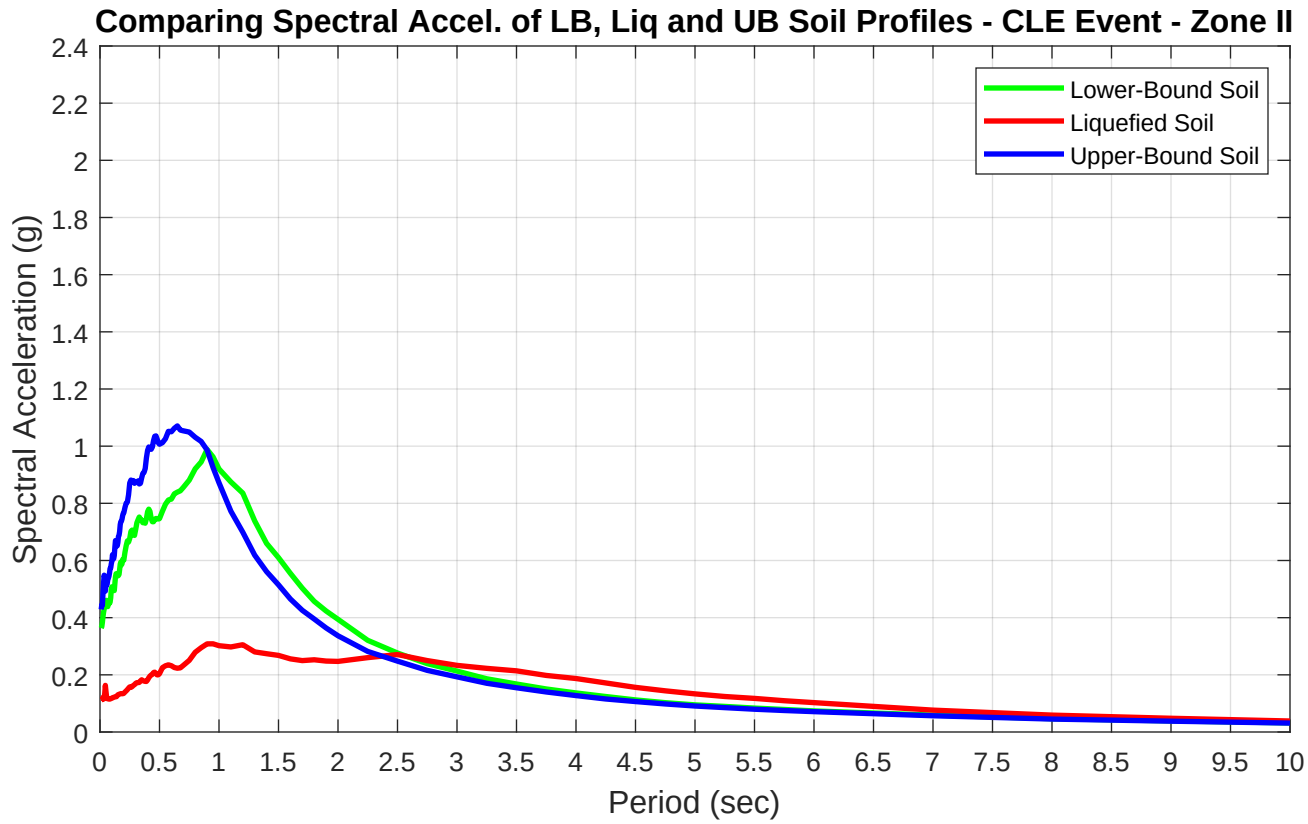

Comparing Pseudo Spectral Disp. of LB, Liq and UB Soil Profiles - OLE Event - Zone III
Lower-Bound Soil
Liquefied Soil
Upper-Bound Soil
Pseudo Relative Disp. (inch)
Period (sec)
0
5
10
15
20
0 0.5 1 1.5 2 2.5 3 3.5 4 4.5 5 5.5 6 6.5 7 7.5 8 8.5 9 9.5 10

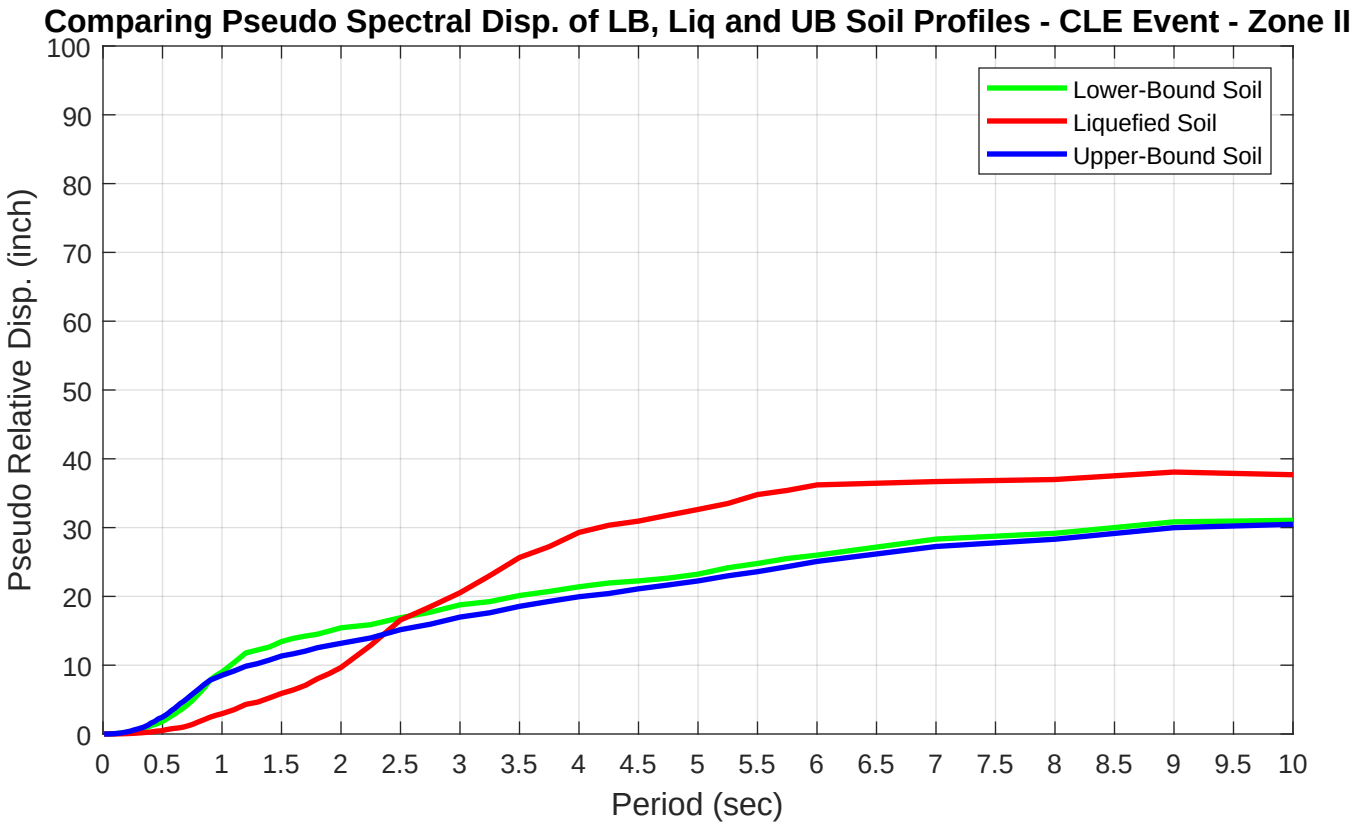

Comparing Spectral Accel. of LB, Liq and UB Soil Profiles - OLE Event - Zone IV
Lower-Bound Soil
Liquefied Soil
Upper-Bound Soil
Spectral Acceleration (g)
Period (sec)
0
0.2
0.4
0.6
0.8
1
0 0.5 1 1.5 2 2.5 3 3.5 4 4.5 5 5.5 6 6.5 7 7.5 8 8.5 9 9.5 10

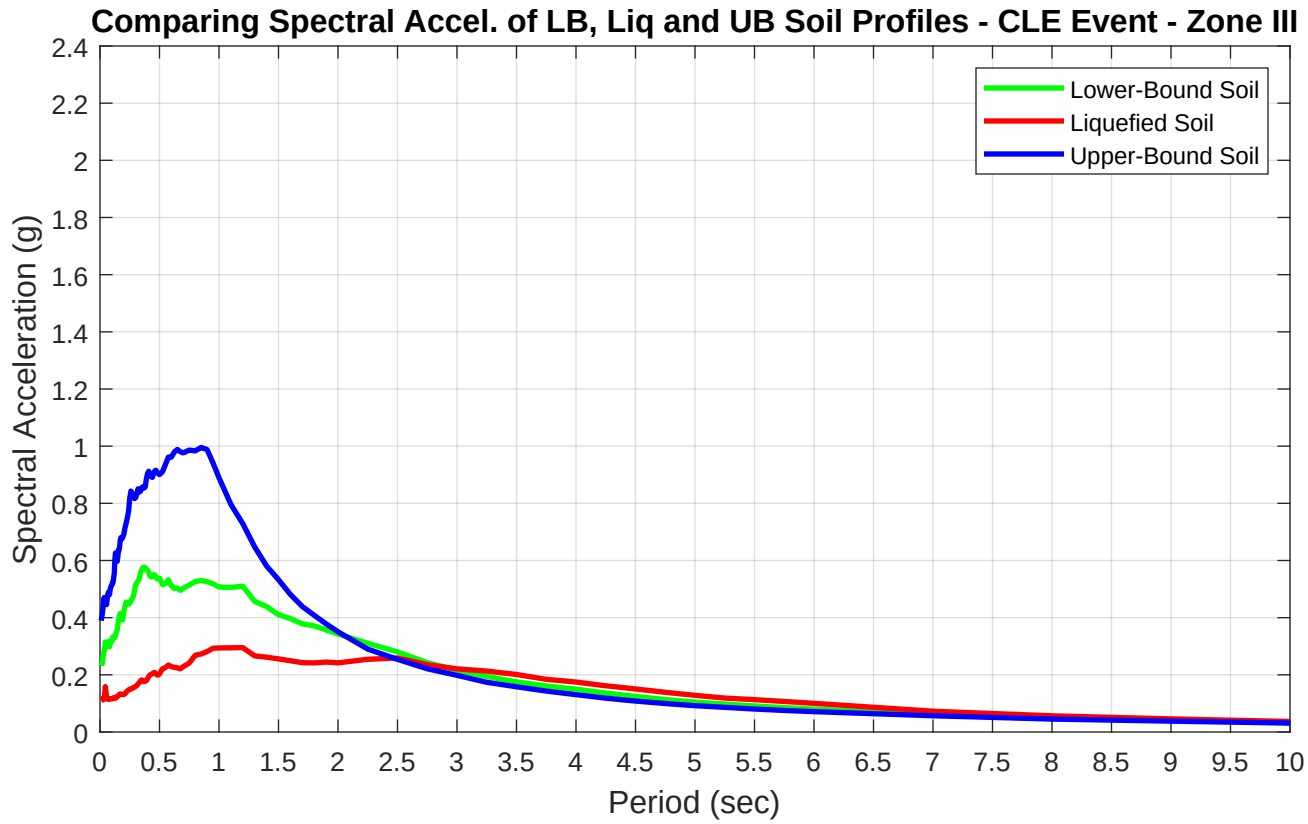

Comparing Pseudo Spectral Disp. of LB, Liq and UB Soil Profiles - OLE Event - Zone IV
Lower-Bound Soil
Liquefied Soil
Upper-Bound Soil
Pseudo Relative Disp. (inch)
Period (sec)
0
5
10
15
20
0 0.5 1 1.5 2 2.5 3 3.5 4 4.5 5 5.5 6 6.5 7 7.5 8 8.5 9 9.5 10

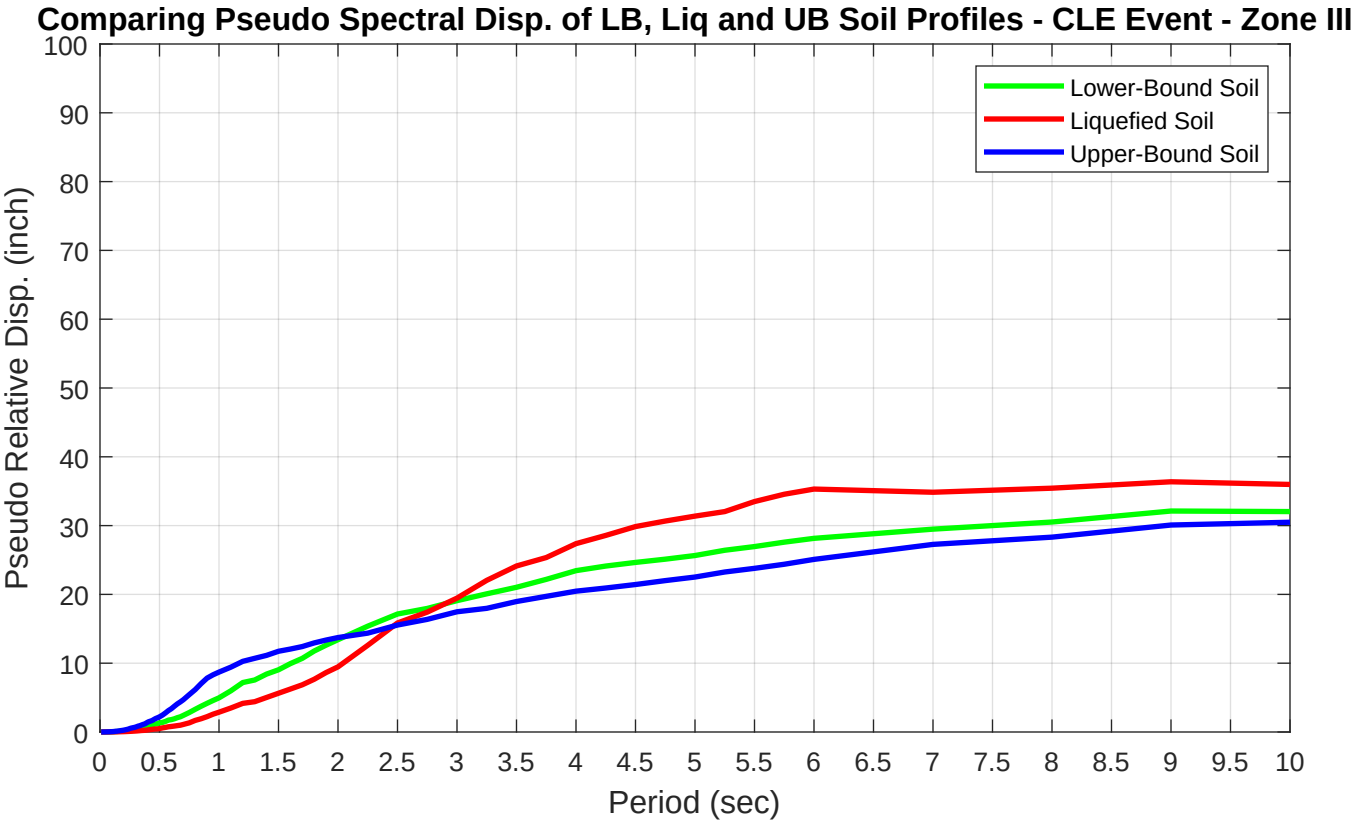

Comparing Spectral Accel. of LB, Liq and UB Soil Profiles - CLE Event - Zone I
Lower-Bound Soil
Liquefied Soil
Upper-Bound Soil
Spectral Acceleration (g)
Period (sec)
0
0.2
0.4
0.6
0.8
1
1.2
1.4
1.6
1.8
2
2.2
2.4
0 0.5 1 1.5 2 2.5 3 3.5 4 4.5 5 5.5 6 6.5 7 7.5 8 8.5 9 9.5 10

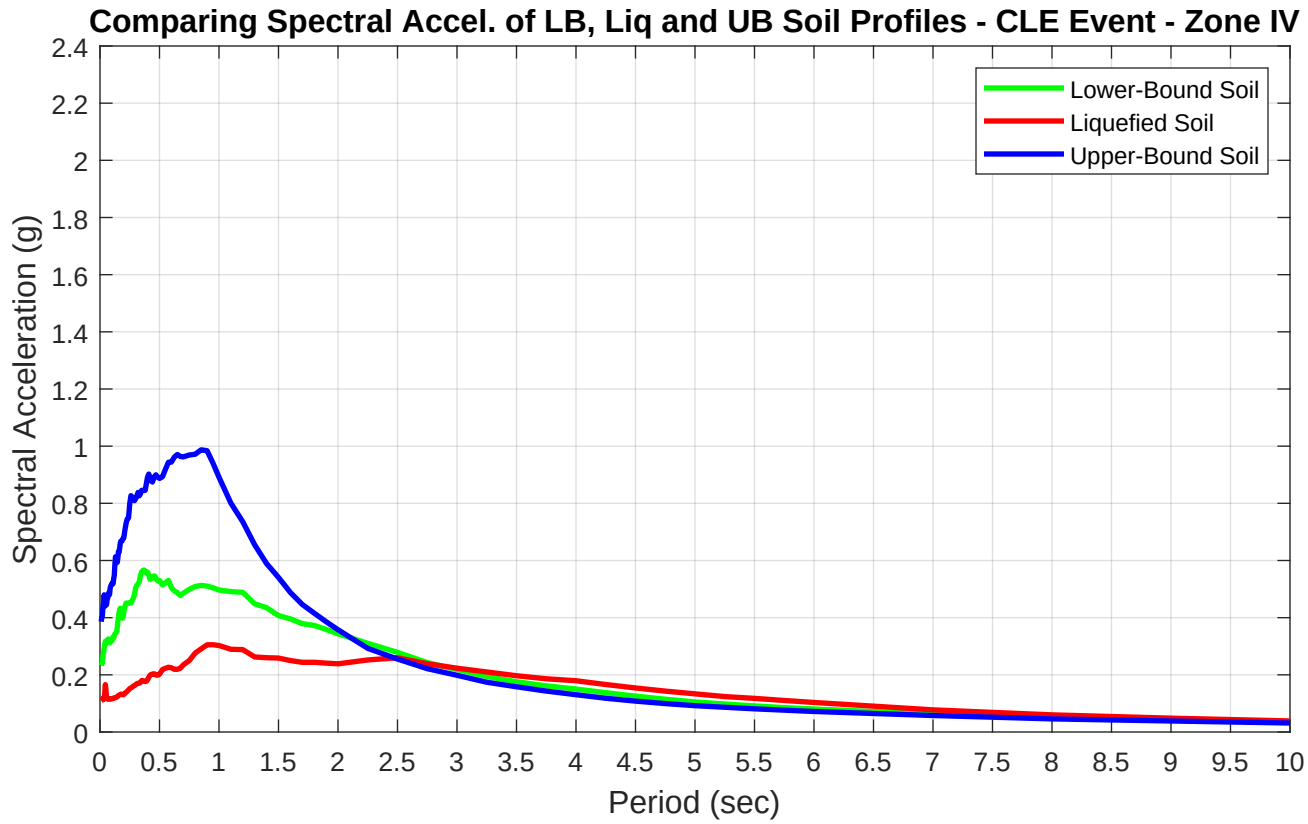

Comparing Pseudo Spectral Disp. of LB, Liq and UB Soil Profiles - CLE Event - Zone I
Lower-Bound Soil
Liquefied Soil
Upper-Bound Soil
Pseudo Relative Disp. (inch)
Period (sec)
0
10
20
30
40
50
60
70
80
90
100
0 0.5 1 1.5 2 2.5 3 3.5 4 4.5 5 5.5 6 6.5 7 7.5 8 8.5 9 9.5 10

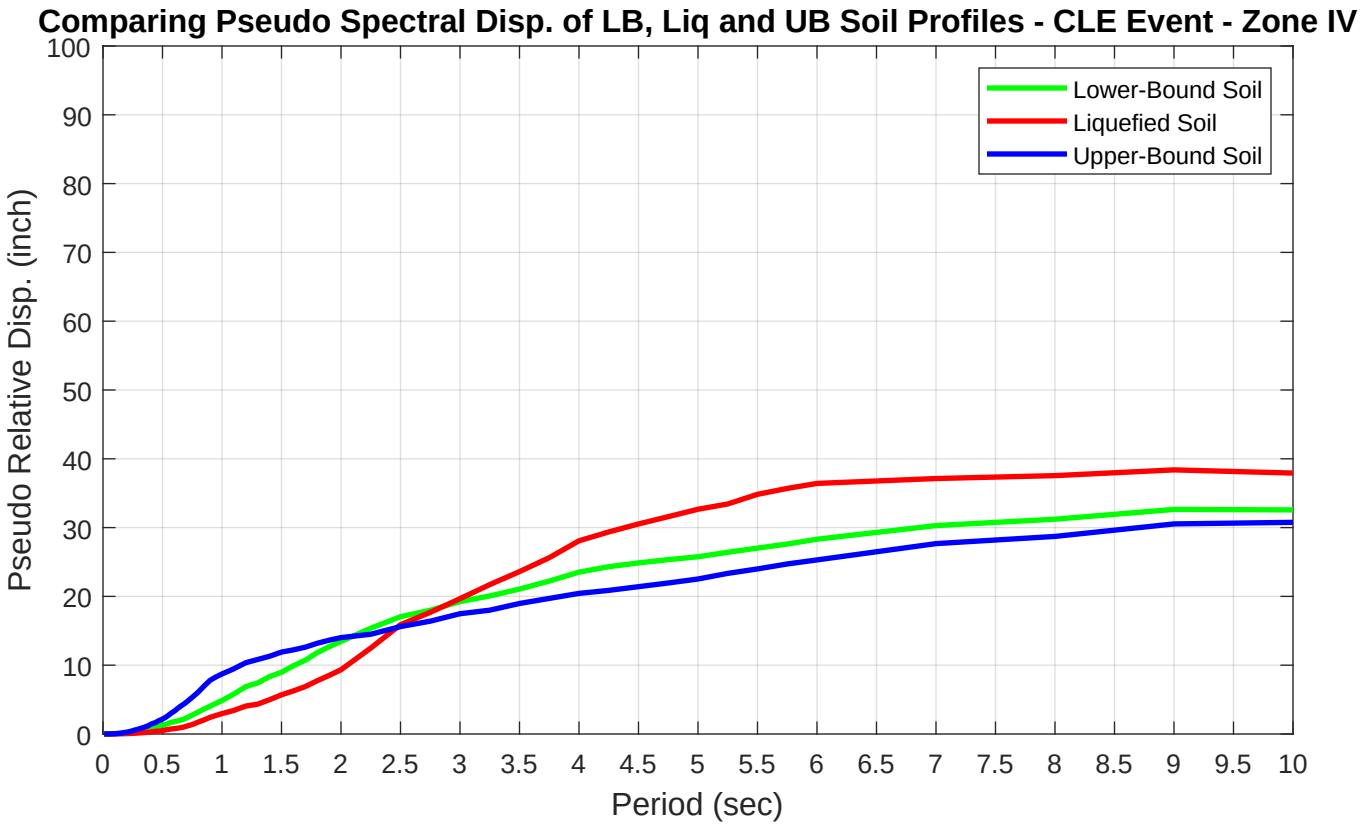

Comparing Spectral Accel. of LB, Liq and UB Soil Profiles - CLE Event - Zone II
Lower-Bound Soil
Liquefied Soil
Upper-Bound Soil
Spectral Acceleration (g)
Period (sec)
0
0.2
0.4
0.6
0.8
1
1.2
1.4
1.6
1.8
2
2.2
2.4
0 0.5 1 1.5 2 2.5 3 3.5 4 4.5 5 5.5 6 6.5 7 7.5 8 8.5 9 9.5 10

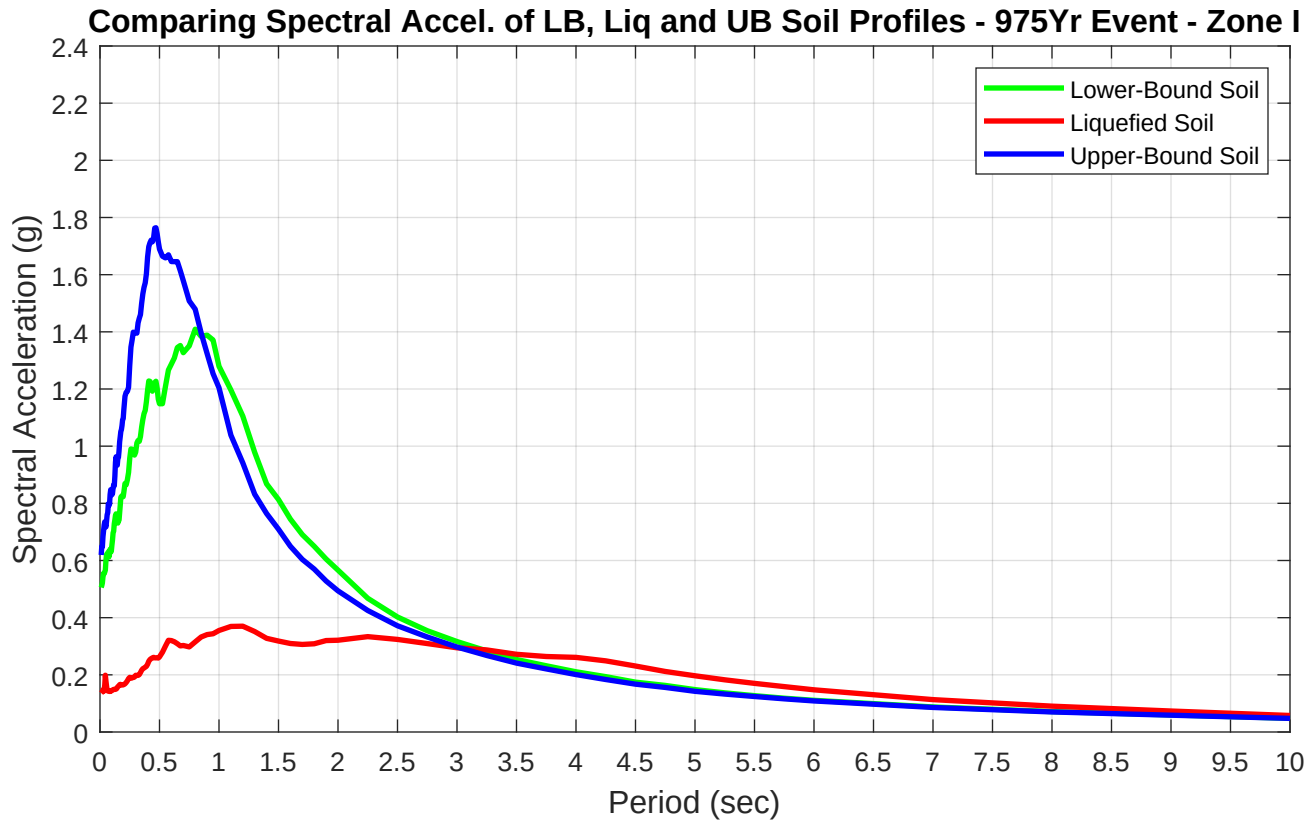

Comparing Pseudo Spectral Disp. of LB, Liq and UB Soil Profiles - CLE Event - Zone II
Lower-Bound Soil
Liquefied Soil
Upper-Bound Soil
Pseudo Relative Disp. (inch)
Period (sec)
0
10
20
30
40
50
60
70
80
90
100
0 0.5 1 1.5 2 2.5 3 3.5 4 4.5 5 5.5 6 6.5 7 7.5 8 8.5 9 9.5 10

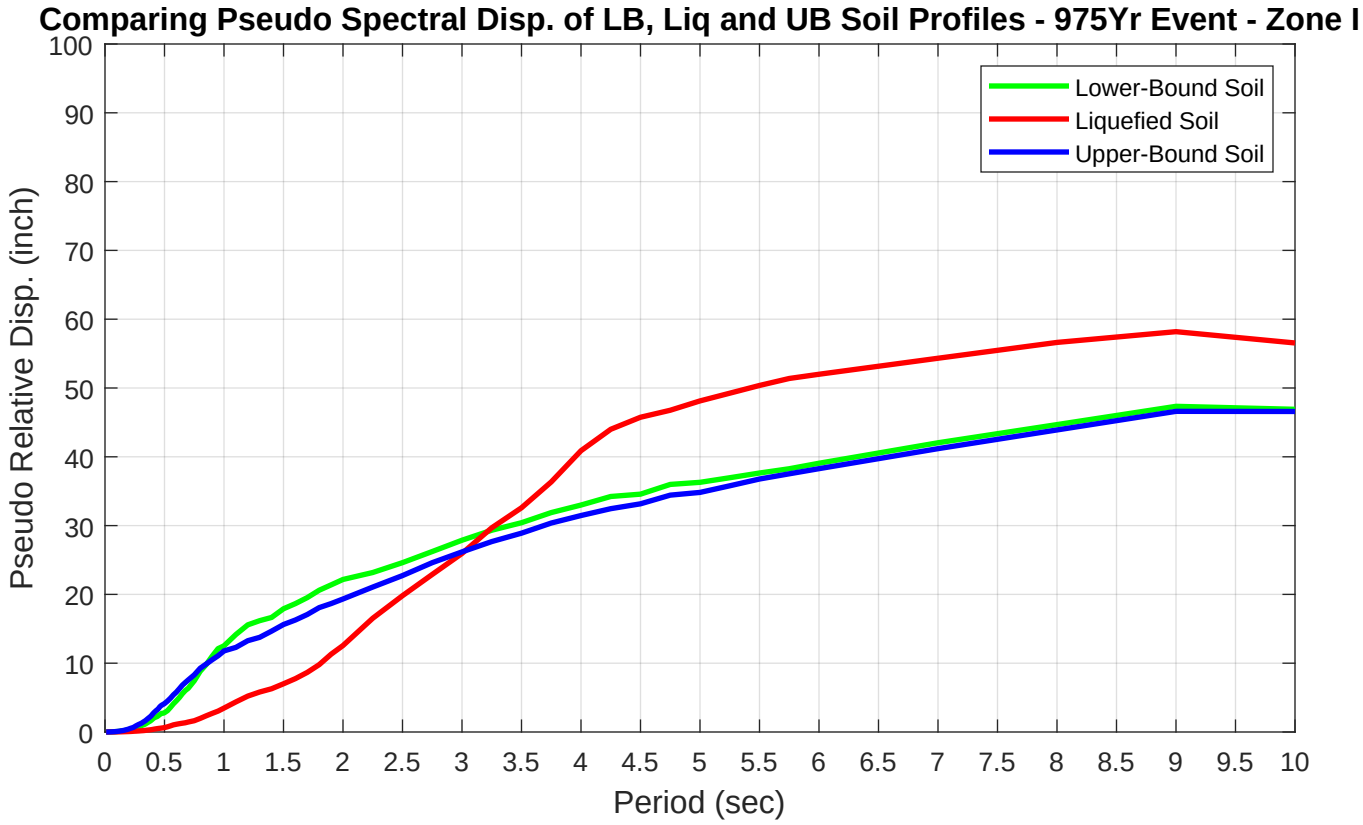

Comparing Spectral Accel. of LB, Liq and UB Soil Profiles - CLE Event - Zone III
Lower-Bound Soil
Liquefied Soil
Upper-Bound Soil
Spectral Acceleration (g)
Period (sec)
0
0.2
0.4
0.6
0.8
1
1.2
1.4
1.6
1.8
2
2.2
2.4
0 0.5 1 1.5 2 2.5 3 3.5 4 4.5 5 5.5 6 6.5 7 7.5 8 8.5 9 9.5 10

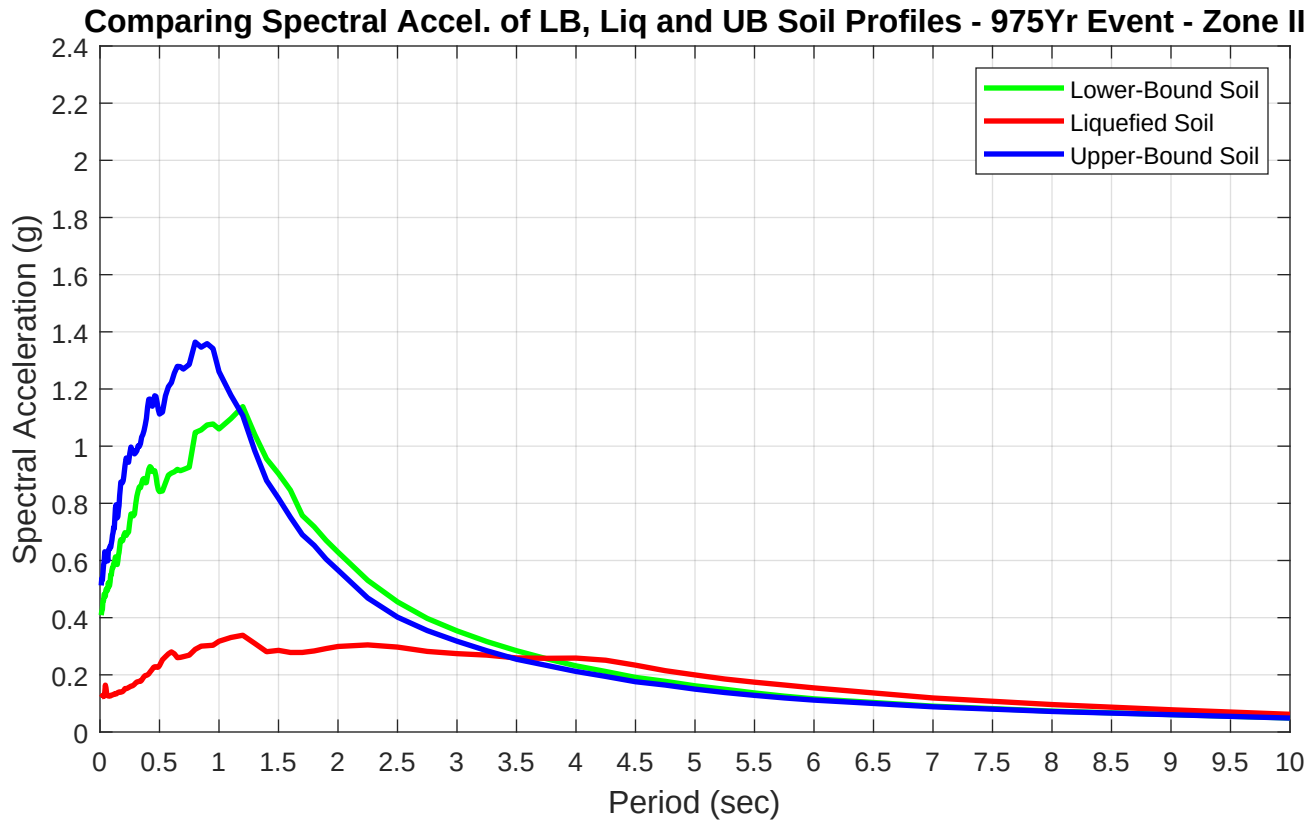

Comparing Pseudo Spectral Disp. of LB, Liq and UB Soil Profiles - CLE Event - Zone III
Lower-Bound Soil
Liquefied Soil
Upper-Bound Soil
Pseudo Relative Disp. (inch)
Period (sec)
0
10
20
30
40
50
60
70
80
90
100
0 0.5 1 1.5 2 2.5 3 3.5 4 4.5 5 5.5 6 6.5 7 7.5 8 8.5 9 9.5 10

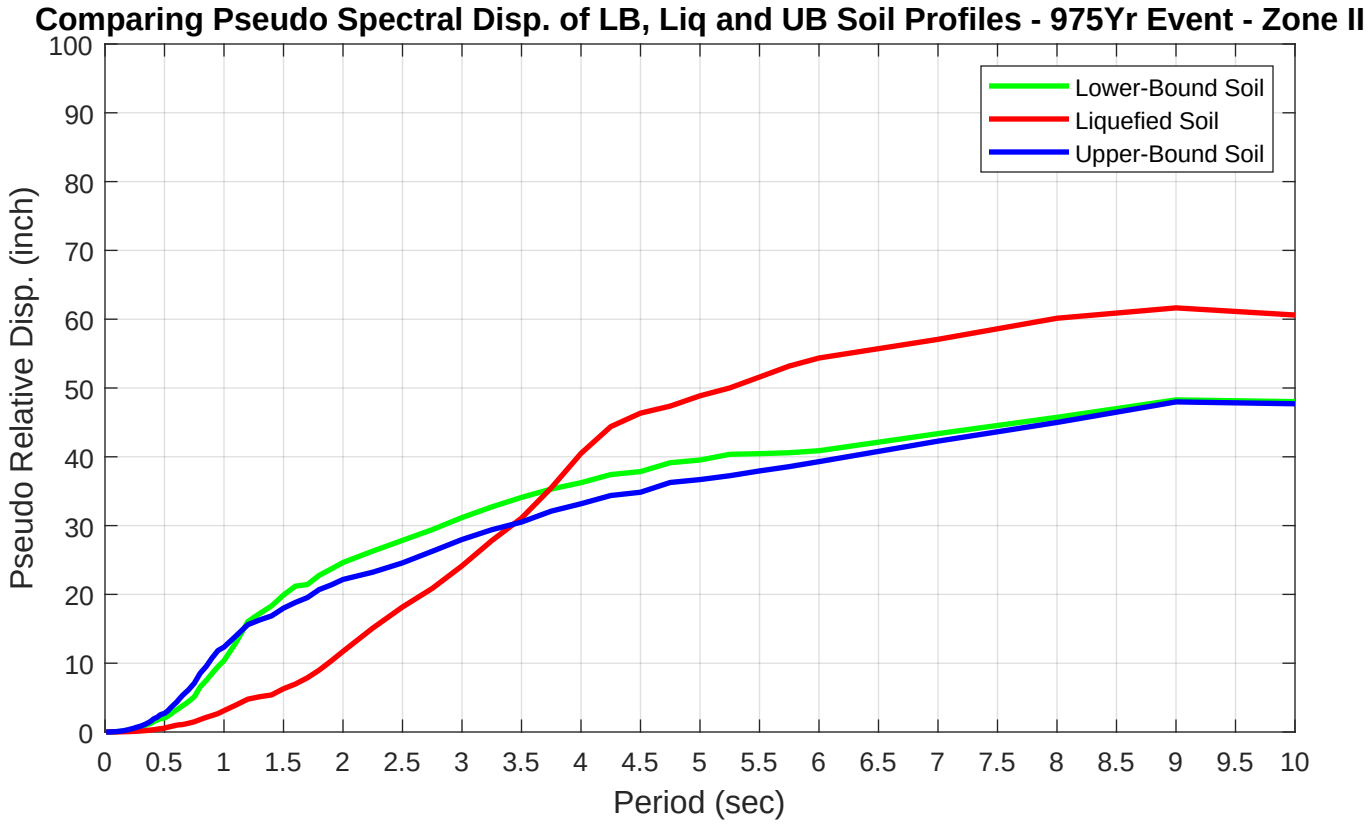

Comparing Spectral Accel. of LB, Liq and UB Soil Profiles - CLE Event - Zone IV
Lower-Bound Soil
Liquefied Soil
Upper-Bound Soil
Spectral Acceleration (g)
Period (sec)
0
0.2
0.4
0.6
0.8
1
1.2
1.4
1.6
1.8
2
2.2
2.4
0.5
1.5
2.5
3
3.5
4
4.5
5
5.5
6
6.5
7
7.5
8
8.5
9
9.5
10

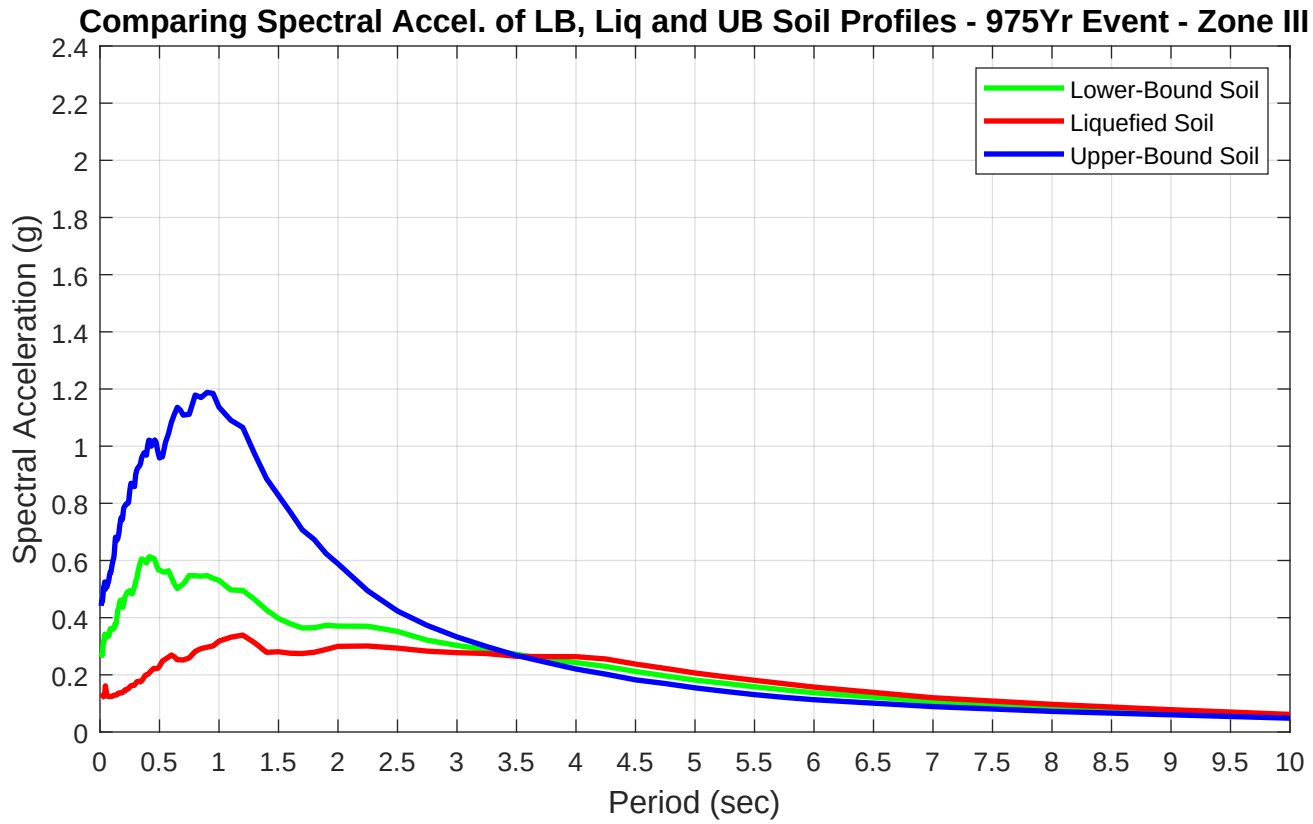

Comparing Pseudo Spectral Disp. of LB, Liq and UB Soil Profiles - CLE Event - Zone IV
Lower-Bound Soil
Liquefied Soil
Upper-Bound Soil
Pseudo Relative Disp. (inch)
Period (sec)
0
10
20
30
40
50
60
70
80
90
100
0.5
1.5
2.5
3
3.5
4
4.5
5
5.5
6
6.5
7
7.5
8
8.5
9
9.5
10

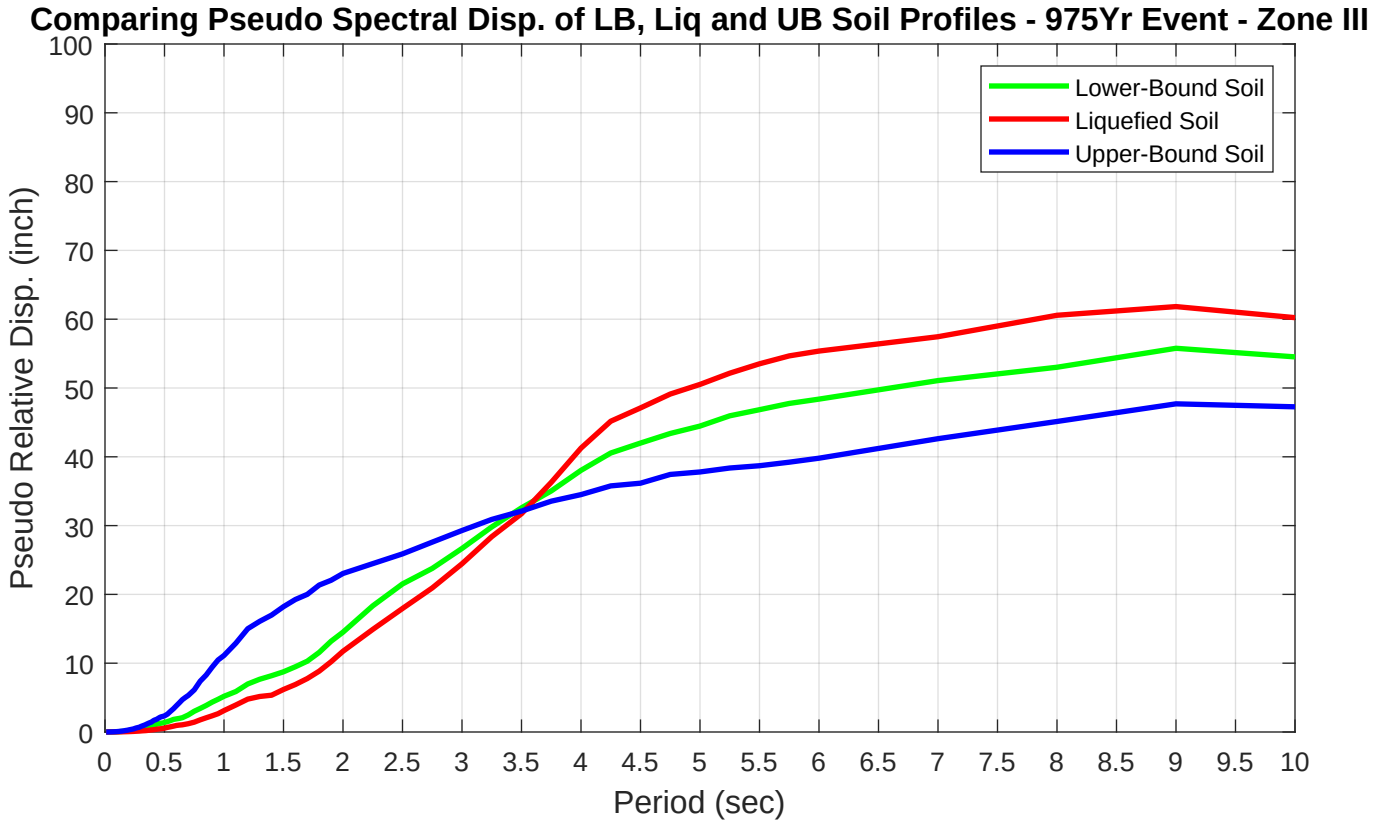

Comparing Spectral Accel. of LB, Liq and UB Soil Profiles - 975Yr Event - Zone I
Lower-Bound Soil
Liquefied Soil
Upper-Bound Soil
Spectral Acceleration (g)
Period (sec)
0
0.2
0.4
0.6
0.8
1
1.2
1.4
1.6
1.8
2
2.2
2.4
0 0.5 1 1.5 2 2.5 3 3.5 4 4.5 5 5.5 6 6.5 7 7.5 8 8.5 9 9.5 10

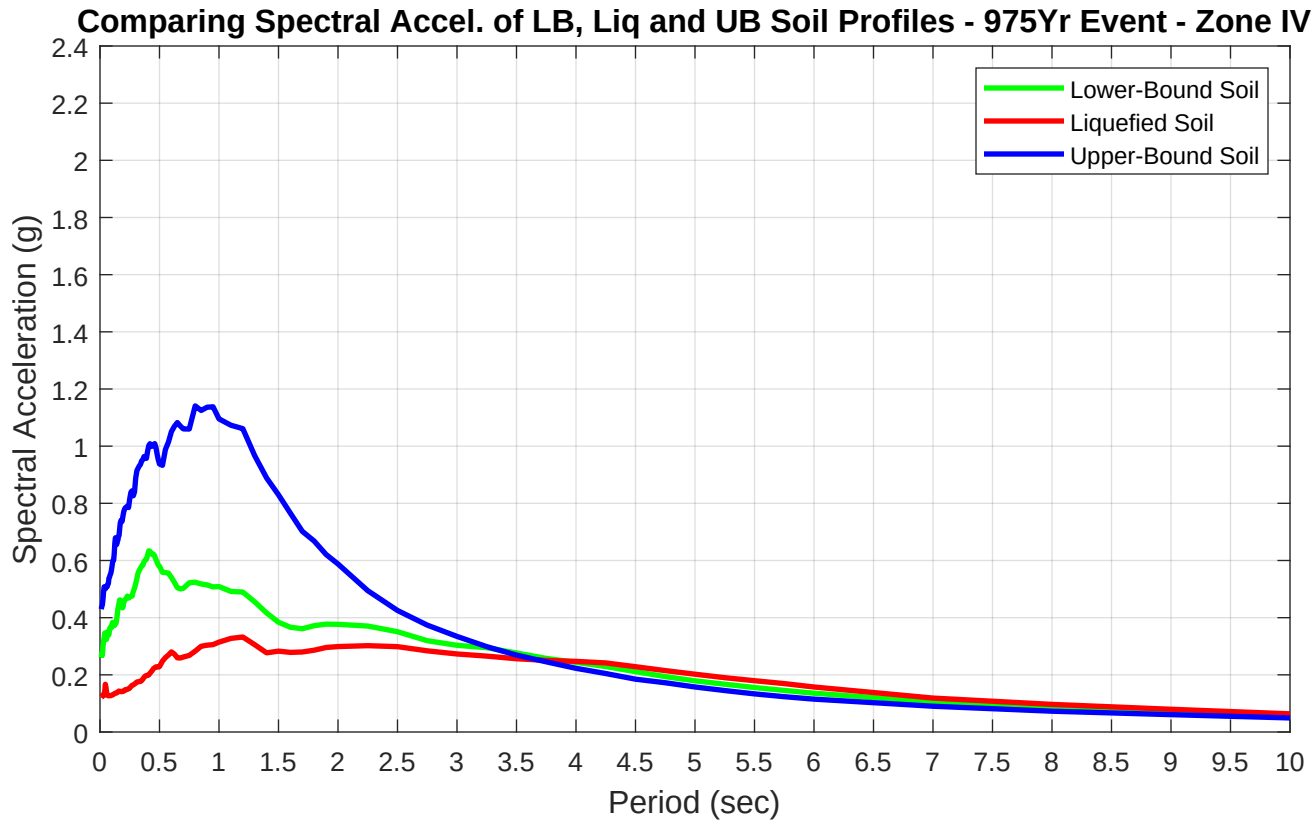

Comparing Pseudo Spectral Disp. of LB, Liq and UB Soil Profiles - 975Yr Event - Zone I
Lower-Bound Soil
Liquefied Soil
Upper-Bound Soil
Pseudo Relative Disp. (inch)
Period (sec)
0
10
20
30
40
50
60
70
80
90
100
0 0.5 1 1.5 2 2.5 3 3.5 4 4.5 5 5.5 6 6.5 7 7.5 8 8.5 9 9.5 10

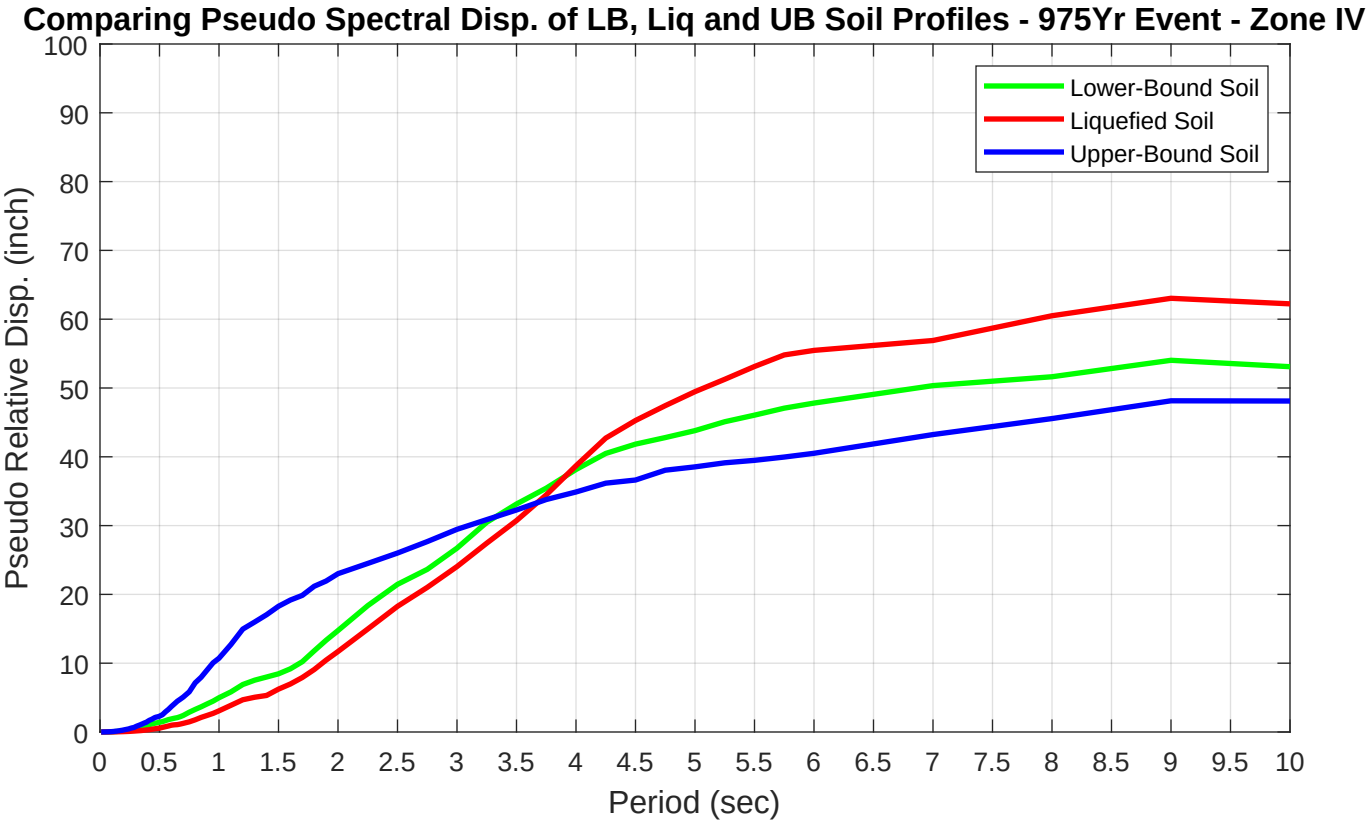

Comparing Spectral Accel. of LB, Liq and UB Soil Profiles - 975Yr Event - Zone II
Lower-Bound Soil
Liquefied Soil
Upper-Bound Soil
Spectral Acceleration (g)
Period (sec)
0
0.2
0.4
0.6
0.8
1
1.2
1.4
1.6
1.8
2
2.2
2.4
0 0.5 1 1.5 2 2.5 3 3.5 4 4.5 5 5.5 6 6.5 7 7.5 8 8.5 9 9.5 10

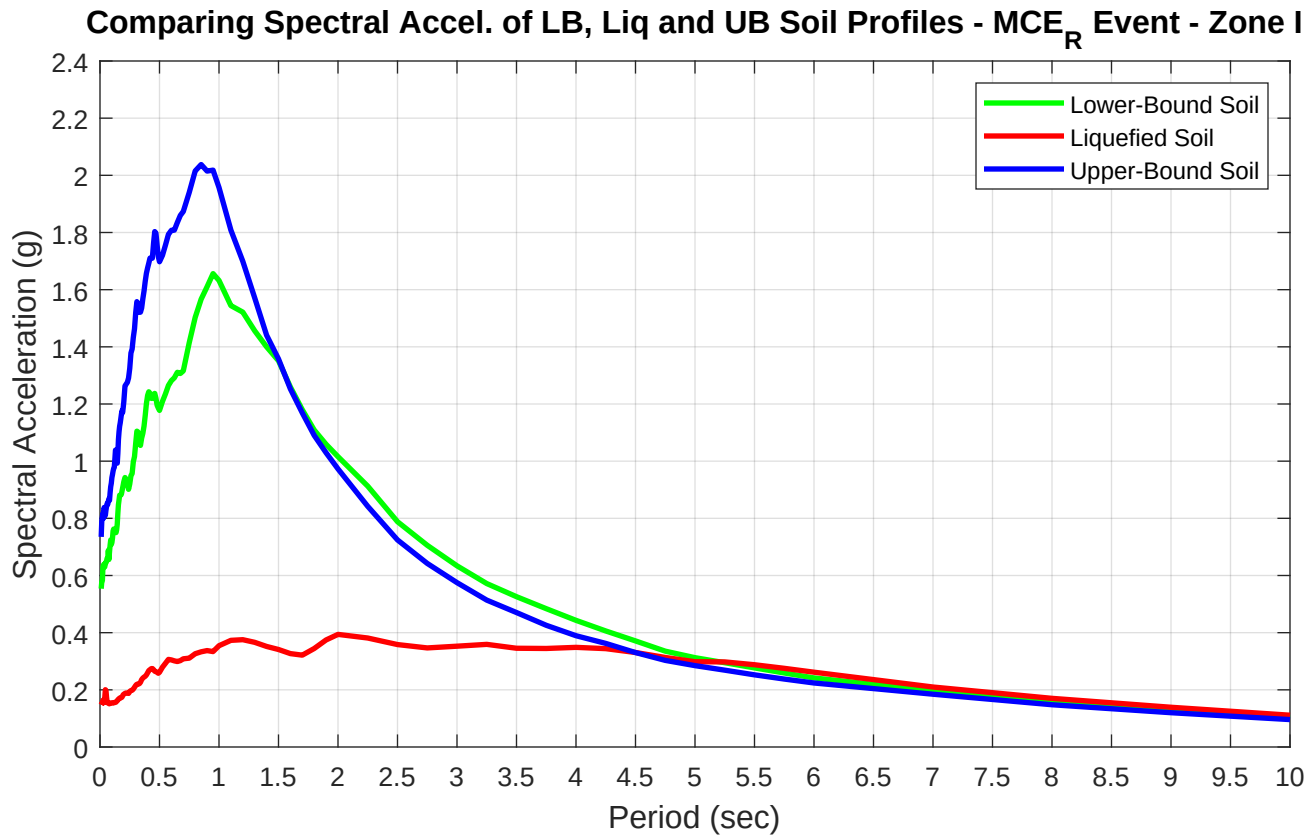

Comparing Pseudo Spectral Disp. of LB, Liq and UB Soil Profiles - 975Yr Event - Zone II
Lower-Bound Soil
Liquefied Soil
Upper-Bound Soil
Pseudo Relative Disp. (inch)
Period (sec)
0
10
20
30
40
50
60
70
80
90
100
0 0.5 1 1.5 2 2.5 3 3.5 4 4.5 5 5.5 6 6.5 7 7.5 8 8.5 9 9.5 10

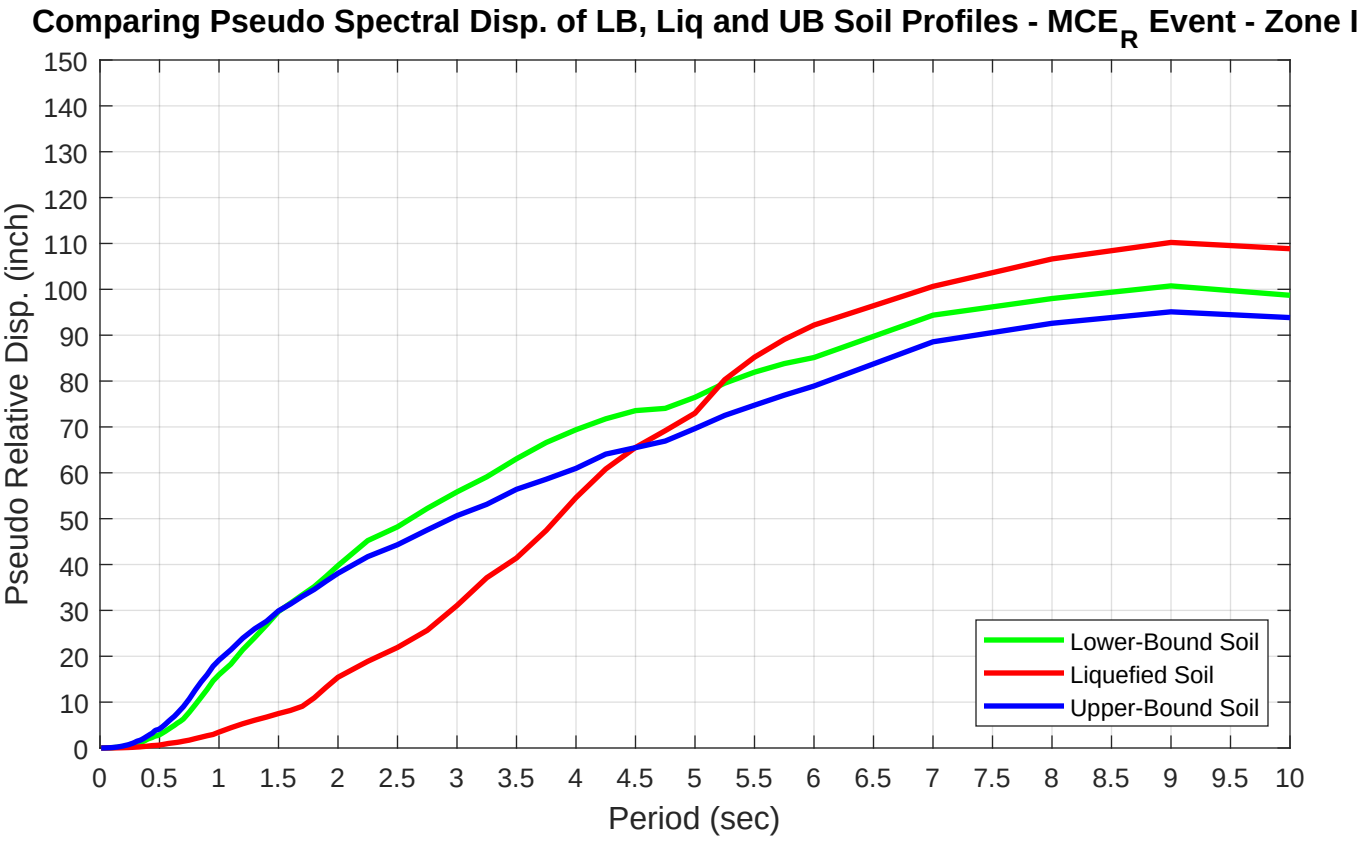

Comparing Spectral Accel. of LB, Liq and UB Soil Profiles - 975Yr Event - Zone III
Lower-Bound Soil
Liquefied Soil
Upper-Bound Soil
Spectral Acceleration (g)
Period (sec)
0
0.2
0.4
0.6
0.8
1
1.2
1.4
1.6
1.8
2
2.2
2.4
0 0.5 1 1.5 2 2.5 3 3.5 4 4.5 5 5.5 6 6.5 7 7.5 8 8.5 9 9.5 10

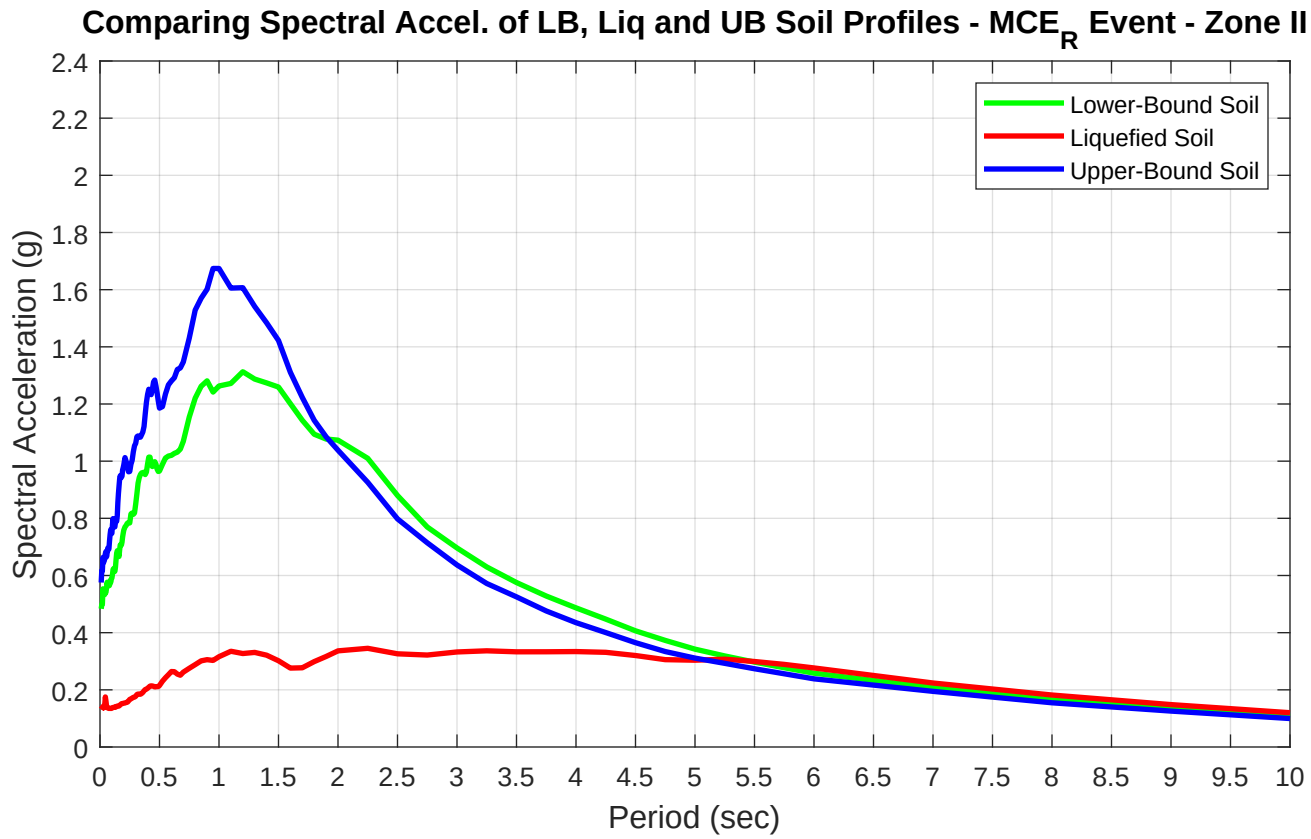

Comparing Pseudo Spectral Disp. of LB, Liq and UB Soil Profiles - 975Yr Event - Zone III
Lower-Bound Soil
Liquefied Soil
Upper-Bound Soil
Pseudo Relative Disp. (inch)
Period (sec)
0
10
20
30
40
50
60
70
80
90
100
0 0.5 1 1.5 2 2.5 3 3.5 4 4.5 5 5.5 6 6.5 7 7.5 8 8.5 9 9.5 10

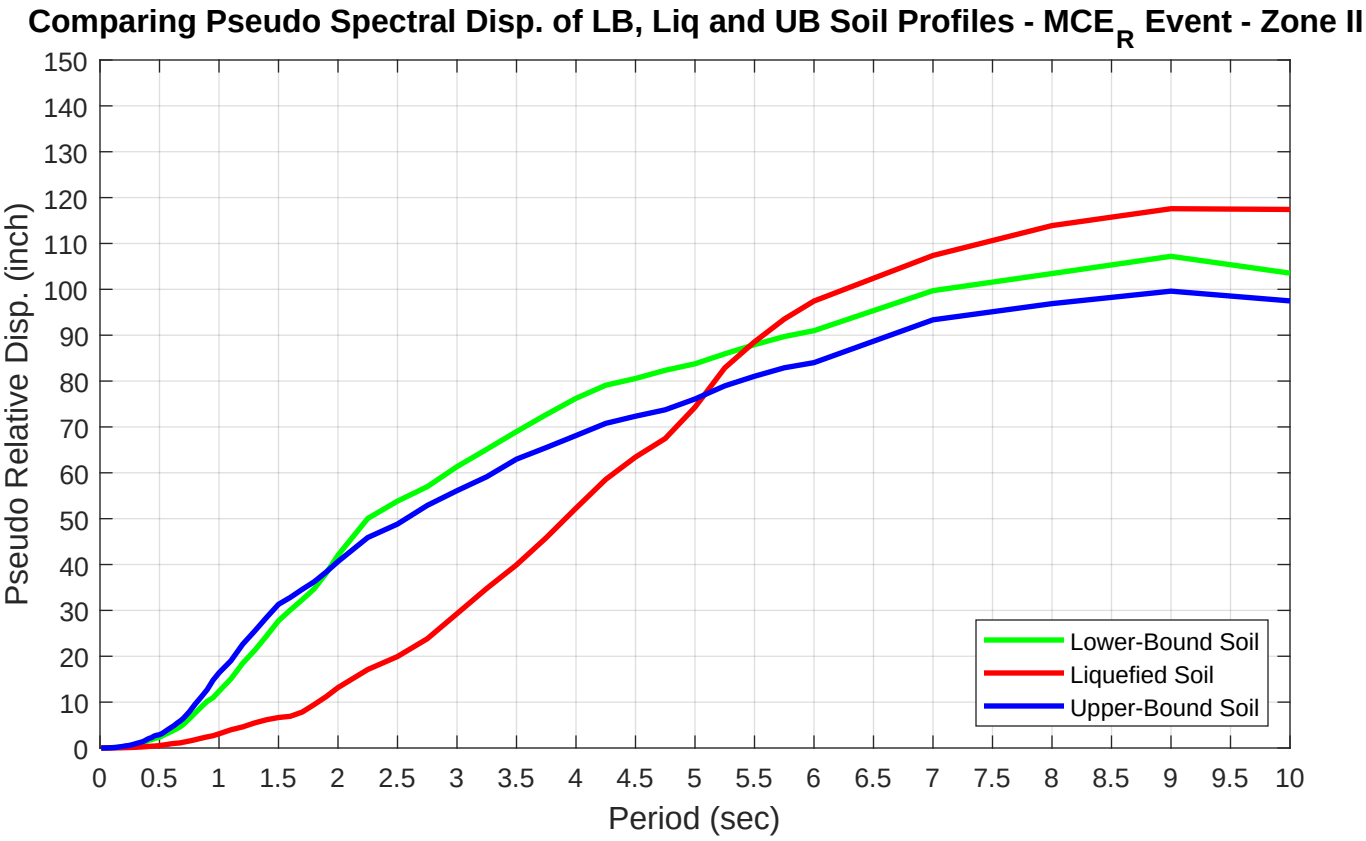

Comparing Spectral Accel. of LB, Liq and UB Soil Profiles - 975Yr Event - Zone IV
Lower-Bound Soil
Liquefied Soil
Upper-Bound Soil
Spectral Acceleration (g)
Period (sec)
0
0.2
0.4
0.6
0.8
1
1.2
1.4
1.6
1.8
2
2.2
2.4
0 0.5 1 1.5 2 2.5 3 3.5 4 4.5 5 5.5 6 6.5 7 7.5 8 8.5 9 9.5 10

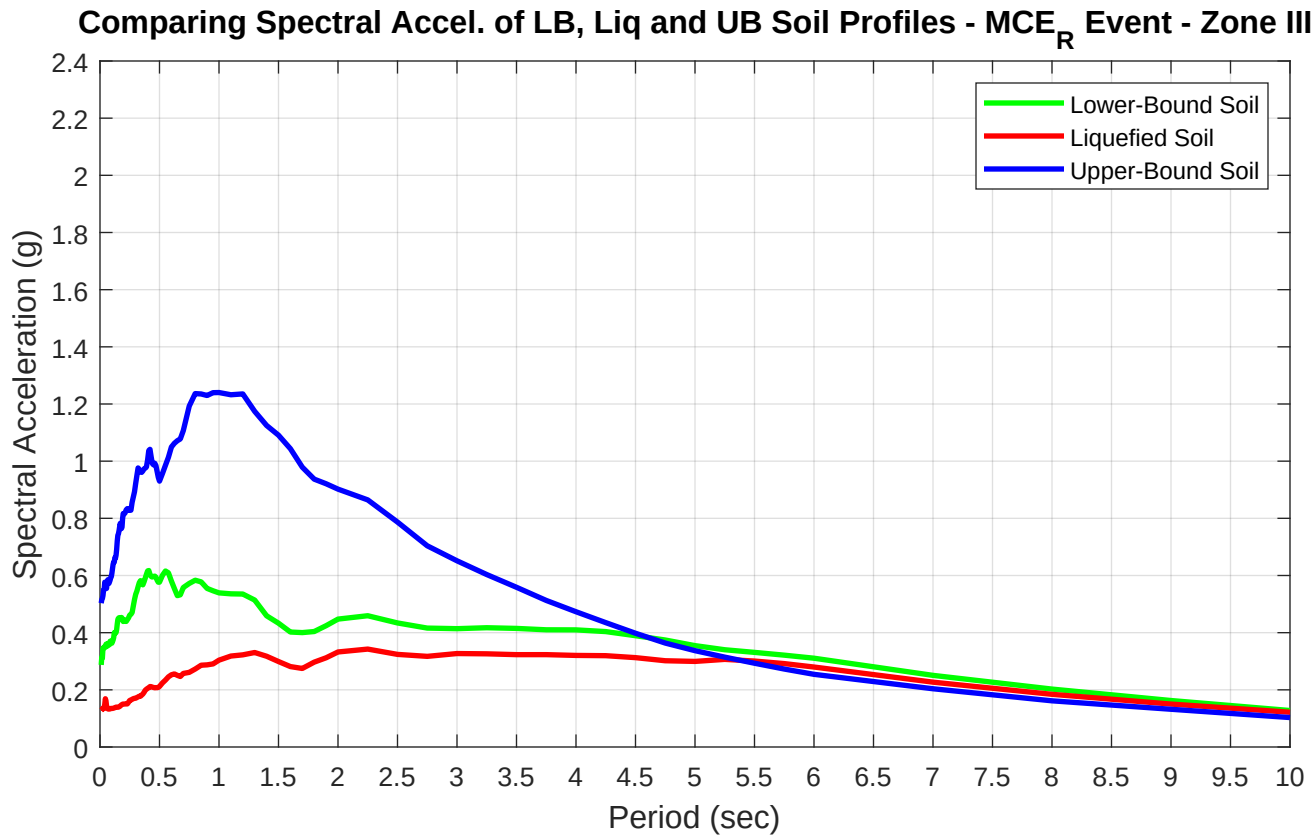

Comparing Pseudo Spectral Disp. of LB, Liq and UB Soil Profiles - 975Yr Event - Zone IV
Lower-Bound Soil
Liquefied Soil
Upper-Bound Soil
Pseudo Relative Disp. (inch)
Period (sec)
0
10
20
30
40
50
60
70
80
90
100
0 0.5 1 1.5 2 2.5 3 3.5 4 4.5 5 5.5 6 6.5 7 7.5 8 8.5 9 9.5 10

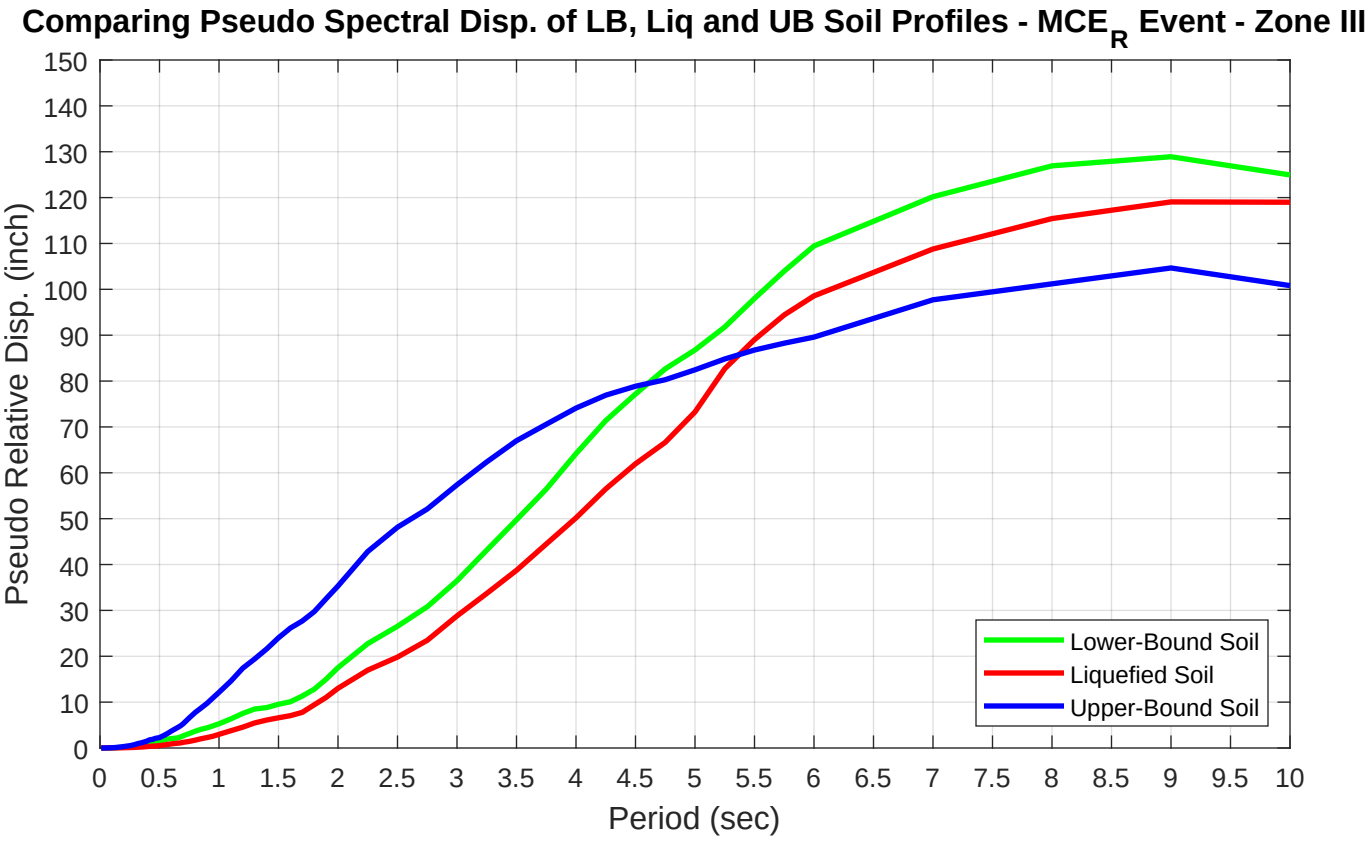

Comparing Spectral Accel. of LB, Liq and UB Soil Profiles - MCE$_R$ Event - Zone I
Spectral Acceleration (g)
Period (sec)
Lower-Bound Soil
Liquefied Soil
Upper-Bound Soil

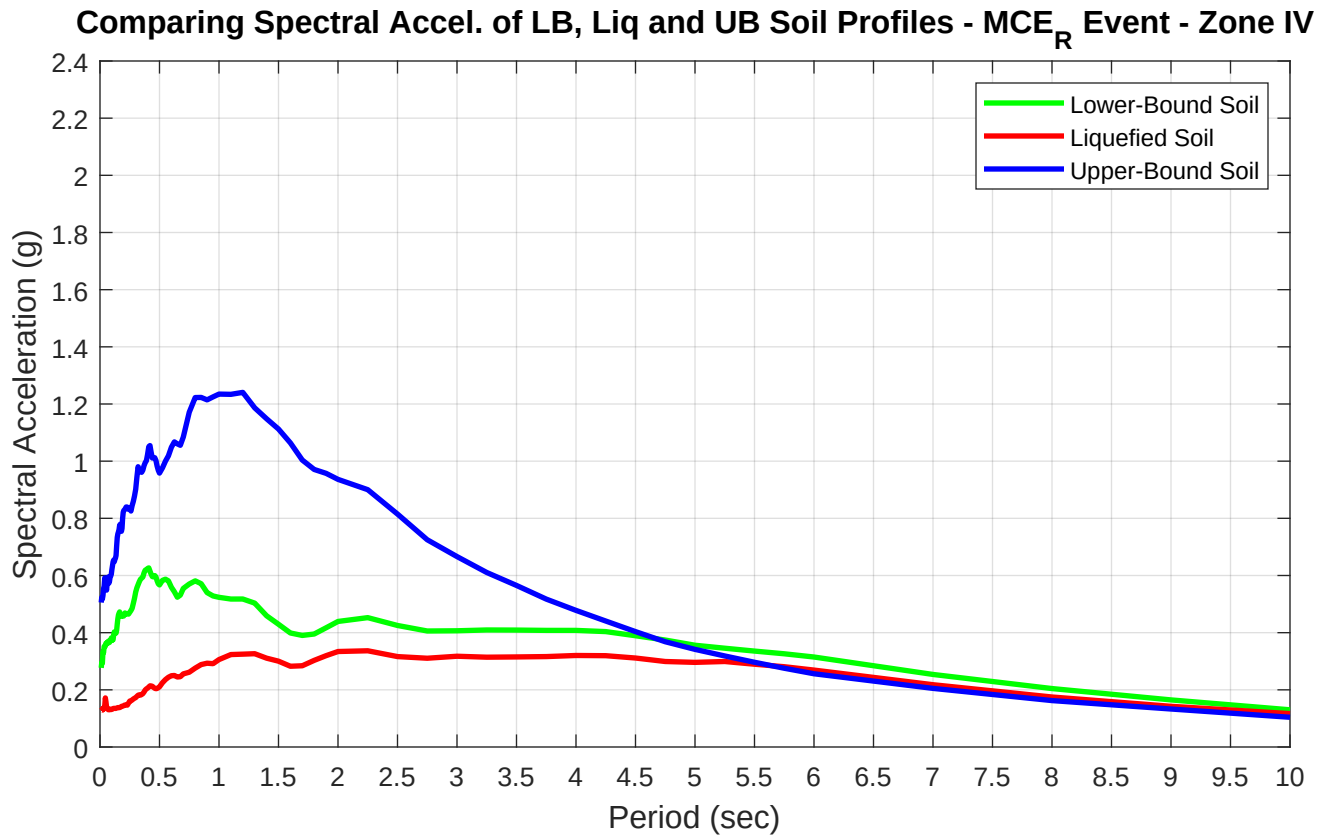

Comparing Pseudo Spectral Disp. of LB, Liq and UB Soil Profiles - MCE$_R$ Event - Zone I
Pseudo Relative Disp. (inch)
Period (sec)
Lower-Bound Soil
Liquefied Soil
Upper-Bound Soil

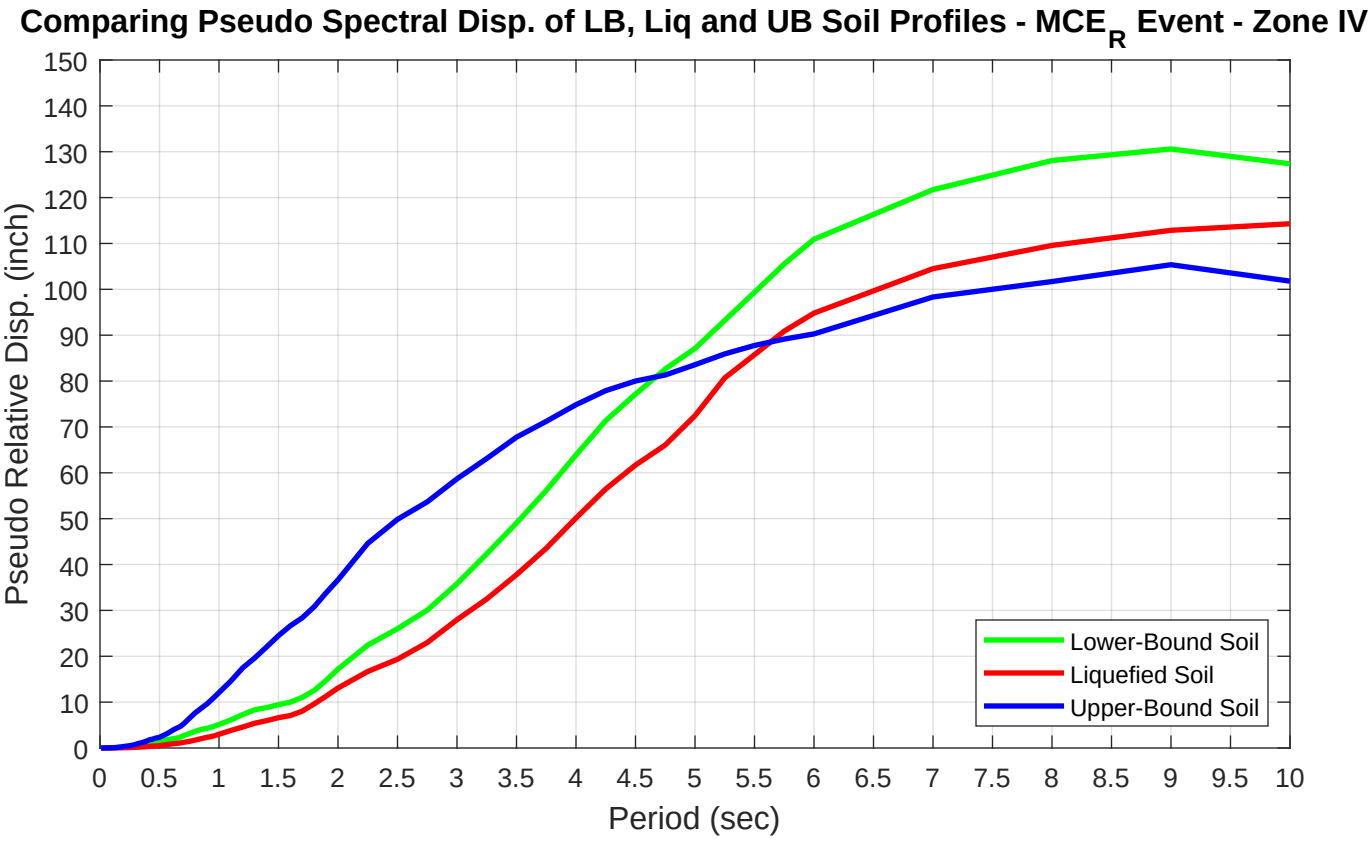

Comparing Spectral Accel. of LB, Liq and UB Soil Profiles - MCE$_R$ Event - Zone II
Spectral Acceleration (g)
Period (sec)
Lower-Bound Soil
Liquefied Soil
Upper-Bound Soil


Comparing Pseudo Spectral Disp. of LB, Liq and UB Soil Profiles - MCE$_R$ Event - Zone II
Pseudo Relative Disp. (inch)
Period (sec)
Lower-Bound Soil
Liquefied Soil
Upper-Bound Soil

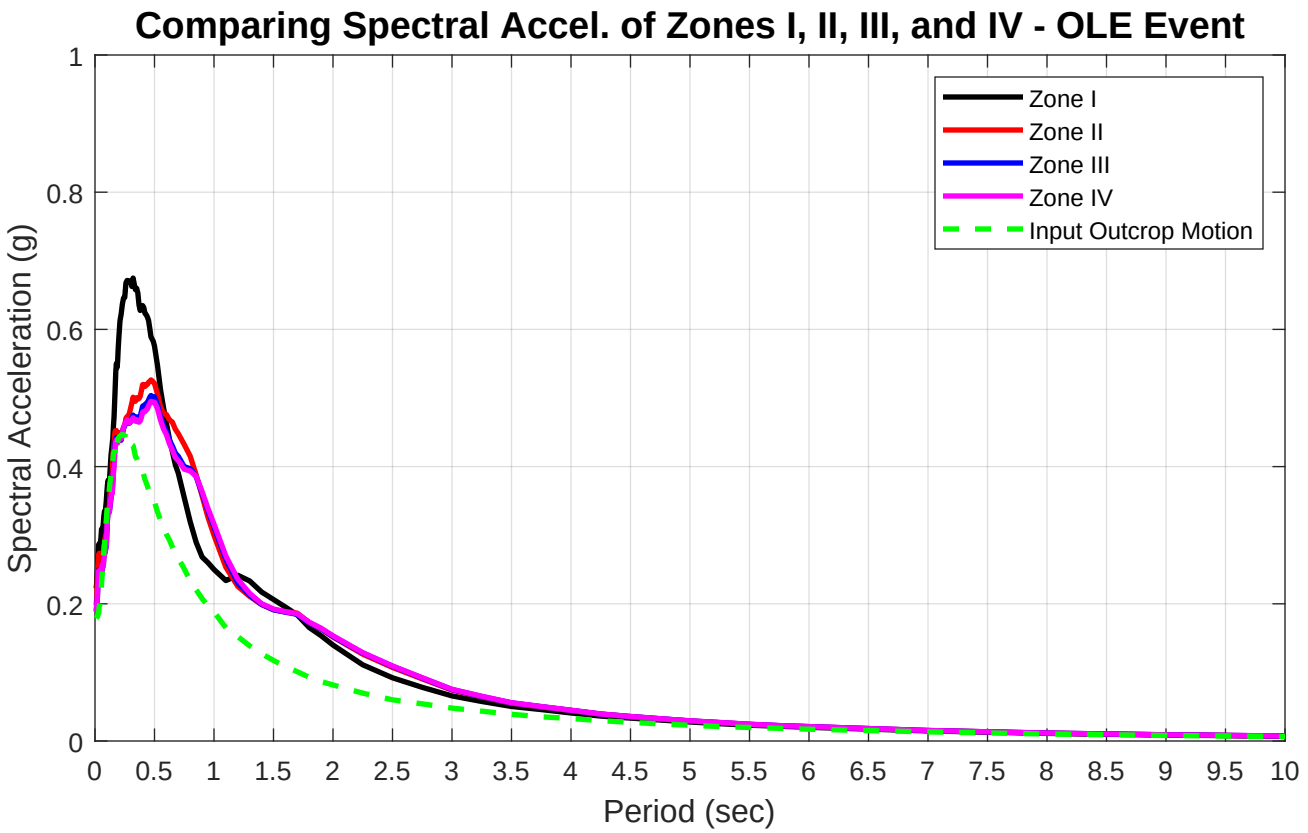

Comparing Spectral Accel. of LB, Liq and UB Soil Profiles - MCE$_R$ Event - Zone III
Spectral Acceleration (g)
Period (sec)
Lower-Bound Soil
Liquefied Soil
Upper-Bound Soil

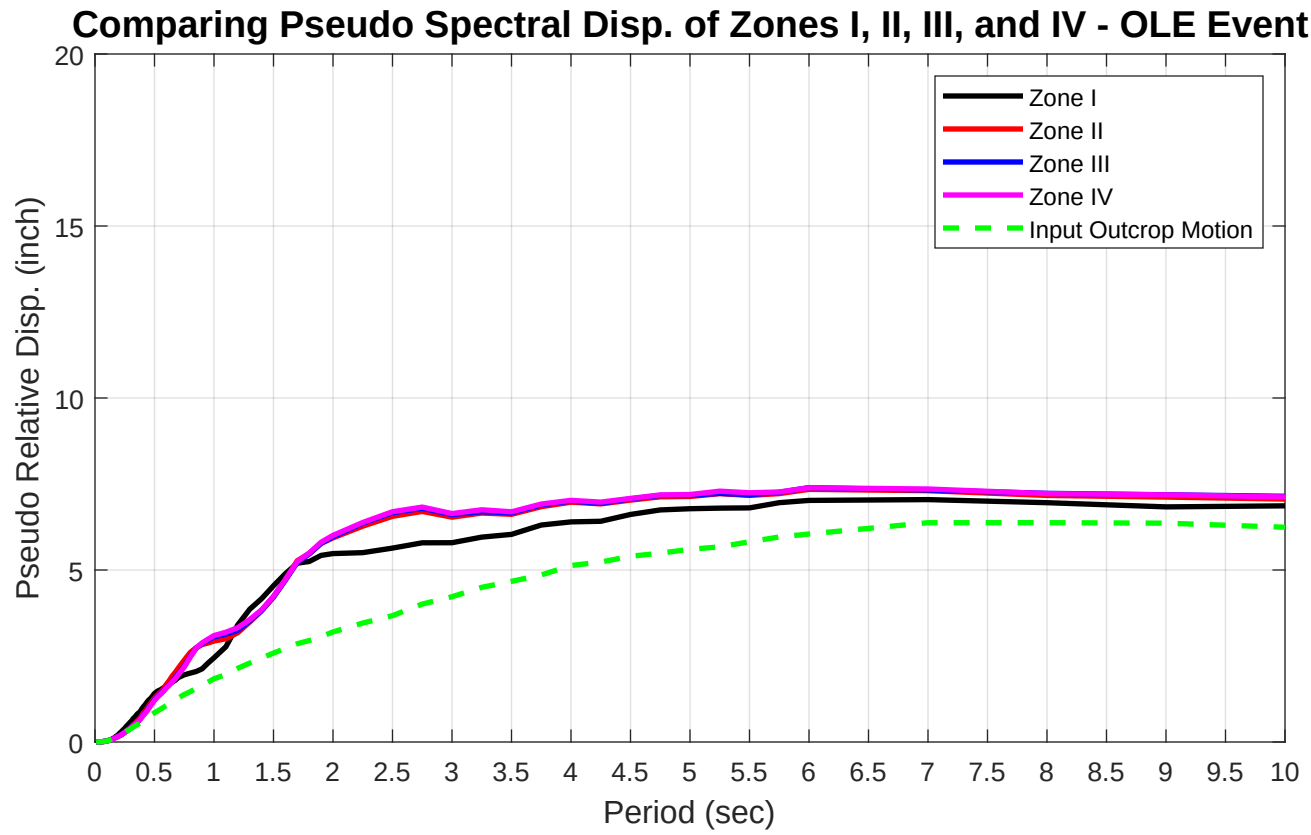

Comparing Pseudo Spectral Disp. of LB, Liq and UB Soil Profiles - MCE$_R$ Event - Zone III
Pseudo Relative Disp. (inch)
Period (sec)
Lower-Bound Soil
Liquefied Soil
Upper-Bound Soil

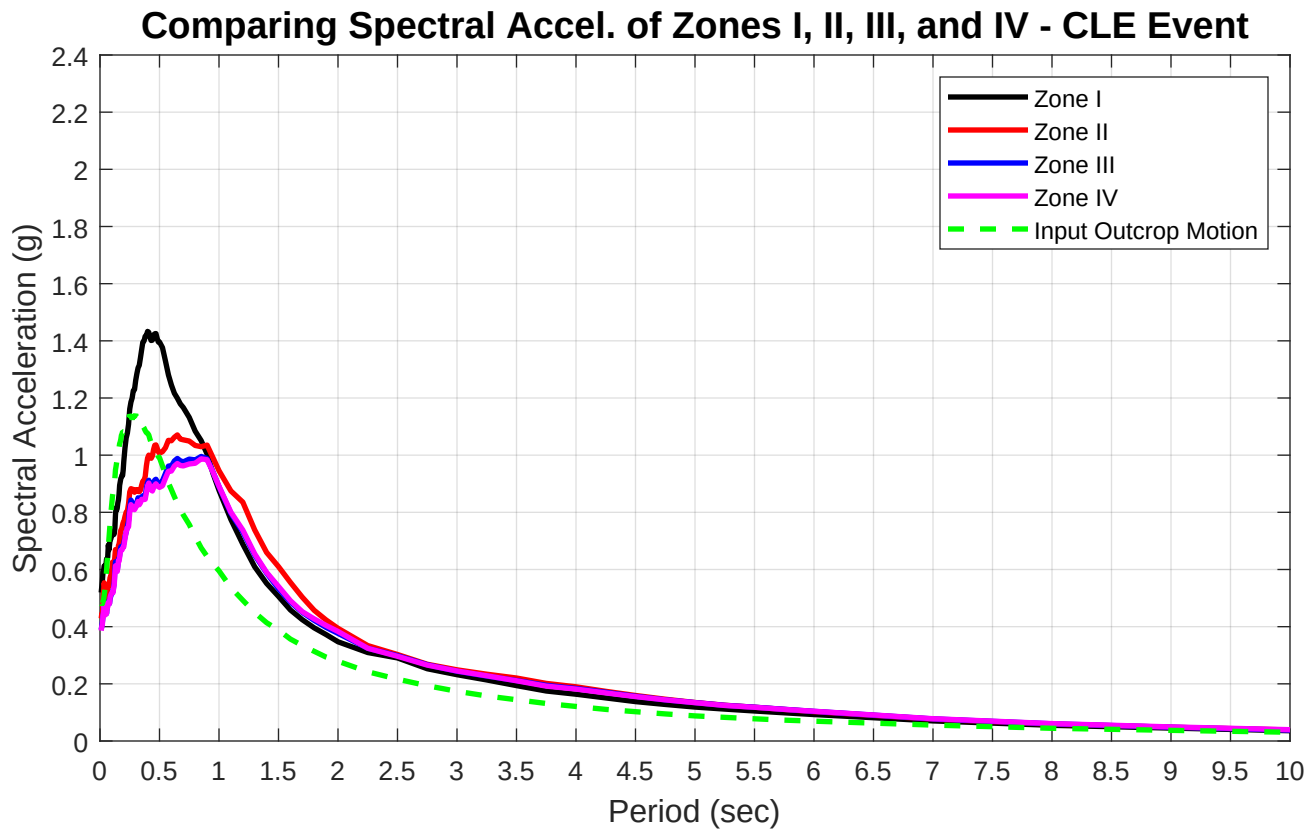

Comparing Spectral Accel. of LB, Liq and UB Soil Profiles - MCE$_R$ Event - Zone IV
Spectral Acceleration (g)
Period (sec)
Lower-Bound Soil
Liquefied Soil
Upper-Bound Soil

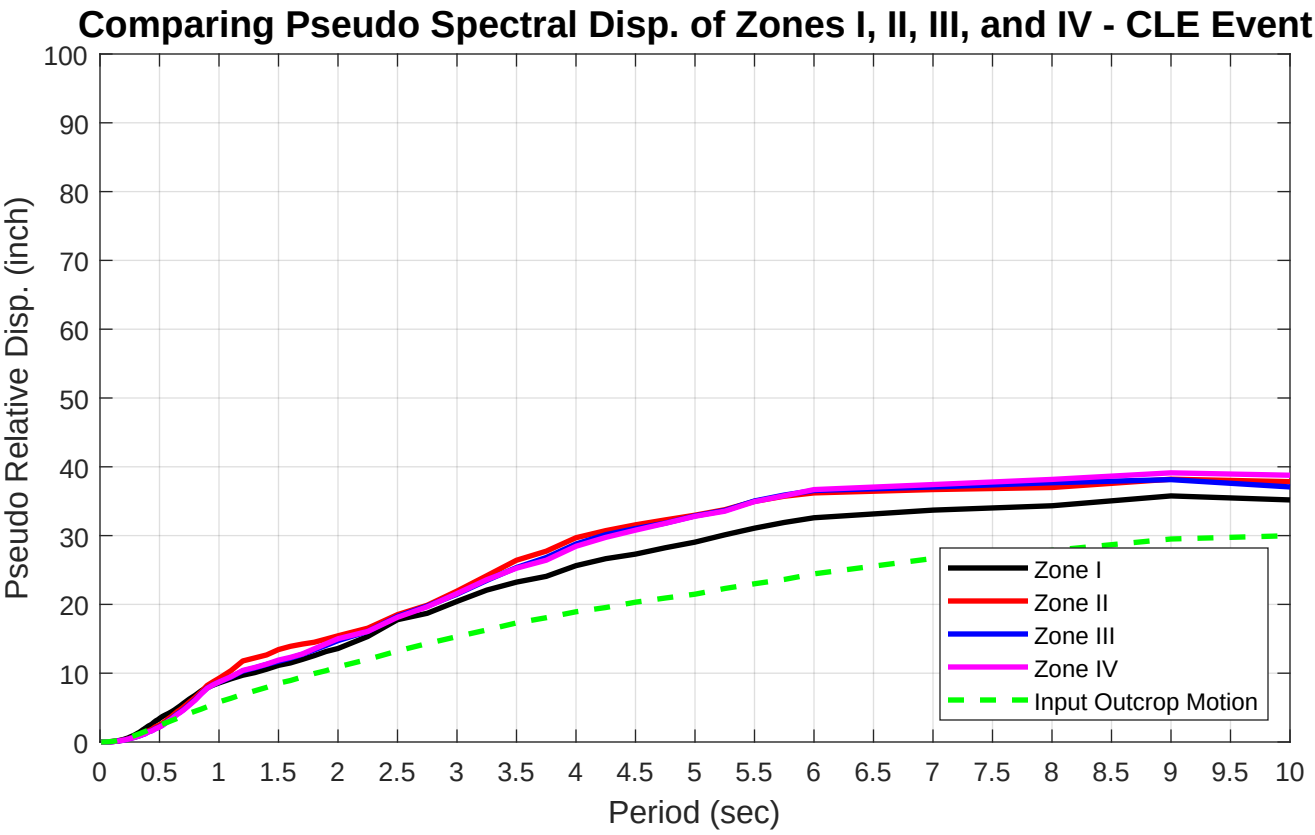

Comparing Pseudo Spectral Disp. of LB, Liq and UB Soil Profiles - MCE$_R$ Event - Zone IV
Pseudo Relative Disp. (inch)
Period (sec)
Lower-Bound Soil
Liquefied Soil
Upper-Bound Soil

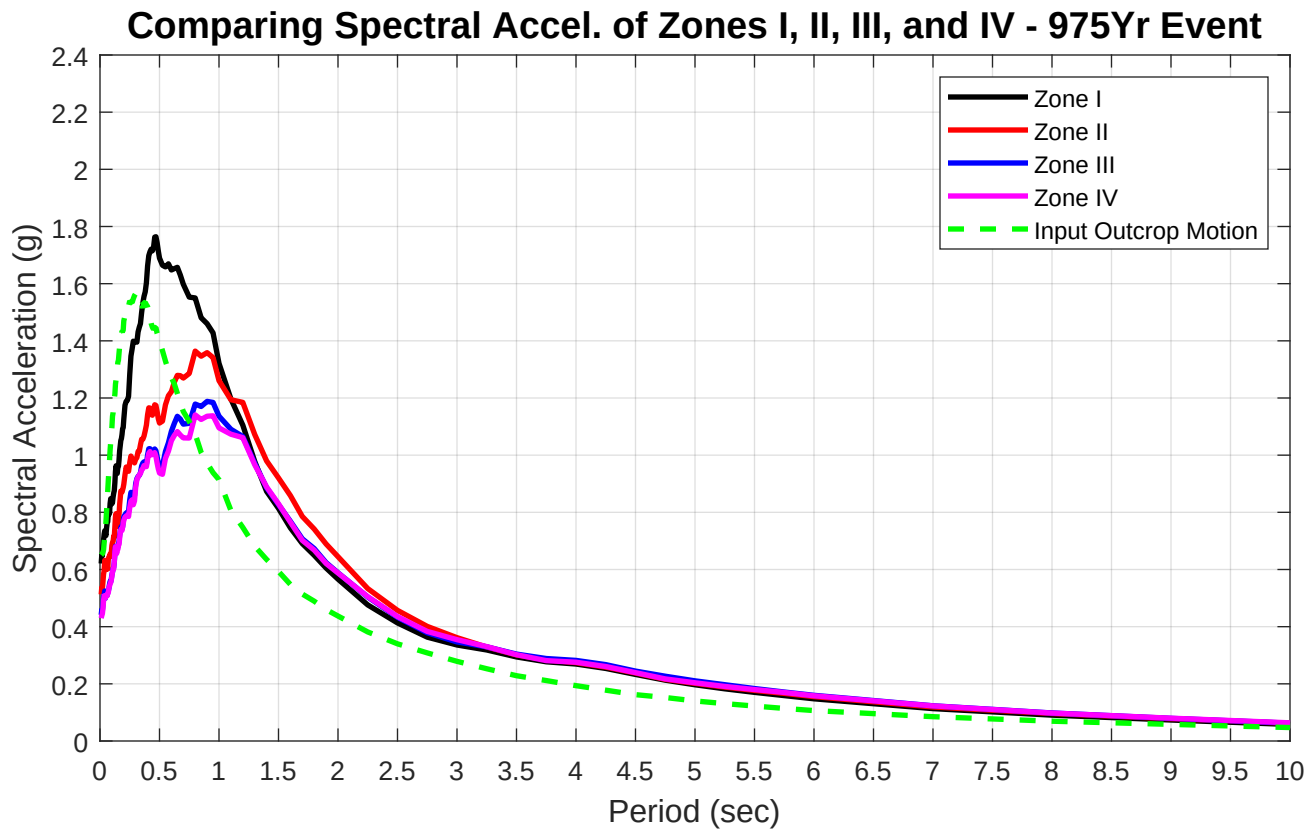
Part II: Enveloped Spectral Acceleration and Pseudo Spectral Displacement Spectra for Zones I, II, III, and IV

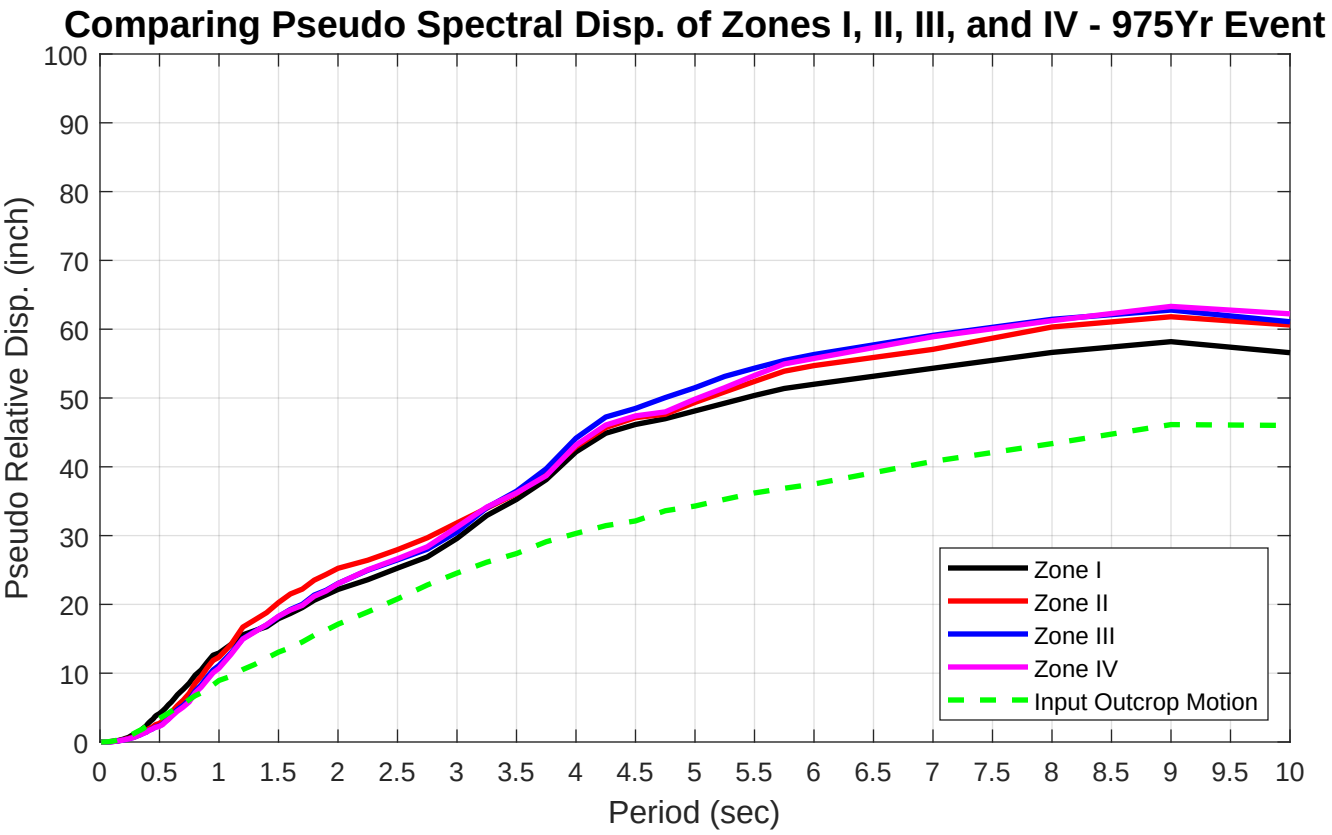

Comparing Spectral Accel. of Zones I, II, III, and IV - OLE Event
Spectral Acceleration (g)
Period (sec)
Zone I
Zone II
Zone III
Zone IV
Input Outcrop Motion
0
0.2
0.4
0.6
0.8
1
0 0.5 1 1.5 2 2.5 3 3.5 4 4.5 5 5.5 6 6.5 7 7.5 8 8.5 9 9.5 10


Comparing Pseudo Spectral Disp. of Zones I, II, III, and IV - OLE Event
Pseudo Relative Disp. (inch)
Period (sec)
Zone I
Zone II
Zone III
Zone IV
Input Outcrop Motion
0
5
10
15
20
0 0.5 1 1.5 2 2.5 3 3.5 4 4.5 5 5.5 6 6.5 7 7.5 8 8.5 9 9.5 10

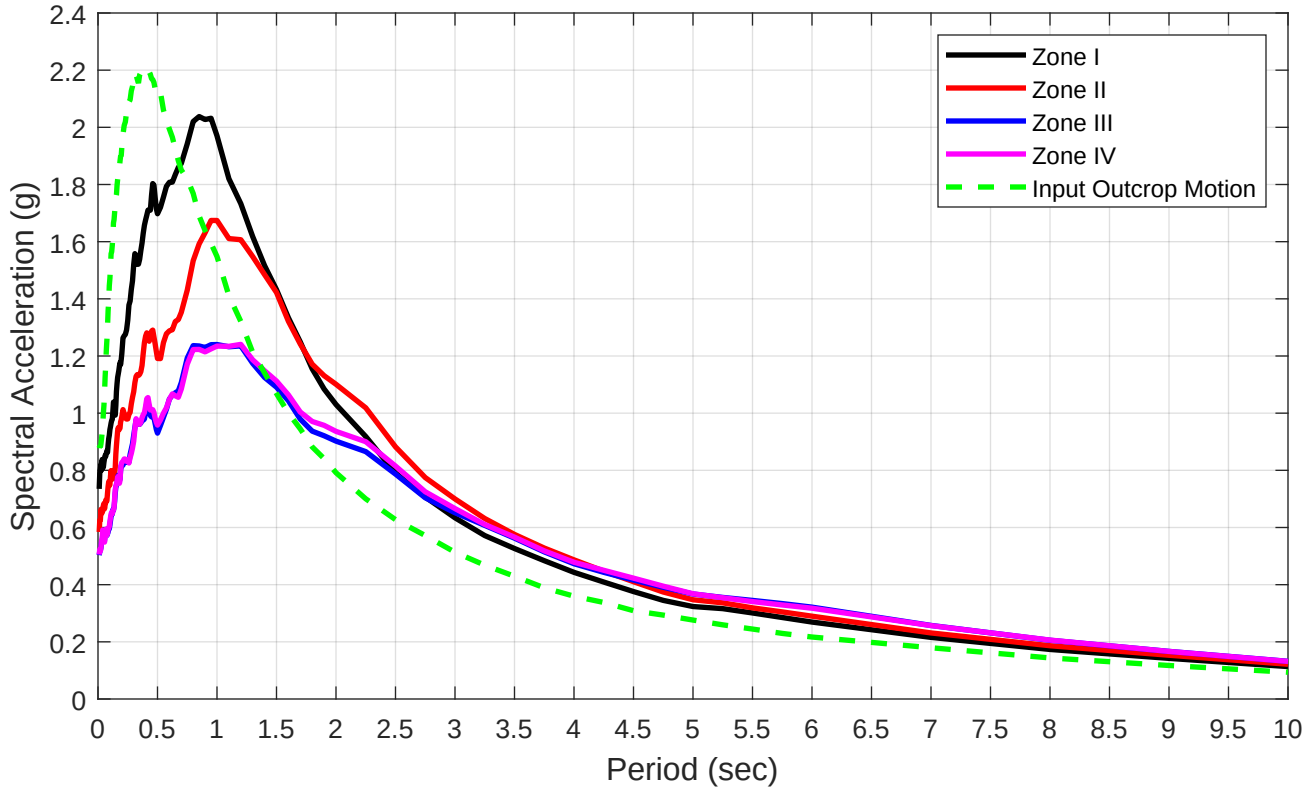

Comparing Spectral Accel. of Zones I, II, III, and IV - CLE Event
Spectral Acceleration (g)
Period (sec)
Zone I
Zone II
Zone III
Zone IV
Input Outcrop Motion


Comparing Pseudo Spectral Disp. of Zones I, II, III, and IV - CLE Event
Pseudo Relative Disp. (inch)
Period (sec)
Zone I
Zone II
Zone III
Zone IV
Input Outcrop Motion

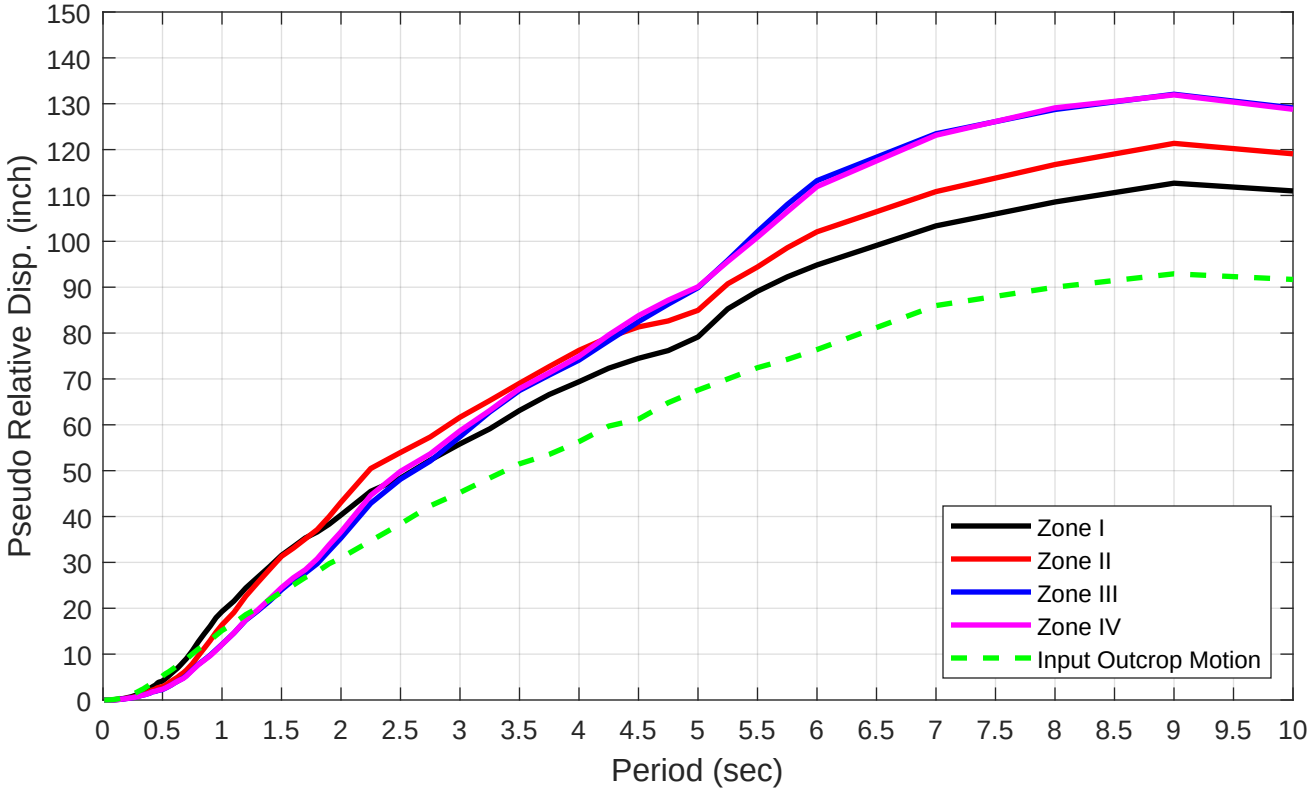

Comparing Spectral Accel. of Zones I, II, III, and IV - 975Yr Event
Spectral Acceleration (g)
Period (sec)
Zone I
Zone II
Zone III
Zone IV
Input Outcrop Motion


Comparing Pseudo Spectral Disp. of Zones I, II, III, and IV - 975Yr Event
Pseudo Relative Disp. (inch)
Period (sec)
Zone I
Zone II
Zone III
Zone IV
Input Outcrop Motion

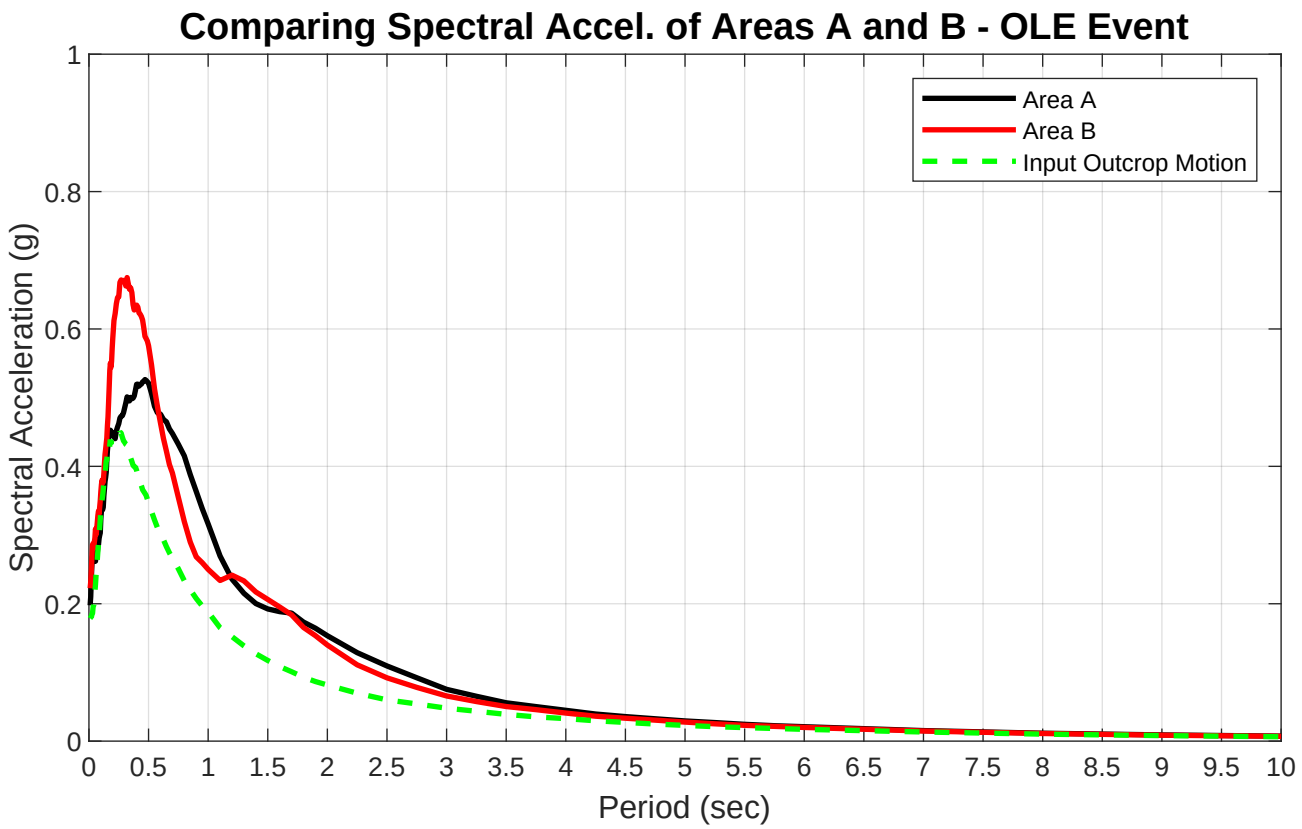
Comparing Spectral Accel. of Zones I, II, III, and IV - MCE_R

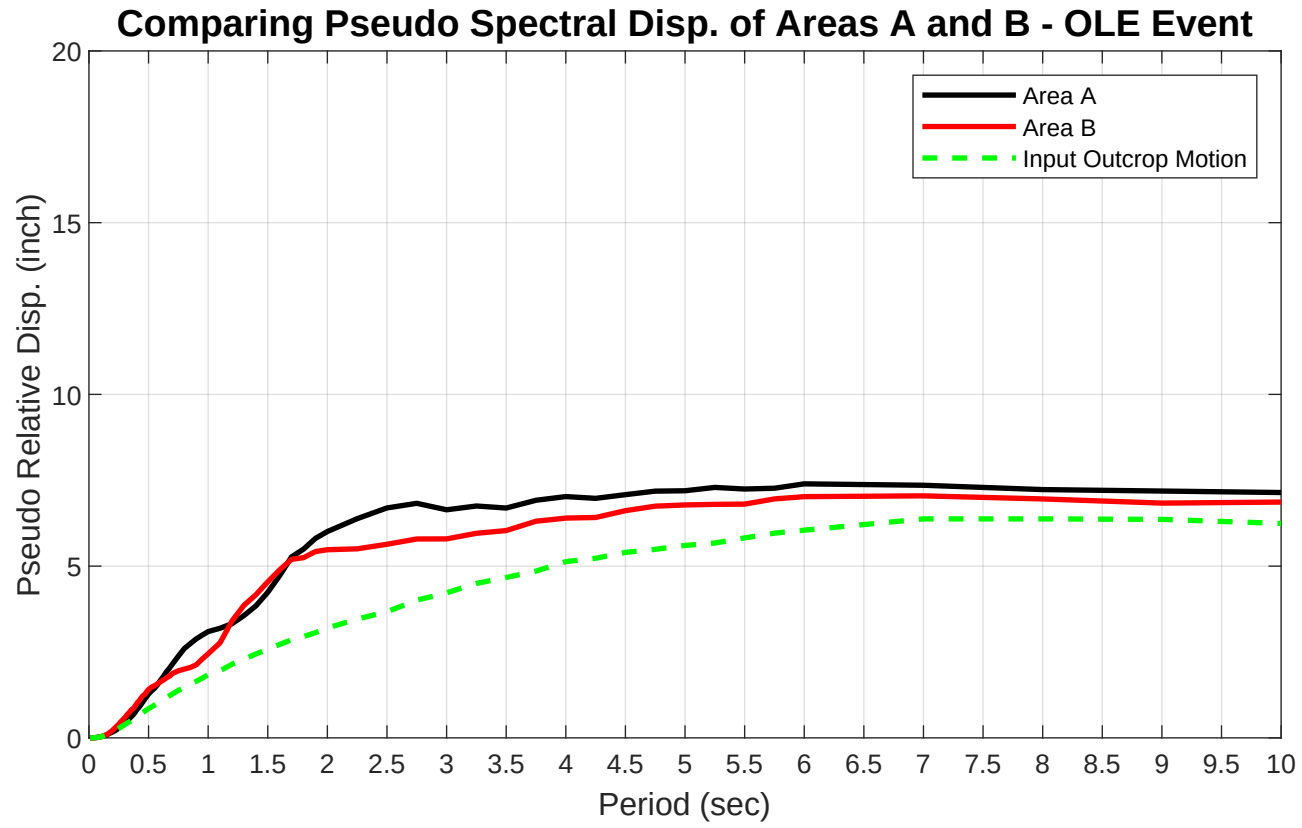


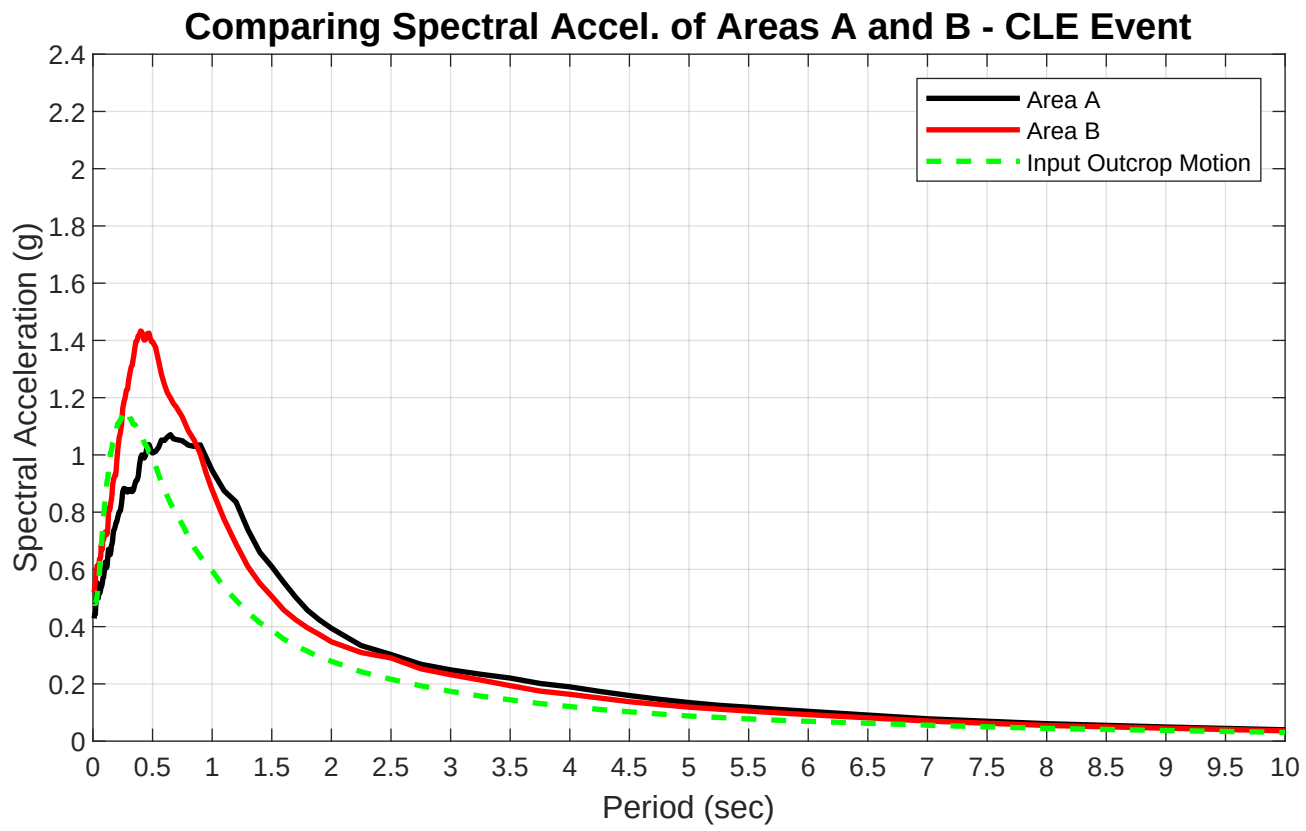
Comparing Pseudo Spectral Disp. of Zones I, II, III, and IV - MCE_R Event

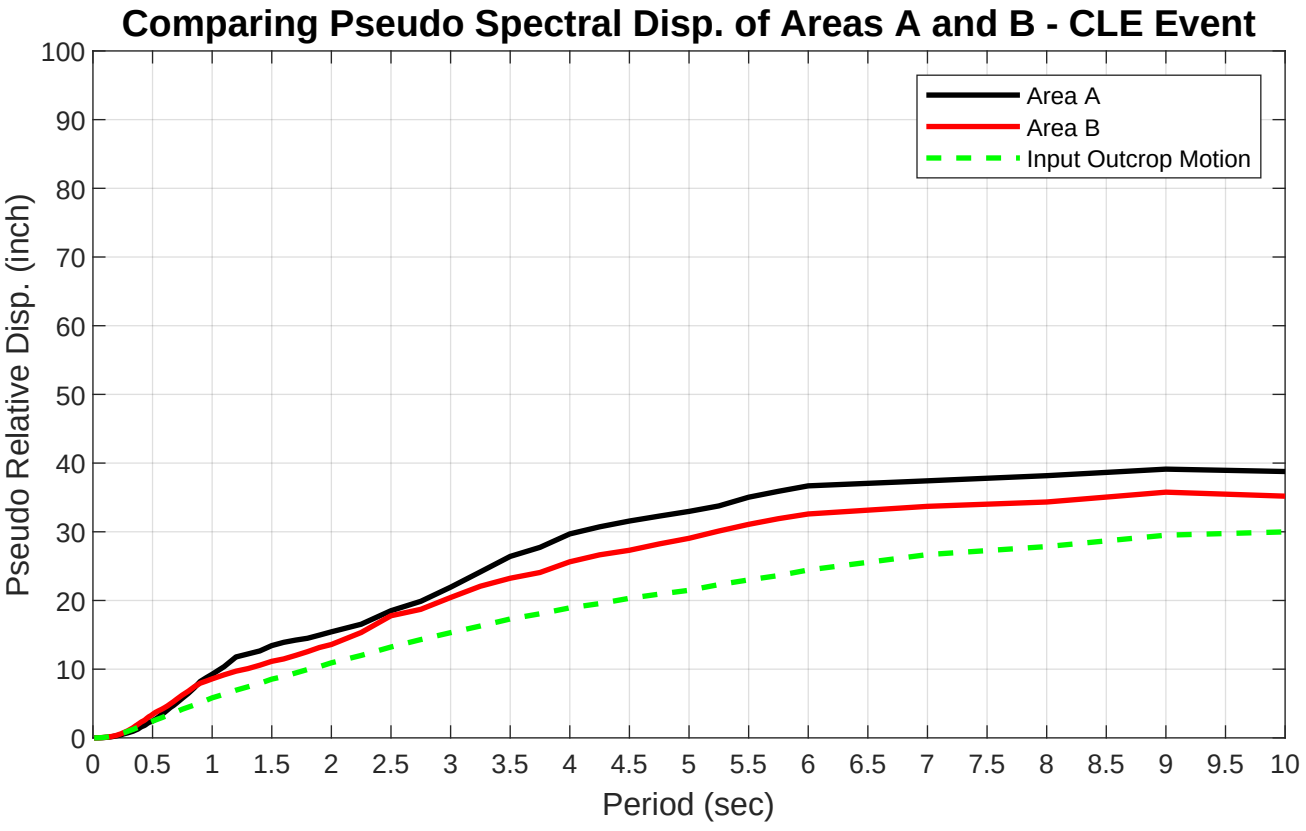


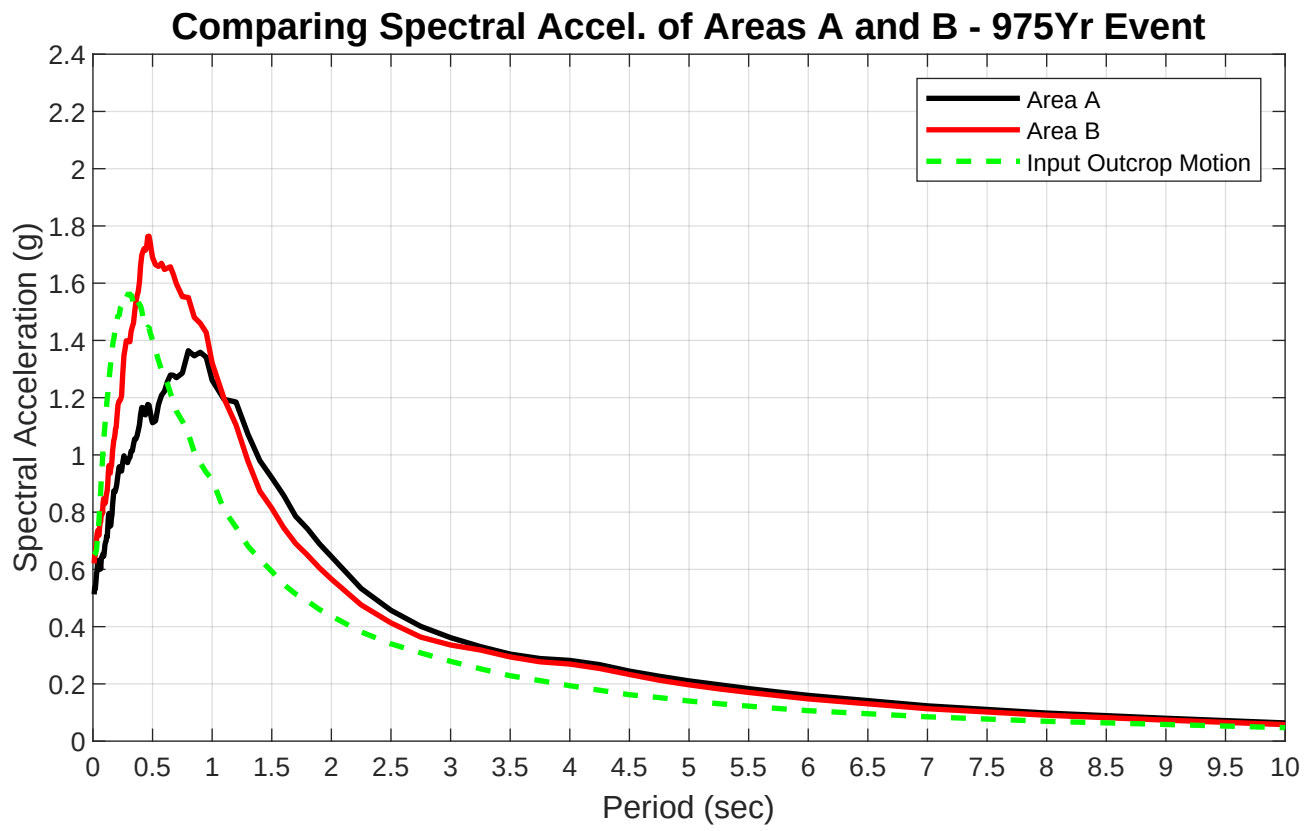
Part III: Enveloped Spectral Acceleration and Pseudo Spectral Displacement Spectra for Areas A and B

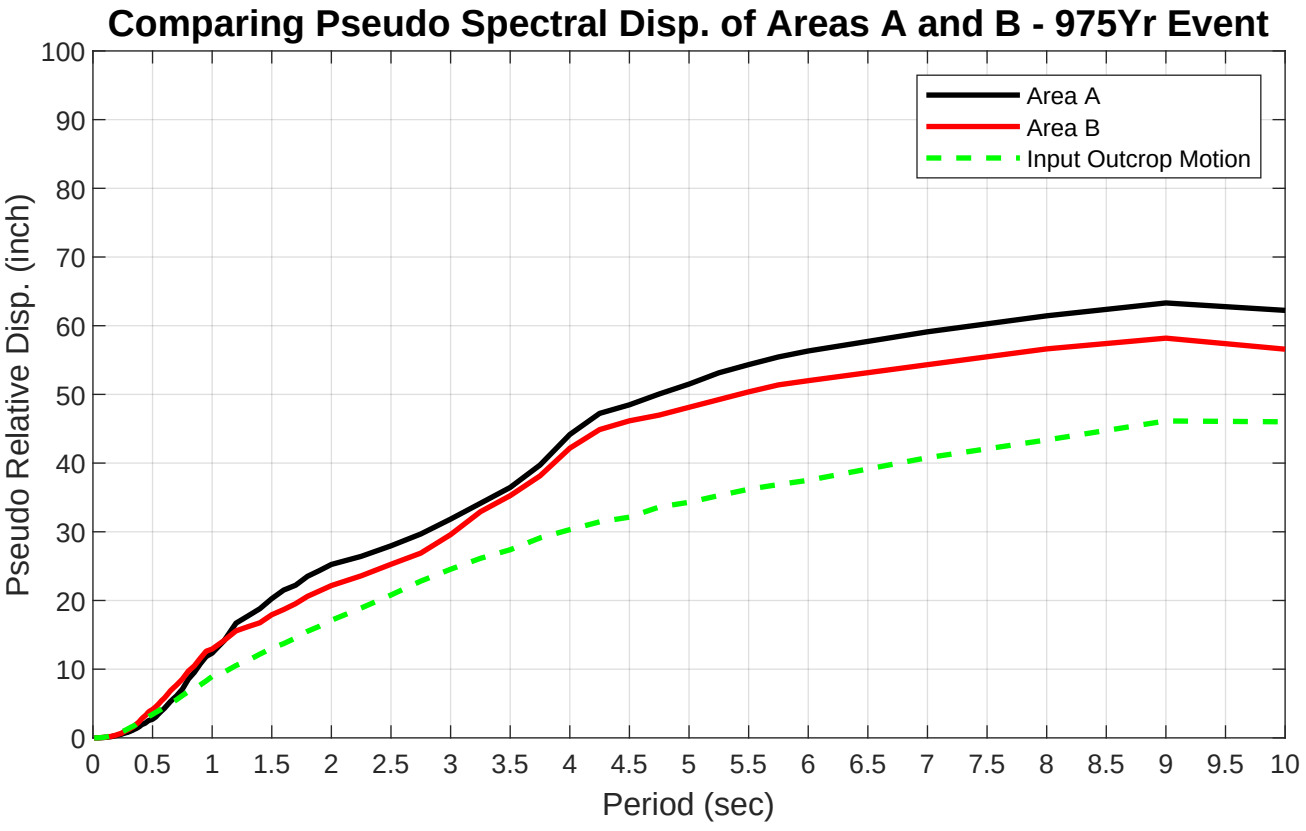

Comparing Spectral Accel. of Areas A and B - OLE Event
Area A
Area B
Input Outcrop Motion
Spectral Acceleration (g)
Period (sec)
0
0.2
0.4
0.6
0.8
1
0 0.5 1 1.5 2 2.5 3 3.5 4 4.5 5 5.5 6 6.5 7 7.5 8 8.5 9 9.5 10

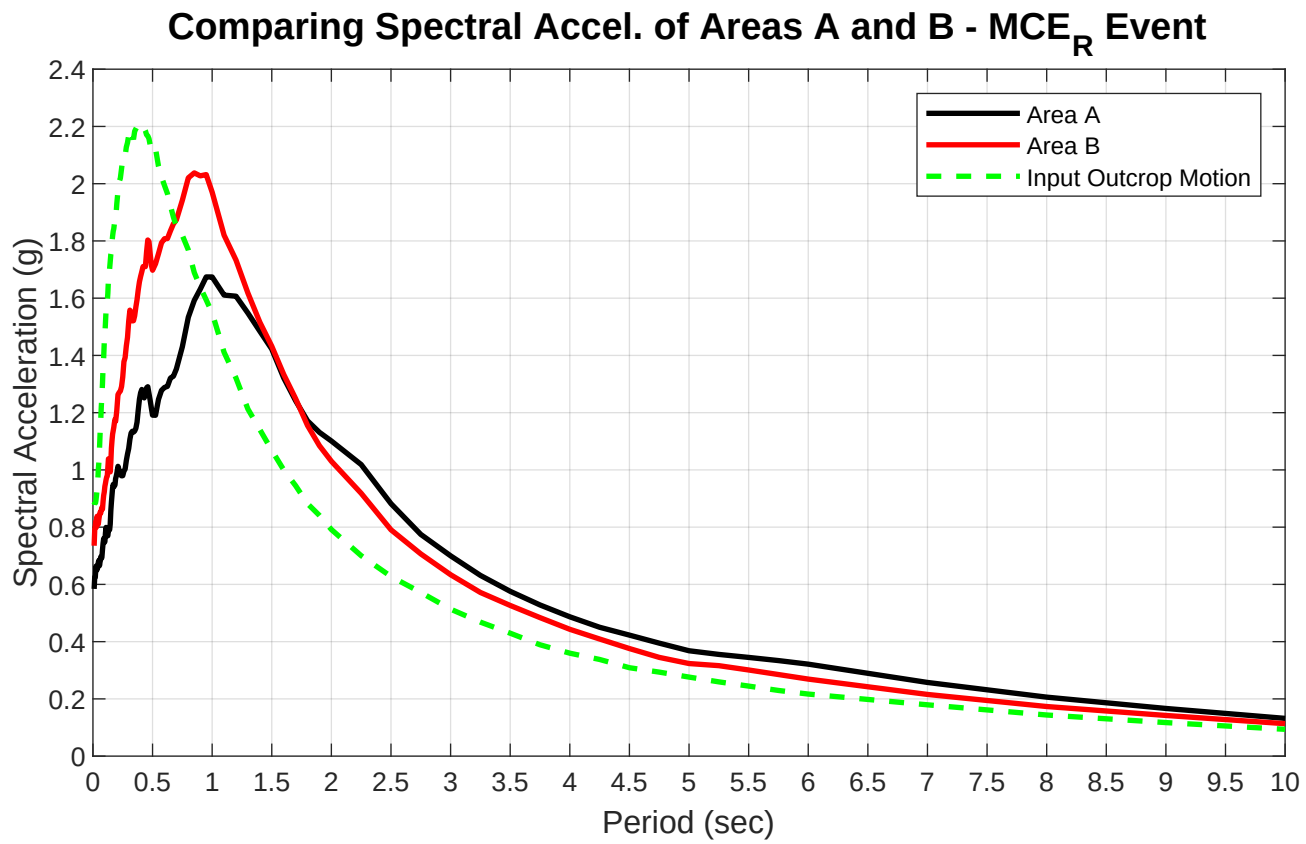

Comparing Pseudo Spectral Disp. of Areas A and B - OLE Event
Area A
Area B
Input Outcrop Motion
Pseudo Relative Disp. (inch)
Period (sec)
0
5
10
15
20
0 0.5 1 1.5 2 2.5 3 3.5 4 4.5 5 5.5 6 6.5 7 7.5 8 8.5 9 9.5 10

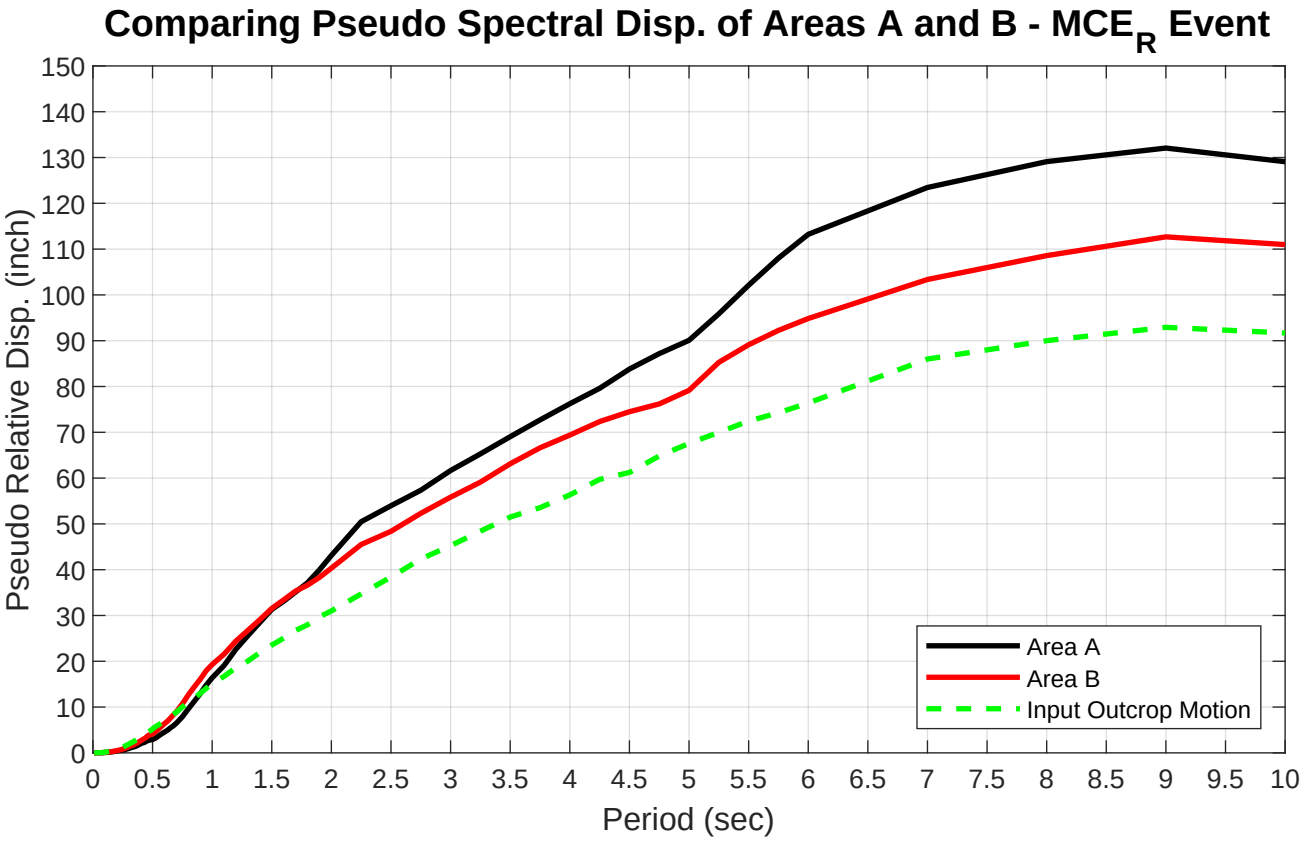

Comparing Spectral Accel. of Areas A and B - CLE Event
Area A
Area B
Input Outcrop Motion
Spectral Acceleration (g)
Period (sec)
0
0.2
0.4
0.6
0.8
1
1.2
1.4
1.6
1.8
2
2.2
2.4
0.5
1.5
2.5
3
3.5
4
4.5
5
5.5
6
6.5
7
7.5
8
8.5
9
9.5
10


Comparing Pseudo Spectral Disp. of Areas A and B - CLE Event
Area A
Area B
Input Outcrop Motion
Pseudo Relative Disp. (inch)
Period (sec)
0
10
20
30
40
50
60
70
80
90
100
0.5
1.5
2.5
3
3.5
4
4.5
5
5.5
6
6.5
7
7.5
8
8.5
9
9.5
10


Comparing Spectral Accel. of Areas A and B - 975Yr Event
Area A
Area B
Input Outcrop Motion
Spectral Acceleration (g)
Period (sec)
0
0.2
0.4
0.6
0.8
1
1.2
1.4
1.6
1.8
2
2.2
2.4
0.5
1.5
2.5
3
3.5
4
4.5
5
5.5
6
6.5
7
7.5
8
8.5
9
9.5
10


Comparing Pseudo Spectral Disp. of Areas A and B - 975Yr Event
Area A
Area B
Input Outcrop Motion
Pseudo Relative Disp. (inch)
Period (sec)
0
10
20
30
40
50
60
70
80
90
100
0.5
1.5
2.5
3
3.5
4
4.5
5
5.5
6
6.5
7
7.5
8
8.5
9
9.5
10


Comparing Spectral Accel. of Areas A and B - MCE$_R$ Event
Spectral Acceleration (g)
Period (sec)
Area A
Area B
Input Outcrop Motion
0
0.2
0.4
0.6
0.8
1
1.2
1.4
1.6
1.8
2
2.2
2.4
0 0.5 1 1.5 2 2.5 3 3.5 4 4.5 5 5.5 6 6.5 7 7.5 8 8.5 9 9.5 10


Comparing Pseudo Spectral Disp. of Areas A and B - MCE$_R$ Event
Pseudo Relative Disp. (inch)
Period (sec)
Area A
Area B
Input Outcrop Motion
0
10
20
30
40
50
60
70
80
90
100
110
120
130
140
150
0 0.5 1 1.5 2 2.5 3 3.5 4 4.5 5 5.5 6 6.5 7 7.5 8 8.5 9 9.5 10

APPENDIX D NEWMARK DISPLACEMENT ANLAYSIS RESULTS

Simplified Newmark sliding block analysis was performed to develop charts of estimated lateral ground displacements as a function of yield acceleration for the OLE, CLE, 975-yr, DE_G, and MCE_G level spectral-matched firm-ground motions.

The seven spectral-matched firm-ground horizontal time histories (i.e., horizontal fault-normal and fault-parallel components, a total of 14 time histories) presented in Appendix B were used in the analyses. The analyses also included all reversed time histories with ground motion acting in the opposite direction. Ground displacement was calculated based on constant yield acceleration levels of 0.01, 0.02, 0.03, 0.05, 0.075, 0.1, 0.125, 0.15, 0.175, 0.2, 0.25, 0.3, 0.35 and 0.4g and down-slope sliding by double-integrating each of the modified time histories. A total of 392 analyses (7 records x 2 components x 2 directions x 14 yield accelerations) were performed for each level of ground motion.

The figures presented in the following pages show the resulting lateral displacement versus yield acceleration curves for all 28 time history components and directions (7 records x 2 components x 2 directions). Since more than seven time histories were used in these evaluations, the geomean curve is judged to be appropriate for screening evaluations. The use of the average values has been recognized as an acceptable practice when seven of more time histories are considered in the analysis.

The start-up ground motions used for Newmark displacement analyses are presented in the Tables D1 and D2. Note that both components of the motions were spectrally matched to the firm (improved) ground ARS curves for each earthquake event. The two components of the motions are denoted as S#N and S#P in the graphs, where # is the ground motion set number.

Table D1. Selected Seed Motion for 72-yr Return Period (OLE) Event

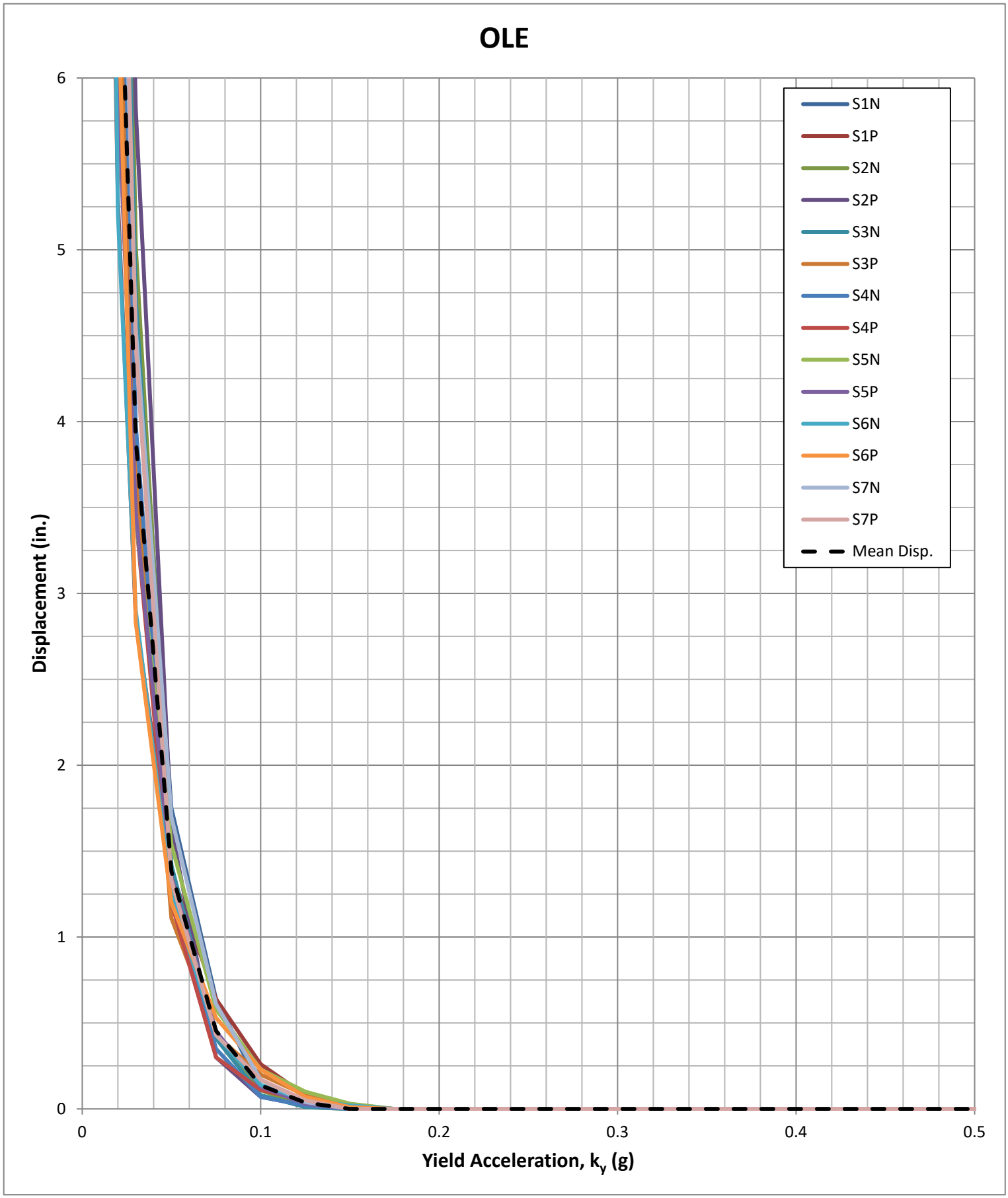
Set	PEER RSN *	Earthquake	Mw	Pulse Motion	Station	Distance, R_{rup} (km)
1	802	1989 Loma Prieta	6.9	Yes	Saratoga – Aloha Ave.	8.5
2	729	1987 Superstition Hill	6.5	No	Wildlife Liquefaction Array	23.9
3	667	1987 Whittier	6.0	No	Northridge-Saticoy St.	41.7
4	170	1979 Imperial Valley	6.5	Yes	EC CO Center FF	7.3
5	4101	2004 Parkfield	6.0	Yes	Parkfield - Vineyard Canyon 3W	5.6
6	821	1992 Erzincan	6.7	No	Erzincan	4.4
7	988	1994 Northridge	6.7	No	Century City, LACC	23.4

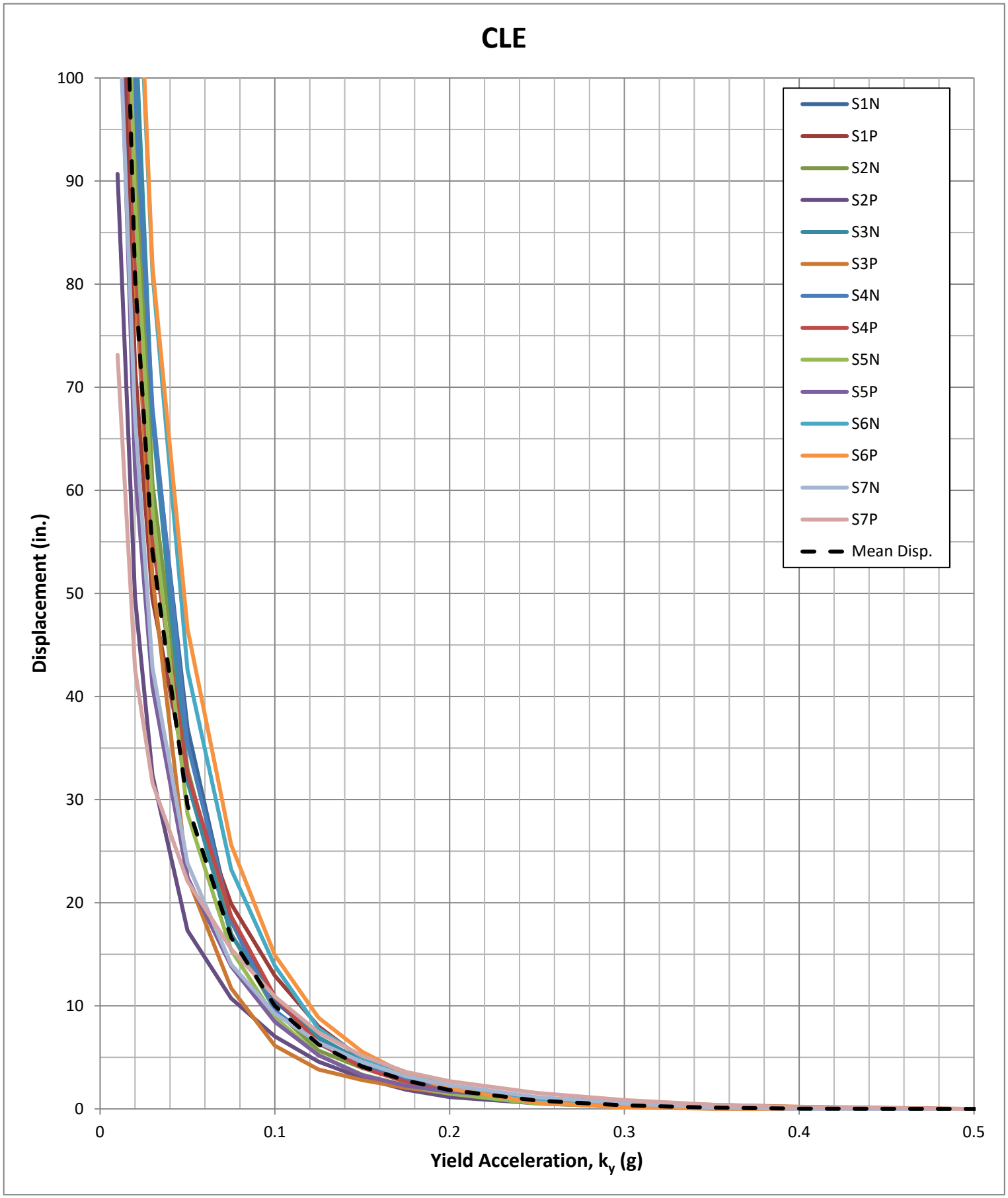
* *PEER ground motion database (https://ngawest2.berkeley.edu/).*

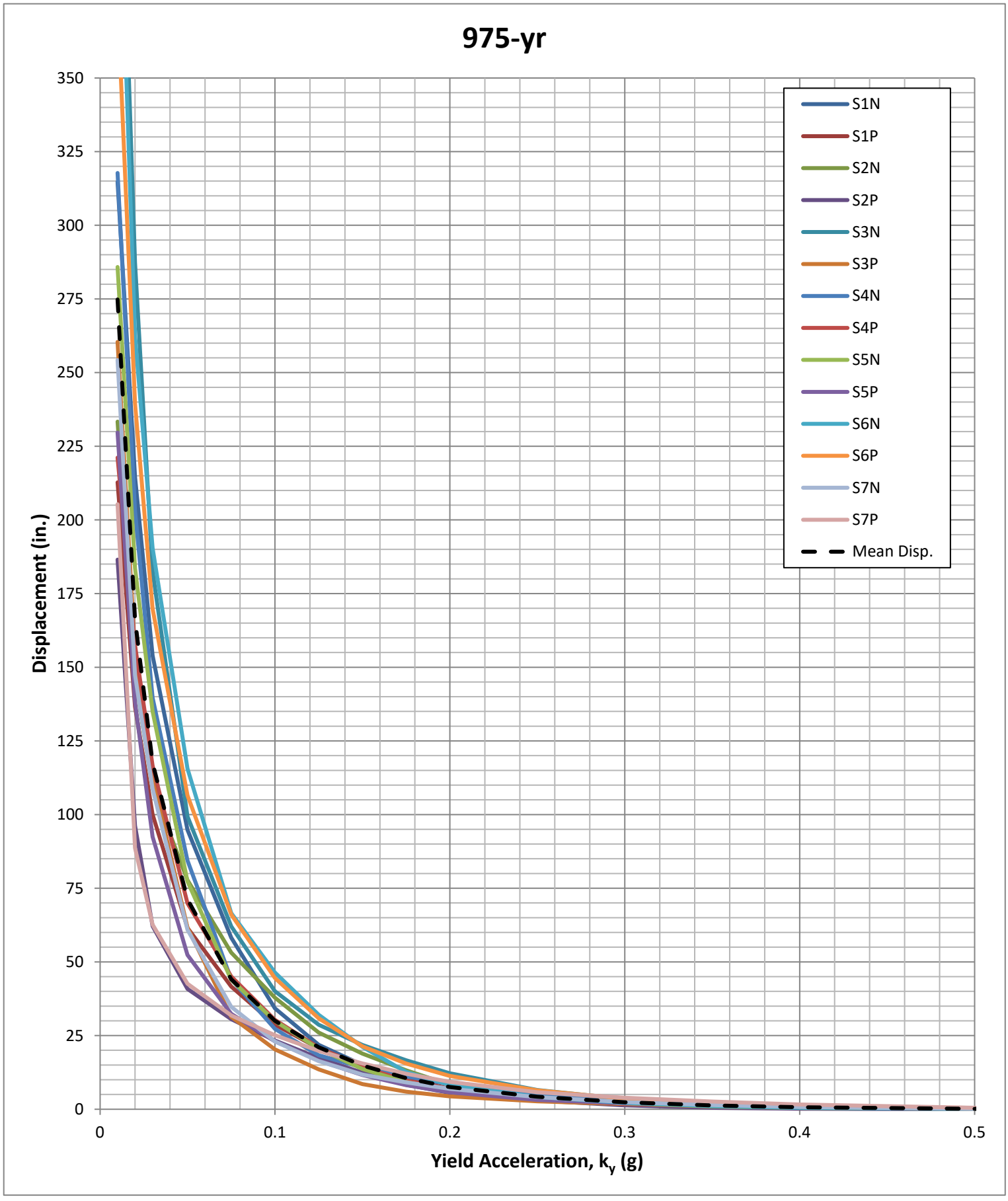
Table D2. Selected Seed Motion for 475-yr (CLE), 975-yr, and 2475-yr Return Period Events

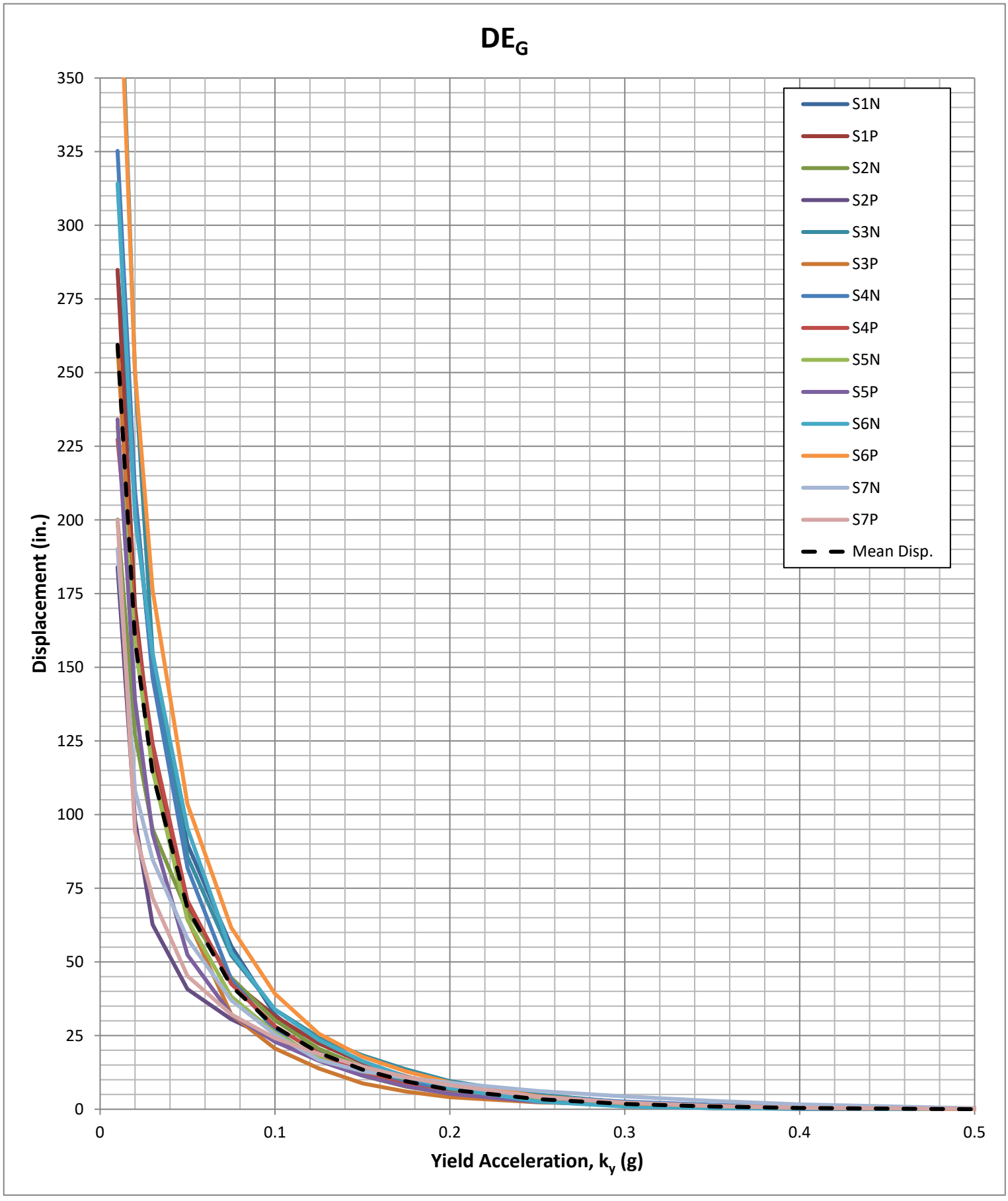
Set	PEER RSN *	Earthquake	Mw	Pulse Motion	Station	Distance, R_{rup} (km)
1	1787	1999 Hector Mine	7.1	No	Hector	11.7
2	767	1989 Loma Prieta	6.9	Yes	Gilroy Array 0#3	12.8
3	2114	2002 Denali, Alaska	7.9	Yes	TAPS Pump Station #10	2.7
4	1612	1999 Duzce, Turkey	7.1	No	Lamont 1059	4.2
5	6906	2010 Darfield, New Zealand	7.0	Yes	GDLC	1.2
6	6	1940 Imperial Valley	6.9	No	El Centro	6.1
7	1108	1995 Kobe, Japan	6.9	No	Kobe University	0.9

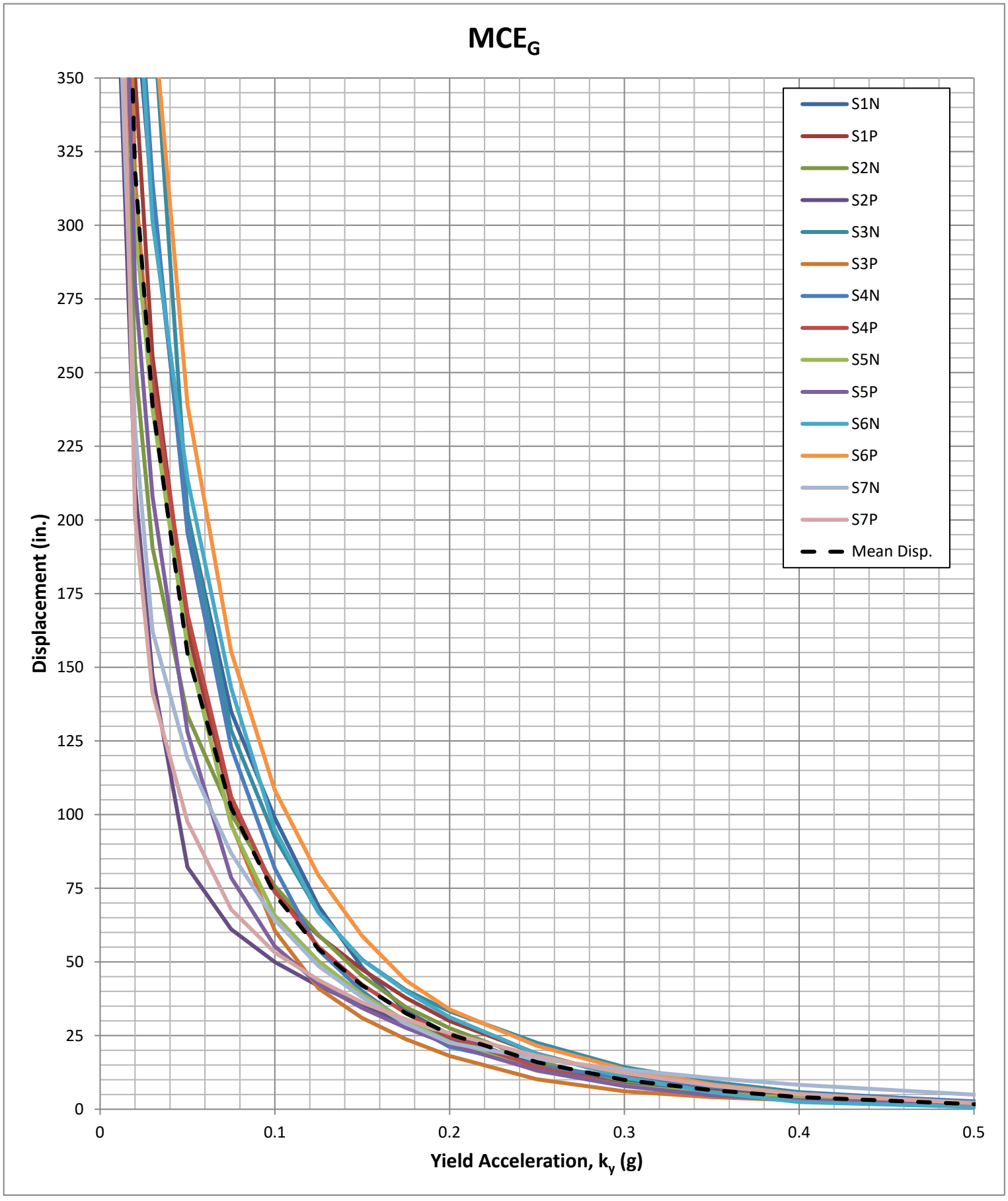
** PEER ground motion database (https://ngawest2.berkeley.edu/).*

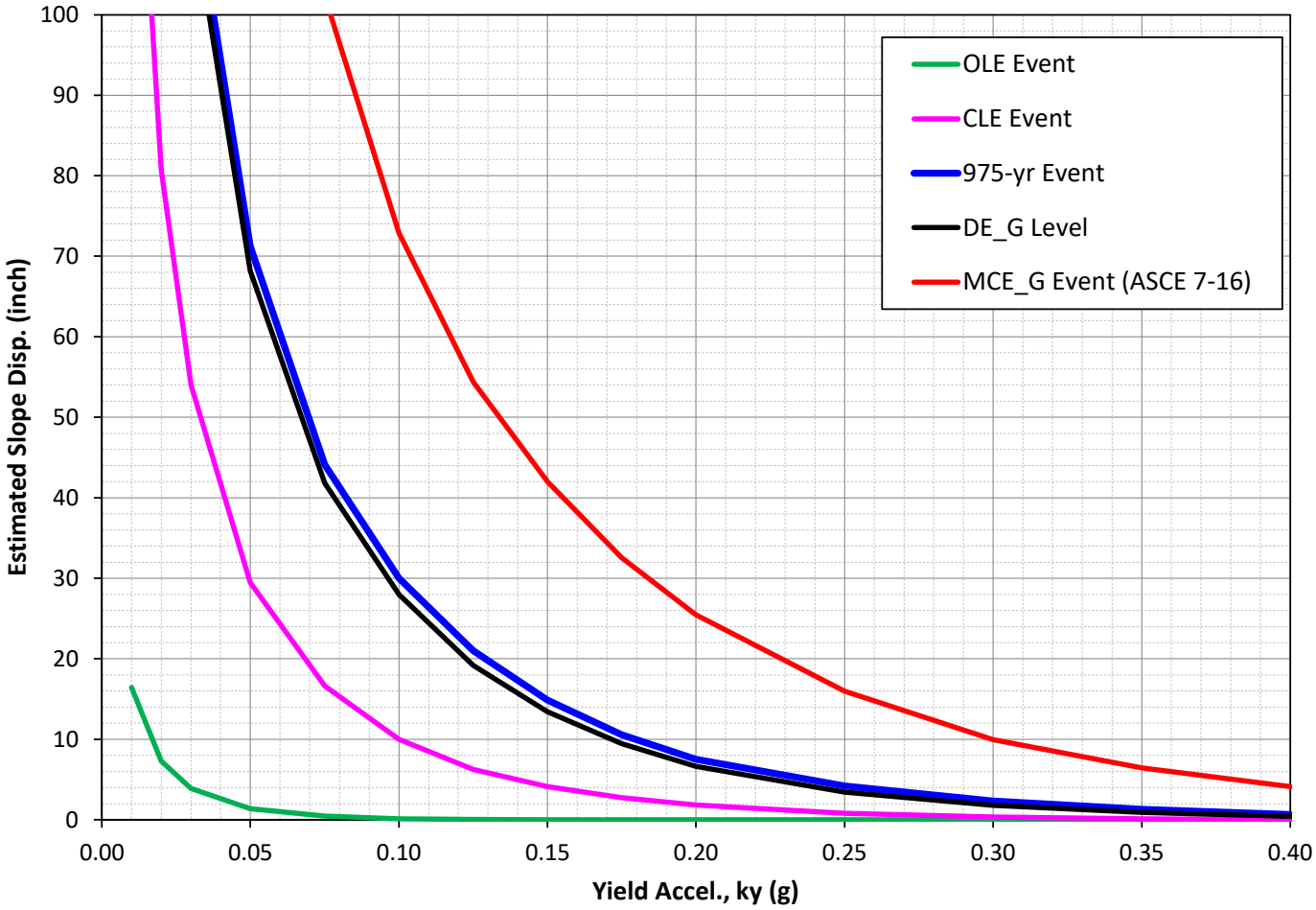

OLE
Displacement (in.)
Yield Acceleration, k_y (g)
0
1
2
3
4
5
6
0
0.1
0.2
0.3
0.4
0.5
S1N
S1P
S2N
S2P
S3N
S3P
S4N
S4P
S5N
S5P
S6N
S6P
S7N
S7P
Mean Disp.


CLE
Displacement (in.)
Yield Acceleration, k_y (g)
0
10
20
30
40
50
60
70
80
90
100
0
0.1
0.2
0.3
0.4
0.5
S1N
S1P
S2N
S2P
S3N
S3P
S4N
S4P
S5N
S5P
S6N
S6P
S7N
S7P
Mean Disp.


975-yr
Displacement (in.)
350
325
300
275
250
225
200
175
150
125
100
75
50
25
0
0
0.1
0.2
0.3
0.4
0.5
Yield Acceleration, k_y (g)
S1N
S1P
S2N
S2P
S3N
S3P
S4N
S4P
S5N
S5P
S6N
S6P
S7N
S7P
Mean Disp.


DE_G
Displacement (in.)
350
325
300
275
250
225
200
175
150
125
100
75
50
25
0
0
0.1
0.2
0.3
0.4
0.5
Yield Acceleration, k_y (g)
S1N
S1P
S2N
S2P
S3N
S3P
S4N
S4P
S5N
S5P
S6N
S6P
S7N
S7P
Mean Disp.


MCE$_G$
Displacement (in.)
350
325
300
275
250
225
200
175
150
125
100
75
50
25
0
0
0.1
0.2
0.3
0.4
0.5
Yield Acceleration, k_y (g)
S1N
S1P
S2N
S2P
S3N
S3P
S4N
S4P
S5N
S5P
S6N
S6P
S7N
S7P
Mean Disp.



Yield Accel., ky (g)	Slope Disp., OLE Event (inch)	Slope Disp., CLE Event (inch)	Slope Disp., 975Yr RP Event (inch)	Slope Disp., DE_G Event (inch)	Slope Disp., MCE_G Event (inch)
0.01	16.4	140	275	259	525
0.02	7.3	80.7	166	159	319
0.03	3.9	54.0	118	114	239
0.05	1.4	29.5	71.2	68.2	155
0.075	0.5	16.6	44.1	41.8	102
0.1	0.1	10.0	30.0	28.0	72.9
0.125	0.0	6.2	21.0	19.2	54.4
0.15	0.0	4.1	14.9	13.4	42.0
0.175	0.0	2.7	10.6	9.5	32.6
0.2	0.0	1.8	7.5	6.6	25.5
0.25	0.0	0.8	4.2	3.4	16.0
0.3	0.0	0.4	2.4	1.8	9.9
0.35	0.0	0.1	1.3	0.9	6.4
0.4	0.0	0.0	0.7	0.4	4.1

APPENDIX E OLE, CLE, 975-YR, AND DE LEVEL UNIMPROVED GROUND MOTION TIME HISTORIES

The seven (7) sets of 2-component horizontal ground motion time histories discussed in Section 3.4 and listed below in Tables E1 and E2 are modified to match the unimproved ground spectra using the time-domain approach. Each set has two (2) components (FN and FP), resulting in a total of 14 time histories for each ground motion level. For each time history, the following is plotted:

- Initial acceleration, velocity and displacement time histories scaled to PGA,
- Modified (spectral-matched) acceleration, velocity and displacement time histories, and
- Comparison of the target acceleration and relative displacement spectra with the spectra of the initial and the modified time histories.

The plots for Area A are shown in Figure E1 through Figure E14 for the OLE, Figure E15 through Figure E28 for the CLE, Figure E29 through Figure E42 for the DE, and Figure E43 through Figure E56 for the 975-yr. Return Period ground motion levels.

The plots for Area B are shown in Figure E57 through Figure E70 for the OLE, Figure E71 through Figure E84 for the CLE, Figure E85 through Figure E98 for the DE, and Figure E99 through Figure E112 for the 975-yr. Return Period ground motion levels.

Table E1. Selected Seed Motion for 72 yr Return Period (OLE) Event

Set	PEER RSN *	Earthquake	Mw	Pulse Motion	Station	Distance, R_{rup} (km)
1	802	1989 Loma Prieta	6.9	Yes	Saratoga – Aloha Ave.	8.5
2	729	1987 Superstition Hill	6.5	No	Wildlife Liquefaction Array	23.9
3	667	1987 Whittier	6.0	No	Northridge-Saticoy St.	41.7
4	170	1979 Imperial Valley	6.5	Yes	EC CO Center FF	7.3
5	4101	2004 Parkfield	6.0	Yes	Parkfield - Vineyard Canyon 3W	5.6
6	821	1992 Erzincan	6.7	No	Erzincan	4.4
7	988	1994 Northridge	6.7	No	Century City, LACC	23.4

* *PEER ground motion database (https://ngawest2.berkeley.edu/).*

Table E2. Selected Seed Motion for 475-yr Return Period (CLE), 975-yr Return Period, and Design Earthquake (DE) Events

Set	PEER RSN *	Earthquake	Mw	Pulse Motion	Station	Distance, R_{rup} (km)
1	1787	1999 Hector Mine	7.1	No	Hector	11.7
2	767	1989 Loma Prieta	6.9	Yes	Gilroy Array 0#3	12.8
3	2114	2002 Denali, Alaska	7.9	Yes	TAPS Pump Station #10	2.7
4	1612	1999 Duzce, Turkey	7.1	No	Lamont 1059	4.2
5	6906	2010 Darfield, New Zealand	7.0	Yes	GDLC	1.2
6	6	1940 Imperial Valley	6.9	No	El Centro	6.1
7	1108	1995 Kobe, Japan	6.9	No	Kobe University	0.9

* *PEER ground motion database (https://ngawest2.berkeley.edu/).*

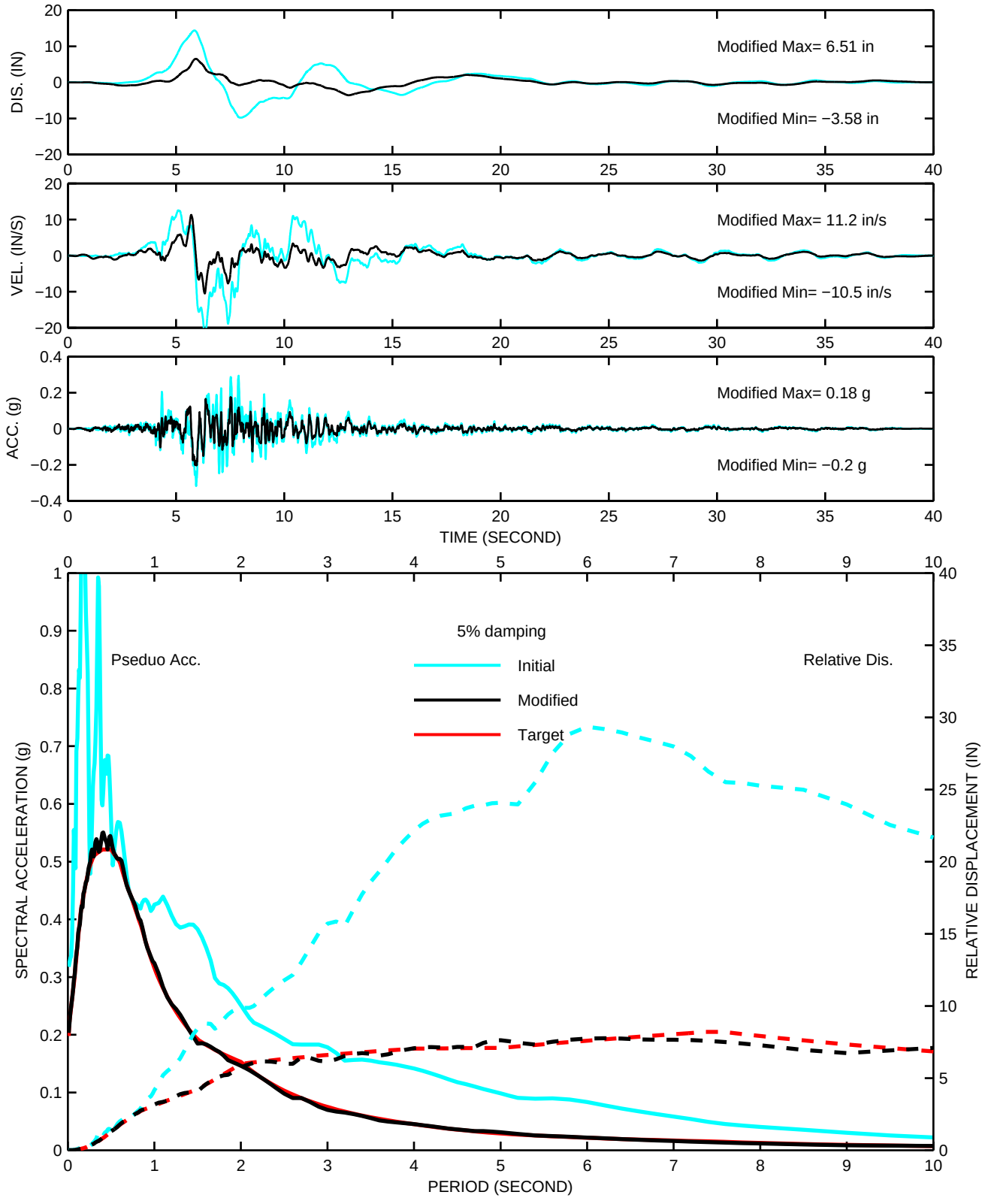


Figure E1. Unimproved Ground Area A OLE Spectrum Compatible Ground Motion (5% Damped)−Set 1 FN

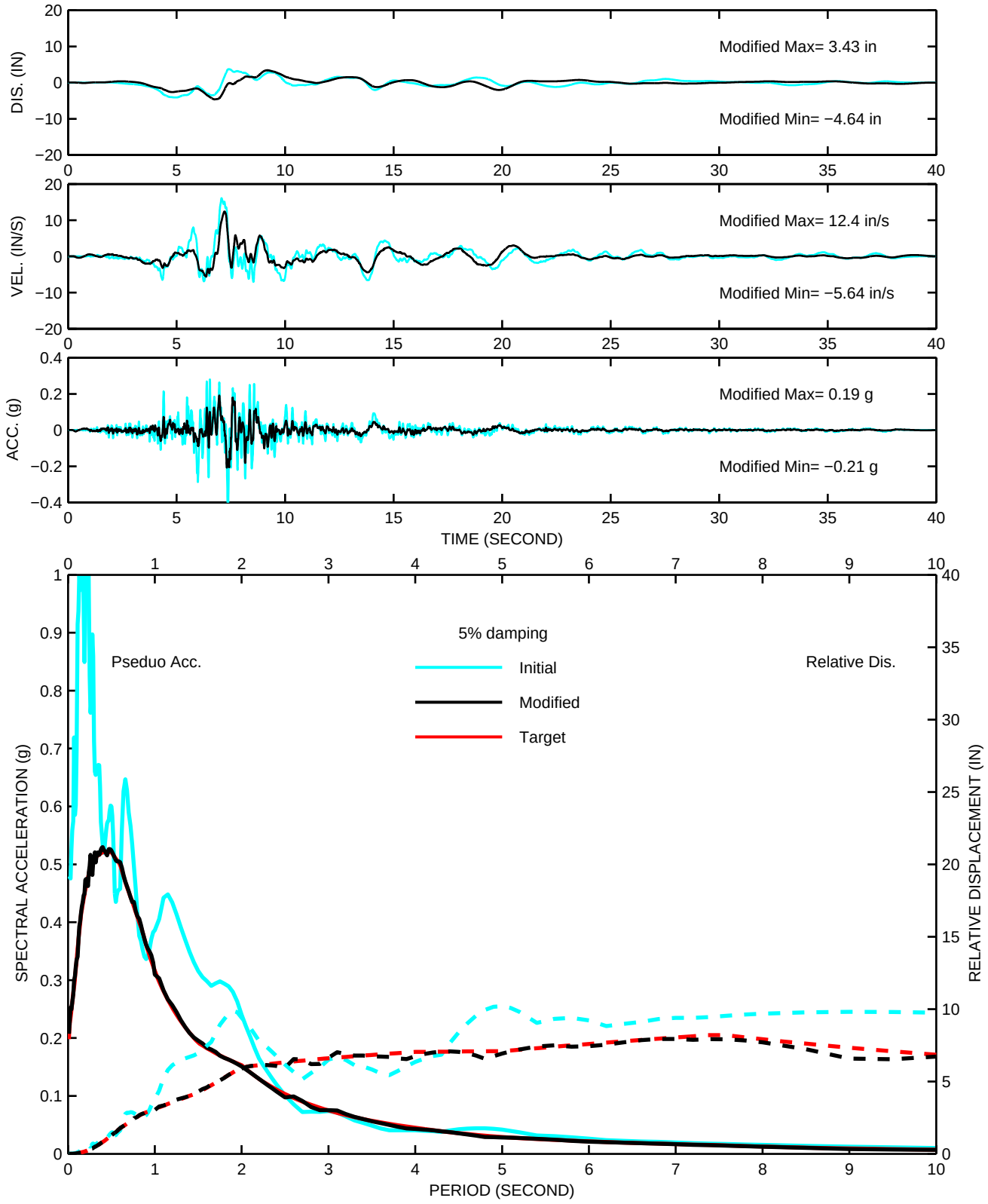


Figure E2. Unimproved Ground Area A OLE Spectrum Compatible Ground Motion (5% Damped)−Set 1 FP

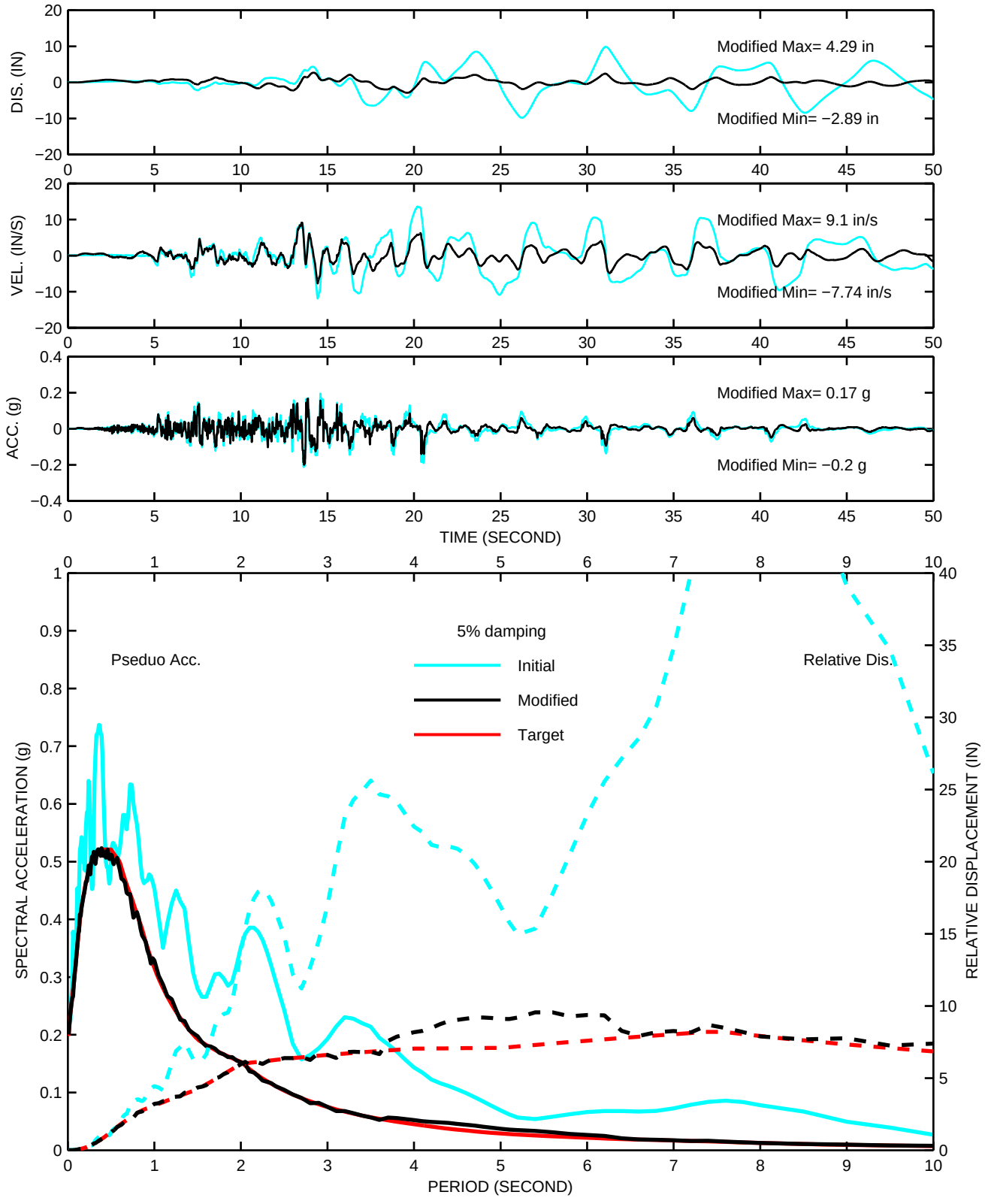


Figure E3. Unimproved Ground Area A OLE Spectrum Compatible Ground Motion (5% Damped)−Set 2 FN

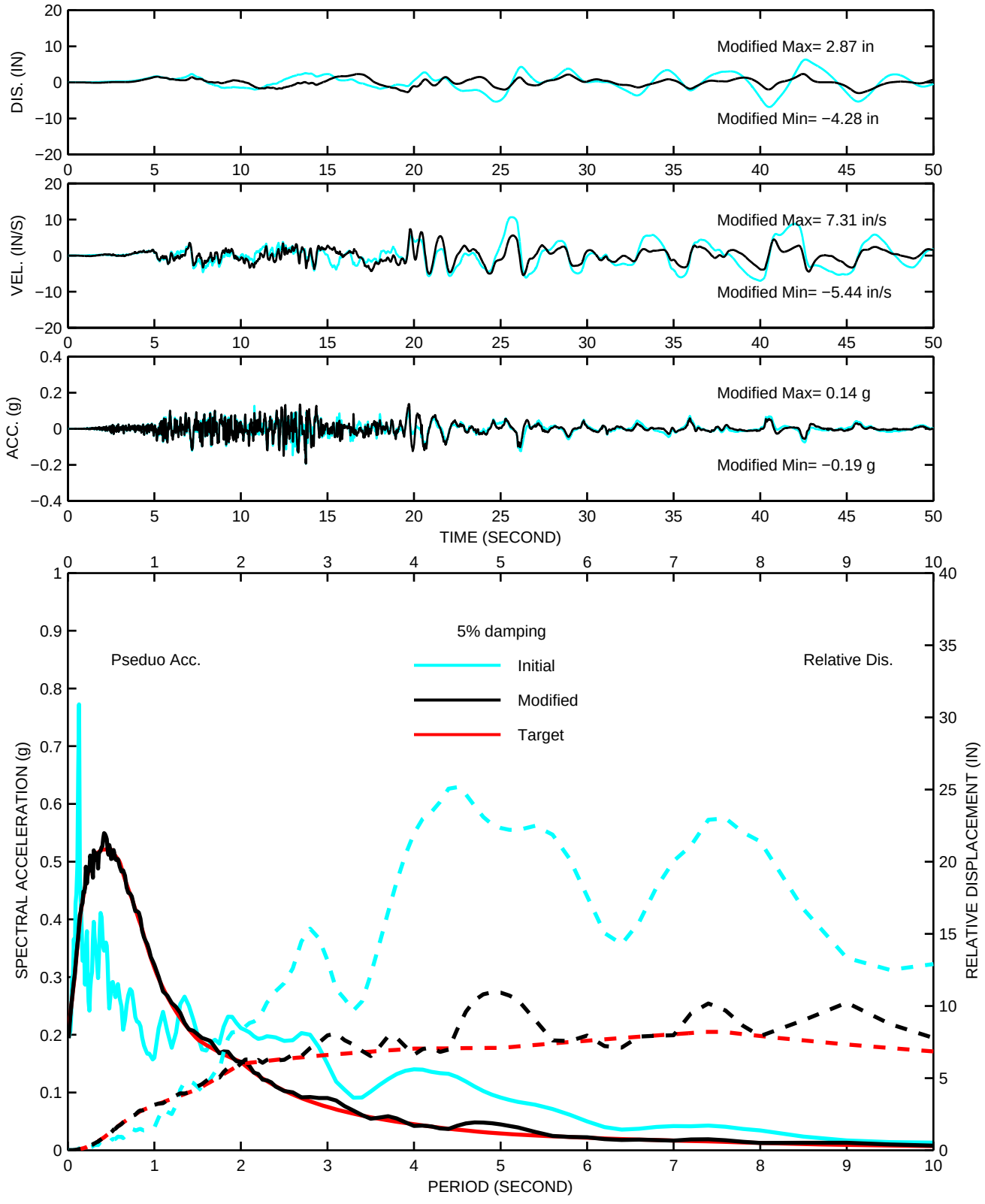


Figure E4. Unimproved Ground Area A OLE Spectrum Compatible Ground Motion (5% Damped)−Set 2 FP

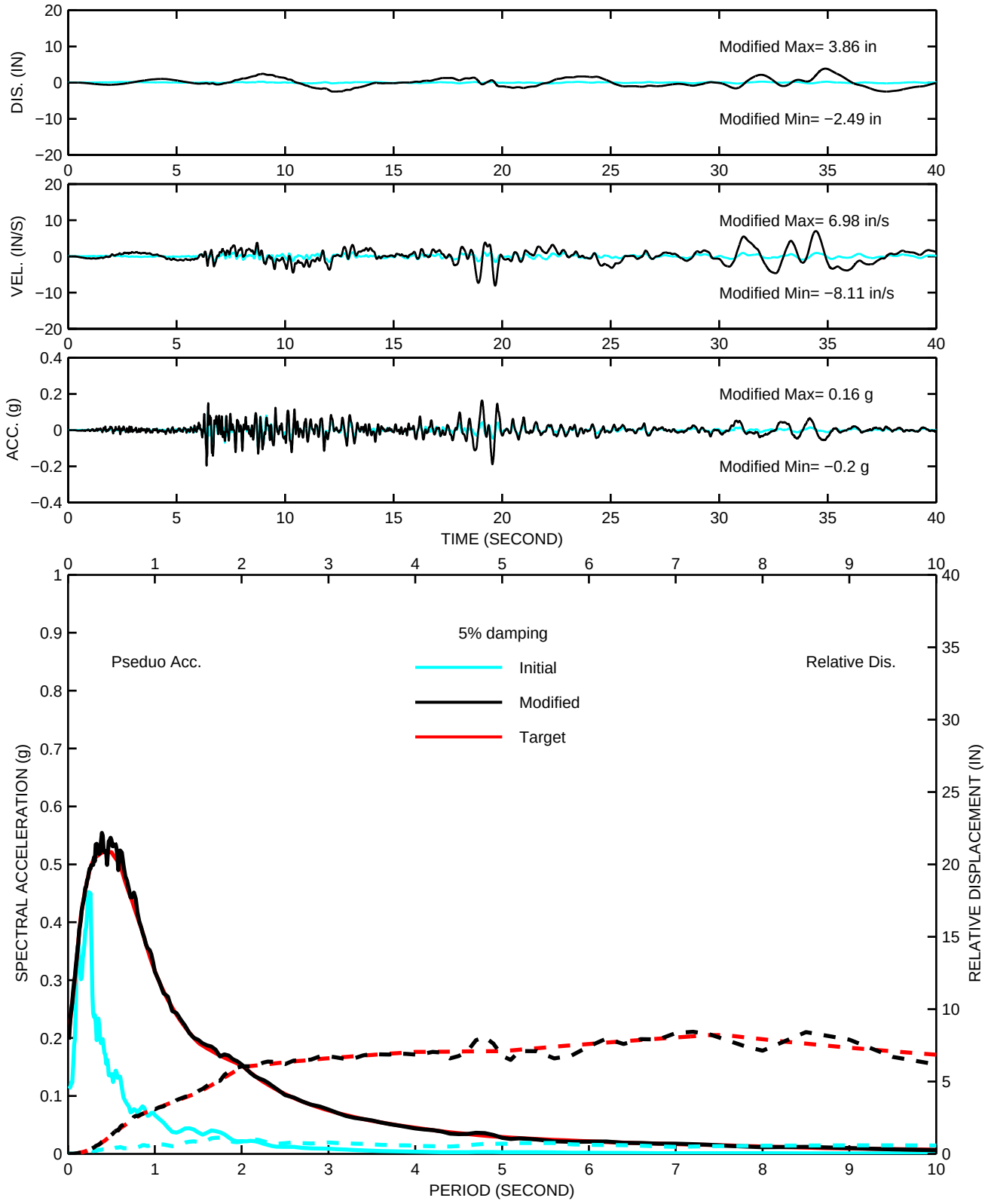


Figure E5. Unimproved Ground Area A OLE Spectrum Compatible Ground Motion (5% Damped)−Set 3 FN

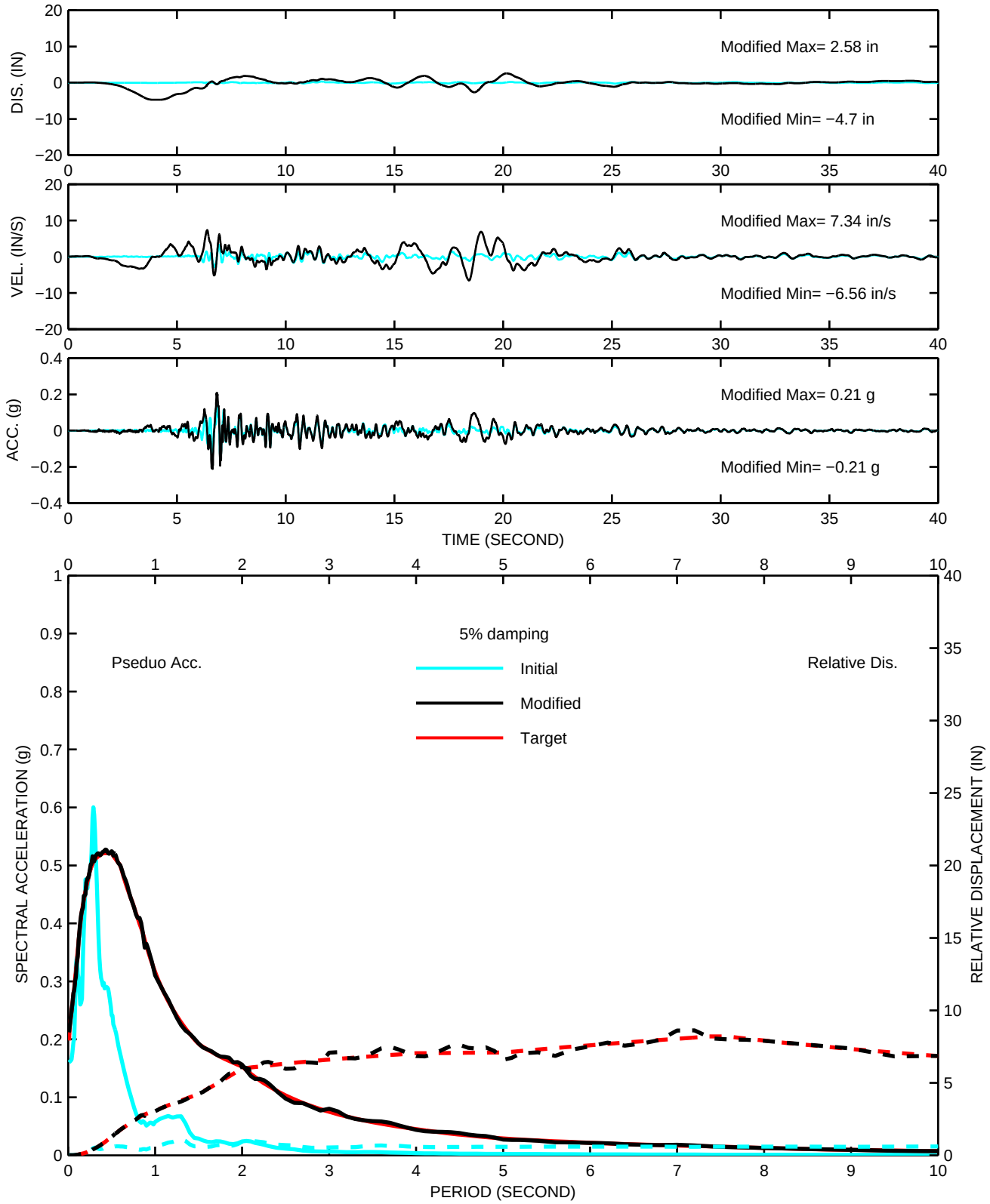


Figure E6. Unimproved Ground Area A OLE Spectrum Compatible Ground Motion (5% Damped)−Set 3 FP

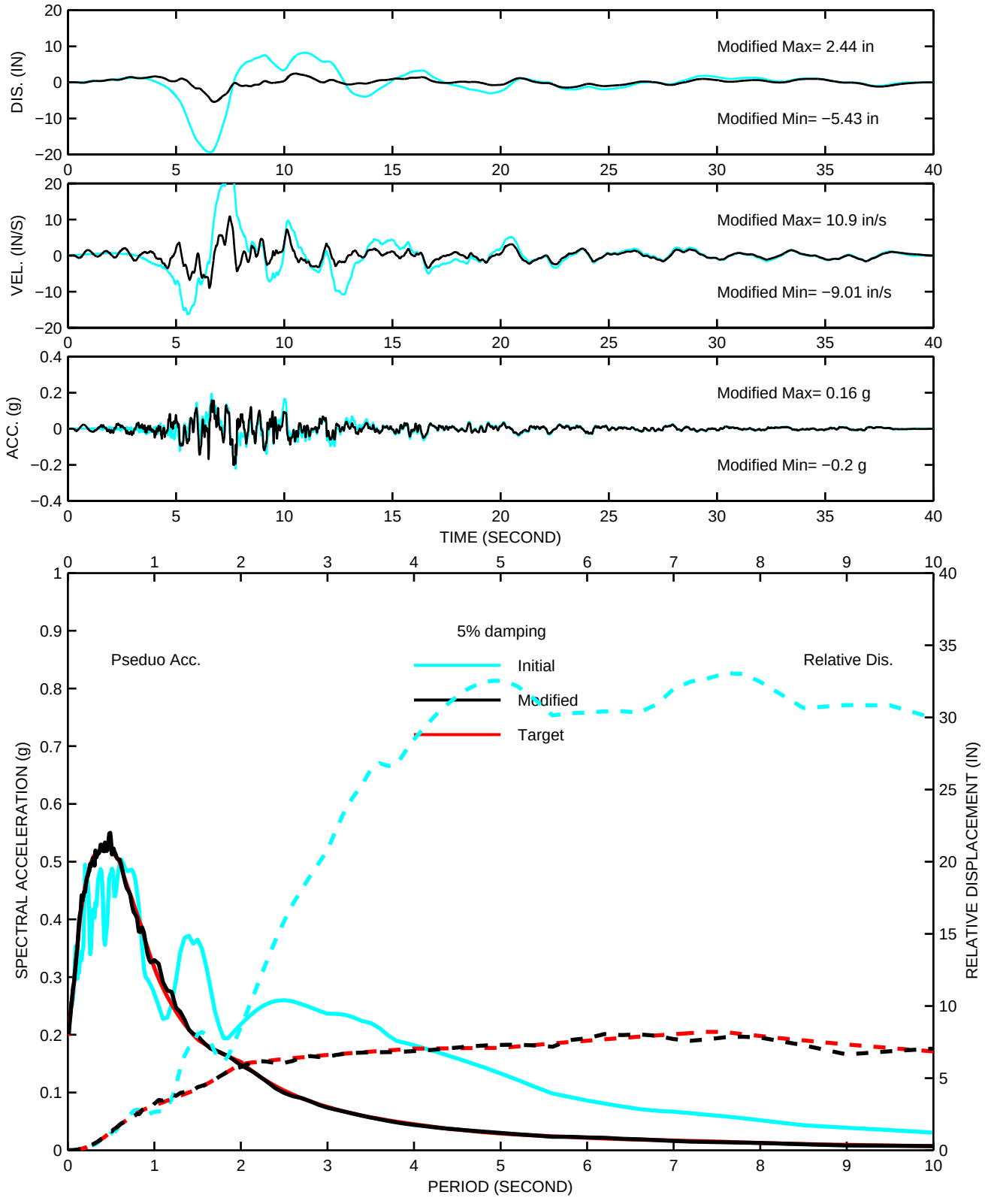


Figure E7. Unimproved Ground Area A OLE Spectrum Compatible Ground Motion (5% Damped)−Set 4 FN

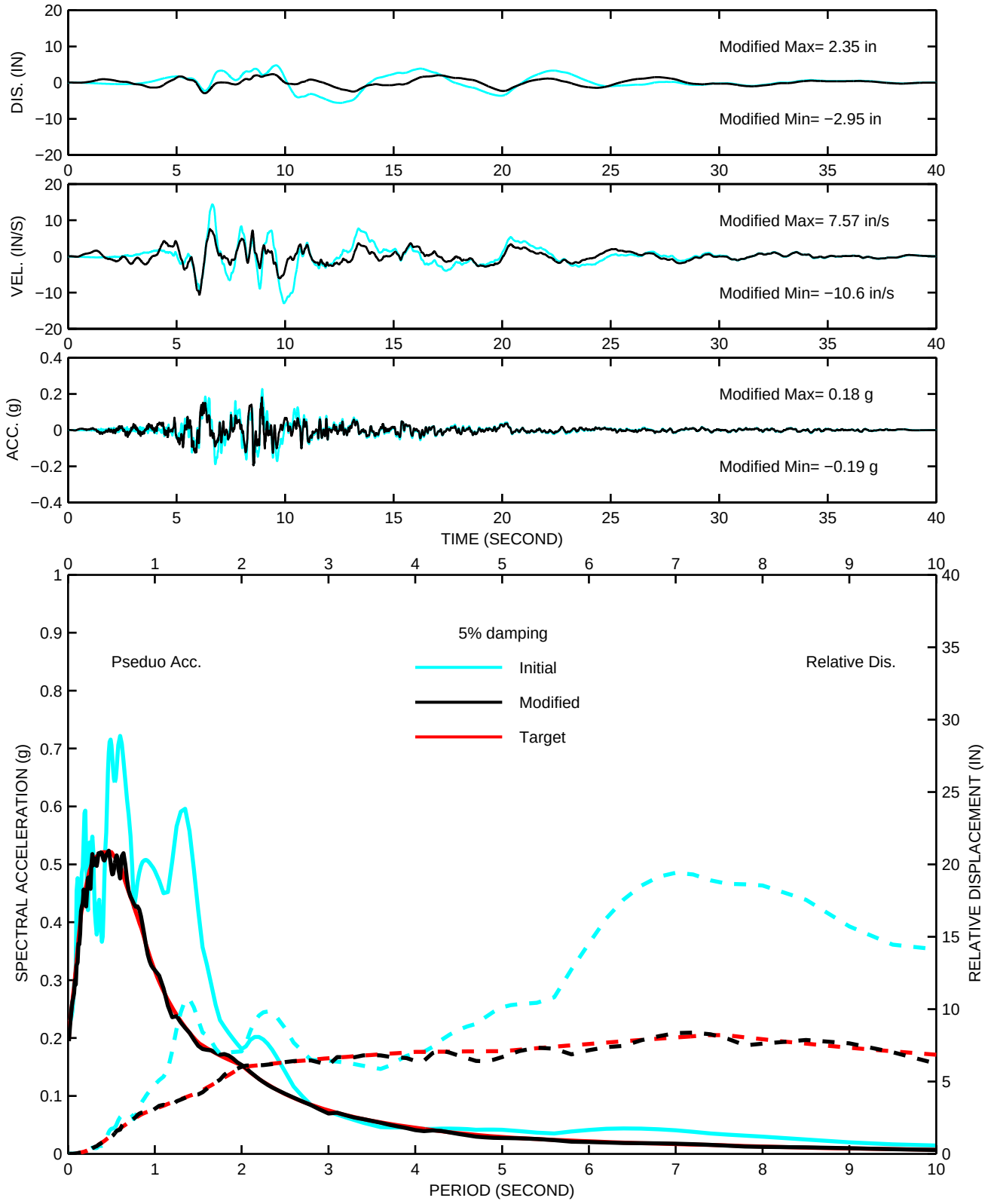


Figure E8. Unimproved Ground Area A OLE Spectrum Compatible Ground Motion (5% Damped)−Set 4 FP

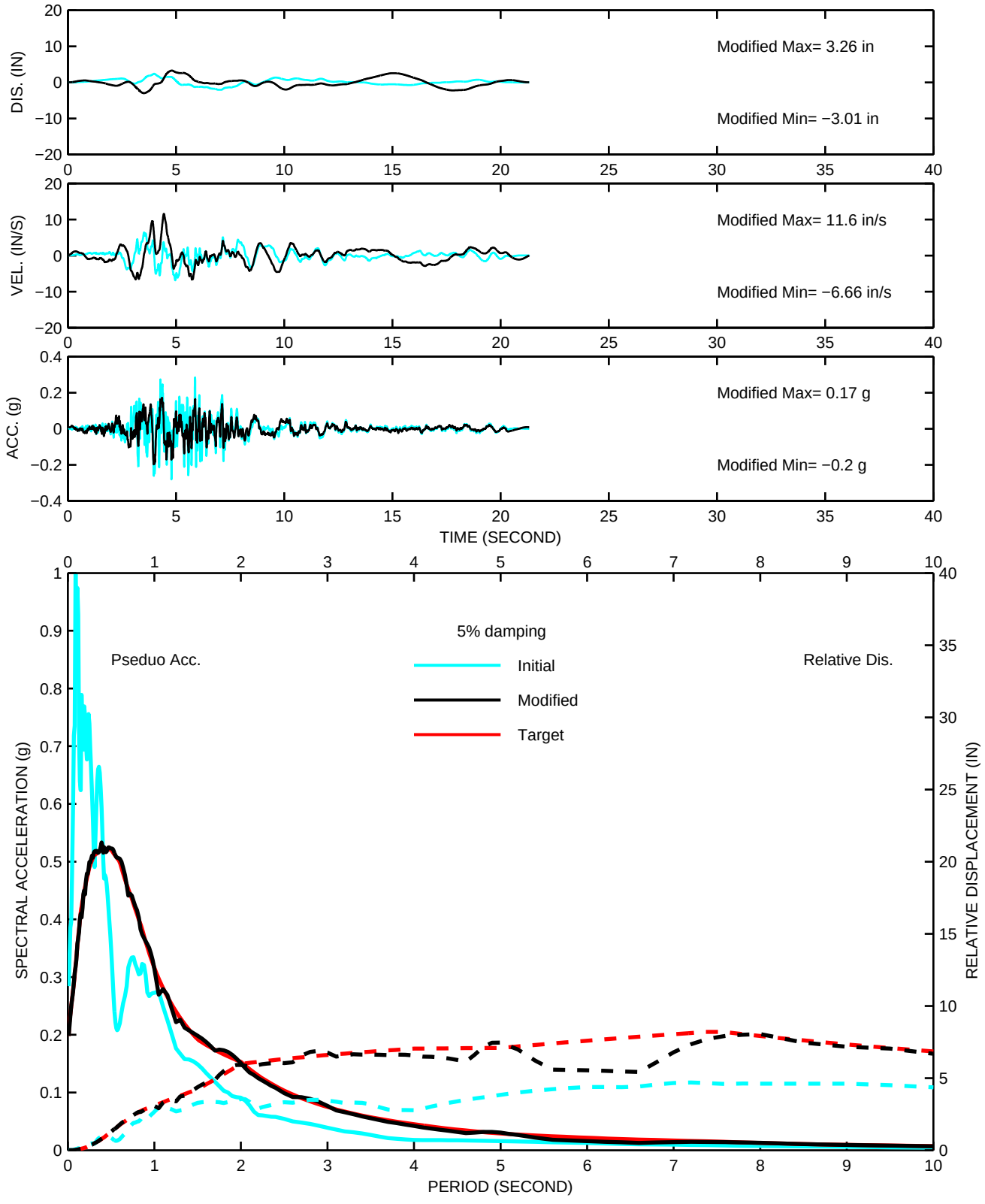


Figure E9. Unimproved Ground Area A OLE Spectrum Compatible Ground Motion (5% Damped)−Set 5 FN

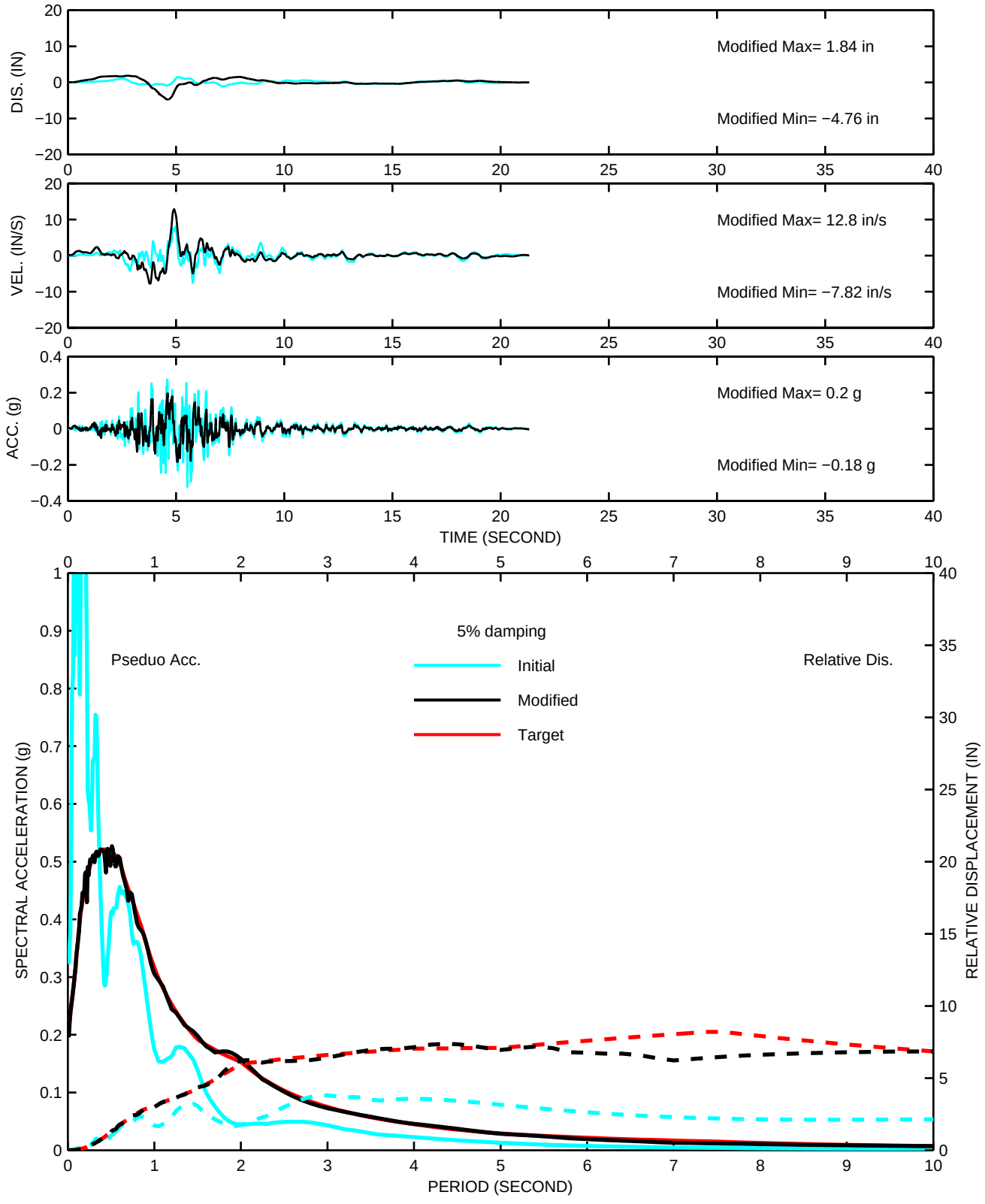


Figure E10. Unimproved Ground Area A OLE Spectrum Compatible Ground Motion (5% Damped)−Set 5 FP

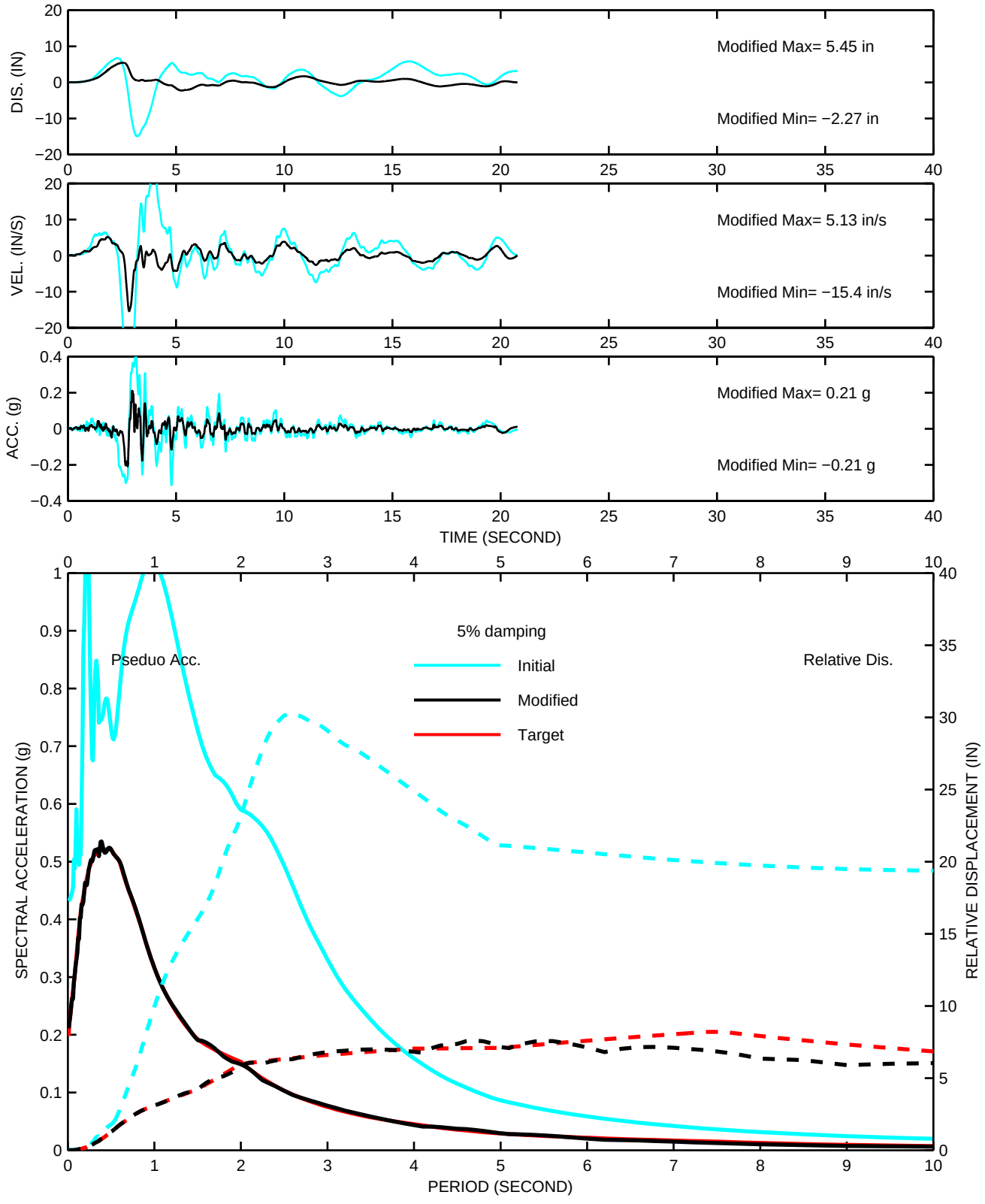


Figure E11. Unimproved Ground Area A OLE Spectrum Compatible Ground Motion (5% Damped)−Set 6 FN

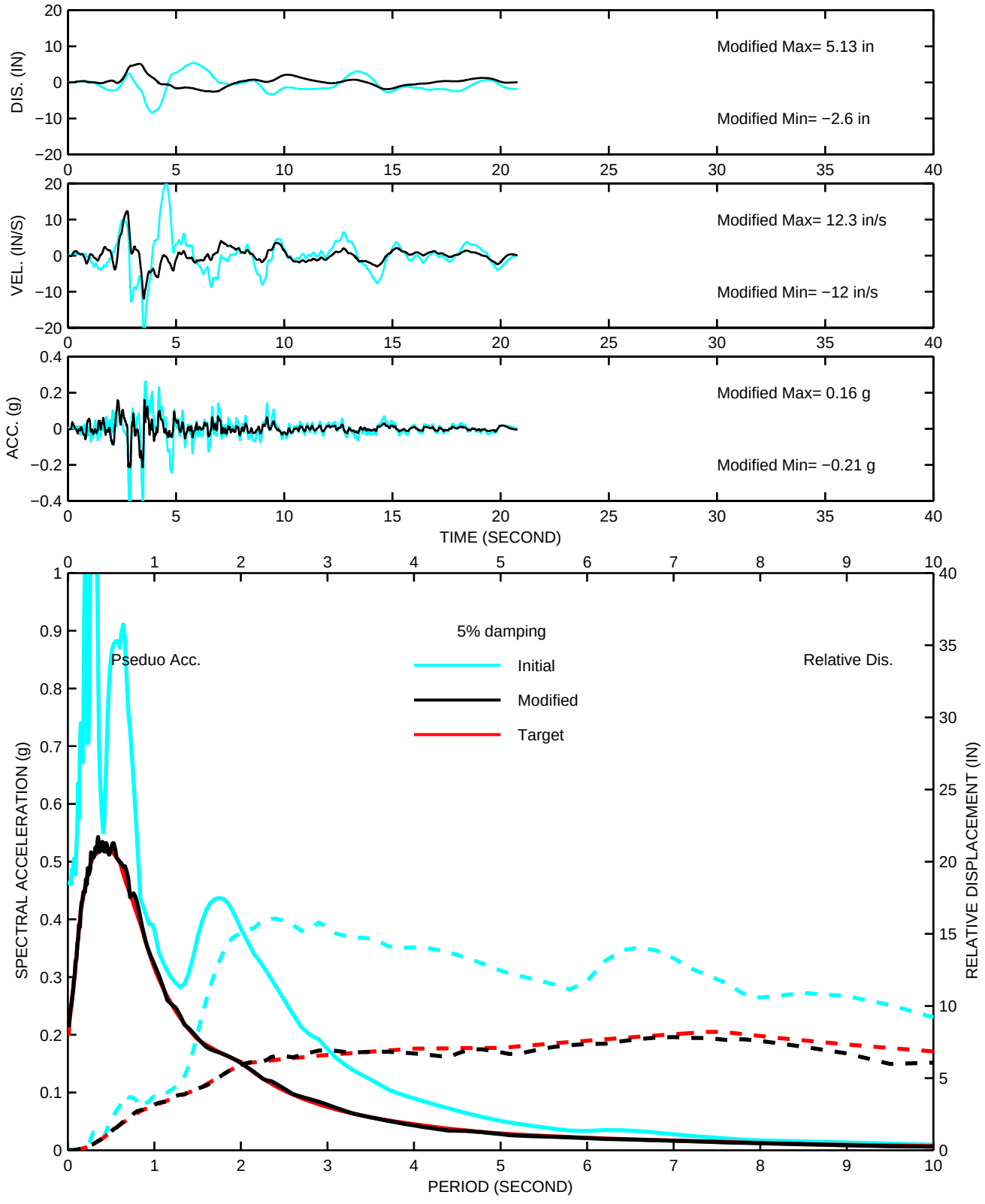


Figure E12. Unimproved Ground Area A OLE Spectrum Compatible Ground Motion (5% Damped)−Set 6 FP

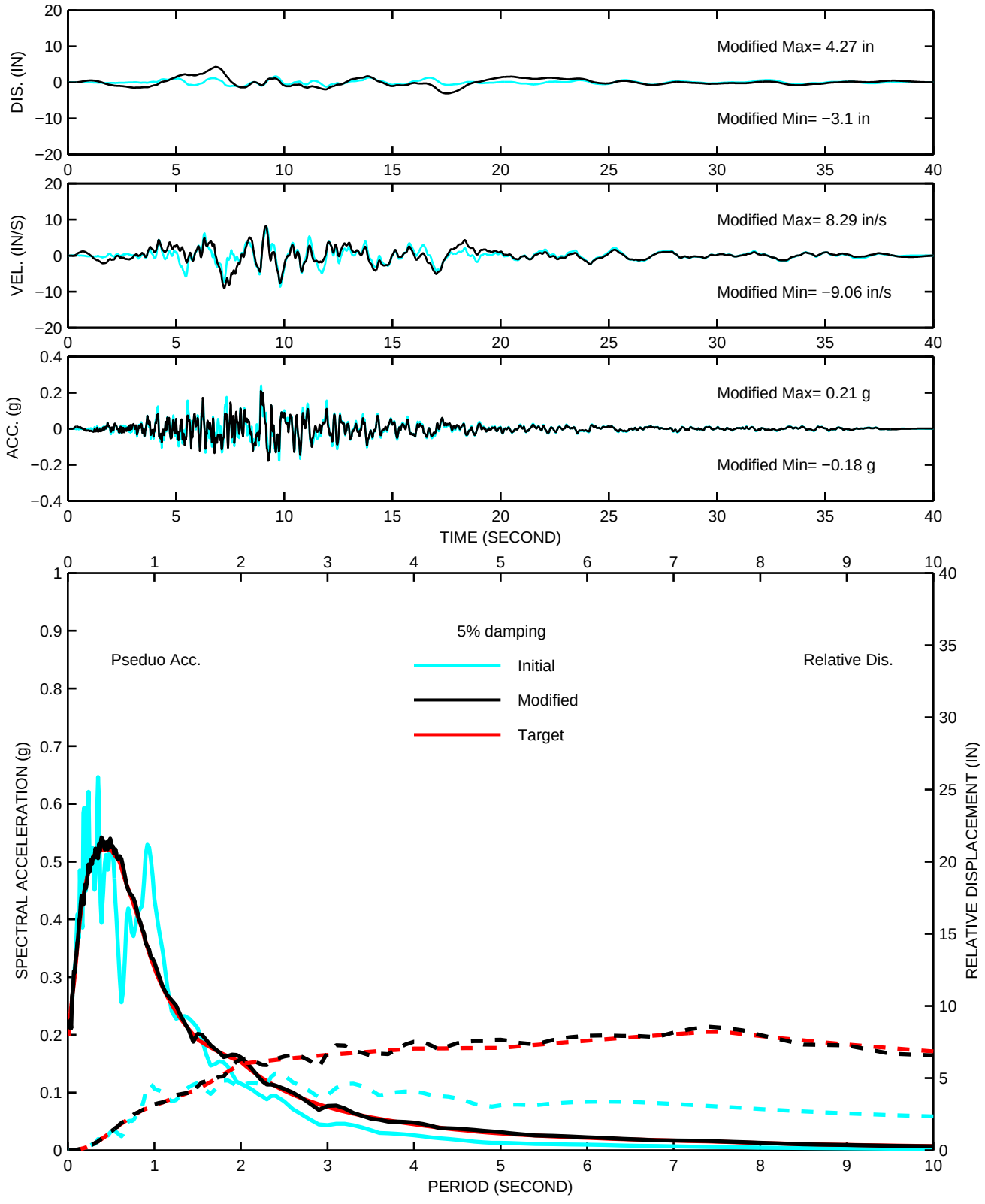


Figure E13. Unimproved Ground Area A OLE Spectrum Compatible Ground Motion (5% Damped)−Set 7 FN

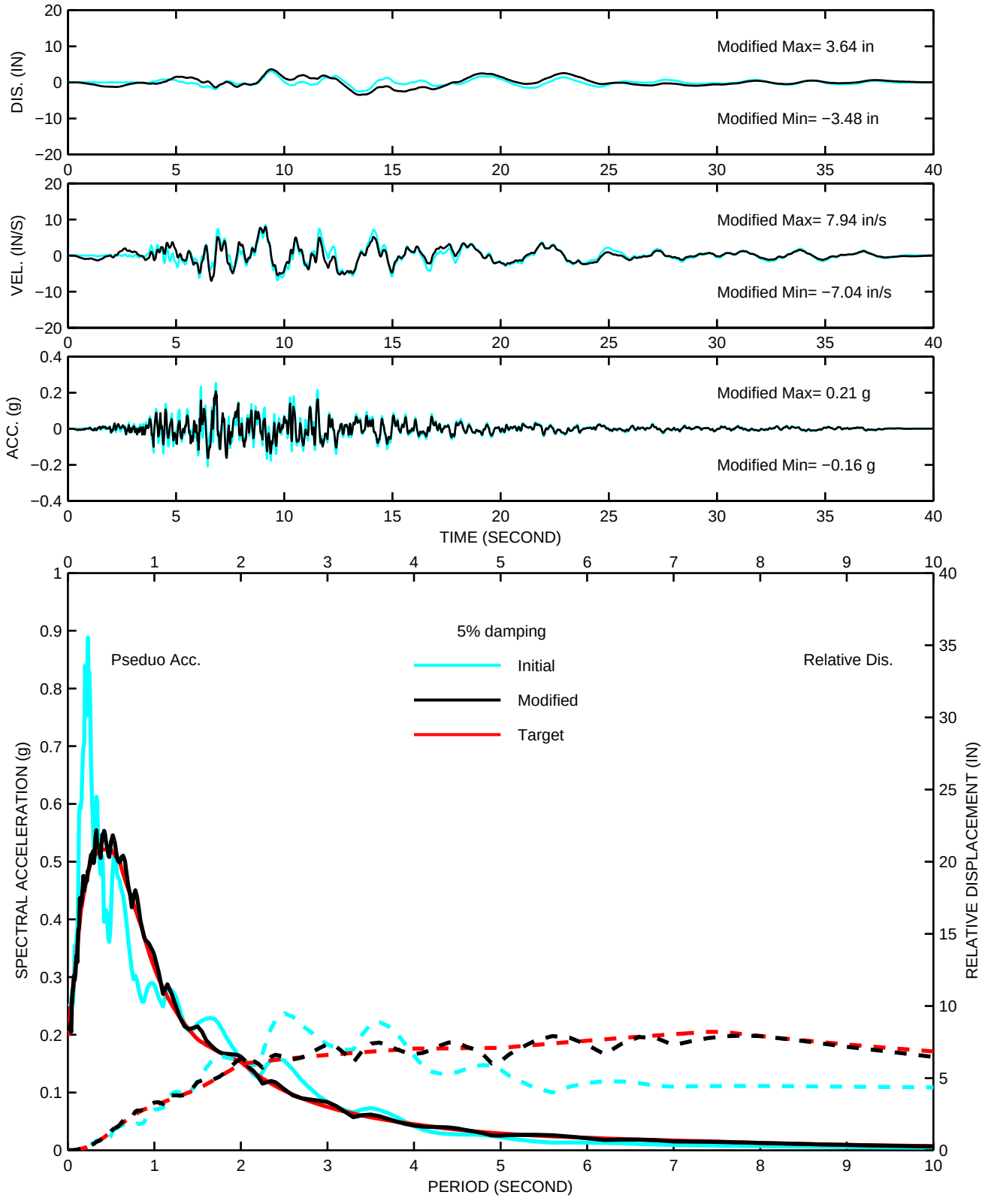


Figure E14. Unimproved Ground Area A OLE Spectrum Compatible Ground Motion (5% Damped)−Set 7 FP

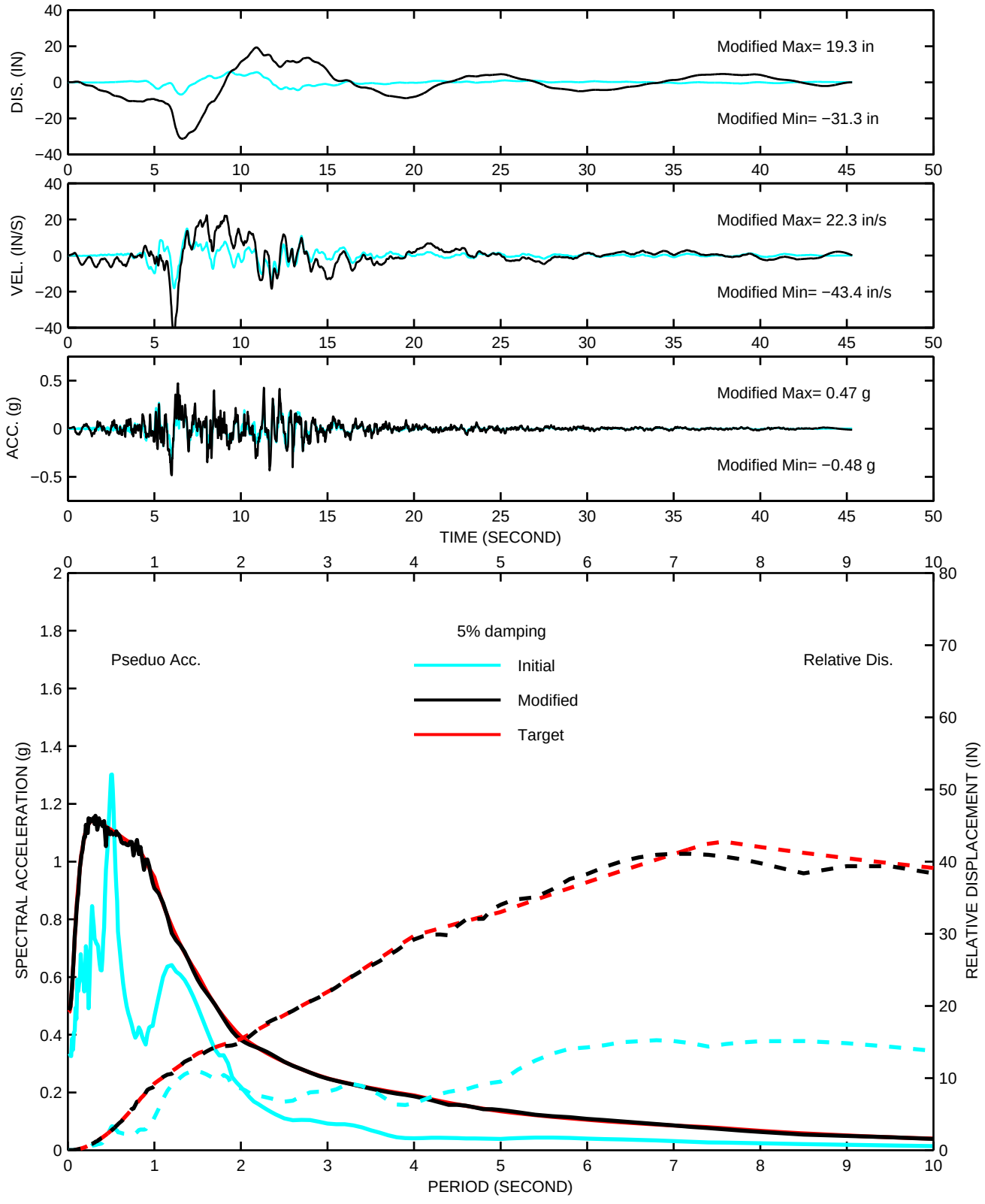


Figure E15. Unimproved Ground Area A CLE Spectrum Compatible Ground Motion (5% Damped)−Set 1 FN

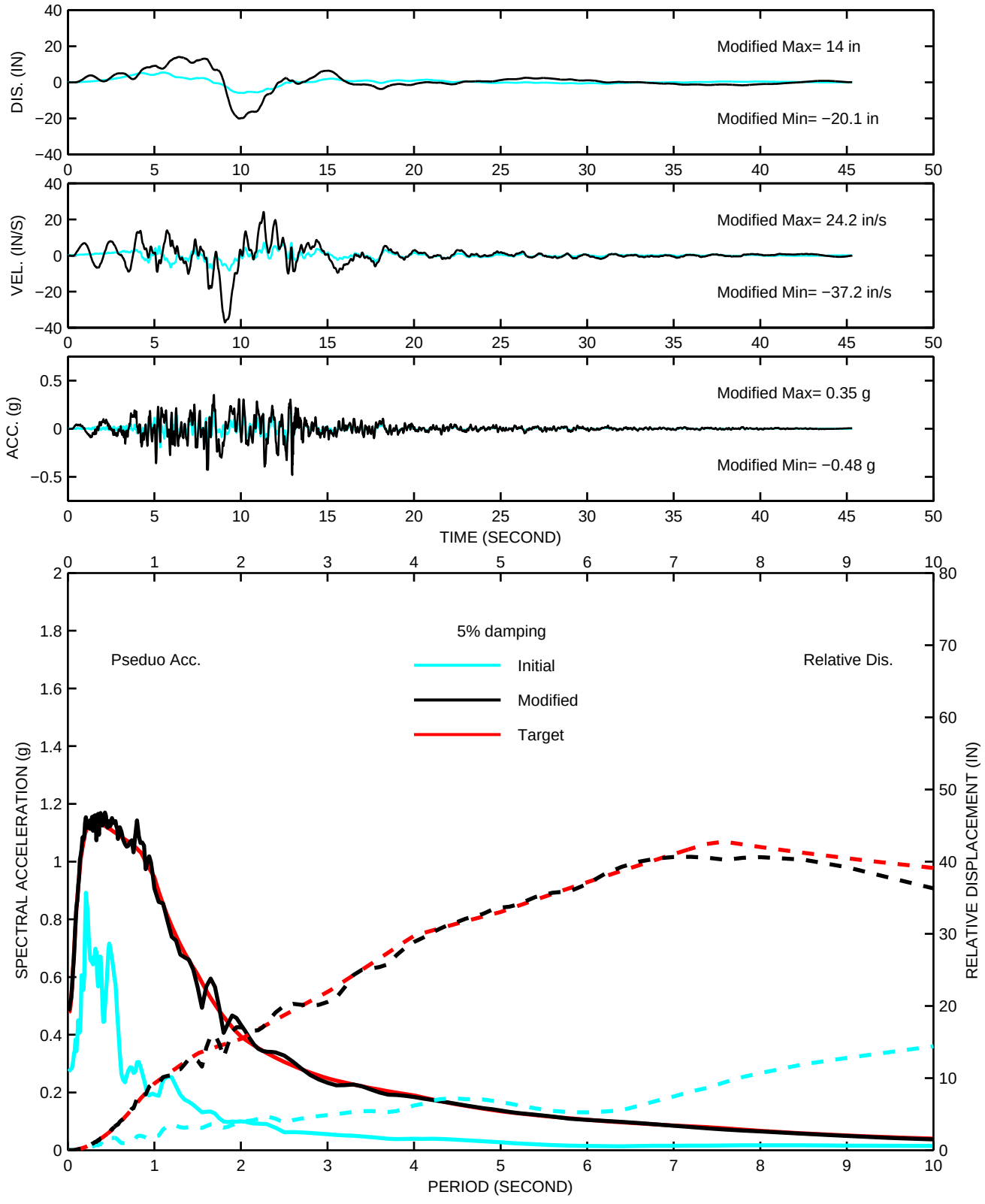


Figure E16. Unimproved Ground Area A CLE Spectrum Compatible Ground Motion (5% Damped)−Set 1 FP

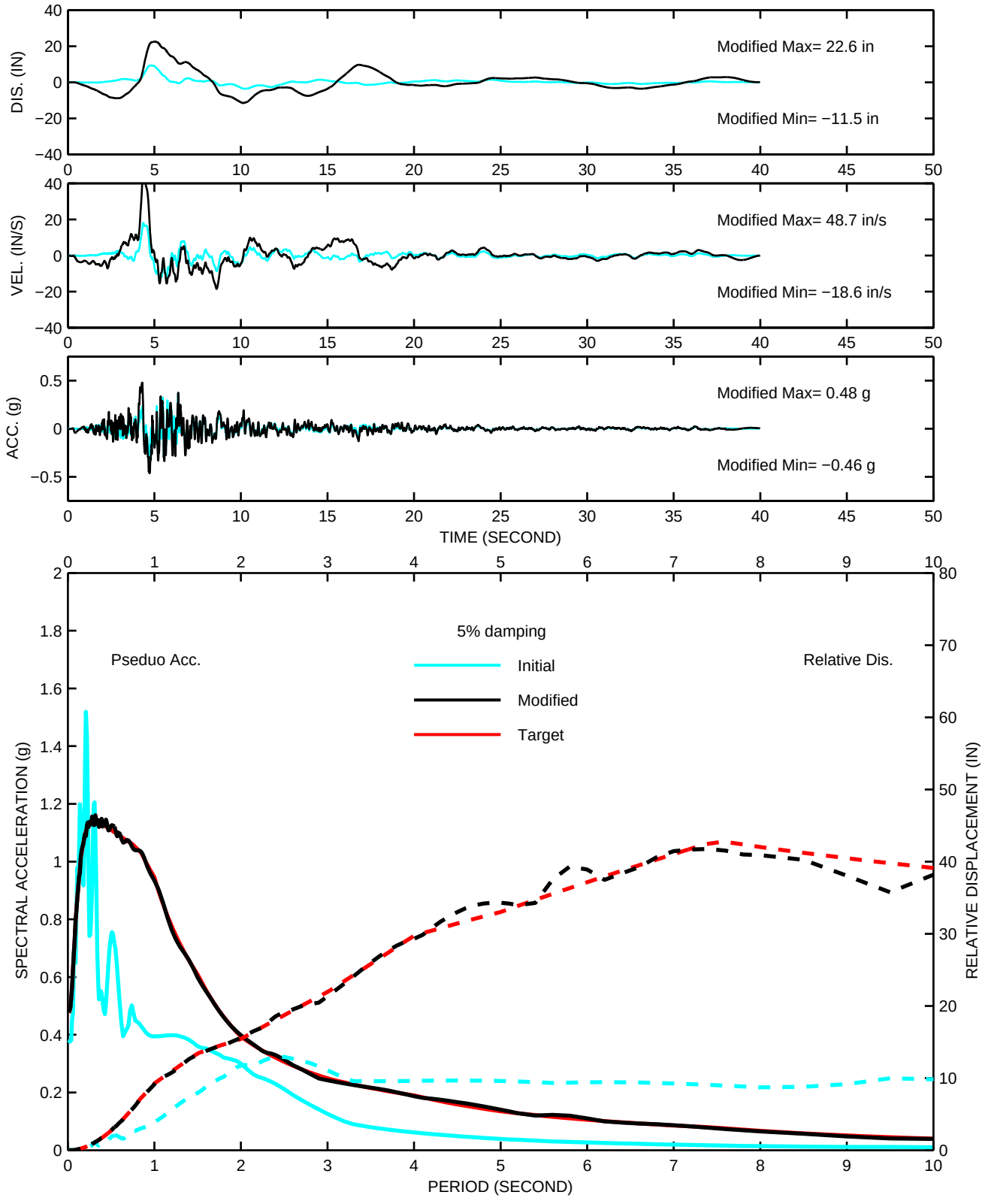


Figure E17. Unimproved Ground Area A CLE Spectrum Compatible Ground Motion (5% Damped)−Set 2 FN

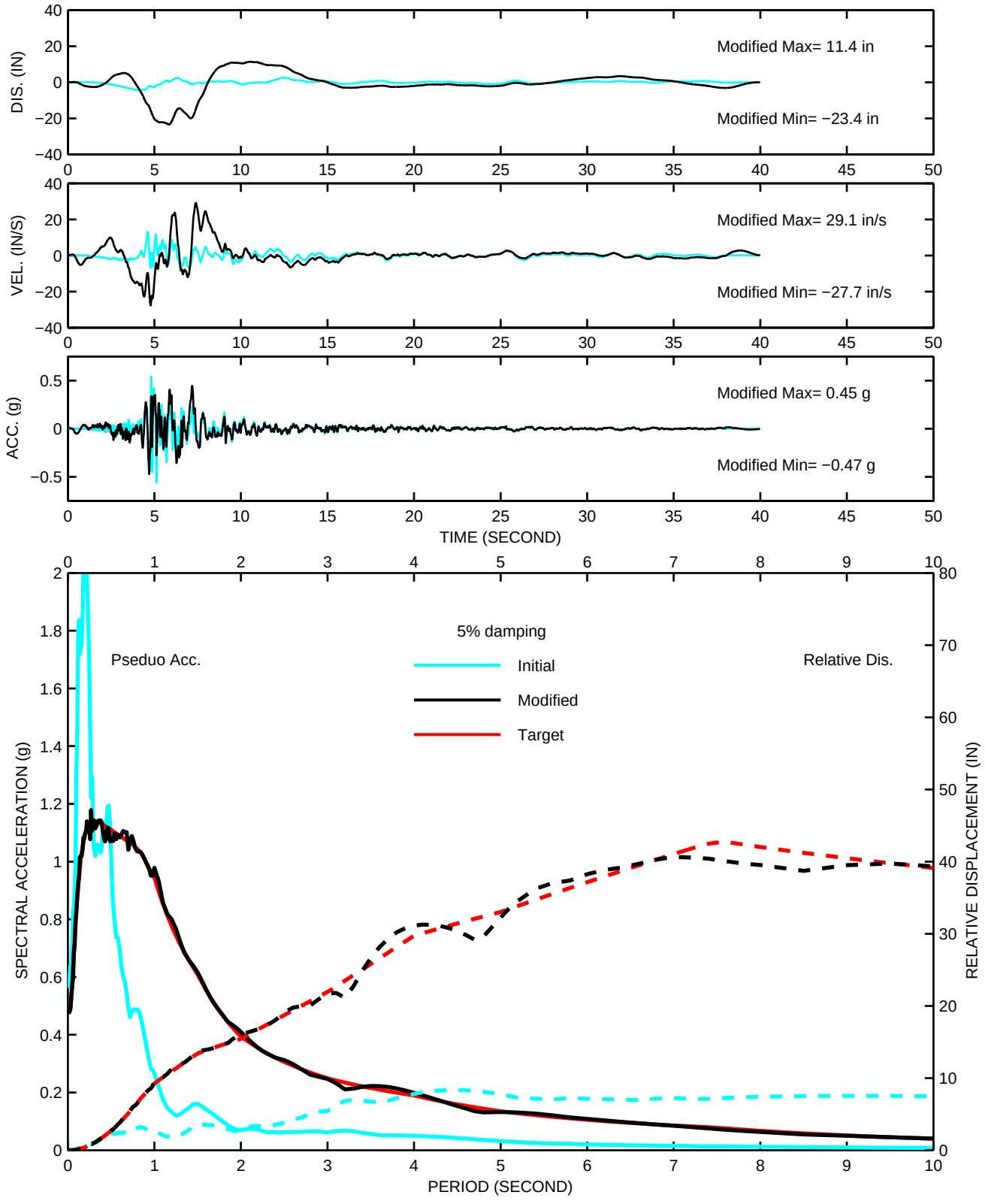


Figure E18. Unimproved Ground Area A CLE Spectrum Compatible Ground Motion (5% Damped)−Set 2 FP

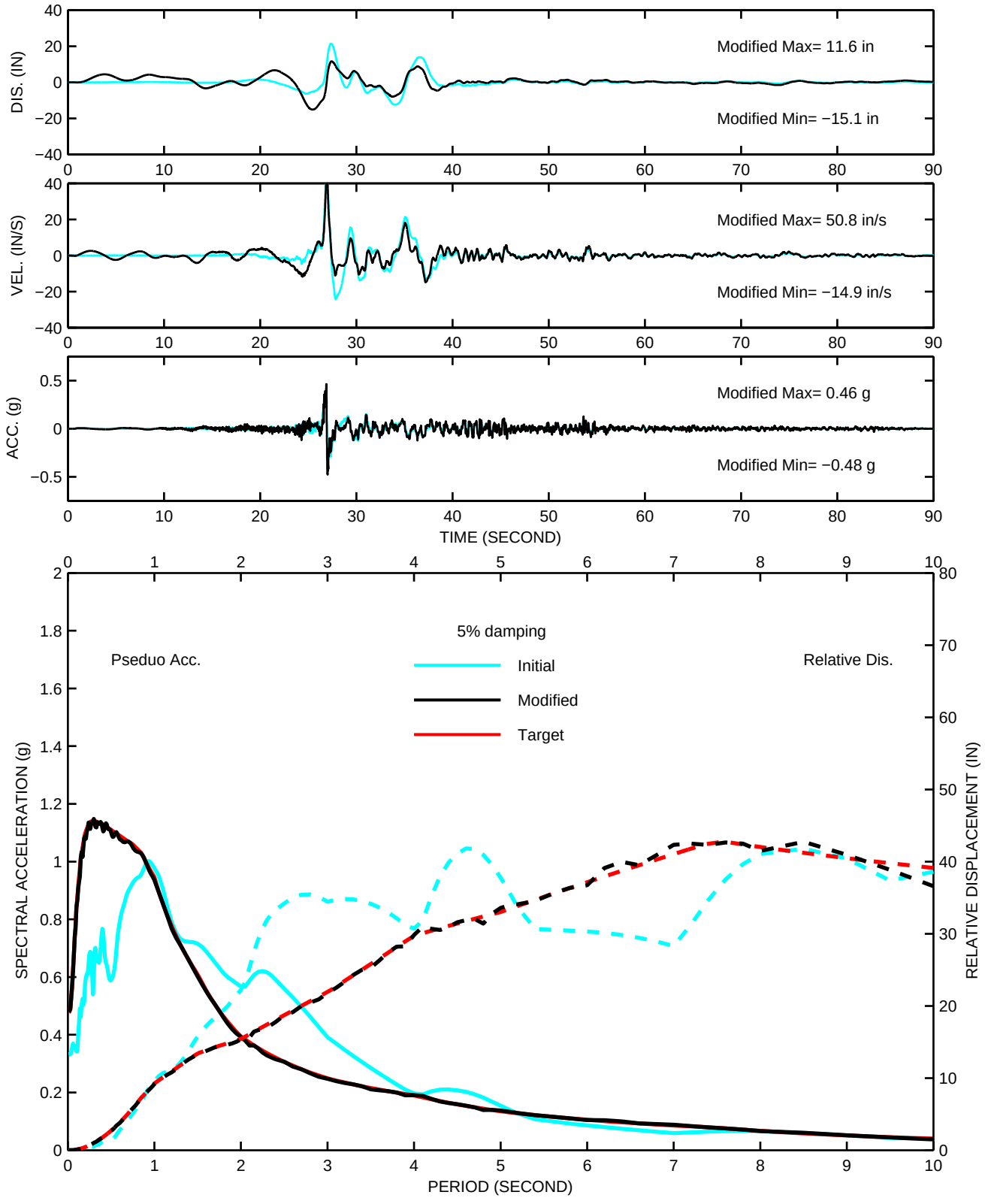


Figure E19. Unimproved Ground Area A CLE Spectrum Compatible Ground Motion (5% Damped)−Set 3 FN

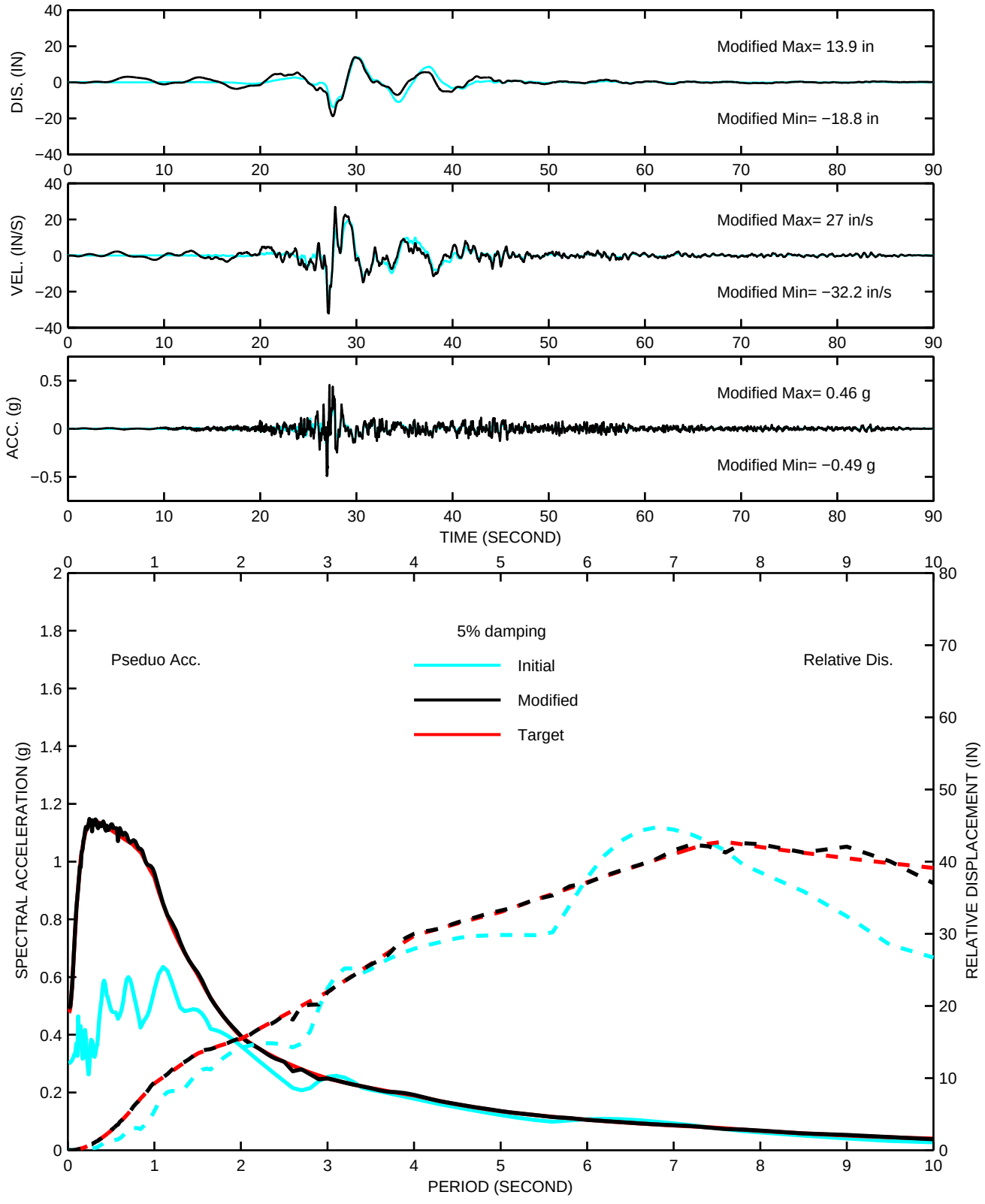


Figure E20. Unimproved Ground Area A CLE Spectrum Compatible Ground Motion (5% Damped)−Set 3 FP

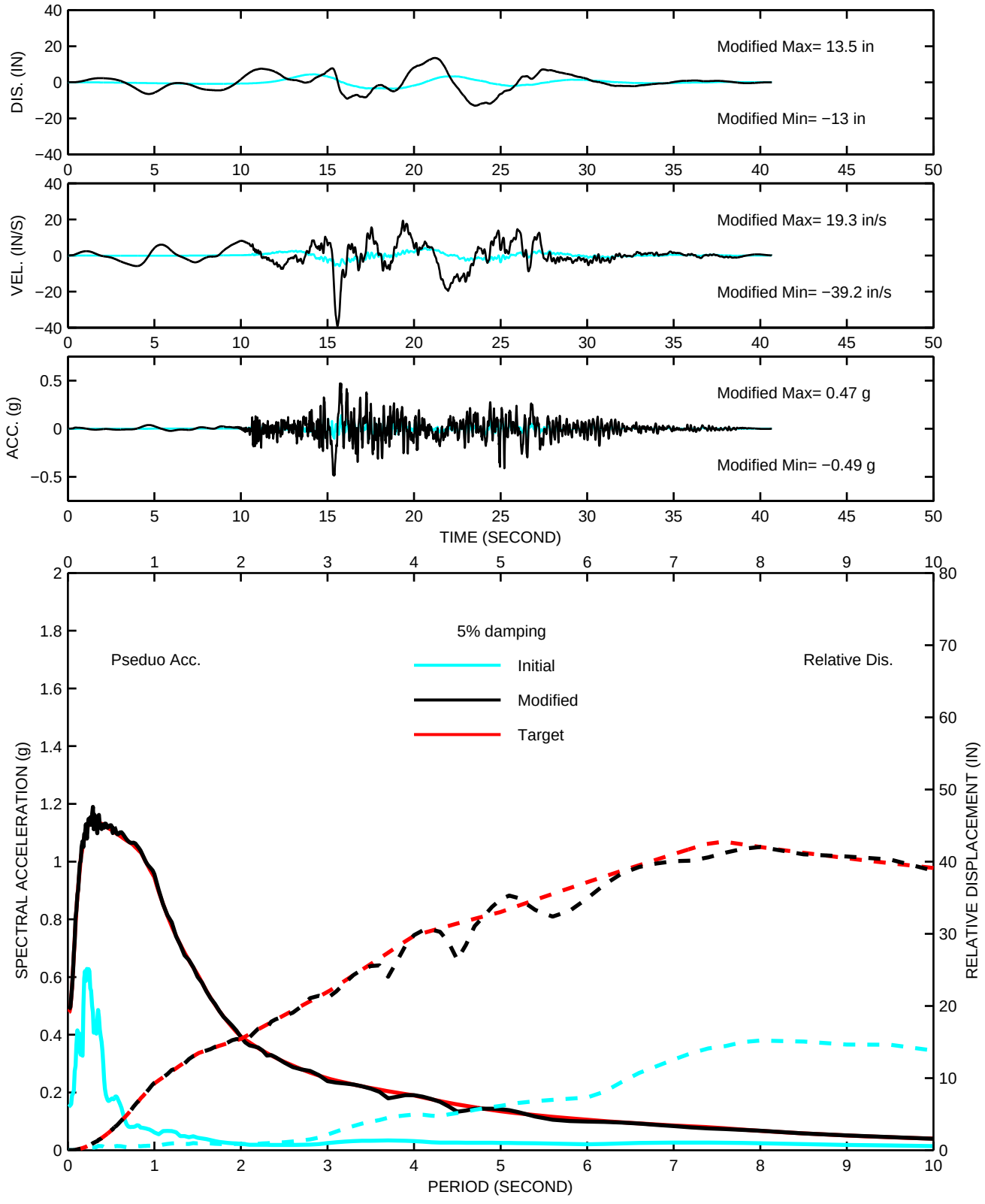


Figure E21. Unimproved Ground Area A CLE Spectrum Compatible Ground Motion (5% Damped)−Set 4 FN

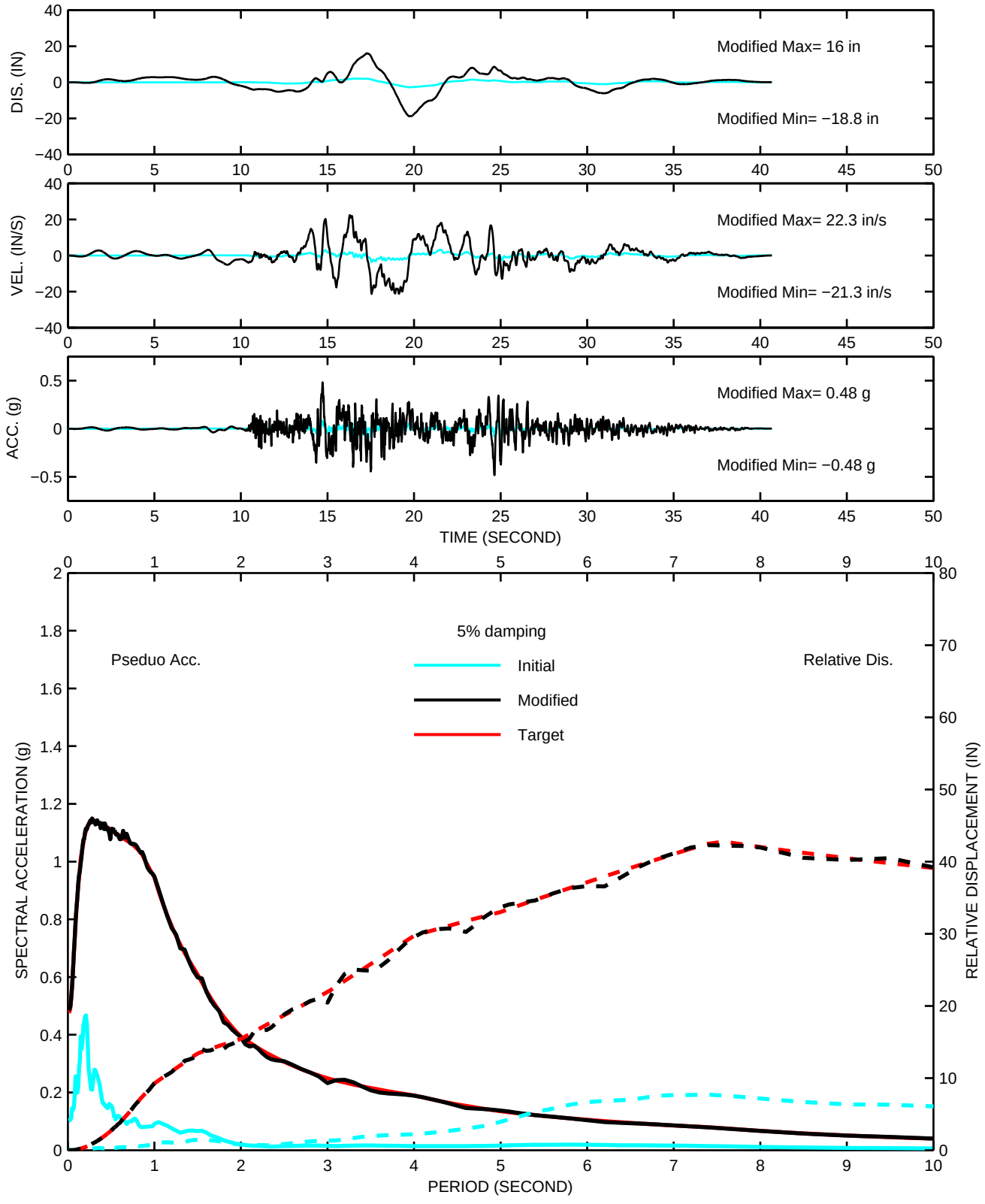


Figure E22. Unimproved Ground Area A CLE Spectrum Compatible Ground Motion (5% Damped)−Set 4 FP

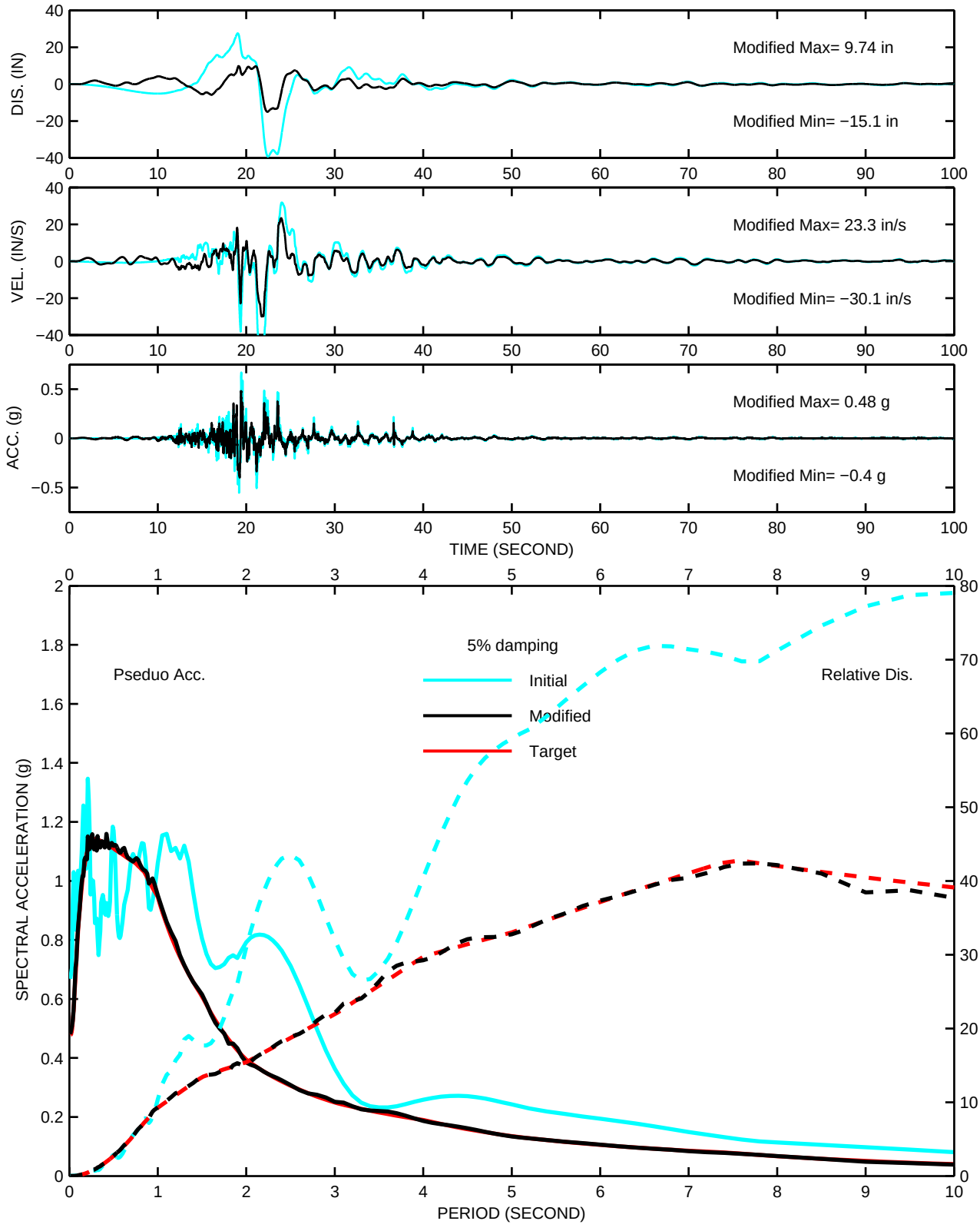


Figure E23. Unimproved Ground Area A CLE Spectrum Compatible Ground Motion (5% Damped)−Set 5 FN

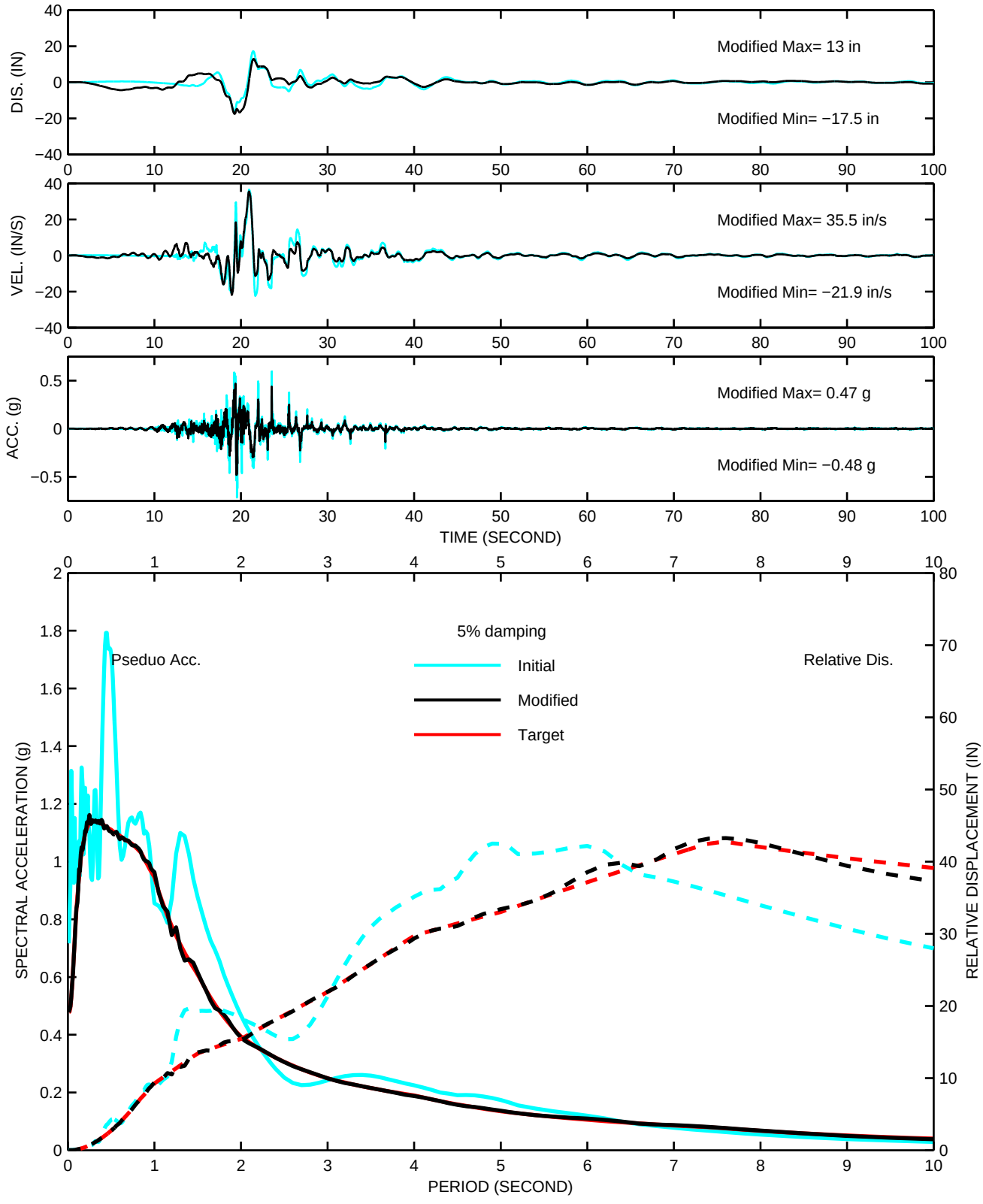


Figure E24. Unimproved Ground Area A CLE Spectrum Compatible Ground Motion (5% Damped)−Set 5 FP

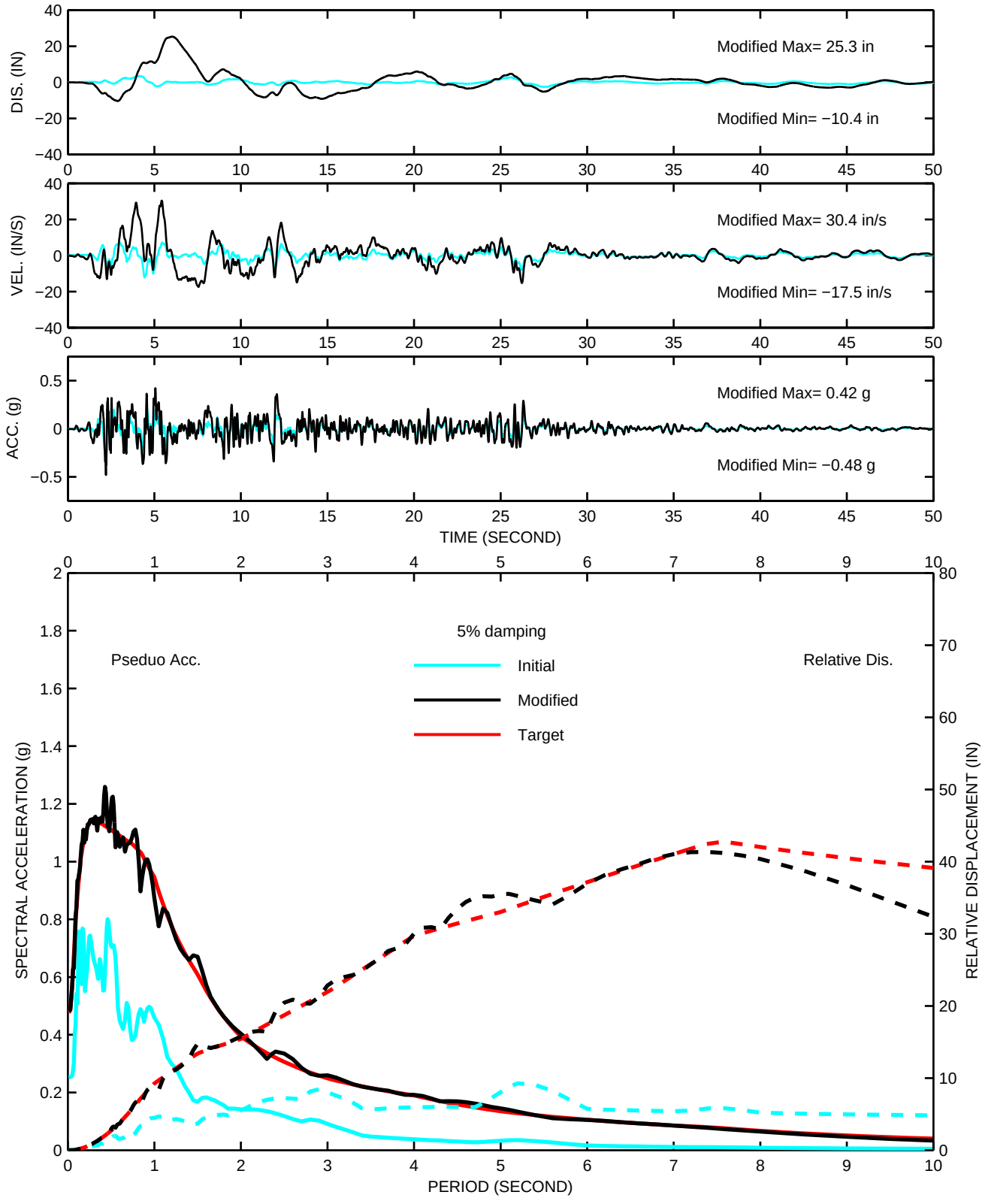


Figure E25. Unimproved Ground Area A CLE Spectrum Compatible Ground Motion (5% Damped)−Set 6 FN

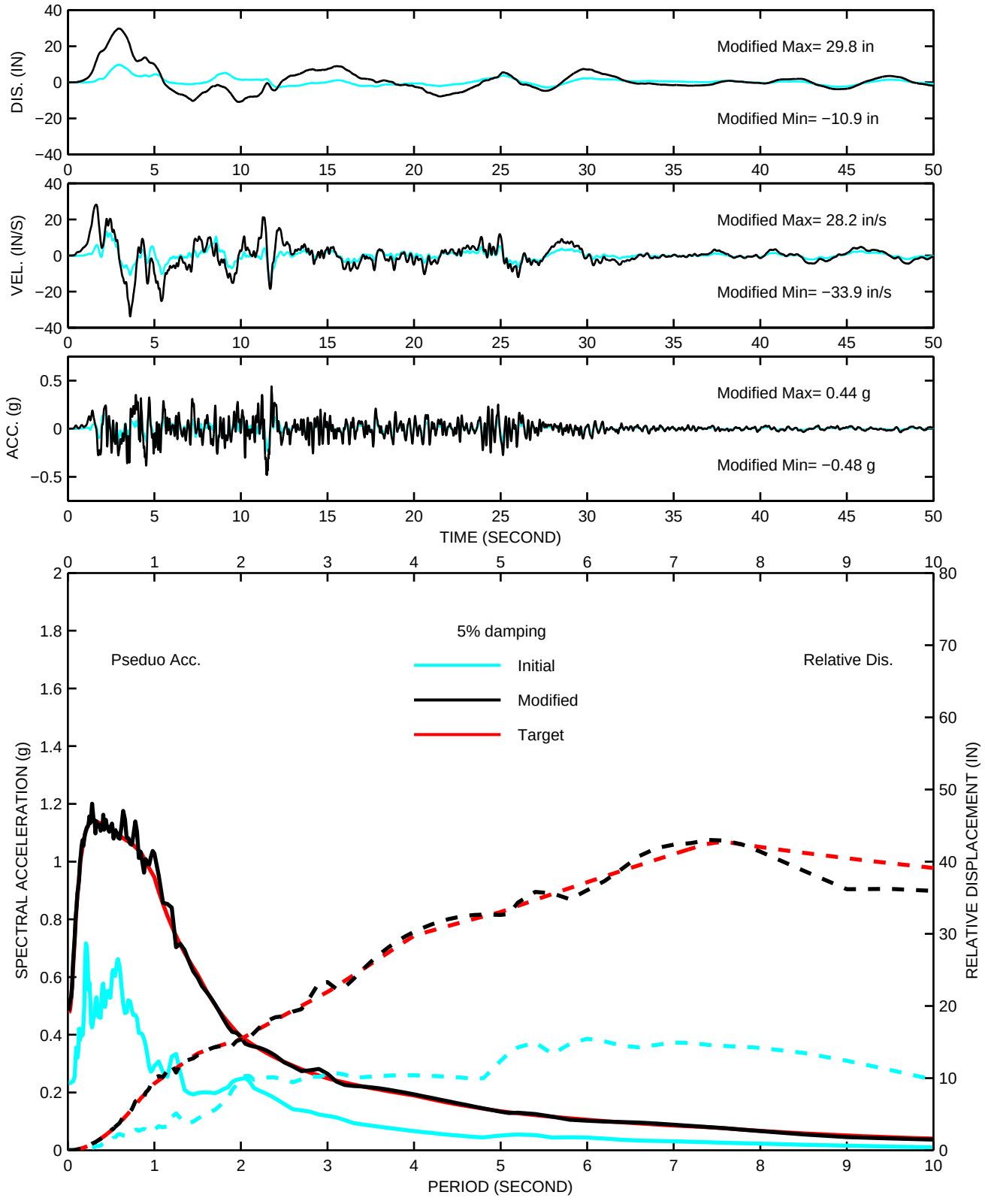


Figure E26. Unimproved Ground Area A CLE Spectrum Compatible Ground Motion (5% Damped)−Set 6 FP

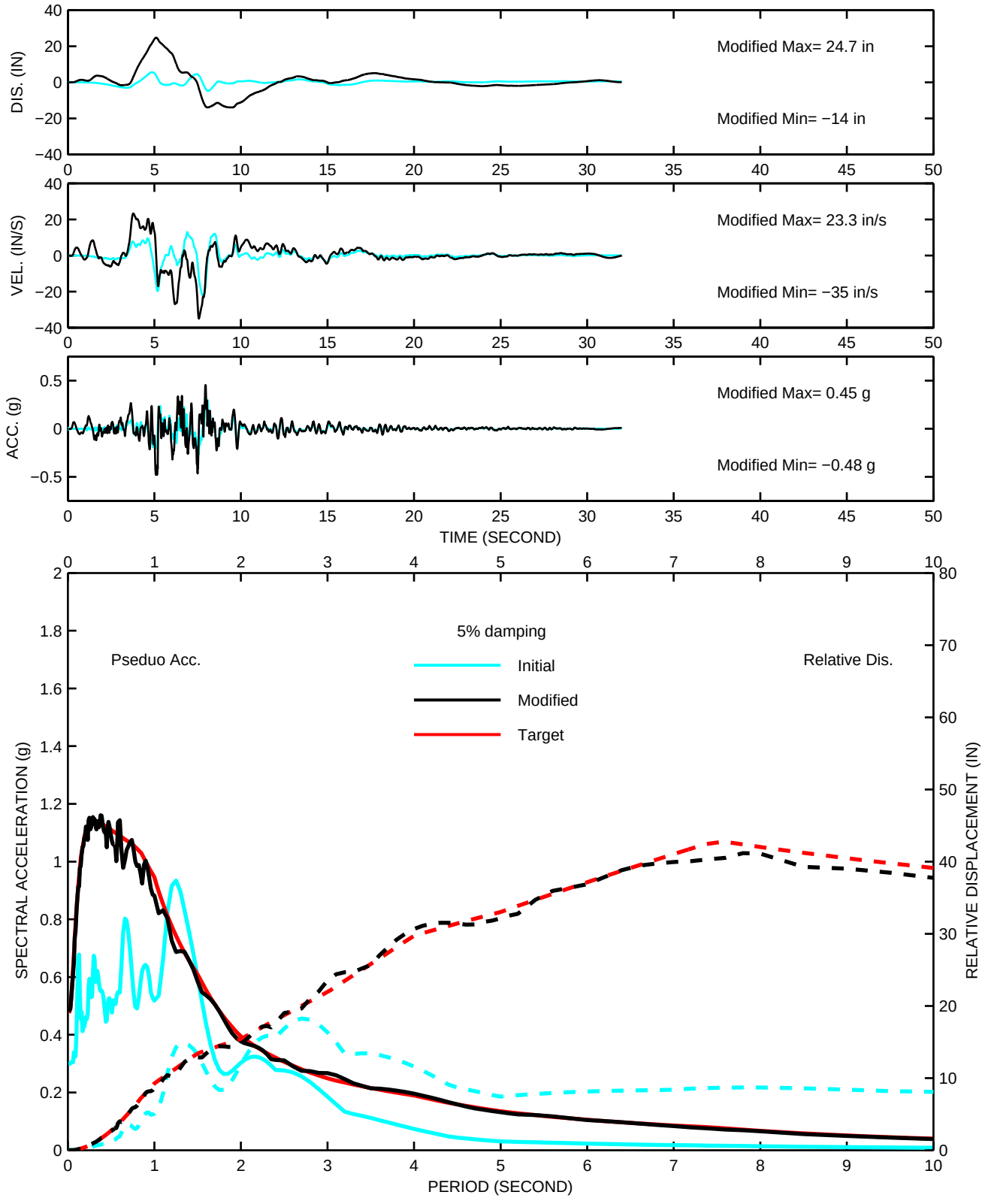


Figure E27. Unimproved Ground Area A CLE Spectrum Compatible Ground Motion (5% Damped)−Set 7 FN

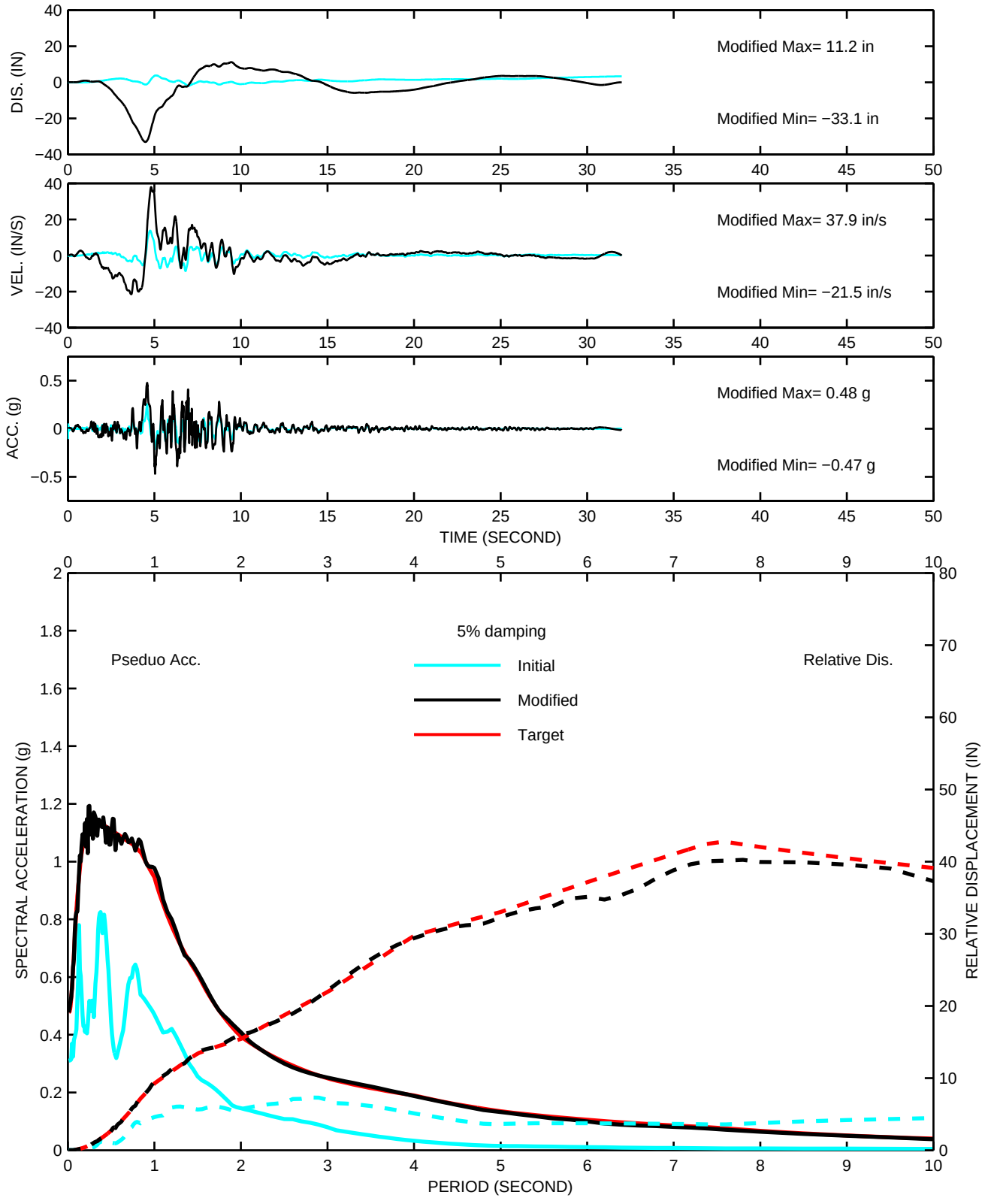


Figure E28. Unimproved Ground Area A CLE Spectrum Compatible Ground Motion (5% Damped)−Set 7 FP

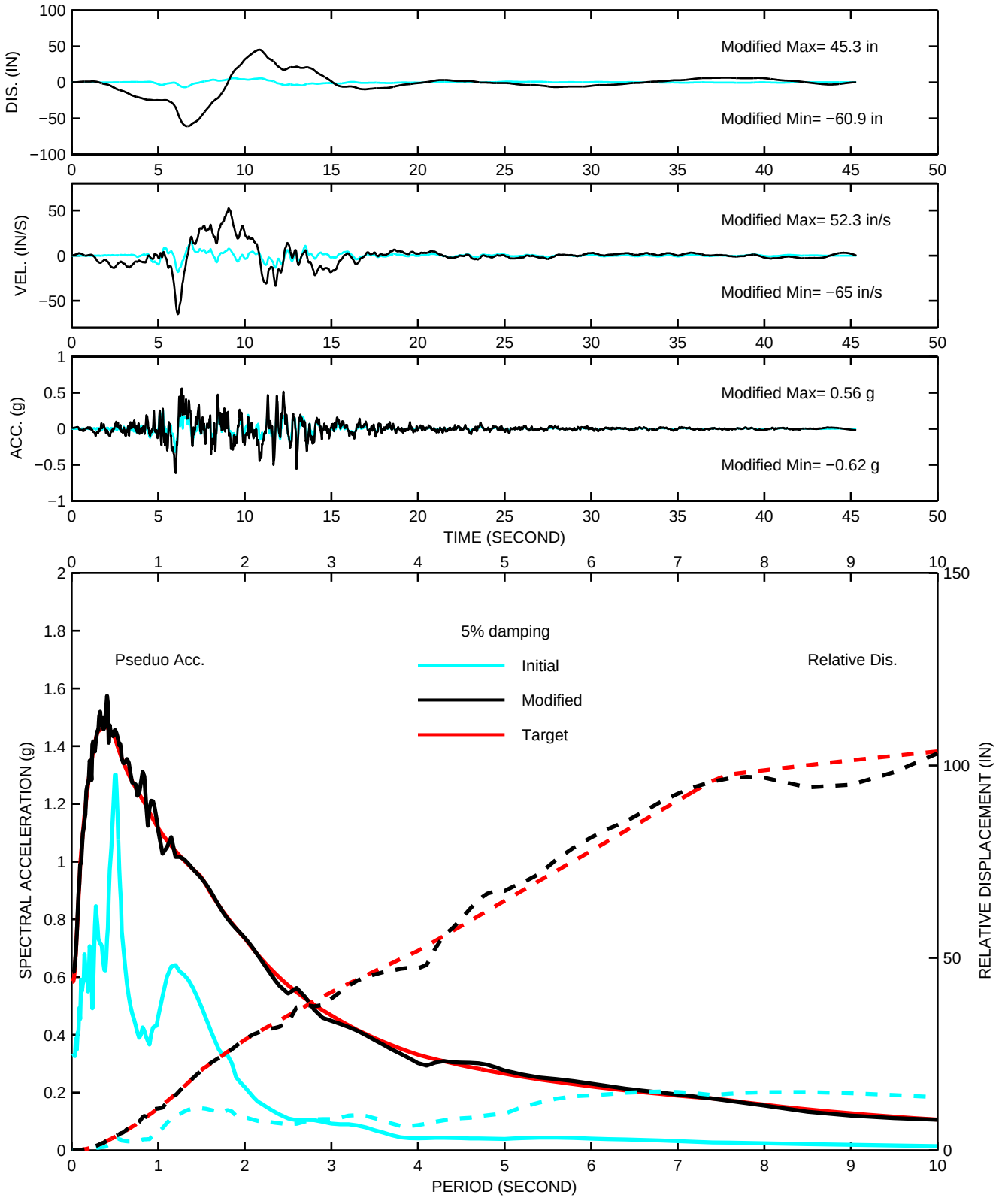


Figure E29. Unimproved Ground Area A DE Spectrum Compatible Ground Motion (5% Damped)−Set 1 FN

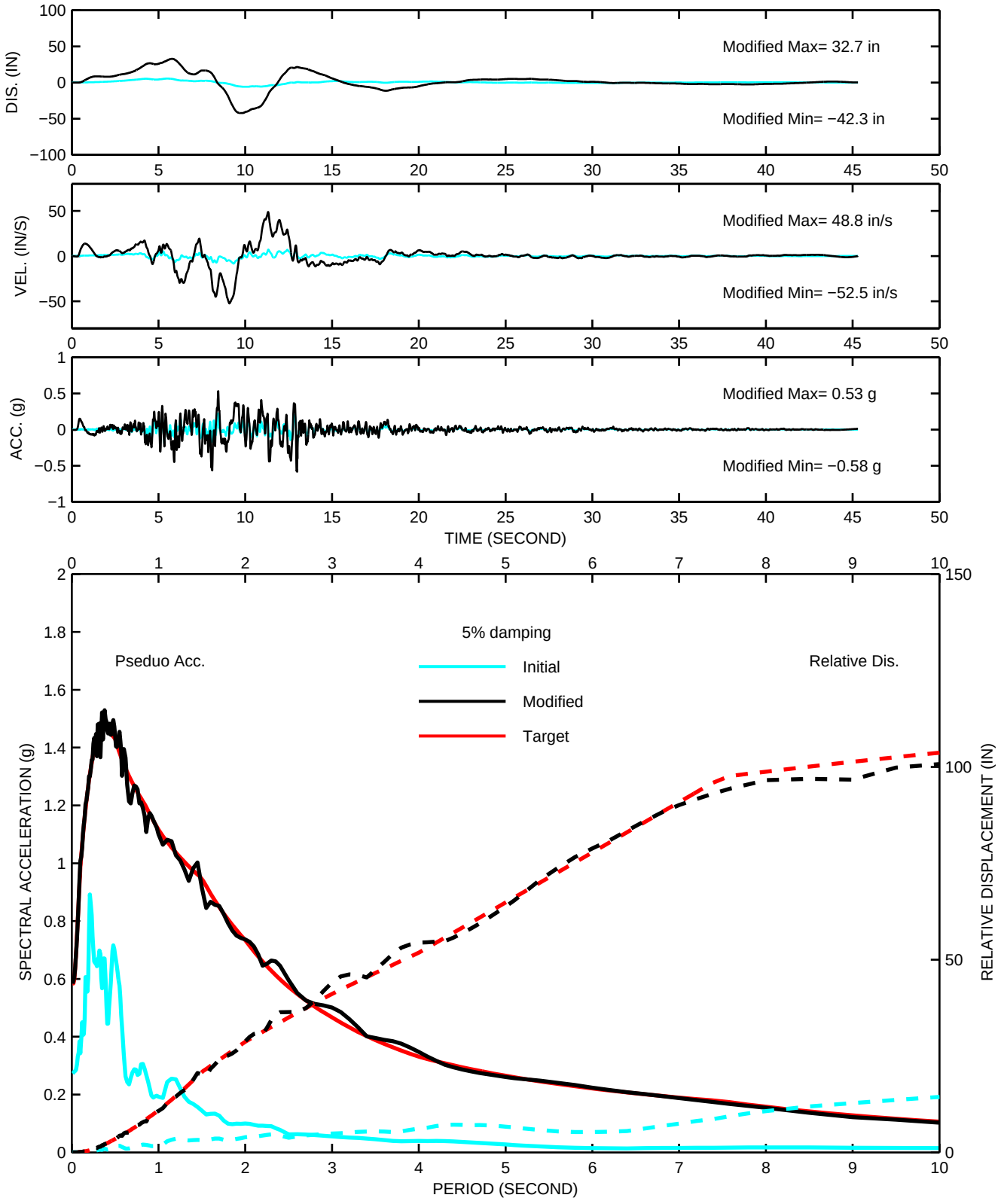


Figure E30. Unimproved Ground Area A DE Spectrum Compatible Ground Motion (5% Damped)−Set 1 FP

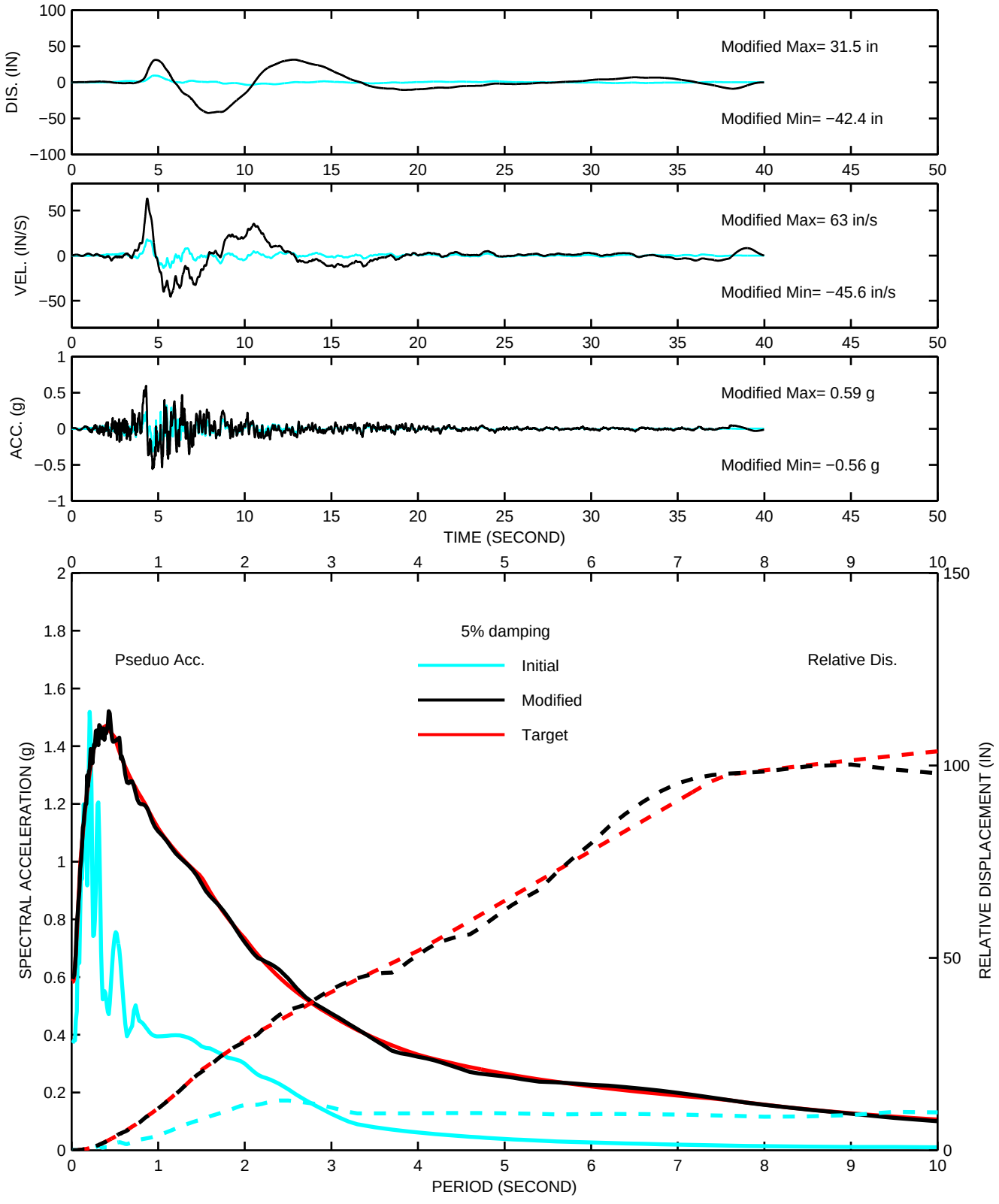


Figure E31. Unimproved Ground Area A DE Spectrum Compatible Ground Motion (5% Damped)−Set 2 FN

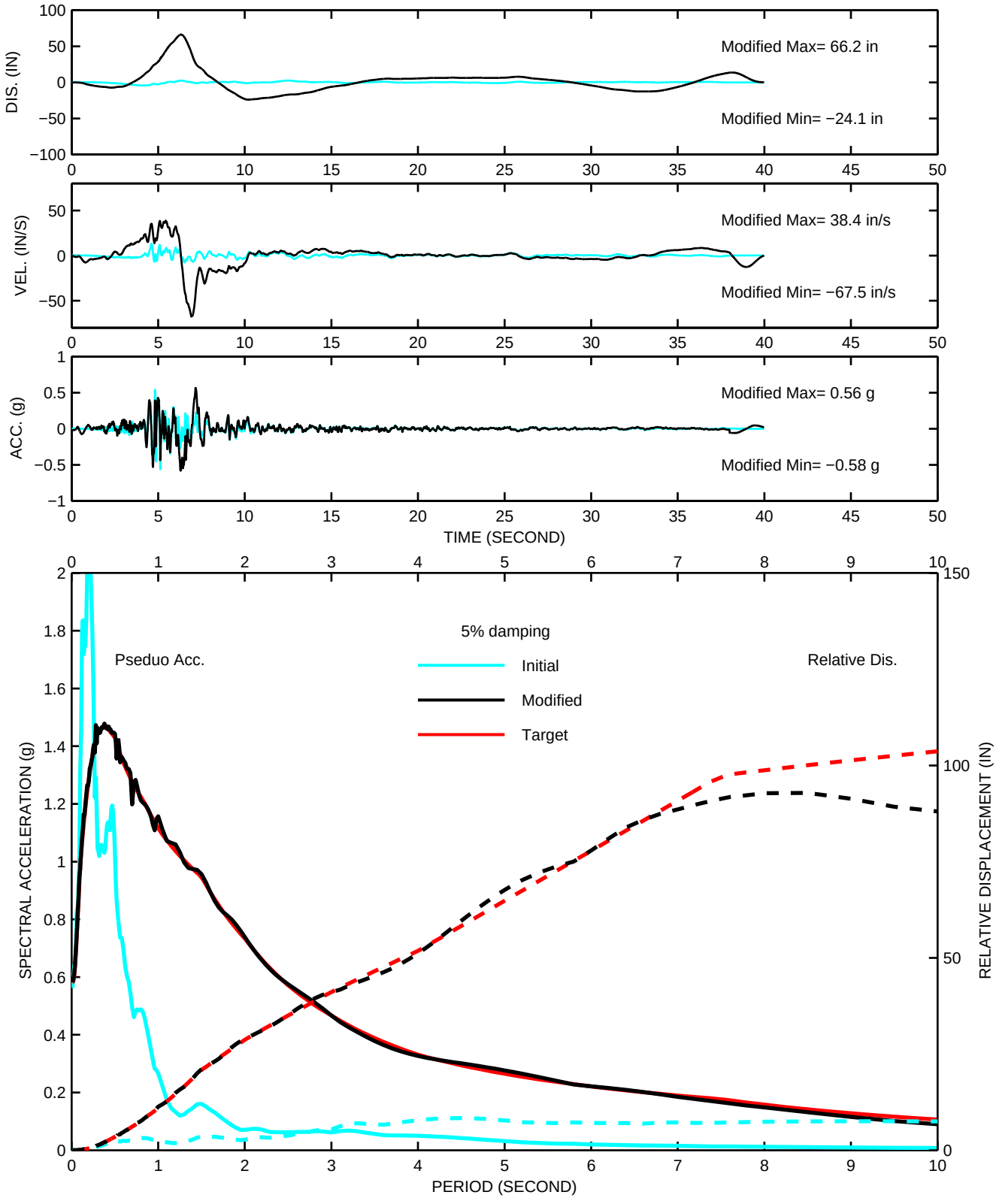


Figure E32. Unimproved Ground Area A DE Spectrum Compatible Ground Motion (5% Damped)−Set 2 FP

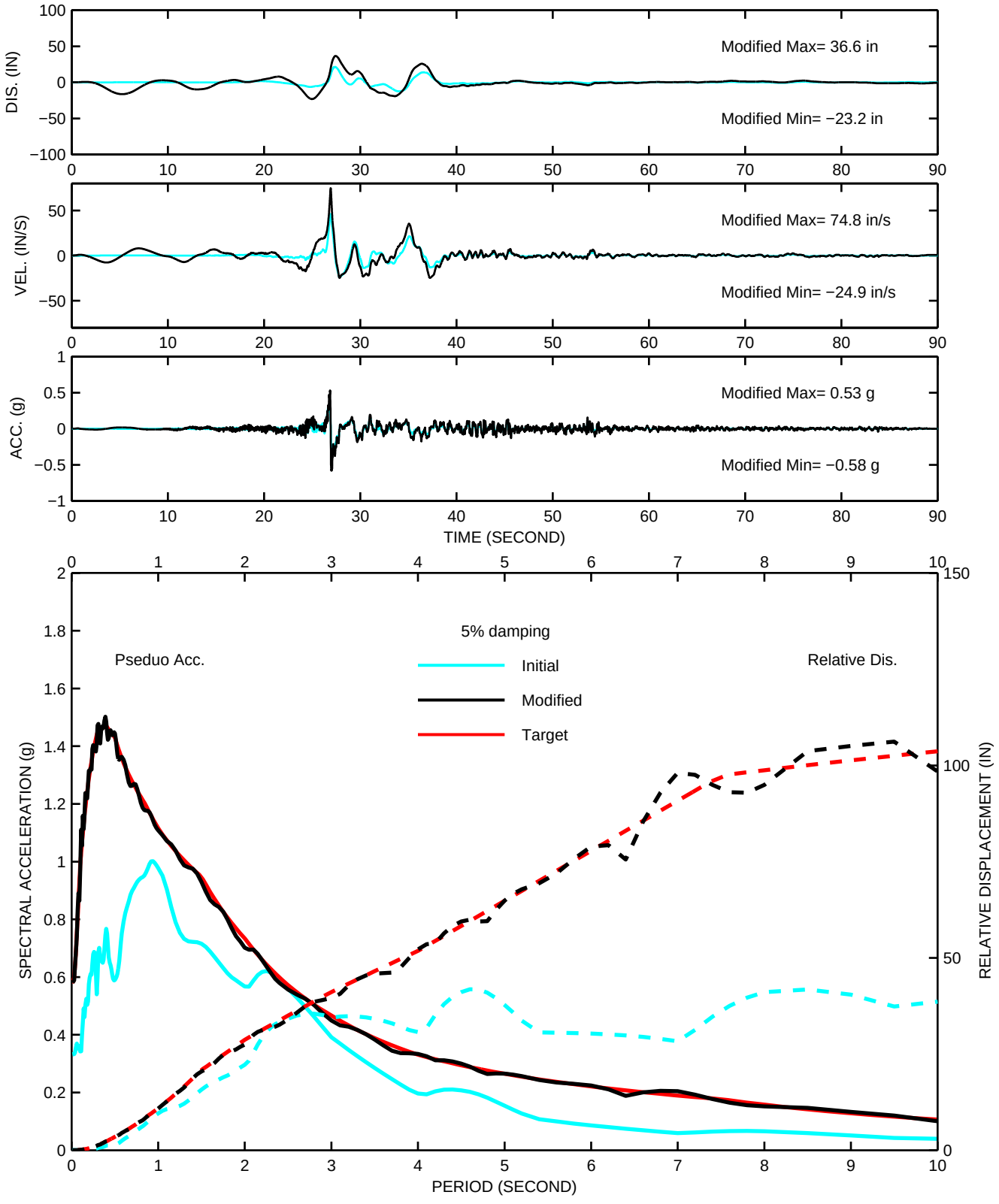


Figure E33. Unimproved Ground Area A DE Spectrum Compatible Ground Motion (5% Damped)−Set 3 FN

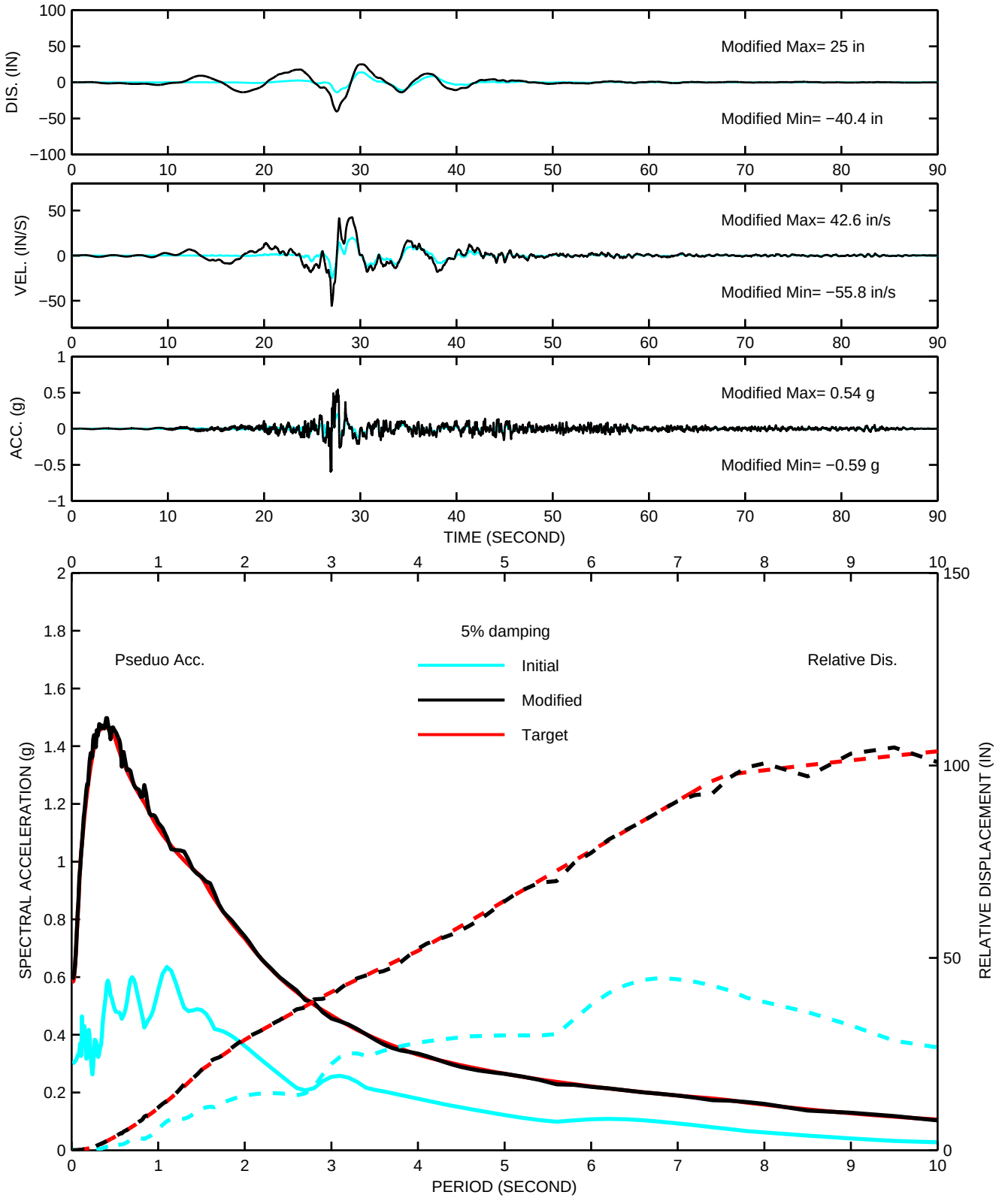


Figure E34. Unimproved Ground Area A DE Spectrum Compatible Ground Motion (5% Damped)−Set 3 FP

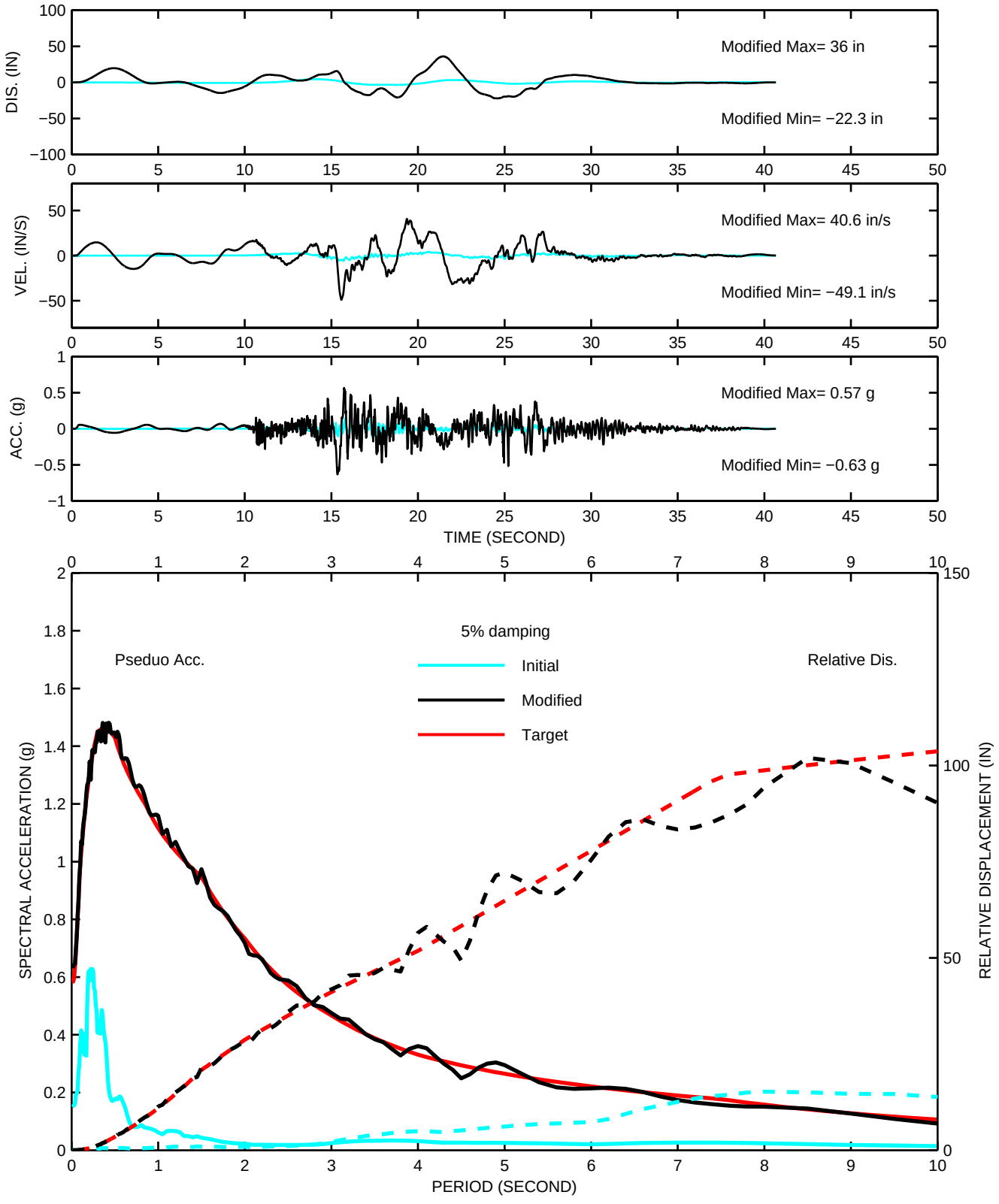


Figure E35. Unimproved Ground Area A DE Spectrum Compatible Ground Motion (5% Damped)−Set 4 FN

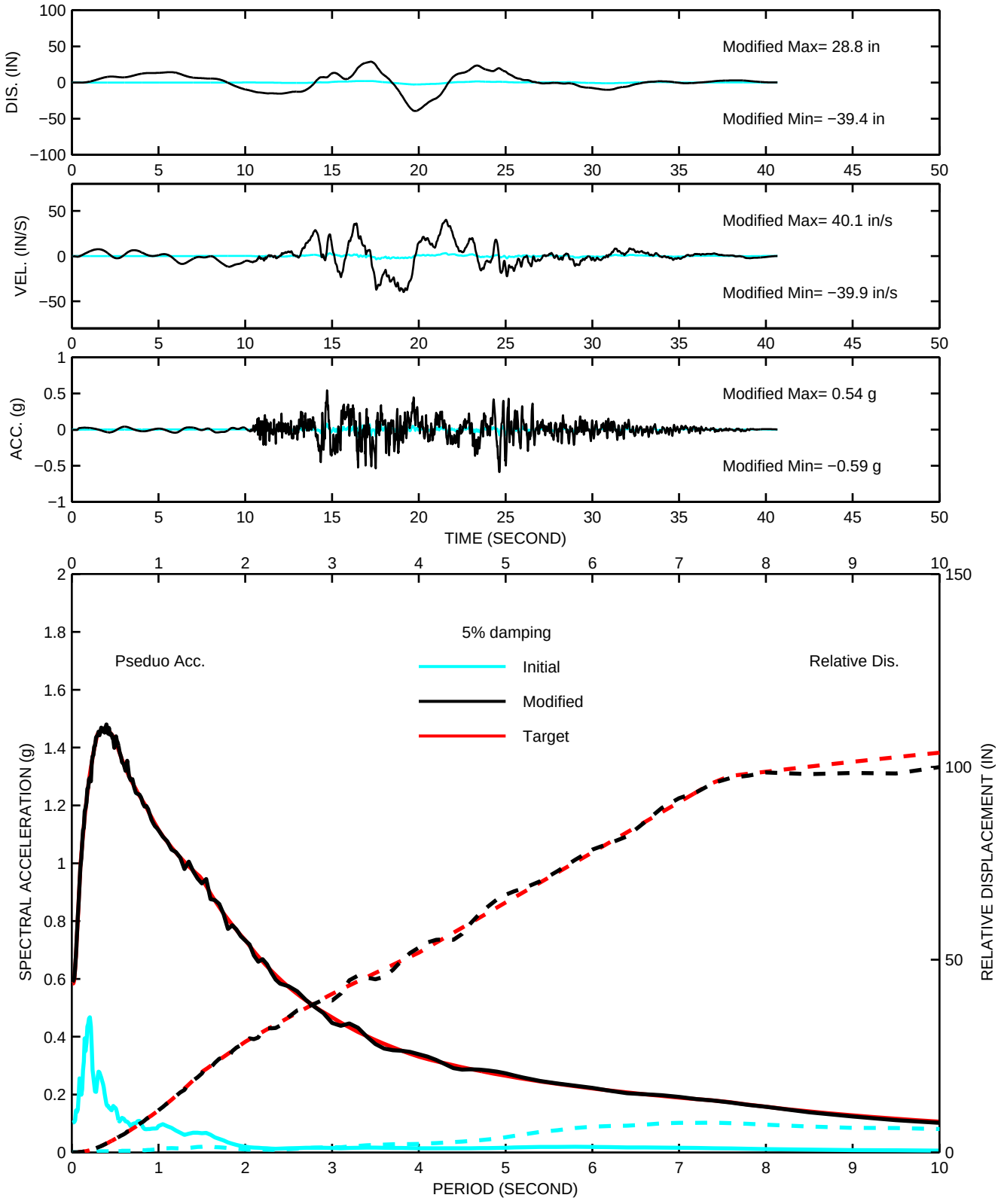


Figure E36. Unimproved Ground Area A DE Spectrum Compatible Ground Motion (5% Damped)−Set 4 FP

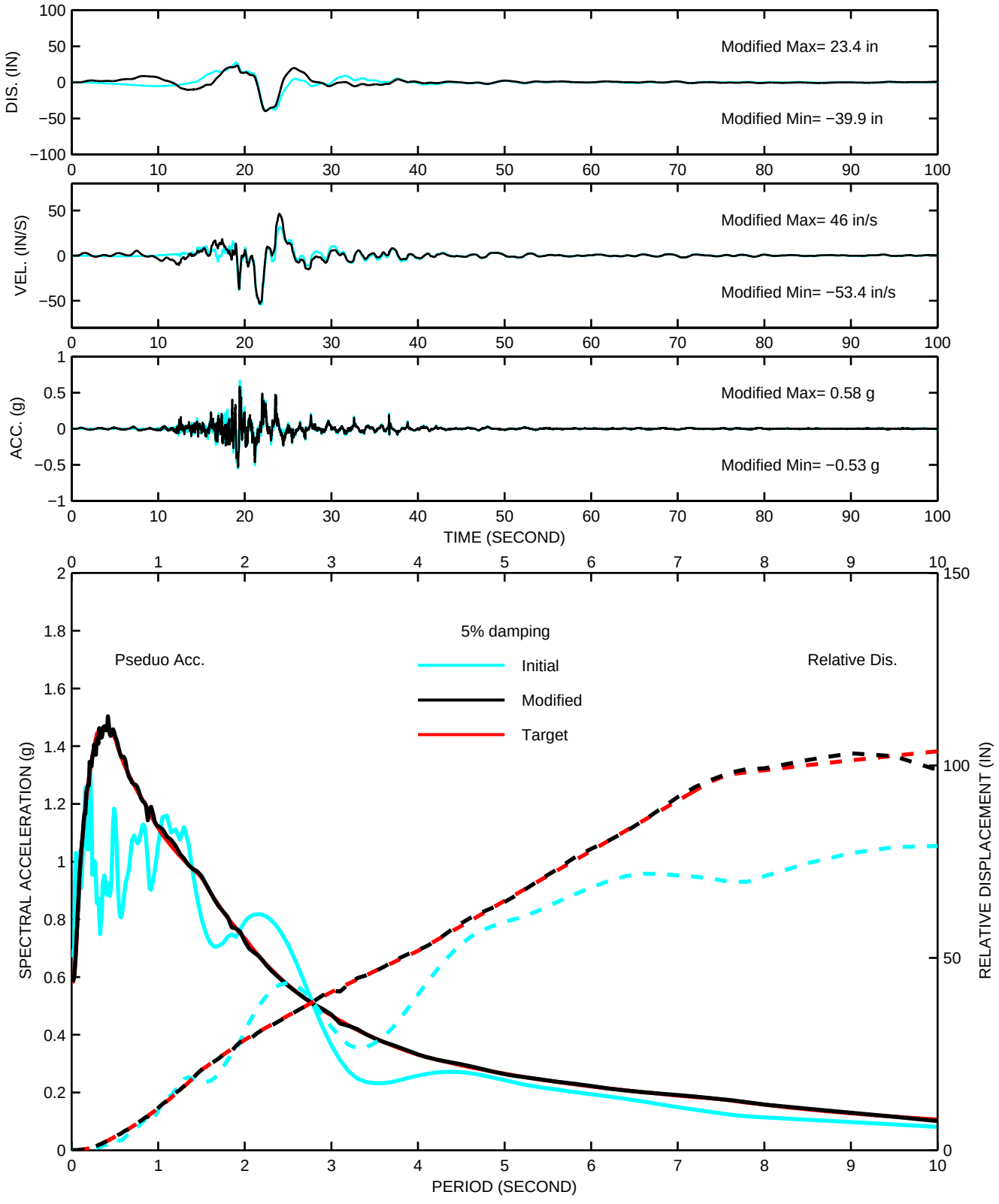


Figure E37. Unimproved Ground Area A DE Spectrum Compatible Ground Motion (5% Damped)−Set 5 FN

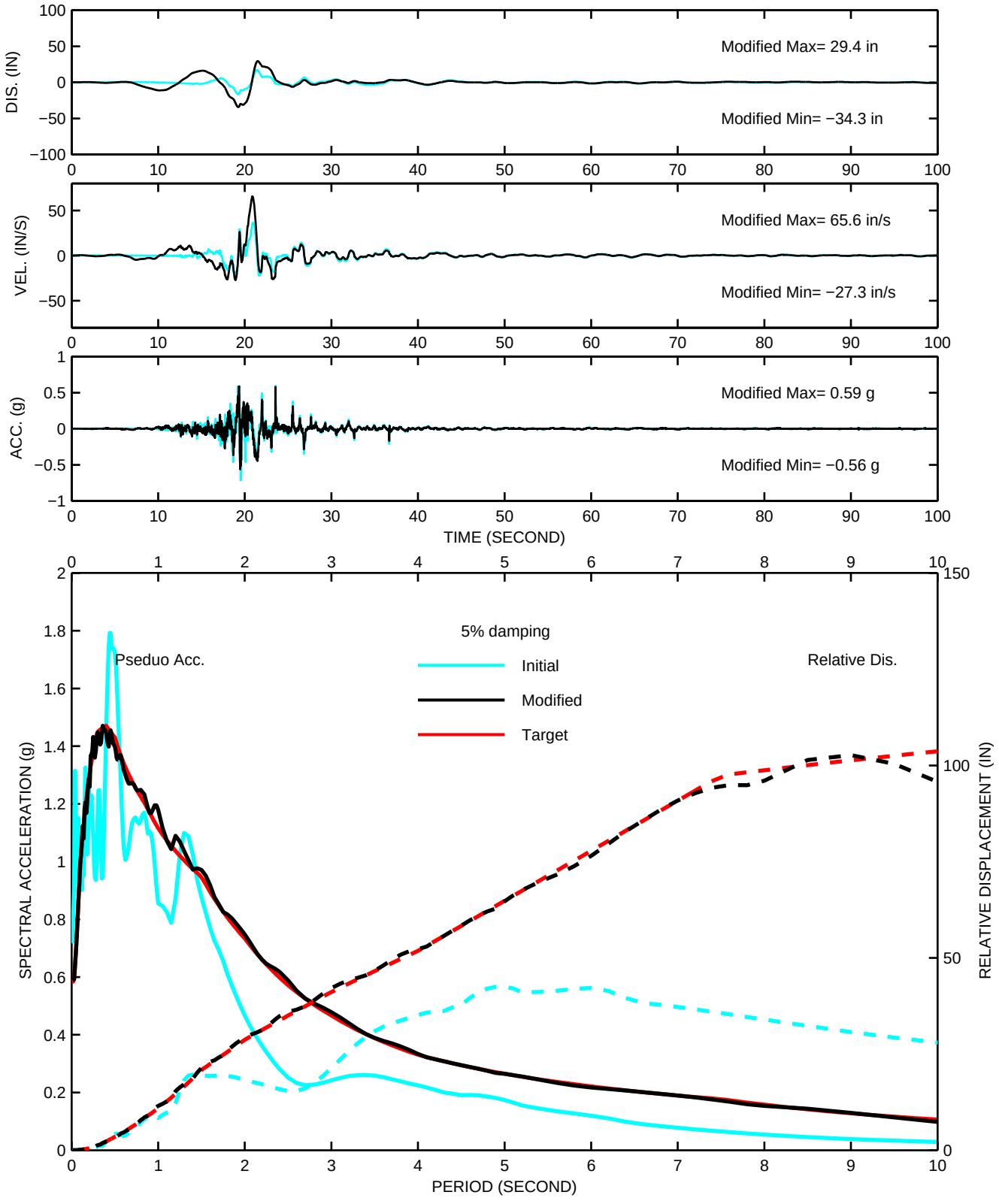


Figure E38. Unimproved Ground Area A DE Spectrum Compatible Ground Motion (5% Damped)−Set 5 FP

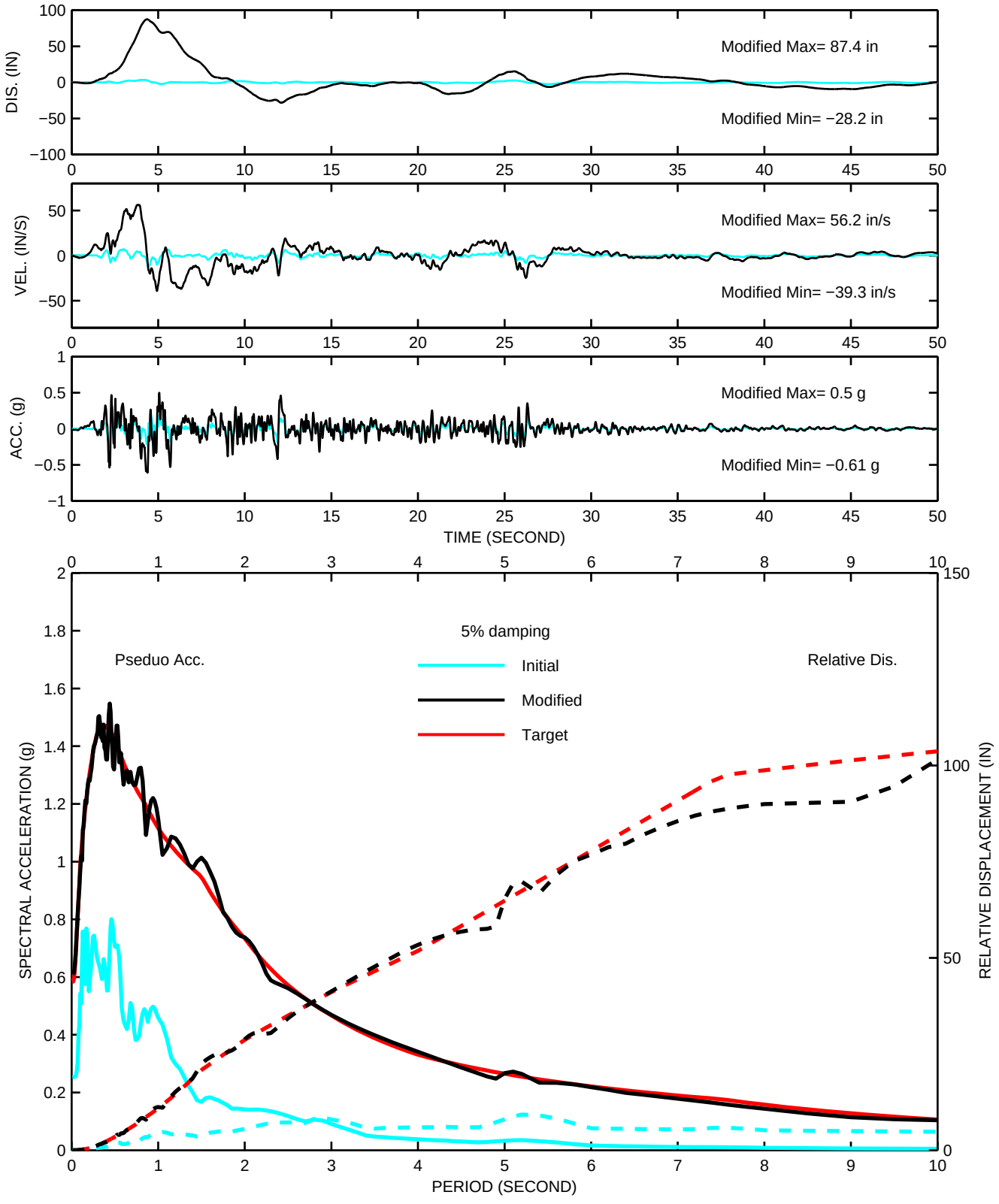


Figure E39. Unimproved Ground Area A DE Spectrum Compatible Ground Motion (5% Damped)−Set 6 FN

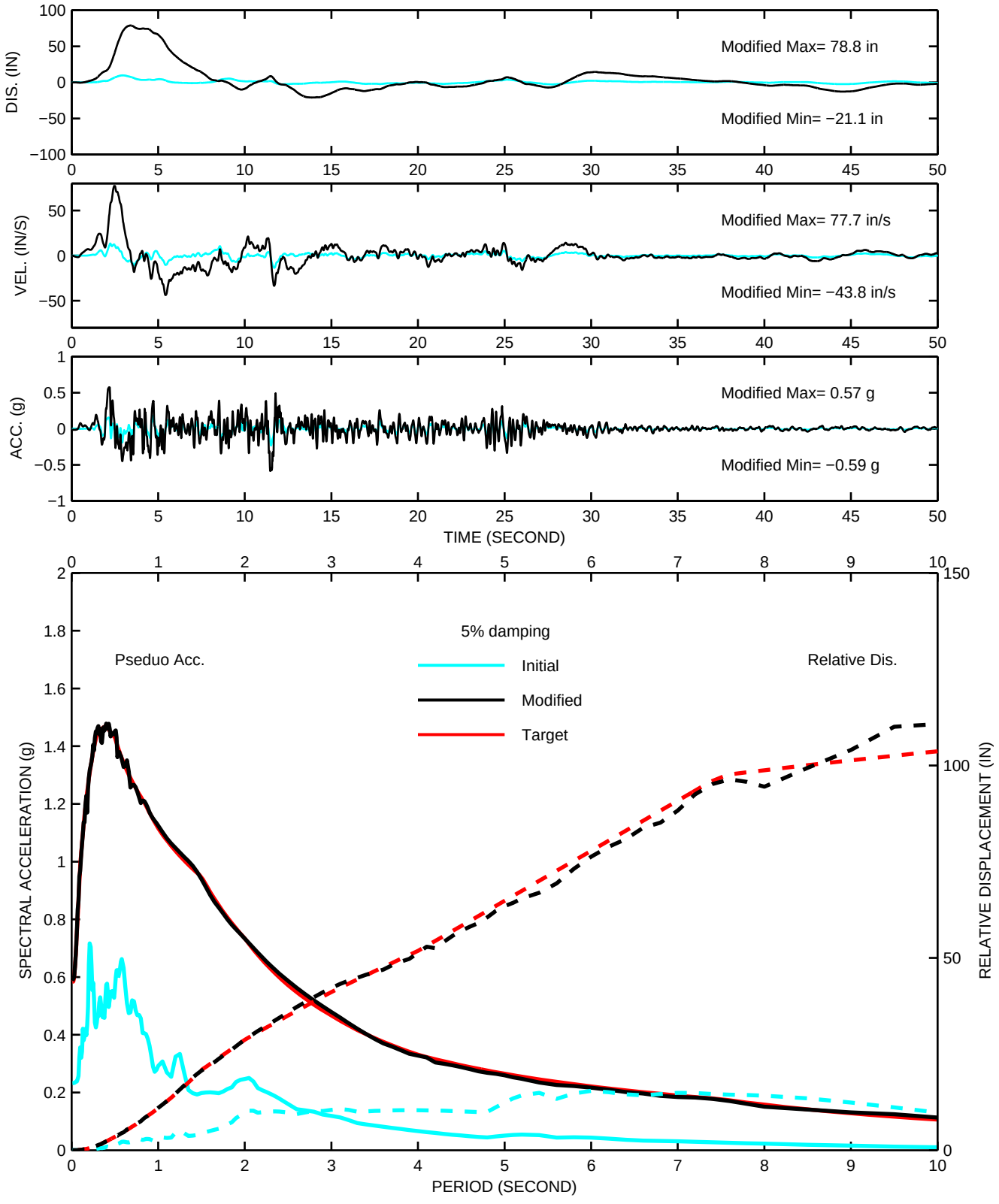


Figure E40. Unimproved Ground Area A DE Spectrum Compatible Ground Motion (5% Damped)−Set 6 FP

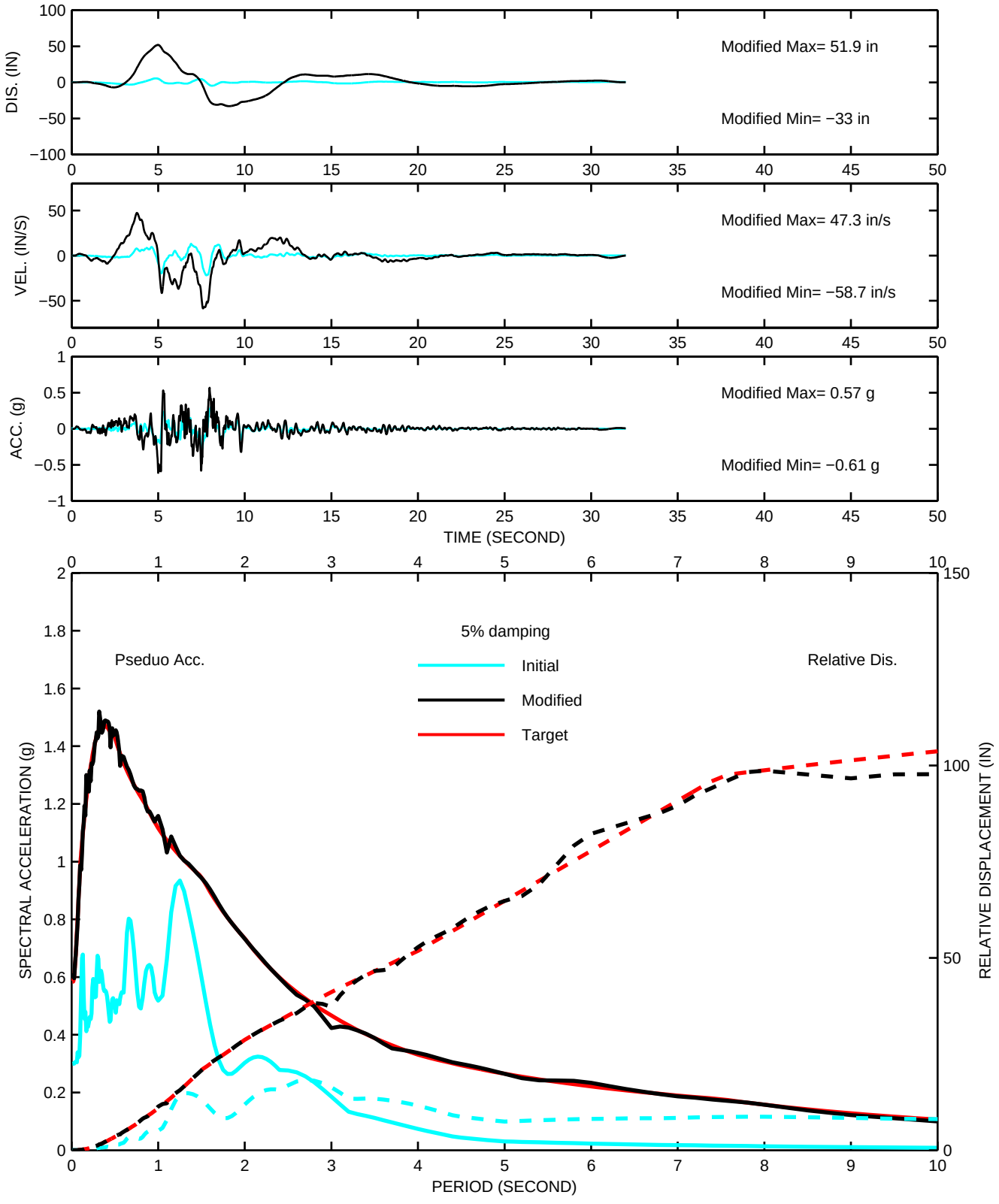


Figure E41. Unimproved Ground Area A DE Spectrum Compatible Ground Motion (5% Damped)−Set 7 FN

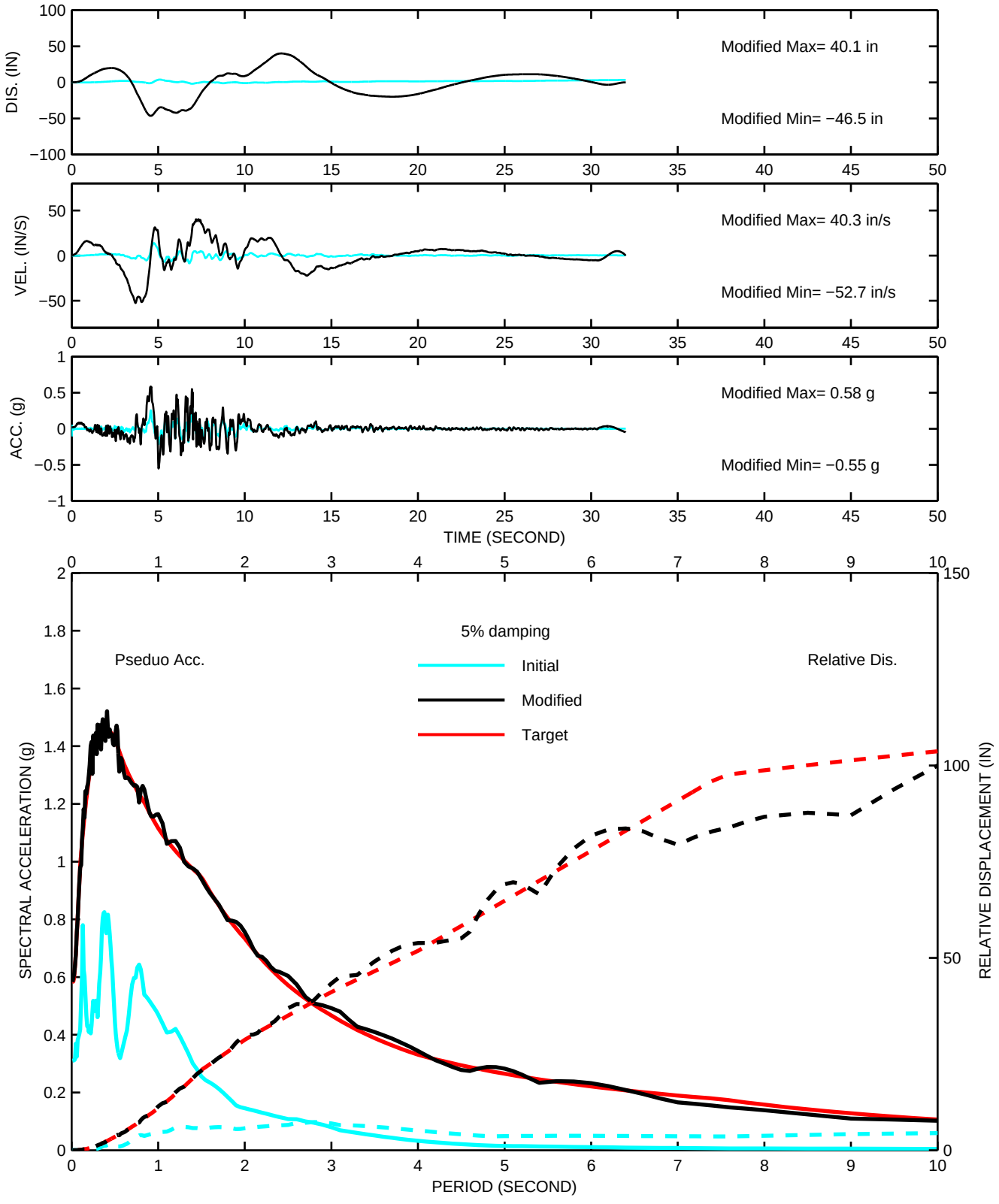


Figure E42. Unimproved Ground Area A DE Spectrum Compatible Ground Motion (5% Damped)−Set 7 FP

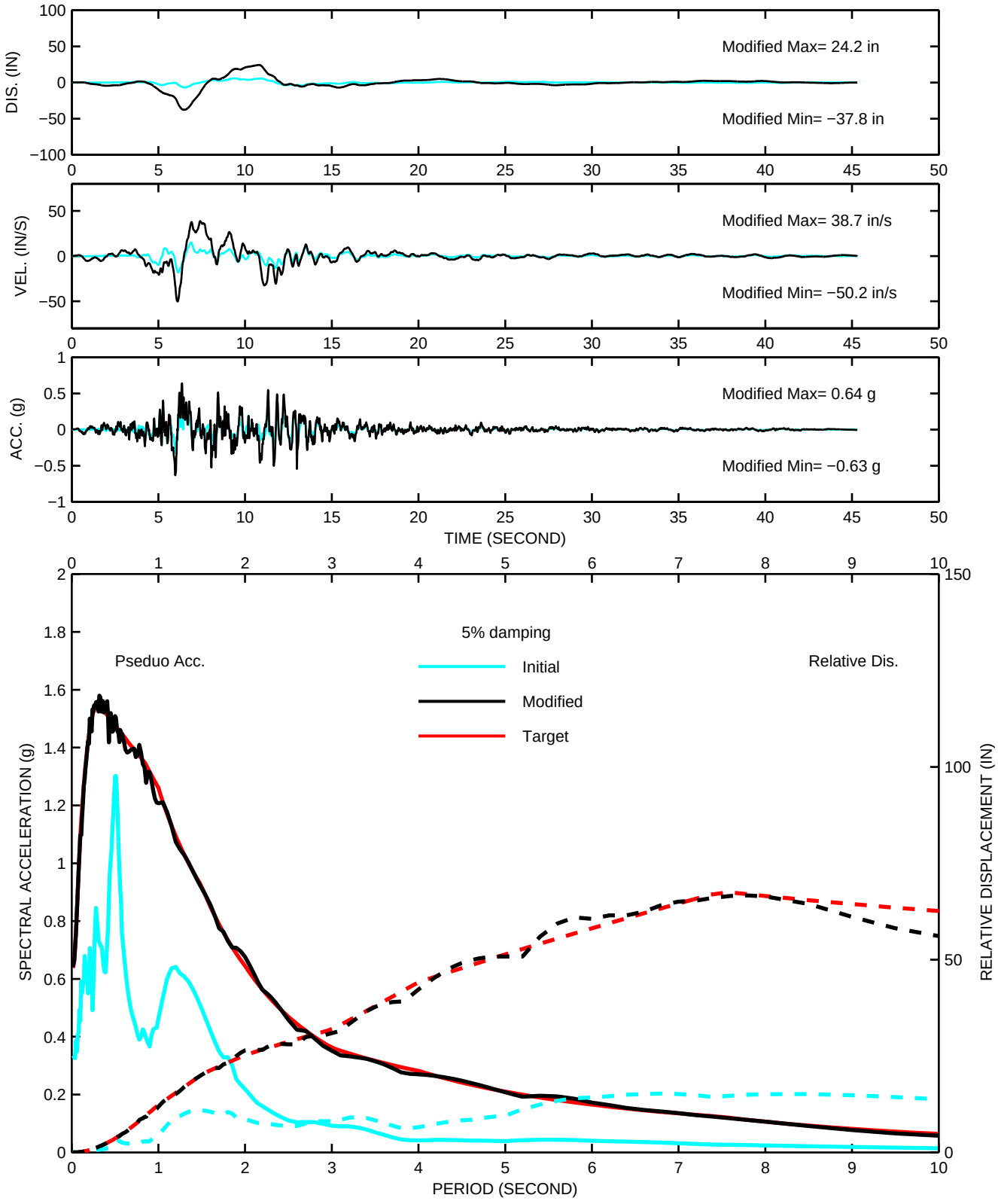


Figure E43. Unimproved Ground Area A 975−Yr Spectrum Compatible Ground Motion (5% Damped)−Set 1 FN

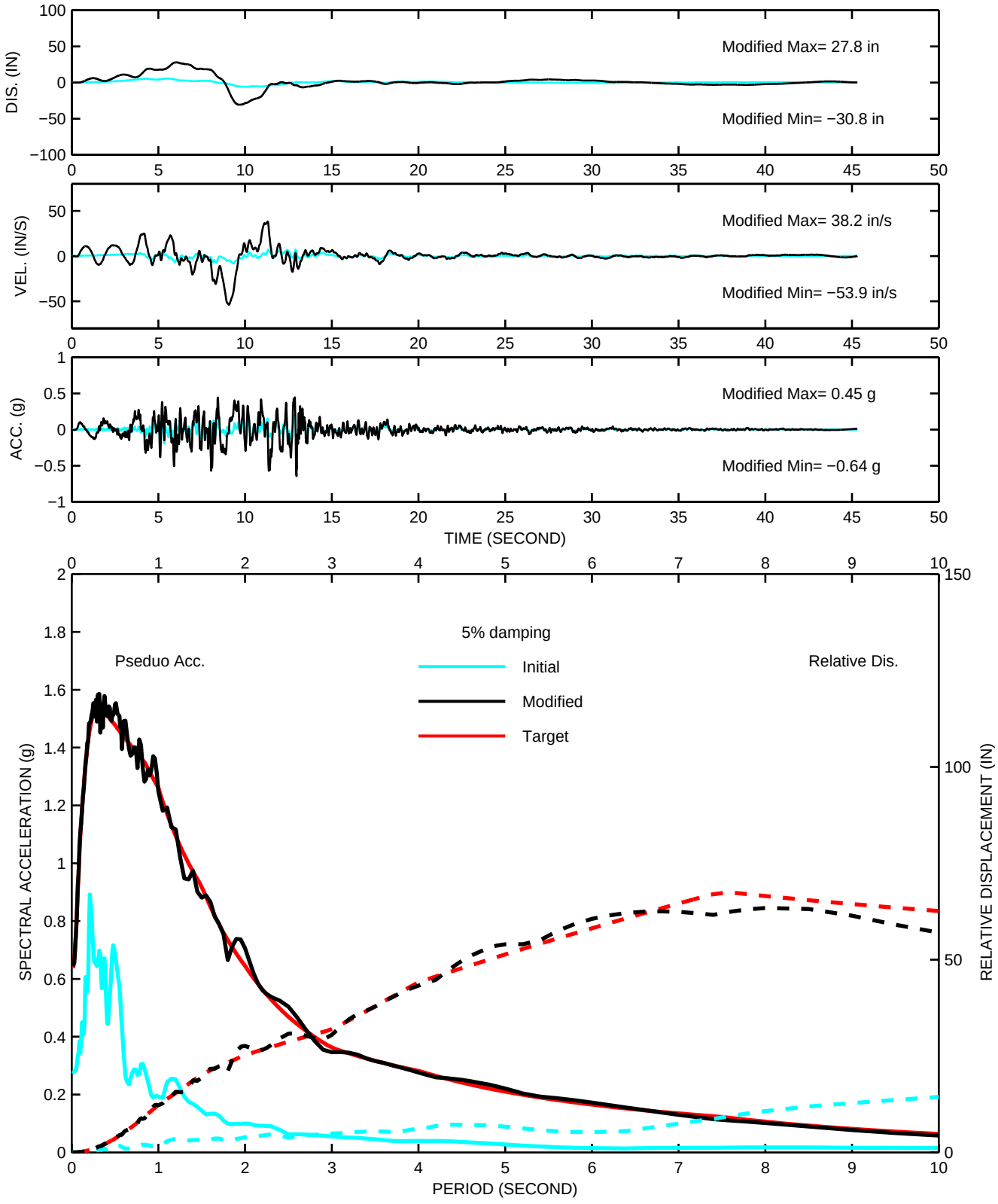


Figure E44. Unimproved Ground Area A 975−Yr Spectrum Compatible Ground Motion (5% Damped)−Set 1 FP

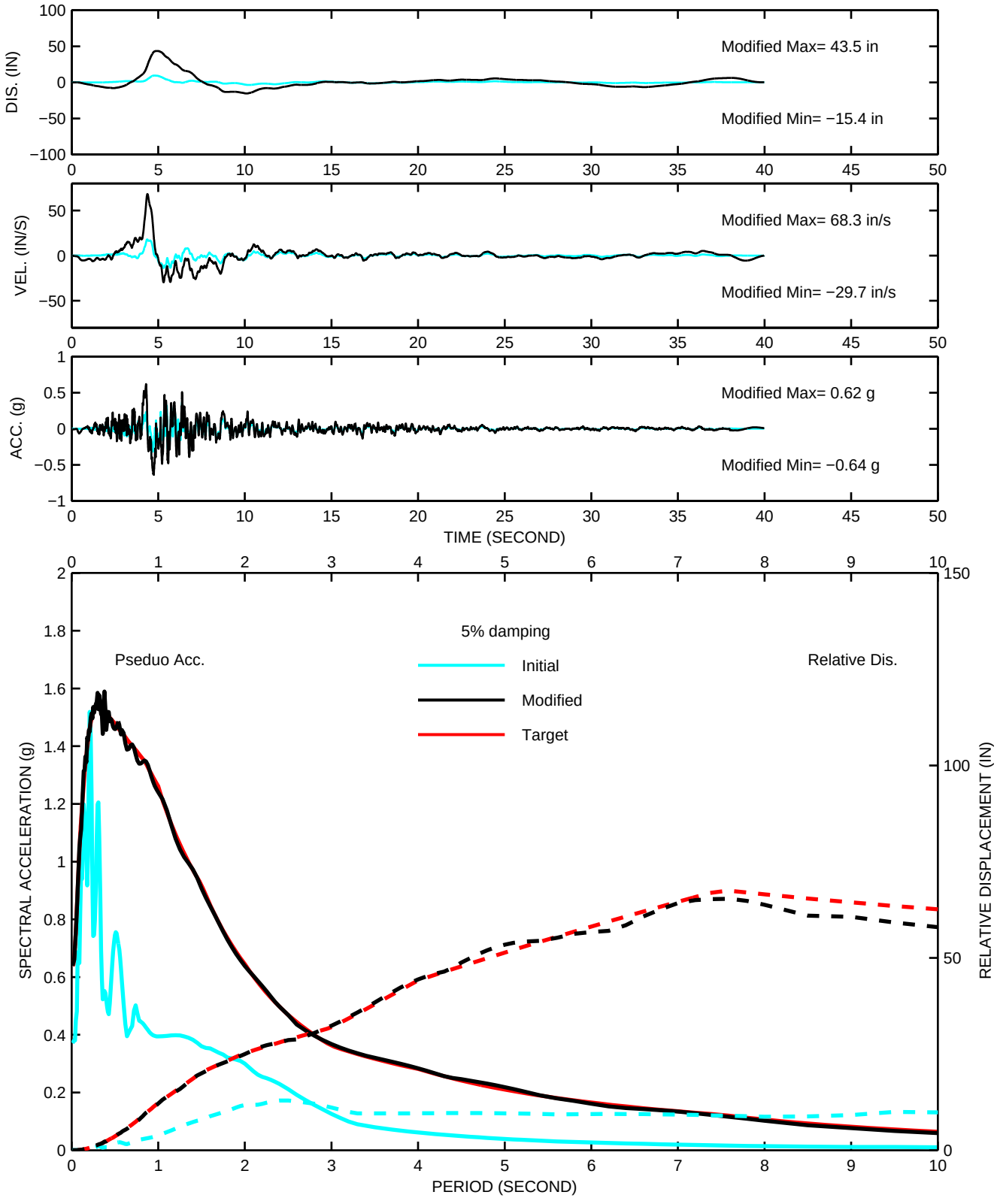


Figure E45. Unimproved Ground Area A 975−Yr Spectrum Compatible Ground Motion (5% Damped)−Set 2 FN

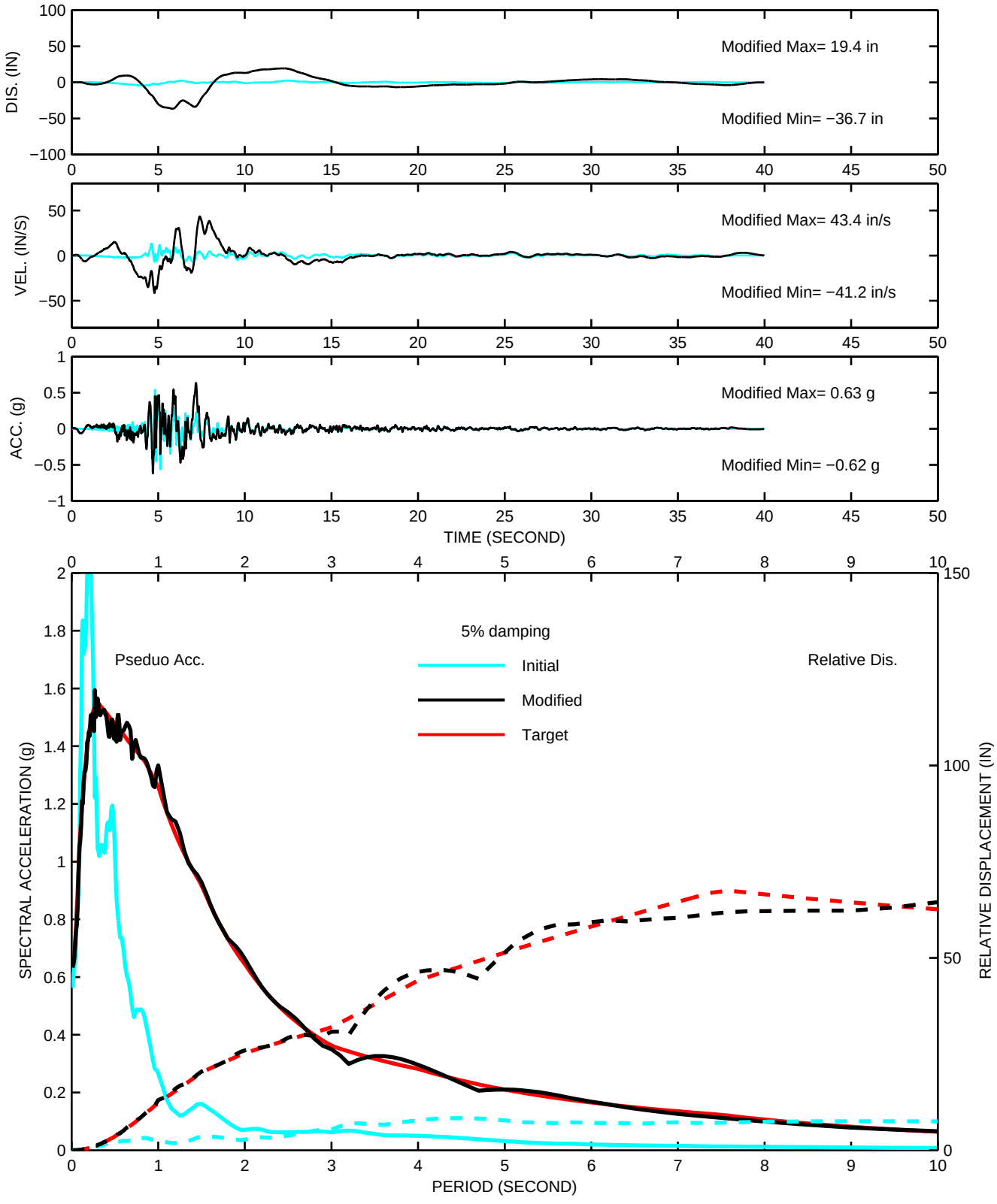


Figure E46. Unimproved Ground Area A 975−Yr Spectrum Compatible Ground Motion (5% Damped)−Set 2 FP

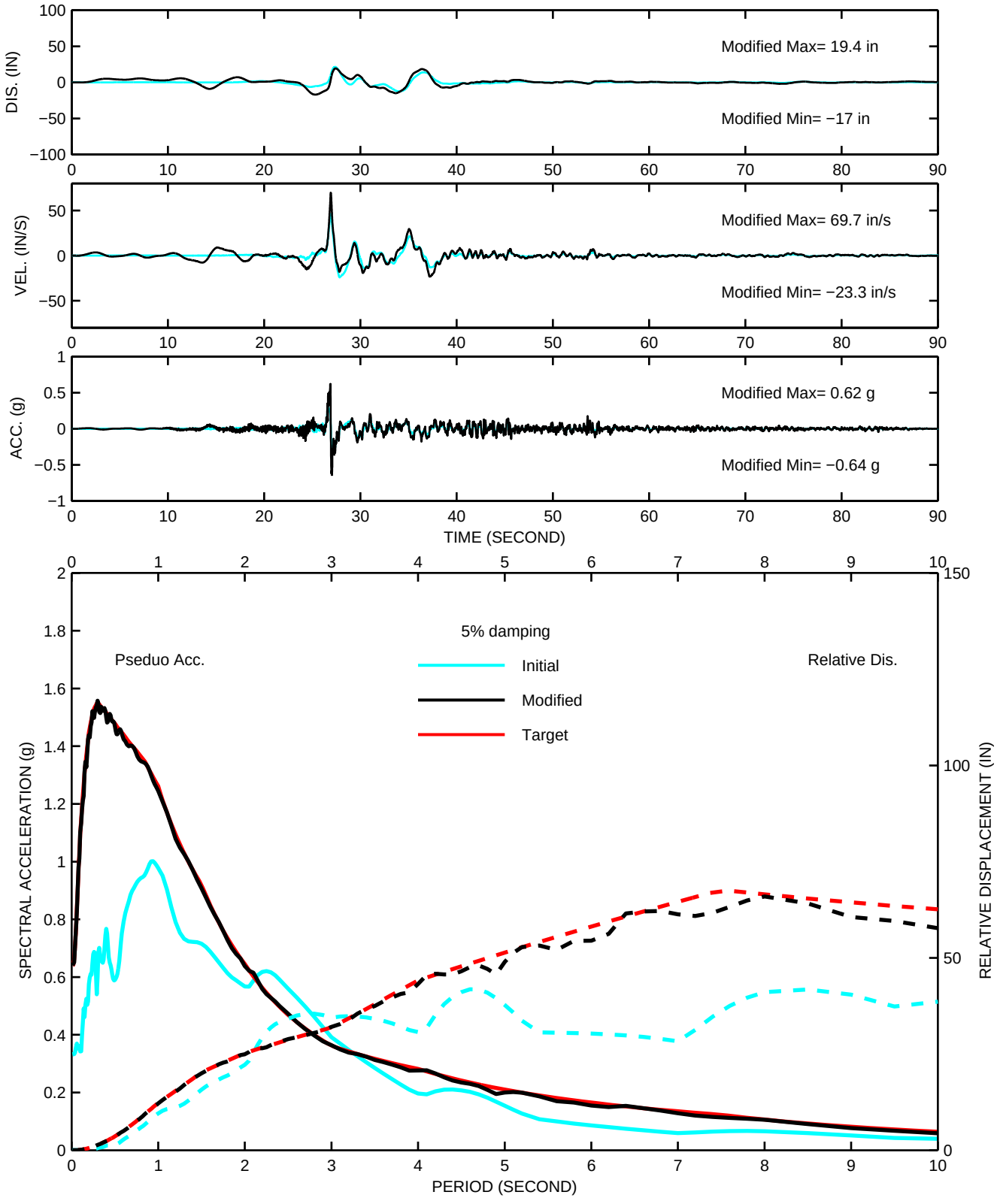


Figure E47. Unimproved Ground Area A 975−Yr Spectrum Compatible Ground Motion (5% Damped)−Set 3 FN

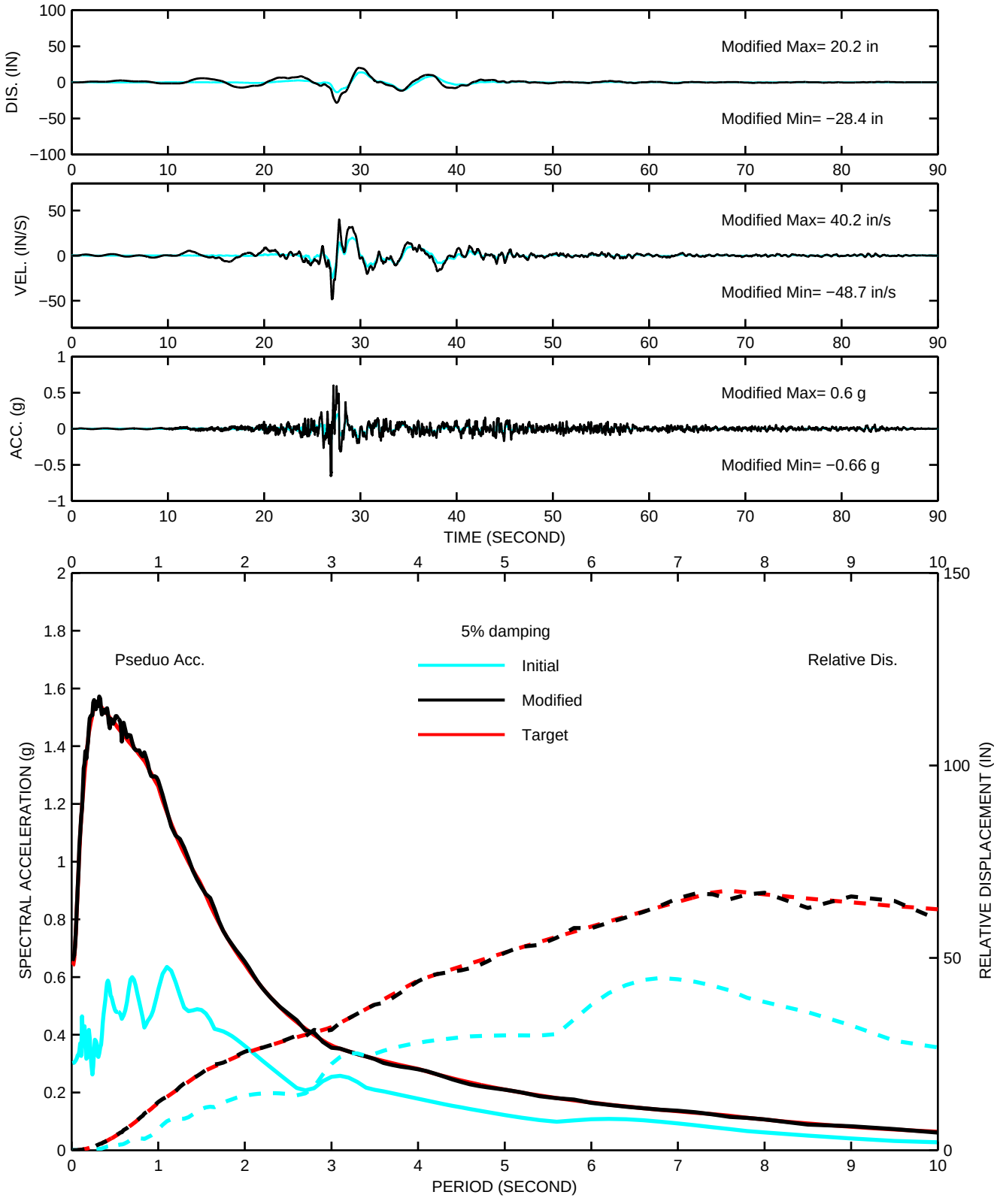


Figure E48. Unimproved Ground Area A 975−Yr Spectrum Compatible Ground Motion (5% Damped)−Set 3 FP

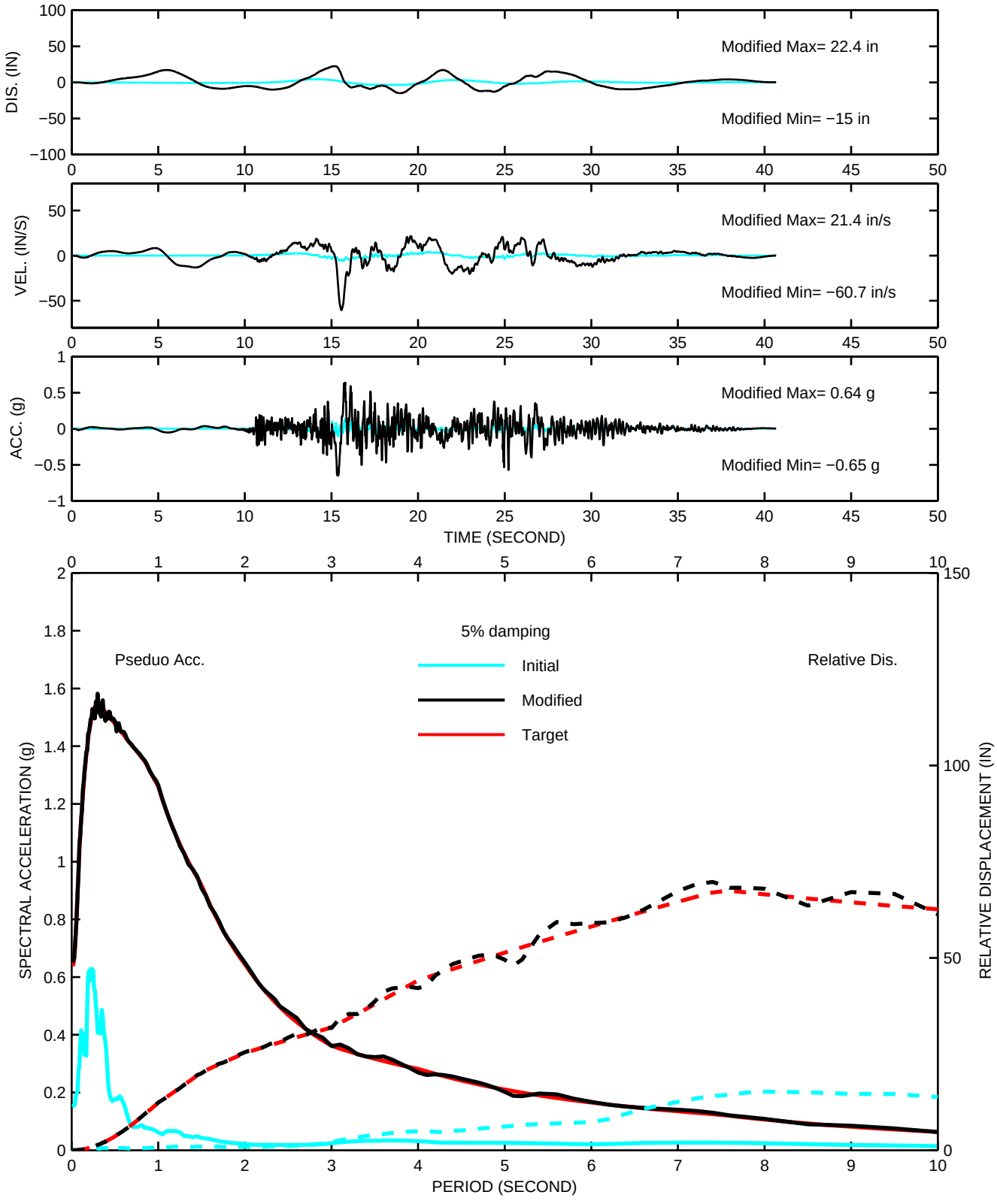


Figure E49. Unimproved Ground Area A 975−Yr Spectrum Compatible Ground Motion (5% Damped)−Set 4 FN

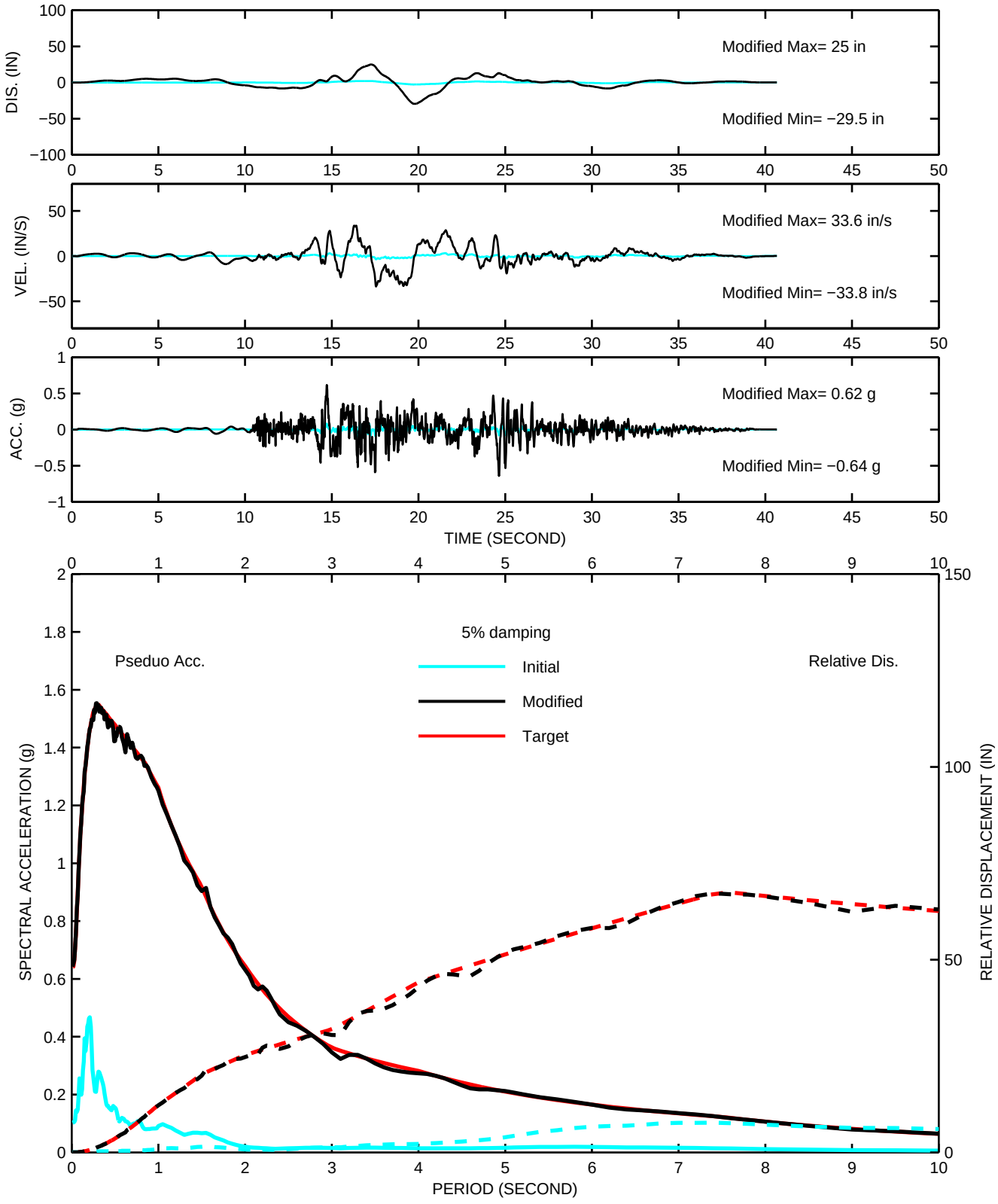


Figure E50. Unimproved Ground Area A 975−Yr Spectrum Compatible Ground Motion (5% Damped)−Set 4 FP

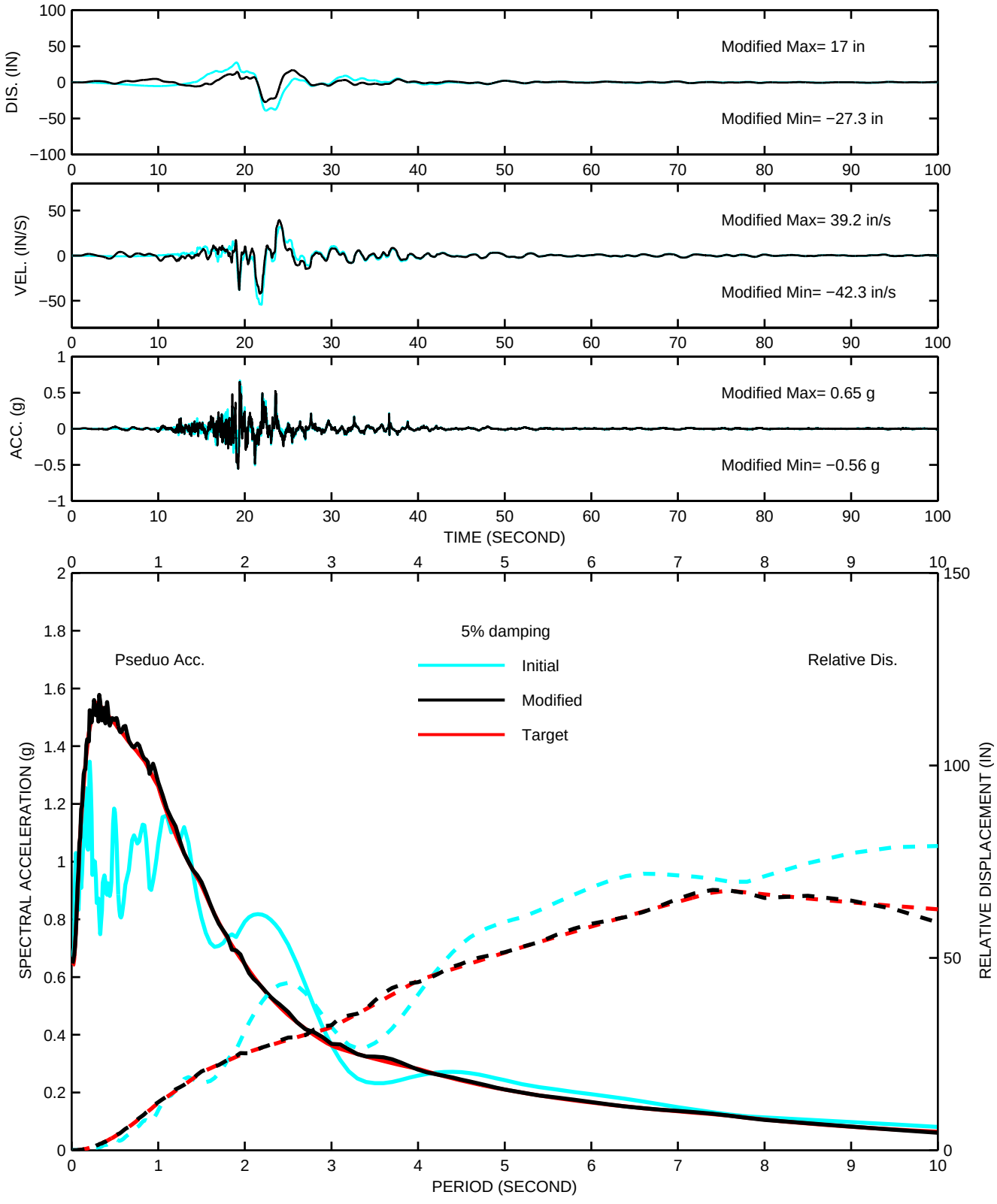


Figure E51. Unimproved Ground Area A 975−Yr Spectrum Compatible Ground Motion (5% Damped)−Set 5 FN

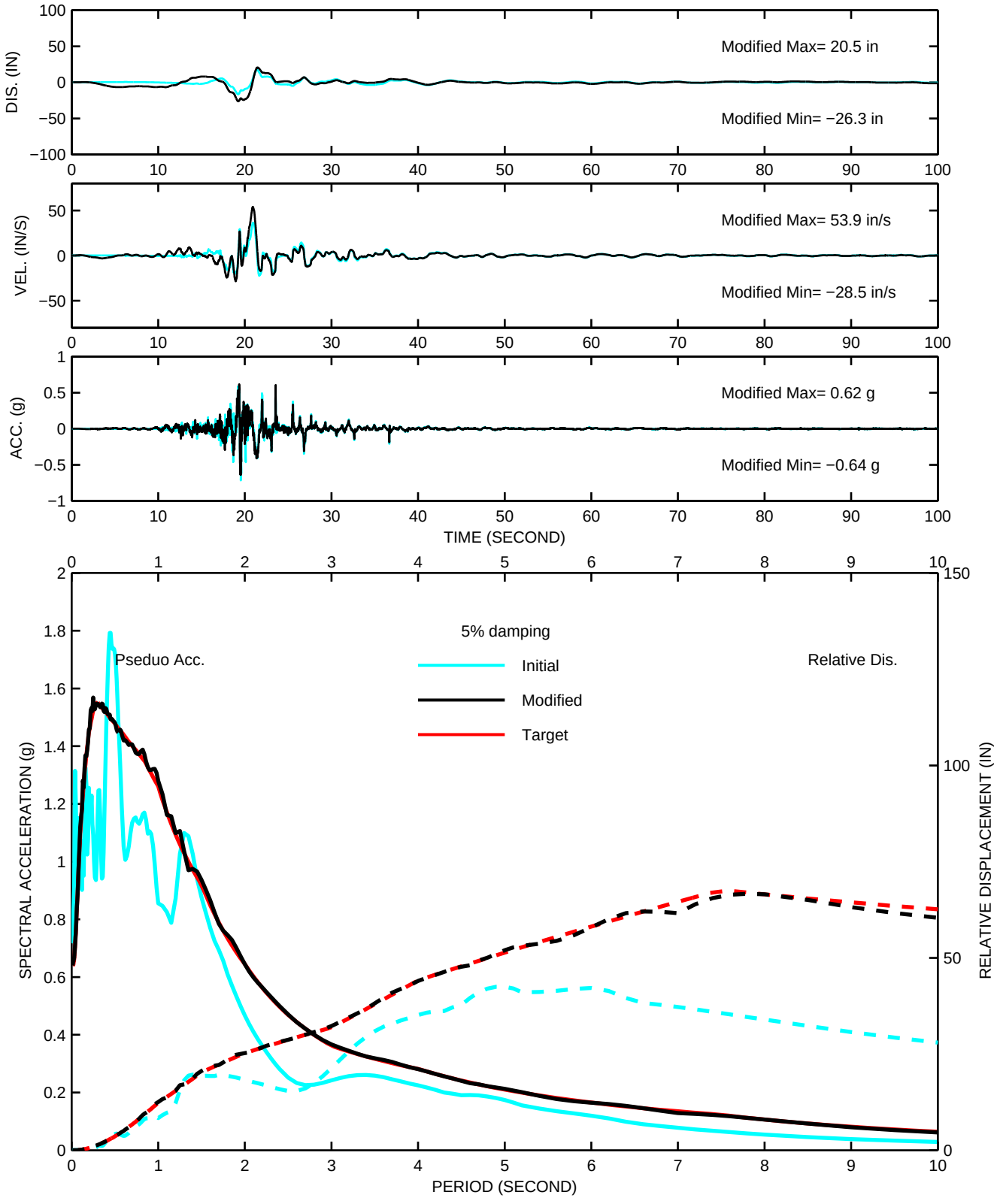


Figure E52. Unimproved Ground Area A 975−Yr Spectrum Compatible Ground Motion (5% Damped)−Set 5 FP

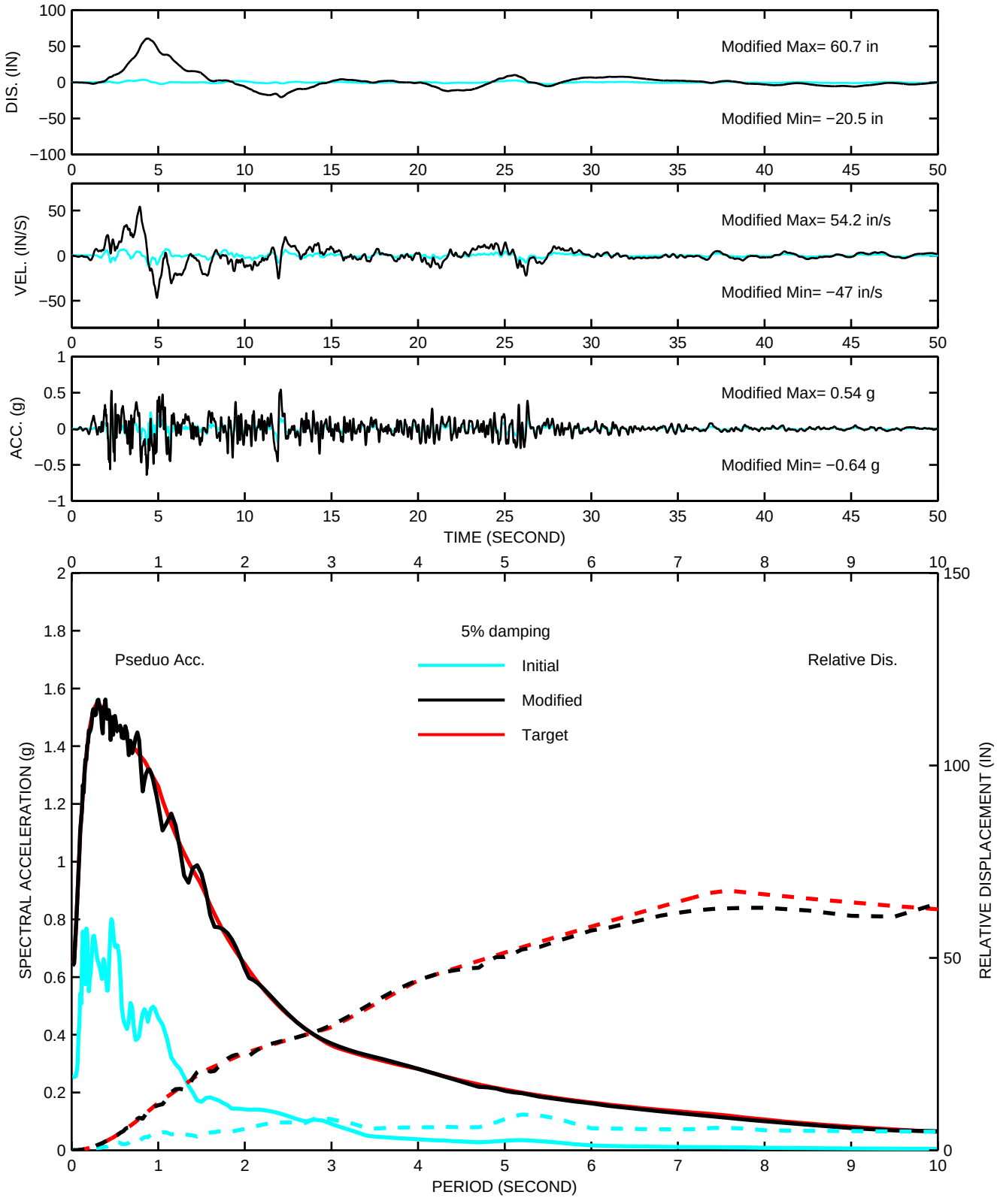


Figure E53. Unimproved Ground Area A 975−Yr Spectrum Compatible Ground Motion (5% Damped)−Set 6 FN

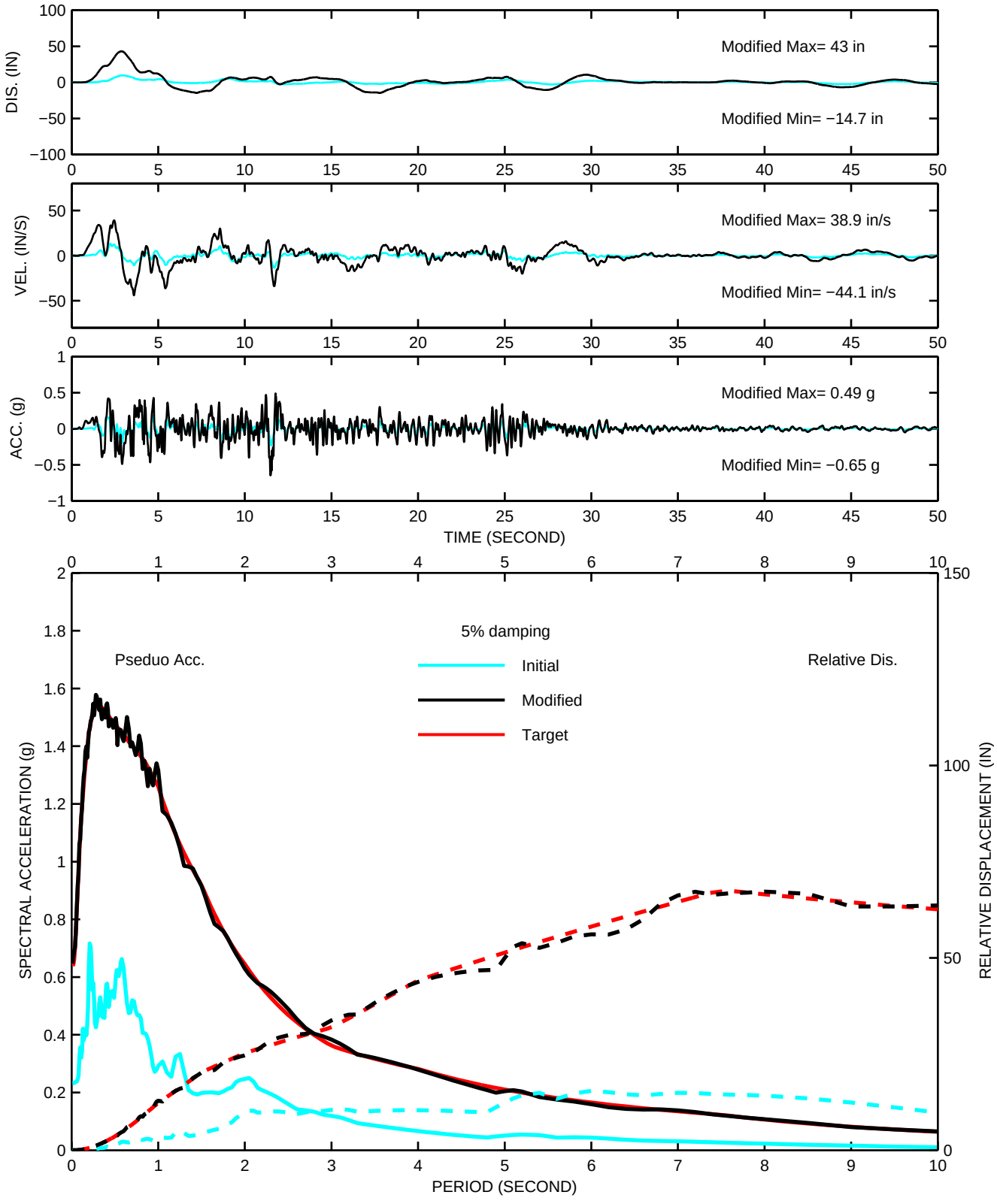


Figure E54. Unimproved Ground Area A 975−Yr Spectrum Compatible Ground Motion (5% Damped)−Set 6 FP

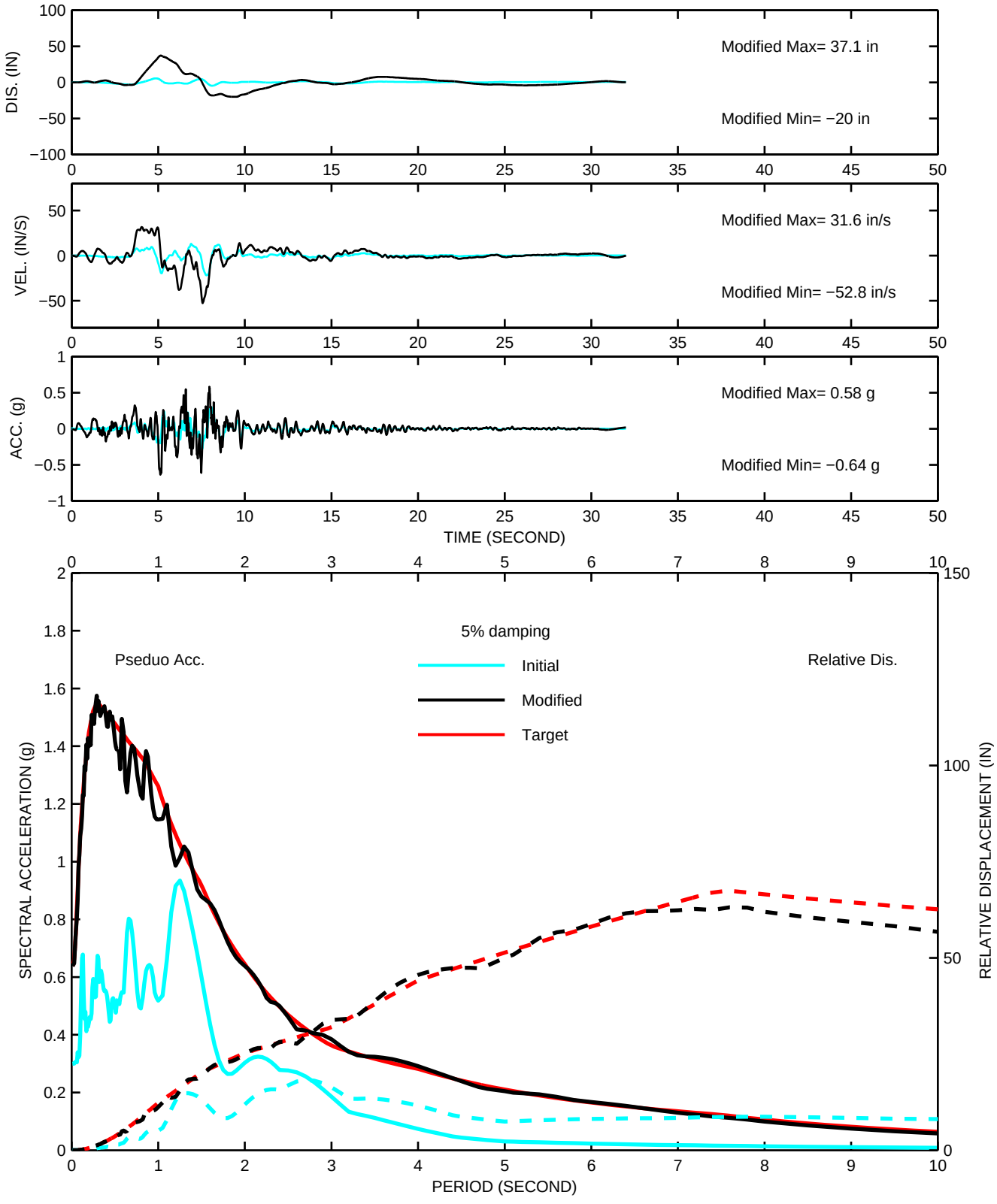


Figure E55. Unimproved Ground Area A 975−Yr Spectrum Compatible Ground Motion (5% Damped)−Set 7 FN

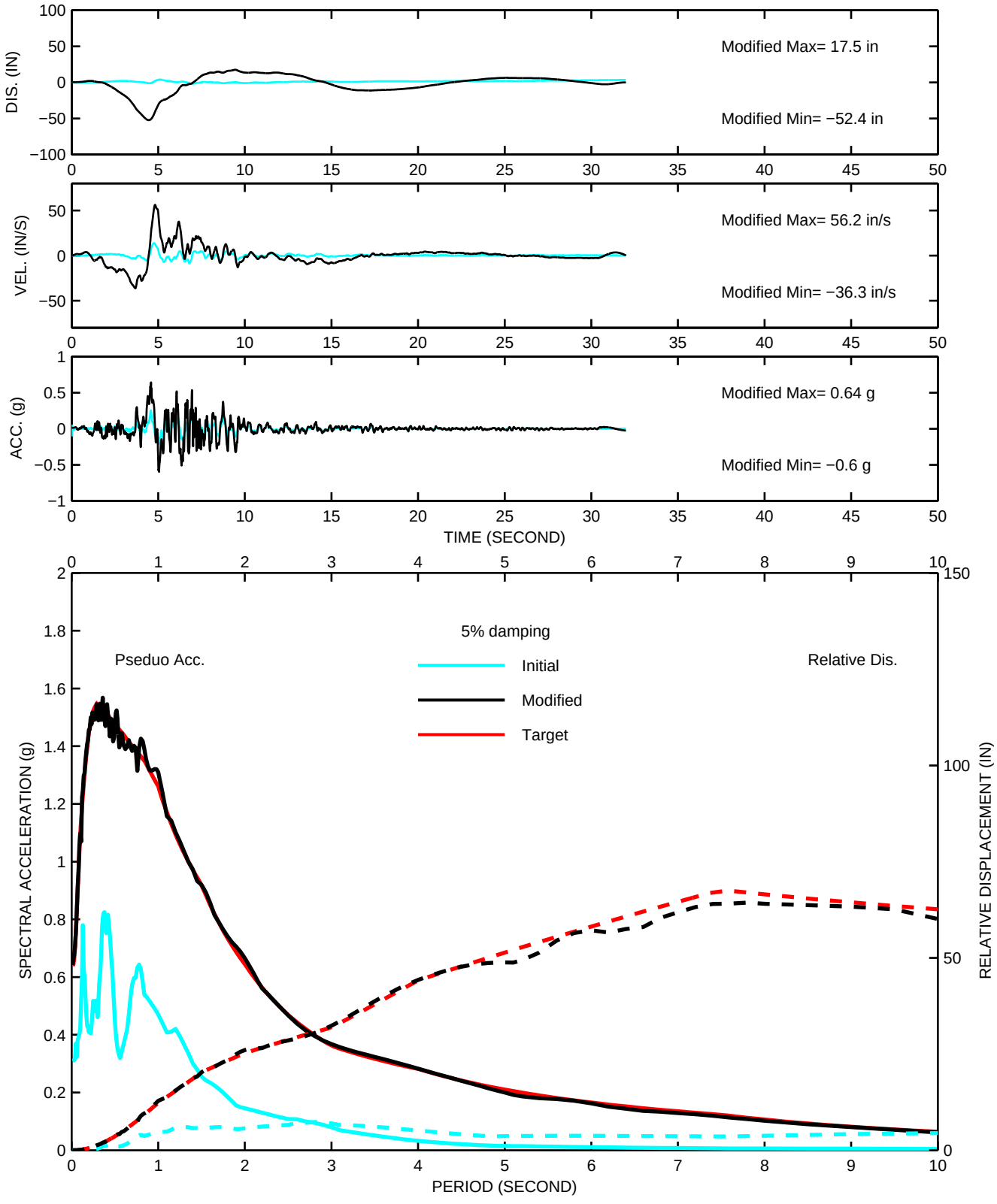


Figure E56. Unimproved Ground Area A 975−Yr Spectrum Compatible Ground Motion (5% Damped)−Set 7 FP

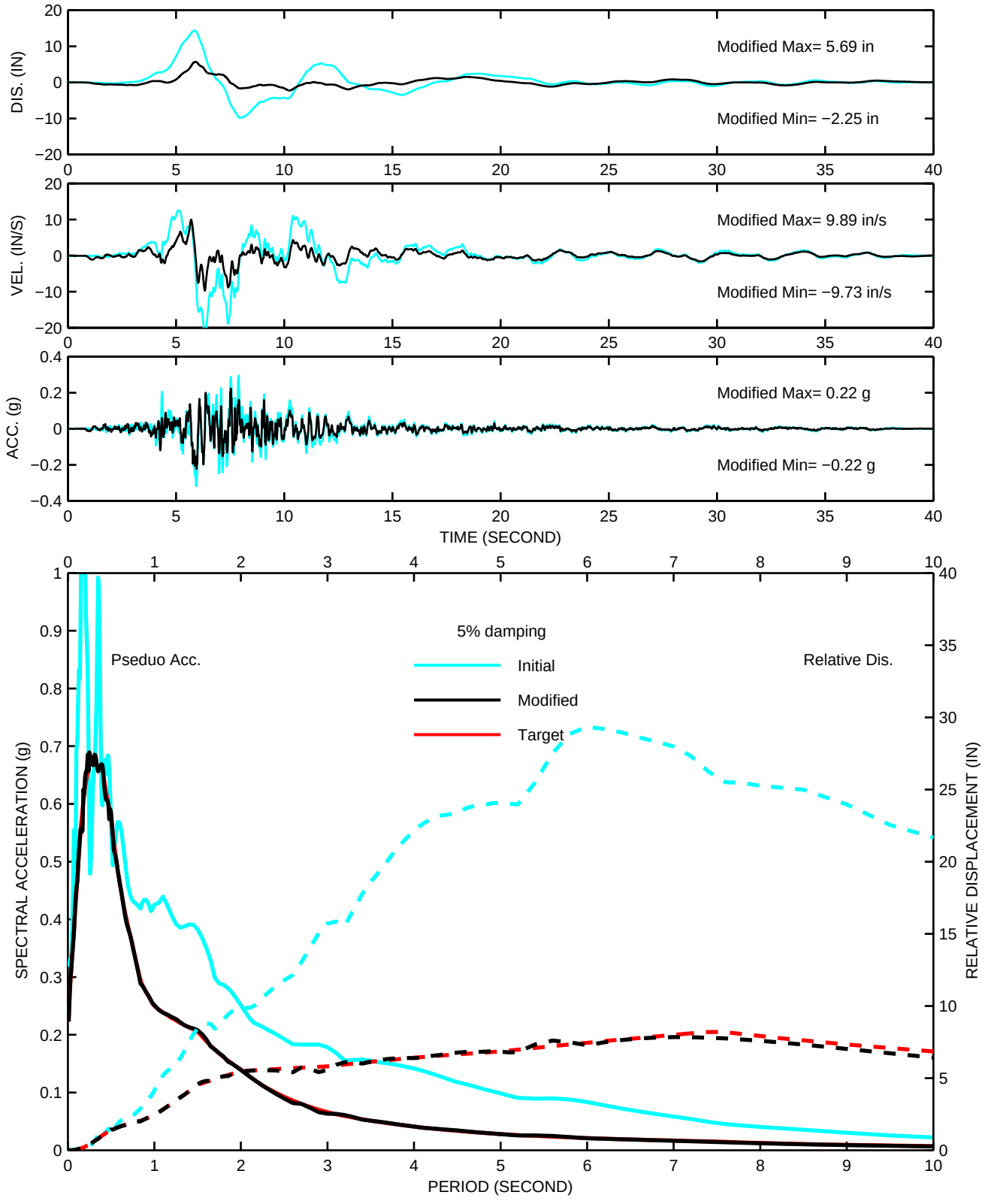


Figure E57. Unimproved Ground Area B OLE Spectrum Compatible Ground Motion (5% Damped)−Set 1 FN

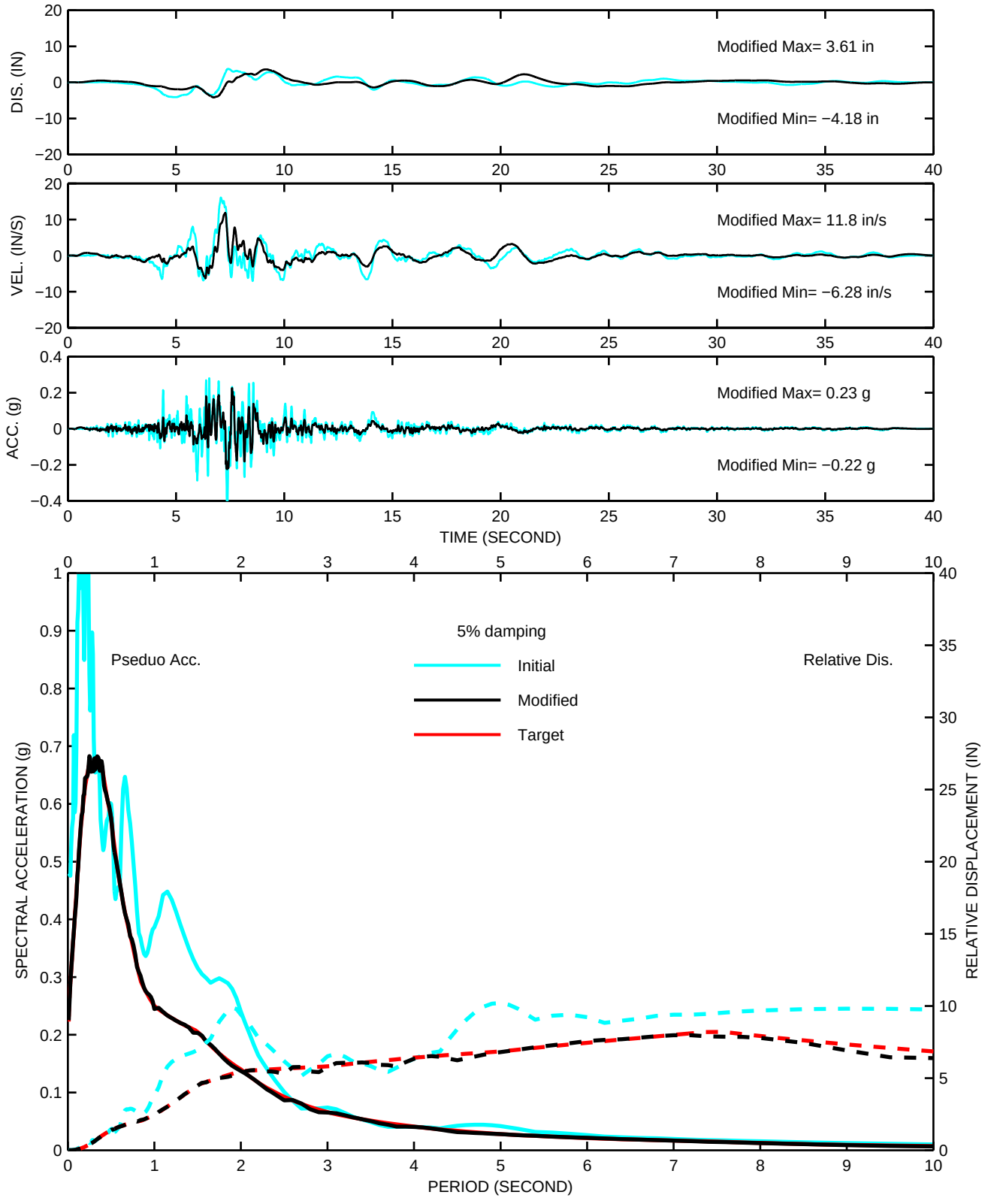


Figure E58. Unimproved Ground Area B OLE Spectrum Compatible Ground Motion (5% Damped)−Set 1 FP

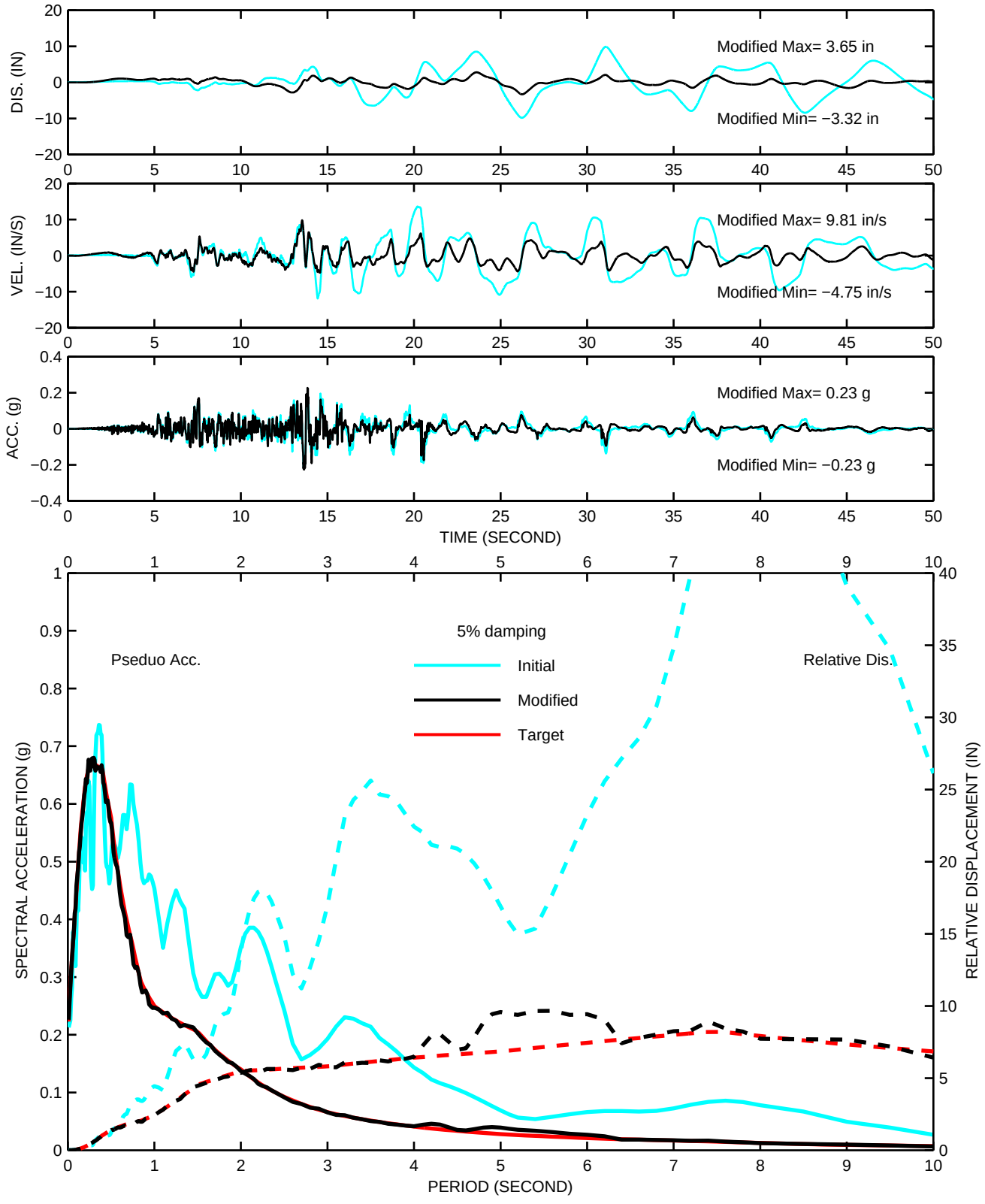


Figure E59. Unimproved Ground Area B OLE Spectrum Compatible Ground Motion (5% Damped)−Set 2 FN

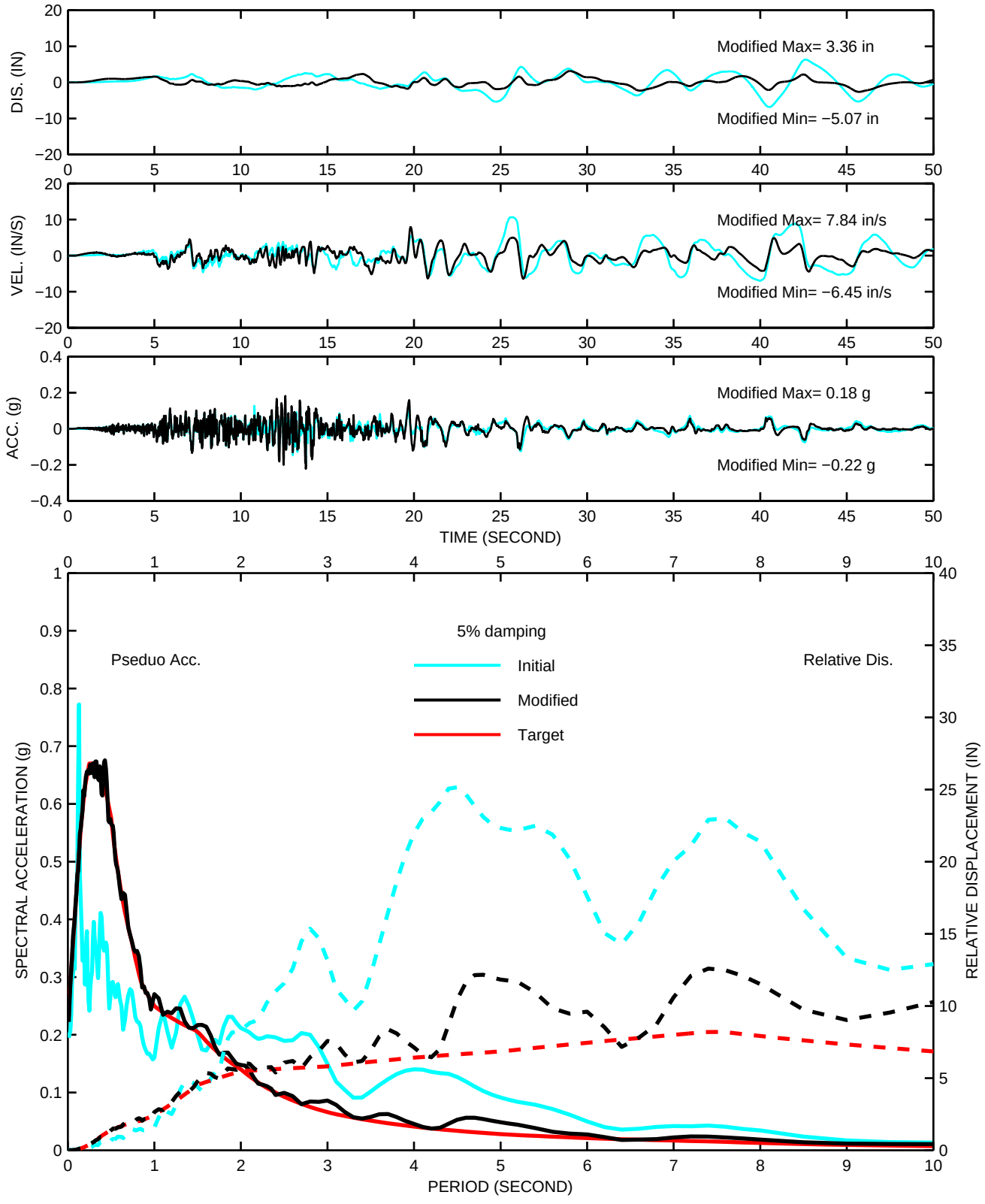


Figure E60. Unimproved Ground Area B OLE Spectrum Compatible Ground Motion (5% Damped)−Set 2 FP

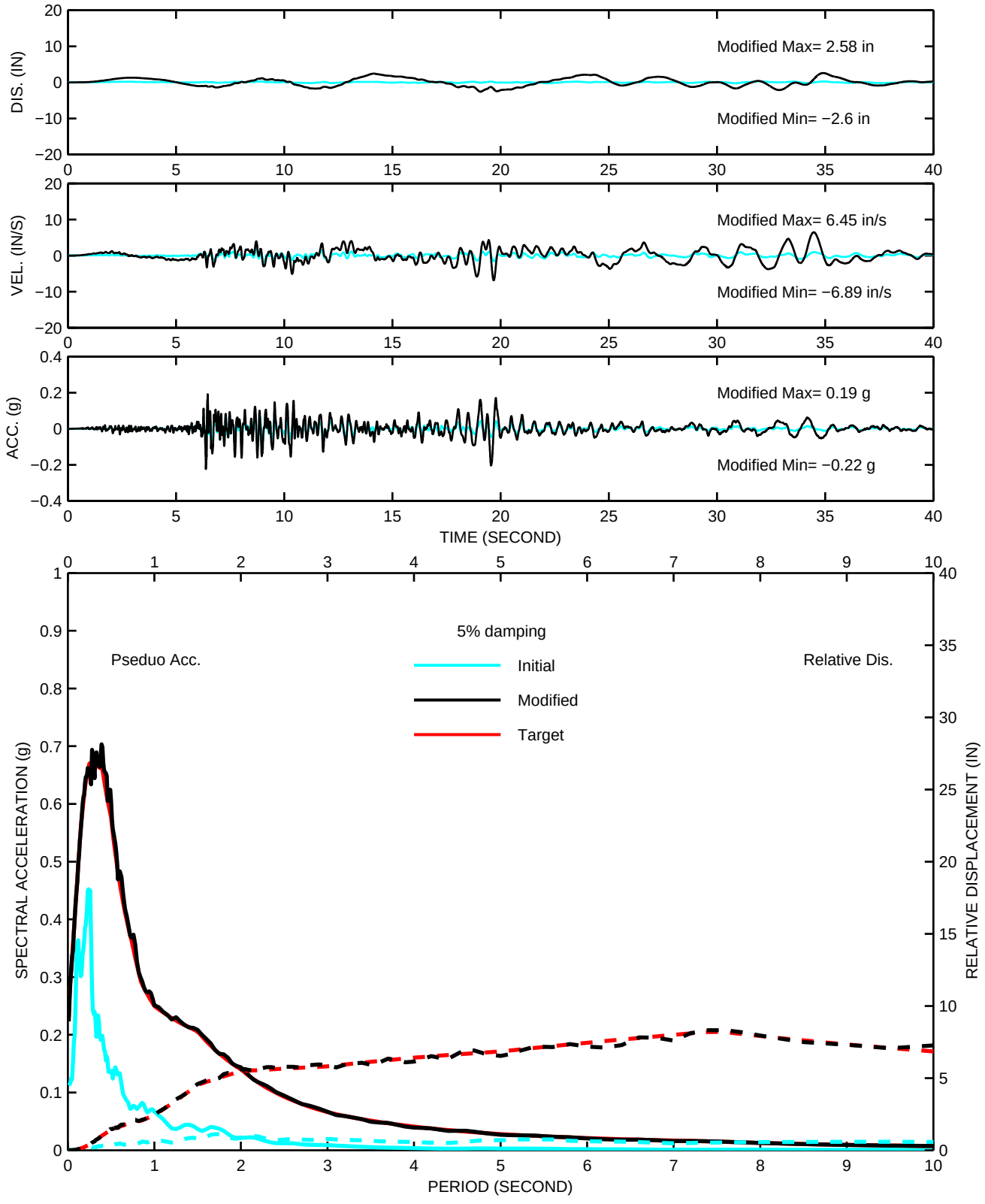


Figure E61. Unimproved Ground Area B OLE Spectrum Compatible Ground Motion (5% Damped)−Set 3 FN

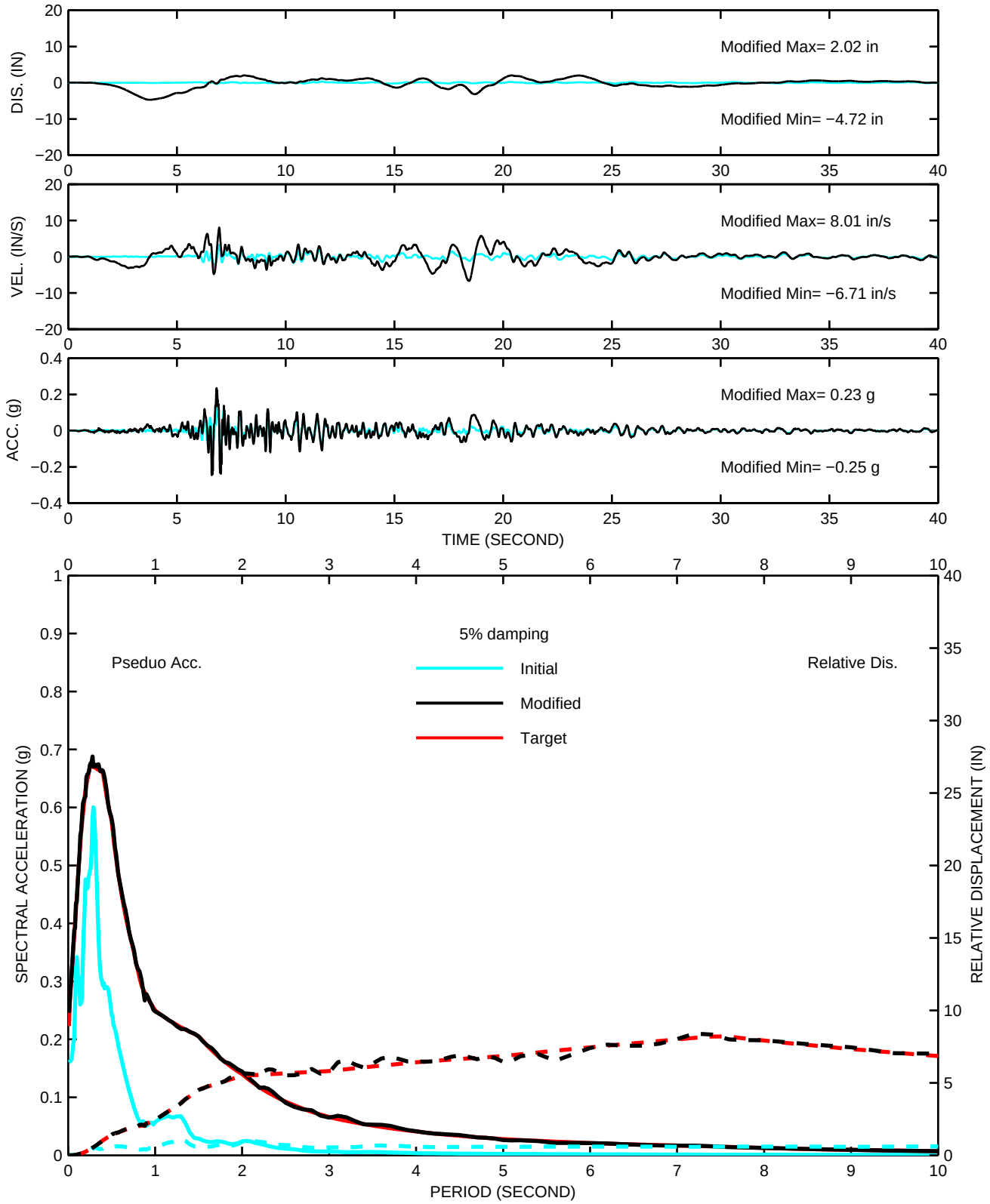


Figure E62. Unimproved Ground Area B OLE Spectrum Compatible Ground Motion (5% Damped)−Set 3 FP

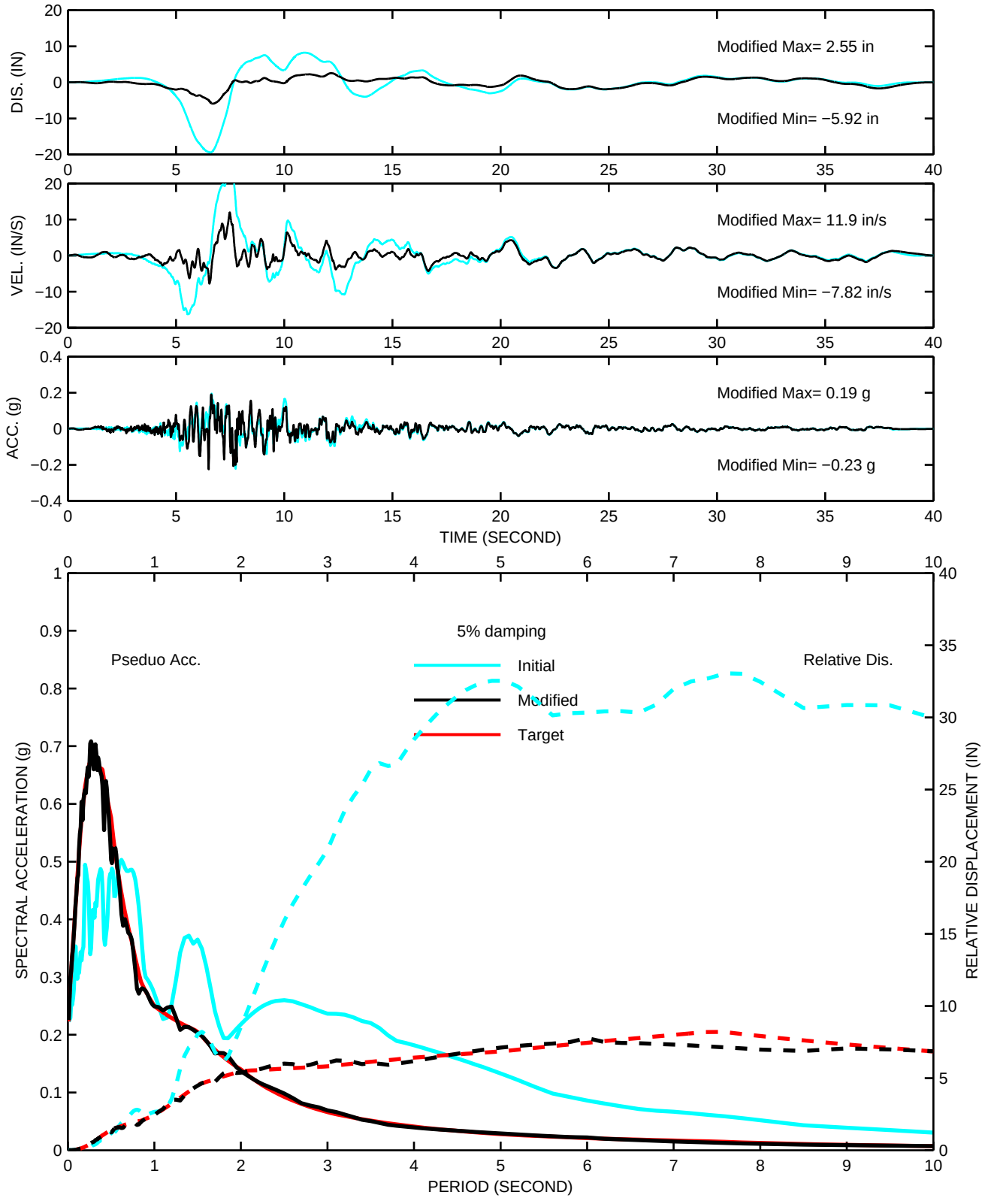


Figure E63. Unimproved Ground Area B OLE Spectrum Compatible Ground Motion (5% Damped)−Set 4 FN

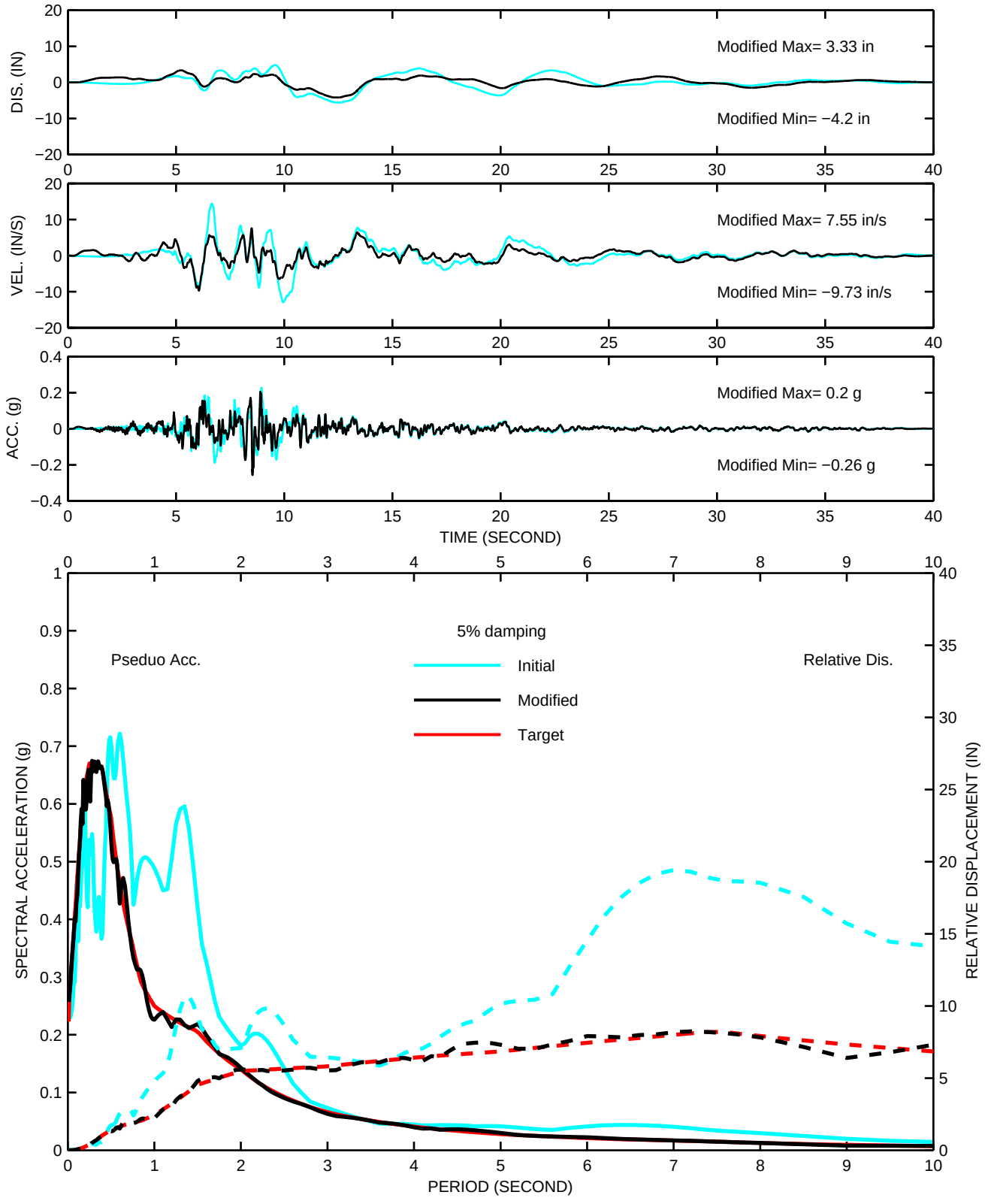


Figure E64. Unimproved Ground Area B OLE Spectrum Compatible Ground Motion (5% Damped)−Set 4 FP

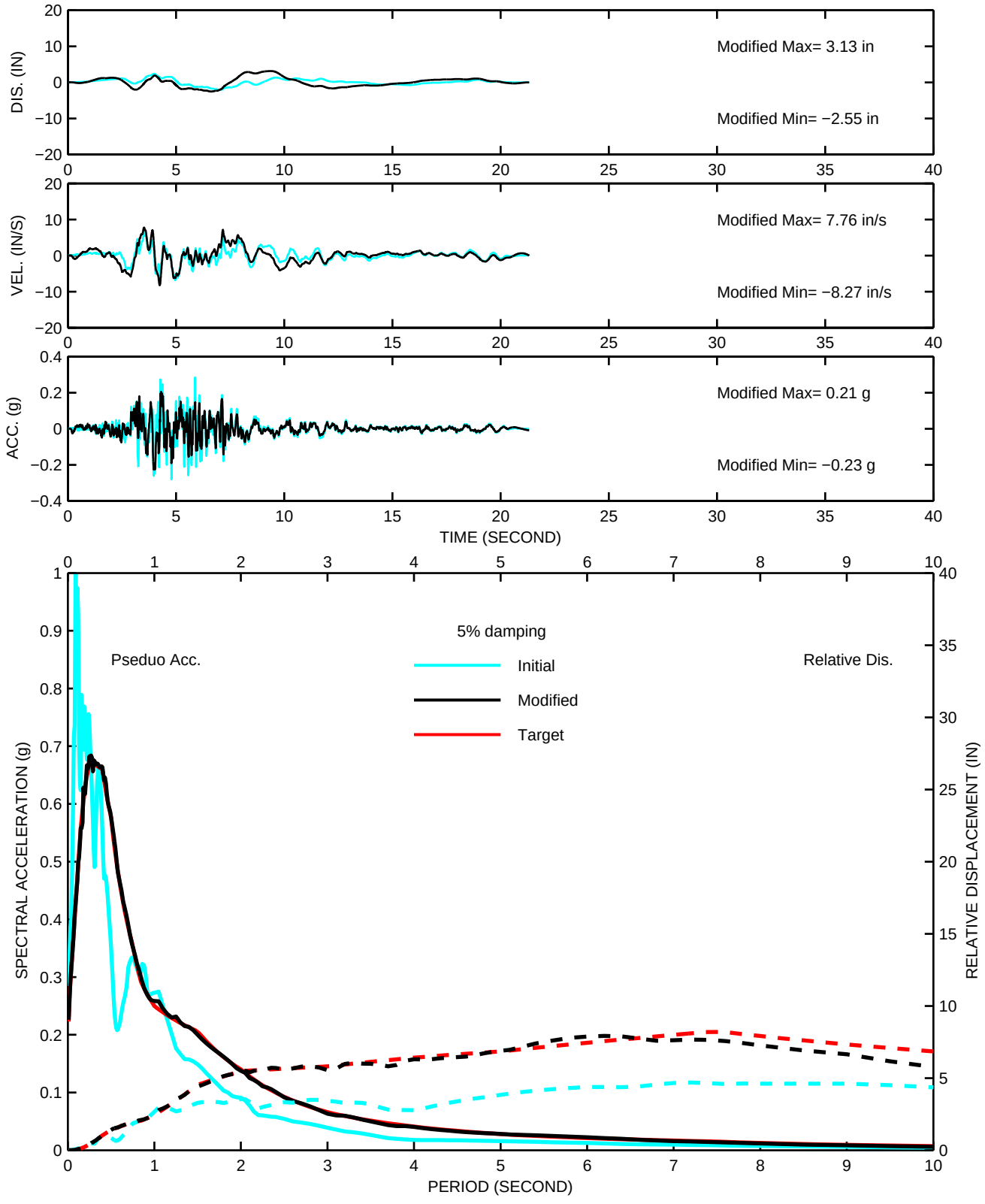


Figure E65. Unimproved Ground Area B OLE Spectrum Compatible Ground Motion (5% Damped)−Set 5 FN

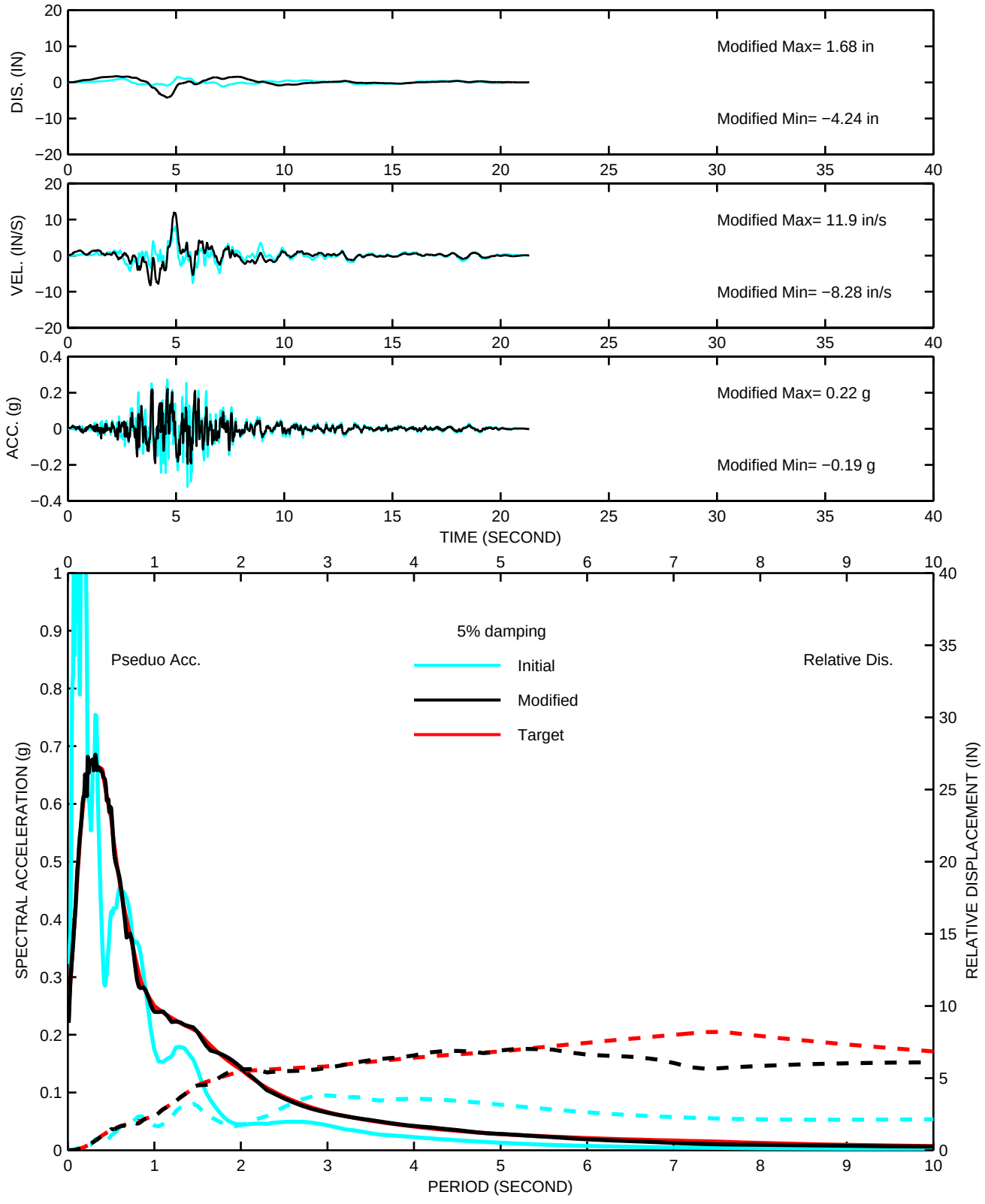


Figure E66. Unimproved Ground Area B OLE Spectrum Compatible Ground Motion (5% Damped)−Set 5 FP

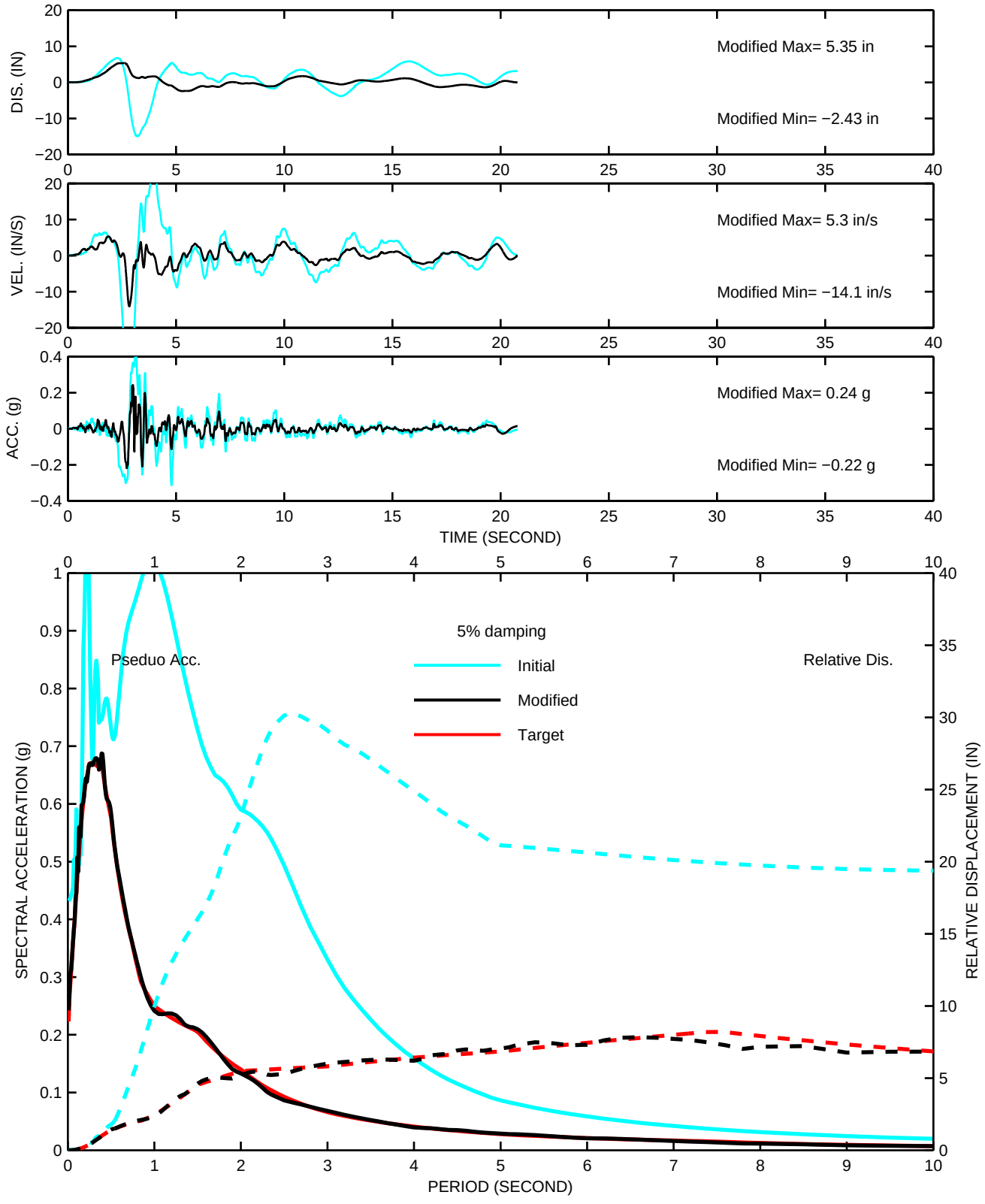


Figure E67. Unimproved Ground Area B OLE Spectrum Compatible Ground Motion (5% Damped)−Set 6 FN

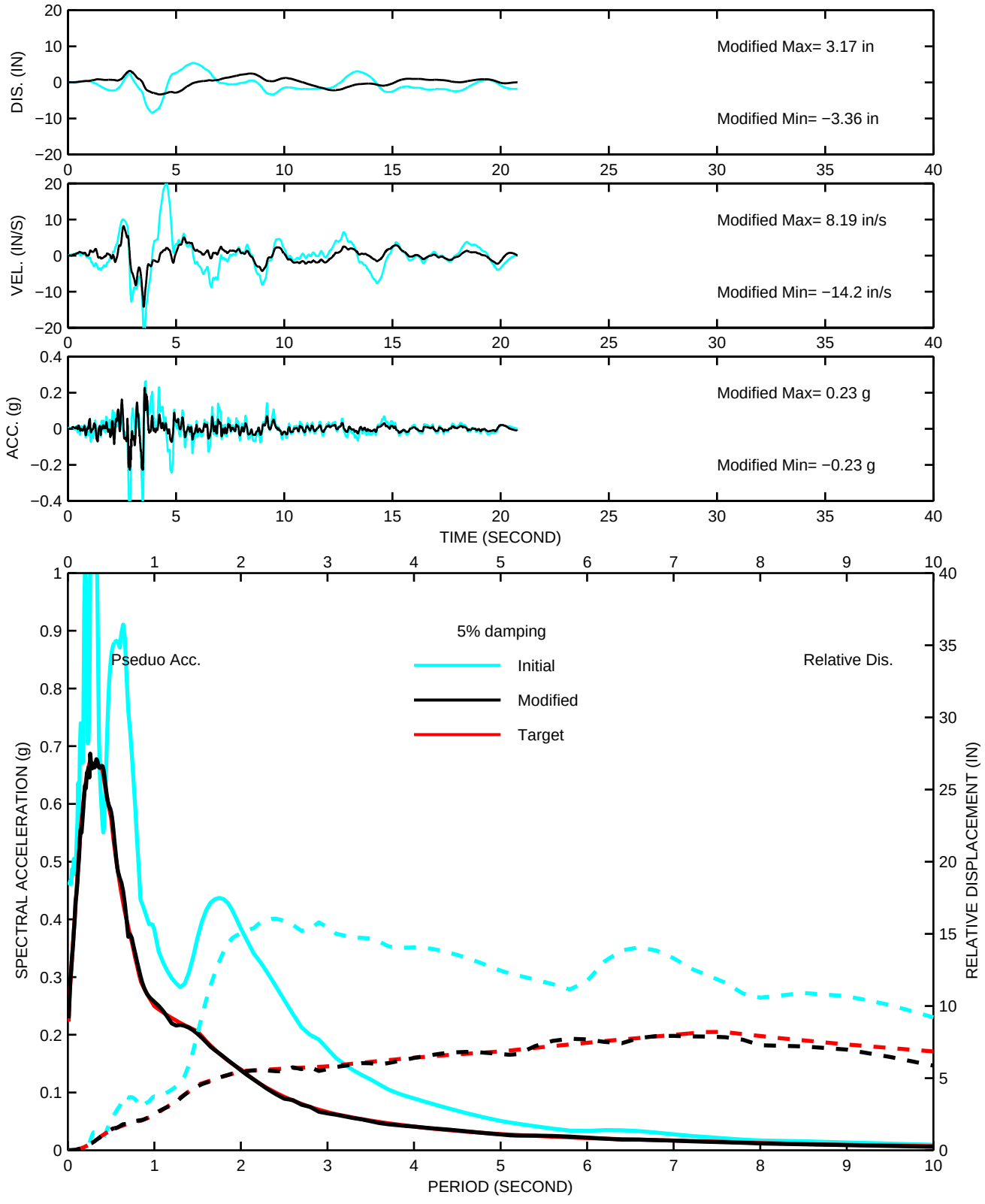


Figure E68. Unimproved Ground Area B OLE Spectrum Compatible Ground Motion (5% Damped)−Set 6 FP

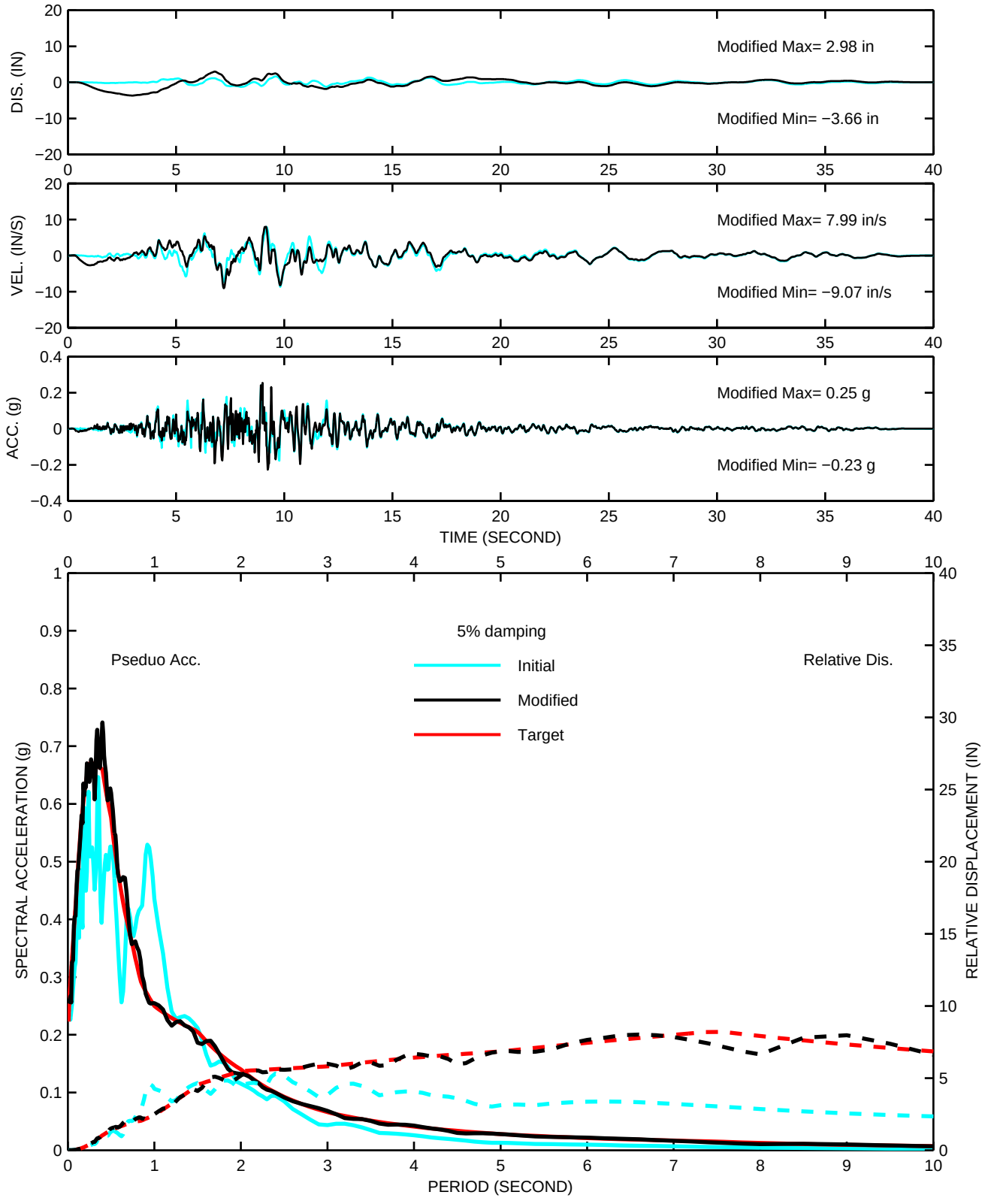


Figure E69. Unimproved Ground Area B OLE Spectrum Compatible Ground Motion (5% Damped)−Set 7 FN

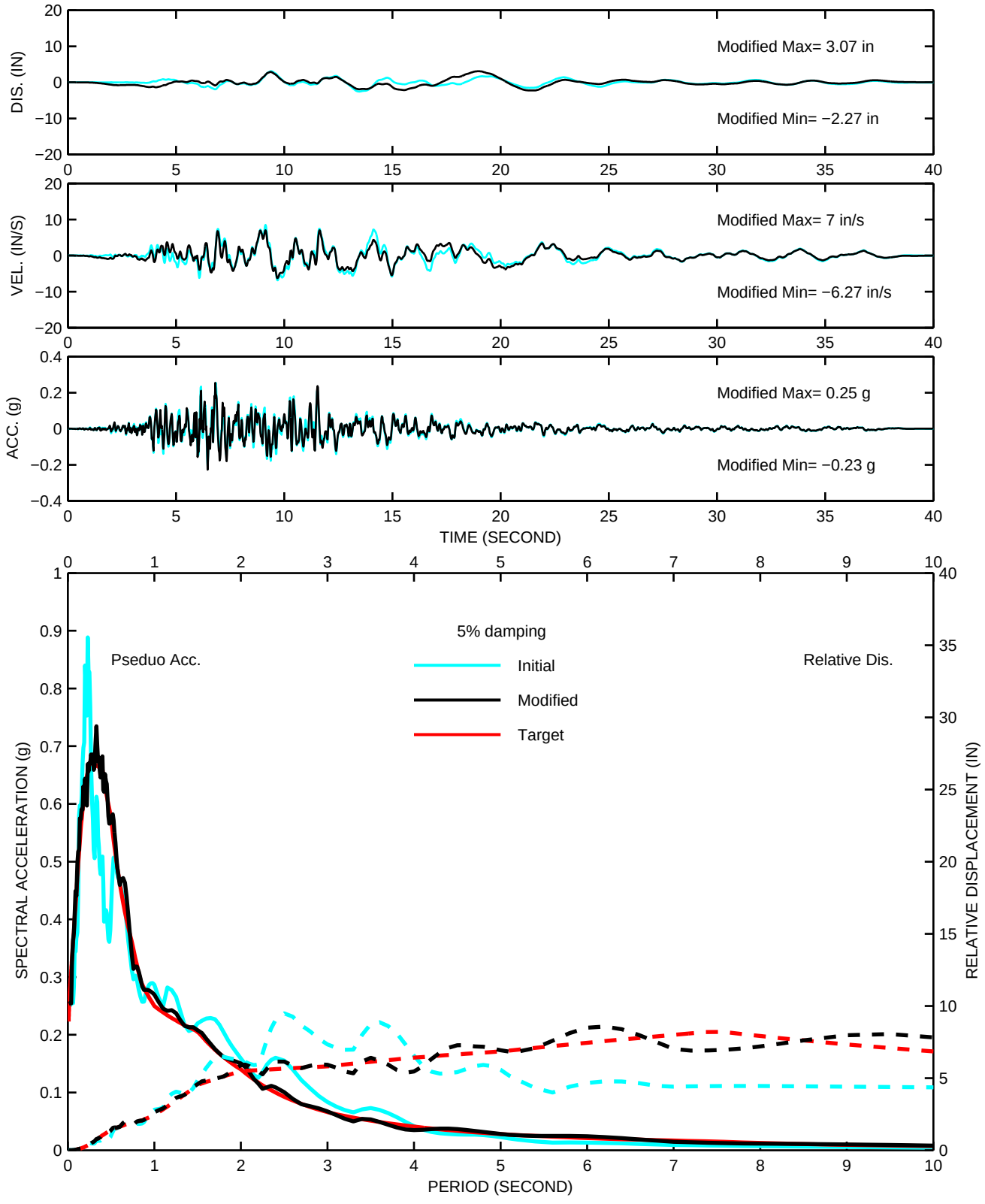


Figure E70. Unimproved Ground Area B OLE Spectrum Compatible Ground Motion (5% Damped)−Set 7 FP

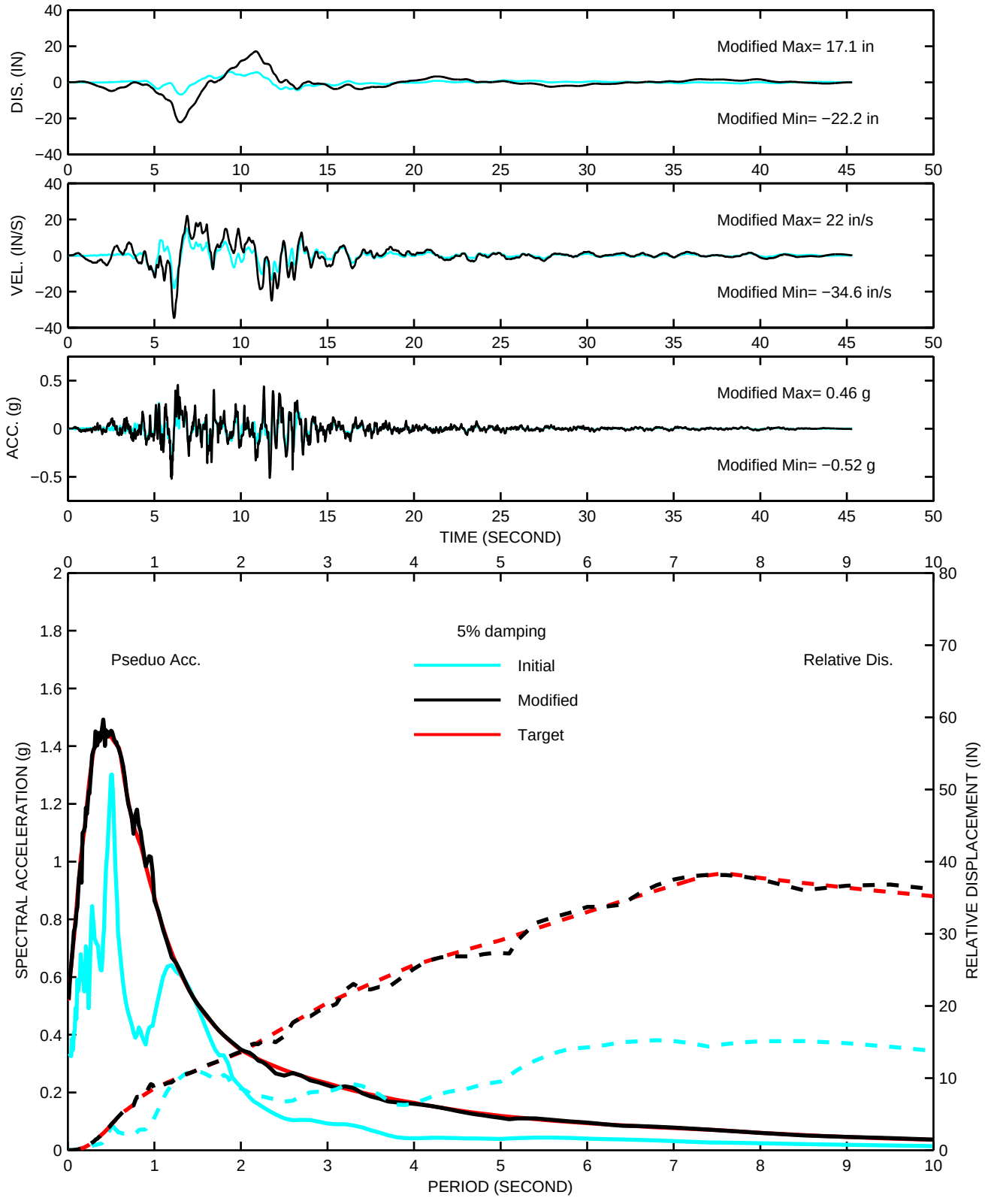


Figure E71. Unimproved Ground Area B CLE Spectrum Compatible Ground Motion (5% Damped)−Set 1 FN

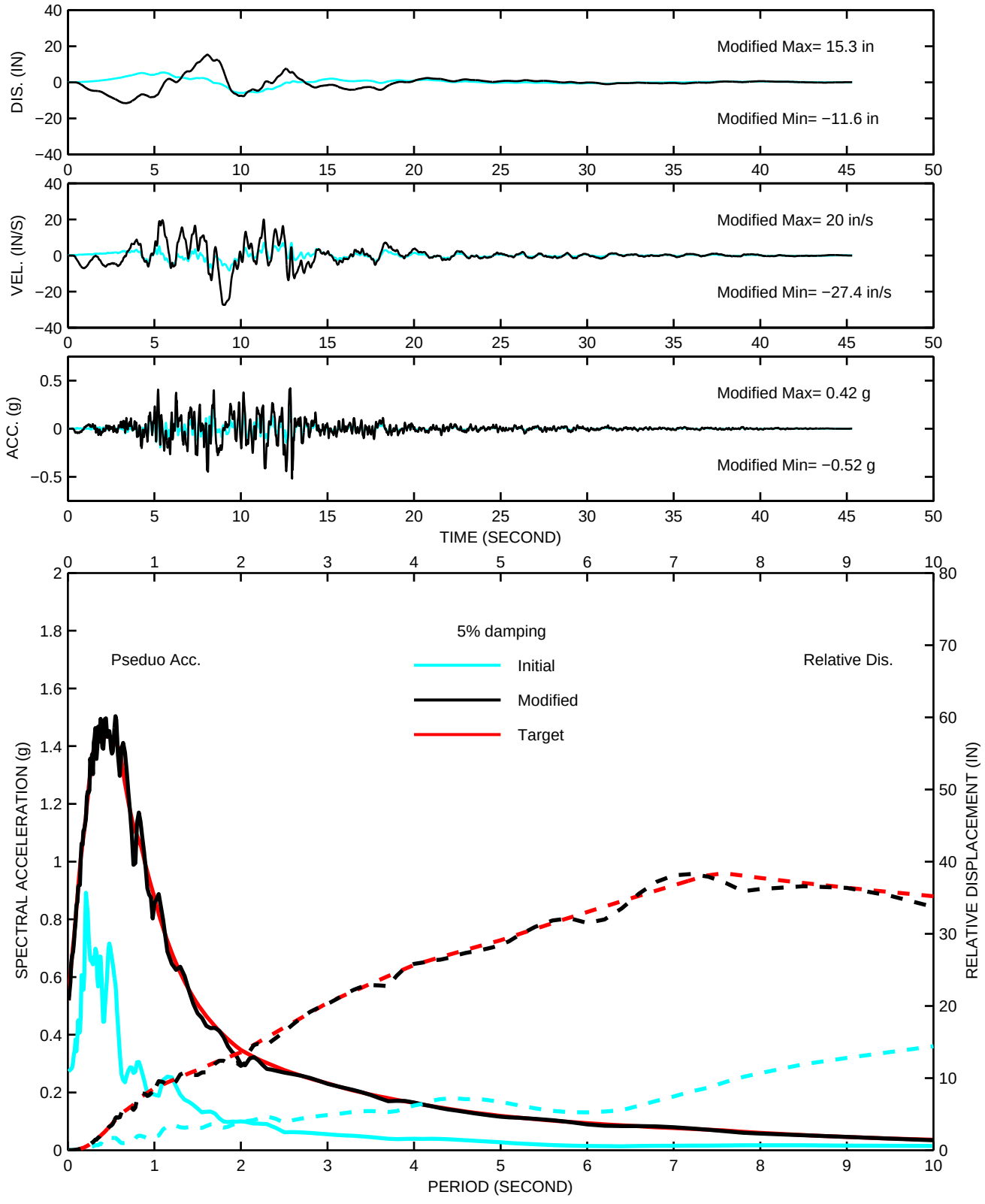


Figure E72. Unimproved Ground Area B CLE Spectrum Compatible Ground Motion (5% Damped)−Set 1 FP

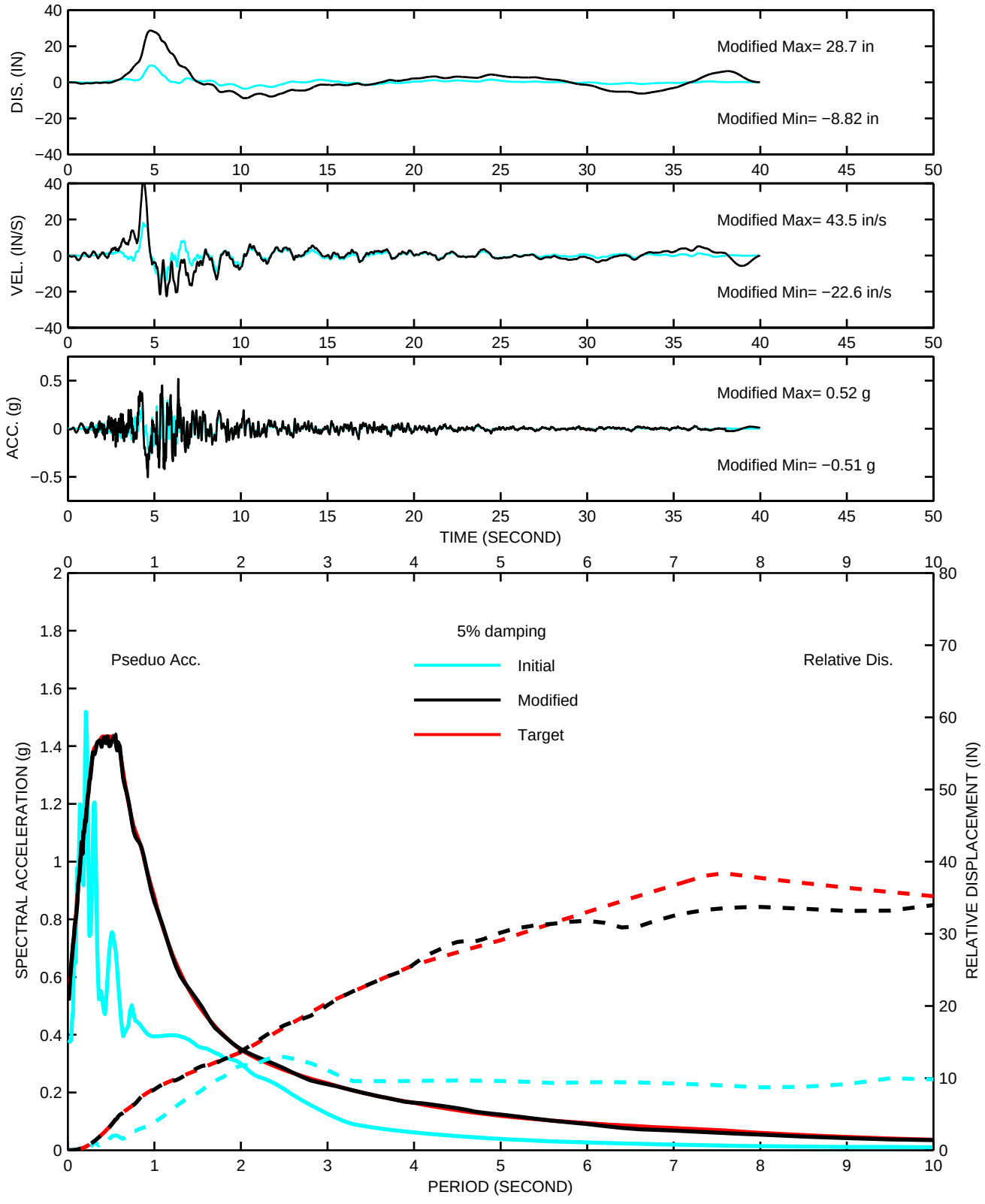


Figure E73. Unimproved Ground Area B CLE Spectrum Compatible Ground Motion (5% Damped)−Set 2 FN

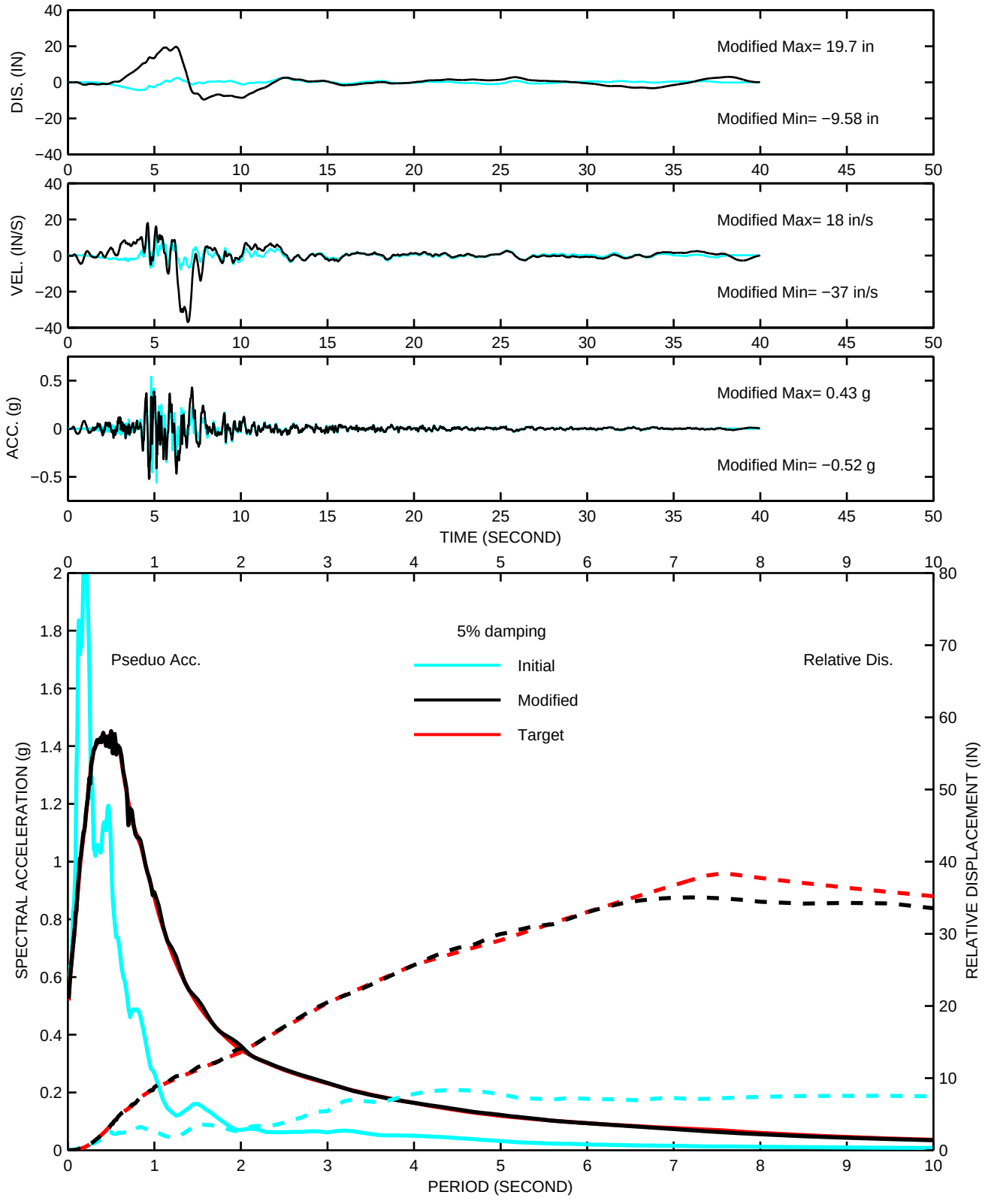


Figure E74. Unimproved Ground Area B CLE Spectrum Compatible Ground Motion (5% Damped)−Set 2 FP

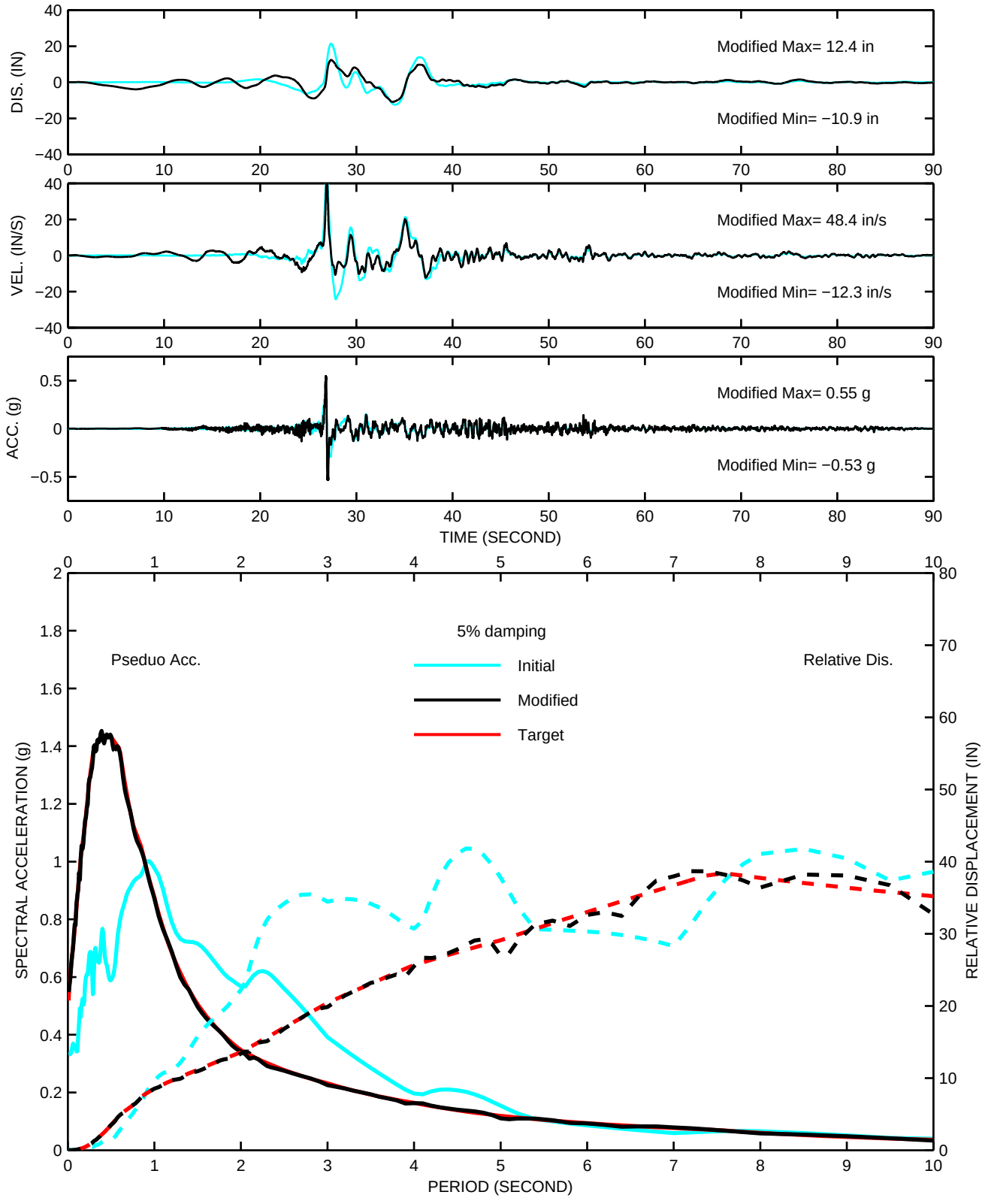


Figure E75. Unimproved Ground Area B CLE Spectrum Compatible Ground Motion (5% Damped)−Set 3 FN

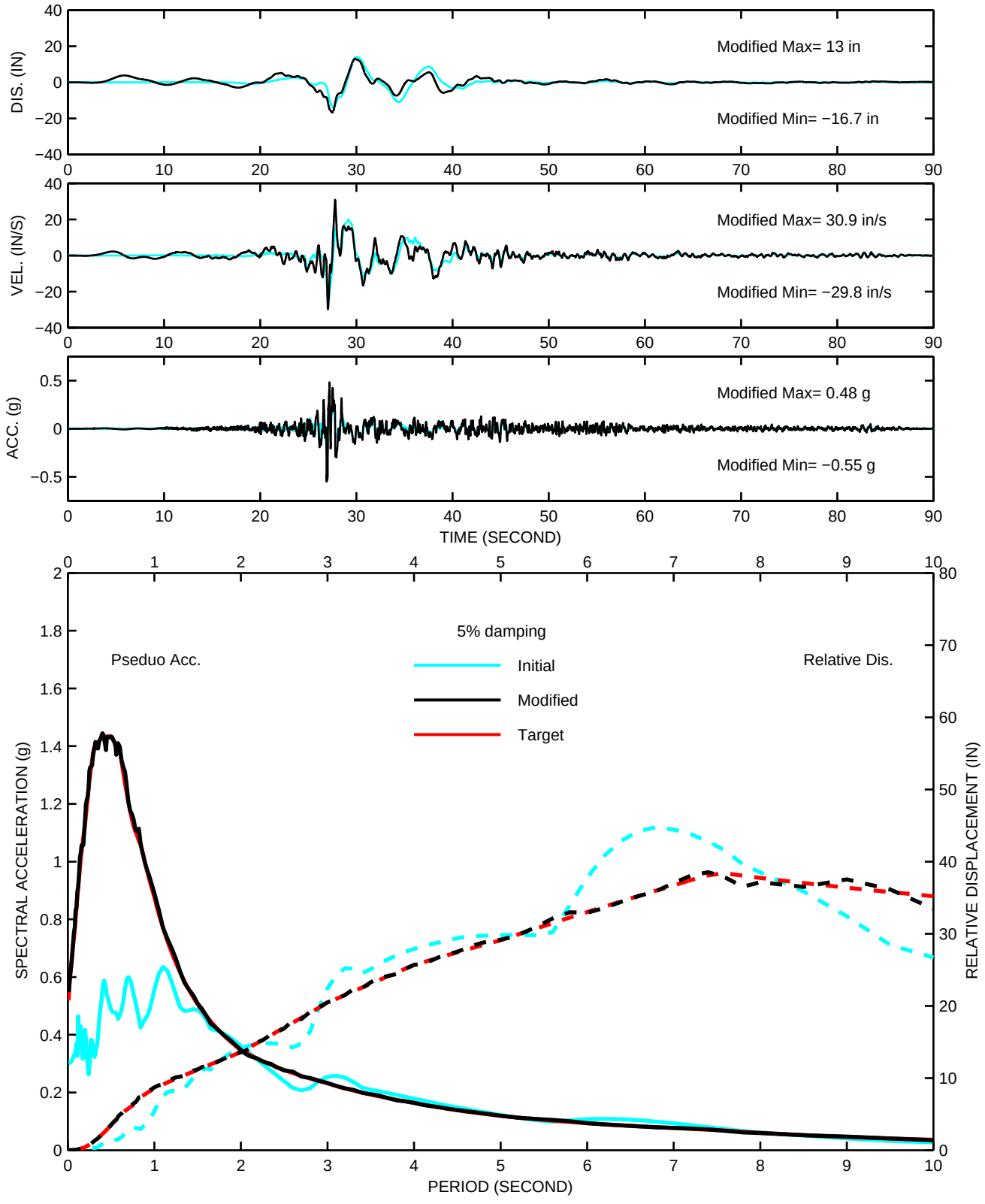


Figure E76. Unimproved Ground Area B CLE Spectrum Compatible Ground Motion (5% Damped)−Set 3 FP

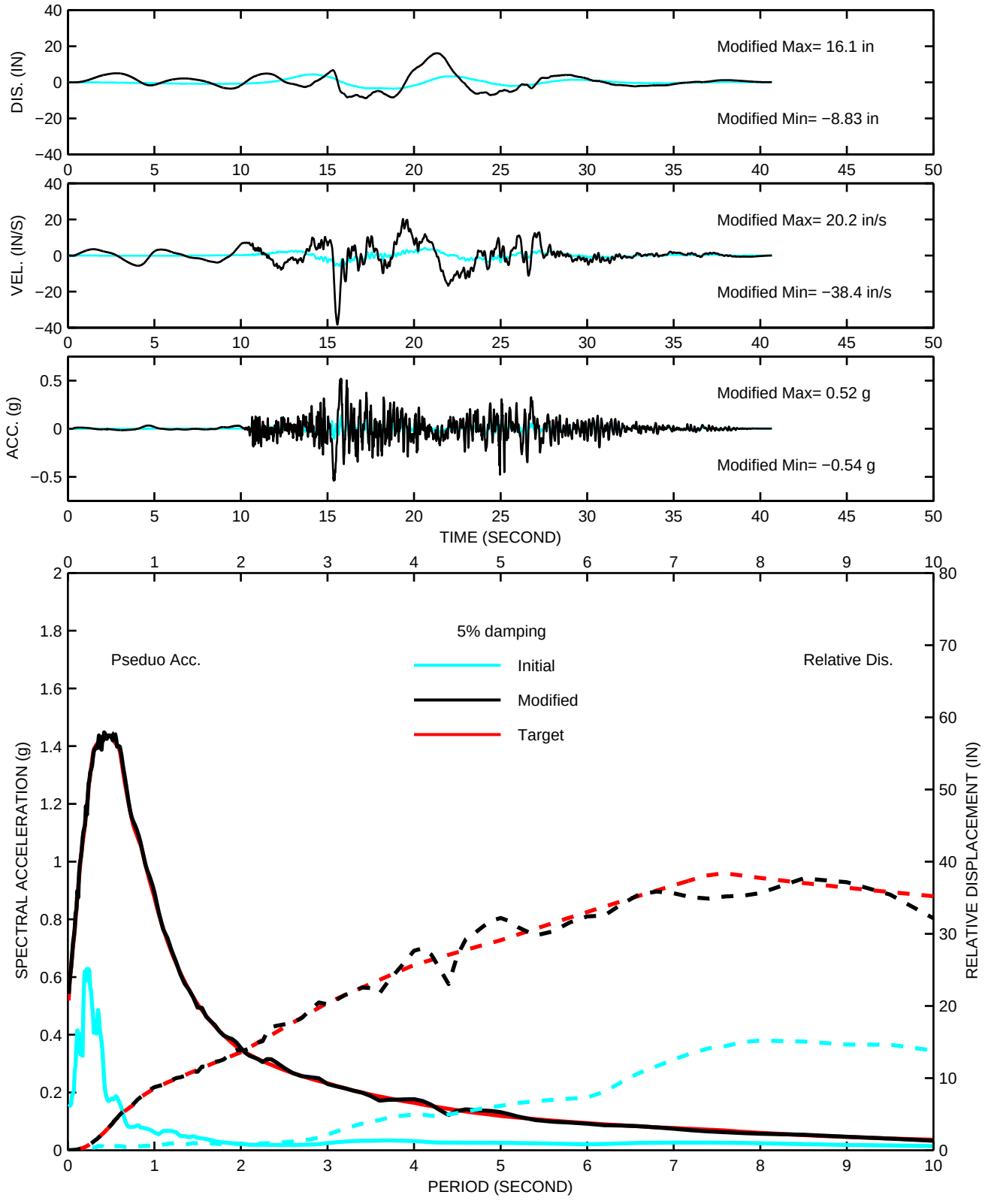


Figure E77. Unimproved Ground Area B CLE Spectrum Compatible Ground Motion (5% Damped)−Set 4 FN

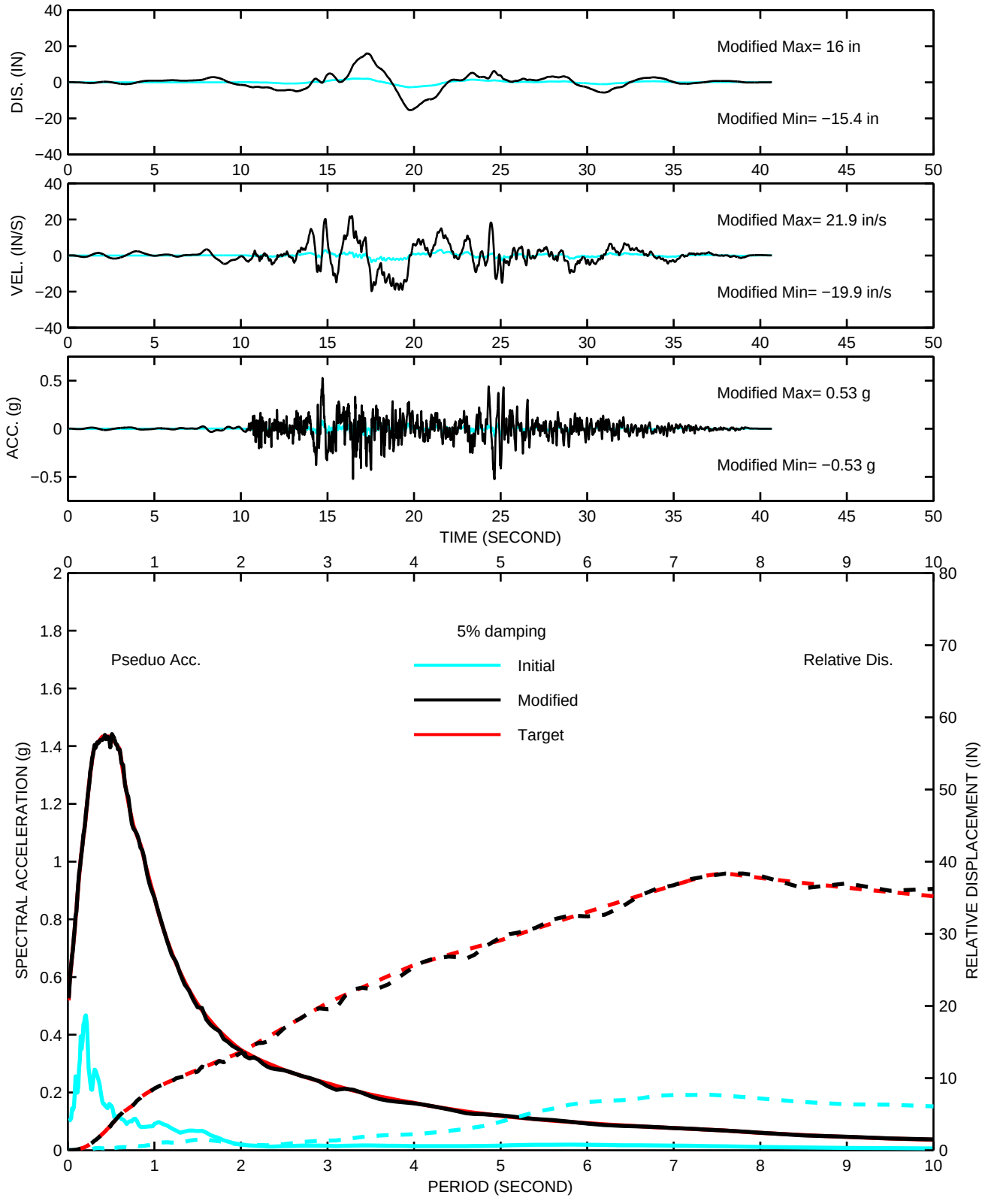


Figure E78. Unimproved Ground Area B CLE Spectrum Compatible Ground Motion (5% Damped)−Set 4 FP

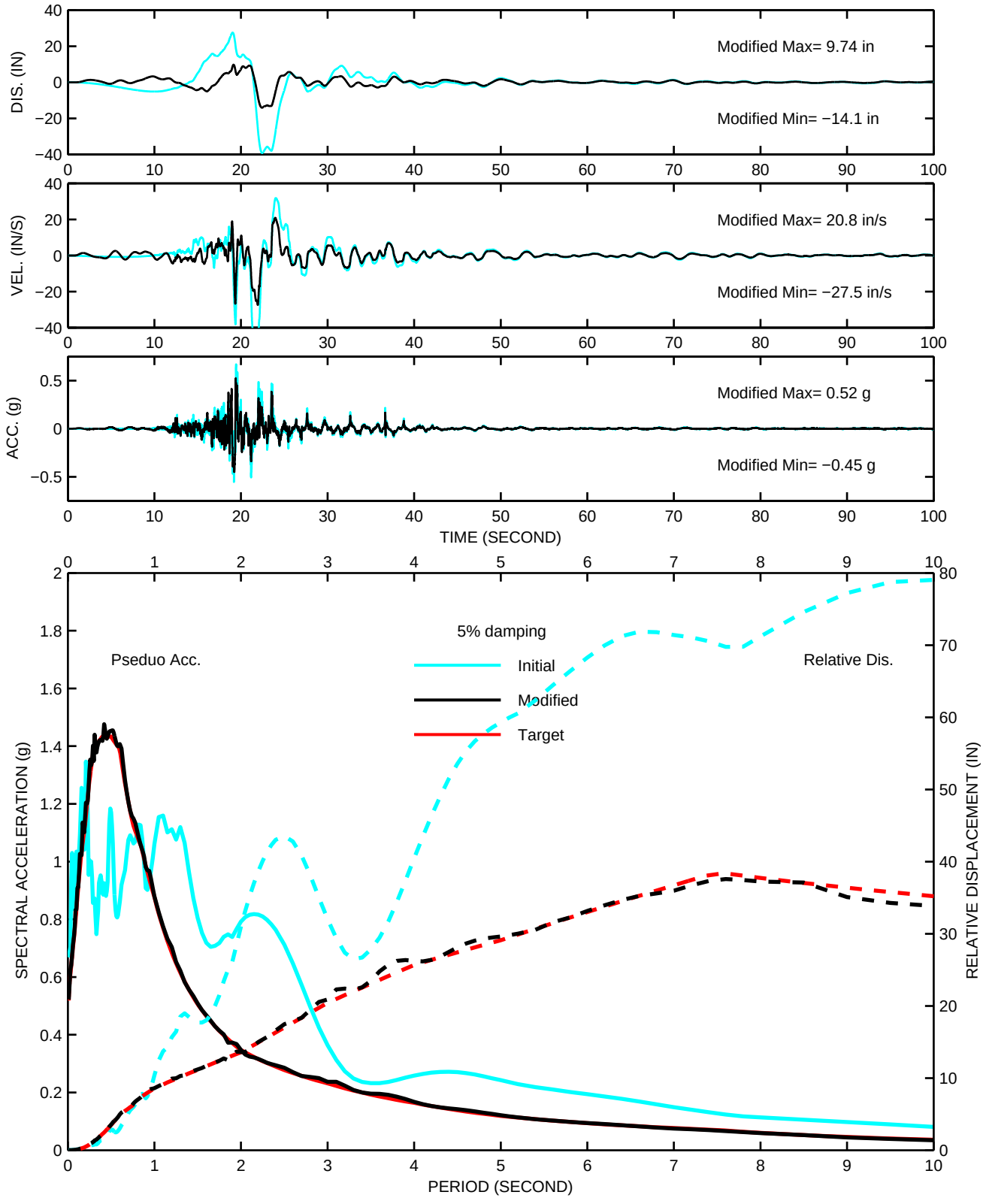


Figure E79. Unimproved Ground Area B CLE Spectrum Compatible Ground Motion (5% Damped)−Set 5 FN

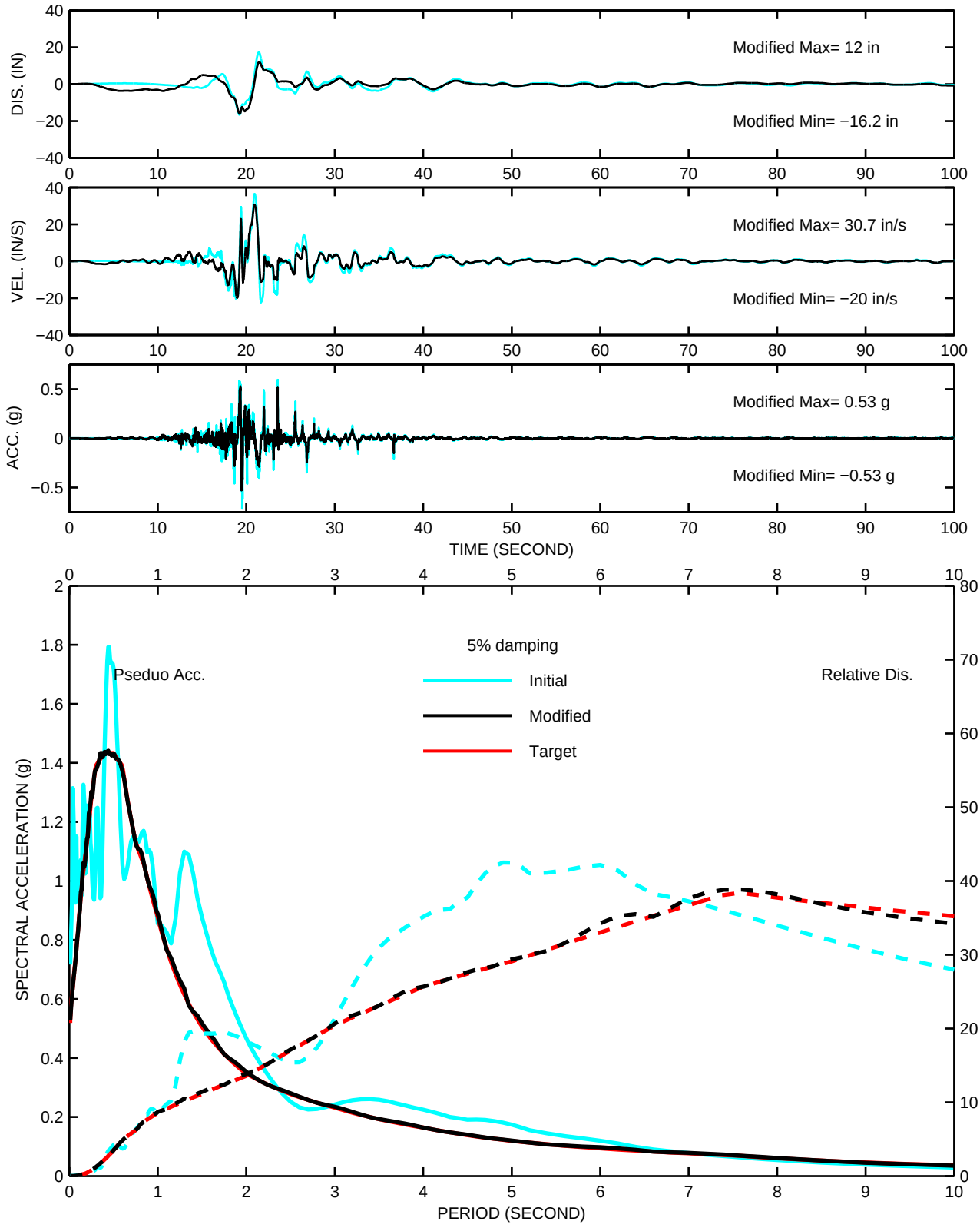


Figure E80. Unimproved Ground Area B CLE Spectrum Compatible Ground Motion (5% Damped)−Set 5 FP

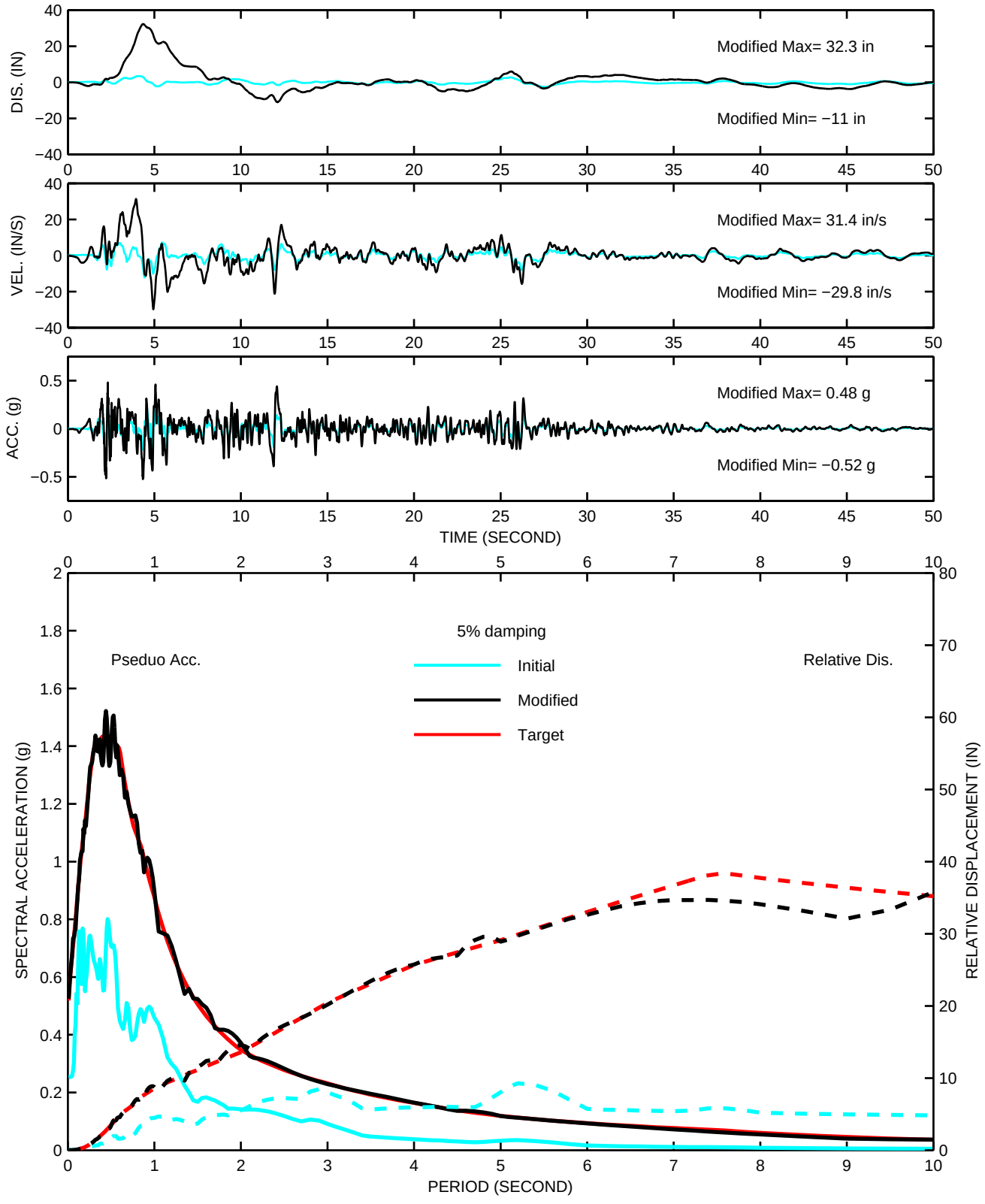


Figure E81. Unimproved Ground Area B CLE Spectrum Compatible Ground Motion (5% Damped)−Set 6 FN

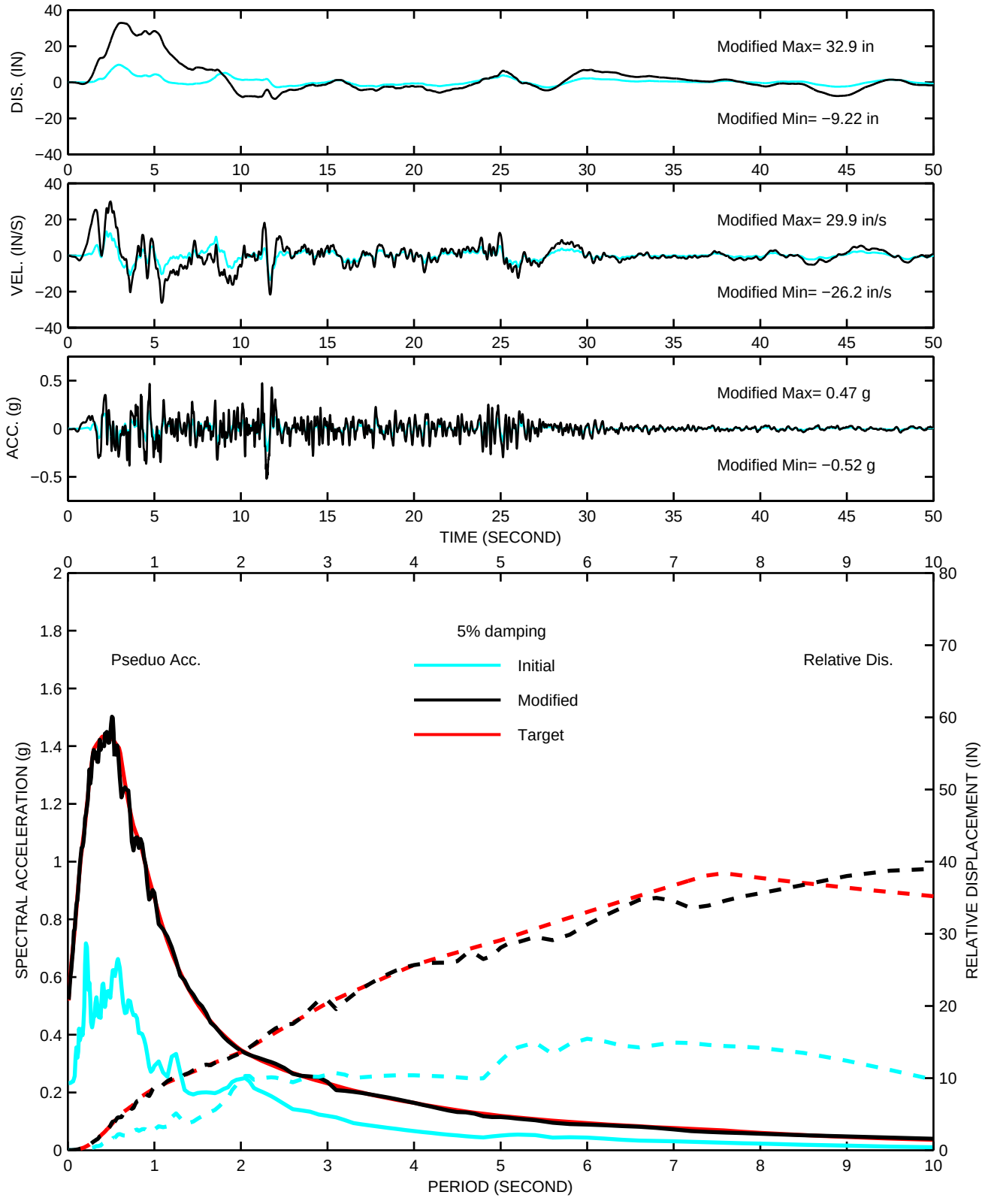


Figure E82. Unimproved Ground Area B CLE Spectrum Compatible Ground Motion (5% Damped)−Set 6 FP

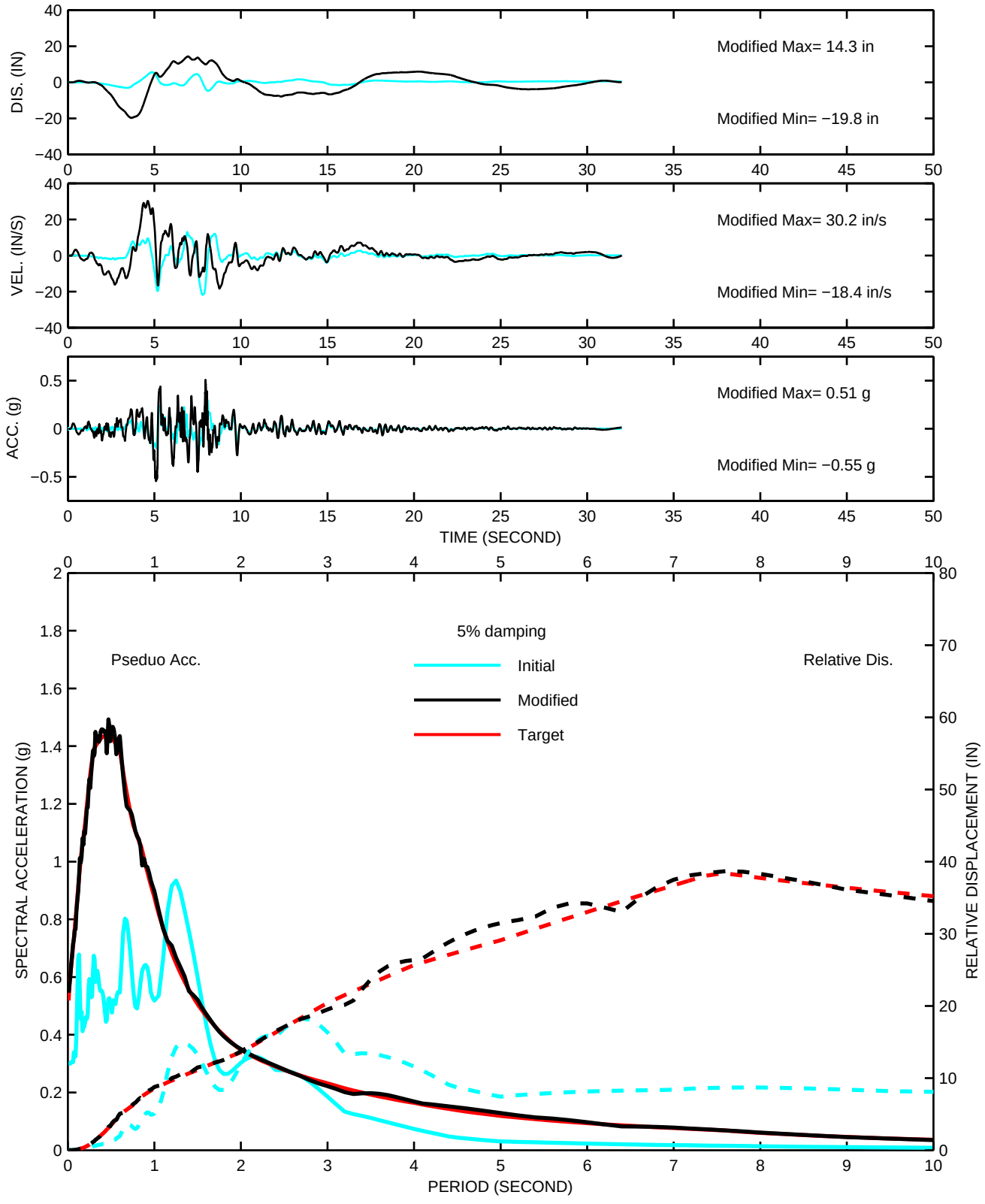


Figure E83. Unimproved Ground Area B CLE Spectrum Compatible Ground Motion (5% Damped)−Set 7 FN

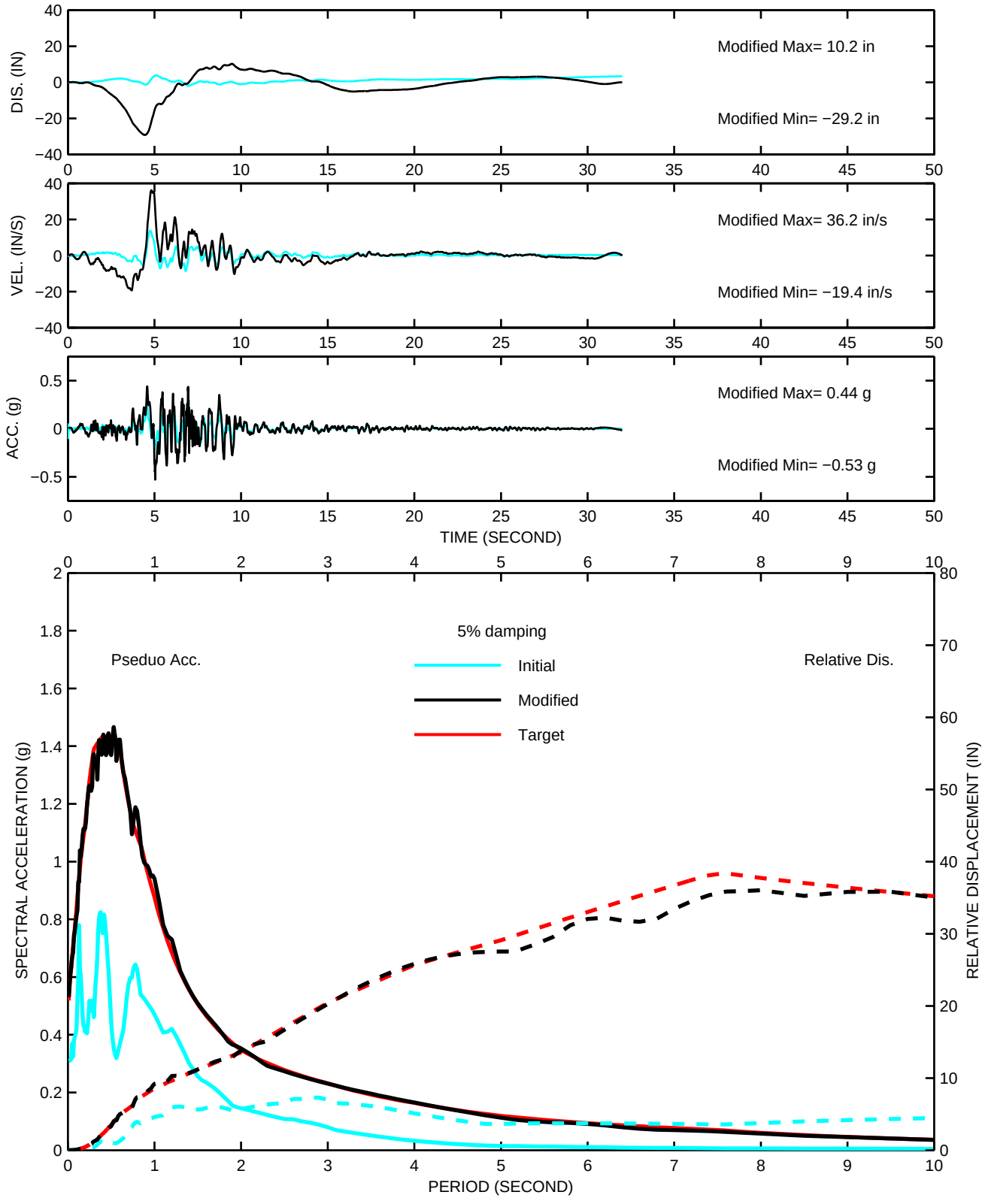


Figure E84. Unimproved Ground Area B CLE Spectrum Compatible Ground Motion (5% Damped)−Set 7 FP

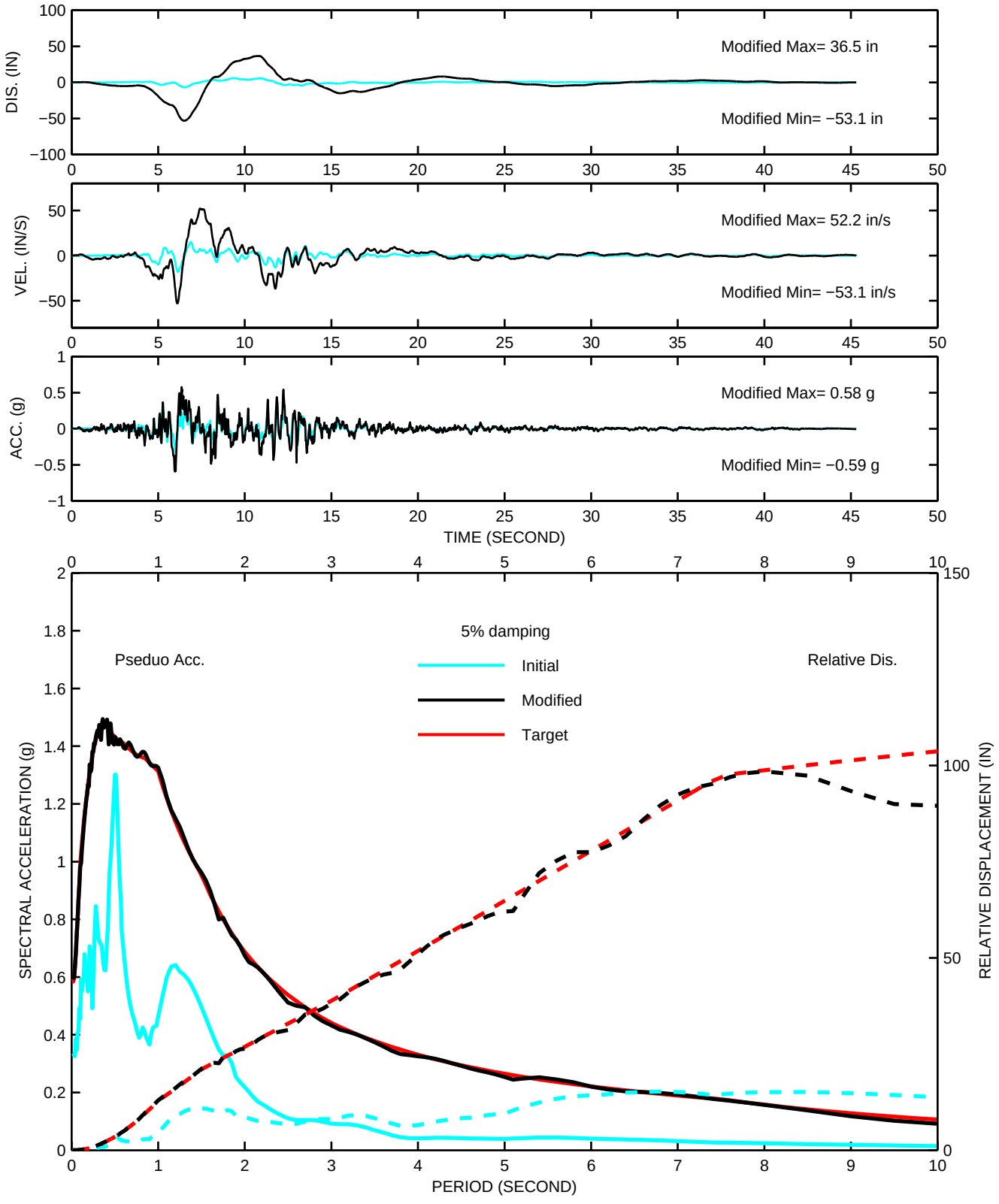


Figure E85. Unimproved Ground Area B DE Spectrum Compatible Ground Motion (5% Damped)−Set 1 FN

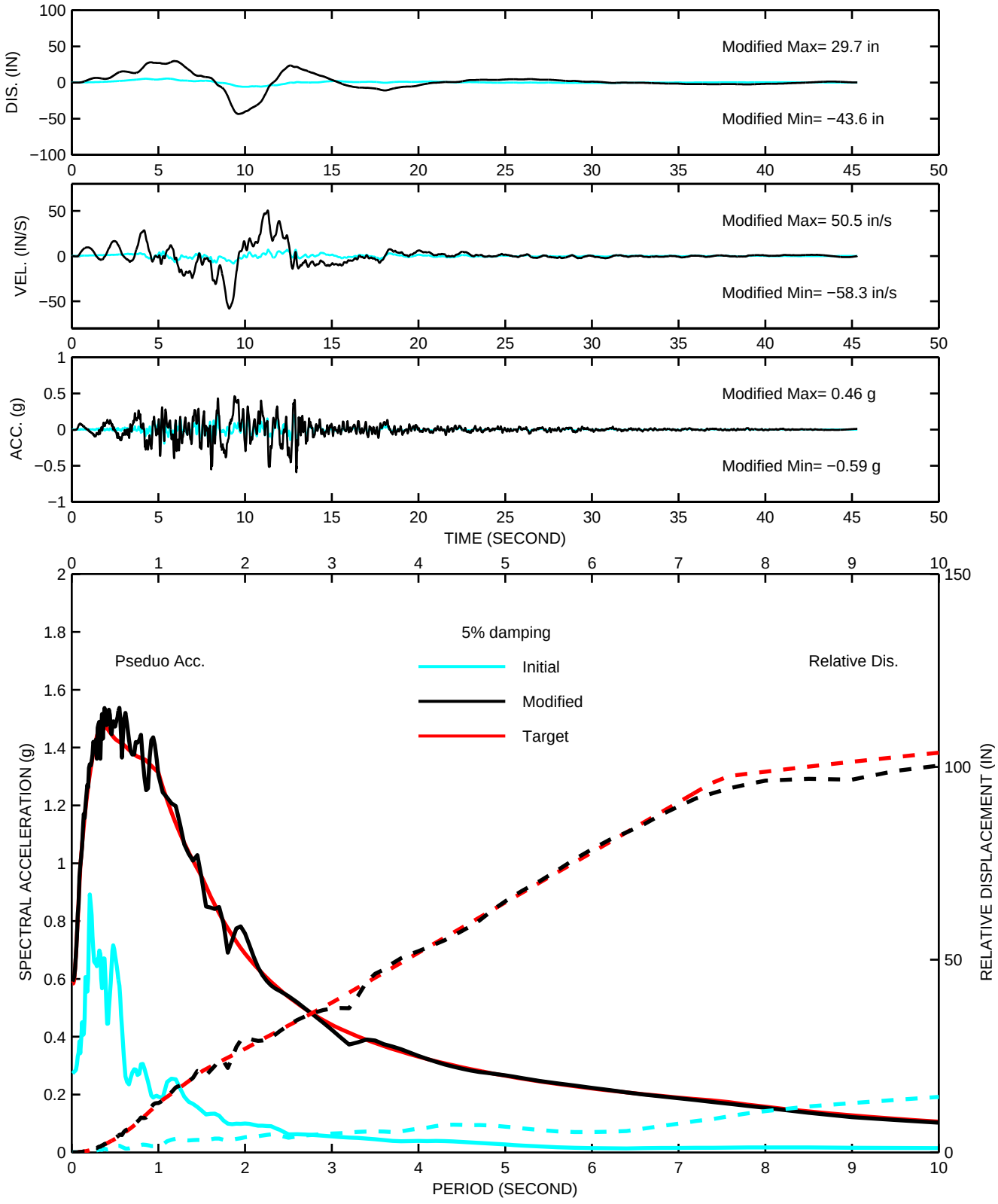


Figure E86. Unimproved Ground Area B DE Spectrum Compatible Ground Motion (5% Damped)−Set 1 FP

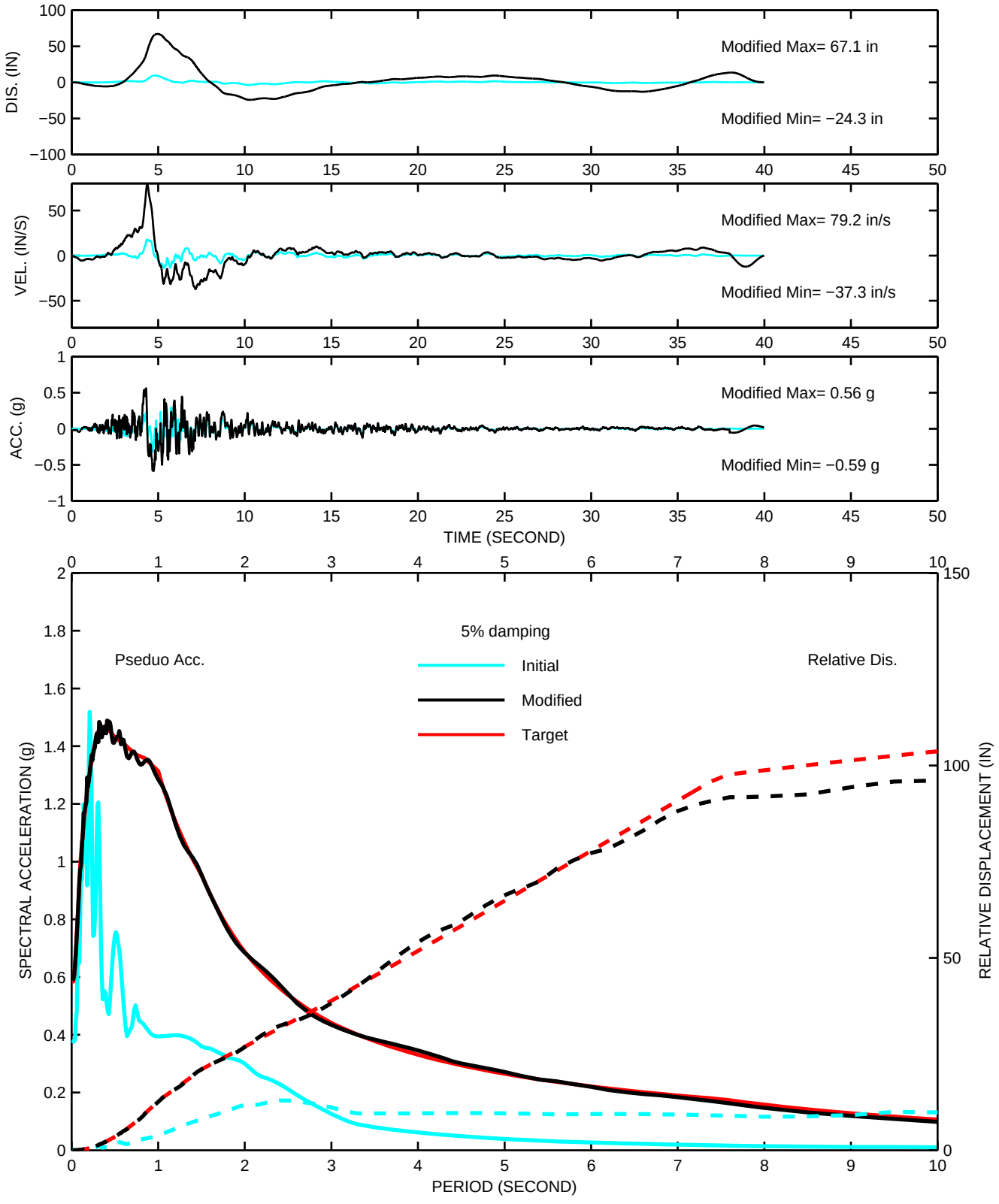


Figure E87. Unimproved Ground Area B DE Spectrum Compatible Ground Motion (5% Damped)−Set 2 FN

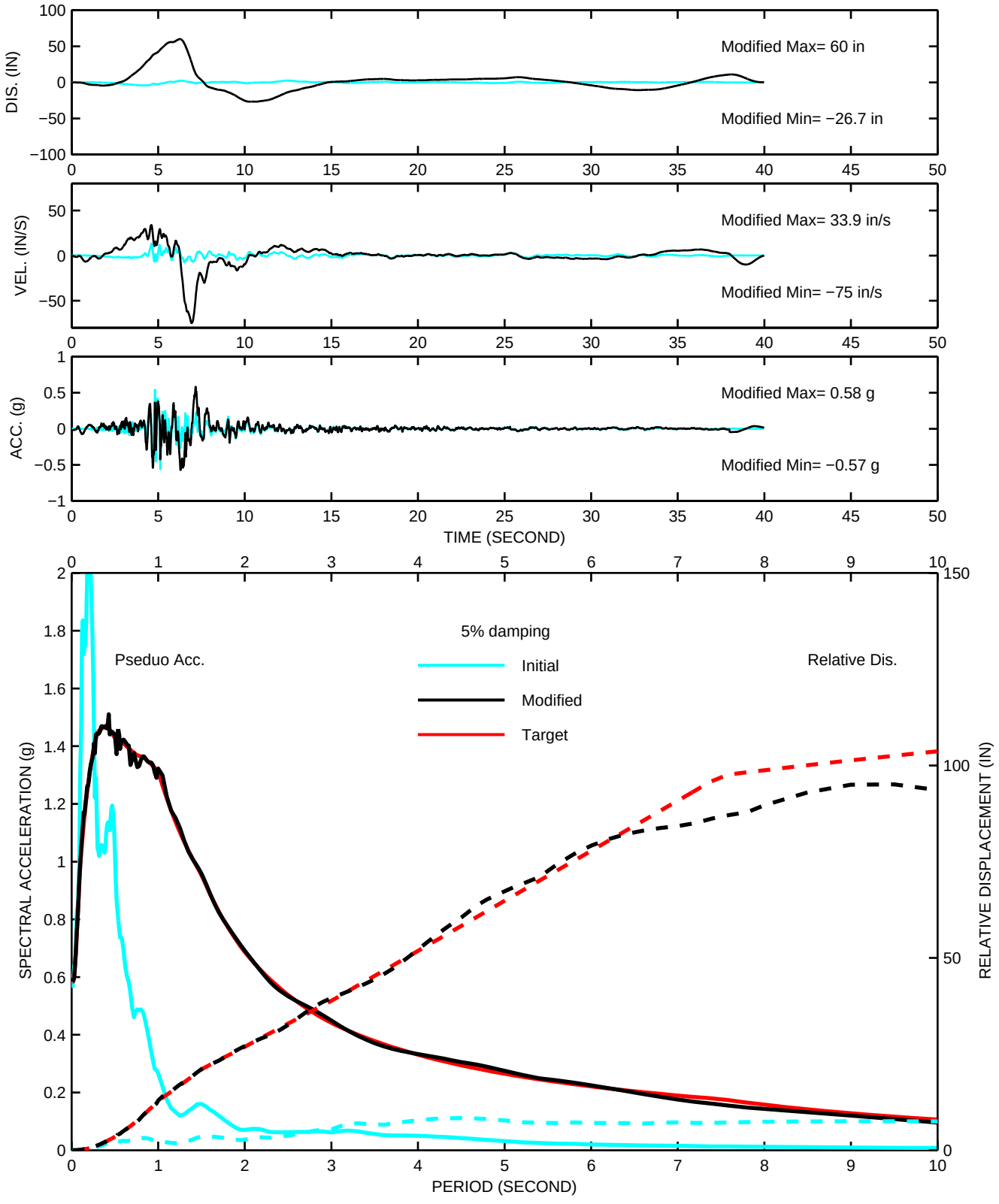


Figure E88. Unimproved Ground Area B DE Spectrum Compatible Ground Motion (5% Damped)−Set 2 FP

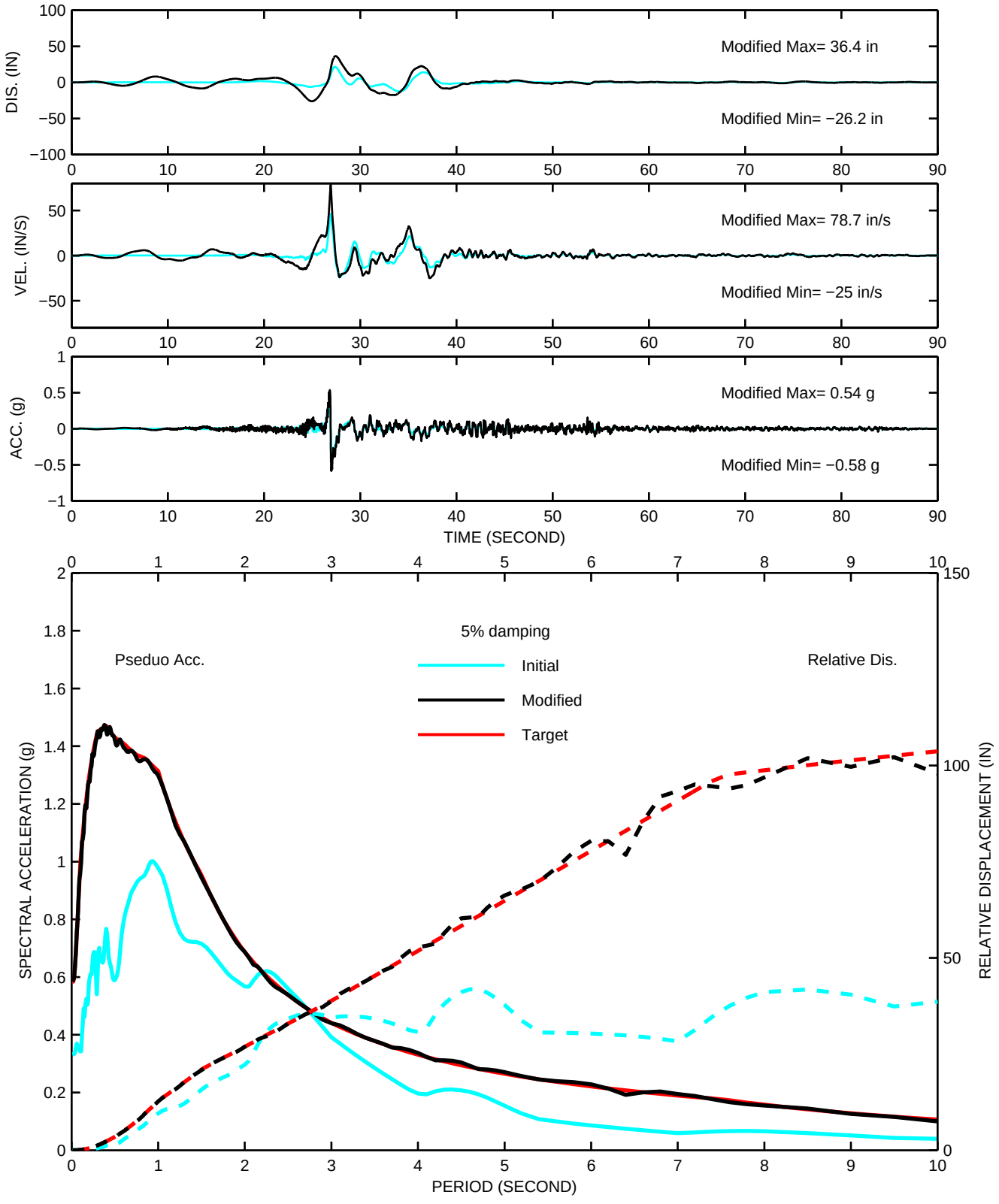


Figure E89. Unimproved Ground Area B DE Spectrum Compatible Ground Motion (5% Damped)−Set 3 FN

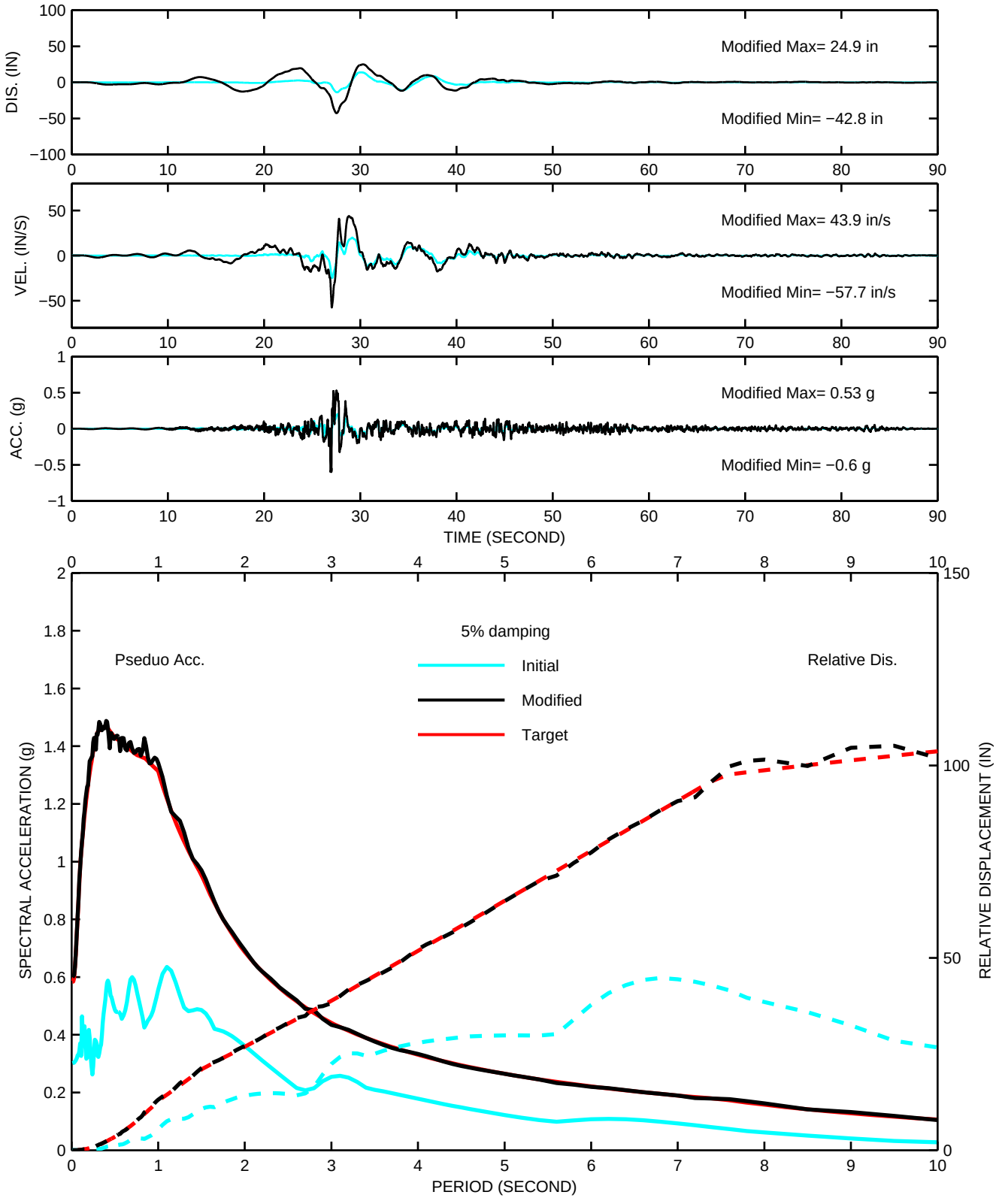


Figure E90. Unimproved Ground Area B DE Spectrum Compatible Ground Motion (5% Damped)−Set 3 FP

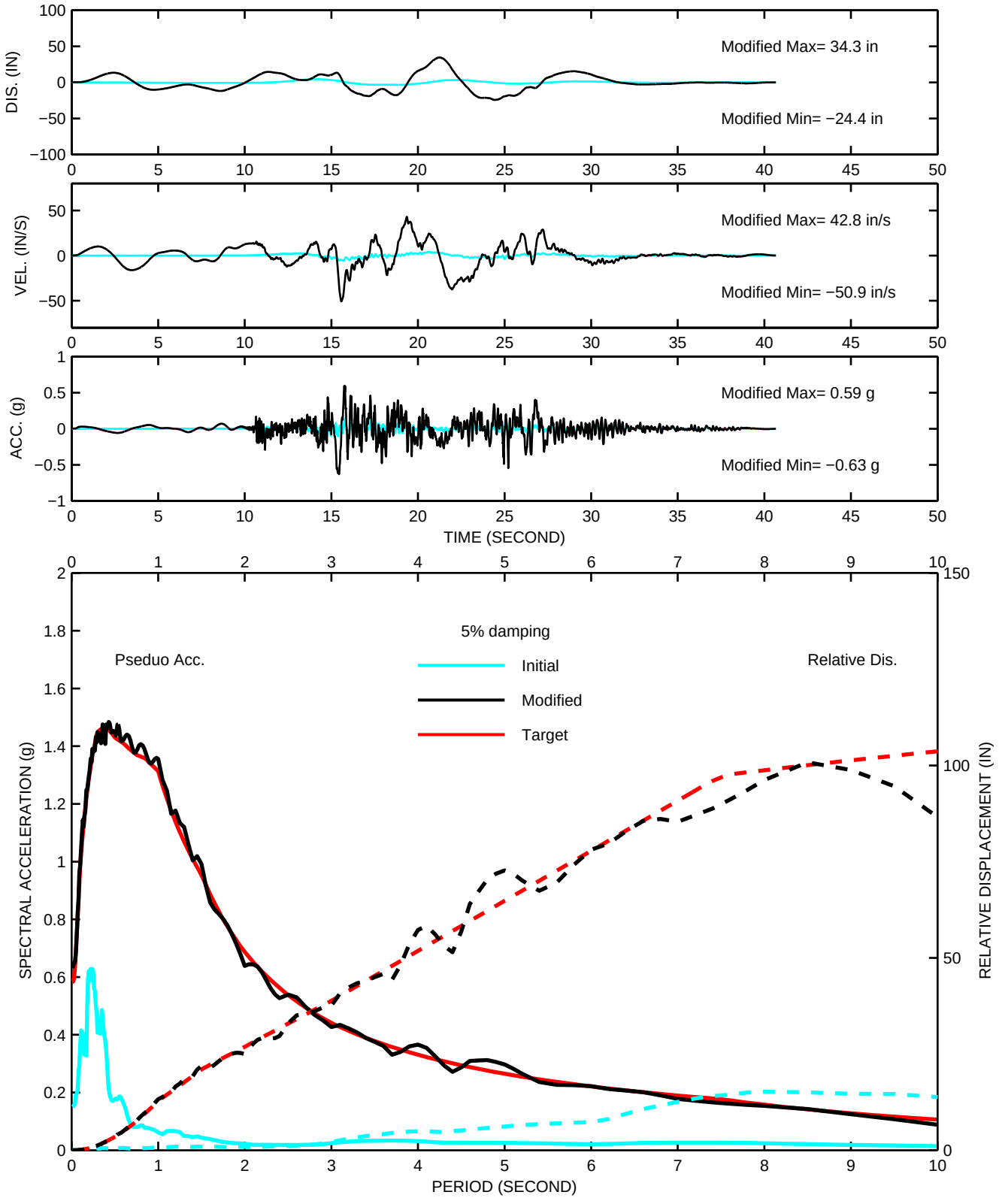


Figure E91. Unimproved Ground Area B DE Spectrum Compatible Ground Motion (5% Damped)−Set 4 FN

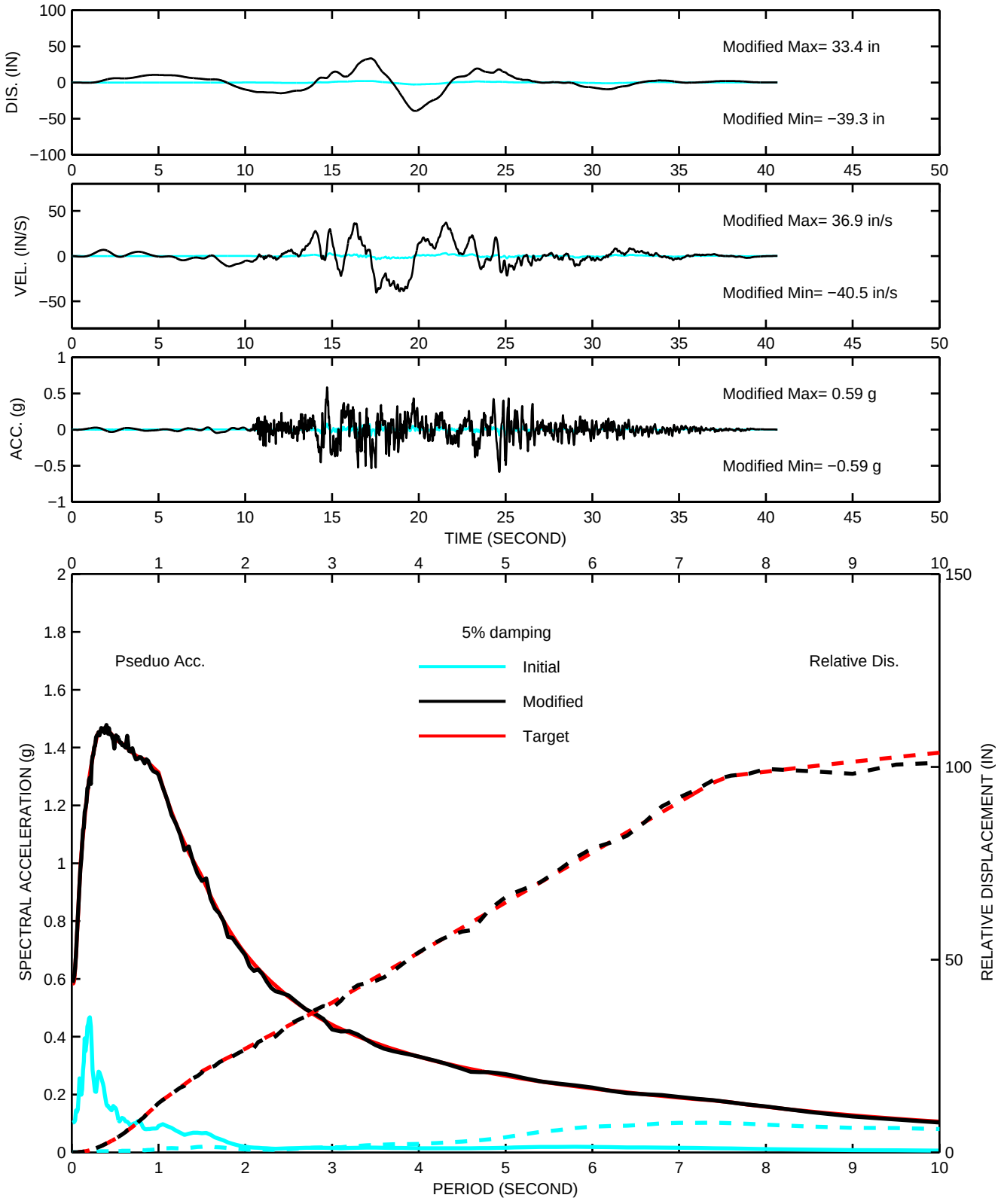


Figure E92. Unimproved Ground Area B DE Spectrum Compatible Ground Motion (5% Damped)−Set 4 FP

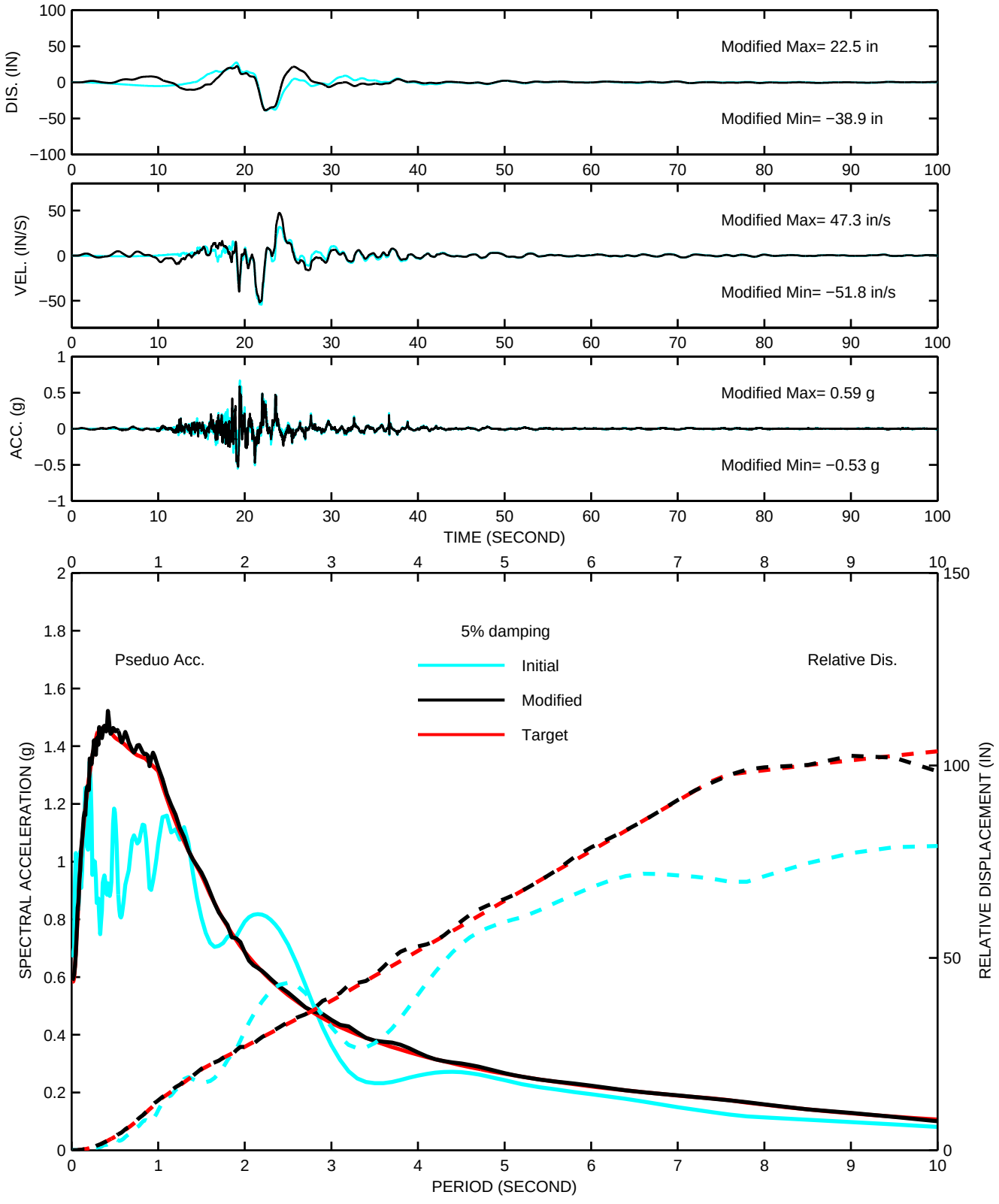


Figure E93. Unimproved Ground Area B DE Spectrum Compatible Ground Motion (5% Damped)−Set 5 FN

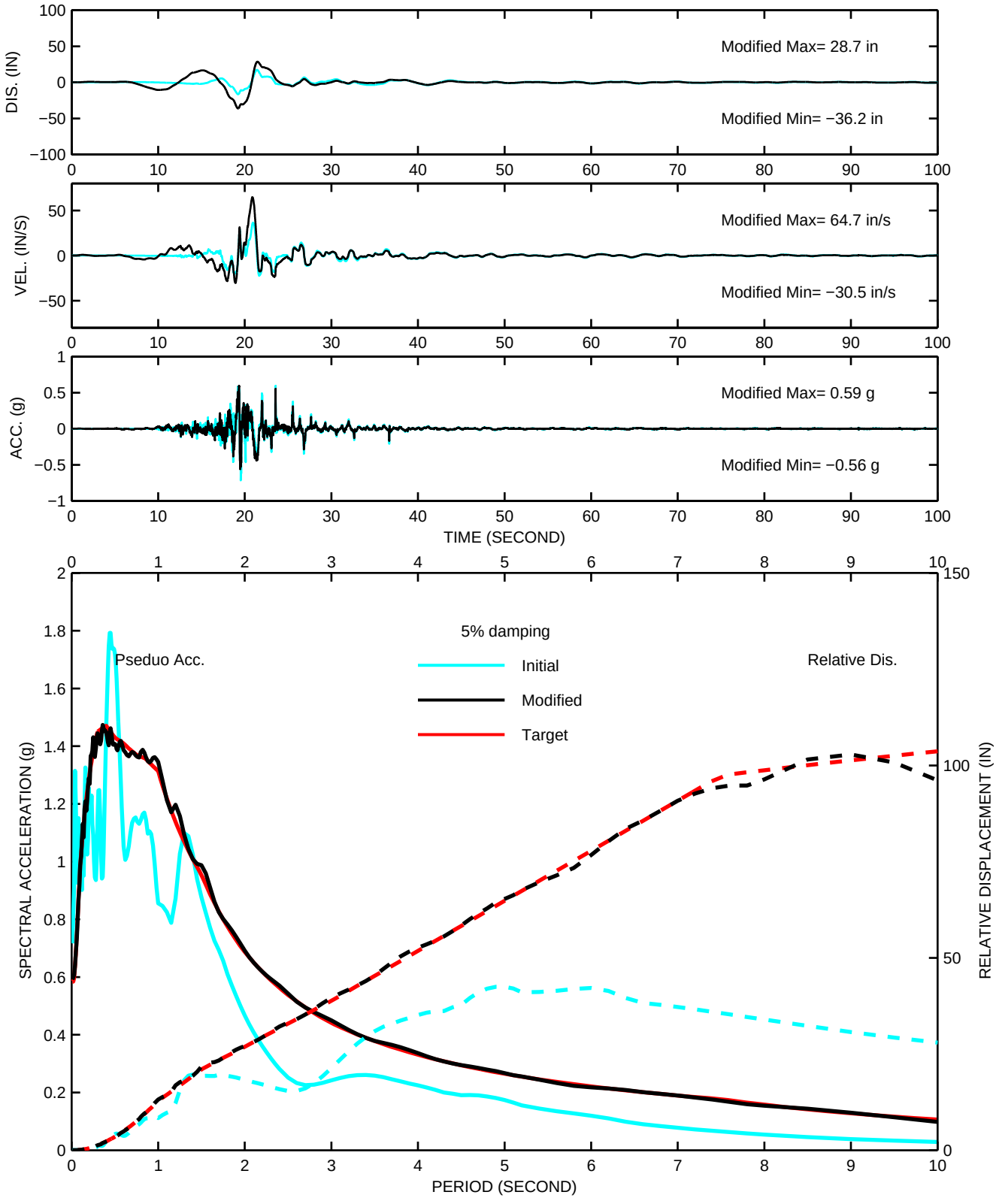


Figure E94. Unimproved Ground Area B DE Spectrum Compatible Ground Motion (5% Damped)−Set 5 FP

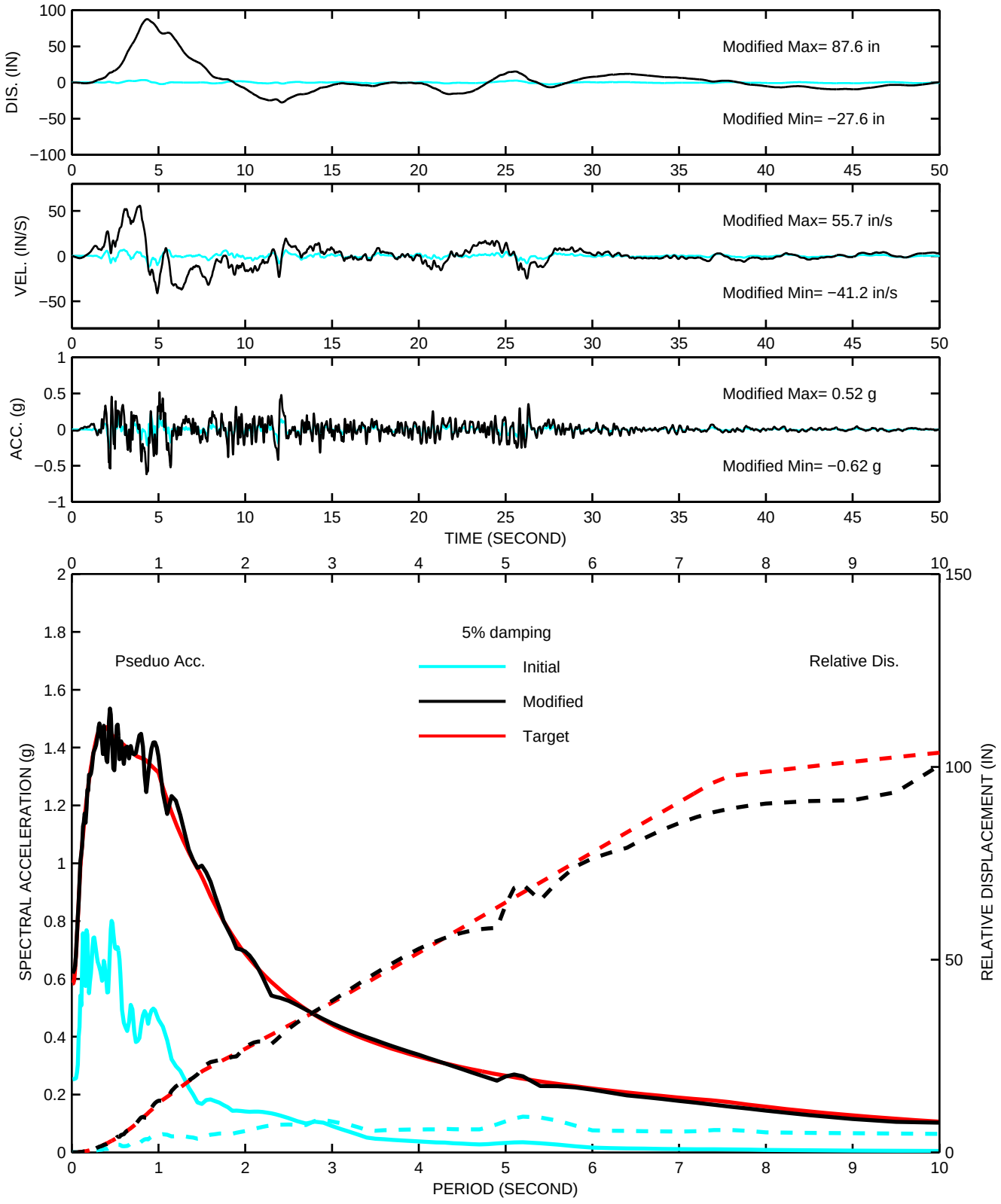


Figure E95. Unimproved Ground Area B DE Spectrum Compatible Ground Motion (5% Damped)−Set 6 FN

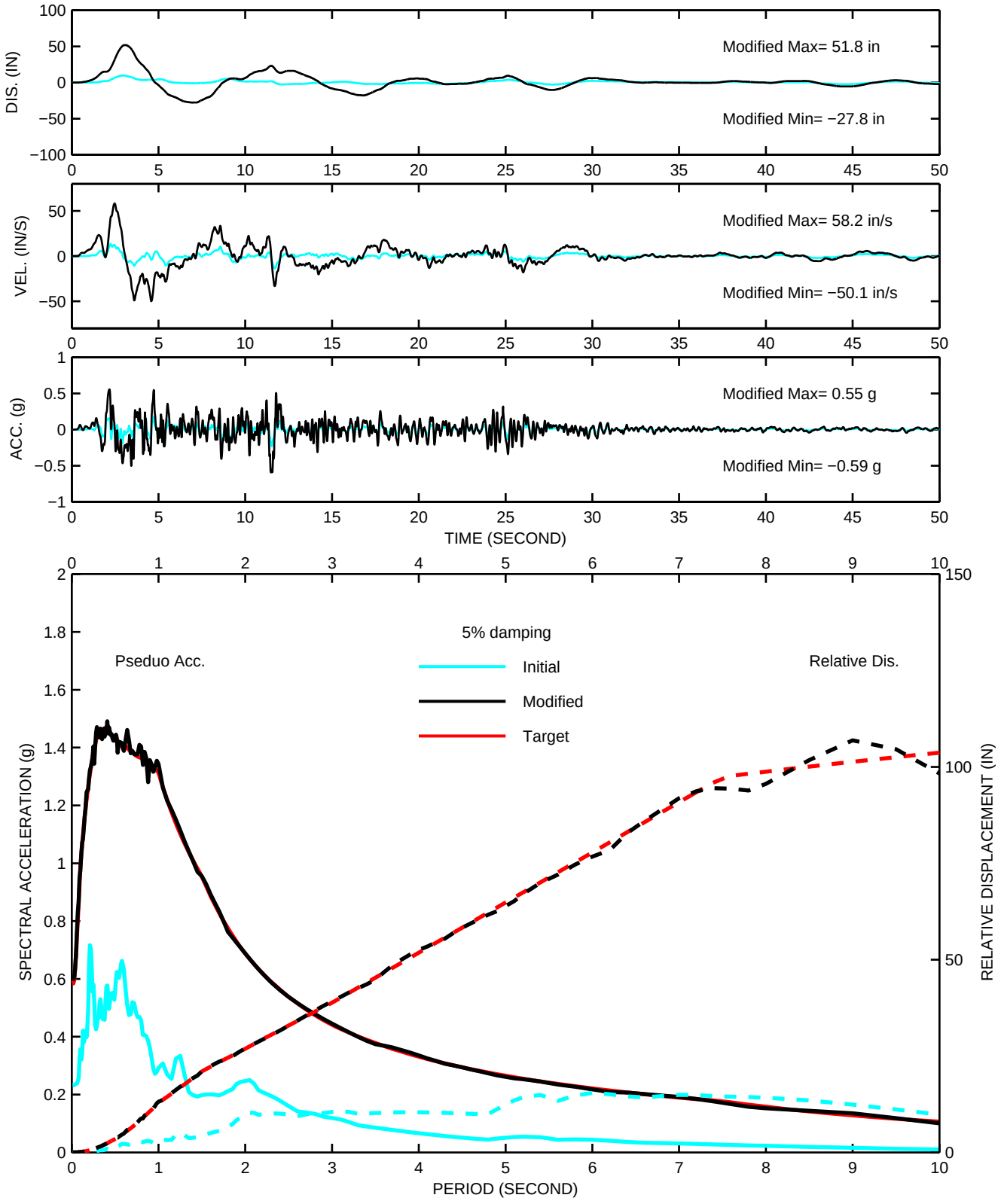


Figure E96. Unimproved Ground Area B DE Spectrum Compatible Ground Motion (5% Damped)−Set 6 FP

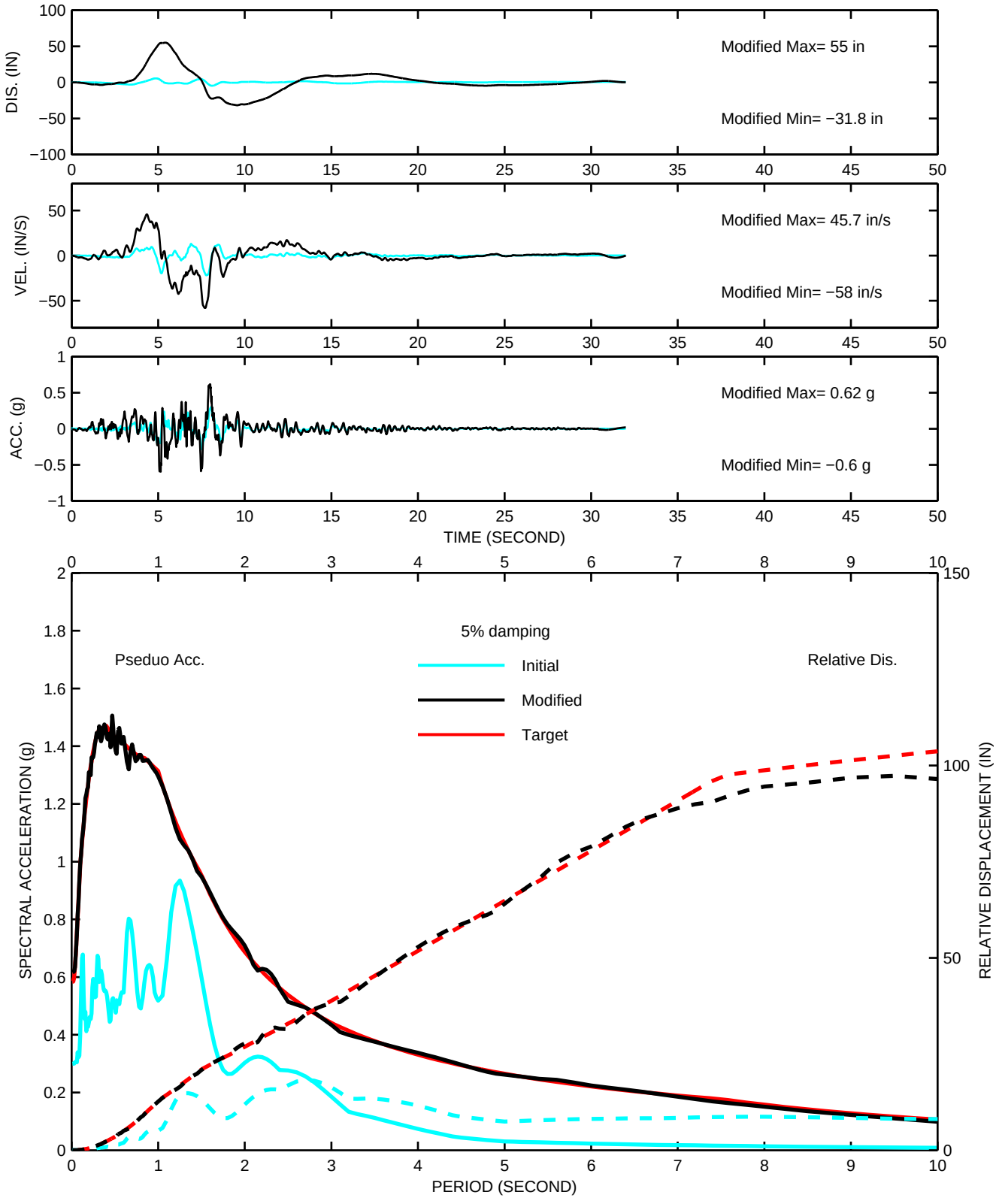


Figure E97. Unimproved Ground Area B DE Spectrum Compatible Ground Motion (5% Damped)−Set 7 FN

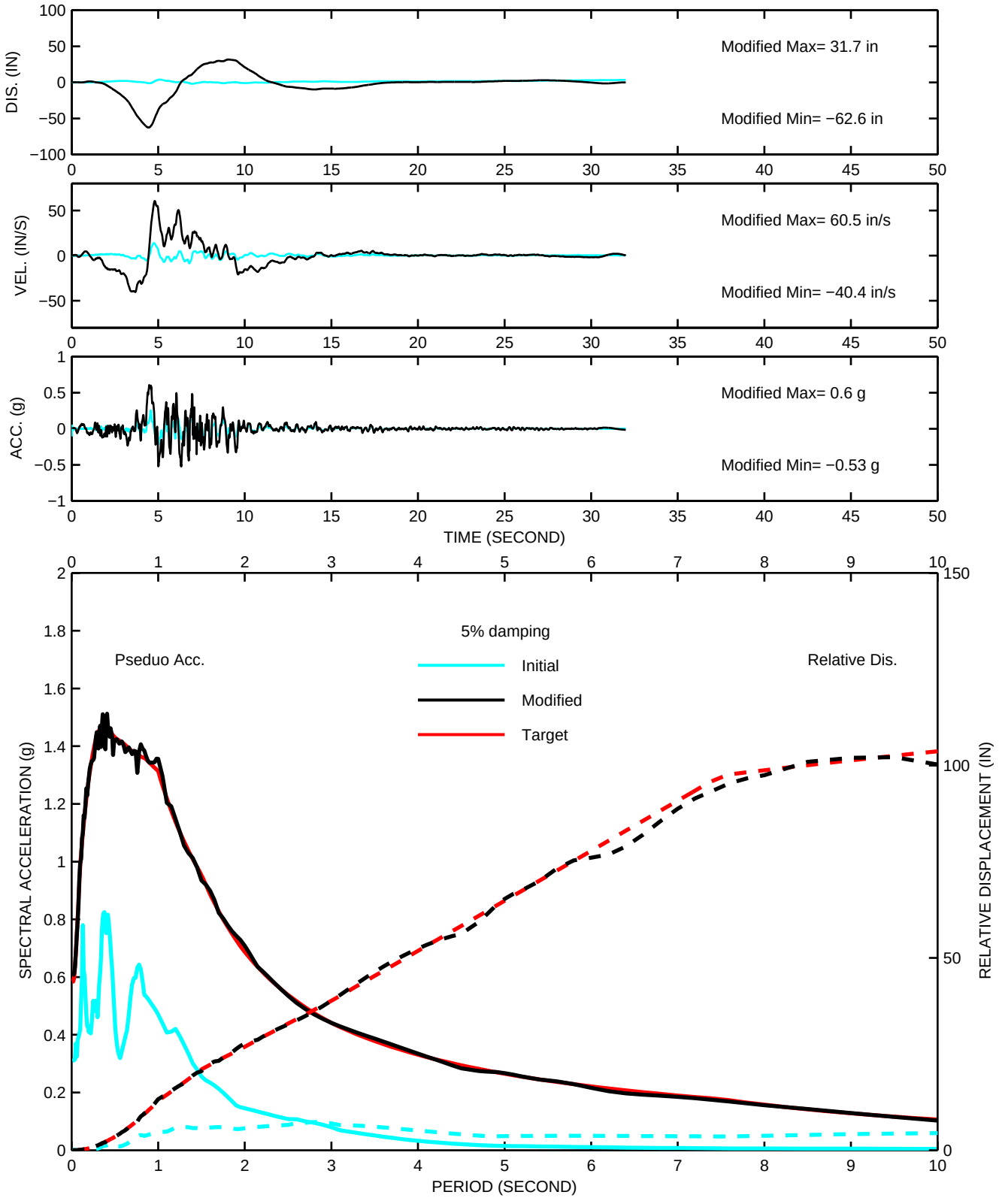


Figure E98. Unimproved Ground Area B DE Spectrum Compatible Ground Motion (5% Damped)−Set 7 FP

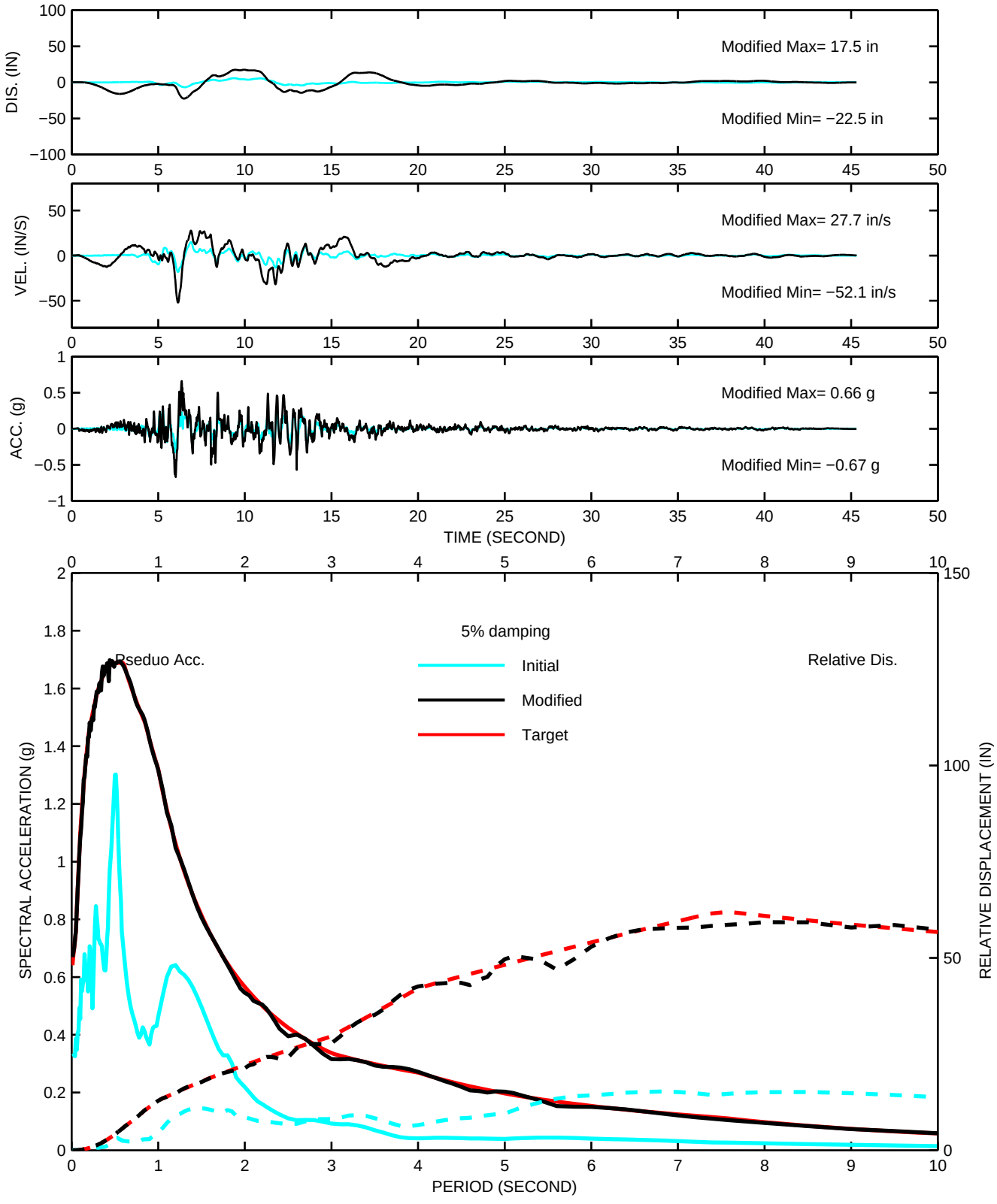


Figure E99. Unimproved Ground Area B 975−Yr Spectrum Compatible Ground Motion (5% Damped)−Set 1 FN

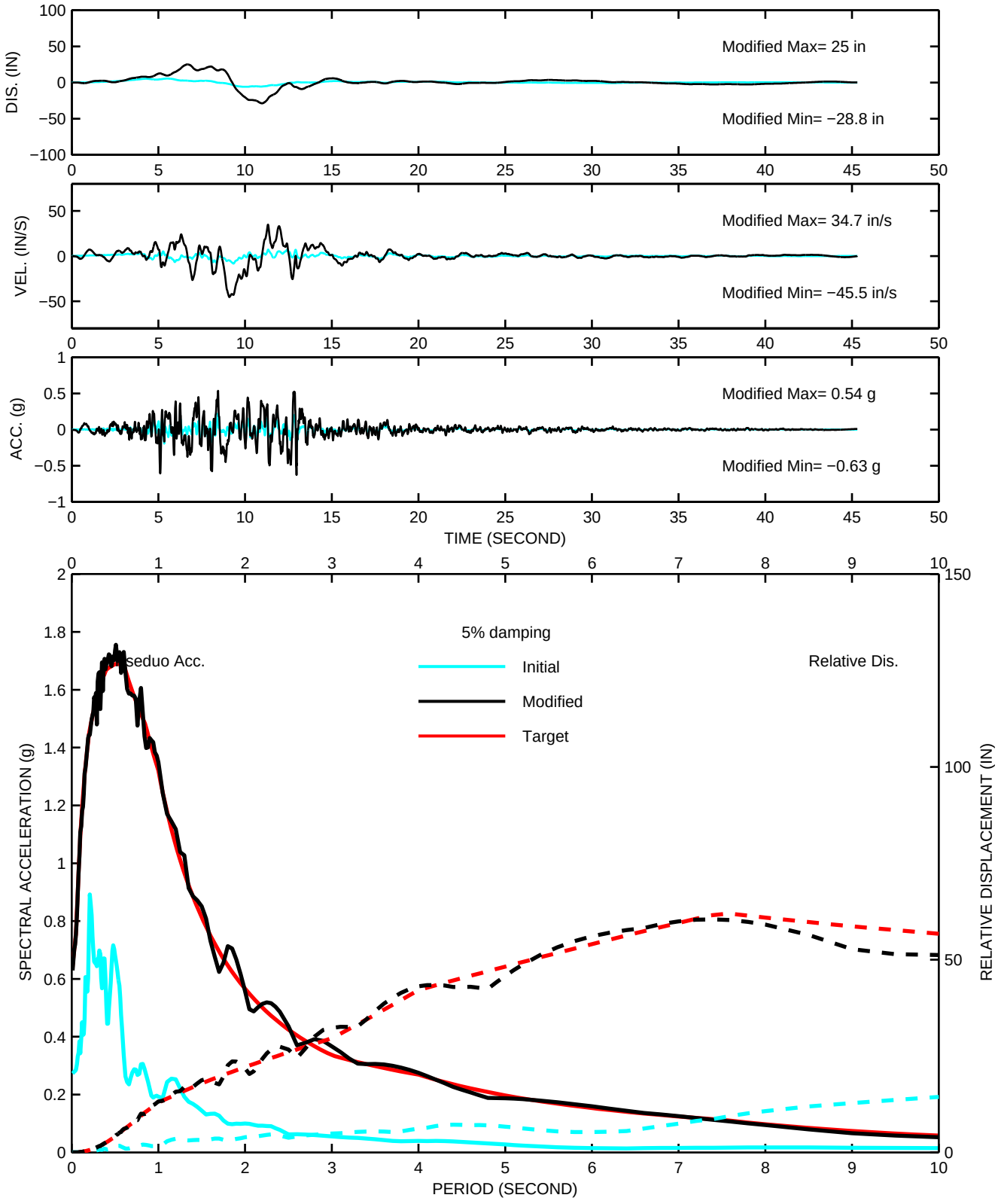


Figure E100. Unimproved Ground Area B 975−Yr Spectrum Compatible Ground Motion (5% Damped)−Set 1 FP

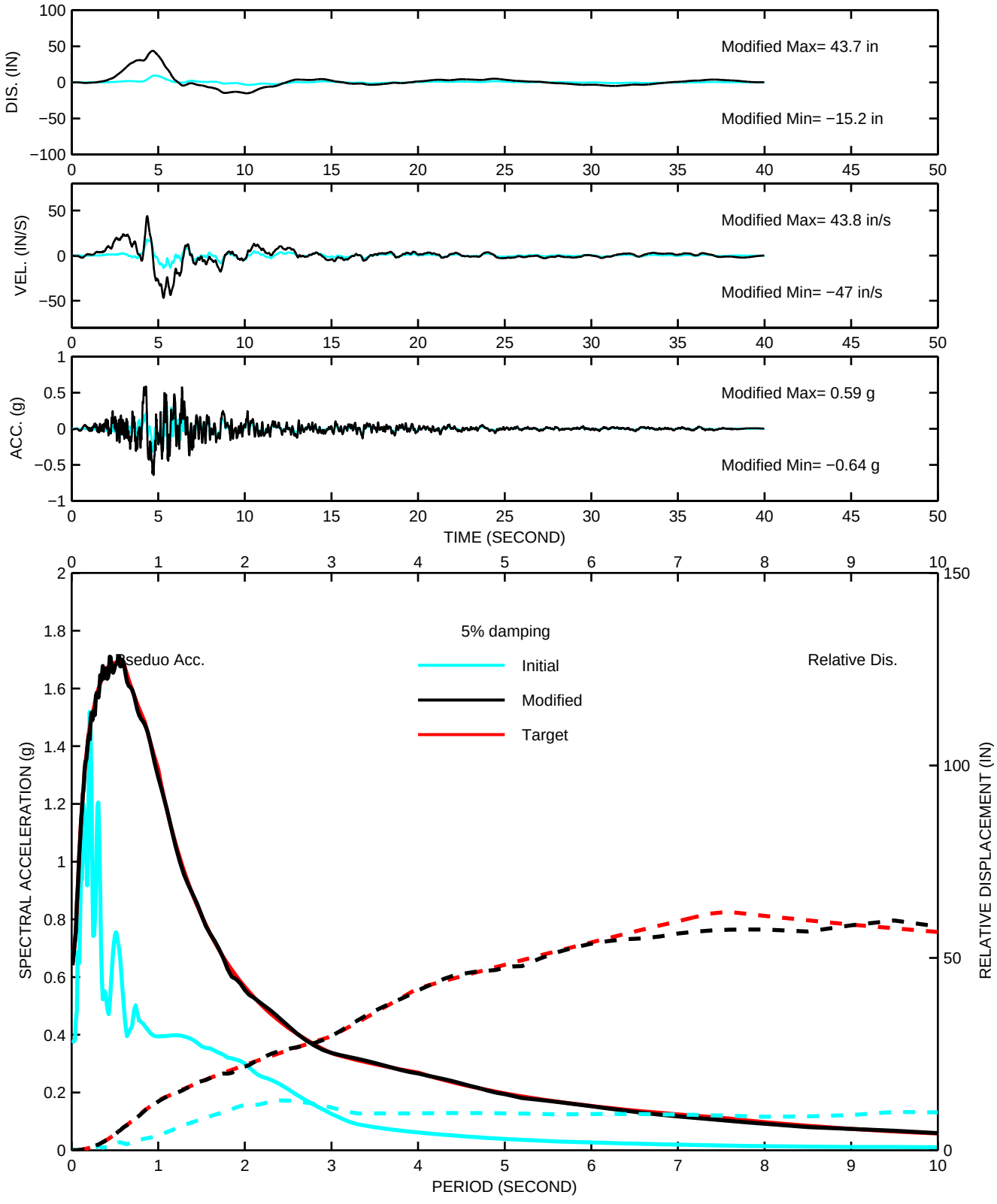


Figure E101. Unimproved Ground Area B 975−Yr Spectrum Compatible Ground Motion (5% Damped)−Set 2 FN

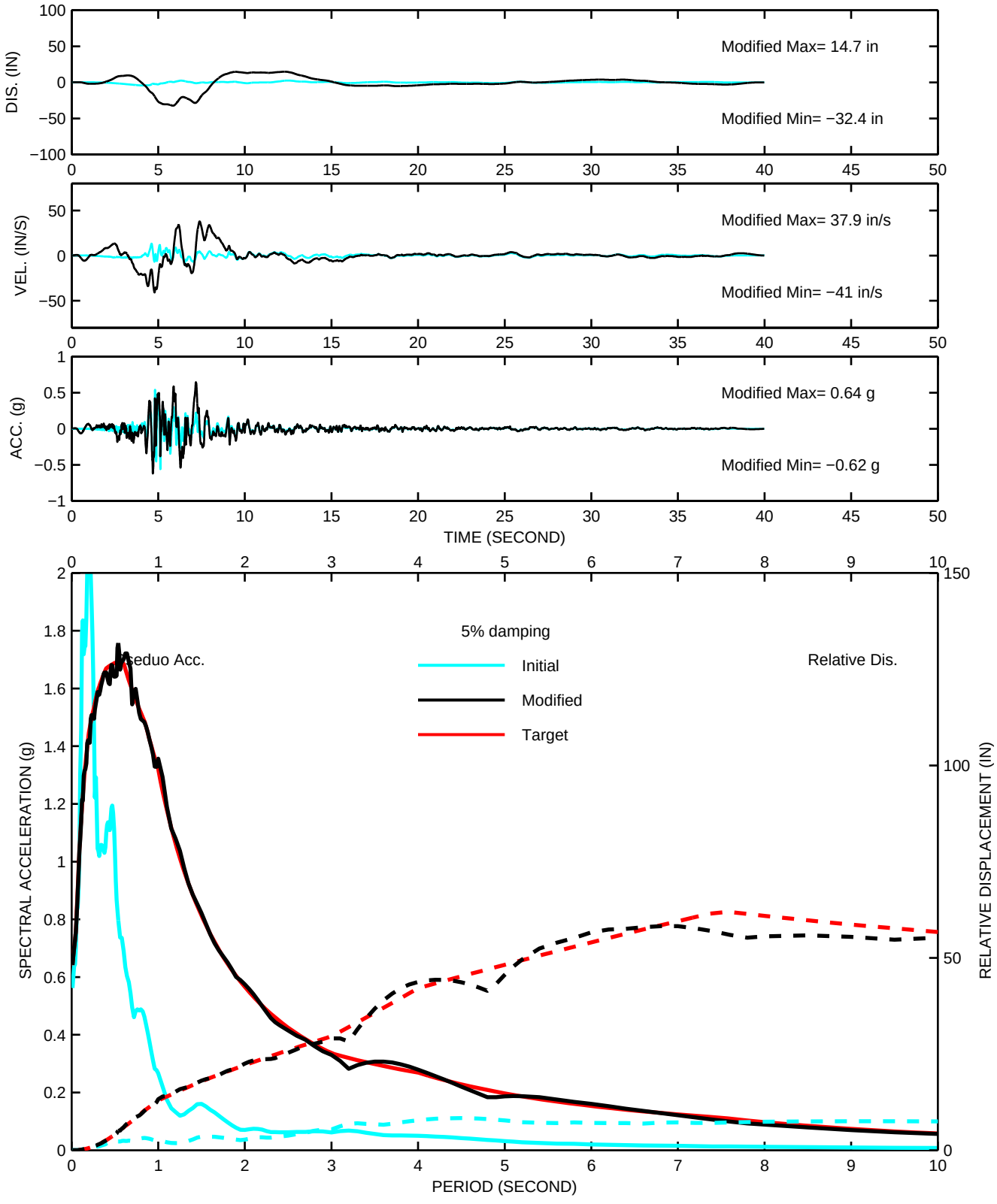


Figure E102. Unimproved Ground Area B 975−Yr Spectrum Compatible Ground Motion (5% Damped)−Set 2 FP

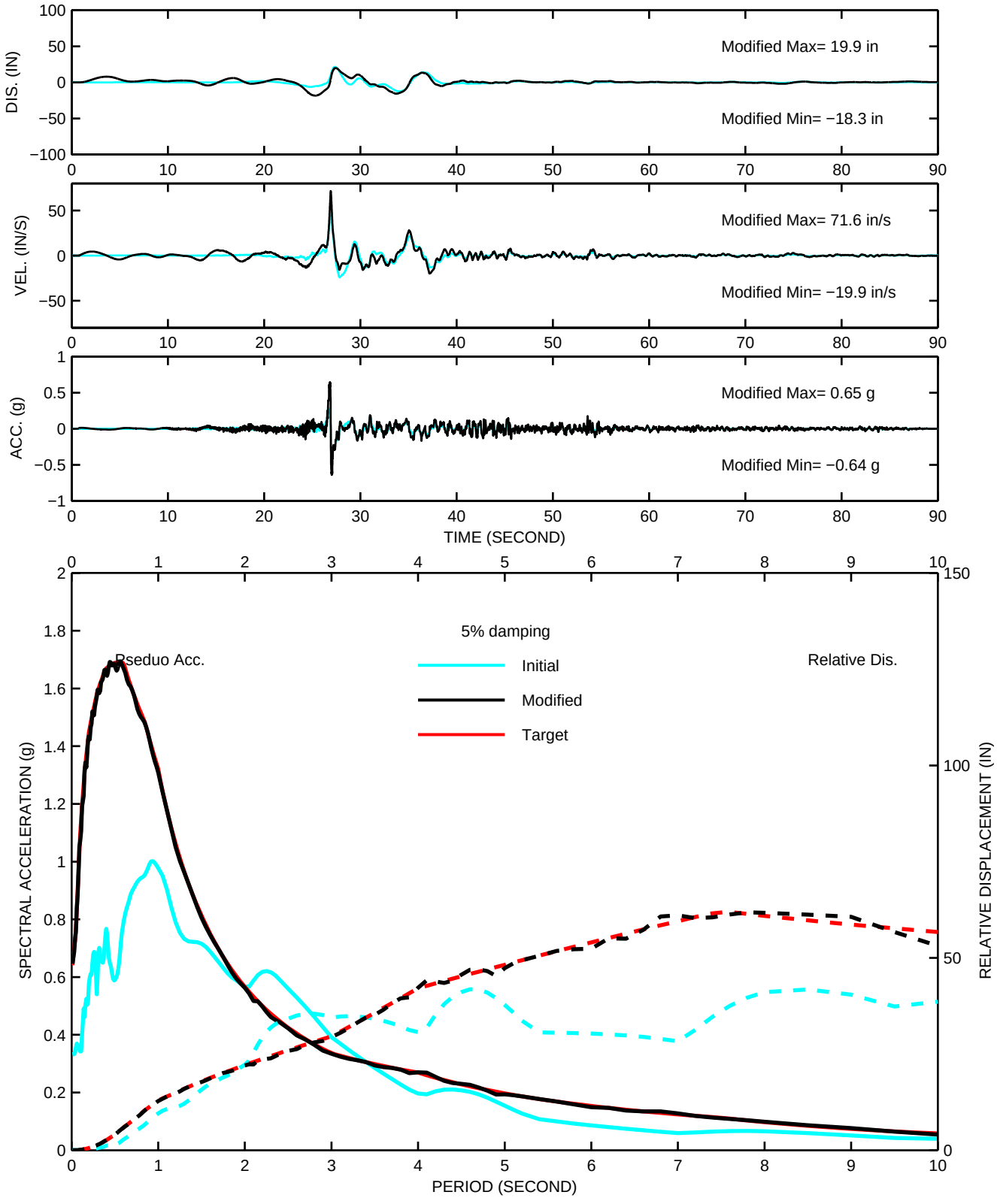


Figure E103. Unimproved Ground Area B 975−Yr Spectrum Compatible Ground Motion (5% Damped)−Set 3 FN

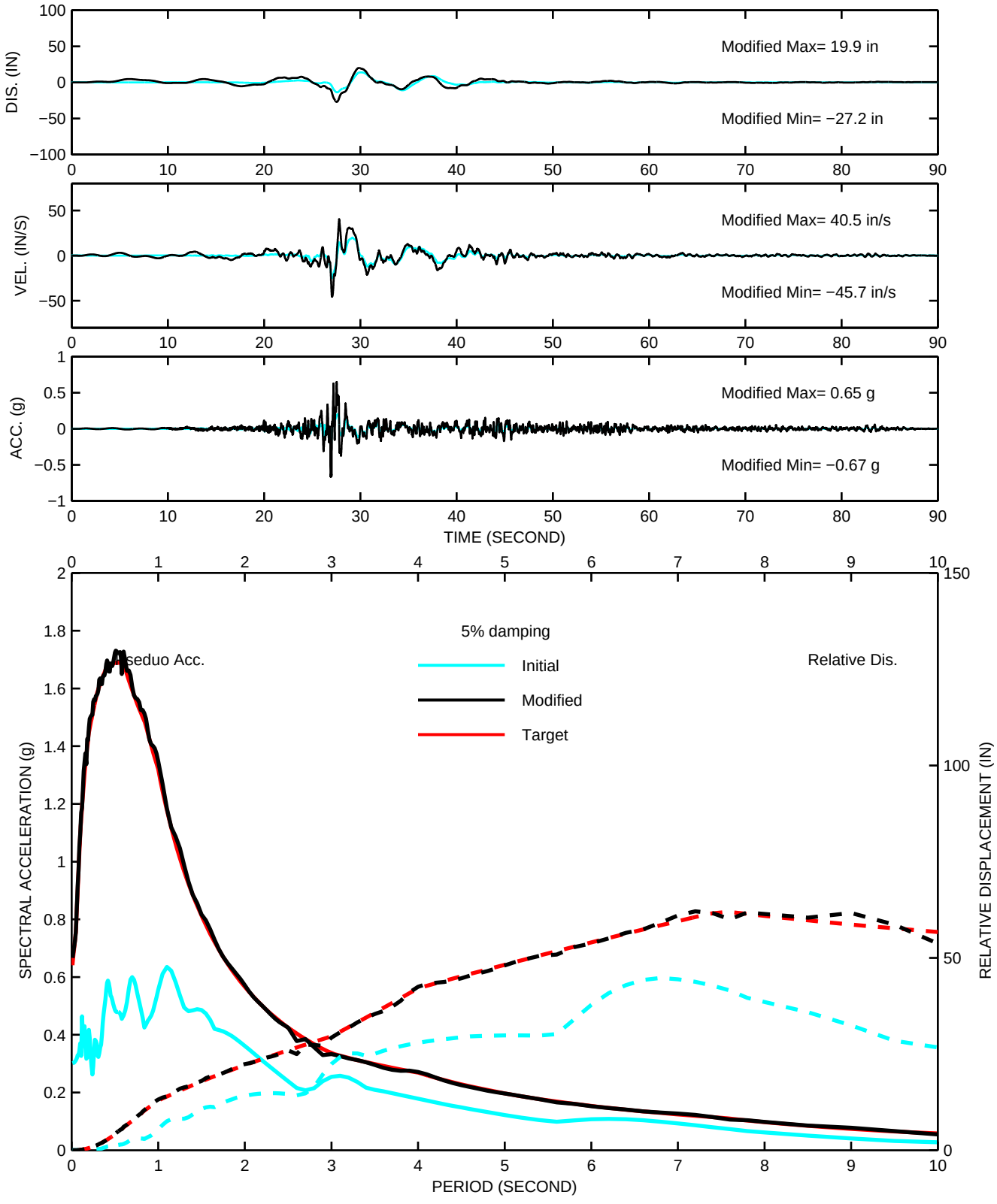


Figure E104. Unimproved Ground Area B 975−Yr Spectrum Compatible Ground Motion (5% Damped)−Set 3 FP

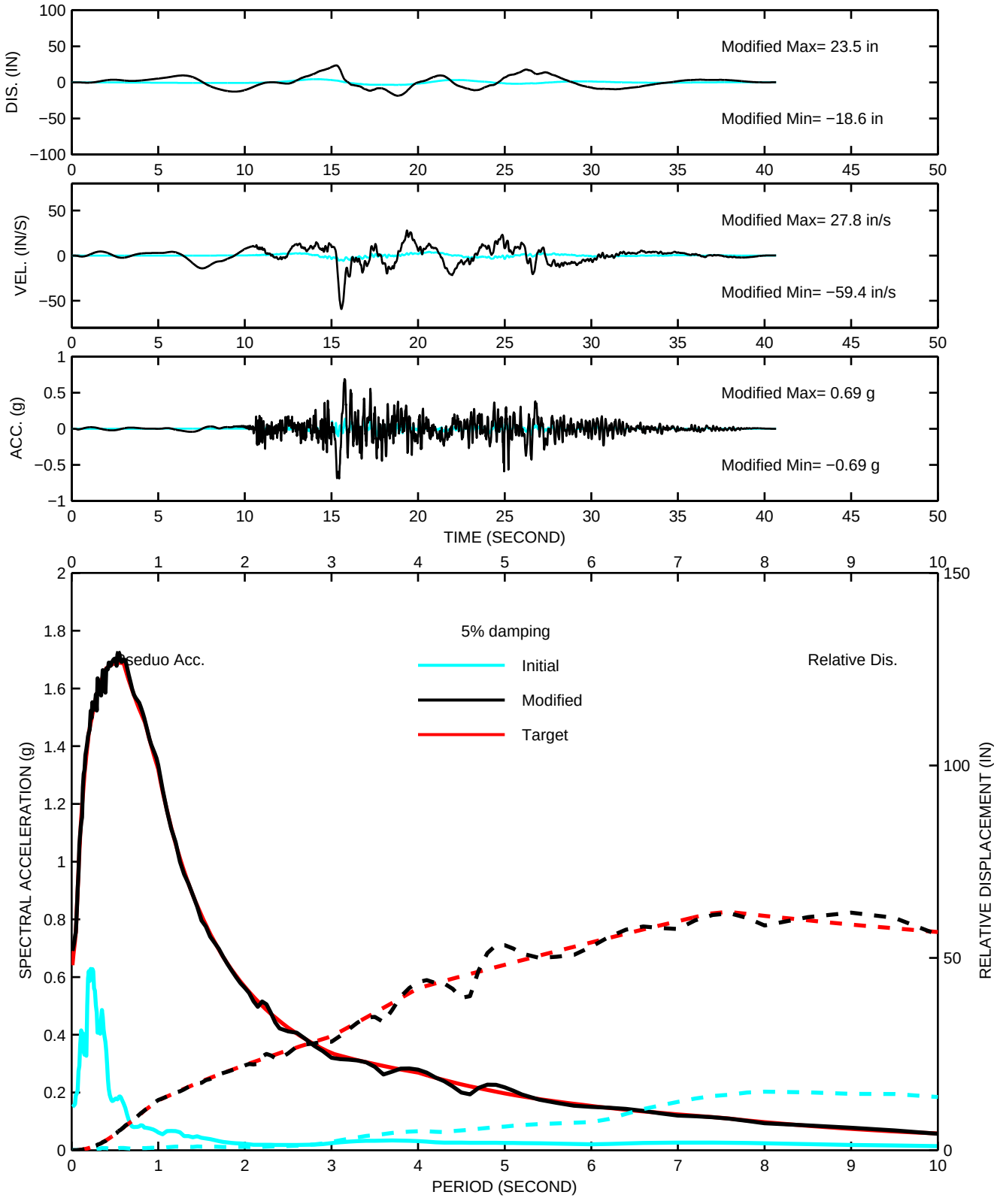


Figure E105. Unimproved Ground Area B 975−Yr Spectrum Compatible Ground Motion (5% Damped)−Set 4 FN

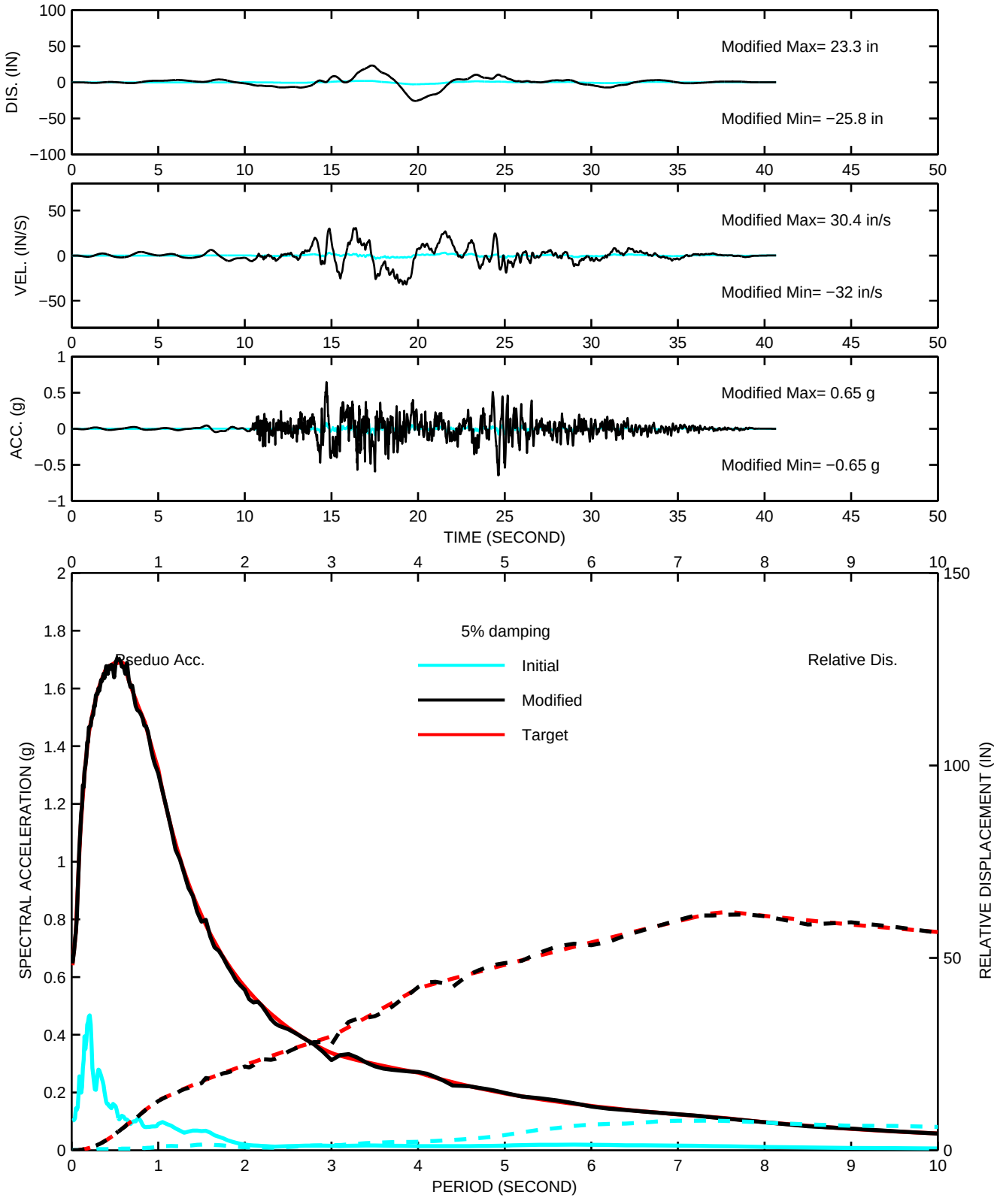


Figure E106. Unimproved Ground Area B 975−Yr Spectrum Compatible Ground Motion (5% Damped)−Set 4 FP

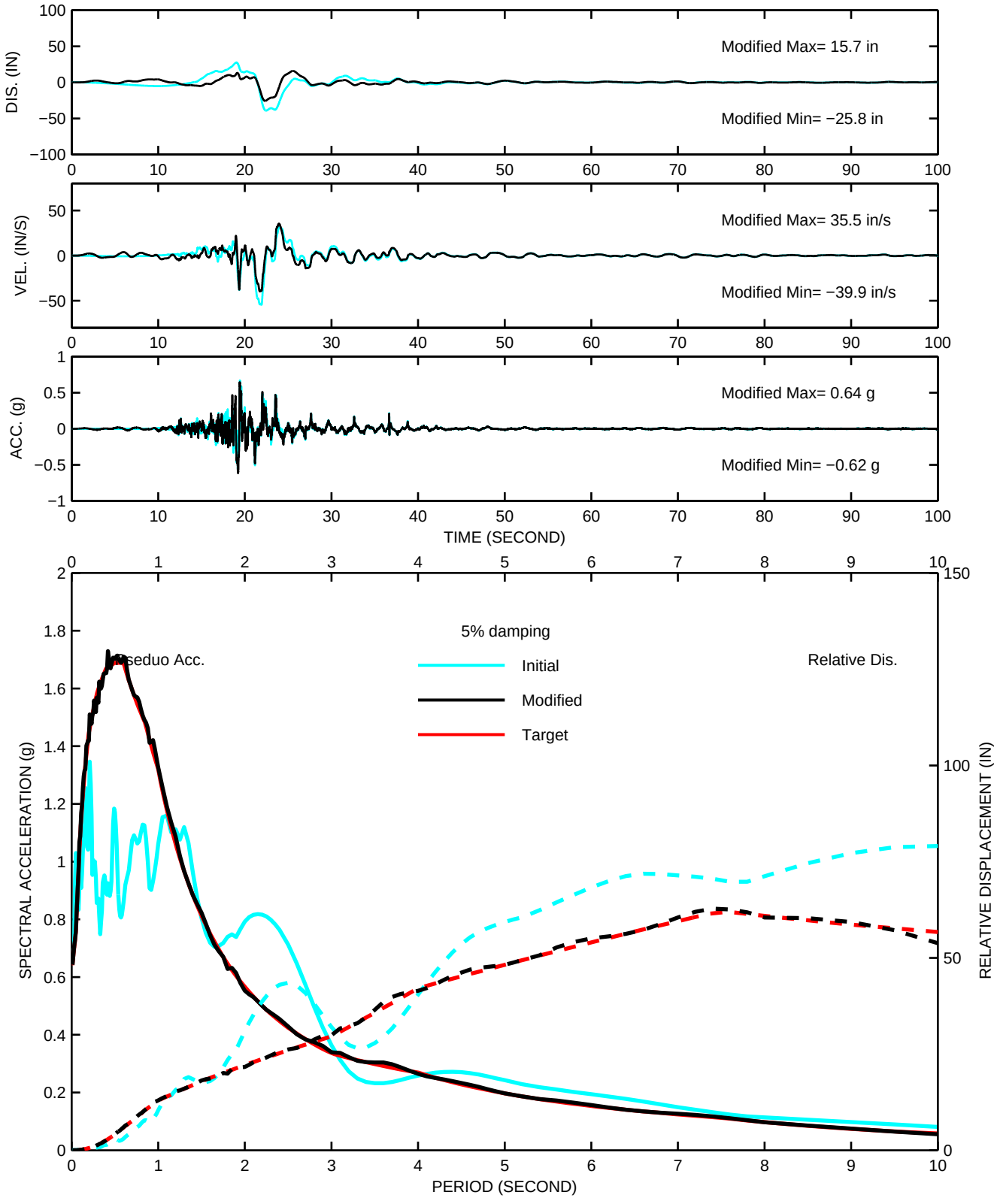


Figure E107. Unimproved Ground Area B 975−Yr Spectrum Compatible Ground Motion (5% Damped)−Set 5 FN

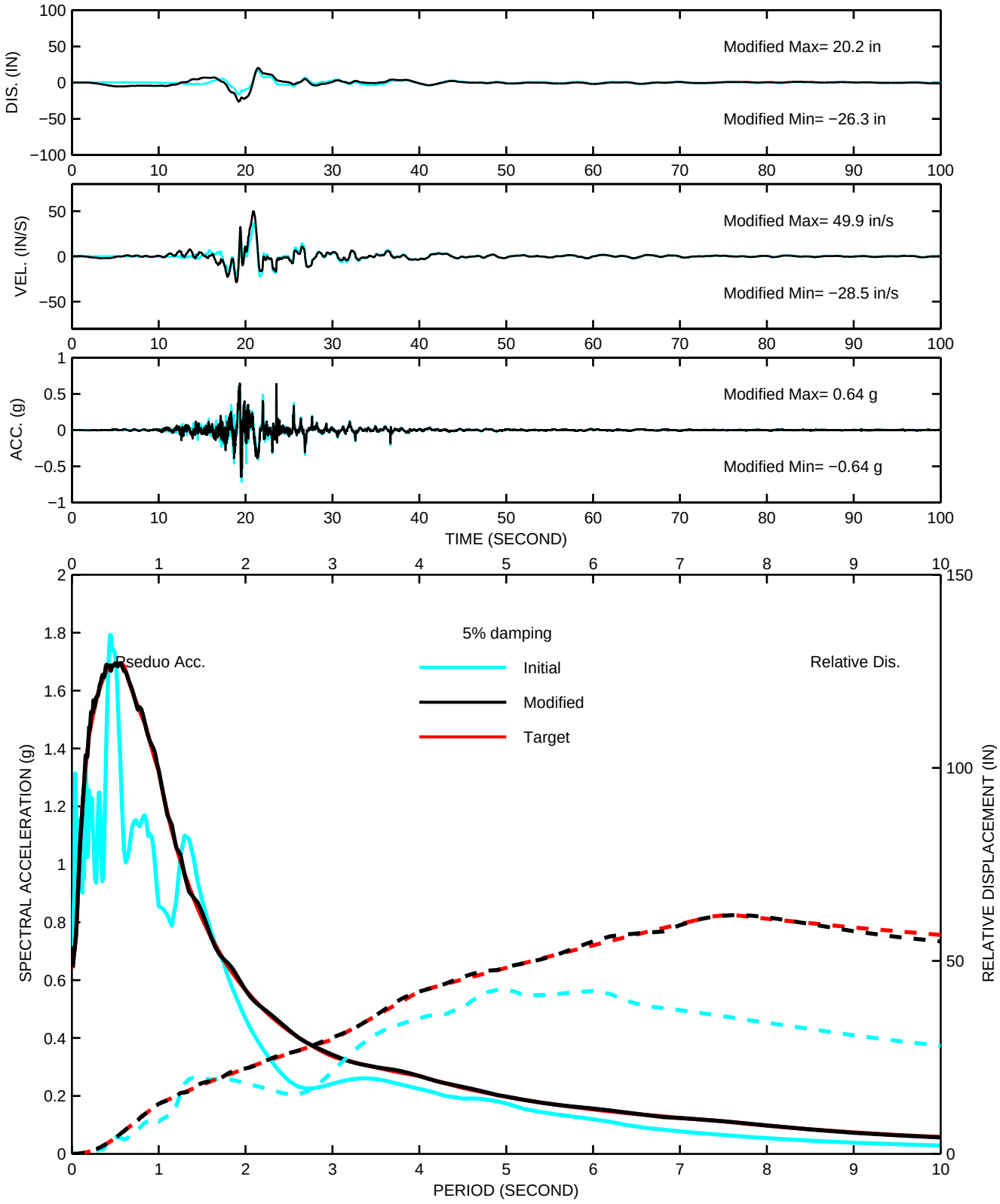


Figure E108. Unimproved Ground Area B 975−Yr Spectrum Compatible Ground Motion (5% Damped)−Set 5 FP

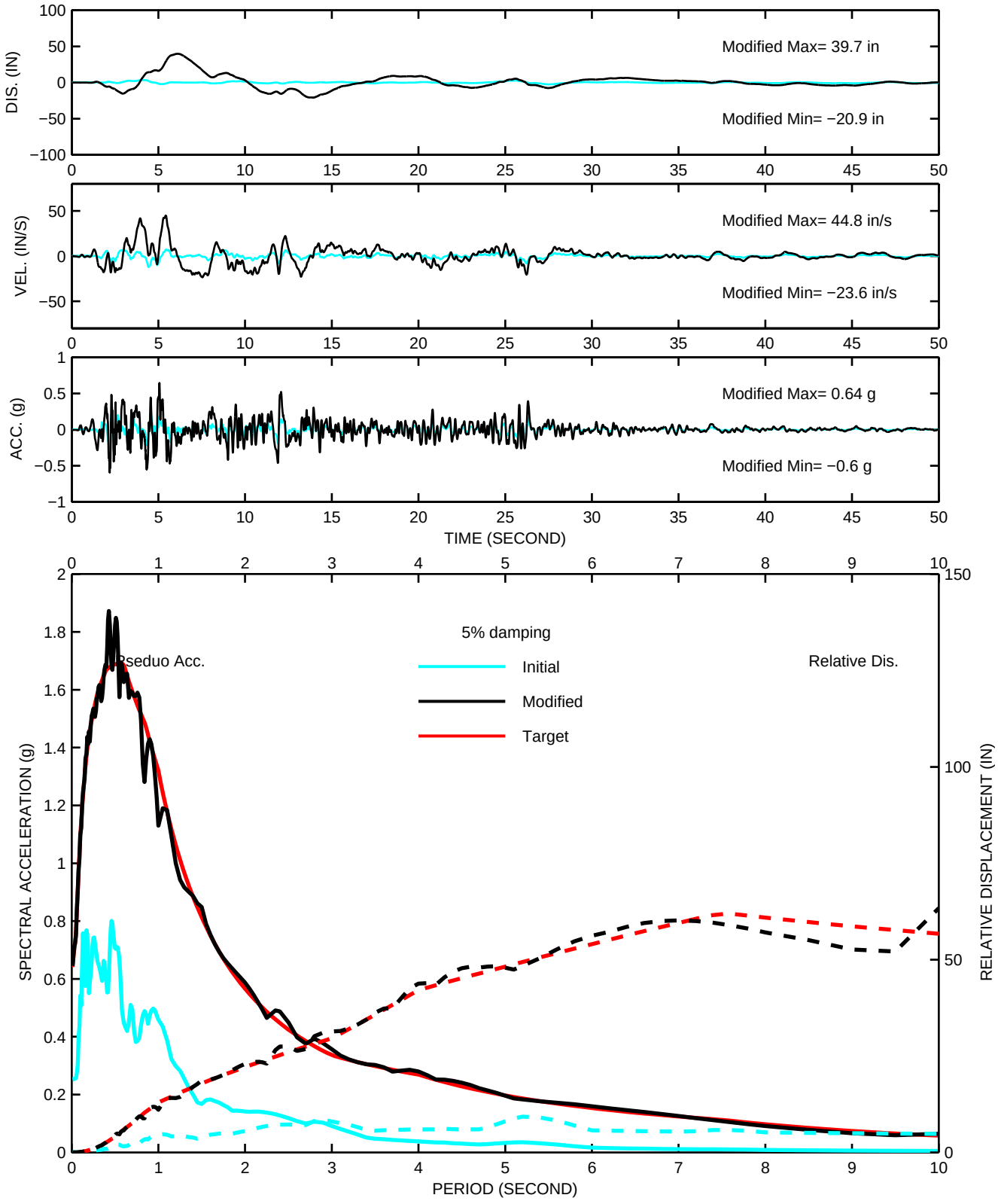


Figure E109. Unimproved Ground Area B 975−Yr Spectrum Compatible Ground Motion (5% Damped)−Set 6 FN

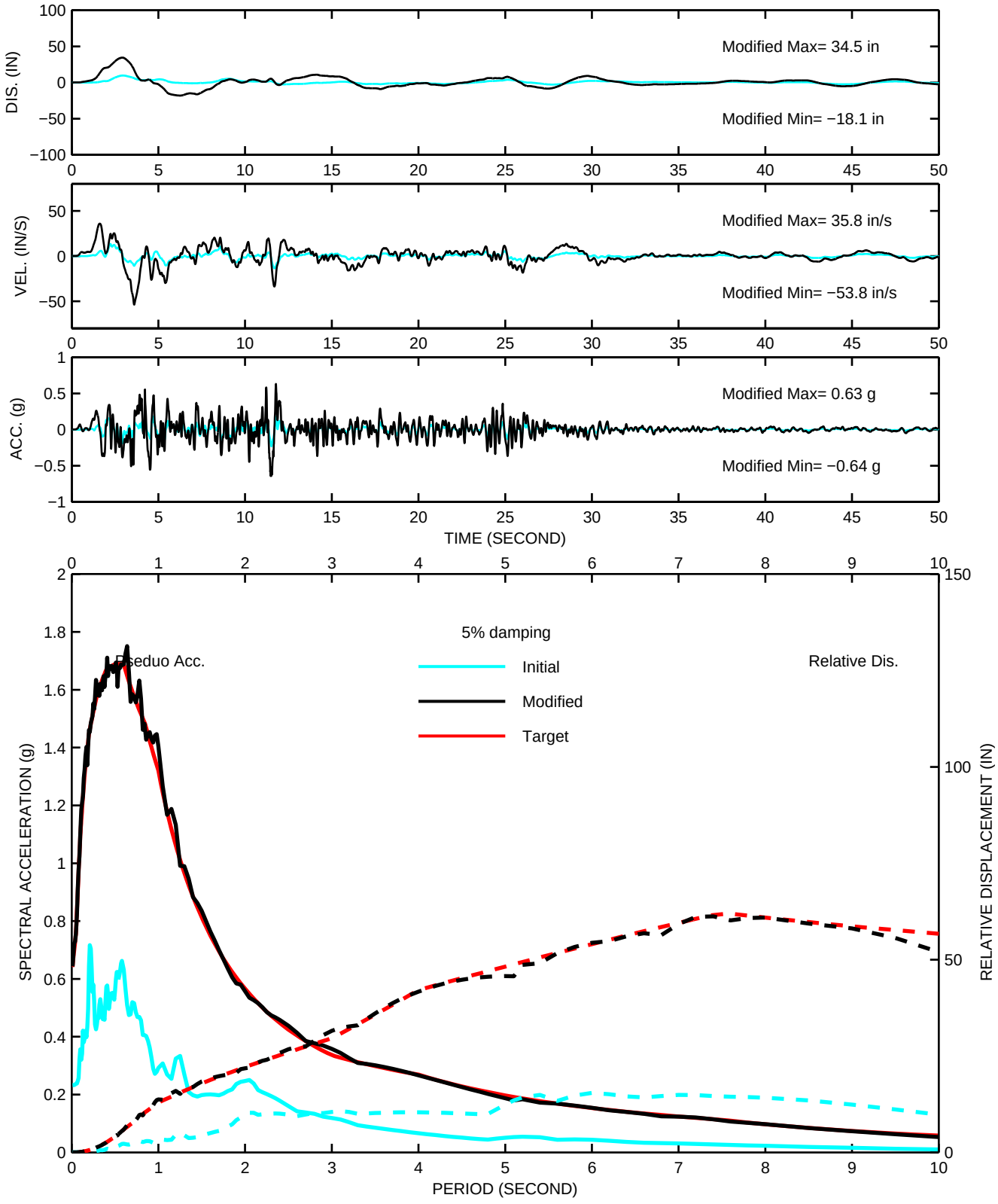


Figure E110. Unimproved Ground Area B 975−Yr Spectrum Compatible Ground Motion (5% Damped)−Set 6 FP

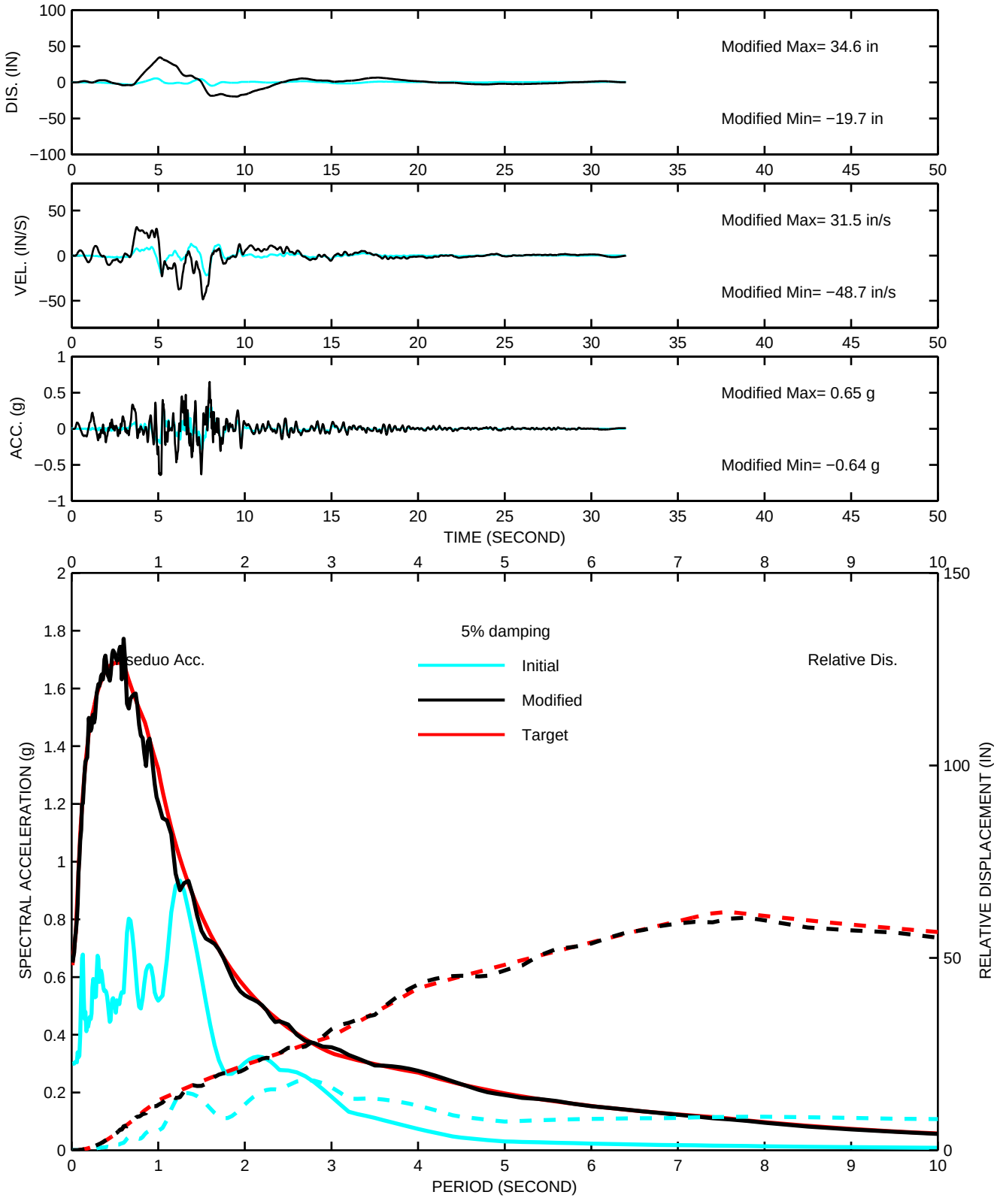


Figure E111. Unimproved Ground Area B 975−Yr Spectrum Compatible Ground Motion (5% Damped)−Set 7 FN

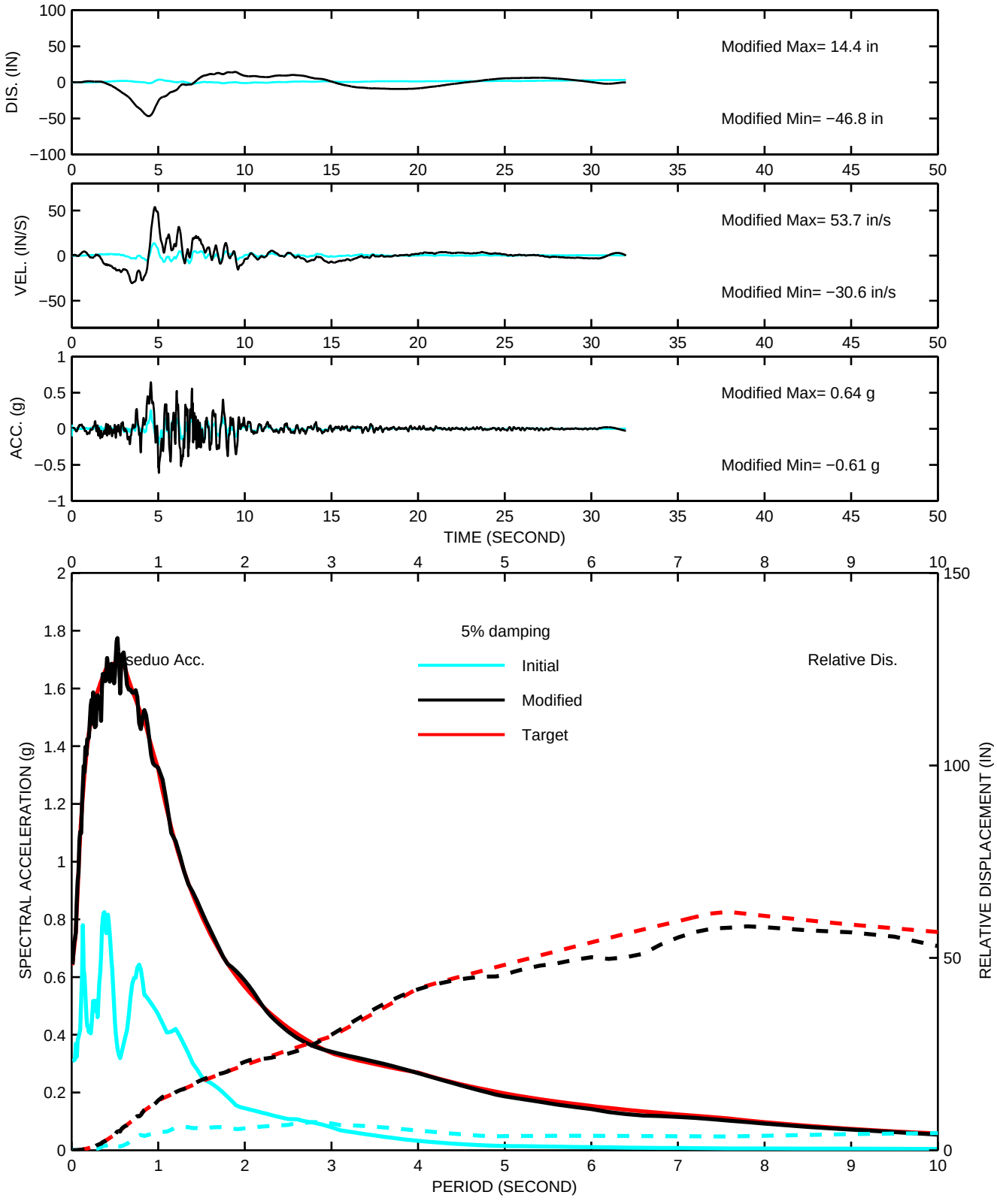


Figure E112. Unimproved Ground Area B 975−Yr Spectrum Compatible Ground Motion (5% Damped)−Set 7 FP